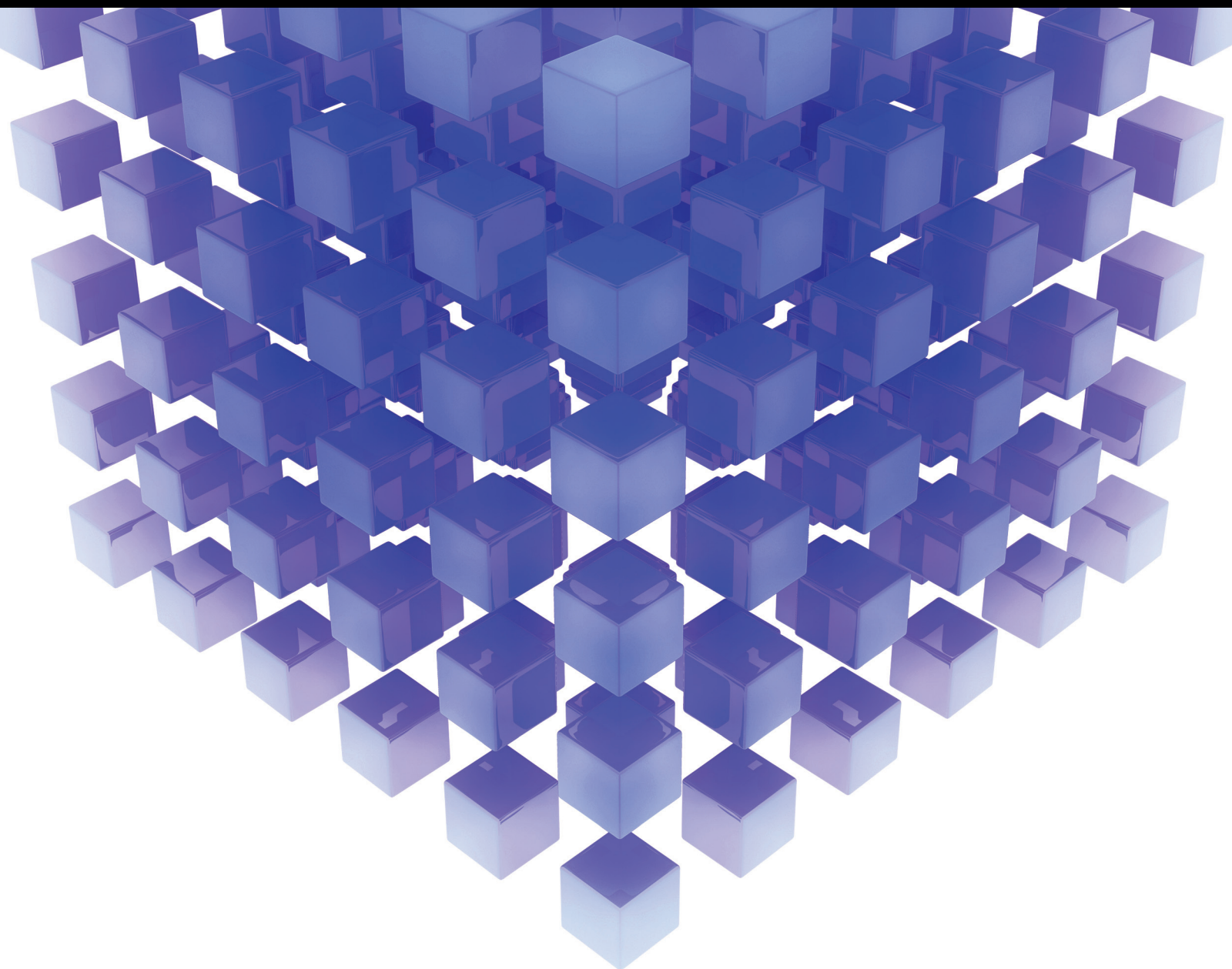


Mathematical Problems in Engineering

# Mathematical Theories and Applications for Nonlinear Control Systems

Special Issue Editor in Chief: Xue-Jun Xie

Guest Editors: Ju H. Park, Hiroaki Mukaidani, and Weihai Zhang





---

# **Mathematical Theories and Applications for Nonlinear Control Systems**

Mathematical Problems in Engineering

---

## **Mathematical Theories and Applications for Nonlinear Control Systems**

Special Issue Editor in Chief: Xue-Jun Xie

Guest Editors: Ju H. Park, Hiroaki Mukaidani, and Weihai Zhang



---

Copyright © 2019 Hindawi. All rights reserved.

This is a special issue published in “Mathematical Problems in Engineering.” All articles are open access articles distributed under the Creative Commons Attribution License, which permits unrestricted use, distribution, and reproduction in any medium, provided the original work is properly cited.

## Editorial Board

- Mohamed Abd El Aziz, Egypt  
AITOUCHE Abdelouhab, France  
Leonardo Acho, Spain  
José A. Acosta, Spain  
Daniela Addressi, Italy  
Paolo Addresso, Italy  
Claudia Adduce, Italy  
Ramesh Agarwal, USA  
Francesco Aggoggeri, Italy  
J. C. Agüero, Australia  
Ricardo Aguilar-Lopez, Mexico  
Tarek Ahmed-Ali, France  
Elias Aifantis, USA  
Muhammad N. Akram, Norway  
Guido Ala, Italy  
Andrea Alaimo, Italy  
Reza Alam, USA  
Nicholas Alexander, UK  
Salvatore Alfonzetti, Italy  
Mohammad D. Aliyu, Canada  
Juan A. Almendral, Spain  
José Domingo Álvarez, Spain  
Cláudio Alves, Portugal  
Juan P. Amezcua-Sanchez, Mexico  
Lionel Amodeo, France  
Sebastian Anita, Romania  
Renata Archetti, Italy  
Felice Arena, Italy  
Sabri Arik, Turkey  
Francesco Aristodemo, Italy  
Fausto Arpino, Italy  
Alessandro Arsie, USA  
Edoardo Artioli, Italy  
Fumihiko Ashida, Japan  
Farhad Aslani, Australia  
Mohsen Asle Zaem, USA  
Romain Aubry, USA  
Matteo Aureli, USA  
Richard I. Avery, USA  
Viktor Avrutin, Germany  
Francesco Aymerich, Italy  
Sajad Azizi, Belgium  
Michele Baccocchi, Italy  
Seungik Baek, USA  
Adil Bagirov, Australia  
Khaled Bahlali, France  
Laurent Bako, France  
Pedro Balaguer, Spain  
Stefan Balint, Romania  
Ines Tejado Balsera, Spain  
Alfonso Banos, Spain  
Jerzy Baranowski, Poland  
Roberto Baratti, Italy  
Andrzej Bartoszewicz, Poland  
David Bassir, France  
Chiara Bedon, Italy  
Azeddine Beghdadi, France  
Denis Benasciutti, Italy  
Ivano Benedetti, Italy  
Rosa M. Benito, Spain  
Elena Benvenuti, Italy  
Giovanni Berselli, Italy  
Giorgio Besagni, Italy  
Michele Betti, Italy  
Jean-Charles Beugnot, France  
Pietro Bia, Italy  
Carlo Bianca, France  
Simone Bianco, Italy  
Vincenzo Bianco, Italy  
Vittorio Bianco, Italy  
Gennaro N. Bifulco, Italy  
David Bigaud, France  
Antonio Bilotta, Italy  
Paul Bogdan, USA  
Guido Bolognesi, UK  
Rodolfo Bontempo, Italy  
Alberto Borboni, Italy  
Paolo Boscariol, Italy  
Daniela Boso, Italy  
Guillermo Botella-Juan, Spain  
Boulaïd Boulkroune, Belgium  
Fabio Bovenga, Italy  
Francesco Braghin, Italy  
Ricardo Branco, Portugal  
Maurizio Brocchini, Italy  
Julien Bruchon, France  
Matteo Bruggi, Italy  
Michele Brun, Italy  
Vasilis Burganos, Greece  
Tito Busani, USA  
Raquel Caballero-Águila, Spain  
Filippo Cacace, Italy  
Pierfrancesco Cacciola, UK  
Salvatore Caddemi, Italy  
Roberto Caldelli, Italy  
Alberto Campagnolo, Italy  
Eric Campos-Canton, Mexico  
Marko Canadija, Croatia  
Salvatore Cannella, Italy  
Francesco Cannizzaro, Italy  
Javier Cara, Spain  
Ana Carpio, Spain  
Caterina Casavola, Italy  
Sara Casciati, Italy  
Federica Caselli, Italy  
Carmen Castillo, Spain  
Inmaculada T. Castro, Spain  
Miguel Castro, Portugal  
Giuseppe Catalanotti, UK  
Nicola Caterino, Italy  
Alberto Cavallo, Italy  
Gabriele Cazzulani, Italy  
Luis Cea, Spain  
Song Cen, China  
Miguel Cerrolaza, Venezuela  
M. Chadli, France  
Gregory Chagnon, France  
Ludovic Chamoin, France  
Ching-Ter Chang, Taiwan  
Qing Chang, USA  
Michael J. Chappell, UK  
Kacem Chehdi, France  
Peter N. Cheimets, USA  
Xinkai Chen, Japan  
Luca Chiapponi, Italy  
Francisco Chicano, Spain  
Nicholas Chileshe, Australia  
Adrian Chmielewski, Poland  
Ioannis T. Christou, Greece  
Hung-Yuan Chung, Taiwan  
Simone Cinquemani, Italy  
Roberto G. Citarella, Italy

Joaquim Ciurana, Spain  
John D. Clayton, USA  
Francesco Clementi, Italy  
Piero Colajanni, Italy  
Giuseppina Colicchio, Italy  
Vassilios Constantoudis, Greece  
Enrico Conte, Italy  
Francesco Conte, Italy  
Alessandro Contento, USA  
Mario Cools, Belgium  
Jean-Pierre Corriou, France  
J.-C. Cortés, Spain  
Carlo Cosentino, Italy  
Paolo Crippa, Italy  
Andrea Crivellini, Italy  
Frederico Cruz, Brazil  
Erik Cuevas, Mexico  
Maria C. Cunha, Portugal  
Peter Dabnichki, Australia  
Luca D'Acerno, Italy  
Weizhong Dai, USA  
Andrea Dall'Asta, Italy  
P. Damodaran, USA  
Bhabani S. Dandapat, India  
Farhang Daneshmand, Canada  
Giuseppe D'Aniello, Italy  
Sergey Dashkovskiy, Germany  
Fabio De Angelis, Italy  
Samuele De Bartolo, Italy  
Abílio De Jesus, Portugal  
Pietro De Lellis, Italy  
Alessandro De Luca, Italy  
Stefano de Miranda, Italy  
Filippo de Monte, Italy  
M. do Rosário de Pinho, Portugal  
Michael Defoort, France  
Alessandro Della Corte, Italy  
Xavier Delorme, France  
Laurent Dewasme, Belgium  
Angelo Di Egidio, Italy  
Roberta Di Pace, Italy  
Ramón I. Diego, Spain  
Yannis Dimakopoulos, Greece  
Zhengtao Ding, UK  
M. Djemai, France  
Alexandre B. Dolgui, France  
Georgios Dounias, Greece  
Florent Duchaine, France  
George S. Dulikravich, USA  
Bogdan Dumitrescu, Romania  
Horst Ecker, Austria  
Saeed Eftekhari Azam, USA  
Ahmed El Hajjaji, France  
Antonio Elipe, Spain  
Fouad Erchiqui, Canada  
Anders Eriksson, Sweden  
R. Emre Erkmen, Canada  
Gilberto Espinosa-Paredes, Mexico  
Leandro F. F. Miguel, Brazil  
Andrea L. Facci, Italy  
Giacomo Falcucci, Italy  
Giovanni Falsone, Italy  
Hua Fan, China  
Nicholas Fantuzzi, Italy  
Yann Favennec, France  
Fiorenzo A. Fazzolari, UK  
Giuseppe Fedele, Italy  
Roberto Fedele, Italy  
Arturo J. Fernández, Spain  
Jesus M. Fernandez Oro, Spain  
Massimiliano Ferraioli, Italy  
Massimiliano Ferrara, Italy  
Francesco Ferrise, Italy  
Eric Feulvarch, France  
Barak Fishbain, Israel  
S. Douwe Flapper, Netherlands  
Thierry Floquet, France  
Eric Florentin, France  
Alessandro Formisano, Italy  
Francesco Franco, Italy  
Elisa Francomano, Italy  
Tomonari Furukawa, USA  
Juan C. G. Prada, Spain  
Mohamed Gadala, Canada  
Matteo Gaeta, Italy  
Mauro Gaggero, Italy  
Zoran Gajic, USA  
Erez Gal, Israel  
J. Gallardo-Alvarado, Mexico  
Ugo Galvanetto, Italy  
Akemi Gálvez, Spain  
Rita Gamberini, Italy  
Maria L. Gandarias, Spain  
Arman Ganji, Canada  
Zhiwei Gao, UK  
Zhong-Ke Gao, China  
Giovanni Garcea, Italy  
Luis Rodolfo Garcia Carrillo, USA  
Jose M. Garcia-Aznar, Spain  
Akhil Garg, China  
Alessandro Gasparetto, Italy  
Gianluca Gatti, Italy  
Oleg V. Gendelman, Israel  
Stylianos Georgantzinou, Greece  
Fotios Georgiades, UK  
Parviz Ghadimi, Iran  
Mergen H. Ghayesh, Australia  
Georgios I. Giannopoulos, Greece  
Agathoklis Giaralis, UK  
Pablo Gil, Spain  
Anna M. Gil-Lafuente, Spain  
Ivan Giorgio, Italy  
Gaetano Giunta, Luxembourg  
Alessio Gizzi, Italy  
Jefferson L.M.A. Gomes, UK  
Emilio Gómez-Déniz, Spain  
Antonio M. Gonçalves de Lima, Brazil  
David González, Spain  
Chris Goodrich, USA  
Rama S. R. Gorla, USA  
Kannan Govindan, Denmark  
Antoine Grall, France  
George A. Gravvanis, Greece  
Fabrizio Greco, Italy  
David Greiner, Spain  
Simonetta Grilli, Italy  
Jason Gu, Canada  
Federico Guarracino, Italy  
Michele Guida, Italy  
Zhaoxia Guo, China  
José L. Guzmán, Spain  
Quang Phuc Ha, Australia  
Petr Hájek, Czech Republic  
Weimin Han, USA  
Zhen-Lai Han, China  
Thomas Hanne, Switzerland  
Mohammad A. Hariri-Ardebili, USA  
Xiao-Qiao He, China  
Luca Heltai, Italy  
Nicolae Herisanu, Romania  
A. G. Hernández-Díaz, Spain

M.I. Herreros, Spain  
 Eckhard Hitzer, Japan  
 Paul Honeine, France  
 Jaromir Horacek, Czech Republic  
 Muneo Hori, Japan  
 András Horváth, Italy  
 S. Hassan Hosseinnia, Netherlands  
 Gordon Huang, Canada  
 Sajid Hussain, Canada  
 Asier Ibeas, Spain  
 Orest V. Iftime, Netherlands  
 Przemyslaw Ignaciuk, Poland  
 Giacomo Innocenti, Italy  
 Emilio Insfran Pelozo, Spain  
 Alessio Ishizaka, UK  
 Nazrul Islam, USA  
 Benoit Jung, France  
 Benjamin Ivorra, Spain  
 Payman Jalali, Finland  
 Mahdi Jalili, Australia  
 Łukasz Jankowski, Poland  
 Samuel N. Jator, USA  
 J. C. Jauregui-Correa, Mexico  
 Reza Jazar, Australia  
 Khalide Jbilou, France  
 Piotr Jędrzejowicz, Poland  
 Isabel S. Jesus, Portugal  
 Linni Jian, China  
 Bin Jiang, China  
 Zhongping Jiang, USA  
 Emilio Jiménez Macías, Spain  
 Ningde Jin, China  
 Xiaoliang Jin, USA  
 Liang Jing, Canada  
 Dylan F. Jones, UK  
 Palle E. Jorgensen, USA  
 Vyacheslav Kalashnikov, Mexico  
 Tamas Kalmar-Nagy, Hungary  
 Tomasz Kapitaniak, Poland  
 Julius Kaplunov, UK  
 Haranath Kar, India  
 Konstantinos Karamanos, Belgium  
 Krzysztof Kecik, Poland  
 Jean-Pierre Kenne, Canada  
 Ch. M. Khaliq, South Africa  
 Do Wan Kim, Republic of Korea  
 Nam-Il Kim, Republic of Korea  
 Jan Koci, Czech Republic  
 Ioannis Kostavelis, Greece  
 Sotiris B. Kotsiantis, Greece  
 Manfred Krafczyk, Germany  
 Frederic Kratz, France  
 Petr Krysl, USA  
 Krzysztof S. Kulpa, Poland  
 Shailesh I. Kundalwal, India  
 Jurgen Kurths, Germany  
 Cedrick A. K. Kwimiy, USA  
 Kyandoghere Kyamakya, Austria  
 Davide La Torre, Italy  
 Risto Lahdelma, Finland  
 Hak-Keung Lam, UK  
 Giovanni Lancioni, Italy  
 Jimmy Lauber, France  
 Antonino Laudani, Italy  
 Hervé Laurent, France  
 Aimé Lay-Ekuakille, Italy  
 Nicolas J. Leconte, France  
 Dimitri Lefebvre, France  
 Eric Lefevre, France  
 Marek Lefik, Poland  
 Yaguo Lei, China  
 Kauko Leiviskä, Finland  
 Thibault Lemaire, France  
 Roman Lewandowski, Poland  
 Chen-Feng Li, China  
 Jian Li, USA  
 Yang Li, China  
 Huchang Liao, China  
 En-Qiang Lin, USA  
 Zhiyun Lin, China  
 Peide Liu, China  
 Peter Liu, Taiwan  
 Wanquan Liu, Australia  
 Bonifacio Llamazares, Spain  
 Alessandro Lo Schiavo, Italy  
 Jean Jacques Loiseau, France  
 Francesco Lolli, Italy  
 Paolo Lonetti, Italy  
 Sandro Longo, Italy  
 António M. Lopes, Portugal  
 Sebastian López, Spain  
 Pablo Lopez-Crespo, Spain  
 Luis M. López-Ochoa, Spain  
 Ezequiel López-Rubio, Spain  
 Vassilios C. Loukopoulos, Greece  
 Jose A. Lozano-Galant, Spain  
 haiyan Lu, Australia  
 Gabriel Luque, Spain  
 Valentin Lychagin, Norway  
 Antonio Madeo, Italy  
 José María Maestre, Spain  
 Alessandro Magnani, Italy  
 Fazal M. Mahomed, South Africa  
 Noureddine Manamanni, France  
 Paolo Manfredi, Italy  
 Didier Maquin, France  
 Giuseppe Carlo Marano, Italy  
 Damijan Markovic, France  
 Francesco Marotti de Sciarra, Italy  
 Rui Cunha Marques, Portugal  
 Rodrigo Martinez-Bejar, Spain  
 Guiomar Martín-Herrán, Spain  
 Denizar Cruz Martins, Brazil  
 Benoit Marx, France  
 Elio Masciari, Italy  
 Franck Massa, France  
 Paolo Massioni, France  
 Alessandro Mauro, Italy  
 Fabio Mazza, Italy  
 Laura Mazzola, Italy  
 Driss Mehdi, France  
 Roderick Melnik, Canada  
 Pasquale Memmolo, Italy  
 Xiangyu Meng, USA  
 Jose Merodio, Spain  
 Alessio Merola, Italy  
 Mahmoud Mesbah, Iran  
 Luciano Mescia, Italy  
 Laurent Mevel, France  
 Mariusz Michta, Poland  
 Aki Mikkola, Finland  
 Giovanni Minafò, Italy  
 Hiroyuki Mino, Japan  
 Pablo Mira, Spain  
 Dimitrios Mitsotakis, New Zealand  
 Vito Mocella, Italy  
 Sara Montagna, Italy  
 Roberto Montanini, Italy  
 Francisco J. Montáns, Spain  
 Gisele Mophou, France  
 Rafael Morales, Spain

Marco Morandini, Italy  
J. Moreno-Valenzuela, Mexico  
Simone Morganti, Italy  
Caroline Mota, Brazil  
Aziz Moukrim, France  
Dimitris Mourtzis, Greece  
Emiliano Mucchi, Italy  
Josefa Mula, Spain  
Jose J. Muñoz, Spain  
Giuseppe Muscolino, Italy  
Marco Mussetta, Italy  
Hakim Naceur, France  
Alessandro Naddeo, Italy  
Hassane Naji, France  
Mariko Nakano-Miyatake, Mexico  
Keivan Navaie, UK  
AMA Neves, Portugal  
Luís C. Neves, UK  
Dong Ngoduy, New Zealand  
Nhon Nguyen-Thanh, Singapore  
Tatsushi Nishi, Japan  
Xesús Nogueira, Spain  
Ben T. Nohara, Japan  
Mohammed Nouari, France  
Mustapha Nourelfath, Canada  
Włodzimierz Ogryczak, Poland  
Roger Ohayon, France  
Krzysztof Okarma, Poland  
Mitsuhiro Okayasu, Japan  
Alberto Olivares, Spain  
Enrique Onieva, Spain  
Calogero Orlando, Italy  
Alejandro Ortega-Moñux, Spain  
Sergio Ortobelli, Italy  
Naohisa Otsuka, Japan  
Erika Ottaviano, Italy  
Pawel Packo, Poland  
Arturo Pagano, Italy  
Alkis S. Paipetis, Greece  
Roberto Palma, Spain  
Alessandro Palmeri, UK  
Pasquale Palumbo, Italy  
Weifeng Pan, China  
Jürgen Pannek, Germany  
Elena Panteley, France  
Achille Paolone, Italy  
George A. Papakostas, Greece  
Xosé M. Pardo, Spain  
Vicente Parra-Vega, Mexico  
Manuel Pastor, Spain  
Petr Páta, Czech Republic  
Pubudu N. Pathirana, Australia  
Surajit Kumar Paul, India  
Sitek Paweł, Poland  
Luis Payá, Spain  
Alexander Paz, Australia  
Igor Pažanin, Croatia  
Libor Pekař, Czech Republic  
Francesco Pellicano, Italy  
Marcello Pellicciari, Italy  
Haipeng Peng, China  
Mingshu Peng, China  
Zhengbiao Peng, Australia  
Zhi-ke Peng, China  
Marzio Pennisi, Italy  
Maria Patrizia Pera, Italy  
Matjaz Perc, Slovenia  
A. M. Bastos Pereira, Portugal  
Ricardo Perera, Spain  
Francesco Pesavento, Italy  
Ivo Petras, Slovakia  
Francesco Petrini, Italy  
Lukasz Pieczonka, Poland  
Dario Piga, Switzerland  
Paulo M. Pimenta, Brazil  
Antonina Pirrotta, Italy  
Marco Pizzarelli, Italy  
Vicent Pla, Spain  
Javier Plaza, Spain  
Kemal Polat, Turkey  
Dragan Poljak, Croatia  
Jorge Pomares, Spain  
Sébastien Poncet, Canada  
Volodymyr Ponomaryov, Mexico  
Jean-Christophe Ponsart, France  
Mauro Pontani, Italy  
Cornelio Posadas-Castillo, Mexico  
Francesc Pozo, Spain  
Christopher Pretty, New Zealand  
Luca Pugi, Italy  
Krzysztof Puszynski, Poland  
Giuseppe Quaranta, Italy  
Vitomir Racic, Italy  
Jose Ragot, France  
Carlo Rainieri, Italy  
Kumbakonam Ramamani Rajagopal, USA  
Ali Ramazani, USA  
Higinio Ramos, Spain  
Alain Rassinieux, France  
S.S. Ravindran, USA  
Alessandro Reali, Italy  
Jose A. Reinoso, Spain  
Oscar Reinoso, Spain  
Carlo Renno, Italy  
Fabrizio Renno, Italy  
Nidhal Rezg, France  
Ricardo Riaza, Spain  
Francesco Riganti-Fulginei, Italy  
Gerasimos Rigatos, Greece  
Francesco Ripamonti, Italy  
Jorge Rivera, Mexico  
Eugenio Roanes-Lozano, Spain  
Bruno G. M. Robert, France  
Ana Maria A. C. Rocha, Portugal  
José Rodellar, Spain  
Luigi Rodino, Italy  
Rosana Rodríguez López, Spain  
Ignacio Rojas, Spain  
Alessandra Romolo, Italy  
Debasish Roy, India  
Gianluigi Rozza, Italy  
Jose de Jesus Rubio, Mexico  
Rubén Ruiz, Spain  
Antonio Ruiz-Cortes, Spain  
Ivan D. Rukhlenko, Australia  
Mazen Saad, France  
Kishin Sadarangani, Spain  
Andrés Sáez, Spain  
Mehrhad Saif, Canada  
John S. Sakellariou, Greece  
Salvatore Salamone, USA  
Vicente Salas, Spain  
Jose Vicente Salcedo, Spain  
Nunzio Salerno, Italy  
Miguel A. Salido, Spain  
Roque J. Saltarén, Spain  
Alessandro Salvini, Italy  
Sylwester Samborski, Poland  
Ramon Sancibrian, Spain  
Giuseppe Sanfilippo, Italy  
Vittorio Sansalone, France

José A. Sanz-Herrera, Spain  
Nickolas S. Sapidis, Greece  
E. J. Sapountzakis, Greece  
Luis Saucedo-Mora, Spain  
Marcelo A. Savi, Brazil  
Andrey V. Savkin, Australia  
Roberta Sburlati, Italy  
Gustavo Scaglia, Argentina  
Thomas Schuster, Germany  
Oliver Schütze, Mexico  
Lotfi Senhadji, France  
Junwon Seo, USA  
Joan Serra-Sagrasta, Spain  
Gerardo Severino, Italy  
Ruben Sevilla, UK  
Stefano Sfarra, Italy  
Mohamed Shaat, Egypt  
Mostafa S. Shadloo, France  
Leonid Shaikhet, Israel  
Hassan M. Shanechi, USA  
Bo Shen, Germany  
Suzanne M. Shontz, USA  
Babak Shotorban, USA  
Zhan Shu, UK  
Nuno Simões, Portugal  
Christos H. Skiadas, Greece  
Konstantina Skouri, Greece  
Neale R. Smith, Mexico  
Bogdan Smolka, Poland  
Delfim Soares Jr., Brazil  
Alba Sofi, Italy  
Francesco Soldovieri, Italy  
Raffaele Solimene, Italy  
Jussi Sopenan, Finland  
Marco Spadini, Italy  
Bernardo Spagnolo, Italy  
Paolo Spagnolo, Italy  
Ruben Specogna, Italy  
Vasilios Spitas, Greece  
Sri Sridharan, USA  
Ivanka Stamova, USA  
Rafał Stanisławski, Poland  
Florin Stoican, Romania  
Salvatore Strano, Italy  
Yakov Strelniker, Israel  
Ning Sun, China  
Sergey A. Suslov, Australia

Thomas Svensson, Sweden  
Andrzej Swierniak, Poland  
Andras Szekrenyes, Hungary  
Kumar K. Tamma, USA  
Yang Tang, Germany  
Hafez Tari, USA  
Alessandro Tasora, Italy  
Sergio Teggi, Italy  
Ana C. Teodoro, Portugal  
Alexander Timokha, Norway  
Gisella Tomasini, Italy  
Francesco Tornabene, Italy  
Antonio Tornambe, Italy  
Javier Martinez Torres, Spain  
Mariano Torrisi, Italy  
George Tsiatas, Greece  
Antonios Tsourdos, UK  
Federica Tubino, Italy  
Nerio Tullini, Italy  
Andrea Tundis, Italy  
Emilio Turco, Italy  
Ilhan Tuzcu, USA  
Efstratios Tzirtzilakis, Greece  
Filippo Ubertini, Italy  
Francesco Ubertini, Italy  
Mohammad Uddin, Australia  
Hassan Ugail, UK  
Giuseppe Vairo, Italy  
Eusebio Valero, Spain  
Pandian Vasant, Malaysia  
Marcello Vasta, Italy  
Carlos-Renato Vázquez, Mexico  
Miguel E. Vázquez-Méndez, Spain  
Josep Vehi, Spain  
Martin Velasco Villa, Mexico  
K. C. Veluvolu, Republic of Korea  
Fons J. Verbeek, Netherlands  
Franck J. Vernerey, USA  
Georgios Veronis, USA  
Vincenzo Vespri, Italy  
Renato Vidoni, Italy  
V. Vijayaraghavan, Australia  
Anna Vila, Spain  
Rafael J. Villanueva, Spain  
Francisco R. Villatoro, Spain  
Uchechukwu E. Vincent, UK  
Gareth A. Vio, Australia

Francesca Vipiana, Italy  
Stanislav Vitek, Czech Republic  
Thuc P. Vo, UK  
Jan Vorel, Czech Republic  
Michael Vynnycky, Sweden  
Hao Wang, USA  
Liliang Wang, UK  
Shuming Wang, China  
Yongqi Wang, Germany  
Roman Wan-Wendner, Austria  
Jaroslaw Wąs, Poland  
P.H. Wen, UK  
Waldemar T. Wójcik, Poland  
Changzhi Wu, China  
Desheng D. Wu, Sweden  
Yuqiang Wu, China  
Michalis Xenos, Greece  
Guangming Xie, China  
Xue-Jun Xie, China  
Gen Q. Xu, China  
Hang Xu, China  
Joseph J. Yame, France  
Xinggang Yan, UK  
Jixiang Yang, China  
Mijia Yang, USA  
Yongheng Yang, Denmark  
Luis J. Yebra, Spain  
Peng-Yeng Yin, Taiwan  
Yuan Yuan, UK  
Qin Yuming, China  
Elena Zaitseva, Slovakia  
Arkadiusz Zak, Poland  
Daniel Zaldivar, Mexico  
Francesco Zammori, Italy  
Vittorio Zampoli, Italy  
Rafał Zdunek, Poland  
Ibrahim Zeid, USA  
Haopeng Zhang, USA  
Huaguang Zhang, China  
Kai Zhang, China  
Qingling Zhang, China  
Xianming Zhang, Australia  
Xuping Zhang, Denmark  
Zhao Zhang, China  
Yifan Zhao, UK  
Jian G. Zhou, UK  
Quanxin Zhu, China



---

Mustapha Zidi, France  
Gaetano Zizzo, Italy

Zhixiang Zou, Germany  
J. A. Fonseca de Oliveira Correia, Portugal

# Contents

## **Mathematical Theories and Applications for Nonlinear Control Systems**

Xue-Jun Xie , Ju H. Park , Hiroaki Mukaidani, and Weihai Zhang   
Editorial (6 pages), Article ID 2065786, Volume 2019 (2019)

## **A Simplified Fractional Order Equivalent Circuit Model and Adaptive Online Parameter Identification Method for Lithium-Ion Batteries**

Jianlin Wang, Le Zhang, Dan Xu , Peng Zhang, and Gairu Zhang  
Research Article (8 pages), Article ID 6019236, Volume 2019 (2019)

## **A Time-Replacement Policy for Multistate Systems with Aging Components under Maintenance, from a Component Perspective**

Chao-Hui Huang  and Chun-Ho Wang   
Research Article (12 pages), Article ID 9651489, Volume 2019 (2019)

## **Research on Instability Boundaries of Control Force for Trajectory Correction Projectiles**

Rupeng Li , Dongguang Li , and Jieru Fan  
Research Article (12 pages), Article ID 6362835, Volume 2019 (2019)

## **Dynamical Analysis and Optimal Harvesting Strategy for a Stochastic Delayed Predator-Prey Competitive System with Lévy Jumps**

Guodong Liu, Kaiyuan Liu , and Xinzhu Meng   
Research Article (14 pages), Article ID 2187274, Volume 2019 (2019)

## **Nonlinear Hybrid Multipoint Model of High-Speed Train with Traction/Braking Dynamic and Speed Estimation Law**

Chao Jia , Hongze Xu, and Longsheng Wang  
Research Article (14 pages), Article ID 1364657, Volume 2019 (2019)

## **Start-Up Process Modelling of Sediment Microbial Fuel Cells Based on Data Driven**

Fengying Ma , Yankai Yin, and Min Li  
Research Article (10 pages), Article ID 7403732, Volume 2019 (2019)

## **A Moving Object Indoor Tracking Model Based on Semiactive RFID**

Hongshan Kong  and Bin Yu   
Research Article (7 pages), Article ID 4812057, Volume 2018 (2019)

## **Iterative Learning Control for Nonlinear Weighing and Feeding Process**

Jianqi An , Fayang You, Min Wu, and Jinhua She  
Research Article (9 pages), Article ID 9425902, Volume 2018 (2019)

## **A High-Precision Rotor Position and Displacement Prediction Method Specially for Bearingless Permanent Magnet Synchronous Motor**

Yukun Sun , Qiang Cui, Yonghong Huang , and Ye Yuan   
Research Article (12 pages), Article ID 9602426, Volume 2018 (2019)

### **Comparative Controlling of the Lorenz Chaotic System Using the SMC and APP Methods**

Ercan Köse  and Aydın Mühürçü 

Research Article (9 pages), Article ID 9612749, Volume 2018 (2019)

### **On an Application of the Absolute Stability Theory to Sampled-Data Stabilization**

Alexander N. Churilov 

Research Article (9 pages), Article ID 3169609, Volume 2018 (2019)

### **Further Results on Sampled-Data Synchronization for Complex Dynamical Networks with Time-Varying Coupling Delay**

Hea-Min Lee , Wookyong Kwon , Sangmoon Lee , and Dongyeop Kang 

Research Article (11 pages), Article ID 4931658, Volume 2018 (2019)

### **Modeling and Stability Analysis for Markov Jump Networked Evolutionary Games**

Guodong Zhao 

Research Article (9 pages), Article ID 5124343, Volume 2018 (2019)

### **Exponential Stability of Antiperiodic Solution for BAM Neural Networks with Time-Varying Delays**

Xiaofei Li , Chuan Qin , and Quanxin Zhu 

Research Article (13 pages), Article ID 3034794, Volume 2018 (2019)

### **Maximum Power Point Tracking of DFIG with DC-Based Converter System Using Coordinated Feedback Linearization Control**

Yuliang Sun, Shaomin Yan, Bin Cai, and Yuqiang Wu 

Research Article (12 pages), Article ID 9642123, Volume 2018 (2019)

### **Fractional-Order Adaptive Backstepping Control of a Noncommensurate Fractional-Order Ferroresonance System**

Yan Wang , Ling Liu, Chongxin Liu, Ziwei Zhu, and Zhenquan Sun

Research Article (10 pages), Article ID 8091757, Volume 2018 (2019)

### **Hot Spot Data Prediction Model Based on Wavelet Neural Network**

Ming Zhang  and Wei Chen 

Research Article (10 pages), Article ID 3719564, Volume 2018 (2019)

### **Optimization Problem of Insurance Investment Based on Spectral Risk Measure and RAROC Criterion**

Xia Zhao , Hongyan Ji , and Yu Shi 

Research Article (7 pages), Article ID 9838437, Volume 2018 (2019)

### **Optimal Control Based on the Polynomial Least Squares Method**

Constantin Bota , Bogdan Căruntu , Mădălina Sofia Pașca, and Marioara Lăpădat

Research Article (8 pages), Article ID 9454160, Volume 2018 (2019)

### **Research on Time-Space Fractional Model for Gravity Waves in Baroclinic Atmosphere**

Yanwei Ren, Huanhe Dong , Xinzhu Meng , and Hongwei Yang 

Research Article (14 pages), Article ID 1345346, Volume 2018 (2019)

**Estimation and Fault Diagnosis of Lithium-Ion Batteries: A Fractional-Order System Approach**

Shulan Kong , Mehrdad Saif, and Guozeng Cui

Research Article (12 pages), Article ID 8705363, Volume 2018 (2019)

**Bipartite Consensus for Multiagent Systems via Event-Based Control**

Cui-Qin Ma  and Wei-Guo Sun

Research Article (8 pages), Article ID 8046576, Volume 2018 (2019)

**$H_\infty$  Control for Nonlinear Infinite Markov Jump Systems**

Yueying Liu and Ting Hou 

Research Article (9 pages), Article ID 2904521, Volume 2018 (2019)

**A New Robust Nonfragile Controller Design Scheme for a Class of Hybrid Systems through Piecewise Affine Models**

Yunsai Chen , Yongjie Pang, Zhao Yang, and Liang Ma

Research Article (13 pages), Article ID 1875610, Volume 2018 (2019)

**A New Stability Criterion for Neutral Stochastic Delay Differential Equations with Markovian Switching**

Wei Hu 

Research Article (8 pages), Article ID 7814974, Volume 2018 (2019)

**A Novel Nonlinear Fault Tolerant Control for Manipulator under Actuator Fault**

Jing Zhao , Sen Jiang, Fei Xie , Zhen He , and Jian Fu 

Research Article (11 pages), Article ID 5198615, Volume 2018 (2019)

**Finite-Time Stabilization for Stochastic Inertial Neural Networks with Time-Delay via Nonlinear Delay Controller**

Deyi Li, Yuanyuan Wang, Guici Chen , and Shasha Zhu

Research Article (11 pages), Article ID 2939425, Volume 2018 (2019)

**Predefined-Time Consensus of Nonlinear First-Order Systems Using a Time Base Generator**

J. Armando Colunga , Carlos R. Vázquez , Héctor M. Becerra , and David Gómez-Gutiérrez 

Research Article (11 pages), Article ID 1957070, Volume 2018 (2019)

**On Leaderless and Leader-Following Consensus for Heterogeneous Nonlinear Multiagent Systems via Discontinuous Distributed Control Protocol**

Fei Wang  and Yongqing Yang

Research Article (10 pages), Article ID 2917954, Volume 2018 (2019)

**$H_\infty$  Robust Tracking Control of Stochastic T-S Fuzzy Systems with Poisson Jumps**

Xiangyun Lin , Weihai Zhang , and Bor-Sen Chen 

Research Article (14 pages), Article ID 5257972, Volume 2018 (2019)

**Global Output Feedback Stabilization of Nonlinear Systems with a Time-Varying Power and Unknown Output Function**

Chao Guo and Kemei Zhang 

Research Article (12 pages), Article ID 2906469, Volume 2018 (2019)

**Unbiased Minimum Variance Estimation for Discrete-Time Systems with Measurement Delay and Unknown Measurement Disturbance**

Yu Guan and Xinmin Song 

Research Article (7 pages), Article ID 2831561, Volume 2018 (2019)

**Trajectory Design and Tracking Control for Nonlinear Underactuated Wheeled Inverted Pendulum**

Shuli Gong , Ancai Zhang , Jinhua She , Xinghui Zhang , and Yuanyuan Liu

Research Article (10 pages), Article ID 6134764, Volume 2018 (2019)

**A Nonhomogeneous Multivariable Grey Prediction NMGM Modeling Mechanism and Its Application**

Haixia Wang  and Lingdi Zhao 

Research Article (8 pages), Article ID 6879492, Volume 2018 (2019)

**Adaptive Fuzzy Command Filtered Control for Chua's Chaotic System**

Lin Wang , Hui Wei , and Chunzhi Yang

Research Article (10 pages), Article ID 9635358, Volume 2018 (2019)

**A New Approach to Adaptive Stabilization of Stochastic High-Order Nonholonomic Systems**

Guangju Li  and Kemei Zhang 

Research Article (13 pages), Article ID 9169367, Volume 2018 (2019)

**Stochastic Stability Analysis of Coupled Viscoelastic Systems with Nonviscously Damping Driven by White Noise**

Di Liu , Yanru Wu, and Xiufeng Xie

Research Article (16 pages), Article ID 6532305, Volume 2018 (2019)

**The Adaptive Neural Control for a Class of High-Order Uncertain Stochastic Nonlinear Systems**

Xiaoyan Qin 

Research Article (10 pages), Article ID 4620125, Volume 2018 (2019)

**Adaptive Parallel Simultaneous Stabilization of a Class of Nonlinear Descriptor Systems via Dissipative Matrix Method**

Liyang Sun  and Renming Yang 

Research Article (13 pages), Article ID 1019569, Volume 2018 (2019)

**Outer Synchronization of a Modified Quorum-Sensing Network via Adaptive Control**

Jianbao Zhang , Wenyan Zhang, Denghua Zhang, Chengdong Yang , Kongwei Zhu, and Jianlong Qiu

Research Article (8 pages), Article ID 2801896, Volume 2018 (2019)

**A Common Value Experimentation with Multiarmed Bandits**

Xiujian Gao , Hao Liang, and Tong Wang 

Research Article (8 pages), Article ID 4791590, Volume 2018 (2019)

**Adaptive Fuzzy Output Feedback Control for Partial State Constrained Nonlinear Pure Feedback Systems**

Liping Wang , Weiwei Sun , and You Wu 

Research Article (12 pages), Article ID 9624938, Volume 2018 (2019)

**Adaptive Synchronization for Uncertain Delayed Fractional-Order Hopfield Neural Networks via Fractional-Order Sliding Mode Control**

Bo Meng  and Xiaohong Wang

Research Article (8 pages), Article ID 1603629, Volume 2018 (2019)

**Stability Analysis of Solutions for a Kind of Integro-Differential Equations with a Delay**

Jing Zhao  and Fanwei Meng 

Research Article (6 pages), Article ID 9519020, Volume 2018 (2019)

**Stochastic Optimal Control of Investment and Dividend Payment Model under Debt Control with Time-Inconsistency**

Dan Zhu  and Chuancun Yin 

Research Article (8 pages), Article ID 7928953, Volume 2018 (2019)

**Strong Solutions and Global Attractors for Kirchhoff Type Equation**

Xiangping Chen 

Research Article (7 pages), Article ID 9349625, Volume 2018 (2019)

**Disturbance Attenuation via Output Feedback for Nonlinear Time-Delay Systems with Input Matching Uncertainty**

Chao Guo and Kemei Zhang 

Research Article (8 pages), Article ID 2870496, Volume 2018 (2019)

**The Dynamic Properties of a Nonlinear Economic Model with Extreme Financial Frictions**

Huan Wang  and WenYi Huang 

Research Article (9 pages), Article ID 9682167, Volume 2018 (2019)

**Global Output Feedback Stabilization for a Class of Nonlinear Cascade Systems**

Cai-Yun Liu, Zong-Yao Sun , Qing-Hua Meng, Chih-Chiang Chen , Bin Cai, and Yu Shao

Research Article (13 pages), Article ID 5185394, Volume 2018 (2019)

**Consensus Control of Multiagent Systems with High-Order Nonlinear Inaccurate Dynamics and Dynamically Switching Undirected Topologies**

Qiang Wang , Qingtian Meng, Xiaonan Fang, and Huaxiang Zhang

Research Article (7 pages), Article ID 5983679, Volume 2018 (2019)

**Exponential Lagrange Stability for Markovian Jump Uncertain Neural Networks with Leakage Delay and Mixed Time-Varying Delays via Impulsive Control**

J. Yogambigai, M. Syed Ali, Quanxin Zhu , and Jingwei Cai

Research Article (15 pages), Article ID 6489517, Volume 2018 (2019)

**Adaptive Tracking Control for a Class of Manipulator Systems with State Constraints and Stochastic Disturbances**

Wei Sun , Wenxing Yuan, Jing Zhang, and Qun Sun 

Research Article (6 pages), Article ID 5080684, Volume 2018 (2019)

**A Novel Fifth-Degree Strong Tracking Cubature Kalman Filter for Two-Dimensional Maneuvering Target Tracking**

Zhaoming Li , Wenge Yang , and Dan Ding 

Research Article (10 pages), Article ID 5918456, Volume 2018 (2019)

## Editorial

# Mathematical Theories and Applications for Nonlinear Control Systems

Xue-Jun Xie <sup>1</sup>, Ju H. Park <sup>2</sup>, Hiroaki Mukaidani,<sup>3</sup> and Weihai Zhang <sup>4</sup>

<sup>1</sup>*Institute of Automation, Qufu Normal University, Qufu, China*

<sup>2</sup>*Department of Electrical Engineering, Yeungnam University, Kyongsan, Republic of Korea*

<sup>3</sup>*Graduate School of Engineering, Hiroshima University, Higashihiroshima, Japan*

<sup>4</sup>*College of Electrical Engineering and Automation, Shandong University of Science and Technology, Qingdao, China*

Correspondence should be addressed to Xue-Jun Xie; [xuejunxie@126.com](mailto:xuejunxie@126.com)

Received 31 March 2019; Accepted 31 March 2019; Published 10 April 2019

Copyright © 2019 Xue-Jun Xie et al. This is an open access article distributed under the Creative Commons Attribution License, which permits unrestricted use, distribution, and reproduction in any medium, provided the original work is properly cited.

Nonlinear control is without doubt a very popular research field in modern control theory. Compared with linear systems, nonlinear control has more applications in practice, and the related problems of nonlinear control exhibit more complexity. Although nonlinear control theory and application have made great progress in recent years, there are still a lot of new and challenging problems existing in the areas of theory analysis and applications, which cover the fields of multiobjective control, design of regulating and tracking systems, fault estimation, nonlinear robust  $H_\infty$  control and filtering, stability and stabilization, etc. These problems merit further study by using more advanced theories and tools.

This special issue will focus on nonlinear control systems together with their applications to control, filtering, communication, manufacturing, fault detection, and systems biology. The collection of papers with different areas of nonlinear systems clearly points to the need for communication between researches of these areas.

The paper entitled “A Time-Replacement Policy for Multistate Systems with Aging Components under Maintenance, from a Component Perspective” by C.-H. Huang and C.-H. Wang studies multistate systems (MSSs) with aging multistate components (MSCs) to construct a time-replacement policy and determine the optimal time. Traditional mathematics cannot acquire accurate explicit expressions. To overcome this difficulty, this paper uses Markov reward models and the bound approximation approach to assess rewards of MSSs with MSCs, including such things as total maintenance costs and the benefits of the system staying in acceptable working states.

R. Li et al. in the paper entitled “Research on Instability Boundaries of Control Force for Trajectory Correction Projectiles” propose a novel method to derive instability boundaries for the control force magnitude. By introducing the concept of angular compensation matrix, the exterior ballistic linearized equations considering control force are established. The necessary prerequisite for a stable flight under control is given by the Routh stability criterion. The instability boundaries for the control force magnitude are derived.

The paper by G. Liu et al. entitled “Dynamical Analysis and Optimal Harvesting Strategy for a Stochastic Delayed Predator-Prey Competitive System with Lévy Jumps” develops a theoretical framework to investigate optimal harvesting control for stochastic delay differential systems. The authors first propose a novel stochastic two-predator and one-prey competitive system subject to time delays and Lévy jumps. Some sufficient conditions for persistence in mean and extinction of three species are obtained by using the stochastic qualitative analysis method. The optimal harvesting effort and the maximum of expectation of sustainable yield are derived from the Hessian matrix method and optimal harvesting theory of delay differential equations.

The paper entitled “Nonlinear Hybrid Multipoint Model of High-Speed Train with Traction/Braking Dynamic and Speed Estimation Law” by C. Jia et al. establishes a nonlinear hybrid multipoint model (NHMPM) for a high-speed train (HST) with the traction/braking dynamic and speed estimation law. A full-order flux observer is designed by using regional pole assignment theory to calculate the

electromagnetic torque. The basic running resistance force is reformulated by considering the aerodynamic drag distribution characteristics, and the nonlinear coupling force is analyzed as well.

F. Ma et al. in the paper entitled “Start-Up Process Modelling of Sediment Microbial Fuel Cells Based on Data Driven” study a typical microbial fuel cell, called sediment microbial fuel cells (SMFCs). This paper uses online monitoring technology to accurately measure the temperature, pH, and voltage of the microbial fuel cell during the start-up process. Experimental results show that the purpose of rapid growth of power production can be achieved at the initial stage of SMFC. At the beginning of SMFC, when the temperature changes drastically, pH will change the same first, and then there will be a certain degree of rebound. In the middle stage of SMFC start-up, even if the temperature will return to normal after the change, a continuous temperature drop in a short time will lead to a continuous decrease in pH value.

The paper by H. Kong and B. Yu entitled “A Moving Object Indoor Tracking Model Based on Semiactive RFID” studies the weak anti-interference and low accuracy problem of moving object indoor tracking based radio frequency identification devices (RFID) and presents a moving object indoor tracking model based on semiactive RFID. This model acquires scene location information through RFID low frequency triggers preinstalled and adopts an improved particle filter algorithm, which can increase the diversity of the particles, overcome the particle impoverishment, and reduce the tracking error.

J. An et al. in the paper entitled “Iterative Learning Control for Nonlinear Weighing and Feeding Process” use a piecewise linearization method for the nonlinear problem and discuss the application of iterative learning control in the weighing and feeding process. The nonlinear problem and the repeatability are discussed based on dynamic analysis of the weighing and feeding process. A linear state space model is established with a piecewise linearization method, and iterative learning controller is presented by utilizing repetitive characteristics.

The paper by Y. Sun et al. entitled “A High-Precision Rotor Position and Displacement Prediction Method Specially for Bearingless Permanent Magnet Synchronous Motor” studies a rotor displacement and position prediction method based on a kernel extreme learning machine. The high performance sensorless performance of the bearingless permanent magnet synchronous motor (BPMSM) is the main direction to improve the reliability of the drive system and reduce the cost of the system. On the basis of the mathematical model of BPMSM, this method predicts the position and displacement of the rotor according to the current and flux linkage of suspension windings and torque windings by a kernel extreme learning machine (KELM).

E. Köse and A. Mühürçü in the paper entitled “Comparative Controlling of the Lorenz Chaotic System Using the SMC and APP Methods” provide two different controller models for the Lorenz chaotic system. Adaptive pole placement and sliding mode control (SMC) methods are proposed for the establishment of the continuous time Lorenz chaotic

system. An improved controller structure is developed first theoretically for both the controller methods and then tested practically using the numerical samples. During the establishment of the adaptive pole placement method for the Lorenz chaotic system, various stages were applied. The chaotic system reached an equilibrium point by using both the SMC and adaptive pole placement methods.

The paper entitled “On an Application of the Absolute Stability Theory to Sampled-Data Stabilization” by A. N. Churilov considers a nonlinear Lur'e-type plant with a sector bound nonlinearity. The plant is stabilized by a discrete-time feedback signal with a nonperiodic uncertain sampling. The sampling control function is nonlinear and also obeys some sectoral constraints at discrete (sampling) times. The linear matrix inequality (LMI) conditions for the stability of the closed-loop system are obtained.

H.-M. Lee et al. in the paper entitled “Further Results on Sampled-Data Synchronization for Complex Dynamical Networks with Time-Varying Coupling Delay” deal with the sampled-data synchronization problem for complex dynamical networks (CDNs) with time-varying coupling delay. The two-sided free-weighting stabilization method is utilized with a novel looped functional by taking the information of the present sampled states and next sampled states, which can more precisely account for the sawtooth shape of the sampling delay. The quadratic generalized free-weighting matrix inequality (QGFWMI) is utilized to calculate the upper limit of the integral term. Based on the novel looped functional and QGFWMI, improved conditions of stability are derived from forms of linear matrix inequalities (LMIs).

The paper by G. Zhao entitled “Modeling and Stability Analysis for Markov Jump Networked Evolutionary Games” investigates the algebraic formulation and stability analysis for a class of Markov jump networked evolutionary games by using the semitensor product method and presents a number of new results. A proper algorithm is constructed to convert the given networked evolutionary games into an algebraic expression. Based on the algebraic expression, the stability of the given game is analyzed and an equivalent criterion is given.

X. Li et al. in the paper entitled “Exponential Stability of Antiperiodic Solution for BAM Neural Networks with Time-Varying Delays” consider a kind of BAM neural networks with leakage delays in the negative feedback terms and time-varying delays in activation functions. By constructing a suitable Lyapunov function and using inequality techniques, some sufficient conditions to ensure the existence and exponential stability of antiperiodic solutions of these neural networks are derived.

Y. Sun et al. entitled in the paper “Maximum Power Point Tracking of DFIG with DC-Based Converter System Using Coordinated Feedback Linearization Control” present a coordinated feedback linearization strategy (CFLS) for a DC-based doubly fed induction generator (DFIG) system to track the maximum power point. The stator and rotor of the DFIG are connected to the DC grid directly by two voltage source converters. Compared with a traditional DFIG system, the DC-based DFIG system has more system inputs

and coupling, which increases the difficulty of vector control strategy.

The paper by Y. Wang et al. entitled “Fractional-Order Adaptive Backstepping Control of a Noncommensurate Fractional-Order Ferroresonance System” applies fractional calculus to establish a novel fractional-order ferroresonance model with fractional-order magnetizing inductance and capacitance. A novel fractional-order adaptive controller is designed in terms of the fractional Lyapunov stability theorem. The proposed control strategy requires only one control input and can force the output of the chaotic system to track the reference signal asymptotically.

The paper entitled “Hot Spot Data Prediction Model Based on Wavelet Neural Network” by M. Zhang and W. Chen improves the performance of data migration between a solid-state hard disk and hard disk. The novel hybrid multilevel storage system will be popular with SSD being integrated into traditional storage systems. The hot data block prediction model based on a wavelet neural network is built and trained by using historical data. Experimental results show that the proposed model has better accuracy and faster learning speed than the BP neural network model. It has better generalization ability and robustness. This model can be applied to the data migration of distributed hybrid storage systems to improve performance.

X. Zhao et al. in the paper entitled “Optimization Problem of Insurance Investment Based on Spectral Risk Measure and RAROC Criterion” introduce spectral risk measure (SRM) into the optimization problem of insurance investment. The authors establish an optimization model aiming at maximizing risk-adjusted return of capital (RAROC) involved with spectral risk measure. The theoretical result is derived and empirical study is displayed under different risk measures and different confidence levels comparatively. The result shows that risk attitude has a significant impact on investment strategy. With the increase of risk aversion factor, the investment ratio of risk asset correspondingly reduces.

The paper entitled “Optimal Control Based on the Polynomial Least Squares Method” by C. Bota et al. presents an approach for computing an optimal control law based on the Polynomial Least Squares Method (PLSM). The initial optimal control problem is reformulated as a variational problem whose corresponding Euler-Lagrange equation is solved by using the PLSM. A couple of examples emphasize the accuracy of the method.

The paper by Y. Ren et al. entitled “Research on Time-Space Fractional Model for Gravity Waves in Baroclinic Atmosphere” derives the integer order mKdV equation to describe the gravity solitary waves which occur in the baroclinic atmosphere. By employing the semi-inverse and variational method, a new model under the Riemann-Liouville derivative definition is obtained. The symmetry analysis and the nonlinear self-adjointness of the space-time fractional mKdV (STFmKdV) equation are carried out and the conservation laws are analyzed. By adopting the  $\exp(-\Phi(\xi))$  method, five different solutions of the STFmKdV equation are obtained.

S. Kong et al. in the paper entitled “Estimation and Fault Diagnosis of Lithium-Ion Batteries: A Fractional-Order

System Approach” investigate the estimation and fault diagnosis of a fractional-order lithium-ion battery system. Two simple and common types of observers are designed to address the design of fault diagnosis and estimation for the fractional-order systems. Fractional-order Luenberger observers are employed to generate residuals which are used to investigate the feasibility of model based fault detection and isolation. The notion of stability in the sense of Mittag-Leffler is first introduced to discuss the state estimation error dynamics. The design of the Luenberger observer as well as the sliding mode observer can accomplish fault detection, fault isolation, and estimation. The effectiveness of the proposed strategy on a three-cell battery string system is demonstrated.

The paper by C.-Q. Ma and W.-G. Sun entitled “Bipartite Consensus for Multiagent Systems via Event-Based Control” studies bipartite consensus for first-order multiagent systems. To improve resource utilization, event-based protocols are considered for bipartite consensus. A new type of control gain is designed in the proposed protocols. By appropriate selection of control gains, the convergence rate of the closed-loop system can be adjusted. It can be found that the system will not show Zeno behavior.

The paper entitled “ $H_\infty$  Control for Nonlinear Infinite Markov Jump Systems” by Y. Liu and T. Hou discusses the infinite horizon  $H_\infty$  control problem for a class of nonlinear stochastic systems with state, control, and disturbance dependent noise. The jumping parameters are modeled as an infinite-state Markov chain. Based on the solvability of a set of coupled Hamilton-Jacobi inequalities (HJIs), the exponential mean square  $H_\infty$  controller for the considered nonlinear stochastic systems is obtained.

Y. Chen et al. in the paper entitled “A New Robust Nonfragile Controller Design Scheme for a Class of Hybrid Systems through Piecewise Affine Models” investigate the robust  $H_\infty$  nonfragile control problem for a class of discrete-time hybrid systems based on piecewise affine models. By employing a state-control augmentation methodology, some new sufficient conditions for the controller synthesis are formulated based on piecewise Lyapunov functions (PLFs). Controller gains can be obtained via solving a set of linear matrix inequalities.

W. Hu in the paper entitled “A New Stability Criterion for Neutral Stochastic Delay Differential Equations with Markovian Switching” investigates a new stability theorem for neutral stochastic delay differential equations with Markovian switching. By applying the stochastic analysis technique and Razumikhin stability approach, a novel criterion of the  $p$ th moment exponential stability is derived for the related systems. The feature of the criterion shows that the estimated upper bound for the diffusion operator of the Lyapunov function is allowed to be indefinite, even if it is unbounded, which can loosen the constraints of the existing results.

Based on the adaptive sliding mode control technique, J. Zhao et al. in the paper entitled “A Novel Nonlinear Fault Tolerant Control for Manipulator under Actuator Fault” propose a fault tolerant control (FTC) scheme for a manipulator with actuator fault. The dynamic model of the manipulator is introduced and its actuator faulty model is established. A fault

tolerant controller is designed, in which both the parameters of actuator fault and external disturbance are estimated and updated by online adaptive technology.

The paper entitled “Finite-Time Stabilization for Stochastic Inertial Neural Networks with Time-Delay via Nonlinear Delay Controller” by D. Li et al. pays close attention to the problem of finite-time stabilization related to stochastic inertial neural networks with or without time delay. By establishing a proper Lyapunov-Krasovskii functional and making use of matrix inequalities, some sufficient conditions on finite-time stabilization are obtained and the stochastic settling-time function is also estimated. In order to achieve the finite-time stabilization, both delayed and nondelayed nonlinear feedback controllers are designed, respectively.

J. A. Colunga et al. in the paper entitled “Predefined-Time Consensus of Nonlinear First-Order Systems Using a Time Base Generator” propose a couple of consensus algorithms for multiagent systems. The proposed consensus protocols are based on the so-called time base generators (TBGs), which are time-dependent functions used to build time-varying control laws. One of the proposed protocols is based on the super-twisting controller, providing robustness against disturbances while maintaining the predefined-time convergence property. It is shown that the proposed TBG protocols represent an advantage not only in the possibility to define a settling time but also in providing smoother and smaller control actions than existing finite-time, fixed-time, and predefined-time consensus.

The paper entitled “On Leaderless and Leader-Following Consensus for Heterogeneous Nonlinear Multiagent Systems via Discontinuous Distributed Control Protocol” by F. Wang and Y. Yang concerns the consensus of heterogeneous nonlinear multiagent systems via distributed control. Both the cases of leaderless and leader-following consensus are systematically investigated. Different from some existing results, completed consensus can be reached in this paper among heterogeneous multiagent network instead of bounded consensus. A novel distributed control protocol is proposed, and some general consensus criteria are derived for multiagent systems without a leader.

The paper by X. Lin et al. entitled “ $H_\infty$  Robust Tracking Control of Stochastic T-S Fuzzy Systems with Poisson Jumps” designs a robust adaptive  $H_\infty$  tracking control for nonlinear stochastic systems with both Brownian motion and Poisson jumps, which is based on Takagi-Sugeno (T-S) type fuzzy techniques. By using the fuzzy systems to approximate the nonlinear systems, an adaptive fuzzy control is employed to achieve the desired  $H_\infty$  tracking performance for stochastic systems with exogenous disturbance.

The paper by C. Guo and K. Zhang entitled “Global Output Feedback Stabilization of Nonlinear Systems with a Time-Varying Power and Unknown Output Function” studies the problem of global output feedback stabilization for a class of nonlinear systems with a time-varying power and unknown output function. For nonlinear systems with a time-varying power and unknown continuous output function, by constructing a new nonlinear reduced-order observer together with adding a power integrator method,

a new function to determine the maximal open sector  $\Omega$  of output function is given. As long as the output function belongs to any closed sector included in  $\Omega$ , it is shown that the equilibrium point of the closed-loop system can be guaranteed to be globally uniformly asymptotically stable by an output feedback controller.

Y. Guan and X. Song in the paper entitled “Unbiased Minimum Variance Estimation for Discrete-Time Systems with Measurement Delay and Unknown Measurement Disturbance” address the state estimation problem for stochastic systems with unknown measurement disturbances any prior information of which is unknown and which has measurement delay resulting from the inherent limited bandwidth. For such complex systems, the Kalman-like one-step predictor independent of unknown measurement disturbances is designed based on the linear unbiased minimum variance criterion and the reorganized innovation analysis approach.

The paper entitled “Trajectory Design and Tracking Control for Nonlinear Underactuated Wheeled Inverted Pendulum” by S. Gong et al. studies an underactuated wheeled inverted pendulum (UWIP) system. The motion planning problem for this nonlinear system is difficult to solve because of the existence of an uncontrollable manifold in the configuration space. A method of designing motion trajectory for this underactuated system is presented. The tracking control of the UWIP for the constructed trajectory is also studied.

H. Wang and L. Zhao in the paper entitled “A Nonhomogeneous Multivariable Grey Prediction NMGM Modeling Mechanism and Its Application” propose a novel nonhomogeneous multivariable grey prediction model termed NMGM( $a, m, k^\alpha$ ) to deal with those data sequences that are not in accord with homogeneous index trend. Based on grey prediction theory, by the least squares method and solutions of differential equations, the modeling mechanism and time response function of the proposed model are expounded. A case study demonstrates that the novel model provides preferable prediction performance compared with the traditional MGM(1,  $m$ ) model.

The paper by L. Wang et al. entitled “Adaptive Fuzzy Command Filtered Control for Chua’s Chaotic System” proposes the command filtered adaptive fuzzy backstepping control (AFBC) approach for Chua’s chaotic system with external disturbance. Based on two proposed first-order command filters, the convergence of tracking errors as well as the problem of “explosion of complexity” in the traditional backstepping design procedure is solved. Fuzzy logic systems (FLSs) are used to identify the system uncertainties in real time. The proposed controller can guarantee that all signals in the closed-loop system remain bounded, and tracking errors converge to a small region eventually.

The paper entitled “A New Approach to Adaptive Stabilization of Stochastic High-Order Nonholonomic Systems” by G. Li and K. Zhang studies the problem of adaptive stabilization for a class of stochastic high-order nonholonomic systems. Under the weaker assumptions, by constructing the appropriate Lyapunov function and combining the sign function technique, an adaptive state feedback

controller is designed to guarantee global asymptotic stability in probability of the closed-loop system. The effectiveness of the controller is demonstrated by a mechanical system.

D. Liu et al. in the paper entitled “Stochastic Stability Analysis of Coupled Viscoelastic Systems with Nonviscously Damping Driven by White Noise” investigate stochastic stability of a coupled viscoelastic system with nonviscous damping driven by white noise through moment Lyapunov exponents. By using the coordinate transformation, coupled Itô stochastic differential equations are obtained. The problem of the moment Lyapunov exponent is transformed to the eigenvalue problem, and then the second-perturbation method is used to derive the moment Lyapunov exponent of the coupled stochastic system.

The paper by X. Qin entitled “The Adaptive Neural Control for a Class of High-Order Uncertain Stochastic Nonlinear Systems” studies the problem of the adaptive neural control for a class of high-order uncertain stochastic nonlinear systems. By using some techniques such as the backstepping recursive technique, Young’s inequality, and approximation capability, a novel adaptive neural control scheme is constructed. The proposed control method can guarantee that the signals of the closed-loop system are bounded in probability, and only one parameter needs to be updated online.

The paper entitled “Adaptive Parallel Simultaneous Stabilization of a Class of Nonlinear Descriptor Systems via Dissipative Matrix Method” by L. Sun and R. Yang investigates the adaptive parallel simultaneous stabilization and robust adaptive parallel simultaneous stabilization problems of a class of nonlinear descriptor systems via the dissipative matrix method. Under an output feedback law, two nonlinear descriptor systems are transformed into two nonlinear differential-algebraic systems by nonsingular transformations, and a sufficient impulse-free condition is given for the two resulting closed-loop systems. Based on the dissipative system, an adaptive parallel simultaneous stabilization controller and a robust adaptive parallel simultaneous stabilization controller are designed for the two systems.

Motivated by the quorum-sensing mechanism of bacteria, J. Zhang et al. in the paper entitled “Outer Synchronization of a Modified Quorum-Sensing Network via Adaptive Control” modify the network model by adding unknown parameters and noise disturbances. There exist three unknown parameters, and updating laws are presented to identify the unknown parameters with help of the Lyapunov stability theory. The negative effects of noise disturbances are also compensated for by designing adaptive controllers.

The paper by X. Gao et al. entitled “A Common Value Experimentation with Multiarmed Bandits” studies value common experimentation with multiarmed bandits and gives an application about the experimentation. The second derivative of value functions at cutoffs is investigated when an agent switches action with multiarmed bandits. The Markov perfect equilibrium and the socially effective allocation in K-armed markets are also discussed.

L. Wang et al. in the paper entitled “Adaptive Fuzzy Output Feedback Control for Partial State Constrained Nonlinear Pure Feedback Systems” address the adaptive fuzzy output feedback control problem for a class of pure feedback systems with partial state constraints. The fuzzy state observers are designed to estimate the unmeasured state while the fuzzy logic systems are used to approximate the unknown nonlinear functions. The proposed adaptive fuzzy output feedback controller can guarantee that the partial state constraints are not violated, and all closed-loop signals remain bounded by use of Barrier Lyapunov Functions (BLFs).

The paper entitled “Adaptive Synchronization for Uncertain Delayed Fractional-Order Hopfield Neural Networks via Fractional-Order Sliding Mode Control” by B. Meng and X. Wang studies adaptive synchronization for a class of uncertain delayed fractional-order Hopfield neural networks (FOHNNs) with external disturbances. For the unknown parameters and external disturbances of the delayed FOHNNs, some adaptive estimations are designed. A fractional-order switched sliding surface is proposed for the delayed FOHNNs. According to the fractional-order extension of the Lyapunov stability criterion, a fractional-order sliding mode controller is constructed to guarantee that the synchronization error of the two uncertain delayed FOHNNs converges to an arbitrary small region of the origin.

The paper by J. Zhao and F. Meng entitled “Stability Analysis of Solutions for a Kind of Integro-Differential Equations with a Delay” analyzes the stability of the zero solution for second-order integrodifferential equations with a delay. By constructing the Lyapunov functional, the corresponding sufficient conditions on stability of the zero solution for two integrodifferential equations are provided.

D. Zhu and C. Yin in the paper entitled “Stochastic Optimal Control of Investment and Dividend Payment Model under Debt Control with Time-Inconsistency” consider the optimal debt ratio, investment, and dividend payment policies for insurers with time-inconsistency. The asset can be invested in a financial market which contains a risky asset and a risk-free asset. The objective is to maximize the expected nonconstant discounted utility of dividend payment until a determinate time. This is a time-inconsistent control problem.

The paper entitled “Strong Solutions and Global Attractors for Kirchhoff Type Equation” by X. Chen studies the long-time behavior of the Kirchhoff type equation with linear damping and proves the existence of a strong solution and the semigroup associated with the solution possesses a global attractor in the higher phase space.

C. Guo and K. Zhang in the paper entitled “Disturbance Attenuation via Output Feedback for Nonlinear Time-Delay Systems with Input Matching Uncertainty” study the problem of output feedback disturbance attenuation for a class of uncertain nonlinear systems with input matching uncertainty and unknown multiple time-varying delays, whose nonlinearities are bounded by unmeasured states multiplying unknown polynomial-of-output growth rate. By skillfully combining the extended state observer, dynamic gain technique, and Lyapunov-Krasovskii theorem,

a delay-independent output feedback controller can be developed with only one dynamic gain to guarantee the boundedness of closed-loop system states and the achievement of global disturbance attenuation in the  $L_2$ -gain sense.

The paper by H. Wang and W.Y. Huang entitled “The Dynamic Properties of a Nonlinear Economic Model with Extreme Financial Frictions” investigates a generalized economic model with two kinds of agents (farmers and landlords). Farmers produce grains by renting lands from landlords. The economy is assumed to be with extreme frictions so that there are no markets for agents to trade grains. The rental rate is determined by the equilibrium of the supply and demand. The psychological anticipation is taken into account in the setting of this model. By using the optimal control theory, the dynamic properties of the rental rate and its influence to the endogenous volatility are analyzed.

The paper entitled “Global Output Feedback Stabilization for a Class of Nonlinear Cascade Systems” by C.-Y. Liu et al. focuses on the problem of global output feedback stabilization for a class of nonlinear cascade systems with time-varying output function. By using the double-domination approach, an output feedback controller is developed to guarantee the global asymptotic stability of the closed-loop system. The novel control strategy successfully constructs a unified Lyapunov function, which is suitable for both upper-triangular and lower-triangular systems.

Q. Wang et al. in the paper entitled “Consensus Control of Multiagent Systems with High-Order Nonlinear Inaccurate Dynamics and Dynamically Switching Undirected Topologies” investigate the consensus control of a class of high-order nonlinear multiagent systems, whose topology is dynamically switching directed graph. The high-order nonlinear dynamics is transformed into the one-order dynamics by structuring a sliding mode plane. Two consensus control protocols of the one-order dynamics are designed by feedback linearization. Under these control protocols, it is proved that the consensus of new variable only requires a weaker topology condition.

The paper by J. Yogambigai et al. entitled “Exponential Lagrange Stability for Markovian Jump Uncertain Neural Networks with Leakage Delay and Mixed Time-Varying Delays via Impulsive Control” studies the problem of exponential Lagrange stability analysis of Markovian jump neural networks with leakage delay and mixed time-varying delays. By utilizing the Lyapunov functional method, employing the free-weighting matrix approach and inequality techniques in matrix form, the novel stability criteria are established such that the suggested neural network is exponentially stable in Lagrange sense.

The paper entitled “Adaptive Tracking Control for a Class of Manipulator Systems with State Constraints and Stochastic Disturbances” by W. Sun et al. constructs an adaptive controller for a class of stochastic manipulator nonlinear systems. A tan-type Barrier Lyapunov Function (BLF) is employed to deal with state constraints. The proposed control scheme guarantees the output error convergence to a small neighborhood of zero. All the signals in the closed-loop system are bounded.

Z. Li et al. in the paper entitled “A Novel Fifth-Degree Strong Tracking Cubature Kalman Filter for

Two-Dimensional Maneuvering Target Tracking” present a novel fifth-degree strong tracking cubature Kalman filter to improve the two-dimensional maneuvering target tracking accuracy. A new fifth-degree cubature rule is used to approximate the intractable nonlinear Gaussian weighted integral in the nonlinear Kalman filtering framework, and a novel fifth-degree cubature Kalman filter is proposed. The suboptimal fading factor is designed for the filter to adjust the filtering gain matrix online and force the residual sequences mutually orthogonal, thus improving the ability of the filter to track the mutation state, and the fifth-degree strong tracking cubature Kalman filter is derived. The suboptimal fading factor is calculated in a new method, which reduces the number of calculations for the cubature points from three times to twice without calculating the Jacobian matrix.

### Conflicts of Interest

The editors declare that they have no conflicts of interest regarding the publication of this special issue.

### Acknowledgments

The guest editorial team would like to express gratitude to all the authors for their interest in selecting this special issue as a venue for disseminating their scholarly work. The editors also wish to thank the anonymous reviewers for their careful reading of the manuscripts submitted to this special issue collection and their many insightful comments and suggestions.

*Xue-Jun Xie  
Ju H. Park  
Hiroaki Mukaidani  
Weihai Zhang*

## Research Article

# A Simplified Fractional Order Equivalent Circuit Model and Adaptive Online Parameter Identification Method for Lithium-Ion Batteries

Jianlin Wang,<sup>1,2</sup> Le Zhang,<sup>1</sup> Dan Xu ,<sup>1</sup> Peng Zhang,<sup>2</sup> and Gairu Zhang<sup>2</sup>

<sup>1</sup>School of Mechanical Engineering, Xi'an Jiaotong University, Xi'an, Shaanxi, China

<sup>2</sup>Department of College of Science, Ningxia Medical University, Yinchuan, NingXia, China

Correspondence should be addressed to Dan Xu; xudan@xjtu.edu.cn

Received 10 September 2018; Revised 25 February 2019; Accepted 19 March 2019; Published 3 April 2019

Academic Editor: Francesc Pozo

Copyright © 2019 Jianlin Wang et al. This is an open access article distributed under the Creative Commons Attribution License, which permits unrestricted use, distribution, and reproduction in any medium, provided the original work is properly cited.

In order to improve the battery management system performance and enhance the adaptability of the system, a fractional order equivalent circuit model of lithium-ion battery based on electrochemical test was established. The parameters of the fractional order equivalent circuit model are identified by the least squares parameter identification method. The least squares parameter identification method needs to rely on the harsh test conditions of the laboratory, and the parameter identification result is static; it cannot adapt to the characteristics of the lithium battery under dynamic conditions. Taking into account the dynamic changes of lithium batteries, a parameter adaptive online estimation algorithm for fractional equivalent circuit model is proposed. Based on the theory of fractional order calculus and indirect Lyapunov method, the stability and convergence of the estimator are analyzed. Finally, simulation experiments show that this method can continuously estimate the parameters of the fractional order equivalent circuit under UDDS conditions.

## 1. Introduction

The battery management system (BMS) is one of the most important technologies in the electric vehicle systems. A good battery management system can fully utilize the battery energy, which can not only prolong the mileage but also improve the performance of the electric vehicle [1–3]. The current electric vehicle's power system is mainly based on lithium batteries, because of their high safety, long life, and high energy density. But the electrochemical reaction of lithium-ion battery is highly nonlinear and uncertain, and conversion of electric energy, chemical energy, and thermal energy is very complex [4, 5]. Therefore, it is impossible to build an accurate, intuitive, and efficient battery model for EVs. As a result, it is difficult to design a battery management system.

According to different modeling mechanism, the commonly used battery models at present are mainly including electrochemical model and equivalent circuit model. The electrochemical model describes the battery characteristics

with high accuracy, but its calculation process is complicated and often contains many complex partial differential equations [6]. The equivalent circuit model is not accurate enough, but it is simple, intuitive, and suitable for electrical design and simulation [7–9]. In [10], GaoPeng and his partners designed an equivalent circuit model for lithium batteries based on electrochemical impedance spectroscopy, which is more accurate but still not simple enough.

In the traditional equivalent circuit model, the integer-order RC networks are used to describe the battery concentration effects based on the electrochemical reaction of lithium-ion batteries. First-order RC equivalent circuit model is the simplest model, and it is suitable for engineering application. However the first-order RC equivalent circuit model cannot accurately simulate the static and dynamic characteristics of the battery in the beginning and the end of charge and discharge. Although the accuracy of the battery model can be improved by increasing the series number of RC networks, it will become difficult to get the model parameters and greatly increase computing tasks. Therefore, satisfying

the engineering requirements and improving the accuracy of the model is mutually restrictive, and we should try to improve the accuracy of the model as much as possible when the RC network is limited [11, 12].

A capacitor is a fractional reactance component with fractional characteristics, and fractional derivatives and integrals can better describe the dynamic behavior of RC networks in a circuit system [13, 14]. Some researchers have established fractional equivalent circuits for the electrochemical performance of lithium batteries, but they mainly consider model accuracy and neglect engineering applications. Such as in [15], the author designed a fractional equivalent circuit model containing 2-RC networks, and there are seven parameters in the circuit that need to be identified so that it is difficult to realize online identification.

In order to balance the accuracy of the fractional equivalent circuit model and the practical application of engineering, a simplified fractional equivalent circuit model is proposed by electrochemical test of lithium battery and combined with equivalent circuit modeling method. This simplified fractional equivalent circuit model contains only one RC network, except that the capacitance is described by a fractional order.

Parameter identification is very important in the modeling and analysis of lithium batteries. The general parameter identification method is based on collecting a large amount of laboratory data and using the fitting method to find the optimal parameter value in an offline situation [16–18]. In practical engineering applications, this offline parameter identification method cannot reflect the influence of operating current, state of charge, temperature, and self-discharge on the battery internal characteristics. Although algorithms such as sliding mode and Kalman filter can compensate a certain model system error by feedback, they do not eliminate the state-of-charge estimation error from the root cause [19, 20].

Therefore, in order to improve the battery management system performance and enhance the adaptability of the system, the battery model parameters need to be estimated online to update the battery models. In [21], the authors propose an adaptive battery model based on online identification of battery parameters to account for changes in the internal characteristics of the battery under variable conditions. The first-order RC integer-order dynamic equivalent model established by this method has good results. In addition, many researchers have given some methods in the field of online identification of fractional parameters, such as [22]. However, online parameter identification of fractional equivalent circuit models is rarely reported.

In this paper, a simplified fractional order equivalent circuit model for lithium-ion batteries and adaptive online parameter identification method are presented. The rest of the paper is organized as follows: Section 2 introduces the electrochemical impedance spectroscopy (EIS) and hybrid pulse power characteristic (HPPC) test and the fractional order equivalent circuit model. Section 3 discusses the parameter identification of fractional equivalent circuit model by least squares method under offline condition. Section 4 deals

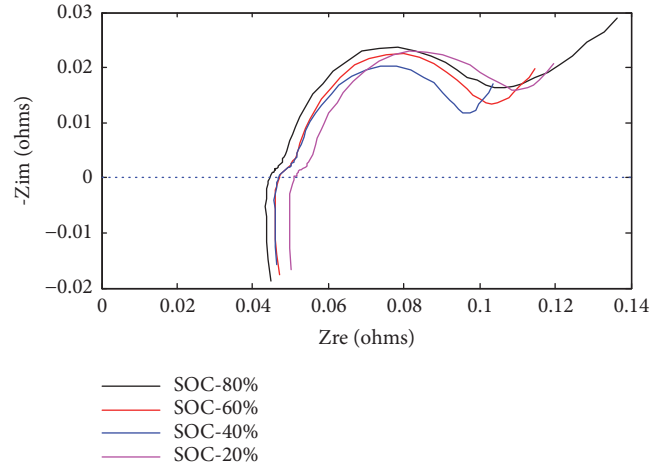


FIGURE 1: EIS curves of lithium-ion batteries with different SOC [15].

with the design of an adaptive online parameter identification method for fractional order equivalent circuit model. Section 5 shows simulation results. Section 6 states some conclusions and guidelines for further works.

## 2. Problem Statement and Fractional Impedance Model

In this study, the NCR18650 lithium-ion battery was applied and tested. It has a rated voltage of 3.7V and a cutoff voltage of 2.8V and 2.9Ah capacity. In order to establish a precise battery model, the battery characterization tests include electrochemical impedance spectroscopy (EIS) and mixed pulse power characteristics (HPPC) [23–25].

The state of health (SOH) of the test battery is 98%. In this case, the EIS test of battery was measured using a Princeton electrochemical workstation, and the battery was under different state of charge (SOC). In the EIS test, the test signal amplitude was set to 5 mV and the frequency range was set to 0.005 Hz to 5000 Hz. Results of the EIS test are shown in Figure 1, and the four curves represent the different test results when the SOC of battery is 20%, 40%, 60%, and 80%, respectively.

Considering the characteristics of ternary lithium-ion battery, the pulse charging current of battery was set to 2C, the discharge current of battery was set to 2.5C, and the sample time of battery current and voltage was set to 0.1S in the hybrid pulse power characteristic (HPPC) test. In order to measure the open circuit voltage of the battery, the battery was left standing for one hour after each pulse test, and the voltage after standing is considered as the open circuit voltage of the battery. Results of the HPPC test are shown in Figure 2.

It can be seen from Figure 1 that the four curves of EIS test have similar shapes when the SOC of battery is different, and the  $Z_{re}$  and  $-Z_{im}$  values also approximately unchanged at the same frequency. When the test frequency exceeds 0.05HZ, the impedance spectrum shows an irregular semicircle that can be modeled by several parallel combinations of a resistor and a CPE. The parallel combination may represent the

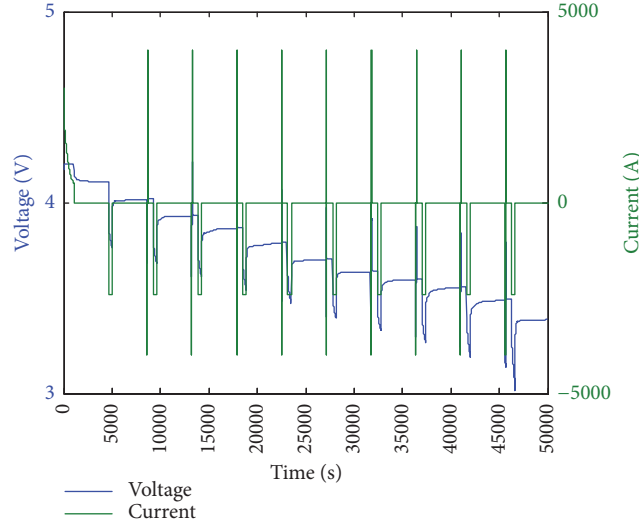


FIGURE 2: HPPC test of lithium-ion battery.

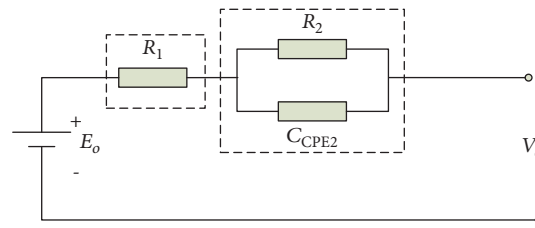


FIGURE 3: Simplified fractional order equivalent circuit model of lithium-ion battery.

charge-transfer reaction on the solid electrolyte interphase layer described by the Butler-Volmer equation.

It can be seen from Figure 2 that the HPPC test includes a rapid voltage rise phase and a voltage ramp stabilization phase. Regarding the battery in the impulse response test voltage rise phase and electrochemical impedance spectroscopy of the high-frequency phase combination analysis, at this stage, the battery voltage is rapidly rising; the main reason for this phenomenon is the battery internal ohmic polarization. In other words, the battery is in the ohmic polarization stage at this stage. When building the battery equivalent model, a resistance element can be used to simulate the battery response to this stage. Combining the cell's ramp stabilization phase of the impulse response test to the mid-frequency and low-frequency sections of the electrochemical impedance spectroscopy, several parallel combinations can be simplified as a parallel representation of one resistor and one CPE element.

On the basis of the EIS analysis and HPPC test, the fractional order equivalent circuit model of lithium-ion battery could be simplified as shown in Figure 3.  $V_1$  denotes the voltage for  $R_1$ , which represents the ohmic voltage.  $V_2$  denotes the voltage for  $R_2$ , which represents the concentration polarization voltage.  $E_0$  is open circuit voltage of the battery and  $C_{CPE2}$  is a constant phase element.

The  $C_{CPE2}$  in Figure 3 could be deciphered by fractional order elements

$$Z_{CPE2}(s) = \frac{1}{C_2 \cdot s^\alpha} \quad (1)$$

where  $\alpha \in \mathbb{R}$  and  $0 < \alpha < 1$ ,  $C_2 \in \mathbb{R}$  and is coefficient as same as capacitance. When  $\alpha = 1$ ,  $C_{CPE2}$  correspond to capacitor with capacitance  $C_2$ ; (1) can be written as

$$Z_{CPE2}(s)|_{\alpha=1} = \frac{1}{C_2 \cdot s} \quad (2)$$

The total impedance of the fractional equivalent circuit model is

$$Z(s) = R_1 + \frac{R_2}{1 + R_2 C_2 \cdot s^\alpha} \quad (3)$$

### 3. Parameter Identification of Least Squares for Fractional Order Equivalent Circuit Model

In the field of parameter identification, since the principle of least squares (LS) is simple and the estimation performance is good, it is considered to be the most basic estimation method.

TABLE 1: Fitting data of every SOC case in fractional equivalent circuit model.

SOC	0.9	0.8	0.7	0.6	0.5	0.4	0.3	0.2	0.1
$R_1/\Omega$	0.0495	0.0498	0.0489	0.0494	0.0491	0.0489	0.0498	0.0512	0.0501
$R_2/\Omega$	0.0092	0.0089	0.0102	0.0097	0.0103	0.0114	0.0121	0.0089	0.0086
$C_2/KF$	0.8031	0.8347	0.8890	0.8912	0.9121	0.9330	0.8062	0.9241	0.9364
$\alpha$	0.7034	0.7002	0.6997	0.0731	0.0726	0.0703	0.0691	0.0701	0.7102

However, it is still difficult to apply the least squares method to the parameter estimation of the fractional order system [15]. Based on the fractional equivalent circuit model, the parameter identification process of the least squares method in the fractional order system is derived, and the parameter identification of the fractional equivalent circuit is completed.

The fractional order equivalent circuit is analyzed based on Kirchhoff's law, available

$$\begin{aligned} V_o &= E_o + IR_1 + V_2 \\ D^\alpha V_2 &= -\frac{V_2}{R_2 C_2} + \frac{I}{C_2} \end{aligned} \quad (4)$$

Performing a Laplace transform on (4) yields an S-domain expression

$$\begin{aligned} V_o(s) &= E_o(s) + I(s) \cdot R_1 + V_2(s) \\ V_2(s) &= \frac{R_2}{R_2 C_2 s^\alpha + 1} I(s) \end{aligned} \quad (5)$$

Defining the input of the fractional order system as  $I$  and the output as  $V_2$ , it means  $Y(s) = V_2(s)$  and  $U(s) = I(s)$ . The transfer function of the S-domain is

$$\frac{Y(s)}{U(s)} = \frac{R_2}{R_2 C_2 s^\alpha + 1} \quad (6)$$

The bilinear transformation relationship of fractional order systems is

$$s^\alpha = \left( \frac{2}{T} \frac{1 - z^{-1}}{1 + z^{-1}} \right)^\alpha, \quad |z| > 1 \quad (7)$$

The bilinear transformation relationship of the fractional order system described by (7) corresponds to the convolution of two binomial sequences corresponding to the numerator and the denominator, as

$$s^\alpha = \left( \frac{2}{T} \right)^\alpha \sum_{k=0}^n \frac{(-a)_k}{k!} \frac{(-1)^{n-k} (a)_{n-k}}{(n-k)!} \quad (8)$$

where  $n! = (-1)^k (-n)_k (n-k)!$ ,  $k \leq n$ ,  $(\alpha)_n = (-1)^k (-\alpha - n + 1)_k (\alpha)_{n-k}$ . So (7) can be rewritten as

$$\begin{aligned} s^\alpha &= \left( \frac{2}{T} \right)^\alpha \frac{(-1)^{n-k} (\alpha)_n}{n!} \sum_{k=0}^n \frac{(-\alpha)_k (-n)_k (-1)^k}{k! (-\alpha - n + 1)_k} \\ &= \left( \frac{2}{T} \right)^\alpha \frac{(-1)^{n-k} (\alpha)_n}{n!} F(-\alpha, -n; -\alpha - n + 1, -1) \end{aligned} \quad (9)$$

where  $F(-\alpha, -n; -\alpha - n + 1, -1)$  is a Gaussian hypergeometric equation obeying the second-order recursive formula.

Using (9), the difference equation of the Z-domain of (5) can be approximated as

$$\begin{aligned} y(k) &= -\frac{T^\alpha - 2R_2 C_2}{T^\alpha + 2R_2 C_2} y(k-1) + \frac{2R_2 T^\alpha}{T^\alpha + 2R_2 C_2} u(k) \\ &\quad + \frac{R_2 T^\alpha}{T^\alpha + 2R_2 C_2} u(k-1) \end{aligned} \quad (10)$$

Define  $\theta = [-(T^\alpha - 2R_2 C_2)/(T^\alpha + 2R_2 C_2), 2R_2 T^\alpha/(T^\alpha + 2R_2 C_2), R_2 T^\alpha/(T^\alpha + 2R_2 C_2)]$  and  $\Phi = [y(k-1), u(k), u(k-1)]$ , the least squares vector expression is

$$y = \Phi \theta + \varepsilon \quad (11)$$

where  $y$  is the output vector at time  $k$ ,  $\Phi$  is a known input and output vector,  $\theta$  is a parameter estimation matrix vector, and  $\varepsilon$  is a residual vector.

By using the least squares method to minimize the sum of the squares of the residuals, the optimal estimate of the parameter matrix can be obtained, as

$$\theta = [\Phi^T \Phi]^{-1} \Phi^T y \quad (12)$$

Since the lithium battery changes at the moment of current change, the voltage change at the battery terminal is equivalent to pure resistance, and the influence of polarization resistance is small enough and can be approximately zero. Therefore, the estimation of the internal resistance of a lithium battery can be equivalent to

$$R_1 = \frac{\Delta V_o}{\Delta t} \quad (13)$$

The fractional equivalent circuit model parameters of the lithium battery are identified by the least squares method under different SOC from HPPC test, and the parameter estimation of the whole discharge interval can be obtained. The parameter identification results are shown in Table 1.

#### 4. Adaptive Online Parameter Identification Method

Although the fractional order equivalent circuits have a more accurate battery performance description, the battery has obvious nonlinear, time-varying characteristics in the actual working condition. In other words, the accurate battery mode is suitable for static performance description, but not for dynamic performance description.

Therefore, in order to improve the estimation accuracy of the state of charge and enhance the adaptability of the system, the battery model parameters need to be estimated online and the battery model should be updated.

According to the fractional order equivalent circuit model, the fractional order is set as  $\alpha = 0.7$  from the contents of the previous section. The model parameters that the internal resistance unit and the polarization impedance unit need to recognize include  $R_1$ ,  $R_2$ , and  $C_2$ . Under normal operating conditions, the battery charge and discharge rate is not high, so the charge state changes slowly. Open circuit voltage ( $E_o$ ) is a function of state of charge (SOC), so the battery open circuit voltage change is relatively slow, in order to obtain a more accurate parameter model, the  $E_o$  also needs to be identified online.

The system of fractional equivalent circuits can be described as a fractional differential equation of (3) and (4). And the derivative of (4) can be rewritten

$$\begin{aligned} D^\alpha V_o &= D^\alpha E_o + D^\alpha I R_1 + D^\alpha V_2 \\ &= R_1 D^\alpha I + \frac{R_1 + R_2}{R_2 C_2} I - \frac{V_o}{R_2 C_2} + \frac{E_o}{R_2 C_2} \\ &= \left[ R_1 \quad \frac{R_1 + R_2}{R_2 C_2} \quad \frac{1}{R_2 C_2} \quad \frac{E_o}{R_2 C_2} \right] [D^\alpha I \quad I \quad -V_o \quad 1] \\ &= \theta \mu^T \end{aligned} \quad (14)$$

where

$$\begin{aligned} \theta &= \left[ R_1 \quad \frac{R_1 + R_2}{R_2 C_2} \quad \frac{1}{R_2 C_2} \quad \frac{E_o}{R_2 C_2} \right] \in \mathbb{R}, \\ \mu &= [D^\alpha I \quad I \quad -V_o \quad 1]^T \in \mathbb{R} \end{aligned} \quad (15)$$

Since the system parameters are unknown to scene  $\theta$ , using its estimation  $\hat{\theta}$  instead, the corresponding estimated output is

$$D^\alpha \hat{V}_o = \hat{\theta} \mu^T \quad (16)$$

Set the output voltage prediction error and the parameter vector estimation error respectively as

$$e(t) = V_o - \hat{V}_o \quad (17)$$

$$\tilde{\theta}(t) = \theta - \hat{\theta} \quad (18)$$

Thus, a model for estimation of parameters is constructed

$$\begin{bmatrix} D^\beta \hat{\theta}_1 \\ D^\beta \hat{\theta}_2 \\ D^\beta \hat{\theta}_3 \\ D^\beta \hat{\theta}_4 \end{bmatrix} = \begin{bmatrix} \rho_1 D^\alpha I \\ \rho_2 I \\ -\rho_3 V_o \\ \rho_4 \end{bmatrix} e(t) \quad (19)$$

where  $\beta$  is the parameter update order limited by inequality  $0 < \beta < 1$ , and  $\rho_1, \rho_2, \rho_3, \rho_4$  are positive constants.

In order to reduce the  $\tilde{\theta}(t)$ , the parameter update law is designed and the normalized quadratic cost function is defined as

$$J(\hat{\theta}) = \frac{e^2(t)}{2\hat{\omega}^2(t)} \quad (20)$$

where  $\hat{\omega}^2(t) = 1 + \mu^T \Lambda \mu$ , and  $\Lambda$  is blamed for the positive definite matrices and it is called the normalizing weighting coefficient matrix.

Design system parameters update law as

$$D^\beta \hat{\theta} = -\Gamma \nabla J \quad (21)$$

where  $\Gamma$  is the positive definite matrix of the appropriate dimension.

Take (17) and (20) into (21), we can obtain

$$D^\beta \tilde{\theta}(t) = -\Gamma \frac{\mu}{1 + \mu^T \Lambda \mu} e(t) \quad (22)$$

Define  $\Theta(t) = \mu \mu^T / \hat{\omega}^2(t) \geq 0$ , so (22) is rewritten as

$$D^\beta \tilde{\theta}(t) = -\Gamma \Theta(t) \tilde{\theta}(t) \quad (23)$$

According to Lemma 2.1 in [22], the corresponding frequency distributed model of the system can be described by

$$\begin{aligned} \frac{\partial z(\omega, t)}{\partial t} &= -\omega z(\omega, t) - \Gamma \Theta(t) \tilde{\theta}(t) \\ \tilde{\theta}(t) &= \int_0^\infty \phi_\beta(\omega) z(\omega, t) d\omega \end{aligned} \quad (24)$$

where  $z(\omega, t) \notin \mathbb{R}$ ,  $\phi_\beta(\omega) = \sin \beta \pi / \pi \omega^\beta$ .

Define the Lyapunov function as

$$V = \frac{1}{2} \int_0^\infty \phi_\beta(\omega) z^T(\omega, t) \Gamma^{-1} z(\omega, t) d\omega \quad (25)$$

The time derivative of (24) can be written as

$$\begin{aligned} \dot{V} &= \int_0^\infty \phi_\beta(\omega) z^T(\omega, t) \Gamma^{-1} \frac{\partial z(\omega, t)}{\partial t} d\omega = \int_0^\infty \phi_\beta(\omega) \\ &\cdot z^T(\omega, t) \Gamma^{-1} (-\omega z(\omega, t) - \Gamma \Theta(t) \tilde{\theta}(t)) d\omega \\ &= - \int_0^\infty \omega \phi_\beta(\omega) z^T(\omega, t) \Gamma^{-1} z(\omega, t) d\omega - \tilde{\theta}^T(t) \\ &\cdot \Theta(t) \tilde{\theta}(t) \end{aligned} \quad (26)$$

It is obvious that  $\dot{V} < 0$ , which means that it satisfies the Lyapunov stability criterion, so the adaptive parameter estimation algorithm is asymptotically stable.

Based on LaSalle Lemma, one can conclude that such a fractional order gradient estimator is asymptotically stable when  $0 < \beta < 1$ . In other words,  $\tilde{\theta}(t)$  can converge to zero

$$\lim_{t \rightarrow \infty} \tilde{\theta} = 0 \quad (27)$$

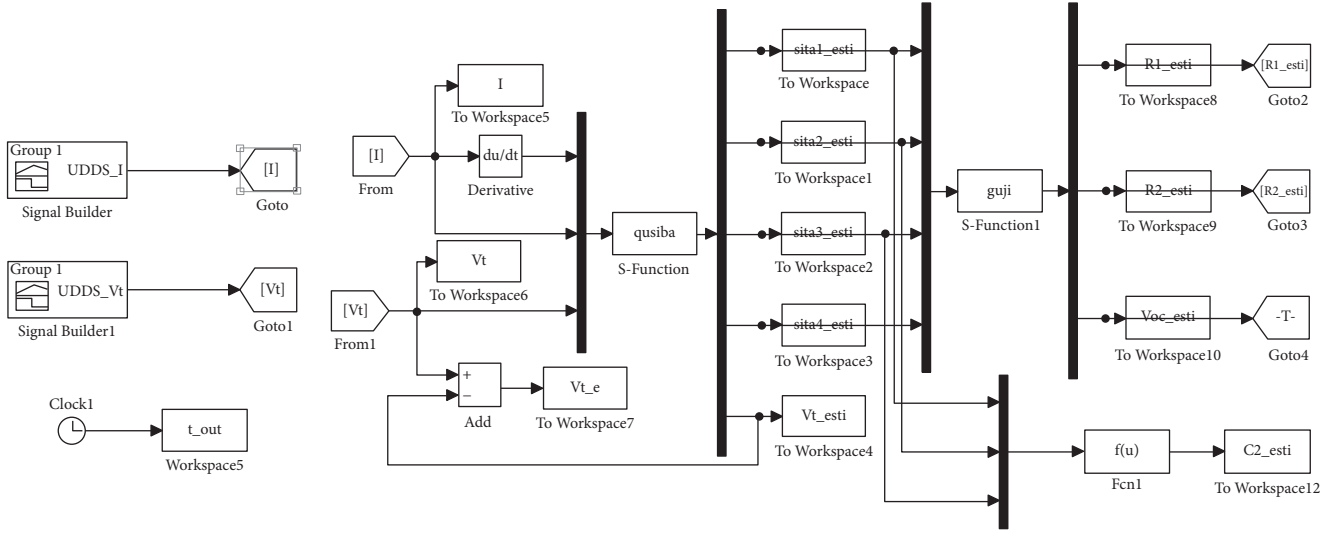


FIGURE 4: Parameter online simulation mode.

Further, the equivalent circuit parameters can be expressed as

$$\begin{bmatrix} \widehat{R}_1 \\ \widehat{R}_2 \\ \widehat{E}_o \\ \widehat{C}_2 \end{bmatrix} = \begin{bmatrix} \widehat{\theta}_1 \\ \frac{\widehat{\theta}_2}{\widehat{\theta}_3} - \widehat{\theta}_1 \\ \frac{\widehat{\theta}_4}{\widehat{\theta}_3} \\ \frac{(\widehat{R}_1 + \widehat{R}_2)I - V_o + \widehat{E}_o}{(\widehat{V}_o - \widehat{R}_1 D^\alpha I) \widehat{R}_2} \end{bmatrix} \quad (28)$$

## 5. Simulation and Experimental Verification

In order to verify the accuracy of the adaptive online parameter identification, a Simulink model is designed in MATLAB/Simulink, as shown in Figure 4. The battery current and voltage data is collected in real time on the battery test platform, according to the discharge requirements of the UDDS driving cycle. The simulation model is used to continuously evaluate the ohmic resistance, polarization resistance, and polarization capacitance of the battery under this condition.

The initial parameters and feedback coefficients of adaptive online parameter identification algorithm are set as follows:  $\widehat{\theta}_{1(0)} = 0.2$ ,  $\widehat{\theta}_{2(0)} = 0.01$ ,  $\widehat{\theta}_{3(0)} = 0.2$ ,  $\widehat{\theta}_{4(0)} = 1$ ,  $\rho_1 = 0.01$ ,  $\rho_2 = 0.002$ ,  $\rho_3 = 0.02$ , and  $\rho_4 = 0.005$ . The results of the adaptive online estimation of fractional equivalent circuit parameters are shown in Figure 5. The blue curves represent the results of the adaptive online identification of the equivalent circuit parameters, and the red curves represent the results of the parameter identification shown in Table 1 under offline conditions.

It can be seen that, under the condition of randomly given initial values, the estimated curve of each parameter quickly converges to the reference curve, and then the fluctuation

tends to be stable. This shows that the proposed algorithm can quickly correct the initial capacity deviation under dynamic conditions, accurately estimate the internal parameters of the battery, and have good rapidity, robustness, and stability.

## 6. Conclusions

In this paper, we analyzed the EIS and the HPPC data of lithium-ion batteries and proposed a simplified fractional order RC equivalent circuit impedance model. By offline identification of fractional order circuit model parameters based on HPPC data, it can be seen that the fractional order equivalent circuit model is more accurate than the integer-order equivalent circuit model. However, there still exists the problem that static battery models cannot match dynamic conditions. In order to solve this problem, an online parameter estimation method for the simplified fractional equivalent circuit model is proposed. Using the Lyapunov stability theorem, the stability and convergence of the method is proved. This method can realize real-time collection of the battery current and voltage data and continuously estimate the ohmic resistance, polarization resistance, and polarization capacitance of the battery under working conditions. Simulation results show that the adaptive online parameter estimation method can be used for parameter identification and parameter updating of the fractional order equivalent circuit model and can well reflect the dynamic characteristics of the battery.

## Data Availability

The data used to support the findings of this study are available from the corresponding author upon request.

## Conflicts of Interest

The authors declare that they have no conflicts of interest.

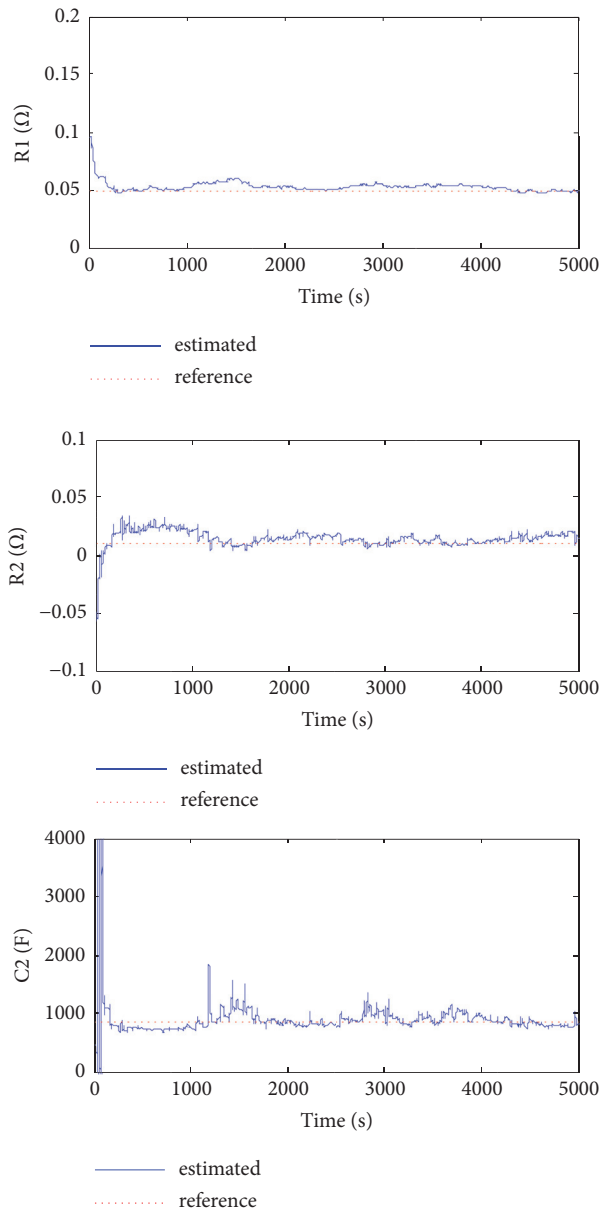


FIGURE 5: Online parameter estimation curves.

## Authors' Contributions

WJL (Jianlin Wang) and XD (Dan Xu) wrote the main manuscript text; ZL (Le Zhang), ZP (Peng Zhang), and ZGR (Gairu Zhang) assisted in electrochemical testing of batteries. All authors reviewed the manuscript.

## References

- [1] L. Lu, X. Han, J. Li, J. Hua, and M. Ouyang, "A review on the key issues for lithium-ion battery management in electric vehicles," *Journal of Power Sources*, vol. 226, pp. 272–288, 2013.
- [2] A. Jossen, V. Späth, H. Döring, and J. Garche, "Reliable battery operation - a challenge for the battery management system," *Journal of Power Sources*, vol. 84, no. 2, pp. 283–286, 1999.
- [3] M. Ortúzar, J. Moreno, and J. Dixon, "Ultracapacitor-based auxiliary energy system for an electric vehicle: implementation and evaluation," *IEEE Transactions on Industrial Electronics*, vol. 54, no. 4, pp. 2147–2156, 2007.
- [4] T. Nukuda and K. Nishiyama, "Technical Trend of Lithium Ion Batteries for EV/PHEV," *The Journal of the Institute of Electrical Engineers of Japan*, vol. 39, no. 1, pp. 228–269, 2013.
- [5] P. Nelson, I. Bloom, K. Amine, and G. Henriksen, "Design modeling of lithium-ion battery performance," *Journal of Power Sources*, vol. 110, no. 2, pp. 437–444, 2012.
- [6] X. Zhang, J. Lu, S. Yuan, J. Yang, and X. Zhou, "A novel method for identification of lithium-ion battery equivalent circuit model parameters considering electrochemical properties," *Journal of Power Sources*, vol. 345, pp. 21–29, 2017.
- [7] M. Chen and G. A. Rincón-Mora, "Accurate electrical battery model capable of predicting runtime and I-V performance," *IEEE Transactions on Energy Conversion*, vol. 21, no. 2, pp. 504–511, 2006.
- [8] R. Rao, S. Vrudhula, and D. N. Rakhmatov, "Battery modeling for energy aware system design," *The Computer Journal*, vol. 36, no. 12, pp. 77–87, 2003.
- [9] H. He, R. Xiong, and J. Fan, "Evaluation of lithium-ion battery equivalent circuit models for state of charge estimation by an experimental approach," *Energies*, vol. 4, no. 4, pp. 582–598, 2011.
- [10] P. Gao, C. Zhang, and G. Wen, "Equivalent circuit model analysis on electrochemical impedance spectroscopy of lithium metal batteries," *Journal of Power Sources*, vol. 294, pp. 67–74, 2015.
- [11] L. Zhang, H. Peng, Z. Ning, Z. Mu, and C. Sun, "Comparative research on RC equivalent circuit models for lithium-ion batteries of electric vehicles," *Applied Sciences*, vol. 7, no. 10, article 1002, 2017.
- [12] J. Jiang, Y. Liang, Q. Ju, L. Zhang, W. Zhang, and C. Zhang, "An equivalent circuit model for lithium-sulfur batteries," *Energy Procedia*, vol. 105, pp. 3533–3538, 2017.
- [13] J. Wang, D. Xu, H. Zhou, and A. Bai, "High-performance fractional order terminal sliding mode control strategy for DC-DC Buck converter," *PLoS ONE*, vol. 12, no. 10, article e0187152, 2017.
- [14] C. Wu, G. Si, Y. Zhang, and N. Yang, "The fractional-order state-space averaging modeling of the Buck-Boost DC/DC converter in discontinuous conduction mode and the performance analysis," *Nonlinear Dynamics*, vol. 79, no. 1, pp. 689–703, 2015.
- [15] Q. Yang, J. Xu, B. Cao, X. Li, and J. Xu, "A simplified fractional order impedance model and parameter identification method for lithium-ion batteries," *PLoS ONE*, vol. 12, no. 2, article e0172424, 2017.
- [16] S. Jiang, "A parameter identification method for a battery equivalent circuit model," *Sae World Congress & Exhibition*, vol. 33, 2011.
- [17] B. Wang, S. E. Li, H. Peng, and Z. Liu, "Fractional-order modeling and parameter identification for lithium-ion batteries," *Journal of Power Sources*, vol. 293, pp. 151–161, 2015.
- [18] Y. Guo, "Study on the parameter identification method of lead-acid battery equivalent circuit model," *Science Technology Engineering*, 2012.
- [19] K. Araki and M. Yamaguchi, "Novel equivalent circuit model and statistical analysis in parameters identification," *Solar Energy Materials & Solar Cells*, vol. 75, no. 3-4, pp. 457–466, 2003.

- [20] T. Feng, L. Yang, X. Zhao, H. Zhang, and J. Qiang, "Online identification of lithium-ion battery parameters based on an improved equivalent-circuit model and its implementation on battery state-of-power prediction," *Journal of Power Sources*, vol. 281, pp. 192–203, 2015.
- [21] B. Ning, J. Xu, B. Cao, B. Wang, and G. Xu, "A sliding mode observer SOC estimation method based on parameter adaptive battery model, the low-carbon cities and urban energy systems," *Energy Procedia*, vol. 88, pp. 619–626, 2016.
- [22] Y. Wei, Z. Sun, Y. Hu, and et al, "On line parameter estimation based on gradient algorithm for fractional order systems," *Journal of Control & Decision*, vol. 2, no. 4, pp. 219–232, 2015.
- [23] J. Huang, H. Ge, Z. Li, and J. Zhang, "Dynamic electrochemical impedance spectroscopy of a three-electrode lithium-ion battery during pulse charge and discharge," *Electrochimica Acta*, vol. 176, no. 176, pp. 311–320, 2015.
- [24] T. Lou, W. Zhang, H. Guo, and J. Wang, "The internal resistance characteristics of lithium-ion battery based on HPPC method," *Advanced Materials Research*, vol. 455-456, pp. 246–251, 2012.
- [25] H. Zhang, H. W. Mu, Y. Zhang, and J. Han, "Calculation and characteristics analysis of lithium ion batteries' internal resistance using HPPC test," *Advanced Materials Research*, vol. 926-930, pp. 915–918, 2014.

## Research Article

# A Time-Replacement Policy for Multistate Systems with Aging Components under Maintenance, from a Component Perspective

Chao-Hui Huang <sup>1</sup> and Chun-Ho Wang <sup>2</sup>

<sup>1</sup>Department of Applied Science, R.O.C. Naval Academy, No. 669, Junxiao Rd., Zuoying District, Kaohsiung City 81345, Taiwan

<sup>2</sup>Department of Power Vehicle and Systems Engineering, Chung Cheng Institute of Technology, National Defense University, No. 75, Shiyuan Rd., Daxi Township, Taoyuan County 33551, Taiwan

Correspondence should be addressed to Chun-Ho Wang; [u8733803@gmail.com](mailto:u8733803@gmail.com)

Received 2 September 2018; Revised 10 January 2019; Accepted 5 February 2019; Published 18 March 2019

Academic Editor: Gen Q. Xu

Copyright © 2019 Chao-Hui Huang and Chun-Ho Wang. This is an open access article distributed under the Creative Commons Attribution License, which permits unrestricted use, distribution, and reproduction in any medium, provided the original work is properly cited.

This study aims for multistate systems (MSSs) with aging multistate components (MSCs) to construct a time-replacement policy and thereby determine the optimal time to replace the entire system. The nonhomogeneous continuous time Markov models (NHCTMMs) quantify the transition intensities among the degradation states of each component. The dynamic system state probabilities are therefore assessed using the established NHCTMMs. Solving NHCTMMs is rather complicated compared to homogeneous continuous time Markov models (HCTMMs) in determining reliability related performance indexes. Often, traditional mathematics cannot acquire accurate explicit expressions, in particular, for multiple components that are involved in designed system configuration. To overcome this difficulty, this study uses Markov reward models and the bound approximation approach to assess rewards of MSSs with MSCs, including such things as total maintenance costs and the benefits of the system staying in acceptable working states. Accordingly, we established a long-run expected benefit (LREB) per unit time, representing overall MSS performance through a lifetime, to determine the optimal time to replace the entire system, at which time the LREB values are maximized. Finally, a simulated case illustrates the practicability of the proposed approach.

## 1. Introduction

Conventional binary-state systems assume that component constituted system configurations involve either only perfect functioning or complete failure. The optimal system reliability design, maintenance policy, and repairing management are thereby determined. However, the design of modern devices tends to be of large scale and complicated; these devices normally confront different kinds of faults and errors, including damage, impacts, and aging factors, throughout their lifetimes. Various systems, such as computer server, telecommunication, and electricity distribution systems, become tolerant to these faults and errors. Even if a fault occurs, these systems continue working at an acceptable or degraded performance level. Accordingly, from being perfectly functioning, systems normally experience multiple intermediate states during the degradation process, before complete failure occurs. Confining systems to binary

states can ignore the intrinsic multistate property of these systems and result in a biased evaluation of actual system performance. Therefore, constructing a multistate reliability theory can provide further insight into the complicated failure theory, lifetime prediction, and improvement of system reliability, which is an essential issue in both practical and theoretical aspects.

Multistate systems (MSSs) are regarded as failures when they degrade into unacceptable performance levels and cannot meet operational requirements. Preventive maintenance (PM) implementation is beneficial to sustain or improve system performance during the planning horizon. Incorporating imperfect maintenance theories into the stochastic process [1, 2] can properly imitate the status of MSS degradation. Although components can exhibit better performance after maintenance, satisfying system performance requirements as these components gradually age is usually necessary. Overly frequent maintenance not only consumes a tremendous

amount of cost but also decreases the marginal effectiveness of system performance improvements and increases maintenance time. This phenomenon induces the essential issue of determining the time-replacement policy for MSSs.

This study extends the work of Wang and Huang [3] which aims for MSSs with aging multistate components (MSCs) to establish an optimal time-replacement policy, given the PM policy from the component perspective. Determining a PM policy from the component perspective has practical applications because the component can be monitored in real time, and its degradation or failure can cause the sudden failure of the system, resulting in catastrophic consequences. A recent case of this occurred when General Motors developed the On Star system, which can monitor car parts and alert drivers before the system needs to be repaired [4]. A performance index regarding the long-run expected benefit (LREB) per unit time for an MSS with aging MSCs was established to evaluate its long-run benefits. The optimal time to replace all the components in MSSs can be determined easily by maximizing the long-run expected benefit (LREB) values. Mathematically, the nonhomogeneous continuous time Markov reward models (NHCTMRMs) [5, 6] for all components and the system are established to evaluate the maintenance costs and benefits of a well-maintained system. Similarly, establishing NHCTMMs mainly calculates the instantaneous state probability distribution of MSSs and thereby determines system availability for MSSs with aging MSCs. Solving the NHCTMMs and NHCTMRMs is more complicated than solving the HCTMMs. This solving difficulty is significantly increased along with the system augmentations, such as the extension of components and their degradation states. Under this consideration, conventional mathematics cannot obtain explicit expressions of NHCTMM and NHCTMRM solutions. Often, using calculators as common mathematical tools, such as MATLAB or Mathcad, may induce the problem of inaccuracy [7–10]. Ding et al. [9] developed the bound approximation approach that can solve the NHCTMMs efficiently. The bound approximation approach partitions the system lifetime into multiple tiny intervals and sets the transition intensities within intervals as constant. The HCTMMs then find the instantaneous probability at the end of each time interval; via iterative procedure, the NHCTMMs can be solved efficiently. This study uses the bound approximation approach [9] to solve the nonlinear simultaneous differential equations corresponding to the established NHCTMMs and NHCTMRMs. The time-dependent LREB index values are then determined throughout lifetime. Maximizing the LREB index values can allow engineers to find the optimal time to replace an MSS given a specified PM policy that is implemented from the component perspective [11]. A simulated case involving execution of sensitivity analysis verifies the efficacy of the proposed approach.

## 2. Literature Review

In general, some indices were proposed in evaluation of dynamic system over time mainly related with system availability; these indices can fall into two categories with

expense-oriented and benefit-oriented indices. These two categories commonly refer to index like “long-run average cost” [12, 13] and “long-run expected profit” [14, 15], respectively, despite other similar measures. Zhang and Wang [12] proposed a replacement policy for a deteriorating system with multifailure modes including nonrepairable failure (catastrophic failure) and  $k$  repairable failure modes. On the basis of a geometric process model to evaluate the aging effect and accumulative wear for a deteriorating system, they established an explicit expression of the long-run average cost (LRAC) per unit time of a system. The system is replaced whenever the number of system failures reaches  $N$  or a nonrepairable failure occurs. The optimal  $N^*$  is determined by minimizing the LRAC. Although the property of system deterioration is considered in the proposed replacement policy [11], their study is confined to a binary system. Wang and Zhang [16] extended the study of Zhang and Wang [12], except that the repair times after failure are assumed to be independent and identically distributed. Two replacement models were proposed: one is based on the limiting availability and the other is based on the LRAC rate of the system. By maximizing the limiting availability  $A(N)$  and minimizing the LRAC rate  $C(N)$ , the optimal replacement policies  $N$  in both cases are determined. Chang et al. [17] proposed a replacement model given the system experiences including a type-I failure (minor), rectified by a minimal repair, and a type-II failure (catastrophic) that calls for a replacement. A long-run expected cost per unit time in operating the system, incorporating costs due to minimal repair and different forms of the replacement state derived, is a determinant to decide whether to repair or replace the system. The maintenance model for replacement policy in Chang et al. [17] is from the perspective of a binary system. Jain and Gupta [18] proposed an optimal replacement policy for a repairable system with multiple vacations and imperfect fault coverage. The reliability analysis of a repairable system consists of a single repair person who can take multiple vacations. A repair system considers two types of failure modes: major and minor. Maintenance policy involves perfect recovery of the system after a minor fault, whereas imperfect recovery with some probability occurs after a major fault. System lifetime and vacation time of the repair person are assumed to be exponentially distributed, whereas the repair time follows a general distribution. By assuming a geometric process for system working/vacation time, the supplementary variable technique and Laplace transform approach derive the reliability indices of the system. Accordingly, a replacement policy to maximize the expected profit after a long run time was proposed.

Liu and Huang [19] constructed an optimal replacement policy for a system consisting of a single multistate element. This study mainly considers scenarios in which the performance rate and transition intensities cannot be crisply determined because of a lack of accuracy or fluctuation of collected data. The optimal threshold value of degradation states related to replacing an element is determined to maximize its objective value of average benefit per unit time. Zhang et al. [20] studied a degenerately simple system with  $k + 1$  states, including  $k$  failure states and one working

state. A replacement policy  $N$  based on the number of system failures was applied given implementation of imperfect maintenance. The objective was to maximize the long-run expected profit per unit time. The explicit expression of the long-run expected profit per unit time was derived and the corresponding optimal solution was determined. Zhang and Wang [13] extended the study of Zhang et al. [20] and proposed a new replacement policy,  $T$ , based on the system age for a multistate degenerative simple system. The model assumes that the system after repair is not “as good as new,” and the degeneration of the system is stochastic. The explicit expression of the long-run average cost per unit time is derived and minimized to determine an optimal replacement policy  $T^*$ . The long-run average cost is mathematically the same measure as the long-run expected cost referred to in Chang *et al.* [17]. Liu and Huang [14] developed an optimal replacement policy for an MSS with imperfect maintenance from the system perspective. There are some efforts aiming at determining the PM policy from the system perspective [9, 21, 22]. Once the system falls into an unacceptable state, the system fails and imperfect maintenance for all components is implemented without considering the states of the components. The established corrective maintenance model assumes that the components recover back to a perfect functioning state after maintenance, whereas degradation intensities increase with the amount of maintenance to characterize the impact of aging factors on components using a quasi-renewal process [15]. An LREB index per unit time associated with the number of MSS failures, denoted as  $N$ , was developed to determine the optimal MSS failure number  $N$  to replace a whole system. Liu and Huang [14] used the NHCTMMs to evaluate the instantaneous multistate probability distribution of aging components. Then, the stochastic process of MSSs was elucidated in terms of their multistate probability distribution, derived by a universal generating function [23]. The maintenance costs of components accounted for in Liu and Huang [14] are independent of their performances levels: no matter the degradation states of the components, maintenance costs are identical. Normally, components at low degradation states cost much more to be restored to perfect functioning than those at high degradation states in maintenance. Furthermore, the components may not need to be restored to perfect status. A rather simple system configuration was illustrated to obtain explicit expressions of system performances in the study.

Much of the previously discussed literatures aimed at binary systems to address the problem of replacement policy given imperfect maintenance from the system implementation perspective. Although some works address the replacement policy problems for multistate systems, the PM from the perspective of a system with binary components is given. Furthermore, in order to deduce the explicit expression of the MSS performance measure, a rather simple system configuration is given to illustrate the theoretical results. Practically, for a safety system, the PM policy from the component perspective can prevent a sudden system failure due to component degradation or failure, avoiding possible catastrophic consequences. In this regard, this study aims at MSSs with aging MSCs to establish an optimal

time-replacement policy, given the implementation of a PM policy from a component perspective. The PM policy involves maintenance actions in the degradation states for aging MSCs. A performance index regarding the long-run expected benefit (LREB) per unit time for MSSs with aging MSCs determined the optimal time to replace an MSS by maximizing the LREB values throughout the lifetime. The term “benefit,” a general designate, corresponds to the profit making with system staying at acceptable states capable of functioning properly with distinct performances in this paper. Alternatively, given other considerations, the term “benefit” could relate to other measures such as productivity and delivery rate in a manufacturing system.

### 3. NHCTMMs

**3.1. NHCTMM for an Aging MSC.** The Lisnianski and Levitin [24, 25] use the homogeneous continuous time Markov model to characterize the degradation process of individual MSC. This approach assumes that the transition intensity to the next state has no age effect only depending on the current state. It is inapplicable for cases that a component’s degradation process does not only rely on the current state but also the age of the component. Taking the aging factors, the NHCTMMs are employed to obtain the stochastic behavior of individual aging components by transition intensities enhanced with age. For a repairable aging MSC, the component degrades to states with lower performance rate from the states with higher performance rate; conversely, it is restored to states with higher performance rate from the states with lower performance rate after appropriate maintenances. Figure 1 shows a typical state-transition diagram of a repairable aging MSC.

For component  $l$ ,  $l = 1, 2, \dots, m$ , the performance degradation is characterized by the stochastic process  $\{G^l(t) \mid t \geq 0\}$ . The intensity  $\lambda_{ij}^l(t)$  of any transition from state  $i$  to state  $j$ ,  $j \in \{i - 1, i - 2, \dots, 1\}$ , is a monotonically increasing function associated with component age, while  $\mu_{ji}^l$  of any transition from state  $j$  to state  $i$  is a repairing rate indicating the repair time is exponentially distributed. The corresponding Chapman-Kolmogorov differential equation of NHCTMM for this repairable aging MSC is expressed as

$$\frac{d}{dt} p_j^l(t) = \sum_{\substack{i=1 \\ i \neq j}}^{K_l} p_i^l(t) \alpha_{ij}^l(t) - p_j^l(t) \sum_{\substack{i=1 \\ i \neq j}}^{K_l} \alpha_{ji}^l(t), \quad (1)$$

$$j = 1, 2, \dots, K_l$$

where  $p_i^l(t)$  and  $p_j^l(t)$  are the instantaneous probabilities of states  $i$  and  $j$  occurring at instant  $t$ , respectively, for component  $l$ .  $\alpha_{ij}^l(t)$  and  $\alpha_{ji}^l(t)$  are time-varying transition intensities from state  $i$  to  $j$  and from  $j$  to  $i$  in terms of  $\lambda_{ij}^l(t)$  and  $\mu_{ji}^l$ , respectively. Equation (1) contains  $K_l$  nonlinear differential equations. Ideally, given the initial probability values of all states, the distribution of states for a component at instant  $t$  can be determined by solving the NHCTMM.

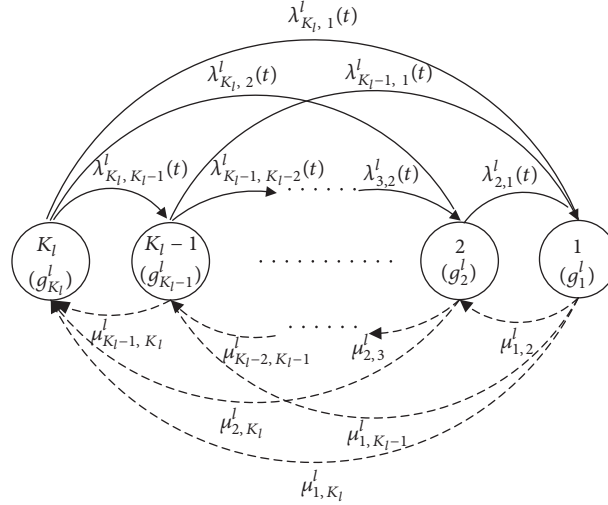


FIGURE 1: State-transition diagram of a component.

However, solving the NHCTMM is a complicated challenge [7–10].

**3.2. The NHCTMM and NHCTMRM for the MSS with Aging MSCs.** When the MSS consists of  $n$  aging MSCs, its performance rate is clearly determined by the performance rates of these MSCs. The state of the entire system is determined by the states of MSCs configured in the system. Let  $L^n = \{g_1^1, \dots, g_{k_1}^1\} \times \{g_1^2, \dots, g_{k_2}^2\} \times \dots \times \{g_1^n, \dots, g_{k_n}^n\}$  be the space of possible combinations of performance rates for all the MSCs. Mapping the space of the components performance rate into the system's performance rate according to MSS structure function can derive the space of possible values of performance rates for the entire system  $M = \{g_1, \dots, g_K\}$ . Mathematically, the space of performance rates for a MSS significantly increases with the augmentation of a MSS such as extension of components and their degradation states. Technically, the MSS states with identical performance rate are united into one state and thereby establish the Markov model to reduce the solving complexity of the established NHCTMMs without calculation inaccuracy. Accordingly, the MSS performance measures are determined. The Chapman-Kolmogorov differential equation of NHCTMM for a MSS is expressed as

$$\frac{d}{dt} p_j(t) = \sum_{\substack{i=1 \\ i \neq j}}^K p_i(t) \alpha_{ij}(t) - p_j(t) \sum_{\substack{i=1 \\ i \neq j}}^K \alpha_{ji}(t), \quad (2)$$

$$j = 1, 2, \dots, K$$

where  $p_i(t)$  and  $p_j(t)$  are the instantaneous probabilities of states  $i$  and  $j$  occurring at instant  $t$ , respectively.  $\alpha_{ij}(t)$  and  $\alpha_{ji}(t)$  are time-varying transition intensities from state  $i$  to  $j$  and from state  $j$  to  $i$  in terms of  $\lambda_{ij}^l(t)$  and  $\mu_{ji}^l$ , respectively, for a MSS. Equation (2) contains  $K$  nonlinear differential equations. Ideally, given the initial probability values of all

MSS states, the MSS states probabilities distribution at instant  $t$  can be determined.

The nonhomogeneous Markov reward model [24, 26] can be used to effectively assess the reliability performances and cost associated measures for an aging MSC/MSS over its lifetime. Basically, the NHCTMRM is a Markov process with rewards; the reward matrix  $\mathbf{r} = [r_{ij}]$  must be constructed according to varied indicators such as maintenance costs, revenue staying at the acceptable states, availability, and mean time to failure. The Chapman-Kolmogorov differential equation corresponding to NHCTMRM for a MSS is expressed as

$$\frac{dV_i(t)}{dt} = r_{ii} + \sum_{\substack{j=1 \\ j \neq i}}^K \alpha_{ij}(t) r_{ij} + \sum_{j=1}^K \alpha_{ij}(t) V_j(t), \quad (3)$$

$$i = 1, 2, \dots, K$$

where  $V_i(t)$  and  $V_j(t)$  are the total expected reward (TER) values accumulated until time  $t$  while in states  $i$  and  $j$ , respectively. Substituting the initial value  $V_i(0) = 0$  into (3), the simultaneous nonlinear differential equations can be solved to derive the TER value for a MSS.

#### 4. Bound Approximation Approach

Solving the NHCTMM to obtain the aging MSC/MSS performance indicators requires a lot of time. Often, the use of calculators embedded in the common mathematical tools, such as MATLAB or MATHCAD, may induce the problem of inaccuracy [8, 13]. The bound approximation approach [9] allows the determination of instantaneous state probabilities for an aging MSC/MSS. This approach divides the lifetime into multiple intervals and sets the failure rate during each interval to be a constant. The HCTMM is then used to find the instantaneous probability at the end of each time interval. As an example of an aging MSC, this numerical approach initially divides the component lifetime  $T$  into  $N$  time intervals. The duration of each time interval is

$\Delta t = T/N$ . Then, two constants  $\lambda_{ij}^{l(n-)}$  and  $\lambda_{ij}^{l(n+)}$  are used to approximate the failure rate  $\lambda_{ij}^l(t)$  in each time interval  $t_n = [\Delta t \cdot (n-1), \Delta t \cdot n]$ ,  $1 \leq n \leq N$ , using the following equations:

$$\lambda_{ij}^{l(n-)} = \lambda_{ij}^l(\Delta t \cdot (n-1)) \quad (4)$$

$$\lambda_{ij}^{l(n+)} = \lambda_{ij}^l(\Delta t \cdot n) \quad (5)$$

where  $\lambda_{ij}^{l(n-)}$  and  $\lambda_{ij}^{l(n+)}$  represent the failure rate of the  $l^{th}$  component at the beginning and end of the  $n^{th}$  time interval. Equations (4) and (5) also give the lower and upper bounds of  $\lambda_{ij}^l(t)$  in the  $n^{th}$  time interval. Using  $\lambda_{ij}^{l(n-)}$  and  $\lambda_{ij}^{l(n+)}$  to solve the component's NHCTMM, the state probabilities  $P_j^{l(n-)}(\Delta t \cdot n)$  and  $P_j^{l(n+)}(\Delta t \cdot n)$  at the end of time interval  $t_n = [\Delta t \cdot (n-1), \Delta t \cdot n]$ ,  $1 \leq n \leq N$ , can be derived. These differential equations [24] are

$$\begin{aligned} \frac{dP_j^{l(n-)}(t)}{dt} &= \sum_{\substack{i=1 \\ i \neq j}}^{K_l} P_i^{l(n-)}(t) \alpha_{ij}^{l(n-)}(t) \\ &\quad - P_j^{l(n-)}(t) \sum_{\substack{i=1 \\ i \neq j}}^{K_l} \alpha_{ji}^{l(n-)}(t), \end{aligned} \quad (6)$$

$j = 1, \dots, K_l$

$$\begin{aligned} \frac{dP_j^{l(n+)}(t)}{dt} &= \sum_{\substack{i=1 \\ i \neq j}}^{K_l} P_i^{l(n+)}(t) \alpha_{ij}^{l(n+)}(t) \\ &\quad - P_j^{l(n+)}(t) \sum_{\substack{i=1 \\ i \neq j}}^{K_l} \alpha_{ji}^{l(n+)}(t), \end{aligned} \quad (7)$$

$j = 1, \dots, K_l$

At each time interval  $t_n$ , the lower bound  $\lambda_{ij}^{l(n-)}$  and upper bound  $\lambda_{ij}^{l(n+)}$  of the failure rate are utilized to determine the lower bound and upper bound intensities  $\alpha_{ij}^{l(n-)}(t)$  and  $\alpha_{ij}^{l(n+)}(t)$  for transitions from state  $i$  to  $j$ . During the first time interval, the initial condition of the component is already known. Hence, given that the component is in state  $K$  at  $t = 0$ , the initial conditions for (6) and (7) during the first time interval  $n = 1$  are as follows:

$$P_{K_l}^{l(1-)}(0) = 1, \quad (8)$$

$$P_{K_l-1}^{l(1-)}(0) = \dots = P_1^{l(1-)}(0) = 0$$

$$P_{K_l}^{l(1+)}(0) = 1, \quad (9)$$

$$P_{K_l-1}^{l(1+)}(0) = \dots = P_1^{l(1+)}(0) = 0$$

The initial conditions for  $t_n$ ,  $n = 2, 3, \dots, N$ , are defined by the following recurrence relations:

$$P_j^{l(n-)}(\Delta t \cdot (n-1)) = P_j^{l(n-1-)}(\Delta t \cdot (n-1)), \quad (10)$$

$j = 1, 2, \dots, K_l \quad n = 1, 2, \dots, N$

$$P_j^{l(n+)}(\Delta t \cdot (n-1)) = P_j^{l(n-1+)}(\Delta t \cdot (n-1)), \quad (11)$$

$j = 1, 2, \dots, K_l \quad n = 1, 2, \dots, N$

This means that the initial conditions for the next interval are defined by the solutions at the end of preceding time interval. By solving the NHCTMRM using the bound approximation approach, the lower bound  $V_i^{l(n-)}$  and upper bound  $V_i^{l(n+)}$  of the TER accumulated at each time interval  $[\Delta t \cdot (n-1), \Delta t \cdot n]$  can be obtained from any state. The equations for the NHCTMRM are

$$\begin{aligned} \frac{dV_i^{l(n-)}(t)}{dt} &= r_{ii}^l + \sum_{\substack{j=1 \\ j \neq i}}^{K_l} \alpha_{ij}^{l(n-)}(t) r_{ij}^l \\ &\quad + \sum_{j=1}^{K_l} a_{ij}^{l(n-)}(t) V_j^{l(n-)}(t), \end{aligned} \quad (12)$$

$i = 1, 2, \dots, K_l, \quad n = 1, \dots, N$

$$\begin{aligned} \frac{dV_i^{l(n+)}(t)}{dt} &= r_{ii}^l + \sum_{\substack{j=1 \\ j \neq i}}^{K_l} \alpha_{ij}^{l(n+)}(t) r_{ij}^l \\ &\quad + \sum_{j=1}^{K_l} a_{ij}^{l(n+)}(t) V_j^{l(n+)}(t), \end{aligned} \quad (13)$$

$i = 1, 2, \dots, K_l, \quad n = 1, \dots, N$

For any state during each time interval, the initial reward is 0; that is,

$$V_i^{l(n-)}(0) = V_i^{l(n+)}(0) = 0, \quad (14)$$

$i = 1, 2, \dots, K_l, \quad n = 1, \dots, N$

Solving (12) and (13) under the initial condition (14) gives the lower and upper bounds of TER accumulated during each time interval for all states. Multiplying  $V_i^{l(n-)}(\Delta t)$  and  $V_i^{l(n+)}(\Delta t)$  by their corresponding state probabilities  $P_i^{l(n-)}(\Delta t \cdot (n-1))$  and  $P_i^{l(n+)}(\Delta t \cdot (n-1))$  gives the system's upper and lower mean reward values for any state during each time interval. The sum of all mean reward values for all states gives the component's overall lower reward bound  $V^{l(n-)}$  and upper

reward bound  $V^{l(n+)}$  for any time interval. These bounds are calculated as

$$V^{l(n-)}(t) = \sum_{i=1}^{k_i} V_i^{l(n-)}(\Delta t) \cdot P_i^{l(n-)}(\Delta t \cdot (n-1)), \quad (15)$$

$$n = 1, \dots, N$$

$$V^{l(n+)}(t) = \sum_{i=1}^{k_i} V_i^{l(n+)}(\Delta t) \cdot P_i^{l(n+)}(\Delta t \cdot (n-1)), \quad (16)$$

$$n = 1, \dots, N$$

where  $t = \Delta t \cdot (n-1)$ . Finally, summing the TER over  $N$  time intervals gives the lower and upper bounds of TER over the component's lifetime:

$$TER^{l(-)}(t) = \sum_{n=1}^N V^{l(n-)}(t) \quad (17)$$

$$TER^{l(+)}(t) = \sum_{n=1}^N V^{l(n+)}(t) \quad (18)$$

The exact  $TER^l(t)$  value falls somewhere between the lower and upper bound; that is,  $TER^{l(-)}(t) \leq TER^l(t) \leq TER^{l(+)}(t)$ . A more accurate  $TER^l(t)$  value can be obtained by dividing  $T$  into smaller intervals.

## 5. Proposed Approach

This study aims for MSSs with aging MSCs to determine the time-replacement policy in which a PM from the component perspective is implemented. The calculation procedure integrates the multiple states of all components to obtain the distinctive states for MSSs and, therefore, to determine MSS performances that are established on the basis of nonhomogeneous Markov models. As mentioned previously, the bound approximation approach [9] can solve the simultaneous Chapman-Kolmogorov differential equations related to the established NHCTMMs. This study develops an LREB per unit time for MSSs with MSCs, taking into consideration maintenance costs, the benefits of a well-maintained system, and system loss due to maintenance. The establishment of the LREB index is as follows:

$$LREB(t) = \frac{V_a(t) - V_r(t) - C_r \cdot t_{rep} - C_{rep}}{t + t_{rep}} \quad (19)$$

where  $LREB(t)$  represents the LREB of a system during  $t$  period;  $V_a(t)$  represents the system benefit for staying at acceptable states during  $t$  period. The benefit mainly relates to the production rate of a system.  $V_r(t)$  represents the total maintenance cost of a system during  $t$  time period.  $C_r$  represents the replacement expense per unit time;  $t_{rep}$  represents the time required to replace a system;  $C_{rep}$  represents material expense related to system replacement. Accordingly, the optimal replacement time is determined by maximizing the LREB values throughout a lifetime. A simulated system

configuration with two distinctive PM policies elucidates the proposed approach. The following sections illustrate the model assumptions and calculation procedures.

### 5.1. Model Assumptions

- (1) The aging MSCs of the system degrade from perfectly functioning to complete failure over multiple states of degradation.
- (2) The failure rate of an individual component is an increasing function of time.
- (3) Components at degradation states can be restored to previous better states by appropriate maintenance.
- (4) Real-time monitoring of the system can identify the performance of individual components within the system.
- (5) A specific PM policy is implemented on the aging MSCs.
- (6) There are five maintenance activities:
  - (1) No service or repair.
  - (2) Minor service: enables restoration to state  $j + 1$  from state  $j$ .
  - (3) Major service: enables restoration to state  $j + 2$  from state  $j$ .
  - (4) Minor repair: enables restoration to state  $j + 3$  from state  $j$ .
  - (5) Major repair: enables restoration to state  $j + 4$  from state  $j$ .

### 5.2. Calculation Procedure of LREB for Numerical Cases.

The proposed approach is elucidated on the basis of a series-parallel system [11]. The structural function of flow transmission is used to model series and parallel links in the system. This simulated system contains three components. Components 1 and 2 are connected in parallel; both are connected to component 3 in series. Each component has five states possessing distinctive output performance, with state 5 being perfectly functioning and state 1 being complete failure. For example, in component 1, the output performances of its five states in descending order are 150, 100, 80, 50, and 0. Each individual component is initially in a perfectly functioning state. Hence, the initial probability of all the states is 0, except for state 5, which has a probability of 1. The minimum acceptable system performance (user demand) is set as 100. Figure 2 shows the system configuration with possible PM implementations at degradation states (the dotted lines) in state-space diagrams of MSCs. Table 1 lists the failure-rate functions of aging MSCs, whereas Table 2 presents the repair rates. Table 3 lists maintenance costs related to PM actions of components, whereas Table 4 presents the replacement-related parameters. Table 5 lists the benefits corresponding to system states with distinct performances.

The calculation procedure involved in the proposed approach has five steps.

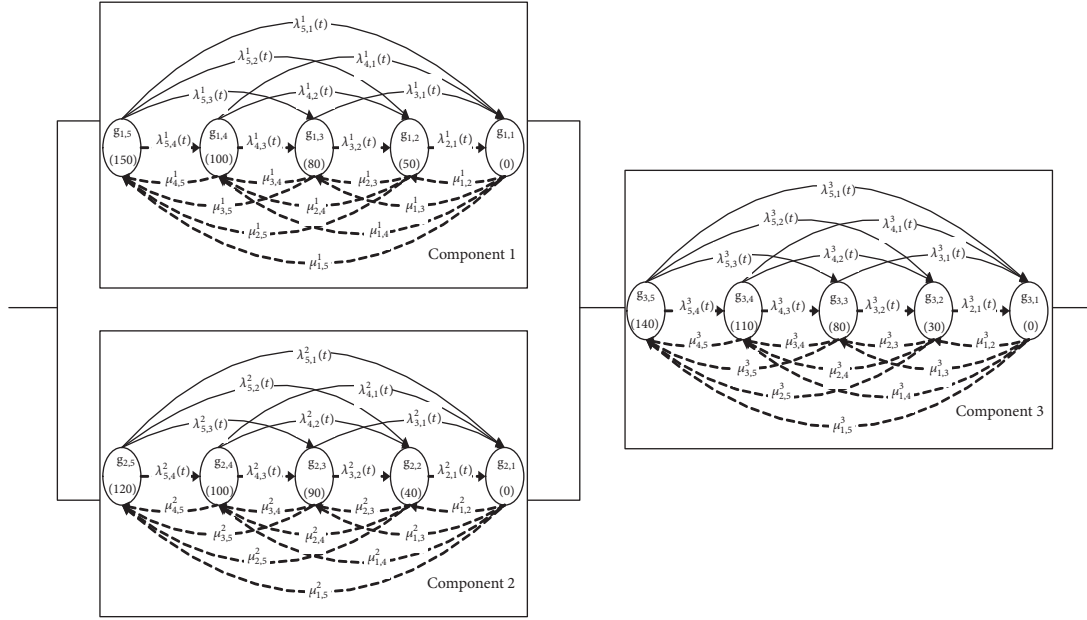


FIGURE 2: MSS configuration with MSC state-space diagrams.

TABLE 1: Failure-rate function of each component between states.

Failure rate	Component		
	1	2	3
$\lambda_{5,4}(t)$	$0.24+0.07 t$	$0.24+0.07 t$	$0.34+0.14 t$
$\lambda_{5,3}(t)$	$0.18+0.04 t$	$0.18+0.04 t$	$0.28+0.08 t$
$\lambda_{5,2}(t)$	$0.14+0.02 t$	$0.14+0.02 t$	$0.24+0.04 t$
$\lambda_{5,1}(t)$	$0.12+0.01 t$	$0.12+0.01 t$	$0.22+0.02 t$
$\lambda_{4,3}(t)$	$0.26+0.08 t$	$0.26+0.08 t$	$0.36+0.16 t$
$\lambda_{4,2}(t)$	$0.20+0.05 t$	$0.20+0.05 t$	$0.30+0.10 t$
$\lambda_{4,1}(t)$	$0.16+0.03 t$	$0.16+0.03 t$	$0.26+0.06 t$
$\lambda_{3,2}(t)$	$0.28+0.09 t$	$0.28+0.09 t$	$0.38+0.18 t$
$\lambda_{3,1}(t)$	$0.22+0.06 t$	$0.22+0.06 t$	$0.32+0.12 t$
$\lambda_{2,1}(t)$	$0.30+0.10 t$	$0.30+0.10 t$	$0.40+0.20 t$

Note:  $\lambda_{i,j}(t)$  is the failure rate at time  $t$  (hrs) of each component from state  $i$  to state  $j$ .

Step 1. Generate the possible states of the MSSs.

The proposed approach initially combines the multistate components constituting the system to form an MSS. For the simulated case, in total, 125 possible states are determined for this system, configuring three components each with five distinctive states with different performances.

Step 2. Obtain the reduced MSS.

Uniting the systems states with an identical performance from step 1 can obtain the reduced MSS. This process can significantly reduce the subsequent calculation complex without loss of system performance information. Accordingly, a total of ten distinctive performance states for this system are determined; the state-transition diagram of this reduced MSS is also constructed. Figure 3 displays the corresponding diagram.

Step 3. Determine the total maintenance cost of the system.

According to the state-transition diagrams for components 1–3 shown in Figure 2, the NHCTMMs and NHCTMRMs of three components are established, respectively. The reward matrix of NHCTMRMs is determined from Table 5. The bound approximation approach [9] then solves the nonlinear simultaneous differential equations related to the established NHCTMMs and NHCTMRMs. Solving NHCTMMs obtains instantaneous state probability distributions of three components, whereas solving NHCTMRMs obtains the total maintenance cost for five states regarding three components. The expected total maintenance costs for these three components are accordingly calculated. Summing up the total maintenance cost of three components derives the total maintenance cost for this system.

Step 4. Determine the MSS benefit.

Initially, the NHCTMMs and NHCTMRMs related to the reduced MSS are established, respectively, on the basis of the state-transition diagrams shown in Figure 3. The reward matrix of NHCTMRMs is determined from the benefit parameters in Table 5. The bound approximation approach [9] again solved the established NHCTMMs and NHCTMRMs; solving NHCTMMs obtains instantaneous probability distributions of ten states for reduced MSS. By using the obtained probability distributions, the expected total system benefit for this system is obtained after complete calculations of the NHCTMRMs.

Step 5. Determine the optimal time to replace the system.

First, using (19), the LREB values over the time horizon can be determined given that specific time can be obtained. Then the optimal time to replace the system is therefore determined by maximizing the LREB value. This study uses

TABLE 2: Repair rate of each component between states (per hour).

Component	Repair rate									
	$\mu_{1,5}$	$\mu_{1,4}$	$\mu_{2,5}$	$\mu_{1,3}$	$\mu_{2,4}$	$\mu_{3,5}$	$\mu_{1,2}$	$\mu_{2,3}$	$\mu_{3,4}$	$\mu_{4,5}$
1	0.125	0.320	0.335	0.410	0.425	0.440	0.455	0.470	0.485	0.500
2	0.080	0.245	0.260	0.275	0.290	0.305	0.350	0.365	0.380	0.395
3	0.065	0.095	0.110	0.140	0.155	0.170	0.185	0.200	0.215	0.230

Note:  $\mu_{j,i}$  is the repair rate of each component from state  $j$  to state  $i$ .

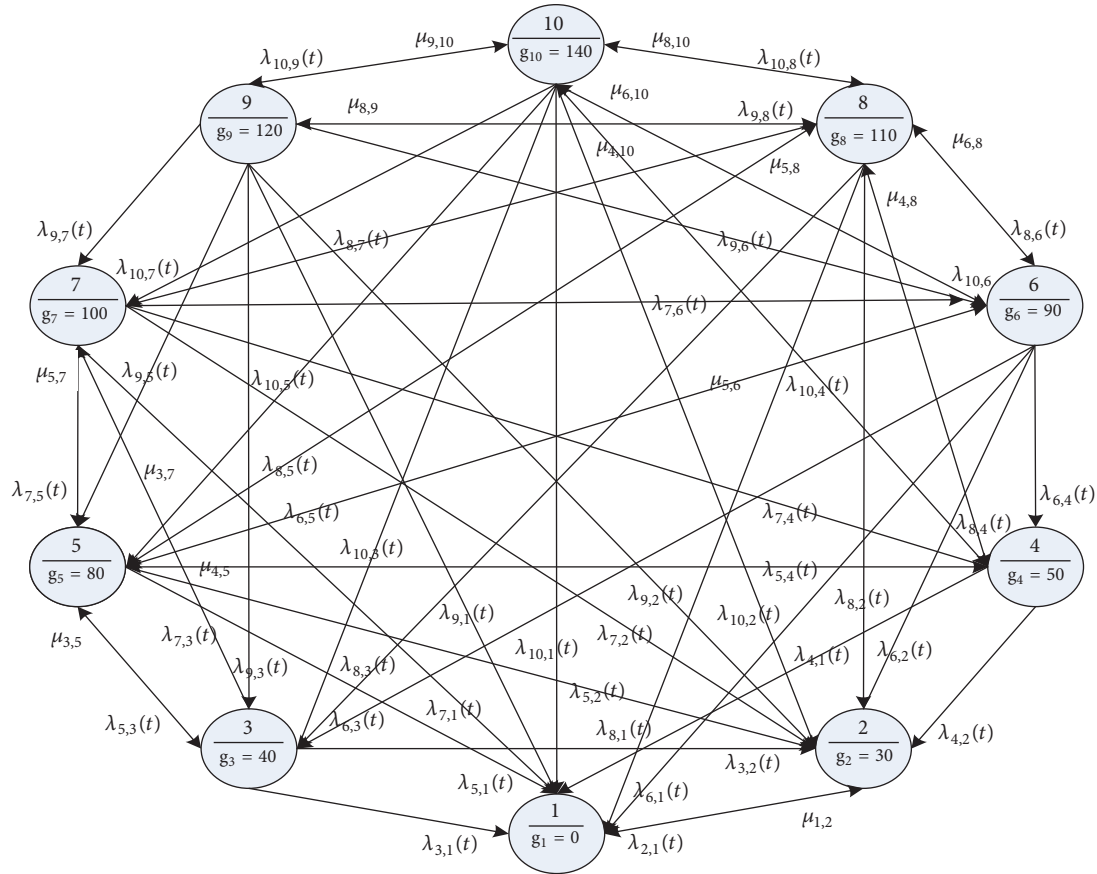


FIGURE 3: State-transition diagram of reduced MSS.

TABLE 3: Cost parameters of maintenance activities.

Maintenance activities	Cost		
	Component 1	Component 2	Component 3
Minor service	54	72	120
Major service	72	96	160
Minor repair	90	120	200
Major repair	180	240	400

TABLE 4: Replacement parameters.

$C_r$ (\$/day)	$t_{rep}$ (day)	$C_{rep}$ (\$)
50	2	200

TABLE 5: MSS performance and benefits.

State	10	9	8	7	6	5	4	3	2	1
Performance	140	120	110	100	90	80	50	40	30	0
Benefit (\$)	1000	800	700	600	500	400	300	200	100	0

MATLAB programs to execute the mathematical calculations involved in the proposed approach.

According to the previously mentioned parameter settings, this study mimics two PM policies to illustrate the ramifications of the proposed approach. The first PM policy

is derived from Huang and Wang [11]. Figures 4–6 show the state-transition diagrams for the three components. Apparently, minor services are implemented in component 1 when this PM policy reaches states 4 and 1; minor repair

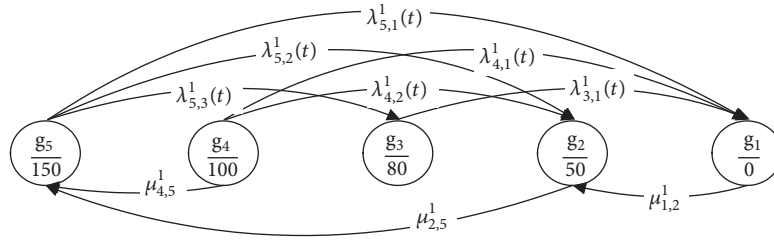


FIGURE 4: State-transition diagram of component 1 with PM policy 1.

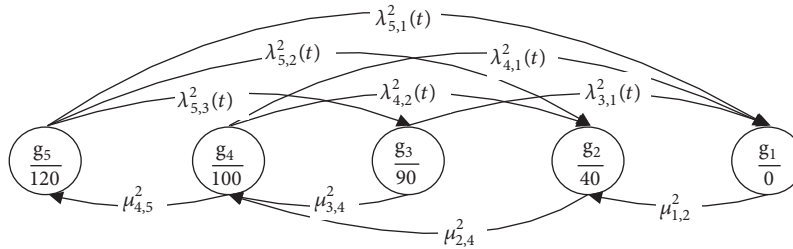


FIGURE 5: State-transition diagram of component 2 with PM policy 1.

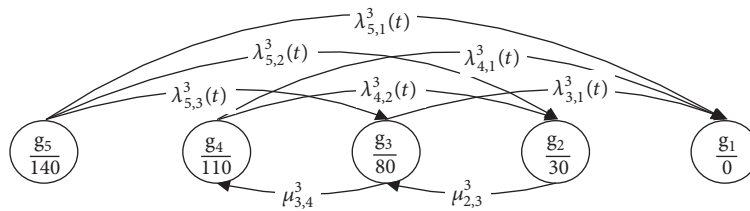


FIGURE 6: State-transition diagram of component 3 with PM policy 1.

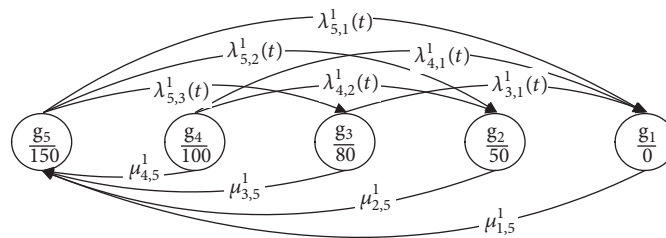


FIGURE 7: State-transition diagram of component 1 with PM policy 2.

is implemented when this policy reaches state 2. However, no maintenance activity is implemented in state 3. In component 2, minor services are undertaken in states 4, 3, and 1; major service is implemented when the PM policy reaches state 2. For component 3, no maintenance activity is performed until states 3 and 2 are reached, at which points minor services are implemented. Figures 7–9 show the state-transition diagrams of the three components for the second PM policy. This PM policy involves restoring the system to the best state whenever a component falls into a degradation state.

Figure 10 shows a trend diagram of the LREB values with time at the continuous time horizon for PM policy 1 and PM policy 2. The time interval for calculation of LREB values is 1 day, which is obtained by dividing the time of 1000 days into

1000 time intervals. Obviously, for policy 1, at the onset of this system's operation, the LREB values increase with time until the 818th day, reaching a maximum average LREB value of 36,046 with lower bound and upper bound 35,501 and 36,590, respectively, and then falling with time dramatically. The gap between lower bound and upper bound of LREB dwindles as the number of intervals  $N$  increases. In this case, the lower bound and upper bound of LREB for the 818th day are 32,724 and 39,368 with  $N=100$ , revealing the difference of 16.88%, while given  $N=1000$ , the difference considerably reduces to 2.88% which is rather small and can be negligible. We can see a similar trend for PM policy 2, which takes until the 635th day to reach its maximum average LREB value of 34,933 with lower bound and upper bound being 34,485 and 35,380, given

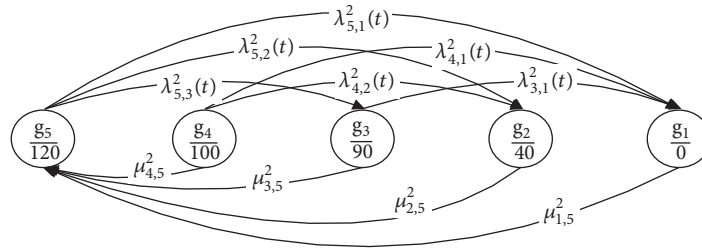


FIGURE 8: State-transition diagram of component 2 with PM policy 2.

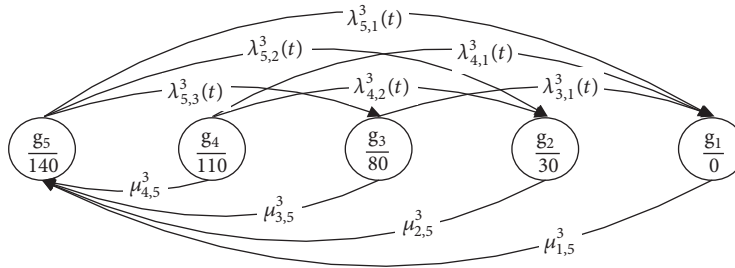


FIGURE 9: State-transition diagram of component 3 with PM policy 2.

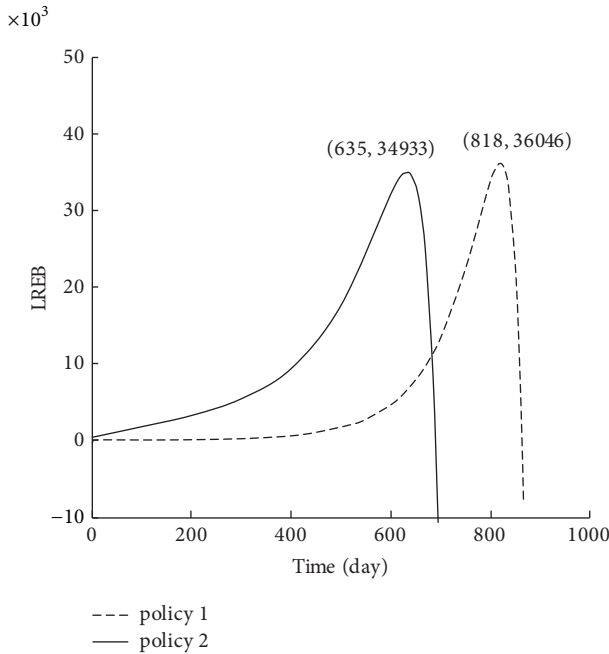


FIGURE 10: LREB trend diagrams through lifetime with two PM policies.

$N=1000$ , respectively. Certainly, Figure 10 reveals that the best time to replace this system is the 818th day and the 635th day for PM policy 1 and PM policy 2, respectively. Both trend diagrams show that more frequent maintenance is necessary for the system to satisfy the performance requirements as the system ages and induces a large maintenance cost. For comparison, PM policy 1 obtains a higher LREB value at a

longer replacement time than does PM policy 2. The main reason is that PM policy 1, derived from Huang and Wang [11], is the result of an optimizing procedure, whereas PM policy 2 mainly characterizes implementing the best maintenance alternative that restores the system to the best state after an MSC falls into any degradation state. From the viewpoint of the PM establishment, PM policy 1 outperforms PM policy 2 in maintenance costs and benefits; excessive maintenance may not be necessary for economic consideration. Certainly, the superiority of the PM policy directly affects the results of the proposed time-replacement policy.

To verify the proposed approach further, a sensitivity analysis with multiple increases in the failure rates for component 3 was performed by a given PM policy 1. Figure 11 shows the corresponding LREB trend diagrams. As expected, the time to replace the MSS decreases with the multiple increases in the failure rates. Furthermore, in contrast, we increase the repair rates multiple times for component 3 given PM policy 1. Figure 12 shows the corresponding trend diagrams. Noticeably, the system requires conducting this MSS replacement a short time after starting the operation with multiple additions of repair rates. We select component 3 to conduct sensitivity analysis because of its importance, being connected in series in the MSS. Additionally, a sensitivity analysis with varied system demands was performed. Table 6 summarizes the ramifications of this analysis. For PM policy 1, the optimal replacement time remains the same at the 818<sup>th</sup> day for all demands, but the corresponding LREB values decrease when demand for system performance increases. For PM policy 2, the result of the sensitivity analysis is similar to PM policy 1: the optimal replacement time is the same at the 632<sup>nd</sup> day, except for demand 100. The desktop computing and executing the proposed approach involves operation

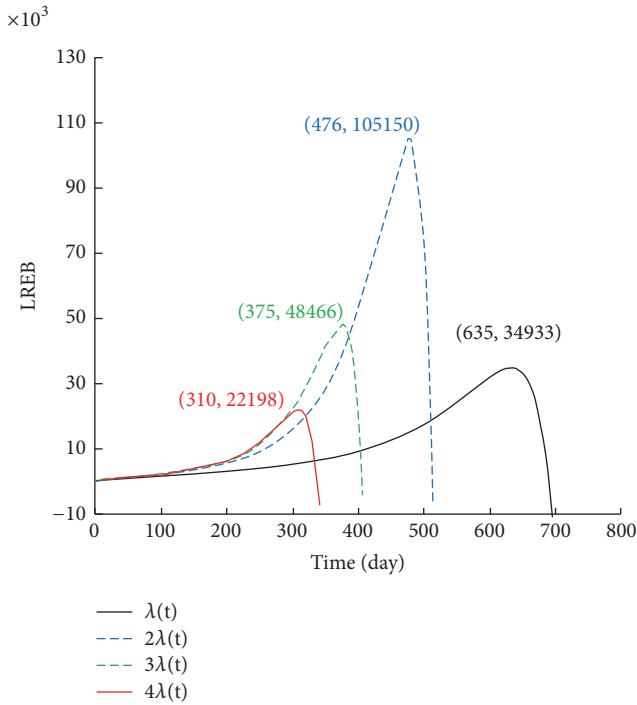


FIGURE 11: LREB trend diagrams with multiple increases in failure rates for component 3 given PM policy 1.

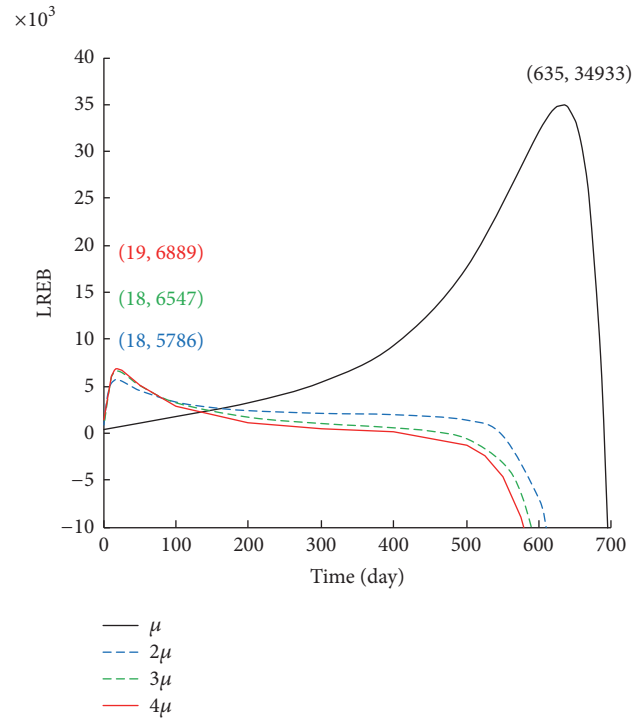


FIGURE 12: LREB trend diagrams with multiple increases in repair rates for component 3 given PM policy 1.

TABLE 6: Optimal replacement time T and LREB versus demand w.

PM policy	Demand w	T (days)	LREB (\$/day)
1	100	818	36,046
	110	818	35,913
	120	818	35,824
	140	818	35,795
2	100	635	34,933
	110	632	34,678
	120	632	34,490
	140	632	34,283

system of Windows 7 (64 bits), Intel i5 CPU of 2.3 GHz, and 8 GB RAM with R2014a version of MATLAB coded. The time is between 600 and 900 seconds.

### 6. Conclusions and Discussions

This study aims at the PM model from the component perspective for the MSS with aging MSCs, in which the maintenance alternatives are implemented when the MSCs fall into degradation states, to propose a time-replacement policy. A time-dependent LREB index of system performance was developed on the basis of the continuous time Markov theory. By maximizing the LREB values throughout the system’s lifetime, we determined the optimal time to replace this type of MSS economically. The proposed approach provides further insight into the relationship between PM policy setting and long-term system benefits; it also verifies a time-replacement policy. For future study, the ramifications of the

current study can be extended to situations that consider the repair difficulties as MSCs age. Namely, the repair rate is a decreasing function of time. Using this method, the analyzed PM models more adequately fulfill the practical requirements. However, the mathematical calculation involved is a difficult challenge in striving to obtain precise results.

### Data Availability

The data used to support the findings of this study are included within the article.

### Conflicts of Interest

The authors declare that they have no conflicts of interest.

### Acknowledgments

This work was supported by the Ministry of Science and Technology of Taiwan (NSC 104-2221-E-606-004 and 107-2221-E-012-001-MY2).

### References

- [1] R. Pascual and J. H. Ortega, “Optimal replacement and overhaul decisions with imperfect maintenance and warranty contracts,” *Reliability Engineering & System Safety*, vol. 91, no. 2, pp. 241–248, 2006.
- [2] R. I. Zequeira and C. Bérenguer, “Periodic imperfect preventive maintenance with two categories of competing failure modes,” *Reliability Engineering & System Safety*, vol. 91, pp. 460–468, 2006.

- [3] C. H. Wang and C. H. Huang, "An optimal replacement policy for systems with multi-state aging components," in *Proceedings of the 21st International Society of Science and Applied Technologies (ISSAT) International Conference on Reliability & Quality in Design*, p. 6, Philadelphia, Pa, USA, 6–8 August 2015.
- [4] A. Fitzpatrick, "Power drive automakers are on the road to smarter cars," *TIME*, 2015.
- [5] R. A. Howard, *Dynamic Programming and Markov Processes*, MIT Press, Cambridge, Mass, USA, 1960.
- [6] H. Mine and S. Osaki, *Markovian Decision Processes*, Elsevier, New York, NY, USA, 1970.
- [7] Y. Liu and K. C. Kapur, "Customer's cumulative experience measures for reliability of non-repairable aging multi-state systems," *Quality, Technology & Quantitative Management*, vol. 4, no. 2, pp. 225–234, 2007.
- [8] Y. Liu and K. C. Kapur, "New model and measurement for reliability of multi-state systems," in *Handbook of Performability Engineering*, Springer, London, UK, 2008.
- [9] Y. Ding, A. Lisnianski, I. Frenkel, and L. Khvatskin, "Optimal corrective maintenance contract planning for aging multi-state system," *Applied Stochastic Models in Business and Industry*, vol. 25, no. 5, pp. 612–631, 2009.
- [10] A. Lisnianski, I. Frenkel, L. Khvatskin, and Y. Ding, "Maintenance contract assessment for aging systems," *Quality and Reliability Engineering International*, vol. 24, no. 5, pp. 519–531, 2008.
- [11] C.-H. Huang and C.-H. Wang, "Optimization of preventive maintenance for a multi-state degraded system by monitoring component performance," *Journal of Intelligent Manufacturing*, vol. 27, no. 6, pp. 1151–1170, 2016.
- [12] Y. L. Zhang and G. J. Wang, "An extended replacement policy for a deteriorating system with multi-failure modes," *Applied Mathematics and Computation*, vol. 218, no. 5, pp. 1820–1830, 2011.
- [13] Y. L. Zhang and G. J. Wang, "An optimal replacement policy for a multistate degenerative simple system," *Applied Mathematical Modelling*, vol. 34, no. 12, pp. 4138–4150, 2010.
- [14] Y. Liu and H.-Z. Huang, "Optimal replacement policy for multi-state system under imperfect maintenance," *IEEE Transactions on Reliability*, vol. 59, no. 3, pp. 483–495, 2010.
- [15] H. Wang and H. Pham, "A quasi renewal process and its applications in imperfect maintenance," *International Journal of Systems Science*, vol. 27, no. 10, pp. 1055–1062, 1996.
- [16] G. J. Wang and Y. L. Zhang, "Optimal repair-replacement policies for a system with two types of failures," *European Journal of Operational Research*, vol. 226, no. 3, pp. 500–506, 2013.
- [17] C.-C. Chang, S.-H. Sheu, and Y.-L. Chen, "Optimal replacement model with age-dependent failure type based on a cumulative repair-cost limit policy," *Applied Mathematical Modelling*, vol. 37, no. 1-2, pp. 308–317, 2013.
- [18] M. Jain and R. Gupta, "Optimal replacement policy for a repairable system with multiple vacations and imperfect fault coverage," *Computers & Industrial Engineering*, vol. 66, no. 4, pp. 710–719, 2013.
- [19] Y. Liu and H.-Z. Huang, "Optimal replacement policy for fuzzy multi-state element," *Journal of Multiple-Valued Logic and Soft Computing*, vol. 17, pp. 69–92, 2010.
- [20] Y. L. Zhang, R. C. M. Yam, and M. J. Zuo, "Optimal replacement policy for a multistate repairable system," *Journal of the Operational Research Society*, vol. 53, no. 3, pp. 336–341, 2002.
- [21] C. M. Tan and N. Raghavan, "A framework to practical predictive maintenance modeling for multi-state systems," *Reliability Engineering & System Safety*, vol. 93, no. 8, pp. 1138–1150, 2008.
- [22] F. Camci, "System maintenance scheduling with prognostics information using genetic algorithm," *IEEE Transactions on Reliability*, vol. 58, no. 3, pp. 539–552, 2009.
- [23] I. Ushakov, "A universal generating function," *Soviet Journal of Computer and Systems Engineering*, vol. 24, pp. 37–49, 1986.
- [24] A. Lisnianski and G. Levitin, *Multi-State System Reliability Assessment, Optimization and Applications*, World Scientific, Singapore, 2003.
- [25] A. Lisnianski, "Extended block diagram method for a multi-state system reliability assessment," *Reliability Engineering & System Safety*, vol. 92, no. 12, pp. 1601–1607, 2007.
- [26] A. Lisnianski, I. Frenkel, and Y. Ding, *Multi-State System Reliability Analysis and Optimization for Engineers and Industrial Managers*, Springer, London, UK, 2010.

## Research Article

# Research on Instability Boundaries of Control Force for Trajectory Correction Projectiles

Rupeng Li , Dongguang Li , and Jieru Fan

*Science and Technology on Electromechanically Dynamic Control Laboratory, Beijing Institute of Technology, Beijing 100081, China*

Correspondence should be addressed to Dongguang Li; [lidongguang@bit.edu.cn](mailto:lidongguang@bit.edu.cn)

Received 29 August 2018; Revised 1 February 2019; Accepted 24 February 2019; Published 11 March 2019

Academic Editor: Kauko Leiviskä

Copyright © 2019 Rupeng Li et al. This is an open access article distributed under the Creative Commons Attribution License, which permits unrestricted use, distribution, and reproduction in any medium, provided the original work is properly cited.

The balance of stability and maneuverability is the foundation of the trajectory correction projectile. For the terminal correction projectile without an attitude feedback loop, a larger control force is expected which may cause an instability. This paper proposes a novel method to derive instability boundaries for the control force magnitude. No additional coordinate system is needed in this method. By introducing the concept of angular compensation matrix, the exterior ballistic linearized equations considering control force are established. The necessary prerequisite for a stable flight under control is given by the Routh stability criterion. The instability boundaries for the control force magnitude are derived. The results of example flights are 13.5% more accurate compared with that in relevant research. Numerical simulations demonstrate that if the control force magnitude lies in the unstable scope derived in this paper, the projectile loses its stability. Furthermore, the effects of the projectile pitch, velocity, and roll rate on flight stability during correction are investigated using the proposed instability boundaries.

## 1. Introduction

Trajectory correction projectiles/fuzes can meet the requirement of low collateral damage and higher delivery accuracy in modern warfare. Moreover, existing stockpiles can be retrofitted and upgraded by just replacing a trajectory correction fuze with a low cost [1–3]. So it is no doubt that trajectory correction technologies have received much attention from researchers. Numerous correction models such as impact point prediction [4–7] and model trajectory prediction [8–10] can be found in the literature. For the pursuit of further improvements in accuracy, the guidance law based on target imager feedback is proposed and becomes a tendency in the future [11, 12]. Unlike the scheme mentioned above, this correction strategy can be used only during the terminal phase with a limited time-to-go. Therefore, a larger control force is expected. However, that may cause an instability for the projectile under control. For a successful terminal correction, the balance between the maneuverability and stability for the projectile under control is studied in this paper.

Many efforts related to stability for ballistic flight have been explored in the literature. McCoy, R. L. [13], and

Murphy [14–16] proposed the stability criteria for flight without control. Costello M [17] extended the gyro stability factor and dynamic stability factor to dual-spin projectile by linearization. In the area of flight stability with control, Wernert [18, 19] found that the control force induced by canards exerted an influence on steady angle of attack compared with conventional projectile without control. Cooper G and Fresconi F [20] regarded the projectile with activating canards asymmetric and investigated its flight stability under control. They established dynamic equations in the body reference frame. The research illustrated that flight instability would be caused when the control frequencies of actuator are close to fast epicyclic motion frequencies or slow epicyclic motion frequencies. Murphy [21] derived the stability boundaries for the maximum trim angles induced by control force. D Zhu [22] extended Murphy's work through Hurwitz stability criterion and derived an analytic solutions of stability boundaries.

The corresponding research made a significant contribution in the field of flight stability for controlled projectile. However, they did not reveal the relationship between control force magnitude and flight stability. Unlike missiles, the trajectory correction projectiles are not provided with a

feedback loop for flight attitude. The investigation of force magnitude influence on the stability is more urgent for such projectiles and is beneficial to the design of actuator (such as the canard deflection or reference area). Lloyd K.H [23] made some efforts in this aspect. By proposing the non-spinning coordinate originally, the research investigated the influence of force magnitude on the flight stability and derived the analytic damping rate expression of the projectile under control by an analogy to non-controlled projectile. However, such an analogy can only get a rough scope of the control force for flight stability.

This paper continues to bridge the gap in the area of controlled projectile stability and extend Lloyd K.H's research without utilizing the non-spinning coordinate. Exterior ballistic differential equations for controlled projectile are expressed in fixed-plane coordinate and rewritten as the form of coefficient matrix. The items of control force are retained in these equations by a novel angular compensation matrix. Routh stability criterion is applied to the coefficient matrix. The magnitude boundaries of the control force that result in flight instability are derived and analyzed.

In Section 2, dynamical equations for projectile under control are established by the proposed compensation matrix. In Section 3, the instability boundaries of the control force are presented on the basis of the Routh stability criterion. In Section 4, an example controlled flight is calculated and 6 DOF numerical simulations are implemented. The results are favorable. The influence of flight parameters on the stability is analyzed by the instability boundaries.

## 2. Projectile Flight Dynamic Model

This section introduces the concept of the trajectory correction projectile, establishes the equations of motion in fixed plane coordinate, and demonstrates the invalidity of the classical linearization in stability research. The cause is analyzed in deep and a novel linearized method based on compensation matrix that is proposed.

*2.1. Concept of the Trajectory Correction Projectile.* The trajectory correction projectile discussed in this paper is used to improve the operational capability of the artillery when attacking the ground targets. The correction actuator is integrated into the projectile fuze in our design. Its appearance is shown in Figure 1. The fuze consists of two parts defined as the forward part and aft part, respectively. The aft part is shown in green. It is fixedly connected with the projectile body by threaded connection. The projectile body is not illustrated here to highlight the fuze appearance. The forward part is shown in purple. It can rotate relative to the aft part of the fuze and the projectile body. The white nose represents the imager and is used for target detection. The blue part is the canard of a waffle style, in which each inner grid has a fixed deflection. It is strapdown with the forward fuze. When the projectile is in its ballistic flight, the canard is attached to the fuze surface. Once the correction is needed, the canard should be unfolded. Because of the oncoming flow and the deflection angle, the canard can produce an aerodynamic

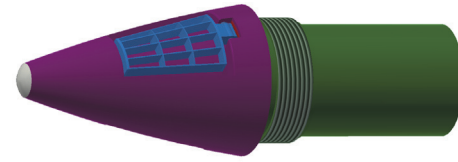


FIGURE 1: Appearance of the projectile fuze.

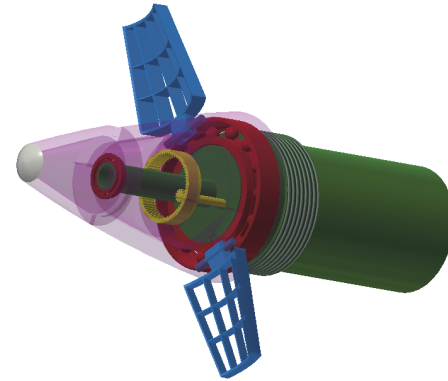


FIGURE 2: Internal structure of the projectile fuze.

force which is used for projectile control. The direction of this control force is determined by roll angle of the forward fuze. Figure 2 illustrates the internal structure of the fuze. The red part represents a pair of bearings, which are used in providing a prerequisite for the relative rotation between the forward and aft part. The yellow part represents the motor shaft and gears, which are used to transfer the motor torque for the rotation.

When the projectile enters its descent trajectory, the detector starts to seek the target. The deviation between the target and the optical axis of detector is presented in detector imaging plane. The target orientation can be directly used to determine the roll angle of the forward fuze and as the input of the control system. The unfolding time of the canard depends on the magnitude of the deviation and the trajectory response under control. It can be seen that the correction actuator can complete the two-dimensional correction by a single motor.

In general, conventional projectiles for artillery can be equipped with the proposed fuze and subsequently obtain a correction capability. Such trajectory correction projectiles work during the terminal trajectory because of the limited detection distance. So the left flight time for correction is constrained. Therefore, a sufficient control force is more necessary here for an effective correction. That is why the canard has a waffle configuration for more frontal area. For stability that is no less important than maneuverability for such projectiles, the balance between them is investigated in this paper.

*2.2. Flight Model of the Projectile.* The projectile flight model is expressed by differential equations in fixed plane coordinate which is defined as follows: the origin of coordinate

system is located at the projectile centroid.  $X$  axis is aligned with the longitudinal axis of projectile, positive direction points to the projectile nose.  $Y$  axis is perpendicular to the longitudinal axis and lies in horizontal plane, positive direction points to right.  $Z$  axis is perpendicular to  $XY$  plane, positive direction points down. Projectile translational motion is written as follows:

$$\begin{aligned} \begin{Bmatrix} \dot{u} \\ \dot{v} \\ \dot{w} \end{Bmatrix} &= \begin{Bmatrix} \frac{F_x}{m} \\ \frac{F_y}{m} \\ \frac{F_z}{m} \end{Bmatrix} + g \begin{Bmatrix} -\sin \theta \\ 0 \\ \cos \theta \end{Bmatrix} + \begin{Bmatrix} \frac{F_{xc}}{m} \\ \frac{F_{yc}}{m} \\ \frac{F_{zc}}{m} \end{Bmatrix} \\ &+ \begin{Bmatrix} 0 & r & -q \\ -r & 0 & -r \tan \theta \\ q & r \tan \theta & 0 \end{Bmatrix} \begin{Bmatrix} u \\ v \\ w \end{Bmatrix} \end{aligned} \quad (1)$$

Projectile angular motion is written as (2).  $F_{yc}$  and  $F_{zc}$  represent the horizontal and vertical components of the control force.  $M_C$  and  $N_C$  represent the corresponding control moments. While the canard is producing the control force, a drag force is also generated due to the canard deflection [18]. The induced drag force is denoted as  $F_{xc}$ . Generally, a small deflection angle is considered for trajectory correction projectiles with canard. In this situation, the induced drag force is far less than the induced control force. So it is always ignored. For the drag force induced by canard that is along the longitudinal axis and through projectile centroid, the corresponding moment is zero.

When the projectile is in a ballistic trajectory, the terms of control force and control moment are set to zero. And when the projectile needs a trajectory correction, these terms would have specific values according to operational requirements.

$$\begin{aligned} \begin{Bmatrix} \dot{p} \\ \dot{q} \\ \dot{r} \end{Bmatrix} &= [I^{-1}] \left\{ \begin{Bmatrix} L \\ M \\ N \end{Bmatrix} + \begin{Bmatrix} 0 \\ M_c \\ N_c \end{Bmatrix} \right\} \\ &- \begin{bmatrix} 0 & -r & q \\ r & 0 & r \tan \theta \\ -q & -r \tan \theta & 0 \end{bmatrix} [I] \begin{Bmatrix} p \\ q \\ r \end{Bmatrix} \end{aligned} \quad (2)$$

Angle of attack  $\alpha$  and sideslip  $\beta$  are introduced and treated as small quantities. The expressions are shown as follows:

$$\alpha = \arctan^{-1} \left( \frac{w}{V} \right) \approx \frac{w}{V} \quad (3)$$

$$\beta = \arctan^{-1} \left( \frac{u}{V} \right) \approx \frac{u}{V} \quad (4)$$

Combining the latter two formulas in (1) and (2) with (3) and (4), a new equation set is completed. It is shown as follows:

$$\begin{aligned} \dot{\beta} &= \frac{F_y}{mv} + \frac{F_{yc}}{mv} - r - r\dot{\alpha} \tan \theta \\ \dot{\alpha} &= \frac{F_z}{mv} + \frac{F_{zc}}{mv} + \frac{g}{v} \cos \theta + q + r\dot{\beta} \tan \theta \\ \dot{q} &= \frac{M + M_c}{I_Y} - pr \frac{I_X}{I_Y} - r^2 \tan \theta \\ \dot{r} &= \frac{N + N_c}{I_Y} + pq \frac{I_X}{I_Y} + qr \tan \theta \end{aligned} \quad (5)$$

The projectile body forces in (1) are composed of drag, lift, and Magnus force (always treated as small quantity and ignored). The projectile body moments in (2) are composed of static moment, pitch/yaw damping moment, and Magnus moment. The specific expressions for projectile body forces and moments are shown as follows:

$$\begin{aligned} F_y &= -\frac{1}{2} \rho S V^2 C_{l\beta} \beta - \frac{1}{2} \rho S V^2 C_{D\beta} \beta - \frac{1}{2} \rho S V^2 C_{yp\alpha} \frac{pl}{V} \alpha \\ F_z &= -\frac{1}{2} \rho S V^2 C_{l\alpha} \alpha - \frac{1}{2} \rho S V^2 C_{D\alpha} \alpha + \frac{1}{2} \rho S V^2 C_{yp\alpha} \frac{pl}{V} \alpha \\ M &= \frac{1}{2} \rho S I V^2 C_{M\alpha} \alpha + \frac{1}{2} \rho S I V^2 C_{Mpq} \frac{pl}{V} \beta \\ &+ \frac{1}{2} \rho S I V^2 C_{Mq} \frac{l}{V} q \\ N &= -\frac{1}{2} \rho S I V^2 C_{M\alpha} \beta + \frac{1}{2} \rho S I V^2 C_{Mpq} \frac{pl}{V} \alpha \\ &+ \frac{1}{2} \rho S I V^2 C_{Mq} \frac{l}{V} r \end{aligned} \quad (6)$$

By comparing with the total projectile velocity  $V$  and the projectile roll rate  $p$ , the magnitude of projectile yaw rate  $r$  and pitch tangent  $\tan \theta$  are several orders inferior. The product of  $r$  and  $\tan \theta$  is a smaller value in (5). Therefore, the neglect of  $r \tan \theta$  is a reasonable simplification. In addition, the total velocity and the roll rate change slowly compared with other parameters and are regarded as constant here. With the simplifications above, the four equations of (5) are largely linearized and uncoupled. Such simplifications and linearized methods are frequently used and helpful in exterior ballistics research. More details can be found in [17, 24].

Based on the linearization, we rewrote (5) in the following form:  $\dot{X} = KX + Q$ , in which the specific expression is shown as (7).  $K$  is the coefficient matrix, which is used to depict the projectile state. Because of the linearization, (7) becomes a set of differential equations with constant coefficients. And each unit in matrix  $K$  is invariable, which makes sure that the coefficients of corresponding eigenvalue equation are

constant and provide a prerequisite for the future analysis of stability.

$$\begin{bmatrix} \dot{\beta} \\ \dot{\alpha} \\ \dot{q} \\ \dot{r} \end{bmatrix} = \begin{bmatrix} A & B & 0 & -1 \\ -B & A & 1 & 0 \\ D & C & E & -p\frac{I_X}{I_Y} \\ -C & D & p\frac{I_X}{I_Y} & E \end{bmatrix} \begin{bmatrix} \beta \\ \alpha \\ q \\ r \end{bmatrix} + \begin{bmatrix} \frac{F_{yc}}{mV} \\ mg \cos \theta + \frac{F_{zc}}{mV} \\ \frac{M_C}{I_Y} \\ \frac{N_C}{I_X} \end{bmatrix} \quad (7)$$

where

$$\begin{aligned} A &= -\frac{\rho S V C_{l\alpha}}{2m} - \frac{\rho S V C_D}{2m} \\ B &= -\frac{\rho S C_{yp\alpha} p l}{2m} \\ C &= \frac{\rho S l V^2 C_{M\alpha}}{2I_Y} \\ D &= \frac{\rho S l^2 V C_{MP\alpha} p}{2I_Y} \\ E &= \frac{\rho S l^2 V C_{Mq}}{2I_Y} \end{aligned} \quad (8)$$

It is remarkable that terms related to control force in (7) consist in matrix Q and its mathematical implications mean that the control force will cause a steady-state trim angle. This is in line with Wernert's research [18]. However, these terms would not appear in the coefficient matrix K. The phenomenon is caused by the linearization according to the definition of the fixed plane coordinate. The fixed plane coordinate should have a roll rate  $-r \tan \theta$  relative to the inertial coordinate and it is the prerequisite to ensure that the  $y$  axis is located in the horizontal plane all the time. For ballistic trajectory without control force, the neglect of  $r \tan \theta$  is a good assumption for linearization. But when control force is considered, the situation is different. Because once the target orientation relative to the projectile is determined, the control force direction would not vary. However, ignoring the item  $-r \tan \theta$  forces the fixed plane coordinate rotate around its longitudinal axis at the roll rate  $r \tan \theta$ . This implies the direction of the control force and is changing along with the fixed plane coordinate constantly. So a contradiction is caused. When it is reflected by the coefficient matrix, there would be no difference in K between the ballistic and controlled trajectory, and the control force would not appear in matrix K. Therefore, for further study of controlled

trajectory, the effect of the neglect of  $-r \tan \theta$  should be compensated before linearization.

**2.3. Compensation Matrix for Control Force.** Based on the analysis in Section 2.1, the paper introduces an angular compensation matrix for control force and gravity to solve the problem above. We define the control force roll angle induced by linearization as  $\Phi$  and express it as (9). The expression for roll angle induced by gravity has the same expression as follows:

$$\dot{\Phi} = r \tan \theta \quad (9)$$

The compensation matrix for control force and gravity is written as follows:

$$T_m = \begin{bmatrix} 1 & 0 & 0 \\ 0 & \cos \Phi & \sin \Phi \\ 0 & -\sin \Phi & \cos \Phi \end{bmatrix} \quad (10)$$

With the compensation matrix, the projectile translational motion is rewritten as follows:

$$\begin{aligned} \begin{Bmatrix} \dot{u} \\ \dot{v} \\ \dot{w} \end{Bmatrix} &= \begin{Bmatrix} \frac{F_x}{m} \\ \frac{F_y}{m} \\ \frac{F_z}{m} \end{Bmatrix} + g \begin{bmatrix} 1 & 0 & 0 \\ 0 & \cos \Phi & \sin \Phi \\ 0 & -\sin \Phi & \cos \Phi \end{bmatrix} \begin{bmatrix} -\sin \theta \\ 0 \\ \cos \theta \end{bmatrix} \\ &+ \begin{bmatrix} 1 & 0 & 0 \\ 0 & \cos \Phi & \sin \Phi \\ 0 & -\sin \Phi & \cos \Phi \end{bmatrix} \begin{bmatrix} \frac{F_{xc}}{m} \\ \frac{F_{yc}}{m} \\ \frac{F_{zc}}{m} \end{bmatrix} \\ &+ \begin{bmatrix} 0 & r & -q \\ -r & 0 & -r \tan \theta \\ q & r \tan \theta & 0 \end{bmatrix} \begin{bmatrix} u \\ v \\ w \end{bmatrix} \end{aligned} \quad (11)$$

The projectile angular motion is rewritten as follows:

$$\begin{aligned} \begin{Bmatrix} \dot{p} \\ \dot{q} \\ \dot{r} \end{Bmatrix} &= [I^{-1}] \left\{ \begin{Bmatrix} L \\ M \\ N \end{Bmatrix} + \begin{bmatrix} 1 & 0 & 0 \\ 0 & \cos \Phi & \sin \Phi \\ 0 & -\sin \Phi & \cos \Phi \end{bmatrix} \begin{bmatrix} L_c \\ M_c \\ N_c \end{bmatrix} \right. \\ &\left. - \begin{bmatrix} 0 & -r & q \\ r & 0 & r \tan \theta \\ -q & -r \tan \theta & 0 \end{bmatrix} [I] \begin{Bmatrix} p \\ q \\ r \end{Bmatrix} \right\} \end{aligned} \quad (12)$$

Then the latter two formulas in (11) and (12) can be linearized with the control force retained after the compensation. The projectile velocity  $V$  and roll rate  $p$  are regarded as constant in a sufficiently short time interval regarding the velocity component  $u$  equal to  $V$ . The pitch angle  $\theta$  is substituted by  $\theta_0 + \theta_d$ .  $\theta_0$  is the initial pitch angle.  $\theta_d$  is a small departure from  $\theta_0$ . It should be noted that this method is

applicable within a few seconds of the selected feature point. Fortunately, the time-to-go for terminal correction is limited to several seconds. The linear ballistic differential equations are eventually expressed as (13)-(16).

$$\dot{\beta} = \frac{F_y}{mV} + \left( \frac{F_{zc}}{mV} + \frac{g}{V} \cos \theta_0 \right) \Phi - r + \frac{F_{yc}}{mV} \quad (13)$$

$$\dot{\alpha} = \frac{F_z}{mV} + \frac{F_{zc}}{mV} + \frac{g}{V} \cos \theta_0 + q - \frac{F_{yc}}{mV} \Phi - \left( \frac{g}{V} \sin \theta_0 \right) \theta_d \quad (14)$$

$$\dot{q} = \frac{M}{I_Y} - pr \frac{I_X}{I_Y} + \frac{M_c}{I_Y} + \frac{N_c}{I_Y} \Phi \quad (15)$$

$$\dot{r} = \frac{N}{I_Y} + pq \frac{I_X}{I_Y} + \frac{N_c}{I_Y} - \frac{M_c}{I_Y} \Phi \quad (16)$$

Combining the four equations above with (9) and supplemental equation (17), the set of equations are completed.

$$\dot{\theta}_d = q \quad (17)$$

### 3. The Instability Boundary for Control Force

The purpose of this section is to derive the boundary for control force that causes an instability and makes some efforts to build the balance between the maneuverability and stability for the projectile under control.

We rewrite the set of equations (13)-(17) as matrix form:  $\dot{X} = KX + Q$ :

$$\begin{bmatrix} \dot{\beta} \\ \dot{\alpha} \\ \dot{q} \\ \dot{r} \\ \dot{\Phi} \\ \dot{\theta}_d \end{bmatrix} = \begin{bmatrix} A & B & 0 & -1 & F & 0 \\ B & A & 1 & 0 & G & H \\ D & C & E & -p \frac{I_X}{I_Y} & R & 0 \\ -C & D & p \frac{I_X}{I_Y} & E & S & 0 \\ 0 & 0 & 0 & \tan \theta_0 & 0 & 0 \\ 0 & 0 & 1 & 0 & 0 & 0 \end{bmatrix} \begin{bmatrix} \beta \\ \alpha \\ q \\ r \\ \Phi \\ \theta_d \end{bmatrix} + \begin{bmatrix} \frac{F_{yc}}{mV} \\ \frac{F_{zc}}{mV} + \frac{g}{V} \cos \theta_0 \\ \frac{M_c}{I_Y} \\ \frac{N_c}{I_Y} \\ \frac{I_X}{0} \\ 0 \end{bmatrix} \quad (18)$$

where the new notations are as follows:

$$\begin{aligned} F &= \frac{F_{zC}}{mV} + \frac{g}{V} \cos \theta_0 \\ G &= -\frac{F_{yC}}{mV} \\ H &= -\frac{g}{V} \sin \theta_0 \\ R &= \frac{N_C}{I_Y} \\ S &= -\frac{M_C}{I_Y} \\ T &= p \frac{I_X}{I_Y} \end{aligned} \quad (19)$$

Terms related to control force are now involved in the coefficient matrix  $K$  with the compensation matrix. The eigenvalue equation for the coefficient matrix in (18) is established as follows:

$$\det(\lambda E - A) = a_6 \lambda^6 + a_5 \lambda^5 + a_4 \lambda^4 + a_3 \lambda^3 + a_2 \lambda^2 + a_1 \lambda + a_0 \quad (20)$$

where  $a_0$ - $a_6$  are consisted of the terms A, B, C, etc. These terms are the combination of physical parameters, state parameters, and aerodynamic coefficients of the projectile. The physical parameters represent the inherent properties of a projectile. So they are constant. State parameters and aerodynamic coefficients could be regarded as constant as well in a short time interval. When a long-duration flight is considered, they should be updated periodically. Each constituent is complex and brings difficulties to calculation and analysis. However, the dominant terms are limited relatively. For simplicity, secondary factors are ignored. The feasibility of this simplification will be verified later. The expressions for  $a_0$ - $a_6$  after simplification are written here directly.

$$\begin{aligned} a_6 &= 1 \\ a_5 &= -2A - 2E \\ a_4 &= T^2 - 2C - S \tan \theta_0 \\ a_3 &= -2AT^2 + 2AC + 2CE + 2DT - RT \tan \theta_0 \\ a_2 &= C^2 + CS \tan \theta_0 - DR \tan \theta_0 + 2ART \tan \theta_0 \\ a_1 &= C^2 H - C^2 F \tan \theta_0 - ACS \tan \theta_0 + CHS \tan \theta_0 \\ a_0 &= -ACHS \tan \theta_0 - C^2 FH \tan \theta_0 \end{aligned} \quad (21)$$

TABLE 1: Initial states and meteorological conditions.

Initial states		Meteorological conditions	
Velocity	250m/s	Ground pressure	1000hPa
Elevation	-43°	Virtual temperature	288.9
Direction	0°	Longitudinal wind	0m/s
Spin-rate	1050rad/s	Lateral wind	0m/s

The Routh matrix corresponding to the eigenvalue equation (20) is established.

$$T_{ROUTH} = \begin{bmatrix} a_6 & a_4 & a_2 & a_0 \\ a_5 & a_3 & a_1 & \\ b_1 = \frac{-1}{a_5}(a_6a_3 - a_5a_4) & b_2 = \frac{-1}{a_5}(a_6a_1 - a_2a_5) & b_3 = a_0 & \\ c_1 = \frac{-1}{b_1}(a_5b_2 - a_3b_1) & c_2 = \frac{-1}{b_1}(a_5b_3 - a_1b_1) & & \\ d_1 = \frac{-1}{c_1}(b_1c_2 - b_2c_1) & d_2 = a_0 & & \\ e_1 = \frac{-1}{d_1}(c_1d_2 - c_2d_1) & & & \\ f_1 = a_0 & & & \end{bmatrix} \quad (22)$$

The necessary prerequisite for a stable flight under control is given according to the Routh stability criterion: The coefficients  $a_0$ - $a_6$  in (20) are positive and the first column elements of the Routh matrix are positive. Furthermore, if the control force magnitude cannot meet (23), the projectile will lose its stability. Then the control force is defined as an unstable force. The set of all unstable forces is called unstable scope. The boundaries of the scope are denoted as the instability boundary. A conclusion is derived evidently that if a control force magnitude belongs to the unstable scope, the flight is definitely unstable.

$$\begin{aligned} a_5 &> 0, \\ a_4 &> 0, \\ a_3 &> 0, \\ a_2 &> 0, \\ a_1 &> 0, \\ a_0 &> 0 \\ b_1 &> 0, \\ c_1 &> 0, \\ d_1 &> 0, \\ e_1 &> 0 \end{aligned} \quad (23)$$

#### 4. Verification and Results

This section demonstrates the feasibility and liability of the theory derived in Section 3. Generally, the flight instability

TABLE 2: Aerodynamic coefficients of the example projectile.

Aerodynamic coefficients	
lift force coefficient	1.7
drag force coefficient	0.13
Magnus force coefficient derivative	-1.5
static moment coefficient derivative	3.8
Magnus moment coefficient derivative	0.2
damping moment coefficient derivative	-8.0

can be clearly shown by numerical simulation. According to the research of Lloyd C.H [23], projectiles under control are the most sensitive to horizontal forces. Therefore, the simulations in this section pay emphasis on the effect of horizontal control force  $F_{yc}$ .

The example projectile mass  $m$  is 15kg, moment of inertia for longitudinal axis  $I_x$  is 0.023kg·m<sup>2</sup>, moment of inertia for projectile transverse axis  $I_y$  is 0.22kg·m<sup>2</sup>, the reference area  $S$  is 0.0087m<sup>2</sup>, and the projectile diameter  $d$  is 0.105m. Initial states and meteorological conditions are shown in Table 1. The aerodynamic coefficients of the example projectile are shown in Table 2

We take the example projectile to calculate the instability boundaries for the flight under control. The result of this unstable scope is  $[-\infty, -35.48] \cup [58.33, +\infty]$ . According to the theory in Section 3, when control force magnitude belongs to the unstable scope ( $F_{yc} \in [-\infty, -35.48] \cup [58.33, +\infty]$ ), the projectile will lose its stability.

Before the verification by simulation, the simplification in Section 3 is recalled. It has been mentioned above that the result is derived from simplified  $a_0$ - $a_6$ . To demonstrate the practicability of this simplification, the instability boundaries are calculated again without any simplification. The result is  $F_{yc} \in [-\infty, -35.63] \cup [58.00, +\infty]$ . It can be seen that the result varies a little compared with that of simplified model.

The projectile angular motion without control force is presented as Figure 3. The angle of attack motion and sideslip motion along with time are presented in Figure 4.

These two figures illustrate that the angular motions for the flight without control force are converging gradually along with time and represent a stable flight.

The projectile angular motion with a -55N force to left is presented as Figure 5. In the same case, the angle of attack motion and sideslip motion along with time are presented in Figure 6.

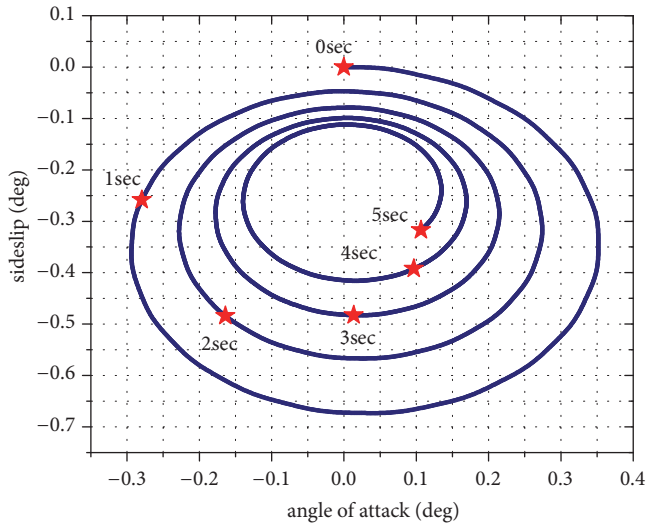


FIGURE 3: Angular motion for the flight without control force.

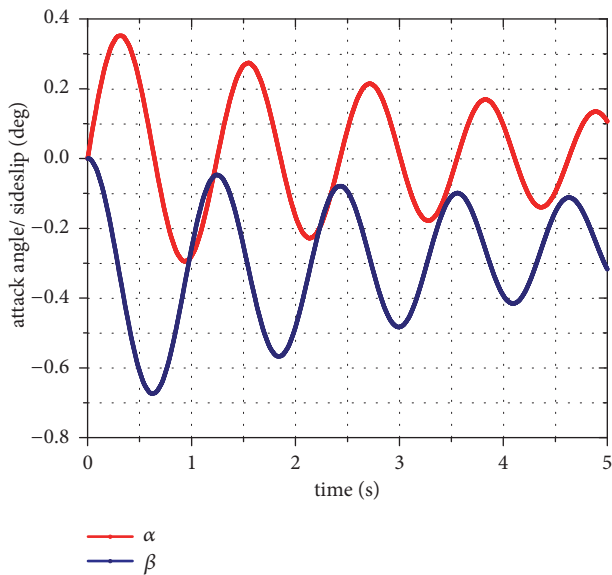


FIGURE 4: Angle of attack and sideslip for the flight without control force.

In Figures 5 and 6, the fast epicyclic motion of the projectile is stable. However, the slow epicyclic motion is diverging along with time obviously. The results have illustrated that the slow epicyclic motion of the projectile is unstable when a -55N control force is exerted to left. The simulation results for  $F_{yc} = -55 \in [-\infty, -35.63] \cup [58.00, +\infty]$  are in conformity to the negative part of the analytic instability boundaries.

Figures 7 and 8 present the numerical simulation results for the flight under an 80N control force. They illustrate that the slow epicyclic motion of the projectile is stable. However, the angle of attack and sideslip are diverging along with time obviously, and the fast epicyclic motion is unstable. For the control force 80N belonging to the unstable scope, the

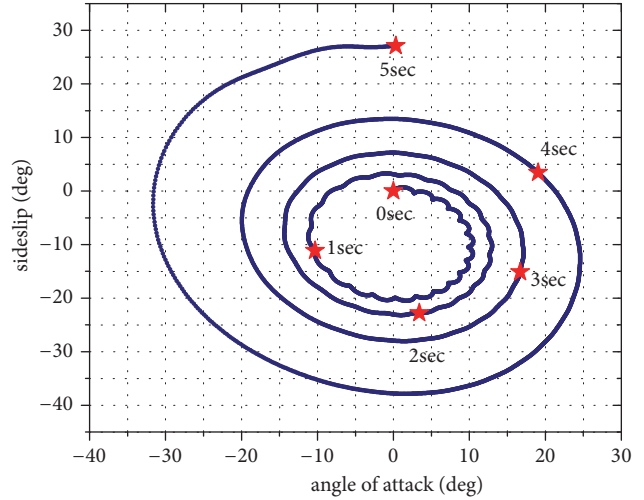


FIGURE 5: Angular motion for the flight with -55N control force.

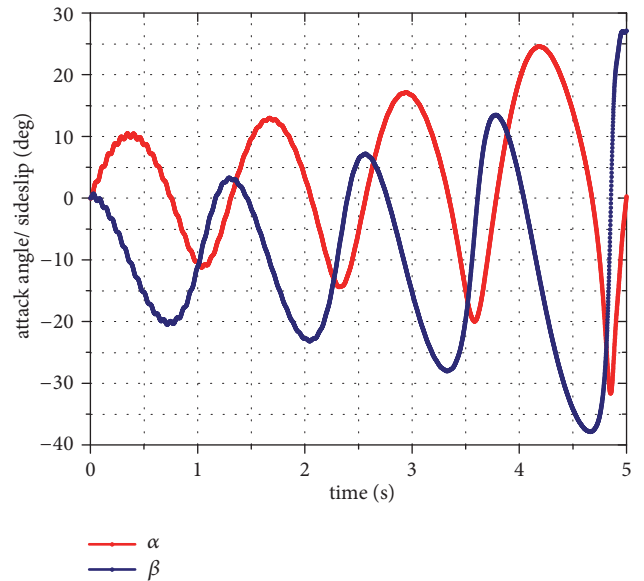


FIGURE 6: Angle of attack and sideslip for the flight with -55N control force.

simulation results demonstrate the validity of the positive part of instability boundaries.

Additionally, the instability boundaries for the flight under control derived in this paper are compared with Lloyd's research. With the same example projectile, initial and meteorological conditions and the instability boundaries under horizontal control force by Lloyd are written as  $F_{yc} \in [-\infty, -44.61] \cup [66.91, +\infty]$ . As is shown in Figure 9, the blue slash represents the scope of horizontal control force that causes an instability derived by Lloyd, and the red slash represents the same scope derived in this paper.

The figure indicates that the instability boundaries in this paper extend the scope by 13.5% compared with Lloyd's research. To further demonstrate the reliability of this

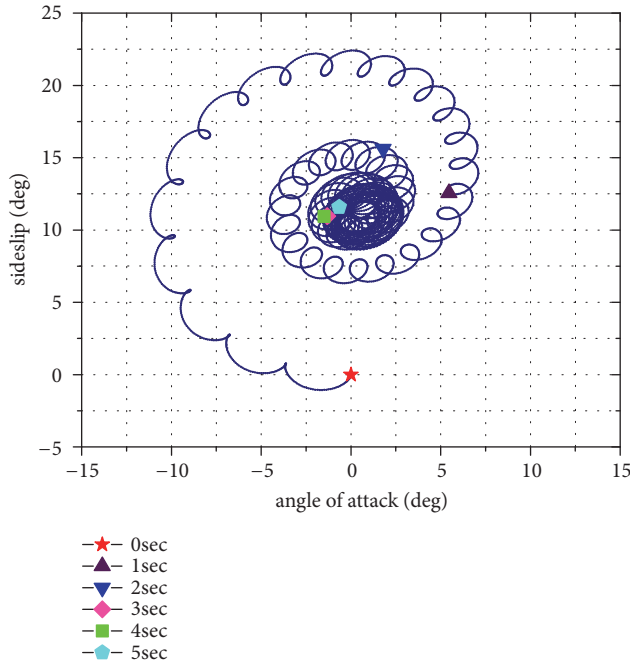


FIGURE 7: Angular motion for the flight with 80N control force.

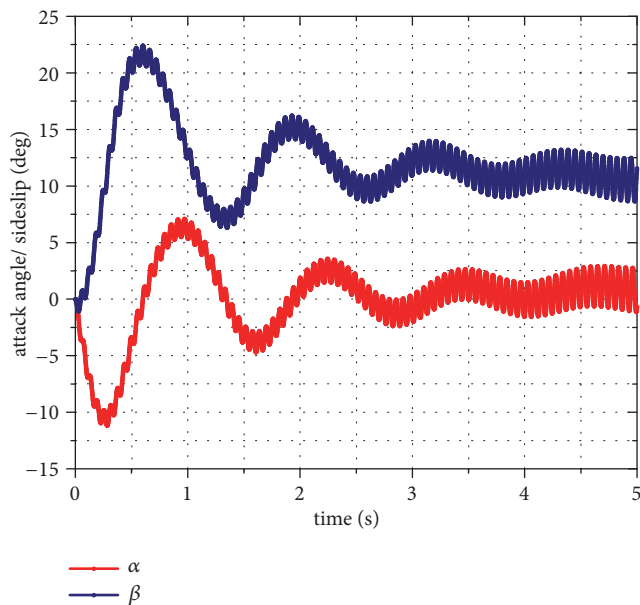


FIGURE 8: Angle of attack and sideslip for the flight with 80N control force.

method, another two simulations are implemented. The control force magnitude is chosen from the extended scope by comparison.

Figures 10 and 11 exhibit the angular motion, angle of attack, and sideslip for the flight with a -40N control force (the value -40 is in the negative extended scope by comparison). The numerical simulation result illustrates clearly that the flight is unstable (specifically, the fast epicyclic motion is stable, while the slow epicyclic motion is unstable).

Similarly, Figures 12 and 13 exhibit the angular motion, angle of attack, and sideslip for the flight with a 60N control force (the value 60 is in the positive extended scope by comparison). The numerical simulation result indicates that the flight is unstable (specifically, the slow epicyclic motion is stable, while the fast epicyclic motion is unstable).

The two simulation results give a further demonstration for the instability boundaries of the flight under control derived in this paper. In addition, it is 13.5% more accurate than Lloyd's research.

## 5. The Effect of Projectile Parameters on Instability Boundaries

The effects of the projectile parameters during flight on stability are analyzed and discussed, respectively, utilizing the instability boundaries when a control force is exerted.

**5.1. The Initial Pitch  $\theta_0$ .** Figure 14 dictates the effect of initial pitch on the instability boundaries. The line of red triangle represents the lower instability boundary variation of the positive control force (denoted as lower boundary for short). The line of blue diamond represents the upper instability boundary variation of the negative control force (denoted as upper boundary for short). As presented in Figure 14, the lower boundary increases progressively as the initial pitch angle decreases in descending flight, while the upper boundary decreases.

The instability boundary variation in this case dictates a decreasing control force unstable scope. That is to say, the increase of the pitch angle in descending flight improves the projectile stability. The reason is that the pitch angle represents the curvature of the trajectory which will induce an aerodynamic trim angle. During the descending flight, the small pitch angle implies a severe trajectory curvature and a large trim angle. Therefore, the flight stability is weakened with the extra aerodynamic drag and lift forces induced by large trim angle.

**5.2. The Projectile Velocity  $V$ .** Figure 15 dictates the effect of projectile velocity on the instability boundaries. The lines of red triangle and blue diamond represent the lower boundary and upper boundary variation, respectively, along with projectile velocity. As illustrated in Figure 15, the increase of projectile velocity causes an increase in lower boundary and a decrease in upper boundary. As discussed in Figure 14, the result illustrates that the flight stability increases as the projectile velocity increases. The conclusion of the analysis is in line with the literature [25].

**5.3. The Projectile Roll Rate  $p$ .** The effect of projectile roll rate on the instability boundaries is illustrated in Figure 16. The expression is almost identical to Figure 15 and to avoid repetition; it is not described here. The increase of projectile velocity causes a lower boundary increase and an upper boundary decrease. That is to say, the flight stability is positively associated with the projectile roll rate. The result

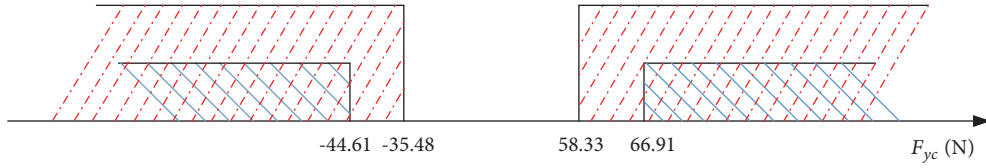


FIGURE 9: The comparison of instability boundaries.

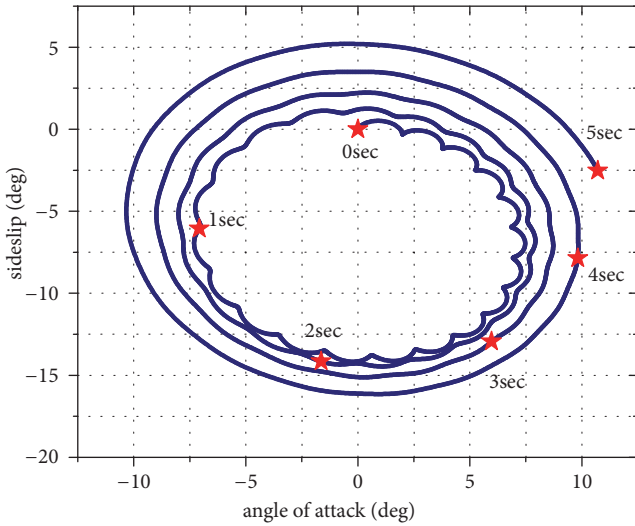
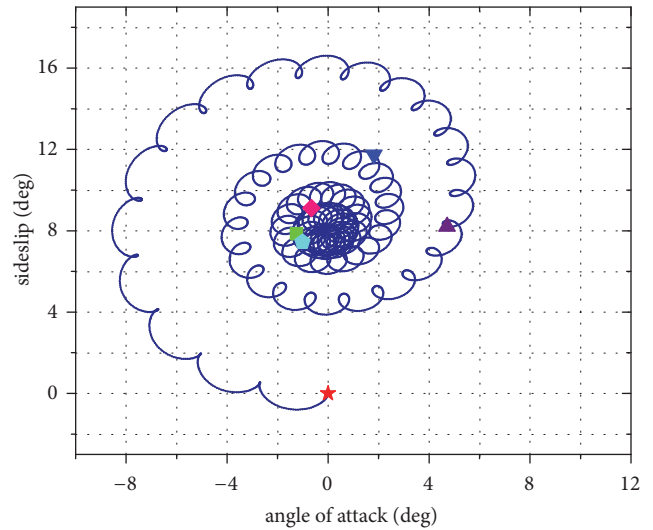


FIGURE 10: Angular motion for the flight with -40N control force.



- ★ 0sec
- ▲ 1sec
- ▼ 2sec
- ◆ 3sec
- 4sec
- 5sec

FIGURE 12: Angular motion for the flight with 60N control force.

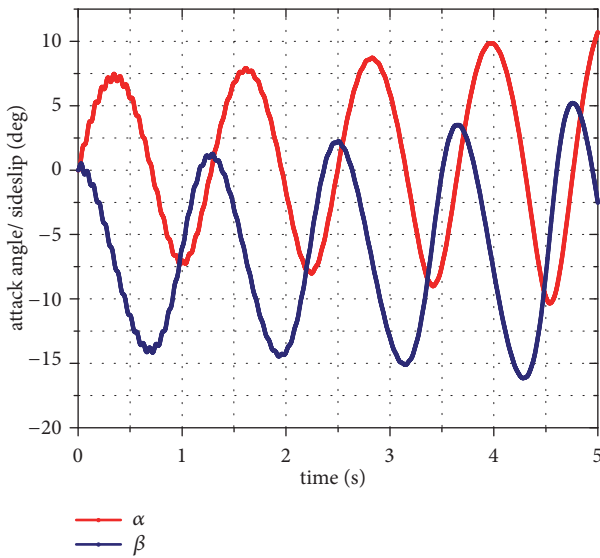


FIGURE 11: Angle of attack and sideslip for the flight with -40N control force.

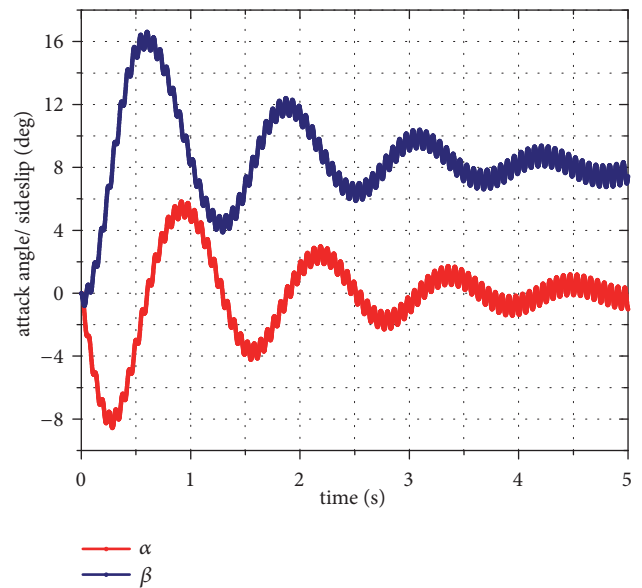


FIGURE 13: Angle of attack and sideslip for the flight with 60N control force.

is in line with the classical ballistic theory: the increase of projectile roll rate will directly improve the gyroscopic stability factor of projectiles.

This section shows the effects of projectile parameters on instability boundaries. The results illustrate that the proposed

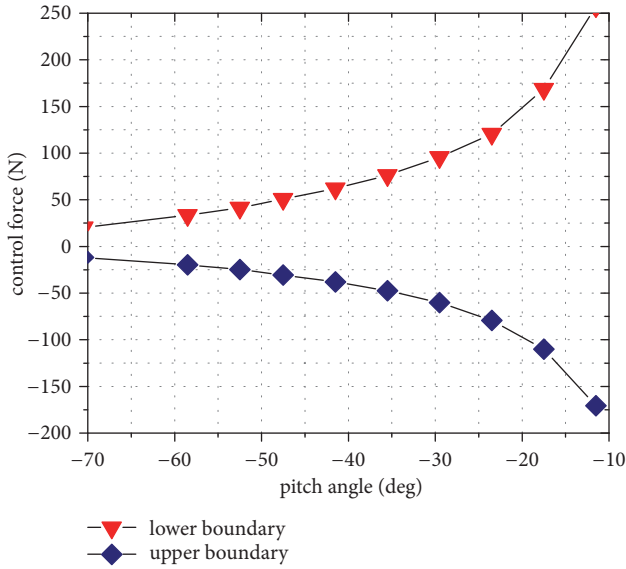


FIGURE 14: The effect of initial pitch angle on the instability boundaries.

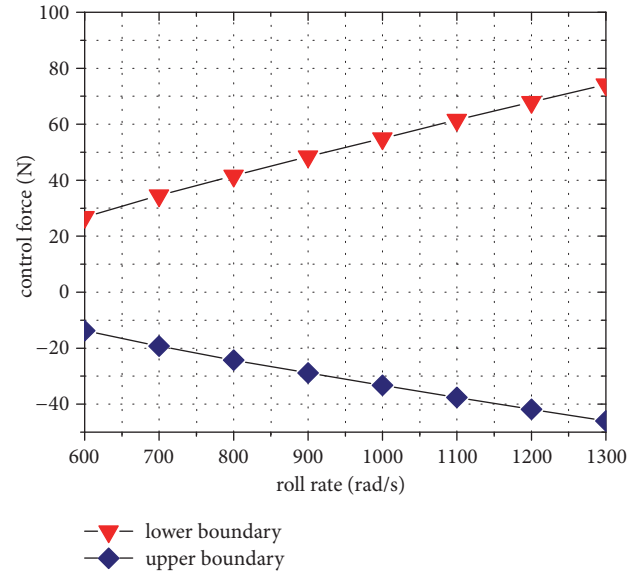


FIGURE 16: The effect of projectile velocity on the instability boundaries.

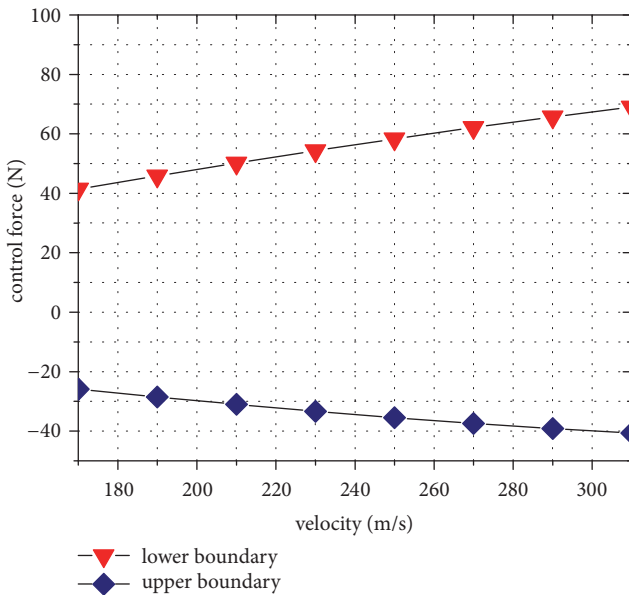


FIGURE 15: The effect of projectile velocity on the instability boundaries.

instability boundaries can be used to predict the stability variation under various flight parameters. The prediction results are in line with the relevant research or theory. Therefore, the validity of instability boundaries is demonstrated once again in this respect.

## 6. Conclusion

This work mainly focuses on the balance between the maneuverability and stability for the projectile under control. With

a deep investigation, this paper indicates the invalidity of classical linearization in stability analysis and reveals the reason. Based on that, the exterior ballistic equations are established with the unique proposed compensation matrix and no additional coordinate system is needed. The necessary prerequisite for a stable flight under control is given by Routh stability criterion and the instability boundaries for the control force are derived. Numerical simulations demonstrate the validity of the analytic relationship between the flight instability boundaries and the control force magnitude. Additionally, the instability boundaries derived in this paper are compared with Lloyd's research. The comparison results dictate that the former is more accurate and extends the scope by 13.5%. The results are also verified by simulations. The effects of the projectile pitch, velocity, and roll rate on the instability boundaries are analyzed, respectively, when a control force is exerted. The results illustrate that the unstable scope is negatively associated with all the three projectile parameters during the descending flight, while the projectile stability is positively associated.

## Nomenclature

$C_L$ :	Lift force coefficient
$C_D$ :	Drag force coefficient
$C_{y p \alpha}$ :	Magnus force coefficient derivative
$C_{M \alpha}$ :	Static moment coefficient derivative
$C_{M p \alpha}$ :	Magnus moment coefficient derivative
$C_{M q}$ :	Damping moment coefficient derivative induced by pitch and yaw rate
$u, v, w$ :	Projectile velocity component of $x, y, z$ axis in fixed plane coordinate, m/s
$F_x, F_y, F_z$ :	Aerodynamic forces component on projectile body of $x, y, z$ axis in fixed plane coordinate, N

$F_{yc}, F_{zc}$ :	Control forces component on projectile body of $y, z$ axis in fixed plane coordinate, N
$p, q, r$ :	Projectile roll rate, pitch rate, yaw rate in fixed plane coordinate, rad/s
L, M, N:	Aerodynamic moments component on projectile body of $x, y, z$ axis in fixed plane coordinate, Nm
$M_c, N_c$ :	Control moments component on projectile body of $y, z$ axis in fixed plane coordinate, Nm
V:	Projectile velocity, m/s
$\theta$ :	Projectile pitch angle, rad
$g$ :	Gravitational acceleration, m/s <sup>2</sup>
$\rho$ :	Atmospheric density, kg/m <sup>3</sup>
S:	Projectile reference area, m <sup>2</sup>
$I_X$ :	Moment of inertia for projectile longitudinal axis, kg·m <sup>2</sup>
$I_Y$ :	Moment of inertia for projectile transverse axis, kg·m <sup>2</sup>
[I] :	Diagonal inertia matrix
l:	Projectile reference length, m.

## Data Availability

The data used to support the findings of this study are available from the corresponding author upon request.

## Disclosure

This research received no specific grant from any funding agency in the public, commercial, or not-for-profit sectors.

## Conflicts of Interest

The authors declare that there are no conflicts of interest regarding the publication of this article.

## References

- [1] E. Gagnon and M. Lauzon, "Course correction fuze concept analysis for in-service 155 mm spin-stabilized gunnery projectiles," in *Proceedings of the AIAA paper 2008-6997, Guidance, Navigation and Control Conference*, 2008.
- [2] P. H. Morrison and D. S. Amberntson, "Guidance and control of a cannon-launched guided projectile," *Journal of Spacecraft and Rockets*, vol. 14, no. 6, pp. 328–334, 1977.
- [3] C. Montalvo and M. Costello, "Effect of canard stall on projectile roll and pitch damping," in *Proceedings of the Institute of Mechanical Engineers, Part G: Journal of Aerospace Engineering*, vol. 225, pp. 703–716, 2011.
- [4] F. Fresconi, "Guidance and control of a projectile with reduced sensor and actuator requirements," *Journal of Guidance, Control, and Dynamics*, vol. 34, no. 6, pp. 1757–1766, 2011.
- [5] F. Fresconi and P. Plostins, "Control mechanism strategies for spin-stabilized projectiles," in *Proceedings of the Institution of Mechanical Engineers, Part G: Journal of Aerospace Engineering*, vol. 224, pp. 979–991, 2010.
- [6] K. Pamadi and E. Ohlmeyer, "Evaluation of two guidance laws for controlling the impact flight path angle of a naval gun launched spinning projectile," in *Proceedings of the AIAA Paper 2006-6081, Guidance, Navigation and Control Conference*, 2006.
- [7] C. A. Phillips, "Guidance algorithm for range maximization and time-of-flight control of a guided projectile," *Journal of Guidance, Control, and Dynamics*, vol. 31, no. 5, pp. 1447–1455, 2008.
- [8] D. Ollerenshaw and M. Costello, "Model predictive control of a direct fire projectile equipped with canards," *Journal of Guidance, Control, and Dynamics*, vol. 130, no. 6, pp. 758–767, 2008.
- [9] T. Jitraphai and M. Costello, "Dispersion reduction of a direct fire rocket using lateral pulse jets," *Journal of Spacecraft and Rockets*, vol. 38, no. 6, pp. 929–936, 2001.
- [10] J. Rogers and M. Costello, "Design of a roll-stabilized mortar projectile with reciprocating canards," *Journal of Guidance, Control, and Dynamics*, vol. 33, no. 4, pp. 1026–1034, 2010.
- [11] F. Fresconi and J. Rogers, "Flight control of a small-diameter spin-stabilized projectile using imager feedback," *Journal of Guidance, Control, and Dynamics*, vol. 38, no. 2, pp. 181–191, 2015.
- [12] F. Fresconi, G. Cooper, I. Celmins, J. DeSpirito, and M. Costello, "Flight mechanics of a novel guided spin-stabilized projectile concept," in *Proceedings of the AIAA 2010-7638, Atmospheric Flight Mechanics Conference*, 2010.
- [13] R. L. McCoy, *Modern Exterior Ballistics: The Launch and Flight Dynamics of Symmetric Projectiles*, Schiffer, Atglen, PA, USA, 1999.
- [14] C. H. Murphy, "Symmetric Missile Dynamic Instabilities: A Survey," in *Proceedings of the 18th AIAA Aerospace Sciences Meeting*, 1980.
- [15] C. H. Murphy, "Angular motion of spinning almost symmetric missiles," *Journal of Guidance, Control, and Dynamics*, vol. 2, no. 6, pp. 504–510, 1978.
- [16] C. H. Murphy, "Gravity-induced angular motion of a spinning missile," in *Proceedings of the AIAA Paper 1970-0968, Guidance, Control and Flight Mechanics Conference*, vol. 8, 1970.
- [17] M. Costello and A. Peterson, "Linear theory of a dual-spin projectile in atmospheric flight," *Journal of Guidance, Control, and Dynamics*, vol. 23, no. 5, pp. 789–797, 2000.
- [18] P. Wernert, "Stability analysis for canard guided dual-spin stabilized projectiles," in *Proceedings of the AIAA Atmospheric Flight Mechanics Conference*, vol. 5843, 2009.
- [19] P. Wernert, F. Leopold, L. Lehmann et al., "Wind tunnel tests and open-loop trajectory simulations for a 155 mm canards guided spin stabilized projectile," in *Proceedings of the AIAA Paper 2008-6881, Atmospheric Flight Mechanics Conference and Exhibit*, 2008.
- [20] G. Cooper, F. Fresconi, and M. Costello, "Flight stability of an asymmetric projectile with activating canards," *Journal of Spacecraft and Rockets*, vol. 49, no. 1, pp. 130–135, 2012.
- [21] C. H. Murphy, "Instability of controlled projectiles in ascending or descending flight," *Journal of Guidance, Control, and Dynamics*, vol. 4, no. 1, pp. 66–69, 1981.
- [22] D. Zhu, S. Tang, J. Guo, and R. Chen, "Flight stability of a dual-spin projectile with canards," in *Proceedings of the Institution of Mechanical Engineers Part G Journal of Aerospace Engineering*, vol. 229, pp. 704–716, 2015.
- [23] K. Lloyd and D. Brown, "Instability of spinning projectiles during terminal guidance," *Journal of Guidance, Control, and Dynamics*, vol. 2, no. 1, pp. 65–70, 1979.

- [24] L. C. Hainz and M. Costello, "Modified projectile linear theory for rapid trajectory prediction," *Journal of Guidance, Control, and Dynamics*, vol. 28, no. 5, pp. 1006–1014, 2005.
- [25] Z. L. Liu, Y. S. Wang, and Q. Weng, "The influence of muzzle velocity on the projectile flight stability," *Journal of Projectiles, Rockets, Missiles and Guidance*, vol. 35, no. 6, pp. 48–52, 2015.

## Research Article

# Dynamical Analysis and Optimal Harvesting Strategy for a Stochastic Delayed Predator-Prey Competitive System with Lévy Jumps

Guodong Liu,<sup>1</sup> Kaiyuan Liu ,<sup>2</sup> and Xinzhu Meng <sup>1</sup>

<sup>1</sup>College of Mathematics and Systems Science, Shandong University of Science and Technology, Qingdao 266590, China

<sup>2</sup>Department of Mathematics, Anshan Normal University, Anshan 114007, China

Correspondence should be addressed to Xinzhu Meng; mxz721106@sdust.edu.cn

Received 26 July 2018; Accepted 27 January 2019; Published 12 February 2019

Academic Editor: Sabri Arik

Copyright © 2019 Guodong Liu et al. This is an open access article distributed under the Creative Commons Attribution License, which permits unrestricted use, distribution, and reproduction in any medium, provided the original work is properly cited.

This paper develops a theoretical framework to investigate optimal harvesting control for stochastic delay differential systems. We first propose a novel stochastic two-predator and one-prey competitive system subject to time delays and Lévy jumps. Then we obtain sufficient conditions for persistence in mean and extinction of three species by using the stochastic qualitative analysis method. Finally, the optimal harvesting effort and the maximum of expectation of sustainable yield (ESY) are derived from Hessian matrix method and optimal harvesting theory of delay differential equations. Moreover, some numerical simulations are given to illustrate the theoretical results.

## 1. Introduction

Optimal control problem in the field of biological mathematics has been widely concerned by researchers. Resource exploitation always aims to maximum sustainable yield (MSY) or the profit associated with the maximum economic yield (MEY) [1]. How to obtain MSY or MEY involves the optimal harvesting control problem. Therefore, it is interesting and meaningful to investigate optimal harvesting control strategies for biological population models, especially stochastic population models. A number of researchers have investigated single-species or two-species population models [2–4]. However, the above two classes of models can not describe some natural phenomena completely and it is believed that models with three or more species can explain the dynamical behaviors of the population accurately [5–8]. Predator-prey models are arguably known as the most fundamental building blocks of the biosystems and ecosystems as the biomasses are grown out of their resource, which have been widely investigated [9–17]. As we all know, after a predator catches and feeds on a prey, the number of the predators will not increase at once, which needs the processes of digestion and absorption. Therefore, the time delays were

considered in many differential systems [18–21], especially stochastic delay models [22–29].

The basic model we consider is based on the delay Lotka-Volterra model with two competitive predators and one prey. We propose the following model by assuming that the random perturbations of intrinsic growth rate are subjected to Gaussian white noise [30]:

$$\begin{aligned} dx(t) &= x(t) [\bar{r}_1 - a_{11}x(t) - a_{12}y_1(t - \tau_{12}) \\ &\quad - a_{13}y_2(t - \tau_{13})] dt + \bar{\sigma}_1 x(t) dB_1(t), \\ dy_1(t) &= y_1(t) [\bar{r}_2 - a_{21}e^{-d_{21}\tau_{21}}x(t - \tau_{21}) - a_{22}y_1(t) \\ &\quad - a_{23}e^{-d_{23}\tau_{23}}y_2(t - \tau_{23})] dt + \bar{\sigma}_2 y_1(t) dB_2(t), \\ dy_2(t) &= y_2(t) [\bar{r}_3 - a_{31}e^{-d_{31}\tau_{31}}x(t - \tau_{31}) \\ &\quad - a_{32}e^{-d_{32}\tau_{32}}y_1(t - \tau_{32}) - a_{33}y_2(t)] dt \\ &\quad + \bar{\sigma}_3 y_2(t) dB_3(t), \end{aligned} \quad (1)$$

with initial value

$$x(\theta) = \varphi_0(\theta),$$

$$\begin{aligned}
y_1(\theta) &= \varphi_1(\theta), \\
y_2(\theta) &= \varphi_2(\theta), \\
\theta &\in [-\tau_0, 0], \\
\tau_0 &= \max_{i,j=1,2,3} \{\tau_{ij}\},
\end{aligned} \tag{2}$$

where  $x(t)$  denotes the number of the prey species at time  $t$  and  $y_i(t)$  ( $i=1, 2$ ) denote the predator species at time  $t$ .  $\bar{r}_1 > 0$  stands for the growth rate of prey.  $\bar{r}_2 < 0$  and  $\bar{r}_3 < 0$  stand for the death rates of the two predators, respectively.  $a_{ii} > 0$  is the interspecific competition rate of species  $i$ ,  $i = 1, 2, 3$ , and  $a_{23}e^{-d_{23}\tau_{23}} > 0$  and  $a_{32}e^{-d_{32}\tau_{32}} > 0$  are the competition rates of two predators.  $a_{12}$  and  $a_{13}$  are positive representing capture rates, and  $a_{21}e^{-d_{21}\tau_{21}}$  and  $a_{31}e^{-d_{31}\tau_{31}}$  are negative representing the growth rates from prey relatively.  $\tau_{ij} \geq 0$  signifies the time delay, and  $\varphi_i(\theta) > 0$  ( $i = 0, 1, 2$ ) are continuous functions on  $[-\tau_0, 0]$ .  $B_i(t)$  ( $i=1,2,3$ ) are mutually independent Brownian motion with  $B_i(0) = 0$  defined on a complete probability space  $(\Omega, \mathcal{F}, \mathcal{P})$  with a filtration  $\{\mathcal{F}_t\}_{t \geq 0}$  that satisfies that it is right continuous and increasing with  $\mathcal{F}_0$  that contains all  $\mathcal{P}$ -null sets.

Various harvesting models have been used to investigate the optimal harvesting policies of renewable resources (e.g., Beddington and May [30], Neubert [31]). Recently, many authors explored the optimal harvesting models [32–37]. According to the catch-per-unit-effort (CPUE) hypothesis, we consider that predators  $y_1$  and  $y_2$  are subject to exploitation with harvesting effort rates  $h_1 > 0$  and  $h_2 > 0$ , respectively.

However, in some cases, models just perturbed by the Gaussian white noise can not effectively and efficiently describe the circumstance when the species suffer sudden catastrophic disturbance in nature. The sudden environmental change can affect the dynamical behavior of the species significantly. Therefore, it is necessary to use the discontinuous stochastic process (e.g., Lévy jump) to model the abrupt nature phenomenon in ecosystem [38–43].

To introduce the Lévy jump into the underlying stochastic model (1), we first give some facts about the Lévy jump [33]. Generally, a Lévy process  $L_i(t)$  can be decomposed into the sum of a linear drift, a Brownian motion  $B_i(t)$ , and a superposition of centered Poisson processes with different jump sizes  $\lambda(dv)$  which is the rate of arrival of the Poisson process with jump of size  $v$ . According to the Lévy decomposition theorem [44], we know that

$$L_i(t) = \bar{a}_i t + \bar{\sigma}_i B_i(t) + \int_{\mathbb{Y}} v \bar{N}(t, dv), \quad i = 1, 2, \dots, n, \tag{3}$$

where  $\bar{a}_i \in R$ ,  $\bar{\sigma}_i > 0$ ,  $\bar{N}(t, dv) = N(t, dv) - \lambda(dv)t$  is a compensated Poisson process, and  $N$  is a Poisson measure with characteristic measure  $\lambda$  on a measurable subset  $\mathbb{Y}$  of  $(0, +\infty)$  with  $\lambda(\mathbb{Y}) < \infty$ . The distribution of a Lévy process  $L_i(t)$  has the property of infinite divisibility and is characterized by its characteristic function  $\phi_{L_i}(t)$ , which is given by the following Lévy-Khintchine formula [45]:

$$\begin{aligned}
\phi_{L_i}(t) &:= \mathbb{E} \left[ e^{tL_i} \right] \\
&= \exp \left\{ \bar{a}_i t - \frac{1}{2} \bar{\sigma}_i^2 t^2 + \int_{\mathbb{Y}} \left[ e^{tv} - 1 - tv I_{|v| < 1} \right] \lambda(dv) \right\},
\end{aligned} \tag{4}$$

where  $I_G$  is the indicator function of set  $G$  and  $\iota$  is the imaginary unit. The distribution of Lévy jump  $L_i(t)$  can be completely parameterized by  $(\bar{a}_i, \bar{\sigma}_i, \lambda)$ .

Motivated by the above discussion, we can assume that the intrinsic growth rate  $\bar{r}_1$  and the death rates  $\bar{r}_2$  and  $\bar{r}_3$  of model (1) perturbed by the Lévy jump to signify the sudden climate change,  $\bar{r}_i \rightarrow \bar{r}_i + \bar{\gamma}_i dL_i(t)$  [42, 46], and then we can obtain the following stochastic model incorporating Lévy jump:

$$\begin{aligned}
dx(t) &= x(t) \left[ r_1 - a_{11}x(t) - a_{12}y_1(t - \tau_{12}) \right. \\
&\quad \left. - a_{13}y_2(t - \tau_{13}) \right] dt + \sigma_1 x(t) dB_1(t) + x(t) \\
&\quad \cdot \int_{\mathbb{Y}} \gamma_1(v) \bar{N}(dt, dv), \\
dx_2(t) &= y_1(t) \left[ r_2 - h_1 - a_{21}e^{-d_{21}\tau_{21}}x(t - \tau_{21}) - a_{22}y_1(t) \right. \\
&\quad \left. - a_{23}e^{-d_{23}\tau_{23}}y_2(t - \tau_{23}) \right] dt + \sigma_2 y_1(t) dB_2(t) + y_1(t) \\
&\quad \cdot \int_{\mathbb{Y}} \gamma_2(v) \bar{N}(dt, dv), \\
dx_3(t) &= y_2(t) \left[ r_3 - h_2 - a_{31}e^{-d_{31}\tau_{31}}x(t - \tau_{31}) \right. \\
&\quad \left. - a_{32}e^{-d_{32}\tau_{32}}y_1(t - \tau_{32}) - a_{33}y_2(t) \right] dt \\
&\quad + \sigma_3 y_2(t) dB_3(t) + y_2(t) \int_{\mathbb{Y}} \gamma_3(v) \bar{N}(dt, dv),
\end{aligned} \tag{5}$$

here  $r_i = \bar{r}_i + \bar{\gamma}_i \bar{a}_i$ ,  $\sigma_i = \bar{\sigma}_i + \bar{\gamma}_i \bar{\sigma}_i$ ,  $\gamma_i(v) = \bar{\gamma}_i(v)$ ,  $i = 1, 2, 3$ , and with initial value (2).

In this paper, we devote our main attention to obtain the optimal harvesting control strategy of system (5). To this end, we firstly investigate the dynamical behavior of the three species including persistence in mean and extinction and asymptotically stable distribution. Then we explore how the time delay, sudden environmental shock expressed by Lévy jump, and other factors affect the optimal harvesting policy and the maximum expectation of sustainable yield.

This paper is organized as follows. We discuss the persistence in mean and extinction of the three species in Section 2. Based on the conclusion of Section 2, we consider the optimal harvesting policy in Section 3. Finally, we conclude our results by numerical simulations and discussions in the last section.

## 2. Persistence in Mean and Extinction

For convenience, we give some notations which will be used for analyzing our main results. Let  $R_+^3 = \{a = (a_1, a_2, a_3) \in R^3 \mid a_i > 0, i = 1, 2, 3\}$  and let  $C([-\tau_0, 0]; R_+^3)$  stand for all continuous functions from  $[-\tau_0, 0]$  to  $R_+^3$ , where  $R^3$  is a 3-dimensional Euclidean space and  $R_+^3$  is the positive cone in  $R^3$ . Correspondingly,  $R_+ = (0, +\infty)$ . Denote  $d_1 = r_1$ ,  $d_2 =$

$r_2 - h_1$ , and  $d_3 = r_3 - h_2$ . To make it more convenient, let  $c_{11} = a_{11}$ ,  $c_{12} = a_{12}$ ,  $c_{13} = a_{13}$ ,  $c_{21} = a_{21}e^{-d_{21}\tau_{21}}$ ,  $c_{22} = a_{22}$ ,  $c_{23} = a_{23}e^{-d_{23}\tau_{23}}$ ,  $c_{31} = a_{31}e^{-d_{31}\tau_{31}}$ ,  $c_{32} = a_{32}e^{-d_{32}\tau_{32}}$ , and  $c_{33} = a_{33}$ . Additionally, denote  $\alpha_1 = (c_{11}, c_{21}, c_{31})^T$ ,  $\alpha_2 = (c_{12}, c_{22}, c_{32})^T$ ,  $\alpha_3 = (c_{13}, c_{23}, c_{33})^T$  and  $\beta = (d_1, d_2, d_3)^T$ , and  $\gamma = (1/2)(\sigma_1^2, \sigma_2^2, \sigma_3^2)^T$ . Accordingly, we define

$$\begin{aligned}
 \Phi &= \det(\alpha_1, \alpha_2, \alpha_3), \\
 \Upsilon &= \det(\alpha_1, \beta, \gamma), \\
 \Phi_1 &= \det(\beta, \alpha_2, \alpha_3), \\
 \tilde{\Phi}_1 &= \det(\gamma, \alpha_2, \alpha_3), \\
 \Phi_2 &= \det(\alpha_1, \beta, \alpha_3), \\
 \tilde{\Phi}_2 &= \det(\alpha_1, \gamma, \alpha_3), \\
 \Phi_3 &= \det(\alpha_1, \alpha_2, \beta), \\
 \tilde{\Phi}_3 &= \det(\alpha_1, \alpha_2, \gamma), \\
 \Delta_1 &= c_{22}d_1 - c_{12}d_2, \\
 \Delta_2 &= c_{11}d_2 - c_{21}d_1, \\
 \Delta_3 &= c_{11}d_3 - c_{31}d_1, \\
 \tilde{\Delta}_1 &= \frac{c_{22}\sigma_1^2}{2} - \frac{c_{12}\sigma_2^2}{2}, \\
 \tilde{\Delta}_2 &= \frac{c_{11}\sigma_2^2}{2} - \frac{c_{21}\sigma_1^2}{2}, \\
 \tilde{\Delta}_3 &= \frac{c_{11}\sigma_3^2}{2} - \frac{c_{31}\sigma_2^2}{2}, \\
 \langle f(t) \rangle &= t^{-1} \int_0^t f(s) ds, \\
 \langle f \rangle^* &= \limsup_{t \rightarrow +\infty} t^{-1} \int_0^t f(s) ds, \\
 \langle f \rangle_* &= \liminf_{t \rightarrow +\infty} t^{-1} \int_0^t f(s) ds.
 \end{aligned} \tag{6}$$

$\Phi_{ij}$  is the complement minor of  $c_{ij}$  in the deterministic  $\Phi$ ,  $i, j = 1, 2, 3$ . Now we give a fundamental assumption of Lévy jump.

**Assumption 1.** Assume that  $\gamma_i(v) > -1$ , and there exists a constant  $K$  such that

$$\int_{\mathbb{Y}} \ln(1 + \gamma_i(v))^2 \lambda(dv) \leq K < \infty. \tag{7}$$

Assumption 1 implies that the intensity of Lévy jump can not be sufficiently large.

**Lemma 2.** For any given initial value  $\varphi(\theta) = (\varphi_0(\theta), \varphi_1(\theta), \varphi_2(\theta))^T \in C([- \tau_0, 0]; \mathbb{R}_+^3)$ , model (5) has a unique global positive solution  $X(t) = (x(t), y_1(t), y_2(t))^T$  on  $t \geq 0$  a.s.

*Proof.* Firstly, we consider the following stochastic model:

$$\begin{aligned}
 d \ln x(t) &= \left[ d_1 - \frac{1}{2}\sigma_1^2 - c_{11}x(t) - c_{12}y_1(t - \tau_{12}) \right. \\
 &\quad \left. - c_{13}y_2(t - \tau_{13}) - \int_{\mathbb{Y}} [\gamma_1 - \ln(1 + \gamma_1)] \lambda(dv) \right] dt \\
 &\quad + \sigma_1 dB_1(t) + \int_{\mathbb{Y}} \ln(1 + \gamma_1) \tilde{N}(dt, dv), \\
 d \ln y_1(t) &= \left[ d_2 - \frac{1}{2}\sigma_2^2 - c_{21}x(t - \tau_{21}) - c_{22}y_1(t) \right. \\
 &\quad \left. - c_{23}y_2(t - \tau_{23}) - \int_{\mathbb{Y}} [\gamma_2 - \ln(1 + \gamma_2)] \lambda(dv) \right] dt \\
 &\quad + \sigma_2 dB_2(t) + \int_{\mathbb{Y}} \ln(1 + \gamma_2) \tilde{N}(dt, dv), \\
 d \ln y_2(t) &= \left[ d_3 - \frac{1}{2}\sigma_3^2 - c_{31}x(t - \tau_{31}) - c_{32}y_1(t - \tau_{32}) \right. \\
 &\quad \left. - c_{33}y_2(t) - \int_{\mathbb{Y}} [\gamma_3 - \ln(1 + \gamma_3)] \lambda(dv) \right] dt \\
 &\quad + \sigma_3 dB_3(t) + \int_{\mathbb{Y}} \ln(1 + \gamma_3) \tilde{N}(dt, dv)
 \end{aligned} \tag{8}$$

with initial value (2). It is easy to see that the coefficients of model (8) satisfy the local Lipschitz condition; therefore model (8) has a unique local solution  $X(t)$  on  $[0, \tau_e]$ , where  $\tau_e$  is the explosion time. According to Itô's formula, we can find that

$$X(t) = (x(t), y_1(t), y_2(t))^T \tag{9}$$

is the unique positive local solution to model (5). Now let us prove  $\tau_e = +\infty$ . Thus, we introduce the following auxiliary model:

$$\begin{aligned}
 du(t) &= u(t) [d_1 - c_{11}u(t)] dt + \sigma_1 u(t) dB_1(t) \\
 &\quad + u(t) \int_{\mathbb{Y}} \gamma_1(v) \tilde{N}(dt, dv), \\
 dv_1(t) &= v_1(t) [d_2 - c_{21}u(t - \tau_{21}) - c_{22}v_1(t)] dt \\
 &\quad + \sigma_2 v_1(t) dB_2(t) \\
 &\quad + v_1(t) \int_{\mathbb{Y}} \gamma_2(v) \tilde{N}(dt, dv), \\
 dv_2(t) &= v_2(t) [d_3 - c_{31}u(t - \tau_{31}) - c_{33}v_2(t)] dt \\
 &\quad + \sigma_3 v_2(t) dB_3(t) + v_2(t) \int_{\mathbb{Y}} \gamma_3(v) \tilde{N}(dt, dv)
 \end{aligned} \tag{10}$$

with initial value

$$\begin{aligned}
 u(\theta) &= \varphi_0(\theta), \\
 v_1(\theta) &= \varphi_1(\theta), \\
 v_2(\theta) &= \varphi_2(\theta), \\
 \theta &\in [-\tau_0, 0].
 \end{aligned} \tag{11}$$

Taking advantage of the comparison theorem for stochastic equation [47] yields that, for  $t \in [0, \tau_e]$ ,

$$\begin{aligned} x(\theta) &< u(\theta), \\ y_i(\theta) &< v_i(\theta) \quad a.s., \quad i = 1, 2. \end{aligned} \tag{12}$$

According to Theorem 4.2 in Jiang and Shi [48], the explicit solution of model (10) is

$$\begin{aligned} u(t) &= \frac{\exp\{b_1 t + \sigma_1 B_1(t) + M_1(t)\}}{u^{-1}(0) + c_{11} \int_0^t \exp\{b_1 s + \sigma_1 B_1(s) + M_1(s)\} ds}, \\ v_1(t) &= \frac{\exp\{b_2 t + c_{21} \int_0^t u(t - \tau_{21}) ds + \sigma_2 B_2(t) + M_2(t)\}}{v_1^{-1}(0) + c_{22} \int_0^t \exp\{b_2 s - \int_0^s c_{21} u(\zeta - \tau_{21}) d\zeta + \sigma_2 B_2(s) + M_2(s)\}}, \tag{13} \\ v_2(t) &= \frac{\exp\{b_3 t + c_{31} \int_0^t u(t - \tau_{31}) ds + \sigma_3 B_3(t) + M_3(t)\}}{v_2^{-1}(0) + c_{33} \int_0^t \exp\{b_3 s - \int_0^s c_{31} u(\zeta - \tau_{31}) d\zeta + \sigma_3 B_3(s) + M_3(s)\}}, \end{aligned}$$

where  $\eta_i = \int_{\mathbb{Y}} [\gamma_i(v) - \ln(1 + \gamma_i(v))] \lambda(dv)$ ,  $b_i = d_i - (1/2)\sigma_i^2 - \eta_i$ , and  $M_i(t) = \int_0^t \int_{\mathbb{Y}} \ln(1 + \gamma_i(v)) \tilde{N}(ds, dv)$ ,  $i = 1, 2, 3$  [33]. It is not difficult to see that  $y_1(t)$ ,  $y_2(t)$ , and  $y_3(t)$  are existent on  $t \geq 0$ ; thereby  $\tau_e = +\infty$ . This completes the proof of Lemma 2.  $\square$

**Lemma 3** (see [22]). *Suppose that  $\phi(t) \in C[\Omega \times [0, +\infty); \mathbb{R}_+]$ . (i) If there exist three constants  $\lambda_0, \lambda$ , and  $T \geq 0$ , such that*

$$\begin{aligned} \ln \phi(t) &\leq \lambda t - \lambda_0 \int_0^t \phi(s) ds + \alpha \sum_{i=1}^3 B_i(t) \\ &+ \sum_{i=1}^3 \delta_i \int_0^t \int_{\mathbb{Y}} \ln(1 + \gamma_i(v)) \tilde{N}(ds, dv), \quad a.s., \end{aligned} \tag{14}$$

for all  $t \geq T$ , where  $\alpha$  and  $\delta_i$  are constants; then

$$\langle \phi \rangle^* \leq \frac{\lambda}{\lambda_0} \quad a.s., \quad \text{if } \lambda \geq 0, \tag{15}$$

$$\lim_{t \rightarrow +\infty} \phi(t) = 0 \quad a.s., \quad \text{if } \lambda \leq 0.$$

(ii) If there exist three constants  $\lambda_0, \lambda$ , and  $T \geq 0$ , such that

$$\begin{aligned} \ln \phi(t) &\geq \lambda t - \lambda_0 \int_0^t \phi(s) ds + \alpha \sum_{i=1}^3 B_i(t) \\ &+ \sum_{i=1}^3 \delta_i \int_0^t \int_{\mathbb{Y}} \ln(1 + \gamma_i(v)) \tilde{N}(ds, dv), \quad a.s., \end{aligned} \tag{16}$$

for all  $t \geq T$ ; then  $\langle \phi \rangle_* \geq \lambda/\lambda_0$  a.s.

**Lemma 4.** For model (10), consider the following:

(a) If  $b_1 < 0$ , then

$$\begin{aligned} \lim_{t \rightarrow +\infty} u(t) &= 0, \\ \lim_{t \rightarrow +\infty} v_i(t) &= 0, \quad a.s., \quad i = 1, 2. \end{aligned} \tag{17}$$

(b) If  $b_1 \geq 0$ ,  $b_2 - c_{21}b_1/c_{11} \geq 0$ , and  $b_3 - c_{31}b_1/c_{11} \geq 0$ , then

$$\begin{aligned} \lim_{t \rightarrow +\infty} \langle u(t) \rangle &= \frac{b_1}{c_{11}}, \\ \lim_{t \rightarrow +\infty} \langle v_1(t) \rangle &= \frac{b_2 - c_{21}b_1/c_{11}}{c_{22}}, \\ \lim_{t \rightarrow +\infty} \langle v_2(t) \rangle &= \frac{b_3 - c_{31}b_1/c_{11}}{c_{33}}, \end{aligned} \tag{18}$$

a.s.;

(c) If  $b_1 \geq 0$ ,  $b_2 - c_{21}b_1/c_{11} < 0$ , and  $b_3 - c_{31}b_1/c_{11} < 0$ , then

$$\begin{aligned} \lim_{t \rightarrow +\infty} \langle u(t) \rangle &= \frac{b_1}{c_{11}}, \\ \lim_{t \rightarrow +\infty} v_1(t) &= 0, \\ \lim_{t \rightarrow +\infty} v_2(t) &= 0, \end{aligned} \tag{19}$$

a.s..

(d) If  $b_1 \geq 0$ ,  $b_2 - c_{21}b_1/c_{11} \geq 0$ , and  $b_3 - c_{31}b_1/c_{11} < 0$ , then

$$\begin{aligned} \lim_{t \rightarrow +\infty} \langle u(t) \rangle &= \frac{b_1}{c_{11}}, \\ \lim_{t \rightarrow +\infty} \langle v_1(t) \rangle &= \frac{b_2 - c_{21}b_1/c_{11}}{c_{22}}, \\ \lim_{t \rightarrow +\infty} v_2(t) &= 0, \end{aligned} \tag{20}$$

a.s..

(e) If  $b_1 \geq 0$ ,  $b_2 - c_{21}b_1/c_{11} < 0$ , and  $b_3 - c_{31}b_1/c_{11} \geq 0$ , then

$$\begin{aligned} \lim_{t \rightarrow +\infty} \langle u(t) \rangle &= \frac{b_1}{c_{11}}, \\ \lim_{t \rightarrow +\infty} v_1(t) &= 0, \\ \lim_{t \rightarrow +\infty} \langle v_2(t) \rangle &= \frac{b_3 - c_{31}b_1/c_{11}}{c_{33}}, \end{aligned} \tag{21}$$

a.s.

*Proof.* Firstly, we prove (a). Applying Itô's formula to model (10), we can get that

$$\begin{aligned} \ln u(t) - \ln u(0) &= b_1 t - c_{11} \int_0^t u(s) ds + \sigma_1 B_1(t) \\ &+ M_1(t), \end{aligned} \tag{22}$$

$$\begin{aligned} \ln v_1(t) - \ln v_1(0) &= b_2 t - c_{21} \int_0^t u(s - \tau_{21}) ds \\ &- c_{22} \int_0^t v_1(s) ds + \sigma_2 B_2(t) \\ &+ M_2(t), \end{aligned} \tag{23}$$

$$\begin{aligned} \ln v_2(t) - \ln v_2(0) &= b_3 t - c_{31} \int_0^t u(s - \tau_{31}) ds \\ &\quad - c_{33} \int_0^t v_2(s) ds + \sigma_3 B_3(t) \\ &\quad + M_3(t). \end{aligned} \quad (24)$$

It follows from (22) that

$$t^{-1} \ln \frac{u(t)}{u(0)} \leq b_1 + \frac{\sigma_1 B_1(t)}{t} + \frac{M_1(t)}{t}. \quad (25)$$

By Assumption 1, the quadratic variation of  $M_1(t)$  is

$$\begin{aligned} \langle M_1(t), M_1(t) \rangle(t) &= \int_0^t \int_{\mathcal{V}} (\ln(1 + \gamma_1(v)))^2 \lambda(dv) ds \\ &\leq t \int_{\mathcal{V}} (\ln(1 + \gamma_1(v)))^2 \lambda(dv) < ct, \end{aligned} \quad (26)$$

where  $\langle M_1(t), M_1(t) \rangle(t)$  is Meyer's angle bracket process. Utilizing the strong law of large numbers for local martingales gives that  $\lim_{t \rightarrow \infty} (B_1(t)/t) = 0$  and  $\lim_{t \rightarrow \infty} (M_1(t)/t) = 0$ . Since  $b_1 < 0$ ,

$$\lim_{t \rightarrow +\infty} u(t) = 0, \quad a.s. \quad (27)$$

Substituting (27) into (23) gives that

$$\begin{aligned} \ln v_1(t) - \ln v_1(0) &\leq b_2 t + \varepsilon t - c_{22} \int_0^t v_1(s) ds + \sigma_2 B_2(t) \\ &\quad + M_2(t), \end{aligned} \quad (28)$$

where  $\varepsilon$  is small enough satisfying  $b_2 + \varepsilon < 0$ . Applying (i) in Lemma 3 gives

$$\lim_{t \rightarrow +\infty} v_1(t) = 0, \quad a.s. \quad (29)$$

Similarly, we can get that

$$\lim_{t \rightarrow +\infty} v_2(t) = 0, \quad a.s. \quad (30)$$

Secondly, we prove (b). Since  $b_1 \geq 0$ , applying Lemma 3 to (22) yields that

$$\lim_{t \rightarrow +\infty} \langle u(t) \rangle = \frac{b_1}{c_{11}}, \quad a.s. \quad (31)$$

We know that

$$t^{-1} \ln \frac{u(t)}{u(0)} = b_1 - c_{11} \langle u(t) \rangle + \frac{\sigma_1 B_1(t)}{t} + \frac{M_1(t)}{t}, \quad (32)$$

$$\begin{aligned} t^{-1} \ln \frac{v_1(t)}{v_1(0)} - t^{-1} c_{21} \left( \int_{t-\tau_{21}}^t u(s) ds - \int_{-\tau_{21}}^0 u(s) ds \right) \\ = b_2 - c_{21} \langle u(t) \rangle - c_{22} \langle v_1(t) \rangle + \frac{\sigma_2 B_2(t)}{t} + \frac{M_2(t)}{t}, \end{aligned} \quad (33)$$

$$\begin{aligned} t^{-1} \ln \frac{v_2(t)}{v_2(0)} - t^{-1} c_{31} \left( \int_{t-\tau_{31}}^t u(s) ds - \int_{-\tau_{31}}^0 u(s) ds \right) \\ = b_3 - c_{31} \langle u(t) \rangle - c_{33} \langle v_2(t) \rangle + \frac{\sigma_3 B_3(t)}{t} + \frac{M_3(t)}{t}. \end{aligned} \quad (34)$$

Using (31) in (32) gives that

$$\lim_{t \rightarrow +\infty} t^{-1} \ln u(0) = 0, \quad a.s. \quad (35)$$

Multiplying (32) and (33) by  $-c_{21}$  and  $c_{11}$ , respectively, and adding them, we can derive that

$$\begin{aligned} t^{-1} c_{11} \ln \frac{v_1(t)}{v_1(0)} - t^{-1} c_{11} c_{21} \left( \int_{t-\tau_{21}}^t u(s) ds - \int_{-\tau_{21}}^0 u(s) ds \right) \\ - t^{-1} \ln \frac{u(t)}{u(0)} \\ = b_2 c_{11} - c_{11} c_{22} \langle v_1(t) \rangle + t^{-1} c_{11} \sigma_2 B_2(t) - b_1 c_{21} \\ - t^{-1} c_{21} \sigma_1 B_1(t) - t^{-1} c_{21} M_1(t) + t^{-1} c_{11} M_2(t). \end{aligned} \quad (36)$$

An application of (31) gives that

$$\begin{aligned} \lim_{t \rightarrow +\infty} t^{-1} \int_{t-\tau_{21}}^t u(s) ds \\ = \lim_{t \rightarrow +\infty} \left( t^{-1} \int_0^t u(s) ds - t^{-1} \int_0^{t-\tau_{21}} u(s) ds \right) = 0, \end{aligned} \quad (37)$$

a.s.

Consequently, utilizing (35), (36), (37), and Lemma 3 yields that

$$\lim_{t \rightarrow +\infty} \langle v_1(t) \rangle = \frac{b_2 - c_{21} b_1 / c_{11}}{c_{22}}, \quad a.s. \quad (38)$$

Similarly, we can get when  $b_3 - c_{31} b_1 / c_{11} \geq 0$ ,

$$\lim_{t \rightarrow +\infty} \langle v_2(t) \rangle = \frac{b_3 - c_{31} b_1 / c_{11}}{c_{33}}, \quad a.s. \quad (39)$$

Thirdly, we prove (c). If  $b_2 - c_{21} b_1 / c_{11} < 0$ , according to (35), (36), (37), and Lemma 3, one can obtain that

$$\lim_{t \rightarrow +\infty} v_1(t) = 0, \quad a.s. \quad (40)$$

Similarly, if  $b_3 - c_{31} b_1 / c_{11} < 0$ , we can obtain

$$\lim_{t \rightarrow +\infty} v_2(t) = 0, \quad a.s. \quad (41)$$

The proofs of (d) and (e) are similar to that of (b) and (c), respectively, and hence are omitted.  $\square$

**Lemma 5.** *The solution of model (5) obeys*

$$\limsup_{t \rightarrow +\infty} \frac{\ln x(t)}{t} \leq 0, \quad (42)$$

$$\limsup_{t \rightarrow +\infty} \frac{\ln y_i(t)}{t} \leq 0, \quad a.s., \quad i = 1, 2.$$

*Proof.* Since  $x(t) \leq u(t)$ ,  $y_i(t) \leq v_i(t)$ ,  $i = 1, 2$ , we only need to prove

$$\limsup_{t \rightarrow +\infty} \frac{\ln u(t)}{t} \leq 0, \quad (43)$$

$$\limsup_{t \rightarrow +\infty} \frac{\ln v_i(t)}{t} \leq 0, \quad a.s., \quad i = 1, 2.$$

According to the proof of Lemma 4, with the same method of [22], we can get (43). Therefore, (42) is obtained.  $\square$

**Theorem 6.** For system (5), if  $\Phi > 0$ ,  $\Phi_i > 0$ ,  $i = 1, 2, 3$ , and  $Y > 0$ , we set  $\rho_1 = 2d_1/\sigma_1^2$ ,  $\rho_2 = \Delta_2/\bar{\Delta}_2$ , and  $\rho_3 = \Phi_3/\bar{\Phi}_3$ , and then  $\rho_1 > \rho_2 > \rho_3$ ; moreover,

(i) if  $\rho_1 < 1$ , then prey species and predator species go to extinction a.s.; i.e.,

$$\begin{aligned} \lim_{t \rightarrow +\infty} x(t) &= 0, \\ \lim_{t \rightarrow +\infty} y_i(t) &= 0, \quad i = 1, 2, \quad a.s.; \end{aligned} \quad (44)$$

(ii) if  $\rho_1 > 1 > \rho_2$ , then two predators go to extinction a.s., and prey is persistent in mean; i.e.,

$$\lim_{t \rightarrow +\infty} \langle x(t) \rangle = \frac{b_1}{c_{11}}, \quad a.s.; \quad (45)$$

(iii) if  $\rho_2 > 1 > \rho_3$ , then predator species  $y_2$  goes to extinction, while prey species  $x$  and predator species  $y_1$  are persistent in mean; i.e.,

$$\begin{aligned} \lim_{t \rightarrow +\infty} \langle x(t) \rangle &= \frac{\Delta_1 - \bar{\Delta}_1}{\Phi_{33}}, \\ \lim_{t \rightarrow +\infty} \langle y_1(t) \rangle &= \frac{\Delta_2 - \bar{\Delta}_2}{\Phi_{33}} \end{aligned} \quad (46)$$

a.s.;

(iv) if  $\rho_3 > 1$ , then three species are persistent in mean; i.e.,

$$\begin{aligned} \lim_{t \rightarrow +\infty} \langle x(t) \rangle &= \frac{\Phi_1 - \bar{\Phi}_1}{\Phi}, \\ \lim_{t \rightarrow +\infty} \langle y_1(t) \rangle &= \frac{\Phi_2 - \bar{\Phi}_2}{\Phi}, \\ \lim_{t \rightarrow +\infty} \langle y_2(t) \rangle &= \frac{\Phi_3 - \bar{\Phi}_3}{\Phi}, \end{aligned} \quad (47)$$

a.s.

*Proof.* It is easy to prove  $\rho_1 > \rho_2 > \rho_3$ . Applying Itô's formula to model (5) yields that

$$\begin{aligned} \ln x(t) - \ln x(0) &= b_1 t - c_{11} \int_0^t x(s) ds \\ &\quad - c_{12} \int_0^t y_1(s - \tau_{12}) ds \\ &\quad - c_{13} \int_0^t y_2(s - \tau_{13}) ds \\ &\quad + \sigma_1 B_1(t) + M_1(t), \end{aligned} \quad (48)$$

$$\begin{aligned} \ln y_1(t) - \ln y_1(0) &= b_2 t - c_{22} \int_0^t y_1(s) ds \\ &\quad - c_{21} \int_0^t x(s - \tau_{21}) ds \end{aligned}$$

$$\begin{aligned} &- c_{23} \int_0^t y_2(s - \tau_{23}) ds \\ &+ \sigma_2 B_2(t) + M_2(t), \end{aligned} \quad (49)$$

$$\begin{aligned} \ln y_2(t) - \ln y_2(0) &= b_3 t - c_{33} \int_0^t y_2(s) ds \\ &- c_{31} \int_0^t x(s - \tau_{31}) ds \\ &- c_{32} \int_0^t y_1(s - \tau_{32}) ds \\ &+ \sigma_3 B_3(t) + M_3(t). \end{aligned} \quad (50)$$

Firstly, we prove (i). Since  $c_{11}$ ,  $c_{12}$ , and  $c_{13}$  are positive, we can get

$$t^{-1} \ln \frac{x(t)}{x(0)} \leq b_1 + \frac{\sigma_1 B_1(t)}{t} + \frac{M_1(t)}{t}. \quad (51)$$

Note that  $\rho_1 = 2d_1/\sigma_1^2 < 1$ ; then  $b_1 < 0$ . By Lemma 3, we get

$$\lim_{t \rightarrow +\infty} x(t) = 0, \quad a.s. \quad (52)$$

Substituting this identity into (49), we can observe that, for sufficiently large  $t$ ,

$$\begin{aligned} \ln y_1(t) - \ln y_1(0) &\leq b_2 t + \varepsilon t - c_{22} \int_0^t y_1(s) ds + \sigma_2 B_2(t) \\ &+ M_2(t), \end{aligned} \quad (53)$$

where  $\varepsilon$  is small enough such that  $b_2 + \varepsilon < 0$ . By Lemma 3, we can get

$$\lim_{t \rightarrow +\infty} y_1(t) = 0, \quad a.s. \quad (54)$$

Similarly, we have

$$\lim_{t \rightarrow +\infty} y_2(t) = 0, \quad a.s. \quad (55)$$

Secondly, we prove (ii). Since  $1 > \rho_2 > \Delta_3/\bar{\Delta}_3$ , we know

$$\frac{\Delta_3}{\bar{\Delta}_3} < 1, \quad (56)$$

$$i.e., \frac{c_{11}d_3 - c_{31}d_1}{c_{11}\sigma_3^2/2 - c_{31}\sigma_1^2/2} < 1.$$

Simplifying the above inequality gives that  $c_{11}b_3 < c_{31}b_1$ , which means  $b_3 - c_{31}b_1/c_{11} < 0$ . Furthermore, from  $\rho_2 < 1$ , we have  $b_2 - c_{21}b_1/c_{11} < 0$ . According to (c) in Lemma 3 and (12), one can observe that

$$\lim_{t \rightarrow +\infty} y_i(t) = 0, \quad a.s., \quad i = 1, 2. \quad (57)$$

Substituting the above identity into (48) and using Lemma 3, we can get

$$\lim_{t \rightarrow +\infty} x(t) = \frac{b_1}{c_{11}}. \quad (58)$$

Thirdly, we prove (iii). Dividing (48), (49), and (50) by  $t$ , we can derive the following equations:

$$\begin{aligned}
 t^{-1} \ln \frac{x(t)}{x(0)} &= b_1 - c_{11} \langle x(t) \rangle - c_{12} \langle y_1(t) \rangle - c_{13} \langle y_2(t) \rangle \\
 &+ t^{-1} c_{12} \left( \int_{t-\tau_{12}}^t y_1(s) ds - \int_{-\tau_{12}}^0 y_1(s) ds \right) \\
 &+ t^{-1} c_{13} \left( \int_{t-\tau_{13}}^t y_2(s) ds - \int_{-\tau_{13}}^0 y_2(s) ds \right) \\
 &+ t^{-1} \sigma_1 B_1(t) + t^{-1} M_1(t),
 \end{aligned} \tag{59}$$

$$\begin{aligned}
 t^{-1} \ln \frac{y_1(t)}{y_1(0)} &= b_2 - c_{22} \langle y_1(t) \rangle - c_{21} \langle x(t) \rangle - c_{23} \langle y_2(t) \rangle \\
 &+ t^{-1} c_{21} \left( \int_{t-\tau_{21}}^t x(s) ds - \int_{-\tau_{21}}^0 x(s) ds \right) \\
 &+ t^{-1} c_{23} \left( \int_{t-\tau_{23}}^t y_2(s) ds - \int_{-\tau_{23}}^0 y_2(s) ds \right) \\
 &+ t^{-1} \sigma_2 B_2(t) + t^{-1} M_2(t),
 \end{aligned} \tag{60}$$

$$\begin{aligned}
 t^{-1} \ln \frac{y_2(t)}{y_2(0)} &= b_3 - c_{33} \langle y_2(t) \rangle - c_{31} \langle x(t) \rangle - c_{32} \langle y_1(t) \rangle \\
 &+ t^{-1} c_{31} \left( \int_{t-\tau_{31}}^t x(s) ds - \int_{-\tau_{31}}^0 x(s) ds \right) \\
 &+ t^{-1} c_{32} \left( \int_{t-\tau_{32}}^t y_1(s) ds - \int_{-\tau_{32}}^0 y_1(s) ds \right) \\
 &+ t^{-1} \sigma_3 B_3(t) + t^{-1} M_3(t).
 \end{aligned} \tag{61}$$

Denote  $m, n$  as the solution of the following equations:

$$\begin{aligned}
 c_{11}m + c_{21}n &= c_{31}, \\
 c_{12}m + c_{22}n &= c_{32}.
 \end{aligned} \tag{62}$$

Consequently,

$$\begin{aligned}
 m &= \frac{-\Phi_{13}}{\Phi_{33}} > 0, \\
 n &= \frac{\Phi_{23}}{\Phi_{33}} > 0.
 \end{aligned} \tag{63}$$

By (12), (43), and Lemma 5, we have

$$\begin{aligned}
 \limsup_{t \rightarrow +\infty} \ln x(t) &\leq 0, \\
 \limsup_{t \rightarrow +\infty} \ln y_i(t) &\leq 0, \quad i = 1, 2.
 \end{aligned} \tag{64}$$

In addition,

$$\begin{aligned}
 \limsup_{t \rightarrow +\infty} t^{-1} \int_{t-\tau_{21}}^t x(s) ds &= \limsup_{t \rightarrow +\infty} t^{-1} \int_{t-\tau_{31}}^t x(s) ds = 0, \\
 \limsup_{t \rightarrow +\infty} t^{-1} \int_{t-\tau_{12}}^t y_1(s) ds &= \limsup_{t \rightarrow +\infty} t^{-1} \int_{t-\tau_{32}}^t y_1(s) ds \\
 &= 0,
 \end{aligned}$$

$$\begin{aligned}
 \limsup_{t \rightarrow +\infty} t^{-1} \int_{t-\tau_{13}}^t y_2(s) ds &= \limsup_{t \rightarrow +\infty} t^{-1} \int_{t-\tau_{23}}^t y_2(s) ds \\
 &= 0.
 \end{aligned} \tag{65}$$

According to Lemma 5, for arbitrarily given  $\varepsilon > 0$ , there exists a  $T_1 > 0$  such that when  $t > T_1$

$$t^{-1} \left( m \ln \frac{x(t)}{x(0)} + n \ln \frac{y_1(t)}{y_1(0)} \right) \leq \varepsilon. \tag{66}$$

Multiplying (59), (60), and (61) by  $-m, -n$ , and  $1$ , respectively, and adding them, one can observe that, for sufficiently large  $t$  such that  $t > T_1$ ,

$$\begin{aligned}
 t^{-1} \ln \frac{y_2(t)}{y_2(0)} &- t^{-1} \left( m \ln \frac{x(t)}{x(0)} + n \ln \frac{y_1(t)}{y_1(0)} \right) \\
 &= \frac{\Phi_3 - \tilde{\Phi}_3}{\Phi_{33}} - \frac{\Phi}{\Phi_{33}} \langle y_2(t) \rangle \\
 &- mt^{-1} c_{12} \left( \int_{t-\tau_{12}}^t y_1(s) ds - \int_{-\tau_{12}}^0 y_1(s) ds \right) \\
 &- mt^{-1} c_{13} \left( \int_{t-\tau_{13}}^t y_2(s) ds - \int_{-\tau_{13}}^0 y_2(s) ds \right) \\
 &- nt^{-1} c_{21} \left( \int_{t-\tau_{21}}^t x(s) ds - \int_{-\tau_{21}}^0 x(s) ds \right) \\
 &- nt^{-1} c_{23} \left( \int_{t-\tau_{23}}^t y_2(s) ds - \int_{-\tau_{23}}^0 y_2(s) ds \right) \\
 &+ t^{-1} c_{31} \left( \int_{t-\tau_{31}}^t x(s) ds - \int_{-\tau_{31}}^0 x(s) ds \right) \\
 &+ t^{-1} c_{32} \left( \int_{t-\tau_{32}}^t y_1(s) ds - \int_{-\tau_{32}}^0 y_1(s) ds \right) \\
 &- t^{-1} (m\sigma_1 B_1(t) + n\sigma_2 B_2(t) - \sigma_3 B_3(t)) \\
 &- t^{-1} (mM_1(t) + nM_2(t) - M_3(t)).
 \end{aligned} \tag{67}$$

Using (43) in (81) yields that

$$\begin{aligned}
 t^{-1} \ln \frac{y_2(t)}{y_2(0)} &\leq \frac{\Phi_3 - \tilde{\Phi}_3}{\Phi_{33}} + 2\varepsilon - \frac{\Phi}{\Phi_{33}} \langle y_2(t) \rangle \\
 &- t^{-1} (m\sigma_1 B_1(t) + n\sigma_2 B_2(t) - \sigma_3 B_3(t)) \\
 &- t^{-1} (mM_1(t) + nM_2(t) - M_3(t)).
 \end{aligned} \tag{68}$$

Since  $\rho_3 = \Phi_3 / \tilde{\Phi}_3 < 1$ , we can choose  $\varepsilon > 0$  to be sufficiently small such that  $(\Phi_3 - \tilde{\Phi}_3) / \Phi_{33} + 2\varepsilon < 0$ . Making use of the arbitrariness  $\varepsilon$  and Lemma 3 gives that

$$\lim_{t \rightarrow +\infty} y_2(t) = 0, \quad a.s. \tag{69}$$

Consequently, model (5) reduces to the following model:

$$\begin{aligned} dx(t) &= x(t) [d_1 - c_{11}x(t) - c_{12}y_1(t - \tau_{12})] dt \\ &\quad + \sigma_1 x(t) dB_1(t) + x(t) \int_{\mathbb{V}} \gamma_1(v) \tilde{N}(dt, dv), \\ dy_1(t) &= y_1(t) [d_2 - c_{21}x(t - \tau_{21}) - c_{22}y_1(t)] dt \\ &\quad + \sigma_2 y_1(t) dB_2(t) \\ &\quad + y_1(t) \int_{\mathbb{V}} \gamma_2(v) \tilde{N}(dt, dv). \end{aligned} \quad (70)$$

For system (70), similarly to the proof of Theorem 1 in [49], the following identities can be derived:

$$\begin{aligned} \lim_{t \rightarrow +\infty} \langle x(t) \rangle &= \frac{\Delta_1 - \tilde{\Delta}_1}{\Phi_{33}}, \\ \lim_{t \rightarrow +\infty} \langle y_1(t) \rangle &= \frac{\Delta_2 - \tilde{\Delta}_2}{\Phi_{33}}, \end{aligned} \quad (71)$$

*a.s.*

Fourthly, we prove (iv). By (68), since  $\rho_3 > 1$ , we know from the arbitrariness of  $\varepsilon$  and Lemma 3 that

$$\langle y_2 \rangle^* \leq \frac{\Phi_3 - \tilde{\Phi}_3}{\Phi}, \quad a.s. \quad (72)$$

Denote  $p, q$  as the solution of the following equations:

$$\begin{aligned} c_{11}p + c_{31}q &= c_{21}, \\ c_{13}p + c_{33}q &= c_{23}. \end{aligned} \quad (73)$$

Then we have

$$\begin{aligned} p &= \frac{-\Phi_{12}}{\Phi_{22}} > 0, \\ q &= \frac{\Phi_{32}}{\Phi_{22}} > 0. \end{aligned} \quad (74)$$

According to Lemma 5, for arbitrarily given  $\varepsilon > 0$ , there exists a  $T_2 > 0$ , such that

$$t^{-1} \left( p \ln \frac{x(t)}{x(0)} + q \ln \frac{y_2(t)}{y_2(0)} \right) \leq \varepsilon. \quad (75)$$

Multiplying (59), (60), and (61) by  $-p, 1$ , and  $-q$ , respectively, and, adding them, we can obtain that, for  $t > T_2$ ,

$$\begin{aligned} t^{-1} \ln \frac{y_1(t)}{y_1(0)} - t^{-1} \left( p \ln \frac{x(t)}{x(0)} + q \ln \frac{y_2(t)}{y_2(0)} \right) \\ = \frac{\Phi_2 - \tilde{\Phi}_2}{\Phi_{22}} - \frac{\Phi}{\Phi_{22}} \langle y_1(t) \rangle \\ - pt^{-1} c_{12} \left( \int_{t-\tau_{12}}^t y_1(s) ds - \int_{-\tau_{12}}^0 y_1(s) ds \right) \\ - pt^{-1} c_{13} \left( \int_{t-\tau_{13}}^t y_2(s) ds - \int_{-\tau_{13}}^0 y_2(s) ds \right) \end{aligned}$$

$$\begin{aligned} - qt^{-1} c_{31} \left( \int_{t-\tau_{31}}^t x(s) ds - \int_{-\tau_{31}}^0 x(s) ds \right) \\ - qt^{-1} c_{32} \left( \int_{t-\tau_{32}}^t y_1(s) ds - \int_{-\tau_{32}}^0 y_1(s) ds \right) \\ + t^{-1} c_{23} \left( \int_{t-\tau_{23}}^t y_2(s) ds - \int_{-\tau_{23}}^0 y_2(s) ds \right) \\ + t^{-1} c_{21} \left( \int_{t-\tau_{21}}^t x(s) ds - \int_{-\tau_{21}}^0 x(s) ds \right) \\ - t^{-1} (p\sigma_1 B_1(t) - \sigma_2 B_2(t) + q\sigma_3 B_3(t)) \\ - t^{-1} (pM_1(t) - M_2(t) + qM_3(t)). \end{aligned} \quad (76)$$

Using (43) in (76) yields that

$$\begin{aligned} t^{-1} \ln \frac{y_1(t)}{y_1(0)} &\leq \frac{\Phi_2 - \tilde{\Phi}_2}{\Phi_{22}} + 2\varepsilon - \frac{\Phi}{\Phi_{22}} \langle x_2(t) \rangle \\ &\quad - t^{-1} (p\sigma_1 B_1(t) - \sigma_2 B_2(t) + q\sigma_3 B_3(t)) \\ &\quad - t^{-1} (pM_1(t) - M_2(t) + qM_3(t)). \end{aligned} \quad (77)$$

Note that  $\Phi_2/\tilde{\Phi}_2 > \Phi_3/\tilde{\Phi}_3 > 1$ . According to the arbitrariness of  $\varepsilon$  and Lemma 3, we have

$$\langle y_1 \rangle^* \leq \frac{\Phi_2 - \tilde{\Phi}_2}{\Phi}, \quad a.s. \quad (78)$$

It follows that, for any sufficiently small  $\varepsilon$ , there exist  $T_3$  and  $T_4$  such that

$$c_{12} \langle y_1(t) \rangle \leq c_{12} \langle y_1 \rangle^* + \varepsilon \leq \frac{c_{12} (\Phi_2 - \tilde{\Phi}_2)}{\Phi} + \varepsilon, \quad t > T_3, \quad (79)$$

$$c_{13} \langle y_2(t) \rangle \leq c_{13} \langle y_2 \rangle^* + \varepsilon \leq \frac{c_{13} (\Phi_3 - \tilde{\Phi}_3)}{\Phi} + \varepsilon,$$

$$t > T_4.$$

Substituting (79) into (59) results in that, for sufficiently large  $t$ ,

$$\begin{aligned} t^{-1} \ln \frac{x(t)}{x(0)} &\geq b_1 - c_{11} \langle x(t) \rangle - \frac{c_{12} (\Phi_2 - \tilde{\Phi}_2)}{\Phi} \\ &\quad - \frac{c_{13} (\Phi_3 - \tilde{\Phi}_3)}{\Phi} - 3\varepsilon + t^{-1} \sigma_1 B_1(t) \\ &\quad + t^{-1} M_1(t) \\ &= \frac{c_{11} (\Phi_1 - \tilde{\Phi}_1)}{\Phi} - c_{11} \langle x(t) \rangle - 3\varepsilon \\ &\quad + t^{-1} \sigma_1 B_1(t) + t^{-1} M_1(t). \end{aligned} \quad (80)$$

According to the arbitrariness of  $\varepsilon$  and Lemma 3, we have

$$\langle x \rangle_* \geq \frac{\Phi_1 - \tilde{\Phi}_1}{\Phi}, \quad a.s. \quad (81)$$

By  $c_{31} < 0$ ,  $c_{32} > 0$ , one can observe that, for every sufficiently small  $\varepsilon$ , there exist  $T_5$  and  $T_6$ , such that

$$\begin{aligned} c_{31} \langle x(t) \rangle &\leq c_{31} \langle x \rangle_* + \varepsilon \leq \frac{c_{31}(\Phi_1 - \tilde{\Phi}_1)}{\Phi} + \varepsilon, \quad t > T_5, \\ c_{32} \langle y_1(t) \rangle &\leq c_{32} \langle y_1 \rangle_* + \varepsilon \leq \frac{c_{32}(\Phi_3 - \tilde{\Phi}_3)}{\Phi} + \varepsilon, \\ & t > T_6. \end{aligned} \quad (82)$$

Using (82) in (61) yields for  $t$  large enough

$$\begin{aligned} t^{-1} \ln \frac{y_2(t)}{y_2(0)} &\geq b_3 - c_{33} \langle y_2(t) \rangle - \frac{c_{31}(\Phi_1 - \tilde{\Phi}_1)}{\Phi} \\ &\quad - \frac{c_{32}(\Phi_2 - \tilde{\Phi}_2)}{\Phi} - 3\varepsilon + t^{-1} \sigma_3 B_3(t) \\ &\quad + t^{-1} M_3(t) \\ &= \frac{c_{33}(\Phi_3 - \tilde{\Phi}_3)}{\Phi} - c_{33} \langle y_2(t) \rangle - 3\varepsilon \\ &\quad + t^{-1} \sigma_3 B_3(t) + t^{-1} M_3(t). \end{aligned} \quad (83)$$

According to the arbitrariness of  $\varepsilon$  and Lemma 3, we have

$$\langle y_2 \rangle_* \geq \frac{\Phi_3 - \tilde{\Phi}_3}{\Phi}, \quad a.s. \quad (84)$$

Combining (72) with (84), one can observe that

$$\lim_{t \rightarrow +\infty} \langle y_2(t) \rangle = \frac{\Phi_3 - \tilde{\Phi}_3}{\Phi}, \quad a.s. \quad (85)$$

In the similar way, using (72), (81), and (60) and then combining them with (78) yield that

$$\lim_{t \rightarrow +\infty} \langle y_1(t) \rangle = \frac{\Phi_2 - \tilde{\Phi}_2}{\Phi}, \quad a.s. \quad (86)$$

Subsequently, we can observe that

$$\lim_{t \rightarrow +\infty} \langle x(t) \rangle = \frac{\Phi_1 - \tilde{\Phi}_1}{\Phi}, \quad a.s. \quad (87)$$

This completes the proof of Theorem 6.  $\square$

### 3. Optimal Harvesting

**Lemma 7.** For any  $p > 1$ , there exists a constant  $K = K(p)$  which makes the solution  $X(t)$  of model (5) satisfy the property that

$$\begin{aligned} \limsup_{t \rightarrow +\infty} \mathbb{E}[x^p(t)] &\leq K, \\ \limsup_{t \rightarrow +\infty} \mathbb{E}[y_i^p(t)] &\leq K, \quad i = 1, 2. \end{aligned} \quad (88)$$

*Proof.* The proof is rather standard and hence is omitted.  $\square$

From Lemma 7, there is a  $T > 0$  such that, for  $t \geq T$ ,  $\mathbb{E}[x^p(t)] \leq 2K$  and  $\mathbb{E}[y_i^p(t)] \leq 2K$ . Note that  $\mathbb{E}[x(t)]$  and  $\mathbb{E}[y_i(t)]$  ( $i = 1, 2$ ) are continuous; thus there is a constant  $K_1 > 0$  such that  $\mathbb{E}[x^p(t)] < K_1$  and  $\mathbb{E}[y_i^p(t)] < K_1$  when  $-\tau_0 \leq t < T$ . Denote  $L = \max\{2K, K_1\}$ ; then we have

$$\begin{aligned} \mathbb{E}[x^p(t)] &\leq L = L(p) \\ \text{and } \mathbb{E}[y_i^p(t)] &\leq L = L(p), \\ & t \geq \tau_0, \quad p > 0, \quad i = 1, 2. \end{aligned} \quad (89)$$

**Lemma 8.** If  $a_{11} > a_{12} + a_{13}$ ,  $a_{22} > -a_{21}e^{-d_{21}\tau_{21}} + a_{23}e^{-d_{23}\tau_{23}}$ , and  $a_{33} > -a_{31}e^{-d_{31}\tau_{31}} + a_{32}e^{-d_{32}\tau_{32}}$ , then model (5) will be asymptotically stable in distribution; i.e., when  $t \rightarrow +\infty$ , there is a unique probability measure  $\mu(\cdot)$  such that the transition probability density  $p(t, \xi, \cdot)$  of  $X(t)$  converges weakly to  $\mu(\cdot)$  with any given initial value  $\xi(\theta) \in C([-\tau, 0]; \mathbb{R}_+^3)$ .

*Proof.* Since the proof of Lemma 8 is rather standard and hence is omitted. The similar proof can be found in [22].  $\square$

We give the following extra notions to get the optimal harvesting policy:

$$P = \begin{pmatrix} a_{22} & a_{23}e^{-d_{23}\tau_{23}} \\ a_{32}e^{-d_{32}\tau_{32}} & a_{33} \end{pmatrix}, \quad (90)$$

$$\Lambda = (\lambda_1, \lambda_2)^T = [P(P^{-1})^T + I]^{-1} Q,$$

where  $Q = (Q_1, Q_2)^T$ ,  $Q_i = r_{i+1} - (1/2)\sigma_{i+1}^2 - \eta_{i+1}$ ,  $i = 1, 2$ , and  $I$  is the unit matrix.

**Theorem 9.** Suppose that  $a_{22} > a_{23}e^{-d_{23}\tau_{23}}$ ,  $a_{33} > a_{32}e^{-d_{32}\tau_{32}}$ ,  $\Phi > 0$ , and  $P^{-1} + (P^{-1})^T$  is positive definite.

(i) If  $\lambda_i \geq 0$  and when  $h_i = \lambda_i$ ,  $i = 1, 2$ , we have  $\Gamma_2 > 0$ ,  $\Gamma_3 > 0$ , and then the optimal harvesting effort is  $H^* = \Lambda = [P(P^{-1})^T + I]^{-1} Q$  and the maximum of ESY is

$$Y^* = \Lambda^T P^{-1} (Q - \Lambda), \quad (91)$$

where  $\Gamma_i = \Phi_i - \tilde{\Phi}_i$ ,  $i = 2, 3$ .

(ii) When  $h_i = \lambda_i$ ,  $i = 1, 2$ , there is a  $\Gamma_i \leq 0$  or  $\lambda_i < 0$ , and then the optimal harvesting strategy does not exist.

*Proof.* Define  $G = \{H = (h_1, h_2)^T \in \mathbb{R}^2 \mid \Gamma_{i+1} > 0, h_i > 0, i = 1, 2\}$ . Therefore, the harvesting effort  $H \in G$ . If the optimal harvesting effort  $H^*$  exists, it must belong to  $G$ .

Firstly, we prove (i). Obviously,  $G$  is not empty, since  $\Lambda \in G$ . By (iv) of Theorem 6, for any  $H \in G$ , we have

$$\begin{aligned} \lim_{t \rightarrow +\infty} t^{-1} \int_0^t H^T X(s) ds &= \sum_{i=1}^2 h_i \lim_{t \rightarrow +\infty} t^{-1} \int_0^t y_i(s) ds \\ &= H^T P^{-1} (Q - H). \end{aligned} \quad (92)$$

According to Lemma 8, we obtain that model (5) has a unique invariant measure  $\mu(\cdot)$  which is strong mixing and ergodic

by Corollary 3.4.3 and Theorem 3.2.6 in [50], respectively. Hence, it can be derived from (3.3.2) in [50] that

$$\lim_{t \rightarrow +\infty} t^{-1} \int_0^t H^T X(s) ds = \int_{\mathbb{R}_+^2} H^T X \mu(dX). \quad (93)$$

Let  $\varrho(X)$  represent the stationary probability density of model (5). Since the invariant measure of model (5) is unique, and then, by the one-to-one correspondence between  $\varrho(x)$  and its corresponding invariant measure  $\mu(\cdot)$ , we obtain

$$\begin{aligned} Y(H) &= \lim_{t \rightarrow +\infty} \sum_{i=1}^2 \mathbb{E}(h_i y_i(t)) = \lim_{t \rightarrow +\infty} \mathbb{E}(H^T X(t)) \\ &= \int_{\mathbb{R}_+^2} H^T X \varrho(X) dX = \int_{\mathbb{R}_+^2} H^T X \mu(dX). \end{aligned} \quad (94)$$

Combining (92) with (94), we can get

$$Y(H) = H^T P^{-1}(Q - H). \quad (95)$$

Let  $\Lambda = (\lambda_1, \lambda_2)^T$  be the unique solution of the following equation:

$$\begin{aligned} \frac{dY(H)}{dH} &= \frac{dH^T}{dH} P^{-1}(Q - H) \\ &\quad + \frac{d}{dH} \left[ (Q - H)^T (P^{-1})^T \right] H \\ &= P^{-1}Q - \left[ P^{-1} + (P^{-1})^T \right] H = 0. \end{aligned} \quad (96)$$

Hence  $\Lambda = [P(P^{-1})^T + I]^{-1}Q$ . Obviously, the following Hessian matrix

$$\begin{aligned} \frac{d}{dH^T} \left[ \frac{dY(H)}{dH} \right] &= \left( \frac{d}{dH} \left[ \left( \frac{dY(H)}{dH} \right)^T \right] \right)^T \\ &= \left( \frac{d}{dH} \left[ Q^T (P^{-1})^T - H^T \left[ P^{-1} + (P^{-1})^T \right] \right] \right)^T \\ &= -P^{-1} - (P^{-1})^T \end{aligned} \quad (97)$$

is negative definite, so  $\Lambda$  is the global maximum point of  $Y(H)$ . In other words, if  $\Lambda \in G$ , i.e.,  $\lambda_i \geq 0$  and  $\Gamma_{i+1} > 0$ ,  $i = 1, 2$ , then the optimal harvesting effort is  $H^* = \Lambda$  and  $Y^*$  is the maximum value of ESY.

Secondly, we prove (ii). Obviously, if there is an  $i$  ( $i = 1, 2$ ) such that  $h_i < 0$ , the optimal harvesting strategy does not exist. Then we suppose that the optimal harvesting effort  $\bar{H}^* = (\bar{h}_1^*, \bar{h}_2^*)^T$  exists. So  $\bar{H}^* \in G$ , i.e.,  $\Gamma_{i+1}|_{h_i=\bar{h}_i^*} > 0$ ,  $\bar{h}_i^* \geq 0$ ,  $i = 1, 2$ . That is to say,  $\bar{H}^*$  is the unique solution of (96). On the other hand,  $\Lambda = (\lambda_1, \lambda_2)^T$  is also the solution of (96). Hence,  $\lambda_i = \bar{h}_i^* \geq 0$ , and  $\Gamma_{i+1}|_{h_i=\lambda_i} = \Gamma_{i+1}|_{h_i=\bar{h}_i^*} > 0$ ,  $i=1,2$ . It is in contradiction with the condition, which implies that the optimal harvesting strategy does not exist.

This completes the proof of Theorem 9.  $\square$

## 4. Numerical Simulations and Discussions

It is imperative to understand the influence of environmental perturbations on the coexistence and extinction of species. In this paper, we consider a stochastic competitive delay model of two predators and one prey, taking both Gaussian white noise and Lévy jump into account. Compared with [24], we consider a model where the prey species predated by two different predators and also we introduce harvesting efforts into the two predator species, which is novel and more realistic. This relationship can be found in Yangtze river. There are two kinds of fishes, sturgeon and siniperca chuatsi, which feed on some shrimps. The two fishes are harvested on spring and our model reflects this phenomenon. Additionally, our main purpose is not only to investigate the dynamical behavior, but also to obtain the optimal harvesting strategy of model (5). How to deal with time delay and jump are two key points. The work [51] used the graph-theoretic approach to deal with the delay and jump in network. In this paper, we utilize variable substitution to eliminate the delay. Quadratic variation and the strong law of large numbers for local martingales are applied to deal with the jump.

Theorem 6 describes sufficient conditions for persistence in mean and extinction of three species, which are derived from the comparison theorem of stochastic differential equations and limit superior theory. When it comes to the harvesting of predators, it is essential to consider the optimal harvesting policy and the maximum expectation of sustainable yield (ESY). Theorem 9 gives the optimal harvesting effort and the maximum of ESY by using Hessian Matrix method and optimal harvesting theory of differential equations.

The authors of [33] have investigated the influence of competition of two species on the optimal harvesting strategy. In contrast to [33], the dynamical behaviors of a three species model are analyzed more sufficiently. Not only do we consider the competition of the species, we also take the predation into account. Our results show that the capture rates can affect the persistence in mean and extinction of the species. Correspondingly, the capture rates also influence the optimal harvesting strategy and the maximum expectation of sustainable yield. To sum up, our main results are summarized as follows:

### (I) Extinction and persistence

Define  $\rho_1 = 2d_1/\sigma_1^2$ ,  $\rho_2 = \Delta_2/\tilde{\Delta}_2$ , and  $\rho_3 = \Phi_3/\tilde{\Phi}_3$ .

(i) If  $\rho_1 < 1$ , then three species go to extinction a.s.; i.e.,

$$\begin{aligned} \lim_{t \rightarrow +\infty} x(t) &= 0, \\ \lim_{t \rightarrow +\infty} y_i(t) &= 0, \quad i = 1, 2, \quad a.s. \end{aligned} \quad (98)$$

(ii) If  $\rho_1 > 1 > \rho_2$ , then two predators go to extinction a.s., and prey is persistent in mean; i.e.,

$$\lim_{t \rightarrow +\infty} \langle x(t) \rangle = \frac{b_1}{c_{11}}, \quad a.s. \quad (99)$$

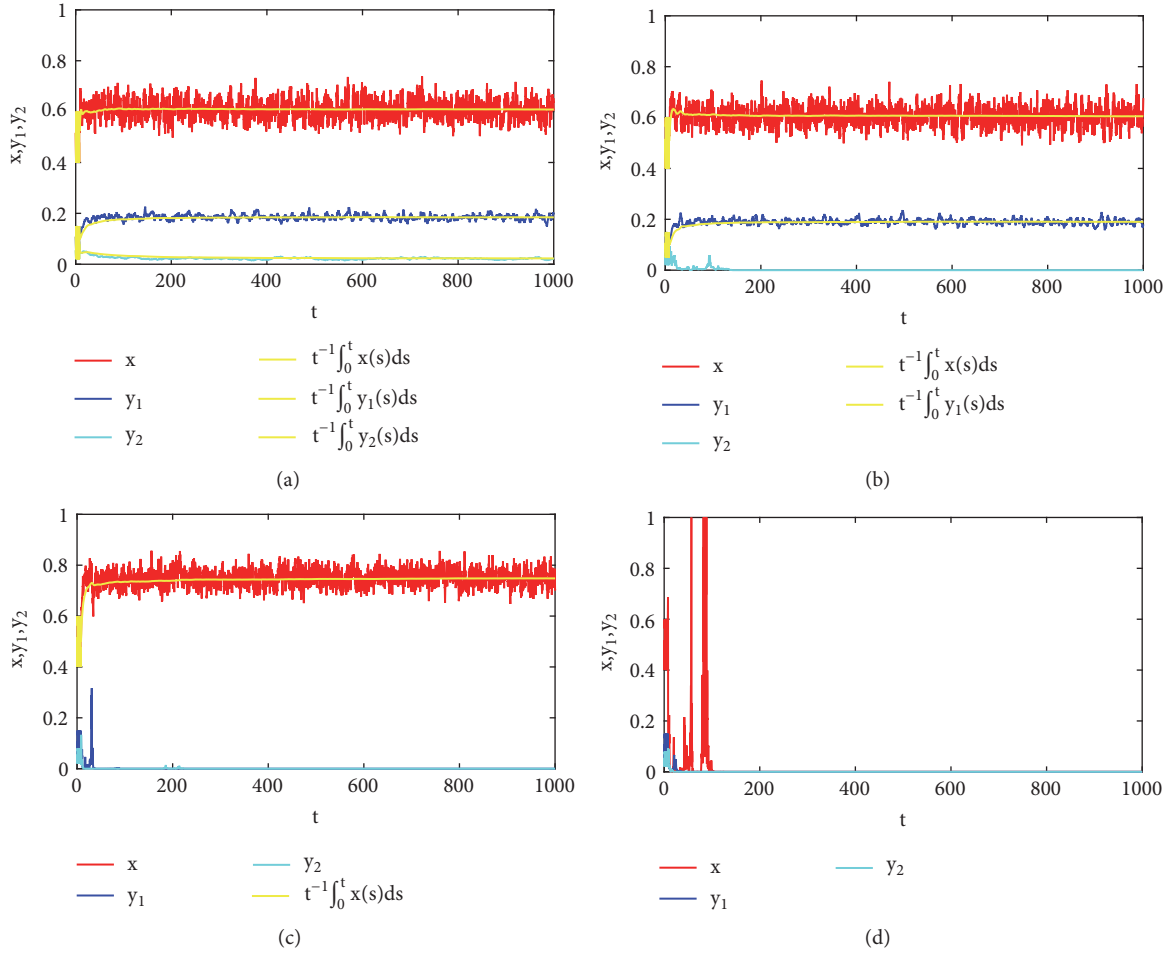


FIGURE 1: The persistence in mean and extinction of three species are given in Theorem 6. The densities of white noises are taken: (a)  $\sigma_1 = 0.77$ ,  $\sigma_2 = 0.32$ , and  $\sigma_3 = 0.32$ , (b)  $\sigma_1 = 0.77$ ,  $\sigma_2 = 0.32$ , and  $\sigma_3 = 5$ , (c)  $\sigma_1 = 0.6$ ,  $\sigma_2 = 10$ , and  $\sigma_3 = 8$ , (d)  $\sigma_1 = 15$ ,  $\sigma_2 = 8$ , and  $\sigma_3 = 10$ .

(iii) If  $\rho_2 > 1 > \rho_3$ , then predator species  $y_2$  goes to extinction, while prey species  $x$  and predator species  $y_1$  are persistent in mean; i.e.,

$$\lim_{t \rightarrow +\infty} \langle x(t) \rangle = \frac{\Delta_1 - \bar{\Delta}_1}{\Phi_{33}},$$

$$\lim_{t \rightarrow +\infty} \langle y_1(t) \rangle = \frac{\Delta_2 - \bar{\Delta}_2}{\Phi_{33}} \quad (100)$$

a.s.

(iv) If  $\rho_3 > 1$ , then three species are persistent in mean; i.e.,

$$\lim_{t \rightarrow +\infty} \langle x(t) \rangle = \frac{\Phi_1 - \bar{\Phi}_1}{\Phi},$$

$$\lim_{t \rightarrow +\infty} \langle y_1(t) \rangle = \frac{\Phi_2 - \bar{\Phi}_2}{\Phi},$$

$$\lim_{t \rightarrow +\infty} \langle y_2(t) \rangle = \frac{\Phi_3 - \bar{\Phi}_3}{\Phi}, \quad (101)$$

a.s.

## (II) Optimal harvesting strategy

Define  $\Lambda = (\lambda_1, \lambda_2)^T = [P(P^{-1})^T + I]^{-1}Q$ .

(i) If  $\lambda_i \geq 0$  and when  $h_i = \lambda_i, i = 1, 2$ , we have  $\Gamma_2 > 0, \Gamma_3 > 0$ , then the optimal harvesting effort is  $H^* = \Lambda = [P(P^{-1})^T + I]^{-1}Q$ , and the maximum of ESY is

$$Y^* = \Lambda^T P^{-1} (Q - \Lambda), \quad (102)$$

where  $\Gamma_i = \Phi_i - \bar{\Phi}_i, i = 2, 3$ .

(ii) If  $\lambda_i < 0$ , then the optimal harvesting strategy does not exist.

Next, we give some numerical simulations to illustrate the biological significance of the results. We choose  $r_1 = 1.2, r_2 = -0.05, r_3 = -0.005, h_1 = 0.1, h_2 = 0.005, a_{11} = 1.6, a_{12} = 1.2, a_{13} = 0.3, a_{21}e^{-d_{21}\tau_{21}} = -0.85, a_{22} = 1.9, a_{23}e^{-d_{23}\tau_{23}} = 0.6, a_{31}e^{-d_{31}\tau_{31}} = -0.4, a_{32}e^{-d_{32}\tau_{32}} = 1, a_{33} = 2.1, \tau_{12} = 3, \tau_{13} = 7, \tau_{21} = 1, \tau_{23} = 5, \tau_{31} = 4, \tau_{32} = 10$ , and  $\gamma_1 = \gamma_2 = \gamma_3 = 1$ . Additionally, we denote  $x(\theta) = 0.5 + 0.1 \sin \theta, y_1(\theta) = 0.1 + 0.05 \sin \theta$ , and  $y_2(\theta) = 0.05 + 0.03 \sin \theta$ . The densities of white noises will be given in Figures 1(a)–1(d).

Figure 1(a) shows that all three species are persistent in mean when  $\rho_3 > 1$ . Figure 1(b) shows that the prey and

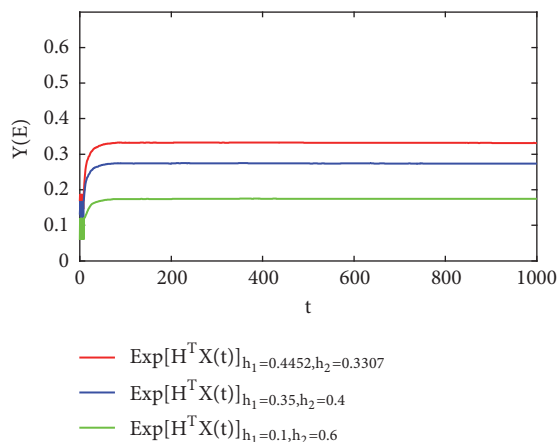


FIGURE 2: The optimal harvesting effort and the maximum of ESY are given in Theorem 9. Red line is with  $h_1 = 0.4452$ ,  $h_2 = 0.3307$ , blue line is with  $h_1 = 0.35$ ,  $h_2 = 0.4$  and green line is with  $h_1 = 0.1$ ,  $h_2 = 0.6$ .

one predator are persistent in mean while another predator is extinct when  $\rho_2 > 1 > \rho_3$ . We can find that only the prey is persistent in mean and the two predators are extinct when  $\rho_1 > 1 > \rho_2$ ; see Figure 1(c). It is obvious that all three species are extinct when  $\rho_1 < 1$ ; see Figure 1(d).

Regarding the optimal harvesting effort, when  $a_{22} = 1.9 > a_{23}e^{-d_{23}\tau_{23}} = 0.6$ ,  $a_{33} = 2.1 > a_{32}e^{-d_{32}\tau_{32}} = 1$ , it is not difficult to estimate that  $P^{-1} + (P^{-1})^T$  is positive definite. Note that  $\Lambda = [P(P^{-1})^T + I]^{-1}Q$ , and we can observe  $\Lambda = (\lambda_1, \lambda_2)^T = (0.4452, 0.3307)^T$ . Then we can find  $\Gamma_2 > 0$ ,  $\Gamma_3 > 0$ . The conditions in Theorem 9 hold; therefore, we have  $h_1 = \lambda_1 = 0.4452$ ,  $h_2 = \lambda_2 = 0.3307$ , and  $Y^* = \Lambda^T P^{-1}(Q - \Lambda) = 0.31$ . Thus the optimal harvesting policy exists (see Figure 2).

In Figure 2, we illustrate not only the optimal harvesting policy but also another two harvesting policies. It is conspicuous that the optimal harvesting policy leads to the maximum of expectation of sustainable yield.

Based on the theoretical analysis and numerical simulations, we present the main biological and ecological meanings of our results.

(1) The perturbations we considered are not only Gaussian white noises but also Lévy jump. The results reveal that the Lévy jump may significantly affect the optimal harvesting effort and the maximum of ESY.

(2) Time delay is imperative in the ecological environment. It has significant relationship with the persistence in mean and optimal harvesting policy of model (5).

(3) We have investigated not only environmental disturbance on the species but harvesting effort affected by human and social factors. The results provide theoretical references for some modern fields, such as fishery management. It is beneficial for people to make a rational exploitation and derive maximum profit.

As a matter of fact, with the environmental pollution continually becoming worse, it is significant to consider the species in the polluted environment [4, 33]. There is no exaggeration that plenty of interesting topics deserve further

investigations, for example, nonautonomous system, Markov process, impulsive effect, and partial differential system [40, 52–56]. We leave these for future investigations.

## Data Availability

No data were used to support this study.

## Conflicts of Interest

The authors declare that there are no conflicts of interest regarding the publication of this paper.

## Acknowledgments

This work was supported by the Research Fund for the Taishan Scholar Project of Shandong Province of China and SDUST Research Fund (2014TDJH102).

## References

- [1] X. Meng, N. L. Lundström, M. Bodin, and Å. Brännström, “Dynamics and management of stage-structured fish stocks,” *Bulletin of Mathematical Biology*, vol. 75, no. 1, pp. 1–23, 2013.
- [2] M. P. Hassell, “Density dependence in single-species population,” *Journal of Animal Ecology*, vol. 44, no. 1, pp. 283–295, 1975.
- [3] X. Y. Song and L. S. Chen, “Optimal harvesting and stability for a two-species competitive system with stage structure,” *Mathematical Biosciences*, vol. 170, no. 2, pp. 173–186, 2001.
- [4] Y. J. Li and X. Z. Meng, “Dynamics of an impulsive stochastic nonautonomous chemostat model with two different growth rates in a polluted environment,” *Discrete Dynamics in Nature and Society*, vol. 2019, 9 pages, 2019.
- [5] A. Hastings and T. Powell, “Chaos in a three-species food chain,” *Ecology*, vol. 72, no. 3, pp. 896–903, 1991.
- [6] S. Ahmad and I. M. Stamova, “Almost necessary and sufficient conditions for survival of species,” *Nonlinear Analysis: Real World Applications*, vol. 5, no. 1, pp. 219–229, 2004.
- [7] X. Fan, Y. Song, and W. Zhao, “Modeling cell-to-cell spread of HIV-1 with nonlocal infections,” *Complexity*, vol. 2018, 10 pages, 2018.
- [8] W. Wang, Y. Cai, J. Li, and Z. Gui, “Periodic behavior in a FIV model with seasonality as well as environment fluctuations,” *Journal of The Franklin Institute*, vol. 354, no. 16, pp. 7410–7428, 2017.
- [9] M. Mimura and J. D. Murray, “On a diffusive prey-predator model which exhibits patchiness,” *Journal of Theoretical Biology*, vol. 75, no. 3, pp. 249–262, 1978.
- [10] W. Zuo and D. Jiang, “Periodic solutions for a stochastic non-autonomous Holling-Tanner predator-prey system with impulses,” *Nonlinear Analysis: Hybrid Systems*, vol. 22, pp. 191–201, 2016.
- [11] M. Chi and W. Zhao, “Dynamical analysis of multi-nutrient and single microorganism chemostat model in a polluted environment,” *Advances in Difference Equations*, vol. 2018, p. 120, 2018.
- [12] T. Zhang, X. Meng, Y. Song, and T. Zhang, “A stage-structured predator-prey SI model with disease in the prey and impulsive effects,” *Mathematical Modelling and Analysis*, vol. 18, no. 4, pp. 505–528, 2013.

- [13] M. Wang, "On some free boundary problems of the prey-predator model," *Journal of Differential Equations*, vol. 256, no. 10, pp. 3365–3394, 2014.
- [14] X.-Z. Meng, S.-N. Zhao, and W.-Y. Zhang, "Adaptive dynamics analysis of a predator-prey model with selective disturbance," *Applied Mathematics and Computation*, vol. 266, pp. 946–958, 2015.
- [15] Y. Zhang, S. Chen, S. Gao, and X. Wei, "Stochastic periodic solution for a perturbed non-autonomous predator-prey model with generalized nonlinear harvesting and impulses," *Physica A: Statistical Mechanics and its Applications*, vol. 486, pp. 347–366, 2017.
- [16] Y. Tian, T. Zhang, and K. Sun, "Dynamics analysis of a pest management prey-predator model by means of interval state monitoring and control," *Nonlinear Analysis: Hybrid Systems*, vol. 23, pp. 122–141, 2017.
- [17] S. Zhang, X. Meng, T. Feng, and T. Zhang, "Dynamics analysis and numerical simulations of a stochastic non-autonomous predator-prey system with impulsive effects," *Nonlinear Analysis: Hybrid Systems*, vol. 26, pp. 19–37, 2017.
- [18] E. Beretta and Y. Takeuchi, "Global stability of single-species diffusion Volterra models with continuous time delays," *Bulletin of Mathematical Biology*, vol. 49, no. 4, pp. 431–448, 1987.
- [19] A. Bahar and X. Mao, "Stochastic delay population dynamics," *International Journal of Pure and Applied Mathematics*, vol. 11, no. 4, pp. 377–400, 2004.
- [20] K. Gopalsamy, *Stability and Oscillations in Delay Differential Equation of Population Dynamics*, vol. 74 of *Mathematics and Its Applications*, Kluwer Academic, Dordrecht, the Netherlands, 1992.
- [21] J. Zhou, C. Sang, X. Li, M. Fang, and Z. Wang, "H<sub>∞</sub> consensus for nonlinear stochastic multi-agent systems with time delay," *Applied Mathematics and Computation*, vol. 325, pp. 41–58, 2018.
- [22] M. Liu, C. Bai, and Y. Jin, "Population dynamical behavior of a two-predator one-prey stochastic model with time delay," *Discrete and Continuous Dynamical Systems - Series A*, vol. 37, no. 5, pp. 2513–2538, 2017.
- [23] M. Liu and M. Fan, "Stability in distribution of a three-species stochastic cascade predator-prey system with time delays," *IMA Journal of Applied Mathematics*, vol. 82, no. 2, pp. 396–423, 2017.
- [24] G. Liu, X. Wang, X. Meng, and S. Gao, "Extinction and persistence in mean of a novel delay impulsive stochastic infected predator-prey system with jumps," *Complexity*, vol. 2017, Article ID 1950970, 15 pages, 2017.
- [25] M. Liu, X. He, and J. Yu, "Dynamics of a stochastic regime-switching predator-prey model with harvesting and distributed delays," *Nonlinear Analysis: Hybrid Systems*, vol. 28, pp. 87–104, 2018.
- [26] X. Xie and M. Jiang, "Output feedback stabilization of stochastic feedforward nonlinear time-delay systems with unknown output function," *International Journal of Robust and Nonlinear Control*, vol. 28, no. 1, pp. 266–280, 2018.
- [27] Y. Wang, Z. Pan, Y. Li, and W. Zhang, "H<sub>∞</sub> control for nonlinear stochastic Markov systems with time-delay and multiplicative noise," *Journal of Systems Science & Complexity*, vol. 30, no. 6, pp. 1293–1315, 2017.
- [28] M.-M. Jiang, K.-M. Zhang, and X.-J. Xie, "Output feedback stabilisation of stochastic nonlinear time-delay systems with unknown output function," *International Journal of Systems Science*, vol. 48, no. 11, pp. 2262–2271, 2017.
- [29] X. Meng, F. Li, and S. Gao, "Global analysis and numerical simulations of a novel stochastic eco-epidemiological model with time delay," *Applied Mathematics and Computation*, vol. 339, pp. 701–726, 2018.
- [30] J. R. Beddington and R. M. May, "Harvesting natural populations in a randomly fluctuating environment," *Science*, vol. 197, no. 4302, pp. 463–465, 1977.
- [31] M. G. Neubert, "Marine reserves and optimal harvesting," *Ecology Letters*, vol. 6, no. 9, pp. 843–849, 2003.
- [32] Z. Jiang, W. Zhang, J. Zhang, and T. Zhang, "Dynamical analysis of a phytoplankton—zooplankton system with harvesting term and holling III functional response," *International Journal of Bifurcation and Chaos*, vol. 28, no. 13, Article ID 1850162, 23 pages, 2018.
- [33] Y. Zhao and S. Yuan, "Optimal harvesting policy of a stochastic two-species competitive model with Lévy noise in a polluted environment," *Physica A: Statistical Mechanics and its Applications*, vol. 477, pp. 20–33, 2017.
- [34] W. X. Li and K. Wang, "Optimal harvesting policy for general stochastic logistic population model," *Journal of Mathematical Analysis and Applications*, vol. 368, no. 2, pp. 420–428, 2010.
- [35] K. Tran and G. Yin, "Optimal harvesting strategies for stochastic competitive Lotka-Volterra ecosystems," *Automatica*, vol. 55, pp. 236–246, 2015.
- [36] L. H. R. Alvarez and L. A. Shepp, "Optimal harvesting of stochastically fluctuating populations," *Journal of Mathematical Biology*, vol. 37, no. 2, pp. 155–177, 1998.
- [37] T. T. Ma, X. Z. Meng, and Z. B. Chang, "Chang, Dynamics and optimal harvesting control for a stochastic one-predator-two-prey time delay system with jumps," *Complexity*, vol. 2019, 2019.
- [38] J. Bao, X. Mao, G. Yin, and C. Yuan, "Competitive Lotka-Volterra population dynamics with jumps," *Nonlinear Analysis: Theory, Methods & Applications*, vol. 74, no. 17, pp. 6601–6616, 2011.
- [39] A. La Cognata, D. Valenti, A. A. Dubkov, and B. Spagnolo, "Dynamics of two competing species in the presence of Lévy noise sources," *Physical Review E: Statistical, Nonlinear, and Soft Matter Physics*, vol. 82, no. 1, Article ID 011121, pp. 1–9, 2010.
- [40] C. Tan and W. H. Zhang, "On observability and detectability of continuous-time stochastic Markov jump systems," *Journal of Systems Science & Complexity*, vol. 28, no. 4, pp. 830–847, 2015.
- [41] Q. Liu, D. Jiang, N. Shi, T. Hayat, and A. Alsaedi, "Stochastic mutualism model with Levy jumps," *Communications in Nonlinear Science and Numerical Simulation*, vol. 43, pp. 78–90, 2017.
- [42] Q. Liu, D. Jiang, N. Shi, and T. Hayat, "Dynamics of a stochastic delayed SIR epidemic model with vaccination and double diseases driven by Lévy jumps," *Physica A: Statistical Mechanics and its Applications*, vol. 492, pp. 2010–2018, 2018.
- [43] X. Leng, T. Feng, and X. Meng, "Stochastic inequalities and applications to dynamics analysis of a novel SIVS epidemic model with jumps," *Journal of Inequalities and Applications*, vol. 2017, no. 138, pp. 1–25, 2017.
- [44] D. Applebaum, *Lévy Processes and Stochastic Calculus*, Cambridge University Press, Cambridge, UK, 2nd edition, 2009.
- [45] K. Sato, *Lévy Processes and Infinitely Divisible Distributions*, Cambridge University Press, Cambridge, UK, 1999.
- [46] X. Zou and K. Wang, "Optimal harvesting for a stochastic N-dimensional competitive Lotka-Volterra model with jumps," *Discrete and Continuous Dynamical Systems - Series B*, vol. 20, no. 2, pp. 683–701, 2015.

- [47] N. Ikeda and S. Watanabe, "A comparison theorem for solutions of stochastic differential equations and its applications," *Osaka Journal of Mathematics*, vol. 14, no. 3, pp. 619–633, 1977.
- [48] D. Jiang and N. Shi, "A note on nonautonomous logistic equation with random perturbation," *Journal of Mathematical Analysis and Applications*, vol. 303, no. 1, pp. 164–172, 2005.
- [49] M. Liu, H. Qiu, and K. Wang, "A remark on a stochastic predator-prey system with time delays," *Applied Mathematics Letters*, vol. 26, no. 3, pp. 318–323, 2013.
- [50] G. Da Prato and J. Zabczyk, *Ergodicity for Infinite Dimensional System*, vol. 229, Cambridge University Press, Cambridge, UK, 1996.
- [51] Y. Xu, H. Zhou, and W. X. Li, "Stabilization of stochastic delayed systems with Lévy noise on networks via periodically intermittent control," *International Journal of Control*, vol. 2018, pp. 1–24, 2018.
- [52] H. Qi, L. Liu, and X. Meng, "Dynamics of a nonautonomous stochastic sis epidemic model with double epidemic hypothesis," *Complexity*, vol. 2017, Article ID 4861391, 14 pages, 2017.
- [53] F. Bian, W. Zhao, Y. Song, and R. Yue, "Dynamical analysis of a class of prey-predator model with beddington-deangelis functional response, stochastic perturbation, and impulsive toxicant input," *Complexity*, vol. 2017, 18 pages, 2017.
- [54] H. K. Qi, X. N. Leng, X. Z. Meng, and T. H. Zhang, "Periodic solution and ergodic stationary distribution of SEIS Dynamical systems with active and latent patients," *Qualitative Theory of Dynamical Systems*, vol. 2018, pp. 1–23, 2018.
- [55] W. Wang and T. Zhang, "Caspase-1-mediated pyroptosis of the predominance for driving  $CD_4^+$  T cells death: a nonlocal spatial mathematical model," *Bulletin of Mathematical Biology*, vol. 80, no. 3, pp. 540–582, 2018.
- [56] M. Guo, H. Dong, J. Liu, and H. Yang, "The time-fractional mZK equation for gravity solitary waves and solutions using sech-tanh and radial basis function method," *Nonlinear Analysis: Modelling and Control*, vol. 24, no. 1, pp. 1–19, 2018.

## Research Article

# Nonlinear Hybrid Multipoint Model of High-Speed Train with Traction/Braking Dynamic and Speed Estimation Law

Chao Jia <sup>1</sup>, Hongze Xu,<sup>1</sup> and Longsheng Wang<sup>2</sup>

<sup>1</sup>School of Electronic and Information Engineering, Beijing Jiaotong University, Beijing, 100044, China

<sup>2</sup>Signal & Communication Research Institute, China Academy of Railway Sciences, Beijing, 100081, China

Correspondence should be addressed to Chao Jia; 15111015@bjtu.edu.cn

Received 7 September 2018; Accepted 31 December 2018; Published 17 January 2019

Academic Editor: Jorge Rivera

Copyright © 2019 Chao Jia et al. This is an open access article distributed under the Creative Commons Attribution License, which permits unrestricted use, distribution, and reproduction in any medium, provided the original work is properly cited.

This paper establishes a NHMPM (Nonlinear Hybrid Multipoint Model) for HST (High-Speed Train) with the traction/braking dynamic and speed estimation law. Firstly, a full-order flux observer is designed using regional pole assignment theory to calculate the electromagnetic torque. The traction and braking forces are obtained according to this electromagnetic torque. Then the basic running resistance force is reformulated by considering the aerodynamic drag distribution characteristics, and the nonlinear in-train coupling force is analyzed as well. Next, the NHMPM including integer variables of running status and car types is built, where an adaptive parameter estimation algorithm and a speed estimation law are proposed to estimate unknown resistance coefficients and train speed, respectively. The effectiveness of the proposed algorithm, law, and NHMPM is verified through numerical simulations last.

## 1. Introduction

HST can operate safely and efficiently mainly depending on the performance of ATO (Automatic Train Operation) system, and the accurate dynamic model is the first step-stone for designing ATO control law [1]; therefore, many researchers have paid more attention to it during the past few decades [2–13]. There are mainly two types of models: single-point model and multipoint model. The former model ignores in-train dynamics and considers the train as a single mass point [2], which is widely used in energy saving optimization [3], automatic driving [4], and precise stopping [5]. However, the train is connected by couplers to transmit large traction and braking force, and this nonlinear force has a strong effect on the longitudinal motion of HST [6]. Therefore, it is necessary to consider the in-train dynamics that leads to the latter one.

The multipoint model was first introduced in 1990 [7] and then several scholars began to research on it [8–11]. In [8], a longitudinal multipoint model was established, in which the couplers were modelled as nonlinear springs, and the aerodynamic drag was assumed to act on the first car only. Reference [9] proposed a longitudinal model for heavy-haul

trains, which took the coupler system as a linear spring with damping to simplify the calculation, and the aerodynamic drag was processed in the same manner as [8]. Reference [10] proposed a single coordinate model to solve the problem that the in-train coupling force was difficult to measure and directly control. In [11], a hybrid integer train model that includes running status integer variable was proposed after piecewise linearization of the train running resistance force.

It is noted that in most existing work, the traction and braking force are treated as control variables; the dynamics of these two forces are ignored, and therefore, the actual dynamic characteristics of the train cannot be accurately reflected [12]. In a recent work, an attempt has been made in accounting for these two forces, where the traction and braking force are linked with the motor current by nonlinear relations and two single-point models about traction and braking dynamics are proposed, respectively, in [13]. It is worth noting that the traction motor is a high-order, strong coupling, multivariable nonlinear system, and a simply nonlinear function cannot describe the traction and braking dynamics comprehensively. In addition, the basic resistance force is obtained by DAVIS formula and the resistance coefficients are available in most existing works. Also, in order

to facilitate the design of the controller, the basic resistance force is linearized. However, the resistance coefficients are variable and unknown due to the change of the line condition and the external environment [14], and the aerodynamic drag is related not only to the speed and resistance coefficients of the train, but also to the location of the car in practice [15].

Furthermore, train speed is the premise of completing ATO control. However, the installation of speed sensors increases the system cost, reduces the reliability of the system, and is not suitable for operating in a harsh environment [16]. By contrast, speed sensorless technology can identify the motor speed from easily measured physical quantities (stator voltage or stator current, for example) [17] and the train speed is obtained through the linear relation between these two speeds. In recent years, full-order flux observer method has received the widespread attention [18–22]. Generally, in order to make the observer converge faster than the traction motor, the observer gain matrix is designed such that the poles of the observer are  $k$  times more than the motor model. Reference [18] presented a method to estimate the motor speed based on adaptive flux observer, and let  $k = 1$ , but it caused the system to be unstable in low-speed range. Thus, [19] linearized the observer at the equilibrium point and increased the speed term; the range of  $k$  that can guarantee the stability of the system was obtained using the Routh stability criterion. An adaptive speed identification scheme for induction motor based on the hyperstability theory was proposed and  $k = 1.2$  was chosen in [20]. In [21], the adaptive speed estimation for IM was analyzed, the necessary and sufficient conditions for stability of the speed estimation system were derived as well. And, furthermore, a novel observer gain was designed to guarantee the stability over the whole speed range by Lyapunov theory in [22]. However, if the observer gain is designed by traditional exact pole assignment method, it will limit the damping speed, deteriorate robustness, and be hard to satisfy multiple performances in some practical applications [23], such as robotic arm movement model [24], uniform damping control of low-frequency oscillations in power system [25], aircraft carrier landing control system [26], and flexible buildings [27]. Therefore, circularly regional pole assignment can be adopted to design the observer gain, which can make the observer have more degrees of freedom.

In this paper, traction and braking dynamics are described in detail, the basic resistance force is reformulated by considering aerodynamic drag distribution characteristics, and the nonlinear in-train coupling force is analyzed as well; the NHMPM including integer variables of running status and car types (locomotives or carriages) is built. An adaptive parameter estimation algorithm and a speed estimated law are proposed to provide unknown resistance coefficients and train speed required in the model, respectively.

The rest of this paper is organized as follows. In Section 2, traction and braking dynamics are discussed. Section 3 reformulates the basic resistance force and analyzes the nonlinear in-train coupling force. In Section 4, integer variables are introduced to represent running status and car types, and the NHMPM is derived, where an adaptive parameter estimation algorithm and speed estimation law are proposed to provide

unknown resistance coefficients and train speed required in the model, respectively. Simulation is conducted in Section 5, and Section 6 draws the conclusion.

## 2. Traction and Braking Dynamics

*2.1. Full-Order Flux Observer.* The traction motor nominal model is described as the following equation in the stationary reference frame.

$$\begin{aligned} \dot{\mathbf{x}}_s &= \mathbf{A}_{m0}\mathbf{x}_s + \mathbf{B}_m\mathbf{u}_s, \\ \mathbf{y}_s &= \mathbf{i}_s = \mathbf{C}_m\mathbf{x}_s. \end{aligned}$$

$$\mathbf{A}_{m0} = \begin{bmatrix} -\lambda(R_{s0}L_r + R_{r0}L_s)\mathbf{I} + \omega_{r0}\mathbf{J} & \lambda R_{r0}\mathbf{I} - \lambda L_r\omega_{r0}\mathbf{J} \\ -R_{s0}\mathbf{I} & \mathbf{0} \end{bmatrix}$$

$$= \begin{bmatrix} \mathbf{A}_{11} & \mathbf{A}_{12} \\ \mathbf{A}_{21} & \mathbf{0} \end{bmatrix} = \begin{bmatrix} a_{11}\mathbf{I} + a'_{11}\mathbf{J} & a_{12}\mathbf{I} + a'_{12}\mathbf{J} \\ a_{21}\mathbf{I} & \mathbf{0} \end{bmatrix},$$

$$\mathbf{B}_m = \begin{bmatrix} b_1\mathbf{I} \\ \mathbf{I} \end{bmatrix} = \begin{bmatrix} \lambda L_r\mathbf{I} \\ \mathbf{I} \end{bmatrix}, \quad (1)$$

$$\mathbf{C}_m = [\mathbf{I} \ \mathbf{0}],$$

$$\mathbf{I} = \begin{bmatrix} 1 & 0 \\ 0 & 1 \end{bmatrix},$$

$$\mathbf{J} = \begin{bmatrix} 0 & -1 \\ 1 & 0 \end{bmatrix},$$

$$\mathbf{0} = \begin{bmatrix} 0 & 0 \\ 0 & 0 \end{bmatrix}.$$

Here,  $\mathbf{x}_s = [\mathbf{i}_s \ \boldsymbol{\psi}_s]^T$ ;  $\mathbf{i}_s = [i_{s\alpha} \ i_{s\beta}]^T$  is stator current;  $\boldsymbol{\psi}_s = [\psi_{s\alpha} \ \psi_{s\beta}]^T$  is stator flux;  $\mathbf{u}_s = [u_{s\alpha} \ u_{s\beta}]^T$  is stator voltage;  $R_s$  is stator resistance;  $R_r$  is rotor resistance;  $L_s$  is stator inductance;  $L_r$  is rotor inductance;  $L_m$  is mutual inductance;  $\lambda = 1/(L_sL_r - L_m^2)$ ;  $\omega_r$  is motor angular speed.

### 2.2. Observer Gain Matrix

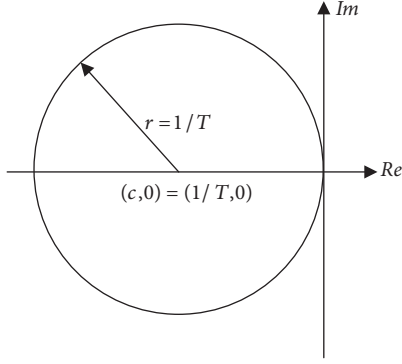
*Definition 1.* For the sake of simplicity, let us introduce the following notations.

$$\mathbf{A}_{ma} = \frac{(\mathbf{A}_{m0} - c\mathbf{I})}{r}, \quad (2)$$

$$\mathbf{C}_{mr} = \frac{\mathbf{C}_m}{r}.$$

$$\mathbf{A}_{mae} = \frac{(\mathbf{A}_{m0} + \mathbf{G}\mathbf{C}_m - c\mathbf{I})}{r}. \quad (3)$$

Here,  $(c, 0)$  is the center of  $D(c, r)$  and  $r$  is radius of  $D(c, r)$  as shown in Figure 1.  $\mathbf{G}$  is observer gain matrix.

FIGURE 1: Circular region  $D(c, r)$ .

Take  $\hat{\mathbf{x}}_s = [\hat{\mathbf{i}}_s \ \hat{\boldsymbol{\psi}}_s]^T$  as the state variable of the observer; the full-order flux observer of traction motor can be written as

$$\dot{\hat{\mathbf{x}}}_s = \mathbf{A}_{m0}\hat{\mathbf{x}}_s + \mathbf{B}_m\mathbf{u}_s + \mathbf{G}(\hat{\mathbf{y}}_s - \mathbf{y}_s) \quad (4)$$

where “ $\hat{\cdot}$ ” denotes observed quantities;  $\hat{\mathbf{y}}_s = \hat{\mathbf{i}}_s = \mathbf{C}_m\hat{\mathbf{x}}_s$ . Using (1) and (4), the actual state estimation error system is

$$\dot{\mathbf{e}} = (\mathbf{A}_{m0} + \mathbf{G}\mathbf{C}_m)\mathbf{e}. \quad (5)$$

Here,  $\mathbf{e} = \hat{\mathbf{x}}_s - \mathbf{x}_s$ .  $\mathbf{G}$  is designed such that all the poles of the observer are assigned in circular region  $D(c, r)$ ; the circular region can be expressed as

$$\left(k_{\max}\sigma_i + \frac{1}{T}\right)^2 + (k_{\max}\Omega_i)^2 \leq \left(\frac{1}{T}\right)^2. \quad (6)$$

Here,  $\sigma_i, \Omega_i$  are the real part and the imaginary part of the  $i_{th}$  pole of the motor model, and they satisfy

$$s_i = \{\sigma_i + j\Omega_i \mid \Omega_i = \max(|\Omega_1|, |\Omega_3|)\}, \quad i = 1, 3. \quad (7)$$

$T$  is the sampling period, and it satisfies the following inequality.

$$T \leq T_c \leq \frac{-2\sigma_i}{\sigma_i^2 + \Omega_i^2}. \quad (8)$$

And  $k_{\max} = -2\sigma_i/T_c(\sigma_i^2 + \Omega_i^2)$ .

**Theorem 2.** Let  $\mathbf{R}$  be a positive definite symmetric matrix of appropriate dimensions. All the eigenvalues of  $\mathbf{A}_{m0} + \mathbf{G}\mathbf{C}_m$  belong to  $D(c, r)$  and the state estimation error system (5) is stable under an observer gain matrix  $\mathbf{G}$  if and only if there exists a positive  $\mathbf{P}$  satisfying the following inequality

$$\begin{bmatrix} -\mathbf{P} & \mathbf{P}\mathbf{A}_{ma} \\ \mathbf{A}_{ma}^T\mathbf{P} & -\mathbf{P} - \mathbf{C}_{mr}^T\mathbf{R}^{-1}\mathbf{C}_{mr} \end{bmatrix} < 0. \quad (9)$$

Then the observer gain matrix  $\mathbf{G}$  is given by

$$\mathbf{G} = -\mathbf{A}_{ma}(\mathbf{P} + \mathbf{C}_{mr}^T\mathbf{R}^{-1}\mathbf{C}_{mr})^{-1}\mathbf{C}_{mr}^T\mathbf{R}^{-1}. \quad (10)$$

*Proof.* By Schur Complement Lemma in [28], (9) implies

$$\mathbf{P}\mathbf{A}_{ma}(\mathbf{P} + \mathbf{C}_{mr}^T\mathbf{R}^{-1}\mathbf{C}_{mr})^{-1}\mathbf{A}_{ma}^T\mathbf{P} - \mathbf{P} < 0. \quad (11)$$

Multiplying  $\mathbf{P}^{-1}$  by both sides of inequality (11), we can get

$$\mathbf{A}_{ma}(\mathbf{P} + \mathbf{C}_{mr}^T\mathbf{R}^{-1}\mathbf{C}_{mr})^{-1}\mathbf{A}_{ma}^T - \mathbf{P}^{-1} < 0. \quad (12)$$

And there exists a positive definite symmetric matrix  $\mathbf{Q}$  such that

$$\mathbf{A}_{ma}(\mathbf{P} + \mathbf{C}_{mr}^T\mathbf{R}^{-1}\mathbf{C}_{mr})^{-1}\mathbf{A}_{ma}^T - \mathbf{P}^{-1} + \mathbf{Q} = 0. \quad (13)$$

Let

$$\mathbf{V} = \mathbf{A}_{mae}\mathbf{P}^{-1}\mathbf{A}_{mae}^T - \mathbf{P}^{-1}. \quad (14)$$

According to (13), we have

$$\mathbf{P}^{-1} = \mathbf{A}_{ma}(\mathbf{P} + \mathbf{C}_{mr}^T\mathbf{R}^{-1}\mathbf{C}_{mr})^{-1}\mathbf{A}_{ma}^T + \mathbf{Q}. \quad (15)$$

Substituting (15) into (14) leads to

$$\begin{aligned} \mathbf{V} &= \mathbf{A}_{mae}\mathbf{P}^{-1}\mathbf{A}_{mae}^T - \mathbf{A}_{ma}(\mathbf{P} + \mathbf{C}_{mr}^T\mathbf{R}^{-1}\mathbf{C}_{mr})^{-1}\mathbf{A}_{ma}^T \\ &\quad - \mathbf{Q}. \end{aligned} \quad (16)$$

Now denote  $\mathbf{U} = \mathbf{A}_{ma}(\mathbf{P} + \mathbf{C}_{mr}^T\mathbf{R}^{-1}\mathbf{C}_{mr})^{-1}$  and notice that

$$\begin{aligned} \mathbf{A}_{ma}(\mathbf{P} + \mathbf{C}_{mr}^T\mathbf{R}^{-1}\mathbf{C}_{mr})^{-1}\mathbf{A}_{ma}^T \\ = \mathbf{U}\mathbf{C}_{mr}^T\mathbf{R}^{-1}\mathbf{C}_{mr}\mathbf{U}^T + \mathbf{U}\mathbf{P}\mathbf{U}^T. \end{aligned} \quad (17)$$

Equation (16) is now given by

$$\mathbf{V} = \mathbf{A}_{mae}\mathbf{P}^{-1}\mathbf{A}_{mae}^T - \mathbf{U}\mathbf{C}_{mr}^T\mathbf{R}^{-1}\mathbf{C}_{mr}\mathbf{U}^T - \mathbf{U}\mathbf{P}\mathbf{U}^T - \mathbf{Q}. \quad (18)$$

When (19) is satisfied,

$$\begin{aligned} \mathbf{G} &= -\mathbf{A}_{ma}(\mathbf{P} + \mathbf{C}_{mr}^T\mathbf{R}^{-1}\mathbf{C}_{mr})^{-1}\mathbf{C}_{mr}^T\mathbf{R}^{-1} \\ &= -\mathbf{U}\mathbf{C}_{mr}^T\mathbf{R}^{-1}, \end{aligned} \quad (19)$$

we have

$$\mathbf{A}_{mae}\mathbf{P}^{-1}\mathbf{A}_{mae}^T = \mathbf{U}\mathbf{P}\mathbf{U}^T. \quad (20)$$

And then

$$\begin{aligned} \mathbf{V} &= \mathbf{U}\mathbf{P}\mathbf{U}^T - \mathbf{U}\mathbf{C}_{mr}^T\mathbf{R}^{-1}\mathbf{C}_{mr}\mathbf{U}^T - \mathbf{U}\mathbf{P}\mathbf{U}^T - \mathbf{Q} \\ &= -\mathbf{U}\mathbf{C}_{mr}^T\mathbf{R}^{-1}\mathbf{C}_{mr}\mathbf{U}^T - \mathbf{Q} = -(\mathbf{G}\mathbf{R}\mathbf{G}^T + \mathbf{Q}) < 0. \end{aligned} \quad (21)$$

That is,

$$\mathbf{V} = \mathbf{A}_{mae}\mathbf{P}^{-1}\mathbf{A}_{mae}^T - \mathbf{P}^{-1} < 0. \quad (22)$$

Or equivalently

$$\mathbf{A}_{mae}^T\mathbf{P}\mathbf{A}_{mae} - \mathbf{P} < 0. \quad (23)$$

That is, by Lemma 1 of [23], all the eigenvalues of  $\mathbf{A}_{m0} + \mathbf{G}\mathbf{C}_m$  belong to  $D(c, r)$ , the error system is stable, and the proof is completed.  $\square$

Then the electromagnetic torque is obtained by the following equation.

$$T_e = n_p (\widehat{\psi}_s^T J i_s) = n_p (\widehat{\psi}_{s\beta} i_{s\alpha} - \widehat{\psi}_{s\alpha} i_{s\beta}). \quad (24)$$

Here,  $n_p$  denotes the number of pole-pairs of traction motor; the electromagnetic torque is different when the train run in traction mode or braking mode, and we denote them as  $T_{et}$  and  $T_{eb}$ , respectively.

**2.3. Traction Force and Braking Force.** In this paper, we assume that the traction force and braking force of HST are all from the electromagnetic torque of traction motor, and they are linked with the motor stator voltage by a nonlinear relation. This nonlinear relation can be written as

$$\begin{aligned} F_{ti} &= \frac{2N_m a \eta}{D} T_{eti} = K_{ti} n_p (\widehat{\psi}_{s\beta} i_{s\alpha} - \widehat{\psi}_{s\alpha} i_{s\beta}) \\ &= K_{ti} \cdot h'_t(u_{si}), \\ F_{bi} &= \frac{2N_m a \eta}{D} T_{ebi} = K_{bi} n_p (\widehat{\psi}_{s\beta} i_{s\alpha} - \widehat{\psi}_{s\alpha} i_{s\beta}) \\ &= K_{bi} \cdot h'_b(u_{si}), \quad i = 1, 2, 3 \dots p. \end{aligned} \quad (25)$$

Here,  $F_{ti}$ ,  $F_{bi}$  are traction force and braking force of  $i_{th}$  car, respectively;  $N_m$  is the number of traction motors;  $a$  is gear ratio;  $\eta$  is transmission efficiency;  $p$  is the number of the locomotives;  $D$  is the diameter of half-worn wheel rolling circle.

### 3. Running Resistance Force and In-Train Coupling Force

In this section, the basic running resistance force is reformulated by analyzing the aerodynamic drag distribution characteristics, and the nonlinear in-train coupling force of each car is described simultaneously.

**3.1. Running Resistance Force with Aerodynamic Resistance Distribution.** The running resistance force  $f_{ri}$  of each car consists of the basic running resistance force  $f_{bi}$  and additional running resistance force  $f_{ai}$ ; the empirical formula (DAVIS formula) is

$$\begin{aligned} f_{ri} &= f_{bi} + f_{ai} \\ &= \underbrace{m_i (c_0 + c_v v_i)}_{\text{rolling resistance force}} + \underbrace{m_i c_a v_i^2}_{\text{aerodynamic drag}} + f_{ai}, \end{aligned} \quad (26)$$

$$i = 1, 2, 3 \dots n.$$

Here,  $m_i$ ,  $v_i$  are the mass and speed of the  $i_{th}$  car, respectively;  $c_0$ ,  $c_v$ ,  $c_a$  denote the resistance coefficients, which are related to the HST type;  $f_{ai}$  includes gradient, tunnel, and curve resistance force. The rolling resistance force is dominant in low-speed range and as the speed increases, the aerodynamic drag becomes dominant.

In fact, the aerodynamic drag consists of friction drag and pressure drag, which account for 24.7% and 75.3%

TABLE 1: The parameters of CRH3.

Symbol	Value	Unit
$m_1 - m_8$	672,69.6,68.8,63.2, 60.8,68.8,69.6,68	t
$k_1 - k_8$	16.1, 19.7, 7.5,9.6, 10.6,7.0,14.1,15.4	%
$c_0, c_v, c_a$	0.42,0.0016,0.000132	-

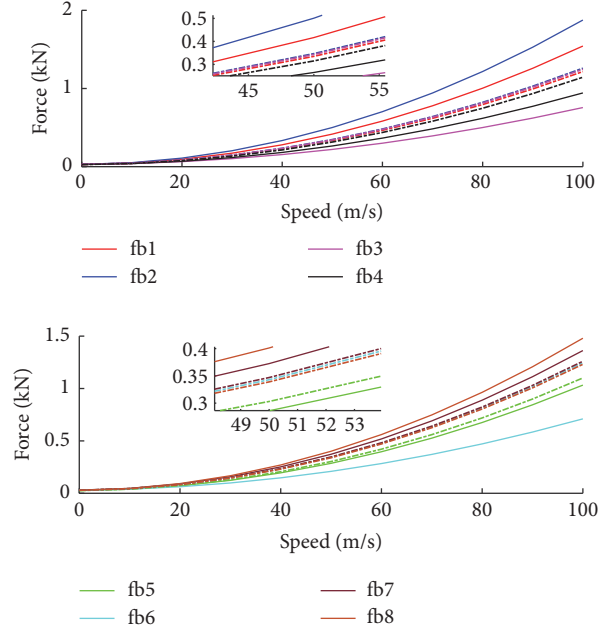


FIGURE 2: Basic running resistance force for CRH3.

of the total aerodynamic drag, respectively. Moreover, the aerodynamic drag of each car is not only related to its own mass and speed, but also related to the location of the car (the first car, the middle car, or the last car, for example) and whether to install air conditioning fairing, pantograph, and compartment connections, bogies, or other parts [15]. Therefore, the running resistance force can be reformulated as

$$f_{ri} = f_{bi} + f_{ai} = m_i (c_0 + c_v v_i) + k_{mi} M c_a v_i^2 + f_{ai}. \quad (27)$$

Here,  $M$  is the total mass of the train;  $k_{mi}$  is the percentage of aerodynamic drag of  $i_{th}$  car in the total aerodynamic drag.

Take CRH3 (China Railway High-Speed 3 series Electric Multiple Unit) as an example; the parameters of CRH3 are shown in Table 1. The basic running resistance force of each car is shown in Figure 2 when the speed varies from 0 m/s to 100 m/s (it is equivalent to the actual train speed from 0 km/h to 350 km/h). The dotted and solid lines represent the forces calculated by the first two items of (26) and (27), respectively.

In addition, the force deviation between these two formulas is shown in Figure 3. From Figure 3, we know that the basic running resistance force of each car has a large deviation before and after the formula modification, and the greater the speed, the larger the deviation. Moreover, the second car has the maximum deviation. Since the second and the seventh car are equipped with pantographs (see Figure 4), the pressure drag of these two cars is relatively greater than other cars

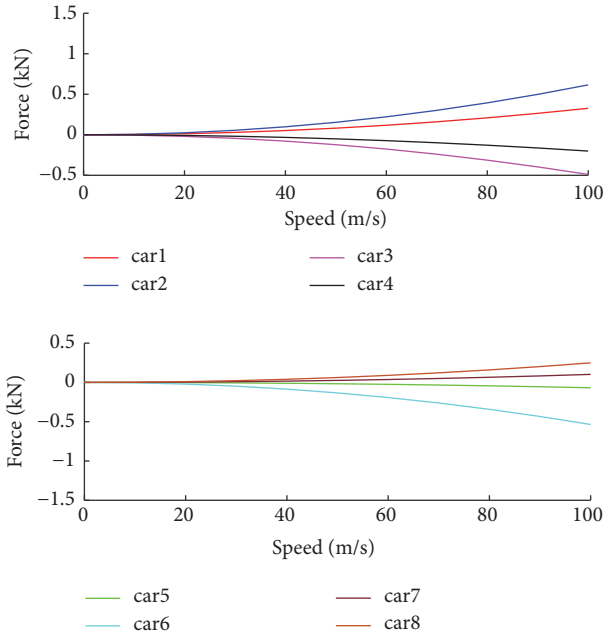


FIGURE 3: Basic running resistance force deviation between (26) and (27) of each car for CRH3.

without pantographs. Moreover, these two pantographs are installed opposite to each other, which results in two different wake flow fields; the intensity of the tail vortex induced by the second car's pantograph is stronger, which leads to the greater pressure drag than the seventh [15]. Thus, the second car has the largest aerodynamic drag and maximum deviation.

**3.2. In-Train Coupling Force.** A train is made up of many cars through springs; the coupling force is divided into two parts: spring part and damping part, and its dynamic equation can be written as

$$u_{ei} = \frac{\gamma \{ |\delta| (F_{ti} + F_{bi}) + \delta (F_{ti} - F_{bi}) \}}{2} = \frac{\gamma \{ |\delta| [K_{ti}h'_t(u_{si}) + K_{bi}h'_b(u_{si})] + \delta [K_{ti}h'_t(u_{si}) - K_{bi}h'_b(u_{si})] \}}{2} \quad (30)$$

$$i = 1, 2, 3, \dots, n; \quad \delta = -1, 0, 1.$$

Now we assume that the displacement of each car is the same when the coupler is not stressed. The force analysis of the other cars is the same except the first and the last car which

$$m_1 \dot{v}_1 = u_{e1} - f_{im12} - f_{r1}$$

$$= \frac{\gamma \{ |\delta| [K_{t1}h'_t(u_{s1}) + K_{b1}h'_b(u_{s1})] + \delta [K_{t1}h'_t(u_{s1}) - K_{b1}h'_b(u_{s1})] \}}{2} - k_0(x_1 - x_2) - k_0\mu(x_1 - x_2)^3$$

$$- k_d(v_1 - v_2) - m_1(c_0 + c_v v_1) - k_{m1} M c_a v_1^2 - f_{a1},$$

$$m_i \dot{v}_i = u_{ei} + f_{in(i-1)i} - f_{in(i)(i+1)} - f_{ri}$$

$$= \frac{\gamma \{ |\delta| [K_{ti}h'_t(u_{si}) + K_{bi}h'_b(u_{si})] + \delta [K_{ti}h'_t(u_{si}) - K_{bi}h'_b(u_{si})] \}}{2} + k_0(x_{i-1} - x_i) + k_0\mu(x_{i-1} - x_i)^3$$

$$f_{in(i)(i+1)} = \underbrace{k_{si}(x_i - x_{i+1})}_{\text{spring part}} + \underbrace{k_d(v_i - v_{i+1})}_{\text{damping part}}. \quad (28)$$

Here,  $f_{in(i)(i+1)}$  is the coupling force between the  $i_{th}$  car and the  $(i+1)_{th}$  car;  $x_i, x_{i+1}$  are displacement of the  $i_{th}$  car and  $(i+1)_{th}$  car, respectively;  $k_{si}, k_d$  are elastic coupling coefficient and damping coupling coefficient, respectively.  $k_{si}$  is the nonlinear function of displacement deviation, that is,

$$k_{si} = k_0 [1 + \mu(x_i - x_{i+1})^2] \quad i = 1, 2, \dots, n-1. \quad (29)$$

Here,  $k_0$  is constant;  $\mu = 0$  denotes linear spring, that is,  $k_{si} = k_0$ , which does not exist in practice;  $\mu < 0$  and  $\mu > 0$  denote softening spring and hardening spring, respectively [8].

#### 4. Nonlinear Multipoint Model of HST

In this section, NHMPM including integer variables of running status and car types is established, where an adaptive parameter estimation algorithm for estimating the unknown resistance coefficients is proposed and a train speed estimated law is derived to get train speed.

**4.1. Nonlinear Hybrid Multipoint Model of HST.** Take CRH3 as an example; it consists of four locomotives equipped with traction units (see Figure 4, the black wheels) and four carriages, and we define the output of traction units as  $u_e$ . Let  $\gamma = 1$  and  $\gamma = 0$  denote locomotives and carriages, respectively. In addition, we define "traction and cruise" states as "traction mode" because both of these two states require traction force; let  $\delta = 1$  denote this mode; define "coasting" and "braking" states as "coast mode" and "braking mode"; let  $\delta = 0$  and  $\delta = -1$  denote these two modes, respectively. Therefore, the output of the execution unit of the  $i_{th}$  car is described as

lack coupling force; the force analysis is shown for the fifth car in Figure 4. According to the Newton's second law, NHMPM can be expressed as (31).

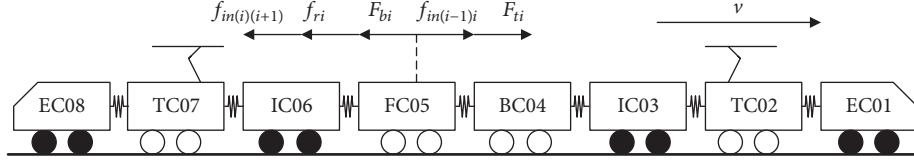


FIGURE 4: The framework of CRH3 series EMU and force analysis for one car.

$$+ k_d (v_{i-1} - v_i) - k_0 (x_i - x_{i+1}) - k_0 \mu (x_i - x_{i+1})^3 - k_d (v_i - v_{i+1}) - m_i (c_0 + c_v v_i) - k_{mi} M c_a v_i^2 - f_{ai},$$

$$(i = 2, 3, \dots, n-1;)$$

$$m_n \dot{v}_n = u_{en} + f_{in(n-1)n} - f_{rn}$$

$$= \frac{\gamma \{ |\delta| [K_{tn} h'_t(u_{sn}) + K_{bn} h'_b(u_{sn})] + \delta [K_{tn} h'_t(u_{sn}) - K_{bn} h'_b(u_{sn})] \}}{2} + k_0 (x_{n-1} - x_n) + k_0 \mu (x_{n-1} - x_n)^3$$

$$+ k_d (v_{n-1} - v_n) - m_n (c_0 + c_v v_n) - k_{mn} M c_a v_n^2 - f_{an} \quad (\gamma = 0, 1; \delta = -1, 0, 1)$$

$$\dot{x}_i = v_i \quad (i = 1, 2, 3, \dots, n)$$
(31)

Sequentially, input variable  $u := [u_{s1}, u_{s2} \dots u_{sn}]_{2n \times 1}^T$  and state variable  $x := [v_1, v_2 \dots v_n, x_1, x_2 \dots x_n]_{2n \times 1}^T$  are defined for transforming (31) to a nonlinear function form, where  $u_{si} = [u_{s\alpha i} \ u_{s\beta i}]^T$  is traction motor stator voltage of the  $i_{th}$  car. In addition, the additional resistance force of the train is not easy to describe in a mathematical form such that it will be regarded as an unknown and bounded disturbance term  $d$ ; furthermore the speed and displacement of the first car are taken as the output variable  $y := [v_1 \ x_1]^T$ . Therefore, (31) can be rewritten as the nonlinear function form.

$$\dot{x} = f'(x, u, d),$$

$$y = Cx. \quad (32)$$

Here,  $C = \begin{bmatrix} 1 & 0 & \dots & 0 & 0 & \dots & 0 \\ 0 & 0 & \dots & 0 & 1 & 0 & \dots & 0 \end{bmatrix}_{2 \times 2n}$ .

**4.2. Adaptive Parameter Estimation.** Resistance coefficients are unknown and time varying, which will affect the accuracy of the model in practice. In this section, an adaptive parameter estimation algorithm is proposed to estimate these coefficients online for NHMPM, and the algorithm is based on the idea of [29].

The nonlinear model (32) is modified as the following form.

$$\dot{x} = f'_0(x, u, d) + C_0 + C_v x + C_a x^2. \quad (33)$$

Here,  $K_m = \begin{bmatrix} k_{m1} & & & \\ & k_{m2} & & \\ & & \dots & \\ & & & k_{mn} \end{bmatrix}$ ,  $M_\Lambda = \begin{bmatrix} m_1 & & & \\ & m_2 & & \\ & & \dots & \\ & & & m_n \end{bmatrix}$ ,  $C_0 = \begin{bmatrix} c_0^p \\ 0_{n \times n} \end{bmatrix}$ ,  $C_v = \begin{bmatrix} C_v^p & 0_{n \times n} \\ 0_{n \times n} & 0_{n \times n} \end{bmatrix}$ ,  $C_a = \begin{bmatrix} (K_m M / M_\Lambda) C_a^p & 0_{n \times n} \\ 0_{n \times n} & 0_{n \times n} \end{bmatrix}$ ,  $C_0^p = -[c_0 \ c_0 \ \dots \ c_0]^T$ ,  $C_v^p = -\text{diag}(c_v, c_v, \dots, c_v)$ ,  $C_a^p = -\text{diag}(c_a, c_a, \dots, c_a)$ .

Now, we define the following vector.

$$O := [C_0, C_v, C_a]^T. \quad (34)$$

$$\Phi := [1, x, x^2]^T. \quad (35)$$

Then (33) can be rewritten as

$$\dot{x} = f'_0(x, u, d) + \Phi^T O. \quad (36)$$

In order to simplify the adaptive parameter estimated algorithm and improve the engineering practicability, the resistance coefficients of each car are assumed to be equal as the train is in the same environment most of the time. Thus, we use the equivalent single-point model to estimate the resistance coefficients. It can be described as

$$\dot{v}_e = f''_0(u_s, d_0) + \varphi^T \theta \quad (37a)$$

$$\dot{x}_e = v_e. \quad (37b)$$

Here,  $d_0$  is bounded disturbance term;  $\varphi = [1, v_e, v_e^2]^T$ ;  $\theta = [c_0, c_v, c_a]^T$ ,  $\theta \in \mathbb{R}^{n\theta}$  is an unknown time-varying parameter. However, we can obtain a rough range from wind tunnel testing. In addition, we give the following assumptions.

**Assumption 3.** There exists an initially known nominal compact set  $\Theta^0 \triangleq B(\theta^0, z_\theta^0)$ , which is described by an initial nominal estimate  $\theta^0$  and associated error bound  $z_\theta^0 = \sup_{s \in \Theta^0} \|s - \theta^0\|$  such that  $\theta \in \Theta^0$ .

Let the state predictor for (37a) be denoted as  $\hat{v}_e$  and define

$$\hat{v}_e = f''_0(u_s, d_0) + \varphi^T \bar{\theta} + k_a e_v + \gamma_\omega \dot{\bar{\theta}}. \quad (38)$$

Here,  $\bar{\theta} := [\bar{c}_0, \bar{c}_v, \bar{c}_a]^T$  is parameter estimate vector;  $k_a > 0$  is constant matrix;  $e_v = v_e - \hat{v}_e$  is prediction error;  $\gamma_\omega$  is the output of the filter and it can be expressed as

$$\dot{\gamma}_\omega = \varphi - k_a \gamma_\omega, \quad \gamma_\omega(t_0) = 0. \quad (39)$$

Let  $\tilde{\theta} = \theta - \bar{\theta}$ ; from (37a) and (38),

$$\dot{e}_v = \varphi^T \tilde{\theta} - k_a e_v - \gamma_\omega \dot{\tilde{\theta}}. \quad (40)$$

Define

$$\varsigma = e_v - \gamma_\omega \tilde{\theta}. \quad (41)$$

From (40) and (41), we can get

$$\begin{aligned} \dot{\varsigma} &= -k_a \varsigma, \\ \varsigma(t_0) &= e_v(t_0). \end{aligned} \quad (42)$$

The adaptive estimation law of parameter  $\bar{\theta}$  is given by (43).

$$\begin{aligned} \dot{\bar{\theta}} &= \kappa \gamma_\omega^T (e_v - \varsigma), \\ \bar{\theta}(t_0) &= \theta^0 \end{aligned} \quad (43)$$

with  $\kappa = \kappa^T > 0$ .

*Definition 4.*

(1)  $Y \in \mathbb{R}^{n_\theta \times n_\theta}$  is generated from

$$\begin{aligned} Y &= \gamma_\omega^T \gamma_\omega, \\ Y(t_0) &= 0. \end{aligned} \quad (44)$$

(2)  $\underline{\kappa} = \underline{\varrho}(\kappa)$ ; excitation index  $\varepsilon(t) = \underline{\varrho}(Y(t))$ ; and contraction factor is

$$0 < \alpha(t) = \frac{1}{1 + \underline{\kappa} \varepsilon(t)} \leq 1. \quad (45)$$

The uncertainty set  $\Theta \triangleq B(\bar{\theta}, z_\theta)$  is updated as the updating of the parameter estimate  $\bar{\theta}$  and its associated error bound  $z_\theta = \sup_{s \in \Theta} \|s - \bar{\theta}\|$ . And  $z_\theta$  is given as

$$z_\theta = z_\theta^\varepsilon = \sqrt{V_\varepsilon}. \quad (46)$$

Here,  $V_\varepsilon(t) = \alpha(t) V_\varepsilon(t_0)$ ,  $V_\varepsilon(t_0) = (1/2)(z_\theta^0)^2$ .

*Algorithm 5* (adaptive estimation algorithm of the parameter  $\bar{\theta}$ ).

*Step 1.* Initialize  $k_a, \varphi, \kappa, \theta^0, v_e(t_0), \gamma_\omega(t_0), \varsigma(t_0)$ , and  $z_\theta(t_0) = z_\theta^0, \bar{\theta}(t_0) = \bar{\theta}^0, \Theta^0 \triangleq B(\bar{\theta}^0, z_\theta^0)$  at time  $t_0$ .

*Step 2.* Measure (or estimate, see Section 4.3) the current value of  $v_e(t_i)$ , and obtain  $\gamma_\omega, e_v, \varsigma$  by (39)-(42).

*Step 3.* Update  $\bar{\theta}(t_i)$  and  $z_\theta(t_i)$  according to (43) and (46).

If the following conditions are met,

$$z_\theta(t_i) \leq z_\theta(t_{i-1}) - \|\bar{\theta}(t_i) - \bar{\theta}(t_{i-1})\|. \quad (47)$$

Otherwise, keep the value of the last time, which is

$$(\bar{\theta}(t_i), z_\theta(t_i)) = (\bar{\theta}(t_{i-1}), z_\theta(t_{i-1})). \quad (48)$$

*Step 4.* Iterate back to Step 2, incrementing  $i = i + 1$ .

*4.3. Train Speed Estimation.* In this section, an adaptive speed estimated law for HST is proposed to get the train speed information instead of speed sensors.

*Assumption 6.*  $\omega_{r0}$  is constant in the control period; that is,  $d\omega_{r0}/dt = 0$ .

In this paper, we assume that the motor parameters are constant except motor speed. Thus, the full-order flux observer of traction motor can be rewritten as

$$\begin{aligned} \dot{\hat{\mathbf{x}}}'_s &= \hat{\mathbf{A}}_m \hat{\mathbf{x}}'_s + \mathbf{B}_m \mathbf{u}_s + \mathbf{G}(\hat{\mathbf{y}}'_s - \mathbf{y}_s) \\ &= (\mathbf{A}_{m0} + \Delta \mathbf{A}_m) \hat{\mathbf{x}}'_s + \mathbf{B}_m \mathbf{u}_s + \mathbf{G}(\hat{\mathbf{y}}'_s - \mathbf{y}_s) \\ \hat{\mathbf{A}}_m &= \begin{bmatrix} \hat{\mathbf{A}}'_{11} & \hat{\mathbf{A}}'_{12} \\ \hat{\mathbf{A}}'_{21} & \mathbf{0} \end{bmatrix} = \begin{bmatrix} a_{11} \mathbf{I} + \hat{a}'_{11} \mathbf{J} & a_{12} \mathbf{I} + \hat{a}'_{12} \mathbf{J} \\ a_{21} \mathbf{I} & \mathbf{0} \end{bmatrix} \\ &= \begin{bmatrix} -\lambda(R_{s0} L_r + R_{r0} L_s) \mathbf{I} + \hat{\omega}_r \mathbf{J} & \lambda R_{r0} \mathbf{I} - \lambda L_r \hat{\omega}_r \mathbf{J} \\ -R_{s0} \mathbf{I} & \mathbf{0} \end{bmatrix} \end{aligned} \quad (49)$$

$$\Delta \mathbf{A}_m = \begin{bmatrix} \Delta \omega_r \mathbf{J} & -b_1 \Delta \omega_r \mathbf{J} \\ 0 & 0 \end{bmatrix}$$

where  $\hat{\mathbf{x}}'_s = [\hat{\mathbf{i}}'_s \ \hat{\boldsymbol{\psi}}'_s]^T$ ;  $\hat{\mathbf{y}}'_s = \hat{\mathbf{i}}'_s = \mathbf{C}_m \hat{\mathbf{x}}'_s$ ;  $\Delta \omega_r = \hat{\omega}_r - \omega_{r0}$ .

According to (49) and (1), the state estimation error system is

$$\dot{\mathbf{e}}_1 = (\mathbf{A}_{m0} + \mathbf{G} \mathbf{C}_m) \mathbf{e}_1 + \Delta \mathbf{A}_m \hat{\mathbf{x}}'_s. \quad (50)$$

Here,  $\mathbf{e}_1 = \hat{\mathbf{x}}'_s - \mathbf{x}_s$ .

Now we define a Lyapunov function candidate.

$$\mathbf{V}_1 = \mathbf{e}_1^T \mathbf{e}_1 + \frac{(\hat{\omega}_r - \omega_{r0})^2}{\lambda_1}. \quad (51)$$

Here,  $\lambda_1$  is a positive constant. The time derivative of  $\mathbf{V}_1$  by Assumption 6 becomes

$$\begin{aligned} \frac{d\mathbf{V}_1}{dt} &= \mathbf{e}_1^T [(\mathbf{A}_{m0} + \mathbf{G} \mathbf{C}_m) \mathbf{e}_1 + \Delta \mathbf{A}_m \hat{\mathbf{x}}'_s] \\ &\quad + [(\mathbf{A}_{m0} + \mathbf{G} \mathbf{C}_m) \mathbf{e}_1 + \Delta \mathbf{A}_m \hat{\mathbf{x}}'_s]^T \mathbf{e}_1 \\ &\quad + 2 \frac{\Delta \omega_r}{\lambda_1} \frac{d\hat{\omega}_r}{dt} \\ &= \mathbf{e}_1^T [(\mathbf{A}_{m0} + \mathbf{G} \mathbf{C}_m)^T + (\mathbf{A}_{m0} + \mathbf{G} \mathbf{C}_m)] \mathbf{e}_1 \\ &\quad + 2 \mathbf{e}_1^T \Delta \mathbf{A}_m \hat{\mathbf{x}}'_s + 2 \frac{\Delta \omega_r}{\lambda_1} \frac{d\hat{\omega}_r}{dt} \\ &= \mathbf{e}_1^T [(\mathbf{A}_{m0} + \mathbf{G} \mathbf{C}_m)^T + (\mathbf{A}_{m0} + \mathbf{G} \mathbf{C}_m)] \mathbf{e}_1 \\ &\quad + 2 \Delta \omega_r [\Delta \hat{\mathbf{i}}_s'^T \mathbf{J} (\hat{\mathbf{i}}'_s - b_1 \hat{\boldsymbol{\psi}}'_s)] + 2 \frac{\Delta \omega_r}{\lambda_1} \frac{d\hat{\omega}_r}{dt}. \end{aligned} \quad (52)$$

By Theorem 2, the first term on the right side of (52) is a seminegative matrix. When (53) is satisfied,

$$\frac{d\hat{\omega}_r}{dt} = \lambda_1 [\Delta \hat{\mathbf{i}}_s'^T \mathbf{J} (b_1 \hat{\boldsymbol{\psi}}'_s - \hat{\mathbf{i}}'_s)]. \quad (53)$$

TABLE 2: The simulation parameters.

Symbol	Value	Unit
$U_d, U_L, P_m, f, n_p$	3200, 2750, 560, 138, 2	V, V, kW, Hz, -
$N_m, D, R_{s0}, R_r0$	16, 0.875, 0.1065, 0.0663	-, m, $\Omega$ , $\Omega$
$L_s, L_r, L_m, c_0, c_v, c_a$	1.31, 1.93, 53.6, 0.42, 0.0016, 0.000132	mH, mH, mH, -, -, -
$k_d, k_0, \mu, a, \eta$	$5 \times 10^6, 2 \times 10^7, -0.1, 2.788, 0.975$	N·s/m, N/m, -, -, -
$k_1, k_2, k_3, m_1, m_2, m_3$	31.4, 38.5, 30.1, 67.2, 69.6, 68	%, %, %, t, t, t

The last two terms on the right side of (52) are equal, which leads to  $dV_1/dt \leq 0$ . Therefore, it satisfies the Lyapunov stability law and guarantees the stability of the speed estimation system. And (53) is the angular speed identification adaptive law; then, PI adaptive law is adopted to satisfy the rapidity of identification, and it can be expressed as

$$\hat{\omega}_r = \left( k_{wp} + k_{wI} \int dt \right) \left( \Delta \mathbf{i}'^T J (b_1 \hat{\psi}'_s - \hat{\mathbf{i}}'_s) \right). \quad (54)$$

Here,  $k_{wp}$ ,  $k_{wI}$  are PI parameters, respectively. Then HST speed is obtained by (55).

$$\begin{aligned} \hat{v} &= \frac{60\pi D}{1000a} \cdot \frac{30}{\pi} \hat{\omega}_r \\ &= \frac{1.8D}{a} \left( k_{wp} + k_{wI} \int dt \right) \left( \Delta \mathbf{i}'^T J (b_1 \hat{\psi}'_s - \hat{\mathbf{i}}'_s) \right). \end{aligned} \quad (55)$$

Here,  $\hat{v}$  is the speed of HST.

## 5. Numerical Simulation

In this section, CRH3 is chosen for the simulation to verify the validity of speed estimation law, adaptive parameters estimation algorithm, and NHMPM. In order to simplify the simulation and not to lose the generality as well, three cars are chosen (the first and last are locomotives and the middle is carriage). The simulation parameters are shown in Table 2 [15, 16, 30, 31].

In Table 2,  $U_L$  is rated line voltage,  $P_m$  is rated power of traction motor, and  $f$  is rated frequency of traction motor.

The verification framework is shown in Figure 5, and the detailed process is as follows.

Firstly, the target speed (see black line in Figure 8) is given which is 15m/s (0-1s), 70 m/s (1-2s), 30 m/s (2-3s), 3 m/s (3-4s). The real speed (see blue line in Figure 8) and the stator current are measured by sensors after traction motor vector control. In addition, the estimated speed is obtained by (55) (see red line in Figure 8). Compare the estimated speed and real speed to verify the validity of the speed estimation law.

Secondly, according to measured stator current and observed stator flux by full-order flux observer, the electromagnetic torque is obtained by (24), so we can get traction force and braking force by (25) and these forces are also taken as input for TPM (Traditional Multipoint Model).

Lastly, the calculated speed of NHMPM is obtained by (31). Compare the real speed and calculated speed to prove the validity of NHMPM. And determine whether the calculated

speed of NHMPM is closer to the real speed than TPM to verify the accuracy of NHMPM.

In addition, determine whether the resistance coefficients estimated by Algorithm 5 converge to the real values to verify the effectiveness of the adaptive parameter estimation algorithm.

5.1. The Validity of Speed Estimation Law. According to Table 2, we can get

$$\begin{aligned} A_{m0} &= \begin{bmatrix} -54.23 & -650.31 & 380 & 2.0496 \times 10^5 \\ -650.31 & -54.23 & -2.0496 \times 10^5 & 380 \\ -0.1065 & 0 & 0 & 0 \\ 0 & -0.1065 & 0 & 0 \end{bmatrix}, \\ B_m &= \begin{bmatrix} 315.167 & 0 \\ 0 & 315.167 \\ 1 & 0 \\ 0 & 1 \end{bmatrix}. \end{aligned} \quad (56)$$

When  $\omega_r = 1.5p.u.$ , the poles of the motor model are  $(-20.64+649.3i)$ ,  $(-20.64-649.3i)$ ,  $(-33.59-1.01i)$ ,  $(-33.59+1.01i)$ . We can get  $T \leq 9.78 \times 10^{-5}$  by (8); let  $T = 9 \times 10^{-5}$  and then  $k_{max} = 1.08$ . Therefore, the circular region  $D(c, r)$  is obtained by (6) with center  $(c, 0) = (-1/9 \times 10^5, 0)$  and  $r = 1/9 \times 10^5$ . Figure 6 shows the trajectories of observer poles when  $\omega_r$  changes from 0 to 1.5p.u. and the circular region  $D(c, r)$ . From the figure, we know that all of the poles of observer belong to the circular region  $D(c, r)$ . The poles of the motor model and observer are shown in Figure 7 when  $\omega_r = 1.5p.u.$

According to the simulation parameter, solving the linear matrix inequality (9), the feasible solution of  $\mathbf{P}$  and observer gain matrix  $\mathbf{G}$  are

$$\begin{aligned} \mathbf{P} &= 10^{-6} \\ &\times \begin{bmatrix} 0.0065 & 0 & -2.0561 & -0.2392 \\ 0 & 0.0065 & 0.2392 & -2.0561 \\ -2.0561 & 0.2392 & 1832.8 & -2.87487 \times 10^{-9} \\ -0.2392 & -2.0561 & -2.87487 \times 10^{-9} & 1832.8 \end{bmatrix}, \end{aligned}$$

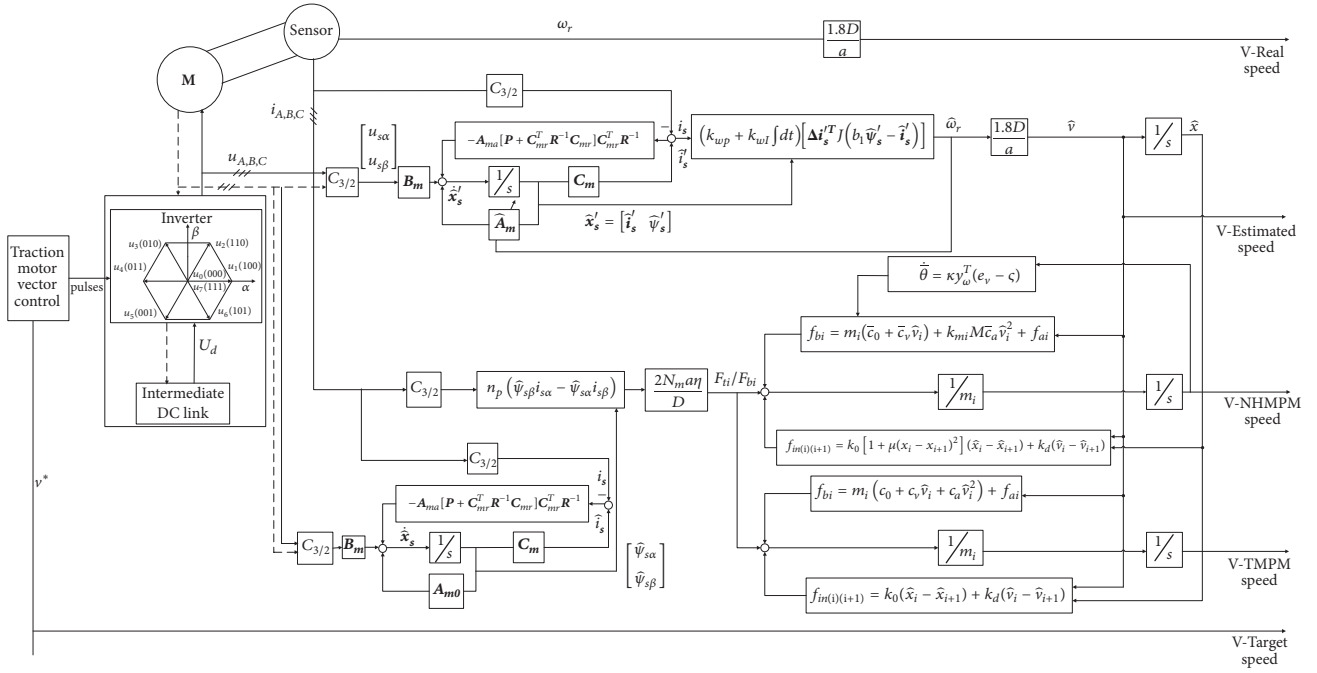


FIGURE 5: The verification framework.

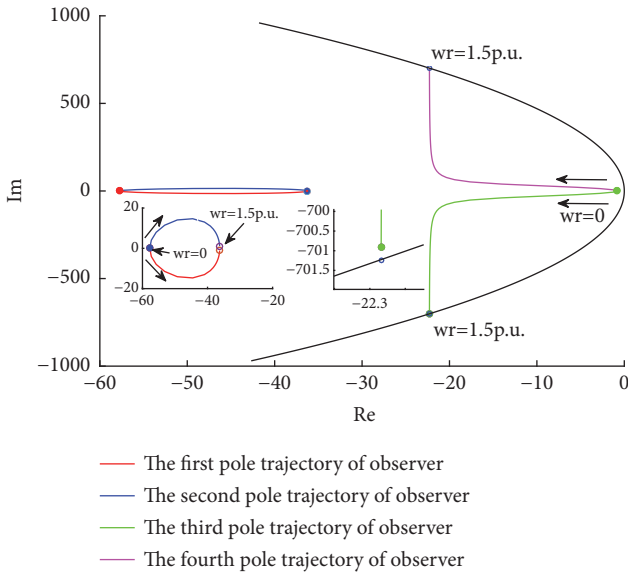


FIGURE 6: The trajectories of observer poles and circular region  $D(c, r)$ .

$$G = \begin{bmatrix} -0.0215 & 0.0008 \\ -0.0008 & 0.0215 \\ -2.3978 \times 10^{-5} & 2.8138 \times 10^{-6} \\ 2.8138 \times 10^{-6} & -2.3978 \times 10^{-5} \end{bmatrix} \quad (57)$$

And then the train speed can be estimated by (55). Figure 8 displays the estimated result which indicates that the estimated speed can converge to real speed after 0.3s at each

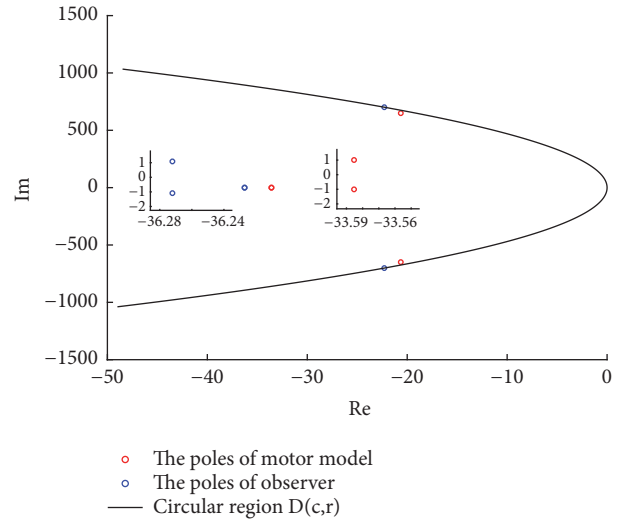


FIGURE 7: The poles of the motor model and observer.

period, and the speed estimation system is stable. The error curve between real speed and estimated speed is shown in Figure 9; the max, min, and mean error value are given in Table 3. From Figure 9 and Table 3, we know that the proposed speed estimation law in this paper can estimate the train speed accurately; the mean error is less than 0.1m/s at each period. In addition, the max error is 2.32m/s and the error rate is 3.32% (the target speed is 70m/s at this period).

5.2. The Validity of NHMPM and Adaptive Parameter Estimation Algorithm. Figure 10 shows the estimated resistance

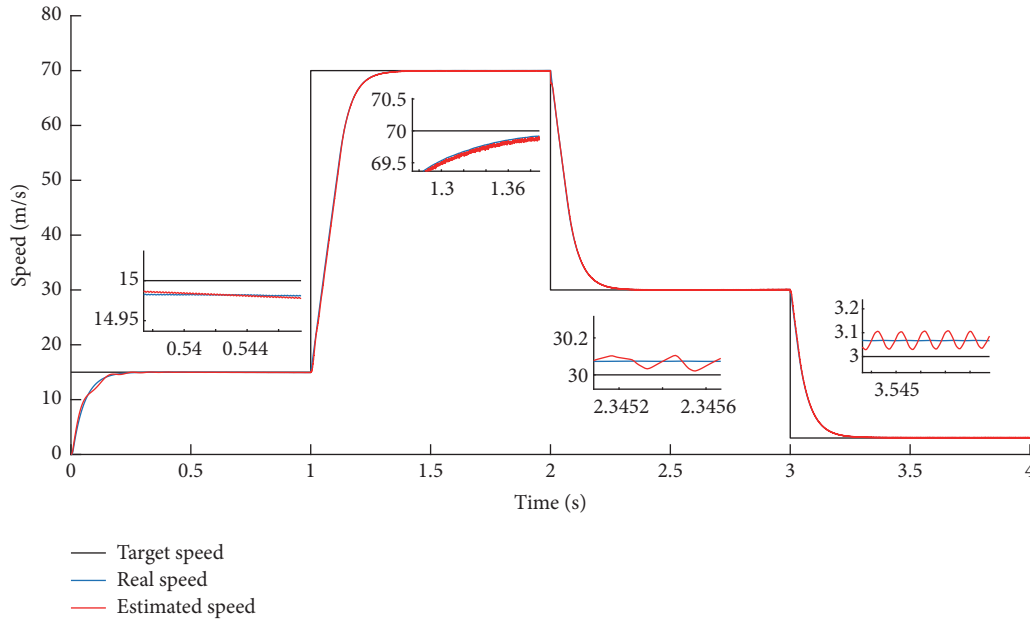


FIGURE 8: The estimated speed of the train.

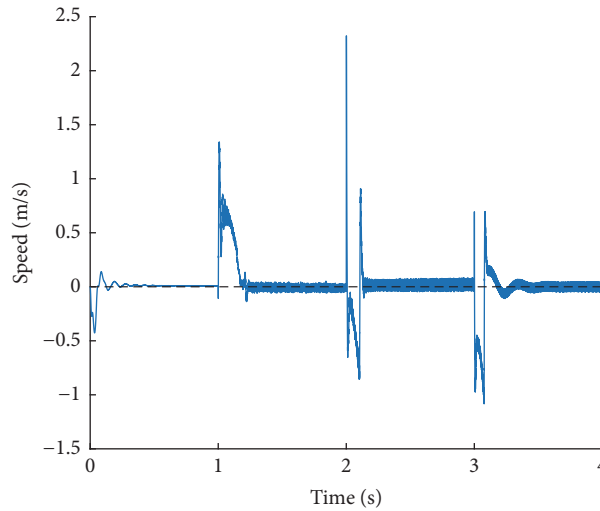


FIGURE 9: The error between real speed and estimated speed.

coefficients using the proposed adaptive parameter estimation algorithm. The unknown resistance parameters can converge to the real value accurately even when the real value changes from  $c_0 = 0.42, c_v = 0.0016, c_a = 0.000132$  to  $c_0 = 0.47, c_v = 0.0026, c_a = 0.001132$ . It verifies the validity of the adaptive estimation algorithm.

Figure 11 and Table 4 show the verification results of NHMPM; it can be seen that the speed of NHMPM (green line) is basically consistent with the real speed that verifies the effectiveness of NHMPM. Moreover, compared with the TPM, the NHMPM speed is closer to the real speed at the same traction and braking force. And the mean error between real speed and NHMPM speed is smaller than the mean error between real speed and TPM speed at all periods

especially at the periods of 2s-3s and 3s-4s, which indicates that NHMPM is more accurate than TPM.

The traction motor stator voltage  $u_{s\alpha}, u_{s\beta}$  and the electromagnetic torque of the first car are shown in Figures 12 and 13, respectively. Figure 14 displays the traction and braking force of three cars. As the second car is a carriage, its traction and braking force are zero. In contrast, the first and the third car are equipped with traction motor; therefore, they can supply traction and braking force in all modes.

### 6. Conclusions

This paper established a NHMPM including the integer variables of running status and car types for HST. As the basis

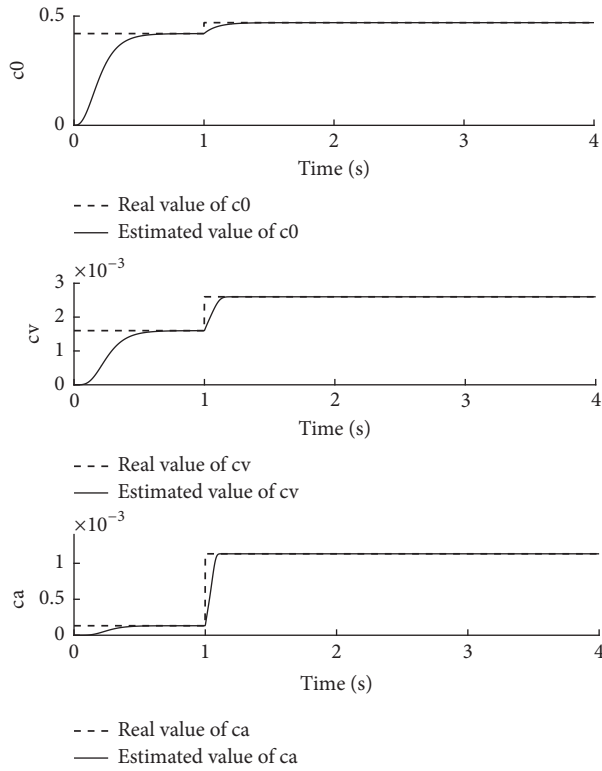


FIGURE 10: The estimated values of resistance coefficients.

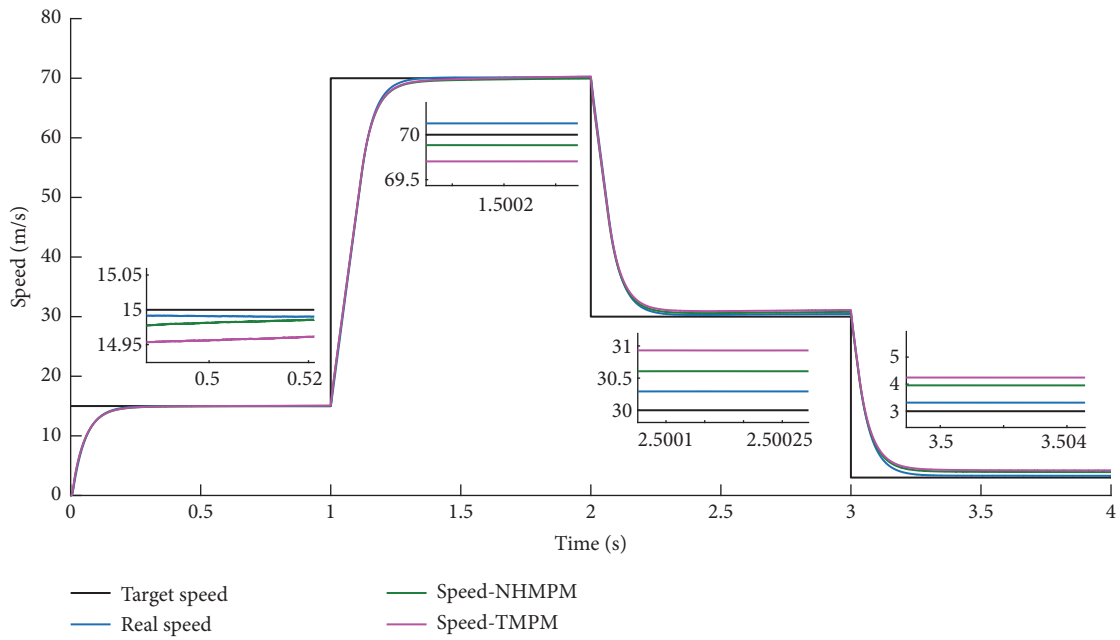


FIGURE 11: Train speed trajectory.

TABLE 3: The error value between real speed and estimated speed.

Value (m/s)	Period (s)			
	0s-1s	1s-2s	2s-3s	3s-4s
Max	0.1394	1.3407	2.3227	0.6965
Min	-0.4277	-0.1374	-0.8565	-1.0835
Mean	-0.0015	0.0910	-0.0128	-0.0378

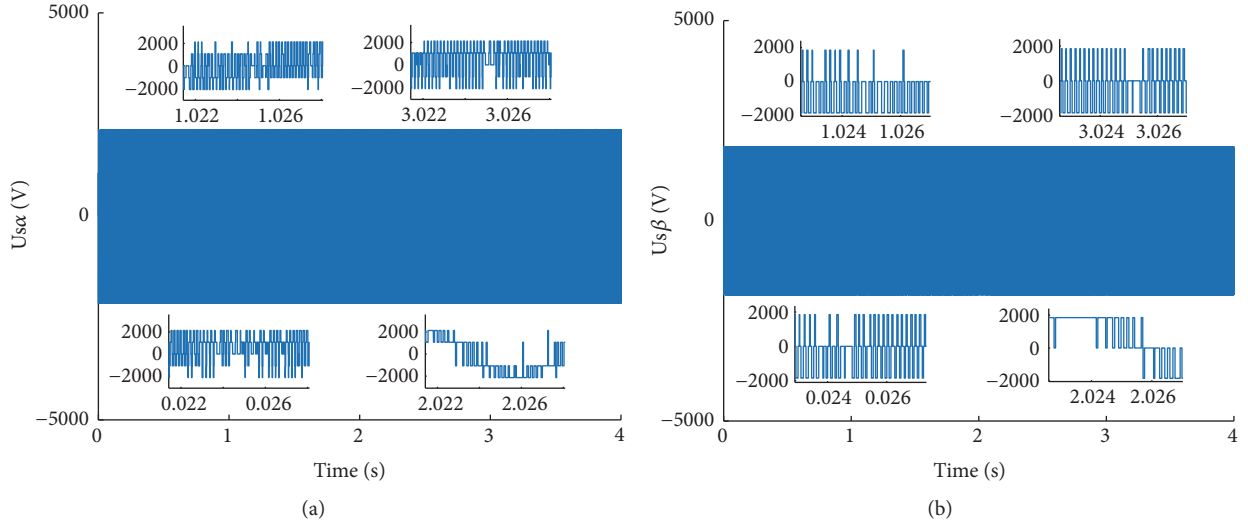
FIGURE 12: Traction motor stator voltage of the first car. (a)  $u_{s\alpha}$ , (b)  $u_{s\beta}$ .

TABLE 4: The max, min, and mean error between real speed and TPM speed, real speed and NHMPM speed.

Period	0s-1s		1s-2s		2s-3s		3s-4s	
	TPM	NHMPM	TPM	NHMPM	TPM	NHMPM	TPM	NHMPM
Value (m/s)								
Max	0.1561	0.1550	0.6063	0.5372	0.9741	0.6317	-0.1487	0.2647
Min	-0.5214	-0.5214	-0.7588	-0.7434	-0.8481	-0.4356	-1.2354	-0.8210
Mean	0.0763	0.0325	0.2871	0.2658	0.714	-0.2734	1.1202	-0.7064

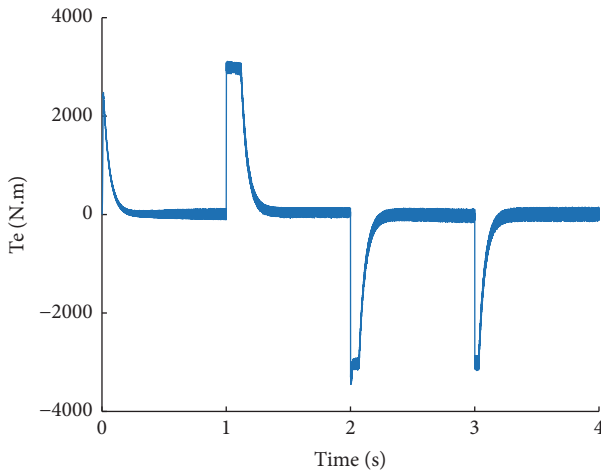


FIGURE 13: The traction motor electromagnetic torque of the first car.

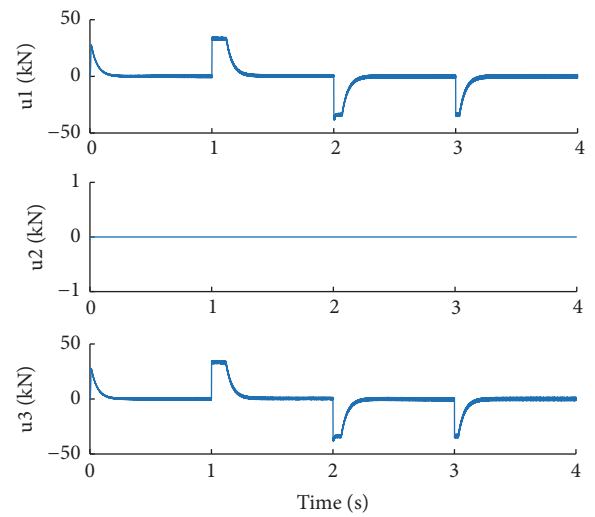


FIGURE 14: Traction and braking force of each car.

of research, the traction/braking dynamics was discussed and the running resistance force was reformulated. The author also analyzed the nonlinear in-train coupling force. Besides, an adaptive parameters estimation algorithm and a train speed estimation law were proposed. The proposed algorithm and law provide the unknown resistance coefficients and train speed required in the model, respectively. At last, numerical simulations are conducted to verify the effectiveness of the proposed algorithm, law, and NHMPM. The results of the

verification are shown as follows. (1) The estimated speed using the proposed estimation law can converge to the real speed accurately. The mean error between real speed and estimated speed is less than 0.1m/s at each period, and the maximum error is 2.32m/s (the target speed is 70m/s at this period). (2) The estimated unknown resistance coefficients can converge to the real value accurately even when the real value changes. (3) The speed of NHMPM is basically

consistent with the real speed. Compared with TPM, it is closer to the real speed at all periods especially at the periods of 2s-3s and 3s-4s.

## Data Availability

The data used to support the findings of this study are included within the article.

## Conflicts of Interest

The authors declare that there are no conflicts of interest regarding the publication of this paper.

## Acknowledgments

This research was supported by the National Key R&D Program of China [2016YFB1200602-26]; the National Key R&D Program of China [2016YFB1200601]; the National Natural Science Foundation of China (Nos. U1734211).

## References

- [1] H. Dong, B. Ning, B. Cai, and Z. Hou, "Automatic train control system development and simulation for high-speed railways," *IEEE Circuits and Systems Magazine*, vol. 10, no. 2, pp. 6–18, 2010.
- [2] L. J. Zhang and X. T. Zhuan, "Optimal operation of heavy-haul trains equipped with electronically controlled pneumatic brake systems using model predictive control methodology," *IEEE Transactions on Control Systems Technology*, vol. 22, no. 1, pp. 13–22, 2014.
- [3] P. G. Howlett, P. J. Pudney, and X. Vu, "Local energy minimization in optimal train control," *Automatica*, vol. 45, no. 11, pp. 2692–2698, 2009.
- [4] H. Luo, H. Xu, and X. Liu, "Immersion and invariance based robust adaptive control of high-speed train with guaranteed prescribed performance bounds," *Asian Journal of Control*, vol. 17, no. 6, pp. 2263–2276, 2015.
- [5] R. S. Luo, Y. H. Wang, Z. Y. Yu et al., "Adaptive Stopping Control of Urban Rail Vehicle," *Journal of the China Railway Society*, vol. 34, no. 4, pp. 64–68, 2012 (Chinese).
- [6] C. Yang and Y. Sun, "Robust cruise control of high speed train with hardening/softening nonlinear coupler," in *Proceedings of the American Control Conference (ACC '99)*, pp. 2200–2204, San Diego, Calif, USA, June 1999.
- [7] B. Wie and D. S. Bernstein, "A benchmark problem for robust control design," in *Proceedings of the 1990 American Control Conference*, pp. 961–962, May 1990.
- [8] C. Yang and Y. Sun, "Mixed  $H_2/H_\infty$  cruise controller design for high speed train," *International Journal of Control*, vol. 74, no. 9, pp. 905–920, 2001.
- [9] M. Chou, X. Xia, and C. Kayser, "Modelling and model validation of heavy-haul trains equipped with electronically controlled pneumatic brake systems," *Control Engineering Practice*, vol. 15, no. 4, pp. 501–509, 2007.
- [10] Q. Song, Y.-D. Song, T. Tang, and B. Ning, "Computationally inexpensive tracking control of high-speed trains with traction/braking saturation," *IEEE Transactions on Intelligent Transportation Systems*, vol. 12, no. 4, pp. 1116–1125, 2011.
- [11] L. S. Wang, H. Z. Xu, M. N. Zhang et al., "Hybrid Model Predictive Control Application to Automatic Train Operation," *Journal of the China Railway Society*, vol. 37, no. 12, pp. 53–60, 2015.
- [12] Z.-Y. Yu and D.-W. Chen, "Modeling and system identification of the braking system of urban rail vehicles," *Journal of the China Railway Society*, vol. 33, no. 10, pp. 37–40, 2011.
- [13] Q. Song, Y. D. Song, and W. Cai, "Adaptive backstepping control of train systems with traction/braking dynamics and uncertain resistive forces," *Vehicle System Dynamics: International Journal of Vehicle Mechanics and Mobility*, vol. 49, no. 9, pp. 1441–1454, 2011.
- [14] Q. Song and Y. D. Song, "Robust and Adaptive Control of High Speed Train," in *Proceedings of Chinese Control and Decision Conference*, vol. 22, pp. 2469–2474, 2010.
- [15] S. B. Yao, D. L. Guo, G. W. Yang et al., "Distribution of High-speed Train Aerodynamic Drag," *Journal of the China Railway Society*, vol. 34, no. 7, pp. 18–23, 2012.
- [16] L. M. Song, *EMU Transmission and Control*, China Railway Publishing House, Beijing, China, 2009.
- [17] J. Wang, W.-H. Gui, X.-H. Nian, and X.-F. Li, "Study on speed sensorless indirect stator-quantities control system of traction motor," *Journal of the China Railway Society*, vol. 32, no. 6, pp. 17–21, 2010.
- [18] H. Kubota, K. Matsuse, and T. Nakano, "DSP-based speed adaptive flux observer of induction motor," *IEEE Transactions on Industry Applications*, vol. 29, no. 2, pp. 344–348, 1993.
- [19] H. Kubota, I. Sato, Y. Tamura, K. Matsuse, H. Ohta, and Y. Hori, "Regenerating-mode low-speed operation of sensorless induction motor drive with adaptive observer," *IEEE Transactions on Industry Applications*, vol. 38, no. 4, pp. 1081–1086, 2002.
- [20] G. Yang and T. Chin, "Adaptive-speed identification scheme for a vector-controlled speed sensorless inverter-induction motor drive," *IEEE Transactions on Industry Applications*, vol. 29, no. 4, pp. 820–825, 1993.
- [21] S. Suwankawin and S. Sangwongwanich, "A speed-sensorless IM drive with decoupling control and stability analysis of speed estimation," *IEEE Transactions on Industrial Electronics*, vol. 49, no. 2, pp. 444–455, 2002.
- [22] S. Suwankawin and S. Sangwongwanich, "Design strategy of an adaptive full-order observer for speed-sensorless induction-motor drives - Tracking performance and stabilization," *IEEE Transactions on Industrial Electronics*, vol. 53, no. 1, pp. 96–119, 2006.
- [23] M. Liu, Y. Jing, and S. Zhang, "Robust state observer design based on regional pole assignment," *International Federation of Automatic Control*, vol. 38, pp. 1263–1268, 2005.
- [24] S. Q. Zhao, Y. F. Ma, and X. P. Gu, "Comparative and analysis of regional poles in the robotic arm movement model," *Computing Technology and Automation*, vol. 31, no. 4, pp. 21–25, 2012.
- [25] K. Y. Guo, F. Z. Wang, and B. Sun, "Uniform damping control of low-frequency oscillations in power systems based on region poles assignment," *Transactions of China electrotechnical Society*, vol. 24, no. 12, pp. 142–148, 2009.
- [26] J. Wang, W. H. Wu, J. T. Liu et al., " $H_2/H_\infty$  control with regional pole placement for carrier landing," *Computer Simulation*, vol. 34, no. 12, pp. 41–44, 2017.
- [27] Z. H. Li, C. J. Chen, J. Teng et al., "Application of State Feedback Control based on Regional Pole-Assignment Method in Flexible Buildings," *Journal of Vibration Engineering*, vol. 31, no. 2, pp. 265–274, 2018.

- [28] L. Yu, *Robust Control-LMI Approach*, Tsinghua University Press, Beijing, China, 2002.
- [29] V. Adetola, D. Dehaan, and M. Guay, "Adaptive model predictive control for constrained nonlinear systems," *Systems & Control Letters*, vol. 58, no. 5, pp. 320–326, 2009.
- [30] Z. Rao, *Train traction calculation*, China Railway Publishing House, Beijing, china, 2012.
- [31] C. B. Zhang and Y. P. Tang, "Research and Simulation on Effect of Gear Ratio on High-Speed EMU Tractive Characterisation," *Journal of Dalian Jiaotong University*, vol. 4, pp. 79–82, 2011.

## Research Article

# Start-Up Process Modelling of Sediment Microbial Fuel Cells Based on Data Driven

Fengying Ma , Yankai Yin, and Min Li

*School of Electrical Engineering and Automation, Qilu University of Technology, Jinan 250000, China*

Correspondence should be addressed to Fengying Ma; mafengy@163.com

Received 7 September 2018; Accepted 24 December 2018; Published 10 January 2019

Academic Editor: Giacomo Falcucci

Copyright © 2019 Fengying Ma et al. This is an open access article distributed under the Creative Commons Attribution License, which permits unrestricted use, distribution, and reproduction in any medium, provided the original work is properly cited.

Sediment microbial fuel cells (SMFCs) are a typical microbial fuel cell without membranes. They are a device developed on the basis of electrochemistry and use microbes as catalysts to convert chemical energy stored in organic matter into electrical energy. This study selected a single-chamber SMFC as a research object, using online monitoring technology to accurately measure the temperature, pH, and voltage of the microbial fuel cell during the start-up process. In the process of microbial fuel cell start-up, the relationship between temperature, pH, and voltage was analysed in detail, and the correlation between them was calculated using SPSS software. The experimental results show that, at the initial stage of SMFC, the purpose of rapid growth of power production can be achieved by a large increase in temperature, but once the temperature is reduced, the power production of SMFC will soon recover to the state before the temperature change. At the beginning of SMFC, when the temperature changes drastically, pH will change the same first, and then there will be a certain degree of rebound. In the middle stage of SMFC start-up, even if the temperature will return to normal after the change, a continuous temperature drop in a short time will lead to a continuous decrease in pH value. The RBF neural network and ELM neural network were used to perform nonlinear system regression in the later stage of SMFC start-up and using the regression network to forecast part of the data. The experimental results show that the ELM neural network is more excellent in forecasting SMFC system. This article will provide important guidance for shortening start-up time and increasing power output.

## 1. Introduction

Microbial fuel cell (MFC) is being viewed as a potential bio-electrochemical device capable of producing energy in the form bioelectricity apart from wastewater treatment [1–3] which has been widely investigated in recent years. Ramanavicius et al. [4] described enzymatic biofuel cell based on enzyme modified anode and cathode electrodes are both powered by ethanol and operate at ambient temperature. Nastro et al. [5] reviewed recent articles about the application of MFCs to solid substrates treatment and valorisation and the contribution that BESs and MFC could give to the development of a more sustainable waste management. Gambino et al. [6] investigated the influence of microelectrogenesis on PAHs degradation and detoxification operated by Pseudomonadaceae, Bacillaceae, Staphylococcaceae, and Enterobacteriaceae in water environment. Compared with MFC, Sediment microbial fuel cells (SMFCs) are a special

application of MFCs for sustainable electricity production [7] and are also the most common membrane free microbial fuel cells which are considered as alternative renewable energy sources for remote environmental monitoring via an energy conversion system. SMFC generates electrical energy through the oxidation of organic matter in the presence of fermentative bacteria under mild operating conditions [8]. The potential (biologically mediated) developed between the bacterial metabolic activity (series of oxidation-reduction reactions generating electrons ( $e^-$ ) and protons ( $H^+$ )) and the electron acceptor conditions generate potential to make bioelectricity [9]. Microorganisms extract energy required to build biomass (anabolic process) from redox reactions (catabolism) through electron donor/acceptor conditions [10]. However, the low output power density of MFC is generally not enough to drive common electronic devices continuously and extremely hinder its practical application [11, 12].

In recent years, researchers in various countries have studied MFC in terms of microorganisms, electrodes, configurations, matrices, operating conditions, and electrochemical properties and found that although microorganisms are the core of MFC, nonbiological factors are more important than biological factors in the production of electricity [13]. The cathode operating conditions play an important part in the overall performance of the MFC [14]. Cathodic pH microenvironment is one of the crucial factors affecting the metabolic activity of the substrate, affecting the electron and  $H^+$  reaction mechanism. Depending on the organism and growth conditions, changes in the external pH can bring about alterations in several primary physiological parameters, including internal pH, concentration of ions, membrane potential, and proton-motive force [15, 16]. Mohan's studies have shown that, under acidic conditions, the MFC system has a smaller internal resistance and a large amount of electricity, but neutral conditions are more suited to matrix degradation [17]. Zhang's research shows that the single-chamber MFC's power generation performance is strongly influenced by temperature, and the operation of a single-chamber MFC should be controlled primarily by temperature [18]. Jannelli et al. [19] assessed the performance of air cathode, single-chambered, Tubular Microbial Fuel Cells (TMFCs) provided with Nafion membrane, according to different operating conditions. Ramanavicius et al. [20] studied the application of heme-c containing enzymes in biofuel cell design. As the principal factor affecting the power generation of SMFC, no one has studied the comprehensive relationship between them and electricity generation. There is also no advanced monitoring method to monitor the minute changes of the parameters in the start-up process on-line. This will lead to the loss of important data in the detection process and will consume a lot of manpower and material resources which will bring inconvenience to the intensive study of SMFC. For the SMFC system, due to its more complex environmental conditions, stronger coupling, and nonlinear characteristics than MFC [21], sometimes it is inconvenient for online detection of certain parameters. Computational methods play a critical role in developing fuel cells with optimum performance in a wide range of operating conditions. Krastev et al. [22] developed algorithms for the simulation of reactive flows through micro- and nanoscale porous media via the Lattice Boltzmann method are presented and for the first time used in the field of microbial fuel cells. Zhang et al. used EKF algorithm to estimate battery parameters in real time [23, 24]. Liu et al. [25] used Gauss-Newton algorithm to solve the parameters iteratively. Liu et al. studied particle filter-based parameter estimation method [26]. Sun et al. Identified the battery parameters through recursive least square method [27, 28]. But due to the lack of precise mathematical models of MFC and the above method only applicable to the condition of constant parameter and slow transformation, it is difficult to apply them to SMFC. The neural network has strong nonlinear fitting ability, can map arbitrarily complex nonlinear relations, and has strong robustness, memory ability, nonlinear mapping ability, and strong self-learning ability [29]. Therefore, it is necessary to

find a suitable neural network to fit the nonlinear model between various parameters in the start-up phase.

As far as we know, there is no study on the relationship between pH, power generation and temperature during the start-up of microbial fuel cells. Therefore, we will focus on the relationship between cathode pH, temperature, and voltage during the start-up of a microbial fuel cell. Due to the successful application of RBF neural network and ELM neural network in other biochemistry fields, we choose them to regress the nonlinear system in the later stage of SMFC start-up, and the regression network was used to predict the pH of that period.

## 2. Data Acquisition and Processing

*2.1. SMFC Configuration and Operation.* The single-chamber microbial fuel cell was employed in this experimental device and a control experiment was conducted. Mixed culture (anaerobic sludge) was collected from Daming Lake (Ji'nan, China) which was at 5 cm under the water. The single-chamber SMFC consisted of an anode and cathode placed in a Plexiglas cylindrical chamber (purchased from Ji'nan lanyo Technology Ltd.) with a length of 49 cm and a diameter of 9 cm (empty bed volume of 2000 mL). The anode and cathode electrodes were made of plain carbon felts (purchased from Beijing Jinglong Special Carbon Technology Co. Ltd.) and pierced in several places, forming holes  $\sim 1$  mm in diameter, so that water motion in the chamber was not blocked when the cathode was placed in the distilled water. Prior to use electrodes were soaked in distilled water and tested for conductivity. Wires were used for contact with electrodes and the contact area was sealed carefully with "epoxy" material. 600 mL of anaerobic sludge was used as the deposit in the anode area and 1400 mL of distilled water was used as the cathode buffer. The anode is buried 8m below the surface of the sediment, and the cathode is located 10 cm below the water level (to prevent evaporation of water), 30 cm from the surface of the sediment. The entire experiment was performed by connecting a 1 mm diameter titanium wire and an external 1000  $\Omega$  resistor to form a loop. A sediment fuel cell was built in the lab as can be seen in Figure 1.

Use data real-time acquisition device to record the SMFC voltage every 1 second through the LabVIEW interface and filter the data. During the one-month test, the voltage of SMFC ascends until it arrives at a stable value. During the entire test period, the system was not supplemented with any buffers and other substrates. The temperature was measured using a LM35DZ temperature sensor (LM35 is a temperature sensor produced by NS company. It has high working accuracy and a wide linear working range). The output voltage is linearly proportional to the Celsius temperature, and it can provide a common room temperature accuracy of  $\pm 1/4^\circ\text{C}$  without external calibration or fine tuning. The pH was measured using the Industrial Online pH and Redox sensors.

*2.2. Correlation Analysis and Neural Network Modelling.* There are various abiotic factors affecting MFC power generation, including pH, temperature, dissolved oxygen, cathode

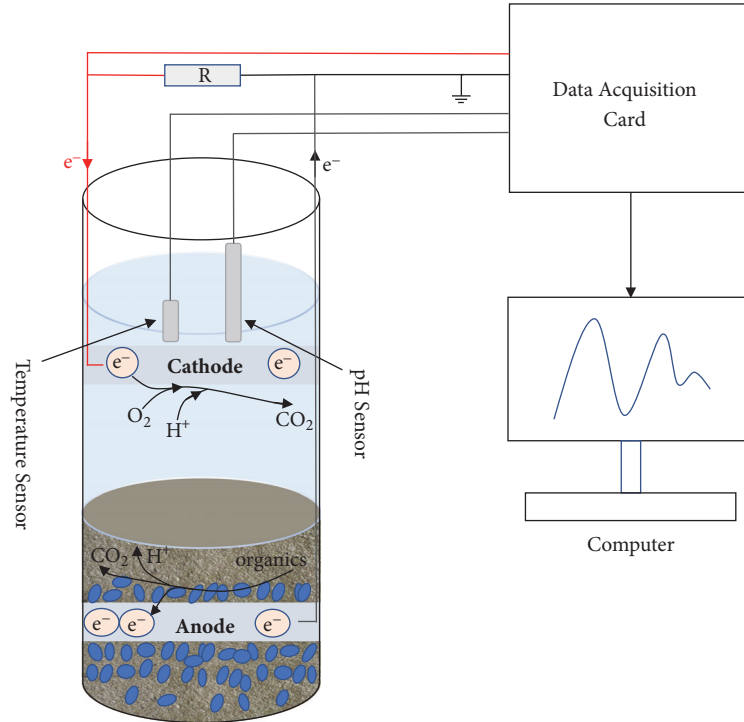


FIGURE 1: Schematic of laboratory SMFC configuration with sensors and data acquisition cards.

liquid and so on. During the experiment, we chose aeration device to support SMFC, but we found that the effect of dissolved oxygen concentration on SMFC power generation is much less than that of temperature. The difference of power generation performance between SMFC in cathode chamber in aeration and natural reoxygenation is not obvious. The initial pH of SMFC is different for diverse cathode fluid, so it is impossible to compare the change trend of pH in the start-up process. To sum up, we chose the pH, temperature and voltage for correlation analysis, and studied the relationship between them during the start-up process. Statistical analysis software SPSS is utilized to analyse the correlation between temperature, pH and electricity generation performance during MFC start-up. This analysis uses Pearson product-moment correlation coefficient as a measure of correlation analysis. The Pearson product-moment correlation coefficient is commonly used in academic research to measure the strength of the linear correlation of two variables and the value is between -1 and 1. The formula is shown in

$$r = \frac{\sum_{i=1}^n (X_i - \bar{X})(Y_i - \bar{Y})}{\sqrt{\sum_{i=1}^n (X_i - \bar{X})^2} \sqrt{\sum_{i=1}^n (Y_i - \bar{Y})^2}} \quad (1)$$

In the formula,  $X_i$  and  $Y_i$  represent two different sets of variables,  $\bar{X}$  represents the average value of  $X_i$ , and  $\bar{Y}$  represents the average value of  $Y_i$ .

It can be seen from the Table 1 that the correlation coefficient between voltage and pH is 0.347, the correlation coefficient between pH and temperature is 0.327, and the correlation coefficient between voltage and temperature is

0.797, which can be regarded as highly correlated, and between any two parameters correlation is significant at the 0.01 level.

MFC is a complex nonlinear model, many variables and parameters in the model will affect the performance of the system. Zeng et al. [30] developed an MFC model based on a two-chamber configuration by integrating biochemical reactions, Butler-Volmer expressions and mass/charge balance. However, this method is based on the ideal state of two-chamber MFC fuelled by acetate, and it doesn't apply to a more complicated SMFC system. Compared to MFC, it is more difficult to establish the model in the start-up process.

Data-driven modelling method is based on process acquisition data. It is widely used in process industry modelling and optimization because it does not need to understand the process mechanism deeply and has strong generality of the algorithm. Neural networks have the ability to approximate arbitrary nonlinear mappings, parallel distributed computations, self-learning capabilities, and fault tolerance, and are therefore commonly used in the modelling and control of nonlinear systems. At present, there is no article modelling, simulation and prediction of the relationship between temperature, pH and voltage in the SMFC start-up process. In this paper, we choose Radical Basis Function (RBF) neural network and Extreme Learning Machine (ELM) neural network respectively to regression and prediction of the system.

**2.3. Problem Formulation and Preliminaries.** RBF neural network has the characteristics of simple structure, simple training and fast learning convergence, and can approximate

TABLE 1: Correlation analysis between voltage, pH, and temperature.

		Voltage [mV]	pH	Temperature [°C]
Voltage [mV]	Pearson Correlation	1	.347**	.797**
	Sig. (2-tailed)		.000	.000
	N	628999	628999	628999
pH	Pearson Correlation	.347**	1	.327**
	Sig. (2-tailed)	.000		.000
	N	628999	628999	628999
Temperature [°C]	Pearson Correlation	.797**	.327*	1
	Sig. (2-tailed)	.000	.000	
	N	628999	628999	628999

Note. \*\* Correlation is significant at the 0.01 level (2-tailed).

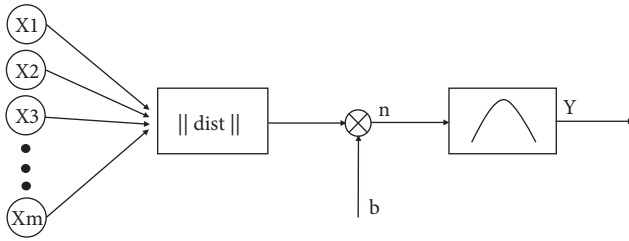


FIGURE 2: Radial basis neuron model.

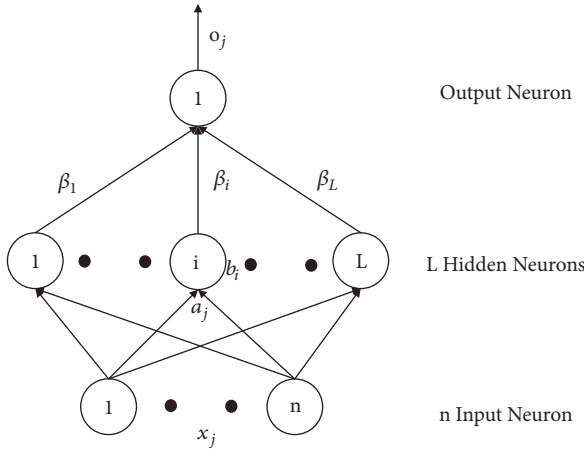


FIGURE 3: Structure diagram of single hidden layer feedforward neural network.

any nonlinear function, this paper selects the RBF neural network to achieve the regression of the nonlinear function of the last 10 days of the SMFC start-up phase. The radial basis neuron model is shown in Figure 2.

In this paper, Gaussian function is used as the radial basis function, so the activation function of radial basis neural network as

$$R(x_p - c_i) = \exp\left(-\frac{1}{2\sigma^2} \|x_p - c_i\|^2\right) \quad (2)$$

In the formula,  $\|x_p - c_i\|$  is a European norm,  $c_i$  is a Gaussian function centre, and  $\sigma$  is a Gaussian function variance.  $x_p = (x_1^p, x_2^p, \dots, x_m^p)$  is the  $p$ th output sample.  $p = 1, 2, 3, \dots, P$ ,  $P$

is the number of sample points.  $c_i$  is the centre of network hidden layer nodes.

The mean square error (MSE) was used to evaluate the prediction accuracy of the model. The mathematical expression is as

$$\text{MSE} = \frac{1}{P} \sum (y - \hat{y})^2 \quad (3)$$

where  $y$  is the actual value,  $\hat{y}$  is the prediction model prediction value, and  $P$  is the number of sample points. The specific steps of the learning algorithm are as follows.

Step one: get the centre of the Radical Base Function.

- (1) Randomly selected  $h$  training samples as cluster centre and expressed by  $c_i (i = 1, 2, \dots, h)$ .
- (2) The input samples are grouped according to the Nearest Neighbor rule. According to Euclidean distance between  $x_p$  and  $c_i$  to assign  $x_p$  to each cluster set  $\vartheta_p (p = 1, 2, 3, \dots, P)$  of the input samples.
- (3) Adjust cluster centre. If the cluster centre no longer changes,  $c_i$  is the final cluster centre; otherwise recalculate.

Step two: Solving the variance of Gauss function according to

$$\sigma_i = \frac{c_{max}}{\sqrt{2h}} \quad (4)$$

In the formula,  $\sigma_i$  is the variance of Gauss function,  $i = 1, 2, 3, \dots, h$ .  $c_{max}$  is the maximum distance between the selected centers.

Step three: Calculate the weights between the hidden layer and the output layer according to

$$\omega = \exp\left(\frac{h}{c_{max}^2} \|x_p - c_i\|^2\right) \quad (5)$$

In the formula,  $i = 1, 2, 3, \dots, h$  and  $p = 1, 2, 3, \dots, P$ .

ELM is an algorithm proposed by Huang et al for solving single hidden layer neural networks. Compared with the traditional neural network, especially the single hidden layer feedforward neural network (SLFN), ELM is faster than the traditional learning algorithm on the premise of

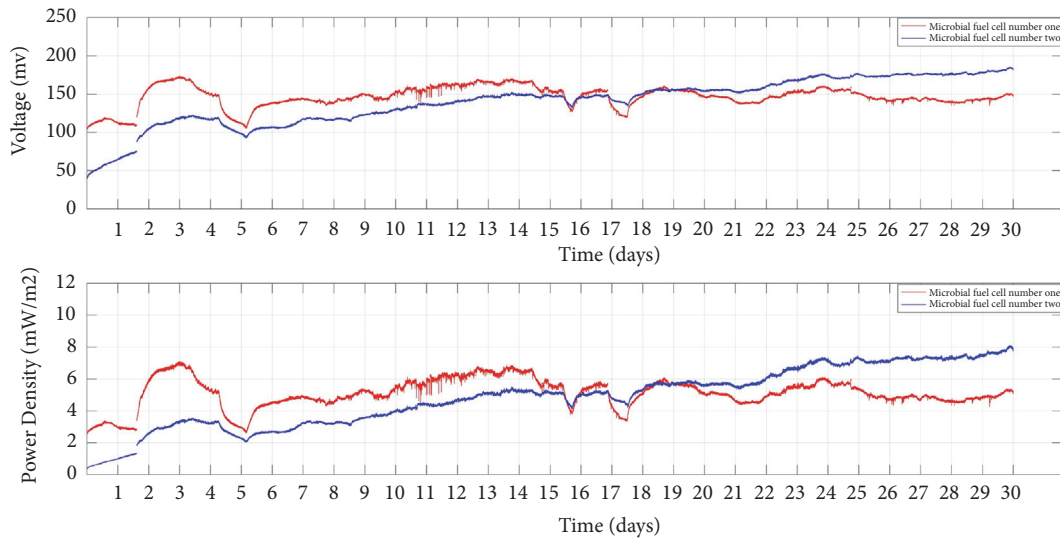


FIGURE 4: The curve of voltage and power density at start-up phase of SMFC.

guaranteeing the learning accuracy. For single hidden layer neural networks, ELM can initialize input weights and offsets randomly to obtain corresponding output weights. Structure diagram of single hidden layer feedforward neural network is given in Figure 3.

The steps of the learning algorithm are as follows:

Step one: Determine the number of hidden layer neurons and randomly set the weight  $\omega$  between the input layer and the hidden layer and the bias  $b$  of hidden layer neurons.

Step two: Select activation function and calculate hidden layer output matrix  $H$ .

Step three: Calculate output layer weights  $\hat{\beta}$ .

### 3. Results and Discussion

**3.1. Changes in Voltage and Power Density.** The SMFC starts after the installation of the experimental equipment. Continuous operation of the system for 30 days when the power generation tends to stabilize which is considered to be the end of the start-up phase. From the analysis of Figure 4, it can be concluded that, during the start-up of SMFC, the voltage does not continuously increase, but rather it has considerable volatility, and this volatility persists. With the increase of time, under the influence of some external factors, electricity production can be increased or decreased rapidly in a short period of time. However, the changes in the production of electricity by the two MFCs are generally in the same trend. The SMFC1 had a maximum electricity production of 170.994 mV and appeared on the third day after the start of the fuel cell (17:57:08). The power density of the SMFC at that moment is 6.89 mW/m<sup>2</sup>. At the same time point, MFC2 also reached the maximum value of 119.972 mV at the beginning of power generation, and the power density was 3.39 mW/m<sup>2</sup>. This shows that, in the early stage of SMFC start-up, the purpose of rapid increase of electricity production can be achieved

through the change of external factors, but once it loses the external field affecting it, SMFC will soon return to what it was before external factors affected it.

**3.2. The Relationship between Temperature, pH, and Voltage.** Because of the high frequency of data recording, this paper divides the data into three phases and is used to carefully compare the voltage, pH, and temperature changes. In the whole process of SMFC starting, the biological and electrochemical reaction in the single chamber SMFC changed the pH of the cathode, while the change trend of temperature and electricity generation is almost the same.

In the 1.5-2 days of first phase (Figure 5), the temperature increased significantly (from 1.5 to 1.7 days) then increased slowly (from 1.7 to 2 days), and the voltage continued to increase with the increase of temperature, but the pH increased only during the sudden increase of temperature (from 8 to 8.3) and then declined slightly and kept steady (from 8.3 to 8.2). This is the same as the change of pH for 4-5 days. The temperature was reduced greatly (from 4 to 4.3 days) and then decreased slowly (from 4.3 to 5 days), and the voltage continued to decrease with the decrease of temperature, but the pH only decreased (from 8.3 to 8.1) during the significant decrease of temperature and then rebounded to 8.3. After analysis, we think that the change of temperature will result in the change of microbial activity, which affects the production of SMFC, but the internal of SMFC is an independent system, and its pH does not continue to increase or decrease with the temperature change, but to adjust itself to a stable value after a short change. It is worth noting that there is a close positive correlation between the power generation and the temperature change during the time when the temperature changes in the first stage of the SMFC start-up. Little or sudden increase in temperature will be reflected in the production of electricity above.

During the 4-7 days of the second stage in SMFC2 start-up (Figure 6), the temperature has undergone two large-scale

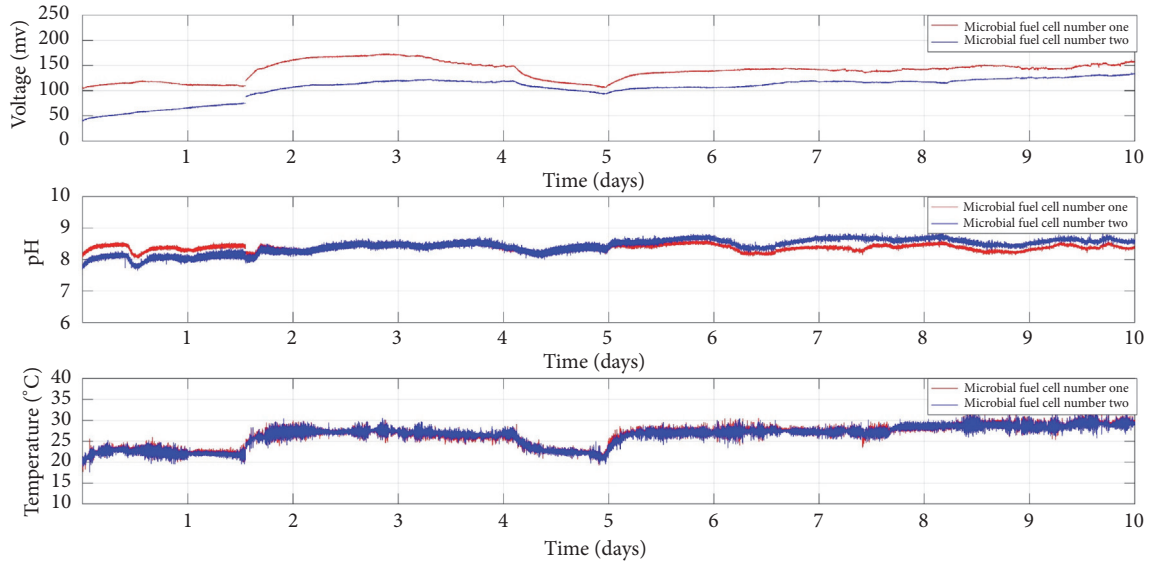


FIGURE 5: The curve of voltage, pH, and temperature at first stage.

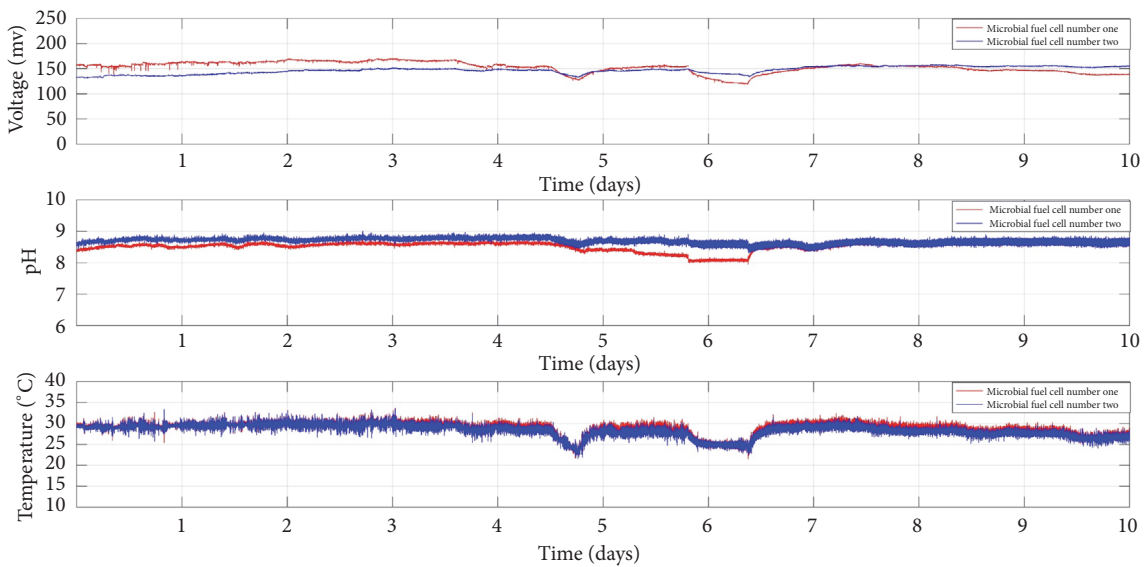


FIGURE 6: The curve of voltage, pH, and temperature at second stage.

reductions in three days and the change of voltage is almost the same as the change of temperature, when the temperature is restored to the value before falling, the voltage also returned to the value before falling. Extraordinarily, the change in pH is not the same; in addition to a slight increase in the 5.5 days, the overall trend is decreasing. This means that even if the temperature will return to normal after the change, a continuous temperature drop in a short time will lead to a continuous decrease in pH value.

In the third stage of the SMFC start-up (Figure 7), since the temperature change is gradually stable, the voltage and the change in the pH do not fluctuate too much, and it is regarded as a successful start.

**3.3. Prediction of pH Based on Neural Network.** From the data of the third stage, 5000 sets of good quality data were selected as training and prediction data, 4500 sets of data were randomly selected for training, and the remaining 500 sets of data were used for prediction. The input variables are time, voltage, and temperature, while the output variable is the pH value. For the RBF neural network, expected output and predictive output are shown in Figure 8. The errors between expected output and predictive output are presented in Figure 9.

From Figures 8 and 9, it can be observed that the pH value is well predicted, the error of most of the data is maintained within the range of -0.005 to 0.005, and the MSE is  $1.6478e-05$ .

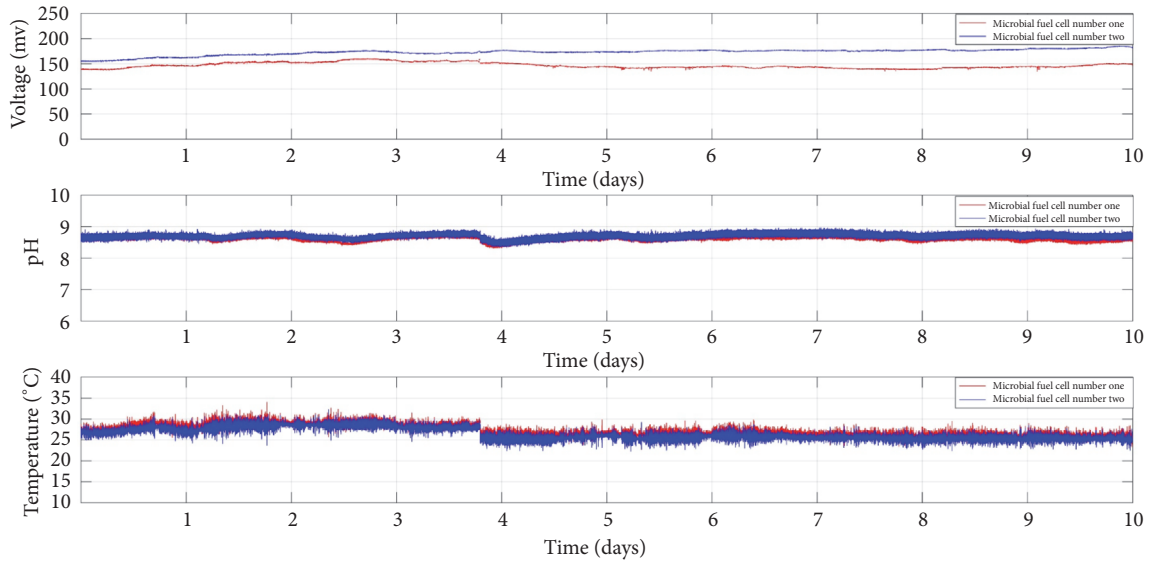


FIGURE 7: The curve of voltage, pH, and temperature at third stage.

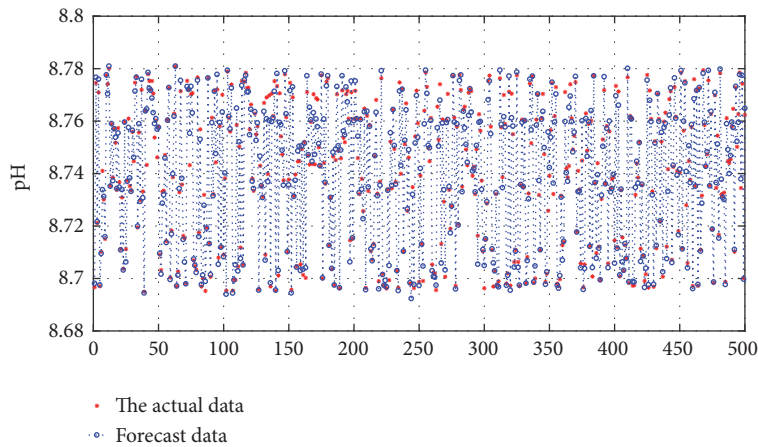


FIGURE 8: Comparison between expected output and predictive output.

It shows that the RBF neural network can fully approximate the complicated nonlinear relationship between temperature, pH, and voltage in SMFC start-up process, and it can be used to model multiparameters in SMFC’s complex internal conditions. Nevertheless, in Figure 9 there are still several absolute errors greater than 0.005. We use the same data to predict the pH based on the ELM algorithm. Because the numbers of hidden layer neurons and activation function have influence on the prediction accuracy of ELM neural network, we choose “sig” as activation function and made several groups of experiments according to different number of neurons in hidden layer. The relationship between the number of neurons in hidden layer, MSE, and computation time is shown in Table 2.

Through the Table 2, we found that the number of neurons in the hidden layer is too big, which will reduce the accuracy of prediction. Therefore, considering the accuracy and computation time of prediction, the most suitable number of neurons is 500. The comparison between expected

TABLE 2: The relationship between the number of neurons in hidden layer, MSE, and computation time.

Number	MSE	Uptime [s]
100	7.7153e-07	0.128385
200	4.0310e-07	0.169729
500	3.5001e-07	0.678840
800	4.0323e-07	0.714896
1100	3.5874e-07	0.881071
1400	3.5081e-07	2.587683
1700	3.5600e-07	3.019430
2000	3.5780e-07	4.588646

outputs and predictive outputs based on the ELM algorithm is shown in Figure 10. The prediction error between expected output and predictive output is given in Figure 11.

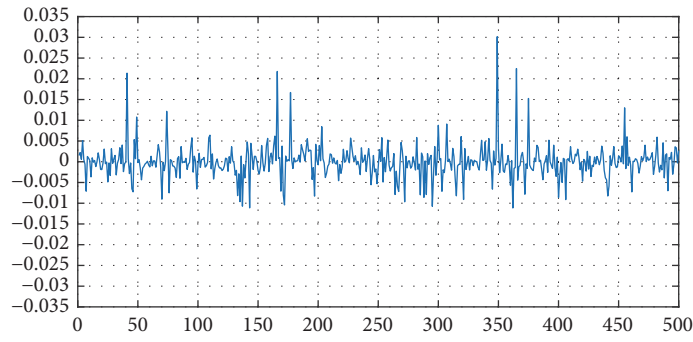


FIGURE 9: Prediction error between expected output and predictive output.

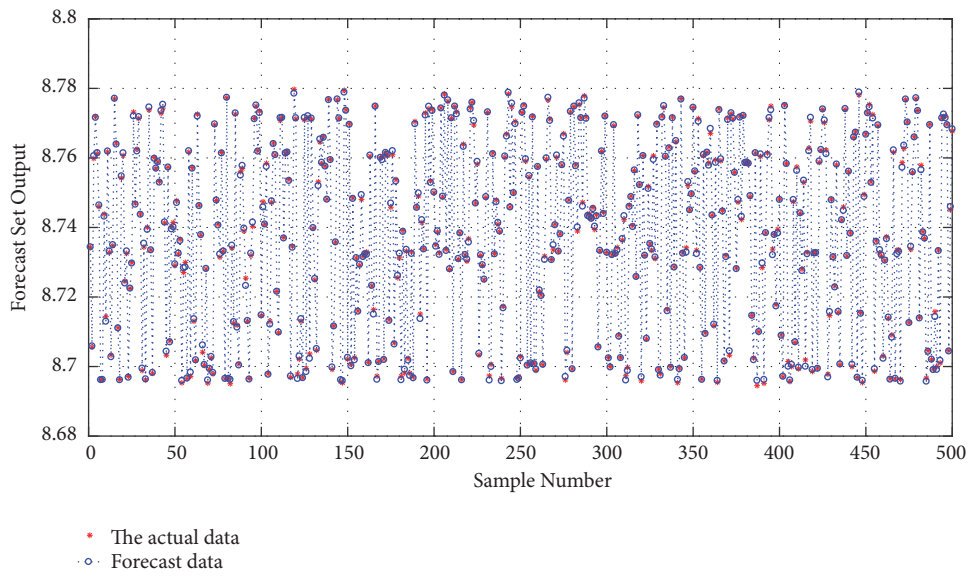


FIGURE 10: Comparison between expected output and predictive output.

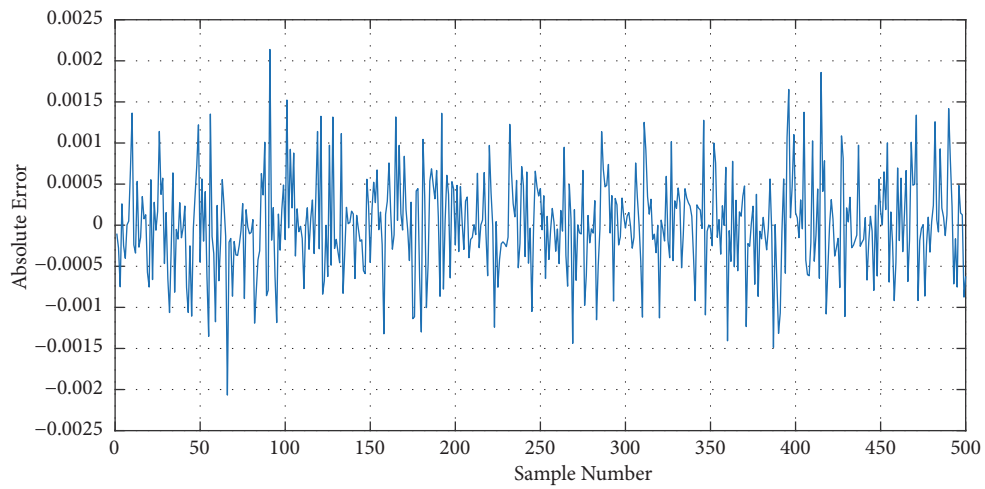


FIGURE 11: Prediction error between expected output and predictive output.

From Figures 10 and 11, it can be seen that the absolute error based on the ELM algorithm is far less than the RBF. This shows that ELM algorithm has better performance in modelling and forecasting of SFMC system than RBF algorithm and the MSE achieved  $3.5001e-07$  which is a great significance for modelling and simulation of SMFC.

#### 4. Conclusions

There is a significant correlation between pH and voltage during the start-up of a single-chamber sediment microbial fuel cell. Changes in temperature at the initial start-up can greatly affect the change in electricity generation. A sudden increase in temperature or a sudden drop may cause a sudden increase in voltage or cut back. This has important guiding significance for increasing the efficiency of generating electricity in the early stage of microbial fuel cell start-up. In the first stage of the SMFC start-up, the pH of the cathode region changes in the same trend as the voltage and temperature change significantly, but after that, pH will rebound to a certain extent. From the second stage of the SMFC start-up, we can make a conclusion that a continuous temperature drop in a short time will lead to a continuous decrease in pH, even though the temperature will go back to normal. Although the temperature during the start-up of microbial fuel cells, pH, and voltage are significantly related to the 0.01 level, the voltage and temperature correlation is much greater than the other, which also proves that the temperature plays an important role in improving the initial production of microbial fuel cells. Microbial fuel cell as a bioelectrochemical system, SMFC system, has the characteristics of complexity, strong coupling, and various parameters cannot be obtained timely and accurately in the process of starting. At this time, it is very important to realize the regression and prediction of the system equation. By comparing the two kinds of neural networks, ELM neural network is more suitable for regression and forecasting of SMFC system. The work in this paper has important guiding significance for deeper understanding and control of the start-up and operation of microbial fuel cells.

#### Data Availability

The data used to support the findings of this study are available from the corresponding author upon request.

#### Conflicts of Interest

The authors declare that there are no conflicts of interest regarding the publication of this paper.

#### Acknowledgments

This work was financially supported by the National Natural Science Foundation of China (Grant: 61773226), the Key Research and Development Program of Shandong Province (Grant: 2018GGX103054, Grant: 2017GSF220005), the Project of Shandong Province Higher Educational Science and Technology Program (Grant: J18KA372), and Independent

Innovation Projects of Colleges and Universities in Jinan City (Grant: 201401210).

#### References

- [1] M. Rahimnejad, A. Adhami, S. Darvari, A. Zirepour, and S.-E. Oh, "Microbial fuel cell as new technology for bioelectricity generation: A review," *Alexandria Engineering Journal*, vol. 54, no. 3, pp. 745–756, 2015.
- [2] S. Choi, "Microscale microbial fuel cells: Advances and challenges," *Biosensors and Bioelectronics*, vol. 69, pp. 8–25, 2015.
- [3] E. Antolini, "Composite materials for polymer electrolyte membrane microbial fuel cells," *Biosensors and Bioelectronics*, vol. 69, pp. 54–70, 2015.
- [4] A. Ramanavicius, A. Kausaite, and A. Ramanaviciene, "Enzymatic biofuel cell based on anode and cathode powered by ethanol," *Biosensors and Bioelectronics*, vol. 24, no. 4, pp. 761–766, 2008.
- [5] R. A. Nastro, G. Falcucci, M. Minutillo et al., *Microbial Fuel Cells in Solid Waste Valorization: Trends and Applications. Modelling Trends in Solid and Hazardous Waste Management*, Springer, Singapore, 2017.
- [6] E. Gambino, M. Toscanesi, F. Del Prete et al., "Polycyclic Aromatic Hydrocarbons (PAHs) Degradation and Detoxification of Water Environment in Single-chamber Air-cathode Microbial Fuel Cells (MFCs)," *Fuel Cells*, vol. 17, no. 5, pp. 618–626, 2017.
- [7] J. An, J. Nam, B. Kim, H.-S. Lee, B. H. Kim, and I. S. Chang, "Performance variation according to anode-embedded orientation in a sediment microbial fuel cell employing a chessboard-like hundred-piece anode," *Bioresour. Technology*, vol. 190, pp. 175–181, 2015.
- [8] N. Li, R. Kakarla, and B. Min, "Effect of influential factors on microbial growth and the correlation between current generation and biomass in an air cathode microbial fuel cell," *International Journal of Hydrogen Energy*, vol. 41, no. 45, pp. 20606–20614, 2016.
- [9] V. B. Oliveira, M. Simões, L. F. Melo, and A. M. F. R. Pinto, "Overview on the developments of microbial fuel cells," *Biochemical Engineering Journal*, vol. 73, no. 8, pp. 53–64, 2013.
- [10] V. Margaria, T. Tommasi, S. Pentassuglia et al., "Effects of pH variations on anodic marine consortia in a dual chamber microbial fuel cell," *International Journal of Hydrogen Energy*, vol. 42, no. 3, pp. 1820–1829, 2017.
- [11] I. A. Ieropoulos, J. Greenman, and C. Melhuish, "Miniature microbial fuel cells and stacks for urine utilisation," *International Journal of Hydrogen Energy*, vol. 38, no. 1, pp. 492–496, 2013.
- [12] D. Zhang, F. Yang, T. Shimotori, K.-C. Wang, and Y. Huang, "Performance evaluation of power management systems in microbial fuel cell-based energy harvesting applications for driving small electronic devices," *Journal of Power Sources*, vol. 217, no. 11, pp. 65–71, 2012.
- [13] Q. Jia, L. Wei, H. Han, and J. Shen, "Factors that influence the performance of two-chamber microbial fuel cell," *International Journal of Hydrogen Energy*, vol. 39, no. 25, pp. 13687–13693, 2014.
- [14] Z. Bi, Y. Hu, and J. Sun, "Simultaneous decolorization of azo dye and bioelectricity generation using a bio-cathode microbial fuel cell," *Acta Scientiae Circumstantiae*, vol. 29, no. 8, pp. 1635–1642, 2009.

- [15] T. K. Sajana, M. M. Ghangrekar, and A. Mitra, "Effect of pH and distance between electrodes on the performance of a sediment microbial fuel cell," *Water Science & Technology A Journal of the International Association on Water Pollution Research*, vol. 68, no. 3, pp. 537–543, 2013.
- [16] S. K. F. Marashi and H.-R. Kariminia, "Performance of a single chamber microbial fuel cell at different organic loads and pH values using purified terephthalic acid wastewater," *Journal of Environmental Health Science and Engineering*, vol. 13, no. 1, pp. 1–6, 2015.
- [17] S. Venkata Mohan, G. Mohanakrishna, B. P. Reddy, R. Saravanan, and P. N. Sarma, "Bioelectricity generation from chemical wastewater treatment in mediatorless (anode) microbial fuel cell (MFC) using selectively enriched hydrogen producing mixed culture under acidophilic microenvironment," *Biochemical Engineering Journal*, vol. 39, no. 1, pp. 121–130, 2008.
- [18] L. Zhang, C. Li, L. Ding et al., "Influence of temperature and pH on performance of microbial fuel cell," *Environmental Pollution & Control*, vol. 32, no. 4, pp. 62–66, 2010.
- [19] N. Jannelli, R. Anna Nastro, V. Cigolotti, M. Minutillo, and G. Falcucci, "Low pH, high salinity: Too much for microbial fuel cells?" *Applied Energy*, vol. 192, pp. 543–550, 2017.
- [20] A. Ramanavicius and A. Ramanaviciene, "Hemoproteins in design of biofuel cells," *Fuel Cells*, vol. 9, no. 1, pp. 25–36, 2009.
- [21] L. Fan, C. Li, and K. Boshnakov, "Performance improvement of a Microbial fuel cell based on adaptive fuzzy control," *Pakistan Journal of Pharmaceutical Sciences*, vol. 27, no. 3, pp. 685–690, 2014.
- [22] V. K. Krastev and G. Falcucci, "Simulating engineering flows through complex porous media via the lattice Boltzmann method," *Energies*, vol. 11, no. 4, p. 715, 2018.
- [23] X. Zhang, Y. Wang, D. Yang, and Z. Chen, "An on-line estimation of battery pack parameters and state-of-charge using dual filters based on pack model," *Energy*, vol. 115, no. 1, pp. 219–229, 2016.
- [24] H. He, R. Xiong, X. Zhang, F. Sun, and J. Fan, "State-of-charge estimation of the lithium-ion battery using an adaptive extended kalman filter based on an improved Thevenin model," *IEEE Transactions on Vehicular Technology*, vol. 60, no. 4, pp. 1461–1469, 2011.
- [25] L. Liu, L. Y. Wang, Z. Chen, C. Wang, F. Lin, and H. Wang, "Integrated system identification and state-of-charge estimation of battery systems," *IEEE Transactions on Energy Conversion*, vol. 28, no. 1, pp. 12–23, 2013.
- [26] X. Liu, Z. Chen, C. Zhang, and J. Wu, "A novel temperature-compensated model for power Li-ion batteries with dual-particle-filter state of charge estimation," *Applied Energy*, vol. 123, no. 3, pp. 263–272, 2014.
- [27] F. Sun and R. Xiong, "A novel dual-scale cell state-of-charge estimation approach for series-connected battery pack used in electric vehicles," *Journal of Power Sources*, vol. 274, pp. 582–594, 2015.
- [28] F. Sun, R. Xiong, and H. He, "A systematic state-of-charge estimation framework for multi-cell battery pack in electric vehicles using bias correction technique," *Applied Energy*, vol. 162, pp. 1399–1409, 2016.
- [29] M. Li and S. Wibowo, "Bayesian Curve Fitting Based on RBF Neural Networks," in *International Conference on Neural Information Processing*, pp. 120–130, 2017.
- [30] Y. Zeng, Y. F. Choo, B.-H. Kim, and P. Wu, "Modelling and simulation of two-chamber microbial fuel cell," *Journal of Power Sources*, vol. 195, no. 1, pp. 79–89, 2010.

## Research Article

# A Moving Object Indoor Tracking Model Based on Semiactive RFID

Hongshan Kong  and Bin Yu 

Zhengzhou Institute of Science and Technology, Zhengzhou, China

Correspondence should be addressed to Hongshan Kong; [m13643861930@163.com](mailto:m13643861930@163.com)

Received 6 September 2018; Accepted 11 December 2018; Published 25 December 2018

Academic Editor: Paolo Addresso

Copyright © 2018 Hongshan Kong and Bin Yu. This is an open access article distributed under the Creative Commons Attribution License, which permits unrestricted use, distribution, and reproduction in any medium, provided the original work is properly cited.

Aimed at the weak anti-interference and low accuracy problem of moving object indoor tracking based RFID, a moving object indoor tracking model based on semiactive RFID is presented. This model acquires scene location information through RFID low frequency triggers preinstalled, which can enhance the anti-interference ability. This model adopts an improved particle filter algorithm, which can increase the diversity of the particles, overcome the particle impoverishment, and reduce the tracking error. Simulation results indicate that the model can achieve better tracking performances. Compared with standard particle filter, the improved algorithm performance is better in the capability of tracking accuracy and robust and is more suitable for indoor tracking application in the complicated environments.

## 1. Introduction

According to the difference in obtaining energy of the electronic tag, RFID technology can be divided into passive, active, and semiactive technologies. The passive electronic tag does not contain a power supply inside and utilizes beam power supply technology. Thomas F Bechteler et al. used passive tags to achieve 2D positioning of indoor targets with positioning errors within 20 cm [1]. Po Yang et al. achieved indoor positioning and tracking of targets in a passive RFID tag environment with an error of about 5 cm [2]. Passive RFID positioning generally uses signal arrival time, signal arrival time difference, and signal arrival angle for positioning, having the advantages of low price and high positioning accuracy. However, passive RFID positioning is not suitable for long-distance indoor positioning because the working distance is relatively close and the positioning accuracy is susceptible to obstacles. The active electronic tag has a power supply inside and an automatic answering function. The LANDMARC system [3] is an active RFID indoor positioning system proposed by Ni L M, etc., with a positioning accuracy of 50% probability of positioning error within 1 meter. The VIRE algorithm [4] is a positioning method improved by Zhao Yi-yang et al. based on the LANDMARC algorithm. By introducing a

virtual reference tag, the positioning accuracy of VIRE is further improved. Active RFID positioning generally uses signal strength for positioning and has the characteristics of long positioning distance but has the problems of poor anti-interference and low positioning accuracy. Semiactive RFID technology utilizes low-frequency close-range activation of tags, high-frequency long-distance identification, and data communication and combines some of the characteristics of passive and active tags. At present, there are few researches on semiactive indoor positioning, but the semiactive RFID technology has the advantages of strong controllability and good anti-interference. The semiactive indoor positioning has a long distance, and the positioning accuracy is high, which has a great development potential.

Mathematically, moving target tracking is defined as the process that estimates the state of a moving target based on observations with noise. The state of a target is generally characterized by one or more of its information such as position, velocity, and acceleration. The real-time tracking problem of moving targets is solved by filtering the current state. The typical filtering algorithm has Bayesian filtering [5], Kalman filtering [6, 7], extended Kalman filtering [8], unscented Kalman filtering [9], and particle filtering [10]. For nonlinear systems with non-Gaussian noise, these methods

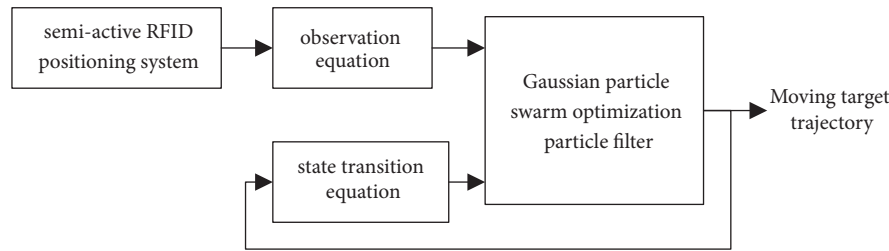


FIGURE 1: System model.

including Kalman filtering, extended Kalman filtering, and unscented Kalman filtering are difficult to obtain the estimated results that meet the requirements. Particle filtering is a filtering method that directly estimates the posterior probability density function sampling and becomes one of the most important solutions to the estimation problem in nonlinear non-Gaussian systems.

P Vorst et al. proposed particle filter algorithm to achieve indoor tracking of moving targets, but the standard particle filtering algorithm has problems such as particle degradation and particle sample depletion, which affects the tracking accuracy of moving targets [11]. Particle swarm optimization (PSO) is an optimization algorithm based on swarm intelligence theory. It is optimized by intelligent information generated by cooperation and competition among particles in the group. In [12], the authors give an improved particle filtering algorithm based on particle swarm optimization and apply the algorithm to target tracking, which can improve particle sample impoverishment. The selection of inertial coefficient, acceleration constant, and other parameters in the particle swarm optimization algorithm is closely related to the actual application and is generally determined by experience or experiment. Improper selection will directly affect the performances, and the optimization purpose cannot be achieved. The Gaussian particle swarm optimization algorithm [13] is an improved algorithm proposed by Krohling in 2004. In Gaussian particle swarm optimization, the Gaussian distribution is used to update the particle velocity and position information, and only one parameter of the number of particles needs to be determined. In this paper, the indoor target tracking system model based on semiactive RFID is studied. The indoor tracking model of moving target based on semiactive RFID and particle filter is given, and a particle filter based on Gaussian particle swarm optimization is designed to improve indoor tracking performance of moving targets.

## 2. The Proposed System Model

The indoor tracking of moving targets can be modeled as a nonlinear state estimation problem. The moving target state is estimated according to the moving equation and the observation equation of the moving target, and the filter is used to smooth the target state. The proposed model of the moving target indoor tracking system based on semiactive RFID technology is shown in Figure 1. It consists of a semiactive RFID positioning system, an observation equation,

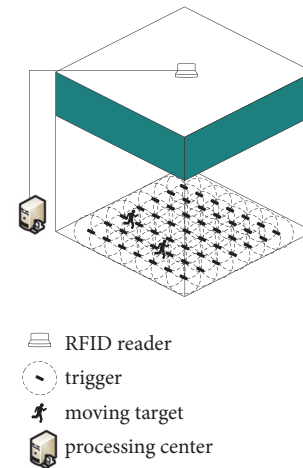


FIGURE 2: Positioning system based on semiactive RFID.

a state transition equation, and a Gaussian particle swarm optimization particle filter.

**2.1. Semiactive RFID Positioning System.** The semiactive RFID positioning system consists of an RFID reader, trigger, dual-band RFID card, moving target, and position processing center, as shown in Figure 2.

The card reader is positioned on the ceiling above the positioning area to automatically identify the RFID card information over long distances. The trigger transmits low-frequency signals in real time and is arranged under the floor according to a certain density according to the positioning accuracy, covering the target positioning area, as shown in Figure 3. The dual-band RFID card integrates two frequencies, low frequency and high frequency, which can be pasted to a moving target or carried by a moving target. The high frequency module of the RFID card is normally in a dormant state. When the RFID card enters the triggering area, the low-frequency module can receive the signal sent by the trigger in the sleep state of the RFID card and activate the high-frequency module, and the dual-frequency RFID card transmits high-frequency signal which contains the identification code and the trigger number information. If the card reader obtains the identification code of the RFID card, the trigger number, and the like, the information, are transmitted to the location processing center through the network port or the serial port, and the location processing

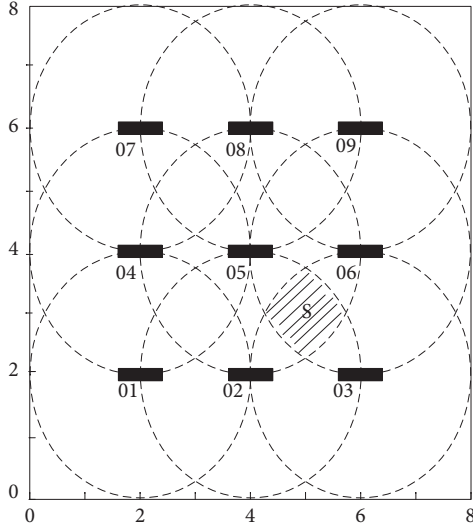


FIGURE 3: The deployment of triggers.

center calculates the location information of the mobile target.

The semiactive RFID positioning acquires the scene position information by presetting the RFID low-frequency trigger and uses the reader to locate the sensing result of the dual-frequency RFID tag in the positioning area. Assume that  $N$  triggers are evenly placed on the floor, which are presented with  $TR = \{tr_i, i = 1, 2, \dots, N\}$ , and the corresponding coordinate positions are  $\{(x_i, y_i), i = 1, 2, \dots, N\}$ . If the moving target is activated by  $M$  triggers at the  $k$  moment, which is presented with  $RFID = \{rfid_k, k = 1, 2, \dots, M\}$ , and  $rfid_k \in TR$ , the corresponding coordinate positions of triggers are  $\{(x_j, y_j), j = 1, 2, \dots, M\}$ . It can be considered that the moving target is in the common area of  $M$  triggers working area; the coordinate position can be estimated by

$$m_{RFID} = (x_{RFID}, y_{RFID}) = \left( \frac{1}{M} \sum_{j=1}^M x_j, \frac{1}{M} \sum_{j=1}^M y_j \right) \quad (1)$$

**2.2. Observation Equation.** The semiactive RFID positioning result is used as the input of the observation equation, but since the effective working area of the trigger is not a standard circular shape, there will be measurement errors in the boundary area. The observation equation can be expressed as

$$z_k = m_{RFID} + q_k \quad (2)$$

where  $z_k$  is observation value and  $q_k$  is observation noise.

**2.3. State Transition Equation.** The state transition process of the moving target in two-dimensional plane coordinates is shown in Figure 4.

Assume that the moving target reaches point A at the  $k$  moment, which is presented with  $x(k) = (x_k, y_k, \theta_k)$ , and  $(x_k, y_k)$  are two-dimensional coordinates;  $\theta_k$  is phase angle. After  $\Delta k$  time interval, the moving target moves to point B,

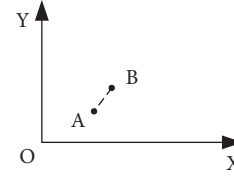


FIGURE 4: The state transition process of a moving object.

which is presented with  $x(k+1) = (x_{k+1}, y_{k+1}, \theta_{k+1})$ , where  $\Delta k$  is sampling interval. If  $\Delta k$  is smaller, the moving target can be regarded as uniform linear motion during  $\Delta k$ ; the distance of movement  $\Delta d_k$  can be expressed as

$$\Delta d_k = \sqrt{(x_k - x_{k-1})^2 + (y_k - y_{k-1})^2} \quad (3)$$

The state transition equation can be expressed as

$$x(k+1) = \begin{bmatrix} x_k + \Delta d_k \cos(\theta_k) \\ y_k + \Delta d_k \sin(\theta_k) \\ \theta_k + \Delta \theta_k \end{bmatrix} + r_k \quad (4)$$

where  $r_k$  is process noise;  $\Delta \theta_k$  is the change in phase angle after  $\Delta k$  time interval.

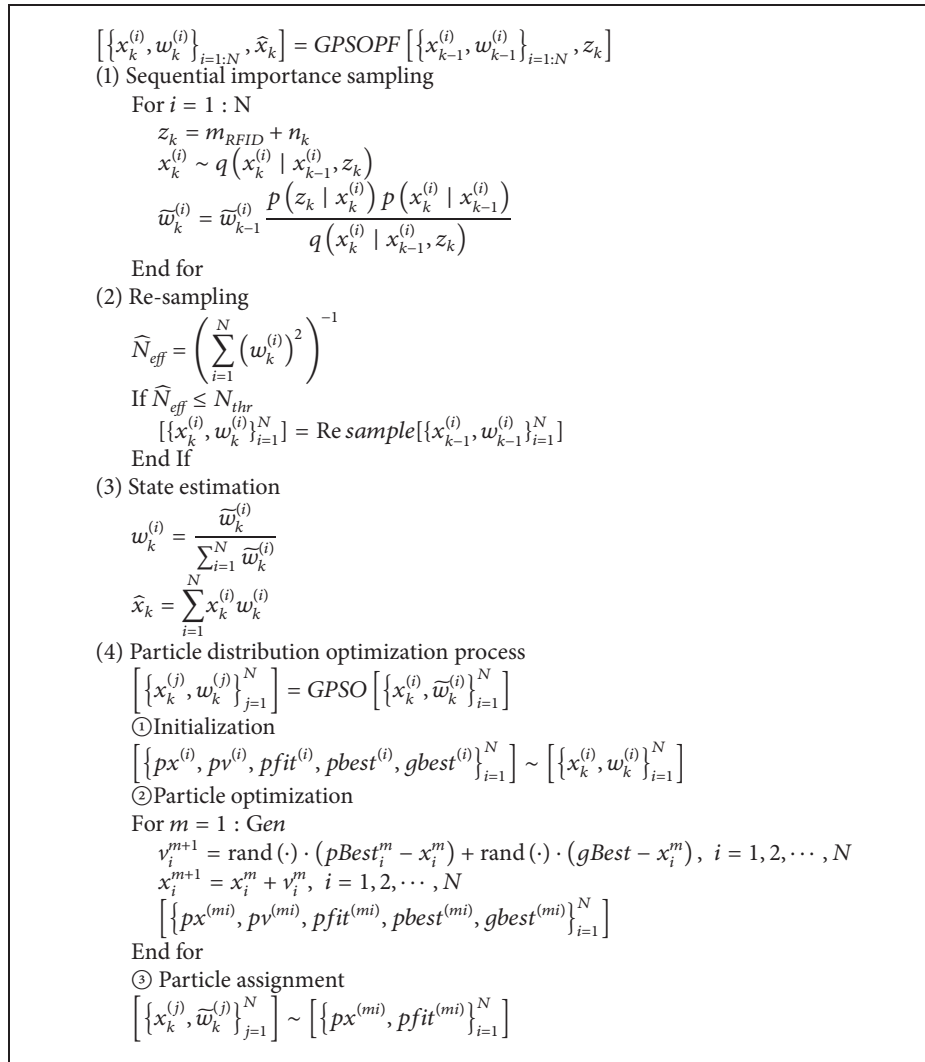
**2.4. Gaussian Particle Swarm Optimization Particle Filter.** Standard particle filters are prone to depletion in particle sampling during the importance sampling process. The Gaussian particle swarm optimization algorithm can be used to improve the performance of the standard particle filter. The Gaussian particle swarm optimization particle filter (GPSO-PF) is obtained by effectively combining the two algorithms. The flow chart is shown in Box 1. GPSO-PF makes the particles move toward the high likelihood region before the weight update, improve the utility of each particle, and alleviate the degradation of the particle weight.

### 3. Simulation Experiment and Evaluation

In order to measure the feasibility and effectiveness of the semiactive RFID based indoor target tracking system model and to evaluate its tracking performance, MATLAB simulation was used for analysis and comparison.

**3.1. Simulation Scene and Parameter Settings.** The simulation test is carried out by using MATLAB software. It is assumed that the simulation experiment is in an 8m\*8m hall. The card reader is deployed on the ceiling above the positioning area, and the RFID card information can be automatically recognized by long distance wireless. The trigger transmits low-frequency signals in real time and is laid on the floor. A total of 7\*7 triggers are deployed. Each trigger area is a circle with a radius of 1 meter, and the distance between the two triggers is 2 meters.

In Figure 5(a), the starting position of the moving target is A (2, 0.5), moving along a straight line to B (6, 4.5) with an angle of  $45^\circ$  to the  $x$ -axis. In Figure 5(b), the starting position



Box 1: Flow chart of GPSO-PF.

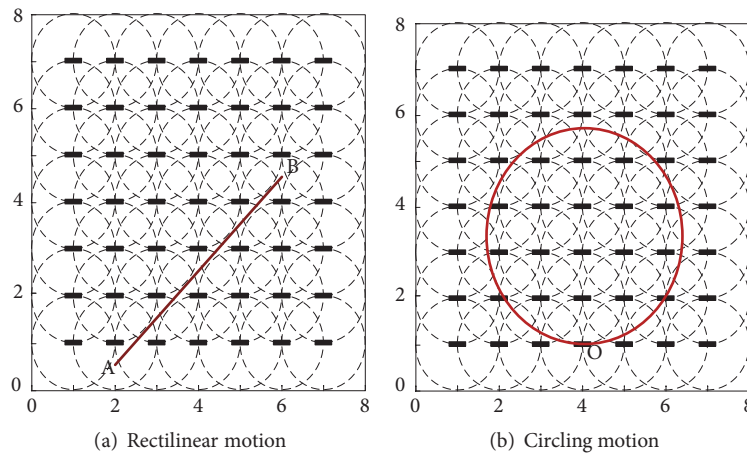


FIGURE 5: Simulation scenario.

TABLE 1: Simulation parameter setting.

Simulation parameter	Description	Setting value
$N$	Number of particles	50
$R$	Process noise variance	0.0025
$Q$	Observed noise variance	0.5
$M$	Number of iterations	5
$L$	Number of simulation steps	100

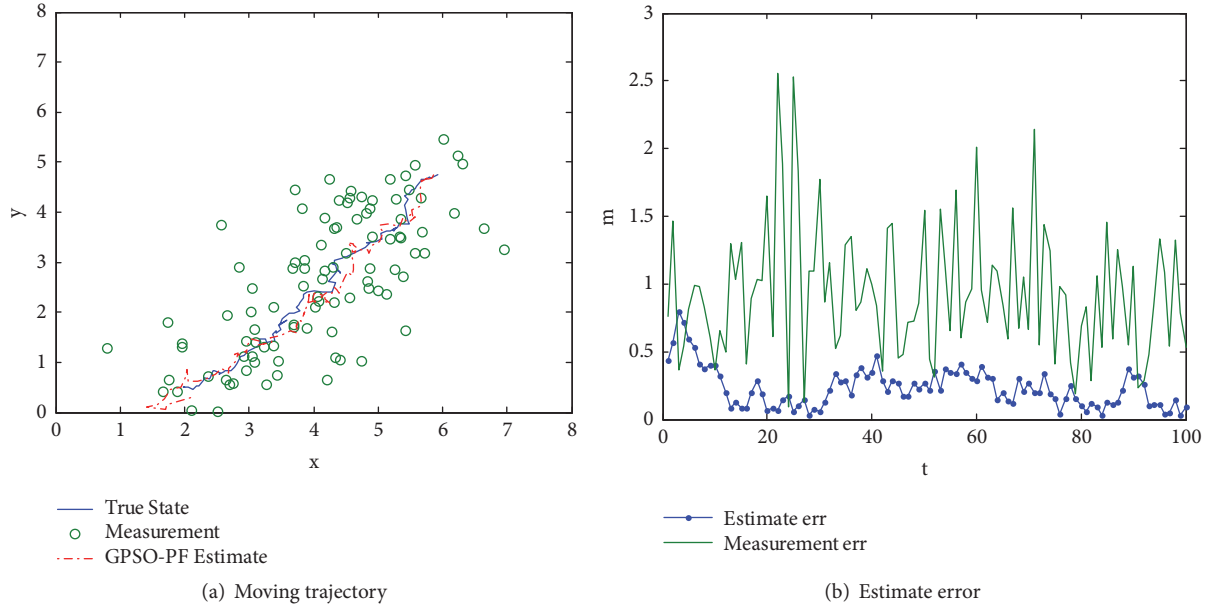


FIGURE 6: Moving trajectory and error of rectilinear motion.

of the moving target is  $O(4, 1)$ , moving counterclockwise along the circumference of a radius of 2.5 meters.

Both process noise and observed noise are Gaussian white noise, and the simulation parameters are set as shown in Table 1.

**3.2. Performance Analysis.** Suppose that the actual coordinates and estimated coordinates of an object are  $(x_0, y_0)$  and  $(x'_0, y'_0)$ . To measure algorithm performance, estimation error  $e$  is defined as

$$e = \sqrt{(x'_0 - x_0)^2 + (y'_0 - y_0)^2} \quad (5)$$

The simulation running track and estimation error of linear motion are shown in Figure 6. The simulation running track and estimation error of circular motion are shown in Figure 7.

It can be seen from Figures 6 and 7 that the moving target is linear motion, the maximum error is 2.5545m, the average error is 0.9414m, and the maximum error is 0.7969m after filtering by GPSO-PF algorithm, and the average estimation error is 0.2340m. While the moving target is circular motion, the maximum error is 2.1745m and the average error is 0.8517m. The maximum error is 0.8166m and the average estimation error is 0.2345m after filtering by GPSO-PF algorithm. For semiactive technology for target

positioning and tracking, whether it is linear motion or circular motion, even though the measurement error is large, the ideal tracking effect can be achieved by using GPSO-PF algorithm, which indicates that the proposed model is feasible and effective.

In order to better explain the performance of the GPSO-PF algorithm, the performance comparison with the standard particle filter PF is performed, and the simulation scene and configuration parameters remain unchanged. Select Root Mean Square Error (RMSE) as an indicator to evaluate the performance of the algorithm; RMSE is defined as

$$RMSE = \sqrt{\frac{1}{T} \cdot \sum_{k=1}^T (x_k - \hat{x}_k)^2} \quad (6)$$

The average of the RMSE is used to represent the filtering accuracy of the algorithm, and the variance of the RMSE is used to measure the stability of the algorithm. For each of the two algorithms, linear motion and circular motion were performed for 1000 Monte Carlo experiments, and the RMSE value curve is shown in Figure 8.

Calculate the mean and variance of RMSE, as shown in Table 2.

It can be seen from Table 1 that, compared with the PF algorithm, the RMSE mean value of the GPSO-PF algorithm

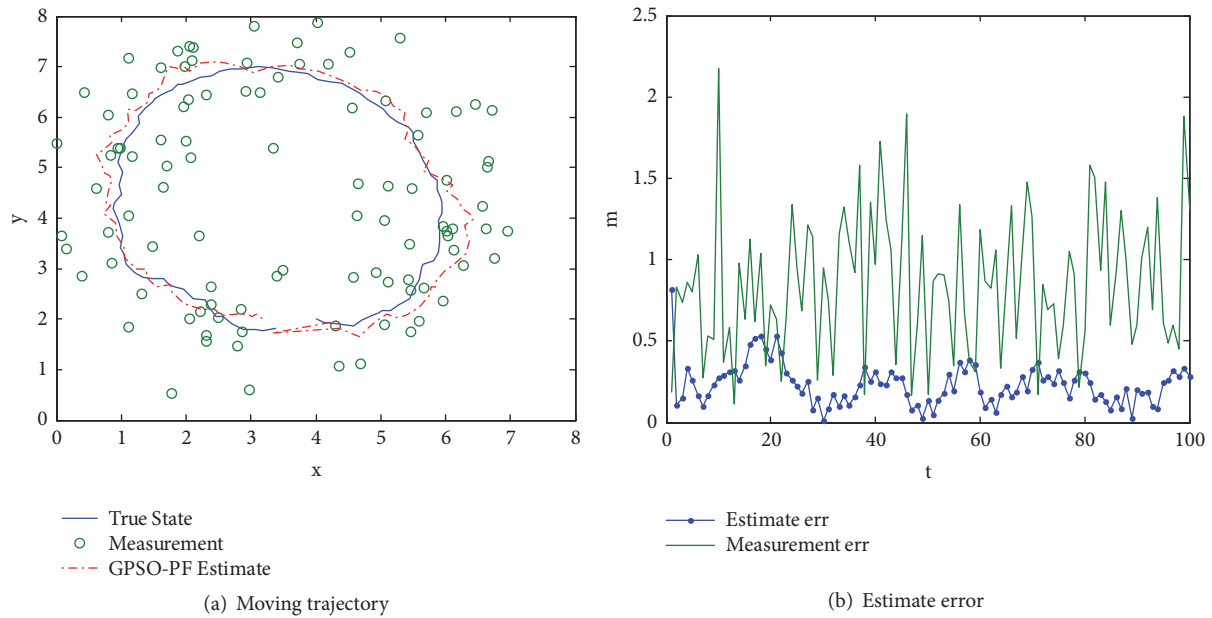


FIGURE 7: Moving trajectory and error of circling motion.

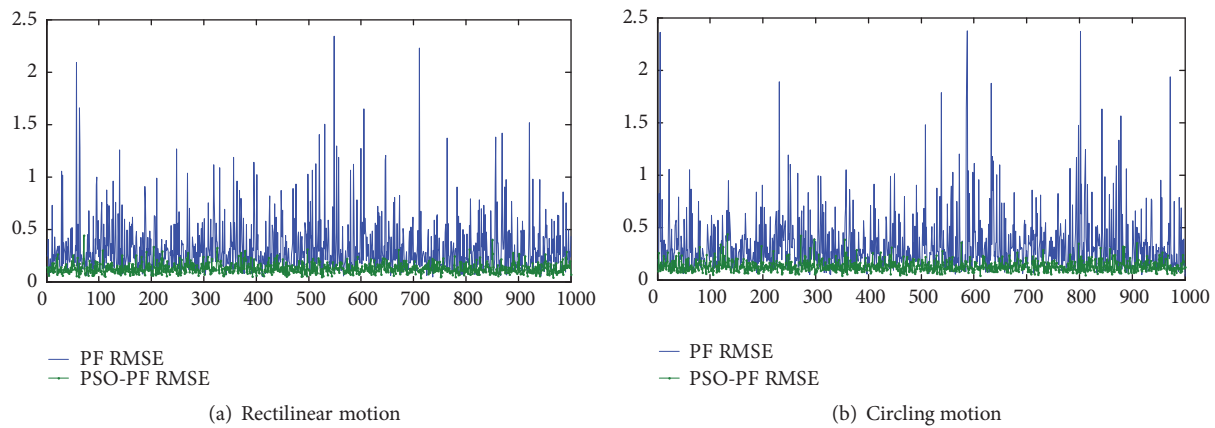


FIGURE 8: RMSE of Monte Carlo simulation.

applied to the moving target for linear motion is increased by 61.8%, and the RMSE mean value of the GPSO-PF algorithm applied to the circular motion of the moving target is increased by 61.3%. Tracking filtering accuracy is greatly improved. The RMSE variance of GPSO-PF algorithm applied to moving targets for linear motion is 3.25% of PF algorithm. The RMSE variance of GPSO-PF algorithm applied to circular motion of moving targets is 3.37% of PF algorithm, and the stability of indoor tracking is greatly improved.

Simulation results indicate that the GPSO-PF algorithm has better performances than the standard particle filter in the capability of tracking accuracy and robust; the reason is that the Gaussian particle swarm optimization algorithm is introduced into the standard particle filter. To the problem of particle impoverishment, GPSO-PF algorithm incorporates the newest observations into sampling process and

also optimizes the particles. Through particles distribution optimization process, the particles are moved toward regions where they have larger values of posterior density function. As a result, the diversity of the particles increases, the particle impoverishment is solved, and the tracking error is reduced dramatically.

The proposed model of this paper is compared with literature [1], literature [3], and literature [11] schemes in four aspects: RFID technology, positioning error, support for moving targets, and filtering algorithm, as shown in Table 3.

It can be seen from Table 2 that the general indoor positioning algorithm is not suitable for tracking of moving targets, and the indoor tracking requires filtering algorithm. The filtering algorithm of this model adopts GPSO-PF. The passive RFID positioning error is small, and the active RFID positioning error is large. The positioning error of this model is only 0.23m, which can achieve higher positioning accuracy.

TABLE 2: Mean value and variance of two algorithms.

Filtering algorithm	Rectilinear motion		Circling motion	
	RMSE mean	RMSE variance	RMSE mean	RMSE variance
PF	0.3300m	0.0708	0.3373m	0.0801
Proposed algorithm	0.1262m	0.0023	0.1304m	0.0027

TABLE 3: Performance comparison of four schemes.

Scheme	[1]	[3]	[11]	Proposed model
RFID technology	Passive	Active	Passive UHF	Semiactive
Positioning error	20cm	1m	0.5m	0.23m
Support for moving targets	No	No	Yes	Yes
Filtering algorithm	-	-	PF	GPSO-PF

## 4. Conclusions

In view of the shortcomings of current passive RFID technology and active RFID technology in indoor positioning in terms of distance and positioning accuracy, a semiactive RFID based indoor target tracking system model is proposed, which can achieve higher positioning and tracking accuracy. It can meet the needs of indoor location tracking in complex environments and has a good application prospect. The next research focus is that, due to the limitations of experimental conditions, the experimental data is obtained through simulation and is not verified in the real environment. The work that the proposed algorithm is tested and applied in the real environment will be done.

## Data Availability

The experiment data used to support the findings of this study were supplied by Hongshan Kong under license and so cannot be made freely available. Requests for access to these data should be made to m13643861930@163.com.

## Conflicts of Interest

The authors declare that there are no conflicts of interest regarding the publication of this paper.

## Acknowledgments

This research work is financially supported by the Fundamental Research Funds of Institute of Science and Technology (no. 2015603503).

## References

- [1] T. F. Bechteler and H. Yenigün, "2-D localization and identification based on SAW ID-tags at 2.5 GHz," *IEEE Transactions on Microwave Theory and Techniques*, vol. 51, no. 5, pp. 1584–1590, 2003.
- [2] P. Yang and W. Wu, "Efficient particle filter localization algorithm in dense passive RFID tag environment," *IEEE Transactions on Industrial Electronics*, vol. 61, no. 10, pp. 5641–5651, 2014.
- [3] L. M. Ni, Y. Liu, Y. C. Lau, and A. P. Patil, "LANDMARC: indoor location sensing using active RFID," *Wireless Networks*, vol. 10, no. 6, pp. 701–710, 2004.
- [4] Y. Zhao, Y. Liu, and L. M. Ni, "VIRE: active RFID-based localization using virtual reference elimination," in *Proceedings of the 36th International Conference on Parallel Processing (ICPP '07)*, p. 56, Xi'an, China, September 2007.
- [5] S. Arulampalam and B. Ristic, "Comparison of the particle filter with range-parameterised and modified polar EKFs for angle-only tracking," in *Proceedings of the Signal and Data Processing of Small Targets*, vol. 4048 of *Proceedings of SPIE*, pp. 288–299, Orlando, Fla, USA, April 2000.
- [6] R. E. Kalman, "A new approach to linear filtering and prediction problems," *Journal of Fluids Engineering*, vol. 82, no. 1, pp. 35–45, 1960.
- [7] Y. Jianmin, *Research on Particle Filter Tracking Method*, Chinese Academy of Sciences, Beijing, 2004.
- [8] A. Doucet and A. M. Johansen, "A tutorial on particle filtering and smoothing: fifteen years later," in *The Oxford handbook of nonlinear filtering*, pp. 656–704, Oxford Univ. Press, Oxford, 2011.
- [9] S. Särkkä, *Bayesian Filtering and Smoothing*, Cambridge University Press, Cambridge, UK, 2013.
- [10] N. Gordon and D. Salmond, "Novel approach to non-linear and non-Gaussian Bayesian state estimation," in *Proceedings of the Institute Electric Engineering*, vol. 14, pp. 107–113, 1993.
- [11] P. Vorst and A. Zell, "Particle filter-based trajectory estimation with passive UHF RFID fingerprints in unknown environments," in *Proceedings of the 2009 IEEE/RSJ International Conference on Intelligent Robots and Systems, IROS 2009*, pp. 395–401, USA, October 2009.
- [12] Z. Caiqian, G. Lei, and H. Dong, "Research on particle swarm particle filter algorithm based on target tracking," *Computer Simulation*, vol. 31, pp. 392–396, 2014.
- [13] R. A. Krohling, "Gaussian swarm: a novel particle swarm optimization algorithm," in *Proceedings of the IEEE Conference on Cybernetics and Intelligent Systems*, vol. 1, pp. 372–376, December 2004.

## Research Article

# Iterative Learning Control for Nonlinear Weighing and Feeding Process

Jianqi An <sup>1,2,3</sup> Fayang You,<sup>1,2</sup> Min Wu,<sup>1,2</sup> and Jinhua She<sup>1,2,3</sup>

<sup>1</sup>School of Automation, China University of Geosciences, Wuhan 430074, China

<sup>2</sup>Hubei Key Laboratory of Advanced Control and Intelligent Automation for Complex Systems, Wuhan 430074, China

<sup>3</sup>School of Engineering, Tokyo University of Technology, Tokyo 192-0982, Japan

Correspondence should be addressed to Jianqi An; [anjianqi@cug.edu.cn](mailto:anjianqi@cug.edu.cn)

Received 7 September 2018; Accepted 25 November 2018; Published 20 December 2018

Academic Editor: AITOU CHE Abdelouhab

Copyright © 2018 Jianqi An et al. This is an open access article distributed under the Creative Commons Attribution License, which permits unrestricted use, distribution, and reproduction in any medium, provided the original work is properly cited.

Due to the nonlinear dynamics in weighing and feeding process, it is difficult to achieve high accuracy with conventional control methods. This paper uses a piecewise linearization method for the nonlinear problem and discusses the application of iterative learning control in weighing and feeding process. First, the nonlinear problem and the repeatability are discussed based on dynamic analysis of weighing and feeding process. Next, a linear state space model is established with a piecewise linearization method. Then, an iterative learning controller is presented by utilizing repetitive characteristics, and the controller parameters are obtained by using a multi-objective optimization method. Finally, simulation results show that the presented control method improves the control performances and the accuracy of feeding.

## 1. Introduction

A weighing and feeding process is a process in which a certain material is weighted and added to a reaction vessel through an actuator, which repeats many times to get more products. It is widely used in modern industries, such as metallurgical industry, pharmaceutical industry, and food processing industry [1]. Vibratory feeders are the main actuators in weighing and feeding processes, which use vibration and gravity to feed material to a weighing hopper. The weight of the material in the weighing hopper is one of the most important control objectives in a weighing and feeding process. However, it is difficult to achieve high accuracy of the weight because of the existence of a nonlinear process of the vibratory feeder [2].

In the past few years, some good methods were researched to establish accurate mathematical models for vibratory feeders. For example, a model of a resonant linear electromagnetic vibratory feeder was established based on the kinetic and potential energies, the dissipative function of the mechanical system, and Lagrangian formulation [3]. Czubak [4] considered the vibratory feeder as a single degree of

freedom system (SDOF). The relations between the structural elements of the mode and the vibratory feeder were analyzed based SDOF [5]. Furthermore, Chandravanshi [6, 7] analyzed the dynamic characteristics of vibratory feeders and examined experimentally the vibration behavior of the particles on the conveying surface. The purposes of these researches are to dynamically analyze the vibratory feeders and the vibration behavior of the particles. These researches reveal the nonlinear relationship between the feed rate and the motor speed (vibratory motors rotate to generate vibration to make the vibratory feeder work). It is obvious that vibratory feeders are nonlinear devices in weighing and feeding processes.

Regarding the control and modeling of weighing and feeding processes, many results were published for one feeding batch, which considered the vibrating feeder as a linear device. For instance, a generalized-predictive-control (GPC)-based PID controller was presented for a linear weighing and feeding process, which considered the relationship between the feed rate and motor speed as a linear model [8]. This method derived PID parameters based on GPC and considered a ramp-type signal as the reference signal. The method presented in [8] was improved in [9], in which the

TABLE I: Some notations used in this paper.

Symbol	Definition
$t, k$	The time and batch index, respectively
$\alpha, \beta$	The time period in a batch and the total number of batches, respectively
$R$	The set of real number
$I, \mathbf{0}$	The identity matrix and the zero matrix with appropriate dimensions, respectively
$f, U$	The output frequency and input voltage of the inverter, respectively
$\omega$	The motor speed
$v$	The feeding rate
$w$	The weight of the material in the weighing hopper

estimated plant parameters are updated when the prediction error increases. A feedback controller was used in the control of an electromagnetic vibratory feeder, in which the vibratory feeder is considered as a linear device [10]. And an amplitude-frequency control method of the vibratory feeder is presented by using a current-controlled power converter [11]. The previous researches on the weighing and feeding processes achieved good results. However, the achieved control accuracy can be further improved by considering the nonlinear characters and the repetitive nature of weighing and feeding processes.

In summary, previous researches on modeling of vibratory feeders had proven that vibratory feeders are nonlinear devices. However, previous researches on the control and modeling of weighing and feeding processes did not consider the nonlinear characters of the weighing and feeding process. In our previous paper [12], the repetitive nature of a weighing and feeding process was considered, and then the feeding accuracy was improved to some extent. However, this performance improvement is limited because the paper did not consider the nonlinear characters of vibratory feeders.

Many good methods were presented to solve nonlinear problems, such as the fixed point index theory in cones which proved the existence of positive solutions of nonlinear boundary value problem [13, 14], the method of upper and lower solutions and different monotone iterative techniques which analyzed a nonlinear third-order differential equation [15], a weighted norm method which analyzed nonlinear Schrodinger equations [16], and using neural networks to approximate the nonlinear function [17, 18]. These researches provide good references for the nonlinear problem of weighing and feeding processes. Iterative learning control (ILC) [19] can improve the control performance with the increasing number of the batch by taking full advantage of the history control information to correct control input. With the effectivity of solving the problems with repetitive characteristics, ILC is widely used in the batch processes [20, 21] and repetitive processes [22, 23].

For the repeatability and the nonlinear problem of weighing and feeding processes, this paper presents an ILC and a piecewise linearization method. The rest of this paper is organized as follows: Section 2 analyzes the dynamic characteristics and the nonlinear problem of the process and then establishes an approximate linear model. Section 3 gives a 2D ILC system based on an improved state space model and a

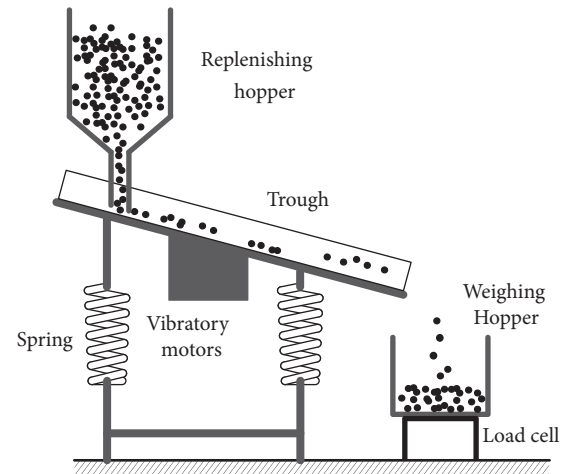


FIGURE 1: Weighing and feeding process.

controller parametrization method by using a multi-objective optimization method. Section 4 gives the simulation results to illustrate the effectiveness of the proposed method. Finally, Section 5 draws a conclusion.

Some notations used in this paper are described in Table 1.

## 2. Analysis and Modeling of Weighing and Feeding Process

This section presents the structure of a weighing and feeding process, analyzes the dynamic characteristic of the weighing and feeding process, discusses its nonlinear problem, and presents an approximate linear model by using a piecewise linearization method.

*2.1. Weighing and Feeding Process.* The schematic diagram of a weighing and feeding process is shown in Figure 1. The vibratory feeder is the main device, which consists of springs for damping, vibration motors for oscillating, and a trough for conveying material. The vibration motors are fixed under the bottom of the trough, which generates an exciting force by driving a rotating unbalanced mass. The trough is inclined at an angle which performs sinusoidal vibration caused by the exciting force. When the trough vibrates due to the exciting force, materials are shaken into the weighing hopper by

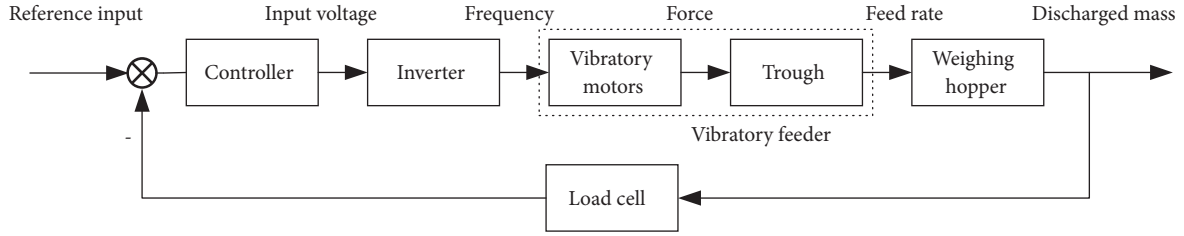


FIGURE 2: Weighing and feeding process control system.

the vibrating trough. Weighing hopper measures materials weight by a load cell. The feed rate of the material is adjusted by changing the exciting force and the vibration frequency. In addition, the replenishing hopper replenishes the loss material on the trough. The spring is installed between the trough and the support unit to reduce damage to the support unit caused by the vibration motors.

The block diagram of weighing and feeding process control system is shown in Figure 2, which consists of a controller, an inverter, a vibratory feeder, a weighing hopper, and a load cell. The controller adjusts the speed of the motor by changing the input voltage of the inverter. When the weight of material reaches the set value, the vibratory feeder stops working and prepares for the next batch. In order to get more products, the feeding process like that repeats many times.

The dynamic characteristics of the inverter are approximated as an amplifier [8], which is expressed as

$$f = K_i U, \quad (1)$$

where  $K_i$  is the gain of the inverter.  $f$  and  $U$  denote the output frequency and input voltage of the inverter, respectively.

The trough of the vibratory feeder vibrates under the drive of double rotating unbalances which produces a periodic force excitation in a definite direction. The electrical model of the motor can be written as a first-order system

$$\dot{\omega} + \frac{1}{T}\omega = \frac{K_m}{T}f, \quad (2)$$

where  $K_m$  is the gain and  $T$  is assumed to be the time constant of the motor.

The exciting forces,  $F_1$  and  $F_2$ , are induced by a single rotating unbalance mass (see Figure 3),  $m$ , respectively. The values of  $F_1$  and  $F_2$  are both given as

$$F_0 = mE\omega^2, \quad (3)$$

where  $E$  is the eccentricity of the unbalance.

Decomposition of excitation force into horizontal and vertical directions

$$F_x = F_0 \cos \omega t + F_0 \cos(\pi - \omega t) = 0, \quad (4)$$

$$F_y = F_0 \sin \omega t + F_0 \sin(\pi - \omega t) = 2F_0 \sin \omega t. \quad (5)$$

The mechanical model of the vibratory feeder is assumed as an SDOF which consists of a mass,  $M$ , spring with stiffness

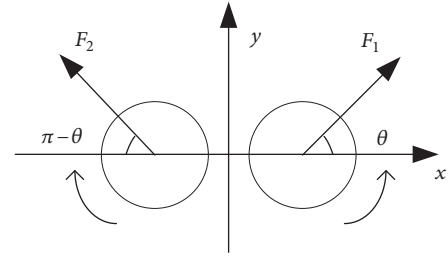


FIGURE 3: The exciting force.

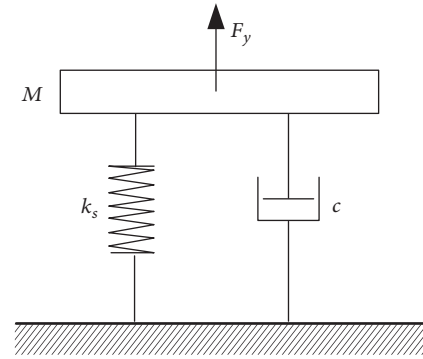


FIGURE 4: The mechanical model of the vibratory feeder.

coefficient,  $k_s$ , and damping with damping coefficient,  $c$ , [5] as shown in Figure 4.

The equation of the vibration is expressed as

$$M \frac{d^2 Y}{dt^2} + c \frac{dY}{dt} + k_s Y = F_y, \quad (6)$$

where  $M$  is the equivalent weight which consists of the weight of the vibratory motor, the trough, and the materials in the trough.  $Y$  denotes the displacement from the balance position in vertical directions. The damping is the consumption of vibratory energy as heat and sound.  $k_s$  is the equivalent stiffness of springs. The exciting force in vertical directions changes sinusoidally. By analyzing (6) through vibration theory, the maximum amplitude,  $Y_{\max}$ , of the vibratory trough is written as

$$Y_{\max} = \frac{2F_0}{\sqrt{(k_s - \omega^2 M)^2 + (\omega c)^2}}. \quad (7)$$

The moving distance of the material in the trough is related to the vibration amplitude in one vibration. During a certain period of time, all the materials in the trough move multiple times to form an average feed rate. The average feed rate,  $v$ , and the maximum amplitude of vibration are approximately proportion

$$v = K \frac{\omega}{2\pi} Y_{\max}, \quad (8)$$

where  $K$  is the structure coefficient, which depends on the width of the trough and the angle of inclination of the trough.

Vibratory feeder adds material to the hopper, which can be approximated as an integrator

$$w = \int v dt, \quad (9)$$

where  $w$  denotes the weight of the material in the weighing hopper.

**2.2. Piecewise Linearization Method.** By substituting (7) into (8), the relationship between the feeding rate and the motor speed is written as

$$v = \frac{K m E \omega^3}{\pi \sqrt{(k_s - \omega^2 M)^2 + (\omega c)^2}}. \quad (10)$$

It is obvious that the feed rate increases first and then decreases when the motor speed increases through mathematic analysis of the relationship between  $v$  and  $\omega$ . And when the vibration frequency of the vibratory motor is equal to the natural frequency,  $\omega_n$ , the vibrating feeder reaches the maximum feeding rate. At this time, the motor speed  $\omega_n$  is

$$\omega_n = \sqrt{\frac{k_s}{M}}. \quad (11)$$

Through the analysis of the relationship between the feeding rate and the motor speed, the feeding rate is decreasing when the motor speed is increasing ( $\omega > \omega_n$ ). It should be avoided to work in this state because increasing the speed of the motor reduces the feeding speed, which is an inefficient production way.

Based on the considerations above, the motor of vibratory feeder should work in motor speed range  $0 < \omega < \omega_n$ . Then, the nonlinear relationship between motor speed and feeding rate is piecewise linearized into proportional relation

$$v = \begin{cases} a_1 \omega + b_1, & 0 \leq \omega < \omega_1 \\ a_2 \omega + b_2, & \omega_1 \leq \omega < \omega_2, \\ a_3 \omega + b_3, & \omega_2 \leq \omega < \omega_3 \end{cases} \quad (12)$$

which can be written as

$$v = a_i \omega + b_i, \quad \omega \in \Omega_i, \quad 1 \leq i \leq 3. \quad (13)$$

The nonlinear character and the piecewise linearization result are shown in Figure 5. In this paper, the motor

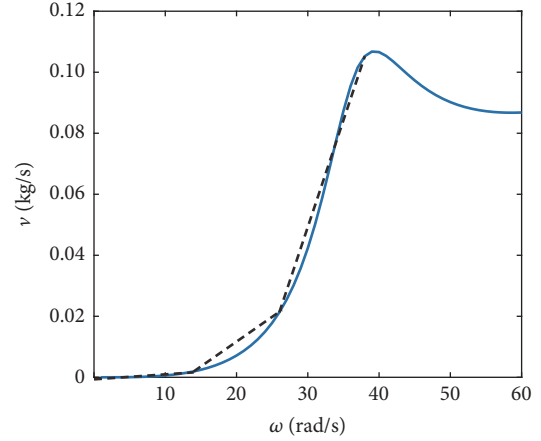


FIGURE 5: The relationship between feeding rate and motor speed.

speed range is divided equally into three intervals. Then the parameters of (13) are obtained by the corresponding motor speed and feeding rate. The accuracy of the piecewise linearized model significantly depends on the number of the intervals and more intervals can increase the accuracy of the piecewise linearized model.

Use the following coordinate transformation

$$\bar{v} = \begin{bmatrix} v \\ 0 \end{bmatrix}, \quad (14)$$

$$\bar{\omega} = \begin{bmatrix} \omega \\ 1 \end{bmatrix}. \quad (15)$$

Then the nonlinear relationship between the feeding rate and the motor speed transforms into an approximate linear model

$$\bar{v} = \begin{bmatrix} a_i & b_i \\ 0 & 0 \end{bmatrix} [\bar{\omega}], \quad \bar{\omega} \in \bar{\Omega}_i, \quad 1 \leq i \leq 3. \quad (16)$$

**2.3. The State Space Model of the Weighing and Feeding Process.** According to the previous analysis, the relationship between motor speed and the input voltage is obtained from (1) and (2), the relationship between motor speed and the feeding rate is obtained from (16), and the relationship between the feeding rate and the weight of the material in the weighing hopper is obtained from (9). They are used as parts of (17) and (18). Then the model of the control object is described as

$$\dot{x} = \begin{bmatrix} \dot{\omega} \\ 0 \\ \dot{w} \end{bmatrix} = \begin{bmatrix} -\frac{1}{T} & 0 & 0 \\ 0 & 0 & 0 \\ a_i & b_i & 0 \end{bmatrix} \begin{bmatrix} \omega \\ 1 \\ w \end{bmatrix} + \begin{bmatrix} \frac{K_m K_i}{T} \\ 0 \\ 0 \end{bmatrix} u, \quad (17)$$

$$1 \leq i \leq 3,$$

$$y = [0 \ 0 \ 1] x. \quad (18)$$

### 3. Iterative Learning Control System

This section discusses the batch characteristic of weighing and feeding process and gives the structure of iterative learning controller based on an improved state space model. Then the controller parameters are found through a multi-objective optimization method.

**3.1. 2D System Representation.** A discrete state space equation which is obtained by using the zero-order hold to discrete (17) and (18) over  $1 \leq t \leq \alpha, k \geq 1$  is

$$x_k(t+1) = A_i x_k(t) + B_i u_k(t), \quad 1 \leq i \leq 3, \quad (19)$$

$$y_k(t) = C x_k(t), \quad (20)$$

where  $u_k(t) \in R$  is the control input,  $y_k(t) \in R$  is the output,  $x_k(t) \in R^2$  is the state vector, including the motor speed  $\omega$ , and the discharged mass  $w$  at time  $t$  in  $k$ th batch.

The discrete dynamic model in the  $k$ th batch is described as above. However, this process will be repeated many times to get more products in practice. Based on the above considerations, define  $x(t, k)$ , and  $y(t, k)$  as the state and output of the process at time  $t$  in  $k$ th batch. The following discrete model can be established from (19) and (20) to describe the relationship between batches:

$$x(t+1, k) = A_i x(t, k) + B_i u(t, k), \quad 1 \leq i \leq 3, \quad (21)$$

$$y(t, k) = C x(t, k). \quad (22)$$

Let  $y_{ref}(t)$  be a vector-valued reference representing desired output behavior. Then the error in the  $k$ th batch is

$$e(t, k) \triangleq y_{ref}(t) - y(t, k). \quad (23)$$

In ILC, a general form of the control law is

$$\Sigma_{ilc} : \begin{cases} u(t, k) = u(t, k-1) + u_e(t, k) \\ u(t, 0) = 0, \end{cases} \quad (24)$$

where  $u(t, k)$  is constructed from the control in previous batch and a correction term  $u_e(t, k)$  from the history control information and  $u(t, 0)$  denotes the initial control.  $u_e(t, k)$  is the updating law to be determined.

Define  $f_e(t, k+1)$  as the difference of  $f$  between two consecutive batches

$$f_e(t, k+1) \triangleq f(t, k+1) - f(t, k), \quad (25)$$

where  $f$  may be state  $x$  or output  $y$  and thus is in accordance with the ILC updating law shown in (24).

The tracking error integral  $\sum e(t, k+1)$  is an additional state variable in ILC design, which is defined as

$$\sum e(t, k+1) \triangleq \sum_{i=0}^t e(i, k+1). \quad (26)$$

It follows from (21), (22) and (25) that

$$x_e(t+1, k+1) = A_i x_e(t, k+1) + B_i u_e(t, k+1), \quad (27)$$

$$1 \leq i \leq 3.$$

Equation (23) can be written as

$$\begin{aligned} e(t+1, k+1) &= y_{ref}(t+1) - y(t+1, k+1) \\ &\quad + y(t+1, k) - y(t+1, k) \\ &= e(t+1, k) - y_e(t+1, k+1). \end{aligned} \quad (28)$$

It follows from (21), (22), (25), and (27) that

$$y_e(t+1, k+1) = C A_i x_e(t, k+1) + C B_i u_e(t, k+1), \quad (29)$$

$$1 \leq i \leq 3.$$

According to (29), (28) can be written as

$$\begin{aligned} e(t+1, k+1) &= e(t+1, k) - C A_i x_e(t, k+1) \\ &\quad - C B_i u_e(t, k+1). \end{aligned} \quad (30)$$

It follows from (26) and (30) that

$$\begin{aligned} \sum e(t+1, k+1) &= \sum e(t, k+1) + e(t+1, k) \\ &\quad - C A_i x_e(t, k+1) \\ &\quad - C B_i u_e(t, k+1), \quad 1 \leq i \leq 3. \end{aligned} \quad (31)$$

Introduce a new state variable as

$$\hat{x}(t+1, k+1) = \begin{bmatrix} x_e(t+1, k+1) \\ e(t+1, k+1) \\ \sum e(t+1, k+1) \end{bmatrix}. \quad (32)$$

Then the corresponding state space model is derived as

$$\begin{aligned} \hat{x}(t+1, k+1) &= A_{i,1} \hat{x}(t, k+1) + A_{i,2} \hat{x}(t+1, k) \\ &\quad + \hat{B}_i u_e(t, k+1), \quad 1 \leq i \leq 3, \end{aligned} \quad (33)$$

where

$$A_{i,1} = \begin{bmatrix} A_i & \mathbf{0} & \mathbf{0} \\ -C A_i & \mathbf{0} & \mathbf{0} \\ -C A_i & \mathbf{0} & \mathbf{I} \end{bmatrix}, \quad (34)$$

$$A_{i,2} = \begin{bmatrix} \mathbf{0} & \mathbf{0} & \mathbf{0} \\ \mathbf{0} & \mathbf{I} & \mathbf{0} \\ \mathbf{0} & \mathbf{I} & \mathbf{0} \end{bmatrix}, \quad (35)$$

$$\hat{B}_i = \begin{bmatrix} B_i \\ -C B_i \\ -C B_i \end{bmatrix}. \quad (36)$$

**3.2. Controller Design.** Design an updating law as

$$u_e(t, k+1) = K_{i,1} \hat{x}(t, k+1) + K_{i,2} \hat{x}(t+1, k), \quad (37)$$

$$1 \leq i \leq 3,$$

where

$$K_{i,1} = [K_{i,11} \ K_{i,12} \ K_{i,13}], \quad (38)$$

$$K_{i,2} = [K_{i,21} \ K_{i,22} \ K_{i,23}]. \quad (39)$$

Then an improved 2D system of (21) and (22) is given by

$$\begin{aligned} \hat{x}(t+1, k+1) &= \widehat{A}_{i,1} \hat{x}(t, k+1) + \widehat{A}_{i,2} \hat{x}(t+1, k), \\ &1 \leq i \leq 3, \end{aligned} \quad (40)$$

where

$$\widehat{A}_{i,1} = \begin{bmatrix} A_i + B_i K_{i,11} & B_i K_{i,12} & B_i K_{i,13} \\ -CA_i - CB_i K_{i,11} & -CB_i K_{i,12} & -CB_i K_{i,13} \\ -CA_i - CB_i K_{i,11} & -CB_i K_{i,12} & I - CB_i K_{i,13} \end{bmatrix}, \quad (41)$$

$$\widehat{A}_{i,2} = \begin{bmatrix} B_i K_{i,21} & B_i K_{i,22} & B_i K_{i,23} \\ -CB_i K_{i,21} & I - CB_i K_{i,22} & -CB_i K_{i,23} \\ -CB_i K_{i,21} & I - CB_i K_{i,22} & -CB_i K_{i,23} \end{bmatrix}. \quad (42)$$

More states information of (21) and (22) is considered, and the control law (37) contains control information of the current and historical batches. The appropriate controller parameters,  $K_{i,1}$ ,  $K_{i,2}$ , will give the system a better control performance.

### 3.3. Stability Analysis

**Theorem 1.** *The closed-loop 2D system in (40) is asymptotically stable and if symmetric positive matrices  $P > Q$  exist, the following linear matrix inequality holds*

$$\psi_i = \begin{bmatrix} -P & PA_{i,1} + Y_1 & PA_{i,2} + Y_2 \\ * & -Q & \mathbf{0} \\ * & * & -P + Q \end{bmatrix} < 0, \quad (43)$$

where

$$Y_1 = P\widehat{B}_i K_{i,1}, \quad (44)$$

$$Y_2 = P\widehat{B}_i K_{i,2}. \quad (45)$$

And the controller parameters  $K_{i,1}$ ,  $K_{i,2}$  can be solved as

$$K_{i,1} = \widehat{B}_i^{-1} P^{-1} Y_1, \quad 1 \leq i \leq 3, \quad (46)$$

$$K_{i,2} = \widehat{B}_i^{-1} P^{-1} Y_2, \quad 1 \leq i \leq 3. \quad (47)$$

*Proof.* Inspired by [20], the following Lyapunov functions are considered

$$V_{1,1} = \hat{x}(t+1, k+1)^T P \hat{x}(t+1, k+1), \quad (48)$$

$$V_{0,1} = \hat{x}(t, k+1)^T Q \hat{x}(t, k+1), \quad (49)$$

$$V_{1,0} = \hat{x}(t+1, k)^T (P - Q) \hat{x}(t+1, k), \quad (50)$$

where  $P$  and  $Q$  are symmetric positive matrices to be determined, and  $P > Q$ .

The state energy increment in both time and batch directions is

$$\Delta V = V_{1,1} - V_{0,1} - V_{1,0}. \quad (51)$$

It follows from (40) and (51) that

$$\Delta V = \xi^T \widehat{\psi} \xi, \quad (52)$$

where

$$\xi = [\hat{x}(t, k+1)^T, \hat{x}(t+1, k)^T]^T, \quad (53)$$

$$\widehat{\psi}_i = \begin{bmatrix} \widehat{A}_{i,1}^T P \widehat{A}_{i,1} - Q & \widehat{A}_{i,1}^T P \widehat{A}_{i,2} \\ \widehat{A}_{i,2}^T P \widehat{A}_{i,1} & \widehat{A}_{i,2}^T P \widehat{A}_{i,2} - P + Q \end{bmatrix}. \quad (54)$$

Therefore,  $\Delta V < 0$  guarantees asymptotic stability of closed-loop 2D system in (40).

Applying Schur's complement  $\Delta V < 0$  is equivalent to

$$\begin{bmatrix} -P & P\widehat{A}_{i,1} & P\widehat{A}_{i,2} \\ * & -Q & \mathbf{0} \\ * & * & -P + Q \end{bmatrix} < 0. \quad (55)$$

Replace  $\widehat{A}_{i,1}$ ,  $\widehat{A}_{i,2}$  with  $A_{i,1} + \widehat{B}_i K_{i,1}$ ,  $A_{i,2} + \widehat{B}_i K_{i,2}$ , and defining  $P\widehat{B}_i K_{i,1} = Y_1$ ,  $P\widehat{B}_i K_{i,2} = Y_2$ , LMI constraints in (43) can be obtained.  $\square$

**3.4. Controller Parametrization.** Theorem 1 is a sufficient and unnecessary condition for system stability, and there are solutions to the LMI Equation (43). The controller with them as parameters stabilizes the system but has different control performance. An efficient combination of linear matrix inequalities and single-objective optimization algorithms was proposed to develop a control law parametrization that guarantees performance [23]. Based on this research, this paper proposes a method of controller parametrization, which combines LMI and multi-objective optimization algorithms.

For the convenience of writing,  $K_{i,1}$ ,  $K_{i,2}$  are described as  $K_1$ ,  $K_2$  in this section.

In order to measure the control performance of the system, the first function is chosen as

$$f_1(K_1, K_2) = \sum_{k=1}^{\beta} \sum_{t=1}^{\alpha} (y - y_{ref})^2, \quad (56)$$

which is the sum of squares of the output error for all samples in all batches.  $f_1(K_1, K_2)$  contains all the system output error information, and the smaller the  $f_1(K_1, K_2)$  is, the better the system's dynamic performance and steady-state performance are.

In order to measure the deviation of the output from the reference signal, the second function is chosen as

$$f_2(K_1, K_2) = \sum_{k=1}^{\beta} \max \left\{ |y(t, k) - y_{ref}(t)|_{t \in [1, \alpha]} \right\}. \quad (57)$$

TABLE 2: The plant parameters.

Plant parameter	Abbreviation	Value
The coefficient of the inverter	$k_i$	5
The weight of the unbalanced mass	$m$	3.5
The eccentricity of weight from the shaft	$E$	0.06
The structure coefficient	$K$	0.882
The equivalent stiffness of springs	$k_s$	76520
Weight of trough	$M$	60
The coefficient damping	$c$	752
The gain of the motor	$k_m$	0.6
The time-constant of the motor	$T$	1

TABLE 3: The parameters of the controller.

Controller parameter	Value
$K_{1,1}$	[-1.862, -0.050, 0.150, -0.027, -0.605]
$K_{1,2}$	[0.035, 0.055, 0.020, 0.081, 0.206]
$K_{2,1}$	[-1.959, 0.054, -0.087, 0.052, -0.192]
$K_{2,2}$	[0.034, 0.060, -0.072, -0.124, 0.282]
$K_{3,1}$	[-1.757, 0.005, -0.082, -0.033, 0.015]
$K_{3,2}$	[0.076, 0.052, 0.020, 0.029, 0.291]

After the above discussion, the controller parametrization problem is transformed into the following multi-objective optimization problem:

$$\begin{aligned} \min \quad & [f_1(K_1, K_2), f_2(K_1, K_2)], \\ \text{s.t.} \quad & \psi_i < 0, \quad 1 \leq i \leq 3. \end{aligned} \quad (58)$$

Based on multi-objective simulated annealing [24], the following steps are proposed.

*Step 1.* Initialize parameters, the initial temperature,  $T$ , and the lowest temperature,  $T_l$ .

*Step 2.* Solve the LMI  $\psi_i < 0$ , apply (46) and (47) to calculate  $K_1, K_2$ , set  $K_{1,opt} = K_1, K_{2,opt} = K_2$ , simulate (21) and (22) and the nonlinear system with the control law (37), and calculate and set  $f_{1,opt} = f_1(K_1, K_2), f_{2,opt} = f_2(K_1, K_2)$ .

*Step 3.* Alter the controller matrices  $K_{1,opt}, K_{2,opt}$ , obtain the new matrices  $K_1, K_2$ , simulate (21) and (22) and the nonlinear system with the control law (37), and calculate the  $f_{1,new} = f_1(K_1, K_2), f_{2,new} = f_2(K_1, K_2)$ .

*Step 4.* If  $f_{1,new} < f_{1,opt}$ , and  $f_{2,new} < f_{2,opt}$ , set  $K_{1,opt} = K_1, K_{2,opt} = K_2, f_{1,opt} = f_{1,new}, f_{2,opt} = f_{2,new}$ . If it does not, calculate  $\mu = (1 - \alpha) \cdot (f_{1,new} - f_{1,opt}) / (f_{1,new} + f_{1,opt}) + \alpha \cdot (f_{2,new} - f_{2,opt}) / (f_{2,new} + f_{2,opt})$ , and set  $K_{1,opt} = K_1, K_{2,opt} = K_2, f_{1,opt} = f_{1,new}, f_{2,opt} = f_{2,new}$  with the probability  $P_{accept} = \exp(-(1 - \mu)/T)$ .

*Step 5.* Reduce the temperature  $T$ . If  $T > T_l$ , go to Step 3. If it does not, go to Step 6.

*Step 6.* Verify  $K_{1,opt}, K_{2,opt}$  subject to  $\psi_i < 0, 1 \leq i \leq 3$ , using  $K_{1,opt}, K_{2,opt}$ .

## 4. Simulation

This section gives numerical simulation results, which show that more accurate feed accuracy is obtained after several feeding batches.

The plant parameters are set in Table 2. The discrete state space model is obtained with a sampling period of  $T_s = 1$  s. And the weight of material in one batch is set: 20 kg. The duration of a batch is set to 200 s. Then the reference trajectory is obtained

$$y_{ret} = 0.1t, \quad 1 \leq t \leq 200. \quad (59)$$

The controller parameters  $K_{i,1}$  and  $K_{i,2}$  are obtained by using the controller parameterization method presented in Section 3.4, which is shown as Table 3.

The updating law is obtained by substituting the controller parameters into (37). Then the input voltage is calculated based on (24) and (37), which is the control input applied to the inverter. Then the output response and the process state are obtained in this sampling time. The output responses in all batches are shown in Figure 6.

Figure 6 shows that the output response curve has large fluctuations in the first batch, which means the feeding performance is not good enough. However, the feeding performance is improved. Figure 6 shows that the fluctuation of the output response curve in the latter batch is smaller than the previous.

Figure 7 shows the output response in the first, fourth, and eighth batches, which shows that the errors between the output responses and the reference signal are decreased with the number of batch increasing.

Two performance indicators, the squared error, and the maximum error are presented to evaluate the control performance of the ILC for the weighing and feeding process. The

TABLE 4: Two performance indicators in first 9 batches.

$k$	1	2	3	4	5	6	7	8	9
Squared error	555	276	123	53	40	35	36	39	34
Maximum error	2.34	2.21	1.56	1.38	1.26	1.17	1.09	1.03	0.98

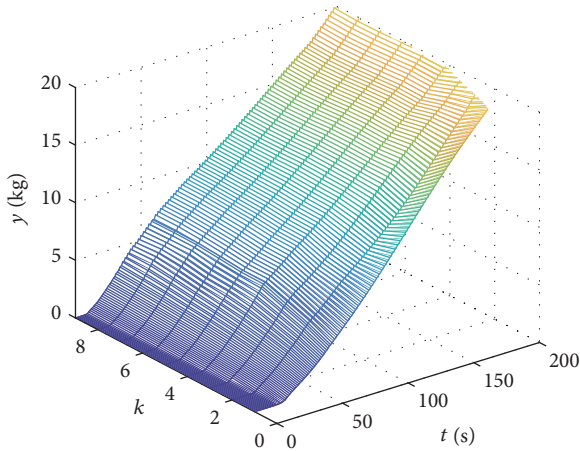
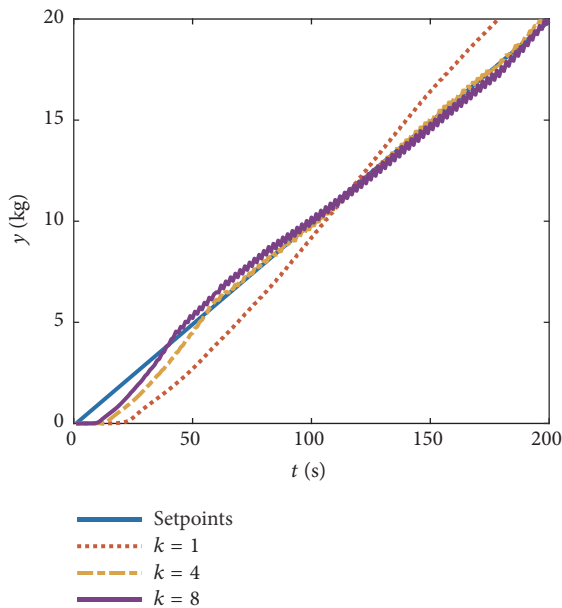


FIGURE 6: Output responses (all batches).

FIGURE 7: Output responses ( $k = 1, 4, 8$ ).

squared error denotes the output error in all sampling time in one batch. The small squared error means good steady-state performance. The maximum error denotes the maximum output error in one batch. The small maximum error means good dynamic state performance. Two performance indicators in the first 9 batches are shown in Table 4. Two values of performance indicators decrease with the number of batch increasing.

Figure 8 shows the change of two performance indicators in the first 9 batches, which demonstrates intuitively that

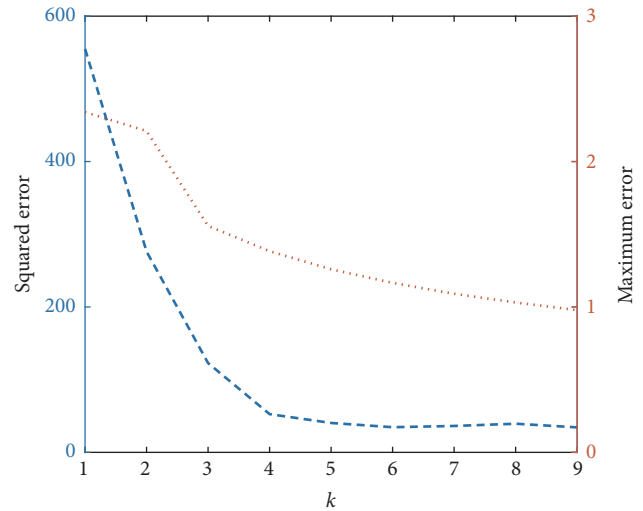


FIGURE 8: Changes in performance indicators.

the two performance indicators decrease with the number of batch increasing. It means that the control performances and the accuracy of feeding are improved with the number of batches increasing, and the accuracy of feeding is acceptable after 3-4 batches.

## 5. Conclusions

This paper presented an ILC method and a piecewise linearization method for a weighing and feeding process with the nonlinear problem. A piecewise linearization method was presented to establish an approximate linear model. Then an iterative learning controller was designed and the controller parametrization method was given. The simulation result showed that ILC and piecewise linearization effectively solved the control problem of weighing and control process.

Our future work will design a new control method considering the changes in the parameters of the weighing and feeding process model, caused by changes in the properties of the material. And we plan to develop a control system to apply the control method in a real-world weighing and feeding process.

## Data Availability

The data used to support the findings of this study are included within the article.

## Conflicts of Interest

The authors declare that there are no conflicts of interest regarding the publication of this paper.

## Acknowledgments

This work was supported by the Hubei Provincial Natural Science Foundation of China, under Grants 2016CFB480 and 2015CFA010; the National Natural Science Foundation of China, under Grants 61333002 and 61203017; and the 111 Project, under Grant B17040. The first author is an overseas researcher under Postdoctoral Fellowship of Japan Society for the Promotion of Science (JSPS) and his JSPS Fellowship ID is P16799.

## References

- [1] S. R. Gopireddy, C. Hildebrandt, and N. A. Urbanetz, "Numerical simulation of powder flow in a pharmaceutical tablet press lab-scale gravity feeder," *Powder Technology*, vol. 302, pp. 309–327, 2016.
- [2] M. A. Parameswaran and S. Ganapathy, "Vibratory conveying-analysis and design: A review," *Mechanism and Machine Theory*, vol. 14, no. 2, pp. 89–97, 1979.
- [3] Ž. V. Despotović, D. Urukalo, M. R. Lečić, and A. Ćosića, "Mathematical modeling of resonant linear vibratory conveyor with electromagnetic excitation: simulations and experimental results," *Applied Mathematical Modelling*, vol. 41, pp. 1–24, 2017.
- [4] P. Czubak, "Analysis of the new solution of the vibratory conveyor," *Archives of Metallurgy and Materials*, vol. 58, no. 4, pp. 1037–1043, 2013.
- [5] M. L. Chandravanshi and A. K. Mukhopadhyay, "Experimental modal analysis of the vibratory feeder and its structural elements," *International Journal of Applied Engineering Research*, vol. 10, no. 13, pp. 33303–33310, 2015.
- [6] M. L. Chandravanshi and A. K. Mukhopadhyay, "Dynamic analysis of vibratory feeder and their effect on feed particle speed on conveying surface," *Measurement*, vol. 101, pp. 145–156, 2017.
- [7] M. L. Chandravanshi and A. K. Mukhopadhyay, "Analysis of variations in vibration behavior of vibratory feeder due to change in stiffness of helical springs using FEM and EMA methods," *Journal of the Brazilian Society of Mechanical Sciences and Engineering*, vol. 39, no. 9, pp. 3343–3362, 2017.
- [8] T. Sato, "Design of a GPC-based PID controller for controlling a weigh feeder," *Control Engineering Practice*, vol. 18, no. 2, pp. 105–113, 2010.
- [9] T. Sato, T. Yamamoto, N. Araki, and Y. Konishi, "Performance-adaptive generalized predictive control-based proportional-integral-derivative control system and its application," *Journal of Dynamic Systems, Measurement, and Control*, vol. 136, no. 6, p. 061003, 2014.
- [10] A. I. Ribić and Ž. V. Despotović, "High-performance feedback control of electromagnetic vibratory feeder," *IEEE Transactions on Industrial Electronics*, vol. 57, no. 9, pp. 3087–3094, 2010.
- [11] Ž. V. Despotović, A. I. Ribić, and V. M. Šinik, "Power current control of a resonant vibratory conveyor having electromagnetic drive," *Journal of Power Electronics*, vol. 12, no. 4, pp. 677–688, 2012.
- [12] F. You and J. An, "Iterative learning control for batch weighing and feeding process," in *Proceedings of the 2018 37th Chinese Control Conference (CCC)*, pp. 2904–2908, Wuhan, China, July 2018.
- [13] X. Hao, L. Liu, Y. Wu, and Q. Sun, "Positive solutions for nonlinear  $n$ th-order singular eigenvalue problem with nonlocal conditions," *Nonlinear Analysis, Theory, Methods and Applications*, vol. 73, no. 6, pp. 1653–1662, 2010.
- [14] P. Zhang, L. Liu, and Y. Wu, "Existence and uniqueness of solution to nonlinear boundary value problems with sign-changing Greens function," *Abstract and Applied Analysis*, vol. 2013, no. 1, pp. 1–7, 2013.
- [15] X. L. Lin and Z. Q. Zhao, "Iterative technique for a third-order differential equation with three-point nonlinear boundary value conditions," *Electronic Journal of Qualitative Theory of Differential Equations*, vol. 12, pp. 1–10, 2016.
- [16] Y. Sun, L. Liu, and Y. Wu, "The existence and uniqueness of positive monotone solutions for a class of nonlinear Schrödinger equations on infinite domains," *Journal of Computational and Applied Mathematics*, vol. 321, pp. 478–486, 2017.
- [17] C. Hua, L. Zhang, and X. Guan, "Decentralized output feedback adaptive NN tracking control for time-delay stochastic nonlinear systems with prescribed performance," *IEEE Transactions on Neural Networks and Learning Systems*, vol. 26, no. 11, pp. 2749–2759, 2015.
- [18] C. Hua, L. Zhang, and X. Guan, "Distributed Adaptive Neural Network Output Tracking of Leader-Following High-Order Stochastic Nonlinear Multiagent Systems with Unknown Dead-Zone Input," *IEEE Transactions on Cybernetics*, vol. 47, no. 1, pp. 177–185, 2017.
- [19] M. Uchiyama, "Formulation of high-speed motion pattern of a mechanical arm by trial," *Transactions of the Society of Instrument and Control Engineers*, vol. 14, no. 6, pp. 706–712, 1978.
- [20] T. Liu and F. Gao, "Robust two-dimensional iterative learning control for batch processes with state delay and time-varying uncertainties," *Chemical Engineering Science*, vol. 65, no. 23, pp. 6134–6144, 2010.
- [21] J. Lu, Z. Cao, R. Zhang, and F. Gao, "Nonlinear Monotonically Convergent Iterative Learning Control for Batch Processes," *IEEE Transactions on Industrial Electronics*, vol. 65, no. 7, pp. 5826–5836, 2018.
- [22] J. Emelianova, P. Pakshin, K. Galkowski, and E. Rogers, "Stability of nonlinear discrete repetitive processes with Markovian switching," *Systems and Control Letters*, vol. 75, pp. 108–116, 2015.
- [23] L. Hladowski, K. Galkowski, W. Nowicka, and E. Rogers, "Repetitive process based design and experimental verification of a dynamic iterative learning control law," *Control Engineering Practice*, vol. 46, pp. 157–165, 2016.
- [24] A. Haidine and R. Lehnert, "Multi-Case Multi-Objective Simulated Annealing (MC-MOSA): new approach to adapt simulated annealing to multi-objective optimization," *Engineering and Technology*, vol. 48, no. 12, pp. 705–713, 2008.

## Research Article

# A High-Precision Rotor Position and Displacement Prediction Method Specially for Bearingless Permanent Magnet Synchronous Motor

Yukun Sun , Qiang Cui, Yonghong Huang , and Ye Yuan 

*School of Electrical and Information Engineering, Jiangsu University, Zhenjiang 212013, China*

Correspondence should be addressed to Yonghong Huang; [hyh@ujs.edu.cn](mailto:hyh@ujs.edu.cn)

Received 24 July 2018; Revised 5 November 2018; Accepted 6 November 2018; Published 9 December 2018

Academic Editor: Roberto Fedele

Copyright © 2018 Yukun Sun et al. This is an open access article distributed under the Creative Commons Attribution License, which permits unrestricted use, distribution, and reproduction in any medium, provided the original work is properly cited.

The high performance sensorless performance of the bearingless permanent magnet synchronous motor is the main direction to improve the reliability of the drive system and reduce the cost of the system, and the high-precision rotor position and displacement prediction method is the key technology to realize the high performance sensorless operation. In view of the above problems, a rotor displacement and position prediction method based on kernel extreme learning machine is studied in this paper. On the basis of the mathematical model of BPMSM, this method predicted the position and displacement of the rotor according to the current and flux linkage of suspension windings and torque windings by KELM. The construction method of rotor position and displacement prediction model was described; meanwhile the implementation steps of offline training and online prediction were given. Finally, the error between the method and the actual value was compared by simulation and experiment. The results showed that the proposed method had high accuracy and could achieve real-time rotor position and displacement and then provides the basis for realizing sensorless operation control of BPMSM.

## 1. Introduction

Bearingless motors have a wide application prospect because of its low energy consumption, high speed and no lubrication. Among all kinds of bearingless motors, bearingless permanent magnet synchronous motor [1] (BPMSM) has been highly influenced by domestic and foreign scholars because of its high power factor, low heat generation, and high reliability. The key to the stable rotation and suspension of BPMSM is to accurately detect the position and radial displacement of the rotor in real time. Generally, sensors such as eddy current and Hall type are used for detecting the position and displacement of the BPMSM rotor, and the detection method increases the cost of the motor. The complexity of the system hardware makes the installation and maintenance cumbersome and the failure rate is high and, even worse, the critical speed of the motor is reduced. Because sensors are susceptible to the environment, they seriously affect the reliability of the system. Therefore, the research of BPMSM's high-performance sensorless control system has high practical significance.

At present, the global researches on sensorless operation of bearingless motors have achieved initial results. For instance, with the linear relationship between the self-inductance of suspension windings and the displacement of the rotor, an extra high frequency excitation signal was injected into the suspension windings to detect the high frequency differential voltage signal of the suspension windings to track the radial displacement of the rotor in literature [2–4]. However, the extraction and processing of high frequency signal were complex; furthermore, dynamic performance was poor, so it was not suitable for high-speed operation. In literatures [5–7], sensorless control technology establishes a series of state observers to detect rotor position and velocity by detecting relevant electrical signals in the motor windings. This type of method relies on the back EMF of PMSM for position and speed estimation. Since the motor operates at zero speed and low speed, the useful signal-to-noise ratio is very low and is often difficult to extract.

In recent years, with the rise of machine learning algorithm, it shows certain superiority in modeling complex systems. As literatures [8, 9], the support vector machine

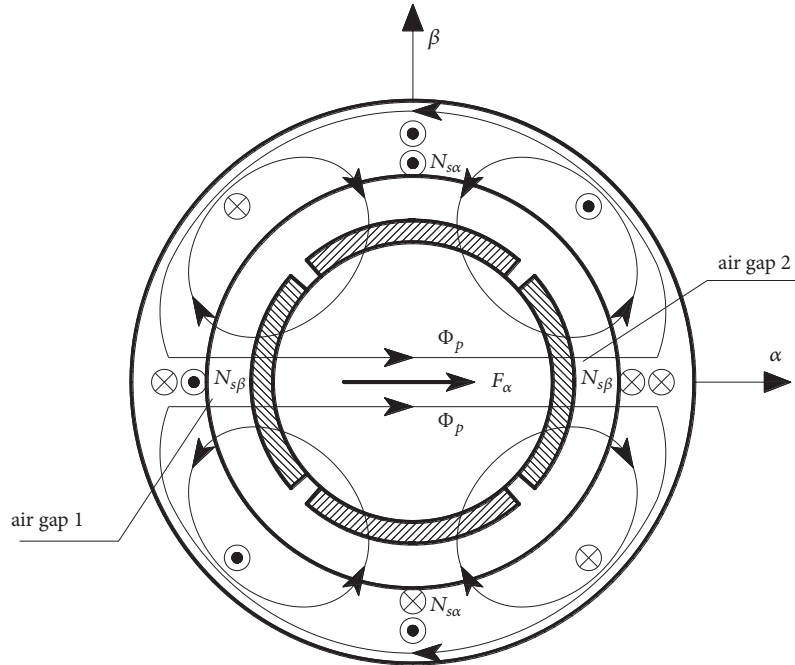


FIGURE 1: Principle of alpha axis radial force production.

(SVM) was used to obtain the prediction model among the rotor position, displacement and the magnetic levitation switched reluctance motor parameters. In literature [10], the author adopts a novel windowed least algorithm to estimate the parameters with fixed value or the parameter with time varying characteristic.

In this regard, a rotor position and displacement prediction model for bearingless permanent magnet synchronous motor based on kernel extreme learning machine is proposed in the paper. According to the mathematical model of BPMSM, it can be known that there is a nonlinear relationship among the current, flux linkage, rotor position and displacement. Therefore the stability and generalization ability of the kernel extreme learning machine (KELM) can be used to predict the rotor position  $\theta_r$  and radial displacement  $x$  and  $y$ . Based on the simulation data, the feasibility and effectiveness of KELM for BPMSM position and displacement prediction are analyzed. Meanwhile, the parameters of KELM are optimized by the particle swarm optimization (PSO) algorithm [11]. The method does not depend on the mathematical model of the motor. Compared with the traditional limit learning machine, it uses the kernel function mapping instead of the hidden layer random mapping. It improves the linear degree of the data and does not need to adjust the parameters of the hidden layer repeatedly. The traditional parameter training problem is converted into a linear equation group to solve the problem, so the training and prediction time are greatly shortened.

## 2. Bearingless Permanent Magnet Synchronous Motor

The BPMSM's stator adopts 24 slots, and the rotor adopts 4 poles surface mounted structure. The stator slot is embedded

with two sets of windings with the polar logarithm difference of 1, which are torque windings and suspension windings respectively. The rotating magnetic field is generated in the torque windings, which drives the permanent magnet on the rotor surface to rotate along the tangent direction. The rotor of the motor is rotated. After the suspension windings are energized, a floating magnetic field is generated in the air gap, which is superposed with the rotating magnetic field and the bias magnetic field generated by the permanent magnet. The synthetic magnetic field generates radial forces of a certain direction and magnitude on the rotor, which achieves the suspension of the motor rotor.

The suspension forces generation principle of the bearing permanent magnet synchronous motor in the static two phase coordinate system is shown in Figure 1, in which  $N_{s\alpha}$  and  $N_{s\beta}$  are 2 pole suspension windings, and  $N_{m\alpha}$  and  $N_{m\beta}$  are 4 pole torque windings.

When the BPMSM windings  $N_{s\alpha}$  and  $N_{s\beta}$  are not energized, the internal flux of the motor is balanced with no levitation force. At this time, the motor is similar to the common permanent magnet synchronous motor. When the suspension winding  $N_{s\alpha}$  is connected to the corresponding polarity current as shown in Figure 1, the controlled flux  $\Phi_{s\alpha}$  produced by the  $N_{s\alpha}$  in the air gap 2 is in the same direction as the  $\Phi_f$  produced by the permanent magnet, and the magnetic flux density in the air gap 2 increases. While the flux  $\Phi_{s\alpha}$  is opposite to the  $\Phi_f$  of the permanent magnet in the air gap 1, the flux density decreases in the air gap 1. The flux density on both sides is different, resulting in the suspension force  $F_\alpha$  in the direction shown in Figure 1, causing radial displacement of the motor rotor. Similarly, the suspension of the motor rotor in the beta direction can be adjusted by adjusting the current in the  $N_{s\beta}$ . By controlling the current in  $N_{s\alpha}$

and  $N_{s\beta}$ , the suspension force in the radial direction can be synthesized; thus the stable suspension control of the bearingless permanent magnet synchronous motor can be realized.

### 3. Design of Position Displacement and Prediction System Based on Kelm

**3.1. Principle of Rotor Position Estimation.** BPMSM is essentially PMSM, so rotor field oriented control ( $i_{md}^*=0$ ) can also be used. Under the control method, the example is the surface-mounted BPMSM with 2 pairs of pole torque windings and 1 pairs of pole suspension windings. The electromagnetic torque equation of the motor is as follows [1]:

$$T_e = P_1 \psi_f i_{mq} = 2\psi_f i_{mq} = 2\psi_{md} i_{mq} \quad (1)$$

According to the dynamic equation of the rotor of BPMSM, it can be obtained [1, 12]:

$$T_e = \frac{J}{2} \frac{d\omega}{dt} + T_L \quad (2)$$

$$\dot{\theta}_r = \omega(t)$$

Combined with (1) and (2), the expression of rotor position angle can be obtained [1]:

$$\frac{J}{2} \ddot{\theta}_r = 2\psi_{md} i_{mq} - T_L \quad (3)$$

where  $T_e$  is the electromagnetic torque of the motor. When  $i_{md}^*=0$ , permanent-magnet magnetic flux linkage  $\psi_f$  is equal to magnetic flux linkage  $d$  axis component of torque windings  $\psi_{md}$ .  $i_{mq}$  is the current  $d$  axis component of torque windings.  $u_{md}$  is the voltage  $d$  axis component of torque windings.  $\psi_{md}(0)$  is the initial  $d$  axis magnetic flux linkage component of torque windings (its value is 0).  $\theta_r$  is the angle of the rotor position.  $T_L$  is the load torque;  $J$  is the moment of inertia.

In order to get the relationship between the rotor position angle  $\theta_r$  and the direct acquisition of the motor parameters, (3) could be represented in the static coordinate system as follows:

$$\frac{J}{2} \ddot{\theta}_r = 2(\psi_{m\alpha} \cos \theta_r + \psi_{m\beta} \sin \theta_r)(i_{m\alpha} \cos \theta_r + i_{m\beta} \sin \theta_r) - T_L \quad (4)$$

where  $\psi_{m\alpha}$  and  $\psi_{m\beta}$  are the  $\alpha$  and  $\beta$  axis components of the torque windings flux linkage.  $i_{m\alpha}$  and  $i_{m\beta}$  are the  $\alpha$  and  $\beta$  axis components of the torque windings current.

According to the principle of electromechanics, the torque windings flux linkage  $\psi_{m\alpha}$ ,  $\psi_{m\beta}$  can be obtained by  $U-I$  flux linkage identification [6]:

$$\psi_{m\alpha} = \int_0^t (u_{m\alpha} - R_m i_{m\alpha}) + \psi_{m\alpha}(0) \quad (5)$$

$$\psi_{m\beta} = \int_0^t (u_{m\beta} - R_m i_{m\beta}) + \psi_{m\beta}(0)$$

where  $u_{m\alpha}$  and  $u_{m\beta}$  are the  $\alpha$  and  $\beta$  axis components of the torque windings voltage;  $R_m$  is the torque windings resistance;  $\psi_{m\alpha}(0)$  and  $\psi_{m\beta}(0)$  are the initial values of the flux linkage of the torque windings.

When the motor model is determined, the load torque  $T_L$  and the moment of inertia  $J$  in (4) can be regarded as constants. Therefore, the rotor position prediction system can be  $\{\psi_{m\alpha}, \psi_{m\beta}, i_{m\alpha}, i_{m\beta}\}$  as input and the rotor position angle  $\{\theta_r\}$  as output. KELM is used to train the rotor position angle model to realize the real-time prediction of rotor position  $\theta_r$ . Equation (4) ensures the feasibility of the KELM prediction rotor position angle model.

**3.2. Principle of Rotor Displacement Estimation.** The flux linkage of the bearingless permanent magnet synchronous motor in the  $\alpha$ - $\beta$  coordinate system can be expressed [13, 14]:

$$\begin{bmatrix} \psi_{m\alpha} \\ \psi_{m\beta} \\ \psi_{s\alpha} \\ \psi_{s\beta} \end{bmatrix} = \begin{bmatrix} L_{m\alpha} & 0 & M_{\alpha\alpha} & -M_{\alpha\beta} \\ 0 & L_{m\beta} & M_{\beta\beta} & M_{\beta\alpha} \\ M_{\alpha\alpha} & M_{\beta\beta} & L_{s\alpha} & 0 \\ -M_{\alpha\beta} & M_{\beta\alpha} & 0 & L_{s\beta} \end{bmatrix} \begin{bmatrix} i_{m\alpha} + i_{f\alpha} \\ i_{m\beta} + i_{f\beta} \\ i_{s\alpha} \\ i_{s\beta} \end{bmatrix} \quad (6)$$

where  $\alpha$  and  $\beta$  are the radial displacement components of the rotor in the stationary coordinate system.  $\psi_{m\alpha}$  and  $\psi_{m\beta}$  are the  $\alpha$  and  $\beta$  axis components of the torque windings flux linkage.  $\psi_{s\alpha}$  and  $\psi_{s\beta}$  are the  $\alpha$  and  $\beta$  axis components of the suspension windings flux linkage.  $L_{m\alpha}$  and  $L_{m\beta}$  are the self-inductance coefficients  $\alpha$  and  $\beta$  axis components of the torque windings.  $L_{s\alpha}$  and  $L_{s\beta}$  are the self-inductance coefficients  $\alpha$  and  $\beta$  axis components of the suspension windings.  $M_{\alpha\alpha}$ ,  $M_{\beta\beta}$  are the mutual inductance coefficients  $\alpha$  and  $\beta$  axis components of the suspension windings.  $i_{m\alpha}$  and  $i_{m\beta}$  are  $\alpha$  and  $\beta$  axis components of the torque windings current.  $i_{s\alpha}$  and  $i_{s\beta}$  are the  $\alpha$  and  $\beta$  axis components of the floating windings current.  $i_{f\alpha}$  and  $i_{f\beta}$  are the  $\alpha$  and  $\beta$  axis components of the permanent magnet equivalent excitation current.

From the third and fourth lines of (6), the rotor radial displacement expression can be derived as [13, 14]

$$\alpha = \frac{M_{\alpha}(i_{m\alpha} + i_{f\alpha})(\psi_{s\alpha} - L_{s\alpha}i_{s\alpha}) + M_{\beta}(i_{m\beta} + i_{f\beta})(\psi_{s\beta} - L_{s\beta}i_{s\beta})}{M_{\alpha}^2(i_{m\alpha} + i_{f\alpha})^2 + M_{\beta}^2(i_{m\beta} + i_{f\beta})^2} \quad (7)$$

$$\beta = \frac{M_{\beta}(i_{m\beta} + i_{f\beta})(\psi_{s\alpha} - L_{s\alpha}i_{s\alpha}) - M_{\alpha}(i_{m\alpha} + i_{f\alpha})(\psi_{s\beta} - L_{s\beta}i_{s\beta})}{M_{\alpha}^2(i_{m\alpha} + i_{f\alpha})^2 + M_{\beta}^2(i_{m\beta} + i_{f\beta})^2}$$

where the suspension windings flux linkages  $\psi_{s\alpha}$  and  $\psi_{s\beta}$  are obtained by the  $U-I$  flux linkage identification method similar to (5).

It can be known from (7) that the rotor radial displacement of BPMSM can be represented nonlinearly by the suspension windings currents  $i_{s\alpha}$  and  $i_{s\beta}$ , the suspension windings flux linkages  $\psi_{s\alpha}$  and  $\psi_{s\beta}$ , the torque windings currents  $i_{m\alpha}$  and  $i_{m\beta}$ , and the permanent magnet equivalent current  $i_f$ . Therefore, the rotor radial displacement prediction system can be  $\{\psi_{s\alpha}, \psi_{s\beta}, i_{s\alpha}, i_{s\beta}, i_{m\alpha}, i_{m\beta}, i_f\}$  as the input, and the rotor radial displacement  $\{\alpha, \beta\}$  is the output. Real-time prediction of rotor displacement can be achieved by using KELM to train the rotor displacement model. Equation (7) guarantees the feasibility of KELM predicting the rotor displacement model.

**3.3. Principle of Kernel Extreme Learning Machine.** Extreme learning machine [15] (ELM) is a training method for a single-hidden layer feedforward neural network. Given a training sample  $T=\{(x_n, y_n), n = 1, 2 \dots N\}$ , its input data is  $x_n$  and its target output value is  $y_n$ . For  $K$  hidden nodes, the ELM network model with activation function  $g_n(x_n)$  can be expressed as [15]

$$y_j = \sum_{n=1}^K \sigma_n g_n(\omega_n \cdot x_j + b_i), \quad j = 1, 2, \dots, N \quad (8)$$

where  $\omega_n$  is the weight between the  $n$ -th hidden layer node and input node.  $b_n$  is the offset of the  $n$ -th hidden layer of the network.  $\sigma_n$  is the  $n$ -th output weight of the connection hidden layer and output layer.  $y_j$  is the network output value.

When the activation function  $g_n(x_n)$  can approximate the target output value of any  $N$  samples, namely,  $\sum_{n=1}^K \|y_n - t_n\| = 0$ , with zero error, at this time there are [15]

$$t_j = \sum_{n=1}^K \sigma_n g_n(\omega_n x_j + b_n), \quad j = 1, 2, \dots, N \quad (9)$$

The matrix form of the above  $N$  equations can be expressed as [15]

$$H\sigma = T \quad (10)$$

Among them [15]

$$H = \begin{bmatrix} g_n(\omega_1 x_1 + b_1) & \cdots & g_n(\omega_K x_1 + b_K) \\ \vdots & \dots & \vdots \\ g_n(\omega_1 x_N + b_1) & \cdots & g_n(\omega_K x_N + b_K) \end{bmatrix}_{N \times K} \quad (11)$$

where  $H$  is the hidden layer output matrix of ELM.  $T$  is the desired output vector.

The above equation is equivalent to finding the least squares solution of the linear system, that is, to find the optimal weight  $\sigma^*$ , which makes the sum of the squares of the difference between the actual and the expected value minimum. According to the theory of generalized inverse matrix, the solution is as follows [15]:

$$\sigma^* = H^+ T \quad (12)$$

where  $H^+$ , which can be obtained by orthogonal projection method or singular value decomposition, represents the

generalized inverse matrix of the hidden layer output matrix  $H$ .

When the number of hidden layer nodes and the number of samples in the ELM model are equal, the network can approach the trained samples with zero error, but in actual use, the calculation time is lengthy in the fitting of larger samples. Therefore, the number of hidden nodes is often set less than the number of training samples, but the data samples may have complex collinear problems at this time, which will make the output of the ELM model fluctuate randomly. The stability and generalization ability of ELM are deteriorated.

In the ELM research process, due to the introduction of the kernel function, ELM can obtain the performance of the least squares support vector machine. The use of kernel mapping to replace the hidden layer feature random mapping, which makes that KELM not only has the superior performance of SVM, but also has a very high operating speed.

Given a training sample  $T=\{(x_n, y_n), n = 1, 2 \dots N\}$ , its regression function and the link weights between the hidden layer and the output layer are as follows [16, 17]:

$$\begin{aligned} \hat{y} &= f(x) = h(x) \delta = H\delta \\ \delta &= H^T \left( \frac{I}{C} + HH^T \right)^{-1} G \end{aligned} \quad (13)$$

where  $\hat{y}=f(x)$  is the network output.  $x$  is the sample input.  $h$  is a hidden layer random feature mapping matrix.  $\delta$  is the connection weight between the hidden layer and the output layer, and the  $\delta$  value can be solved according to the generalized inverse matrix.  $I$  is a diagonal matrix.  $C$  is the regularization coefficient.  $G$  is the output of target value.

Huang combined kernel learning with ELM in literature [16] and proposed the KELM algorithm. KELM kernel matrix  $\Omega_{ELM}$  is defined as follows [16, 17]:

$$\begin{aligned} \Omega_{ELM} &= HH^T \\ \Omega_{ELM,ij} &= h(x_i) h(x_j) = K(x_i, x_j) \end{aligned} \quad (14)$$

where  $x_i, x_j$  is the sample input vector, where  $i$  and  $j$  are any integers in  $[1, N]$ .  $K(x_i, x_j)$  is a kernel function, which is usually replaced by a radial basis function (RBF), namely [16, 17],

$$K(x_i, x_j) = \exp(-\gamma \|x_i, x_j\|^2) \quad (15)$$

where  $\|x_i, x_j\|$  is the Euclidean norm between samples.  $\gamma > 0$ , which is the kernel parameter.

Combining (13), (14), and (15) gives the output and output weight of the KELM network as follows [17]:

$$\hat{y} = f(x) = \begin{bmatrix} K(x, x_1) \\ \vdots \\ K(x, x_N) \end{bmatrix} \left( \frac{I}{C} + \Omega_{ELM} \right)^{-1} G \quad (16)$$

$$\delta = \left( \frac{I}{C} + \Omega_{ELM} \right)^{-1} G$$

According to (16), KELM transforms the random feature mapping matrix  $H$  in ELM to a stable kernel function  $K(x_i, x_j)$

mapping. Compared with the traditional ELM, the function output value can be obtained without setting the number of nodes in the hidden layer, and the generalization ability and stability of the model are enhanced. Considering the advantages of KELM, this paper proposes a BPMSM rotor position and displacement prediction model based on KELM.

**3.4. Particle Swarm Optimization Algorithm for Optimizing KELM Parameters.** The kernel parameter and the regularization coefficient of KELM have been selected by random or experience, which makes KELM very complicated and inefficient in fitting some complex networks. At present, the optimization of kernel parameter by particle swarm optimization is the main research direction in the KELM field. The PSO algorithm can globally optimize, ensuring that the KELM network parameters are in the optimal state, which makes the robustness and prediction accuracy of KELM improved.

**3.4.1. Principle of PSO Algorithm.** PSO algorithm is a lightweight algorithm with fewer parameters, faster convergence speed and easy to find global optimal solution. It has been applied in the parameter optimization and training of KELM in literatures [17–19].

In the optimization process, all particles are determined by a fitness-function to judge the good or bad of the current position, meanwhile each particle has two attributes: position and speed. The initial cluster size is  $N$ . In a  $D$ -dimensional target search space, the position of the particle  $i$  is represented as  $X_i = (X_{i1}, X_{i2}, \dots, X_{iD})^T$  and the velocity is expressed as  $v_i = (v_{i1}, v_{i2}, \dots, v_{iD})^T$ . The best position that the particle currently searches for is represented as  $pbest_i = (p_{i1}, p_{i2}, \dots, p_{iD})^T$ , and the global optimal position of the current population is represented as  $gbest = (p_{g1}, p_{g2}, \dots, p_{gD})^T$ . Then the following equations are used to simulate the change of particle velocity and position [11, 19]:

$$v_{iD}^{t+1} = v_{iD}^t + c_1 r_{1D} (p_{iD}^t - X_{iD}^t) + c_2 r_{2D} (p_{gD}^t - X_{iD}^t) \quad (17)$$

$$X_{iD}^{t+1} = X_{iD}^t + v_{iD}^{t+1} \quad (18)$$

where  $1 \leq i \leq N$ .  $T$  represents the number of iterations.  $c_1$  and  $c_2$  are acceleration constants that determine the particle velocity change, where  $c_1$  acts on the particle's individual optimal solution and  $c_2$  affects the particle's global optimal solution.  $r_{1D}$  and  $r_{2D}$  are two independent 0~1 random coefficients used to constrain the velocity of the particles. In order to balance the global search ability and local search ability of the particle swarm algorithm, the inertia weight coefficient  $w$ [20] is introduced. The particle velocity changes after introduction are as follows [11, 19]:

$$v_{iD}^{t+1} = w v_{iD}^t + c_1 r_{1D} (p_{iD}^t - X_{iD}^t) + c_2 r_{2D} (p_{gD}^t - X_{iD}^t) \quad (19)$$

When  $w > 1$ , the global search ability of the particle is increased. When  $w < 1$ , the particle performs deceleration

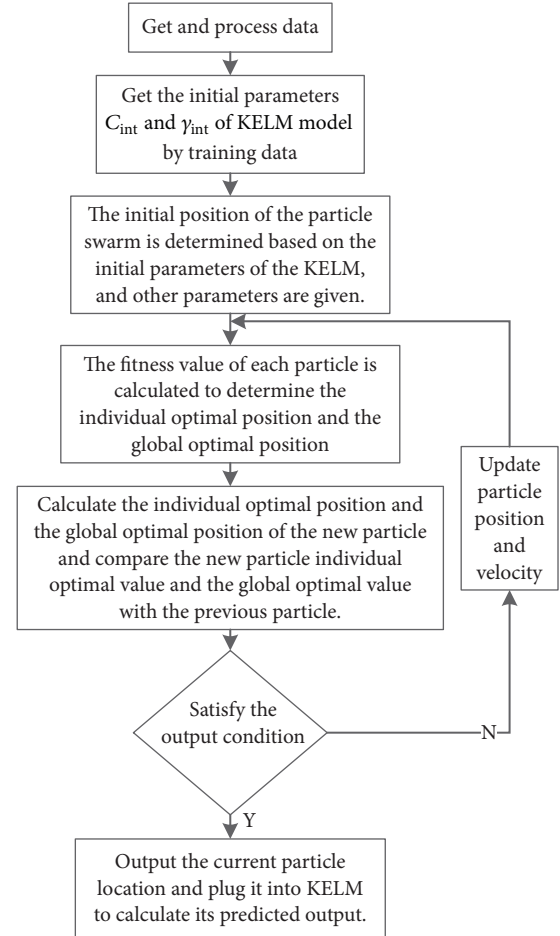


FIGURE 2: The flow chart of PSO optimizing KELM.

motion, the search range of the particle reduces, and the local search ability of the particle increases.

**3.4.2. Steps to Optimize KELM Parameters with PSO Algorithm.** The flowchart of particle swarm optimization KELM is shown in Figure 2.

**Step 1.** The diachronic data obtained by the BPMSM simulation model is selected and divided into training set and test set, and then the training set and test set are normalized to  $[-1, 1]$ .

**Step 2.** The kernel function of the KELM model is RBF kernel, and it is taken into further processing the training set data to get the initial regularization coefficient and kernel parameter.

**Step 3.** Initialize the particle swarm parameters, including setting the population number to  $N$ , the initial particle position to  $(\gamma_{int}, C_{int})$ , and setting the search range. When the particle crosses the boundary, the position of the particle is set to the boundary value and its velocity is set in the opposite direction. Set the upper limit of the iteration. The mean square error (MSE) of rotor position and displacement prediction by KELM is set as fitness function. The smaller

TABLE 1: Simulation parameters of BPMSM.

Motor parameters	Values	Motor parameters	Values
Rated voltage	242 V	Rated torque	5 N·m
Rated speed	3000 r/min	Moment of inertia	$1.5 \times 10^{-3}$ kg·m <sup>2</sup>
Torque windings resistance	7.136 $\Omega$	Pole number of torque windings	4
Suspension windings resistance	1.85 $\Omega$	Pole number of suspension windings	2

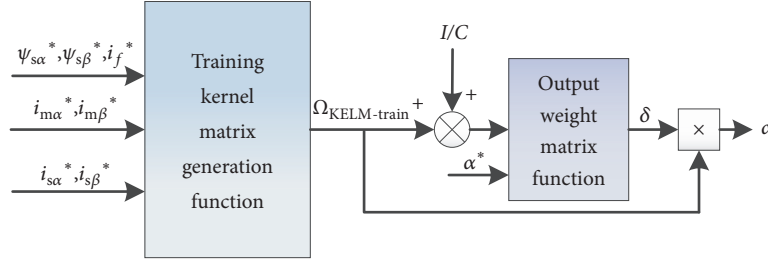


FIGURE 3: Rotor alpha axis radial displacement training function flow.

the MSE value, the better the fitness. Meanwhile the initial velocity, the optimal location, and the global optimal location are given randomly.

*Step 4.* The particle swarm optimization is carried out. According to the objective function, the fitness of each particle is calculated in each iteration. Then the speed and individual and global optimal position are updated.

*Step 5.* The individual and global optimum values of the new particles are compared with the previous ones. If they are better, they are updated. Otherwise they will not be updated.

*Step 6.* If the number of iterations exceeds the upper limit of iteration, the algorithm is terminated. Otherwise Steps 4 and 5 are repeated.

*Step 7.* The global optimal position ( $\gamma_{best}$ ,  $C_{best}$ ) of the particle is outputted, and the fitness value corresponding to the global optimal position is saved.

**3.5. Design Steps of Position and Displacement Prediction Models.** In order to verify the effectiveness of the designed prediction model, simulation study is carried out in Matlab/Simulink, and the BPMSM simulation parameters in simulation are shown in Table 1. The sampling time is 0.15s, and the sampling mode is variable step ode45, which can obtain the simulation data.

The torque windings current  $\alpha$ ,  $\beta$  axis component data, the torque windings flux  $\alpha$ ,  $\beta$  axis component data, the suspension windings current  $\alpha$ ,  $\beta$  axis component data, the suspension windings flux  $\alpha$ ,  $\beta$  axis component data, and the permanent magnet equivalent excitation current data are used to simulate actual rotor position and displacement data. 1000 sets of training samples are selected as rotor position and displacement prediction models at equal time interval, and 1000 groups are selected as rotor position and displacement test samples. Since the single-kernel KELM can only be used

for the fitting problem of a single output function, in order to achieve multioutput prediction of rotor position and radial displacement, three prediction models based on KELM are established.

Respectively, the rotor position angle prediction model is  $\{\psi_{m\alpha}, \psi_{m\beta}, i_{m\alpha}, i_{m\beta}\}$  as the input set and  $\{\theta_r\}$  is the output set. The rotor  $\alpha$ -axis radial displacement prediction model is  $\{\psi_{s\alpha}, \psi_{s\beta}, i_{s\alpha}, i_{s\beta}, i_{m\alpha}, i_{m\beta}, i_f\}$  as the input set, and  $\{\alpha\}$  is the output set. The rotor  $\beta$ -axis radial displacement prediction model is  $\{\psi_{s\alpha}, \psi_{s\beta}, i_{s\alpha}, i_{s\beta}, i_{m\alpha}, i_{m\beta}, i_f\}$  as the input set, and  $\{\beta\}$  is the output set.

**3.5.1. Optimization of KELM Kernel Parameters.** Given the parameters of PSO algorithm, the MSE of training samples is set as fitness function. For the rotor position angle  $\theta_r$  training model, the acceleration factors  $c_1$  and  $c_2$  are set to 2,  $w$  is set to 0.5, the population number is set to 25, and the maximum iteration number  $t_{max}$  is 100. Finally, the parameter optimization result can be obtained as  $(\gamma_{best}, C_{best}) = (0.001, 10000)$ .

For the rotor  $\alpha$ -axis radial displacement  $\alpha$  training model, the acceleration factors  $c_1$  and  $c_2$  are set to 2,  $w$  is set to 0.6, the population number is set to 25, and the maximum iteration number  $t_{max}$  is 100. Finally, the parameter optimization result can be obtained as  $(\gamma_{best}, C_{best}) = (0.008, 200000)$ .

For the rotor  $\beta$ -axis radial displacement  $\alpha$  training model, the acceleration factors  $c_1$  and  $c_2$  are set to 2,  $w$  is set to 0.6, the population number is set to 25, and the maximum iteration number  $t_{max}$  is 100. Finally, the parameter optimization result can be obtained as  $(\gamma_{best}, C_{best}) = (0.002, 20000)$ .

**3.5.2. Training Model Offline.** As shown in Figure 3, the establishment process of the radial displacement training model of the rotor  $\alpha$ -axis is taken as an example.

During the training process of the model, according to the training sample input  $\{\psi_{s\alpha}^*, \psi_{s\beta}^*, i_{s\alpha}^*, i_{s\beta}^*, i_{m\alpha}^*, i_{m\beta}^*, i_f^*\}$ , the samples are trained offline by Matlab. After the training

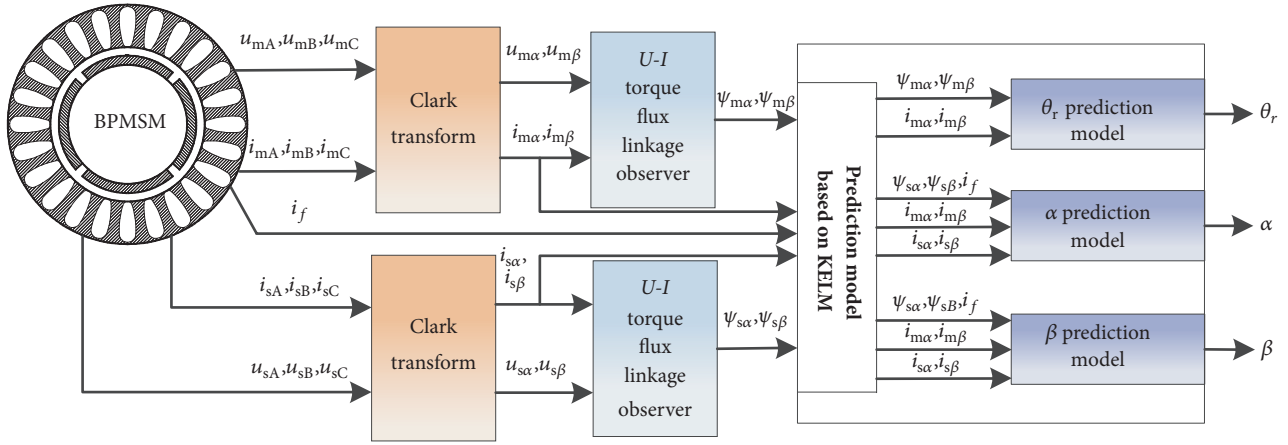


FIGURE 4: Rotor position/displacement prediction process based on KELM.

kernel matrix  $\Omega_{\text{ELM}_{\text{train}}}$  is obtained, a matrix  $I/C$  is added, which is substituted into the output weight matrix function together with the output  $\{\alpha^*\}$  of the training sample, and finally an output weight matrix  $\delta$  is obtained. Among them,  $I$  is the unit matrix with the same order of training kernel matrix. Multiplication of  $\Omega_{\text{ELM}_{\text{train}}}$  and  $\delta$  is the predicted output of training samples  $\{\alpha\}$ . After obtaining the mean square error, it is trained several times to get the minimum mean square error and finally get the most suitable output weight matrix  $\delta$ . The establishment of the rotor position angle  $\theta_r$  and the rotor  $\beta$ -axis radial displacement training model is similar to the rotor  $\alpha$ -axis radial displacement. It will not be described in detail here.

**3.5.3. Prediction of Rotor Position and Displacement Online.** According to Figure 4, the Matlab/Simulink simulation model is built. The current and voltage signals obtained by real-time simulation are firstly identified to obtain the torque and the floating flux linkage, and then the flux linkage signal and the current signal are used as the corresponding inputs of the three prediction models; finally the predictions are obtained.

In the online prediction, the offline trained weight matrix  $\delta$  is stored in advance in an external data file. The construction of the predictive model is written in the Matlab Function module. The real-time sampling of current and flux signals is stored in a variable array. Then the predicted kernel matrix  $\Omega_{\text{ELM}_{\text{predict}}}$  corresponds to the input at this time, and finally the Matlab Function module calls the external weight matrix  $\delta$  directly. The products of the two are the real-time prediction output under the sampling time point.

## 4. Analysis of Simulation Results

Figures 5 and 6 show the actual value, predicted value, and prediction error of the rotor position and displacement when BPMSM is unloaded and given a constant speed of 3000 r/min.

It can be seen from Figure 5(a) that the rotor position prediction value is basically consistent with the measured value when the motor no-load constant speed was 3000 r/min. It can be seen from Figure 5(b) that the maximum position angle  $\theta_r$  prediction error of the rotor position prediction model based on KELM is  $3.48e-03$  rad, which is within an acceptable range.

It can be seen from Figures 6(a) and 6(c) that, during the motor starting phase, the rotor suspension state of the motor fluctuates because the operating conditions of the motor are not stable enough. In the  $\beta$  direction, it is greatly affected by gravity. When the motor starts, the rotor position starts from  $-3 \times 10^{-4}$  m, and the suspension control accuracy is slightly lower too, which is  $10^{-4}$  m. The prediction error of the rotor displacement prediction model based on KELM is more obvious in the motor starting stage. When the operating condition of the motor is stable, the prediction error was gradually reduced to close to 0. When the no-load constant speed was 3000 r/min, the displacement error in the maximum  $\alpha$  direction is  $4.99 \times 10^{-9}$  m, and the displacement error in the maximum  $\beta$  direction is  $4.94 \times 10^{-7}$  m, which are much smaller than the set allowable value.

Figure 7 shows the change of the rotational speed and the rotor position prediction error at the time when the BPMSM is given a constant speed of 3000 r/min under the condition of a load torque  $T_L = 5$  N·m at 0.1 s.

It can be seen from Figure 7(b) that, in the case of sudden load, although the rotor position prediction stability was slightly lower than before the load torque was added, the overall error was within the acceptable range, so the rotor position prediction model based on KELM still had good reliability.

When the BPMSM is given a constant speed of 3000 r/min, Figures 8(a) and 8(b) exert interference forces on the  $\alpha$ -axis at 0.12s and Figures 8(c) and 8(d) exert interference forces on the  $\beta$ -axis at 0.08s.

It can be seen from Figure 8 that the accuracy of the rotor displacement prediction model decreased slightly when the disturbance is added, but the overall predicted displacement accuracy is within an acceptable range. When the rotor

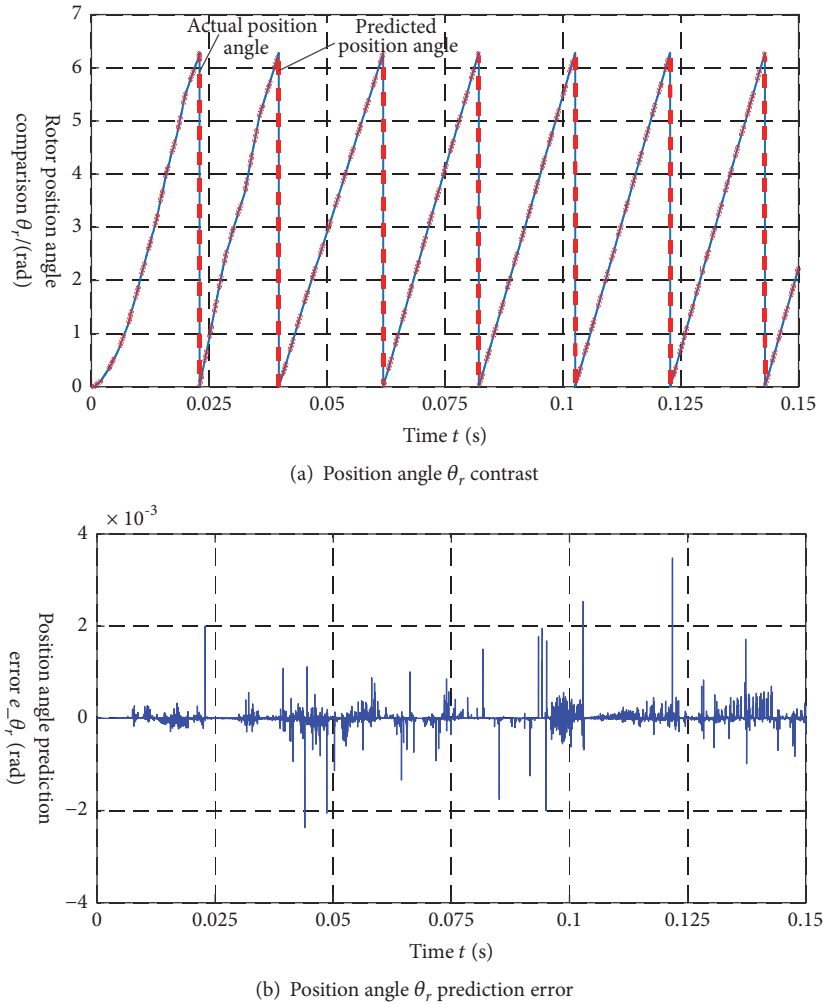


FIGURE 5: Rotor position and predicted error at 3000 r/min.

position returns to the equilibrium position, the accuracy will increase accordingly.

The comprehensive simulation results show that the rotor position and displacement prediction models based on KELM can meet the high-precision requirements of the BPMSM control system and have certain robustness when the BPMSM is running with load or displacement disturbance at a given speed.

## 5. Comparison of Algorithm Performance

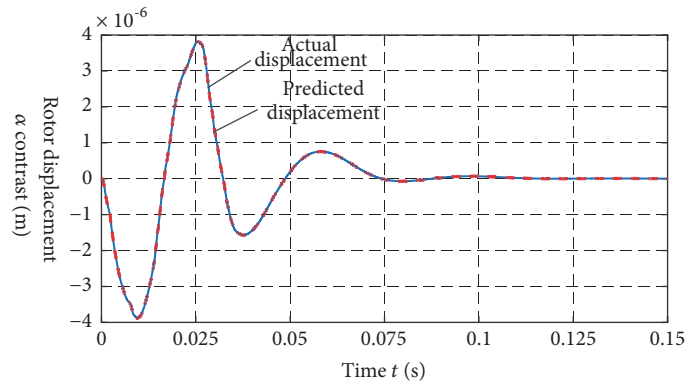
In order to test the performance of KELM algorithm, ELM and LS-SVM are used as comparison algorithms to establish BPMSM rotor position and displacement offline training models for three algorithms. According to the original training set data, the maximum error and the mean square error of the prediction model are used as indicators to compare the algorithms.

In the ELM training models, “sawtooth” is used as all the activation functions. The number of hidden neurons is adjusted with the establishment of different models, but they

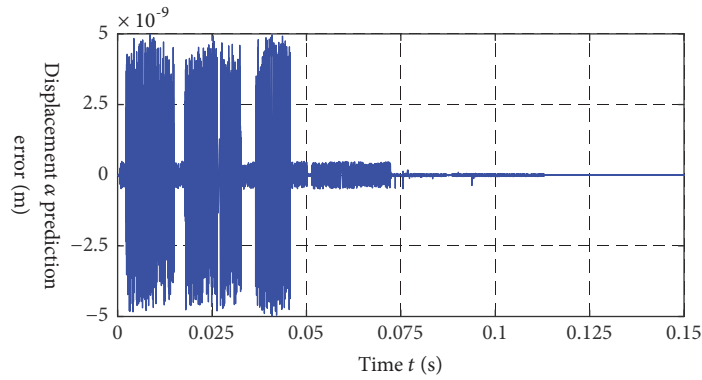
are basically adjusted within the range of 2500~3000. When the LS-SVM training models are used, “RBF” is used as all the kernel functions. Under different training models, the sigma kernel parameters of the RBF kernel function are different.

Because it is only to test the superiority of the KELM algorithm in rotor position and displacement prediction accuracy, this section collects the correlation quantities of the Matlab/Simulink model after simulation into the “.mat” files and only calculates the predicted output under each algorithm offline. The training samples and prediction samples of each algorithm are completely consistent. After selecting the optimal parameters of each model, the computer program is programmed by Matlab, and the simulation is performed on the PC. The final results of each algorithm are shown in Table 2.

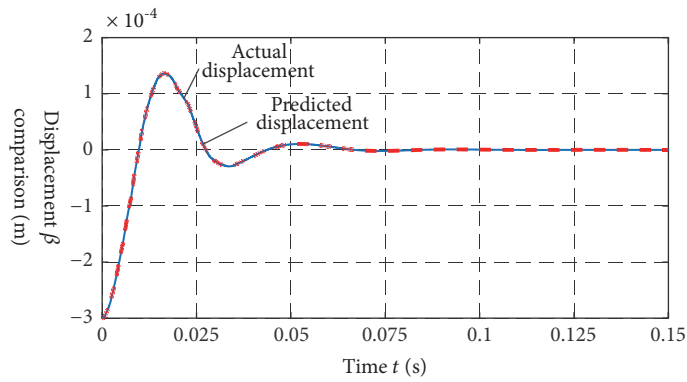
Comparing the algorithms, it can be seen that KELM is slightly higher than LS-SVM in terms of prediction accuracy, but both are much higher than ELM prediction accuracy. This is because ELM is a random given parameter of the algorithm hidden layer, which leads to its poor generalization ability and stability. KELM replaces the random mapping in ELM with nuclear mapping, which effectively solves such problems



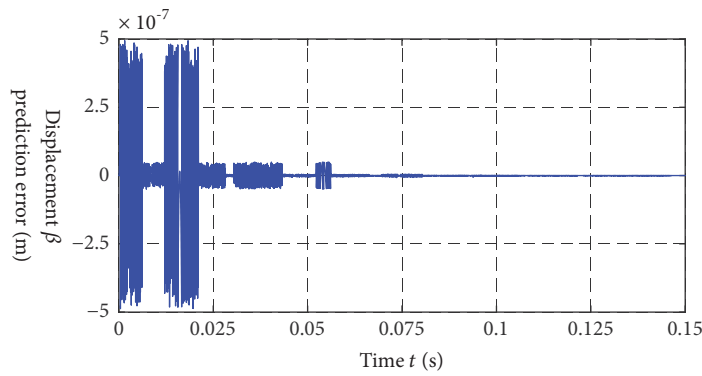
(a) Comparison of displacement on the  $\alpha$ -axis



(b) Displacement prediction error on the  $\alpha$ -axis

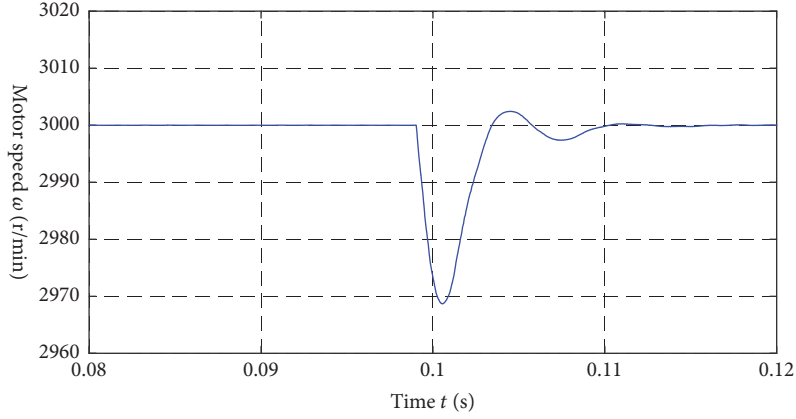


(c) Comparison of displacement on the  $\beta$ -axis

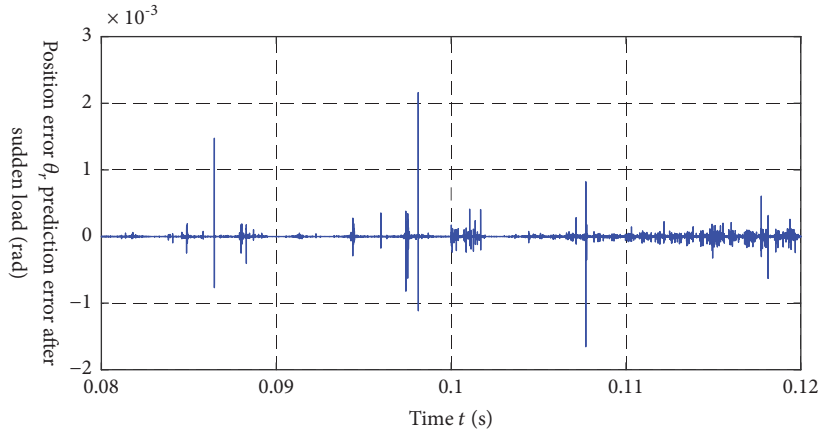


(d) Displacement prediction error on the  $\beta$ -axis

FIGURE 6: Rotor displacement and predicted error at 3 000 r/min.



(a) Speed change at 0.1 s sudden load



(b) Position angle prediction error at 0.1 s sudden load

FIGURE 7: Speed and rotor position prediction error under load torque  $T_L=5$  N·m.

TABLE 2: Comparison of prediction results of various algorithms at 3 000 r/min.

	Algorithm	Maximum error	Mean square error	Calculating time /s
Rotor position angle $\theta_r$ , prediction /rad	KELM	3.48e-03	1.56e-04	0.575
	ELM	0.0368	0.0033	2.734
	LS-SVM	6.96e-03	5.09e-04	0.781
Displacement $\alpha$ prediction /m	KELM	4.99e-09	5.52e-10	0.531
	ELM	7.62e-08	4.03e-09	2.653
	LS-SVM	7.27e-09	8.58e-10	0.688
Displacement $\beta$ prediction /m	KELM	4.94e-07	4.34e-08	0.609
	ELM	4.02e-06	5.49e-07	2.375
	LS-SVM	6.57e-07	7.01e-08	0.719

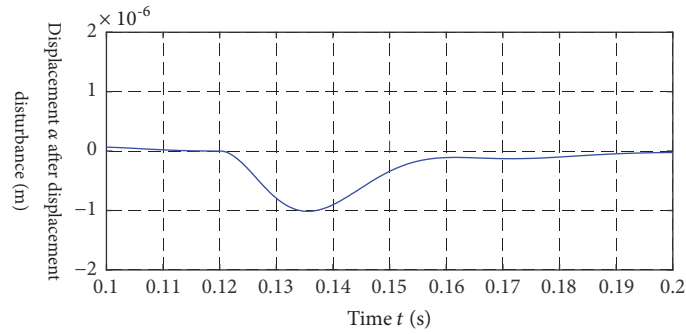
and obtains the least squares optimal solution. At the same time, KELM has relatively weak optimization constraints compared with LS-SVM.

In the prediction time, the difference between KELM and LS-SVM is not significant, which is obviously better than that of ELM. The time of calculation of ELM is not only limited by the size of the sample size but also influenced by the number of neurons in the hidden layer. KELM does not need to input the number of hidden layer neurons and only needs to

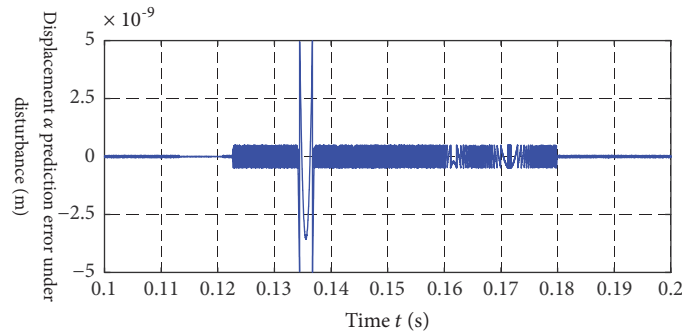
adjust the kernel parameters and regularization coefficients. Its calculation time is only related to the number of samples, so KELM has an advantage in system response.

## 6. Conclusion

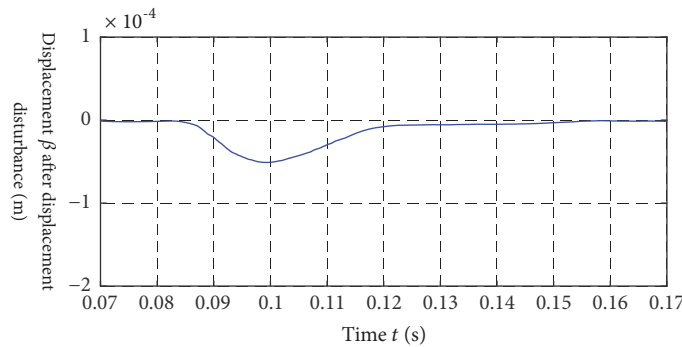
In this paper, a high-precision prediction method based on KELM is proposed for the prediction of rotor position and displacement of BPMSM. The mathematical model of



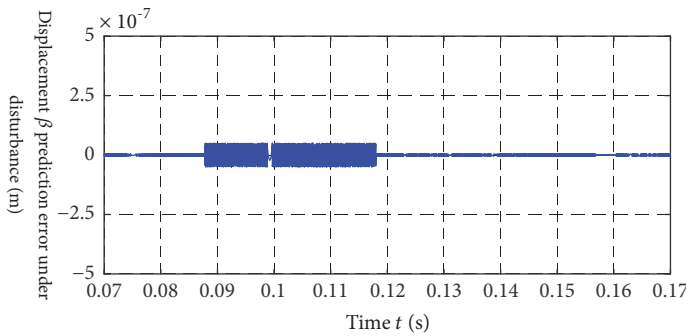
(a) Displacement  $\alpha$  at 0.12s with disturbance



(b) Prediction error of displacement  $\alpha$  under disturbance



(c) Displacement  $\beta$  at 0.08s with disturbance



(d) Prediction error of displacement  $\beta$  under disturbance

FIGURE 8: Prediction and error of rotor displacement under external displacement disturbance.

BPMSM is used to determine the input required by the prediction method. KELM prediction models are established by the data obtained in the simulation model. Finally, in order to prove the superiority of KELM algorithm, the

performance index of KELM algorithm is compared with other algorithms.

Simulation results show that (1) the KELM-based predictive model design method is efficient and convenient

and can well fit the nonlinear relationship between various parameters of the motor; (2) the designed prediction model can accurately predict the position and displacement of the rotor, which provides the basis for the realization of BPMSM sensorless operation control; (3) compared to traditional ELM, KELM has a shorter prediction time and more stability. Compared to LS-SVM, KELM has better generalization performance. In summary, the BPMSM rotor position and displacement high-precision prediction method based on KELM provide a reliable and key technology for sensorless operation control of BPMSM.

## Data Availability

Requests for data, [6/12 months] after publication of this article, will be considered by the corresponding author.

## Conflicts of Interest

The authors declare that they have no conflicts of interest.

## Acknowledgments

The work is sponsored by the National Natural Science Foundation of China (51877101) and Priority Academic Program Development of Jiangsu Higher Education Institutions.

## References

- [1] H. Q. Zhu, Q. L. Cheng, and C. B. Wang, "Modeling of bearingless permanent magnet synchronous motor based on mechanical to electrical coordinates transformation," *Science in China, Series E: Technological Sciences*, vol. 52, no. 12, pp. 3736–3744, 2009.
- [2] K. Muronoi, N. Andoh, A. Chiba, and T. Fukao, "Characteristics of Induction type Self-Sensing Bearingless Motors," in *Proceedings of the IPEC-Tokyo*, pp. 2109–2114, 2000.
- [3] T. Kuwajima, T. Nobe, K. Ebara, A. Chiba, and T. Fukao, "An estimation of the rotor displacements of bearingless motors based on a high frequency equivalent circuit," in *Proceedings of the 4th IEEE International Conference on Power Electronics and Drive Systems*, pp. 725–731, 2001.
- [4] H. Nian, Y. He, F. Qin, and Y. Liu, "Sensorless operation of permanent magnet bearingless motor," *Proceedings of the CSEE*, vol. 24, no. 11, pp. 101–105, 2004.
- [5] P. P. Xia, Y. T. Deng, Z. Q. Wang, and H. W. Li, "Speed Adaptive Sliding Mode Control with an Extended State Observer for Permanent Magnet Synchronous Motor," *Mathematical Problems in Engineering*, vol. 2018, Article ID 6405923, 13 pages, 2018.
- [6] H. Kim, J. Son, and J. Lee, "A high-speed sliding-mode observer for the sensorless speed control of a PMSM," *IEEE Transactions on Industrial Electronics*, vol. 58, no. 9, pp. 4069–4077, 2011.
- [7] Y. A.-R. I. Mohamed, "Design and implementation of a robust current-control scheme for a PMSM vector drive with a simple adaptive disturbance observer," *IEEE Transactions on Industrial Electronics*, vol. 54, no. 4, pp. 1981–1988, 2009.
- [8] Z. Zhu, Y. Sun, X. Ji, and Y. Huang, "Displacement and Position Observers Designing for Bearingless Switched Reluctance Motor," *Proceedings of the CSEE*, vol. 32, no. 12, pp. 83–89, 2012.
- [9] C. Xia, Z. He, Y. Zhou, and X. Xie, "Rotor Position Estimation for Switched Reluctance Motors Based on Support Vector Machine," *Transactions of China Electrotechnical Society*, vol. 22, no. 10, pp. 12–17, 2007.
- [10] S. Wang, "Windowed Least Square Algorithm Based PMSM Parameters Estimation," *Mathematical Problems in Engineering*, vol. 2013, Article ID 131268, 11 pages, 2013.
- [11] R. Poil, J. Kennedy, and T. Blackwell, "Particle Swarm Optimization," *IEEE Swarm Intelligence Symposium*, vol. 107, no. 1, pp. 120–127, 2007.
- [12] J. Qian, A. Xiong, and W. Ma, "Extended State Observer-Based Sliding Mode Control with New Reaching Law for PMSM Speed Control," *Mathematical Problems in Engineering*, vol. 2016, Article ID 6058981, 10 pages, 2016.
- [13] S. Zhang, A. Wu, and T. Li, "Direct Control for Rotor Eccentric Displacement of Bearingless Permanent Magnet-type Synchronous Motors," *Proceedings of the CSEE*, vol. 27, no. 12, pp. 65–70, 2007.
- [14] Y. Zhang and X. F. Cheng, "Sensorless Control of Permanent Magnet Synchronous Motors and EKF Parameter Tuning Research," *Mathematical Problems in Engineering*, vol. 2016, Article ID 3916231, 12 pages, 2016.
- [15] G. B. Huang, Q. Y. Zhu, and C. K. Siew, "Extreme learning machine: a new learning scheme of feedforward neural networks," in *Proceedings of the IEEE International Joint Conference on Neural Networks*, vol. 2, pp. 985–990, 2005.
- [16] M. Li, G. Huang, P. Saratchandran, and N. Sundararajan, "Channel Equalization Using Complex Extreme Learning Machine with RBF Kernels," in *Proceedings of the International Conference on Advances in Neural Networks – ISNN*, vol. 3973, pp. 114–119, 2006.
- [17] K. Li, X. Qi, B. Wei, H. Huang, J. Wang, and J. Zhang, "Prediction of Transformer Top Oil Temperature Based on Kernel Extreme Learning Machine Error Prediction and Correction," *High Voltage Engineering*, vol. 43, no. 12, pp. 4045–4053, 2017.
- [18] X. Yang, W. Guan, Y. Liu, and Y. Xiao, "Prediction Intervals Forecasts of Wind Power based on PSO-KELM," *Proceedings of the CSEE*, vol. 35, 1, pp. 146–153, 2015.
- [19] X. Qi, K. Li, X. Yu, Z. Zhang, and J. Lou, "Transformer Top Oil Temperature Interval Prediction Based on Kernel Extreme Learning Machine and Bootstrap Method," *Proceedings of the CSEE*, vol. 37, no. 19, pp. 5821–5828, 2017.
- [20] M. Clerc and J. Kennedy, "The particle swarm-explosion, stability, and convergence in a multidimensional complex space," *IEEE Transactions on Evolutionary Computation*, vol. 6, no. 1, pp. 58–73, 2002.

## Research Article

# Comparative Controlling of the Lorenz Chaotic System Using the SMC and APP Methods

Ercan Köse <sup>1</sup> and Aydın Mühürçü <sup>2</sup>

<sup>1</sup>Department of Mechatronic Engineering, Tarsus University, Tarsus, Mersin, Turkey

<sup>2</sup>Department of Mechatronic Engineering, Kırklareli University, Kırklareli, Turkey

Correspondence should be addressed to Ercan Köse; [ekose@mersin.edu.tr](mailto:ekose@mersin.edu.tr)

Received 4 September 2018; Revised 16 November 2018; Accepted 22 November 2018; Published 6 December 2018

Academic Editor: Xinkai Chen

Copyright © 2018 Ercan Köse and Aydın Mühürçü. This is an open access article distributed under the Creative Commons Attribution License, which permits unrestricted use, distribution, and reproduction in any medium, provided the original work is properly cited.

The Lorenz chaotic system is based on a nonlinear behavior and this causes the system to be unstable. Therefore, two different controller models were developed and named as the adaptive pole placement and sliding mode control (SMC) methods for the establishment of continuous time nonlinear Lorenz chaotic system. In order to achieve this, an improved controller structure was developed first theoretically for both the controller methods and then tested practically using the numerical samples. During the establishment of adaptive pole placement method for the Lorenz chaotic system, various stages were applied. The nonlinear chaotic system was also linearized by means of Taylor Series expansion processes. In addition, the feedback matrix of the adaptive pole placement method was determined using linear Jacobian matrix. The chaotic system reached an equilibrium point by using both the SMC and adaptive pole placement methods; however the simulation results of the SMC had better success than adaptive pole placement control technique.

## 1. Introduction

Several studies have been conducted to analyze and control the chaotic structure since it has been found [1–4]. These studies are mainly focused on obtaining different chaotic structures, development process in the fields of applications on chaotic structures, and controlling the chaos with different procedures [5].

Lorenz, Chua, Rössler, Rikitake, Rucklidge, Chen, Lü, and Genesio developed the most important chaotic systems. These systems were applied to many control methods, such as OGY [6], nonlinear feedback control [7], delay feedback control [8], sliding mode control [9], switching control [10], fuzzy sliding mode control [11], and adaptive backstepping control [12].

Chaos is illustrated by nonlinear behaviors; therefore SMC technique can be used to control of the chaotic systems. SMC technique has been used by many different system controls, such as robotic, mechatronic, machine driver, chemical processes, wind turbine systems, and DC/DC converter [13].

The structure of the SMC must be known in order to understand the applications of the SMC technology. SMC has two different stages known as reaching and sliding phase. Firstly, a proper slip surface is the choice for the sliding mode technique. Switching technique forms the basic structure of SMC. In contrast to the switching ratio ideal, SMC is limited by physical reasons. The most important problem in these systems is chattering which is caused by fast switching. Switching functions such as relay, sigmoid, saturation, hysteresis-saturation, and hyperbolic functions could be used to reduce the chattering level [13, 14].

Abundant literature is available regarding the linearization considered as an important method for controlling of nonlinear systems. One of the most important studies about time-invariant systems linearization was conducted by Khalil [15]. Another study also addressed the problem of approximate linearization of a nonlinear control system [16].

The adaptive pole placement-based controller technique is another important method used in this work. A

zero equilibrium point was selected for APPM. The system which is nonlinear is linearized around this point, and required feedback vector is obtained from Taylor's series.

The applications of the pole placement-based controller techniques were examined in literature. Some of important applications related to this topic are as follows. Chilali and Gahinet have presented a novel LMI characterization for general convex subregions of the complex plane and proved its practicality for H<sub>∞</sub> synthesis with closed-loop pole clustering constraints [17]. Another study presented a PPM using both the improved Jacobian and the corresponding system transfer function matrices [18].

On the other hand, the control of chaotic systems with nonlinear behavior has become an important engineering problem recently. At the same time, chaotic systems have been widely used to explain the events and systems involving nonlinear behaviors such as Lorenz's description of weather events. In addition, chaotic systems provide a very important infrastructure for encrypting and sending electronic data that are widely used in communication systems. The aim of this study is to present a different approach to control the chaotic system of Lorenz, which is one of the basic studies for chaotic systems. The performances of two different control methods to accomplish this aim have been compared. The results of such comparisons would be a good example of the application of new control techniques on chaotic systems. It will also give a different approach to the chaotic structures used industrially.

This paper has been organized as follows. First, a brief definition of a Lorenz chaos system is given in Section 2. Then, design of sliding mode controller is given in Section 3. Afterward, numerical simulations for chaos control by way of sliding mode control and adaptive pole placement methods are given. Finally, conclusion is given in Section 5.

## 2. The Modeling of the Lorenz Chaotic System

The Lorenz system with a nonlinear structure is described by (1) given below. While positive constant parameters are  $a$ ,  $b$ , and  $c$ , state variables are  $x$ ,  $y$ , and  $z$ . The typical literature parameter values of the  $a$ ,  $b$ , and  $c$  constants are  $a=10$ ,  $b=8/3$ , and  $c=28$ , respectively.

$$\begin{aligned}\dot{x} &= a \cdot (-x + y) \\ \dot{y} &= (c - z) \cdot x - y \\ \dot{z} &= x \cdot y - b \cdot z\end{aligned}\quad (1)$$

The Lorenz chaotic system of the  $xy$ ,  $xz$ ,  $yz$ , and  $xyz$  phase portraits were obtained by using a MATLAB/Simulink program as indicated in Figure 1, when  $x_0 = 0.001$ ,  $y_0 = 0.001$ , and  $z_0 = 0$ . The initial values of the chaotic system were selected as values close or similar to the values in the literature. The choice of initial values is very important because of the change in all dynamic behavior.

## 3. SMC Design for Lorenz Chaotic System

SMC may be practiced for the Lorenz chaotic system. Stability of the Lorenz system was improved using only one controller. The system can be presented with

$$\begin{aligned}\dot{x} &= a \cdot (y - x) \\ \dot{y} &= x \cdot (c - z) - y + u \\ \dot{z} &= x \cdot y - b \cdot z\end{aligned}\quad (2)$$

where  $u$  is the control input.

After choosing of a sliding surface like (3), equations indicated below might be established:

$$s = \dot{e} + \lambda \cdot e \quad (3)$$

$$\dot{s} = \ddot{e} + \lambda \cdot \dot{e} \quad (4)$$

The trajectory error state could be selected like  $e = y_r - y$ , where  $y_r$  is constant, so  $\dot{y}_r = \ddot{y}_r = 0$ .  $\dot{y}_r$  and  $\ddot{y}_r$  are obtained as  $\dot{e} = \dot{y}_r - \dot{y} = 0 - \dot{y} = -\dot{y}$  and  $\ddot{e} = \ddot{y}_r - \ddot{y} = 0 - \ddot{y} = -\ddot{y}$ .

$$\dot{s} = -\rho \cdot \text{sign}(s) \quad (5)$$

After a proportional reachability rule as (5) is selected, equations below may be inscribed.

$$\dot{s} = \ddot{e} + \lambda \cdot \dot{e} = \ddot{y}_r - \ddot{y} + \lambda \cdot (\dot{y}_r - \dot{y})$$

$$= -\rho \cdot \text{sign}(s)$$

$$-\ddot{y} - \lambda \cdot \dot{y} = -\rho \cdot \text{sign}(s) \quad (6)$$

$$\dot{y}_{new} = \dot{y} + u$$

$$-\ddot{y} - \lambda \cdot \dot{y} - \lambda \cdot u = -\rho \cdot \text{sign}(s)$$

The control input is provided like

$$u = -\frac{\ddot{y}}{\lambda} - \dot{y} + \frac{\rho \cdot \text{sign}(s)}{\lambda} \quad (7)$$

The stability analysis is significant for evaluating the design of nonlinear controller. Therefore, Lyapunov stability analysis is selected and applied to SMC stability analysis. The stability is guaranteed, after the derivation of the Lyapunov function is negative definite [17].

$$\begin{aligned}\dot{v}(t) &= s \cdot \dot{s} \leq 0, s(t) \neq 0 \\ s \cdot \dot{s} &= s \cdot (-\rho \cdot \text{sign}(s)) \leq |s| \cdot (-\rho \cdot \text{sign}(s)) < 0\end{aligned}\quad (8)$$

According to the Lyapunov 2<sup>nd</sup> method,  $n$  to be constant, if  $\lim_{t \rightarrow \infty} y(t) = n$  is provided, then the systems is considered to be stable [19].

## 4. Adaptive Pole Placement Method Definitions

In the modern control theory and design, pole placement control techniques have been widely used. Firstly, the nonlinear Lorenz chaotic system is linearized by means of using

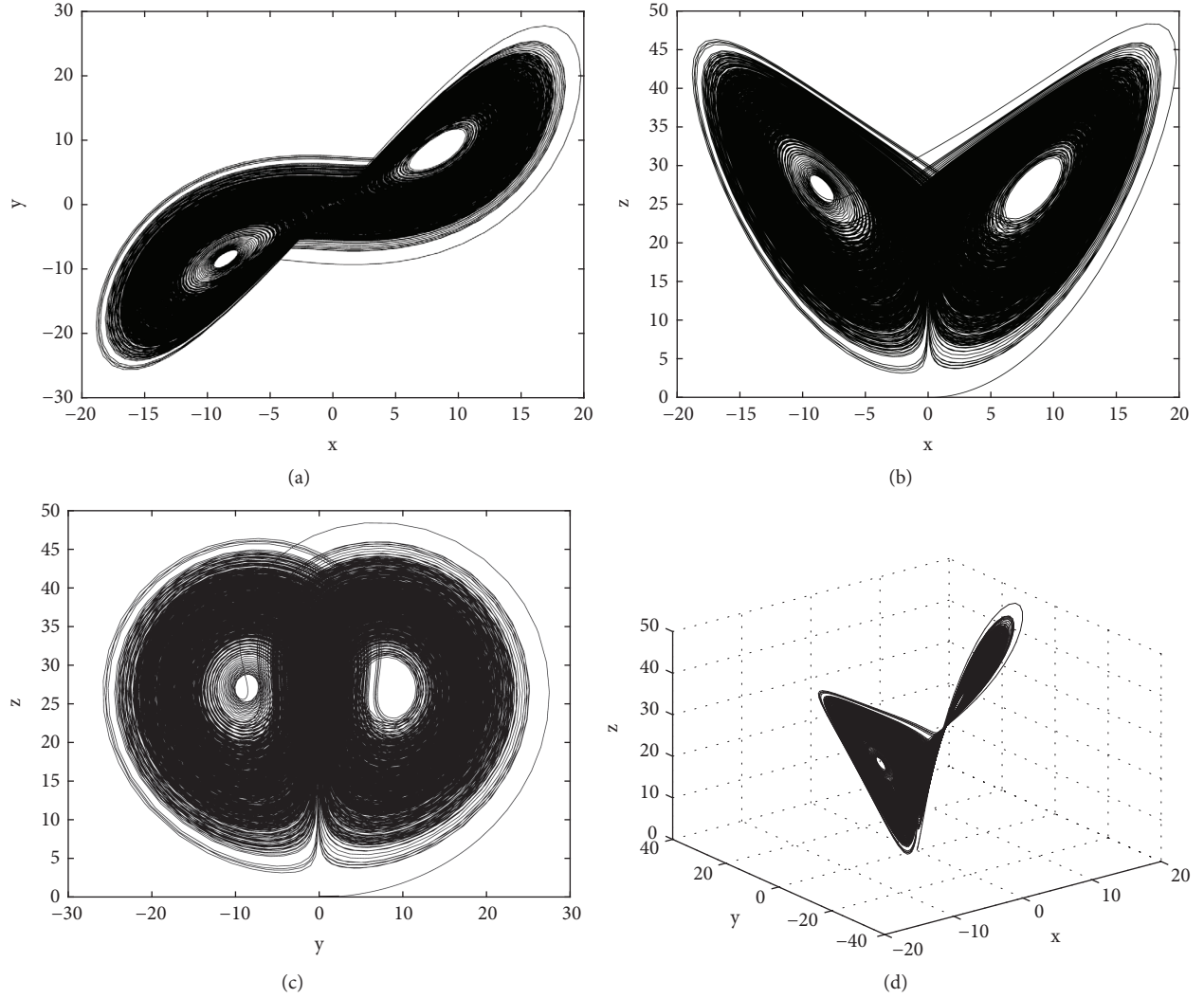


FIGURE 1: Phase portrait of the Lorenz systems in (a) xy, (b) xz, (c) yz, and (d) xyz.

Jacobian matrix, and then the feedback vector  $\mathbf{K}[\mathbf{k}_1 \ \mathbf{k}_2 \ \mathbf{k}_3]$  is determined by using embedded programming including linear matrix. The feedback linearized system may be defined:

$$\mathbf{u}(t) = -\mathbf{K}\mathbf{x}(t) \quad (9)$$

Modifying the system equation too:

$$\dot{\mathbf{x}}(t) = (\mathbf{A} - \mathbf{BK})\mathbf{x}(t) + \mathbf{B}r(t) \quad (10)$$

The desired eigenvalues are to be at

$$|s\mathbf{I} - \mathbf{A} + \mathbf{BK}| = (s - \gamma_1)(s - \gamma_2) \dots (s - \gamma_n) \quad (11)$$

## 5. Numerical Simulation

The control input signal is obtained by using (9), where  $\ddot{y} = -1$ ,  $\dot{y} = 28x - x.z + y$ , and SMC gains have been selected as  $\lambda = 3$ ,  $\rho = 0.01$  with the initial conditions  $x_0 = 0.001$ ,  $y_0 = 0.001$ , and  $z_0 = 0$ . The controllers are activated at  $t = 40$  seconds in all simulations. The system was linearized by means of Taylor's

series and then the Jacobian matrix was obtained by using the first terms of linear elements. A function is expressed in a great ratio by the first terms of the expansion. Therefore, higher degree terms can be ignored.

$$u = -\frac{1}{\lambda} - 28x + xz + y + \frac{\rho \cdot \text{sign}(s)}{\lambda} \quad (12)$$

$$u = -\frac{1}{3} - 28x + xz + y + \frac{0.01 \cdot \text{sign}(s)}{3}$$

$$f_1 = \dot{x} = a \cdot (y - x)$$

$$f_2 = \dot{y} = x \cdot (c - z) - y \quad (13)$$

$$f_3 = \dot{z} = x \cdot y - b \cdot z$$

$$f(x) = f(\bar{x})$$

$$= \left. \frac{df}{dx} \right|_{x=\bar{x}} (x - \bar{x}) + \text{Higher degree terms} \quad (14)$$

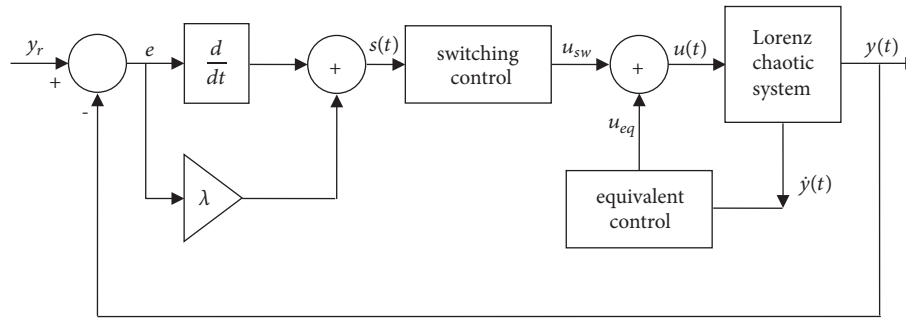


FIGURE 2: The SMC model for the Lorenz chaotic system.

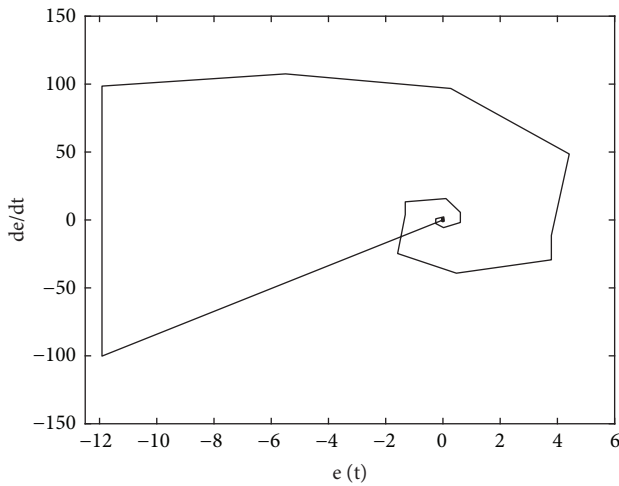


FIGURE 3: The phase planes  $e(t)$  and  $\dot{e}(t)$  in the Lorenz chaotic system.

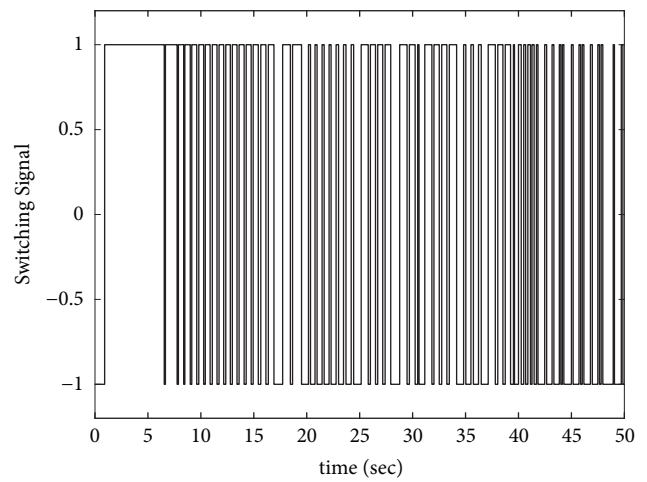


FIGURE 4: Switching signal for sliding mode control.

The eigenvalues are calculated by means of solving the characteristic equation:

$$A = |\lambda I - J| = \begin{vmatrix} \lambda - (-10) & -10 & 0 \\ z - 28 & 1 + \lambda & x \\ -y & -x & \lambda + \left(\frac{8}{3}\right) \end{vmatrix} = 0 \quad (15)$$

Initial eigenvalues of  $\lambda_1 = 22.8277$ ,  $\lambda_2 = -11.8277$ ,  $\lambda_3 = 2.6667$  for  $x_0 = 0.001$ ,  $y_0 = 0.001$ , and  $z_0 = 0$ .

A suggested control model based on the equivalent control  $u_{eq}(t)$  and switching control  $u_{sw}(t)$  is indicated in Figure 2 and (16), (17), and (18), where  $\rho_{sw}$  is a positive constant.

$$u(t) = u_{eq}(t) + u_{sw}(t) \quad (16)$$

$$u_{sw}(t) = -\rho_{sw} \text{sign}(s(t)) \quad (17)$$

$$u_{eq}(t) = u(t) - u_{sw}(t) \quad (18)$$

In Figure 3, the phase system controlling sliding mode reached the third region from second region at fourth second. Then, the error of system reached the equilibrium point (zero point) after sliding phase.

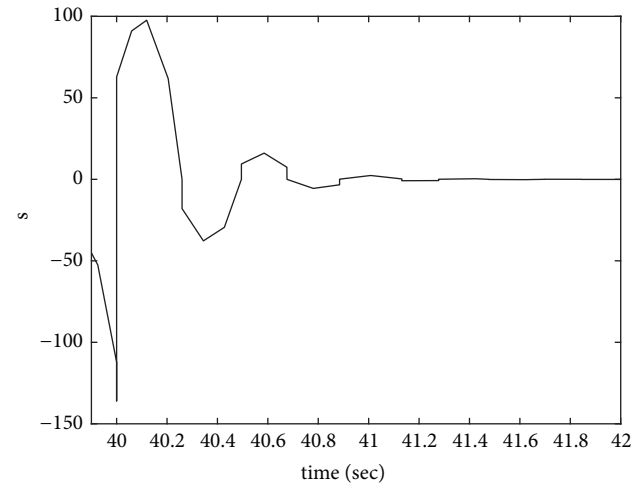


FIGURE 5: The time variation of the sliding surface.

High frequency control signal was applied to input of chaos system as shown in Figures 4, 5, and 6.

After the controller enters the system at 40th second as shown in Figure 7, the state variables reached an equilibrium point  $E_0(0, 0, 0)$ . This phenomenon is clearer in Figure 8 of the phase portrait.

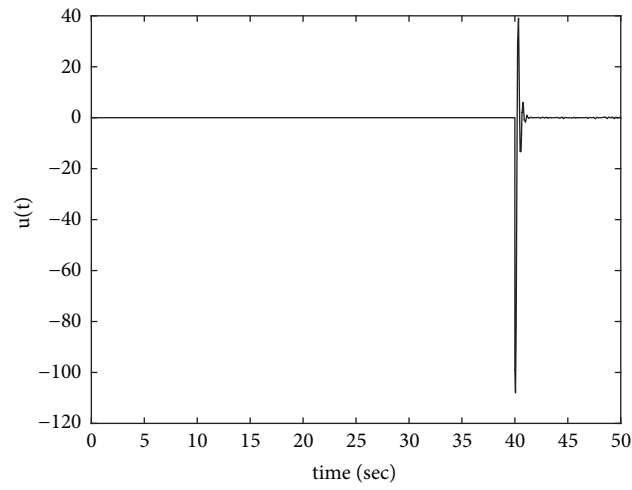


FIGURE 6: The control signals for sliding mode.

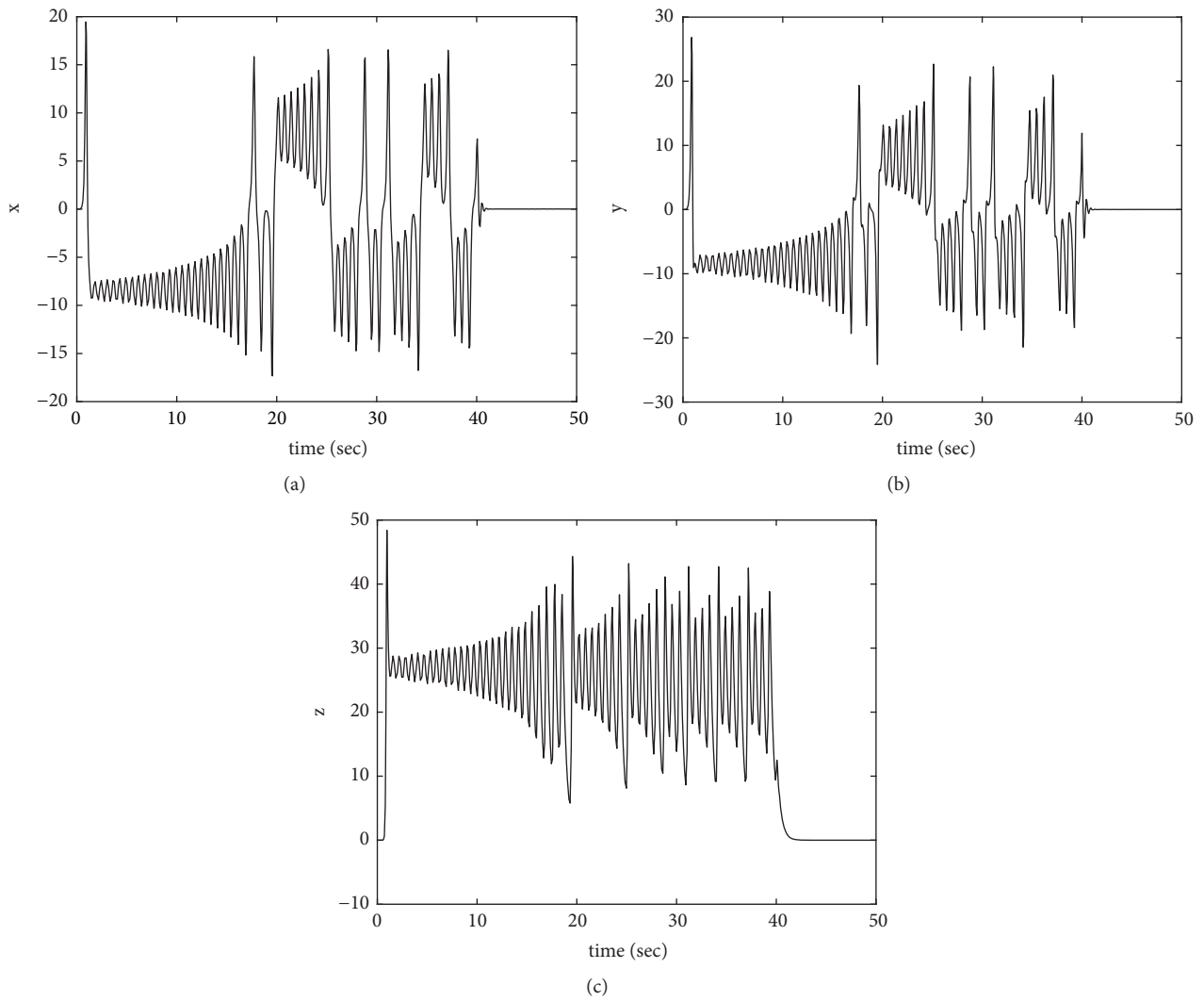


FIGURE 7: The time response of (a)  $x$ , (b)  $y$ , and (c)  $z$  state variables with the SMC activated at  $t = 40$  seconds.

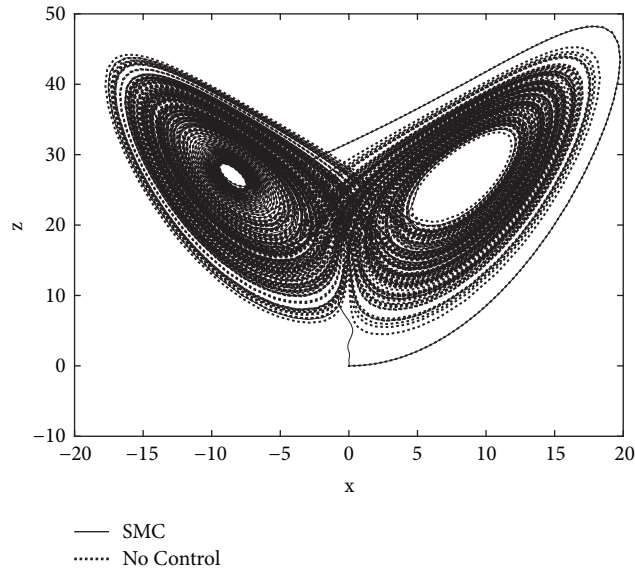


FIGURE 8:  $xz$  portraits with and without sliding mode control.

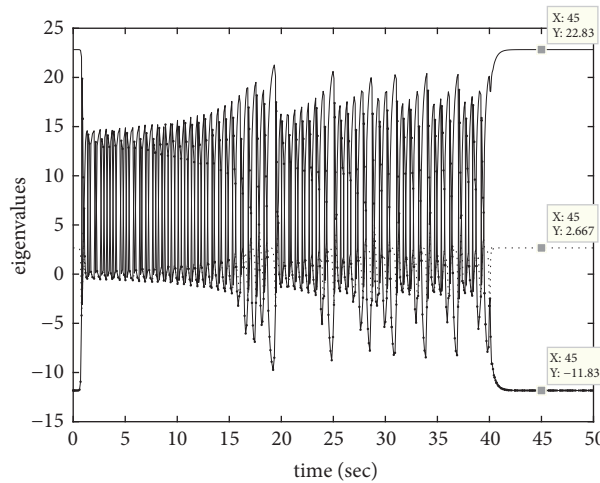


FIGURE 9: Eigenvalues changes with controller active at  $t=40$  seconds.

In Figure 9, the eigenvalues of  $E_0(0, 0, 0)$  are 22.83, 2.667, and -11.83, which are given respectively. The same values can also be reached at the equilibrium point due to the existence of the controller at 40th second. According to Lyapunov stability theorem, the criterion of  $s.\dot{s} \leq 0$  was applied at fourth second and the system reached the stability. Initial eigenvalues of  $\gamma_1 = 22.8277$ ,  $\gamma_2 = -11.8277$ , and  $\gamma_3 = 2.6667$  were chosen for the adaptive pole placement system design. Using (14) adaptive pole placement method was improved as shown in Figure 10.

In Figure 11, the state variables reached the equilibrium point  $E_0(0, 0, 0)$  quickly with an error. These conditions were also confirmed in both Figures 12 and 13 with attained eigenvalues, 22.81, 2.667, and -11.81, respectively. Also,  $\mathbf{k}_1$ ,  $\mathbf{k}_2$ , and  $\mathbf{k}_3$  are adaptive controller gains as shown in Figure 14. While the  $\mathbf{k}_2$  feedback vector was fixed, the feedback vectors  $\mathbf{k}_1$  and  $\mathbf{k}_3$  varied intensively with the existence of the controller especially at 40<sup>th</sup> second.

## 6. Conclusion

In this study, the controllers were developed by way of the SMC and APP methods for continuous time nonlinear Lorenz chaotic system. The simulation results of the SMC technique are more influential than APP technique. While the SMC method reached an equilibrium point, adaptive pole placement method reached an equilibrium point with greater error. According to SMC, the signal responses given by APPM are quite noisy and the steady-state errors have quite high values. Moreover, the results of the study showed that the system behaviors based on Lyapunov stability analysis were unstable and nonlinear at 0th to 40th second. The SMC, which is widely preferred in the literature, has performed very well in the control of the Lorenz chaotic system. Another recommended control method is APPM. This method can be used to control the Lorenz chaotic system but has a lower level of performance.

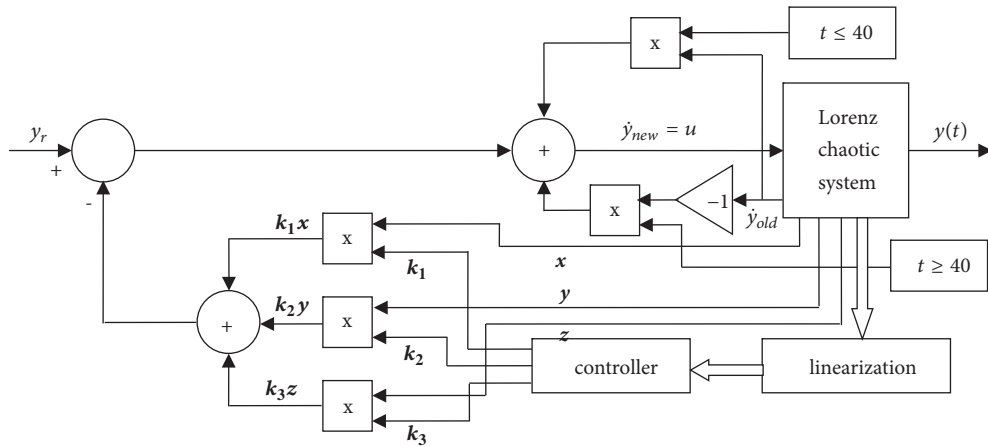


FIGURE 10: Proposed adaptive pole placement control method.

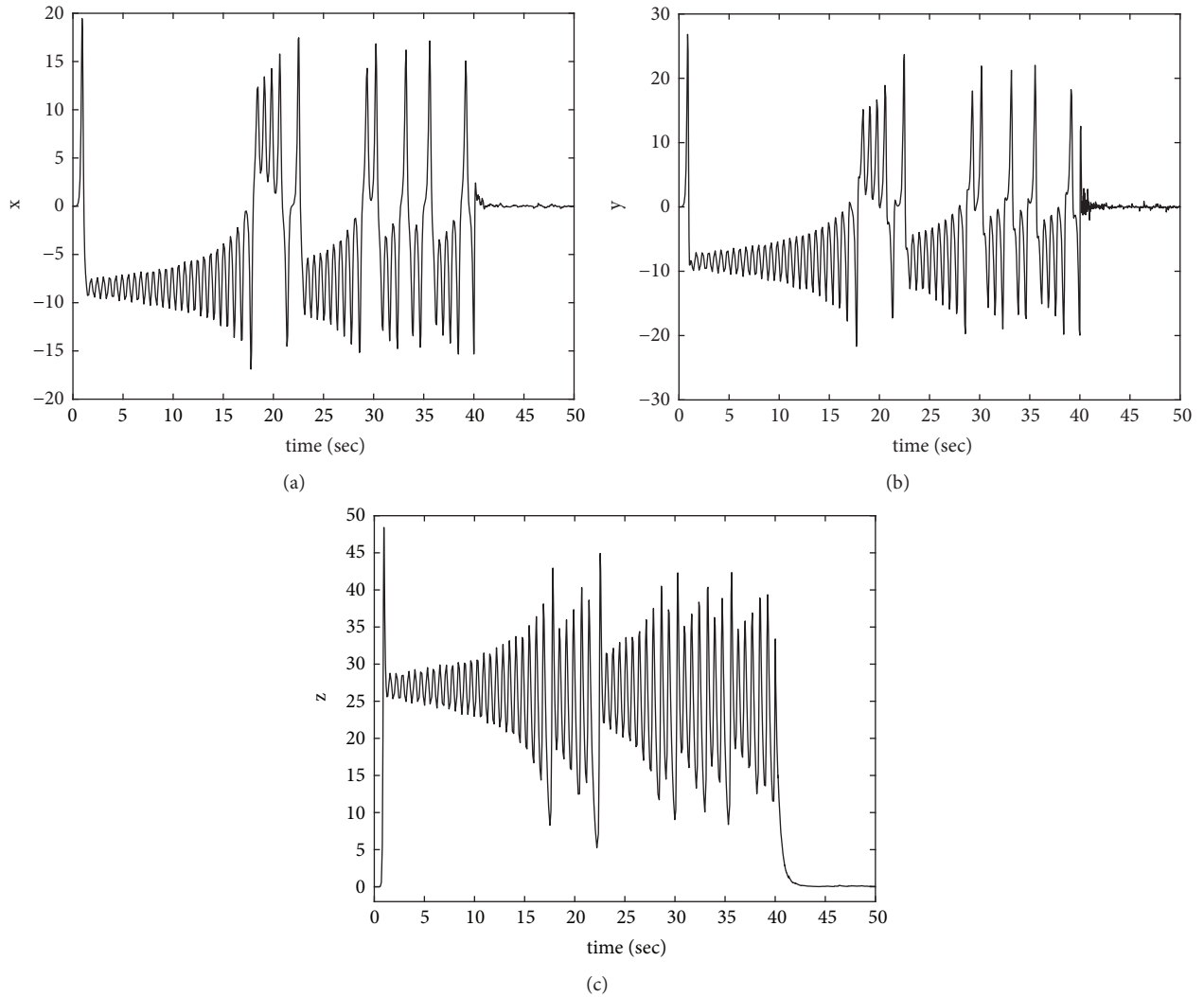


FIGURE 11: The time response of (a)  $x$ , (b)  $y$ , and (c)  $z$  state variables with the APPM activated at  $t = 40$  seconds.

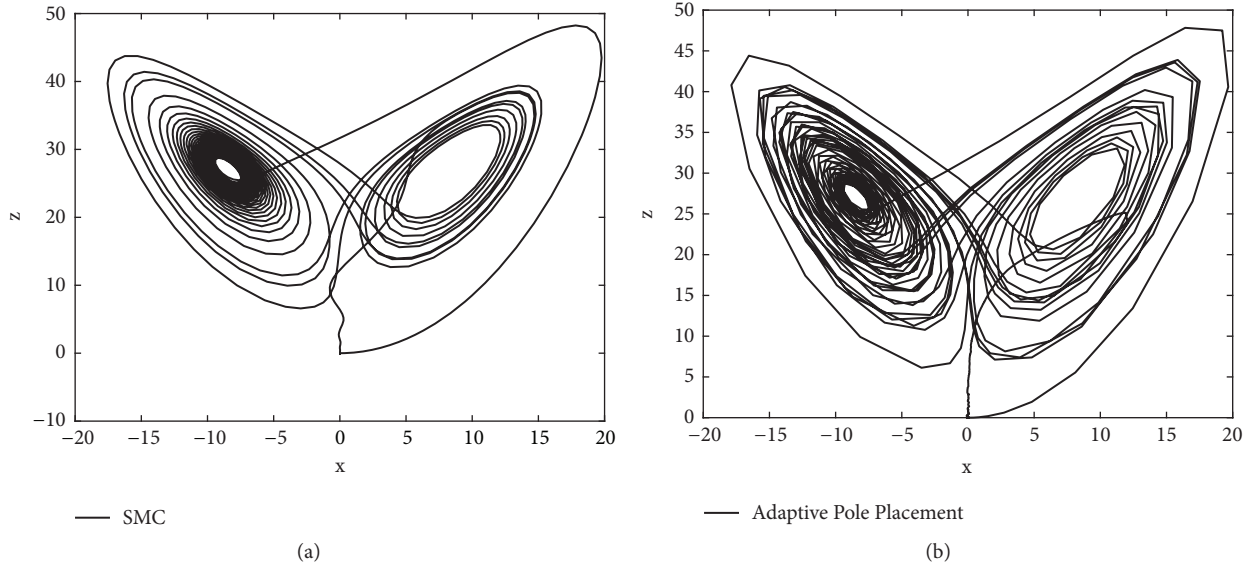


FIGURE 12: xz portraits obtained with SMC (a) and APP (b) control methods.

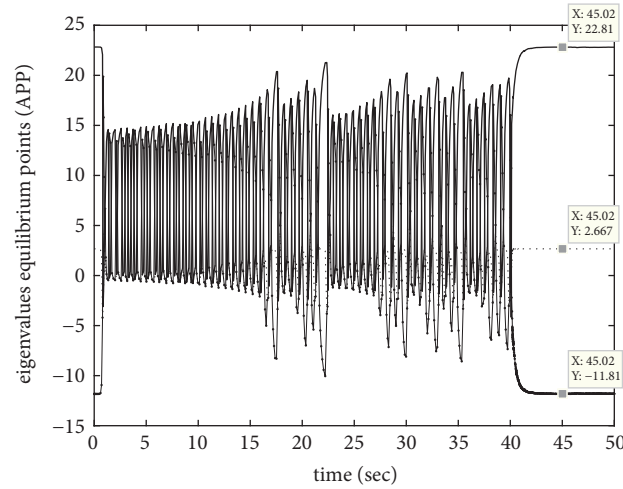


FIGURE 13: Eigenvalues values changes with controller active at t=40 seconds.

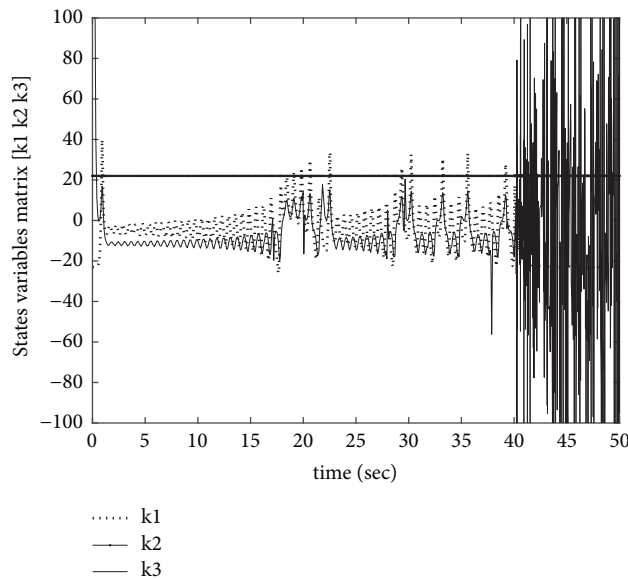


FIGURE 14: The change of adaptive control gain matrix  $K$  [ $k_1$   $k_2$   $k_3$ ].

## Data Availability

The data used to support the findings of this study are available from the corresponding author upon request.

## Conflicts of Interest

The authors declare that they have no conflicts of interest.

## References

- [1] E. N. Lorenz, "Deterministic nonperiodic flow," *Journal of the Atmospheric Sciences*, vol. 20, no. 2, pp. 130–141, 1963.
- [2] O. E. Rössler, "An equation for continuous chaos," *Physics Letters A*, vol. 57, no. 5, pp. 397–398, 1976.
- [3] K. Ito, "Chaos in the Rikitake two-disc dynamo system," *Earth and Planetary Science Letters*, vol. 51, no. 2, pp. 451–456, 1980.
- [4] L. O. Chua, M. Komuro, and T. Matsumoto, "The double scroll family," *IEEE Transactions on Circuits and Systems II: Express Briefs*, vol. 33, no. 11, pp. 1072–1118, 1986.
- [5] J. Lü, G. Chen, and S. Zhang, "The compound structure of a new chaotic attractor," *Chaos, Solitons & Fractals*, vol. 14, no. 5, pp. 669–672, 2002.
- [6] E. Ott, C. Grebogi, and J. A. Yorke, "Controlling chaos," *Physical Review Letters*, vol. 64, no. 11, pp. 1196–1199, 1990.
- [7] J. Alvarez-Ramírez, "Nonlinear feedback for controlling the Lorenz equation," *Physical Review E: Statistical, Nonlinear, and Soft Matter Physics*, vol. 50, no. 3, pp. 2339–2342, 1994.
- [8] Y. Ding, W. Jiang, and H. Wang, "Delayed feedback control and bifurcation analysis of Rossler chaotic system," *Nonlinear Dynamics*, vol. 61, no. 4, pp. 707–715, 2010.
- [9] U. E. Kocamaz, Y. Uyaroglu, and H. Kizmaz, "Controlling hyperchaotic Rabinovich system with single state controllers: Comparison of linear feedback, sliding mode, and passive control methods," *Optik - International Journal for Light and Electron Optics*, vol. 130, pp. 914–921, 2017.
- [10] S.-J. Cho, M. Jin, T.-Y. Kuc, and J. S. Lee, "Control and synchronization of chaos systems using time-delay estimation and supervising switching control," *Nonlinear Dynamics*, vol. 75, no. 3, pp. 549–560, 2014.
- [11] M. M. Fateh, A. Alfi, M. Moradi, and H. Modarres, "Sliding mode control of lorenz chaotic system on a moving fuzzy surface," in *Proceedings of the IEEE EUROCON 2009, EUROCON 2009*, pp. 964–970, Russia, May 2009.
- [12] J. H. Park, "Synchronization of Genesio chaotic system via backstepping approach," *Chaos, Solitons & Fractals*, vol. 27, no. 5, pp. 1369–1375, 2006.
- [13] I. Eker, "Sliding mode control with PID sliding surface and experimental application to an electromechanical plant," *ISA Transactions*, vol. 45, no. 1, pp. 109–118, 2006.
- [14] E. Kose, H. Kizmaz, K. Abaci et al., "Control of SVC based on the sliding mode control method," *Turkish Journal Of Electrical Engineering Computer*, vol. 22, pp. 605–619, 2014.
- [15] K. H. Khalil, *Nonlinear Systems*, Prentice Hall, 1996.
- [16] W. Kang, "Approximate linearization of nonlinear control systems," *System & Control Letters*, vol. 23, pp. 43–52, 1994.
- [17] M. Chilali and P. Gahinet, "H $\infty$  design with pole placement constraints: an LMI approach," *IEEE Transactions on Automatic Control*, vol. 41, no. 3, pp. 358–367, 1996.
- [18] P. Bueno De Araujo and L. C. Zanetta Jr., "Pole placement method using the system matrix transfer function and sparsity," *International Journal of Electrical Power & Energy Systems*, vol. 23, no. 3, pp. 173–178, 2001.
- [19] E. Köse, "Controller design by using non-linear control methods for satellite chaotic system," *Electrical Engineering*, vol. 99, no. 2, pp. 763–773, 2017.

## Research Article

# On an Application of the Absolute Stability Theory to Sampled-Data Stabilization

Alexander N. Churilov 

*Faculty of Mathematics and Mechanics, St. Petersburg State University, St. Petersburg, Russia*

Correspondence should be addressed to Alexander N. Churilov; [a\\_churilov@mail.ru](mailto:a_churilov@mail.ru)

Received 7 July 2018; Revised 6 October 2018; Accepted 18 November 2018; Published 3 December 2018

Guest Editor: Weihai Zhang

Copyright © 2018 Alexander N. Churilov. This is an open access article distributed under the Creative Commons Attribution License, which permits unrestricted use, distribution, and reproduction in any medium, provided the original work is properly cited.

A nonlinear Lur'e-type plant with a sector bound nonlinearity is considered. The plant is stabilized by a discrete-time feedback signal with a nonperiodic uncertain sampling. The sampling control function is nonlinear and also obeys some sectoral constraints at discrete (sampling) times. The linear matrix inequality (LMI) conditions for the stability of the closed-loop system are obtained.

## 1. Introduction

Absolute stability theory of nonlinear systems with sectoral constraints goes back to works of A. I. Lur'e (see [1], some historical reviews can be found in [2, 3]). In [4] and subsequent papers the Lur'e problem was reduced to feasibility of a special system of Linear Matrix Inequalities (LMIs). Later, the advantage of the LMI approach to different problems of applied mathematics was comprehensively discussed in monograph [5] that launched a broad development of a specific computer software for exploring LMIs. In [6–8] the Lur'e theory was extended to multiple nonlinearities.

We will mention two basic concepts put forward by V. A. Yakubovich in 1960s–1970s. The first one is S-procedure [2, 9, 10] that is especially useful when we have to deal with several nonlinearities. The second one is integral-quadratic constraint (IQC), the concept that was initially introduced by V. A. Yakubovich in connection with the study of pulse-width modulated systems (a special class of sampled-data systems) [11]. Regrettably, the last paper was never translated and is almost unknown for a non-Russian reader. Notice that the impact of the early works of V. A. Yakubovich on the modern IQC theory was recognized in the review part of a widely known paper [12]. Sectoral constraints and IQCs proved to be instrumental for stability analysis of various classes of nonlinear control systems (see, e.g., [2]).

The third type of constraints, that can be named discrete-time constraints, was put forward by A. Kh. Gelig for nonlinear sampled-data systems [13]. Unlike the usual sectoral constraints, discrete-time constraints are valid not at all times, by only at some discrete-time instants lying in the sampling interval. The exact position of these instants depends on the type of a pulse modulation. In the further development of this approach it was proposed to exploit a Lyapunov–Krasovskii functional [14], but later it was found that for the stability analysis it is more convenient to combine discrete-time constraints with IQCs. Namely, in [15] it was proposed to employ the IQC based on Wirtinger integral inequality [16]. Since that time, the Wirtinger-based IQCs were used in a great number of publications for various types of sampled-data systems [17–26]. In particular, the problem of stabilization of a linear plant by means of a pulse-modulated signal was considered [21, 22]. The statements of the above works were formulated in terms of frequency-domain inequalities, but later some of them were restated in terms of LMIs [23–26].

The main idea of the Gelig's approach is a substitution of the initial train of pulses for a sequence of the average values of these pulses, with a supposition that these averages satisfy some instant constraints. The errors of such a substitution are estimated with the help of IQCs. Unlike other averaging theorems, the results of Gelig were not asymptotical, but

could be used for an estimation of the sampling frequency from below. For sufficiently high sampling frequencies the Gelig-type stability conditions reduce to the conventional absolute stability criteria (the circle criterion, the Popov criterion, and some others).

The problem of stabilization of a continuous-time plant by a sampled-data signal attracted much attention last decade; see a review paper [27] where the existing modern approaches are outlined. We can distinguish two main competing methods. The input delay approach was contributed by E. Fridman [28, 29] who considered a sampled-data signal as a special case of delayed signal. If  $t_n, n \geq 0$ , are sampling times, then a sampled signal  $x(t_n)$  can be reformulated as a delayed signal  $x(t - \tau(t))$  with  $\tau(t) = t - t_n, t_n < t < t_{n+1}$ , then Lyapunov–Krasovskii functionals can be applied.

An alternative is the IQCs approach that is more closely related to the absolute stability theory [30–33]. In [30] it was firstly proved that specially chosen IQCs give the same results as those previously obtained by the input delay method. In [31] it was demonstrated that by extending the IQC approach these results can be refined. Notice that the estimate for a  $L^2$ -gain used in [30] can be considered as a reformulated Wirtinger inequality. In [32, 33] the stability problem was reduced to feasibility of an infinite number of LMIs with coefficients depending on time  $t$ . It was shown that under certain assumptions they can be checked only at a finite number of points. Though being more laborious, this approach leads to improvements of the previous results.

The most publications on sampled-data stabilization treat the case when the plant is linear and the discrete-time control implements the zero-order hold strategy. As for nonlinear plants (with single or multiple nonlinearities), their stabilization problem by a linear zero-order hold sampled-data control was considered in [34–37]. The technique used in these papers was based on the method of input delays and on constructing special Lyapunov–Krasovskii functionals. The paper [38] considered a multiple nonlinearity Lur'e system stabilized by a multirate discrete-data control. The consideration was based on the integral estimate from [39]; the result was formulated in the form of a frequency-domain inequality.

This paper aims to demonstrate how the classical absolute stability technique (Yakubovich's S-procedure, Lur'e sectoral constraints, IQCs, and Gelig's discrete-time constraints) can be applied to stability analysis of a nonlinear Lur'e-type plant under a sampled-data nonlinear stabilizing signal. The results thus obtained are parsimonious and easily verifiable, but they are compatible with those obtained by more sophisticated mathematical methods.

The paper is organized as follows. Firstly we describe a model that consists of a Lur'e-type nonlinear plant under a sampled-data nonlinear control. The sampling is supposed to be nonuniform, with a known upper bound of dwell-times. Further, we demonstrate how the sampled-data stabilization problem for a Lur'e system can be treated in the frame of the Gelig–Yakubovich approach to the absolute stability theory. The key role is played by the Yakubovich's S-procedure that in fact provides an alternative technique to using Lyapunov–Krasovski functionals. It is proved that for

a sufficiently high sampling frequency the stability criterion obtained is reduced to the circle criterion for absolute stability of continuous-time systems. Thus for high sampling frequencies the conservatism of the considered method is the same as that of the classical absolute stability criteria. Finally the main result is illustrated by an application to a simple first-order problem and to a sampled-data control of a mathematical pendulum.

## 2. System Model

Here we address a sampling-data counterpart of the circle stability criterion (see, e.g., [2, 40, 41]).

Consider a nonlinear Lur'e-type plant with a sectoral bound uncertainty

$$\begin{aligned}\dot{x}(t) &= Ax(t) + Bv(t), \\ \sigma(t) &= Cx(t), \\ v(t) &= \varphi(\sigma(t), t).\end{aligned}\tag{1}$$

Here the nonlinearity  $\varphi(\cdot, \cdot)$  describes an intrinsic nonlinear feedback; it is continuous and obeys the sectoral bound

$$\mu_1 \leq \frac{\varphi(y, t)}{y} \leq \mu_2 \tag{2}$$

for all real  $y, t$ . In other words,  $v(t)$  satisfies a quadratic constraint [2]

$$(\mu_2\sigma(t) - v(t))(v(t) - \mu_1\sigma(t)) \geq 0 \tag{3}$$

for all  $t$ . Here  $\mu_1, \mu_2$  are scalars, and  $A, B, C$  are constant matrices of sizes  $p \times p, p \times 1, 1 \times p$ , respectively. Obviously, system (1) has a zero equilibrium  $x(t) \equiv 0$ , whose stability can be investigated with the help of the circle criterion of absolute stability [2]. However, we will be interested in the case when the zero equilibrium is unstable, so a sampled-data external feedback is used for its stabilization.

Let plant (1) be governed by a sampled-data external signal. Assume that we have a strictly increasing sequence of sampling times  $t_0 < t_1 < t_2 < \dots$  with the lengths of the sampling intervals (dwell-times)  $T_n = t_{n+1} - t_n$  estimated as

$$\delta_0 T \leq T_n \leq T, \quad \forall n \geq 0, \tag{4}$$

where  $\delta_0, T$  are some positive constants. The sequence  $\{t_n\}$  is uncertain, and it does not need to be periodic, and only estimates (4) matter. The ratio  $1/T_n$  can be considered as an instant sampling frequency. Let plant (1) be controlled by a zero-order hold signal  $u(t)$ :

$$\begin{aligned}\dot{x}(t) &= Ax(t) + Bv(t) + B_u u(t), \\ \sigma_u(t) &= Kx(t),\end{aligned}\tag{5}$$

$$u(t) = u_n, \quad t_n \leq t < t_{n+1}, \tag{6}$$

$$u_n = F(\sigma_u(t_n)). \tag{7}$$

Here  $B_u$ ,  $K$  are vectors of sizes  $p \times 1$ ,  $1 \times p$ , respectively, and  $F(\cdot)$  is a nonlinear function (a modulation characteristic) that satisfies a sectoral constraint

$$\nu_1 \leq \frac{F(y)}{y} \leq \nu_2 \quad (8)$$

for all real  $y$  and some scalars  $\nu_1, \nu_2$ , hence

$$(\nu_2 \sigma_u(t_n) - u_n)(u_n - \nu_1 \sigma_u(t_n)) \geq 0 \quad (9)$$

for all  $n \geq 0$ . Thus the quadratic constraint (9) holds not for all times  $t$ , but only for discrete times  $t_n$  (see [13]).

The zero-order hold signal  $u(t)$  defined by (6), (7) can be considered as a special case of a square (rectangular) pulse

$$u(t) = \begin{cases} u_n, & t_n \leq t < t_n + \tau_n, \\ 0, & t_n + \tau_n \leq t < t_{n+1}, \end{cases} \quad (10)$$

where  $u_n$ ,  $\tau_n$ , and  $1/T_n$  (with  $T_n = t_{n+1} - t_n$ ) are the amplitude, the width and the instant frequency, respectively. The specific of the zero-order hold is that  $\tau_n \equiv T_n$ ; thus all the three impulse parameters, the amplitude, the width, and the frequency, are modulated. The average of the pulse signal  $u(t)$  considered on the  $n$ th sampling interval is

$$\bar{u}_n = \frac{1}{T_n} \int_{t_n}^{t_{n+1}} u(t) dt = u_n. \quad (11)$$

Hence  $u(t) = \bar{u}_n$ ,  $t_n < t < t_{n+1}$ ; i.e., the error of a substitution of a pulse for its average is equal to zero.

Formula (7) reads that the amplitude modulation is of the first kind [20, 42], so discrete constraints can be imposed at the points  $t = t_n$ . (In the theory of hybrid systems this type of modulation is termed as self-triggered control [43, 44].) Notice that for more elaborate types of pulse modulation the averaging method considers discrete constraints at some intermediate points  $t = \tilde{t}_n$ ,  $t_n < \tilde{t}_n < t_{n+1}$ . Then the value  $\sigma_u(\tilde{t}_n)$  can be interpreted as a signal with a deviating argument that can be not only delayed, but also advanced:  $\sigma_u(t - \tau(t))$  with  $\tau(t) = t - \tilde{t}_n$ ,  $t_n < t < t_{n+1}$ .

Here we will demonstrate how the approach developed in Theorem 3.3 [20] can be reformulated for this special case. We will use not the frequency-domain inequalities (as in [20]), but LMIs. The result will be augmented by an additional IQC taken from [31].

### 3. The Main Statement

Let us make an additional assumption on the nonlinearity  $\varphi_0(\sigma, t)$ . Suppose that there exists a scalar  $\mu$  such that the function

$$\varphi_0(\sigma, t) = \varphi(\sigma, t) - \mu\sigma \quad (12)$$

is bounded for all  $\sigma, t$ . The following theorem presents LMI conditions for the zero asymptotic of the closed-loop system (5), (6), (7).

**Theorem 1.** Consider a nonlinear system (5), (6), (7) with a nonlinearity  $v(t) = \varphi(\sigma(t), t)$  satisfying (3) and with a sampled-data control satisfying (4) and (9). Assume that there exist a symmetric  $p \times p$  matrix  $H$  and scalars  $\tau \geq 0$ ,  $\varepsilon \geq 0$ ,  $\vartheta \geq 0$  such that the following set of matrix inequalities is feasible:

$$H > 0, \quad (13)$$

$$\Pi = \begin{bmatrix} \Pi_{11} & \Pi_{12} & \Pi_{13} & \Pi_{14} \\ * & \Pi_{22} & \Pi_{23} & \Pi_{24} \\ * & * & \Pi_{33} & \Pi_{34} \\ * & * & * & \Pi_{44} \end{bmatrix} < 0 \quad (14)$$

with

$$\begin{aligned} \Pi_{11} &= HA + A^\top H - \varepsilon \mu_1 \mu_2 C^\top C - \tau \nu_1 \nu_2 K^\top K \\ &\quad + A^\top K^\top KA, \\ \Pi_{12} &= HB_u + \frac{1}{2} \tau (\nu_1 + \nu_2) K^\top + A^\top K^\top KB_u, \\ \Pi_{13} &= HB + \frac{1}{2} \varepsilon (\mu_1 + \mu_2) C^\top + A^\top K^\top KB, \\ \Pi_{14} &= \tau \nu_1 \nu_2 K^\top + \vartheta A^\top K^\top, \\ \Pi_{22} &= -\tau + (KB_u)^2, \\ \Pi_{23} &= KBKB_u, \\ \Pi_{24} &= -\frac{1}{2} \tau (\nu_1 + \nu_2) + \vartheta KB_u, \\ \Pi_{33} &= -\varepsilon + (KB)^2, \\ \Pi_{34} &= \vartheta KB, \\ \Pi_{44} &= -\tau \nu_1 \nu_2 - \gamma. \end{aligned} \quad (15)$$

Here  $\gamma = \pi^2/(4T^2)$ ,  $\top$  denotes matrix transpose and asterisks stand for the matrix blocks symmetric with respect to the main diagonal. Inequalities (13), (14) are understood in the sense of positive and negative definiteness of quadratic forms. Then any solution of (5), (6), (7) is asymptotically zero:  $x(t) \rightarrow 0$  as  $t \rightarrow +\infty$  and  $u_n \rightarrow 0$  as  $n \rightarrow +\infty$ .

Notice that if we abandon the above assumption on the function  $\varphi_0(\sigma, t)$  we can assert only that any solution  $x(t)$  is square integrable that is a weaker property than the zero asymptotic.

If the control gains vector  $K$  is given and fixed, inequalities (14), (15) present LMIs with respect to variables  $H$ ,  $\tau$ ,  $\varepsilon$ ,  $\vartheta$ ,  $\gamma$ . However, if  $K$  is considered as a design parameter and needs to be chosen, then we get a problem with nonlinear constraints.

### 4. Proof of the Main Statement

Let us introduce an auxiliary function

$$\xi(t) = \sigma_u(t) - \sigma_u(t_n) = K(x(t) - x(t_n)) \quad (16)$$

for  $t_n \leq t < t_{n+1}$ . As well as  $u(t)$ , the function  $\xi(t)$  is discontinuous with jumps at the points  $t = t_n, n \geq 0$ .

The proof follows the mathematical technique conventional for the absolute stability theory (see, e.g., [2]). The three types of constraints will be used. Firstly, we will use a quadratic (Lur'e-type) constraint (3) that can be rewritten as

$$(\mu_2 Cx(t) - v(t))(v(t) - \mu_1 Cx(t)) \geq 0 \quad (17)$$

for all  $t$ . Secondly, consider a discrete-time (Gelig-type) constraint (9). With the help of (16) it can be rewritten as

$$\begin{aligned} & (\nu_2 \sigma_u(t_n) - u(t))(u(t) - \nu_1 \sigma_u(t_n)) \\ &= (\nu_2 \sigma_u(t) - \nu_2 \xi(t) - u(t)) \\ & \cdot (u(t) - \nu_1 \sigma_u(t) - \nu_1 \xi(t)) = (\nu_2 \sigma_u(t) - u(t)) \\ & \cdot (u(t) - \nu_1 \sigma_u(t)) - (\nu_1 + \nu_2) u(t) \xi(t) \\ &+ 2\nu_1 \nu_2 \sigma_u(t) \xi(t) - \nu_1 \nu_2 \xi^2(t) \geq 0 \end{aligned} \quad (18)$$

for  $t_n < t < t_{n+1}, n \geq 0$ . Recall that  $\sigma_u(t) = Kx(t)$ .

Thirdly, let us take two integral-quadratic (Yakubovich type) constraints. The first one is based on the Wirtinger integral inequality (see [15, 17, 19, 20])

$$\int_{t_n}^{t_{n+1}} (\sigma_u(t) - \sigma_u(t_n))^2 dt \leq \frac{4T_n^2}{\pi^2} \int_{t_n}^{t_{n+1}} \dot{\sigma}_u^2(t) dt \quad (19)$$

for all  $n \geq 0$ . From (4) the last inequality implies

$$\int_{t_n}^{t_{n+1}} (\sigma_u(t) - \sigma_u(t_n))^2(t) dt \leq \Delta \int_{t_n}^{t_{n+1}} \dot{\sigma}_u^2(t) dt \quad (20)$$

with  $\Delta = 4T^2/\pi^2$ .

The second IQC can be extracted from [31]. Since  $\dot{\sigma}_u(t) = \dot{\xi}(t), t_n < t < t_{n+1}$ , and  $\xi(t_n^+) = 0$ , we get

$$\int_{t_n}^t \dot{\sigma}_u(s) \xi(s) ds = \int_{t_n}^t \dot{\xi}(s) \xi(s) ds = \frac{1}{2} \xi^2(t) \quad (21)$$

for  $t_n < t < t_{n+1}$ . Thus

$$\int_{t_n}^{t_{n+1}} \dot{\sigma}_u(s) \xi(s) ds = \frac{1}{2} \xi^2(t_{n+1}^-) \geq 0. \quad (22)$$

Following the S-procedure (see [2, 9]), let us define a quadratic form

$$\begin{aligned} G(x, u, v, \xi) &= \varepsilon (\mu_2 Cx - v)(v - \mu_1 Cx) \\ &+ \tau \left[ (\nu_2 Kx - u)(u - \nu_1 Kx) - (\nu_1 + \nu_2) u\xi \right. \\ &+ 2\nu_1 \nu_2 Kx\xi - \nu_1 \nu_2 \xi^2 \left. \right] + \left[ (KAx + KBv + KB_u u)^2 \right. \\ &\left. - \frac{\xi^2}{\Delta} \right] + 2\vartheta (KAx + KBv + KB_u u) \xi, \end{aligned} \quad (23)$$

where  $\tau, \varepsilon, \vartheta$  are some nonnegative parameters. From (17), (18), (20), (22) it follows that

$$\int_{t_n}^{t_{n+1}} G(x(t), u(t), v(t), \xi(t)) dt \geq 0 \quad (24)$$

for any solution of (5), (6), (7) and any  $n \geq 0$  (see also [11]).

Let us define a quadratic Lyapunov function  $V(x) = x^T Hx$ , where  $H$  is a symmetric matrix satisfying (14). Denote  $X = \text{col}\{x, u, v, \xi\}$ . Since

$$2x^T H(Ax + Bv + B_u u) + G(x, u, v, \xi) = X^T \Pi X, \quad (25)$$

linear matrix inequality (14) can be rewritten in terms of quadratic forms as

$$\begin{aligned} & 2x^T H(Ax + Bv + B_u u) + G(x, u, v, \xi) \\ & \leq -\varepsilon_0 (\|x\|^2 + u^2 + v^2 + \xi^2) \end{aligned} \quad (26)$$

for all vectors  $x$  and scalars  $u, v, \xi$ , where  $\varepsilon_0$  is some (sufficiently small) positive number and  $\|\cdot\|$  is the Euclidean vector norm. Along the solutions of (5), (6), (7) inequality (26) implies

$$\begin{aligned} & \dot{V}(x(t)) + G(x(t), u(t), v(t), \xi(t)) \\ & \leq -\varepsilon_0 (\|x(t)\|^2 + u(t)^2) \end{aligned} \quad (27)$$

for all  $t_n < t < t_{n+1}, n \geq 0$ . Notice the vector function  $x(t)$  is continuous in  $t$ ; hence  $V(x(t))$  is also continuous for all  $t \geq t_0$ . Integrating (27) and using (24) we get

$$\begin{aligned} V(x(t_n)) - V(x(t_0)) & \leq -\varepsilon_0 \int_{t_0}^{t_n} \|x(s)\|^2 ds \\ & - \varepsilon_0 \sum_{k=0}^{n-1} T_k u_k^2 \end{aligned} \quad (28)$$

for all  $n \geq 1$ . Since  $H > 0$ , (28) implies

$$\int_{t_0}^{t_n} \|x(s)\|^2 ds + \sum_{k=0}^{n-1} T_k u_k^2 \leq \frac{1}{\varepsilon_0} V(x(t_0)). \quad (29)$$

From (29) and (4) it follows that

$$\int_{t_0}^{+\infty} \|x(s)\|^2 ds < +\infty, \quad (30)$$

$$\sum_{k=0}^{\infty} u_k^2 < +\infty$$

that implies  $u_n \rightarrow 0$  as  $n \rightarrow \infty$ .

Let us prove that  $x(t)$  is asymptotically zero. From (28) we get  $V(x(t_n)) \leq V(x(t_0))$  for  $n \geq 0$ . Since  $H > 0$ , we conclude that the sequence  $\|x(t_n)\|$  is bounded for  $n \geq 0$ . The sequence  $u_n$  vanishes as  $n \rightarrow \infty$ , thus it is bounded, and the function  $u(t)$  is also bounded for  $t \geq t_0$ . Introduce the matrix  $A_\mu = A + \mu BC$ . Then the first equation (5) can be rewritten as

$$\dot{x} = A_\mu x(t) + Bv_0(t) + B_u u(t) \quad (31)$$

where  $A_\mu = A + \mu BC$ ,  $v_0(t) = v(t) - \mu\sigma(t)$  and the function  $v_0(t)$  is bounded for  $t \geq t_0$ . Integrating (31), we get

$$x(t) = e^{A_\mu(t-t_n)} x(t_n) + \int_{t_n}^t e^{A_\mu(t-s)} (Bv_0(s) + B_u u(s)) ds \quad (32)$$

for  $t_n \leq t \leq t_{n+1}$ . Hence

$$\|x(t)\| \leq e^{\|A_\mu\|T} \|x(t_n)\| + T e^{\|A_\mu\|T} \sup_{t \geq t_0} \|Bv_0(t) + B_u u(t)\| \quad (33)$$

for  $t_n \leq t \leq t_{n+1}$ . Because  $\|x(t_n)\|$  is bounded, estimate (33) implies that  $\|x(t)\|$  is bounded for  $t \geq t_0$ . Thus the right-hand side of (31) is also bounded, and so the function  $\|x(t)\|^2$  is uniformly continuous. Applying Barbalat's lemma (see, e.g., [8]) we conclude that  $x(t) \rightarrow 0$  as  $t \rightarrow +\infty$ .

## 5. Some Remarks to Theorem 1

*Remark 2.* Let us multiply formulas (15) elementwise by  $T$  and change the variables

$$\begin{aligned} H_0 &= TH, \\ \tau_0 &= T\tau, \\ \varepsilon_0 &= T\varepsilon, \\ \vartheta_0 &= T\vartheta, \\ \gamma_0 &= T\gamma. \end{aligned} \quad (34)$$

Using the Schur complement [5] inequality (14) can be rewritten as

$$\tilde{\Pi} + TL_1^T L_1 + \frac{1}{\tau_0 \nu_1 \nu_2 + \gamma_0} L_2^T L_2 < 0 \quad (35)$$

with

$$\begin{aligned} L_1 &= \begin{bmatrix} A^T K^T \\ KB_u \\ KB \end{bmatrix}, \\ L_2 &= \begin{bmatrix} \tau_0 \nu_1 \nu_2 K^T + \vartheta_0 A^T K^T \\ -\frac{1}{2} \tau_0 (\nu_1 + \nu_2) + \vartheta_0 KB_u \\ \vartheta_0 KB \end{bmatrix}, \\ \tilde{\Pi} &= \begin{bmatrix} \tilde{\Pi}_{11} & \tilde{\Pi}_{12} & \tilde{\Pi}_{13} \\ * & \tilde{\Pi}_{22} & \tilde{\Pi}_{23} \\ * & * & \tilde{\Pi}_{33} \end{bmatrix}, \end{aligned} \quad (36)$$

where

$$\begin{aligned} \tilde{\Pi}_{11} &= H_0 A + A^T H_0 - \varepsilon_0 \mu_1 \mu_2 C^T C - \tau_0 \nu_1 \nu_2 K^T K, \\ \tilde{\Pi}_{12} &= H_0 B_u + \frac{1}{2} \tau_0 (\nu_1 + \nu_2) K^T, \\ \tilde{\Pi}_{13} &= H_0 B + \frac{1}{2} \varepsilon_0 (\mu_1 + \mu_2) C^T, \\ \tilde{\Pi}_{22} &= -\tau_0, \\ \tilde{\Pi}_{23} &= 0, \\ \tilde{\Pi}_{33} &= -\varepsilon_0. \end{aligned} \quad (37)$$

Assume that the sampling frequency is sufficiently high; i.e.

$$\begin{aligned} T &\rightarrow +0, \\ \gamma_0 &= \frac{\pi^2}{4T} \rightarrow +\infty. \end{aligned} \quad (38)$$

Then (35) can be reduced to  $\tilde{\Pi} < 0$ . The last inequality ensures the fulfillment of the circle criterion of absolute stability for a continuous-time system

$$\begin{aligned} \dot{x} &= Ax(t) + Bv(t) + B_u u(t), \\ v(t) &= \varphi(Cx(t)), \\ u(t) &= F(Kx(t)) \end{aligned} \quad (39)$$

with quadratic constraints (17) and

$$(\nu_2 Kx(t) - u(t))(u(t) - \mu_1 Kx(t)) \geq 0 \quad (40)$$

for all  $t$ .

*Remark 3.* Let the conditions of Theorem 1 be satisfied. As it was shown above, this implies inequality (26). Let us set  $v = \hat{\mu}Cx$ ,  $u = \hat{\nu}Kx$ ,  $\xi = 0$  in (26), where  $\hat{\mu}$ ,  $\hat{\nu}$  are some numbers such that

$$\begin{aligned} \mu_1 &\leq \hat{\mu} \leq \mu_2, \\ \nu_1 &\leq \hat{\nu} \leq \nu_2. \end{aligned} \quad (41)$$

Then from (26) we obtain  $HA_L + A_L^T H < 0$  with

$$A_L = A + \hat{\mu}BC + \hat{\nu}B_u K. \quad (42)$$

Since  $H > 0$ , we conclude that the matrix  $A_L$  defined by (42) is Hurwitz stable for any numbers  $\hat{\mu}$ ,  $\hat{\nu}$  satisfying (41). This gives necessary conditions for the fulfillment of Theorem 1.

*Remark 4.* Let us discuss a relation of Theorem 1 of this paper to Theorem 3.2 [38]. The difference of the problem setting in Theorem 3.2 with that considered in this paper is threefold. Firstly, Theorem 3.2 studies not zero asymptotic, but a stronger property of exponential stability. Secondly, Theorem 3.2 considers a more general case of multiple nonlinearities and a multirate control. Thirdly, Theorem 3.2

is formulated not as an LMI, but as a frequency-domain inequality. However, a reformulation of Theorem 1 to this more general case presents no problem. (Frequency-domain counterparts of the LMI problem given here can be found in Chapter 3 [20].) The more interesting is to compare integral estimates used in both works. The proof of Theorem 3.2 is based on an inequality from Lemma 1 [39] that can be written as

$$(\sigma_u(t) - \sigma_u(t - \tau(t)))^2 \leq T \int_{t-\tau(t)}^t \dot{\sigma}_u^2(s) ds, \quad (43)$$

where  $\tau(t) \leq T$ . The advantage of estimate (43) is that it is valid for any function  $\tau(t)$ ,  $0 \leq \tau(t) \leq T$ . However, for a special type of delay  $\tau(t) = t - t_n$ ,  $t_n \leq t < t_{n+1}$ , the estimate based on (43) can be refined. Integrating (43) with this special delay we obtain

$$\int_{t_n}^{t_{n+1}} (\sigma_u(s) - \sigma_u(t_n))^2 \leq T^2 \int_{t_n}^{t_{n+1}} \dot{\sigma}_u^2(s) ds. \quad (44)$$

Obviously, (44) is more conservative than the Wirtinger inequality (20) with the multiplier  $4T^2/\pi^2$  in the right-hand side.

## 6. Example: First-Order System

Consider a simplest first-order model

$$\dot{x}(t) = -F(x(t_n)), \quad t_n \leq t < t_{n+1}, \quad (45)$$

where  $x(t)$  is a scalar function and the nonlinearity  $F(\cdot)$  satisfies the sectoral bounds (8) with some scalars  $\nu_1, \nu_2, 0 < \nu_1 < \nu_2$ .

Let us apply Theorem 1. Equation (45) can be rewritten in the form (5) with  $A = 0, B = 0, C = 0, B_u = -1, K = 1$ . Let us take  $\vartheta = 0$ . Then inequality (14) takes the form

$$\begin{bmatrix} -\tau\nu_1\nu_2 & -H + \frac{1}{2}\tau(\nu_1 + \nu_2) & 0 & \tau\nu_1\nu_2 \\ * & 1 - \tau & 0 & -\frac{1}{2}\tau(\nu_1 + \nu_2) \\ 0 & 0 & -\varepsilon & 0 \\ * & * & 0 & -\tau\nu_1\nu_2 - \gamma \end{bmatrix} < 0, \quad (46)$$

where the asterisks stand for the symmetric entries with respect to the main diagonal. Take any positive number for  $\varepsilon$  and

$$\begin{aligned} H &= \nu_2, \\ \tau &= \frac{2\nu_2}{\nu_2 - \nu_1}. \end{aligned} \quad (47)$$

Then  $H - (1/2)\tau(\nu_1 + \nu_2) = -\tau\nu_1$ , and inequality (46) is reduced to

$$\begin{bmatrix} \nu_1\nu_2 & -\nu_1 & -\nu_1\nu_2 \\ * & 1 - \alpha & \frac{1}{2}(\nu_1 + \nu_2) \\ * & * & \nu_1\nu_2 + \gamma\alpha \end{bmatrix} > 0, \quad (48)$$

where  $\alpha = 1/\tau$ . By applying Sylvester's criterion we conclude that (48) is satisfied provided that  $\gamma > \nu_2^2$ . The latter inequality can be rewritten as

$$T < \frac{\pi}{2\nu_2} \approx \frac{1.57}{\nu_2}. \quad (49)$$

Let us estimate the conservatism of estimate (49). Introduce notation  $x_n = x(t_n)$ . Integrating (45) we come to a discrete-time map

$$x_{n+1} = \left(1 - \frac{F(x_n)}{x_n} T_n\right) x_n. \quad (50)$$

Map (50) is contracting if

$$\left|1 - \frac{F(x_n)}{x_n} T_n\right| < 1 \quad (51)$$

that is guaranteed if  $T < 2/\nu_2$ .

The case when the function  $F(\cdot)$  is linear was considered previously in [29, 30]. Assume  $F(x) = x$ , then we can apply Theorem 1 with  $\nu_2 = 1, \nu_1 \rightarrow 1 - 0$ , then we come to the estimate  $T < \pi/2$ . This inequality is consistent with the result obtained in [30] (with the help of IQCs), but Proposition 1 of [29] gives the more accurate estimate  $T < 1.99$  (with the help of Lyapunov–Krasovskii functionals).

Notice that unlike the linear case, the model considered in Theorem 1 is much more general. Observe also that from the practical standpoint the systems' stability is not the only issue that should be taken into account. If a sampling frequency is close to the boundary of the stability region, the decay rate of solutions may decrease dramatically. On the other hand, (50) reduces to

$$x_{n+1} = (1 - T_n) x_n \quad (52)$$

for the linear system considered. Thus if the sampling period is chosen  $T_n = 1$ , the zero equilibrium is attained in one iteration.

## 7. Numerical Example: Mathematical Pendulum

Following [34], consider an equation of a computer controlled pendulum

$$\ddot{\theta}(t) = -\frac{g}{l} \sin \theta(t) + \frac{1}{ml^2} u(t), \quad (53)$$

$$u(t) = F(k_1\theta(t_n) + k_2\dot{\theta}(t_n)), \quad t_n \leq t < t_{n+1},$$

for  $n \geq 0$ . Let the sampling times satisfy the bound  $|t_{n+1} - t_n| \leq T, n \geq 0$ . The parameters of (53) are  $g = 9.8 \text{ m/s}^2, l = 1 \text{ m}, m = 2 \text{ kg}$ . The function  $\varphi(\sigma) = \sin \sigma$  is bounded and satisfies a sectoral constraint (2) with  $\mu_1 = -0.2173, \mu_2 = 1$  (see [34]). Assume that the function  $F(\cdot)$  obeys (8) with  $\nu_1 = 0.95, \nu_2 = 1.05$  (i.e., its slope can deviate as  $1 \pm 5\%$ ).

Define  $x_1 = \theta, x_2 = \dot{\theta}$ . Then we have

$$\begin{aligned} A &= \begin{bmatrix} 0 & 1 \\ 0 & 0 \end{bmatrix}, \\ B &= \begin{bmatrix} 0 \\ -b_1 \end{bmatrix}, \\ B_u &= \begin{bmatrix} 0 \\ b_2 \end{bmatrix}, \\ C &= [1 \ 0], \\ K &= [k_1 \ k_2], \end{aligned} \tag{54}$$

where  $b_1 = g/l, b_2 = 1/(ml^2)$ . With the help of Remark 3 let us obtain upper bounds for feasible values of feedback gains  $k_1, k_2$ . Suppose that numbers  $\hat{\mu}, \hat{\nu}$  satisfy (41). Then the matrix  $A_L$  defined by (42) must be Hurwitz stable. Since

$$A_L = \begin{bmatrix} 0 & 1 \\ -\hat{\mu}b_1 + \hat{\nu}b_2k_1 & \hat{\nu}b_2k_2 \end{bmatrix}. \tag{55}$$

The conditions for Hurwitz stability of the matrix  $A_L$  are

$$\begin{aligned} k_1 &< \mu_1 \frac{gml}{\nu_2} \approx -4.056, \\ k_2 &< 0. \end{aligned} \tag{56}$$

Let us apply MATLAB software with YALMIP package for interface and SeDuMi solver for semidefinite programming [45, 46]. Feasible values of  $k_1, k_2$  were found by a manual search within region (56), then  $k_1, k_2$  were fixed while  $\gamma$  was minimized. It was discovered that the conditions of Theorem 1 are fulfilled for

$$\begin{aligned} T &= 0.2336, \\ k_1 &= -23.6, \\ k_2 &= -11.4 \end{aligned} \tag{57}$$

with

$$\begin{aligned} H &= \begin{bmatrix} 12731 & 2034 \\ 2034 & 554 \end{bmatrix}, \\ \varepsilon &= 78496, \\ \tau &= 1002.7, \\ \vartheta &= 0, \\ \gamma &= 45.1981. \end{aligned} \tag{58}$$

Thus the lower bound for the sampling frequency is  $1/T = 4.28$  Hz.

Let us compare the above result with Example 4.1 of [34], where the linear discrete-time control of (53) was treated (in our notation  $F(\sigma_u) = \sigma_u$ , so  $\nu_1 = \nu_2 = 1$ ). We are primarily

interested in the case of a nonuniform sampling which was considered in Theorem 1 [34]. From that theorem it was found that the pendulum system is stable with  $T = 0.191$  and  $k_1 = -23.6, k_2 = -6$ . It is seen that even for this special case the lower bound for the sampling frequency provided in [34] is  $1/T = 5.23$  Hz, which is greater than ours. However, for the case of a periodic sampling and a linear discrete-time control the estimate given in [34] is better than ours:  $1/0.302 = 3.31$  Hz. Notice that the simulation for the case of a periodic sampling and a linear discrete-time control gave the minimal sampling rate  $1/0.432 = 2.31$  Hz (see Table 1 [34]).

## 8. Conclusion

The paper discusses an application of the absolute stability theory to a sampled-data stabilization of a nonlinear Lur'e-type system. The design of the stabilizing feedback is reduced to optimization problem for some system of matrix inequalities. The mathematical considerations are based on the Gel'g-Yakubovich approach to the stability of sampled-data systems, including S-procedure and specific integral-quadratic constraints. When the sampling frequency is sufficiently high, the main statement of this paper reduces to the circle criterion of absolute stability with two nonlinearities. Illustrative examples demonstrate sufficiently good agreement with the previously known results on linear sampled-data control.

## Data Availability

All data generated or analysed during this study are included in the present article.

## Conflicts of Interest

The author declares that there are no conflicts of interest regarding the publication of this paper.

## Acknowledgments

Alexander N. Churilov was supported by the Russian Foundation for Basic Research, Grant 17-01-00102-a.

## References

- [1] A. I. Lur'e, *Some Non-linear Problems in the Theory of Automatic Control*, H. M. Stationery Office, London, 1957.
- [2] V. A. Yakubovich, G. A. Leonov, and A. Kh. Gel'g, *Stability of Stationary Sets in Control Systems with Discontinuous Nonlinearities*, vol. 14 of *Series on Stability, Vibration and Control of Systems. Series A: Textbooks, Monographs and Treatises*, World Scientific Publishing Co., Inc., River Edge, NJ, 2004.
- [3] M. R. Liberzon, "Essays on the absolute stability theory," *Automation and Remote Control*, vol. 67, no. 10, pp. 1610–1644, 2006.
- [4] V. A. Yakubovich, "The solution of certain matrix inequalities in automatic control theory," *Soviet Mathematics - Doklady*, vol. 3, no. 2, pp. 620–623, 1962.

- [5] S. Boyd, L. El Ghaoui, E. Feron, and V. Balakrishnan, *Linear Matrix Inequalities in System and Control Theory*, SIAM, Philadelphia, Pa, USA, 1994.
- [6] V. M. Popov, "Hyperstability and optimality of automatic systems with several control functions," *Revue roumain des sci. techn., sér. électrotechn. et énergét.*, vol. 9, no. 4, pp. 629–690, 1964.
- [7] V. A. Yakubovich, "Frequency domain conditions for absolute stability of control systems with several nonlinear or linear nonstationary blocks," *Automation and Remote Control*, no. 6, pp. 857–880, 1967.
- [8] V. M. Popov, *Hyperstability of Control Systems*, Springer, New York, NY, USA, 1973.
- [9] V. A. Yakubovich, "The S-procedure in nonlinear control theory," *Vestnik Leningrad University. Mathematics*, vol. 4, pp. 62–77, 1971.
- [10] A. L. Fradkov and V. A. Yakubovich, "The S-procedure and duality relations in nonconvex problems of quadratic programming," *Vestnik Leningrad University. Mathematics*, vol. 6, pp. 101–109, 1979.
- [11] V. A. Yakubovich, "On impulsive control systems with a pulse width modulation," *Doklady Akademii Nauk SSSR*, vol. 180, pp. 283–285, 1968 (Russian).
- [12] A. Megretski and A. Rantzer, "System analysis via integral quadratic constraints," *IEEE Transactions on Automatic Control*, vol. 42, no. 6, pp. 819–830, 1997.
- [13] A. Ch. Gelig, "Frequency criterion for nonlinear pulse systems stability," *Systems & Control Letters*, vol. 1, no. 6, pp. 409–412, 1981/82.
- [14] A. N. Churilov, "A frequency criterion for stability of nonlinear impulse systems," *Automation and Remote Control*, vol. 52, no. 6, pp. 824–833, 1991.
- [15] A. Kh. Gelig and A. N. Churilov, *Oscillations and Stability of Nonlinear Impulsive Systems*, St. Petersburg State Univ., St. Petersburg, 1993 (Russian).
- [16] G. H. Hardy, J. E. Littlewood, and G. Pólya, *Inequalities*, Cambridge University Press, 1934.
- [17] A. Kh. Gelig and A. N. Churilov, "Popov-type stability criterion for the functional-differential equations describing pulse modulated control systems," in *Functional-Differential Equations*, vol. 1 of *Funct. Differential Equations Israel Sem.*, pp. 95–107, Coll. Judea Samaria, Ariel, 1993.
- [18] A. Kh. Gelig and A. N. Churilov, "Frequency-domain criteria for absolute stability of nonlinear systems with various types of pulse modulation," in *Proceedings of the the third European Control Conference ECC 95*, vol. 58, pp. 2251–2255, Roma, Italy, 1995.
- [19] A. Kh. Gelig and A. N. Churilov, "Stability and oscillations in pulse-modulated systems: a review of mathematical approaches," *Functional Differential Equations*, vol. 3, no. 3–4, pp. 287–320 (1997), 1996.
- [20] A. Kh. Gelig and A. N. Churilov, *Stability and Oscillations of Nonlinear Pulse-Modulated Systems*, Birkhäuser Boston, Inc., Boston, MA, 1998.
- [21] A. N. Churilov, "Stabilization of a linear system by means of a combined pulse modulation," in *Proceedings of the In 6th Saint Petersburg Symposium on Adaptive Systems Theory*, vol. 1, pp. 47–50, St.Petersburg, 1999.
- [22] A. N. Churilov, "Stabilization of a linear system by combined impulse modulation," *Automation and Remote Control*, vol. 61, no. 10, pp. 1650–1654, 2000.
- [23] A. Churilov and A. Gessen, "LMI technique for stabilization of a linear plant by a pulse-modulated signal," in *Proceedings of the 2003 International Conference Physics and Control.*, pp. 1267–1272, Saint Petersburg, Russia.
- [24] A. N. Churilov, "Local stabilization of a linear plant by a pulse signal," *Vestnik St. Petersburg University. Mathematics*, vol. 36, no. 1, pp. 44–49 (2004), 2003.
- [25] A. N. Churilov and A. V. Gessen, "LMI approach to stabilization of a linear plant by a pulse modulated signal," *International Journal of Hybrid Systems*, vol. 3, no. 4, pp. 375–388, 2003.
- [26] A. Kh. Gelig and A. N. Churilov, "Frequency methods in the theory of stability of pulse-modulated control systems," *Automation and Remote Control*, vol. 67, no. 11, pp. 1752–1765, 2006.
- [27] L. Hetel, C. Fiter, H. Omran et al., "Recent developments on the stability of systems with aperiodic sampling: an overview," *Automatica*, vol. 76, pp. 309–335, 2017.
- [28] E. Fridman, A. Seuret, and J. Richard, "Robust sampled-data stabilization of linear systems: an input delay approach," *Automatica*, vol. 40, no. 8, pp. 1441–1446, 2004.
- [29] E. Fridman, "A refined input delay approach to sampled-data control," *Automatica*, vol. 46, no. 2, pp. 421–427, 2010.
- [30] L. Mirkin, "Some remarks on the use of time-varying delay to model sample-and-hold circuits," *IEEE Transactions on Automatic Control*, vol. 52, no. 6, pp. 1109–1112, 2007.
- [31] H. Fujioka, "Stability analysis of systems with aperiodic sample-and-hold devices," *Automatica*, vol. 45, no. 3, pp. 771–775, 2009.
- [32] C.-Y. Kao and D.-R. Wu, "On robust stability of aperiodic sampled-data systems—An Integral Quadratic Constraint approach," in *Proceeding of American Control Conference*, pp. 4871–4876, Portland, Oregon, USA, 2014.
- [33] C.-Y. Kao, "An IQC approach to robust stability of aperiodic sampled-data systems," *IEEE Transactions on Automatic Control*, vol. 61, no. 8, pp. 2219–2225, 2016.
- [34] R. E. Seifullaev and A. L. Fradkov, "Sampled-data control of nonlinear oscillations based on Fridman's analysis and passification design," *IFAC Proceedings Volumes*, vol. 46, no. 12, pp. 95–100, 2013.
- [35] R. E. Seifullaev and A. L. Fradkov, "Linear matrix inequality-based analysis of the discrete-continuous nonlinear multivariable systems," *Automation and Remote Control*, vol. 76, no. 6, pp. 989–1004, 2015.
- [36] R. E. Seifullaev and A. L. Fradkov, "Robust nonlinear sampled-data system analysis based on Fridman's method and S-procedure," *International Journal of Robust and Nonlinear Control*, vol. 26, no. 2, pp. 201–217, 2016.
- [37] R. E. Seifullaev and A. L. Fradkov, "Sampled-data control of nonlinear systems based on Fridman's analysis and passification Design," *IFAC-PapersOnLine*, vol. 48, no. 11, pp. 685–690, 2015.
- [38] T. A. Bryntseva and F. L. Fradkov, "Frequency-domain estimates of the sampling interval in multirate nonlinear systems by time-delay approach," *International Journal of Control*, 2018.
- [39] M. Yu. Churilova, "An analogue of the circular criterion of absolute stability for systems with variable delay," *Automation and Remote Control*, vol. 56, no. 2, pp. 195–198, 1995.
- [40] G. Zames, "On the input-output stability of time-varying nonlinear systems—Part II. Conditions involving circles on the frequency plane and sector nonlinearities," *IEEE Transactions on Automatic Control*, vol. 11, no. 3, pp. 465–476, 1966.
- [41] H. K. Khalil, *Nonlinear Systems*, Prentice-Hall, Upper Saddle River, 3rd edition, 2002.

- [42] V. M. Kuntsevich and Yu. N. Chekhovoi, "Fundamentals of nonlinear control systems with pulse-frequency and pulse-width modulation," *Automatica*, vol. 7, no. 1, pp. 73–81, 1971.
- [43] J. Mazo, A. Anta, and P. Tabuada, "An ISS self-triggered implementation of linear controllers," *Automatica*, vol. 46, no. 8, pp. 1310–1314, 2010.
- [44] U. Tiberi and K. H. Johansson, "A simple self-triggered sampler for perturbed nonlinear systems," *Nonlinear Analysis: Hybrid Systems*, vol. 10, pp. 126–140, 2013.
- [45] J. Löfberg, "YALMIP: a toolbox for modeling and optimization in MATLAB," in *Proceedings of the IEEE International Symposium on Computer Aided Control System Design (CACSD '04)*, pp. 284–289, IEEE, Taipei, Taiwan, September 2004.
- [46] J. F. Sturm, "Using SeDuMi 1.02, a Matlab toolbox for optimization over symmetric cones," *Optimization Methods and Software*, vol. 11, no. 1–4, pp. 625–653, 1999.

## Research Article

# Further Results on Sampled-Data Synchronization for Complex Dynamical Networks with Time-Varying Coupling Delay

Hea-Min Lee <sup>1</sup>, Wookyong Kwon <sup>1</sup>, Sangmoon Lee <sup>2</sup>, and Dongyeop Kang <sup>1</sup>

<sup>1</sup>Smart Vehicles Laboratory, Electronics and Telecommunications Research Institute, Daegu 42994, Republic of Korea

<sup>2</sup>School of Electronics Engineering, Kyungpook National University, Daegu 41566, Republic of Korea

Correspondence should be addressed to Sangmoon Lee; [moony@knu.ac.kr](mailto:moony@knu.ac.kr)

Received 5 September 2018; Revised 7 November 2018; Accepted 12 November 2018; Published 26 November 2018

Guest Editor: Hiroaki Mukaidani

Copyright © 2018 Hea-Min Lee et al. This is an open access article distributed under the Creative Commons Attribution License, which permits unrestricted use, distribution, and reproduction in any medium, provided the original work is properly cited.

This paper deals with the sampled-data synchronization problem for complex dynamical networks (CDNs) with time-varying coupling delay. To get improved results, two-sided free-weighting stabilization method is utilized with a novel looped functional taking the information of the present sampled states and next sampled states, which can more precisely account for the sawtooth shape of the sampling delay. Also, the quadratic generalized free-weighting matrix inequality (QGFWMI), which provides additional degree of freedom (DoF), is utilized to calculate the upper limit of the integral term. Based on the novel looped functional and QGFWMI, improved conditions of stability are derived from forms of linear matrix inequalities (LMIs). The numerical examples show the validity and effectiveness.

## 1. Introduction

Complex dynamical networks (CDNs) are an attempt to model a set of interconnected dynamic properties of nodes with specific contents. For example, there are human interaction networks, ad hoc networks, secure communications, harmonic oscillations, biological systems, and chaotic systems, financial systems, social networks, and neural networks. CDNs are faced with the problems of expressing structural complexity and connection diversity at the same time. Furthermore, the dynamic characteristics of the network make it difficult to provide a solution to the real world because modeling should be done with the node's insufficient information from the network. Nevertheless, CDNs have attracted lots of attention in various fields of engineering [1–4]. Especially, the problem of synchronization has been focused by many researchers [5–7], as the synchronization of CDNs is a fundamental phenomenon. In nature, complex networks in the synchronization encounter time delay in biological and physical networks, because of the limited speed of network transmission, traffic jams, and signal propagation. The time delay is a source of degradation synchronization performance and instability, and thus complex networks with time-varying delay are of importance and generality [8, 9].

The design of control has been developed including pinning control [10], impulsive control [11], hybrid control [12], fuzzy adaptive output feedback control [13], and sampled-data control [5] to accomplish stable synchronization. Among these methods, sampled-data control for the synchronization of CDNs has been studied extensively with the development of digital communication since sampled-data offers many benefits in modern control systems. The advantages of sampled-data control are as follows: Firstly, the sampled-data control is more realistic than continuous control in that it can be implemented in practical systems. Secondly, in the case of the signal in the form of pulse data, the information is supplied immediately with a small outlay. Lastly, the control system for better performance is generally achieved by a sampled-data control. For continuous systems, the differentiator not only improves the existing noise but also generate additional noise. In the sampled-data system, the differential operation can be implemented without increasing noise problem. For that reason, sampled-data control was used because of these benefits: practicality, immediacy, economics, and accuracy. In sampled-data control systems, it is the main issue to design controllers that can get larger sampling interval. Increasing maximum sampling interval is very important because it not only enlarges the stable region

but also improves performance when considered with other aspects:  $H_\infty$  [14] and dissipativity [15].

Several criteria for CDNs with time delay are developed to derive stability conditions on sampled-data intervals. Sampled-data signals which are discontinuous at every sampling time can be treated as continuous time-varying delayed signals. In [5], the problem of sampled-data synchronization control for a class of general complex networks with time-varying coupling delay is firstly handled using Jensen's inequality found in the input delay approach. The time-dependent Lyapunov functional and convex combination techniques are used in [16] to derive a less conservative condition for the sampled-data synchronization. The synchronization in memory neural networks with time-varying delays was studied in [2, 17, 18]. In [17], a sampled-data feedback controller was proposed by using the Lyapunov function theory and Jensen's inequality method to guarantee the synchronization of memristive Bidirectional Associative Memory (BAM) neural networks with leakage and two additive time-varying delays. The authors in [18] obtained less conservative results by constructing a Lyapunov function and using the stochastic differential inclusions and some inequality techniques. Recently, Wirtinger's inequality is used in [19, 20]. Also, the augmented Lyapunov function approach and Lyapunov function with triple integral have been reported in the literature [15, 21, 22]. In [23], a looped-functional-based approach was proposed for the stability analysis of linear impulsive systems. This approach easily formulates sampling interval result for discrete time stability using a continuous time's approach. In [24], a new looped-functional for stability analysis was proposed. This functional entirely uses the information on both interval  $t_k$  and  $t_{k+1}$ , which improved stability condition. However, there are still more rooms for improvement, which motivates our research. To consider the information of sampling time at  $t_k$  and  $t_{k+1}$ , the modified looped-functional is proposed by using the augmented vector for two-sided sampling time.

In this paper, enhanced results on sampled-data synchronization criteria and controller design are given for the complex dynamical networks with time-varying coupling delay. The stability and stabilization criteria are presented in forms of linear matrix inequalities (LMIs). The superiority of the proposed scheme is shown through numerical examples. The main contribution of this note is summarized as follows:

- (i) Free-weighting matrices at time sequence  $t_k$  and  $t_{k+1}$  are separately employed with an additional scalar parameter in consideration of system dynamics in CDN satisfying convexity.
- (ii) In order to fully consider the information of sawtooth shape sampling pattern at  $t_k$  and  $t_{k+1}$ , novel looped functional is employed with augmented vectors which become zero by constructing the vector crossly aligned at each sampling time  $t_k$  or  $t_{k+1}$ . Namely, the dimension of the LMI variable extends from  $R^{2 \times 2}$  ( $2 \times 2$  dimensional Euclidean space) to  $R^{4 \times 4}$ . Therefore, augmented vectors provide an increased degrees of freedom (DoF) and improved results.

- (iii) QGFMI is firstly applied to sampled-data synchronization. QGFMI estimates the upper limit of the integral term more tightly. Thus it contributes to deriving a less conservative result.

## 2. Preliminaries

CDNs composed of  $N$  identical coupled nodes with  $n$ -dimensional dynamics are described as follows:

$$\begin{aligned} \dot{x}_i(t) = & f(x_i(t)) + c \sum_{j=1}^N G_{ij} D x_j(t) \\ & + c \sum_{j=1}^N G_{ij} A x_j(t - \tau(t)) + u_i(t), \end{aligned} \quad (1)$$

*for*  $i = 1, 2, \dots, N$

where  $f(\cdot)$  is the continuous vector-valued nonlinear function,  $G_{ij}$  is the outer coupling matrix from node  $i$  to  $j$  with weight,  $A$  and  $D$  are the inner coupling matrix,  $x_i(t)$  is the state variable of node  $i$ ,  $u_i(t)$  is input variable  $e$  of node  $i$ , and  $c > 0$  is the coupling strength.  $G_{ij}$  is defined as follows:

$$\begin{aligned} G_{ij} &> 0 \\ &\text{if there is connection between node } i \text{ and } j \\ G_{ij} &= 0 \\ &\text{if there is no connection between node } i \text{ and } j \end{aligned} \quad (2)$$

The diagonal elements of  $G_{ij}$  are denoted as  $G_{ij} = -\sum_{i=1, j=i}^N G_{ij}$  for  $i = 1, 2, \dots, N$ . The bounded time-varying delay  $\tau(t)$  satisfies

$$\begin{aligned} 0 &\leq \tau(t) \leq \tau_M, \\ -\mu &\leq \dot{\tau}(t) \leq \mu, \end{aligned} \quad (3)$$

where  $\tau_M$  and  $\mu$  are positive known constants. Without loss of generality, the nonlinear function  $f(\cdot)$  is assumed to satisfy a sector-bounded condition as

$$\begin{aligned} [f(x) - f(y) - W_1(x - y)]^T \\ \cdot [f(x) - f(y) - W_2(x - y)] \leq 0, \end{aligned} \quad (4)$$

where  $W_1$  and  $W_2$  are matrices with appropriate dimensions. Let  $r(t)$  be an unforced isolated node,  $\dot{r}(t) = f(r(t))$ , then the error dynamics of each dynamical system is derived as

$$\begin{aligned} \dot{e}_i(t) = & g(e_i(t), r(t)) + c \sum_{j=1}^N G_{ij} D x_j(t) \\ & + c \sum_{j=1}^N G_{ij} A x_j(t - \tau(t)) + u_i(t), \end{aligned} \quad (5)$$

*for*  $i = 1, 2, \dots, N$ ,

where  $e_i(t) = x_i - r(t)$  and  $g(e_i(t), r(t)) = f(x_i(t)) - f(r(t))$ . Utilizing Kronecker product, the whole CDN is represented as

$$\begin{aligned} \dot{e}_i(t) = & \widehat{g}(e(t), r(t)) + c(G \otimes D)e(t) \\ & + c(G \otimes A)e(t - \tau(t)) + u(t) \end{aligned} \quad (6)$$

where

$$\begin{aligned} e(t) &= \begin{bmatrix} e_1(t) \\ e_2(t) \\ \dots \\ e_N(t) \end{bmatrix}, \\ e(t - \tau(t)) &= \begin{bmatrix} e_1(t - \tau(t)) \\ e_2(t - \tau(t)) \\ \dots \\ e_N(t - \tau(t)) \end{bmatrix}, \\ \widehat{g}(e(t), r(t)) &= \begin{bmatrix} g(e_1(t), r(t)) \\ g(e_2(t), r(t)) \\ \dots \\ g(e_N(t), r(t)) \end{bmatrix}, \\ u(t) &= \begin{bmatrix} u_1(t) \\ u_2(t) \\ \dots \\ u_N(t) \end{bmatrix}. \end{aligned} \quad (7)$$

For the given system, our objective is to design a sampled-data controller which makes the error systems converge to zero. When considering that the measurement sensor generates a signal, discretized sampled signals are only sent to the controller through the network in system topology, and

the control input can be utilized using zero order function. The control input signals using sampler are generated with a sequence of hold time  $0 = t_0 < t_1 < \dots < t_k < \dots$  where  $\lim_{k \rightarrow \infty} t_k = \infty$  and  $k$  is a positive integer. The sampling intervals are represented as

$$t_{k+1} - t_k \leq h_k \leq h_M \quad (8)$$

where  $h_M$  is the maximum sampling instant. Then, the sampled-data controller is designed as

$$u(t) = u(t_k) = K(e(t_k)), \quad \text{for } t_k \leq t \leq t_{k+1}. \quad (9)$$

where  $k = \text{diag}\{K_1, K_2, \dots, K_N\}$  is the control gain matrix and  $e(t_k)$  is the sampled error signal. The closed-loop error systems with sampled-data control are rewritten as

$$\begin{aligned} \dot{e}_i(t) = & \widehat{g}(e(t), r(t)) + c(G \otimes D)e(t) \\ & + c(G \otimes A)e(t - \tau(t)) + Ku(t_k) \end{aligned} \quad (10)$$

To develop main results, useful lemmas are introduced.

**Lemma 1** (Wirtinger's inequalities; [25]). *For given a matrix  $R > 0$  and a continuous differentiable function  $\omega(t)$  in  $[a, b]$ , the following inequality holds:*

$$\int_a^b \omega^T(s) R \omega(s) ds \geq \frac{1}{b-a} \eta_1^T R \eta_1 + \frac{3}{b-a} \eta_2^T R \eta_2 \quad (11)$$

where  $\eta_1 = \int_a^b \omega(s) ds$  and  $\eta_2 = \int_a^b \omega(s) ds - (2/(b-a)) \int_a^b \int_s^b \omega(u) du ds$ .

**Lemma 2** (reciprocally convex combination method; [26]). *For a given scalar  $0 < \theta < 1$ , vectors  $\omega_1, \omega_2$ , and matrices  $M > 0, N$  satisfying  $\begin{bmatrix} M & N \\ N & M \end{bmatrix} > 0$ , then the following holds:*

$$\frac{1}{\theta} \omega_1^T M \omega_1 + \frac{1}{1-\theta} \omega_2^T M \omega_2 \leq \begin{bmatrix} \omega_1 \\ \omega_2 \end{bmatrix}^T \begin{bmatrix} M & N \\ N & M \end{bmatrix} \begin{bmatrix} \omega_1 \\ \omega_2 \end{bmatrix}. \quad (12)$$

**Lemma 3** (QGFMI). *Given matrices  $X, Y$  and positive semi-definite matrix  $R$ , the inequality is given by*

$$\int_a^b \omega^T(s) R \omega(s) ds \geq - \begin{bmatrix} \eta_0 \\ \eta_3 \end{bmatrix}^T \begin{bmatrix} (b-a) X R^{-1} X^T & X [I \ 0] \\ * & \frac{(b-a)}{3} Y R^{-1} Y^T + \text{sym}(Y [-I \ 2I]) \end{bmatrix} \begin{bmatrix} \eta_0 \\ \eta_3 \end{bmatrix} \quad (13)$$

where  $\eta_0$  is any vector and  $\eta_3 = [\int_a^b \omega^T(s) ds, (1/(b-a)) \int_a^b \int_s^b \omega(u)^T du ds]^T$ , and  $\omega(t)$  is a differentiable function which is a continuous on  $[a, b]$ .

*Proof.* The proof of Lemma 3 is omitted as it is similar to that of [27].  $\square$

**Remark 4.** The QGFMI is used to calculate the upper limit of integral term in the derivative of Lyapunov-Krasovskii function, which increases freedom to choose a free-selectable vector [27]. Furthermore, the new free-weighting matrix plays a vital role in filling in the diagonal element and corresponding augmented vector provides additional flexibility.

*Remark 5.* The control technique using the sample value data in (9) can be applied to systems such as event-triggered communication as in [28, 29].

### 3. Main Results

The matrices  $I_i = R^{11n \times n}$  for  $i = 1, 2, \dots, 11$  are denoted to represent matrices composed of  $(n - 1)$  zero elements matrices with  $i_{th}$  identity matrix. For example,  $I_1 = [I \ 0 \ 0 \ 0 \ 0 \ 0 \ 0 \ 0 \ 0 \ 0 \ 0]^T$  and  $I_5 = [0 \ 0 \ 0 \ 0 \ I \ 0 \ 0 \ 0 \ 0 \ 0 \ 0]^T$ . Moreover, the following are declared:

$$\begin{aligned} \zeta(t) = & \left[ e(t), \dot{e}(t), e(t_k), \frac{1}{(t-t_k)} \right. \\ & \cdot \int_{t_k}^t e^T(\alpha) d\alpha, e(t_{k+1}), \frac{1}{(t_{k+1}-t)} \\ & \cdot \int_t^{t_{k+1}} e^T(\alpha) d\alpha, e(t-\tau(t)), e(t-\tau_M), \frac{1}{\tau(t)} \\ & \cdot \int_{t-\tau(t)}^t e^T(\alpha) d\alpha, \frac{1}{(\tau_M-\tau(t))} \\ & \left. \cdot \int_{t-\tau_M}^{t-\tau(t)} e^T(\alpha) d\alpha, \widehat{g}^T(e(t), s(t)) \right], \\ \kappa_1 = & [I_1, I_3 + I_5, I_4 + I_6, I_2], \\ \kappa_2 = & [I_1 - I_3, I_1 - I_4], \\ \kappa_3 = & [I_5 - I_1, I_5 - I_6], \\ \kappa_4 = & [I_1 - I_7, I_1 + I_7 - I_9, I_7 - I_8, I_7 + I_8 - I_{10}], \\ \eta_1 = & [I_1 - I_3, (t-t_k)I_5, (t-t_k)I_3, (t-t_k)I_4], \\ \eta_2 = & [I_5 - I_1, (t_{k+1}-t)I_3, (t_{k+1}-t)I_5, (t_{k+1}-t)I_6], \\ \eta_{1d} = & [I_2, I_5, I_3, I_1], \\ \eta_{2d} = & [-I_2, -I_3, -I_5, -I_1], \end{aligned} \quad (14)$$

$$S_1(t) = \begin{bmatrix} (t-t_k)S_{10} - (t_{k+1}-t)S_{11} & S_{12} \\ S_{12}^T & S_{13} \end{bmatrix} \in R^{4n \times 4n},$$

$$S_{10} \in R^{n \times n},$$

$$S_{11} \in R^{n \times n},$$

$$S_{12} \in R^{n \times 3n},$$

$$S_{13} \in R^{3n \times 3n},$$

$$S_{1d} = \begin{bmatrix} S_{10} - S_{11} & 0_{n \times n} \\ 0_{n \times n} & 0_{n \times n} \end{bmatrix},$$

$$\widehat{R} = \begin{bmatrix} R & 0 \\ 0 & R \end{bmatrix}.$$

**Theorem 6.** For a given scalar parameter  $h_M$  and a gain matrix  $K$ , if there exist a positive scalar  $\delta$ , symmetric matrices  $P > 0$ ,  $Q_1 > 0$ ,  $Q_2 > 0$ ,  $R > 0$ ,  $T_1 > 0$ , and  $T_2 > 0$ , any matrices  $G_1, G_2, G_3, G_4, S_1(t), S_2, X_1, X_2, Y_1, Y_2$ , and  $\widehat{M}$ , and a scalar  $\delta > 0$  satisfying the inequalities

$$\begin{bmatrix} \Pi_{1,h(t)=0} & \kappa_1 X_2 & \kappa_3 Y_2 \\ * & -h_M T_2 & 0 \\ * & 0 & -3h_M T_2 \end{bmatrix} \leq 0 \quad (15)$$

$$\begin{bmatrix} \Pi_{1,h(t)=h} & \kappa_1 X_1 & \kappa_2 Y_1 \\ * & -h_M T_1 & 0 \\ * & 0 & -3h_M T_1 \end{bmatrix} \leq 0 \quad (16)$$

$$\begin{bmatrix} \widehat{R} & \widehat{M} \\ \widehat{M} & \widehat{R} \end{bmatrix} \geq 0 \quad (17)$$

where

$$\begin{aligned} \Pi_{1,h(t)} = & \text{sym} \{I_1 P I_2^T\} + I_1 Q_1 I_1^T - (1-\mu) I_7 Q_1 I_7^T \\ & + I_1 Q_2 I_1^T - I_8 Q_2 I_8^T + \tau_M I_2 R I_2^T - \kappa_4 \begin{bmatrix} \widehat{R} & \widehat{M} \\ \widehat{M} & \widehat{R} \end{bmatrix} \kappa_4^T \\ & + \text{sym} \{ \eta_1 S_1(t) \eta_{2d}^T + \eta_{1d} S_1(t) \eta_2^T + \eta_1 S_{1d} \eta_{2d}^T \} \\ & + \text{sym} \left\{ [I_1 - I_3 \ (t-t_k) I_4] S_2 \begin{bmatrix} -I_2^T \\ -I_1^T \end{bmatrix} \right\} \\ & + [I_2 \ I_1] S_2 \begin{bmatrix} I_5^T - I_1^T \\ (t_{k+1}-t) I_6 \end{bmatrix} \left\} + (t_{k+1}-t) I_2 T_1 I_2^T \right. \\ & + (t-t_k) I_2 T_2 I_2^T + \text{sym} \{ \kappa_1 X_1 [I \ 0] \kappa_2^T \\ & + \kappa_2 Y_1 [-I \ 2I] \kappa_3^T \} + \text{sym} \{ \kappa_1 X_2 [I \ 0] \kappa_3^T \\ & + \kappa_1 Y_2 [-I \ 2I] \kappa_3^T \} - \delta [I_1 \ I_{11}] \begin{bmatrix} \widehat{W}_1 & \widehat{W}_2 \\ * & 2I \end{bmatrix} \begin{bmatrix} I_1^T \\ I_{11}^T \end{bmatrix} \\ & + (t-t_k) \text{sym} \{ (I_1 G_1 + I_2 G_2) \\ & \cdot (c(C \otimes D) I_1^T + c(C \otimes A) I_7^T + K I_3^T - I_2^T + I_{11}^T) \} \\ & + (t_{k+1}-t) \text{sym} \{ (I_1 G_3 + I_2 G_4) \\ & \cdot (c(C \otimes D) I_1^T + c(C \otimes A) I_7^T + K I_3^T - I_2^T + I_{11}^T) \} \end{aligned} \quad (18)$$

and  $\widehat{W}_1 = (I \otimes W_1 W_2) + (W_1 W_2 \otimes I)$ ,  $\widehat{W}_2 = -I \otimes (W_1^T + W_2^T)$ , then CDNs are asymptotically stable.

*Proof.* Construct the following Lyapunov-Krasovskii function for  $t \in [t_k, t_{k+1})$ :

$$\begin{aligned} V(x_t) = & V_1(t) + V_2(t) + V_3(t) + V_{11}(t) + V_{12}(t) \\ & + V_{13}(t) + V_{14}(t), \end{aligned} \quad (19)$$

where

$$\begin{aligned}
 V_1(t) &= e^T(t) P e(t), \\
 V_2(t) &= \int_{t-\tau(t)}^t e^T(\alpha) Q_1 e(\alpha) d\alpha + \int_{t-\tau_M}^t e^T(\alpha) Q_2 e(\alpha) d\alpha, \\
 V_3(t) &= \int_{t-\tau_M}^t \int_{\beta}^t \dot{e}^T(\alpha) R \dot{e}(\alpha) d\alpha d\beta, \\
 V_{11}(t) &= 2 \begin{bmatrix} e(t) - e(t_k) \\ (t - t_k) e(t_{k+1}) \\ (t - t_k) e(t_k) \\ \int_{t_k}^t e(\alpha) d\alpha \end{bmatrix}^T S_1 \begin{bmatrix} e(t_{k+1}) - e(t) \\ (t_{k+1} - t) e(t_k) \\ (t_{k+1} - t) e(t_{k+1}) \\ \int_t^{t_{k+1}} e(\alpha) d\alpha \end{bmatrix}, \\
 V_{12}(t) &= 2 \begin{bmatrix} e(t) - e(t_k) \\ \int_{t_k}^t e(\alpha) d\alpha \end{bmatrix}^T S_2 \begin{bmatrix} e(t_{k+1}) - e(t) \\ \int_t^{t_{k+1}} e(\alpha) d\alpha \end{bmatrix}, \\
 V_{13}(t) &= (t_{k+1} - t) \int_{t_k}^t \dot{e}^T(\alpha) T_1 \dot{e}(\alpha) d\alpha, \\
 V_{14}(t) &= -(t - t_k) \int_t^{t_{k+1}} \dot{e}^T(\alpha) T_2 \dot{e}(\alpha) d\alpha.
 \end{aligned} \tag{20}$$

Differentiating each LKF in equation (20) provides

$$\begin{aligned}
 \dot{V}(x_t) &= \dot{V}_1(t) + \dot{V}_2(t) + \dot{V}_3(t) + \dot{V}_{11}(t) + \dot{V}_{12}(t) \\
 &\quad + \dot{V}_{13}(t) + \dot{V}_{14}(t),
 \end{aligned} \tag{21}$$

where

$$\begin{aligned}
 \dot{V}_1(t) &= 2e(t) P \dot{e}(t) = \text{sym} \{I_1^T P I_2\}, \\
 \dot{V}_2(t) &= e^T(t) Q_1 e(t) - (1 - \mu) e^T(t - \tau(t)) Q_1 e(t - \tau(t)) + e^T(t) Q_2 e(t) - e^T(t - \tau_M) Q_2 e(t - \tau_M) \\
 &= I_1 Q_1 I_1^T - (1 - \mu) I_7 Q_1 I_7^T + I_1 Q_2 I_1^T - I_8 Q_2 I_8^T, \\
 \dot{V}_3(t) &= \tau_M \dot{e}^T(t) R \dot{e}(t) - \int_{t-\tau_M}^t \dot{e}^T(\alpha) R \dot{e}(\alpha) d\alpha \\
 &= \tau_M I_2 R I_2^T - \int_{t-\tau_M}^t \dot{e}^T(\alpha) R \dot{e}(\alpha) d\alpha, \\
 \dot{V}_{11}(t) &= 2 \begin{bmatrix} e(t) - e(t_k) \\ (t - t_k) e(t_{k+1}) \\ (t - t_k) e(t_k) \\ \int_{t_k}^t e(\alpha) d\alpha \end{bmatrix}^T S_1 \begin{bmatrix} -\dot{e}(t) \\ -e(t_k) \\ -e(t_{k+1}) \\ -e(t) \end{bmatrix}
 \end{aligned}$$

$$\begin{aligned}
 &+ 2 \begin{bmatrix} \dot{e}(t) \\ e(t_{k+1}) \\ e(t_k) \\ e(t) \end{bmatrix}^T S_1(t) \begin{bmatrix} e(t_{k+1}) - e(t) \\ (t_{k+1} - t) e(t_k) \\ (t_{k+1} - t) e(t_{k+1}) \\ \int_t^{t_{k+1}} e(\alpha) d\alpha \end{bmatrix} \\
 &+ 2 \begin{bmatrix} e(t) - e(t_k) \\ (t - t_k) e(t_{k+1}) \\ (t - t_k) e(t_k) \\ \int_{t_k}^t e(\alpha) d\alpha \end{bmatrix}^T \\
 &\cdot S_{1d} \begin{bmatrix} e(t_{k+1}) - e(t) \\ (t_{k+1} - t) e(t_k) \\ (t_{k+1} - t) e(t_{k+1}) \\ \int_t^{t_{k+1}} e(\alpha) d\alpha \end{bmatrix} = \text{sym} \{ \eta_1 S_1(t) \eta_{2d}^T \\
 &+ \eta_{1d} S_1(t) \eta_2^T + \eta_1 S_{1d} \eta_{2d}^T \}, \\
 \dot{V}_{12}(t) &= 2 \begin{bmatrix} e(t) - e(t_k) \\ \int_{t_k}^t e(\alpha) d\alpha \end{bmatrix}^T S_2 \begin{bmatrix} -\dot{e}(t) \\ -e(t) \end{bmatrix} + 2 \begin{bmatrix} \dot{e}(t) \\ e(t) \end{bmatrix}^T \\
 &\cdot S_2 \begin{bmatrix} e(t_{k+1}) - e(t) \\ \int_t^{t_{k+1}} e(\alpha) d\alpha \end{bmatrix} \\
 &= \text{sym} \left\{ [I_2 - I_3 \quad (t - t_k) I_4] S_2 \begin{bmatrix} -I_2^T \\ -I_1^T \end{bmatrix} \right. \\
 &\left. + [I_2 \quad I_1] S_2 \begin{bmatrix} I_5^T - I_1^T \\ (t_{k+1} - t) I_6^T \end{bmatrix} \right\}, \\
 \dot{V}_{13}(t) &= (t_{k+1} - t) \dot{e}^T(t) T_1 \dot{e}(t) - \int_{t_k}^t \dot{e}^T(\alpha) \\
 &\cdot T_1 \dot{e}(\alpha) d\alpha = (t_{k+1} - t) I_2 T_1 I_2^T - \int_{t_k}^t \dot{e}^T(\alpha) \\
 &\cdot T_1 \dot{e}(\alpha) d\alpha, \\
 \dot{V}_{14}(t) &= (t - t_k) \dot{e}^T(t) T_2 \dot{e}(t) - \int_t^{t_{k+1}} \dot{e}^T(\alpha) \\
 &\cdot T_2 \dot{e}(\alpha) d\alpha = (t - t_k) I_2 T_2 I_2^T - \int_t^{t_{k+1}} \dot{e}^T(\alpha) \\
 &\cdot T_2 \dot{e}(\alpha) d\alpha.
 \end{aligned} \tag{22}$$

Separating the integral in  $\dot{V}_2$  for two sides and applying Lemmas 1 and 2, we have

$$\begin{aligned} & - \int_{t-\tau_M}^t \dot{e}^T(\alpha) R \dot{e}(\alpha) d\alpha \\ & = - \int_{t-\tau(t)}^t \dot{e}^T(\alpha) R \dot{e}(\alpha) d\alpha \\ & \quad - \int_{t-\tau_M}^{t-\tau(t)} \dot{e}^T(\alpha) R \dot{e}(\alpha) d\alpha \end{aligned}$$

$$- \int_{t_k}^t \dot{e}^T(\alpha) T_1 \dot{e}(\alpha) d\alpha \leq \zeta^T(t) \begin{bmatrix} \kappa_1^T \\ \kappa_2^T \end{bmatrix}^T \begin{bmatrix} (t-t_k) X_1 T_1^{-1} X_1^T & X_1 [1 \ 0] \\ * & \frac{(t-t_k)}{3} Y_1 T_1^{-1} Y_1^T + \text{sym}(Y_1 [-I \ 2I]) \end{bmatrix} \begin{bmatrix} \kappa_1^T \\ \kappa_2^T \end{bmatrix} \zeta(t), \quad (24)$$

$$- \int_t^{t_{k+1}} \dot{e}^T(\alpha) T_2 \dot{e}(\alpha) d\alpha \leq \zeta^T(t) \begin{bmatrix} \kappa_1^T \\ \kappa_3^T \end{bmatrix}^T \begin{bmatrix} (t_{k+1}-t) X_2 T_2^{-1} X_2^T & X_2 [1 \ 0] \\ * & \frac{(t_{k+1}-t)}{3} Y_2 T_2^{-1} Y_2^T + \text{sym}(Y_2 [-I \ 2I]) \end{bmatrix} \begin{bmatrix} \kappa_1^T \\ \kappa_3^T \end{bmatrix} \zeta(t), \quad (25)$$

Then, the following is satisfied with the given nonlinear function as

$$\begin{aligned} & [g(e_i(t), s_i(t)) - W_1 e_i(t)]^T \\ & \cdot [g(e_i(t), s_i(t)) - W_2 e_i(t)] \leq 0. \end{aligned} \quad (26)$$

Equation (13) is equivalent to

$$-\delta \begin{bmatrix} e(t) \\ \widehat{g}(e(t), r(t)) \end{bmatrix}^T \begin{bmatrix} \widehat{W}_1 & \widehat{W}_2 \\ * & 2I \end{bmatrix} \begin{bmatrix} e(t) \\ \widehat{g}(e(t), r(t)) \end{bmatrix} \geq 0 \quad (27)$$

where  $\widehat{W}_1 = (I \otimes W_1 W_2) + (W_1 W_2 \otimes I)$ ,  $\widehat{W}_2 = -I \otimes (W_1^T + W_2^T)$ , and  $\delta$  is a constant scalar. Considering the dynamic equations (6) with auxiliary matrices  $G_1, G_2, G_3, G_4$ , the following holds:

$$\begin{aligned} & 2(((t-t_k) G_1 + (t_{k+1}-t) G_2) I_1 \\ & + ((t-t_k) G_3 + (t_{k+1}-t) G_4) I_2) \cdot (c(C \otimes D) I_1 \\ & + c(C \otimes A) I_7 + K I_3 - I_2 + I_{11}) = 0, \end{aligned} \quad (28)$$

Summing up (21), (24), (25), (27), and (28), the derivative of LKF is expressed as

$$\dot{V}(x_t) = \zeta^T(t) \Lambda_{h(t)} \zeta(t) \quad (29)$$

$$\begin{aligned} & \leq -\zeta^T(t) \Sigma \begin{bmatrix} \widehat{R} & \widehat{M} \\ \widehat{M} & \widehat{R} \end{bmatrix} \Sigma^T \zeta(t) \\ & = -\zeta^T(t) \kappa_4 \begin{bmatrix} \widehat{R} & \widehat{M} \\ \widehat{M} & \widehat{R} \end{bmatrix} \kappa_4^T \zeta(t) \end{aligned} \quad (23)$$

where  $\Sigma = [I_1 - I_6 \ I_1 + I_6 - I_8 \ I_1 - I_7 \ I_1 + I_7 - I_9]$ ,  $\widehat{R} = \begin{bmatrix} R & 0 \\ 0 & R \end{bmatrix}$ .

Using Lemma 3, the upper bound of each integrals in  $\dot{V}_{13}(t), \dot{V}_{14}(t)$  is estimated as follows:

where

$$\begin{aligned} \Lambda_{h(t)} & = \Pi_{1,h(t)} + (t-t_k) \Pi_2 + (t_{k+1}-t) \Pi_3 \\ \Pi_{1,h(t)} & = \text{sym} \{I_1 P I_2^T\} + I_1 Q_1 I_1^T - (1-\mu) I_7 Q_1 I_7^T \\ & \quad + I_1 Q_2 I_1^T - I_8 Q_2 I_8^T + \tau_M I_2 R I_2^T - \kappa_4 \begin{bmatrix} \widehat{R} & \widehat{M} \\ \widehat{M} & \widehat{R} \end{bmatrix} \kappa_4^T \\ & \quad + \text{sym} \{ \eta_1 S_1(t) \eta_{2d}^T + \eta_{1d} S_1(t) \eta_2^T + \eta_1 S_{1d}(t) \eta_{2d}^T \} \\ & \quad + \text{sym} \left\{ [I_1 - I_3 \ (t-t_k) I_4] S_2 \begin{bmatrix} -I_2^T \\ -I_1^T \end{bmatrix} \right. \\ & \quad \left. + [I_2 \ I_1] S_2 \begin{bmatrix} I_5^T - I_1^T \\ (t_{k+1}-t) I_6^T \end{bmatrix} \right\} + (t_{k+1}-t) I_2 T_1 I_2^T \\ & \quad + (t-t_k) I_2 T_2 I_2^T + \text{sym} \{ \kappa_1 X_1 [I \ 0] \kappa_2^T \\ & \quad + \kappa_2 Y_1 [-I \ 2I] \kappa_2^T \} + \text{sym} \{ \kappa_1 X_2 [I \ 0] \kappa_3^T \\ & \quad + \kappa_2 Y_2 [-I \ 2I] \kappa_3^T \} - \delta [I_1 \ I_{11}] \begin{bmatrix} \widehat{W}_1 & \widehat{W}_2 \\ * & 2I \end{bmatrix} \begin{bmatrix} I_1^T \\ I_{11}^T \end{bmatrix} \\ & \quad + \text{sym} \{ (I_1 G_1 + I_2 G_2) \\ & \quad \cdot (c(C \otimes D) I_1^T + c(C \otimes A) I_7^T + K I_3^T - I_2^T + I_{11}^T) \} \end{aligned} \quad (30)$$

$$\Pi_2 = \kappa_1 X_1 T_1^{-1} X_1^T \kappa_1^T + \frac{1}{3} \kappa_2 Y_1 T_1^{-1} Y_1^T \kappa_2^T$$

$$\Pi_3 = \kappa_1 X_2 T_2^{-1} X_2^T \kappa_1^T + \frac{1}{3} \kappa_3 Y_2 T_2^{-1} Y_2^T \kappa_3^T$$

Therefore, the conditions  $\zeta^T(t)\Lambda_{h(t)}\zeta(t) < 0$  implies that  $\dot{V} < 0$  for  $t \in [t_k, t_{k+1})$ . From the convex combination method,  $\Lambda_{h(t)} < 0$  for  $h(t) \in [0, h_M]$  is equivalent to the conditions in Theorem 6 using Schur complements, and thus the synchronization error system is asymptotically stable for given sampling time  $h_M$ . This is the end of the proof.  $\square$

*Remark 7.* The constructed Lyapunov functionals include novel looped functionals, which are  $V_{l1}$ ,  $V_{l2}$ ,  $V_{l3}$ , and  $V_{l4}$ . Those functionals satisfy  $V_{l1} = V_{l2} = V_{l3} = 0$  at every sampling instances  $t_k, t_{k+1}$  so it is looped functional as defined in [23].

*Remark 8.* The additional consideration of  $t_{k+1}$  in Lyapunov-Krasovskii functional (LKF) results in deriving less conservative results, which reflect more information for sampling time. The idea is motivated by the two-sided looped-functional [24], which is applied to CDNs with time-varying coupling delay to achieve more stable synchronization between two or more nodes. In the stability analysis of the sampled-data system using looped-functional, it is important to take into account the sampled-time-dependent vectors which become zero at each end point of each sampling time. However, in [24], the product term between the vectors  $x(t) - x(t_k)$  and  $x(t_{k+1}) - x(t)$  and the product term between  $x(t_k)$  and  $x(t_{k+1})$  are separately considered. In this paper, more generalized results are derived by defining the vector as  $\eta$  which provides each cross terms at the same time.

*Remark 9.* The novelty of the proposed looped functional is in the formation of  $V_{l1}$ . In  $V_{l1}$ , the variables are chosen as  $\eta_1, \eta_2$  and  $S(t)$  is composed of sampled-time-dependent matrix. The dimension of the LMI variable  $S_1(t)$  is extended to  $R^{4 \times 4}$ . Therefore, augmented vectors provide an increased degrees of freedom (DoF) and improved results compared with the existing results. Herein, the DoF is the number of independent variables or equations that must be specified to solve the problem uniquely. It extends the range of the solution and provides less conservative conditions.

*Remark 10.* In Theorem 6, a sufficient condition for the synchronization is derived in terms of LMIs which is obtained by constructing new looped functional. The results are sufficient conditions, which imply that there is still room for further improvement. Some approaches to reducing the conservatism are available. The conservativeness will be reduced by augmented vector or segmenting formulas. Also, new Lyapunov functions such as Lyapunov-Krasovskii or discontinuous Lyapunov [30] may play an essential role in the further reduction of the conservativeness.

Based on Theorem 6, the following corollary is constructed for the stabilization problem.

**Corollary 11.** For given scalars  $\alpha, 0 \leq \beta \leq 1$ , and  $h_M$ , if there exist a positive scalar  $\delta$ , symmetric matrices  $P > 0, Q_1 > 0, Q_2 > 0, R > 0, T_1 > 0$ , and  $T_2 > 0$ , and any matrices  $S_1(t), S_2, X_1, X_2, Y_1, Y_2, \widehat{M}, H_a, H_b, G_a = \text{diag}\{G_{a1}, G_{a2}, \dots, G_{an}\}, G_b = \text{diag}\{G_{b1}, G_{b2}, \dots, G_{bn}\}$ ,

$$\begin{bmatrix} \widehat{\Pi}_{1,h(t)=0} & \kappa_1 X_2 & \kappa_3 Y_2 \\ * & -h_M T_2 & 0 \\ * & 0 & -3h_M T_2 \end{bmatrix} \leq 0, \quad (31)$$

$$\begin{bmatrix} \widehat{\Pi}_{1,h(t)=h} & \kappa_1 X_1 & \kappa_2 Y_1 \\ * & -h_M T_1 & 0 \\ * & 0 & -3h_M T_1 \end{bmatrix} \leq 0, \quad (32)$$

$$\begin{bmatrix} \widehat{R} & \widehat{M} \\ \widehat{M} & \widehat{R} \end{bmatrix} \geq 0, \quad (33)$$

where

$$\begin{aligned} \widehat{\Pi}_{1,h(t)} = & \text{sym} \{I_1 P_1 I_2^T\} + I_1 Q_1 I_1^T - (1 - \mu) I_7 Q_1 I_7^T \\ & + I_1 Q_2 I_1^T - I_8 Q_2 I_8^T + \tau_M I_2 R I_2^T - \kappa_4 \begin{bmatrix} \widehat{R} & \widehat{M} \\ \widehat{M} & \widehat{R} \end{bmatrix} \kappa_4^T \\ & + \text{sym} \{ \eta_1 S_1(t) \eta_{2d}^T + \eta_{1d} S_1(t) \eta_2^T + \eta_1 S_{1d}(t) \eta_2^T \} \\ & + \text{sym} \left\{ [I_1 - I_3 \quad (t - t_k) I_4] S_2 \begin{bmatrix} -I_2^T \\ -I_1^T \end{bmatrix} \right. \\ & \left. + [I_2 \quad I_1] S_2 \begin{bmatrix} I_5^T - I_1^T \\ (t_{k+1} - t) I_6^T \end{bmatrix} \right\} + (t_{k+1} - t) I_2 T_1 I_2^T \\ & + (t - t_k) I_2 T_2 I_2^T + \text{sym} \{ \kappa_1 X_1 [I \quad 0] \kappa_2^T \\ & + \kappa_2 Y_1 [-I \quad 2I] \kappa_2^T \} + \text{sym} \{ \kappa_1 X_2 [I \quad 0] \kappa_3^T \\ & + \kappa_1 Y_2 [-I \quad 2I] \kappa_3^T \} - \delta [I_1 \quad I_{11}] \begin{bmatrix} \widehat{W}_1 & \widehat{W}_2 \\ * & 2I \end{bmatrix} \begin{bmatrix} I_1^T \\ I_{11}^T \end{bmatrix} \\ & + (t - t_k) \text{sym} \{ (\beta_1 I_1 + \alpha I_2) \cdot (G_a I_{11}^T \\ & + c G_a (C \otimes D) I_1^T + c G_a (C \otimes A) I_7^T + H_a I_3^T \\ & - G I_2^T) \} + (t_{k+1} - t) \text{sym} \{ (\beta_2 I_1 + \alpha I_2) \cdot (G_a I_{11}^T \\ & + c G_b (C \otimes D) I_1^T + c G_b (C \otimes A) I_7^T + H_b I_3^T \\ & - G_b I_2^T) \}, \end{aligned} \quad (34)$$

then the control gain is given by  $h = G_a^{-1} H_a$  which stabilizes the error dynamics.

*Proof.* Substituting the variables  $G_1, G_2, G_3$ , and  $G_4$  in the zero equation (28) into  $\beta_1 G_a, \beta_2 G_b, \alpha G_a$ , and  $\alpha G_b$ , respectively, the following are obtained:

$$\begin{aligned} 2(t - t_k) & \left[ (\beta_1 I_1 + \alpha I_2) \cdot (c G_a (C \otimes D) I_1^T \right. \\ & \left. + c G_a (C \otimes A) I_7^T + H_a I_3^T - G_a I_2^T + G_a I_{11}^T) \right] = 0, \end{aligned} \quad (35)$$

$$2(t_{k+1} - t) \left[ (\beta_2 I_1 + \alpha I_2) \cdot (c G_b (C \otimes D) I_1^T + c G_b (C \otimes A) I_7^T + H_b I_3^T - G_b I_2^T + G_b I_{11}^T) \right] = 0. \quad (36)$$

where  $H_a = G_a K$  and  $H_b = G_b K$ . The other part of the proof is omitted for brevity as it is similar to that of Theorem 6.  $\square$

#### 4. Numerical Examples

In this section, two examples are revisited from literature [5].

*Example 12.* Let us consider the CDNs composed of 3 nodes with the following matrices and parameters:

$$A = \begin{bmatrix} 1 & 0 \\ 0 & 1 \end{bmatrix}, \quad (37)$$

$$D = \begin{bmatrix} 0 & 0 \\ 0 & 0 \end{bmatrix},$$

$$G = \begin{bmatrix} -1 & 0 & 1 \\ 0 & -1 & 1 \\ 1 & 1 & 2 \end{bmatrix},$$

$$c = 0.5,$$

$$\tau_M = 0.5,$$

$$\mu = 0.25.$$

The nonlinear function is defined as

$$f(x_i(t)) = \begin{bmatrix} -0.5x_{i1} + \tanh(0.2x_{i1}) + 0.2x_{i1} \\ 0.95x_{i2} - \tanh(0.75x_{i2}) \end{bmatrix}, \quad (38)$$

satisfying the condition in (3) by the following matrices:

$$W_1 = \begin{bmatrix} -0.5 & 0.2 \\ 0 & 0.95 \end{bmatrix}, \quad (39)$$

$$W_2 = \begin{bmatrix} -0.3 & 0.2 \\ 0 & 0.2 \end{bmatrix}.$$

For  $\alpha = 1.2$ ,  $h_M = 2.01$ , the corresponding gain matrices are given by

$$K_1 = \begin{bmatrix} 0.1117 & -0.1514 \\ -0.0761 & -0.8361 \end{bmatrix},$$

$$K_2 = \begin{bmatrix} 0.1117 & -0.1514 \\ -0.0761 & -0.8361 \end{bmatrix}, \quad (40)$$

$$K_3 = \begin{bmatrix} 0.2682 & -0.1716 \\ -0.0949 & -0.8335 \end{bmatrix}.$$

$K$  are designed using the toolbox YALMIP 3.0 and SeDuMi 1.3 of MATLAB. The time-varying delay is chosen as  $\tau(t) = 0.25 + 0.1 \sin^2(5t)$ . The initial state is  $x(0) = [4, -3, -2, 1, 2, -5]^T$ .

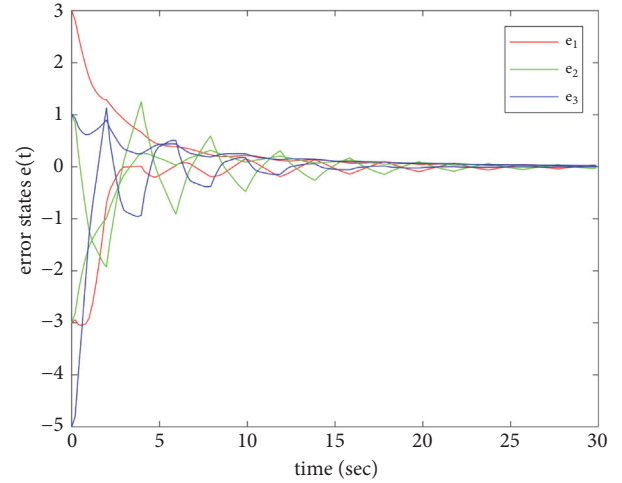


FIGURE 1: The state trajectories of the system (38) with  $c = 0.5$ ,  $\tau_M = 0.5$ , and  $\mu = 0.25$ .

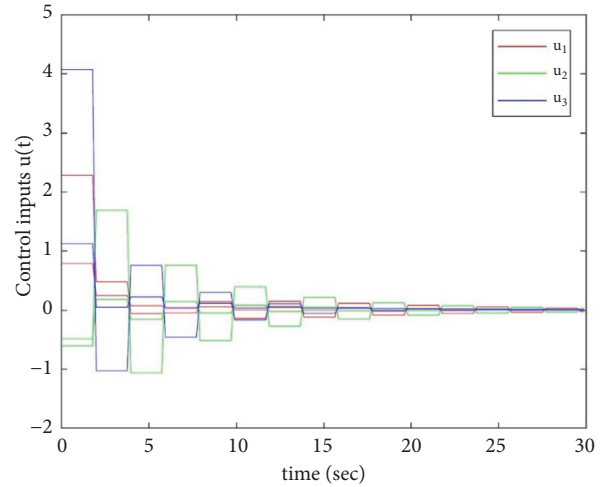


FIGURE 2: The input signals of the system (38) with  $c = 0.5$ ,  $\tau_M = 0.5$ , and  $\mu = 0.25$ .

The state trajectories of error system and the sampled-data input signals are, respectively, presented in Figures 1 and 2, which show stable convergence. Figure 1 shows the trajectories of error dynamics which is controlled by using the gain matrices at the simulation time from 0 to 30 seconds. The input signals ( $u_1$ ,  $u_2$ , and  $u_3$ ) converge, respectively, to 0 in Figure 2.

*Example 13.* Consider Chua's circuit composed of 4 nodes. The dynamics of Chua's circuit is represented as

$$\begin{aligned} \dot{x}_1(t) &= \epsilon_1 (-x_1(t) + x_2(t) - h(x_1(t))) \\ \dot{x}_2(t) &= -x_1(t) - x_2(t) + x_3(t) \\ \dot{x}_3(t) &= -\epsilon_2 x_2(t) \end{aligned} \quad (41)$$

where  $h(x_1(t)) = m_2 x_1(t) + 0.5(m_1 + m_2)(\|x_1(t) + 1\| - \|x_1(t) - 1\|)$  with the parameters  $\epsilon_1 = 10$ ,  $\epsilon_2 = 14.87$ ,  $m_1 = -1.27$ ,

and  $m_2 = -0.68$ . Then, the nonlinear function is denoted as

$$f(x_i(t)) = \begin{bmatrix} -\epsilon_1(1+m_2) & \epsilon_1 & 0 \\ 1 & -1 & 1 \\ 0 & -\epsilon_2 & 0 \end{bmatrix} x_i(t) + \begin{bmatrix} -\epsilon_1(m_1+m_2)(\|x_{i1}(t)+1\| - \|x_{i1}(t)-1\|) \\ 0 \\ 0 \end{bmatrix} \quad (42)$$

From (4), the matrices are given as

$$W_1 = \begin{bmatrix} 2.7 & 10 & 0 \\ 1 & -1 & 0 \\ 0 & -14.87 & 0 \end{bmatrix}, \quad (43)$$

$$W_2 = \begin{bmatrix} -3.2 & 10 & 0 \\ 1 & -1 & 1 \\ 0 & -14.87 & 0 \end{bmatrix}.$$

For given systems, the inner coupling matrix  $A$ , the outer coupling  $D$ , and parameters are chosen as

$$A = I_N,$$

$$D = 0_n,$$

$$G = \begin{bmatrix} -3 & 1 & 1 & 1 \\ 1 & -2 & 1 & 0 \\ 1 & 1 & -2 & 0 \\ 1 & 0 & 0 & -1 \end{bmatrix}, \quad (44)$$

$$c = 0.5,$$

$$\tau_M = 0.5,$$

$$\mu = 0.1.$$

The controller gain of Example 13 was calculated using toolbox YALMIP 3.0 and SeDuMi 1.3 of MATLAB in the same manner of Example 12. The corresponding gain with  $\alpha = 0.7$ ,  $h_M = 0.2138$  is given as

$$K_1 = \begin{bmatrix} -6.7314 & -4.1356 & 1.0795 \\ -0.0834 & -1.1048 & -0.7895 \\ 6.6711 & 7.6457 & -2.1652 \end{bmatrix},$$

$$K_2 = \begin{bmatrix} -7.7827 & -3.5618 & 1.0721 \\ -0.1367 & -2.0333 & -0.5521 \\ 6.6458 & 7.3950 & -3.0248 \end{bmatrix},$$

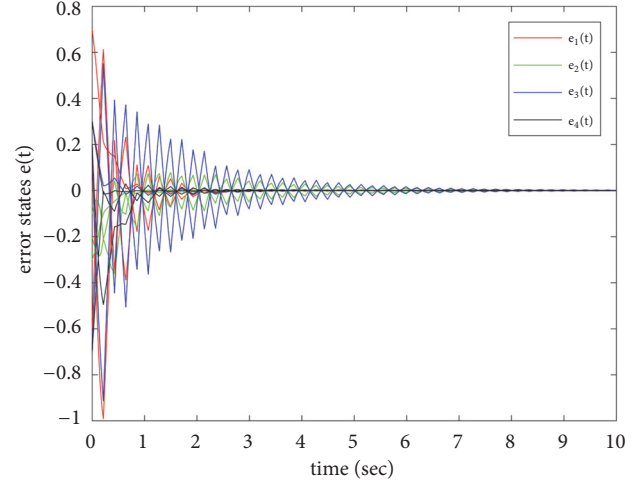


FIGURE 3: The error trajectories of system (41) with  $c = 0.5$ ,  $\tau_M = 0.5$ , and  $\mu = 0.1$ .

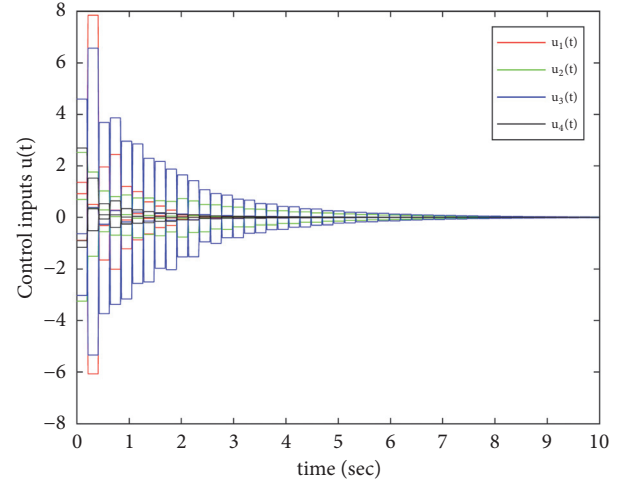


FIGURE 4: The sampled-data input signals of system (41) with  $c = 0.5$ ,  $\tau_M = 0.5$ , and  $\mu = 0.1$ .

$$K_3 = \begin{bmatrix} -7.7821 & -3.5679 & 1.0678 \\ -0.1372 & -2.0340 & -0.5508 \\ 6.6346 & 7.4183 & -3.0214 \end{bmatrix},$$

$$K_4 = \begin{bmatrix} -7.8447 & -3.4030 & 1.1874 \\ -0.0468 & -2.3492 & -0.5990 \\ 6.4107 & 7.2538 & -3.3484 \end{bmatrix}.$$

(45)

The trajectories of error dynamics and the sampled-data input signals are represented in Figures 3 and 4, respectively.

The maximum allowable sampling time is computed; the result using Corollary 11 is compared with existing results in Table 1. The results show that Corollary 11 provides more considerable maximum sampling period. It means that the synchronized error system guarantees stability in the broader

TABLE 1: The allowable maximum sampling time for Examples 12 and 13.

	ref. [5]	ref. [31]	ref. [16]	ref. [19]	Corollary 11
$h_M$	0.5409	0.5573	0.9016	1.3756	1.9789
$h_M$	0.0790	0.0793	0.1607	0.1833	0.2138
Nov	$3t^2 + (4+n)t + 1$	$3.5t^2 + 3.5t + 1$	$11.5t^2 + 3.5t + 1$	$7t^2 + (4+n)t + 1$	$34t^2 + 5t + 1$

sampling region. The last line of Table 1 represents a number of decision variables (NoV). It can be expressed as the product of the number of node and dimension of the node, which is defined as  $\iota = N \times n$ . Our method has higher complexity due to a larger NoV than ones of other methods. However, the proposed method is efficient on offline work with a more considerable allowable maximum sampling time.

## 5. Conclusions

This paper provides the new stabilization criteria to increase the maximum sampling interval for the synchronization of CDN with time-varying coupling delay. Novel two-sided looped functional and QGFWI are presented to obtain the enhanced results. The two-sided stabilization method is formulated by additional free matrices for present and next sampling time. The proposed looped functional, which vanishes at current sampling time and the next one, is constructed by using the augmented states to consider the information of sawtooth shape sampling pattern. Finally, simulation results show that the proposed synchronization approach provides a larger maximum sampling interval than one of the existing results. In other words, the proposed method contributes to extending the stable region and deriving a less conservative result. Also, the effectiveness of the proposed sampled-data control scheme has been demonstrated by numerical examples.

In future work, practical situations will be considered in sampled-data control for CDNs. For example, the proposed scheme could be applied to the synchronization of CDN systems with heterogeneous time-varying delay or with asynchronous and aperiodic sampling characteristics.

## Data Availability

The simulation result data used to support the findings of this study are included within the article.

## Conflicts of Interest

The authors declare that there are no conflicts of interest regarding the publication of this paper.

## Acknowledgments

This work was supported by Electronics and Telecommunications Research Institute (ETRI) grant funded by the Korean Government (18ZD1120, Support Project for Advanced ICT Convergence Technology based on Regional Industry) and Basic Science Research Program through the National Research Foundation of Korea (NRF) funded

by the Ministry of Education, Science and Technology (2016R1D1A1B03930623).

## References

- [1] A. Arenas, A. Díaz-Guilera, and C. J. Pérez-Vicente, "Synchronization processes in complex networks," *Physica D: Nonlinear Phenomena*, vol. 224, no. 1-2, pp. 27–34, 2006.
- [2] M. Yuan, W. Wang, X. Luo, L. Liu, and W. Zhao, "Finite-time anti-synchronization of memristive stochastic BAM neural networks with probabilistic time-varying delays," *Chaos, Solitons & Fractals*, vol. 113, pp. 244–260, 2018.
- [3] M. Yuan, X. Luo, W. Wang, L. Li, and H. Peng, "Pinning synchronization of coupled memristive recurrent neural networks with mixed time-varying delays and perturbations," *Neural Processing Letters*, 2018.
- [4] M. Yuan, W. Wang, X. Luo et al., "Synchronization of a class of memristive stochastic bidirectional associative memory neural networks with mixed time-varying delays via sampled-data control," *Mathematical Problems in Engineering*, vol. 2018, Article ID 9126183, 24 pages, 2018.
- [5] N. Li, Y. Zhang, J. Hu, and Z. Nie, "Synchronization for general complex dynamical networks with sampled-data," *Neurocomputing*, vol. 74, no. 5, pp. 805–811, 2011.
- [6] Z. Li and G. Chen, "Global synchronization and asymptotic stability of complex dynamical networks," *IEEE Transactions on Circuits and Systems II: Express Briefs*, vol. 53, no. 1, pp. 28–33, 2006.
- [7] B. Wang and Z.-H. Guan, "Chaos synchronization in general complex dynamical networks with coupling delays," *Nonlinear Analysis: Real World Applications*, vol. 11, no. 3, pp. 1925–1932, 2010.
- [8] C. P. Li, W. G. Sun, and J. Kurths, "Synchronization of complex dynamical networks with time delays," *Physica A: Statistical Mechanics and its Applications*, vol. 361, no. 1, pp. 24–34, 2006.
- [9] J. Lu and G. Chen, "A time-varying complex dynamical network model and its controlled synchronization criteria," *IEEE Transactions on Automatic Control*, vol. 50, no. 6, pp. 841–846, 2005.
- [10] W. Yu, G. Chen, and J. Lv, "On pinning synchronization of complex dynamical networks," *Automatica*, vol. 45, no. 2, pp. 429–435, 2009.
- [11] Z.-H. Guan, Z.-W. Liu, G. Feng, and Y.-W. Wang, "Synchronization of complex dynamical networks with time-varying delays via impulsive distributed control," *IEEE Transactions on Circuits and Systems I: Regular Papers*, vol. 57, no. 8, pp. 2182–2195, 2010.
- [12] X. Yang, J. Cao, and J. Lu, "Stochastic synchronization of complex networks with nonidentical nodes via hybrid adaptive and impulsive control," *IEEE Transactions on Circuits and Systems I: Regular Papers*, vol. 59, no. 2, pp. 371–384, 2012.
- [13] S. Tong, S. Sui, and Y. Li, "Fuzzy adaptive output feedback control of MIMO nonlinear systems with partial tracking errors constrained," *IEEE Transactions on Fuzzy Systems*, vol. 23, no. 4, pp. 729–742, 2014.

- [14] L. Su and H. Shen, "Mixed  $H_{\infty}$ /passive synchronization for complex dynamical networks with sampled-data control," *Applied Mathematics and Computation*, vol. 259, pp. 931–942, 2015.
- [15] L. Su, D. Ye, and X. Yang, "Dissipative-based sampled-data synchronization control for complex dynamical networks with time-varying delay," *Journal of The Franklin Institute*, vol. 354, no. 15, pp. 6855–6876, 2017.
- [16] Z.-G. Wu, P. Shi, H. Su, and J. Chu, "Sampled-Data exponential synchronization of complex dynamical networks with time-varying coupling delay," *IEEE Transactions on Neural Networks and Learning Systems*, vol. 24, no. 8, pp. 1177–1187, 2013.
- [17] W. Wang, M. Yu, X. Luo, L. Liu, M. Yuan, and W. Zhao, "Synchronization of memristive BAM neural networks with leakage delay and additive time-varying delay components via sampled-data control," *Chaos, Solitons & Fractals*, vol. 104, pp. 84–97, 2017.
- [18] W. Wang, X. Yu, X. Luo, and J. Kurths, "Synchronization control of memristive multidirectional associative memory neural networks and applications in network security communication," *IEEE Access*, vol. 6, pp. 36002–36018, 2018.
- [19] Y. Liu and S. M. Lee, "Improved results on sampled-data synchronization of complex dynamical networks with time-varying coupling delay," *Nonlinear Dynamics*, vol. 81, no. 1-2, pp. 931–938, 2015.
- [20] X. Wang, K. She, S. Zhong, and H. Yang, "New result on synchronization of complex dynamical networks with time-varying coupling delay and sampled-data control," *Neurocomputing*, vol. 214, pp. 508–515, 2016.
- [21] Z. Chen, K. Shi, and S. Zhong, "New synchronization criteria for complex delayed dynamical networks with sampled-data feedback control," *ISA Transactions*, vol. 63, pp. 154–169, 2016.
- [22] S. H. Lee, M. J. Park, O. M. Kwon, and R. Sakthivel, "Advanced sampled-data synchronization control for complex dynamical networks with coupling time-varying delays," *Information Sciences*, vol. 420, pp. 454–465, 2017.
- [23] C. Briat and A. Seuret, "A looped-functional approach for robust stability analysis of linear impulsive systems," *Systems & Control Letters*, vol. 61, no. 10, pp. 980–988, 2012.
- [24] H.-B. Zeng, K. L. Teo, and Y. He, "A new looped-functional for stability analysis of sampled-data systems," *Automatica*, vol. 82, pp. 328–331, 2017.
- [25] A. Seuret and F. Gouaisbaut, "Wirtinger-based integral inequality: application to time-delay systems," *Automatica*, vol. 49, no. 9, pp. 2860–2866, 2013.
- [26] P. G. Park, J. W. Ko, and C. Jeong, "Reciprocally convex approach to stability of systems with time-varying delays," *Automatica*, vol. 47, no. 1, pp. 235–238, 2011.
- [27] H.-B. Zeng, Y. He, M. Wu, and S.-P. Xiao, "Stability analysis of generalized neural networks with time-varying delays via a new integral inequality," *Neurocomputing*, vol. 161, pp. 148–154, 2015.
- [28] D. Zhang, Q.-L. Han, and X. Jia, "Network-based output tracking control for T-S fuzzy systems using an event-triggered communication scheme," *Fuzzy Sets and Systems*, vol. 273, pp. 26–48, 2015.
- [29] C. Peng, Q.-L. Han, and D. Yue, "To transmit or not to transmit: a discrete event-triggered communication scheme for networked takagi-sugeno fuzzy systems," *IEEE Transactions on Fuzzy Systems*, vol. 21, no. 1, pp. 164–170, 2013.
- [30] N. Eghbal, N. Pariz, and A. Karimpour, "Discontinuous piecewise quadratic Lyapunov functions for planar piecewise affine systems," *Journal of Mathematical Analysis and Applications*, vol. 399, no. 2, pp. 586–593, 2013.
- [31] Z. Wu, J. H. Park, H. Su, B. Song, and J. Chu, "Exponential synchronization for complex dynamical networks with sampled-data," *Journal of The Franklin Institute*, vol. 349, no. 9, pp. 2735–2749, 2012.

## Research Article

# Modeling and Stability Analysis for Markov Jump Networked Evolutionary Games

Guodong Zhao 

*School of Mathematics and Statistics, Shandong Normal University, Jinan 250014, China*

Correspondence should be addressed to Guodong Zhao; [zgd\\_qufu@126.com](mailto:zgd_qufu@126.com)

Received 3 September 2018; Accepted 2 October 2018; Published 19 November 2018

Guest Editor: Weihai Zhang

Copyright © 2018 Guodong Zhao. This is an open access article distributed under the Creative Commons Attribution License, which permits unrestricted use, distribution, and reproduction in any medium, provided the original work is properly cited.

This paper investigates the algebraic formulation and stability analysis for a class of Markov jump networked evolutionary games by using the semitensor product method and presents a number of new results. Firstly, a proper algorithm is constructed to convert the given networked evolutionary games into an algebraic expression. Secondly, based on the algebraic expression, the stability of the given game is analyzed and an equivalent criterion is given. Finally, an example works out to support the new results.

## 1. Introduction

The importance of networked evolutionary games (NEGs) [1] has been recognized many scholars recently. Unlike traditional  $n$ -player game, an NEG consists of a network graph and a basic game. The nodes in the network represent players and the edges in the network represent interaction relationship among players. Every player in the given game only plays with its neighbors. Furthermore, in the given game, players have the specialized strategy updating rules to adjust their own strategy choices. They are only affected by their neighbors. It coincides with an obvious fact that, in many practical economic activities, each individual is only in contract with its trade partners. This distinguishing feature makes NEGs theory be a very appealing research topic in recent years [2].

In the last decades, a very useful mathematical tool, called the semitensor product method (STP) of matrices, has been proposed by [3]. With this tool, [3] proposed a method to transform Boolean networks, Boolean control networks, and mix-valued logical networks into some kinds of difference equations. Then, one could investigate them by using mathematical tools in control theory.

Up to now, this method has been successfully applied to the analysis and control of Boolean networks and mix-valued logical networks, and many essential results have been obtained, such as the calculation of fixed points and cycles and the controllability and observability of Boolean networks;

see [3–19] for details. References [17, 20] presented the recent applications for STP method in engineering and finite-valued systems, respectively. See [20–29] for more recent developments about the application of STP method in logical networks.

In recent years, many scholars have attempted to study NEGs via STP method. For many specific NEGs, they transformed the given NEGs into some proper algebraic expressions, logical networks, for example. Based on “the myopic best response adjustment rule”, [30] designed a proper algorithm to construct the structural matrices of the updating laws for every players in the given NEG. Reference [31] gave the description of the NEG and investigated the relationship between the given NEG and the given logical networks. NEGs defined on finite networks were considered by [32], which converted the given NEGs to a kind of logical networks and solved the optimization problem when one player was regarded as a control. Reference [33] investigated evolutionary game theoretic demand-side management and control for a class of networked smart grid. A class of event-triggered control for finite evolutionary networked games was studied by [34]. Reference [16] studied stochastic set stabilization of  $n$ -person random evolutionary Boolean games and its applications.

It is worth noting that all of the above results are concentrated on NEGs with pure strategy dynamics except [16]. However, the fact that most evolutionary games are related to random dynamics more or less cannot be neglected. The

work [35] considered an interesting evolutionary game. In the game, major player is with infinite time horizon and the other players, called minor players, are with finite time horizons. At any time, when some new players enter the evolutionary game, the number of them is a random variable, which has a distribution depending on the number of the players who have entered the game at that moment. This situation is called random entrance, which is modeled as a Markov chain. In random entrance, there exists a long living player which has interaction relationships with the other players and the interactions are existing for a certain period. This situation is very common, University-Student Games [36], for example.

Actually, we can model the above evolutionary games with random entrance as a kind of networked evolutionary defined on finite networks. For every time, the entered players make up a network. The given game evolves on these finite networks. Thus, this paper considers this kind of networked evolutionary games as Markov jump networked evolutionary games (MJNEGs). In this paper, we would give the formal description of MJNEGs and analyze the stability of MJNEGs.

The main works of this paper are as follows: (1) The STP method is firstly applied to the study of MJNEGs. (2) The method to formulate the given MJNEGs as an algebraic expression is proposed. (3) The stability analysis of MJNEGs is presented in this paper, and an equivalent test criterion is given.

**Notations:**  $\mathbb{R}_{m \times n}$  denotes the set of  $m \times n$  real matrices.  $\mathbb{R}_{m \times n}^+$  denotes the set of  $m \times n$  nonnegative real matrices.  $\Delta_n := \{\delta_n^i \mid i = 1, 2, \dots, n\}$ , where  $\delta_n^i$  is the  $i$ -th column of the identity matrix  $I_n$ . An  $n \times t$  matrix  $M$  is called a logical matrix, if  $M = [\delta_n^{i_1} \delta_n^{i_2} \dots \delta_n^{i_t}]$  and denote  $M$  briefly by  $M = \delta_n[i_1 \ i_2 \ \dots \ i_t]$ . Define the set of  $n \times t$  logical matrices as  $\mathcal{L}_{n \times t}$ .  $Col_i(L)$  ( $Row_i(L)$ ) is the  $i$ -th column (row) of matrix  $L$ .  $r = (r_1, \dots, r_k)^T \in \mathbb{R}_k$  is a probabilistic vector, if  $r_i \geq 0$ ,  $i = 1, \dots, k$ , and  $\sum_{i=1}^k r_i = 1$ .  $\Upsilon_k$  denotes the set of  $k$  dimensional probabilistic vectors. If  $M \in \mathbb{R}_{m \times n}^+$  and  $Col(M) \subset \Upsilon_m$ ,  $M$  is called a probabilistic matrix.  $\Upsilon_{m \times n}$  denotes the set of  $m \times n$  probabilistic matrices.  $\times$  denotes the default matrix product throughout this paper. Please refer to [3] for the definition and properties of STP. Because  $\times$  is a generalization of the ordinary matrix product. We omit “ $\times$ ” without confusion and call it “product”.  $M * N$  denotes Khatri-Rao product of  $M$  and  $N$ .

## 2. Preliminaries

This section gives some necessary mathematic tools, which will be used in this paper.

**Lemma 1** (see [3]).

- (1) Consider  $X \in \mathbb{R}_m$  and  $Y \in \mathbb{R}_n$  as two column vectors. Then,  $W_{[m,n]}XY = YX$ , where  $W_{[m,n]}$  is the swap matrix. Especially  $W_{[n,n]} := W_{[n]}$ .
- (2) Define  $X \in \mathbb{R}_t$  and  $A \in \mathbb{R}_{m \times n}$ . Then, one gets  $XA = (I_t \otimes A)X$ .

**Lemma 2** (see [31]). Consider  $X \in \Upsilon_p$  and  $Y \in \Upsilon_q$ . Define dummy matrices, called “front-maintaining operator” and “rear-maintaining operator”, respectively, as

$$D_f^{p,q} = \delta_p \left[ \underbrace{1 \ 1 \ \dots \ 1}_q \ \underbrace{2 \ 2 \ \dots \ 2}_q \ \dots \ \underbrace{p \ p \ \dots \ p}_q \right], \quad (1)$$

$$D_r^{p,q} = \delta_q \left[ \underbrace{1 \ 2 \ \dots \ q}_p \ \underbrace{1 \ 2 \ \dots \ q}_p \ \dots \ \underbrace{1 \ 2 \ \dots \ q}_p \right].$$

Then  $D_f^{p,q}XY = X$ ,  $D_r^{p,q}XY = Y$ .

**Lemma 3** (see [37]). Consider  $f : \Delta_k^n \rightarrow \mathbb{R}$  (or  $f : \Delta_k^n \rightarrow \Delta_m$ ) as a pseudological (or logical) function. Then, there exists a unique matrix  $M_f \in \mathbb{R}_{1 \times k^n}$  (or  $M_f \in \mathcal{L}_{m \times k^n}$ ), called the structural matrix of  $f$ , such that

$$f(x_1, x_2, \dots, x_n) = M_f \times_{i=1}^n x_i, \quad (2)$$

where  $x_i \in \Delta_k$ ,  $i = 1, 2, \dots, n$ ,  $Col_j(M_f) = f(\delta_k^j)$ , and  $j = 1, 2, \dots, k^n$ .

In the rest of this section, we present some basic concepts in networked evolutionary games.

**Definition 4** (see [31]). A normal game with two players is a fundamental network game (FNG), if the strategy set is  $\{1, 2, \dots, k\}$  and player’s payoff function is  $c = c(x, y)$ .

## 3. Main Results

This section firstly gives the description of MJNEGs. Then, the method to formulate the given MJNEGs is given. Finally, this section analyzes the stability of the MJNEG based on its corresponding algebraic expression.

**3.1. Description of MJNEGs.** At first, we give the description of an MJNEG as follows:

- (a) A set of finite networks  $\mathcal{M} := \{1, 2, \dots, m\}$ : the topological structure of each network is a connected undirected graph  $(N_z, \mathcal{E}_z)$ , where  $\emptyset \neq N_z \subset \{1, 2, \dots, n\}$  is the set of nodes in network  $z$ ,  $\mathcal{E}_z = \{(i, j) \mid \text{there exists interaction between node } i \text{ and node } j \text{ in network } z\}$  is the set of edges, and  $z \in \mathcal{M}$ .
- (b) An FNG: if  $(i, j) \in \mathcal{E}_z$ , then node  $i$  and node  $j$  play the FNG in network  $z$  with strategies  $x_i(t)$  and  $x_j(t)$  at time  $t$ , respectively.
- (c) Players’ strategy updating rule: in network  $z$ , the rule can be expressed as

$$x_i(t) = f_{i,z}(x_i(0), x_i(1), \dots, x_i(t-1), x_j(0), x_j(1), \dots, x_j(t-1) \mid j \in \mathcal{N}_{i,z}), \quad (3)$$

where  $x_j(\tau) \in S_0$  is the strategy of player  $j$  at time  $\tau$ ,  $\tau = 0, 1, \dots, t-1$ , and  $\mathcal{N}_{i,z}$  is the neighborhood of

player  $i$  in the network  $z$ , that is,  $j \in \mathcal{N}_{i,z}$  if and only if  $(i, j) \in \mathcal{E}_z$ ,  $i \in \mathcal{N}$ , and  $z \in \mathcal{M}$ . Obviously,  $i \notin \mathcal{N}_{i,z}$  and  $j \in \mathcal{N}_{i,z} \iff i \in \mathcal{N}_{j,z}$ .

- (d) Network evolve process:  $\{\theta(t) : t \in \mathbb{N}\}$  represents the discrete-time homogeneous Markov chain taking values in a finite set  $\mathcal{M}$  with a transition probability matrix  $P = (p_{ij})_{m \times m}$  as

$$p_{ij} = Pr \{ \theta(t+1) = j \mid \theta(t) = i \}, \quad (4)$$

where  $p_{ij} \geq 0$ , for  $\forall i, j \in \mathcal{M}$ ,  $\sum_{j=1}^m p_{ij} = 1$  for any  $i \in \mathcal{M}$ , and  $\theta(t) = k$  represents that the MJNEG evolves on network  $k$  at time  $t$ .

In network  $z$ , at each time, node  $i$  only plays with its neighbors, and its aggregate payoff  $p_{i,z} : S_0^{|\mathcal{N}_{i,z}|+1} \rightarrow \mathbb{R}$  is the sum of payoffs gained by playing with all its neighbors, i.e.,

$$p_{i,z}(x_i, x_j \mid j \in \mathcal{N}_{i,z}) = \sum_{j \in \mathcal{N}_{i,z}} c(x_i, x_j) \quad (5)$$

in which  $c$  is the payoff function of the given FNG and  $x_i, x_j \in S_0$ .

In this paper, we adopt *the myopic best response adjustment rule* [38], that is, every player forecasts that its neighbors will repeat their last-step strategy choice, and the strategy choice at present time is the best response against its neighbors' strategies choice of the last one. Based on that, one has

$$x_i(t) \in Q_{i,z} := \arg \max_{x_i \in S} p_{i,z}(x_i, x_{-i}(t-1)), \quad (6)$$

$$i \in \mathcal{N}_{i,z}, z \in \mathcal{M}.$$

When player  $i$  may have more than one best strategies to choose, define a priority for the strategy choice as follows:  $x \in S_0$  has priority over  $y \in S_0$ , if and only if  $x > y$ . Thus, player  $i$  updates its strategy according to the following expression:

$$x_i(t) = \max \{ x \mid x \in Q_{i,z} \}, \quad i \in \mathcal{N}_z, z \in \mathcal{M}. \quad (7)$$

We let the initial state  $\bar{x}_0$  for nodes  $j \notin \mathcal{N}_z$ , which are not activated at that moment in the network  $z$ ; i.e.,  $x_j(t) = \bar{x}_0$  holds.

*Remark 5.* We assign the initial state  $\bar{x}_0$  for the new participators. It implies an obvious fact that every new participator has the same conditions when they enter the evolutionary game.

In addition to the evolution of strategies for players, the Markov chain  $\{\theta(t) \mid t \in \mathbb{N}\}$  decides the probability with which network the given MJNEG stays at a specific time  $t$ .

The aim of this paper is to study the algebraic formulation and stability analysis of the given MJNEG as a  $k$ -valued switched logical system with a given switching signal as a Markov chain.

*3.2. Algebraic Expression of the Given MJNEG.* This subsection algebraically formulates the given MJNEG as Markov jump  $k$ -valued logical system. To achieve it, we can take the following steps: (i) Find the proper structural matrices of the payoff function for every node in each networks. (ii) Find the proper structural matrix of the updating law for every node in each networks. (iii) Via the obtained structural matrices and the transition probability matrix of Markov chain  $\{\theta(t), t \in \mathbb{N}\}$ , we construct the algebraic formulation for the given MJNEGs.

Step (i), using the vector form of logical variables, we identify  $S_0 \sim \Delta_k$ , where  $|S_0| = k$ , " $\sim$ " denotes that the strategy  $j \in S_0$  is equivalent to  $\delta_k^j \in \Delta_k$ ,  $j = 1, 2, \dots, k$ . Then, when  $i \in \mathcal{N}_z$  holds, by Lemmas 1, 2, and 3, and (5), the payoff function of player  $i$  in network  $z$  can be rewritten as

$$\begin{aligned} p_{i,z}(x_i(t), x_j(t) \mid j \in \mathcal{N}_{i,z}) &= M_c \sum_{j \in \mathcal{N}_{i,z}} x_i(t) x_j(t) \\ &= M_c \sum_{j \in \mathcal{N}_{i,z}} W_{[k]} x_j(t) x_i(t) \\ &= M_c W_{[k]} \left( \sum_{j < i, j \in \mathcal{N}_{i,z}} x_j(t) x_i(t) \right. \\ &\quad \left. + \sum_{j > i, j \in \mathcal{N}_{i,z}} x_j(t) x_i(t) \right) \\ &= M_c W_{[k]} D_r^{k^{n-2}, k^2} \left( \sum_{j < i, j \in \mathcal{N}_{i,z}} W_{[k^j, k^{n-j-1}]} \right. \\ &\quad \left. + \sum_{j > i, j \in \mathcal{N}_{i,z}} W_{[k^{j-1}, k^{n-j}]} \right) x_{-i}(t) x_i(t) := M_{i,z} x_{-i}(t) \\ &\quad \cdot x_i(t), \end{aligned} \quad (8)$$

where  $M_c \in \mathbb{R}_{1 \times k^2}$  is the structural matrix of the FNG's payoff function and  $M_{i,z} \in \mathbb{R}_{1 \times k^n}$  is the structural matrix of  $p_{i,z}$ ,  $x_i(t) \in \Delta_k$  is the strategy of player  $i$  at time  $t$ ,  $x_{-i}(t) := x_1(t) \times x_2(t) \times \dots \times x_{i-1}(t) \times x_{i+1}(t) \times \dots \times x_n(t) \in \Delta_{k^{n-1}}$ , and  $z \in \mathcal{M}$ .

In Step (ii), we consider the following two cases.

*Case I.* If  $i \in \mathcal{N}_z$ , divide  $M_{i,z}$  into  $k^{n-1}$  equal blocks as

$$M_{i,z} = [Blk_1(M_{i,z}), Blk_2(M_{i,z}), \dots, Blk_{k^{n-1}}(M_{i,z})], \quad (9)$$

where  $Blk_l(M_{i,z})$  is all possible benefits of player  $i$  with other players' strategy  $x_{-i}(t) = \delta_{k^{l-1}}^l$ ,  $l = 1, 2, \dots, k^{n-1}$ .

Next, we find the best response of player  $i$  to make its benefit maximum. For all  $l = 1, 2, \dots, k^{n-1}$ , let the column index set  $\Xi_{i,l,z}$ , such that

$$\begin{aligned} \Xi_{i,l,z} &= \left\{ \xi_l \mid Col_{\xi_l}(Blk_l(M_{i,z})) \right. \\ &\quad \left. = \max_{1 \leq \xi \leq k} Col_{\xi}(Blk_l(M_{i,z})) \right\}. \end{aligned} \quad (10)$$

If there are more than one maximum columns, i.e.,  $|\Xi_{i,l,z}| > 1$ , one can choose the unique column index  $\xi_{i,l,z}$  with the help of the priority of strategy choice given in (7).

By Lemma 2, letting  $\tilde{L}_{i,z} = \delta_k[\xi_{i,1,z}, \dots, \xi_{i,k^{n-1},z}]$ , we can construct the algebraic form of the updating law for node  $i$  in network  $z$  as

$$\begin{aligned} x_i(t+1) &= \tilde{L}_{i,z} x_{-i}(t) = \tilde{L}_{i,z} D_r^{k,k^{n-1}} W_{[k^{i-1},k]} x(t) \\ &:= L_{i,z} x(t). \end{aligned} \quad (11)$$

*Case II.* If  $i \notin N_z$ , by Lemma 2, we define

$$\begin{aligned} x_j(t+1) &= \bar{x}_0 = D_f^{k,k^n} \bar{x}_0 x_1(t) x_2(t) \cdots x_n(t) \\ &:= L_{j,z} x(t), \end{aligned} \quad (12)$$

where  $x(t) = x_1(t)x_2(t)\cdots x_n(t)$ . Then, each new player entering the MJNEG would have the initial state  $\bar{x}_0$ .

Thus, by (11) and (12), one gets the MJNEGs evolving on fixed network  $z$  as follows:

$$x(t+1) = L_z x(t), \quad (13)$$

where  $x(t) = x_1(t)x_2(t)\cdots x_n(t)$  and  $L_z = L_{1,z} * L_{2,z} * \cdots * L_{n,z}$ .

In Step (iii), by the aforementioned analysis, we formulate the given MJNEG as follows:

$$x(k+1) = L_{\theta(t)} x(k), \quad (14)$$

where  $\{\theta(t) : t \in \mathbb{N}\}$  is the discrete-time Markov chain and  $x(k) = x_1(k)x_2(k)\cdots x_n(k)$ .

Based on the aforementioned analysis, the following algorithm is constructed to formulate the MJNEG.

*Algorithm 6.* This algorithm contains four steps:

- (1) Calculate the structural matrix,  $M_{i,z}$ , of the payoff functions of the player in node  $i$ , when  $\mathcal{N}_{i,z} \neq \emptyset$ , for each network  $z$  by

$$\begin{aligned} M_{i,z} &= M_c W_{[k]} D_r^{k^{n-2}, k^2} \left( \sum_{j < i, j \in \mathcal{N}_{i,z}} W_{[k^j, k^{n-j-1}]} \right. \\ &\quad \left. + \sum_{j > i, j \in \mathcal{N}_{i,z}} W_{[k^{j-1}, k^{n-j}]} \right). \end{aligned} \quad (15)$$

- (2) For each network  $z$ , divide the matrices  $M_{i,z}$  into  $k^{n-1}$  equal blocks as

$$M_{i,z} = [\text{Blk}_1(M_{i,z}), \text{Blk}_2(M_{i,z}), \dots, \text{Blk}_{k^{n-1}}(M_{i,z})], \quad (16)$$

and for all  $l = 1, 2, \dots, k^{n-1}$ , find the column index  $\xi_{i,l,z}$ , such that  $\xi_{i,l,z} = \max\{j \mid \text{Col}_j(\text{Blk}_l(M_{i,z})) = \max_{1 \leq \xi \leq k} \text{Col}_\xi(\text{Blk}_l(M_{i,z}))\}$ ;

- (3) Formulate the MJNEG evolving on network  $z$  under study as

$$x(t+1) = L_z x(t), \quad (17)$$

where  $L_z = L_{1,z} * L_{2,z} * \cdots * L_{n,z}$ ,  $\tilde{L}_{i,z} = \delta_k[\xi_{i,1,z}, \xi_{i,2,z}, \dots, \xi_{i,k^{n-1},z}]$ ,  $i \in N_z$ ,  $L_{j,z} = D_f^{k,k^n} \bar{x}_0$ , and  $j \notin N_z$ .

- (4) Finally, one has the algebraic formulation as follows:

$$x(k+1) = L_{\theta(t)} x(k), \quad (18)$$

where  $x(k) = x_1(k)x_2(k)\cdots x_n(k)$ .

*3.3. Stability Analysis.* This subsection investigates the stochastic global stability of the given MJNEG as

$$x(t+1) = L_{\theta(t)} x(t), \quad (19)$$

where  $x(t) = \kappa_{i=1}^n x_i(t)$  and  $\{\theta(t) : t \in \mathbb{N}\}$  denotes the given Markov chain. In an evolutionary game, some strategy profile  $x_e$  has specific meaning, Nash equilibrium, for example. This subsection analyzes the globally stability at  $x_e$  in stochastic sense. In addition, because of transformation of coordinates, we assume that  $x_e = \delta_{k^n}^k \in \Delta_{k^n}$  holds.

In the following, we give the definition for MJNEG of global stability in stochastic sense.

*Definition 7.* The given MJNEG with algebraic form (19) is said to be globally stable in stochastic sense at  $x_e = \delta_{k^n}^k \in \Delta_{k^n}$ , if, for  $\forall x(0)$  and  $\forall \theta(t)$ ,  $\lim_{t \rightarrow +\infty} E\{x(t) \mid x(0), \theta(0)\} = \delta_{k^n}^k$  holds.

Denote  $z_j(t) = E\{x(t) 1_{\{\theta(t)=j\}}\}$ , where  $1_{\{\theta(t)=j\}}$  represents the Dirac measure over the set  $\{\theta(t) = j\}$  with  $j \in \mathcal{M}$ . Since  $\{\theta(t) = j\}$  is independent from  $\{x(t) = \delta_{k^n}^i\}$ , one has

$$\begin{aligned} E\{x(t)\} &= \sum_{i=1}^{k^n} \delta_{k^n}^i P\{x(t) = \delta_{k^n}^i\} \\ &= \sum_{i=1}^{k^n} \delta_{k^n}^i \sum_{j=1}^m P\{x(t) = \delta_{k^n}^i \mid \theta(t) = j\} P\{\theta(t) = j\} \end{aligned} \quad (20)$$

$$= \sum_{j=1}^m \sum_{i=1}^{k^n} \delta_{k^n}^i P\{x(t) = \delta_{k^n}^i\} P\{\theta(t) = j\} = \sum_{j=1}^m z_j(t).$$

Then, we have

$$\begin{aligned} z_j(t+1) &= E\{x(t+1) 1_{\{\theta(t+1)=j\}}\} \\ &= \sum_{i=1}^m E\{x(t+1) 1_{\{\theta(t+1)=j\}} 1_{\{\theta(t)=i\}}\} \\ &= \sum_{i=1}^m p_{ij} L_i z_i(t). \end{aligned} \quad (21)$$

Rewrite  $z_j(t)$  as  $z_j(t) = (w_j^T(t), \mu_j(t))^T$ , where  $w_j(t) \in \mathbb{R}_{k^{n-1},1}$ ,  $\mu_j(t) \in \mathbb{R}$  and  $j \in \mathcal{M}$ ; one has

$$\begin{aligned} w_j(t+1) &= \sum_{i=1}^m p_{i,j} L_i^{1,1} w_i(t) + \sum_{i=1}^m p_{i,j} L_i^{1,2} \mu_i(t), \\ \mu_j(t+1) &= \sum_{i=1}^m p_{i,j} L_i^{2,1} w_i(t) + \sum_{i=1}^m p_{i,j} L_i^{2,2} \mu_i(t), \end{aligned} \quad (22)$$

where  $j \in \mathcal{M}$  and

$$\begin{pmatrix} L_i^{1,1} & L_i^{1,2} \\ L_i^{2,1} & L_i^{2,2} \end{pmatrix} = L_i, \quad L_i^{1,1} \in \Upsilon_{(k^n-1) \times (k^n-1)}, \quad i \in \mathcal{M}. \quad (23)$$

Thus, via (22), the following result reveals some property for the given MJNEG.

**Theorem 8.** *The given MJNEG with algebraic form (19) is globally stable at  $x_e = \delta_{k^n}^{k^n}$  in stochastic sense if and only if,  $\forall x(0)$  and  $\forall \theta(t)$ ,*

$$\lim_{t \rightarrow +\infty} w_i(t) = \mathbf{0}_{k^n-1}, \quad \forall i \in \mathcal{M}. \quad (24)$$

*Proof. Sufficient.* If,  $\forall x(0)$  and  $\forall \theta(t)$ , (24) holds, then  $\lim_{t \rightarrow +\infty} \sum_{i=1}^m \mu_i(t) = 1$  according to that  $1 = \mathbf{1}_{k^n}^T E\{x(t)\} = \mathbf{1}_{k^n}^T \sum_{j=1}^m z_j(t)$ . It is easy to see that  $\lim_{t \rightarrow +\infty} E\{x(t)\} = \lim_{t \rightarrow +\infty} \sum_{j=1}^m z_j(t) = \delta_{k^n}^{k^n}$ .

*Necessity.* If system (19) is globally stable in stochastic sense at  $x_e = \delta_{k^n}^{k^n}$ , then using Definition 7, for  $\forall x(0)$  and initial distribution of  $\theta(t)$ ,  $\lim_{t \rightarrow +\infty} E\{x(t)\} = \delta_{k^n}^{k^n}$ , which yields that  $\lim_{t \rightarrow +\infty} \sum_{i=1}^m w_i(t) = \mathbf{0}_{k^n-1}$ . Note that  $w_i(t) \geq 0$ , then one has, for every  $i \in \mathcal{M}$ ,  $\lim_{t \rightarrow +\infty} w_i(t) = \mathbf{0}_{k^n-1}$ .  $\square$

With the help of the above theorem, we can get the main result in this paper. The following theorem gives an equivalent criterion for the stability of the given NEG.

**Theorem 9.** *The given system with algebraic form (19) is globally stable in stochastic sense at  $x_e = \delta_{k^n}^{k^n}$  if and only if there exist vectors  $\lambda_i \in \mathbb{R}^{k^n}$ ,  $i \in \mathcal{M}$  such that the following conditions hold:*

$$\begin{aligned} \lambda_i^T \delta_{k^n}^{k^n} &= 0, \\ \lambda_i^T \delta_{k^n}^t &> 0, \\ \sum_{j=1}^m p_{i,j} \lambda_j^T L_i \delta_{k^n}^{k^n} &= 0, \\ \left( \sum_{j=1}^m p_{i,j} \lambda_j^T L_j - \lambda_i^T \right) \delta_{k^n}^t &< 0, \end{aligned} \quad (25)$$

for  $i = 1, 2, \dots, m$ , and  $t = 1, 2, \dots, k^n - 1$ .

*Proof. Sufficient.* To prove the part of sufficient, we need first prove the fact that each network has a common fixed point as  $x_e$  under conditions (25).

Assume that  $x_e$  is not a fixed point of network  $i_0$ , then  $L^{i_0} x_e \neq x_e$ , i.e.,  $Col_{k^n}(L^{i_0}) = \delta_{k^n}^s$ , for some  $s \neq k^n$ . Subsequently, by the second equation in (25), one has that for every  $j \in \mathcal{M}$ ,  $\lambda_j^T L^{i_0} \delta_{k^n}^{k^n} = \lambda_j^T \delta_{k^n}^s > 0$ . Note that  $\sum_{j=1}^m p_{i_0,j} \geq 0$ , then there exists at least one integer  $j^*$  such that  $p_{i_0,j^*} > 0$ . Therefore,

$$\sum_{j=1}^m p_{i_0,j} \lambda_j^T L^{i_0} \delta_{k^n}^{k^n} = \sum_{j=1}^m \lambda_j^T \delta_{k^n}^s \geq p_{i_0,j^*} * \lambda_{j^*}^T * \delta_{k^n}^s > 0, \quad (26)$$

which is contradictory to the third equation in (25). Thus,  $x_e$  is a common fixed point of each network, which implies that  $Col_{k^n}(L^i) = \delta_{k^n}^{k^n}$ , for  $\forall i \in \mathcal{M}$ . Therefore,  $L_i^{1,2} = \mathbf{0}_{k^n-1}$  and  $L_i^{2,2} = 1$  for  $\forall i \in \mathcal{M}$  in (23). Then, the first equation of (22) can be rewritten as

$$w_j(t+1) = \sum_{i=1}^m p_{i,j} L_i^{1,1} w_i(t), \quad j \in \mathcal{M}. \quad (27)$$

Let  $w(t) = (w_1^T(t), w_2^T(t), \dots, w_m^T(t)) \in \mathbb{R}_{m(k^n-1)}$ , then

$$w(t+1) = Qw(t), \quad (28)$$

where

$$Q = (P^T \otimes I_{2^n-1}) \begin{pmatrix} L_1^{11} & \mathbf{0} & \cdots & \mathbf{0} \\ \mathbf{0} & L_2^{11} & \cdots & \mathbf{0} \\ \vdots & \vdots & \ddots & \vdots \\ \mathbf{0} & \mathbf{0} & \cdots & L_m^{11} \end{pmatrix} \in \Upsilon_{m(2^n-1) \times m(2^n-1)}. \quad (29)$$

It is worth noting that  $Q \geq 0$ . Thus, from Lemma 1 in [39] system, (28) is a positive system. Rewrite  $\lambda_i$  as  $\lambda_i = (\widehat{\lambda}_i^T, 0)^T$ , where  $\widehat{\lambda}_i \in \mathbb{R}^{k^n-1}$ ,  $i \in \mathcal{M}$ , then by (25) and denoting  $\widehat{\lambda} = (\widehat{\lambda}_1^T, \widehat{\lambda}_2^T, \dots, \widehat{\lambda}_m^T)^T \in \mathbb{R}_{k^n-1}$ , one has  $\widehat{\lambda} \gg 0$  and  $\widehat{\lambda}^T(Q - I_{s(k^n-1)}) \ll 0$ . Therefore, system (28) is stable by Proposition 1 in [39]. By Theorem 8, network (19) is stochastically globally stable.

*Necessity.* Because system (19) is stochastically globally stable. From Theorem 8, we have (24). For Markov process  $\{\theta(k), k \geq 0\}$  is ergodic, one get that there exists  $K \in \mathbb{N}^+$  such that the probability of reaching every mode  $i \in \mathcal{M}$  is positive after time  $K$ . Thus, for all networks,  $x_e$  is a common fixed point. Otherwise, if  $x_e$  is not a fixed point of network  $i_0$ , then  $L_{i_0}^{2,2} = 0$  and  $L_i^{2,2} = 1$  for  $i \neq i_0$ . By (22) and (24), one has

$$\begin{aligned} \lim_{k \rightarrow +\infty} \sum_{j=1}^s \mu_j(k+1) &= \lim_{k \rightarrow +\infty} \sum_{j=1}^s \sum_{i=1}^s p_{ij} F_{22}^i \mu_i(k) \\ &= \lim_{k \rightarrow +\infty} \sum_{j=1}^s \sum_{i=1, i \neq i_0}^s p_{ij} F_{22}^i \mu_i(k) \\ &= \lim_{k \rightarrow +\infty} \sum_{i=1, i \neq i_0}^s \sum_{j=1}^s p_{ij} F_{22}^i \mu_i(k) \\ &= \lim_{k \rightarrow +\infty} \sum_{i=1, i \neq i_0}^s \mu_i(k). \end{aligned} \quad (30)$$

With  $\lim_{k \rightarrow +\infty} \mu_i(k) = 1$  in hands, one obtains that  $\lim_{k \rightarrow +\infty} \mu_0(k) = 0$ , which implies that  $\lim_{k \rightarrow +\infty} z_{i_0}(k) = \mathbf{0}_{k^n}$  holds. It is contrary to that the probability of every reaching mode  $i \in \mathcal{M}$  is positive after time  $K$ . Therefore, for each  $i \in \mathcal{M}$ ,  $F_{22}^i = 1$  and  $F_{12}^i = 0_{k^n-1}$ . So,  $w(k)$  satisfies (28). System (28) is a positive and stable system. Then, by Proposition 1 in [39], there exists a vector  $\widehat{\lambda} = (\widehat{\lambda}_1^T, \widehat{\lambda}_2^T, \dots, \widehat{\lambda}_m^T)^T \in \mathbb{R}^{m(k^n-1)}$ ,

TABLE 1: Payoff bimatrix.

Player1\Player2	M	F
M	(2, 2)	(1, 0)
F	(0, 1)	(3, 3)

where  $\hat{\lambda}_i \in \mathbb{R}^{k^n-1}$  and  $\hat{\lambda}_i \gg 0$ ,  $i \in \mathcal{M}$  such that  $\hat{\lambda}^T(Q - I_{m(k^n-1)}) \ll 0$ . Define  $\lambda_i = (\hat{\lambda}_i^T, 0)^T$ ,  $i \in \mathcal{M}$ , then (25) holds. The proof is completed.  $\square$

*Remark 10.* It worth noting that this manuscript consists of two important part: (1) The modeling and algebraic formulation of the given MJNEGs; (2) Based on the obtained algebraic expressions, we investigate the stability analysis for the given MJNEGs. Actually, this paper can be considered as a further research of [40]. Compared with the model adopted in [40], the description of MJNEGs is more general, i.e., the MJNEGs given in this paper can include the research target in [40] as a special case. In addition to that, the stability analysis for the MJNEGs in this paper is deeper than the stability analysis in [40]. We obtain better results in this paper.

#### 4. An Illustrative Example

In this section, we use a classical example University-students game [36] to show the effective of our results.

*Example 1.* In an evolutionary game  $\mathcal{G}$  with random entrance, minor players have time horizon 2.  $n_m = 2$  denotes the maximum possible number of active players in  $\Xi$ . At the time  $t$ , the number of the minor players is modelled by the vector

$$y(t) = (n_0(t), n_1(t)), \quad (31)$$

where  $n_l(t) = |I_l(t)|$ ,  $I_l(t)$  is the set of players with entrance time  $t - l$ ,  $l = 0, 1$ . Furthermore, major player plays game with minor players and minor players do not player game with each other. Thus, the random entrance is denoted by a Markov chain with states: (0, 1), (1, 0), and (1, 1).

Define an MJNEG as follows:

- (i) Network topological structures, denote by  $(N_z, \mathcal{E}_z)$ , where  $N_1 = \{1, 3\}$ ,  $N_2 = \{2, 3\}$ ,  $N_3 = \{1, 2, 3\}$ ,  $\mathcal{E}_1 = \{(1, 3)\}$ ,  $\mathcal{E}_2 = \{(2, 3)\}$ ,  $\mathcal{E}_3 = \{(1, 3), (2, 3)\}$  node 3 represents the major player, and  $z \in \mathcal{M} = \{1, 2, 3\}$ . See in Figure 1.

- (ii) The FNG's payoff is shown in Table 1.

- (iii) The updating rule is MBRA.

- (iv) Network evolve process:  $\{\theta(t) : t \in \mathbb{N}\}$  with a transition probability matrix

$$P = \begin{pmatrix} 0 & 0 & 1 \\ 0.4 & 0 & 0.6 \\ 0 & 0 & 1 \end{pmatrix}. \quad (32)$$

Firstly, we rewrite the MJNEG into an algebraic expression. Denote  $M \sim \delta_2^1$ ,  $F \sim \delta_2^2$ ,  $(0, 1) \sim \delta_3^1$ , network  $j \sim \delta_3^j$ , and  $j = 1, 2, 3$ . Using the vector form of logical variables, we have  $p_{i,z} = M_{i,z}x_{-i}(t)x_i(t)$ ,  $x(t) = (x_1(t), x_2(t), x_3(t))$ ,  $x_i(t) \in \Delta_2$ , and  $z \in \mathcal{M}$ .

With (11), one obtains

$$\begin{aligned} M_{3,1} &= [2 \ 0 \ 2 \ 0 \ 1 \ 3 \ 1 \ 3], \\ M_{3,2} &= [2 \ 0 \ 1 \ 3 \ 2 \ 0 \ 1 \ 3], \\ M_{3,3} &= [4 \ 0 \ 3 \ 3 \ 3 \ 3 \ 2 \ 6], \\ M_c &= [2 \ 0 \ 1 \ 3], \quad i \in \{1, 2\}, \quad z \in \mathcal{M}. \end{aligned} \quad (33)$$

Then, by (11) and (12), we have

$$\begin{aligned} L_{3,1} &= \delta_2 [1 \ 1 \ 1 \ 1 \ 2 \ 2 \ 2 \ 2], \\ L_{3,2} &= \delta_2 [1 \ 1 \ 2 \ 2 \ 1 \ 1 \ 2 \ 2], \\ L_{3,3} &= \delta_2 [1 \ 1 \ 2 \ 2 \ 2 \ 2 \ 2 \ 2], \\ L_{i,z} &= \delta_2 [1 \ 2 \ 1 \ 2 \ 1 \ 2 \ 1 \ 2], \\ L_{j,z} &= \delta_2 [2 \ 2 \ 2 \ 2 \ 2 \ 2 \ 2 \ 2]. \end{aligned} \quad (34)$$

where  $i \in N_z \cap \{1, 2\}$ ,  $j \notin N_z \cap \{1, 2\}$ , and  $z \in \mathcal{M}$ .

Thus, by (13), one has

$$\begin{aligned} L_1 &= \delta_8 [3 \ 7 \ 3 \ 7 \ 4 \ 8 \ 4 \ 8], \\ L_2 &= \delta_8 [5 \ 7 \ 6 \ 8 \ 5 \ 7 \ 6 \ 8], \\ L_3 &= \delta_8 [1 \ 7 \ 2 \ 8 \ 2 \ 8 \ 2 \ 8]. \end{aligned} \quad (35)$$

Solving (25), we have

$$\begin{aligned} \lambda_1 &= [156.5833 \ 93.8453 \ 130.6051 \ 87.0810 \ 103.0636 \ 51.2119 \ 69.1398 \ 0]^T, \\ \lambda_2 &= [154.2605 \ 96.0248 \ 107.3501 \ 56.5912 \ 154.3603 \ 118.9928 \ 79.4038 \ 0]^T, \\ \lambda_3 &= [186.6039 \ 89.6133 \ 120.7651 \ 45.4087 \ 121.5054 \ 51.2119 \ 93.5792 \ 0]^T \end{aligned} \quad (36)$$

Therefore, it follows from Theorem 9 that the given game is globally stable at  $x_e = \delta_8^8$  in stochastic sense. Figure 2

demonstrates the effective of the calculation of  $\lambda_1$ ,  $\lambda_2$ , and  $\lambda_3$ .

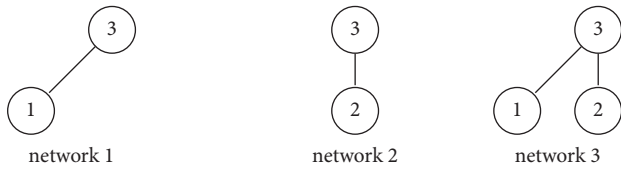


FIGURE 1: The networks.

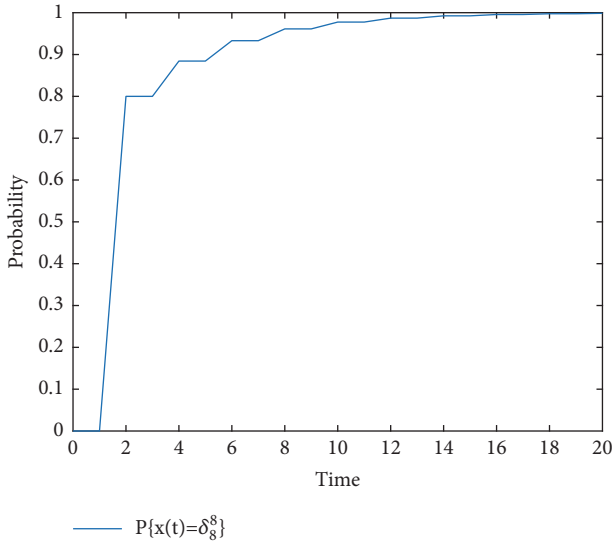


FIGURE 2: The trajectory of the given game.

**5. Conclusion**

This paper has investigated the algebraic formulation and stability analysis for a class of MJNEG. A proper algorithm has been constructed to convert the given MJNEG into an algebraic expression. Based on the above results, the stability of the given game has been analyzed and an equivalent criterion is given. Finally, an interesting example has proved the effectiveness of our results.

In the future work, we could consider the given MJNEG with time delay. Actually, time delay is a very common situation. Many great works in the community of control and engineering have reached towards this kind of systems. See [41–60] for details.

**Data Availability**

No data were used to support this study.

**Conflicts of Interest**

The authors declare that they have no conflicts of interest.

**Acknowledgments**

The research was supported by the Natural Science Foundation of Shandong Province under Grants ZR2018BA001 and ZR2015FQ003, the National Natural Science Foundation of China under Grants 61503225 and 61873150, and the Natural

Science Fund for Distinguished Young Scholars of Shandong Province under Grant JQ201613. The material in this paper was not presented at any conference.

**References**

- [1] M. A. Nowak and R. M. May, “Evolutionary games and spatial chaos,” *Nature*, vol. 359, no. 6398, pp. 826–829, 1992.
- [2] S. R. Gyö and A. C. Toke, “Evolutionary prisoner’s dilemma game on a square lattice,” *Physical Review E*, vol. 58, no. 1, pp. 69–73, 1998.
- [3] D. Cheng, H. Qi, and Z. Li, *Analysis and Control of Boolean Network: A Semi-Tensor Product Approach*, Communications and Control Engineering Series, Springer, London, UK, 2011.
- [4] D. Z. Cheng, H. S. Qi, and Y. Zhao, “Analysis and control of Boolean networks: a matrix semi-tensor product approach,” *Zidonghua Xuebao/Acta Automatica Sinica*, vol. 37, no. 5, pp. 529–540, 2011.
- [5] H. Li, Y. Wang, and L. Xie, “Output tracking control of Boolean control networks via state feedback: Constant reference signal case,” *Automatica*, vol. 59, article 6422, pp. 54–59, 2015.
- [6] H. Li and Y. Wang, “Controllability analysis and control design for switched Boolean networks with state and input constraints,” *SIAM Journal on Control and Optimization*, vol. 53, no. 5, pp. 2955–2979, 2015.
- [7] H. Li, L. Xie, and Y. Wang, “On robust control invariance of Boolean control networks,” *Automatica*, vol. 68, pp. 392–396, 2016.
- [8] H. Li and Y. Wang, “Output tracking of switched Boolean networks under open-loop/closed-loop switching signals,” *Nonlinear Analysis: Hybrid Systems*, vol. 22, pp. 137–146, 2016.
- [9] H. Li, Y. Wang, and P. Guo, “State feedback based output tracking control of probabilistic Boolean networks,” *Information Sciences*, vol. 349/350, pp. 1–11, 2016.
- [10] H. Li and Y. Wang, “Minimum-time state feedback stabilization of constrained Boolean control networks,” *Asian Journal of Control*, vol. 18, no. 5, pp. 1688–1697, 2016.
- [11] G. Zhao, Y. Wang, and H. Li, “Invertibility of higher order  $k$ -valued logical control networks and its application in trajectory control,” *Journal of The Franklin Institute*, vol. 353, no. 17, pp. 4667–4679, 2016.
- [12] H. Li and Y. Wang, “Robust stability and stabilisation of Boolean networks with disturbance inputs,” *International Journal of Systems Science*, vol. 48, no. 4, pp. 750–756, 2017.
- [13] H. Li, P. Song, and Q. Yang, “Pinning control design for robust output tracking of  $k$ -valued logical networks,” *Journal of The Franklin Institute*, vol. 354, no. 7, pp. 3039–3053, 2017.
- [14] H. Li, L. Xie, and Y. Wang, “Output regulation of Boolean control networks,” *Institute of Electrical and Electronics Engineers Transactions on Automatic Control*, vol. 62, no. 6, pp. 2993–2998, 2017.
- [15] H. Li and Y. Wang, “Further results on feedback stabilization control design of Boolean control networks,” *Automatica*, vol. 83, pp. 303–308, 2017.
- [16] X. Ding, H. Li, Q. Yang, Y. Zhou, A. Alsaedi, and F. E. Alsaedi, “Stochastic stability and stabilization of  $n$ -person random evolutionary Boolean games,” *Applied Mathematics and Computation*, vol. 306, pp. 1–12, 2017.
- [17] J. Lu, H. Li, Y. Liu, and F. Li, “Survey on semi-tensor product method with its applications in logical networks and other

- finite-valued systems,” *IET Control Theory & Applications*, vol. 11, no. 13, pp. 2040–2047, 2017.
- [18] H. Li and Y. Wang, “Lyapunov-based stability and construction of Lyapunov functions for Boolean networks,” *SIAM Journal on Control and Optimization*, vol. 55, no. 6, pp. 3437–3457, 2017.
- [19] Y. Zheng, H. Li, X. Ding, and Y. Liu, “Stabilization and set stabilization of delayed Boolean control networks based on trajectory stabilization,” *Journal of The Franklin Institute*, vol. 354, no. 17, pp. 7812–7827, 2017.
- [20] H. Li, G. Zhao, M. Meng, and J. Feng, “A survey on applications of semi-tensor product method in engineering,” *Science China Information Sciences*, vol. 61, no. 1, 010202, 17 pages, 2018.
- [21] Y. Li, W. Dou, H. Li, and X. Liu, “Controllability, Reachability, and Stabilizability of Finite Automata: A Controllability Matrix Method,” *Mathematical Problems in Engineering*, vol. 2018, Article ID 6719319, 6 pages, 2018.
- [22] S. Fu, H. Li, and G. Zhao, “Modelling and strategy optimisation for a kind of networked evolutionary games with memories under the bankruptcy mechanism,” *International Journal of Control*, vol. 91, no. 5, pp. 1104–1117, 2018.
- [23] Y. Li, H. Li, and P. Duan, “Synchronization of switched logical control networks via event-triggered control,” *Journal of The Franklin Institute*, vol. 355, no. 12, pp. 5203–5216, 2018.
- [24] S. Fu, G. Zhao, and H. Li, “Model and control for a class of networked evolutionary games with finite memories and time-varying networks,” *Circuits Systems & Signal Processing*, vol. 37, no. 7, pp. 3093–3114, 2018.
- [25] Y. Li, H. Li, X. Ding, and G. Zhao, “Leader-follower consensus of multi-agent systems with time delays over finite fields,” *IEEE Transactions on Cybernetics*, 2018.
- [26] Y. Li, H. Li, and W. Sun, “Event-triggered control for robust set stabilization of logical control networks,” *Automatica*, vol. 95, pp. 556–560, 2018.
- [27] Y. Li, H. Li, and X. Xu, “A semi-tensor product approach to minimal-agent consensus control of networked evolutionary games,” *IET Control Theory Applications*, pp. 10–1049, 2018.
- [28] G. Zhao and S. Fu, “Matrix approach to trajectory control of higher-order  $k$ -valued logical control networks,” *IET Control Theory & Applications*, vol. 11, no. 13, pp. 2110–2115, 2017.
- [29] G. Zhao, H. Li, W. Sun, and F. . Alsaadi, “Modelling and strategy consensus for a class of networked evolutionary games,” *International Journal of Systems Science*, vol. 49, no. 12, pp. 2548–2557, 2018.
- [30] P. Guo, Y. Wang, and H. Li, “Algebraic formulation and strategy optimization for a class of evolutionary networked games via semi-tensor product method,” *Automatica*, vol. 49, no. 11, pp. 3384–3389, 2013.
- [31] D. Cheng, F. He, H. Qi, and T. Xu, “Modeling, analysis and control of networked evolutionary games,” *Institute of Electrical and Electronics Engineers Transactions on Automatic Control*, vol. 60, no. 9, pp. 2402–2415, 2015.
- [32] G. Zhao and Y. Wang, “Formulation and optimization control of a class of networked evolutionary games with switched topologies,” *Nonlinear Analysis: Hybrid Systems*, vol. 22, pp. 98–107, 2016.
- [33] B. Zhu, X. Xia, and Z. Wu, “Evolutionary game theoretic demand-side management and control for a class of networked smart grid,” *Automatica*, vol. 70, pp. 94–100, 2016.
- [34] P. Guo, H. Zhang, F. E. Alsaadi, and T. Hayat, “Semi-tensor product method to a class of event-triggered control for finite evolutionary networked games,” *IET Control Theory & Applications*, vol. 11, no. 13, pp. 2140–2145, 2017.
- [35] I. Kordonis and G. P. Papavassilopoulos, “LQ Nash games with random entrance: an infinite horizon major player and minor players of finite horizons,” *Institute of Electrical and Electronics Engineers Transactions on Automatic Control*, vol. 60, no. 6, pp. 1486–1500, 2015.
- [36] G. P. Papavassilopoulos, “University-students game,” *Dynamic Games and Applications*, vol. 3, no. 3, pp. 387–418, 2013.
- [37] H. Li, Y. Wang, and Z. Liu, “A semi-tensor product approach to pseudo-BOOlean functions with application to BOOlean control networks,” *Asian Journal of Control*, vol. 16, no. 4, pp. 1073–1081, 2014.
- [38] G. Ellison, “Learning, local interaction, and coordination,” *Econometrica*, vol. 61, no. 5, pp. 1047–1071, 1993.
- [39] X. Chen, J. Lam, P. Li, and Z. Shu, “ $l_1$ -induced norm and controller synthesis of positive systems,” *Automatica*, vol. 49, no. 5, pp. 1377–1385, 2013.
- [40] G. Zhao, Y. Wang, and H. Li, “A matrix approach to modeling and optimization for dynamic games with random entrance,” *Applied Mathematics and Computation*, vol. 290, pp. 9–20, 2016.
- [41] X. Li and J. Wu, “Stability of nonlinear differential systems with state-dependent delayed impulses,” *Automatica*, vol. 64, pp. 63–69, 2016.
- [42] X. Li and S. Song, “Stabilization of Delay Systems: delay-dependent Impulsive Control,” *IEEE Transactions on Automatic Control*, vol. 62, no. 1, pp. 406–411, 2017.
- [43] X. Zhang and X. Li, “Input-to-state stability of non-linear systems with distributed-delayed impulses,” *IET Control Theory & Applications*, vol. 11, no. 1, pp. 81–89, 2017.
- [44] R. Rakkiyappan, G. Velmurugan, X. Li, and D. O’Regan, “Global dissipativity of memristor-based complex-valued neural networks with time-varying delays,” *Neural Computing and Applications*, vol. 27, no. 3, pp. 629–649, 2016.
- [45] X. Li, X. Zhang, and S. Song, “Effect of delayed impulses on input-to-state stability of nonlinear systems,” *Automatica*, vol. 76, pp. 378–382, 2017.
- [46] X. Li and J. Cao, “An impulsive delay inequality involving unbounded time-varying delay and applications,” *Institute of Electrical and Electronics Engineers Transactions on Automatic Control*, vol. 62, no. 7, pp. 3618–3625, 2017.
- [47] X. Li and J. Wu, “Sufficient stability conditions of nonlinear differential systems under impulsive control with state-dependent delay,” *Institute of Electrical and Electronics Engineers Transactions on Automatic Control*, vol. 63, no. 1, pp. 306–311, 2018.
- [48] X. Li and Y. Ding, “Razumikhin-type theorems for time-delay systems with Persistent impulses,” *Systems & Control Letters*, vol. 107, pp. 22–27, 2017.
- [49] J. Hu, G. Sui, S. Du, and X. Li, “Finite-Time Stability of Uncertain Nonlinear Systems with Time-Varying Delay,” *Mathematical Problems in Engineering*, vol. 2017, Article ID 2538904, 9 pages, 2017.
- [50] X. Zhang, X. Lv, and X. Li, “Sampled-data-based lag synchronization of chaotic delayed neural networks with impulsive control,” *Nonlinear Dynamics*, vol. 90, no. 3, pp. 2199–2207, 2017.
- [51] X. Lv and X. Li, “Finite time stability and controller design for nonlinear impulsive sampled-data systems with applications,” *ISA Transactions*, vol. 70, pp. 30–36, 2017.
- [52] E. A. Alzahrani, H. Akca, and X. Li, “New synchronization schemes for delayed chaotic neural networks with impulses,” *Neural Computing and Applications*, vol. 28, no. 9, pp. 2823–2837, 2017.

- [53] H. Zhang, R. Ye, J. Cao, A. Ahmed, X. Li, and Y. Wan, "Lyapunov Functional Approach to Stability Analysis of Riemann-Liouville Fractional Neural Networks with Time-Varying Delays," *Asian Journal of Control*, vol. 20, no. 5, pp. 1938–1951, 2018.
- [54] X. Li, P. Li, and Q. Wang, "Input/output-to-state stability of impulsive switched systems," *Systems Control Letters*, p. 116, 2018.
- [55] X. Yang, X. Li, and J. Cao, "Robust finite-time stability of singular nonlinear systems with interval time-varying delay," *Journal of The Franklin Institute*, vol. 355, no. 3, pp. 1241–1258, 2018.
- [56] X. Tan, J. Cao, X. Li, and A. Alsaedi, "Leader-following mean square consensus of stochastic multi-agent systems with input delay via event-triggered control," *IET Control Theory & Applications*, vol. 12, no. 2, pp. 299–309, 2018.
- [57] X. Tan, J. Cao, and X. Li, "Consensus of Leader-Following Multiagent Systems: A Distributed Event-Triggered Impulsive Control Strategy," *IEEE Transactions on Cybernetics*, 2018.
- [58] X. Lv, R. Rakkiyappan, and X. Li, " $\mu$ -stability criteria for nonlinear differential systems with additive leakage and transmission time-varying delays," *Nonlinear Analysis: Modelling and Control*, vol. 23, no. 3, pp. 380–400, 2018.
- [59] Y. Wang, J. Cao, X. Li, and A. Alsaedi, "Edge-based epidemic dynamics with multiple routes of transmission on random networks," *Nonlinear Dynamics*, vol. 91, no. 1, pp. 403–420, 2018.
- [60] B. S. Vadivoo, R. Ramachandran, J. Cao, H. Zhang, and X. Li, "Controllability analysis of nonlinear neutral-type fractional-order differential systems with state delay and impulsive effects," *International Journal of Control, Automation and Systems*, pp. 1–11, 2018.

## Research Article

# Exponential Stability of Antiperiodic Solution for BAM Neural Networks with Time-Varying Delays

Xiaofei Li <sup>1</sup>, Chuan Qin <sup>2</sup>, and Quanxin Zhu <sup>3</sup>

<sup>1</sup>School of Information and Mathematics, Yangtze University, Jingzhou 434023, Hubei, China

<sup>2</sup>College of Technology and Engineering, Yangtze University, Jingzhou 434020, Hubei, China

<sup>3</sup>College of Mathematics and Statistics, Hunan Normal University, Changsha 410081, Hunan, China

Correspondence should be addressed to Quanxin Zhu; zqx22@126.com

Received 10 September 2018; Accepted 4 November 2018; Published 14 November 2018

Academic Editor: Ju H. Park

Copyright © 2018 Xiaofei Li et al. This is an open access article distributed under the Creative Commons Attribution License, which permits unrestricted use, distribution, and reproduction in any medium, provided the original work is properly cited.

In this paper, a kind of BAM neural networks with leakage delays in the negative feedback terms and time-varying delays in activation functions was considered. By constructing a suitable Lyapunov function and using inequality techniques, some sufficient conditions to ensure the existence and exponential stability of antiperiodic solutions of these neural networks were derived. These conditions extend some results recently appearing in recent papers. Lastly, an example is given to show the feasibility of these conditions.

## 1. Introduction

It is known that neural networks have been applied in numerous fields, such as pattern recognition, classification, associative memory, optimization, signal and image processing, parallel computation, and nonlinear optimization problems. Up to now, there are many works focusing on the dynamical nature of various kinds of neural networks, such as stability, periodic solution, almost periodic solution, bifurcation, and chaos (see [1–11]). However, since significant time delays are ubiquitous, it is necessary to introduce delays into communication channels which leads to delayed neural networks models. Kosko [12] proposed a new kind of neural networks named bidirectional associative memory (BAM) neural networks with time delays which was given by the following:

$$\begin{aligned} \frac{dx_i(t)}{dt} &= -a_i x_i(t) + \sum_{j=1}^m a_{ji} f_j(y_j(t - \sigma_{ji}(t))) + I_i, \\ \frac{dy_i(t)}{dt} &= -b_i y_i(t) + \sum_{j=1}^m b_{ji} g_j(x_j(t - \tau_{ji}(t))) + J_i, \end{aligned} \quad (1)$$

where  $i = 1, \dots, m$ ,  $m$  is the number of neurons in layers. In model (1),  $x_i$  and  $y_i$  stand for the activations of  $i$ th neurons;

positive constants  $a_i$  and  $b_i$  represent the rate with which the  $i$ th neuron will reset its potential to the resting state in isolation when they are disconnected from the network and the external inputs at time  $t$ ; time delays  $\tau_{ji}(t)$  and  $\sigma_{ji}(t)$  are nonnegative functions; and  $I_i$  and  $J_i$  denote the components of external input source introduced from outside the network. *The authors in this paper applied this model to image processing.*

There are many papers about BAM neural networks and stochastic BAM neural networks; for details, see [13–18]. *It is known that the existence-uniqueness and stability is an important theoretical problem in the field of dynamics systems and one can find this topic in these papers [19–22].* Always, leakage delays appear in the negative feedback term of neural networks. Based on this, Gopalsmay [23] proposed the following BAM neural networks and studied the stability of the equilibrium and periodic solutions

$$\begin{aligned} \frac{dx_i(t)}{dt} &= -a_i x_i(t - \delta_{1i}) + \sum_{j=1}^m a_{ji} f_j(y_j(t - \sigma_{ji})) + I_i, \\ \frac{dy_i(t)}{dt} &= -b_i y_i(t - \delta_{2i}) + \sum_{j=1}^m b_{ji} g_j(x_j(t - \tau_{ji})) + J_i. \end{aligned} \quad (2)$$

In this system, time delays  $\delta_{1i}$  and  $\delta_{2i}$  are positive constants, where  $i = 1, \dots, m$ . By constructing Lyapunov-Kravsovskii functionals, using inequalities and  $M$ -matrices technology, the author gave two sets of delay dependent sufficient conditions on the existence of a unique equilibrium as well as its asymptotic and exponential stability to system (2). Because of time-varying delays in the real world, Liu [24] proposed the following BAM neural networks and discussed the global exponential stability of the network:

$$\begin{aligned} \frac{dx_i(t)}{dt} &= -a_i x_i(t - \delta_{1i}) + \sum_{j=1}^m a_{ij} f_j(y_j(t - \sigma_{ji}(t))) \\ &\quad + I_i, \\ \frac{dy_i(t)}{dt} &= -b_i y_i(t - \delta_{2i}) + \sum_{j=1}^m b_{ij} g_j(x_j(t - \tau_{ji}(t))) \\ &\quad + J_i. \end{aligned} \quad (3)$$

By constructing a Lyapunov functional, some sufficient conditions on the global exponential stability of the equilibrium for system (3) were established. There are few papers considering the variable external input. It is significative to consider time-varying delays and external input in neural networks.

Recently, Li et al. [25] considered the following BAM neural networks with time-varying external input:

$$\begin{aligned} \frac{dx_i(t)}{dt} &= -a_i x_i(t) + \sum_{j=1}^m s_{ji}(t) f_j[x_j(t), y_j(t - \tau_{ji})] \\ &\quad + I_i(t), \\ \frac{dy_i(t)}{dt} &= -b_i y_i(t) + \sum_{j=1}^m t_{ji}(t) g_j[x_j(t - \delta_{ji}), y_j(t)] \\ &\quad + J_i(t). \end{aligned} \quad (4)$$

To the best of our knowledge, there are few papers focusing on the existence and stability of antiperiodic solution to BAM neural networks with time-varying delays in the leakage terms in the negative feedback term. Motivated by the above discussions, in this paper, we propose a kind of BAM neural networks with time-varying delays and external input as follows:

$$\begin{aligned} \frac{dx_i(t)}{dt} &= -a_i x_i(t - \delta_i(t)) + \sum_{j=1}^m a_{ji}(t) f_j(x_j(t)) \\ &\quad + \sum_{j=1}^m b_{ji}(t) g_j(y_j(t - \tau_{ji}(t))) + I_i(t), \\ \frac{dy_i(t)}{dt} &= -b_i y_i(t - \sigma_i(t)) + \sum_{j=1}^m s_{ji}(t) h_j(y_j(t)) \\ &\quad + \sum_{j=1}^m t_{ji}(t) \varphi_j(x_j(t - \xi_{ji}(t))) + J_i(t). \end{aligned} \quad (5)$$

We can easily find that model (5) extends the above models. In model (5), we consider the time-varying leakage delays in negative feedback terms and time-varying delays in activation functions. And the activation functions in model (5) are more general. If the parameters  $\delta_i(t)$  are all equal to 0, then model (5) will deduce to special model in (4). And if  $\delta_i(t)$  are all constants, then model (5) will extend the models in (2) and (3). Therefore, it is important to investigate the stability of model (5). In this paper, by constructing a suitable Lyapunov functional, we give some sufficient conditions to ensure the existence and global exponential stability of antiperiodic solutions of system (5).

The rest of this paper is organized as follows. In Section 2, we introduce some notations and give some lemmas. In Section 3, we obtain some sufficient conditions on the existence and global exponential stability of antiperiodic solution of system (5). In Section 4, we give some examples to illustrate the efficiency. In Section 5, some conclusions are given.

## 2. Notations and Preliminary Results

First, we give some notations. We denote

$$\begin{aligned} \delta_i^+ &= \sup_{t \in \mathbb{R}} \delta_i(t), \\ a_{ji}^+ &= \sup_{t \in \mathbb{R}} a_{ji}(t), \\ b_{ji}^+ &= \sup_{t \in \mathbb{R}} b_{ji}(t), \\ \tau_{ji}^+ &= \sup_{t \in \mathbb{R}} \tau_{ji}(t), \\ I_i^+ &= \sup_{t \in \mathbb{R}} I_i(t), \\ \sigma_i^+ &= \sup_{t \in \mathbb{R}} \sigma_i(t), \\ s_{ji}^+ &= \sup_{t \in \mathbb{R}} s_{ji}(t), \\ t_{ji}^+ &= \sup_{t \in \mathbb{R}} t_{ji}(t), \\ \xi_{ji}^+ &= \sup_{t \in \mathbb{R}} \xi_{ji}(t), \\ J_i^+ &= \sup_{t \in \mathbb{R}} J_i(t). \end{aligned} \quad (6)$$

For vector  $U = (u_1, \dots, u_m)^T$  and matrix  $M = (m_{ij})_{m \times m}$ , we define the following norms:

$$\begin{aligned} \|U\| &= \left( \sum_{i=1}^m u_i^2 \right)^{1/2}, \\ \|M\| &= \left( \sum_{i,j=1}^m m_{ij}^2 \right)^{1/2}, \end{aligned} \quad (7)$$

respectively. For

$$\begin{aligned} \phi(s) &= (\phi_1(s), \dots, \phi_m(s))^T, \\ \phi_i(s) &\in C([-\delta, 0], R), \quad i = 1, \dots, m, \\ \psi(s) &= (\psi_1(s), \dots, \psi_m(s))^T, \\ \psi_i(s) &\in C([-\tau, 0], R), \quad i = 1, \dots, m, \end{aligned} \quad (8)$$

where  $\delta = \max_{1 \leq i, j \leq m} \{\delta_i^+, \xi_{ji}^+\}$ ,  $\tau = \max_{1 \leq i, j \leq m} \{\sigma_i^+, \tau_{ji}^+\}$ , we denote

$$\begin{aligned} \|\phi\| &= \sup_{-\delta \leq s \leq 0} \left( \sum_{i=1}^m |\phi_i(s)|^2 \right)^{1/2}, \\ \|\psi\| &= \sup_{-\tau \leq s \leq 0} \left( \sum_{i=1}^m |\psi_i(s)|^2 \right)^{1/2}. \end{aligned} \quad (9)$$

The initial conditions of the system (5) are given by

$$\begin{aligned} x_{i0}(s) &= \phi_i(s), \quad -\delta \leq s \leq 0, \\ y_{i0}(s) &= \psi_i(s), \quad -\tau \leq s \leq 0. \end{aligned} \quad (10)$$

Let  $(x(t), y(t))^T$  be the solution of system (5) with initial conditions (10), where  $x(t) = (x_1(t), \dots, x_m(t))^T$ ,  $y(t) = (y_1(t), \dots, y_m(t))^T$ . We say the solution  $(x(t), y(t))^T$  is  $T$ -antiperiodic if  $x_i(t+T) = -x_i(t)$ ,  $y_i(t+T) = -y_i(t)$  ( $i = 1, \dots, m$ ) for all  $t \in R$ , where  $T$  is a positive constant.

Throughout this paper, we assume that the following conditions hold.

(H1) For  $f_j, g_j, h_j, \varphi_j \in C(R, R)$ ,  $j = 1, \dots, m$ , there exist positive constants  $L_{jf}, L_{jg}, L_{jh}, L_{j\varphi}$  and  $M_{jf}, M_{jg}, M_{jh}, M_{j\varphi}$  such that

$$\begin{aligned} |f_j(u) - f_j(v)| &\leq L_{jf} |u - v|, \\ |f_j(u)| &\leq M_{jf}, \\ |g_j(u) - g_j(v)| &\leq L_{jg} |u - v|, \\ |g_j(u)| &\leq M_{jg}, \\ |h_j(u) - h_j(v)| &\leq L_{jh} |u - v|, \\ |h_j(u)| &\leq M_{jh}, \\ |\varphi_j(u) - \varphi_j(v)| &\leq L_{j\varphi} |u - v|, \\ |\varphi_j(u)| &\leq M_{j\varphi}. \end{aligned} \quad (11)$$

for all  $u, v \in R$ .

(H2) For all  $t, u \in R$ ,

$$\begin{aligned} a_{ji}(t+T) f_j(u) &= -a_{ji}(t) f_j(-u), \\ b_{ji}(t+T) g_j(u) &= -b_{ji}(t) g_j(-u), \\ s_{ji}(t+T) h_j(u) &= -s_{ji}(t) h_j(-u), \\ t_{ji}(t+T) \varphi_j(u) &= -t_{ji}(t) \varphi_j(-u), \\ I_i(t+T) &= -I_i(t), \\ J_i(t+T) &= -J_i(t), \\ \delta_i(t+T) &= \delta_i(t), \\ \sigma_i(t+T) &= \sigma_i(t), \end{aligned} \quad (12)$$

where  $i, j = 1, \dots, m$  and  $T$  is a positive constant.

**Definition 1.** The solution  $(x^*(t), y^*(t))^T$  of system (5) is said to be globally exponentially stable if there exist constants  $\beta > 0$  and  $M > 1$  such that

$$\begin{aligned} \sum_{i=1}^m |x_i(t) - x_i^*(t)|^2 + \sum_{i=1}^m |y_i(t) - y_i^*(t)|^2 \\ \leq M e^{-\beta t} [\|\phi - \phi^*\|^2 + \|\psi - \psi^*\|^2] \end{aligned} \quad (13)$$

for each solution  $(x(t), y(t))^T$  of system (5).

**Lemma 2** (see [25]). *Let*

$$\begin{aligned} A &= \begin{pmatrix} -a_i & 0 \\ 0 & -b_j \end{pmatrix}, \\ \alpha &= \min_{1 \leq i, j \leq m} \{a_i, b_j\}, \end{aligned} \quad (14)$$

and then

$$\|\exp At\| \leq \sqrt{2} e^{-\alpha t}, \quad \forall t \geq 0. \quad (15)$$

**Lemma 3.** *Suppose that (H3)*

$$\begin{aligned} -2a_i + 2a_i^2 \delta_i^+ + t_{ji}^+ L_{j\varphi}^{2(1-\zeta_j)} \\ + (a_i \delta_i^+ + 1) \left( \sum_{j=1}^m b_{ji}^+ L_{jg}^{2\xi_j} + \sum_{j=1}^m a_{ji}^+ (L_{jf}^{2\xi_j} + L_{jf}^{2(1-\xi_j)}) \right) \\ + \sum_{j=1}^m b_i \sigma_i^+ t_{ji}^+ L_{j\varphi}^{2(1-\zeta_j)} < 0, \\ -2b_i + 2b_i^2 \sigma_i^+ + b_{ji}^+ L_{jg}^{2(1-\xi_j)} \\ + (b_i \sigma_i^+ + 1) \left( \sum_{j=1}^m t_{ji}^+ L_{j\varphi}^{2\zeta_j} + \sum_{j=1}^m s_{ji}^+ (L_{jh}^{2\zeta_j} + L_{jh}^{2(1-\zeta_j)}) \right) \\ + \sum_{j=1}^m a_i \delta_i^+ b_{ji}^+ L_{jg}^{2(1-\xi_j)} < 0, \end{aligned} \quad (16)$$

where  $0 \leq \xi_j, \varsigma_j < 1 (j = 1, \dots, m)$  are any constants. Then there exists  $\beta > 0$  such that

$$\begin{aligned} & \beta - 2a_i + a_i^2 \delta_i^+ \left( e^{\beta \delta_i^+} + 1 \right) + t_{ji}^+ L_{j\varphi}^{2(1-\varsigma_j)} e^{\beta \xi_{ji}^+} \\ & + (a_i \delta_i^+ + 1) \left( \sum_{j=1}^m b_{ji}^+ L_{jg}^{2\xi_j} + \sum_{j=1}^m a_{ji}^+ \left( L_{jf}^{2\xi_j} + L_{jf}^{2(1-\xi_j)} \right) \right) \\ & + \sum_{j=1}^m b_i \sigma_i^+ t_{ji}^+ L_{j\varphi}^{2(1-\varsigma_j)} e^{\beta \xi_{ji}^+} \leq 0, \\ & \beta - 2b_i + b_i^2 \sigma_i^+ \left( e^{\beta \sigma_i^+} + 1 \right) + b_{ji}^+ L_{jg}^{2(1-\xi_j)} e^{\beta \tau_{ji}^+} \\ & + (b_i \sigma_i^+ + 1) \left( \sum_{j=1}^m t_{ji}^+ L_{j\varphi}^{2\varsigma_j} + \sum_{j=1}^m s_{ji}^+ \left( L_{jh}^{2\varsigma_j} + L_{jh}^{2(1-\varsigma_j)} \right) \right) \\ & + \sum_{j=1}^m a_i \delta_i^+ t_{ji}^+ L_{jg}^{2(1-\xi_j)} e^{\beta \tau_{ji}^+} \leq 0. \end{aligned} \quad (17)$$

*Proof.* Let

$$\begin{aligned} \varrho_{1i}(\beta) &= \beta - 2a_i + a_i^2 \delta_i^+ \left( e^{\beta \delta_i^+} + 1 \right) + t_{ji}^+ L_{j\varphi}^{2(1-\varsigma_j)} e^{\beta \xi_{ji}^+} \\ & + (a_i \delta_i^+ + 1) \left( \sum_{j=1}^m b_{ji}^+ L_{jg}^{2\xi_j} + \sum_{j=1}^m a_{ji}^+ \left( L_{jf}^{2\xi_j} + L_{jf}^{2(1-\xi_j)} \right) \right) \\ & + \sum_{j=1}^m b_i \sigma_i^+ t_{ji}^+ L_{j\varphi}^{2(1-\varsigma_j)} e^{\beta \xi_{ji}^+}, \\ \varrho_{2i}(\beta) &= \beta - 2b_i + b_i^2 \sigma_i^+ \left( e^{\beta \sigma_i^+} + 1 \right) + b_{ji}^+ L_{jg}^{2(1-\xi_j)} e^{\beta \tau_{ji}^+} \\ & + (b_i \sigma_i^+ + 1) \left( \sum_{j=1}^m t_{ji}^+ L_{j\varphi}^{2\varsigma_j} + \sum_{j=1}^m s_{ji}^+ \left( L_{jh}^{2\varsigma_j} + L_{jh}^{2(1-\varsigma_j)} \right) \right) \\ & + \sum_{j=1}^m a_i \sigma_i^+ b_{ji}^+ L_{jg}^{2(1-\xi_j)} e^{\beta \tau_{ji}^+}. \end{aligned}$$

Clearly,  $\varrho_{1i}(\beta), \varrho_{2i}(\beta) (i = 1, \dots, m)$  are continuously differential functions and satisfy that

$$\begin{aligned} \frac{d\varrho_{1i}(\beta)}{d\beta} &> 0, \\ \lim_{\beta \rightarrow +\infty} \varrho_{1i}(\beta) &= +\infty, \end{aligned}$$

$$\varrho_{1i}(0) < 0,$$

$$\frac{d\varrho_{2i}(\beta)}{d\beta} > 0,$$

$$\lim_{\beta \rightarrow +\infty} \varrho_{2i}(\beta) = +\infty,$$

$$\varrho_{2i}(0) < 0.$$

(19)

According to the intermediate value theorem, it is clear that there exist constants  $\beta_i > 0, \beta_i^* > 0$  such that

$$\varrho_{1i}(\beta_i) = 0,$$

$$\varrho_{2i}(\beta_i^*) = 0,$$

(20)

$$i = 1, \dots, m.$$

Let  $\beta_0 = \min\{\beta_1, \dots, \beta_m, \beta_1^*, \dots, \beta_m^*\}$ ; then it follows that  $\beta_0 > 0$  and

$$\varrho_{1i}(\beta_0) \leq 0,$$

$$\varrho_{2i}(\beta_0) \leq 0,$$

(21)

$$i = 1, \dots, m.$$

The proof of Lemma 3 is complete.  $\square$

(18) **Lemma 4.** Suppose that (H1) holds true. Then, for any solution  $(x(t), y(t))^T$  of system (5), there exists a constant

$$\begin{aligned} \gamma &= \left[ 1 - \frac{\sqrt{2}}{\alpha} (a_i^2 \delta_i^+ + b_i^2 \sigma_i^+) \right]^{-1} \left[ \sqrt{2} (\|\phi\|^2 + \|\psi\|^2) \right. \\ & + \frac{\sqrt{2}}{\alpha} \left( a_i \delta_i^+ \sum_{j=1}^m a_{ji}^+ M_{jf} + a_i \delta_i^+ \sum_{j=1}^m b_{ji}^+ M_{jg} + a_i \delta_i^+ I_i^+ \right. \\ & + \sum_{j=1}^m a_{ji}^+ M_{jf} + \sum_{j=1}^m b_{ji}^+ M_{jg} + I_i^+ + b_i \sigma_i^+ \sum_{j=1}^m s_{ji}^+ M_{jh} \\ & + b_i \sigma_i^+ \sum_{j=1}^m t_{ji}^+ M_{j\varphi} + b_i \sigma_i^+ J_i^+ + \sum_{j=1}^m s_{ji}^+ M_{jh} + \sum_{j=1}^m t_{ji}^+ M_{j\varphi} \\ & \left. \left. + J_i^+ \right) \right], \end{aligned} \quad (22)$$

such that

$$\begin{aligned} |x_i(t)| &\leq \gamma, \\ |y_i(t)| &\leq \gamma, \\ i &= 1, \dots, m, \quad \forall t > 0. \end{aligned} \quad (23)$$

*Proof.* From system (5), we conclude that

$$\begin{aligned} \frac{dx_i(t)}{dt} &= -a_i x_i(t) + a_i \int_{t-\delta_i(t)}^t \left[ -a_i x_i(s - \delta_i(s)) \right. \\ &+ \sum_{j=1}^m a_{ji}(s) f_j(x_j(s)) \\ &+ \sum_{j=1}^m b_{ji}(s) g_j(y_j(s - \tau_{ji}(s))) + I_i(s) \left. \right] ds \\ &+ \sum_{j=1}^m a_{ji}(t) f_j(x_j(t)) + \sum_{j=1}^m b_{ji}(t) \\ &\cdot g_j(y_j(t - \tau_{ji}(t))) + I_i(t), \\ \frac{dy_i(t)}{dt} &= -b_i y_i(t) + b_i \int_{t-\sigma_i(t)}^t \left[ -b_i y_i(s - \sigma_i(s)) \right. \\ &+ \sum_{j=1}^m s_{ji}(s) h_j(y_j(s)) \\ &+ \sum_{j=1}^m t_{ji}(s) \varphi_j(x_j(s - \sigma_{ji}(s))) + J_i(s) \left. \right] ds \\ &+ \sum_{j=1}^m s_{ji}(t) h_j(y_j(t)) + \sum_{j=1}^m t_{ji}(t) \\ &\cdot \varphi_j(x_j(t - \xi_{ji}(t))) + J_i(t). \end{aligned} \quad (24)$$

Let

$$\begin{aligned} z_{ii}(t) &= \begin{pmatrix} x_i(t) \\ y_i(t) \end{pmatrix}, \\ A &= \begin{pmatrix} -a_i & 0 \\ 0 & -b_i \end{pmatrix}, \\ B_{ii}(t) &= \begin{pmatrix} I_i(t) \\ J_i(t) \end{pmatrix}, \end{aligned}$$

$$F(x_i(t), y_i(t)) = \begin{pmatrix} f_1(x_i(t), y_i(t)) \\ f_2(x_i(t), y_i(t)) \end{pmatrix}, \quad (25)$$

where

$$\begin{aligned} f_1(x_i(t), y_i(t)) &= a_i \int_{t-\delta_i(t)}^t \left[ -a_i x_i(s - \delta_i(s)) \right. \\ &+ \sum_{j=1}^m a_{ji}(s) f_j(x_j(s)) \\ &+ \sum_{j=1}^m b_{ji}(s) g_j(y_j(s - \tau_{ji}(s))) + I_i(s) \left. \right] ds \\ &+ \sum_{j=1}^m a_{ji}(t) f_j(x_j(t)) + \sum_{j=1}^m b_{ji}(t) \\ &\cdot g_j(y_j(t - \tau_{ji}(t))), \\ f_2(x_i(t), y_i(t)) &= b_i \int_{t-\sigma_i(t)}^t \left[ -b_i y_i(s - \sigma_i(s)) \right. \\ &+ \sum_{j=1}^m s_{ji}(s) h_j(y_j(s)) \\ &+ \sum_{j=1}^m t_{ji}(s) \varphi_j(x_j(s - \sigma_{ji}(s))) + J_i(s) \left. \right] ds \\ &+ \sum_{j=1}^m s_{ji}(t) h_j(y_j(t)) + \sum_{j=1}^m t_{ji}(t) \\ &\cdot \varphi_j(x_j(t - \xi_{ji}(t))), \end{aligned} \quad (26)$$

and then system (5) has the following form:

$$z'_{ii}(t) \leq A z_{ii}(t) + F(x_i(t), y_i(t)) + B_{ii}(t). \quad (27)$$

By (27), we get

$$\begin{aligned} z_{ii}(t) &\leq e^{At} z_{ii}(0) \\ &+ \int_0^t e^{A(t-s)} [F(x_i(s), y_j(s)) + B_{ii}(s)] ds. \end{aligned} \quad (28)$$

In view of Lemma 2, we have

$$\begin{aligned}
& \|z_{ii}(t)\| \leq \sqrt{2}e^{-\alpha t} \|z_{ii}(0)\| \\
& + \sqrt{2} \int_0^t e^{-\alpha(t-s)} [\|F(x_i(s), y_i(s))\| \\
& + \|B_{ii}(s)\|] ds \leq \sqrt{2} (\|\phi\|^2 + \|\psi\|^2) + \frac{\sqrt{2}}{\alpha} (1 \\
& - e^{-\alpha t}) \left[ a_i \delta_i^+ \left( a_i |x_i(t - \delta_i(t))| + \sum_{j=1}^m a_{ji}^+ M_{jf} \right. \right. \\
& \left. \left. + \sum_{j=1}^m b_{ji}^+ M_{jg} + I_i^+ \right) + \sum_{j=1}^m a_{ji}^+ M_{jf} + \sum_{j=1}^m b_{ji}^+ M_{jg} + I_i^+ \right. \\
& \left. + b_i \sigma_i^+ \left( b_i |y_i(t - \sigma_i(t))| + \sum_{j=1}^m s_{ji}^+ M_{jh} + \sum_{j=1}^m t_{ji}^+ M_{j\varphi} \right. \right. \\
& \left. \left. + J_i^+ \right) + \sum_{j=1}^m s_{ji}^+ M_{jh} + \sum_{j=1}^m t_{ji}^+ M_{j\varphi} + J_i^+ \right] \leq \sqrt{2} (\|\phi\|^2 \quad (29) \\
& + \|\psi\|^2) + \frac{\sqrt{2}}{\alpha} \left[ a_i^2 \delta_i^+ \|z_{ii}(t)\| + a_i \delta_i^+ \sum_{j=1}^m a_{ji}^+ M_{jf} \right. \\
& \left. + a_i \delta_i^+ \sum_{j=1}^m b_{ji}^+ M_{jg} + a_i \delta_i^+ I_i^+ + \sum_{j=1}^m a_{ji}^+ M_{jf} + \sum_{j=1}^m b_{ji}^+ M_{jg} \right. \\
& \left. + I_i^+ + b_i^2 \sigma_i^+ \|z_{ii}(t)\| + b_i \sigma_i^+ \sum_{j=1}^m s_{ji}^+ M_{jh} \right. \\
& \left. + b_i \sigma_i^+ \sum_{j=1}^m t_{ji}^+ M_{j\varphi} + b_i \sigma_i^+ J_i^+ + \sum_{j=1}^m s_{ji}^+ M_{jh} + \sum_{j=1}^m t_{ji}^+ M_{j\varphi} \right. \\
& \left. + J_i^+ \right].
\end{aligned}$$

Let

$$\begin{aligned}
\gamma & = \left[ 1 - \frac{\sqrt{2}}{\alpha} (a_i^2 \delta_i^+ + b_i^2 \sigma_i^+) \right]^{-1} \left[ \sqrt{2} (\|\phi\|^2 + \|\psi\|^2) \right. \\
& \left. + \frac{\sqrt{2}}{\alpha} \left( a_i \delta_i^+ \sum_{j=1}^m a_{ji}^+ M_{jf} + a_i \delta_i^+ \sum_{j=1}^m b_{ji}^+ M_{jg} + a_i \delta_i^+ I_i^+ \right. \right. \\
& \left. \left. + \sum_{j=1}^m a_{ji}^+ M_{jf} + \sum_{j=1}^m b_{ji}^+ M_{jg} + I_i^+ + b_i \sigma_i^+ \sum_{j=1}^m s_{ji}^+ M_{jh} \right. \right. \quad (30) \\
& \left. \left. + b_i \sigma_i^+ \sum_{j=1}^m t_{ji}^+ M_{j\varphi} + b_i \sigma_i^+ J_i^+ + \sum_{j=1}^m s_{ji}^+ M_{jh} + \sum_{j=1}^m t_{ji}^+ M_{j\varphi} \right. \right. \\
& \left. \left. + J_i^+ \right) \right],
\end{aligned}$$

and it follows from (29) that  $\|z_{ii}(t)\| \leq \gamma$ . That is,  $|x_i(t)| \leq \gamma$  and  $|y_i(t)| \leq \gamma$ . This completes the proof of Lemma 4.  $\square$

### 3. Main Results

In this section, we give our main results for system (5).

**Theorem 5.** Suppose that (H1)-(H3) are satisfied. Then any solution  $(x^*(t), y^*(t))^T$  of system (5) is globally exponentially stable.

*Proof.* First, we denote  $u_i(t) = x_i(t) - x_i^*(t)$ ,  $v_i(t) = y_i(t) - y_i^*(t)$ ,  $i = 1, \dots, m$ . By system (5), we have

$$\begin{aligned}
\frac{du_i(t)}{dt} & = -a_i u_i(t) + a_i \int_{t-\delta_i(t)}^t \left[ -a_i u_i(s - \delta_i(s)) \right. \\
& \left. + \sum_{j=1}^m a_{ji}(s) (f_j(x_j(s)) - f_j(x_j^*(s))) + \sum_{j=1}^m b_{ji}(s) \right. \\
& \cdot (g_j(y_j(s - \tau_{ji}(s)))) \\
& \left. - g_j(y_j^*(s - \tau_{ji}(s))) \right] ds + \sum_{j=1}^m a_{ji}(t) \\
& \cdot (f_j(x_j(t)) - f_j(x_j^*(t))) + \sum_{j=1}^m b_{ji}(t) (g_j(y_j(s \\
& - \tau_{ji}(s))) - g_j(y_j^*(s - \tau_{ji}(s))))), \quad (31)
\end{aligned}$$

$$\begin{aligned}
\frac{dv_i(t)}{dt} & = -b_i v_i(t) + b_i \int_{t-\sigma_i(t)}^t \left[ -b_i v_i(s - \sigma_i(s)) \right. \\
& \left. + \sum_{j=1}^m s_{ji}(s) (h_j(y_j(s)) - h_j(y_j^*(s))) + \sum_{j=1}^m t_{ji}(s) \right. \\
& \cdot (\varphi_j(x_j(s - \xi_{ji}(s)))) \\
& \left. - \varphi_j(x_j^*(s - \xi_{ji}(s))) \right] ds + \sum_{j=1}^m s_{ji}(t) \\
& \cdot (h_j(y_j(t)) - h_j(y_j^*(t))) + \sum_{j=1}^m t_{ji}(t) (\varphi_j(x_j(t \\
& - \xi_{ji}(t))) - \varphi_j(x_j^*(t - \xi_{ji}(t))))),
\end{aligned}$$

which leads to

$$\begin{aligned}
\frac{1}{2} \frac{du_i^2(t)}{dt} & = -a_i u_i^2(t) + a_i u_i(t) \int_{t-\delta_i(t)}^t \left[ -a_i u_i(s \right. \\
& \left. - \delta_i(s)) + \sum_{j=1}^m a_{ji}(s) (f_j(x_j(s)) - f_j(x_j^*(s))) \right.
\end{aligned}$$

$$\begin{aligned}
 & + \sum_{j=1}^m b_{ji}^-(s) \left( g_j(y_j(s - \tau_{ji}(s))) \right. \\
 & \left. - g_j(y_j^*(s - \tau_{ji}(s))) \right) ds + u_i(t) \sum_{j=1}^m a_{ji}^-(t) \\
 & \cdot (f_j(x_j(t)) - f_j(x_j^*(t))) + u_i(t) \sum_{j=1}^m b_{ji}^-(t) \\
 & \cdot (g_j(y_j(s - \tau_{ji}(s))) - g_j(y_j^*(s - \tau_{ji}(s))))), \\
 \frac{1}{2} \frac{dv_i^2(t)}{dt} & = -b_i v_i^2(t) + b_i v_i(t) \int_{t-\sigma_i(t)}^t \left[ -b_i v_i(s \right. \\
 & - \sigma_i(s) + \sum_{j=1}^m s_{ji}^-(s) (h_j(y_j(s)) - h_j(y_j^*(s))) \\
 & + \sum_{j=1}^m t_{ji}^-(s) (\varphi_j(x_j(s - \xi_{ji}(s))) \\
 & \left. - \varphi_j(x_j^*(s - \xi_{ji}(s)))) \right] ds + v_i(t) \sum_{j=1}^m s_{ji}^-(t) \\
 & \cdot (h_j(y_j(t)) - h_j(y_j^*(t))) + v_i(t) \sum_{j=1}^m t_{ji}^-(t) \\
 & \cdot (\varphi_j(x_j(t - \xi_{ji}(t))) - \varphi_j(x_j^*(t - \xi_{ji}(t)))).
 \end{aligned} \tag{32}$$

Then

$$\begin{aligned}
 \frac{du_i^2(t)}{dt} & \leq -2a_i u_i^2(t) + 2a_i u_i(t) \delta_i^+ \left[ a_i |u_i(t - \delta_i(t))| \right. \\
 & \left. + \sum_{j=1}^m a_{ji}^+ L_{jf} u_j(t) + \sum_{j=1}^m b_{ji}^+ L_{jg} v_j(t - \tau_{ji}(t)) \right] \\
 & + 2u_i(t) \sum_{j=1}^m a_{ji}^+ L_{jf} u_j(t) + 2u_i(t) \sum_{j=1}^m b_{ji}^+ L_{jg} v_j(t \\
 & - \tau_{ji}(t)) \leq -2a_i u_i^2(t) \\
 & + a_i \delta_i^+ \left[ a_i (u_i^2 + u_i^2(t - \delta_i(t))) \right. \\
 & + \sum_{j=1}^m a_{ji}^+ (L_{jf}^{2\xi_j} u_i^2(t) + L_{jf}^{2(1-\xi_j)} u_j^2(t)) \\
 & \left. + \sum_{j=1}^m b_{ji}^+ (L_{jg}^{2\xi_j} u_i^2(t) + L_{jg}^{2(1-\xi_j)} v_j^2(t - \tau_{ji}(t))) \right]
 \end{aligned}$$

$$\begin{aligned}
 & + \sum_{j=1}^m a_{ji}^+ (L_{jf}^{2\xi_j} u_i^2(t) + L_{jf}^{2(1-\xi_j)} u_j^2(t)) + \sum_{j=1}^m b_{ji}^+ \\
 & \cdot (L_{jg}^{2\xi_j} u_i^2(t) + L_{jg}^{2(1-\xi_j)} v_j^2(t - \tau_{ji}(t))).
 \end{aligned} \tag{33}$$

With the same method, we have

$$\begin{aligned}
 \frac{dv_i^2(t)}{dt} & \leq -2b_i v_i^2(t) + b_i \sigma_i^+ \left[ b_i (v_i^2 + v_i^2(t - \sigma_i(t))) \right. \\
 & + \sum_{j=1}^m s_{ji}^+ (L_{jh}^{2\xi_j} v_i^2(t) + L_{jh}^{2(1-\xi_j)} v_j^2(t)) \\
 & \left. + \sum_{j=1}^m t_{ji}^+ (L_{j\varphi}^{2\xi_j} v_i^2(t) + L_{j\varphi}^{2(1-\xi_j)} u_j^2(t - \xi_{ji}(t))) \right] \\
 & + \sum_{j=1}^m s_{ji}^+ (L_{jh}^{2\xi_j} v_i^2(t) + L_{jh}^{2(1-\xi_j)} v_j^2(t)) + \sum_{j=1}^m t_{ji}^+ \\
 & \cdot (L_{j\varphi}^{2\xi_j} v_i^2(t) + L_{j\varphi}^{2(1-\xi_j)} u_j^2(t - \xi_{ji}(t))),
 \end{aligned} \tag{34}$$

where  $0 \leq \xi_j, \zeta_j < 1, j = 1, \dots, m$ . Now we define a Lyapunov function as follows:

$V(t)$

$$\begin{aligned}
 & = e^{\beta t} \left( \sum_{i=1}^m u_i^2(t) + \sum_{i=1}^m v_i^2(t) \right) \\
 & + \sum_{i=1}^m \sum_{j=1}^m a_i \delta_i^+ b_{ij}^+ L_{jg}^{2(1-\xi_j)} \int_{t-\tau_{ji}(t)}^t e^{\beta(s+\tau_{ji}(t))} v_j^2(s) ds \\
 & + \sum_{i=1}^m a_i^2 \delta_i^+ \int_{t-\delta_i(t)}^t e^{\beta(s+\delta_i(t))} u_i^2(s) ds \\
 & + \sum_{i=1}^m b_{ij}^+ L_{jg}^{2(1-\xi_j)} \int_{t-\tau_{ji}(t)}^t e^{\beta(s+\tau_{ji}(t))} v_j^2(s) ds \\
 & + \sum_{i=1}^m b_i^2 \sigma_i^+ \int_{t-\sigma_i(t)}^t e^{\beta(s+\sigma_i(t))} v_i^2(s) ds \\
 & + \sum_{i=1}^m t_{ij}^+ L_{j\varphi}^{2(1-\xi_j)} \int_{t-\xi_{ji}(t)}^t e^{\beta(s+\xi_{ji}(t))} u_j^2(s) ds \\
 & + \sum_{i=1}^m \sum_{j=1}^m b_i \sigma_i^+ t_{ij}^+ L_{j\varphi}^{2(1-\xi_j)} \int_{t-\xi_{ji}(t)}^t e^{\beta(s+\xi_{ji}(t))} u_j^2(s) ds,
 \end{aligned} \tag{35}$$

where  $\beta$  is defined by Lemma 3. Differentiating  $V(t)$  along solutions to system (5), together with (33) and (34), we have

$$\begin{aligned}
\frac{dV(t)}{dt} &\leq \beta e^{\beta t} \left( \sum_{i=1}^m u_i^2(t) + \sum_{i=1}^m v_i^2(t) \right) \\
&+ e^{\beta t} \sum_{i=1}^m \left\{ -2a_i u_i^2(t) + a_i \delta_i^+ \left[ a_i u_i^2(t) + a_i u_i^2(t) \right. \right. \\
&- \delta_i(t) + \sum_{j=1}^m a_{ji}^+ \left( L_{jf}^{2\xi_j} u_i^2(t) + L_{jf}^{2(1-\xi_j)} u_j^2(t) \right) \\
&+ \left. \left. \sum_{j=1}^m b_{ji}^+ \left( L_{jg}^{2\xi_j} u_i^2(t) + L_{jg}^{2(1-\xi_j)} v_j^2(t - \tau_{ji}(t)) \right) \right] \right. \\
&+ \left. \sum_{j=1}^m a_{ji}^+ \left( L_{jf}^{2\xi_j} u_i^2(t) + L_{jf}^{2(1-\xi_j)} u_j^2(t) \right) + \sum_{j=1}^m b_{ji}^+ \right. \\
&\cdot \left. \left( L_{jg}^{2\xi_j} u_i^2(t) + L_{jg}^{2(1-\xi_j)} v_j^2(t - \tau_{ji}(t)) \right) \right\} \\
&+ e^{\beta t} \sum_{i=1}^m \left\{ -2b_i v_i(t) + b_i \sigma_i^+ \left[ b_i v_i^2(t - \sigma_i(t)) + \sum_{j=1}^m s_{ji}^+ \right. \right. \\
&\cdot \left. \left. \left( L_{jh}^{2\zeta_j} v_i^2(t) + L_{jh}^{2(1-\zeta_j)} v_j^2(t) \right) + \sum_{j=1}^m t_{ji}^+ \left( L_{j\varphi}^{2\zeta_j} v_i^2(t) \right. \right. \right. \\
&+ \left. \left. \left. L_{jh}^{2(1-\zeta_j)} u_j^2(t - \xi_{ji}(t)) \right) \right] \right\} + \sum_{i=1}^m a_i^2 \delta_i^+ \\
&\cdot \left( e^{\beta t + \beta \delta_i(t)} u_i(t) - e^{\beta t} u_i(t - \delta_i(t)) \right) + \sum_{i=1}^m b_{ij}^+ \\
&\cdot L_{jg}^{2(1-\xi_j)} \left( e^{\beta t + \beta \tau_{ji}(t)} v_j(t) - e^{\beta t} v_j(t - \delta_i(t)) \right) \\
&+ \sum_{i=1}^m b_i^2 \sigma_i^+ \left( e^{\beta t + \beta \sigma_i(t)} v_i^2(t) - e^{\beta t} v_i^2(t - \sigma_i(t)) \right) \\
&+ \sum_{i=1}^m \sum_{j=1}^m b_i \sigma_i^+ t_{ij}^+ L_{j\varphi}^{2(1-\zeta_j)} \left( e^{\beta t + \beta \xi_{ji}(t)} u_j^2(t) - e^{\beta t} u_j^2(t - \right. \\
&- \xi_{ji}(t)) + \sum_{i=1}^m t_{ij}^+ L_{j\varphi}^{2(1-\zeta_j)} \left( e^{\beta t + \beta \xi_{ji}(t)} u_j^2(t) - e^{\beta t} u_j^2(t - \right. \\
&- \xi_{ji}(t)) + \sum_{i=1}^m \sum_{j=1}^m a_i \delta_i^+ b_{ij}^+ L_{jg}^{2(1-\xi_j)} \left( e^{\beta t + \beta \tau_{ji}(t)} v_j(t) \right. \\
&- \left. e^{\beta t} v_j(t - \tau_{ji}(t)) \right) = e^{\beta t} \sum_{i=1}^m \left[ \beta - 2a_i \right. \\
&+ a_i^2 \delta_i^+ \left( e^{\beta \delta_i^+} + 1 \right) + t_{ji}^+ L_{j\varphi}^{2(1-\zeta_j)} e^{\beta \xi_{ji}^+} + (a_i \delta_i^+ + 1)
\end{aligned}$$

$$\begin{aligned}
&\cdot \sum_{j=1}^m b_{ji}^+ L_{jg}^{2\xi_j} + (a_i \delta_i^+ + 1) \sum_{j=1}^m a_{ji}^+ \left( L_{jf}^{2\xi_j} + L_{jf}^{2(1-\xi_j)} \right) \\
&+ \sum_{j=1}^m b_i \sigma_i^+ t_{ji}^+ L_{j\varphi}^{2(1-\zeta_j)} e^{\beta \xi_{ji}^+} \left. \right] u_i^2(t) + e^{\beta t} \sum_{i=1}^m \left[ \beta - 2b_i \right. \\
&+ b_i^2 \sigma_i^+ \left( e^{\beta \sigma_i^+} + 1 \right) + b_{ji}^+ L_{jg}^{2(1-\xi_j)} e^{\beta \tau_{ji}^+} + (b_i \sigma_i^+ + 1) \\
&\cdot \sum_{j=1}^m t_{ji}^+ L_{j\varphi}^{2\zeta_j} + (b_i \sigma_i^+ + 1) \sum_{j=1}^m s_{ji}^+ \left( L_{jh}^{2\zeta_j} + L_{jh}^{2(1-\zeta_j)} \right) \\
&+ \left. \left. \sum_{j=1}^m a_i \delta_i^+ b_{ji}^+ L_{jg}^{2(1-\xi_j)} e^{\beta \tau_{ji}^+} \right] v_i^2(t) \right. \\
&\left. \right] \quad (36)
\end{aligned}$$

In view of Lemma 3, we have  $dV(t)/dt \leq 0$ . That is to say,  $V(t) \leq V(0)$  for all  $t > 0$ . Thus

$$\begin{aligned}
e^{\beta t} \left[ \sum_{i=1}^m u_i^2(t) + \sum_{j=1}^m v_j^2(t) \right] &\leq V(t) \leq V(0) \leq \|\phi\| \\
&- \phi^* \|^2 + \|\psi - \psi^*\|^2 + \frac{1}{\beta} \sum_{i=1}^m a_i^2 \delta_i^+ e^{\beta \delta_i^+} \|\phi - \phi^*\|^2 \\
&+ \frac{1}{\beta} \sum_{i=1}^m \sum_{j=1}^m a_i \delta_i^+ b_{ji}^+ L_{jg}^{2(1-\xi_j)} e^{\beta \tau_{ji}^+} \|\psi - \psi^*\|^2 + \frac{1}{\beta} \\
&\cdot \sum_{i=1}^m b_{ji}^+ L_{jg}^{2(1-\xi_j)} e^{\beta \tau_{ji}^+} \|\psi - \psi^*\|^2 + \frac{1}{\beta} \sum_{i=1}^m b_i^2 \sigma_i^+ e^{\beta \sigma_i^+} \|\psi \\
&- \psi^*\|^2 + \frac{1}{\beta} \sum_{i=1}^m \sum_{j=1}^m t_{ji}^+ L_{j\varphi}^{2(1-\zeta_j)} e^{\beta \tau_{ji}^+} \|\phi - \phi^*\|^2 + \frac{1}{\beta} \sum_{i=1}^m \sum_{j=1}^m b_i \\
&\cdot \sigma_i^+ t_{ji}^+ L_{j\varphi}^{2(1-\zeta_j)} e^{\beta \xi_{ji}^+} \|\phi - \phi^*\|^2 = \left[ 1 + \frac{1}{\beta} \sum_{i=1}^m a_i^2 \delta_i^+ e^{\beta \delta_i^+} \right. \\
&+ \frac{1}{\beta} \sum_{i=1}^m \sum_{j=1}^m b_i \sigma_i^+ t_{ij}^+ L_{j\varphi}^{2(1-\zeta_j)} e^{\beta \xi_{ji}^+} \\
&+ \frac{1}{\beta} \sum_{i=1}^m \sum_{j=1}^m b_i \sigma_i^+ t_{ji}^+ L_{j\varphi}^{2(1-\zeta_j)} e^{\beta \xi_{ji}^+} \left. \right] \|\phi - \phi^*\|^2 + \left[ 1 \right. \\
&+ \frac{1}{\beta} \sum_{i=1}^m b_i^2 \sigma_i^+ e^{\beta \sigma_i^+} + \frac{1}{\beta} \sum_{i=1}^m b_{ji}^+ L_{jg}^{2(1-\xi_j)} e^{\beta \tau_{ji}^+} \\
&+ \left. \frac{1}{\beta} \sum_{i=1}^m \sum_{j=1}^m a_i \delta_i^+ b_{ji}^+ L_{jg}^{2(1-\xi_j)} e^{\beta \tau_{ji}^+} \right] \|\psi - \psi^*\|^2. \quad (37)
\end{aligned}$$

Let

$$\begin{aligned}
 M = \max & \left\{ 1 + \frac{1}{\beta} \sum_{i=1}^m a_i^2 \delta_i^+ e^{\beta \delta_i^+} \right. \\
 & + \frac{1}{\beta} \sum_{i=1}^m \sum_{j=1}^m b_i \sigma_i^+ t_{ji}^+ L_{j\varphi}^{2(1-\zeta_j)} e^{\beta \xi_{ji}^+} \\
 & + \frac{1}{\beta} \sum_{i=1}^m \sum_{j=1}^m b_i \sigma_i^+ t_{ji}^+ L_{j\varphi}^{2(1-\zeta_j)} e^{\beta \xi_{ji}^+}, 1 + \frac{1}{\beta} \sum_{i=1}^m b_i^2 \sigma_i^+ e^{\beta \sigma_i^+} \\
 & + \frac{1}{\beta} \sum_{i=1}^m b_{ji}^+ L_{jg}^{2(1-\xi_j)} e^{\beta \tau_{ji}^+} \\
 & \left. + \frac{1}{\beta} \sum_{i=1}^m \sum_{j=1}^m a_i \delta_i^+ b_{ji}^+ L_{jg}^{2(1-\xi_j)} e^{\beta \tau_{ji}^+} \right\} > 1.
 \end{aligned} \tag{38}$$

By (37), one has

$$\sum_{i=1}^m u_i^2(t) + \sum_{i=1}^m v_i^2(t) \leq M e^{-\beta t} [\|\varphi - \varphi^*\|^2 + \|\psi - \psi^*\|^2] \tag{39}$$

for all  $t > 0$ . Then

$$\begin{aligned}
 & \sum_{i=1}^m |x_i(t) - x_i^*(t)|^2 + \sum_{i=1}^m |y_i(t) - y_i^*(t)|^2 \\
 & \leq M e^{-\beta t} [\|\varphi - \varphi^*\|^2 + \|\psi - \psi^*\|^2]
 \end{aligned} \tag{40}$$

for all  $t > 0$ . Thus the solution  $(x^*(t), y^*(t))^T$  of system (5) is globally exponentially stable.  $\square$

**Theorem 6.** Suppose that (H1)–(H3) hold. Then system (5) has exactly one  $T$ -antiperiodic solution which is globally stable.

*Proof.* By system (5) and (H2), for each  $k \in N$ , we get

$$\begin{aligned}
 & \frac{d}{dt} [(-1)^{k+1} x_i(t + (k+1)T)] = (-1)^{k+1} \\
 & \cdot \left[ -a_i x_i(t + (k+1)T - \delta_i(t + (k+1)T)) + \sum_{j=1}^m a_{ji} \right. \\
 & \cdot (t + (k+1)T) f_j(x_i(t + (k+1)T)) + \sum_{j=1}^m b_{ji} \\
 & \cdot (t + (k+1)T) \\
 & \cdot g_j(y_i(t + (k+1)T - \tau_{ji}(t + (k+1)T))) \\
 & \left. + I_i(t + (k+1)T) \right] = -a_i (-1)^{k+1} x_i(t + (k+1)T) \\
 & - \delta_i(t) + \sum_{j=1}^m a_{ji}(t) f_j((-1)^{k+1} x_j(t + (k+1)T))
 \end{aligned}$$

$$\begin{aligned}
 & + \sum_{j=1}^m b_{ji}(t) g_j((-1)^{k+1} y_j(t + (k+1)T - \tau_{ji}(t))) \\
 & + I_i(t).
 \end{aligned} \tag{41}$$

In a similar way, we have

$$\begin{aligned}
 & \frac{d}{dt} [(-1)^{k+1} y_i(t + (k+1)T)] \\
 & = -b_i (-1)^{k+1} y_i(t + (k+1)T - \sigma_i(t)) \\
 & + \sum_{j=1}^m s_{ji}(t) h_j((-1)^{k+1} y_j(t + (k+1)T)) \\
 & + \sum_{j=1}^m t_{ji}(t) \varphi_j((-1)^{k+1} x_j(t + (k+1)T - \xi_{ji}(t))) \\
 & + J_i(t).
 \end{aligned} \tag{42}$$

Let

$$\begin{aligned}
 \bar{x}(t) & = ((-1)^{k+1} x_1(t + (k+1)T), \dots, (-1)^{k+1} \\
 & \cdot x_m(t + (k+1)T))^T, \\
 \bar{y}(t) & = ((-1)^{k+1} y_1(t + (k+1)T), \dots, (-1)^{k+1} \\
 & \cdot y_m(t + (k+1)T))^T.
 \end{aligned} \tag{43}$$

It follows that, for any  $k \in N$ ,  $(\bar{x}^T(t), \bar{y}^T(t))^T$  is also the solution of system (5). If the initial functions  $\phi_i(s), \psi_i(s), i = 1, \dots, m$ , are bounded, we conclude from Theorem 5 that there exists a constant  $\gamma > 1$  such that

$$\begin{aligned}
 & |(-1)^{k+1} x_i(t + (k+1)T) - (-1)^k x_i(t + kT)| \\
 & \leq M e^{-\beta(t+kT)} \sup_{-\tau \leq s \leq 0} \sum_{i=1}^m |x_i(t+T) + x_i(s)|^2 \\
 & \leq \gamma e^{-\beta(t+kT)},
 \end{aligned} \tag{44}$$

where  $t + kT > 0, i = 1, \dots, m$ , and  $\beta$  is a positive constant. For any  $k \in N$  we have

$$\begin{aligned}
 & (-1)^{k+1} x_i(t + (k+1)T) = x_i(t) \\
 & + \sum_{j=0}^k [(-1)^{j+1} x_i(t + (j+1)T) \\
 & - (-1)^j x_i(t + jT)].
 \end{aligned} \tag{45}$$

Then

$$\begin{aligned}
 & (-1)^{k+1} x_i(t + (k+1)T) \leq |x_i(t)| \\
 & + \sum_{j=0}^k |(-1)^{j+1} x_j(t + (j+1)T) \\
 & - (-1)^j x_j(t + jT)|.
 \end{aligned} \tag{46}$$

In view of Lemma 4, we know that the solutions of system (5) are bounded. In view of (4) and (5), we can easily know that  $\{(-1)^{k+1}x_i(t+(k+1)T)\}$  uniformly converges to a continuous function  $x^*(t) = (x_1^*(t), \dots, x_m^*(t))^T$  on any compact set of  $R$ . In a similar way, we can easily prove that  $\{(-1)^{k+1}y_i(t+(k+1)T)\}$  uniformly converges to a continuous function  $y^*(t) = (y_1^*(t), \dots, y_m^*(t))^T$  on any compact set of  $R$ . Now we will show that  $(x^*(t), y^*(t))^T$  is  $T$ -antiperiodic solution of system (5). Since

$$\begin{aligned} x^*(t+T) &= \lim_{k \rightarrow \infty} (-1)^k x(t+T+kT) \\ &= - \lim_{(k+1) \rightarrow \infty} (-1)^{k+1} x(t+(k+1)T) \quad (47) \\ &= -x^*(t). \end{aligned}$$

thus  $x^*(t)$  is  $T$ -antiperiodic solution. Similarly,  $y^*(t)$  is also  $T$ -antiperiodic solution. Thus we know that  $(x^*(t), y^*(t))^T$  is a solution of system (5). In fact, together with the continuity of the right side of system (5), letting  $k \rightarrow \infty$ , we can easily get

$$\begin{aligned} \frac{dx_i^*(t)}{dt} &= -a_i x_i^*(t - \delta_i(t)) + \sum_{j=1}^m a_{ji}(t) f_j(x_j^*(t)) \\ &\quad + \sum_{j=1}^m b_{ji}(t) g_j(y_j^*(t - \tau_{ji}(t))) + I_i(t), \\ \frac{dy_i^*(t)}{dt} &= -b_i y_i^*(t - \sigma_i(t)) + \sum_{j=1}^m s_{ji}(t) h_j(y_j^*(t)) \\ &\quad + \sum_{j=1}^m t_{ji}(t) \varphi_j(x_j^*(t - \xi_{ji}(t))) + J_i(t). \end{aligned} \quad (48)$$

Therefore,  $(x^*(t), y^*(t))^T$  is the  $T$ -periodic solution of system (5). Finally, by applying Theorem 5, it is easy to check that  $(x^*(t), y^*(t))^T$  is globally exponentially stable. The proof of Theorem 6 is completed.  $\square$

*Remark 7.* There are a large number of papers about neural networks with delays. The main topic of these papers is exponential stability. For example, the authors in [26–28] considered the exponential stability of neural networks with constants delays. The authors in [29–31] considered the exponential stability of neural networks with time-varying delays and [32–35] with distributed delays. But these are few results on stability of BAM neural networks with leakage terms. This paper constructs a kind of BAM neural networks with time-varying delay and leakage terms and the results in our paper extend the results in the above papers.

### 4. An Example

In this section, to illustrate the efficiency of our results obtained in Section 3, we give an example. Consider the

following BAM neural networks with time-varying delays and external input:

$$\begin{aligned} \frac{dx_1(t)}{dt} &= -a_1 x_1(t - \delta_1(t)) + \sum_{j=1}^2 a_{j1}(t) f_j(x_j(t)) \\ &\quad + \sum_{j=1}^2 b_{j1}(t) g_j(y_j(t - \tau_{j1}(t))) + I_1(t), \\ \frac{dx_2(t)}{dt} &= -a_2 x_2(t - \delta_2(t)) + \sum_{j=1}^2 a_{j2}(t) f_j(x_j(t)) \\ &\quad + \sum_{j=1}^2 b_{j2}(t) g_j(y_j(t - \tau_{j2}(t))) + I_2(t), \\ \frac{dy_1(t)}{dt} &= -b_1 y_1(t - \sigma_1(t)) + \sum_{j=1}^2 s_{j1}(t) h_j(y_j(t)) \\ &\quad + \sum_{j=1}^2 t_{j1}(t) \varphi_j(x_j(t - \xi_{j1}(t))) + J_1(t), \\ \frac{dy_2(t)}{dt} &= -b_2 y_2(t - \sigma_2(t)) + \sum_{j=1}^m s_{j2}(t) h_j(y_j(t)) \\ &\quad + \sum_{j=1}^2 t_{j2}(t) \varphi_j(x_j(t - \xi_{j2}(t))) + J_2(t), \end{aligned} \quad (49)$$

where

$$\begin{aligned} \begin{pmatrix} a_1 & a_2 \\ b_1 & b_2 \end{pmatrix} &= \begin{pmatrix} 2 & 2 \\ 2 & 2 \end{pmatrix}, \\ \begin{pmatrix} \delta_1(t) & \delta_2(t) \\ \sigma_1(t) & \sigma_2(t) \end{pmatrix} &= \begin{pmatrix} 0.04 |\sin t| & 0.04 |\sin t| \\ 0.03 |\cos t| & 0.03 |\cos t| \end{pmatrix}, \\ \begin{pmatrix} a_{11}(t) & a_{12}(t) \\ a_{21}(t) & a_{22}(t) \end{pmatrix} &= \begin{pmatrix} 0.2 |\cos t| & 0.3 |\sin t| \\ 0.2 |\cos t| & 0.3 |\sin t| \end{pmatrix}, \\ \begin{pmatrix} b_{11}(t) & b_{12}(t) \\ b_{21}(t) & b_{22}(t) \end{pmatrix} &= \begin{pmatrix} 0.1 |\cos t| & 0.2 |\sin t| \\ 0.1 |\cos t| & 0.2 |\sin t| \end{pmatrix}, \\ \begin{pmatrix} s_{11}(t) & s_{12}(t) \\ s_{21}(t) & s_{22}(t) \end{pmatrix} &= \begin{pmatrix} 0.2 |\sin t| & 0.3 |\cos t| \\ 0.2 |\sin t| & 0.3 |\cos t| \end{pmatrix}, \\ \begin{pmatrix} I_1 & I_2 \\ J_1 & J_2 \end{pmatrix} &= \begin{pmatrix} 0.3 \sin t & 0.3 \sin t \\ 0.4 \cos t & 0.4 \cos t \end{pmatrix}. \end{aligned} \quad (50)$$

We also set

$$\begin{aligned} f_j(u) &= g_j(u) = h_j(u) = \varphi_j(u) \\ &= \frac{1}{2} (|u+1| - |u-1|), \quad j = 1, 2. \end{aligned} \quad (51)$$

Then we find that  $L_{jf} = L_{jg} = L_{jh} = L_{j\varphi} = 1$ , and  $M_{jf} = M_{jg} = M_{jh} = M_{j\varphi} = 1, j = 1, 2$ . Also we have

$$\begin{aligned} \begin{pmatrix} \delta_1^+ & \delta_2^+ \\ \sigma_1^+ & \sigma_2^+ \end{pmatrix} &= \begin{pmatrix} 0.04 & 0.04 \\ 0.03 & 0.03 \end{pmatrix}, \\ \begin{pmatrix} a_{j1}^+ & a_{j2}^+ \\ b_{j1}^+ & b_{j2}^+ \end{pmatrix} &= \begin{pmatrix} 0.2 & 0.3 \\ 0.1 & 0.2 \end{pmatrix}, \\ \begin{pmatrix} s_{j1}^+ & s_{j2}^+ \\ t_{j1}^+ & t_{j2}^+ \end{pmatrix} &= \begin{pmatrix} 0.2 & 0.3 \\ 0.1 & 0.2 \end{pmatrix}. \end{aligned} \tag{52}$$

for  $j = 1, 2$ .

It is easy to verify that

$$\begin{aligned} &-2a_1 + 2a_1^2\delta_1^+ + t_{j1}^+L_{j\varphi}^{2(1-\varsigma_j)} + (a_1\delta_1^+ + 1) \\ &\cdot \left( \sum_{j=1}^2 b_{j1}^+L_{jg}^{2\xi_j} + \sum_{j=1}^2 a_{j1}^+ \left( L_{jf}^{2\xi_j} + L_{jf}^{2(1-\xi_j)} \right) \right) + \sum_{j=1}^2 b_1\sigma_1^+ \\ &\cdot t_{j1}^+L_{j\varphi}^{2(1-\varsigma_j)} = -2.488 < 0, \\ &-2a_2 + 2a_2^2\delta_2^+ + t_{j2}^+L_{j\varphi}^{2(1-\varsigma_j)} + (a_2\delta_2^+ + 1) \\ &\cdot \left( \sum_{j=1}^2 b_{j2}^+L_{jg}^{2\xi_j} + \sum_{j=1}^2 a_{j2}^+ \left( L_{jf}^{2\xi_j} + L_{jf}^{2(1-\xi_j)} \right) \right) + \sum_{j=1}^2 b_2\sigma_2^+ \\ &\cdot t_{j2}^+L_{j\varphi}^{2(1-\varsigma_j)} = -1.728 < 0, \\ &-2b_1 + 2b_1^2\sigma_1^+ + b_{j1}^+L_{jg}^{2(1-\xi_j)} + (b_1\sigma_1^+ + 1) \\ &\cdot \left( \sum_{j=1}^2 t_{j1}^+L_{j\varphi}^{2\varsigma_j} + \sum_{j=1}^2 s_{j1}^+ \left( L_{jh}^{2\varsigma_j} + L_{jh}^{2(1-\varsigma_j)} \right) \right) + \sum_{j=1}^2 a_1\delta_1^+ \\ &\cdot b_{j1}^+L_{jg}^{2(1-\xi_j)} = -2.584 < 0, \\ &-2b_2 + 2b_2^2\sigma_2^+ + b_{j2}^+L_{jg}^{2(1-\xi_j)} + (b_2\sigma_2^+ + 1) \\ &\cdot \left( \sum_{j=1}^2 t_{j2}^+L_{j\varphi}^{2\varsigma_j} + \sum_{j=1}^2 s_{j2}^+ \left( L_{jh}^{2\varsigma_j} + L_{jh}^{2(1-\varsigma_j)} \right) \right) + \sum_{j=1}^2 a_2\delta_2^+ \\ &\cdot b_{j2}^+L_{jg}^{2(1-\xi_j)} = -1.832 < 0. \end{aligned} \tag{53}$$

Then all the conditions (H1)–(H3) hold. Thus system (49) has exactly one  $\pi$ -antiperiodic solution which is globally exponentially stable. The numerical result is shown in Figure 1. And system (49) is exponentially stable when all inputs are equal to 0, which can also be seen from Figure 2.

### 5. Conclusions

In this paper, a kind of BAM neural networks with time-varying delays and external input has been dealt with. By constructing a suitable Lyapunov-Kravsovskii functional

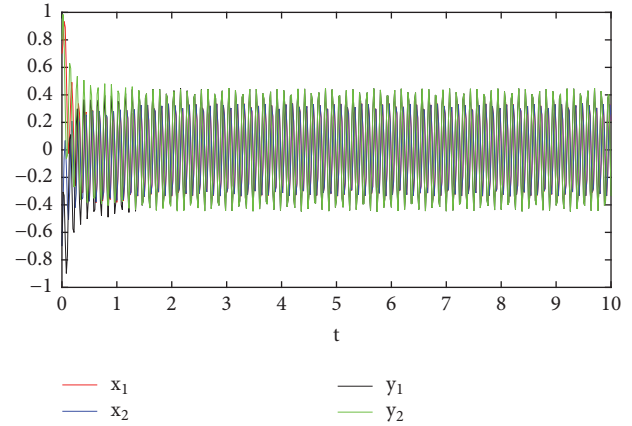


FIGURE 1: The state response of BAM neural network in (49).

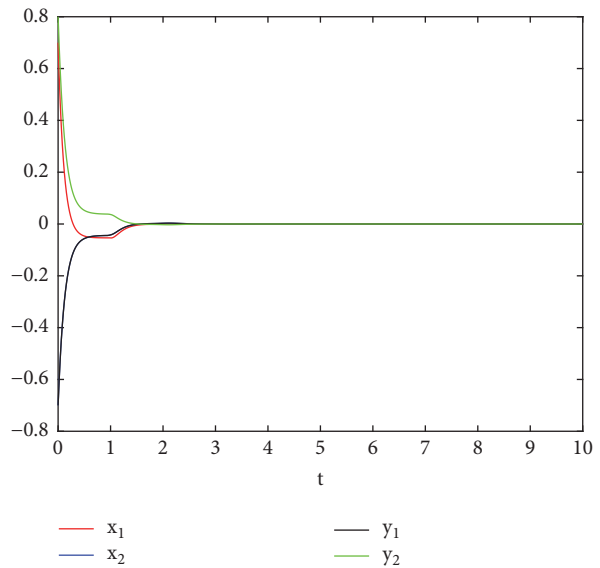


FIGURE 2: The state response of BAM neural network with inputs equal to 0 in (49).

and using matrix theory and inequality technique, a series of sufficient criteria to guarantee the existence and global exponential stability of antiperiodic solutions for this system have been established. And the criteria are easy to check in practice. We also give an example to illustrate the feasibility and effectiveness. In real life, many BAM neural networks are affected by external perturbation. There are many papers concerned with stochastic BAM neural networks, e.g., [36–41]. In the future, we will give our research on these networks.

### Data Availability

No data were used to support this study.

### Conflicts of Interest

The authors declare that they have no conflicts of interest.

## Authors' Contributions

The authors have made the same contribution. All authors read and approved the final manuscript.

## Acknowledgments

This work was jointly supported by the National Natural Science Foundation of China (61773217, 61374080), the Natural Science Foundation of Jiangsu Province (BK20161552), Qing Lan Project of Jiangsu Province, Research Foundation of Hubei Province (B2018413), Development Funding from Yangtze University (18100200018), and Yangtze University College of Technology and Engineering (2017KY09, 2017KY10).

## References

- [1] Y. Song, Y. Han, and Y. Peng, "Stability and Hopf bifurcation in an unidirectional ring of  $n$  neurons with distributed delays," *Neurocomputing*, vol. 121, pp. 442–452, 2013.
- [2] Y. Bai and X. Mu, "Global asymptotic stability of a generalized SIRS epidemic model with transfer from infectious to susceptible," *Journal of Applied Analysis and Computation*, vol. 8, no. 2, pp. 402–412, 2018.
- [3] W. Qi, Y. Kao, X. Gao, and Y. Wei, "Controller design for time-delay system with stochastic disturbance and actuator saturation via a new criterion," *Applied Mathematics and Computation*, vol. 320, pp. 535–546, 2018.
- [4] L. Gao, D. Wang, and G. Wang, "Further results on exponential stability for impulsive switched nonlinear time-delay systems with delayed impulse effects," *Applied Mathematics and Computation*, vol. 268, pp. 186–200, 2015.
- [5] R. Rakkiyappan, V. Preethi Latha, Q. Zhu, and Z. Yao, "Exponential synchronization of Markovian jumping chaotic neural networks with sampled-data and saturating actuators," *Nonlinear Analysis: Hybrid Systems*, vol. 24, pp. 28–44, 2017.
- [6] Y. Guo, "Exponential stability analysis of travelling waves solutions for nonlinear delayed cellular neural networks," *Dynamical Systems. An International Journal*, vol. 32, no. 4, pp. 490–503, 2017.
- [7] Y. Liu, J. H. Park, B.-Z. Guo, F. Fang, and F. Zhou, "Event-triggered dissipative synchronization for Markovian jump neural networks with general transition probabilities," *International Journal of Robust and Nonlinear Control*, vol. 28, no. 13, pp. 3893–3908, 2018.
- [8] Y.-H. Feng and C.-M. Liu, "Stability of steady-state solutions to Navier-Stokes-Poisson systems," *Journal of Mathematical Analysis and Applications*, vol. 462, no. 2, pp. 1679–1694, 2018.
- [9] Y. Liu, J. H. Park, and F. Fang, "Global exponential stability of delayed neural networks based on a new integral inequality," *IEEE Transactions on Systems, Man, and Cybernetics: Systems*, 2018.
- [10] K. Matsuoka, "Stability conditions for nonlinear continuous neural networks with asymmetric connection weights," *Neural Networks*, vol. 5, no. 3, pp. 495–500, 1992.
- [11] X. Cao and J. Wang, "Finite-time stability of a class of oscillating systems with two delays," *Mathematical Methods in the Applied Sciences*, vol. 41, no. 13, pp. 4943–4954, 2018.
- [12] B. Kosko, "Adaptive bidirectional associative memories," *Applied Optics*, vol. 26, no. 23, pp. 4947–4960, 1987.
- [13] J. H. Park, C. H. Park, O. M. Kwon, and S. M. Lee, "A new stability criterion for bidirectional associative memory neural networks of neutral-type," *Applied Mathematics and Computation*, vol. 199, no. 2, pp. 716–722, 2008.
- [14] W. Sun, Y. Wang, and R. Yang, "L2 disturbance attenuation for a class of time delay Hamiltonian systems," *Journal of Systems Science & Complexity*, vol. 24, no. 4, pp. 672–682, 2011.
- [15] S. Arik and V. Tavsanoğlu, "Global asymptotic stability analysis of bidirectional associative memory neural networks with constant time delays," *Neurocomputing*, vol. 68, no. 1–4, pp. 161–176, 2005.
- [16] R. Samidurai, R. Sakthivel, and S. M. Anthoni, "Global asymptotic stability of BAM neural networks with mixed delays and impulses," *Applied Mathematics and Computation*, vol. 212, no. 1, pp. 113–119, 2009.
- [17] G. Liu, S. Xu, Y. Wei, Z. Qi, and Z. Zhang, "New insight into reachable set estimation for uncertain singular time-delay systems," *Applied Mathematics and Computation*, vol. 320, pp. 769–780, 2018.
- [18] C. Bai, "Stability analysis of Cohen-Grossberg BAM neural networks with delays and impulses," *Chaos, Solitons & Fractals*, vol. 35, no. 2, pp. 263–267, 2008.
- [19] G. Wang, "Existence-stability theorems for strong vector set-valued equilibrium problems in reflexive Banach spaces," *Journal of Inequalities and Applications*, vol. 239, pp. 1–14, 2015.
- [20] L. Li, F. Meng, and P. Ju, "Some new integral inequalities and their applications in studying the stability of nonlinear integro-differential equations with time delay," *Journal of Mathematical Analysis and Applications*, vol. 377, no. 2, pp. 853–862, 2011.
- [21] Y. Guo, "Nontrivial periodic solutions of nonlinear functional differential systems with feedback control," *Turkish Journal of Mathematics*, vol. 34, no. 1, pp. 35–44, 2010.
- [22] X. Zheng, Y. Shang, and X. Peng, "Orbital stability of periodic traveling wave solutions to the generalized Zakharov equations," *Acta Mathematica Scientia*, vol. 37, no. 4, pp. 998–1018, 2017.
- [23] K. Gopalsamy, "Leakage delays in BAM," *Journal of Mathematical Analysis and Applications*, vol. 325, no. 2, pp. 1117–1132, 2007.
- [24] B. Liu, "Global exponential stability for BAM neural networks with time-varying delays in the leakage terms," *Nonlinear Analysis: Real World Applications*, vol. 14, no. 1, pp. 559–566, 2013.
- [25] X. Li, D. Ding, J. Feng, and S. Hu, "Existence and exponential stability of anti-periodic solutions for interval general bidirectional associative memory neural networks with multiple delays," *Advances in Difference Equations*, vol. 190, 2016.
- [26] M. Li and J. Wang, "Representation of solution of a Riemann-Liouville fractional differential equation with pure delay," *Applied Mathematics Letters*, vol. 85, pp. 118–124, 2018.
- [27] H. Bao and J. Cao, "Exponential stability for stochastic BAM networks with discrete and distributed delays," *Applied Mathematics and Computation*, vol. 218, no. 11, pp. 6188–6199, 2012.
- [28] H. Bao, J. H. Park, and J. Cao, "Exponential synchronization of coupled stochastic memristor-based neural networks with time-varying probabilistic delay coupling and impulsive delay," *IEEE Transactions on Neural Networks and Learning Systems*, vol. 27, no. 1, pp. 190–201, 2016.
- [29] H. Bao, J. Cao, J. Kurths, A. Alsaedi, and B. Ahmad, " $H_\infty$  state estimation of stochastic memristor-based neural networks with time-varying delays," *Neural Networks*, vol. 99, pp. 79–91, 2018.

- [30] Y. Guo, "Mean square exponential stability of stochastic delay cellular neural networks," *Electronic Journal of Qualitative Theory of Differential Equations*, vol. 34, pp. 1–10, 2013.
- [31] L. Li, W. Qi, X. Chen, Y. Kao, X. Gao, and Y. Wei, "Stability analysis and control synthesis for positive semi-Markov jump systems with time-varying delay," *Applied Mathematics and Computation*, vol. 332, pp. 363–375, 2018.
- [32] Y. Guo, "Mean square global asymptotic stability of stochastic recurrent neural networks with distributed delays," *Applied Mathematics and Computation*, vol. 215, no. 2, pp. 791–795, 2009.
- [33] W. Sun and L. Peng, "Observer-based robust adaptive control for uncertain stochastic Hamiltonian systems with state and input delays," *Lithuanian Association of Nonlinear Analysts. Nonlinear Analysis: Modelling and Control*, vol. 19, no. 4, pp. 626–645, 2014.
- [34] M. Li and J. Wang, "Exploring delayed Mittag-Leffler type matrix functions to study finite time stability of fractional delay differential equations," *Applied Mathematics and Computation*, vol. 324, pp. 254–265, 2018.
- [35] Y. Guo, "Globally robust stability analysis for stochastic Cohen-Grossberg neural networks with impulse and time-varying delays," *Ukrainian Mathematical Journal*, vol. 69, no. 8, pp. 1049–1060, 2017.
- [36] Y. Guo, "Global stability analysis for a class of Cohen-Grossberg neural network models," *Bulletin of the Korean Mathematical Society*, vol. 49, no. 6, pp. 1193–1198, 2012.
- [37] Y. Guo, "Global asymptotic stability analysis for integro-differential systems modeling neural networks with delays," *Zeitschrift für Angewandte Mathematik und Physik*, vol. 61, no. 6, pp. 971–978, 2010.
- [38] F. Li and Y. Bao, "Uniform stability of the solution for a memory-type elasticity system with nonhomogeneous boundary control condition," *Journal of Dynamical and Control Systems*, vol. 23, no. 2, pp. 301–315, 2017.
- [39] J. Hu and A. Xu, "On stability of F-Gorenstein flat categories," *Algebra Colloquium*, vol. 23, no. 2, pp. 251–262, 2016.
- [40] X. Zheng, Y. Shang, and X. Peng, "Orbital stability of solitary waves of the coupled Klein-Gordon-Zakharov equations," *Mathematical Methods in the Applied Sciences*, vol. 40, no. 7, pp. 2623–2633, 2017.
- [41] C. Liu and Y.-J. Peng, "Stability of periodic steady-state solutions to a non-isentropic Euler-Maxwell system," *Zeitschrift für Angewandte Mathematik und Physik*, vol. 68, no. 5, pp. 1–17, 2017.

## Research Article

# Maximum Power Point Tracking of DFIG with DC-Based Converter System Using Coordinated Feedback Linearization Control

Yuliang Sun,<sup>1,2</sup> Shaomin Yan,<sup>1</sup> Bin Cai,<sup>1</sup> and Yuqiang Wu <sup>1</sup>

<sup>1</sup>School of Engineering, Qufu Normal University, Rizhao, China

<sup>2</sup>Shandong Water Conservancy Vocational College, Rizhao, China

Correspondence should be addressed to Yuqiang Wu; [yu-qiang\\_wu@126.com](mailto:yu-qiang_wu@126.com)

Received 28 August 2018; Accepted 22 October 2018; Published 11 November 2018

Guest Editor: Weihai Zhang

Copyright © 2018 Yuliang Sun et al. This is an open access article distributed under the Creative Commons Attribution License, which permits unrestricted use, distribution, and reproduction in any medium, provided the original work is properly cited.

This paper presents a coordinated feedback linearization strategy (CFLS) for DC-based doubly-fed induction generator (DFIG) system to track the maximum power point. The stator and rotor of DFIG are connected to DC grid directly by two voltage source converters. Compared with a traditional DFIG system, the DC-based DFIG system has more system inputs and coupling, which increases the difficulty of vector control strategy. Accordingly, CFLS is proposed to make DFIG operate at the maximum power point (MPP), and two aspects are improved: first a single-loop control is adopted to make DFIG operate steady and accurate under coordinated the control of RSC and SSC. Second system control laws are obtained by the feedback linearization strategy that achieves DC-based DFIG system decoupling fully during the MPPT and system control. Simulations are carried out the comparison between CFLS and conventional vector control (VC), and it shows that the control performance of CFLS is superior.

## 1. Introduction

In recent years, the technology of wind power generation has developed rapidly, due to its freely available and renewable resource. Variable speed constant frequency doubly fed induction generator (DFIG) is often selected in wind power generation [1]. Compared with the traditional AC transmission, the DC transmission is more economical and stable for the long distance high voltage transmission [2]. The traditional DFIG stator windings are connected to an AC grid by transformer, and the rotor windings is connected to the AC grid by back to back converters. Therefore, the traditional DFIG is used into the DC grid and additional converter will be needed, which is bound to increase the cost [3].

Accordingly, the new converter system is adopted for DFIG in DC grid. A diode-based stator converter interfaces a DFIG with a DC grid, which has the advantages of low cost and simple structure [4–7]. But harmonic may reach from 5.97% to 11.66% [8]. An IGBT-based converters system consisting of a rotor side converter (RSC) and a stator side converter (SSC) connects rotor and stator with DC grid,

respectively [9–13]. This structure has the advantages that it can reduce the current harmonic effectively and regulate the stator flux and current flexibly according to the needs of the system, not limited to AC grid.

However, the above improved structure results in that the state variables and the system outputs of DFIG with DC-based converters system are twice that of the traditional system, which greatly increases the complexity and coupling of the system and also increases the control difficulty of the system. Therefore, the traditional vector control (VC), which is based on approximate linear model, is difficult to achieve the global optimal control requirements of the new system [14]. Reference [9] adopts indirect air gap flux linkage orientation strategy to control DFIG in a DC grid, but air gap flux linkage is not suitable for measurement. Model predictive control for DFIG in a DC grid is adopted by [13], which requires high precision of system model.

Nowadays, Feedback linearization control (FLC) has been widely used in power electronics and power systems [15–21]. It adopts a dual-loop control strategy of FLC and PI to control DFIG in an AC grid in [22]. The advantage of

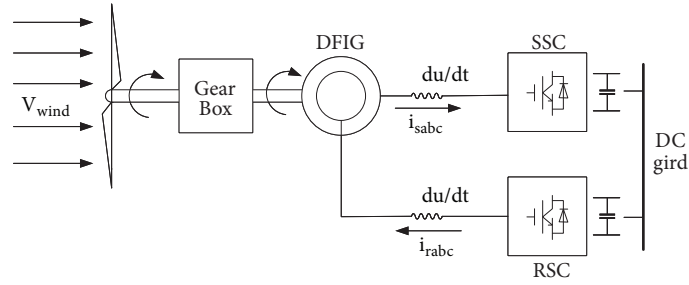


FIGURE 1: DFIG with its DC-based converter system in a DC grid.

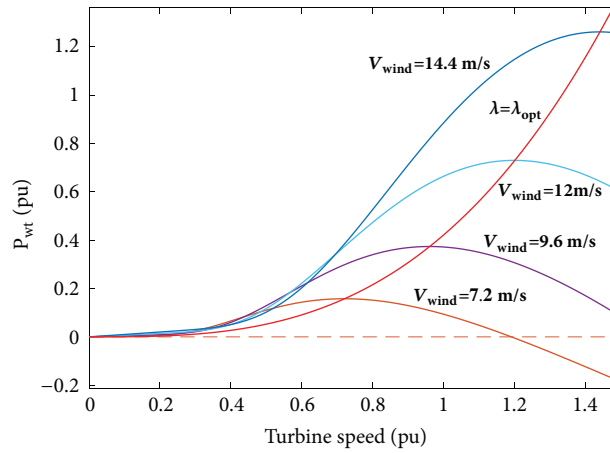


FIGURE 2: The output mechanical power, optimal power, and rotor speed.

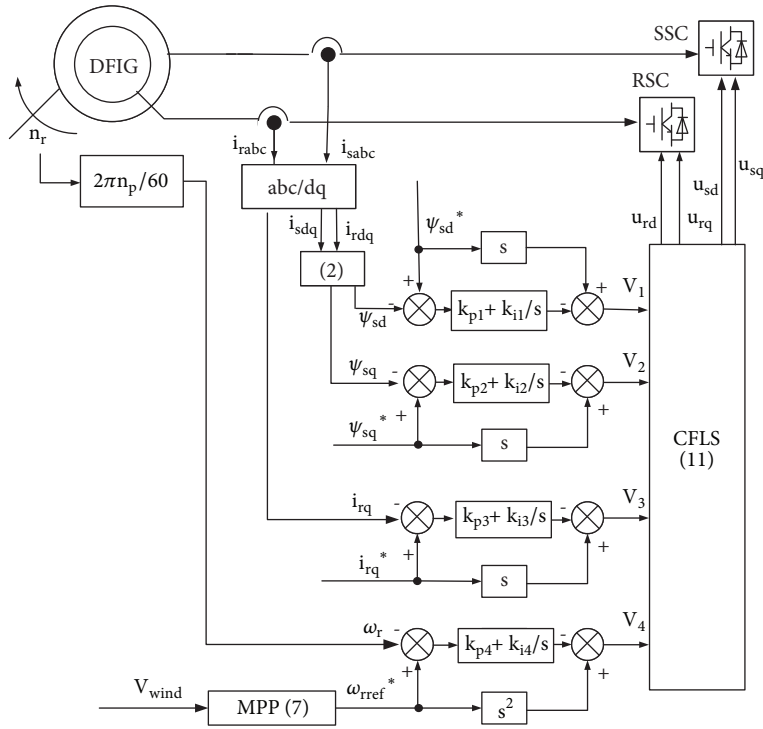


FIGURE 3: Control scheme for RSC and SSC.

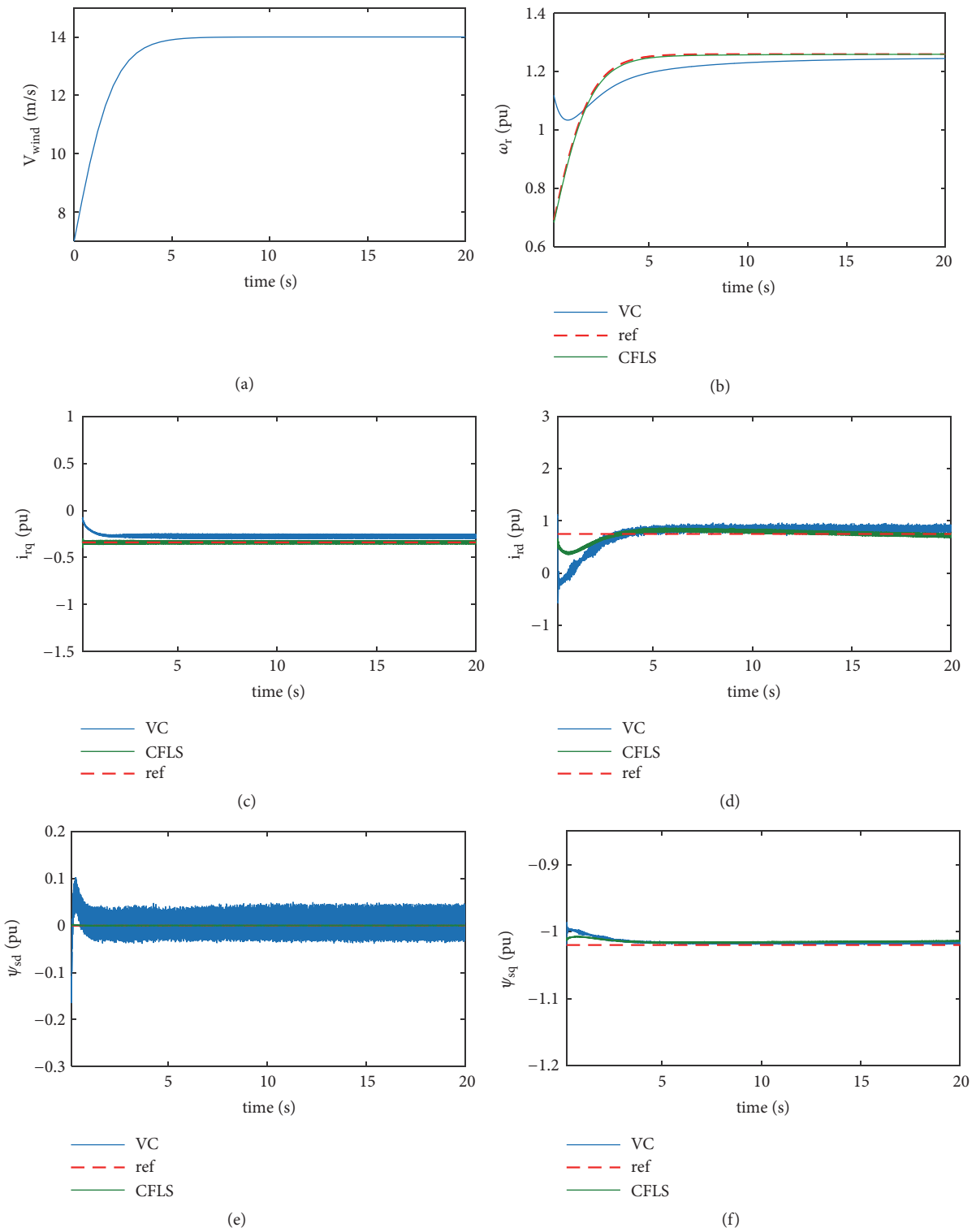


FIGURE 4: Performance response to the ramp-change wind speed.

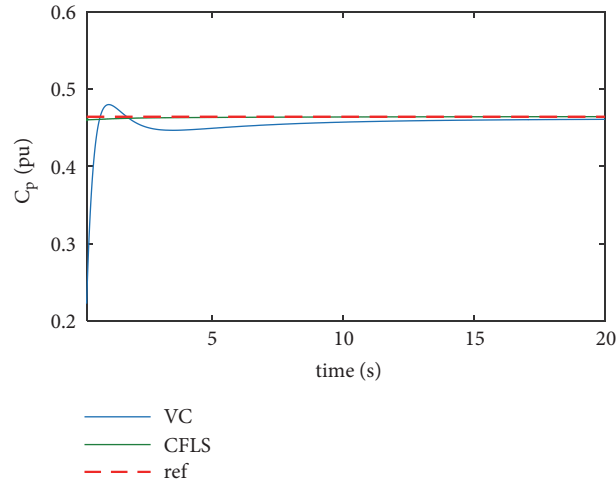


FIGURE 5:  $C_p$  at the ramp-change wind speed.

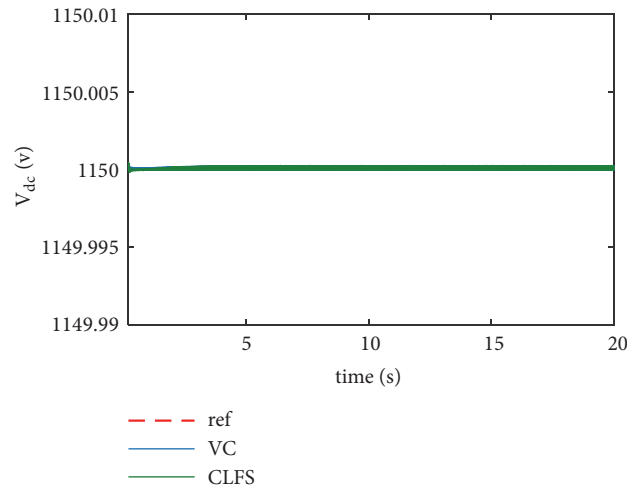


FIGURE 6:  $V_{dc}$  at the ramp-change wind speed.

this method is simple to calculate, but the disadvantage is that could not achieve full system decoupling. Article [23] adopts rotor speed and stator reactive power of DFIG in an AC grid as state variables for FLC, which computationally complex and does not select direct system parameters to controller which affects control accuracy [24].

This paper designs a CFLS for DC-based DFIG to achieve maximum power point tracking (MPPT). This control strategy employs stator flux, rotor speed, and rotor current as system inputs, applies FLC to make up a single-loop control, and achieves complete decoupling of the system, which attains coordinated optimal control performance between the SSC and the RSC. This proposed control strategy has better control accuracy and tracking speed than the traditional VC strategy.

The paper is organized as follows. In Section 2, the model of DFIG based on DC grid is introduced. In Section 3, the maximum wind power is achieved by designing CFLS.

In Section 4, simulation studies are evaluate the control performance of the proposed control strategy on a DC-based DFIG system. Finally there is conclusion of this paper.

## 2. Modeling of DFIG System

**2.1. System Configuration.** DFIG with its DC-based converters system in a DC grid is shown in Figure 1 [12]. The stator and the rotor of DFIG are connected to a DC grid through SSC and RSC. The stator voltage and frequency are completely unrestricted by the power grid. SSC can adjust stator voltage and frequency to control stator current and compensate stator reactive power. RSC can adjust rotor voltage to control rotor flux. The  $du/dt$  filter inductors are connected to stator and rotor, respectively, to prevent sharp voltage caused by converters and smooth currents.

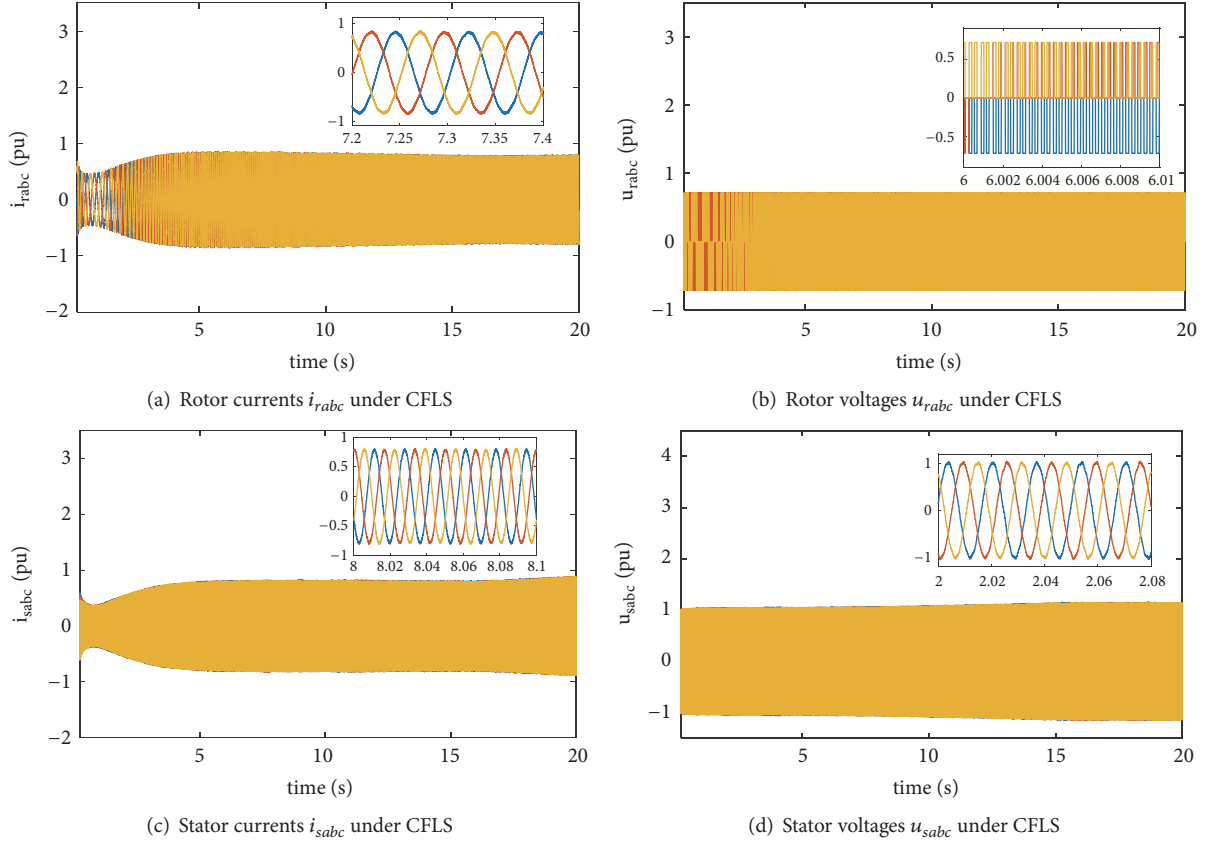


FIGURE 7: Performance response to the ramp-change wind speed.

**2.2. DFIG Model Description.** In this paper, DFIG model is adopted according to the motor direction in a d-q synchronous frame that can be expressed as [24, 25]

$$\begin{aligned}
 u_{sd} &= \frac{d\psi_{sd}}{dt} - \omega_1 \psi_{sq} + R_s i_{sd} \\
 u_{sq} &= \frac{d\psi_{sq}}{dt} + \omega_1 \psi_{sd} + R_s i_{sq} \\
 u_{rd} &= \frac{d\psi_{rd}}{dt} - \omega_s \psi_{rq} + R_r i_{rd} \\
 u_{rq} &= \frac{d\psi_{rq}}{dt} + \omega_s \psi_{rd} + R_r i_{rq} \\
 \psi_{sd} &= L_s i_{sd} + L_m i_{rd} \\
 \psi_{sq} &= L_s i_{sq} + L_m i_{rq} \\
 \psi_{rd} &= L_r i_{rd} + L_m i_{sd} \\
 \psi_{rq} &= L_r i_{rq} + L_m i_{sq} \\
 T_e - T_m &= J \frac{d\omega_m}{dt} = \frac{J}{n_p} \frac{d\omega_r}{dt} \\
 T_e &= \frac{3L_m n_p}{2L_s} (\psi_{sd} i_{rq} - \psi_{sq} i_{rd})
 \end{aligned} \tag{1}$$

where  $u_{sd}$ ,  $u_{sq}$ ,  $i_{sd}$ ,  $i_{sq}$ ,  $\psi_{sd}$ , and  $\psi_{sq}$  are the d-q components of stator voltage, current, and flux, respectively;  $u_{rd}$ ,  $u_{rq}$ ,  $i_{rd}$ ,  $i_{rq}$ ,  $\psi_{rd}$ , and  $\psi_{rq}$  are the d-q components of rotor voltage, current, and flux, respectively;  $\omega_1$ ,  $\omega_s$ ,  $\omega_r$ , and  $\omega_m$  are synchronous, slip, rotor, and mechanical angular frequency, respectively;  $L_s$ ,  $L_r$ , and  $L_m$  are the stator, rotor, and mutual inductance respectively;  $R_r$  and  $R_s$  are the rotor and stator resistance, respectively;  $T_e$  is electromagnetic torque;  $J$  is generator rotational inertia; and  $n_p$  is the number of pairs of poles.

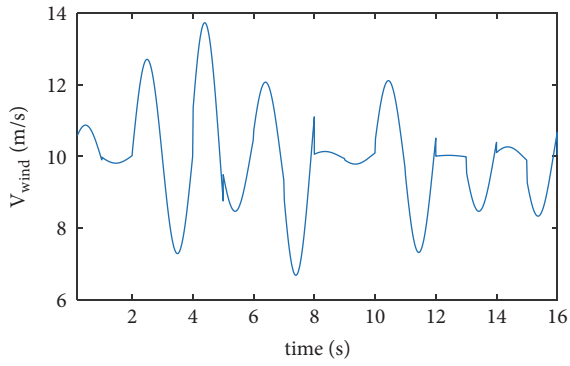
### 3. Control Strategy Description

**3.1. MPPT Control Strategy.** Usually the maximum kinetic power captured from the wind by a wind turbine is expressed as follows [26]:

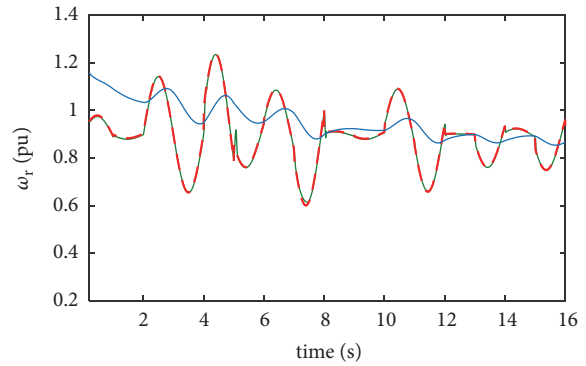
$$P_{wtmax} = \frac{1}{2} \rho \pi R_{wt} C_{pmax} V_{wind}^3 \tag{4}$$

where  $\rho$  is air density,  $R_{wt}$  is radius of wind turbine,  $V_{wind}$  is wind speed, and  $C_{pmax}$  is maximum power coefficient.

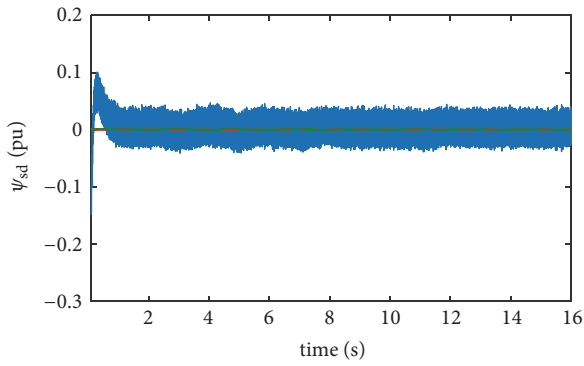
To capture the maximum wind power, the power coefficient  $C_p$  should maintain maximum  $C_{pmax}$  at any wind speed



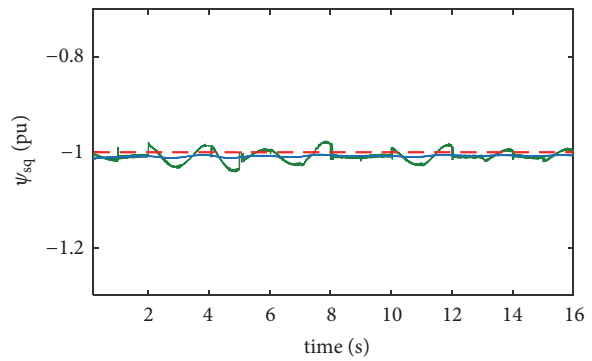
(a) Wind speed



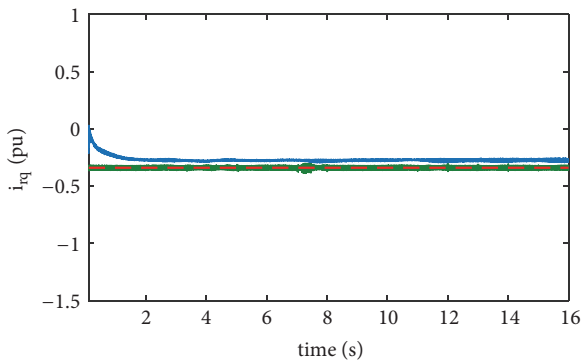
(b) Rotor speed  $\omega_r$



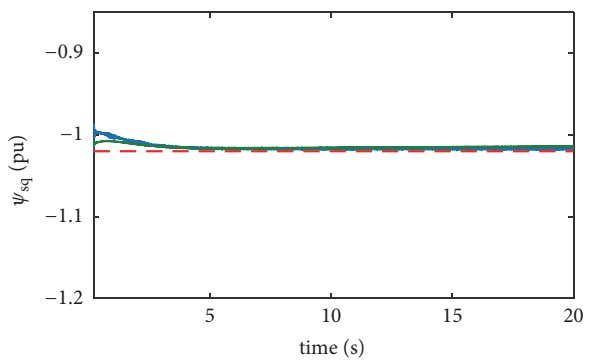
(c)  $\psi_{sd}$



(d)  $\psi_{sq}$

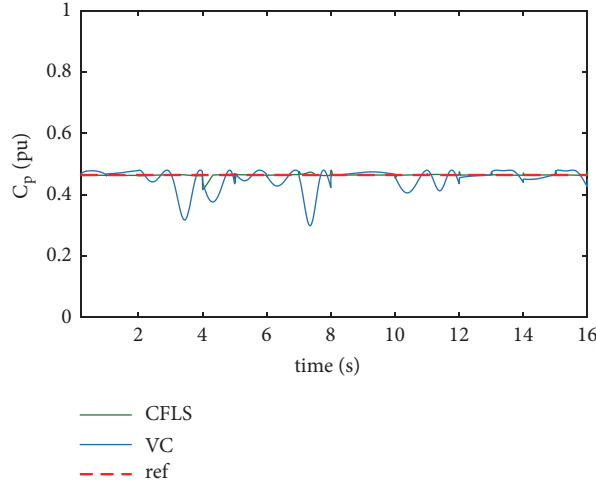


(e)  $i_{rq}(x_3)$



(f)  $i_{rd}$  under the CFLS

FIGURE 8: Performance response to the random-change wind speed.


 FIGURE 9:  $C_p$  at the random-change wind speed.

within the operating range. Maximum  $C_{pmax}$  is achieved by maintaining the tip speed ratio  $\lambda$  equal to optimal value  $\lambda_{opt}$  and the pitch angle  $\beta$  at a fixed value.

$$\begin{aligned} C_{pmax} &= C_p(\lambda_{opt}) \\ &= 0.5176 \left( \frac{116}{\lambda_i} - 0.4\beta - 5 \right) e^{-21/\lambda_i} \\ &\quad + 0.0068\lambda_{opt} \\ \frac{1}{\lambda_i} &= \frac{1}{\lambda_{opt} + 0.08\beta} - \frac{0.035}{\beta^3 + 1} \end{aligned} \quad (5)$$

The tip speed ratio  $\lambda$  indicates the state of the wind wheel under different wind speeds, as

$$\lambda = \frac{\omega_r R_{wt}}{K_1 V_{wind}} \quad (6)$$

When  $\lambda$  is equal to  $\lambda_{opt}$ , the optimal reference  $\omega_r^*$  is

$$\omega_r^* = \frac{K_1 \lambda_{opt}}{R_{wt}} V_{wind} \quad (7)$$

In this paper, the pitch angle is  $\beta = 0^\circ$ , the optimal tip speed ratio is  $\lambda_{opt} = 9.7$ , and the maximum power coefficient is  $C_{pmax} = 0.4642$ .  $P_{wtmax}$  is shown in the Figure 2.

3.2. CFLS of DFIG. From (1)-(3), the DFIG model can be derived in the form

$$\begin{aligned} \dot{x} &= f(x) + g(x)u \\ y &= h(x) \end{aligned} \quad (8)$$

where

$$\begin{aligned} x &= [x_1 \ x_2 \ x_3 \ x_4 \ x_5]^T \\ &= [\psi_{sd} \ \psi_{sq} \ i_{rd} \ i_{rq} \ \omega_r]^T \\ u &= [u_1 \ u_2 \ u_3 \ u_4]^T = [u_{sd} \ u_{sq} \ u_{rd} \ u_{rq}]^T \\ y &= [h_1(x) \ h_2(x) \ h_3(x) \ h_4(x)]^T \\ &= [x_1 \ x_2 \ x_4 \ x_5]^T = [\psi_{sd} \ \psi_{sq} \ i_{rq} \ \omega_r]^T \\ f(x) &= \begin{bmatrix} f_1(x) \\ f_2(x) \\ f_3(x) \\ f_4(x) \\ f_5(x) \end{bmatrix} \\ &= \begin{bmatrix} -\frac{R_s}{L_s}x_1 + \omega_1 x_2 + \beta R_s x_3 \\ -\omega_1 x_1 - \frac{R_s}{L_s}x_2 + \beta R_s x_4 \\ \frac{\beta R_s}{\alpha L_s}x_1 - \frac{\beta}{\alpha}x_2 x_5 - \frac{R_r + \beta^2 R_s}{\alpha}x_3 + \omega_s x_4 \\ \frac{\beta}{\alpha}x_1 x_5 + \frac{\beta R_s}{\alpha L_s}x_2 - \omega_s x_3 - \frac{R_r + \beta^2 R_s}{\alpha}x_4 \\ \frac{3L_m n_p^2}{2JL_s}(x_1 x_4 - x_2 x_3) - \frac{n_p}{J}T_m \end{bmatrix} \end{aligned}$$

$$g(x) = \begin{bmatrix} g_1(x) \\ g_2(x) \\ g_3(x) \\ g_4(x) \end{bmatrix}^T = \begin{bmatrix} 1 & 0 & 0 & 0 \\ 0 & 1 & 0 & 0 \\ -\frac{\beta}{\alpha} & 0 & \frac{1}{\alpha} & 0 \\ 0 & -\frac{\beta}{\alpha} & 0 & \frac{1}{\alpha} \\ 0 & 0 & 0 & 0 \end{bmatrix} \begin{cases} \alpha = \frac{(L_r L_s - L_m^2)}{L_s} \\ \beta = \frac{L_m}{L_s} \end{cases} \quad (9)$$

This is a multi-input multioutput (MIMO) system. An approach to obtain the input/output linearization of the

MIMO system is to differentiate the output  $y_i$  of the system until the inputs  $u_j$  appear, assuming that the corresponding relation degree  $r_i$  is the smallest integer such that at least one of the inputs explicitly appears in [27]

$$y_i^{(r_i)} = L_f^{r_i} h_i + \sum_{j=1}^m L_{g_j} L_f^{r_i-1} h_i u_j \quad (10)$$

where  $y_i^{(r_i)}$  denotes the  $r_i$ th-order derivative of  $y_i$ .

In (8),  $x$  is 5 dimensional state phase quantity,  $f_i(x)$  ( $i = 1, 2, \dots, 5$ ) is 5d smooth vector field, and  $g_i(x)$  ( $i = 1, 2, 3, 4$ ) is 4d smooth vector field. Each output  $y_i$  has a  $r_i$ , and by calculating that is 1, 1, 1 and 2. The system relation degree is  $r = 1 + 1 + 1 + 2 = 5 = n$ ; therefore, the system has no nontrivial zero dynamics, which can be linearized by feedback linearization. According to (10) and  $r_i$  of each output  $y_i$ , the Lie Derivative of  $h$  with along  $f$  and the Lie Derivative of  $L_f h(x)$  with along  $g(x)$  are obtained, and they are

$$\begin{bmatrix} \dot{y}_1 \\ \dot{y}_2 \\ \dot{y}_3 \\ \dot{y}_4 \end{bmatrix} = \begin{bmatrix} L_f h_1(x) \\ L_f h_2(x) \\ L_f h_3(x) \\ L_f^2 h_4(x) \end{bmatrix} + \begin{bmatrix} L_{g_1} L_f^0 h_1(x) & L_{g_2} L_f^0 h_1(x) & L_{g_3} L_f^0 h_1(x) & L_{g_4} L_f^0 h_1(x) \\ L_{g_1} L_f^0 h_2(x) & L_{g_2} L_f^0 h_2(x) & L_{g_3} L_f^0 h_2(x) & L_{g_4} L_f^0 h_2(x) \\ L_{g_1} L_f^0 h_3(x) & L_{g_2} L_f^0 h_3(x) & L_{g_3} L_f^0 h_3(x) & L_{g_4} L_f^0 h_3(x) \\ L_{g_1} L_f^1 h_4(x) & L_{g_2} L_f^1 h_4(x) & L_{g_3} L_f^1 h_4(x) & L_{g_4} L_f^1 h_4(x) \end{bmatrix} \begin{bmatrix} u_1 \\ u_2 \\ u_3 \\ u_4 \end{bmatrix} \quad (11)$$

According to (8) and (11), the system can be described in the following matrix form:

$$[\dot{y}_1 \quad \dot{y}_2 \quad \dot{y}_3 \quad \dot{y}_4]^T = A(x) + E(x)u \quad (12)$$

where

$$A(x) = \begin{bmatrix} -\frac{R_s}{L_s} x_1 + \omega_1 x_2 + \beta R_s x_3 \\ -\omega_1 x_1 - \frac{R_s}{L_s} x_2 + \beta R_s x_4 \\ \frac{\beta}{\alpha} x_1 x_5 + \frac{\beta R_s}{\alpha L_s} x_2 - \omega_s x_3 - \frac{R_r + \beta^2 R_s}{\alpha} x_4 \\ \xi \left[ \left( -\frac{R_s}{L_s} - \frac{R_r + \beta^2 R_s}{\alpha} \right) x_1 x_4 + (\omega_1 - \omega_s) (x_2 x_4 + x_1 x_3) \right. \\ \left. + \left( \frac{R_s}{L_s} + \frac{R_r + \beta^2 R_s}{\alpha} \right) x_2 x_3 + \frac{\beta}{\alpha} x_5 (x_1^2 + x_2^2) \right] \end{bmatrix}$$

$E(x)$

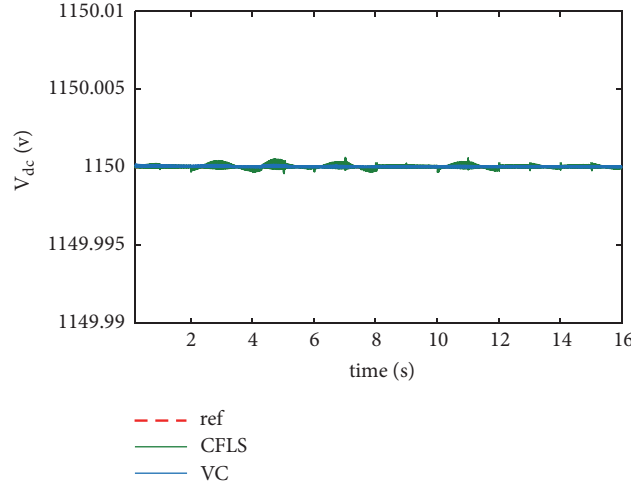
$$E(x) = \begin{bmatrix} 1 & 0 & 0 & 0 \\ 0 & 1 & 0 & 0 \\ 0 & -\frac{\beta}{\alpha} & 0 & \frac{1}{\alpha} \\ 2\xi \left( x_4 + \frac{\beta}{\alpha} x_2 \right) & -2\xi \left( x_3 + \frac{\beta}{\alpha} x_1 \right) & -2\xi \left( \frac{1}{\alpha} x_2 \right) & 2\xi \left( \frac{1}{\alpha} x_1 \right) \end{bmatrix}$$

$$\xi = \frac{3L_m n_p^2}{2JL_s} \quad (13)$$

There is  $\det(E(x)) = 2\xi x_2 / \alpha^2 \neq 0$ , so the inverse matrix  $E(x)^{-1}$  exists. A new input variable is defined for input-output feedback linearization, as  $v = [v_1 \quad v_2 \quad v_3 \quad v_4]^T$ . The conversion relation between the original input variable and the new input variable is as follows:

$$u = E(x)^{-1} (-A(x) + v) \quad (14)$$

where  $[\dot{y}_1 \quad \dot{y}_2 \quad \dot{y}_3 \quad \dot{y}_4]^T = [v_1 \quad v_2 \quad v_3 \quad v_4]^T$ . Thus, the input-output mapping of (8) can be simplified as (14), which realizes the linear decoupling between the system output and input variables. According to the MTPP control strategy, and the output is stabilized at  $\sigma^* = [\psi_{sd}^* \quad \psi_{sq}^* \quad i_{rq}^* \quad \omega_r^*]^T$ , where  $\psi_{sd}^*$ ,  $\psi_{sq}^*$ ,  $i_{rq}^*$ ,  $\omega_r^*$  are the MPP reference value of the system. Through variable substitution  $e = \sigma^* - y$  the equilibrium


 FIGURE 10:  $V_{dc}$  at the random-change wind speed.

point is moved to the origin, and the input variable can be redesigned into (14)

$$\begin{bmatrix} v_1 \\ v_2 \\ v_3 \\ v_4 \end{bmatrix} = \begin{bmatrix} \dot{\psi}_{sd}^* - k_{p1}e_1 - k_{i1} \int e_1 dt \\ \dot{\psi}_{sq}^* - k_{p2}e_2 - k_{i2} \int e_2 dt \\ \dot{i}_{rq}^* - k_{p3}e_3 - k_{i3} \int e_3 dt \\ \dot{\omega}_r^* - k_{p4}e_4 - k_{i4} \int e_4 dt \end{bmatrix} \quad (15)$$

$$\ddot{e}_i + k_{pi}\dot{e}_i + k_{ii}e_i = 0 \quad (16)$$

In the controller design we can choose the parameters  $k_{pi}$  and  $k_{ii}$  ( $i = 1, 2, 3, 4$ ) in (15) and (16) to ensure the convergence and stability of the  $e_i$  ( $i = 1, 2, 3, 4$ ). Now we have derived that the partial states  $x_1$   $x_2$   $x_3$   $x_4$  track the setting reference points.

Therefore, from the above analysis, the whole control scheme is shown in Figure 3.

**3.3. Reference Points of Controller.** The rotor flux and stator current are the control targets; the method determined in this paper is that, when a stator-oriented flux frame is adopted with its vector direction aligned with the q-axis, from (2), the stator flux reference value ( $\psi_s^*$ ) and its d-q components are given by

$$\begin{aligned} \psi_{sd}^* &= 0 \\ \psi_{sq}^* &= \psi_s^* = -\frac{V_s}{\omega_1} = -1 \end{aligned} \quad (17)$$

where  $V_s$  is generator rated voltage amplitude,  $\omega_1$  is synchronous speed. In this paper,  $V_s = 1.0$  pu,  $\omega_1 = 1.0$  pu. Substituting (17) into (2), the rotor current are obtained:

$$i_{rq}^* = -\frac{\psi_s^*}{L_m} = -0.34 \quad (18)$$

**3.4. Stability Analysis of State Variable  $x_3$ .** From the error equation (16), we obtain that the partial states  $x_1$   $x_2$   $x_4$   $x_5$  are bounded around the reference point. Next we will analyze the boundedness of the state  $x_3$ . From (8), the equation about  $x_3$  is extracted

$$\begin{aligned} \dot{x}_3 &= \frac{\beta R_s}{\alpha L_s} x_1 - \frac{\beta}{\alpha} x_2 x_5 - \frac{R_r + \beta^2 R_s}{\alpha} x_3 + \omega_s x_4 - \frac{\beta}{\alpha} u_{sd} \\ &\quad + \frac{1}{\alpha} u_{rd} \end{aligned} \quad (19)$$

Substituting (14) into (19), that can be derived as

$$\begin{aligned} \dot{x}_3 &= \left( \frac{3\beta^2 R_s - R_r}{2\alpha} + \frac{2R_s}{2L_s} \right. \\ &\quad \left. + \frac{2\omega_1 x_1 - (\beta R_s + 1)x_4 + v_2}{x_2} - \frac{x_5 x_1}{2x_2} \right) x_3 \\ &\quad - \frac{\beta x_2 x_5}{2\alpha} + \left( \frac{R_s}{L_s} + \frac{R_r + \beta^2 R_s}{\alpha} \right) \frac{x_1 x_4}{2x_2} - \frac{x_5 x_4}{2} \\ &\quad - \frac{\beta x_5 x_1^2}{2\alpha x_2} + \frac{x_4 v_1 + x_1 v_3}{x_2} - \frac{1}{2\xi x_2} v_4 \end{aligned} \quad (20)$$

From (15), the states  $x_1$   $x_2$   $x_4$   $x_5$  are convergent to  $\psi_{sd}^*$   $\psi_{sq}^*$   $i_{rq}^*$   $\omega_r^*$ , and further from (17), (18), and (7) know that their values are  $0$   $-1$   $-0.34$   $0.09V_{wind}$ , so that dynamics (20) can be approximated as

$$\dot{x}_3 = -0.0588x_3 + 0.14355V_{wind} + 0.0243\ddot{V}_{wind} \quad (21)$$

In this paper, the rated wind speed of wind turbine is  $V_{wind,nom} = 13$  m/s, and the variable wind speed range is focus on 6-14 m/s. And the high frequency components in the wind speed measurement  $V_{wind}$  may cause undesired noise; therefore the measured wind speed is passed through low-pass filter to attenuate its effect [28]. It is assumed that the

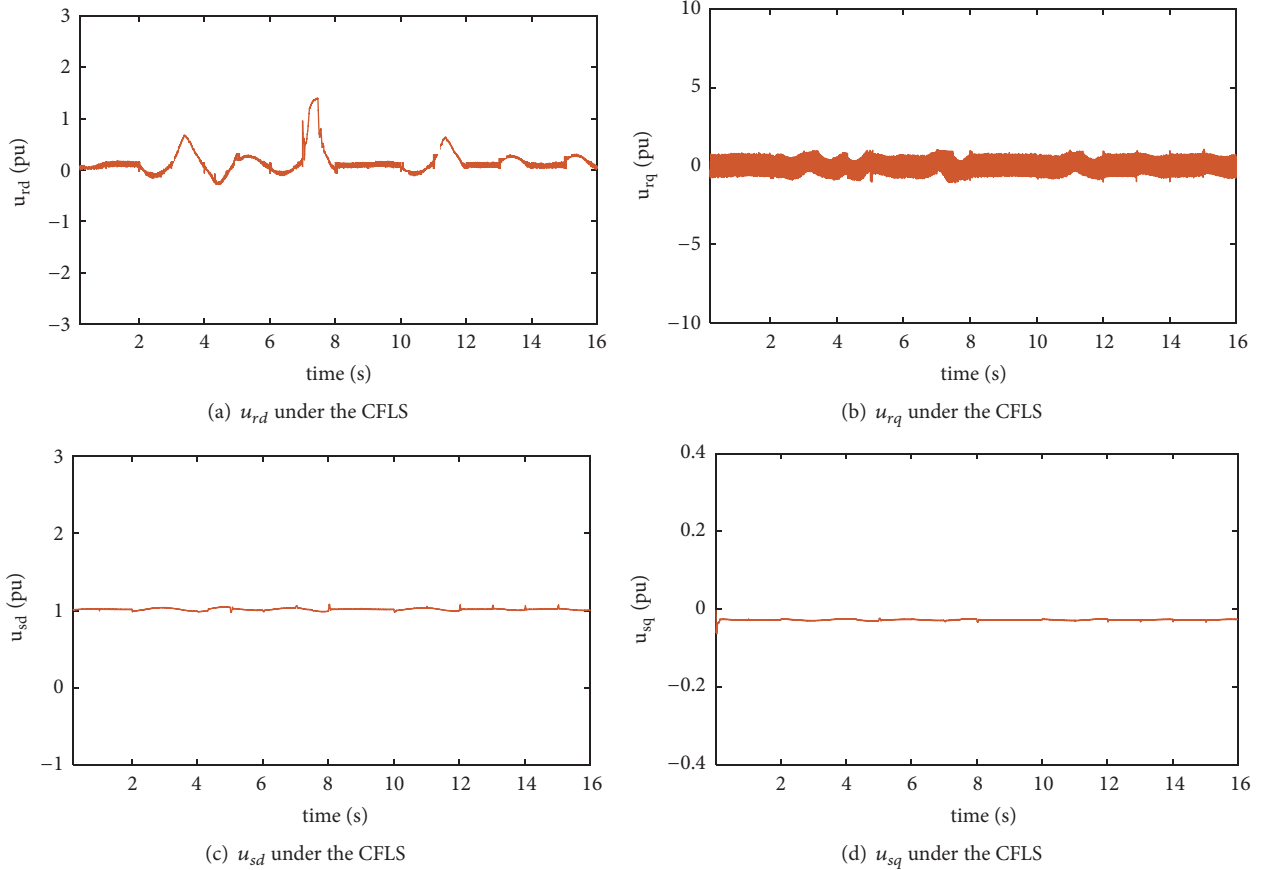


FIGURE 11: The output control signals response to the random-change wind speed.

magnitude of its derivative  $|\ddot{V}_{wind}|$  is bounded as  $|\ddot{V}_{wind}| \leq 5$ ; it becomes

$$\dot{x}_3 = -0.0588x_3 + M \quad 0.7385 \leq M \leq 2.1215 \quad (22)$$

The above can be known, the state variable  $x_3(i_{rd})$  is bounded, when  $t \rightarrow \infty$ .

#### 4. Simulation Results

In this section, simulation results are carried out in MATLAB/SIMULINK, to verify the coordinated optimal control performance in a wide range operating conditions. There are two tests performed: case one shows the accuracy of CFLS compare with the VC under the ramp-change wind and case two is the system that operates at random-change wind to show the tracking speed of controller. The DFIG system parameters in the following simulation are listed in Appendix A.

**4.1. Ramp-Change Wind.** Figures 4–7 shows the performance of a DFIG in DC-grid controlled by the VC and CFLS under the ramp-change wind. The wind speed condition is depicted in Figure 4(a). The wind speed rises from 7 m/s to 14 m/s and then remains 14 m/s. It can be seen from Figure 4(b) that the optimal reference rotor speed  $\omega_r^*$  is well tracked by the CFLS,

while the response of the VC with larger overshoots is slower. Figures 4(c), 4(e), and 4(f) show that the tracking references performance of VC and CFLS and the tracking accuracy of CFLS are better than that of VC. The state variable  $x_3(i_{rd})$  is shown in Figure 4(d), as it keep stable in both VC and CFLS under ramp-change wind.

As shown in Figure 5, the CFLS can well capture the maximum power coefficient  $C_{pmax}$  value, but the VC needs long time to catch  $C_{pmax}$ . It means that the wind turbine maintains the maximum output power under the proposed control strategy.

Figure 6 shows the system output DC-voltage  $V_{dc}$  that connected to a stable DC-grid. It can be seen that the DC voltage remains stable under the control of CFLS and VC, when the wind ramp changes.

The rotor currents and voltages  $(i_{rabc}, u_{rabc})$ , and the stator currents and voltages  $(i_{sabc}, u_{sabc})$  can be seen that the DFIG is operated at the rated value while under the CFLS in Figure 7.  $i_{sabc}$  and  $u_{sabc}$  are sine wave with frequency of 60 Hz, and their amplitudes are 1.0 pu and 0.8 pu.  $i_{rabc}$  is sine wave with amplitude of 0.85 pu.  $u_{rabc}$  is the RSC output pulse wave, and its amplitude is 0.7 pu.

**4.2. Random-Change Wind.** The performance of a DC-based DFIG system controlled by the VC and CFLS under random-change wind is shown in Figures 8–11. The wind speed

condition is depicted in Figure 8(a), which fluctuates between 6.8 m/s and 13.4 m/s. As shown in Figures 8(b), 8(c), 8(d), and 8(e), the tracking speed and accuracy of CFLS are obviously better than VC when the wind speed is time-varying. The state variable  $x_3(i_{rd})$  in the CFLS is shown in Figure 8(f), as it can stay mostly stable under the influence of random-change wind.

When the wind speed changes at any time, the power coefficient  $C_p$  should be kept at the maximum value in order to extract the maximum wind power. As shown in Figure 9, the maximum power coefficient  $C_{pmax}$  can be well captured by the CFLS. However, the change of the wind speed will affect the maximum power coefficient  $C_{pmax}$  obtained by the VC strategy. This means that the CFLS maximum power tracking performance is much better than VC in a wide range operating conditions.

System output DC-voltage  $V_{dc}$  connected to a stable DC-grid in the random-change wind speed is shown in Figure 10; it remains stable under the control of CFLS and VC.

The output control signals  $u_{rd}$   $u_{rq}$   $u_{sd}$   $u_{sq}$  of controllers are listed in Figure 11. Under the CFLS, because of the rotor speed  $\omega_r$  tracking the optimal reference rotor speed  $\omega_r^*$  that fluctuates follow the random-change wind, so the rotor side output signals  $u_{rd}$   $u_{rq}$  are fluctuated near the working point. But the stator side output signals  $u_{sd}$   $u_{sq}$  less fluctuant and operate steadily at working point. This shows that the proposed control strategy achieves the complete decoupling of DC-based DFIG system and that the stator side and rotor side have each performs its own functions, and coordinate the work.

## 5. Conclusion

From the simulation results and analysis, the following conclusions may be drawn out:

(1) A coordinated feedback linearization strategy is applied to achieve the complete decoupling and linearization for the DFIG with DC-based converter system.

(2) This paper gives up the traditional indirect dual-loop control method of power and current and selects stator flux ( $\psi_{sd}$   $\psi_{sq}$ ), rotor speed ( $\omega_r$ ), and rotor current ( $i_{rq}$ ) as state variables. A direct single-loop coordinated control method is implemented, which achieves the division cooperation between stator side and rotor side, and enhances the robustness of the system.

(3) The maximum power point tracking performance of the proposed control strategy is better than traditional VC. The CFLS kept power coefficient ( $C_p$ ) at its maximum, to make DFIG operate at the maximum power point (MPP).

In further study, this experiment will be extended to verify the effectiveness of the system in case of failure.

## Appendix

### A.

A.1. DFIG Parameters [29].  $P_{rated} = 1.5$  MW,  $f_{nom} = 60$  Hz,  $v_{s,nom} = 1.0$  pu,  $\omega_s = 1.0$  pu,  $R_s = 0.00706$  pu,

$$R_r = 0.005 \text{ pu}, L_{ls} = 0.171 \text{ pu}, L_{ms} = 2.9 \text{ pu}, n_p = 3.$$

A.2. Wind Turbine Parameters.  $\rho = 1.225$  kg/m<sup>3</sup>,  $R_{wt} = 40$  m<sup>2</sup>,  $k_1 = 3.711$ ,  $H = 5.04$  S,  $V_{wind,nom} = 13$  m/s.

A.3. VC Parameters [11]. RSC:

$$\text{Outer-loop: } k_{pp} = 4, k_{pi} = 0.1;$$

$$\text{Inner-loop: } k_{rp} = 0.496, k_{ri} = 0.0128.$$

SSC:

$$\text{Outer-loop: } k_{up} = 4, k_{ui} = 0.1;$$

$$\text{Inner-loop: } k_{sp} = 0.496, k_{si} = 0.0128.$$

## Data Availability

The data used to support the findings of this study are available from the corresponding author upon request.

## Conflicts of Interest

The authors declare that they have no conflicts of interest.

## Acknowledgments

This work was supported by National Natural Science Foundation of China (61473170).

## References

- [1] F. Akel, T. Ghennam, E. M. Berkouk, and M. Laour, "An improved sensorless decoupled power control scheme of grid connected variable speed wind turbine generator," *Energy Conversion and Management*, vol. 78, pp. 584–594, 2014.
- [2] X. She, A. Q. Huang, S. Lukic, and M. E. Baran, "On integration of solid-state transformer with zonal DC microgrid," *IEEE Transactions on Smart Grid*, vol. 3, no. 2, pp. 975–985, 2012.
- [3] W. Chen, A. Q. Huang, C. Li, G. Wang, and W. Gu, "Analysis and comparison of medium voltage high power DC/DC converters for offshore wind energy systems," *IEEE Transactions on Power Electronics*, vol. 28, no. 4, pp. 2014–2023, 2013.
- [4] M. F. Iacchetti, G. D. Marques, and R. Perini, "A scheme for the power control in a DFIG connected to a DC bus via a diode rectifier," *IEEE Transactions on Power Electronics*, vol. 30, no. 3, pp. 1286–1296, 2015.
- [5] G. D. Marques and M. F. Iacchetti, "Inner control method and frequency regulation of a DFIG connected to a dc link," *IEEE Transactions on Energy Conversion*, vol. 29, no. 2, pp. 435–444, 2014.
- [6] M. F. Iacchetti, G. D. Marques, and R. Perini, "Torque Ripple Reduction in a DFIG-DC System by Resonant Current Controllers," *IEEE Transactions on Power Electronics*, vol. 30, no. 8, pp. 4244–4254, 2015.
- [7] G. D. Marques and M. F. Iacchetti, "A Self-Sensing Stator-Current-Based Control System of a DFIG Connected to a DC-Link," *IEEE Transactions on Industrial Electronics*, vol. 62, no. 10, pp. 6140–6150, 2015.
- [8] R. Zhu, Z. Chen, and X. Wu, "Diode rectifier bridge-based structure for DFIG-based wind turbine," in *Proceedings of the IEEE Applied Power Electronics Conference and Exposition (APEC '15)*, pp. 1290–1295, Charlotte, NC, USA, March 2015.

- [9] H. Nian and X. Yi, "Coordinated control strategy for doubly-fed induction generator with DC connection topology," *IET Renewable Power Generation*, vol. 9, no. 7, pp. 747–756, 2015.
- [10] S. Yan, A. Zhang, H. Zhang, J. Wang, and B. Cai, "An Optimum Design for a DC-Based DFIG System by Regulating Gearbox Ratio," *IEEE Transactions on Energy Conversion*, vol. 33, no. 1, pp. 223–231, 2018.
- [11] S. Yan, A. Zhang, H. Zhang, and J. Wang, "Control scheme for DFIG converter system based on DC-transmission," *IET Electric Power Applications*, vol. 11, no. 8, pp. 1441–1448, 2017.
- [12] S. Yan, A. Zhang, H. Zhang, J. Wang, and B. Cai, "Transient stability enhancement of DC-connected DFIG and its converter system using fault protective device," *Journal of Modern Power Systems and Clean Energy*, vol. 5, no. 6, pp. 887–896, 2017.
- [13] S. Yan, A. Zhang, H. Zhang, J. Wang, and B. Cai, "Optimized and coordinated model predictive control scheme for DFIGs with DC-based converter system," *Journal of Modern Power Systems and Clean Energy*, vol. 5, no. 4, pp. 620–630, 2017.
- [14] W. Qiao, L. Qu, and R. G. Harley, "Control of IPM synchronous generator for maximum wind power generation considering magnetic saturation," *IEEE Transactions on Industry Applications*, vol. 45, no. 3, pp. 1095–1105, 2009.
- [15] N. Reddy Naguru, A. Karthikeyan, C. Nagamani, and V. Sravan Kumar, "Comparative study of power control of DFIG using PI control and feedback linearization control," in *Proceedings of the International Conference on Advances in Power Conversion and Energy Technologies (APCET '12)*, pp. 1–6, August 2012.
- [16] L. Jiang and Q. Wu, "Nonlinear adaptive control via sliding-mode state and perturbation observer," *IEEE Proceedings - Control Theory and Applications*, vol. 149, no. 4, pp. 269–277, 2002.
- [17] Z. Zhang, Y. Wu, and J. Huang, "Differential-flatness-based finite-time anti-swing control of underactuated crane systems," *Nonlinear Dynamics*, vol. 87, no. 3, pp. 1749–1761, 2017.
- [18] L. Gao and D. Wang, "Input-to-state stability and integral input-to-state stability for impulsive switched systems with time-delay under asynchronous switching," *Nonlinear Analysis: Hybrid Systems*, vol. 20, pp. 55–71, 2016.
- [19] X. Yan, X. Song, and X. Wang, "Global output-feedback stabilization for nonlinear time-delay systems with unknown control coefficients," *International Journal of Control, Automation, and Systems*, vol. 16, no. 4, pp. 1550–1557, 2018.
- [20] X. Xie, N. Duan, and C. Zhao, "A combined homogeneous domination and sign function approach to output-feedback stabilization of stochastic high-order nonlinear systems," *IEEE Transactions on Automatic Control*, vol. 59, no. 5, pp. 1303–1309, 2014.
- [21] Y. Wu, J. Yu, and Y. Zhao, "Output feedback regulation control for a class of cascade nonlinear systems and its application to fan speed control," *Nonlinear Analysis: Real World Applications*, vol. 13, no. 3, pp. 1278–1291, 2012.
- [22] X. Lin, K. S. Xiahou, Y. Liu, Y. B. Zhang, and Q. H. Wu, "Maximum power point tracking of DFIG-WT using feedback linearization control based current regulators," in *Proceedings of the IEEE Innovative Smart Grid Technologies - Asia (ISGT-Asia '16)*, pp. 718–723, Melbourne, Australia, November 2016.
- [23] B. Yang, L. Jiang, L. Wang, W. Yao, and Q. Wu, "Nonlinear maximum power point tracking control and modal analysis of DFIG based wind turbine," *International Journal of Electrical Power & Energy Systems*, vol. 74, pp. 429–436, 2016.
- [24] R. Cardenas, R. Pena, S. Alepuz, and G. Asher, "Overview of control systems for the operation of DFIGs in wind energy applications," *IEEE Transactions on Industrial Electronics*, vol. 60, no. 7, pp. 2776–2798, 2013.
- [25] M. Tazil, V. Kumar, R. C. Bansal et al., "Three-phase doubly fed induction generators: an overview," *IET Electric Power Applications*, vol. 4, no. 2, pp. 75–89, 2010.
- [26] W. Qiao, "Dynamic modeling and control of doubly fed induction generators driven by wind turbines," in *Proceedings of the IEEE/PES Power Systems Conference and Exposition (PSCE '09)*, pp. 1–8, March 2009.
- [27] H. K. Khalil, *Nonlinear Systems*, 3rd edition, 2002.
- [28] W. Qiao, W. Zhou, J. M. Aller, and R. G. Harley, "Wind speed estimation based sensorless output maximization control for a wind turbine driving a DFIG," *IEEE Transactions on Power Electronics*, vol. 23, no. 3, pp. 1156–1169, 2008.
- [29] N. W. Miller et al., "Dynamic modeling of GE 1.5 and 3.6 MW wind turbine-generators for stability simulations," *Power Engineering Society General Meeting IEEE*, vol. 3, pp. 1977–1983, 2004.

## Research Article

# Fractional-Order Adaptive Backstepping Control of a Noncommensurate Fractional-Order Ferroresonance System

Yan Wang <sup>1</sup>, Ling Liu,<sup>1</sup> Chongxin Liu,<sup>1</sup> Ziwei Zhu,<sup>1</sup> and Zhenquan Sun<sup>2</sup>

<sup>1</sup>State Key Laboratory of Electrical Insulation and Power Equipment, School of Electrical Engineering, Xi'an Jiaotong University, Xi'an 710049, China

<sup>2</sup>Shaanxi Provincial Electric Power Design and Research Institute, Xi'an 710065, China

Correspondence should be addressed to Yan Wang; 1142716188@qq.com

Received 30 July 2018; Revised 3 October 2018; Accepted 29 October 2018; Published 7 November 2018

Academic Editor: S. Hassan Hosseinnia

Copyright © 2018 Yan Wang et al. This is an open access article distributed under the Creative Commons Attribution License, which permits unrestricted use, distribution, and reproduction in any medium, provided the original work is properly cited.

In this paper, fractional calculus is applied to establish a novel fractional-order ferroresonance model with fractional-order magnetizing inductance and capacitance. Some basic dynamic behaviors of this fractional-order ferroresonance system are investigated. And then, considering noncommensurate orders of inductance and capacitance and unknown parameters in an actual ferroresonance system, this paper presents a novel fractional-order adaptive backstepping control strategy for a class of noncommensurate fractional-order systems with multiple unknown parameters. The virtual control laws and parameter update laws are designed in each step. Thereafter, a novel fractional-order adaptive controller is designed in terms of the fractional Lyapunov stability theorem. The proposed control strategy requires only one control input and can force the output of the chaotic system to track the reference signal asymptotically. Finally, the proposed method is applied to a noncommensurate fractional-order ferroresonance system with multiple unknown parameters. Numerical simulation confirms the effectiveness of the proposed method. In addition, the proposed control strategy also applies to commensurate fractional-order systems with unknown parameters.

## 1. Introduction

Fractional calculus is a generalization of ordinary integration and differentiation to arbitrary order [1]. In recent years, some scholars pointed out that there exist a large number of fractal phenomena in nature [2], which should not be modeled and analyzed by the classical calculus but fractional calculus. Two main outstanding advantages of fractional calculus have drawn great attention of scholars. The first advantage is that fractional calculus has unlimited memory and can take into account the previous responses up to the present time. Fractional calculus can provide clearer and more accurate description than the classical calculus methods without memory which is only a particular case. Furthermore, with the help of fractional-order calculus, we can obtain more accurate descriptions of the physical phenomena, such as electrical circuit [3, 4], power system [5, 6], signal processing [7], secure communication [8], bioengineering [9], and image encryption [10]. Second, the

fractional-order  $\alpha$  can enhance the flexibility of parameters and reveal various unusual characteristics of the fractional-order system and fractional-order controllers which remain concealed in the integer-order method. It has been confirmed that the controller based on fractional calculus leads to better closed-loop performance by improving transient and steady-state responses than integer-order approaches [11, 12]. One of the most striking applications of fractional calculus is fractional-order controllers. In recent years, some excellent fractional-order controllers have been investigated, such as fractional-order PID control [13], fractional-order sliding mode control [5], fractional fuzzy control [14], and fractional-order backstepping control [15].

As a complex nonlinear phenomenon in a power system, ferroresonance can result in chaotic oscillation and push the power system to instability, which may cause overvoltage and overcurrent, voltage collapse, and even large-scale blackout [16–18]. At present, the trend of establishing a large-scale power grid, which may cause more uncertainties

and disturbances in the power system, results in some ferroresonance incidents. Thus, it is necessary to suppress the chaotic oscillation caused by ferroresonance and many scholars have studied some excellent methods [19–21] to eliminate ferroresonance. In fact, the actual inductance and capacitance modeled by fractional calculus are more accurate than the classical integer method [3, 4]. In addition, the fractional-order model can provide clear description of real systems with unmodeled dynamics, uncertainties, and noise, which the integer-order model fails to do. Many real dynamical circuits, like RLC circuit, resonance circuits with ultracapacitors, fractional-order Chua's circuit, and so on, have been investigated by the fractional-order model [22–26]. However, to the best of our knowledge, there are almost no reports about the fractional-order ferroresonance system, especially the more general noncommensurate case. Thus, it is necessary to investigate, study, and suppress ferroresonance by the novel and interesting fractional-order method.

Within the aforementioned fractional-order control method, the backstepping control strategy, which can simplify the controller, is an effective control technique for the systems with strict-feedback structure. Various excellent fractional-order backstepping strategies have been investigated and proposed in recent studies. In [15], a fractional-order backstepping controller to realize the stabilization of a fractional-order chaotic system was proposed via fractional Lyapunov functions. In [27], an adaptive backstepping controller to stabilize fractional-order Chua's circuit was designed. Ref. [28] promoted the adaptive backstepping technique to the system which does not have strict-feedback structure and avoided singularity effectively in the proposed controller. In [14], an adaptive fuzzy backstepping controller was designed for the fractional-order system with unknown external disturbances. In [29], an adaptive backstepping controller was designed for the noncommensurate fractional-order system via the fractional-order Lyapunov indirect method. In [12], a finite time fractional-order adaptive backstepping controller was applied to robotic manipulators with uncertainties and external disturbances.

In fact, the orders of actual inductance and capacitance of the ferroresonance system are not all the same which means that the fractional-order ferroresonance system is a noncommensurate fractional-order system. Nevertheless, most of the aforementioned fractional-order backstepping methods only apply to the commensurate fractional-order systems. Though the fractional-order extension of the Lyapunov direct method proposed in [30] has been used in some present works, designing an excellent controller for noncommensurate fractional-order systems is still an open and challenging problem [31]. To the best of our knowledge, there are almost no reports about noncommensurate fractional-order backstepping control for noncommensurate fractional-order via the fractional-order Lyapunov direct method. Furthermore, considering the uncertainties of a real ferroresonance system in practice, investigation of fractional-order adaptive backstepping control for noncommensurate fractional-order systems with unknown parameters is necessary.

Motivated by the above considerations, we establish a novel noncommensurate fractional-order ferroresonance model. And then, to suppress undesirable chaotic behaviors of the proposed system, a novel fractional-order adaptive controller is designed for the noncommensurate fractional-order system with unknown parameters via the fractional-order Lyapunov direct method. Virtual control laws and parameter update laws are designed in terms of the backstepping procedures. The stability of the system under control is guaranteed by the fractional Lyapunov stability theorem. Finally, chaotic behaviors of the noncommensurate and commensurate fractional-order ferroresonance systems with multiple unknown parameters are eliminated, which illustrates the effectiveness and feasibility of the proposed method.

The rest of this paper is organized as follows. Section 2 contains preliminary knowledge throughout this paper. Dynamic analysis and the adaptive controller of the fractional-order ferroresonance system are presented in Section 3. Section 4 contains the simulation results. Finally, the conclusion is drawn in Section 5.

## 2. Preliminary

In the development of fractional calculus theory, many kinds of definitions were proposed. At present, the widely accepted fractional definitions are the Riemann-Liouville definition and Caputo definition. The initial value conditions of the Caputo fractional-order differential equations are clearer than the Riemann-Liouville definition. Thus, in this paper, the Caputo fractional calculus definition is employed.

*Definition 1* (see [11]). The  $\alpha$ th-order Caputo fractional derivative of function  $f(t)$  is defined as

$${}^C D_t^\alpha f(t) = \begin{cases} \frac{1}{\Gamma(m-\alpha)} \int_{t_0}^t \frac{f^m(\tau)}{(t-\tau)^{\alpha-m+1}} d\tau, & m-1 < \alpha < m \\ \frac{d^m f(t)}{dt^m}, & \alpha = m, \end{cases} \quad (1)$$

where  $m$  is the smallest integer number larger than or equal to  $\alpha$ ,  $\Gamma(\cdot)$  is the Gamma function, and  $C$  represents the Caputo definition. In this paper,  ${}^C D_t^\alpha$  is abbreviated as  $D^\alpha$  when  $t_0 = 0$ .

Properties 2 and 3 hold for both the Caputo derivative and Riemann-Liouville derivative.

*Property 2* (see [2]). For  $\alpha = 0$ , it has

$${}_0 D_t^0 f(t) = f(t). \quad (2)$$

*Property 3* (see [2]). The additive index law:

$${}_0 D_t^\alpha {}_0 D_t^\beta f(t) = {}_0 D_t^\beta {}_0 D_t^\alpha f(t) = {}_0 D_t^{\alpha+\beta} f(t). \quad (3)$$

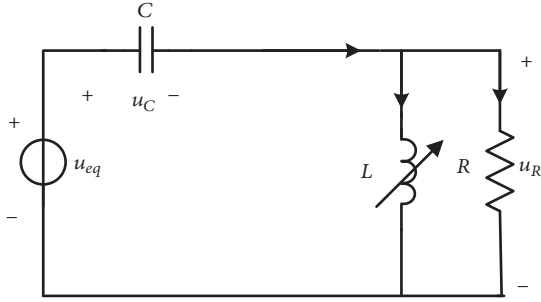


FIGURE 1: The simplified ferroresonance system circuit model.

**Lemma 4** (see [32]). Let  $x(t) \in \mathbb{R}$  be a continuous and derivable function. Then, for any  $t \geq t_0$ , it has

$$\frac{1}{2} {}^C D_t^\alpha x^2(t) \leq x(t) {}^C D_t^\alpha x(t), \quad \forall \alpha \in (0, 1). \quad (4)$$

**Lemma 5** (see [33]). Let  $\mathbf{x} = 0$  be an equilibrium point of the following nonautonomous fractional-order system:

$${}_0 D_t^\alpha \mathbf{x} = f(t, \mathbf{x}), \quad (5)$$

where  $\alpha \in (0, 1]$ , the symbol  $D$  can denote both the Caputo and Riemann-Liouville fractional operators, and  $f(t)$  satisfies the Lipschitz condition. Assume that there exists a Lyapunov function  $V(t, \mathbf{x}(t))$  which satisfies

$$\alpha_1(\|\mathbf{x}\|) \leq V(t, \mathbf{x}(t)) \leq \alpha_2(\|\mathbf{x}\|) \quad (6)$$

$$D^\beta V(t, \mathbf{x}(t)) \leq -\alpha_3(\|\mathbf{x}\|), \quad (7)$$

where  $\beta \in (0, 1)$  and there exists three class  $K$  functions  $\alpha_i$ ,  $i = 1, 2, 3$ . Then system (5) is Mittag-Leffler stable, asymptotically.

### 3. Main Results

**3.1. Dynamic Analysis.** A classic two-order nonautonomous ferroresonance chaotic circuit model [17, 18] is shown in Figure 1. The circuit is derived by a sinusoidal voltage source  $u_{eq} = (C_g / (C_b + C_g)) u_{SY}$ , where  $C_b$  is the grading capacitance of circuit breaker,  $C_g$  is the bus-to-ground capacitance, and note  $C = C_b + C_g$  as equivalent capacitance.  $u_{SY}$  is the system voltage and it has  $u_{SY} = U_m \sin \omega t$ ,  $L$  is magnetizing inductance, and  $R$  is the equivalent resistance corresponding to the system losses. For very high currents, the transformer coil is saturated and the flux-current characteristic  $\psi - i$  of the transformer becomes highly nonlinear which is approximated by  $i = a\psi + b\psi^n$ , where  $\psi$  represents the flux of the nonlinear inductance and  $n$  is the index of nonlinearity of the curve.

With the help of fractional calculus, losses of actual magnetizing inductance and capacitance can be described more accurately [3, 4]. Therefore, we try to investigate some dynamic behaviors of the ferroresonance system with noncommensurate fractional-order magnetizing inductance and

capacitance. The system shown in Figure 1 can be described as

$$\begin{aligned} \frac{d^{q_1} \psi}{dt^{q_1}} &= u_R \\ \frac{d^{q_2} u_R}{dt^{q_2}} &= \omega \frac{U_m C_b}{C} \cos \omega t - \frac{u_R}{RC} - \frac{a\psi + b\psi^n}{C}, \end{aligned} \quad (8)$$

where  $q_1$  is the order of fractional-order magnetizing inductance  $L$  and  $q_2$  is the order of fractional-order capacitance  $C$ . For the general case, it usually has  $q_1 \neq q_2$  and  $q_1, q_2 \in (0, 1)$ . Let  $x_1 = \psi$ ,  $x_2 = u_R / \omega$ , and  $\tau = \omega t$ . Then, (8) can be rewritten as

$$\frac{d^{q_1} x_1}{d\tau^{q_1}} = x_2 \quad (9)$$

$$\frac{d^{q_2} x_2}{d\tau^{q_2}} = q \cos(\tau) - p x_2 - p_1 x - p_2 x^n,$$

where  $q = U_m C_b / \omega C$ ,  $p = 1 / \omega C R$ ,  $p_1 = a / \omega^2 C$ , and  $p_2 = b / \omega^2 C$ . According to most actual 110kV transformer substations in China, set  $p = 1.155 \times 10^{-2}$ ,  $p_1 = 1.94 \times 10^{-4}$ ,  $p_2 = 4.99 \times 10^{-4}$ , and  $n = 11$ . The simulation in this paper is based on the Adams-Bashforth-Moulton method.

**Remark 6.** The fractional-order magnetizing inductance  $L$  and fractional-order capacitance  $C$  are fractance devices which can be approximately equivalent to the tree or chain structure of ideal inductance, capacitance, and resistance [34–36]. Due to the resistance of the equivalent tree or chain structure, impedance and capacitance of fractance devices contain both real and imaginary parts. The real parts will increase the loss of the fractional-order system. Furthermore, the fractance devices will result in more complicated dynamic behaviors than the integer-order model.

To investigate dynamic behaviors with different orders of the proposed system, set  $q_1 = 0.99$  and  $q_2 = 0.98$ . As the bifurcation diagram with  $q$  varying from 0 to 10 shown in Figure 2, the periodic and chaotic states appear alternately. Phase portraits and time series of states of  $q = 5.85$  shown in Figures 3–5 indicate that the noncommensurate fractional-order ferroresonance system exhibits chaotic oscillation. For the integer-order case  $q_1 = q_2 = 1$ , the bifurcation diagram with  $q$  varying from 0 to 10 is shown in Figure 6 which indicates that the integer-order ferroresonance system exhibits chaotic oscillation with  $q > 0.841$ . As the phase portraits and time series of states of  $q = 5.85$  shown in Figures 7–9, the system also exhibits chaotic oscillation. Although there exists some difference of bifurcation behaviors between Figures 2 and 6, serious overvoltage occurs in both the integer-order and noncommensurate fractional-order case.

**3.2. Controller Design.** In an actual ferroresonance system, it is difficult to obtain accurate values of bus-to-ground capacitance  $C_g$  and parameters  $a$  and  $b$  which results in that parameters  $q$ ,  $p$ ,  $p_1$ , and  $p_2$  are actually unknown parameters. To suppress undesirable chaotic behaviors in the power

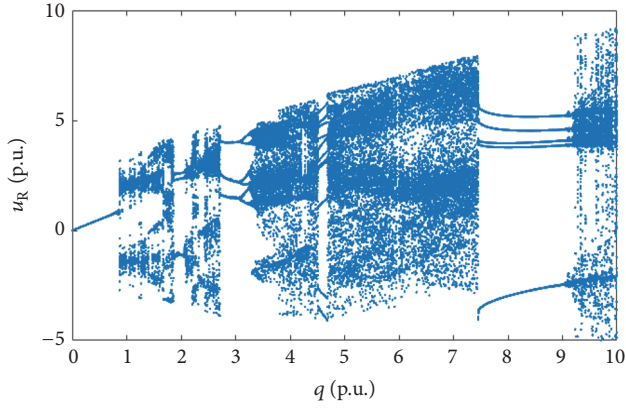
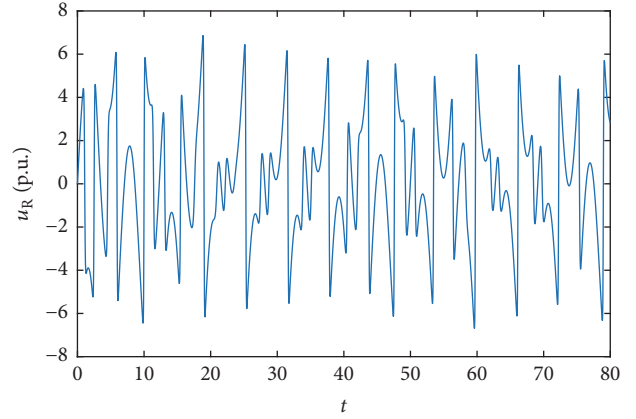
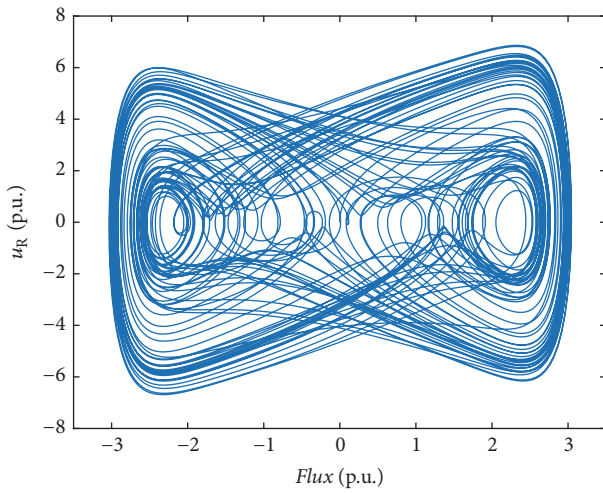
FIGURE 2: Bifurcation diagram with  $q$ .FIGURE 5: Time series with  $x_2$ .

FIGURE 3: The phase portraits.

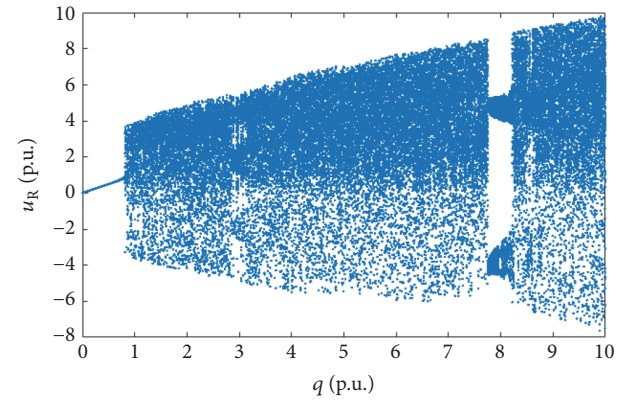
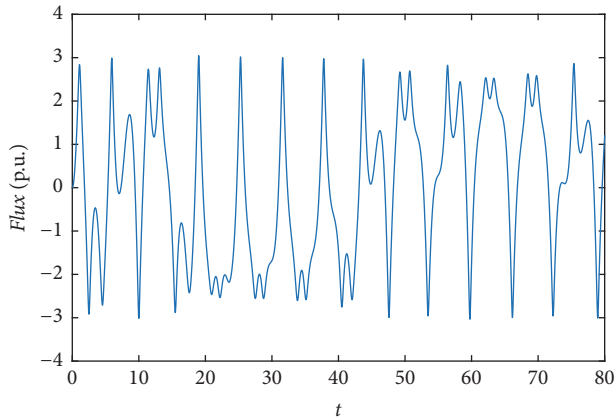
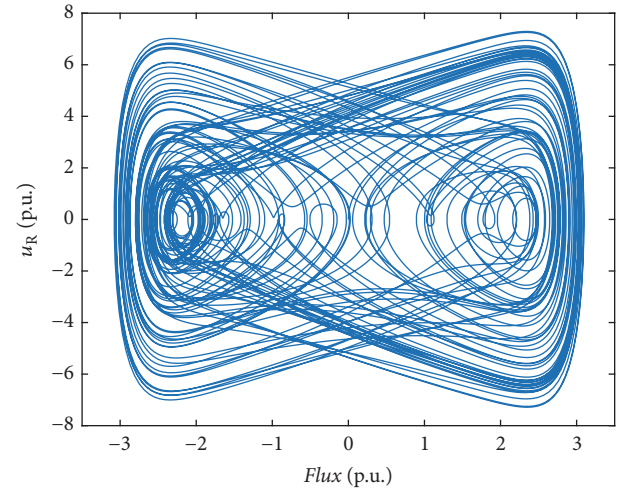
FIGURE 6: Bifurcation diagram with  $q$ .FIGURE 4: Time series with  $x_1$ .

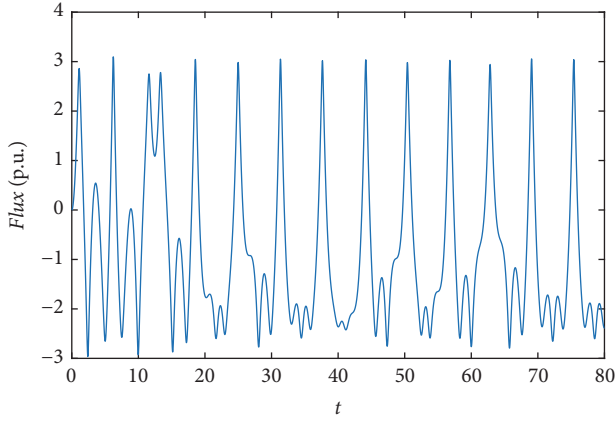
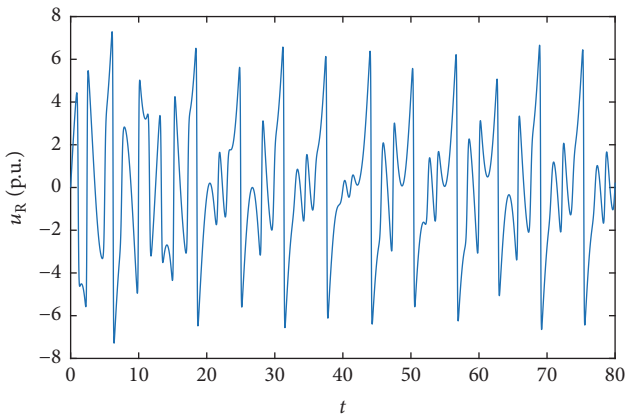
FIGURE 7: The phase portraits.

system and design an effective controller for such noncommensurate fractional-order systems with multiple unknown parameters, let us consider the following strict-feedback noncommensurate fractional-order system with unknown parameters:

$$D^{\alpha_i} x_i = c_i x_{i+1} + \theta_i^T F_i(x_1 \cdots x_i, t) + f_i(x_1 \cdots x_i, t)$$

$$\begin{aligned} D^{\alpha_n} x_n &= c_n u + \theta_n^T F_n(x_1 \cdots x_n, t) + f_n(x_1 \cdots x_n, t) \\ y &= x_1, \quad i = 1, \dots, n-1, \end{aligned} \quad (10)$$

where system orders  $\alpha_i \in (0, 1)$  are not all the same.  $\mathbf{x} = [x_1, \dots, x_n]^T$  is the state vector,  $u$  is controller input, and  $y$


 FIGURE 8: Time series with  $x_1$ .

 FIGURE 9: Time series with  $x_2$ .

is the output of system (10).  $\theta_i \in \mathbb{R}^q$  ( $i = 1, \dots, n-1$ ) is the vector of unknown constant parameters.  $c_i \in \mathbb{R}$  ( $i = 1, \dots, n$ ) is a known constant.  $F_i(x_1 \dots x_i, t)$  and  $f_i(x_1 \dots x_i, t)$  are known smooth nonlinear or linear functions and they are abbreviated as  $F_i$  and  $f_i$  in this paper.

Obviously, noncommensurate fractional-order ferroresonance system (8) is a particular case of the strict-feedback noncommensurate fractional-order system with unknown parameters (10). To design an excellent adaptive backstepping controller for system (10), in each step, a virtual controller and parameter update law are designed systematically until the last equation which contains the controller.

The result is stated by the following theorem.

**Theorem 7.** For system (10), let the following designs:

The tracking error variables:

$$e_i = r_i - x_i, \quad i = 1, 2, \dots, n. \quad (11)$$

The virtual control laws:

$$\begin{aligned} r_2 &= \frac{1}{c_1} \left[ D^{\alpha_1} r_1 - \hat{\theta}_1^T F_1 - f_1 + k_1 D^{\alpha_1 - \alpha_\xi} e_1 \right] \\ r_{i+1} &= \frac{1}{c_i} \left[ D^{\alpha_i} r_i - \hat{\theta}_i^T F_i - f_i + k_i D^{\alpha_i - \alpha_\xi} e_i \right. \\ &\quad \left. + c_{i-1} e_i \operatorname{sign} \left( D^{\alpha_{i-1} - \alpha_\xi} e_{i-1} \right) \operatorname{sign} \left( D^{\alpha_i - \alpha_\xi} e_i \right) \right] \\ &\quad i = 2, \dots, n-1. \end{aligned} \quad (12)$$

The parameter update laws:

$$D^{\alpha_\xi} \hat{\theta}_i^T = -\Lambda \cdot F_i \operatorname{sign} \left( D^{\alpha_i - \alpha_\xi} e_i \right), \quad i = 1, \dots, n. \quad (13)$$

The adaptive control law:

$$\begin{aligned} u &= \frac{1}{c_n} \left[ D^{\alpha_n} r_n - \hat{\theta}_n^T F_n - f_n + k_n D^{\alpha_n - \alpha_\xi} e_n \right. \\ &\quad \left. + c_{n-1} e_n \operatorname{sign} \left( D^{\alpha_{n-1} - \alpha_\xi} e_{n-1} \right) \operatorname{sign} \left( D^{\alpha_n - \alpha_\xi} e_n \right) \right]. \end{aligned} \quad (14)$$

Then the tracking error is stable asymptotically and globally as

$$\lim_{t \rightarrow \infty} (y - r_1) = 0, \quad (15)$$

where  $\alpha_\xi$  is the smallest order of  $\alpha_i$ .  $r_1$  is a smooth reference signal and its  $(\alpha_1, \dots, \sum_{i=1}^n \alpha_i)$ -th-order derivatives are bounded and continuous.  $k_i$  is a positive constant and  $\Lambda = \operatorname{diag}(k, k, \dots, k)$ ,  $k > 0$ .

*Proof.*

*Step 1.* Find the smallest order  $\alpha_\xi$  of noncommensurate fractional-order system (10); let  $e_1 = r_1 - x_1$ ,  $e_2 = r_2 - x_2$ .  $\tilde{\theta}_1 = \hat{\theta}_1 - \theta_1$  is the adaptive parameter tracking error and  $r_2$  is the first virtual controller. The first subsystem is given as

$$D^{\alpha_1} x_1 = c_1 (r_2 - e_2) + \theta_1^T F_1 + f_1. \quad (16)$$

Choose the Lyapunov function candidate as

$$V_1 = |D^{\alpha_1 - \alpha_\xi} e_1| + \frac{1}{2} \tilde{\theta}_1^T \Lambda^{-1} \tilde{\theta}_1. \quad (17)$$

Note  $\mathbf{z}^T = [D^{\alpha_1 - \alpha_\xi} e_1, \tilde{\theta}_1^T]$  and the K-class functions  $\alpha_1$  and  $\alpha_2$  are selected as  $\alpha_1(\mathbf{z}) = \min(|\mathbf{z}|, (1/2)\mathbf{z}^T \Lambda^{-1} \mathbf{z})$ ,  $\alpha_2(\mathbf{z}) = |\mathbf{z}| + (1/2)\mathbf{z}^T \Lambda^{-1} \mathbf{z}$ . Thus, (17) satisfies condition (6). And then, take the  $\alpha_\xi$  order derivative of Lyapunov function (17) and use Lemma 4; we obtain

$$\begin{aligned} D^{\alpha_\xi} V_1 &= D^{\alpha_1} e_1 \cdot \operatorname{sign} \left( D^{\alpha_1 - \alpha_\xi} e_1 \right) + D^{\alpha_\xi} \left( \frac{1}{2} \tilde{\theta}_1^T \Lambda^{-1} \tilde{\theta}_1 \right) \\ &\leq D^{\alpha_1} (r_1 - x_1) \operatorname{sign} \left( D^{\alpha_1 - \alpha_\xi} e_1 \right) + \tilde{\theta}_1^T \Lambda^{-1} D^{\alpha_\xi} \tilde{\theta}_1 \\ &\leq \left( D^{\alpha_1} r_1 + c_1 e_2 - c_1 r_2 - \theta_1^T F_1 - f_1 \right) \\ &\quad \times \operatorname{sign} \left( D^{\alpha_1 - \alpha_\xi} e_1 \right) + \tilde{\theta}_1^T \Lambda^{-1} D^{\alpha_\xi} \tilde{\theta}_1. \end{aligned} \quad (18)$$

Then choose the first virtual control law  $r_2$  as

$$r_2 = \frac{1}{c_1} \left( D^{\alpha_1} r_1 - \hat{\theta}_1^T F_1 - f_1 + k_1 D^{\alpha_1 - \alpha_\xi} e_1 \right) \quad (19)$$

which leads to

$$\begin{aligned} D^{\alpha_\xi} V_1 &\leq \left( c_1 e_2 + \hat{\theta}_1^T F_1 - k_1 D^{\alpha_1 - \alpha_\xi} e_1 \right) \\ &\quad \times \operatorname{sign} \left( D^{\alpha_1 - \alpha_\xi} e_1 \right) + \tilde{\theta}_1^T \Lambda^{-1} D^{\alpha_\xi} \tilde{\theta}_1 \\ &\leq -k_1 |D^{\alpha_1 - \alpha_\xi} e_1| + \left( c_1 e_2 + \hat{\theta}_1^T F_1 \right) \\ &\quad \times \operatorname{sign} \left( D^{\alpha_1 - \alpha_\xi} e_1 \right) + \tilde{\theta}_1^T \Lambda^{-1} D^{\alpha_\xi} \tilde{\theta}_1. \end{aligned} \quad (20)$$

Choose the first parameter update law  $\hat{\theta}_1$  as

$$D^{\alpha_\xi} \hat{\theta}_1 = -\Lambda \cdot F_1 \text{sign}(D^{\alpha_1 - \alpha_\xi} e_1). \quad (21)$$

Substitute (21) into (20), which leads to

$$D^{\alpha_\xi} V_1 \leq -k_1 |D^{\alpha_1 - \alpha_\xi} e_1| + c_1 e_2 \text{sign}(D^{\alpha_1 - \alpha_\xi} e_1). \quad (22)$$

*Step 2.* For the second subsystem given as

$$D^{\alpha_2} x_2 = c_2 (r_3 - e_3) + \theta_2^T F_2 + f_2, \quad (23)$$

choose the second Lyapunov function candidate which is similar to (17) as

$$V_2 = V_1 + |D^{\alpha_2 - \alpha_\xi} e_2| + \frac{1}{2} \tilde{\theta}_2^T \Lambda^{-1} \tilde{\theta}_2. \quad (24)$$

Similarly, take the  $\alpha_\xi$  order derivative of Lyapunov function (24) and use Lemma 4, which leads to

$$\begin{aligned} D^{\alpha_\xi} V_2 &= D^{\alpha_\xi} V_1 + D^{\alpha_2} e_2 \cdot \text{sign}(D^{\alpha_2 - \alpha_\xi} e_2) \\ &\quad + D^{\alpha_\xi} \left( \frac{1}{2} \tilde{\theta}_2^T \Lambda^{-1} \tilde{\theta}_2 \right) \\ &\leq -k_1 |D^{\alpha_1 - \alpha_\xi} e_1| + c_1 e_2 \text{sign}(D^{\alpha_1 - \alpha_\xi} e_1) \\ &\quad + D^{\alpha_2} (r_2 - x_2) \text{sign}(D^{\alpha_2 - \alpha_\xi} e_2) \\ &\quad + \tilde{\theta}_2^T \Lambda^{-1} D^{\alpha_\xi} \tilde{\theta}_2 \\ &\leq -k_1 |D^{\alpha_1 - \alpha_\xi} e_1| + c_1 e_2 \text{sign}(D^{\alpha_1 - \alpha_\xi} e_1) \\ &\quad + (D^{\alpha_2} r_2 + c_2 e_3 - c_2 r_3 - \theta_2^T F_2 - f_2) \\ &\quad \times \text{sign}(D^{\alpha_2 - \alpha_\xi} e_2) + \tilde{\theta}_2^T \Lambda^{-1} D^{\alpha_\xi} \tilde{\theta}_2. \end{aligned} \quad (25)$$

Choose the second virtual control law  $r_3$  as

$$\begin{aligned} r_3 &= \frac{1}{c_2} \left[ D^{\alpha_2} r_2 - \tilde{\theta}_2^T F_2 - f_2 + k_2 D^{\alpha_2 - \alpha_\xi} e_2 \right. \\ &\quad \left. + c_1 e_2 \text{sign}(D^{\alpha_1 - \alpha_\xi} e_1) \text{sign}(D^{\alpha_2 - \alpha_\xi} e_2) \right]. \end{aligned} \quad (26)$$

Substituting (26) into (25), we obtain

$$\begin{aligned} D^{\alpha_\xi} V_2 &\leq -k_1 |D^{\alpha_1 - \alpha_\xi} e_1| + c_1 e_2 \text{sign}(D^{\alpha_1 - \alpha_\xi} e_1) + \left[ c_2 e_3 \right. \\ &\quad \left. + \tilde{\theta}_2^T F_2 - k_2 D^{\alpha_2 - \alpha_\xi} e_2 \right. \\ &\quad \left. - c_1 e_2 \text{sign}(D^{\alpha_1 - \alpha_\xi} e_1) \text{sign}(D^{\alpha_2 - \alpha_\xi} e_2) \right] \\ &\quad \times \text{sign}(D^{\alpha_2 - \alpha_\xi} e_2) + \tilde{\theta}_2^T \Lambda^{-1} D^{\alpha_\xi} \tilde{\theta}_2 \leq -k_1 |D^{\alpha_1 - \alpha_\xi} e_1| \\ &\quad - k_2 |D^{\alpha_2 - \alpha_\xi} e_2| + (c_2 e_3 + \tilde{\theta}_2^T F_2) \text{sign}(D^{\alpha_2 - \alpha_\xi} e_2) \\ &\quad + \tilde{\theta}_2^T \Lambda^{-1} D^{\alpha_\xi} \tilde{\theta}_2. \end{aligned} \quad (27)$$

Choose the second parameter update law  $\hat{\theta}_2$  as

$$D^{\alpha_\xi} \hat{\theta}_2^T = -\Lambda \cdot F_2 \text{sign}(D^{\alpha_2 - \alpha_\xi} e_2). \quad (28)$$

Substituting (28) into (27), we obtain

$$\begin{aligned} D^{\alpha_\xi} V_2 &\leq -k_1 |D^{\alpha_1 - \alpha_\xi} e_1| - k_2 |D^{\alpha_2 - \alpha_\xi} e_2| \\ &\quad + c_2 e_3 \text{sign}(D^{\alpha_2 - \alpha_\xi} e_2). \end{aligned} \quad (29)$$

*Step i = (2, \dots, n-1).* Consider the *i*th subsystem given as

$$D^{\alpha_i} x_i = c_i (r_{i+1} - e_{i+1}) + \theta_i^T F_i + f_i. \quad (30)$$

Similarly, select the *i*th Lyapunov function candidate as

$$V_i = V_{i-1} + |D^{\alpha_i - \alpha_\xi} e_i| + \frac{1}{2} \tilde{\theta}_i^T \Lambda^{-1} \tilde{\theta}_i. \quad (31)$$

Take the  $\alpha_\xi$  order derivative of Lyapunov function (31) and use Lemma 4, which leads to

$$\begin{aligned} D^{\alpha_\xi} V_i &= D^{\alpha_\xi} V_{i-1} + D^{\alpha_i} e_i \text{sign}(D^{\alpha_i - \alpha_\xi} e_i) \\ &\quad + D^{\alpha_\xi} \left( \frac{1}{2} \tilde{\theta}_i^T \Lambda^{-1} \tilde{\theta}_i \right) \\ &\leq -\sum_{j=1}^{i-1} (k_j |D^{\alpha_j - \alpha_\xi} e_j|) \\ &\quad + c_{i-1} e_i \text{sign}(D^{\alpha_{i-1} - \alpha_\xi} e_{i-1}) \\ &\quad + D^{\alpha_i} (r_i - x_i) \text{sign}(D^{\alpha_i - \alpha_\xi} e_i) + \tilde{\theta}_i^T \Lambda^{-1} D^{\alpha_\xi} \tilde{\theta}_i \\ &\leq -\sum_{j=1}^{i-1} (k_j |D^{\alpha_j - \alpha_\xi} e_j|) \\ &\quad + c_{i-1} e_i \text{sign}(D^{\alpha_{i-1} - \alpha_\xi} e_{i-1}) \\ &\quad + (D^{\alpha_i} r_i + c_i e_{i+1} - c_i r_{i+1} - \theta_i^T F_i - f_i) \\ &\quad \times \text{sign}(D^{\alpha_i - \alpha_\xi} e_i) + \tilde{\theta}_i^T \Lambda^{-1} D^{\alpha_\xi} \tilde{\theta}_i. \end{aligned} \quad (32)$$

Choose the *i*th virtual control law  $r_{i+1}$  as

$$\begin{aligned} r_{i+1} &= \frac{1}{c_i} \left[ D^{\alpha_i} r_i - \tilde{\theta}_i^T F_i - f_i + k_i D^{\alpha_i - \alpha_\xi} e_i \right. \\ &\quad \left. + c_{i-1} e_i \text{sign}(D^{\alpha_{i-1} - \alpha_\xi} e_{i-1}) \text{sign}(D^{\alpha_i - \alpha_\xi} e_i) \right]. \end{aligned} \quad (33)$$

Substituting (33) into (32), we obtain

$$\begin{aligned} D^{\alpha_\xi} V_i &\leq -\sum_{j=1}^i (k_j |D^{\alpha_j - \alpha_\xi} e_j|) \\ &\quad + (c_i e_{i+1} + \tilde{\theta}_i^T F_i) \text{sign}(D^{\alpha_i - \alpha_\xi} e_i) \\ &\quad + \tilde{\theta}_i^T \Lambda^{-1} D^{\alpha_\xi} \tilde{\theta}_i. \end{aligned} \quad (34)$$

In a similar way, the  $i$ th parameter update law is chosen as

$$D^{\alpha_\xi} \hat{\theta}_i^T = -\Lambda \cdot F_i \text{sign}(D^{\alpha_i - \alpha_\xi} e_i), \quad i = 2, \dots, n-1. \quad (35)$$

Substituting (35) into (34), we obtain

$$D^{\alpha_\xi} V_i \leq -\sum_{j=1}^i (k_j |D^{\alpha_j - \alpha_\xi} e_j|) + c_i e_{i+1} \text{sign}(D^{\alpha_i - \alpha_\xi} e_i) \quad (36)$$

$$i = 2, \dots, n-1.$$

*Step n.* Finally, the overall Lyapunov function for system (10) is chosen as

$$V_n = V_{n-1} + |D^{\alpha_n - \alpha_\xi} e_n| + \frac{1}{2} \tilde{\theta}_n^T \Lambda^{-1} \tilde{\theta}_n. \quad (37)$$

Take the  $\alpha_\xi$  order derivative of Lyapunov function (37) and use Lemma 4, which leads to

$$\begin{aligned} D^{\alpha_\xi} V_n &= D^{\alpha_\xi} V_{n-1} + D^{\alpha_n} e_n \text{sign}(D^{\alpha_n - \alpha_\xi} e_n) \\ &\quad + D^{\alpha_\xi} \left( \frac{1}{2} \tilde{\theta}_n^T \Lambda^{-1} \tilde{\theta}_n \right) \\ &\leq -\sum_{j=1}^{n-1} (k_j |D^{\alpha_j - \alpha_\xi} e_j|) \\ &\quad + c_{n-1} e_n \text{sign}(D^{\alpha_{n-1} - \alpha_\xi} e_{n-1}) \\ &\quad + D^{\alpha_n} (r_n - x_n) \text{sign}(D^{\alpha_n - \alpha_\xi} e_n) \\ &\quad + \tilde{\theta}_n^T \Lambda^{-1} D^{\alpha_\xi} \tilde{\theta}_n \\ &\leq -\sum_{j=1}^{n-1} (k_j |D^{\alpha_j - \alpha_\xi} e_j|) \\ &\quad + c_{n-1} e_n \text{sign}(D^{\alpha_{n-1} - \alpha_\xi} e_{n-1}) \\ &\quad + (D^{\alpha_\xi} r_n - c_n u - \theta_n^T F_n - f_n) \\ &\quad \times \text{sign}(D^{\alpha_n - \alpha_\xi} e_n) + \tilde{\theta}_n^T \Lambda^{-1} D^{\alpha_\xi} \tilde{\theta}_n. \end{aligned} \quad (38)$$

If the parameter update law and adaptive control law are designed as (13) and (14), the negative terms in (38) can be left, which leads to

$$D^{\alpha_\xi} V_n \leq -\sum_{j=1}^n (k_j |D^{\alpha_j - \alpha_\xi} e_j|). \quad (39)$$

Therefore, according to Lemma 5, all the states of system (10) are globally and asymptotically stable, and tracking errors  $e_i$  ( $i = 1, \dots, n$ ) will converge to zero asymptotically under the proposed control scheme. The proof is completed.  $\square$

*Remark 8.* The unsmooth Lyapunov function  $V = \|x\|_1$  is selected to analyze the stability of fractional-order systems in recent literature [5, 12, 37]. In this paper, the unsmooth Lyapunov function candidate is selected as  $V_i = V_{i-1} +$

$|D^{\alpha_i - \alpha_\xi} e_i| + (1/2) \tilde{\theta}_i^T \Lambda^{-1} \tilde{\theta}_i$ . The term  $|D^{\alpha_i - \alpha_\xi} e_i|$  is used to solve the problem brought by the noncommensurate orders, and the term  $(1/2) \tilde{\theta}_i^T \Lambda^{-1} \tilde{\theta}_i$  can simplify the forms of parameter update laws effectively.

*Remark 9.* When system orders satisfy  $\alpha_i = \alpha$  ( $i = 1, \dots, n$ ), system (10) becomes a strict-feedback commensurate fractional-order system with unknown parameters. It can be described as

$$D^\alpha x_i = c_i x_{i+1} + \theta_i^T F_i(x_1 \cdots x_i, t) + f_i(x_1 \cdots x_i, t).$$

$$D^\alpha x_n = c_n u + \theta_n^T F_n(x_1 \cdots x_n, t) + f_n(x_1 \cdots x_n, t) \quad (40)$$

$$y = x_1, \quad i = 1, \dots, n-1$$

For system (40), according to Property 2, adaptive control law (14), and parameter update laws, (13) can be rewritten as

$$u = \frac{1}{c_n} \left[ D^\alpha r_n - \tilde{\theta}_n^T F_n - f_n + k_n e_n \right. \\ \left. + c_{n-1} e_n \text{sign}(e_{n-1}) \text{sign}(e_n) \right] \quad (41)$$

$$D^\alpha \tilde{\theta}_i^T = -\Lambda \cdot F_i \text{sign}(e_i), \quad i = 1, \dots, n. \quad (42)$$

For system (40), in each step, the Lyapunov function candidate is selected as

$$V_i = V_{i-1} + |e_i| + \frac{1}{2} \tilde{\theta}_i^T \Lambda^{-1} \tilde{\theta}_i, \quad i = 2, \dots, n. \quad (43)$$

Similar to the noncommensurate case, consider system (40) with adaptive control law (41) and parameter update law (42), and take the  $\alpha$  order derivative of the overall Lyapunov function  $V_n$ . Finally, it concludes as

$$D^\alpha V_n \leq -\sum_{j=1}^n (k_j |e_j|). \quad (44)$$

For the commensurate fractional-order system with unknown parameters, according to Lemma 5, all the states are stable globally and tracking errors  $e_i$  ( $i = 1, \dots, n$ ) will converge to zero asymptotically under the proposed control method.

*Remark 10.* To illustrate the advantages of the proposed control method, the main contributions of our work are presented here as follows:

(1) More common conditions for the strict-feedback system are considered, including the noncommensurate orders, nonautonomous system, and multiple unknown parameters

(2) A novel Lyapunov function candidate  $V_i = V_{i-1} + |D^{\alpha_i - \alpha_\xi} e_i| + (1/2) \tilde{\theta}_i^T \Lambda^{-1} \tilde{\theta}_i$  for the noncommensurate fractional-order system with unknown parameters is presented and the proposed Lyapunov function also applies to the commensurate fractional-order system

(3) Compared with existing methods, the proposed adaptive control strategy requires only one controller input which reduces the complexity and eases the implementation

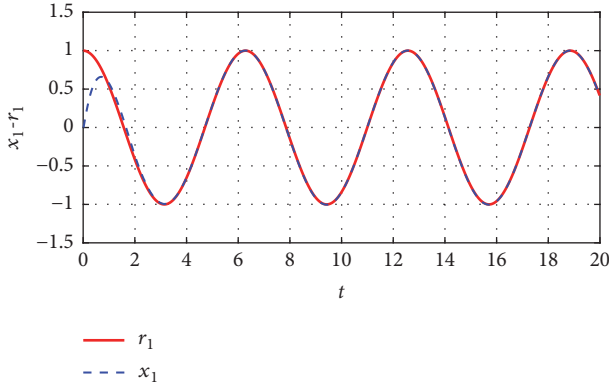


FIGURE 10: The tracking performance  $x_1 - r_1$  of  $q_1 = 0.99$  and  $q_2 = 0.98$ .

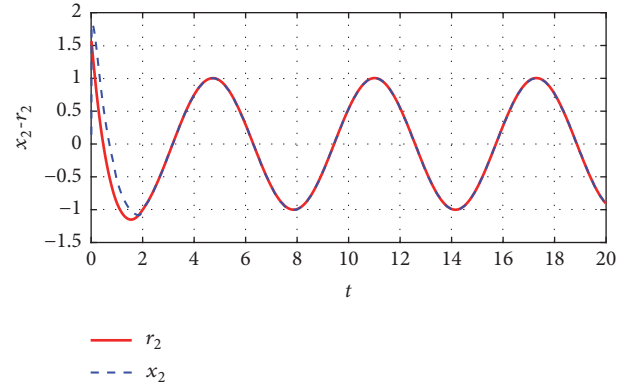


FIGURE 11: The tracking performance  $x_2 - r_2$  of  $q_1 = 0.99$  and  $q_2 = 0.98$ .

#### 4. Simulation Results

In this section, the proposed control strategy is applied to both the noncommensurate and commensurate fractional-order ferroresonance system with unknown parameters. The system is described as

$$\begin{aligned} \frac{d^{q_1} x_1}{d\tau^{q_1}} &= x_2 \\ \frac{d^{q_2} x_2}{d\tau^{q_2}} &= q \cos(\tau) - p x_2 - p_1 x - p_2 x^{11} + u, \end{aligned} \quad (45)$$

where  $p, p_1, p_2$ , and  $q$  are unknown parameters and  $u$  is the controller. Applying the control strategy proposed in Section 3, adaptive control law is selected as

$$\begin{aligned} u &= D^{q_2} r_2 + k_2 D^{q_2 - \delta} e_2 \\ &+ e_2 \operatorname{sign}(D^{q_1 - \delta} e_1) \operatorname{sign}(D^{q_2 - \delta} e_2) \\ &- (\hat{p} x_2 + \hat{p}_1 x_1 + \hat{p}_2 x_1^{11} + \hat{q} \cos \tau). \end{aligned} \quad (46)$$

The parameter update laws are selected as

$$\begin{aligned} D^\delta \hat{p} &= -k x_2 \operatorname{sign}(D^{q_2 - \delta} e_2) \\ D^\delta \hat{p}_1 &= -k x_2 \operatorname{sign}(D^{q_2 - \delta} e_2) \\ D^\delta \hat{p}_2 &= -k x_1^{11} \operatorname{sign}(D^{q_2 - \delta} e_2) \\ D^\delta \hat{q} &= -k \cos(\tau) \operatorname{sign}(D^{q_2 - \delta} e_2), \end{aligned} \quad (47)$$

where  $\delta$  is the smallest order between  $q_1$  and  $q_2$ ,  $r_1 = \cos t$  is the reference signal,  $r_2 = D^{q_1} r_1 + k_1 D^{q_1 - \delta} e_1$  is the virtual control law, and  $e_1 = r_1 - x_1$  and  $e_2 = r_2 - x_2$  are the tracking errors. The constants are selected as  $k_1 = 1.5$ ,  $k_2 = 8$ , and  $k = 3$ . The initial condition is selected as  $(x_1(0), x_2(0)) = (0, 0)$ . *Case 1:* Tracking performance of the noncommensurate fractional-order ferroresonance system of  $q_1 = 0.99$  and  $q_2 = 0.98$  under control is shown in Figures 10 and 11. *Case 2:* Tracking performance of the commensurate fractional-order

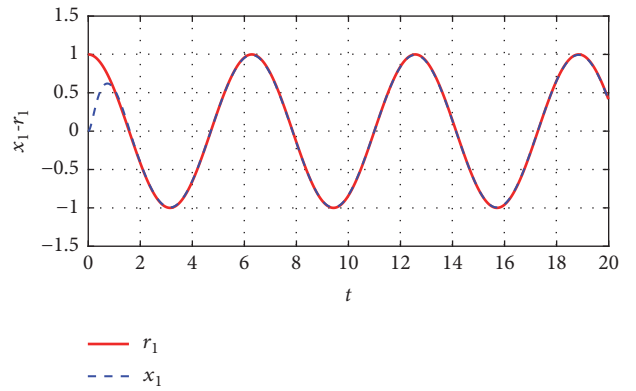


FIGURE 12: The tracking performance  $x_1 - r_1$  of  $q_1 = q_2 = 0.99$ .

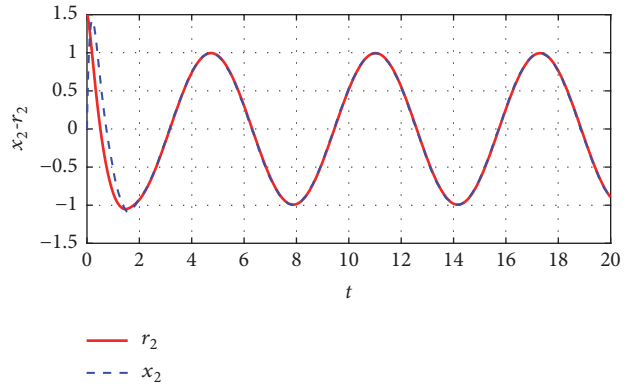


FIGURE 13: The tracking performance  $x_2 - r_2$  of  $q_1 = q_2 = 0.99$ .

ferroresonance system of  $q_1 = q_2 = 0.99$  under control is shown in Figures 12 and 13.

From Figures 10–13, it can be seen that the state  $x_1$  can track the reference signal  $r_1 = \cos t$  within 2 s. Under the proposed control method, the system voltage and flux are restored to the normal level gradually. In addition, the proposed control method applies to both the noncommensurate case and commensurate fractional-order ferroresonance system with multiple unknown parameters by just one control input.

## 5. Conclusions

In this paper, fractional calculus is applied to investigate the dynamic behaviors of a ferroresonance system with noncommensurate fractional-order magnetizing inductance and capacitance. The simulations illustrate that chaotic oscillation could occur in both the integer-order and noncommensurate fractional-order case. Considering the unknown parameters of a real system and the different orders of actual magnetizing inductance and capacitance, a novel fractional-order adaptive backstepping control method is proposed to suppress chaotic behaviors of noncommensurate fractional-order strict-feedback chaotic systems with unknown parameters via the fractional-order Lyapunov direct method. Parameter update laws and virtual control laws are designed in each step. And then, a novel adaptive backstepping controller is designed to force the system output to track the reference signal. Asymptotic stability of the fractional-order chaotic system under control is guaranteed by the fractional Lyapunov stability theorem. Compared with existing methods, the proposed control scheme not only applies to the noncommensurate case, but also requires just one control input which can simplify implementation in practice. Finally, the proposed control strategy is applied to the noncommensurate fractional-order ferroresonance system with unknown parameters. Simulation results demonstrate the effectiveness of the proposed method. In addition, it is worth noting that the proposed method also applies to the commensurate fractional-order ferroresonance system with unknown parameters.

## Data Availability

The data used to support the findings of this study are included within the article.

## Conflicts of Interest

There are no conflicts of interest regarding the publication of this paper.

## Acknowledgments

This project was supported by the National Natural Science Foundation of China (Grant No. 51877162) and the Science Fund for Creative Research Groups of the National Natural Science Foundation of China (Grant No. 51521065).

## References

- [1] M. S. Tavazoei, M. Haeri, S. Jafari, S. Bolouki, and M. Siami, "Some applications of fractional calculus in suppression of chaotic oscillations," *IEEE Transactions on Industrial Electronics*, vol. 55, no. 11, pp. 4094–4101, 2008.
- [2] I. Petráš, *Fractional-Order Nonlinear Systems: Modeling, Analysis and Simulation*, Higher Education Press, Beijing, China, 2011.
- [3] S. Westerlund and L. Ekstam, "Capacitor theory," *IEEE Transactions on Dielectrics and Electrical Insulation*, vol. 1, no. 5, pp. 826–839, 1994.
- [4] I. Schäfer and K. Krüger, "Modelling of lossy coils using fractional derivatives," *Journal of Physics D: Applied Physics*, vol. 41, no. 4, 2008.
- [5] J. Ni, L. Liu, C. Liu, and X. Hu, "Fractional order fixed-time nonsingular terminal sliding mode synchronization and control of fractional order chaotic systems," *Nonlinear Dynamics*, vol. 89, no. 3, pp. 2065–2083, 2017.
- [6] W. Zheng, Y. Luo, Y. Chen, and Y. Pi, "Fractional-order modeling of permanent magnet synchronous motor speed servo system," *Journal of Vibration and Control*, vol. 22, no. 9, pp. 2255–2280, 2016.
- [7] S.-C. Pei and J.-J. Ding, "Relations between Gabor transforms and fractional Fourier transforms and their applications for signal processing," *IEEE Transactions on Signal Processing*, vol. 55, no. 10, pp. 4839–4850, 2007.
- [8] I. N'Doye, H. Voos, and M. Darouach, "Observer-based approach for fractional-order chaotic synchronization and secure communication," *IEEE Journal on Emerging and Selected Topics in Circuits and Systems*, vol. 3, no. 3, pp. 442–450, 2013.
- [9] R. L. Magin, "Fractional calculus in bioengineering: A tool to model complex dynamics," in *Proceedings of the 13th International Carpathian Control Conference (ICCC '12)*, pp. 464–469, May 2012.
- [10] J. Hou, R. Xi, P. Liu, and T. Liu, "The switching fractional order chaotic system and its application to image encryption," *IEEE/CAA Journal of Automatica Sinica*, vol. 4, no. 2, pp. 381–388, 2017.
- [11] I. Petráš, *Fractional Differential Equations*, Academic Press, New York, NY, USA, 1999.
- [12] N. Nikdel, M. Badamchizadeh, V. Azimirad, and M. A. Nazari, "Fractional-Order Adaptive Backstepping Control of Robotic Manipulators in the Presence of Model Uncertainties and External Disturbances," *IEEE Transactions on Industrial Electronics*, vol. 63, no. 10, pp. 6249–6256, 2016.
- [13] A. Dumlu and K. Erenturk, "Trajectory tracking control for a 3-DOF parallel manipulator using fractional-order  $PI^1D^{\mu}$  control," *IEEE Transactions on Industrial Electronics*, vol. 61, no. 7, pp. 3417–3426, 2014.
- [14] H. Liu, Y. Pan, S. Li, and Y. Chen, "Adaptive Fuzzy Backstepping Control of Fractional-Order Nonlinear Systems," *IEEE Transactions on Systems, Man, and Cybernetics: Systems*, vol. 47, no. 8, pp. 2209–2217, 2017.
- [15] M. K. Shukla and B. B. Sharma, "Backstepping based stabilization and synchronization of a class of fractional order chaotic systems," *Chaos, Solitons & Fractals*, vol. 102, pp. 274–284, 2017.
- [16] C. Charalambous, Z. D. Wang, M. Osborne, and P. Jarman, "Sensitivity studies on power transformer ferroresonance of a 400kV double circuit," *IET Generation, Transmission & Distribution*, vol. 2, no. 2, pp. 159–166, 2008.
- [17] S. Mozaffari, M. Sameti, and A. C. Soudack, "Effect of initial conditions on chaotic ferroresonance in power transformers," *IEE Proceedings - Generation, Transmission and Distribution*, vol. 144, no. 5, pp. 456–460, 1997.
- [18] A. E. A. Araujo, A. C. Soudack, and J. R. Marti, "Ferroresonance in power systems: chaotic behaviour," *IEE Proceedings Part C: Generation, Transmission and Distribution*, vol. 140, no. 3, pp. 237–240, 1993.
- [19] S.-J. Huang and C.-H. Hsieh, "Relation analysis for ferroresonance of bus potential transformer and circuit breaker grading capacitance," *International Journal of Electrical Power & Energy Systems*, vol. 51, no. 3, pp. 61–70, 2013.

- [20] M. Yang, W. Sima, Q. Yang, J. Li, M. Zou, and Q. Duan, "Non-linear characteristic quantity extraction of ferroresonance overvoltage time series," *IET Generation, Transmission & Distribution*, vol. 11, no. 6, pp. 1427–1433, 2017.
- [21] S. Rezaei, "Adaptive overcurrent protection against ferroresonance," *IET Generation, Transmission & Distribution*, vol. 12, no. 7, pp. 1573–1588, 2018.
- [22] J. Walczak and A. Jakubowska, "Resonance in series fractional order  $RL_\beta C_\alpha$  circuit," *Przegląd Elektrotechniczny*, vol. 4, pp. 210–213, 2014.
- [23] J. Walczak and A. Jakubowska, "Analysis of resonance phenomena in series RLC circuit with supercapacitor," *Lecture Notes in Electrical Engineering: Analysis and Simulation of Electrical and Computer System*, vol. 324, pp. 27–34, 2015.
- [24] A. Jakubowska-Ciszek and J. Walczak, "Analysis of the transient state in a parallel circuit of the class  $RL_\beta C_\alpha$ ," *Applied Mathematics and Computation*, vol. 319, pp. 287–300, 2018.
- [25] I. Petrá, "A note on the fractional-order Chua's system," *Chaos, Solitons & Fractals*, vol. 38, no. 1, pp. 140–141, 2008.
- [26] D. Sierociuk, G. Sarwas, and M. Twardy, "Resonance phenomena in circuits with ultracapacitors," in *Proceedings of the 12th International Conference on Environment and Electrical Engineering (EEEIC '13)*, pp. 197–202, Wroclaw, Poland, May 2013.
- [27] M. K. Shukla and B. B. Sharma, "Stabilization of a class of uncertain fractional order chaotic systems via adaptive backstepping control," in *Proceedings of the 3rd Indian Control Conference (ICC '17)*, pp. 462–467, Guwahati, India, January 2017.
- [28] M. K. Shukla and B. B. Sharma, "Stabilization of a class of fractional order chaotic systems via backstepping approach," *Chaos, Solitons & Fractals*, vol. 98, pp. 56–62, 2017.
- [29] Y. Wei, P. W. Tse, D. Sheng, and Y. Wang, "Fractional order adaptive backstepping output feedback control: The incommensurate case," in *Proceedings of the 32nd Youth Academic Annual Conference of Chinese Association of Automation (YAC '17)*, pp. 366–372, Hefei, China, May 2017.
- [30] Y. Li, Y. Chen, and I. Podlubny, "Stability of fractional-order nonlinear dynamic systems: Lyapunov direct method and generalized Mittag-Leffler stability," *Computers & Mathematics with Applications*, vol. 59, no. 5, pp. 1810–1821, 2010.
- [31] M. P. Aghababa, "Stabilization of a class of fractional-order chaotic systems using a non-smooth control methodology," *Nonlinear Dynamics*, vol. 89, no. 2, pp. 1357–1370, 2017.
- [32] N. Aguila-Camacho, M. A. Duarte-Mermoud, and J. A. Gallegos, "Lyapunov functions for fractional order systems," *Communications in Nonlinear Science and Numerical Simulation*, vol. 19, no. 9, pp. 2951–2957, 2014.
- [33] Y. Li, Y. Chen, and I. Podlubny, "Mittag-Leffler stability of fractional order nonlinear dynamic systems," *Automatica*, vol. 45, no. 8, pp. 1965–1969, 2009.
- [34] M. Nakagawa and K. Sorimachi, "Basic characteristics of a fractance device," *IEICE Transactions on Fundamentals of Electronics, Communications and Computer Sciences*, vol. 75, pp. 1814–1819, 1992.
- [35] G. E. Carlson and C. A. Halijak, "Approximation of fractional capacitors  $(1/s)^{1/n}$  by a regular Newton process," *IEEE Transactions on Circuit Theory*, vol. 11, no. 2, pp. 210–213, 1964.
- [36] Z. Jia and C. Liu, "Fractional-order modeling and simulation of magnetic coupled boost converter in continuous conduction mode," *International Journal of Bifurcation and Chaos*, vol. 28, no. 05, 2018.
- [37] M. P. Aghababa, "Stabilization of a class of fractional-order chaotic systems using a non-smooth control methodology," *Nonlinear Dynamics*, vol. 69, no. 1-2, pp. 247–261, 2012.

## Research Article

# Hot Spot Data Prediction Model Based on Wavelet Neural Network

Ming Zhang <sup>1,2</sup> and Wei Chen <sup>2</sup>

<sup>1</sup>School of Information Science and Engineering, Linyi University, Linyi, Shandong 276005, China

<sup>2</sup>School of Information Engineering, Wuhan University of Technology, Wuhan, Hubei 430070, China

Correspondence should be addressed to Ming Zhang; zhangming2000225@163.com

Received 24 August 2018; Accepted 16 October 2018; Published 30 October 2018

Guest Editor: Weihai Zhang

Copyright © 2018 Ming Zhang and Wei Chen. This is an open access article distributed under the Creative Commons Attribution License, which permits unrestricted use, distribution, and reproduction in any medium, provided the original work is properly cited.

The novel hybrid multilevel storage system will be popular with SSD being integrated into traditional storage systems. To improve the performance of data migration between solid-state hard disk and hard disk according to the characteristics of each storage device, identifying the hot data block is significant issue. The hot data block prediction model based on wavelet neural network is built and trained by using historical data. This prediction model can overcome the cumulative effect of traditional statistical methods and has strong sensitivity to I/O loads with random variations. The experimental results show that the proposed model has better accuracy and faster learning speed than BP neural network model. In addition, it has less dependence on sample data and has better generalization ability and robustness. This model can be applied to the data migration of distributed hybrid storage systems to improve performance.

## 1. Introduction

The hybrid storage system with traditional hard disk drive (HDD) and solid-state drive (SSD) has become a significant storage system in large-scale data processing [1]. HDD have been broadly used as the primary storage medium in the past decades due to their relatively low cost per gigabyte and large storage capacities. However, the access performance of HDD has been improving slowly and the performance gap between HDD and CPU has been becoming bigger. The HDD has become the performance bottleneck of the computer system, even in the datacenter [2, 3]. The SSD is flash-based electronic storage device with low read delay and high writing delay [4]. So the SSDs are installed into the traditional HDD-based storage systems to build the HDD/SSD hybrid storage system [5]. To exploit the high random read performance owned by SSD, the hybrid storage systems focus on identifying hot data from cold data accurately. These systems perform data migration operation to copy hot data from HDD to SSD and cold ones from SSD into HDD for improving the access performance. Several authors analyzed the convergence and oscillatory properties of data using differential equations and

dynamic equations on time scales; see, e.g., [6–9]. So the identification of data status in hybrid storage is a significant issue. Here we proposed a prediction model to identify the hot data in hybrid storage system and this model can be used in data migration in cloud storage system or distribution storage systems [10].

To identify the hot data in storage system, the current researches focus on statistical method that logs and counts the number of accessing for each data block. Kgil [11] and Koltidas [12] proposed data block classification model based on data page I/O statistics to guide data migration strategy. Yang put forward to a novel method for increasing intermediate state to reduce occasional read tendency page classification error and the caused false migration in order to reduce the error in the classification of data pages [1]. Chai et al. used data block temperature to qualify the data block status and identify hot data block by sorting data block temperature [13]. However, the above mentioned models belong to statistical method that has a congenital deficiency. This is because these statistical models calculate the accessing requests from the data block creation. It has a certain time accumulation effect, which will cause classification model to be insensitive to the

change of random access load. There is a large number of I/O random access loads in complex application environments where large data is stored and calculated. This statistical classification model cannot respond quickly to changes in storage load and inevitably affects the accuracy and cost of data migration in hybrid storage systems. To solve the cumulative effect of statistical method and improve the response for random access workloads, we build a prediction model based on wavelet neural network to identify the hot and cold data block. Our contributions can be summarized as follows.

(1) We predict the data block status based on the wavelet neural network that has better nonlinear learning and generalization capacity. This model is very suitable for the small training data set and can learn with high resolution in sparse training data set. Additionally, the prediction model generates the thermal degree of data block, which is a continuous value within  $[0, 1]$ . So it is more flexible for data migration mechanism than previous models.

(2) The prediction model can solve the shortcoming of statistical method and response of the variation of hot data faster than those statistical models. This model is more suitable to deal with the uncertain workloads in distribution storage system.

This paper is organized as follows: in Section 2 we briefly describe the problem of identifying hot data. Section 3 introduces the features and qualifying model. Section 4 provides the detailed prediction model. Section 5 we evaluate the prediction model by experiments and analyze the results. Finally, Section 6 concludes this paper with discussion of future work.

## 2. Problem Description

In this section, we introduce the problem firstly. Accessing Data block rules are very complex in large-scale data distributed storage environment. According to historical data access trends, the current data block read operation heat degree is predicted to provide basic basis for data migration in hybrid storage system. Distributed big data storage system is a multitenant computing platform. On the platform a large number of users launch random computing tasks, so a lot of data's reading and writing requests will be produced. For the convenience of later discussion, some of the important concepts are defined as follows.

*Definition 1.* Data block  $B$ . A data block is a triple:  $B = \langle F, S, P \rangle$ , where  $F$  is the file that the data block belongs to.  $S$  is the size of the attached file.  $P$  is the set of data block access rule attributes.

*Definition 2.* Data block access attribute set  $P$ . Data block access attribute set  $P = (\delta, \theta, T, \varsigma)$ , where  $\delta$  is the data block unit time access frequency.  $\theta$  is the access density in statistical period.  $T$  is the data block inertia;  $\varsigma$  is the data block concurrency.

*Definition 3.* The access frequency per unit time  $\delta$  is the access frequency per unit time in a statistical cycle. For example, the

statistical period for a data block is 30 days and 240 times of access happens in this statistical cycle. They happen in 3 days, respectively, and then  $\delta = 240/3$ .

*Definition 4.*  $\theta$  is the access density in statistical period. The ratio of the number of unit times of data access in a statistical period to the length of the statistical period. It reflects the distribution of data block access. For example, a month is calculated by 30 days, a total of 240 times of access happen, they happen in different 3 days respectively, then  $\theta = 3/30$ ; if happen in 18 days, then  $\theta = 18/30$ .

*Definition 5.* The recent data block inertia  $T$ . In distributed storage system, from the beginning of the creation of data block, the set of time for each access is  $\langle t_1, t_2, \dots, t_n \rangle$ . The time interval for each access is  $t_2 - t_1, t_3 - t_2, t_n - t_{n-1}$ . For easy measurement and use, this paper uses the most recent access interval of data block as the inertia value of data block. For example, if current time is  $t_i$ , data inertia is  $T = t_i - t_{i-1}$ .

*Definition 6.* Data block concurrency  $\varsigma$  is the number of processes which access data block. This index reflects the degree of concurrent access to data block to a certain extent.

*Definition 7.* Life of data blocks  $L$ . Time interval between current time and the time of data block creation. Usually the longer the life of the data block is, the lower the probability of being accessed is.

In this case, the future access probability of data block is predicted according to the access characteristics and laws of large number of data blocks. The data blocks with high access probability are hot data. On the contrary, the data blocks with low access probability are cold data. Then whether the data state is hot or cold is determined to prepare for further data migration.

## 3. Data Heat and Eigenvector

First, create an index to quantify data block heat degree, and this index can express the frequency that a data block is accessed.

*Definition 8.* Data heat degree  $h$ . Using data block access frequency and access density, two important access attributes and weighting them to build data heat degree index, as shown in

$$h = w\delta + (1 - w)\theta, \quad h \in [0, 1]. \quad (1)$$

In Equation (1),  $\delta$  and  $\theta$  are the two dimensionless indexes with same direction. The larger the value is, the greater the heat of data block is. In addition, the maximum method is used to normalize  $\delta$ , that is  $\delta = \delta_{cur}/\delta_{max}$ ,  $\delta \in [0, 1]$ .  $\theta$  is a real number in interval  $[0, 1]$ . This method of describing data block heat mainly focuses on the main indexes of data block access. It has advantages of simpleness and intuitiveness. Because the weight is assigned value with subjective method,  $w = 0.7$ , this weight identification has a certain subjective shortcomings.

In order to establish the prediction model of thermal data, we need to construct training data set from large number of data block access history data. First, we select eigenvalues which can reflect access rule and is easy to measure from sample data, and construct eigenvector for each data sample. The following lists the specific eigenvectors  $\langle T, \zeta, S, L \rangle$ : the recent data block inertia  $T$ , concurrency  $\zeta$ , data block life, etc. They are indexes which have more significant correlation with data block heat. Data block inertia is normalized by maximum value method, that is,  $T = T_{cur}/T_{max}$ ,  $T \in [0, 1]$ . Then the method is used to perform co-oriented treatment for characteristic indexes,  $T = T_{max}/T_{cur}$ . Data block concurrency also needs to be normalized with maximum value, that is,  $\zeta = \zeta_{cur}/\zeta_{max}$ ,  $\zeta \in [0, 1]$ .  $S$  the size of the file associated by data block is looked as a supplementary eigenvalue, after normalization,  $S = S_{cur}/S_{max}$ ,  $\zeta \in [0, 1]$ . Data block life value is also normalized with maximum value.  $L = L_{cur}/L_{max}$ ,  $L \in [0, 1]$ . Then this method is used to co-orient index value. According to the observation on training data set, the maximum value of the above eigenvalues is selected by artificial experience for normalization, where  $\delta_{max} = 500$ ,  $T_{max} = 200$  statistical time points,  $\zeta_{max} = 30$  concurrent users,  $S_{max} = 500\text{MB}$ , and  $T_{max} = 1$  year.

#### 4. Data Block Heat Degree Prediction Model

Data heat degree prediction model is a nonlinear function relationship  $f(T, \zeta, S, L) = h$ . The input of the prediction model is a quaternary real number vector. The model output is the heat state of data block  $h \in [0, 1]$ . By training the prediction model, the nonlinear function relation between the features vector of data block access and the heat degree is fitted. We choose wavelet neural network (WNN) to construct the prediction model. The wavelet neural network integrates the advantages of wavelet analysis and artificial neural network, and has excellent nonlinear mapping ability and generalization ability [14]. In addition, the experimental observation data show that the training sample data has obvious sparsity. A large number of sample data show similar access characteristics. A small number of sample characteristics has diversity. Therefore, the wavelet neural network has obvious advantages in learning. Due to the multiscale time-frequency analysis capability of the wavelet function in wavelet neural network, the local singularity function can be studied with high accuracy by adjusting the expansion and translation of the wavelet function in training data-intensive region. In training data sparse area, low-scale parameters are used to learn smooth function. The characteristics of training data are the main reason to select wavelet neural network for fitting nonlinear prediction model. WNN has better adaptability and better prediction accuracy than traditional BP neural network [15].

**4.1. Fuzzy Preprocessing Eigenvalues.** In feature vector  $\langle T, \zeta, S, L \rangle$ , relevant file size  $S$  and data block life  $L$  have obvious uncertainty. The value difference of various sample data is larger. So if using the means of standard quantification, the value of two indexes will affect the proportion of other

indexes and reduce the accuracy of training model. In order to solve this problem, these two indexes are quantified by fuzzy evaluation method, and the output of fuzzy processing is taken as the input of wavelet neural network [16].

The concrete method is as follows: Firstly, we define the fuzzy set  $A = \{(a, \mu_A(a)), a \in R, \mu_A(a) \in [0, 1]\}$ , where  $\mu_A(a)$  is the appurtenant degree function of the fuzzy set, which reflects the degree of the element  $a$  belonging to the fuzzy set  $A$ . For example, the data block-related file size is set to three levels: small, medium, and large. The appurtenant degree function of large file is  $\mu_{great}(e(s)), \{(e(s), \mu_{great}(e(s))), e(s) \in [0, 1], \mu_{great}(e(s)) \in [0, 1]\}$ , and it is expressed as the extent that the data block size  $e(s)$  belongs to the fuzzy set large file. In order to blur file size index, we use fuzzy appurtenant function as in

$$\mu_A(a) = \begin{cases} 0, & a < l \\ \frac{a-l}{b-l}, & l \leq a < b \\ 1, & b \leq a < c \\ \frac{h-a}{h-c}, & c \leq a < h. \end{cases} \quad (2)$$

First normalize file size with maximum method, normalize it into  $[0, 1]$ . Then use Equation (2) to process. For example, if  $e(s) = 0.47$ , then  $\mu_{small}(0.47) = 0.12$ ,  $\mu_{median}(0.47) = 0.72$ ,  $\mu_{great}(0.47) = 0.16$ ; therefore  $E(s) = 0.47$  represents the fuzzy set  $\{(0.47, \mu_{small}(0.47)), (0.47, \mu_{median}(0.47)), (0.47, \mu_{great}(0.47))\} = \{(0.47, 0.12), (0.47, 0.72), (0.47, 0.16)\}$ . Design three fuzzy sets  $U_s$ ,  $U_m$ , and  $U_g$  for data block association file size index; they represent small files, medium files, and large files, respectively (denoted as Small, Median, and Great). Then, the same method is used to define three fuzzy sets (old data, middle-aged data, and new data) for data block life index, so as to solve the fuzzy processing of this index.

**4.2. Wavelet Neural Network Structure.** The main idea of wavelet neural network is to combine wavelet function with traditional BP neural network, replace the sigmoid function in BP neural network with nonlinear wavelet basis function, and use the linear superposition of nonlinear wavelet basis to fit the nonlinear function [14]. In this paper, the wavelet neural network structure is shown in Figure 1.

The wavelet neural network in Figure 1 consists of input layer, fuzzy layer, inference layer, wavelet layer, and output layer. The number of neuron nodes in each layer is  $n$ ,  $n \times M$ ,  $M$ ,  $M$ , and 1, respectively.

(1) Input layer (Layer 1): Each node of this layer is directly connected to each input component  $x_j$  of the eigenvector, and passes the input value  $X = [x_1, x_2, x_3, \dots, x_n]$  to the next layer. Here the eigenvector is  $\langle T, \zeta, S, L \rangle$ ,  $n=4$ ;

(2) Fuzzy layer (Layer 2): Through the fuzzy rules, the input vector is transformed into fuzzy values. Here Gaussian function is used to complete the work of the fuzzy appurtenant function, as shown in

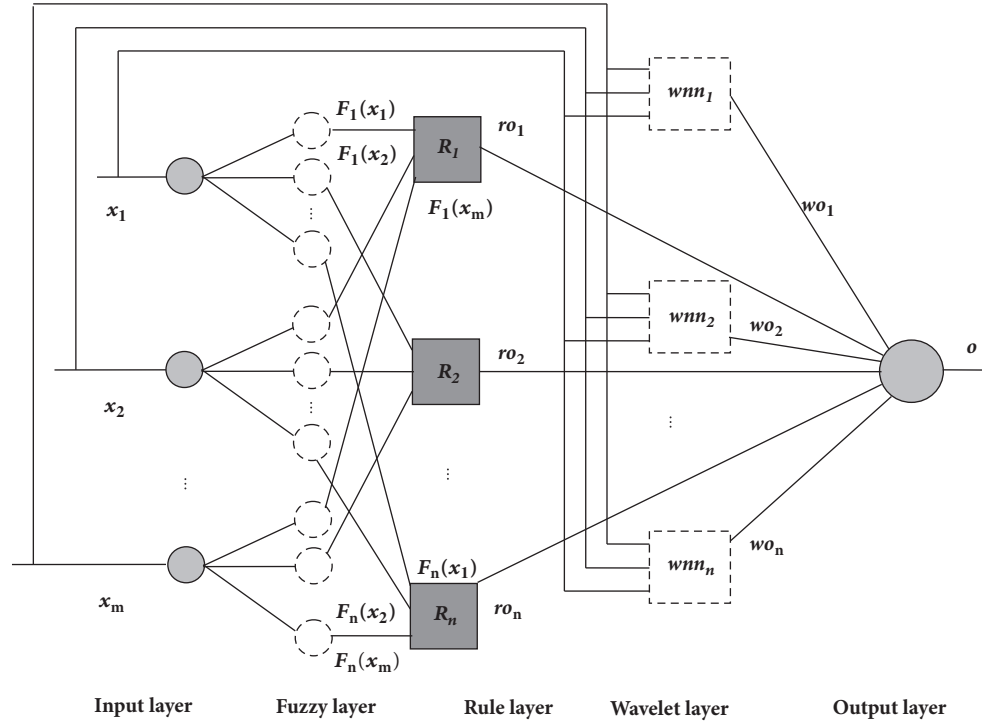


FIGURE 1: Architecture of wavelet neural networks.

$$F_j(x_i) = \exp\left(-\frac{(x_i - c_{ij})^2}{2\sigma_{ij}^2}\right) \quad (3)$$

$(j = 1, 2, \dots, n, i = 1, 2, \dots, m),$

where  $i$  is the component of input vector,  $j$  is the ordinal number of fuzzy rule,  $c_{ij}$  and  $\sigma_{ij}$  are the center position and distribution parameter of Gaussian function, respectively. In addition, the fuzzy rule can be described as  $R_i$ : if  $x_1$  is  $A_{i1}$  then  $y_i = B_{i1}$ .

(3) Rule layer (Layer 3): Rule layer is also known as inference layer. Each neuron corresponds to a fuzzy rule. Then we use the following formula to calculate the fitness degree of fuzzy rules.

$$\mu_j(x) = \prod_{j=1}^n F_j(x_i) \quad (i = 1, \dots, m). \quad (4)$$

In (4),  $n$  is the rule ordinal number and  $\mu_j(x)$  is the input value of next layer.

(4) Wavelet layer (Layer 4): The wavelet network layer output is mainly used for output compensation. The output of the neurons of this layer is calculated by using

$$wo_j = w_j \Psi_j(z)$$

$$\Psi_j(z) = \sum_{i=1}^m \frac{1}{\sqrt{|a_{ij}|}} (1 - z_{ij}^2) e^{-z_{ij}^2/2}, \quad (5)$$

where  $z_{ij} = (x_i - b_{ij})/a_{ij}$  is the weight of the connection from the  $i$ th node of input layer to the  $j$ th node of wavelet layer;  $w_j$

is the weight of the connection from the  $j$ th node of wavelet layer to output layer;  $a_{ij}$  is the extension and contraction parameter of wavelet function;  $b_{ij}$  is the translation parameter of wavelet function.

(5) Output layer (Layer 5): This layer is the final output layer of wavelet neural network. It will produce prediction results of predictive model. As a result of using fuzzy rules to quantify eigenvector index, this layer also perform defuzzy calculation, so it is also known as anti-fuzzy layer.

4.3. Training Algorithm. The wavelet neural network model in the previous section can be expressed as follows:

$$Q(X) = \sum_{j=1}^N W_{ij}^{(j)} \Psi_j(z) + \bar{\theta}, \quad (6)$$

where  $X = [x_1, x_2, x_3, \dots, x_M]^T$  is input vector; as shown in (5) and  $\Psi_j(z)$  is the neuron wavelet activation function of wavelet layer;  $W_{ij}$  is the weight of the connection from the  $j$ th node of wavelet layer to output layer and  $\bar{\theta}$  is the average estimated value of output sequence;  $Q(X)$  is the output value of wavelet neural network. The purpose of wavelet neural network training is to use sample data to determine the important parameters. This model parameters to be trained are  $Z_{ij}$ ,  $W_j$ ,  $a_j$ ,  $b_j$ , and  $\bar{\theta}$ . We do not use the batch approach of traditional BP for training. Here we use genetic algorithm for repeated approximation to actual measurement data in sample space to obtain. Firstly, the parameters to be trained in model are constructed into parameter vector with string structure by their order. Each vector is a chromosome for

genetic operation. Each chromosome is encoded with a real number. The initial value of the parameter is determined by the following method:

(1) *Determination of Stretching and Translation Parameters.* According to the nature of wavelet function, the window center position and width of the wavelet function are fixed values. Given that the initial center of the wavelet window is  $x_{0j}$  and the window width is  $\Delta x_{0j}$ , then the scaling factor  $a_j$  is given by the following formula:

$$a_j = \frac{\sum_{j=1}^M x_{j\max} - \sum_{j=1}^M x_{j\min}}{\Delta x_{0j}}. \quad (7)$$

The translation factor  $b_j$  is determined by Equation (8):

$$b_j = 0.5 \times \left( \sum_{j=1}^M x_{j\max} + \sum_{j=1}^M x_{j\min} \right) - a_j \times x_{0j}, \quad (8)$$

$M$  in (7) and (8) are the number of input vectors.  $x_{j\max}$  and  $x_{j\min}$  are the maximum and minimum sample values of the  $j$ -th neuron of the input layer, respectively.

(2) *Determination of Network Weights.* The initial value of the weight from input layer to wavelet layer  $Z_{ij}$  and the weight from wavelet layer to output layer  $W_j$  is to select a uniformly distributed random number in  $[-1, 1]$  and to ensure that the various values are not zero.

(3) *Determination of the Parameter  $\bar{\theta}$ .* It is obtained according to the calculated mean of partial sample data. Then it is constantly updated and corrected during calculation.

Before the start of wavelet neural network training, the genetic population size was set to  $L = 200$ , the maximum number of iterations was  $J = 300$ , the network convergence accuracy was  $\varepsilon = 3 \times 10^{-3}$ , the probability of selection was  $p_s = 0.65$ , the crossover probability was  $p_c = 0.8$ , and the probability of variation is  $p_m = 0.03$ . The specific training algorithm is as follows [17]:

*Step 1.* Set the initial value of the iteration variable,  $J = 0$ , and then base on the determination method of parameter initial value to create  $L$  initial parent classes  $T_1^{(0)}, T_2^{(0)}, \dots, T_L^{(0)}$ ;

*Step 2.* Calculate fitness function, as shown in (9). When the smaller the value of the adaptive function is, it means the better the network training effect is [18].

$$E(T_l^{(j)}) = \frac{1}{2 \sum_{k=1}^K [Q(X_k, T_l^{(j)}) - Q'_k]^2}, \quad (9)$$

where  $Q(X_k, T_l^{(j)})$  is the wavelet neural network output value calculated by (6),  $Q'_k$  is the expected output value of prediction model, and  $K$  is the number of elements in training sample set.

*Step 3.* Cross and mutate the  $j$ th generation of chromosomes, and select  $N$  individuals to enter the next generation of evolution.

*Step 4 (determine convergence).* When the condition  $(E_{\max} - E_{\min})/E_{\text{avg}} \leq \varepsilon$  or  $J > J_{\max}$  is satisfied, the training algorithm ends; otherwise update the variable  $J$ ,  $J = J + 1$  and then return to Step 3.  $E_{\max}$ ,  $E_{\min}$ , and  $E_{\text{avg}}$  represent the maximum, minimum, and average value of the calculated fitness function, respectively.

*Step 5.* Select the best combination of parameters that has reached best fitness accuracy in the previous step and then perform real-time prediction.

By now, the data block hotspot prediction model with wavelet neural network as core has been completed. The training and learning of the predictive model is described in a concrete example. First, the eigenvector  $d_1 = \langle T, \varsigma, S, L \rangle$  of a data block is obtained by measuring,  $d_1 = (0.47, 0.38, 0.6, 0.3)$  after normalization. Then the heat degree of data block is calculated by the heat degree equation,  $h = 0.45$ . The calculated heat degree value is the expected output value of the sample. The sample data is denoted as  $d_1 = \langle (0.47, 0.38, 0.6, 0.3), 0.45 \rangle$ . After selecting 1000 such sample data, the training algorithm is used to obtain the main parameters of wavelet neural network. The constructed wavelet neural network model is used to predict. For example, the input vector of the data block to be predicted is  $d_2 = (0.37, 0.18, 0.3, 0.3)$ ; then the model output value  $\tilde{h} = 0.39$  is the predicted heat degree of the data block.

## 5. Experiment and Analysis

Since the existing disk load dataset does not provide detailed I/O information, we use the disk access data in actual production environment to train the prediction model and perform performance analysis. The experimental environment is Linux operating system, and the file system is ext2, each data block is 4KB. The following methods are used to measure the access character data of data blocks in disk: Blktrace is used to collect I/O data of disk data blocks in Linux system. Blktrace can monitor the I/O events of a particular disk block device, capture and record events such as reading, writing, and synchronous operations [19]. Then blkparse is used to analyze blktrace log data, and we can obtain the attributes such as the processes which accessed the data block, the associated file node, and timestamp. Writing script analysis program based on this tool software, access feature attributes of any one data block of the monitored disk such as access frequency, access density, associated file size, and concurrent program number can be obtained.

*5.1. Performance Analysis.* In this section, we mainly validate the advantages of the prediction model constructed by wavelet neural network. In this paper, we use traditional BP neural network as the benchmark model to compare. First observe the distribution of access attributes of sample data block, as shown in Figure 2.

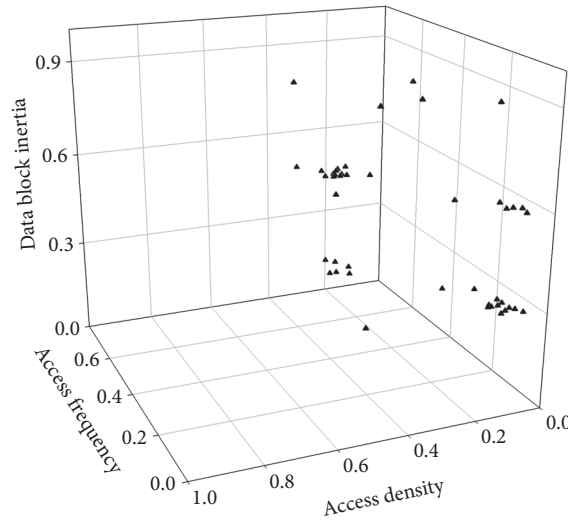


FIGURE 2: Sample data attribute distribution diagram.

In Figure 2,  $x$ ,  $y$  and  $z$  denotes the access frequency, access density and data block inertia within unit time in data block respectively, and the data range is  $[0, 1]$  after normalization. It can be seen from the figure that the access property has a certain extent of regularity. There is obvious aggregation phenomenon. In BP model, the excitation function of neuron is  $S$  function. The common sample data of two models is used to train the batch model. The weights and coefficients in BP network are adjusted adaptively. The minimum mean square error energy function is used to optimize network parameters. The error is as follows:

$$E = \frac{1}{2 \sum_{l=1}^L (y_l - \hat{y}_l)^2}, \quad (10)$$

where  $l$  is the number of samples and  $y_l$  and  $\hat{y}_l$  are the actual value and the predicted value, respectively. The gradient descent method is used to calculate the instantaneous gradient vector. The learning rate parameter in the reverse propagation process  $\eta = 0.05$ . In order to facilitate distinction, the proposed model is denoted as WNN and the benchmark model is BP neural network. The two models use same sample data to train and test. The training speed of the two predictive models is compared. Firstly, 300 sample data are randomly selected to train the two prediction models. The data preprocessing modes are same. The error of WNN and BP model is shown in Figure 3. The error accuracy of WNN is lower than the pre-set value after 57 iterations. BP is not lower than the preset value until after 217 iterations.

In addition to adjusting network weights, the WNN model can adjust the scaling factor and translation factor of wavelet function. It has better adaptability and elasticity than BP model and has more sensitive nonlinear fitting ability.

**5.2. Comparison of Prediction Accuracy.** In this section, we use the trained prediction model in previous section for

identifying hot data block. The main purpose is to compare prediction accuracy of the two models. The accuracy of wavelet neural network and BP is compared by selecting 10 actual measured data, as shown in Table 1. Table 1 lists the predicted values (average values) and the variance of predicted values generated by the two models.

The experimental results show that the prediction error of WNN is 1.6%, while the prediction error of BP is 3.1%. This indicates that WNN has better nonlinear fitting ability. In addition, the variance of the predicted value of WNN is 3.3%, while the variance of BP is 7.1%. This indicates that WNN prediction model has better fault tolerance capacity. This is because that BP neural network excitation function uses conventional  $S$  function. This excitation function is relatively smooth. It cannot quickly respond to those sample data which changes rapidly from wave peak to wave trough, resulting in that the trained model is not stable enough in real-time prediction.

**5.3. Model Robustness.** In this section, we can verify that WNN has multi-dimensional learning ability, train the learning with high frequency by adjusting scaling and translation factors in data dense area and train the learning with low frequency in data sparse area. So it has the ability to automatically adapt to sample data. Here 300 samples of sample data intensive area are selected to train the two prediction models. Then 10 testing data of previous section are used to verify prediction accuracy. Training and comparison is shown in Figure 4.

As shown in Figure 4, the WNN model reaches the preset error value after 56 iterations. The BP model is lower than the pre-set error after 75th iteration. Comparing Figure 4 and Figure 3, it can be found that the convergence rate of BP model is greatly improved. This is mainly due to the better

TABLE 1: Comparison of predicted results.

ID	measured value	WNN		BP	
		predicted	variance	predicted	variance
1	0.592	0.583	0.019	0.610	0.044
2	0.081	0.082	0.003	0.010	0.001
3	0.453	0.446	0.015	0.467	0.034
4	0.403	0.409	0.013	0.415	0.03
5	0.102	0.103	0.003	0.098	0.007
6	0.073	0.071	0.002	0.075	0.005
7	0.415	0.421	0.014	0.402	0.029
8	0.524	0.515	0.017	0.540	0.039
9	0.173	0.175	0.006	0.167	0.012
10	0.393	0.386	0.013	0.380	0.027

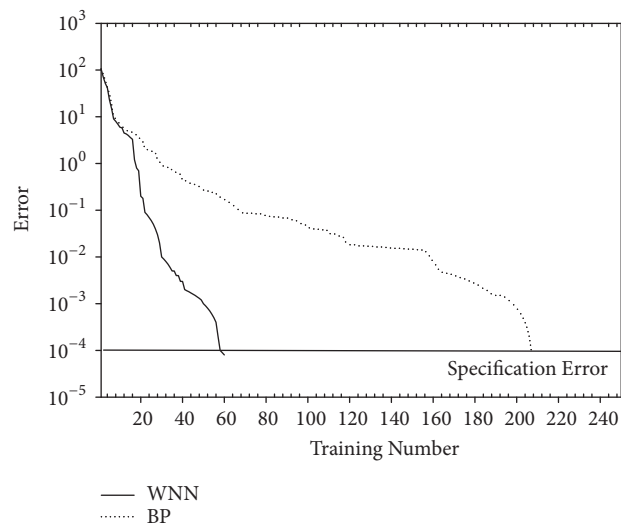


FIGURE 3: Training comparisons of WNN and BP.

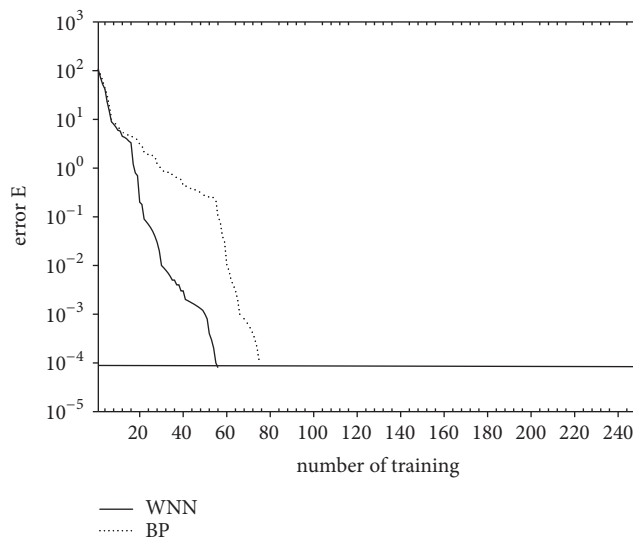


FIGURE 4: Training comparisons of dense sample data of WNN and BP.

TABLE 2: Comparison of predictive results of dense area data after training.

ID	Measured value	WNN		BP	
		predicted	variance	predicted	variance
1	0.592	0.581	0.019	0.580	0.020
2	0.081	0.083	0.003	0.079	0.003
3	0.453	0.447	0.015	0.463	0.016
4	0.403	0.406	0.013	0.395	0.014
5	0.102	0.104	0.003	0.104	0.004
6	0.073	0.074	0.002	0.071	0.002
7	0.415	0.422	0.014	0.424	0.015
8	0.524	0.517	0.017	0.513	0.018
9	0.173	0.174	0.006	0.177	0.006
10	0.393	0.387	0.013	0.385	0.013

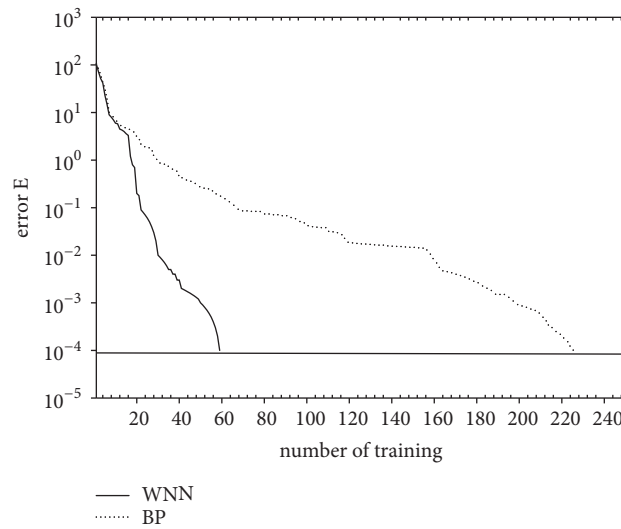


FIGURE 5: Training comparisons of sparse sample data of WNN and BP.

training effect of dense sample. The prediction accuracy comparison is shown in Table 2.

As shown in Table 2, the prediction error of WNN is basically the same, while the prediction error of BP is reduced to 2.1%. This indicates that BP model is better trained in the dense data area. So the prediction accuracy is improved. In addition, the predicted variance of BP model decreases from 7.1% in previous section to 3.5%, which is basically similar to the predicted variance of WNN. The above results show that the training effect of BP is improved and the prediction ability is enhanced in the area with dense sample data. In order to highlight the advantages that WNN has better adaptive ability to sample data, another 100 data are selected from the sparse area of sample data to retrain the two prediction models. Finally, the verification data is used to compare the prediction accuracy and stability.

As shown in Figure 5, when using sparse area sample data to train the prediction model, WNN converges into the pre-set error range at the 61st iteration, while BP model is just lower than the pre-set error at 225th iteration. This indicates that BP model has a poorer adaptive ability to sparse area

sample data. The comparison of prediction accuracy is shown in Table 3.

In prediction accuracy, the predicted mean value and variance of WNN are kept stable. The prediction accuracy of BP is reduced from 3.1% to 3.3%. Especially, the variance of the predicted value is reduced to 9.7%. This indicates that the prediction robustness of BP is lower than that of WNN. The dependence on sample data is stronger. It indicates that the generalized learning ability of WNN prediction model is better than that of the prediction model constructed with BP neural network.

*5.4. Comparison with Statistical Method.* In literature [13], the identifying hot data block is used as a Data-block temperature model. This model called EESDC was applied to reducing data migration overhead and improving energy-efficient of large-scale streaming media storage systems. Note that we used the identifying hot data method as benchmark model, which belongs to the statistical model. To compare with EESDC, we further demonstrate that our proposed model is better than the traditional statistical models. This experiment

TABLE 3: Comparison of predicted results of sparse area data after training.

ID	Measured value	WNN		BP	
		predicted	variance	predicted	variance
1	0.592	0.584	0.019	0.612	0.057
2	0.081	0.083	0.003	0.078	0.007
3	0.453	0.444	0.015	0.468	0.044
4	0.403	0.408	0.013	0.390	0.036
5	0.102	0.104	0.003	0.105	0.010
6	0.073	0.070	0.002	0.071	0.007
7	0.415	0.422	0.014	0.429	0.040
8	0.524	0.514	0.017	0.507	0.047
9	0.173	0.175	0.006	0.179	0.017
10	0.393	0.385	0.013	0.380	0.035

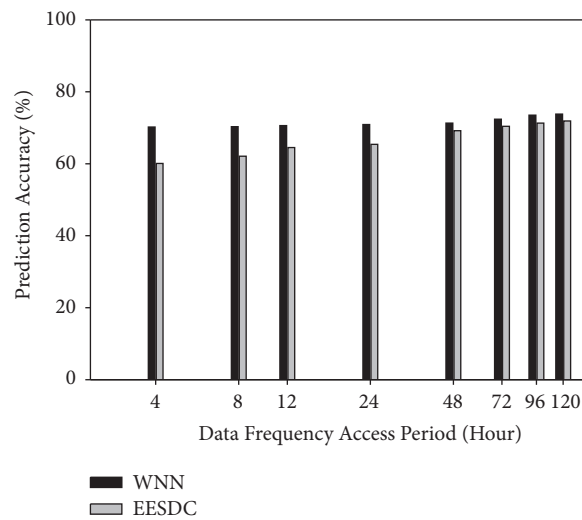


FIGURE 6: Prediction accuracy comparison of WNN and traditional statistical model.

is designed on a video learning website of campus. The hybrid storage system of website has large-scale stream video files for students. These video files have different hot degree for users. Such as some videos may be popular for one or two hours, some videos even keep hot for many days. Here we select different kind's videos to verify our model and benchmark model.

As shown in Figure 6, x axis represents the data block frequency period. As  $x$  equals 4, this means that this kind video files are accessed frequently in four hours. Here 100 file of each kind of stream video is selected and used two prediction models to identify the data block status.  $y$  axis shows the prediction accuracy. The WNN prediction model is stable for different kinds of video files. However, EESDC is not well in handling video files, whose hot degree change fast in short period. The prediction accuracy of EESDC gradually increases while increasing the frequency access period. This comparison shows that our proposed model overcomes the cumulative effect of traditional statistical methods and is suitable to prediction short-term variation data block.

## 6. Conclusion

To handle the large-scale data migration in distribution storage system and improve the performance of migration, a novel prediction model of data block status was provided to judge the heat degree of data block. We extracted the access features of data block and used those features as input vector to train the prediction model. The kernel of prediction model is wavelet neural network that has better capacity than other models. Additionally, we used the fuzzy rule to deal with the uncertain of sampling data. Compared with BP neural network, our proposed prediction model has better nonlinear fitting capacity due to the fact that wavelet neural network can learn with low frequency in sparse sample area and with high frequency in dense sample area. The experimental results show that our proposed prediction model has better generalization capacity and robustness than BP model and relevant model. In the future, we will integrate this prediction model into the data migration model and verify the prediction accuracy in the production environment.

## Data Availability

The data used to support the findings of this study are available from the corresponding author upon request.

## Disclosure

Ming Zhang (1983- ), male, is with a Ph.D. degree and is a lecturer. His research interests include distributed intelligent computing and distributed multisensor data fusion system. Wei Chen (1963- ), male, is with a Ph.D and is a Professor and a Doctoral supervisor. His major research interests include mobile communication, signal processing, and distributed system.

## Conflicts of Interest

The authors declare that they have no conflicts of interest.

## Acknowledgments

This project is supported by the Shandong Provincial Natural Science Foundation, China (nos. ZR2017MF050 and ZR2014FL008), Shandong Province Key Research and Development Program of China (nos. 2018GGX101005, 2017CXGC0701, and 2016GGX109001), and Project of Shandong Province Higher Educational Science and Technology Program (no. J17KA049).

## References

- [1] P.-Y. Yang, P.-Q. Jin, and L.-H. Yue, "A time-sensitive and efficient hybrid storage model involving SSD and HDD," *Jisuanji Xuebao/Chinese Journal of Computers*, vol. 35, no. 11, pp. 2294–2305, 2012.
- [2] Y. Yamato, "Cloud storage application area of HDD–SSD hybrid storage, distributed storage, and HDD storage," *IEEJ Transactions on Electrical and Electronic Engineering*, vol. 11, no. 5, pp. 674–675, 2016.
- [3] H. Dongmei, D. Yanling, and H. Qi, "Research on Ocean Large Data Migration Algorithm in Hybrid Cloud Storage," *Journal of Computer Research and Development*, vol. 51, no. 1, pp. 199–205, 2014.
- [4] C. Zhiguang, N. Xiao et al., "A high-performance and reliable storage system for backing up SSDs with disks," *Journal of Computer Research and Development*, vol. 50, no. 1, pp. 80–89, 2013.
- [5] S. Zhenlong, L. Qiong et al., "Design and Implementation of Hybrid Storage System for High Performance Computing," *Journal of Shanghai Jiaotong University*, vol. 47, no. 1, pp. 113–118, 2013.
- [6] P. Wang and X. Liu, "Rapid convergence for telegraph systems with periodic boundary conditions," *Journal of Function Spaces*, vol. 2017, Article ID 1982568, 10 pages, 2017.
- [7] L. H. Liu and Y. Z. Bai, "New oscillation criteria for second-order nonlinear neutral delay differential equations," *Journal of Computational and Applied Mathematics*, vol. 231, no. 2, pp. 657–663, 2009.
- [8] M. Bohner, T. S. Hassan, and T. Li, "Fite-Hille-Wintner-type oscillation criteria for second-order half-linear dynamic equations with deviating arguments," *Indagationes Mathematicae*, vol. 29, no. 2, pp. 548–560, 2018.
- [9] T. Li and Y. V. Rogovchenko, "Oscillation criteria for second-order superlinear Emden-Fowler neutral differential equations," *Monatshefte für Mathematik*, vol. 184, no. 3, pp. 489–500, 2017.
- [10] J. Luo, L. Fan, Z. Li, and C. Tsu, "A new big data storage architecture with intrinsic search engines," *Neurocomputing*, vol. 181, pp. 147–152, 2016.
- [11] T. Kgil, D. Roberts, and T. Mudge, "Improving NAND flash based disk caches," in *Proceedings of the ISCA 2008, 35th International Symposium on Computer Architecture*, pp. 327–338, China, June 2008.
- [12] I. Koltsidas and S. D. Viglas, "Designing a Flash-Aware Two-Level Cache," in *Advances in Databases and Information Systems*, vol. 6909 of *Lecture Notes in Computer Science*, pp. 153–169, Springer Berlin Heidelberg, Berlin, Heidelberg, 2011.
- [13] Y. Chai, Z. Du, D. A. Bader, and X. Qin, "Efficient data migration to conserve energy in streaming media storage systems," *IEEE Transactions on Parallel and Distributed Systems*, vol. 23, no. 11, pp. 2081–2093, 2012.
- [14] F.-J. Lin, Y.-C. Hung, and K.-C. Ruan, "An intelligent second-order sliding-mode control for an electric power steering system using a wavelet fuzzy neural network," *IEEE Transactions on Fuzzy Systems*, vol. 22, no. 6, pp. 1598–1611, 2014.
- [15] T. Hieu, X. Zhang et al., "Passive-Islanding detection method using the wavelet packet transform in grid-connected photovoltaic system," *IEEE Transactions on Power Electronics*, vol. 31, no. 10, pp. 6955–6967, 2016.
- [16] A. Albanese, S. K. Pal, and A. Petrosino, "Rough sets, kernel set, and spatiotemporal outlier detection," *IEEE Transactions on Knowledge and Data Engineering*, vol. 26, no. 1, pp. 194–207, 2014.
- [17] L. Quan, W. Xiaoyan et al., "Double Elite Coevolutionary Genetic Algorithm," *Journal of Software*, vol. 23, no. 4, pp. 765–775, 2014.
- [18] Y. Liang and C. Nie, "The Optimization of Genetic Algorithm Configuration Parameter Generated by Coverage Table," *Chinese Journal of Computers*, vol. 35, no. 7, pp. 1522–1537, 2012.
- [19] G. Casale, S. Kraft, and D. Krishnamurthy, "A Model of Storage I/O Performance Interference in Virtualized Systems," in *Proceedings of the 2011 31st International Conference on Distributed Computing Systems Workshops (ICDCS Workshops)*, pp. 34–39, Minneapolis, MN, USA, June 2011.

## Research Article

# Optimization Problem of Insurance Investment Based on Spectral Risk Measure and RAROC Criterion

Xia Zhao <sup>1</sup>, Hongyan Ji <sup>2</sup>, and Yu Shi <sup>1</sup>

<sup>1</sup>School of Statistics and Information, Shanghai University of International Business and Economics, Shanghai 201620, China

<sup>2</sup>School of Statistics, Shandong University of Finance and Economics, Jinan, Shandong 250014, China

Correspondence should be addressed to Xia Zhao; zhaoxia-w@163.com

Received 7 September 2018; Accepted 15 October 2018; Published 30 October 2018

Academic Editor: Xue-Jun Xie

Copyright © 2018 Xia Zhao et al. This is an open access article distributed under the Creative Commons Attribution License, which permits unrestricted use, distribution, and reproduction in any medium, provided the original work is properly cited.

This paper introduces spectral risk measure (SRM) into optimization problem of insurance investment. Spectral risk measure could describe the degree of risk aversion, so the underlying strategy might take the investor's risk attitude into account. We establish an optimization model aiming at maximizing risk-adjusted return of capital (RAROC) involved with spectral risk measure. The theoretical result is derived and empirical study is displayed under different risk measures and different confidence levels comparatively. The result shows that risk attitude has a significant impact on investment strategy. With the increase of risk aversion factor, the investment ratio of risk asset correspondingly reduces. When the aversive level increases to a certain extent, the impact on investment strategies disappears because of the marginal effect of risk aversion. In the case of VaR and CVaR without regard for risk aversion, the investment ratio of risk asset is increasing significantly.

## 1. Introduction

Underwriting business and investment business are two main fund sources of an insurance company. In recent years, more and more insurers have paid attention to the efficiency of investment business because of increasing competition among insurance companies, continuing decline in underwriting profits and gradual relaxation of insurance investment policies.

The relationship between return and risk needs to be fully balanced in insurance investment, in which mean-risk optimization is the most commonly used criterion. For the measurement of risk, variance is a common choice. Early studies, for example, Lambert and Hofflander [1], Kahane and Nye [2], and Briys [3], established optimal portfolio model for property insurance under mean-variance criterion. Later, due to the limitation of variance, new risk measures were proposed constantly and mean-risk models were also extended in various backgrounds; see [4–9]. In particular, ruin probability and some down-side risk measures such as VaR and CaR were introduced into insurance business to find the optimal investment strategy. Guo and Li [10] used

mean-VaR model to analyze the choice of optimal portfolios for insurers. Chen et al. [11] investigated an investment-reinsurance problem under dynamic Value-at-Risk (VaR) constraint. Zeng et al. [12] established two mean-CaR models to study reinsurance-investment problem of insurers and obtained the explicit expressions of the optimal deterministic rebalance reinsurance-investment strategies and mean-CaR efficient frontiers.

Risk measures used in the above literatures indeed describe different risk characteristics of the assets, but they do not take investors' risk attitude into account. Spectral risk measures (SRM) proposed by Acerbi et al. [13] characterize investors' risk aversion and have been applied to fields of banks and securities, for example, Adam et al. [14] and Diao et al. [15] and the references therein. However, to the best of our knowledge, there is no literature which studied optimal investment problem in insurance business based on SRM. On the other hand, mean is generally used to describe the return, but the insurer needs to determine the amount of capital based on entire risk situation of company. The risk-adjusted return on capital (RAROC) takes into account the capital return adjusted by risk, which makes up for the shortcomings

from average-return principle; see [16–18] and the references therein.

This paper will introduce spectral risk measure into optimal investment model with RAROC as optimization target, construct optimization model, and give its theoretical and empirical study. The rest of this paper is organized as follows. Section 2 illustrates spectral risk measure and insurance return model used here. Section 3 finds the solution of the optimization problem. The empirical application is displayed in Section 4. Section 5 concludes the paper.

## 2. Spectral Risk Measure and Insurance Return Model

### 2.1. Spectral Risk Measure

*Definition 1* (see [19]). Suppose that random variable  $X$  represents the loss of assets, and its distribution function can be denoted as  $F(x) = Pr(X \leq x)$ . Spectral risk measure with confidence level  $p = 1 - \alpha$  ( $\alpha \in (0, 1)$ ) is defined as follows:

$$\rho = \int_0^1 \phi(p) q_p dp, \quad (1)$$

where  $\phi(p) : (0, 1) \mapsto \mathcal{R}$  is a weight function or risk spectral function and  $q_p = \inf\{x \mid F(x) \geq p\}$  is  $p$ -quantile of distribution function. SRM is a coherent risk measure when  $\phi(p)$  satisfies nonnegativity, normalization, and increasingness.

Specially,  $\rho$  is Value at Risk (VaR) if  $\phi(p) = \{0, p \neq 1 - \alpha; \infty, p = 1 - \alpha\}$ .  $\rho$  corresponds to Conditional Value at Risk (CVaR) if  $\phi(p) = (1/\alpha)I_{\{p \geq 1 - \alpha\}}$ . If  $\phi(p) = (\gamma e^{-(1-p)\gamma/\alpha} / \alpha(1 - e^{-\gamma}))I_{\{1 - \alpha \leq p \leq 1\}}$ ,  $\rho$  is exponential spectral risk measure; if  $\phi(p) = \{(\beta(\alpha - 1 + p)^{\beta-1} / \alpha^\beta)I_{\{1 - \alpha \leq p \leq 1\}}, \beta > 1; (\beta(1 - p)^{\beta-1} / \alpha^\beta)I_{\{1 - \alpha \leq p \leq 1\}}, 0 < \beta < 1\}$ ,  $\rho$  is power spectral risk measure, where  $\gamma > 0$  is the coefficient of absolute risk aversion and  $\beta > 0$  is the coefficient of relative risk aversion.

**Proposition 2** (see [20]). *Suppose that  $R$  denotes income variable, and then  $X = -R$  denotes the loss variable. If  $R$  follows normal distribution assumption, we can get*

$$SRM(R) = -E(R) + T(\alpha)\sigma(R). \quad (2)$$

$$\text{Specially: } VaR(R) = -E(R) + \Phi^{-1}(p)\sigma(R) \quad (3)$$

$$\text{and } CVaR(R) = -E(R) + \frac{f(\Phi^{-1}(p))}{\alpha}\sigma(R), \quad (4)$$

where  $T(\alpha) = \int_0^1 \Phi^{-1}(p)\phi(p)dp$ ,  $\Phi^{-1}(p)$  is  $p$ -quantile of standard normal distribution and  $f(\cdot)$  is probability density function of standard normal distribution.

**2.2. Insurance Return Model.** Suppose that insurers invest in  $N$  assets, one of which is risk-free asset, and others are risk assets. Therefore, the total profit is given as

$$R_p = r_b R_0 + gR_0 \left(1 - \sum_{i=1}^{N-1} k_i\right) r_0 + gR_0 \sum_{i=1}^{N-1} k_i r_i, \quad (5)$$

where  $R_0$ ,  $r_b$ ,  $g$  denote premium charged by insurers, the rate of underwriting profit, and investment ratio, respectively. Constant  $r_0$  denotes the rate of risk-free asset return. And random variable  $r_i$  ( $i = 1, 2, \dots, N-1$ ) denotes the rate of risk asset return with  $N(\mu_i, \sigma_i^2)$  assumption.  $k_i$  is the investment weight of the  $i$ -th risk asset and we assume that  $0 < \sum_{i=1}^{N-1} k_i < 1$ .

Let  $K = (R_0, gR_0k_1, gR_0k_2, \dots, gR_0k_{N-1})^T$  and  $r = (r_b + gr_0, r_1 - r_0, \dots, r_{N-1} - r_0)^T$  with mean  $\mu$  and covariance matrix  $\Sigma$ . Then we have  $R = r^T K$ , and  $E(R) = \mu^T K$ ,  $\sigma(R) = \sqrt{K^T \Sigma K}$ .  $\rho_c$  is the upper limit of risk the insurer can bear, that is,  $SRM(R_p) \leq \rho_c$ .

## 3. Optimal Investment Strategy for Insurers Based on SRM-RAROC Criterion

In this section, we establish SRM-RAROC optimization model and derive the optimal solution under normal distribution assumption.

**3.1. Optimization Model.** Here the investment performance evaluation is measured by risk-adjusted return on capital (RAROC) instead of the absolute amount of income as follows:

$$RAROC = \frac{E(R_p)}{SRM(R_p)}. \quad (6)$$

Thus, the optimization model can be formulated as

$$\begin{aligned} \max \quad & RAROC = \frac{E(R_p)}{SRM(R_p)} \\ \text{s.t.} \quad & 0 < \sum_{i=1}^{N-1} k_i < 1 \end{aligned} \quad (7)$$

$$SRM(R_p) = -E(R_p) + T(\alpha)\sigma(R_p) \leq \rho_c$$

$$E(R_p) = \mu^T K$$

$$\sigma(R_p) = \sqrt{K^T \Sigma K}.$$

### 3.2. Solution of Optimization Model

**Step 1** (simplifying optimization model). Define  $\theta$  as  $n$ -dimension vector,  $\theta = (\theta_1, \theta_2, \dots, \theta_n)^T$ , where  $\theta_1 = 1/(1 + g \sum_{j=1}^{N-1} k_j)$ ,  $\theta_i = gk_{i-1}/(1 + g \sum_{j=1}^{N-1} k_j)$ ,  $i = 2, 3, \dots, n$ . And then  $K$  can be rewritten as  $K = R_0(1 + g \sum_{j=1}^{N-1} k_j)\theta$ ,  $I^T \theta = 1$ , where  $I$  is  $n$ -dimension vector,  $I = (1, 1, \dots, 1)^T$ .

Let  $r_p = r^T \theta$ , then  $\mu_p = E(r_p) = \mu^T \theta$ ,  $\sigma_p = var(r_p) = \sqrt{\theta^T \Sigma \theta}$ . With  $1 - \alpha$  confidence level,  $SRM(r_p) = -\mu^T \theta + T(\alpha)\sqrt{\theta^T \Sigma \theta}$ . Then we have

$$\begin{aligned} E(R_p) &= \mu^T K = \mu^T R_0 \left( 1 + g \sum_{j=1}^{N-1} k_j \right) \theta \\ &= R_0 \left( 1 + g \sum_{j=1}^{N-1} k_j \right) E(r_p) \end{aligned} \quad (8)$$

$$\begin{aligned} \text{and } SRM(R_p) &= -E(R_p) + T(\alpha) \sigma(R_p) \\ &= R_0 \left( 1 + g \sum_{j=1}^{N-1} k_j \right) SRM(r_p). \end{aligned} \quad (9)$$

So RAROC can be rewritten as

$$\begin{aligned} RAROC &= \frac{E(R_p)}{SRM(R_p)} \\ &= \frac{R_0 \left( 1 + g \sum_{j=1}^{N-1} k_j \right) E(r_p)}{R_0 \left( 1 + g \sum_{j=1}^{N-1} k_j \right) SRM(r_p)} \\ &= \frac{E(r_p)}{SRM(r_p)} \end{aligned} \quad (10)$$

And model (7) can be transformed as

$$\begin{aligned} \max \quad RAROC &= \frac{E(r_p)}{SRM(r_p)} \\ \text{s.t.} \quad I^T \theta &= 1 \\ SRM(r_p) &= -\mu_p + T(\alpha) \sigma_p \leq \rho_c \\ \mu_p &= E(r_p) = \mu^T \theta \\ \sigma_p &= \sigma(r_p) = \sqrt{\theta^T \Sigma \theta} \end{aligned} \quad (11)$$

*Step 2* (effective frontier curve equation of mean-SRM space). Effective frontier in mean-risk space refers to the portfolio that maximizes the return at a certain level of risk or minimizes the risk at a certain level of return. Therefore, mathematical expression of curve equation of effective frontier can be given as

$$\begin{aligned} \min \quad & \left( -\mu^T \theta + T(\alpha) \sqrt{\theta^T \Sigma \theta} \right) \\ \text{s.t.} \quad & \mu_p = \mu^T \theta \\ & I^T \theta = 1. \end{aligned} \quad (12)$$

Solving model (12) by Lagrange multiplier method yields

$$\theta = \frac{1}{d} \Sigma^{-1} \left( (c\mu_p - b)\mu + (a - b\mu_p)I \right), \quad (13)$$

where  $a = \mu^T \Sigma^{-1} \mu$ ,  $b = \mu^T \Sigma^{-1} I = I^T \Sigma^{-1} \mu$ ,  $c = I^T \Sigma^{-1} I$ ,  $d = ac - b^2$ .

So then,  $\sigma_p^2 = \theta^T \Sigma \theta = (c\mu_p^2 - 2b\mu_p + a)/d$ . Therefore the effective frontier curve equation is

$$SRM(r_p) = -\mu_p + T(\alpha) \sqrt{\frac{1}{d} (c\mu_p^2 - 2b\mu_p + a)}. \quad (14)$$

Assume that  $\mu_{opt}$  be the optimal return for a given risk  $\rho$  based on formula (14); the corresponding optimal portfolio weights on effective frontier curve can be solved as

$$\theta_{opt} = \frac{1}{d} \Sigma^{-1} \left( (c\mu_{opt} - b)\mu + (a - b\mu_{opt})I \right). \quad (15)$$

*Step 3* (RAROC maximized portfolio under SRM constraints). Let  $RAROC = \mu_p / SRM(r_p) = u$ ; that is, the slope  $u$  of line  $\mu_p = u SRM(r_p)$  will be maximized in the processing of optimization. From portfolio theory in finance, we know that maximum value is obtained when the line is tangent to the effective leading edge. The tangent point is the optimal portfolio when the tangent point is on the left of the constraint line while the intersection of the constraint line and the effective frontier is the optimal portfolio when the tangent point is on the right of the constraint line.

Let  $(SRM_T, \mu_T)$  denote the intersection portfolio. It is obvious that  $SRM_T = \rho_c$  at the intersection point. From effective frontier curve equation, we can find that

$$\mu_T = \frac{(bT^2 + d\rho_c) + T\sqrt{d(2b\rho_c + c\rho_c^2 + a - T^2)}}{cT^2 - d}. \quad (16)$$

Let  $(SRM_{tg}, \mu_{tg})$  denote tangent portfolio. The formula  $\partial SRM / \partial \mu_p = 1/u$  is true for tangent point when the line is tangent to the effective frontier. So it follows that

$$\begin{aligned} -1 + \frac{T(\alpha)(c\mu_p - b)}{d\sqrt{(1/d)(c\mu_p^2 - 2b\mu_p + a)}} \\ = \frac{-\mu_p + T(\alpha)\sqrt{(1/d)(c\mu_p^2 - 2b\mu_p + a)}}{\mu_p}, \end{aligned} \quad (17)$$

which results in the following tangent point portfolio:

$$(SRM_{tg}, \mu_{tg}) = \left( \frac{\sqrt{a}}{b} (T - \sqrt{a}), \frac{a}{b} \right). \quad (18)$$

Summarily, the optimal solution of optimization model can be expressed as

$$(SRM_{opt}, \mu_{opt}) = \begin{cases} (SRM_{tg}, \mu_{tg}) & \text{if } \rho_{tg} \leq \rho_c \\ (SRM_T, \mu_T) & \text{if } \rho_{tg} > \rho_c \end{cases} \quad (19)$$

and the optimal portfolio weight is

$$\theta_{opt} = \frac{1}{d} \Sigma^{-1} \left( (c\mu_{opt} - b)\mu + (a - b\mu_{opt})I \right). \quad (20)$$

Therefore, the optimal investment ratio of each risk asset is

$$k_{i-1} = \frac{\theta_i}{g\theta_1} \quad i = 2, 3, \dots, N, \quad (21)$$

TABLE 1: Descriptive statistical analysis of risk assets.

	Chang'an Vehicle (000625)	JoinTo Energy (000600)	Yili (600887)
Median	0.196729	0.005992	-0.070959
Maximum	1.341006	1.124433	1.299169
Minimum	-1.631535	-1.184555	-1.196948
Standard deviation	0.866075	0.632811	0.698381
Skewness	-0.545350	-0.132884	0.049686
Kurtosis	2.653994	2.993299	2.709674
J-B statistic	0.545562	0.034779	0.039235
p value	0.761260	0.982761	0.980574

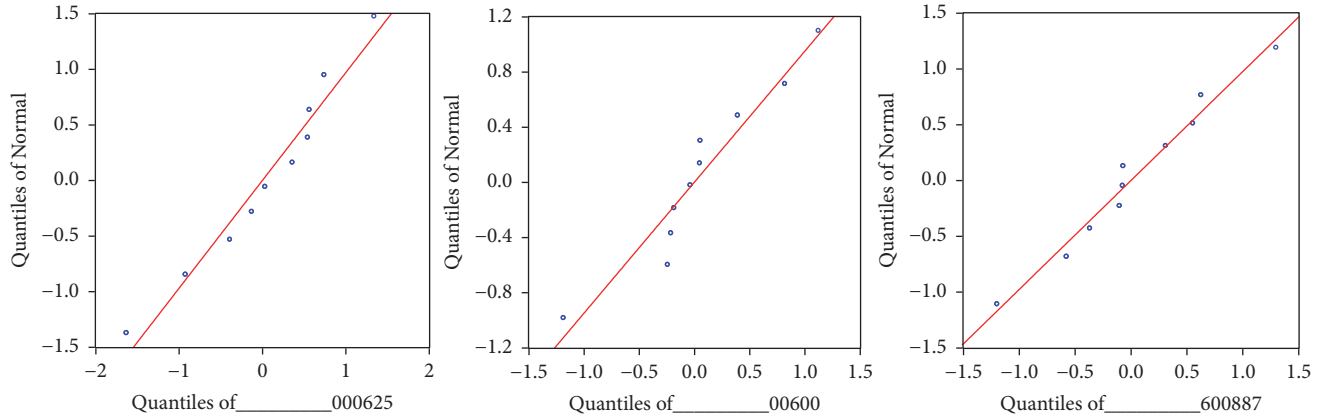


FIGURE 1: QQ chart of each risky asset's return.

and the corresponding proportion of investment in risk-free assets is

$$1 - \sum_{i=1}^{N-1} k_i = 1 - \frac{1 - \theta_1}{g\theta_1} = \frac{g\theta_1 + \theta_1 - 1}{g\theta_1}. \quad (22)$$

## 4. Data Analysis

**4.1. Data Selection.** In this section, we assume that insurers invest in one risk-free asset and three security risk assets. Bank deposit is regarded as risk-free asset and the selected risk assets are JoinTo Energy (000600), Chang'an Vehicle (000625), and Yili (600887). Yearly data is chosen from January 1, 2006, to December 31, 2016. The data for China Life Insurance Company Ltd is calculated from the company's annual report and semi-annual report. Data of risk assets is obtained from Guotai An CSMAR series of research databases.

**4.2. Descriptive Statistics of Risk Asset Data.** We conduct descriptive statistical analysis of risk assets; see Table 1 and Figure 1.

It can be found from Table 1 that the distribution of return for three risk assets presents a certain degree of skewness and flatter peak than normal distribution. From QQ chart and the fact that JB statistic of each risky asset return rate is less than 5.99, which is 95% quantile of  $\chi^2(2)$ , we can conclude that the return of each risky asset is subject to a normal distribution approximately.

## 4.3. Calculation of Related Variables

**(1) Investment Ratio and Rate of Underwriting Profit.** The investment ratio is an important indicator to measure the level of capital utilization of an insurance company, which can be calculated by investment assets divided by total assets. The rate of underwriting profit can be calculated by the difference between total profit and investment profit divided by underwriting income. Based on investment data and underwriting data of China Life Insurance Company Ltd, we obtain that  $g = 94.08\%$  and  $r_b = -0.1776$  here.

**(2) Rate of Return for Risk-Free Asset and Risky Asset.** From China Life Insurance Company Ltd's data of the amount of bank deposit and bank deposit return in 2006–2016, we can calculate the mean of the return rate  $E(r_0) = 0.0428$  as risk-free return rate. Each risky asset return is calculated by  $r_i = \ln(P_{it}/P_{it-1})$ , where  $P_{it}$  and  $P_{it-1}$  denote  $i$ -th asset's price at time  $t$  and  $t-1$ , respectively. So it can be calculated from Guotai An CSMAR Series Research Database that the average return of JoinTo Energy (000600), Chang'an Vehicle (000625), and Yili (600887) are 0.0580, 0.0516 and 0.0409, respectively.

**4.4. Optimal Insurance Investment Strategy Based on SRM-RAROC Criterion.** In this section, we conduct empirical analysis for optimal insurance investment strategy. The confidence level is set to 90% and 95% and the upper limit of risk is assumed to be 0.02. Based on formulas in Section 2, we calculate the optimal weights of the assets under different confidence levels. The results are displayed in Table 2.

TABLE 2: Optimal investment strategy under confidence level.

$\alpha = 0.05, \rho_c = 0.02$					
Risk measure	Factor of risk aversion	Risk-free asset	JoinTo Energy (000600)	Chang'an Vehicle (000625)	Yili (600887)
VaR	—	0.7136	0.2538	-0.0903	0.1229
CVaR	—	0.8062	0.1812	-0.0674	0.0799
Exponential SRM	$\gamma = 0.2$	0.8150	0.1743	-0.0652	0.0758
	$\gamma = 0.4$	0.8261	0.1657	-0.0625	0.0707
	$\gamma > 0.6$	0.8400	0.1548	-0.0590	0.0642
Power SRM	$\beta = 1.1$	0.8177	0.1723	-0.0646	0.0746
	$\beta = 1.2$	0.8342	0.1594	-0.0605	0.0669
	$\beta > 1.3$	0.8400	0.1548	-0.0590	0.0642
$\alpha = 0.1, \rho_c = 0.02$					
Risk measure	Factor of risk aversion	Risk-free asset	JoinTo Energy (000600)	Chang'an Vehicle (000625)	Yili (600887)
VaR	—	0.6357	0.3148	-0.1096	0.1591
CVaR	—	0.7350	0.2370	-0.0850	0.1130
Exponential SRM	$\gamma = 0.2$	0.7393	0.2336	-0.0840	0.1110
	$\gamma = 0.4$	0.7437	0.2302	-0.0829	0.1089
	$\gamma \geq 3.5$	0.8335	0.1599	-0.0606	0.0673
Power SRM	$\beta = 1.1$	0.7405	0.2327	-0.0837	0.1104
	$\beta = 1.2$	0.7457	0.2286	-0.0824	0.1080
	$\beta \geq 3$	0.8335	0.1599	-0.0606	0.0673

Remark: the negative value means short-selling.

From Table 2, we can obtain the following conclusion.

(1) Generally, the optimal investment proportion in risk asset is decreasing as the factor of risk aversion increases, which reflects the effect of risk attitude on investment strategy. When the factor of risk aversion reaches some fix value, the optimal investment proportion stays in a roughly identical level, which shows the existence of marginal effect from risk aversion extent.

(2) Compared with the results under different risk measures, risk aversion attitude shows a significant effect on the choice and assignment among risk assets and risk-free asset; and hence the risk attitude should not be ignored.

(3) As confidence level becomes bigger, the optimal investment proportion in risky asset increases and the one in risk-free asset decreases. This is a natural conclusion since bigger confidence level will make the value of risk be smaller, which results in the increasing trend of investing in risk assets.

## 5. Conclusions

This paper constructed an insurance optimization model including spectral risk measure and risk-adjusted return of capital and conducted theoretical and empirical analysis. The main innovation of this paper is introduction of spectral risk measure in insurance business, which makes the risk attitude of the investor be considered in decision-making. The result tells us that more risk aversion will decrease the investment ratio in risk asset and increase the interest of investing in risk-free asset. However, the impact on investment strategies will disappear when the level of risk aversion increases to a certain extent. Furthermore, both confidence level and the threshold of risk play a significant role on optimal strategy. For convenience, here we suppose that the underwriting insurance return follows a deterministic process and the policy constraints for insurance investment are not involved. It may be also of interest to extend the research to the case with stochastic insurance surplus process and/or the government policy constraint. We will explore these problems in the following studies.

## Data Availability

The data used to support the findings of this study are available from the corresponding author upon request.

## Conflicts of Interest

The authors declare that they have no conflicts of interest.

## Acknowledgments

This work was partially supported by NSFC (71671104), Project of Humanities Social Sciences of MOE, China (16YJA910003, 18YJC630220), Key Project of National Social Science of China (16AZD019), Special Funds of Taishan Scholar Project (tsqn20161041) and SUIBE Postgraduate Innovative Talents Training Project.

## References

- [1] E. W. Lambert and A. E. Hofflander, "Impact of New Multiple Line Underwriting on Investment Portfolios of Property-Liability Insurers," *Journal of Risk and Insurance*, vol. 33, no. 2, p. 209, 1966.
- [2] Y. Kahane and D. Nye, "A Portfolio Approach to the Property-Liability Insurance Industry," *Journal of Risk and Insurance*, vol. 42, no. 4, p. 579, 1975.
- [3] E. P. Briys, "Investment portfolio behavior of non-life insurers: a utility analysis," *Insurance: Mathematics & Economics*, vol. 4, no. 2, pp. 93–98, 1985.
- [4] A. J. Frost, "Implications of modern portfolio theory for life assurance companies [J]," *Journal of the Institute of Actuaries*, vol. 26, pp. 47–68, 1983.
- [5] W. Guo, "Optimal portfolio choice for an insurer with loss aversion," *Insurance: Mathematics & Economics*, vol. 58, pp. 217–222, 2014.
- [6] Y. Zeng, Z. Li, and Y. Lai, "Time-consistent investment and reinsurance strategies for mean-variance insurers with jumps," *Insurance: Mathematics & Economics*, vol. 52, no. 3, pp. 498–507, 2013.
- [7] C. Weng, "Constant proportion portfolio insurance under a regime switching exponential Levy process," *Insurance: Mathematics & Economics*, vol. 52, no. 3, pp. 508–521, 2013.
- [8] P. Artzner, F. Delbaen, and J.-M. Eber, "Coherent measures of risk," *Mathematical Finance*, vol. 9, no. 3, pp. 203–228, 1999.
- [9] R. G. Emanuela, "Risk measures via g-expectations [J]," *Insurance: Mathematics & Economics*, vol. 39, pp. 19–34, 2006.
- [10] W. Guo and X. Li, "Optimal insurance investment strategy under VaR restriction [J]," *Journal of Systems & Management*, vol. 18, no. 5, pp. 118–124, 2009.
- [11] S. Chen, Z. Li, and K. Li, "Optimal investment-reinsurance policy for an insurance company with VaR constraint," *Insurance: Mathematics & Economics*, vol. 47, no. 2, pp. 144–153, 2010.
- [12] Y. Zeng and Z. Li, "Optimal reinsurance-investment strategies for insurers under mean-CaR criteria," *Journal of Industrial and Management Optimization*, vol. 8, no. 3, pp. 673–690, 2012.
- [13] C. Acerbi, "Spectral measures of risk: a coherent representation of subjective risk aversion," *Journal of Banking & Finance*, vol. 26, no. 7, pp. 1505–1518, 2002.
- [14] A. Adam, M. Houkari, and J.-P. Laurent, "Spectral risk measures and portfolio selection," *Journal of Banking & Finance*, vol. 32, no. 9, pp. 1870–1882, 2008.
- [15] X. Diao, B. Tong, and C. Wu, "Spectral risk measurement based on EVT and its application in risk management [J]," *Journal of Systems Engineering*, vol. 6, no. 30, pp. 354–405, 2015.
- [16] A. Milne and M. Onorato, "Risk-Adjusted Measures of Value Creation in Financial Institutions," *European Financial Management*, vol. 18, no. 4, pp. 578–601, 2012.
- [17] L. Wang and J. Li, "Research on Insurance Investment Strategy Based on Risk-Adjusted Return Rate under Policy Constraints [J]," *Chinese Journal of Management Science*, vol. 20, pp. 16–22, 2012.
- [18] X. Chen, Z. Han, and K. Tang, "Research on the Optimization Model of Insurance Investment Based on VaR and RAROC [J]," *The Journal of Quantitative & Technical Economics*, vol. 4, pp. 111–117, 2006.

- [19] K. Dowd and D. Blake, "After VaR: The theory, estimation, and insurance applications of quantile-based risk measures," *Journal of Risk and Insurance*, vol. 73, no. 2, pp. 193–229, 2006.
- [20] X. Li and X. Liu, "The mean-spectral measures of risk efficient frontier of portfolio and its empirical test [J]," *Chinese Journal of Management Science*, vol. 5, no. 13, pp. 6–11, 2005.

## Research Article

# Optimal Control Based on the Polynomial Least Squares Method

Constantin Bota , Bogdan Căruntu , Mădălina Sofia Pașca, and Marioara Lăpădat

Department of Mathematics “Politehnica” University of Timișoara, P-ta Victoriei, 2, Timișoara 300006, Romania

Correspondence should be addressed to Constantin Bota; [constantin.bota@upt.ro](mailto:constantin.bota@upt.ro)

Received 23 August 2018; Accepted 17 October 2018; Published 28 October 2018

Guest Editor: Hiroaki Mukaidani

Copyright © 2018 Constantin Bota et al. This is an open access article distributed under the Creative Commons Attribution License, which permits unrestricted use, distribution, and reproduction in any medium, provided the original work is properly cited.

In this paper an approach for computing an optimal control law based on the Polynomial Least Squares Method (PLSM) is presented. The initial optimal control problem is reformulated as a variational problem whose corresponding Euler-Lagrange equation is solved by using PLSM. A couple of examples emphasize the accuracy of the method.

## 1. Introduction

Optimal control problems occur in many areas of science and engineering such as system mechanics, hydrodynamics, elasticity theory, geometrical optics, and aerospace engineering, and they are one of the several applications and extensions of the calculus of variations.

The beginning of optimal control is represented by the Brachistochrone problem formulated by Galileo in 1683: A mass material point  $m$  moves without friction along a vertical curve joining the points  $(x_0, y_0)$  and  $(x_1, y_1)$ . There is the question of finding such a curve for which the scroll time is minimal, curve called brachistochrone. Galileo's attempts to resolve it were incorrect [1, 2]. The problem raised great interest at that time and solutions were proposed by many mathematicians like Bernoulli, Leibnitz, l'Hopital, and Newton [1]. These results were published by Euler in 1744, who concluded “nothing at all takes place in the universe in which some rule of maximum or minimum does not appear.” Euler also formulated the problem in general terms as the problem of finding the curve  $y(t)$  over the interval  $[a, b]$  (with  $y(a)$  and  $y(b)$  known) which minimizes:

$$J = \int_a^b F(t, y(t), y'(t)) dt \quad (1)$$

for some given function  $F(t, y(t), y'(t))$ , where  $y' = dy/dt$ .

Euler presented a necessary condition of optimality for the curve  $y(t)$ :

$$\frac{d}{dt} F_{y'}(t, y(t), y'(t)) = F_y(t, y(t), y'(t)) \quad (2)$$

where  $F_{y'}$  and  $F_y$  represent the partial derivatives with respect to  $y'$  and  $y$ , respectively.

The solution techniques proposed initially had been of a geometric nature until 1755 when Lagrange described an analytical approach, based on perturbations or “variations” of the optimal curve and using his “undetermined multipliers,” which led directly to Euler's necessary condition, now known as the “Euler-Lagrange equation.” Euler also adopted this approach and renamed the subject “the calculus of variations” [3].

In the years to come, considerable efforts have been made to develop optimal control techniques. A classification of methods for solving optimal control problems is presented by Berkani et al. in [3]. Among the most used ones we mention the following.

(i) The Dynamic Programming method, based on the principle of optimality, was first formulated by Bellman [4] and often used in the analysis and design of automatic control systems. Bellman's partial differential equation and the boundary conditions included are necessary conditions for obtaining the minimum of the optimal control problem.

(ii) The Pontryagin Minimum Principle [5] is built on defining the Hamiltonian function by introducing adjoint variables. The optimal control law is obtained by solving the canonical differential equations (the Hamilton equations) which are the necessary conditions of optimality according to the minimum principle [6]. The optimality conditions are in general not able to provide the exact optimum since the resulting two-point boundary value problem (Bellman partial differential equation) is not easy to be solved

analytically and usually computational methods are employed [7–9].

In this paper we apply the Polynomial Least Squares Method (PLSM) in order to compute approximate analytical polynomial solutions for a optimal control problems. This method was used by C. Bota and B. Căruntu in 2014 to compute approximate analytical solutions for the Brusselator system which is a fractional-order system of nonlinear differential equations [10]. In the following years the accuracy of the method is emphasized by its use in solving several types of differential equations [11–13].

The optimal control problem approached in this paper is the computation of the optimal control law  $u(t) : [0, t_f] \subset \mathcal{R} \rightarrow \mathcal{R}$  which minimizes the performance index:

$$J = \int_0^{t_f} F(y(t), u(t), t) dt \quad (3)$$

where the state equation is

$$y'(t) = f(y(t), u(t), t) \quad (4)$$

and the state variable  $y(t)$  satisfies the constraints  $y(0) = y_0$  and  $y(t_f) = y_f$ .

We will assume that  $F$  is of class  $C^1$ , so the solution of the optimal control problem exists and is unique for the given conditions. The state equation (4) may be linear or nonlinear but we also assume that  $u(t)$  can be explicitly obtained from (4) as a function of  $y(t)$ . In this case solving the optimal control problem is equivalent to solving the variational problem of finding the minimum of functional:

$$J = \int_0^{t_f} G(t, y(t), y'(t)) dt \quad (5)$$

with

$$\begin{aligned} y(0) &= y_0, \\ y(t_f) &= y_f \end{aligned} \quad (6)$$

where the relation (5) is obtained from (3) by substituting the expression for  $u(t)$  as a function of  $y(t)$  (4).

The necessary condition for the uniqueness of the solution to the problem (5)-(6) is that  $y(t)$  satisfies the conditions (6) and the Euler-Lagrange equation:

$$\frac{\partial G(t, y(t), y'(t))}{\partial y(t)} = \frac{d}{dt} \left( \frac{\partial G(t, y(t), y'(t))}{\partial y'(t)} \right). \quad (7)$$

## 2. Approximate Solution for an Optimal Control Problem Using the Polynomial Least Squares Method

2.1. *The Polynomial Least Squares Method.* The Euler-Lagrange equation associated with the optimal problem (5)-(6) may have the expression:

$$y''(t) = \mathcal{F}(y'(t), y(t), t) \quad (8)$$

where  $\mathcal{F}$  may be linear or nonlinear. We associate with this equation the following operator:

$$D(y(t)) = y''(t) - \mathcal{F}(y'(t), y(t), t) \quad (9)$$

If we denote by  $\tilde{y}(t)$  an approximate solution of (8), the error obtained by replacing the exact solution  $y(t)$  with the approximation  $\tilde{y}(t)$  is given by the remainder:

$$\mathcal{R}(t, \tilde{y}(t)) = D(\tilde{y}(t)), \quad t \in [0, t_f]. \quad (10)$$

Taking into account the boundary conditions (6), for  $\epsilon \in R_+$ , we will compute approximate polynomial solutions  $\tilde{y}$  of the problem (8), (6) on the interval  $[0, t_f]$  as follows.

*Definition 1.* We call an  $\epsilon$ -approximate polynomial solution of the problem (8), (6) an approximate polynomial solution  $\tilde{y}$  satisfying the relations

$$|\mathcal{R}(t, \tilde{y})| < \epsilon \quad (11)$$

$$\tilde{y}(0) = y_0, \quad (12)$$

$$\tilde{y}(t_f) = y_f$$

We call a *weak  $\epsilon$ -approximate polynomial solution* of the problem (8), (6) an approximate polynomial solution  $\tilde{y}$  satisfying the relation

$$\int_0^{t_f} |\mathcal{R}(t, \tilde{y})| dt \leq \epsilon \quad (13)$$

together with the initial conditions (6)

*Definition 2.* Let  $P_m(t) = c_0 + c_1 t + c_2 t^2 + \dots + c_m t^m$ ,  $c_i \in \mathbb{R}$ ,  $i = 0, 1, \dots, m$ , be a sequence of polynomials satisfying the conditions  $P_m(0) = y_0$ ,  $P_m(t_f) = y_f$ .

We call the sequence of polynomials  $P_m(t)$  convergent to the solution of the problem (8), (6) if  $\lim_{m \rightarrow \infty} D(P_m(t)) = 0$ .

We observe that from the hypothesis of the initial problem (8), (6) it follows that there exists a sequence of polynomials  $P_m(t)$  which converges to the solution of the problem. We will compute a weak  $\epsilon$ -approximate polynomial solution, in the sense of the Definition 1, of the type

$$\tilde{y}(t) = \sum_{k=0}^m d_k t^k \quad (14)$$

where  $d_0, d_1, \dots, d_m$  are constants which are calculated using the following steps:

- (i) By substituting the approximate solution (14) in (8) we obtain the remainder:

$$\mathcal{R}(t, \tilde{y}) = \tilde{y}''(t) - \mathcal{F}(\tilde{y}'(t), \tilde{y}(t), t) \quad (15)$$

We remark that if we could find  $d_0, d_1, \dots, d_m$  such that  $\mathcal{R}(t, \tilde{y}) = 0$ ,  $\tilde{y}(0) = y_0$ ,  $\tilde{y}(t_f) = y_f$ , then by substituting  $d_0, d_1, \dots, d_m$  in (14) we would obtain the exact solution of the problem (8), (6). This is not generally possible, unless the exact solution is actually a polynomial

- (ii) We attach to the problem (8), (6) the following functional:

$$\mathcal{J}(d_2, d_3 \dots, d_m) = \int_0^{t_f} \mathcal{R}^2(t, \bar{y}(t)) dt \quad (16)$$

where  $d_0, d_1$  are computed as functions of  $d_2, d_3 \dots d_m$  using the conditions (6).

- (iii) We compute the values  $d_2^0, d_3^0, \dots, d_m^0$  as the values which give the minimum of the functional  $\mathcal{J}$  and the values of  $d_0^0$  and  $d_1^0$  as functions of  $d_2^0, d_3^0, \dots, d_m^0$  using the conditions (6).
- (iv) Using the constants  $d_2^0, d_3^0, \dots, d_m^0$  previously determined we compute the polynomial

$$M_m(t) = \sum_{k=0}^m d_k^0 t^k \quad (17)$$

**Theorem 3.** *The sequence of polynomials  $M_m(t)$  from (17) satisfies the property*

$$\lim_{t \rightarrow \infty} \int_0^{t_f} \mathcal{R}^2(t, M_m(t)) dt = 0 \quad (18)$$

Moreover, if  $\forall \epsilon > 0, \exists m_o \in \mathbf{N}, m > m_o$ , it follows that  $M_m(t)$  is a weak  $\epsilon$ -approximate polynomial solution of the problem (8), (6)

*Proof.* Based on the way the polynomials  $M_m(t)$  are computed and taking into account the relations (15)-(17), the following inequalities are satisfied:

$$0 \leq \int_0^{t_f} \mathcal{R}^2(t, M_m(t)) dt \leq \int_0^{t_f} \mathcal{R}^2(t, P_m(t)) dt, \quad (19)$$

$\forall m \in \mathbf{N}$ ,

where  $P_m(t)$  is the sequence of polynomials introduced in Definition 2.

It follows that

$$\begin{aligned} 0 &\leq \lim_{t \rightarrow \infty} \int_0^{t_f} \mathcal{R}^2(t, M_m(t)) dt \\ &\leq \lim_{t \rightarrow \infty} \int_0^{t_f} \mathcal{R}^2(t, P_m(t)) dt = 0. \end{aligned} \quad (20)$$

We obtain

$$\lim_{t \rightarrow \infty} \int_a^b \mathcal{R}^2(t, M_m(t)) dt = 0. \quad (21)$$

From this limit we obtain that  $\forall \epsilon > 0, \exists m_o \in \mathbf{N}, m > m_o$  and it follows that  $M_m(t)$  is a weak  $\epsilon$ -approximate polynomial solution of the problem (8), (6).  $\square$

*Remark 4.* In order to find  $\epsilon$ -approximate polynomial solutions of the problem (8), (6) by using the Polynomial Least Squares Method we will first determine weak approximate polynomial solutions,  $\bar{y}$ . If  $|\mathcal{R}(t, \bar{y})| < \epsilon$  then  $\bar{y}$  is also an  $\epsilon$ -approximate polynomial solution of the problem.

**2.2. Application of the Polynomial Least Squares Method for an Optimal Control Problem.** We will find the approximate solution of the optimal control problem (3)-(4) using the following steps:

- (i) We transform the optimal control problem (3)-(4) in a variational problem (5)-(6) as described in the introduction.
- (ii) We attach to the variational problem (5)-(6) the corresponding Euler-Lagrange equation (7), (8).
- (iii) We compute the approximate solution  $\bar{y}(t)$  of the Euler-Lagrange equation using PLSM as described in the previous section. Thus  $\bar{y}(t)$  is an approximation of the state variable  $y(t)$  of the optimal control problem.
- (iv) Finally we compute an approximation  $\bar{u}(t)$  of the optimal control law  $u(t)$  by means of the state equation (4).

### 3. Applications

In this section we apply the Polynomial Least Squares Method in order to compute analytical approximate optimal control laws for three optimal control problems.

**3.1. Application 1.** We consider the following optimal control problem [3]:

$$\min_{u(t)} \int_0^1 [(2 - y(t))^2 + u^2(t)] dt \quad (22)$$

where the state equation is

$$y'(t) = u(t) - \frac{1}{4} \sqrt{y(t)} \quad (23)$$

and the boundary conditions are

$$\begin{aligned} y(0) &= 0, \\ y(1) &= 2 \end{aligned} \quad (24)$$

The exact solution of this problem is [3]

$$\begin{aligned} y(t) &= \frac{e^{-t} (-e - 63e^2 - 63e^t + 63e^{2t} + 63e^{2+t} + e^{1+2t})}{32(-1 + e^2)} \end{aligned} \quad (25)$$

In order to apply PLSM we follow the steps presented in the previous section:

- (i) From the state equation (23) we obtain the optimal control law  $u(t)$  as a function of the state variable  $y(t)$ :

$$u(t) = y'(t) + \frac{1}{4} \sqrt{y(t)} \quad (26)$$

Replacing this expression of  $u(t)$  in the performance index (22) we transform the initial optimal control problem into the following variational problem:

(a) Find the minimum of the functional

$$\int_0^1 \left[ (2 - y(t))^2 + \left( y'(t) + \frac{1}{4} \sqrt{y(t)} \right)^2 \right] dt \quad (27)$$

subject to the boundary conditions (24).

(ii) The corresponding Euler-Lagrange equation is

$$y''(t) - y(t) + \frac{63}{32} = 0 \quad (28)$$

(iii) We compute using PLSM an approximate analytical solution of the type

$$\begin{aligned} \tilde{y}(t) = & d_0 + d_1 \cdot t + d_2 \cdot t^2 + d_3 \cdot t^3 + d_4 \cdot t^4 + d_5 \cdot t^5 \\ & + d_6 \cdot t^6 + d_7 \cdot t^7 + d_8 \cdot t^8 + d_9 \cdot t^9. \end{aligned} \quad (29)$$

From the boundary conditions (24) we obtain  $\tilde{d}_0 = 0$  and  $d_1 = 2 - d_2 - d_3 - d_4 - d_5 - d_6 - d_7 - d_8 - d_9$ .

The corresponding remainder (15) is

$$\begin{aligned} \mathcal{R}(t) = & -\frac{63}{16} - 2 \cdot (2 \cdot d_2 + 6 \cdot d_3 \cdot t + 12 \cdot d_4 \cdot t^2 + 20 \\ & \cdot d_5 \cdot t^3 + 30 \cdot d_6 \cdot t^4 + 42 \cdot d_7 \cdot t^5 + 56 \cdot d_8 \cdot t^6 \\ & + 72 \cdot d_9 \cdot t^7) + 2 \\ & \cdot ((2 - d_2 - d_3 - d_4 - d_5 - d_6 - d_7 - d_8 - d_9) \cdot t \\ & + d_2 \cdot t^2 + d_3 \cdot t^3 + d_4 \cdot t^4 + d_5 \cdot t^5 + d_6 \cdot t^6 + d_7 \\ & \cdot t^7 + d_8 \cdot t^8 + d_9 \cdot t^9). \end{aligned} \quad (30)$$

By minimizing the functional (16)  $\mathcal{F}(d_2, d_3, \dots, d_9)$  (too large to be included here) we obtain the values for  $d_2, d_3, \dots, d_9$ . We compute the corresponding values of  $d_0$  and  $d_1$  using again the conditions (24) and we replace all these values in  $\tilde{y}(t)$  to obtain our approximation:

$$\begin{aligned} \tilde{y}(t) = & 2.6116294098342876 \cdot t \\ & + 0.9843749991096482 \cdot t^2 \\ & + 0.43527154661696676 \cdot t^3 \\ & + 0.08203105649571096 \cdot t^4 \\ & + 0.021762704663334236 \cdot t^5 \\ & + 0.0027321111314777993 \cdot t^6 \\ & + 0.0005146366961518619 \cdot t^7 \\ & + 0.0000454584242327247 \cdot t^8 \\ & + 0.000005327350329483319 \cdot t^9. \end{aligned} \quad (31)$$

TABLE 1: Absolute errors of the approximations of the state variable  $\tilde{y}(t)$  and the optimal control law  $\tilde{u}(t)$  obtained by using PLSM for Application 1.

$t$	$\tilde{y}(t)$	$\tilde{u}(t)$
0	0	$4.440892099 \cdot 10^{-16}$
0.1	$2.317035452 \cdot 10^{-13}$	$2.194910920 \cdot 10^{-11}$
0.2	$6.393774399 \cdot 10^{-13}$	$1.921662829 \cdot 10^{-11}$
0.3	$1.423638984 \cdot 10^{-12}$	$7.726264073 \cdot 10^{-12}$
0.4	$7.804867863 \cdot 10^{-14}$	$2.682920552 \cdot 10^{-11}$
0.5	$1.620037438 \cdot 10^{-12}$	$1.299405028 \cdot 10^{-12}$
0.6	$2.264854970 \cdot 10^{-13}$	$2.589484183 \cdot 10^{-11}$
0.7	$1.334266031 \cdot 10^{-12}$	$9.465761508 \cdot 10^{-12}$
0.8	$6.727951529 \cdot 10^{-13}$	$1.677147310 \cdot 10^{-11}$
0.9	$1.718625242 \cdot 10^{-13}$	$2.004618693 \cdot 10^{-11}$
1.0	$2.220446049 \cdot 10^{-16}$	0

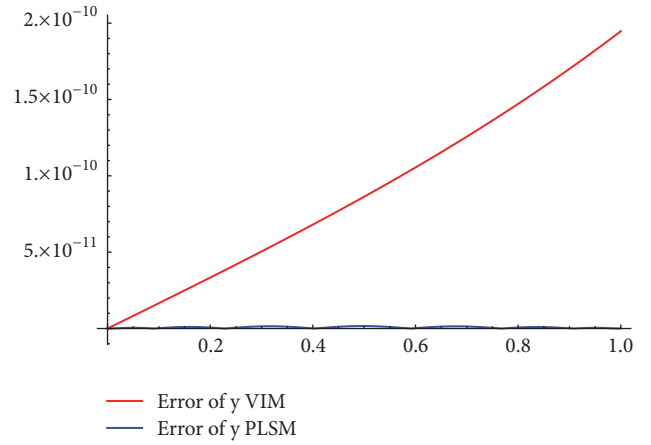


FIGURE 1: The absolute errors corresponding to the approximations of the state variable  $\tilde{y}(t)$  in Application 1: approximate solution from [3] given by VIM (red curve) and approximate solution given by PLSM (blue curve).

(iv) Finally we can easily compute an approximation for  $\tilde{u}(t)$  (also not included here because of its large size) by means of (26):

$$\tilde{u}(t) = \tilde{y}'(t) + \frac{1}{4} \sqrt{\tilde{y}(t)} \quad (32)$$

Table 1 presents the absolute errors (as differences in absolute value between the exact value and the approximate one) corresponding to our approximations of the state variable  $\tilde{y}(t)$  and of the optimal control law  $\tilde{u}(t)$  obtained by using PLSM.

Figures 1 and 2 present the comparison between our results and previous ones computed in [3] by using the Variational Iteration Method (VIM). It can be easily observed that not only is our approximation more precise, but while the error function corresponding to the VIM approximations shows a sizeable increase with  $t$ , the error function corresponding to PLSM does not. Moreover, another advantage of PLSM is the fact that, evidently, the approximation has the

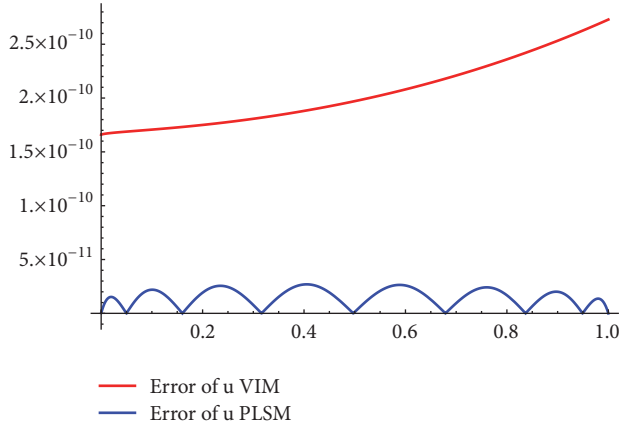


FIGURE 2: The absolute errors corresponding to the approximations of the optimal control law  $\tilde{u}(t)$  in Application 1: approximate solution from [3] given by VIM (red curve) and approximate solution given by PLSM (blue curve).

simplest possible form, namely, a polynomial, and thus is very easy to use in any further computations. Finally, we mention the fact that by increasing the degree of the polynomial  $\tilde{y}(t)$  we can obtain higher accuracy: for example, using a 10-th degree polynomial we obtain an overall error of  $10^{-14}$ .

3.2. *Application 2.* Our second application is the optimal control problem:

$$\min_{u(t)} \int_0^1 \frac{1 + y^2(t)}{u^2(t)} dt \quad (33)$$

where there state equation is

$$y'(t) = u(t) \quad (34)$$

and the boundary conditions are

$$\begin{aligned} y(0) &= 0, \\ y(1) &= 0.5 \end{aligned} \quad (35)$$

(i) Replacing the expression of  $u(t)$  from (34) in the performance index (33) we obtain the variational problem [6]:

$$\min_{y(t)} \int_0^1 \frac{1 + y^2(t)}{y'^2(t)} dt \quad (36)$$

with the same boundary conditions  $y(0) = 0$ ,  $y(1) = 0.5$ .

The exact solution of this problem is [6]

$$y(t) = \sinh \left( t \cdot \sinh^{-1} \left( \frac{1}{2} \right) \right) \quad (37)$$

We apply the same steps as in the previous application:

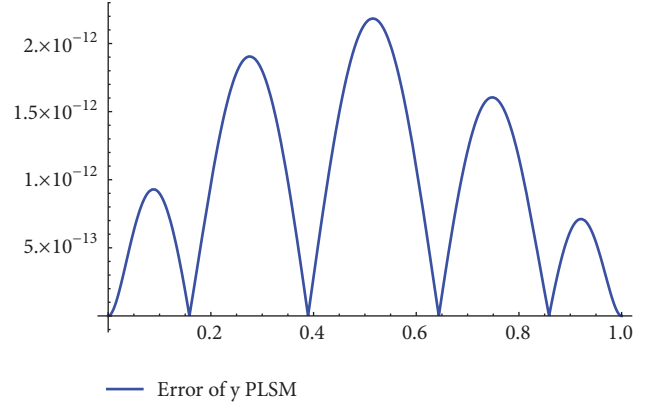


FIGURE 3: The absolute error corresponding to the approximation of the state variable  $\tilde{y}(t)$  in Application 2: approximate solution given by PLSM.

(ii) The corresponding nonlinear Euler Lagrange equation is

$$y''(t)(1 + y^2(t)) - y'(t)y(t) = 0 \quad (38)$$

(iii) We compute using PLSM an approximate analytical solution of the type

$$\begin{aligned} \tilde{y}(t) &= d_0 + d_1 \cdot t + d_2 \cdot t^2 + d_3 \cdot t^3 + d_4 \cdot t^4 + d_5 \cdot t^5 \\ &\quad + d_6 \cdot t^6 + d_7 \cdot t^7. \end{aligned} \quad (39)$$

From the boundary conditions (35) we obtain  $\tilde{d}_0 = 0$  and  $d_1 = 1/2 - d_2 - d_3 - d_4 - d_5 - d_6 - d_7$ .

We compute again the corresponding reminder (15) and by minimizing the functional (16)  $\mathcal{F}(d_2, d_3, \dots, d_7)$  we obtain the values for  $d_2, \dots, d_7$ . Using the conditions (35) and replacing all the values in  $\tilde{y}$ , our approximation of the state variable is

$$\begin{aligned} \tilde{y} &= 0.4812118250596084 \cdot t - 5.310800720418878 \\ &\quad \cdot 10^{-10} \cdot t^2 + 0.018571962082159076 \cdot t^3 \\ &\quad - 3.347040175284603 \cdot 10^{-8} \cdot t^4 \\ &\quad + 0.00021510474426296038 \cdot t^5 \\ &\quad - 8.131321771683893 \cdot 10^{-8} \cdot t^6 \\ &\quad + 1.2234286690670117 \cdot 10^{-6} \cdot t^7 \end{aligned} \quad (40)$$

(iv) Using the state equation (34) we compute an approximation for the optimal control law  $\tilde{u}(t)$ .

In Figures 3 and 4 we present the absolute errors corresponding to our approximations of the state variable  $\tilde{y}(t)$  and of the optimal control law  $\tilde{u}(t)$  for the problem (33)-(35) obtained by using PLSM.

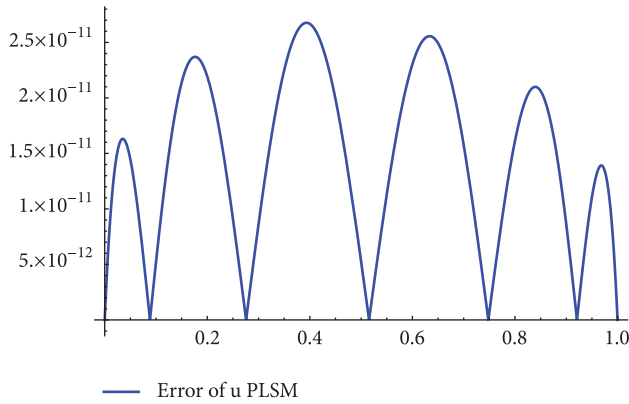


FIGURE 4: The absolute error corresponding to the approximation of the optimal control law  $\tilde{u}(t)$  in Application 2: approximate solution given by PLSM.

**3.3. Application 3.** Our third application is the well-known linear quadratic regulator (LQR), more precisely the finite-horizon, continuous-time LQR. LQRs have a wide range of applications in engineering such as trajectory tracking and optimization in robotics, control system design for various types of vehicles, automatic voltage regulators in electrical generators, and optimal controls for various types of motors.

The corresponding optimal control problem may be formulated as

$$J = \frac{1}{2} x(t_f)^T S x(t_f) + \frac{1}{2} \int_{t_0}^{t_f} (x^T P x + 2x^T Q u + u^T R u) dt \quad (41)$$

$$x'(t) = A x(t) + B u(t) \quad (42)$$

$$x(t_0) = x_0,$$

$$x(t_f) = x_f, \quad (43)$$

$$t \in [t_0, t_f].$$

We consider the following particular case of the problem (41)-(43) corresponding to the values  $A=1$ ,  $B=1$ ,  $S=8$ ,  $P=3$ ,  $Q=0$ ,  $R=1$ , and  $t_f=1$  [14, 15]:

The performance index is

$$J = 4 \cdot y^2(1) + \frac{1}{2} \int_0^1 (3 \cdot y^2(t) + u^2(t)) dt \quad (44)$$

the state equation is

$$y'(t) = u(t) \quad (45)$$

and the boundary conditions are

$$y(0) = 3 + \frac{20}{9e^4 - 5}, \quad (46)$$

$$y(1) = 8$$

Approximate solutions for this problem were proposed in [14] using the Homotopy Analysis Method and in [15] using the Optimal Homotopy Analysis Method. The exact solution of the problem is

$$y(t) = \frac{e^{-2t} \left( (5 + 45e^2 + 72e^4) e^{4t} + e^2 (-40 - 45e^2 + 27e^4) \right)}{(1 + e^2)(9e^4 - 5)} \quad (47)$$

The corresponding expression of the control is

$$u(t) = \frac{e^{-2t} \left( (5 + 45e^2 + 72e^4) e^{4t} + 3e^2 (40 + 45e^2 - 27e^4) \right)}{(1 + e^2)(9e^4 - 5)} \quad (48)$$

Using the same steps presented in the previous examples we computed the following approximation of the state variable:

$$\begin{aligned} \tilde{y}(t) = & 3.041119828603783 - 1.8976676950657474 \\ & \cdot t + 6.08223965125759 \cdot t^2 \\ & - 1.2651116099552036 \cdot t^3 \\ & + 2.027411010322069 \cdot t^4 \\ & - 0.2530087549866359 \cdot t^5 \\ & + 0.2702720790557366 \cdot t^6 \\ & - 0.02398312502575098 \\ & \cdot t^7 + 0.01913989850290996 \cdot t^8 \\ & - 0.0011806615481455588 \cdot t^9 \\ & + 0.0007696532612724977 \cdot t^{10} \\ & - 0.00002286154490479068 \cdot t^{11} \\ & + 0.000022587123028528187 \cdot t^{12}. \end{aligned} \quad (49)$$

In Figures 5 and 6 we present the absolute errors corresponding to our approximations of the state variable  $\tilde{y}(t)$  and of the optimal control law  $\tilde{u}(t)$  for the problem (44)-(46) obtained by using PLSM.

The accuracy of our method is emphasized by a comparison with approximate solutions for Application 3 previously computed by means of other well-known methods. Table 2 presents a comparison of the absolute errors corresponding to the approximations of the state variable  $\tilde{y}(t)$  obtained by using the Homotopy Analysis Method (HAM [14]) and by using the Optimal Homotopy Analysis Method (OHAM [15]).

## 4. Conclusion

In this paper the application of the Polynomial Least Squares Method to optimal control problems is presented.

TABLE 2: Comparison of the absolute errors corresponding to the approximations of the state variable  $\bar{y}(t)$  obtained by using HAM, OHAM, and PLSM for Application 3.

$t$	$\bar{y}(t)_{HAM}$	$\bar{y}(t)_{OHAM}$	$\bar{y}(t)_{PLSM}$
0	$3.8034 \cdot 10^{-4}$	$2.2926 \cdot 10^{-7}$	$4.4409 \cdot 10^{-16}$
0.2	$3.7677 \cdot 10^{-4}$	$8.7067 \cdot 10^{-7}$	$1.7306 \cdot 10^{-12}$
0.4	$1.2227 \cdot 10^{-4}$	$3.1004 \cdot 10^{-7}$	$3.8681 \cdot 10^{-12}$
0.6	$1.5453 \cdot 10^{-4}$	$6.0923 \cdot 10^{-8}$	$9.6811 \cdot 10^{-13}$
0.8	$2.1309 \cdot 10^{-4}$	$7.4523 \cdot 10^{-9}$	$1.6227 \cdot 10^{-12}$
1.0	0	$3.7303 \cdot 10^{-14}$	0

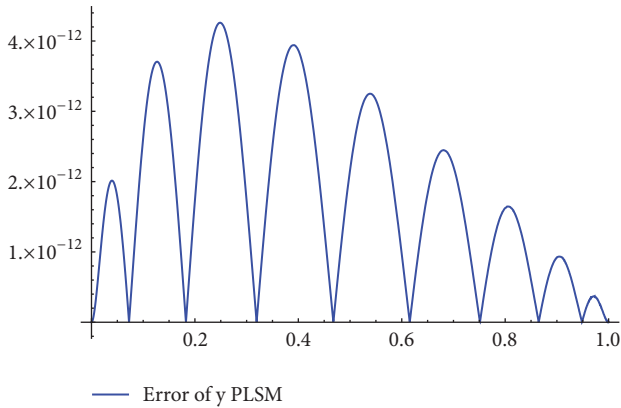


FIGURE 5: The absolute error corresponding to the approximation of the state variable  $\bar{y}(t)$  in Application 3: approximate solution given by PLSM.

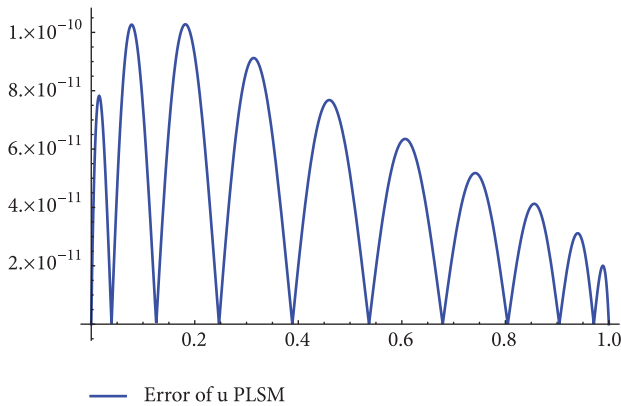


FIGURE 6: The absolute error corresponding to the approximation of the optimal control law  $\bar{u}(t)$  in Application 3: approximate solution given by PLSM.

In order to apply PLSM the optimal problem is transformed to a variational problem by substituting in the performance index the expression of the control variable given by the state equation. PLSM is able to find accurate approximations of the state variable by computing approximate analytical polynomial solutions of the Euler-Lagrange equation corresponding to the variational problem. The optimal control law is then computed by using the state equation.

The numerical examples included clearly illustrate the accuracy of the method by means of a comparison with solutions previously computed by other methods.

### Data Availability

The data used to support the findings of this study are included within the article.

### Conflicts of Interest

The authors declare that they have no conflicts of interest.

### References

- [1] R. W. Sargent, "Optimal control," *Journal of Computational and Applied Mathematics*, vol. 124, no. 1-2, pp. 361–371, 2000.
- [2] H. J. Sussmann and J. C. Willems, "300 years of optimal control: from the brachistochrone to the maximum principle," *IEEE Control Systems Magazine*, vol. 17, no. 3, pp. 32–44, 1997.
- [3] S. Berkani, F. Manseur, and A. Maida, "Optimal control based on the variational iteration method," *Computers & Mathematics with Applications. An International Journal*, vol. 64, no. 4, pp. 604–610, 2012.
- [4] R. Luus, "On the application of iterative dynamic programming to singular optimal control problems," *Institute of Electrical and Electronics Engineers Transactions on Automatic Control*, vol. 37, no. 11, pp. 1802–1806, 1992.
- [5] M. J. Sewell, *Maximum and Minimum Principles. A Unified Approach, with Applications*, Cambridge University Press, New York, NY, USA, 1987.
- [6] M. Tatari and M. Dehghan, "Solution of problems in calculus of variations via He's variational iteration method," *Physics Letters A*, vol. 362, no. 5-6, pp. 401–406, 2007.
- [7] B. van Brunt, *The Calculus of Variations*, Springer, New York, NY, USA, 2004.
- [8] J.-H. He, "Variational iteration method for autonomous ordinary differential systems," *Applied Mathematics and Computation*, vol. 114, no. 2-3, pp. 115–123, 2000.
- [9] I. Kucuk, "Active Optimal Control of the KdV Equation Using the Variational Iteration Method," *Mathematical Problems in Engineering*, vol. 2010, Article ID 929103, 10 pages, 2010.
- [10] C. Bota and B. Căruntu, "Approximate Analytical Solutions of the Fractional-Order Brusselator System Using the Polynomial Least Squares Method," *Advances in Mathematical Physics*, vol. 2015, Article ID 450235, 5 pages, 2015.
- [11] C. Bota and B. Caruntu, "Analytic approximate solutions for a class of variable order fractional differential equations using

- the polynomial least squares method,” *Fractional Calculus and Applied Analysis*, vol. 20, no. 4, pp. 1043–1050, 2017.
- [12] C. Bota and B. Caruntu, “Analytical approximate solutions for quadratic Riccati differential equation of fractional order using the polynomial least squares method,” *Chaos, Solitons & Fractals*, vol. 102, pp. 339–345, 2017.
- [13] B. Caruntu and C. Bota, “Approximate Analytical Solutions of the Regularized Long Wave Equation Using the Optimal Homotopy Perturbation Method,” *The Scientific World Journal*, vol. 201, Article ID 721865, 6 pages, 2014.
- [14] M. S. Zahedi and H. S. Nik, “On homotopy analysis method applied to linear optimal control problems,” *Applied Mathematical Modelling: Simulation and Computation for Engineering and Environmental Systems*, vol. 37, no. 23, pp. 9617–9629, 2013.
- [15] W. Jia, X. He, and L. Guo, “The optimal homotopy analysis method for solving linear optimal control problems,” *Applied Mathematical Modelling: Simulation and Computation for Engineering and Environmental Systems*, vol. 45, pp. 865–880, 2017.

## Research Article

# Research on Time-Space Fractional Model for Gravity Waves in Baroclinic Atmosphere

Yanwei Ren,<sup>1</sup> Huanhe Dong ,<sup>2</sup> Xinzhu Meng ,<sup>2</sup> and Hongwei Yang <sup>2</sup>

<sup>1</sup>College of Economics and Management, Shandong University of Science and Technology, Qingdao, Shandong 266590, China

<sup>2</sup>College of Mathematics and Systems Science, Shandong University of Science and Technology, Qingdao, Shandong 266590, China

Correspondence should be addressed to Hongwei Yang; [hwyang1979@163.com](mailto:hwyang1979@163.com)

Received 8 August 2018; Accepted 14 October 2018; Published 24 October 2018

Academic Editor: Ivo Petras

Copyright © 2018 Yanwei Ren et al. This is an open access article distributed under the Creative Commons Attribution License, which permits unrestricted use, distribution, and reproduction in any medium, provided the original work is properly cited.

The research of gravity solitary waves movement is of great significance to the study of ocean and atmosphere. Baroclinic atmosphere is a complex atmosphere, and it is closer to the real atmosphere. Thus, the study of gravity waves in complex atmosphere motion is becoming increasingly essential. Deriving fractional partial differential equation models to describe various waves in the atmosphere and ocean can open up a new window for us to understand the fluid movement more deeply. Generally, the time fractional equations are obtained to reflect the nonlinear waves and few space-time fractional equations are involved. In this paper, using multiscale analysis and perturbation method, from the basic dynamic multivariable equations under the baroclinic atmosphere, the integer order mKdV equation is derived to describe the gravity solitary waves which occur in the baroclinic atmosphere. Next, employing the semi-inverse and variational method, we get a new model under the Riemann-Liouville derivative definition, i.e., space-time fractional mKdV (STFmKdV) equation. Furthermore, the symmetry analysis and the nonlinear self-adjointness of STFmKdV equation are carried out and the conservation laws are analyzed. Finally, adopting the  $\exp(-\Phi(\xi))$  method, we obtain five different solutions of STFmKdV equation by considering the different cases of the parameters  $(\eta, \sigma)$ . Particularly, we study the formation and evolution of gravity solitary waves by considering the fractional derivatives of nonlinear terms.

## 1. Introduction

With the intercross and penetration of different knowledge, Rossby solitary waves have been applied to many fields successfully, such as physical oceanography, atmospheric science, hydraulic engineering, and communication engineering. Particularly, Rossby solitary waves have important theoretical significance and research value in marine atmospheric science. They have largely determined the impact of the oceans on the atmosphere and other climate change. On the time scale, the energy of Rossby waves determines the ocean energy spectrum, which makes the energy spread from east to west to form and maintain a strong ocean boundary flow, such as Kuroshio, Gulfstream, and East Australian flow. Great achievements have been made in this regard.

As we know, Rossby solitary waves in the westerly shear flow were first found by Long [1]. He found that the amplitude

of the Rossby waves satisfied KdV equation by the  $\beta$ -plane approximation

$$u_t + \mu u u_x + \delta u_{xxx} = 0. \quad (1)$$

With the development of Rossby waves theory, Wadati [2] derived the modified KdV equation

$$u_t + \mu u^2 u_x + \delta u_{xxx} = 0. \quad (2)$$

In view of the barotropic fluid and stratified fluid model, the KdV model and the mKdV model are also generated to describe the generation and evolution of Rossby solitary waves by Redekopp [3]. Apart from the KdV model and the mKdV model, for other initial disturbance, employing a different time and space stretching transform, Boussinesq equation was derived by Meng and Lv [4]. Afterwards, the Rossby parameters  $\beta$  along with the changes of latitude were discussed by Luo [5] and generalized  $\beta$ -plane approximation

was obtained. In recent years, in the theoretical study of Rossby waves, many new wave equations were obtained to describe the generation and evolution of various types of fluctuations in the ocean [6, 7], such as NLS equation, ILW-Burgers equation, and ZK-Burgers equation. In the past, predecessors studied wave equations in the barotropic atmospheric environment by using the  $\beta$ -plane approximation. But we know that the basic dynamic equations for describing the baroclinic atmospheric movement are more in line with the actual situation and are very complicated. And the baroclinic problem in real atmosphere is inevitable [8]. In this paper, starting with the basic equations adopting the Bousinesq approximation [9] and under the baroclinic atmospheric environment, using multiscale analysis and turbulence method, we get a new model (mKdV) to describe the Rossby solitary waves. The advantages of basic equations are as follows:

(1) The equations are multivariate, and the physical meaning of each variable is clear;

(2) The baroclinic atmosphere problem is considered to help us understand the generation and evolution of isolated waves in the ocean.

In recent years, the study of integer partial differential equations has yielded many brilliant achievements [10–15]. Simultaneously, it has been found that fractional order partial differential equations also play an important role in many fields [16–22]. The fractional differentiation calculus [23, 24] was first developed by Liouville primary. Liouville expands the function into an exponential form and defines the  $q$ -order derivatives of this expanded form term by term. Afterwards, Riemann proposed a different definition that can be implemented to a power series with a negative power term. Finally, Ross and Oldham [25, 26] unified the two definitions, so that the application of fractional differential was further developed. Subsequently, a version of the Euler-Lagrange equations for problems of calculus of variation with fractional derivatives was formulated by Riewe in 1990s [27, 28]. Recently, Agrawal [29, 30] studied the fractional Euler-Lagrange equation deeper and a series of new methods have been put forward in his research, which provide a new idea for us to study fractional partial differential equations [31, 32]. The fact has shown that the new fractional equation is more suitable than the integer order equation due to the precise description of the nonlinear phenomena [33, 34]. At the same time, in the field of oceanography, the fractional partial differential equation can better describe the generation and evolution of solitary waves, which is more favorable for us to study the theory of fluctuation.

Similar to the study of integer order differential equation, the conservation laws of the fractional differential equation are an important branch. As we know, if the fractional differential equation is an Euler-Lagrange equation, then conservation laws can be found using Noether's theorem by variational Lie point symmetries of this equation [35–37]. Lie symmetry analysis was proposed by Sophus Lie. The main idea of this method is that the infinitesimal transformation keeps the solution set of the partial differential equation unchanged. The Lie symmetry analysis offers an efficient and powerful tool for the study of conservation laws of fractional

partial differential equation [38–42]. For this reason, the researchers are very interested in studying the symmetry analysis of fractional differential equations. As far as we know, in the past, the symmetric method was only used for time fraction partial differential equations (TFPDE), but has not been used to analyze space and time fraction partial differential equations (STFPDE) [43, 44]. In this paper, the Lie symmetry analysis was used to study the conservation law of the STFmKdV equation [45, 46].

By studying the work of predecessors, we can find that several methods have been used to solve nonlinear partial differential equations, such as the trial equation method [47, 48], Hirota bilinear method [49], binary nonlinearization method [50], Darboux transformation method [51], Jacobi iteration method [52],  $(G'/G)$ -expansion method [53–55], exp-function method [48], sub-equation method [56], and others [57, 58]. Therefore, it is an important task to find an accurate and effective method to solve the fractional differential equation.

This paper is organized as follows: In Section 2, using multiscale analysis and turbulence method, from the basic dynamic multivariable equations under the baroclinic atmosphere [59, 60], the integer order mKdV equation is derived. In Section 3, we use the semi-inverse method to derive the Lagrangian form of the mKdV equation [61, 62] firstly. Then the Lagrangian space and time operator of the mKdV equation have been transformed into the fractional domain of the left Riemann-Liouville fractional differential operator. Finally, applying the variational method, we derive the STFmKdV from this Euler-Lagrangian equation. In Section 4, we first study the symmetry analysis of the fractional equation to obtain the corresponding infinitesimal generator of the equation. Then we discuss the nonlinear self-adjointness of the STFmKdV equation and finally get the conservation vectors of the equation. In Section 5, based on the STFmKdV equation, employing the  $\exp(-\Phi(\xi))$  method, and considering the different cases of the parameters  $(\eta, \sigma)$ , we obtain five different solutions of the equation.

## 2. Derivation of the mKdV Equation

Using the sum of disturbance pressure gradient force and buoyancy force expressing the vertical pressure gradient force and gravity force, and adopting the Bousinesq approximation [60], the dimensionless basic dynamic equations of atmospheric motion are as follows [59]:

$$\begin{aligned} \frac{\partial u'}{\partial t'} + \frac{U}{fL} \left( u' \frac{\partial u'}{\partial x'} + v' \frac{\partial u'}{\partial y'} + w' \frac{\partial u'}{\partial z'} \right) &= -\frac{1}{\rho_s} \frac{\partial p'}{\partial x'} + v', \\ \frac{\partial v'}{\partial t'} + \frac{U}{fL} \left( u' \frac{\partial v'}{\partial x'} + v' \frac{\partial v'}{\partial y'} + w' \frac{\partial v'}{\partial z'} \right) &= -\frac{1}{\rho_s} \frac{\partial p'}{\partial y'} - u', \\ \frac{\partial w'}{\partial t'} + \frac{U}{fL} \left( u' \frac{\partial w'}{\partial x'} + v' \frac{\partial w'}{\partial y'} + w' \frac{\partial w'}{\partial z'} \right) \\ &= \frac{gL\delta\theta}{DfU\theta_0} \left( -\frac{1}{\rho_s} \frac{\partial p'}{\partial z'} + \theta' \right), \end{aligned}$$

$$\begin{aligned} \frac{\partial \theta'}{\partial t'} + \frac{U}{fL} \left( u' \frac{\partial \theta'}{\partial x'} + v' \frac{\partial \theta'}{\partial y'} \right) + \frac{\sigma UD}{fL \delta \theta} w' &= 0, & \frac{\partial}{\partial y} &= \frac{\partial}{\partial y'}, \\ \frac{\partial (\rho_s u')}{\partial x'} + \frac{\partial (\rho_s v')}{\partial y'} + \frac{\partial (\rho_s w')}{\partial z'} &= 0. & \frac{\partial}{\partial z} &= \frac{\partial}{\partial z'}. \end{aligned} \quad (7)$$

where  $u'$ ,  $v'$  are the level of the air speed,  $w'$  is the vertical velocity,  $p'$  is the atmospheric pressure,  $\theta$  is the temperature field, and  $f$  is the Coriolis parameter.  $\theta_0$  is the potential of environmental flow field and  $\rho_s$  is the density of environmental flow field; they are both the height functions.

Because the second term of the fourth formula in the left side is lesser, we get the following approximation:

$$\begin{aligned} \delta \theta &\sim \frac{\sigma UD}{fL}, \\ \frac{U}{fL} &\sim o(1). \end{aligned} \quad (4)$$

Let the parameter  $\varepsilon = f^2/N^2$  ( $\varepsilon \ll 1$ ),  $N^2 = g\sigma/\theta_0$ . By varying, (3) transforms to

$$\begin{aligned} \frac{\partial u'}{\partial t'} + u' \frac{\partial u'}{\partial x'} + v' \frac{\partial u'}{\partial y'} + w' \frac{\partial u'}{\partial z'} &= -\frac{1}{\rho_s} \frac{\partial p'}{\partial x'} + v', \\ \frac{\partial v'}{\partial t'} + u' \frac{\partial v'}{\partial x'} + v' \frac{\partial v'}{\partial y'} + w' \frac{\partial v'}{\partial z'} &= -\frac{1}{\rho_s} \frac{\partial p'}{\partial y'} - u', \\ \frac{\partial w'}{\partial t'} + u' \frac{\partial w'}{\partial x'} + v' \frac{\partial w'}{\partial y'} + w' \frac{\partial w'}{\partial z'} &= \varepsilon^{-1} \left( -\frac{1}{\rho_s} \frac{\partial p'}{\partial x'} + \theta' \right), \\ \frac{\partial \theta'}{\partial t'} + u' \frac{\partial \theta'}{\partial x'} + v' \frac{\partial \theta'}{\partial y'} + w' &= 0, \\ \frac{\partial (\rho_s u')}{\partial x'} + \frac{\partial (\rho_s v')}{\partial y'} + \frac{\partial (\rho_s w')}{\partial z'} &= 0. \end{aligned} \quad (5)$$

We introduce the multiscale variables (omitting the sign at the top right corner of the variables)

$$\begin{aligned} t &= \varepsilon^{3/2} t', \\ x &= \varepsilon^{1/2} x', \\ y &= y', \\ z &= z', \end{aligned} \quad (6)$$

so long time and space scales are defined as

$$\begin{aligned} \frac{\partial}{\partial t} &= \varepsilon^{3/2} \frac{\partial}{\partial t'}, \\ \frac{\partial}{\partial x} &= \varepsilon^{1/2} \frac{\partial}{\partial x'}, \end{aligned}$$

Further, according to the small parameter  $\varepsilon$ ,  $u'$ ,  $v'$ ,  $w'$ ,  $p'$ ,  $\theta'$  in (5) can be expended:

$$\begin{aligned} u' &= - \int_0^y (U(\zeta, z) - c + \varepsilon \lambda) d\zeta + \varepsilon^{1/2} u_0 + \varepsilon u_1 \\ &\quad + \varepsilon^{3/2} u_2 + \varepsilon^2 u_3 + \dots, \\ v' &= \varepsilon v_0 + \varepsilon^{3/2} v_1 + \varepsilon^2 v_2 + \varepsilon^{5/2} v_3 + \dots, \\ w' &= \varepsilon w_0 + \varepsilon^{3/2} w_1 + \varepsilon^2 w_2 + \varepsilon^{5/2} w_3 + \dots, \\ \theta' &= \Theta(y, z) + \varepsilon^{1/2} \theta_0 + \varepsilon \theta_1 + \varepsilon^{3/2} \theta_2 + \varepsilon^2 \theta_3 + \dots, \\ p' &= P(y, z) + \varepsilon^{1/2} p_0 + \varepsilon p_1 + \varepsilon^{3/2} p_2 + \varepsilon^2 p_3 + \dots, \end{aligned} \quad (8)$$

where  $U$ ,  $P$ ,  $\Theta$  are the function of  $y$ ,  $z$ .  $U$  is the speed of the basic flow,  $P$  is the air pressure, and  $\Theta$  is the temperature field. Obviously, the zonal flow is in the following forms:

$$U = \begin{cases} U_y = 0, & \text{as } 0 \leq y < y_0, \\ \text{costant}, & \text{as } y \geq y_0, \end{cases} \quad (9)$$

and the boundary conditions of (3) are

$$\begin{aligned} p' &= 0, \\ \text{as } y &= 0, \\ p' &\rightarrow 0, \\ \text{as } y &\rightarrow \infty. \end{aligned} \quad (10)$$

Substituting (7) and (8) into (3), we get each order form for  $\varepsilon$  as follows:

$$O(\varepsilon^0): \begin{cases} \frac{1}{\rho_s} \frac{\partial p}{\partial y} - \int_0^y (U - c) d\zeta = 0, \\ \frac{1}{\rho_s} \frac{\partial p}{\partial z} - \Theta = 0. \end{cases} \quad (11)$$

Assuming  $|1/\rho_s^2| \ll 1$ , we have

$$\frac{\partial}{\partial z} \left( \int_0^y U d\zeta \right) = \Theta_y. \quad (12)$$

Next, we write the first-, second-, and third-order approximation for  $\varepsilon$  as the following form:

$$\begin{aligned} \int_0^y (U - c) d\zeta \frac{\partial u_i}{\partial x} + (U - c + 1) v_i + \Theta y w_i - \frac{1}{\rho_s} \frac{\partial p_i}{\partial x} \\ = A u_i, \end{aligned}$$

$$\begin{aligned}
\frac{1}{\rho_s} \frac{\partial p_i}{\partial y} + u_i &= Av_i, \\
\frac{1}{\rho_s} \frac{\partial p_i}{\partial z} - \theta_i &= Aw_i, \\
\int_0^y (U - c) d\zeta \frac{\partial \theta_i}{\partial x} - \Theta y v_i - w_i &= A\theta_i, \\
\frac{\partial \rho_s u_i}{\partial x} + \frac{\partial \rho_s v_i}{\partial y} + \frac{\partial \rho_s w_i}{\partial z} &= 0,
\end{aligned}$$

$i = 0, 1, 2, 3 \dots$

(13)

where

$$Au_0 = Av_0 = Aw_0 = A\theta_0 = 0. \quad (14)$$

By eliminating  $u_0, v_0, w_0, \theta_0$  in (13), we can obtain the equation for  $p_0$

$$L_{y,z} \left( \frac{\partial p_0}{\partial x} \right) = 0, \quad (15)$$

where

$$\begin{aligned}
\Omega &= U_y - 1 + U_z^2, \\
\Omega_y &= \frac{\partial \Omega}{\partial y}, \\
\Omega_z &= \frac{\partial \Omega}{\partial z}, \\
L_{y,z} &= \frac{\partial^2}{\partial y^2} - (U_y - 1) \frac{\partial^2}{\partial z^2} + 2U_z \frac{\partial^2}{\partial y \partial z} \\
&+ \left[ U_{zz} - \frac{\Omega_y}{\Omega} - U_z \frac{\Omega_z}{\Omega} \right] \frac{\partial}{\partial y} \\
&+ \left[ (U_y - 1) \frac{\Omega_z}{\Omega} - U_z \frac{\Omega_y}{\Omega} \right] \frac{\partial}{\partial z} \\
&- \frac{1}{U} \left[ U_{zz} - \frac{\Omega_y}{\Omega} - U_z \frac{\Omega_z}{\Omega} \right].
\end{aligned} \quad (16)$$

Clearly, (15) is a variable separable equation. Assume its solution is

$$p_0 = \widetilde{p}_0(y, z) A(t, x), \quad (17)$$

and under a certain definite solution condition, we can get  $\widetilde{p}_0$ . Further, all the solutions of (15) can be obtained:

$$\begin{aligned}
u_0 &= \widetilde{u}_0(y, z) A(t, x), \\
v_0 &= \widetilde{v}_0(y, z) A_x(t, x), \\
w_0 &= \widetilde{w}_0(y, z) A_x(t, x), \\
\theta_0 &= \widetilde{\theta}_0(y, z) A(t, x).
\end{aligned} \quad (18)$$

Further, we know that

$$\begin{aligned}
Au_1 &= u_0 \frac{\partial u_0}{\partial x} + v_0 \frac{\partial u_0}{\partial y} + w_0 \frac{\partial u_0}{\partial z}, \\
Av_1 &= 0, \\
Aw_1 &= 0, \\
A\theta_1 &= u_0 \frac{\partial \theta_0}{\partial x} + v_0 \frac{\partial \theta_0}{\partial y}.
\end{aligned} \quad (19)$$

Similarly, we cannot get the equation for  $A(x, t)$ . So, we eliminate  $u_1, v_1, w_1, \theta_1$  in (13) and (19), and we can obtain the equation of  $p_1$

$$L_{y,z} \left( \frac{\partial p_1}{\partial x} \right) = \ell_{1y,z} (Au_1) + \ell_{2y,z} (A\theta_1), \quad (20)$$

where

$$\begin{aligned}
\ell_{1y,z} &= - \left[ -\frac{\partial}{\partial y} - U_{zz} - U_z \frac{\partial}{\partial z} - \frac{1}{U - c} \right. \\
&\quad \left. - \frac{1}{\Delta} (\Delta_y + U_z \Delta_z) \right], \\
\ell_{2y,z} &= \frac{-1}{U - c} \left[ \frac{\partial}{\partial y} + U_{zz} + U_z \frac{\partial}{\partial z} \right. \\
&\quad \left. - \frac{1}{\Delta} (\Delta_y + U_z \Delta_z) \right]
\end{aligned} \quad (21)$$

Substituting (19) into (20) and observing both ends of (20), we can get the solutions for the variables as follows:

$$\begin{aligned}
u_1 &= \widetilde{u}_1(y, z) A^2(t, x), \\
v_1 &= \widetilde{v}_1(y, z) A(t, x) A_x(t, x), \\
w_1 &= \widetilde{w}_1(y, z) A(x, t) A_x(t, x), \\
\theta_1 &= \widetilde{\theta}_1(y, z) A^2(t, x), \\
p_1 &= \widetilde{p}_1(y, z) A^2(t, x).
\end{aligned} \quad (22)$$

Next, we have a further discussion,

$$\begin{aligned}
Au_2 &= \frac{\partial u_0}{\partial t} + \alpha \frac{\partial u_0}{\partial x} + u_0 \frac{\partial u_1}{\partial x} + u_1 \frac{\partial u_0}{\partial x} + v_0 \frac{\partial u_1}{\partial y} \\
&\quad + v_1 \frac{\partial u_0}{\partial y} + w_0 \frac{\partial u_1}{\partial z} + w_1 \frac{\partial u_0}{\partial z}, \\
Av_2 &= \int_0^y (U - c) d\zeta \frac{\partial v_0}{\partial x}, \\
Aw_2 &= 0, \\
A\theta_2 &= \frac{\partial \theta_0}{\partial t} + u_0 \frac{\partial \theta_1}{\partial x} + u_1 \frac{\partial \theta_0}{\partial x} + v_0 \frac{\partial \theta_1}{\partial y} + v_1 \frac{\partial \theta_0}{\partial y},
\end{aligned} \quad (23)$$

Simplify (13) and (23) to the following form:

$$L_{y,z} \left( \frac{\partial p_2}{\partial x} \right) \equiv \ell_{3y,z} \left( \frac{\partial A v_2}{\partial x} \right) + \ell_{1y,z} (A u_2) + \ell_{2y,z} (A \theta_2), \quad (24)$$

where

$$\begin{aligned} \ell_{1y,z} &= - \left[ - \frac{\partial}{\partial y} - U_{zz} - U_z \frac{\partial}{\partial z} - \frac{1}{U-c} \right. \\ &\quad \left. - \frac{1}{\Delta} (\Delta_y + U_z \Delta_z) \right] \\ \ell_{2y,z} &= \frac{-1}{U-c} \left[ \frac{\partial}{\partial y} + U_{zz} + U_z \frac{\partial}{\partial z} \right. \\ &\quad \left. - \frac{1}{\Delta} (\Delta_y + U_z \Delta_z) \right] \\ \ell_{3y,z} &= \frac{-1}{U-c} \left[ -U_z \frac{\partial}{\partial y} + (U_y - 1) \frac{\partial}{\partial z} \right. \\ &\quad \left. + \frac{1}{\Delta} (U_z \Delta_y + (U_y - 1) \Delta_z) \right]. \end{aligned} \quad (25)$$

We know that the homogeneous part in (24) is the same as (15). Substituting (18) and (22) into (19) and (23), and according to (13)  $\times \partial p_0 / \partial x$  - (20)  $\times \partial p_2 / \partial x$ , we can get

$$\begin{aligned} A_{u_2} &= \bar{u}_0 A_t + \lambda A_x + (3\bar{u}_0 \bar{u}_1 + \bar{v}_0 \bar{u}_{1y} + \bar{v}_1 \bar{u}_{0y} \\ &\quad + \bar{w}_0 \bar{u}_{1z} + \bar{w}_1 \bar{u}_{0z}) A^2 A_x, \\ A_{v_2} &= \int_0^y (U-c) d\zeta \bar{v}_0 A_{xx}, \\ A_{w_2} &= 0, \\ A_{\theta_2} &= \bar{\theta}_0 A_t + (2\bar{u}_0 \bar{\theta}_1 + \bar{u}_1 \bar{\theta}_0 + \bar{v}_0 \bar{\theta}_{1y} + \bar{v}_1 \bar{\theta}_{0y}) A^2 A_x, \\ \frac{d}{dy} \left[ \frac{\partial p_2}{\partial x} \frac{d\bar{p}_0}{dy} - \bar{p}_0 \frac{d}{dy} \left( \frac{\partial p_2}{\partial x} \right) \right] &- \left[ L_{y,z} (\bar{p}_0) \frac{\partial p_2}{\partial x} \right. \\ &\quad \left. - L_{y,z} \left( \frac{\partial p_2}{\partial x} \right) \bar{p}_0 \right] = -\bar{p}_0 \left\{ \left[ \ell_{1y,z} (\bar{u}_0) + \ell_{2y,z} (\bar{\theta}_0) \right] \right. \\ &\quad \cdot A_t + \ell_{1y,z} \lambda A_x + \left[ \ell_{1y,z} (3\bar{u}_0 \bar{u}_1 + \bar{v}_0 \bar{u}_{1y} + \bar{v}_1 \bar{u}_{0y} \right. \\ &\quad \left. + \bar{w}_0 \bar{u}_{1z} + \bar{w}_1 \bar{u}_{0z}) + \ell_{2y,z} (2\bar{u}_0 \bar{\theta}_1 + \bar{u}_1 \bar{\theta}_0 + \bar{v}_0 \bar{\theta}_{1y} \right. \\ &\quad \left. \left. + \bar{v}_1 \bar{\theta}_{0y}) \right] A^2 A_x + \left[ \ell_{3y,z} (U-c) \bar{v}_0 \right] A_{xxx} \right\}. \end{aligned} \quad (26)$$

Integrating (27) over the domain  $[0, y_0]$  leads to

$$\begin{aligned} &\int \left[ \bar{p}_0 (y_0, z) \frac{d}{dy} \left( \frac{\partial p_2}{\partial x} \right) - \left( \frac{\partial p_2}{\partial x} \right) \frac{d\bar{p}_0 (y_0, z)}{dy} \right] dz + \int \int_0^{y_0} \left[ L (\bar{p}_0 (y_0, z)) \left( \frac{\partial p_2}{\partial x} \right) - L \left( \frac{\partial p_2}{\partial x} \right) \bar{p}_0 (y_0, z) \right] dy dz \\ &= \int \int_0^{y_0} -\bar{p}_0 \left\{ \left[ \ell_{1y,z} (\bar{u}_0) + \ell_{2y,z} (\bar{\theta}_0) \right] A_t + \ell_{1y,z} (\bar{u}_0) \lambda A_x \right. \\ &\quad \left. + \left[ \ell_{1y,z} (3\bar{u}_0 \bar{u}_1 + \bar{v}_0 \bar{u}_{1y} + \bar{v}_1 \bar{u}_{0y} + \bar{w}_0 \bar{u}_{1z} + \bar{w}_1 \bar{u}_{0z}) + \ell_{2y,z} (2\bar{u}_0 \bar{\theta}_1 + \bar{u}_1 \bar{\theta}_0 + \bar{v}_0 \bar{\theta}_{1y} + \bar{v}_1 \bar{\theta}_{0y}) \right] A^2 A_x \right. \\ &\quad \left. + \left[ \ell_{3y,z} (U-c) \bar{v}_0 \right] A_{xxx} \right\} dy dz. \end{aligned} \quad (28)$$

We know that the two ends of (28) are identically zero, so we can write the simple form as the following form:

$$A_t + a_0 \lambda A_x + a_1 A^2 A_x + a_2 A_{xxx} = 0, \quad (29)$$

where

$$\begin{aligned} a_0 &= \frac{\ell_{1y,z} (\bar{u}_0)}{\ell_{1y,z} (\bar{u}_0) + \ell_{2y,z} (\bar{\theta}_0)}, \\ a_1 &= \frac{\ell_{1y,z} (3\bar{u}_0 \bar{u}_1 + \bar{v}_0 \bar{u}_{1y} + \bar{v}_1 \bar{u}_{0y} + \bar{w}_0 \bar{u}_{1z} + \bar{w}_1 \bar{u}_{0z}) + \ell_{2y,z} (2\bar{u}_0 \bar{\theta}_1 + \bar{u}_1 \bar{\theta}_0 + \bar{v}_0 \bar{\theta}_{1y} + \bar{v}_1 \bar{\theta}_{0y})}{\ell_{1y,z} (\bar{u}_0) + \ell_{2y,z} (\bar{\theta}_0)}, \\ a_2 &= \frac{\ell_{3y,z} (U-c) \bar{v}_0}{\ell_{1y,z} (\bar{u}_0) + \ell_{2y,z} (\bar{\theta}_0)}. \end{aligned} \quad (30)$$

*Remark.* According to the above study, we obtain a new model in baroclinic atmosphere. Based on the nonlinear

term  $A^2 A_x$ , the new model is called the generalized mKdV equation. Compared to the model which is obtained in the

barotropic atmosphere, the new mKdV equation is more likely to describe the movement of solitary waves.

### 3. Formulation of the STFMKdV Equation

First we introduce the definition of Riemann-Liouville fractional derivatives and Caputo fractional derivatives [41, 63].

*Definition 1* (Riemann-Liouville fractional derivative [41, 63]).  $f(t)$  is a function defined in the  $[a, b]$ , for any nonnegative real  $\alpha$ , satisfying  $n - 1 \leq \alpha < n$ ,

$$\begin{aligned} {}_a^R D_t^\alpha f(t) &:= D^n {}_a^R D_t^{\alpha-n} f(t) \\ &= \frac{1}{\Gamma(n-\alpha)} \frac{d^n}{dt^n} \int_a^t \frac{f(\tau)}{(t-\tau)^{\alpha+1-n}} d\tau, \end{aligned} \quad (31)$$

$$\forall t \in [a, b],$$

and this formula is called the  $\alpha$ -order left Riemann-Liouville fractional derivative. And

$$\begin{aligned} {}_t^R D_b^\alpha f(t) &:= (-1)^n D^n {}_t^R D_b^{\alpha-n} f(t) \\ &= \frac{(-1)^n}{\Gamma(n-\alpha)} \frac{d^n}{dt^n} \int_t^b \frac{f(\tau)}{(\tau-t)^{\alpha+1-n}} d\tau, \end{aligned} \quad (32)$$

$$\forall t \in [a, b],$$

and this formula is the  $\alpha$ -order right Riemann-Liouville fractional derivative.

*Remark 2.* We note that if the function  $f(t)$  is  $n$ -order continuous derivable on the interval of  $[a, b]$ , when  $\alpha$  tends to  $n$ , the left fractional derivative is the traditional  $n$ -order derivative. In addition, if the function  $f(t)$  is  $n$ -order continuous derivable on the interval of  $[a, b]$ , when  $\alpha$  tends to  $n$ , the right fractional derivative is the traditional  $n(n-1)$ -order derivative multiplied by  $(-1)^n$ .

*Definition 3* (Caputo fractional derivative [41, 63]).  $f(t)$  is a function defined in the  $[a, b]$ , for any nonnegative real  $\alpha$ , satisfying  $n - 1 \leq \alpha < n$ ,

$$\begin{aligned} {}_a^C D_t^\alpha f(t) &:= {}_a^R D_t^{\alpha-n} D^n f(t) \\ &= \frac{1}{\Gamma(n-\alpha)} \int_a^t \frac{f^{(n)}(\tau)}{(t-\tau)^{\alpha+1-n}} d\tau, \end{aligned} \quad (33)$$

$$\forall t \in [a, b],$$

and this formula is the  $\alpha$ -order left Caputo fractional derivative.

$$\begin{aligned} {}_t^C D_b^\alpha f(t) &:= (-1)^n {}_t^R D_b^{(\alpha-n)} D^n f(t) \\ &= \frac{(-1)^n}{\Gamma(n-\alpha)} \int_t^b \frac{f^{(n)}(\tau)}{(\tau-t)^{\alpha+1-n}} d\tau, \end{aligned} \quad (34)$$

$$\forall t \in [a, b],$$

and this formula is the  $\alpha$ -order right Caputo fractional derivative.

**Lemma 4** (see [61, 62]). *Riemann-Liouville fractional derivative and Caputo fractional derivative have the following relationship:*

$${}^R D_t^\alpha f(t) = {}^C D_t^\alpha f(t) + \sum_{j=0}^{n-1} \frac{f^{(j)}(a)(t-a)^{j-\alpha}}{\Gamma(1+j-\alpha)}. \quad (35)$$

In this section, based on the generalized mKdV equation obtained in Section 2, we use semi-inverse method and variational method [63] to construct the generalized STFMKdV equation under the Riemann-Liouville derivative definition. Let  $a_{0,3} = 1$ , so that (29) transforms to the following form:

$$A_t + \lambda A_x + a_1 A^2 A_x + a_2 A_{xxx} = 0, \quad (36)$$

where  $a_1, a_2$  are arbitrary constants,  $A(x, t)$  denotes the amplitude of the Rossby waves,  $x \in R$  is the space variable in the propagation of the field, and  $t \in T (= [0, T_0])$  is the time variable. The main steps are arranged as follows [62].

First of all, we introduce  $u(x, t)$  as a potential function. Let  $A(x, t) = u_x(x, t)$ , so that (36) can be written as

$$u_{xt} + \lambda u_{xx} + a_1 u_x^2 u_{xx} + a_2 u_{xxx} = 0. \quad (37)$$

The Lagrangian form of (36) can be defined using the semi-inverse method.  $\mu A$  is considered as a fixed function. The functional of the potential equation (37) can be represented by

$$\begin{aligned} J(u) &= \int_R dx \int_T dt \left\{ u(x, t) \right. \\ &\quad \left. \cdot [c_1 u_{xt} + c_2 \lambda u_{xx} + c_3 a_1 u_x^2 u_{xx} + c_4 a_2 u_{xxx}] \right\}, \end{aligned} \quad (38)$$

where  $c_1, c_2, c_3$ , and  $c_4$  are Lagrangian multipliers to be determined later. Integrating (38) by parts and taking  $u_t|_R = u_x|_R = u_{xx}|_R = u_{xxx}|_R = 0$  lead to

$$\begin{aligned} J(u) &= \int_R dx \int_T dt \left\{ -c_1 u_x u_t - c_2 \lambda u_x^2 - \frac{1}{3} c_3 a_1 u_x^4 \right. \\ &\quad \left. + c_4 a_2 u_{xx}^2 \right\}. \end{aligned} \quad (39)$$

Secondly, by applying the variation of this functional with respect to  $u(x, t)$ , and integrating each term by parts, optimizing the variation  $\delta J(u) = 0$ , we have

$$2c_1 u_{xt} + 2c_2 \lambda u_{xx} + 4c_3 a_1 u_x^2 u_{xx} + 2c_4 a_2 u_{xxx} = 0. \quad (40)$$

Equation (40) is equivalent to (37), so we can get

$$\begin{aligned} c_1 &= \frac{1}{2}, \\ c_2 &= \frac{1}{2}, \\ c_3 &= \frac{1}{4}, \\ c_4 &= \frac{1}{2}. \end{aligned} \quad (41)$$

A functional relation (39) is given to produce the direct Lagrange form of the mKdV equation.

$$L(u_t, u_x, u_{xx}, \dots) = -\frac{1}{2}u_x u_t - \frac{1}{2}\lambda u_x^2 - \frac{1}{12}a_1 u_x^4 + \frac{1}{2}a_2 u_{xx}^2. \quad (42)$$

Thirdly, according to the Lagrangian form of the integer order, we can obtain the Lagrangian form of the space-time fractional order similarly.

$$F(D_t^\alpha * D_x^\beta u, D_x^\beta u, D_x^{2\beta} u, \dots) = -\frac{1}{2}D_t^\alpha u * D_x^\beta u - \frac{1}{2}\lambda (D_x^\beta u)^2 - \frac{1}{12}a_1 (D_x^\beta u)^4 + \frac{1}{2}a_2 (D_x^{2\beta} u)^2, \quad (43)$$

where  $0 \leq \alpha, \beta < 1$ . The fractional derivative  $D_t^\alpha u(x, t)$  or  $D_x^\beta u(x, t)$  in terms of the left Riemann-Liouville fractional derivative is defined by

$$D_\zeta^\gamma f(\zeta) = \frac{1}{\Gamma(k-\gamma)} \frac{d^k}{d\zeta^k} \left[ \int ds (\zeta-s)^{k-\gamma-1} f(s) \right], \quad (44)$$

$$k-1 \leq \gamma \leq k, \quad \zeta = \zeta(t, x).$$

Then, the STFMKdV-Burgers equation takes the following form:

$$J_F(u) = \int_R (dx)^\beta \int_T (dt)^\alpha F^* (D_t^\alpha * D_x^\beta u, D_x^\beta u, D_x^{2\beta} u). \quad (45)$$

The variation of (45) with respect to  $u(x, t)$  leads to

$$\delta J_F(u) = \int_R (dx)^\beta \int_T (dt)^\alpha \left[ \frac{\partial F^*}{\partial u} \delta u + \frac{\partial F^*}{\partial D_t^\alpha u} \delta D_t^\alpha u + \frac{\partial F^*}{\partial D_x^\beta u} \delta D_x^\beta u + \frac{\partial F^*}{\partial D_x^{2\beta} u} \delta D_x^{2\beta} u \right]. \quad (46)$$

Adopting the fractional integration rule and the right Riemann-Liouville fractional derivative,  $\delta J_{F^*}(u)$  is written as

$$\delta J_F(u) = \int_R (dx)^\beta \int_T (dt)^\alpha \left[ \frac{\partial F}{\partial u} - D_t^\alpha \left( \frac{\partial F}{\partial D_t^\alpha u} \right) - D_x^\beta \left( \frac{\partial F}{\partial D_x^\beta u} \right) + D_x^{2\beta} \left( \frac{\partial F}{\partial D_x^{2\beta} u} \right) \right] \delta u. \quad (47)$$

Optimizing the variation of the functional, i.e.,  $\delta J_{F^*}(u) = 0$ , the Euler-Lagrange form for the STFMKdV equation leads to

$$\frac{\partial F}{\partial u} - D_t^\alpha \left( \frac{\partial F}{\partial D_t^\alpha u} \right) - D_x^\beta \left( \frac{\partial F}{\partial D_x^\beta u} \right) + D_x^{2\beta} \left( \frac{\partial F}{\partial D_x^{2\beta} u} \right) = 0. \quad (48)$$

Substituting (43) into (48), we have

$$D_t^\alpha D_x^\beta u + \lambda D_x^\beta (D_x^\beta u) + a_1 (D_x^\beta u)^2 D_x^{2\beta} u + a_2 D_x^{2\beta} (D_x^{2\beta} u) = 0. \quad (49)$$

Substituting  $D_x^\beta u(x, t) = A(x, t)$  into (49), we have the STFMKdV equation

$$D_t^\alpha A + \lambda D_x^\beta A + a_1 A^2 D_x^{2\beta} A + a_2 D_x^{3\beta} A = 0. \quad (50)$$

In this paper, in order to make the content more complete, then we will study the conservation laws and the solutions of the STFMKdV equation.

#### 4. Lie Symmetry Analysis and Conservation Laws of the STFMKdV Equation

In this section, we employ Lie symmetry analysis to discuss the conservation laws[64, 65] of STFMKdV equation which does not contain dissipation item. The details are as follows.

**4.1. Lie Symmetry Analysis.** The STFPDE of a function  $f(x, t)$  with two independent variables considered in the Riemann-Liouville sense is defined as the following form:

$$D_t^\alpha u = \frac{\partial^\alpha u}{\partial t^\alpha} = \begin{cases} \frac{1}{\Gamma(n-\alpha)} \frac{\partial^n}{\partial t^n} \int_0^t (t-s)^{n-\alpha-1} f(x, s) ds, & n-1 < \alpha < n \in N, \\ \frac{\partial^n f(x, t)}{\partial t^n}, & \alpha = n \in N. \end{cases} \quad (51)$$

First, we define a Lie group of point transformations under one parameter

$$\begin{aligned} x^* &= x + \varepsilon \xi(x, t, A) + o(\varepsilon^2), \\ t^* &= t + \varepsilon \tau(x, t, A) + o(\varepsilon^2), \\ u^* &= u + \varepsilon \eta(x, t, A) + o(\varepsilon^2), \end{aligned} \quad (52)$$

where  $\xi, \tau, \eta$  are infinitesimal functions and  $\varepsilon$  is a small continuous parameter. The associated Lie algebra is spanned by

$$X = \xi(x, t, A) \frac{\partial^\beta}{\partial x^\beta} + \tau(x, t, A) \frac{\partial^\alpha}{\partial t^\alpha} + \eta(x, t, A) \frac{\partial}{\partial A}. \quad (53)$$

The prolonged generator can be defined

$$\begin{aligned} Pr^{(\alpha, \beta, 2)} X &= \xi(x, t, A) \frac{\partial^\beta}{\partial x^\beta} + \tau(x, t, A) \frac{\partial^\alpha}{\partial t^\alpha} \\ &+ \eta(x, t, A) \frac{\partial}{\partial A} + \eta^{\alpha, t} \frac{\partial}{\partial (D_t^\alpha A)} \\ &+ \eta^{\beta, x} \frac{\partial}{\partial (D_x^\beta A)} + \eta^{\beta, xx} \frac{\partial}{\partial (D_x^{2\beta} A)}. \end{aligned} \quad (54)$$

On the basis of the infinitesimal invariance criterion, one can get

$$Pr^{(n)} X [F] \Big|_{F=0} = 0, \quad (55)$$

where

$$F = D_t^\alpha A + \lambda D_x^\beta A + a_1 A^2 D_x^\beta A + a_2 D_x^{3\beta} A. \quad (56)$$

The operators  $\eta^{\alpha,t}$ ,  $\eta^{\beta,x}$ ,  $\eta^{\beta,xx}$  are fractional extended symmetry operators defined as follows[64]:

$$\begin{aligned} \eta^{\alpha,t} &= D_t^\alpha (\eta) + \xi D_t^\alpha (A_x) - D_t^\alpha (\xi A_x) \\ &\quad + D_t^\alpha (A (D_t \tau)) - D_t^{\alpha+1} (\tau A) + \tau D_t^{\alpha+1} A, \\ \eta^{\beta,x} &= D_x^\beta (\eta) + D_x^\beta (A (D_x \xi)) - D_x^{\beta+1} (\xi A) \\ &\quad + \xi D_x^{\beta+1} (A) + \tau D_x^\beta (A_t) - D_x^\beta (\tau A_t), \\ \eta^{\beta,xx} &= D_x^\beta (\eta^{\beta,x}) - A_{xx} D_x^\beta (\xi) - A_{xt} D_x^\beta (\tau), \end{aligned} \quad (57)$$

where the symbols  $D_t$ ,  $D_x$  represent the total derivative operators defined by

$$\begin{aligned} D_t &= \partial_t + A_t \partial_A + A_{tt} \partial_{A_t} + A_{xt} \partial_{A_x} + \dots, \\ D_x &= \partial_x + A_x \partial_A + A_{xx} \partial_{A_x} + A_{xt} \partial_{A_t} + \dots. \end{aligned} \quad (58)$$

Second, the conserved vectors of the STFMkdv equation are investigated as follows. Applying the second prolongation  $Pr^{(\alpha,\beta,2)} X$ , we get

$$\eta^{\alpha,t} + \lambda \eta^{\beta,x} + 2a_1 A \eta D_x^\beta A + a_1 A^2 \eta^{\beta,x} + a_2 \eta^{\beta,xxx} = 0 \quad (59)$$

Substituting (57) and (58) into (59), and equating the coefficients of alike partial derivatives of  $u$ , we can obtain the determining equations

$$\begin{aligned} \xi_t &= \xi_A = \tau_x = \tau_A = \eta_{AA} = 0, \\ \alpha \tau_t - 3\beta \xi_x &= 0, \\ \binom{\alpha}{n} \partial_t^\alpha \eta_A - \binom{\alpha}{n+1} D_t^{n+1} \tau &= 0, \\ \binom{\beta}{n} \partial_x^\beta \eta_A - \binom{\beta}{n+1} D_x^{n+1} \xi &= 0, \\ \partial_t^\alpha \eta - A \partial_t^\alpha \eta_A + \lambda (\partial_t^\alpha \eta - A) \partial_t^\alpha \eta_A + a_0 A^2 \eta_x + a_1 \eta_{xxx} &= 0. \end{aligned} \quad (60)$$

Solving these equations, the infinitesimals can be derived in the following form:

$$\begin{aligned} \xi &= \frac{c_1}{\beta} x + c_2, \\ \tau &= \frac{3c_1}{\alpha} t + c_3, \\ \eta &= \frac{3c_1 (\beta - 1)}{\beta} A. \end{aligned} \quad (61)$$

where  $c_1, c_2, c_3$  are arbitrary constants. Thus, the corresponding infinitesimal generator can be written

$$X = \frac{x}{\beta} \frac{\partial}{\partial x} + \frac{3t}{\alpha} \frac{\partial}{\partial t} + \frac{3A(\beta-1)}{\beta} \frac{\partial}{\partial A} \quad (62)$$

**4.2. Nonlinear Self-Adjointness.** The concept of nonlinear self adjoint is proposed in the application of new conservation theorem to the conservation laws of equations. This concept is extended to the space-time fractional partial differential equations. The lagrangian form of nondissipative STFMkdv equation is given by

$$\mathcal{L} = v(x, t) [D_t^\alpha A + \lambda D_x^\beta A + a_1 A^2 D_x^\beta A + a_2 D_x^{3\beta} A], \quad (63)$$

where  $v(x, t)$  is a new dependent variable. The adjoint equation of the STFMkdv equation is defined by

$$F^* \equiv \frac{\delta \mathcal{L}}{\delta A} = 0, \quad (64)$$

where  $\delta/\delta A$  is the Euler-Lagrange operator. According to (63) and (64), the adjoint equation of STFMkdv equation can be obtained as follows:

$$\begin{aligned} F^* &= (D_t^\alpha)^* v + (a_1 A^2 - \lambda) (D_x^\beta)^* v - a_2 (D_x^{3\beta})^* v \\ &= 0. \end{aligned} \quad (65)$$

Here,  $(D_t^\alpha)^*$ ,  $(D_x^\beta)^*$  are the adjoint operators of  $D_t^\alpha$ ,  $D_x^\beta$ . For the Riemann-Liouville fractional differential operators, the corresponding adjoint operators[41] have the following form:

$$\begin{aligned} ({}_0 D_t^\alpha)^* &= (-1)_t^n I_T^{n-\alpha} (D_t^n) = {}_t^C D_T^\alpha, \\ ({}_0 D_x^\beta)^* &= (-1)_x^m I_R^{m-\beta} (D_x^m) = {}_x^C D_R^\beta, \end{aligned} \quad (66)$$

where  $I_T^{n-\alpha}$ ,  $I_R^{m-\beta}$  are the right fractional integral operators of order  $n - \alpha$ ,  $m - \beta$ , defined by

$$\begin{aligned} I_T^{n-\alpha} f(x, t) &= \frac{1}{\Gamma(n-\alpha)} \int_t^T \frac{f(x, \tau)}{(\tau-t)^{\alpha+1-n}} d\tau, \\ I_R^{m-\beta} f(x, t) &= \frac{1}{\Gamma(m-\beta)} \int_x^R \frac{f(\zeta, t)}{(\zeta-x)^{\beta+1-m}} d\zeta, \end{aligned} \quad (67)$$

$$n = [\alpha] + 1, \quad m = [\beta] + 1.$$

For nonlinear self-adjointness, let us assume  $v = \psi(x, t, A)$ , where  $\psi(x, t, A) \neq 0$ .

Substituting  $v = \psi(x, t, A)$  into (65)

$$\begin{aligned} (D_t^\alpha)^* \psi + (a_1 A^2 - \lambda) (D_x^\beta)^* \psi - a_2 [(D_x^{3\beta})^* \psi \\ + 3 (D_x^{2\beta})^* \psi_A A_x + 3 (D_x^\beta)^* \psi_{AA} (A_x)^2 \\ + 3 (D_x^\beta)^* \psi_{Ax} A_{xx} + 3 \psi_{AA} A_x A_{xx} + \psi_A A_{xxx} \\ + \psi_{AAA} A_x^3] \equiv F^*. \end{aligned} \quad (68)$$

By using the method of undetermined coefficients, we obtain the following cases[64, 65]:

$$\begin{aligned} \text{case 1: } & 0 < \beta < 1, \\ & v(x, t) = C_0 \\ & \text{for } D_t^\alpha = {}_0D_t^\alpha, \end{aligned} \tag{69}$$

$$\begin{aligned} \text{case 2: } & 0 < \beta < 1, \\ & v(x, t) = C_1x + C_2 \\ & \text{for } D_t^\alpha = {}^c_0D_t^\alpha. \end{aligned}$$

Here,  $C_0, C_1, C_2$  are arbitrary constants. These solutions of  $v(x, t)$  are introduced in the Lagrangian form for the construction of conserved vectors in the next subsection.

4.3. Conservation Laws. It is well known that  $C = (C^t, C^x)$  is called the conserved vector that satisfies the conservation equation

$$D_t(C^t) + D_x(C^x) = 0, \tag{70}$$

Noether's theorem is widely adopted to construct the conserved vectors. Using this method, the conserved vectors are obtained by using the Noether operators for the Lagrangian form. According to[40], the fractional Noether operator for the variable  $x, t$  has been given.

Before constructing the conserved vectors, we should consider the Lie characteristic function for the Lie symmetry infinitesimal generator  $X = \xi(\partial^\beta/\partial x^\beta) + \tau(\partial^\alpha/\partial t^\alpha) + \eta(\partial/\partial A)$ . The Lie characteristic function is defined by

$$W = \eta - \xi A_x - \tau A_t = \frac{3A(\beta - 1)}{\beta} - \frac{x}{\beta} A_x - \frac{3t}{\alpha} A_t, \tag{71}$$

Then, the fractional Noether operator for  $t$  of the STFMKdV-Burgers equation is

$$C^t = \sum_{k=0}^{n-1} (-1)^k D_t^{\alpha-1-k} (W) D_t^k \left( \frac{\partial F^*}{\partial (D_t^\alpha A)} \right), \tag{72}$$

Similarly, the fractional Noether operator for  $x$  of the STFMKdV-Burgers equation is

$$C^x = \sum_{k=0}^{m-1} (-1)^k D_x^{\beta-1-k} (W) D_x^k \left( \frac{\partial F^*}{\partial (D_x^\beta A)} \right), \tag{73}$$

Substituting the Lagrangian form (65) and (71) into (72) with case 1 in (69), let  $C_0 = 1$ ; the  $t$ -component of the conserved vectors can be obtained:

$$\begin{aligned} C^t &= \frac{3(\beta - 1)}{\beta} I_t^{1-\alpha} (A) - \frac{x}{\beta} I_t^{1-\alpha} (A_x) - \frac{3}{\alpha} I_t^{1-\alpha} (tA_t), \\ & \text{as } 0 < \alpha < 1, \end{aligned} \tag{74}$$

$$\begin{aligned} C^t &= \frac{3(\beta - 1)}{\beta} D_t^{\alpha-1} (A) - \frac{x}{\beta} D_t^{\alpha-1} (A_x) \\ & - \frac{3}{\alpha} D_t^{\alpha-1} (tA_t), \text{ as } 1 < \alpha < 2, \end{aligned} \tag{75}$$

The  $x$ -component of the conserved vectors is

$$\begin{aligned} C^x &= \left[ \frac{3(\beta - 1)}{\beta} D_x^{\beta-1} (A) - \frac{1}{\beta} D_x^{\beta-1} (xA_x) \right. \\ & \left. - \frac{3t}{\alpha} D_x^{\beta-1} (A_t) \right], \text{ as } 1 < \alpha < 2, \end{aligned} \tag{76}$$

In case 2 in (69), let  $C_1 = 1, C_2 = 0$ ; the  $t$ -component of the conserved vectors can be obtained as follows:

$$\begin{aligned} C^t &= x \times \left[ \frac{3(\beta - 1)}{\beta} I_t^{1-\alpha} (A) - \frac{x}{\beta} I_t^{1-\alpha} (A_x) \right. \\ & \left. - \frac{3}{\alpha} I_t^{1-\alpha} (tA_t) \right], \text{ as } 0 < \alpha < 1, \end{aligned} \tag{77}$$

$$\begin{aligned} C^t &= x \times \left[ \frac{3(\beta - 1)}{\beta} D_t^{\alpha-1} (A) - \frac{x}{\beta} D_t^{\alpha-1} (A_x) \right. \\ & \left. - \frac{3}{\alpha} D_t^{\alpha-1} (tA_t) \right], \text{ as } 1 < \alpha < 2, \end{aligned} \tag{78}$$

The  $x$ -component of the conserved vectors is

$$\begin{aligned} C^x &= x \times \left[ \frac{3(\beta - 1)}{\beta} D_x^{\beta-1} (A) - \frac{1}{\beta} D_x^{\beta-1} (xA_x) \right. \\ & \left. - \frac{3t}{\alpha} D_x^{\beta-1} (A_t) \right] - \left[ \frac{3(\beta - 1)}{\beta} I_x^{2-\beta} (A) \right. \\ & \left. - \frac{1}{\beta} I_x^{2-\beta} (xA_x) - \frac{3t}{\alpha} I_x^{2-\beta} (A_t) \right]. \end{aligned} \tag{79}$$

### 5. The Exact Solutions of the STFMKdV Equation

In this part, we deal with the exact solutions [66–68] of (50). Using  $\exp(-\Phi(\xi))$  method, the main steps of this method to solve the space time fractional partial equation can be given as follows.

Firstly, we introduce the fractional complex transform:

$$\begin{aligned} A(x, t) &= U(\xi), \\ \xi &= \frac{x^\beta}{\Gamma(1 + \beta)} - \frac{\nu t^\alpha}{\Gamma(1 + \alpha)}, \end{aligned} \tag{80}$$

where  $\nu$  is the wave speed. Substitute (80) into the STFMKdV equation as follows:

$$D_t^\alpha A + \lambda D_x^\beta A + a_1 A^2 D_x^\beta A + a_2 D_x^{3\beta} A = 0 \tag{81}$$

Equation (81) transforms to an ordinary differential equation

$$-\nu U' + \lambda U' + a_1 U^2 U' + a_2 U''' = 0. \tag{82}$$

Integrating (82) with respect to  $\xi$  and setting the integration constant to zero, we have the following equation:

$$(-\nu + \lambda)U + \frac{a_1}{3}U^3 + a_2U'' = 0. \tag{83}$$

Secondly, balancing the highest order derivative term and the highest order nonlinear term in (83), we get the balancing number  $n = 1$ . Thus the solution of (83) takes the form

$$U(\xi) = k_0 + k_1 e^{-\Phi(\xi)}, \tag{84}$$

where  $k_0, k_1$  are constants to be determined later. And  $\Phi(\xi)$  satisfies the following auxiliary ordinary differential equation:

$$\Phi'(\xi) = \exp(-\Phi(\xi)) + \eta \exp(\Phi(\xi)) + \sigma. \tag{85}$$

Substitute (84) and (81) into (83) and collect all terms with the same degree of  $\exp(-\Phi(\xi))^n$  together. Equating each coefficient of the same degree of  $\exp(-\Phi(\xi))^n$  to zero, a set of algebraic equations for  $k_0, k_1, \eta, \sigma, \nu$  can be obtained.

$$e^{0\Phi(\xi)}: (\lambda - \nu) a_0 + \eta \sigma a_1^2 + \frac{a_0^4}{3} = 0,$$

$$e^{-\Phi(\xi)}: (\lambda - \nu) a_1 + a_0^3 a_1 + (\sigma^2 + 2\eta) a_1^2 = 0,$$

$$e^{-2\Phi(\xi)}: a_0 62 a_1^2 + 3 a_1^2 \sigma = 0,$$

$$e^{-3\Phi(\xi)}: \frac{a_0 a_1^3}{3} + 2 a_1^2 = 0. \tag{86}$$

Solving the algebraic equation system, we can get the solutions. Let  $\rho = \pm \sqrt{\sigma}$ ; the solutions of (86) are expressed by

$$a_0 = \sqrt{3} \rho,$$

$$a_1 = \frac{2\sqrt{3}}{\rho}, \tag{87}$$

$$\nu = \lambda + \frac{\sqrt{3}(4\eta + \rho^4)}{\rho},$$

Different solutions of the auxiliary equation (85) have been given in [68], so we get the solutions of (81). Different cases are discussed as follows.

*Case 1* (hyperbolic function solutions). When  $\sigma^2 - 4\eta > 0, \eta \neq 0,$

$$A_1(x, t) = \sqrt{3}\rho + \frac{2\eta}{\sqrt{\sigma^2 - 4\eta} \tanh \left\{ \left( \sqrt{\sigma^2 - 4\eta} / 2 \right) \left[ x^\beta / \Gamma(1 + \beta) - \left[ \lambda + \sqrt{3}(4\eta + \rho^4) / \rho \right] t^\alpha / \Gamma(1 + \alpha) + c \right] \right\} + \sigma} \tag{88}$$

*Case 2* (trigonometric function solutions). When  $\sigma^2 - 4\eta < 0, \eta \neq 0,$

$$A_2(x, t) = \sqrt{3}\rho + \frac{2\eta}{\sqrt{4\eta - \sigma^2} \tan \left\{ \left( \sqrt{4\eta - \sigma^2} / 2 \right) \left[ x^\beta / \Gamma(1 + \beta) - \left[ \lambda + \sqrt{3}(4\eta + \rho^4) / \rho \right] t^\alpha / \Gamma(1 + \alpha) + c \right] \right\} - \sigma}, \tag{89}$$

*Case 3* (hyperbolic function solutions). When  $\sigma^2 - 4\eta > 0, \eta = 0, \sigma \neq 0,$

$$A_3(x, t) = \sqrt{3}\rho + \frac{\sigma}{\cosh \left\{ \sigma \left[ x^\beta / \Gamma(1 + \beta) - \left[ \lambda + \sqrt{3}(4\eta + \rho^4) / \rho \right] t^\alpha / \Gamma(1 + \alpha) + c \right] \right\} + \sinh \left\{ \sigma \left[ x^\beta / \Gamma(1 + \beta) - \left[ \lambda + \sqrt{3}(4\eta + \rho^4) / \rho \right] t^\alpha / \Gamma(1 + \alpha) + c \right] \right\} - 1}, \tag{90}$$

*Case 4* (rational function solutions). When  $\sigma^2 - 4\eta = 0, \eta \neq 0, \sigma \neq 0,$

$$A_4(x, t) = \sqrt{3}\rho - \frac{\sigma^2 \left\{ x^\beta / \Gamma(1 + \beta) - \left[ \lambda + \sqrt{3}(4\eta + \rho^4) / \rho \right] t^\alpha / \Gamma(1 + \alpha) + c \right\}}{2\sigma \left\{ x^\beta / \Gamma(1 + \beta) - \left[ \lambda + \sqrt{3}(4\eta + \rho^4) / \rho \right] t^\alpha / \Gamma(1 + \alpha) + c \right\} + 4}, \tag{91}$$

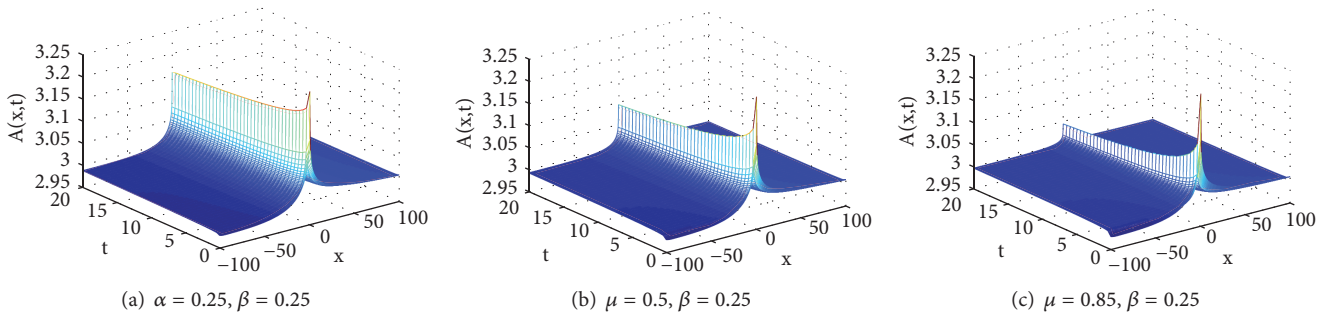


FIGURE 1: The effect of the variation of the dissipation coefficient on the amplitude if the space and time derivative are determined.

Case 5. When  $\sigma^2 - 4\eta = 0$ ,  $\eta = 0$ ,  $\sigma = 0$ ,

$$A_5(x, t) = \frac{1}{x^\beta / \Gamma(1 + \beta) - [\lambda + \sqrt{3}(4\eta + \rho^4) / \rho] t^\alpha / \Gamma(1 + \alpha) + c} \tag{92}$$

We take the solution of Case 1 as an example to discuss the influence of fractional derivatives  $\alpha$  and  $\beta$  on the wave, respectively.

Figure 1 shows that when the space and time derivative are determined, the amplitude of the wave decreases as time increases.

In Figures 2 and 3, we investigate how the parameters  $\alpha$ ,  $\beta$  affect the nonlinear solitary waves; the corresponding physical interpretations can be given as follows:

(1) From Figure 2, we can see that the amplitude of solitary wave increases with increase of  $\beta$  value, while the width of the wave decreases.

(2) Figure 3 shows that when the values of  $\alpha$  increase, the amplitude of solitary waves has an increasing trend; however, the amplitude of the wave declines more and more quickly.

### 6. Conclusions

In this paper, using multiscale analysis and turbulence method, from the basic dynamic multivariable equations under the baroclinic atmosphere, the integer order mKdV equation is derived. In Section 3, we use the semi-inverse method and variational method to derive the STFmKdV equation under the Riemann-Liouville definition. In Section 4, we extend the symmetry analysis of the fractional equation to obtain the corresponding infinitesimal generator of the equation. Then we discuss the nonlinear self-adjointness of the STFmKdV equation and finally get the conservation vectors of the equation. In Section 5, based on the STFmKdV equation, employing the  $\exp(-\Phi(\xi))$  method, and considering the different cases of the parameters  $(\eta, \sigma)$ , we obtain five different solutions of the equation.

Note 5. In this paper, we only study the space-time fractional order equation under the Riemann-Liouville derivative definition. In future studies, we can also consider the fractional equation under the Caputo derivative definition.

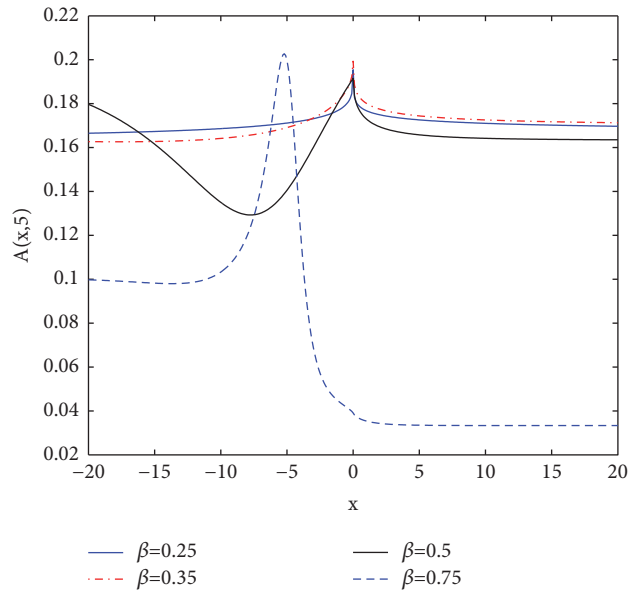


FIGURE 2: The amplitude of solitary wave  $A(x, 10)$  at  $t = 10$ ,  $\beta = 0.5$ , for different value of  $\alpha$ .

Note 6. In future studies, we can also consider the conservation laws of fractional equations under the Caputo derivative definition.

### Data Availability

No data were used to support this study.

### Conflicts of Interest

The authors declare that there are no conflicts of interest regarding the publication of this paper.

### Acknowledgments

This project was supported by National Natural Science Foundation of China (No. 41576023), Nature Science Foundation of Shandong Province of China (No. ZR2018MA017), and China Postdoctoral Science Foundation funded project

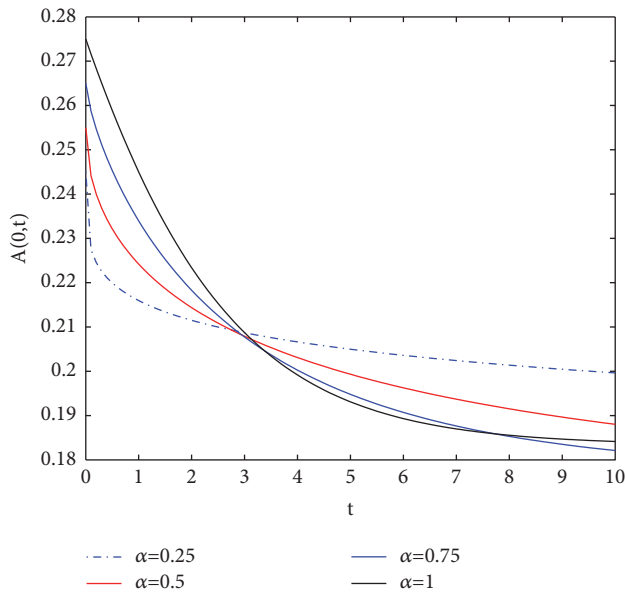


FIGURE 3: The amplitude of solitary wave  $A(0, t)$  at  $x = 0$ ,  $\alpha = 0.5$ , for different value of  $\beta$ .

(No. 2017M610436). The authors sincerely thank Xin Chen, Min Guo, Qiulan Zhao, and Jianxin Liu for their contribution to the research.

## References

- [1] R. R. Long, "Solitary waves in one and two-fluids system," *Journal of the Atmospheric Sciences*, vol. 21, no. 2, pp. 197–200, 1964.
- [2] M. Wadati, "The modified Korteweg-de Vries equation," *Journal of the Physical Society of Japan*, vol. 34, pp. 1289–1296, 1973.
- [3] L. G. Redekopp, "On the theory of solitary Rossby waves," *Journal of Fluid Mechanics*, vol. 82, no. 4, pp. 725–745, 1977.
- [4] J. M. Mihaljan, "A rigorous exposition of the Boussinesq approximations applicable to a thin layer of fluid," *The Astrophysical Journal*, vol. 136, pp. 1126–1133, 1962.
- [5] L. Meng and K. L. Lv, "Nonlinear long-wave disturbances excited by localized forcing," *Chinese Journal of Computation Physics*, vol. 17, p. 259, 2000.
- [6] D. H. Luo, "The nonlinear schrodinger equation rotating barotropic atmosphere and atmospheric blocking," *Acta Meteorologica Sinica*, vol. 48, p. 265, 1990.
- [7] H. Yang, Q. Zhao, Ba. Yin, and H. Dong, "A new integro-differential equation for rossby solitary waves with topography effect in deep rotational fluids," *Abstract and Applied Analysis*, vol. 2013, Article ID 597807, 8 pages, 2013.
- [8] H. W. Yang, Z. H. Xu, D. Z. Yang, X. R. Feng, B. S. Yin, and H. H. Dong, "ZK-Burgers equation for three-dimensional Rossby solitary waves and its solutions as well as chirp effect," *Advances in Difference Equations*, vol. 2016, p. 167, 2016.
- [9] M. C. Li and J. S. Xue, "The nonlinear evolution process of squall lines in a baroclinic atmosphere and the KdV equation," *Chinese Journal of Atmospheric Sciences*, vol. 8, no. 2, pp. 143–152, 1984.
- [10] M. Guo, Y. Zhang, M. Wang, Y. Chen, and H. Yang, "A new ZK-ILW equation for algebraic gravity solitary waves in finite depth stratified atmosphere and the research of squall lines formation mechanism," *Computers & Mathematics with Applications. An International Journal*, vol. 75, no. 10, pp. 3589–3603, 2018.
- [11] H. W. Yang, X. Chen, M. Guo, and Y. D. Chen, "A new ZK-BO equation for three-dimensional algebraic Rossby solitary waves and its solution as well as fission property," *Nonlinear Dynamics*, vol. 91, pp. 2019–2032, 2017.
- [12] S. Manukure, Y. Zhou, and W.-X. Ma, "Lump solutions to a (2+1)-dimensional extended KP equation," *Computers & Mathematics with Applications*, vol. 75, no. 7, pp. 2414–2419, 2018.
- [13] W.-X. Ma, X. Yong, and H.-Q. Zhang, "Diversity of interaction solutions to the (2+1)-dimensional Ito equation," *Computers & Mathematics with Applications*, vol. 75, no. 1, pp. 289–295, 2018.
- [14] X.-Y. Li, Y.-X. Li, and H.-X. Yang, "Two families of Liouville integrable lattice equations," *Applied Mathematics and Computation*, vol. 217, no. 21, pp. 8671–8682, 2011.
- [15] R. Zhang, L. Yang, J. Song, and H. Yang, "(2+1) dimensional Rossby waves with complete Coriolis force and its solution by homotopy perturbation method," *Computers & Mathematics with Applications*, vol. 73, no. 9, pp. 1996–2003, 2017.
- [16] H. H. Dong, B. Y. Guo, and B. S. Yin, "Generalized fractional supertrace identity for Hamiltonian structure of NLS-MKdV hierarchy with self-consistent sources," *Analysis and Mathematical Physics*, vol. 6, no. 2, pp. 199–209, 2016.
- [17] Y. Wang and L. Liu, "Positive properties of the Green function for two-term fractional differential equations and its application," *Journal of Nonlinear Sciences and Applications*, vol. 10, no. 4, pp. 2094–2102, 2017.
- [18] C. Lu, C. Fu, and H. Yang, "Time-fractional generalized Boussinesq equation for Rossby solitary waves with dissipation effect in stratified fluid and conservation laws as well as exact solutions," *Applied Mathematics and Computation*, vol. 327, pp. 104–116, 2018.
- [19] Y. J. Cui, W. J. Ma, X. Z. Wang, and X. W. Su, "Uniqueness theorem of differential system with coupled integral boundary conditions," *Electronic Journal of Qualitative Theory of Differential Equations*, vol. 9, pp. 1–10, 2018.
- [20] M. Mirzazadeh, M. Ekici, A. Sonmezoglu, S. Ortakaya, M. Eslami, and A. Biswas, "Soliton solutions to a few fractional nonlinear evolution equations in shallow water wave dynamics," *The European Physical Journal Plus*, vol. 5, pp. 131–166, 2016.
- [21] Q. Zhou, A. Sonmezoglu, M. Ekici, and M. Mirzazadeh, "Optical solitons of some fractional differential equations in nonlinear optics," *Journal of Modern Optics*, vol. 64, no. 21, pp. 2345–2349, 2017.
- [22] T. Qi, Y. Liu, and Y. Zou, "Existence result for a class of coupled fractional differential systems with integral boundary value conditions," *Journal of Nonlinear Sciences and Applications*, vol. 10, no. 7, pp. 4034–4045, 2017.
- [23] Y. Guo, "Solvability for a nonlinear fractional differential equation," *Bulletin of the Australian Mathematical Society*, vol. 80, no. 1, pp. 125–138, 2009.
- [24] Y. Wang, L. Liu, and Y. Wu, "Positive solutions for a nonlocal fractional differential equation," *Nonlinear Analysis: Theory, Methods & Applications*, vol. 74, no. 11, pp. 3599–3605, 2011.
- [25] B. Ross, *The Fractional Calculus and Its Application*, Lecture Notes in Mathematics, Springer, Berlin, Germany, 1975.
- [26] K. B. Oldham and J. Spanier, *The Fractional Calculus*, Academic Press, New York, NY, USA, 1974.

- [27] F. Riewe, "Nonconservative Lagrangian and Hamiltonian mechanics," *Physical Review E: Statistical, Nonlinear, and Soft Matter Physics*, vol. 53, no. 2, pp. 1890–1899, 1996.
- [28] F. Riewe, "Mechanics with fractional derivatives," *Physical Review E: Statistical, Nonlinear, and Soft Matter Physics*, vol. 55, no. 3, pp. 3581–3592, 1997.
- [29] O. P. Agrawal, "Formulation of Euler-Lagrange equations for fractional variational problems," *Journal of Mathematical Analysis and Applications*, vol. 272, no. 1, pp. 368–379, 2002.
- [30] O. P. Agrawal, "A general finite element formulation for fractional variational problems," *Journal of Mathematical Analysis and Applications*, vol. 337, no. 1, pp. 1–12, 2008.
- [31] A. Biswas, A. Sonmezoglu, M. Ekici et al., "Optical soliton perturbation with fractional temporal evolution by generalized Kudryashov's method," *Optik - International Journal for Light and Electron Optics*, vol. 164, pp. 303–310, 2018.
- [32] M. Ekici, M. Mirzazadeh, Q. Zhou, S. P. Moshokoa, A. Biswas, and M. Belic, "Solitons in optical metamaterials with fractional temporal evolution," *Optik - International Journal for Light and Electron Optics*, vol. 127, no. 22, pp. 10879–10897, 2016.
- [33] M. Ekici, M. Mirzazadeh, M. Eslami et al., "Optical soliton perturbation with fractional-temporal evolution by first integral method with conformable fractional derivatives," *Optik - International Journal for Light and Electron Optics*, vol. 127, no. 22, pp. 10659–10669, 2016.
- [34] Q. Huang and R. Zhdanov, "Symmetries and exact solutions of the time fractional Harry-Dym equation with Riemann-Liouville derivative," *Physica A: Statistical Mechanics and its Applications*, vol. 409, pp. 110–118, 2014.
- [35] S. Sahoo, G. Garai, and S. Saha Ray, "Lie symmetry analysis for similarity reduction and exact solutions of modified KdV-Zakharov-KUZnetsov equation," *Nonlinear Dynamics*, vol. 87, no. 3, pp. 1995–2000, 2017.
- [36] C. Fu, C. N. Lu, and H. W. Yang, "Time-space fractional (2+1) dimensional nonlinear Schrodinger equation for envelope gravity waves in baroclinic atmosphere and conservation laws as well as exact solutions," *Advances in Difference Equations*, vol. 2018, p. 56, 2018.
- [37] W.-X. Ma, "Conservation laws by symmetries and adjoint symmetries," *Discrete and Continuous Dynamical Systems - Series S*, vol. 11, no. 4, pp. 707–721, 2018.
- [38] R. Sahadevan and P. Prakash, "On Lie symmetry analysis and invariant subspace methods of coupled time fractional partial differential equations," *Chaos, Solitons & Fractals*, vol. 104, pp. 107–120, 2017.
- [39] A. R. Adem, "Symbolic computation on exact solutions of a coupled Kadomtsev-Petviashvili equation: Lie symmetry analysis and extended tanh method," *Computers & Mathematics with Applications. An International Journal*, vol. 74, no. 8, pp. 1897–1902, 2017.
- [40] G. Wang, A. H. Kara, and K. Fakhar, "Symmetry analysis and conservation laws for the class of time-fractional nonlinear dispersive equation," *Nonlinear Dynamics*, vol. 82, no. 1-2, pp. 281–287, 2015.
- [41] S. Y. Lukashchuk, "Conservation laws for time-fractional sub-diffusion and diffusion-wave equations," *Nonlinear Dynamics*, vol. 80, no. 1-2, pp. 791–802, 2015.
- [42] R. K. Gazizov, N. H. Ibragimov, and S. Y. Lukashchuk, "Non-linear self-adjointness, conservation laws and exact solutions of time-fractional Kompaneets equations," *Communications in Nonlinear Science and Numerical Simulation*, vol. 23, no. 1-3, pp. 153–163, 2015.
- [43] J. Hu, Y. Ye, S. Shen, and J. Zhang, "Lie symmetry analysis of the time fractional KdV-type equation," *Applied Mathematics and Computation*, vol. 233, pp. 439–444, 2014.
- [44] M. Guo, C. Fu, Y. Zhang, J. Liu, and H. Yang, "Study of ion-acoustic solitary waves in a magnetized plasma using the three-dimensional time-space fractional Schamel-KdV equation," *Complexity*, vol. 2018, Article ID 6852548, 17 pages, 2018.
- [45] H. Jafari, N. Kadkhoda, and D. Baleanu, "Fractional Lie group method of the time-fractional Boussinesq equation," *Nonlinear Dynamics*, vol. 81, no. 3, pp. 1569–1574, 2015.
- [46] M. S. Hashemi and D. Baleanu, "Lie symmetry analysis and exact solutions of the time fractional gas dynamics equation," *Journal of Optoelectronics and Advanced Materials*, vol. 18, pp. 383–388, 2016.
- [47] A. Biswas, M. Ekici, A. Sonmezoglu, and R. T. Alqahtani, "Sub-pico-second chirped optical solitons in mono-mode fibers with Kaup-Newell equation by extended trial function method," *Optik - International Journal for Light and Electron Optics*, vol. 168, pp. 208–216, 2018.
- [48] A. Biswas, M. Ekici, A. Sonmezoglu, and R. T. Alqahtani, "Optical solitons with differential group delay for coupled Fokas-Lenells equation by extended trial function scheme," *Optik - International Journal for Light and Electron Optics*, vol. 165, pp. 102–110, 2018.
- [49] H.-Q. Zhao and W.-X. Ma, "Mixed lump-kink solutions to the KP equation," *Computers & Mathematics with Applications. An International Journal*, vol. 74, no. 6, pp. 1399–1405, 2017.
- [50] X. Li and Q. Zhao, "A new integrable symplectic map by the binary nonlinearization to the super AKNS system," *Journal of Geometry and Physics*, vol. 121, pp. 123–137, 2017.
- [51] X.-X. Xu, "A deformed reduced semi-discrete Kaup-Newell equation, the related integrable family and Darboux transformation," *Applied Mathematics and Computation*, vol. 251, pp. 275–283, 2015.
- [52] Z. Tian, M. Tian, Z. Liu, and T. Xu, "The Jacobi and Gauss-Seidel-type iteration methods for the matrix equation  $AXB=C$ ," *Applied Mathematics and Computation*, vol. 292, pp. 63–75, 2017.
- [53] A. Bekir, Ö. Güner, A. H. Bhrawy, and A. Biswas, "Solving nonlinear fractional differential equations using exp-function and  $G'/G$ -expansion methods," *Romanian Journal of Physics*, vol. 60, no. 3-4, pp. 360–378, 2015.
- [54] M. Foroutan, J. Manafian, and A. Ranjbaran, "Solitons in optical metamaterials with anti-cubic law of nonlinearity by generalized  $G'/G$ -expansion method," *Optik - International Journal for Light and Electron Optics*, vol. 162, pp. 86–94, 2018.
- [55] A. Biswas, A. Sonmezoglu, M. Ekici et al., "Optical soliton perturbation with fractional temporal evolution by extended  $G'/G$ -expansion method," *Optik - International Journal for Light and Electron Optics*, vol. 161, pp. 301–320, 2018.
- [56] A. Bekir, Ö. Güner, and A. C. Cevikel, "Fractional complex transform and exp-function methods for fractional differential equations," *Abstract and Applied Analysis*, vol. 2013, Article ID 426462, 8 pages, 2013.
- [57] A. Bekir, E. Aksoy, and Ö. Güner, "A generalized fractional sub-equation method for nonlinear fractional differential equations," in *Proceedings of the 2nd International Conference on Analysis and Applied Mathematics, ICAAM '14*, vol. 1611, pp. 78–83, 2014.
- [58] W.-X. Ma and Y. Zhou, "Lump solutions to nonlinear partial differential equations via Hirota bilinear forms," *Journal of Differential Equations*, vol. 264, no. 4, pp. 2633–2659, 2018.

- [59] M. McAnally and W.-X. Ma, "An integrable generalization of the D-Kaup–Newell soliton hierarchy and its bi-Hamiltonian reduced hierarchy," *Applied Mathematics and Computation*, vol. 323, pp. 220–227, 2018.
- [60] M. Tao and H. Dong, "Algebro-geometric solutions for a discrete integrable equation," *Discrete Dynamics in Nature and Society*, pp. 1–9, 2017.
- [61] M. C. Li, "Non-linear process of the formation of the squall and KdV equation," *Scientia Sinica*, vol. 3, pp. 341–350, 1981.
- [62] S. A. El-Wakil, E. M. Abulwafa, and M. A. Zahran, "Time-fractional KdV equation: formulation and solution using variational methods," *Nonlinear Dynamics*, vol. 65, no. 1-2, pp. 55–63, 2011.
- [63] J. H. He, "A tutorial and heuristic review on Lagrange multiplier for optimal problems," *Nonlinear Science Letters A*, vol. 2, pp. 121–148, 2017.
- [64] W. Rui and X. Zhang, "Lie symmetries and conservation laws for the time fractional Derrida-Lebowitz-Speer-SPOhn equation," *Communications in Nonlinear Science and Numerical Simulation*, vol. 34, pp. 38–44, 2016.
- [65] X. L. Yong, W. X. Ma, Y. H. Huang, and Y. Liu, "Lump solutions to the Kadomtsev–Petviashvili I equation with a self-consistent source," *Computers & Mathematics with Applications*, vol. 75, no. 9, pp. 3414–3419, 2018.
- [66] J.-B. Zhang and W.-X. Ma, "Mixed lump-kink solutions to the BKP equation," *Computers & Mathematics with Applications. An International Journal*, vol. 74, no. 3, pp. 591–596, 2017.
- [67] M. Mirzazadeh, M. Ekici, and A. Sonmezoglu, "On the solutions of the space and time fractional Benjamin-BONa-Mahony equation," *Iranian Journal of Science & Technology*, vol. 41, no. 3, pp. 819–836, 2017.
- [68] M. Kaplan and A. Bekir, "A novel analytical method for time-fractional differential equations," *Optik - International Journal for Light and Electron Optics*, vol. 127, no. 20, pp. 8209–8214, 2016.

## Research Article

# Estimation and Fault Diagnosis of Lithium-Ion Batteries: A Fractional-Order System Approach

Shulan Kong <sup>1</sup>, Mehrdad Saif,<sup>2</sup> and Guozeng Cui<sup>3</sup>

<sup>1</sup>*School of Mathematics Science, Qufu Normal University, Qufu 273165, China*

<sup>2</sup>*Department of Electrical and Computer Engineering, University of Windsor, Windsor, ON N9B 3P4, Canada*

<sup>3</sup>*School of Electronic and Information Engineering, Suzhou University of Science and Technology, Suzhou 215009, China*

Correspondence should be addressed to Shulan Kong; [shulank@163.com](mailto:shulank@163.com)

Received 20 July 2018; Revised 1 October 2018; Accepted 10 October 2018; Published 24 October 2018

Guest Editor: Hiroaki Mukaidani

Copyright © 2018 Shulan Kong et al. This is an open access article distributed under the Creative Commons Attribution License, which permits unrestricted use, distribution, and reproduction in any medium, provided the original work is properly cited.

This study investigates estimation and fault diagnosis of fractional-order Lithium-ion battery system. Two simple and common types of observers are designed to address the design of fault diagnosis and estimation for the fractional-order systems. Fractional-order Luenberger observers are employed to generate residuals which are then used to investigate the feasibility of model based fault detection and isolation. Once a fault is detected and isolated, a fractional-order sliding mode observer is constructed to provide an estimate of the isolated fault. The paper presents some theoretical results for designing stable observers and fault estimators. In particular, the notion of stability in the sense of Mittag-Leffler is first introduced to discuss the state estimation error dynamics. Overall, the design of the Luenberger observer as well as the sliding mode observer can accomplish fault detection, fault isolation, and estimation. The effectiveness of the proposed strategy on a three-cell battery string system is demonstrated.

## 1. Introduction

Lithium-ion (Li-ion) batteries are an integral part of electrified vehicles and have found many other areas of applications in consumer products, space, marine, and other applications. They however remain a costly and safety critical subsystem in many areas that they are used in. As a result, reliability, safety, and efficient operation of Li-ion batteries in high power applications, such as in electrified vehicles, and challenging problems such as modeling, state estimation, monitoring, diagnostics, and pyrognostics capabilities are critical areas for research [1–8].

With the development of natural science and complex engineering applications, it has been found that many real-world physical systems show fractional-order dynamical behavior. And fractional calculus theories have been increasingly applied to many practical systems of a variety of scientific and engineering fields. The first application of the fractional calculus was accomplished by Abel in 1823 while investigating the solution of the famous problem of tautochrone [9]. For almost two hundred years, fractional-order models have been used to describe biology systems [10]

in bioengineering, financial markets [11–13] in economics, and diffusion wave [14–17] and lead-acid battery or Li-ion battery [18–21] in physical engineering. Due to inherent properties of fractional-order calculus, fractional-order differential systems sometimes have a more appropriate mathematical description than integer-order differential systems for managing lithium-ion batteries. In integer-order models of Li-ion batteries, constant phase elements are either approximated by ideal capacitors, or a number of resistor-capacitor networks, or relaxation times [21]. The resulting models are commonly not capable of predicting battery dynamics in both the time and frequency domains over the entire operating range. They can not capture the key and accuracy battery characteristics. To address the above problems, a fractional-order model of replacing the ideal capacitor in the first-order resistor-capacitor networks model to a fractional element is explored for Li-ion cells. By using experimental data from time and frequency domains, Alavi et al. [22] found that this model can reproduce a Li-ion battery's behavior better than its integer counterpart, thanks to an additional degree of freedom, namely, the fractionation order. A fractional-order state space model of lithium-ion battery was proposed and

the experiment results showed that it has a better fitness than the classical equivalent circuit models based on the integer differential equations in [20]. In addition, a comprehensive review of fractional-order techniques for Li-ion batteries was referred to [21]. Consequently, the fractional-order modeling methodology may not only improve prediction accuracy but also preserve some physical meanings underlying model parameters.

Catastrophic failures and/or explosion of Li-ion batteries in various applications ranging from cell phones to aircrafts and automobiles are all familiar new stories of the past few years. It is therefore imperative that, at the onset of failures, such events are detected and preventive measures to be taken [23–25]. Model based fault detection and isolation strategies could prove invaluable in this direction. For such techniques to be effective, availability of accurate representative model of the system is necessary. Accordingly, significant progress towards fault diagnosis and estimation of Li-ion batteries modeled as integer-order differential systems have recently been made in [1–7, 26–28] and the references therein. In particular a synthesized design of reduced-order Luenberger observers and Learning observers was presented for the purpose of simultaneous fault isolation and estimation of a three-cell battery string in [1]. As discussed in the previous paragraph, Li-ion battery systems do exhibit the fractional phenomena. The fractional characteristic could give a better description of the mathematical model of the battery system and can potentially lead to more effective fault detection and estimation strategies. Inspired by the abovementioned works and observation, a fractional-order system approach will be considered for estimation and fault diagnosis of fractional-order Li-ion battery system instead of the integer-order system [1].

Observer-based fault diagnosis of fractional-order systems remains problematic due to the lack of well-established and reliable techniques even though the design of observers for fractional-order systems has been reported [29–33]. However, little progress on fault detection and estimation for fractional-order models has been made besides [34, 35]. Reference [35] aims to provide sufficient conditions of the asymptotical convergence for the fractional-order state estimation errors and fault estimation errors via a frequency-distributed fractional integrator equivalent model [36] and employs an indirect Lyapunov method [30, 37, 38]. Recently observer-based tracking control of fractional-order systems is addressed by using Mittag-Leffler function based Lyapunov methods to prove the boundedness of state estimation error in [33]. As such, it is of practical and theoretical importance to focus studies on observer-based fault diagnosis of Li-ion batteries expressed by the fractional-order differential systems.

The main goal of this paper is to propose a strategy for fault detection, isolation, and estimation via fractional-order differential models. The goal is not only in detecting, and if possible isolating and estimating the fault in Li-ion battery system, but also in theoretical development for designing stable observers and estimating faults. Firstly, sources of faults and uncertainties are separated by reorganizing the original system. Towards this, the system is divided into two subsystems. This will allow us to give detectability conditions under which a stable fractional-order observer exists for the second

subsystem. A fault-detection residual is then generated by constructing a fractional-order Luenberger observer. The residual is used to characterize the feasibility of fault detection and isolation. Once a fault occurs in the system, it is possible to detect and isolate it. After that, we attempt to further explore the isolated fault. In this step, a fractional-order sliding-mode observer is designed to provide an estimate of the isolated fault for the first subsystem containing the isolated fault as well as the systems uncertainties. Mittag-Leffler stability of fractional-order estimation error system is defined and the estimation error is proved to be Mittag-Leffler stable. As a result, the synthesized design of the fractional-order Luenberger observers and the fractional-order sliding-mode observer can lead to simultaneous fault isolation and estimation.

The main contribution of the paper is twofold. On one hand, two simple and common types of fractional-order observer-based strategies are derived to satisfactorily accomplish the task of fault detection, isolation, and estimation for the fractional-order Li-ion battery system inspired by the ideas proposed in [1, 39, 40]. On the other hand, Mittag-Leffler stability of fractional-order estimation error system is defined and some other theoretical results are then presented. It is believed that the obtained results can perfectly embody accuracy and practicability properties of fractional calculus describing a real process in physical systems.

The rest of the paper is organized as follows. In Section 2, a fractional-order system based on a Li-ion battery model is formulated to achieve fault diagnosis and estimation and to answer the listed three questions. A strategy for fault detection and isolation is presented in Section 3 and fault estimation strategy is given in Section 4. In Section 5 the proposed strategy is applied to a three-cell battery string system to show the effectiveness of the proposed approach. Finally, some conclusions are drawn in Section 6.

## 2. Problem Formulation

Inspired by the idea of [20], we are ready to present a fractional-order model for a general system in [1]. Consider the following fractional-order pseudostate space description

$$D^\alpha x(t) = Ax(t) + Bu(t) + Ff(t) + Gd(t), \quad 0 < \alpha < 1, \quad (1)$$

$$y(t) = Cx(t)$$

where  $D^\alpha$  denotes the Caputo fractional derivative of order  $\alpha$  on  $[0, t]$ ,  $\alpha$  is the fractional commensurate order,  $x \in R^n$  is the pseudostate vector,  $u \in R^m$  is the input vector,  $y \in R^p$  is the measurable output vector,  $f(t)$  is a bounded  $s$ -dimensional fault vector,  $d(t)$  represents bounded uncertainties/disturbances with dimension of  $q$ , and  $A, B, F, G$ , and  $C$  are  $n \times n$ ,  $n \times m$ ,  $n \times s$ ,  $n \times q$ , and  $p \times n$  constant matrices, respectively.

Define  $F = [F_1 \ F_2 \ \cdots \ F_s]$  and  $G = [G_1 \ G_2 \ \cdots \ G_q]$  for any  $i \in \{1, 2, \dots, s\}$  and  $j \in \{1, 2, \dots, q\}$ , and  $F_i$  and  $G_j$  are the  $i$ -th and  $j$ -th column of  $F$  and  $G$ . Denote also  $G_i'$  as a matrix consisting of  $F_i$  and all columns of  $G$ , that is,  $G_i' = [F_i \ G_1 \ G_2 \ \cdots \ G_q]$  for any  $i \in \{1, 2, \dots, s\}$ .

For the above system, the following assumptions are made.

*Assumption 1.* At most a fault occurs at one time in system (1).

*Assumption 2.* Matrix  $G$  is of full column rank,  $\text{rank}(C) = p$ , and  $\text{rank}(CG_i') = \text{rank}(G_i') = q + 1$  where  $\text{rank}(\cdot)$  denotes the rank of a matrix.

*Assumption 3.* For each  $i = 1, 2, \dots, s$  and for every complex number  $\sigma$ ,

$$\text{rank} \begin{bmatrix} \sigma I_n - A & G_i' \\ C & 0 \end{bmatrix} = n + q + 1 \quad (2)$$

with  $|\arg(\sigma)| \leq \alpha\pi/2$ ,  $I_n$  is the  $n \times n$  identity matrix, and  $\arg(\sigma)$  stands for the argument of  $\sigma$ .

*Remark 4.* Assumption 2 implies that  $G_i'$  is of full column rank and  $q + 1 \leq p$ . Then  $F$  has no zero columns.

The purpose of this paper is to study the fault diagnosis problem. The fault diagnosis problem addressed here is to detect, isolate, and estimate the fault. A systematic study is performed to answer the three following questions under Assumptions 1–3:

- (1) How can a fault be detected or what are the possible conditions for detecting a fault when it occurs?
- (2) How can the detected fault be isolated?
- (3) How can the isolated fault be dealt with or estimated?

### 3. Fault Detection and Isolation

In the section, we will reorganize system (1) and develop an approach to fault diagnosis. To present the conditions for fault detection and isolation, a particular system structure is presented, which is the structure to be built on the following results.

**Lemma 5.**  $\text{rank}(CG_i') = q + 1$  if and only if there exist nonsingular matrices  $T_i$  and  $S_i$  such that

$$T_i^{-1}G_i' = \begin{bmatrix} G_i^1 \\ 0 \end{bmatrix}, \quad (3)$$

$$S_i^{-1}CT_i = \begin{bmatrix} C_i^{11} & 0 \\ 0 & C_i^{22} \end{bmatrix},$$

where  $G_i^1$  and  $C_i^{11}$  are invertible,  $\text{rank}(G_i^1) = \text{rank}(C_i^{11}) = q + 1$ .

*Proof.* Based on Lemma 1 presented in [41], it is obtained that  $\text{rank}(CG_i') = \text{rank}(G_i')$  if and only if there are nonsingular matrices  $T_i$  and  $S_i$  such that

$$T_i^{-1}G_i' = \begin{bmatrix} G_i^1 \\ 0 \end{bmatrix}, \quad (4)$$

$$S_i^{-1}CT_i = \begin{bmatrix} C_i^{11} & 0 \\ 0 & C_i^{22} \end{bmatrix},$$

where  $G_i^1$  and  $C_i^{11}$  have the same number of rows,  $G_i^1$  is of full row rank, and  $C_i^{11}$  is invertible.

Considering Assumption 2 and

$$\begin{aligned} \text{rank}(G_i') &= \text{rank}(T_i^{-1}G_i') = \text{rank}[G_i^{1T} \ 0]^T \\ &= \text{rank}(G_i^1), \end{aligned} \quad (5)$$

where  $T$  means the transpose of a matrix, we can obtain that  $G_i^1$  is of full column rank and  $\text{rank}(G_i^1) = q + 1$ . It is worth noting that  $G_i^1$  is also of full row rank, and then  $G_i^1$  is invertible. Because  $C_i^{11}$  is invertible, and  $G_i^1$  and  $C_i^{11}$  have the same number of rows, then  $\text{rank}(C_i^{11}) = q + 1$ .  $\square$

*Remark 6.* Lemma 5 is equivalent to the existence of state and output transformations. In order to effectively isolate every fault, the original system (1) can be reorganized using Lemma 5.

*3.1. Bank of Reformulated Systems.* This subsection deals with transformation of the system into a proper form containing two subsystems. Define  $f(t) = [f_1(t) \ f_2(t) \ \dots \ f_s(t)]^T$ ,  $\bar{F}_i$  is defined as the matrix after removing the column  $F_i$  from  $F$ , and  $\bar{f}_i(t)$  is the matrix after deleting the  $f_i(t)$  from  $f(t)$ . Then, system (1) is reformulated as a bank of  $s$  systems as follows:

$$\begin{aligned} D^\alpha x(t) &= Ax(t) + Bu(t) + \bar{F}_i \bar{f}_i(t) + F_i f_i(t) \\ &\quad + Gd(t), \end{aligned} \quad (6)$$

$$y(t) = Cx(t), \quad i = 1, 2, \dots, s.$$

According to Lemma 5, for  $i \in \{1, 2, \dots, s\}$ , there exist nonsingular matrices  $T_i$  and  $S_i$  such that state and output transformations are described as

$$x = T_i \begin{bmatrix} \xi_i^1 \\ \xi_i^2 \end{bmatrix}, \quad (7)$$

$$y = S_i \begin{bmatrix} \eta_i^1 \\ \eta_i^2 \end{bmatrix}$$

and (6) can be correspondingly transformed as

$$\begin{aligned} D^\alpha \xi_i^1(t) &= A_i^{11} \xi_i^1(t) + A_i^{12} \xi_i^2(t) + B_i^1 u(t) + \bar{F}_i^1 \bar{f}_i(t) \\ &\quad + G_i^1 \begin{bmatrix} f_i(t) \\ d(t) \end{bmatrix} \\ D^\alpha \xi_i^2(t) &= A_i^{21} \xi_i^1(t) + A_i^{22} \xi_i^2(t) + B_i^2 u(t) + \bar{F}_i^2 \bar{f}_i(t) \\ \eta_i^1(t) &= C_i^{11} \xi_i^1(t) \\ \eta_i^2(t) &= C_i^{22} \xi_i^2(t), \end{aligned} \quad (8)$$

where  $G_i^1$  and  $C_i^{11}$  are  $(q + 1) \times (q + 1)$  matrices,  $\xi_i^1(t)$  and  $\xi_i^2(t)$  are  $(q + 1)$ -dimensional and  $(n - q - 1)$ -dimensional vectors, and

$$\begin{aligned}
T_i^{-1}AT_i &= \begin{bmatrix} A_i^{11} & A_i^{12} \\ A_i^{21} & A_i^{22} \end{bmatrix}, \\
T_i^{-1}B &= \begin{bmatrix} B_i^1 \\ B_i^2 \end{bmatrix}, \\
T_i^{-1}\bar{F}_i &= \begin{bmatrix} \bar{F}_i^1 \\ \bar{F}_i^2 \end{bmatrix}, \\
T_i^{-1}G_i' &= \begin{bmatrix} G_i^1 \\ 0 \end{bmatrix}, \\
S_i^{-1}CT_i &= \begin{bmatrix} C_i^{11} & 0 \\ 0 & C_i^{22} \end{bmatrix},
\end{aligned} \tag{9}$$

where the dimensions of matrices are defined as follows:  $A_i^{11}$  is  $(q+1) \times (q+1)$ ,  $A_i^{12}$  is  $(q+1) \times (n-q-1)$ ,  $A_i^{21}$  is  $(n-q-1) \times (q+1)$ ,  $A_i^{22}$  is  $(n-q-1) \times (n-q-1)$ ,  $\bar{F}_i^1$  is  $(q+1) \times (s-1)$ ,  $\bar{F}_i^2$  is  $(n-q-1) \times (s-1)$ , and  $C_i^{22}$  is  $(p-q-1) \times (n-q-1)$ .

System (8) can be rewritten as two subsystems

$$\begin{aligned}
D^\alpha \xi_i^1(t) &= A_i^{11} \xi_i^1(t) + A_i^{12} \xi_i^2(t) + B_i^1 u(t) + \bar{F}_i^1 \bar{f}_i(t) \\
&\quad + G_i^1 \begin{bmatrix} f_i(t) \\ d(t) \end{bmatrix}
\end{aligned} \tag{10}$$

$$\eta_i^1(t) = C_i^{11} \xi_i^1(t), \quad i = 1, 2, \dots, s$$

and

$$\begin{aligned}
D^\alpha \xi_i^2(t) &= A_i^{21} \xi_i^1(t) + A_i^{22} \xi_i^2(t) + B_i^2 u(t) + \bar{F}_i^2 \bar{f}_i(t) \\
\eta_i^2(t) &= C_i^{22} \xi_i^2(t), \quad i = 1, 2, \dots, s,
\end{aligned} \tag{11}$$

where all variables and matrices here are the same as before.

*Remark 7.* It is important to separate a single fault source and disturbances simultaneously by introducing state and output transformations. As well known, the key of the fault isolation is to isolate the single fault source.

**3.2. Fault Detection Based on a Luenberger Observer.** The observer technique is used to detect and isolate faults in this subsection. We propose to construct an observer for the second subsystem (11) for each  $i$ .

**Lemma 8.** Consider (11) satisfying Assumptions 2 and 3; then

$$\text{rank} \left( \begin{bmatrix} \sigma I_{n-q-1} - A_i^{22} \\ C_i^{22} \end{bmatrix} \right) = n - q - 1. \tag{12}$$

*Proof.* By performing elementary column and row operations on matrix and using Lemma 5, the following equivalence is shown:

$$\begin{bmatrix} \sigma I_n - A & G_i' \\ C & 0 \end{bmatrix} \sim \begin{bmatrix} G_i^1 & 0 & 0 \\ 0 & C_i^{11} & 0 \\ 0 & 0 & \sigma I_{n-q-1} - A_i^{22} \\ 0 & 0 & C_i^{22} \end{bmatrix}, \tag{13}$$

where “ $\sim$ ” means equivalence. It is worth noting that

$$\begin{aligned}
&\text{rank} \left( \begin{bmatrix} \sigma I_n - A & G_i' \\ C & 0 \end{bmatrix} \right) \\
&= \text{rank} \left( \begin{bmatrix} \sigma I_{n-q-1} - A_i^{22} \\ C_i^{22} \end{bmatrix} \right) + 2(q+1),
\end{aligned} \tag{14}$$

and

$$\text{rank} \left( \begin{bmatrix} \sigma I_n - A & G_i' \\ C & 0 \end{bmatrix} \right) = n + (q+1), \tag{15}$$

And then (12) is obtained.

Meanwhile, we can obtain a conclusion in Theorem 9 similar to Lemma 1 presented in [42].  $\square$

**Theorem 9.** With Assumptions 2 and 3, the unobservable polynomial of the pair  $(A_i^{22}, C_i^{22})$  is equal to the invariant zero polynomial of  $(C, A, G_i')$ .

Following Lemmas 2 and 3 in [31], Theorem 10 can be stated.

**Theorem 10.** System (11) satisfying Assumptions 2 and 3 is detectable or the pair  $(A_i^{22}, C_i^{22})$  is detectable.

Considering system (11),  $\xi_i^1$  and  $\eta_i^2$  can be obtained from the measured output  $y$ . In fact, let

$$S_i^{-1} = \begin{bmatrix} S_i^1 \\ S_i^2 \end{bmatrix}, \tag{16}$$

And then they are computed by

$$\begin{aligned}
\xi_i^1 &= (C_i^{11})^{-1} S_i^1 y, \\
\eta_i^2 &= S_i^2 y.
\end{aligned} \tag{17}$$

Moreover, based on Theorem 2 presented in [43] and Theorem 10 in this work, we are ready to design a Luenberger observer for system (11) and select  $L_i^2$  such that  $(A_i^{22} - L_i^2 C_i^{22})$  is a stable matrix; that is, the spectrum of  $(A_i^{22} - L_i^2 C_i^{22})$  can be assigned anywhere in the complex of region of asymptotic stability  $|\arg(\sigma)| > \alpha\pi/2$ . A Luenberger observer is designed as follows:

$$\begin{aligned}
D^\alpha \hat{\xi}_i^2(t) &= A_i^{21} \hat{\xi}_i^1(t) + A_i^{22} \hat{\xi}_i^2(t) + B_i^2 u(t) \\
&\quad + L_i^2 (\eta_i^2(t) - \hat{\eta}_i^2(t)),
\end{aligned} \tag{18}$$

$$\hat{\eta}_i^2(t) = C_i^{22} \hat{\xi}_i^2(t), \quad i = 1, 2, \dots, s,$$

where  $\hat{\cdot}$  indicates estimate.

For each  $i = 1, 2, \dots, s$ , the state estimation error dynamics of the second subsystem (11) can be obtained by subtracting (18) from (11)

$$D_t^\alpha e_i^2(t) = (A_i^{22} - L_i^2 C_i^{22}) e_i^2(t) + \bar{F}_i^2 \bar{f}_i(t), \quad (19)$$

where  $e_i^2(t) = \xi_i^2(t) - \hat{\xi}_i^2(t)$ .

We now define a fault-detection residual as

$$r_i(t) = \|\eta_i^2(t) - \hat{\eta}_i^2(t)\| = \|C_i^{22} e_i^2(t)\|, \quad (20)$$

and then we have Theorem 11.

**Theorem 11.** For system (1) satisfying Assumptions 1-3 with a bank of Luenberger observers in the form of (18), we consider only one single fault scenario. If there exist  $i, j$  and  $i \neq j$  such that  $\lim_{t \rightarrow \infty} r_i(t) = 0$  and  $\lim_{t \rightarrow \infty} r_j(t) = 0$ ,  $i, j \in \{1, 2, \dots, s\}$ , then the system is healthy. If there are  $i, j$  such that  $\lim_{t \rightarrow \infty} r_i(t) = 0$  and  $\lim_{t \rightarrow \infty} r_j(t) \neq 0$  for  $j \neq i$ , then  $f_i(t) \neq 0$ ; that is,  $f_i(t)$  is the only one fault.

*Proof.* If  $\lim_{t \rightarrow \infty} r_i(t) = 0$  and  $\lim_{t \rightarrow \infty} r_j(t) = 0$  when  $i \neq j$ , it follows that  $\bar{f}_i(t) \equiv 0$  and  $\bar{f}_j(t) \equiv 0$  from (20) and the stability of  $(A_i^{22} - L_i^2 C_i^{22})$  in (19), it implies that the system is free from faults, and thus system (1) is healthy.

If  $\lim_{t \rightarrow \infty} r_i(t) = 0$ , it holds that  $\bar{f}_i(t) \equiv 0$  from (20) and the stability of  $(A_i^{22} - L_i^2 C_i^{22})$  of (19). If  $\lim_{t \rightarrow \infty} r_j(t) \neq 0$  when  $j \neq i$ , it follows that  $\bar{F}_j^2 \bar{f}_j(t) \neq 0$  from (19) and (20). Moreover,  $\bar{f}_j(t)$  has one and only one nonzero element, which is  $f_j(t)$ . Thus,  $f_i(t) \neq 0$  and  $f_j(t) = 0$  for all  $j, j \neq i$ .  $\square$

*Remark 12.* Theorem 11 implies that the residual  $r_i(t)$  is not sensitive to the  $i$ th fault  $f_i(t)$  but is sensitive to all other faults.

**3.3. Fault Isolation Based on Fault-Detection Residuals.** Based on the analysis presented in the above subsections, the following fault-detection and isolation algorithm was suggested.

*Step 1.* Design a bank of Luenberger observers of the form (18) for  $i = 1, 2, \dots, s$ .

*Step 2.* Compute the  $s$  fault-detection residuals  $r_i(t), i = 1, 2, \dots, s$ .

*Step 3.* Choose a threshold  $r_0$  (which can be chosen as small as possible theoretically because  $\lim_{t \rightarrow \infty} r_i(t) = 0$  when  $f_i(t) \neq 0$ ).

*Step 4.* If all residuals  $r_i(t), i = 1, 2, \dots, s$  are below the threshold, then, the system is healthy. If there is only one residual, say  $r_{i_0}(t)$  with  $i_0 \in \{1, 2, \dots, s\}$ , which is below the threshold, then it is claimed that a fault has been detected and the fault is isolated as  $f_{i_0}(t)$ .

*Remark 13.* Based on Theorem 11, a fault can be detected when system (1) has only one fault by computing at most  $s$  fault-detection residuals  $r_i(t)$  for the bank of Luenberger observers (18). Performing the above algorithm, the first two questions listed in Section 2 are addressed.

## 4. Fault Estimation Based on Sliding Mode Observers

In this section, fault estimation based on sliding mode observers is addressed and will address the third question posed above. It is assumed that a fault has been detected and isolated as  $f_{i_0}(t)$ .

### 4.1. Design of a Sliding Mode Observer for Fault Estimation.

When the fault  $f_{i_0}(t)$  occurs,  $\lim_{t \rightarrow \infty} r_{i_0}(t) = 0$  and  $\bar{f}_{i_0}(t) = 0$ . For convenience, the isolated fault  $f_{i_0}(t)$  is still denoted as  $f_i(t)$ . The  $i_0$ -th is denoted as  $i$ -th. In fact, the first subsystem (10) and the state estimation error dynamics (19) with fault  $f_{i_0}(t)$  can be described as follows:

$$D_t^\alpha \xi_i^1(t) = A_i^{11} \xi_i^1(t) + A_i^{12} \xi_i^2(t) + B_i^1 u(t) + G_i^1 \begin{bmatrix} f_i(t) \\ d(t) \end{bmatrix} \quad (21)$$

$$\eta_i^1(t) = C_i^{11} \xi_i^1(t), \quad i = 1, 2, \dots, s$$

and

$$D_t^\alpha e_i^2(t) = (A_i^{22} - L_i^2 C_i^{22}) e_i^2(t). \quad (22)$$

For system (21), the following equations are established:

$$\text{rank}(C_i^{11} G_i^1) = \text{rank}(G_i^1) = q + 1, \quad (23)$$

$$\text{rank} \left( \begin{bmatrix} \sigma I_{q+1} - A_i^{11} & G_i^1 \\ C_i^{11} & 0 \end{bmatrix} \right) = q + 1 + \text{rank}(G_i^1) \quad (24)$$

based on Lemma 5 and the equivalence of the following two matrices:

$$\begin{bmatrix} \sigma I_{q+1} - A_i^{11} & G_i^1 \\ C_i^{11} & 0 \end{bmatrix} \sim \begin{bmatrix} 0 & G_i^1 \\ C_i^{11} & 0 \end{bmatrix}. \quad (25)$$

The stability of the fractional-order observer for subsystem (21) can be formulated by the two conditions (23) and (24) according to [35]. Parallel to the  $i$ th Luenberger observer of the form (18), a sliding mode observer can be designed to estimate the fault for (21) as follows:

$$D_t^\alpha \hat{\xi}_i^1(t) = A_i^{11} \hat{\xi}_i^1(t) + A_i^{12} \hat{\xi}_i^2(t) + B_i^1 u(t) + L_i^1 (\eta_i^1(t) - \hat{\eta}_i^1(t)) + G_i^1 \hat{v}_i(t) \quad (26)$$

$$\hat{\eta}_i^1(t) = C_i^{11} \hat{\xi}_i^1(t), \quad i = 1, 2, \dots, s,$$

where  $\hat{v}_i(t)$  is the estimate of  $v_i(t) = [f_i(t) \ d(t)]^T$ . It is defined as

$$\hat{v} = \begin{cases} \rho_i \frac{K_i^1 e_{\eta_i}}{\|K_i^1 e_{\eta_i}\|}, & \|K_i^1 e_{\eta_i}\| \neq 0; \\ 0, & \|K_i^1 e_{\eta_i}\| = 0 \end{cases} \quad (27)$$

with  $e_{\eta_i} = \eta_i^1 - \hat{\eta}_i^1$  and constant matrix  $K_i^1 \in R^{(q+1) \times (q+1)}$ ,  $\rho_i$  should be chosen to be a large enough constant, and  $L_i^1$  can

be selected such that the spectrum of  $(A_i^{11} - L_i^1 C_i^{11})$  is a stable matrix.

Let  $e_i^1(t) = \xi_i^1(t) - \widehat{\xi}_i^1(t)$  be the estimation error of state  $\xi_i^1(t)$ , then the fractional-order state estimation error can be described as follows:

$$D^\alpha e_i^1 = (A_i^{11} - L_i^1 C_i^{11}) e_i^1 + A_i^{12} e_i^2 + G_i^1 (v - \widehat{v}), \quad (28)$$

$$\text{and } e_{\eta_i} = \eta_i^1 - \widehat{\eta}_i^1 = C_i^{11} e_i^1.$$

**4.2. Stability of the Designed Sliding Mode Observer.** Before embarking on the fundamental theorem, we first give some preliminary results on Caputo fractional derivatives.

*Definition 14* (see [9]). The two-parameter Mittag-Leffler function is defined by

$$E_{\alpha,\beta}(z) = \sum_{k=0}^{\infty} \frac{z^k}{\Gamma(\alpha k + \beta)}, \quad \alpha > 0, \beta > 0, z \in C, \quad (29)$$

where  $\Gamma(\cdot)$  is the Gamma function with

$$\Gamma(x) = \int_0^{\infty} t^{x-1} e^{-t} dt. \quad (30)$$

When  $\beta = 1$ , one has  $E_\alpha(z) = E_{\alpha,1}(z)$ .

Let  $e_i(t) = [e_i^1(t) \ e_i^2(t)]^T$ ,  $e_i(0) = [0 \ 0]^T$ . According to the definition in [44],  $[0, 0]^T$  is the equilibrium point of the following dynamic system:

$$D^\alpha e_i^1(t) = (A_i^{11} - L_i^1 C_i^{11}) e_i^1(t) + A_i^{12} e_i^2(t) \quad (31)$$

$$D^\alpha e_i^2(t) = (A_i^{22} - L_i^2 C_i^{22}) e_i^2(t). \quad (32)$$

Then we present the definition of stability for the system formed by (28) and (22) in the sense of Mittag-Leffler similar to those in [44, 45] as follows.

*Definition 15.* The solution  $e_i(t)$  of the system formed by (28) and (22) is said to be Mittag-Leffler stable with respect to the equilibrium point  $e_i(0)$  of system (31) if

$$\|e_i(t)\| \leq \{m[e_i(t_0)] E_\alpha(-\lambda(t-t_0)^\alpha)\}^b, \quad (33)$$

$$\alpha \in (0, 1),$$

where  $t_0 = 0$  is the initial time,  $\lambda > 0$ ,  $b > 0$ ,  $m(0) = 0$ ,  $m(e_i) \geq 0$ , and  $m(e_i)$  is locally Lipschitz with Lipschitz constant.

**Lemma 16** (see [46]). Let  $x(t) \in R^n$  be a differentiable vector; then, for any time instant,

$$\frac{1}{2} D^\alpha (x^T(t) P x(t)) \leq x^T(t) P D^\alpha x(t), \quad (34)$$

$$\forall \alpha \in (0, 1], t \geq 0,$$

where  $P \in R^{n \times n}$  is a positive definite constant matrix.

The following theorem is to present the stability of the designed observers in the sense of Mittag-Leffler.

**Theorem 17.** Consider (1) satisfying Assumptions 1–3,  $f(t)$  and  $d(t)$  are bounded, and the Luenberger observers and the sliding mode observer are designed in (18), (26), and (27). For  $i = 1, 2, \dots, s$ , if there exist matrices  $L_i^1, L_i^2, K_i^1$  and positive definite matrices  $P_1, P_2, Q_i^1, Q_i^2$  such that

$$-Q_i^1 = (A_i^{11} - L_i^1 C_i^{11})^T P_1 + P_1 (A_i^{11} - L_i^1 C_i^{11}) + P_1^2 \quad (35)$$

$$-Q_i^2 = (A_i^{22} - L_i^2 C_i^{22})^T P_2 + P_2 (A_i^{22} - L_i^2 C_i^{22}) + A_i^{12T} A_i^{12} \quad (36)$$

$$P_1 G_i^1 = C_i^{11T} K_i^{1T}, \quad (37)$$

then the observers given by (18), (26), and (27) can ensure that the state estimation error  $e_i(t)$  is Mittag-Leffler stable.

*Proof.* Consider a Lyapunov function candidate as follows:

$$V_i(t, e_i(t)) = e_i^{1T}(t) P_1 e_i^1(t) + e_i^{2T}(t) P_2 e_i^2(t), \quad (38)$$

where  $P_1$  and  $P_2$  are positive definite matrices.

Applying Caputo fractional-order operation  $D^\alpha$  to  $V_i$  with respect to  $t$  along (22) and (28), by Lemma 16, it is obtained that

$$\begin{aligned} D^\alpha V_i &= D^\alpha (e_i^{1T} P_1 e_i^1) + D^\alpha (e_i^{2T} P_2 e_i^2) \\ &\leq 2e_i^{1T} P_1 (D^\alpha e_i^1) + 2e_i^{2T} P_2 (D^\alpha e_i^2) \\ &= [(A_i^{11} - L_i^1 C_i^{11}) e_i^1 + A_i^{12} e_i^2 + G_i^1 e_v]^T P_1 e_i^1 \\ &\quad + e_i^{1T} P_1 [(A_i^{11} - L_i^1 C_i^{11}) e_i^1 + A_i^{12} e_i^2 + G_i^1 e_v] \\ &\quad + e_i^{2T} [(A_i^{22} - L_i^2 C_i^{22})^T P_2 + P_2 (A_i^{22} - L_i^2 C_i^{22})] e_i^2 \\ &\leq e_i^{1T} [(A_i^{11} - L_i^1 C_i^{11})^T P_1 + P_1 (A_i^{11} - L_i^1 C_i^{11}) \\ &\quad + P_1^2] e_i^1 + e_i^{2T} [(A_i^{22} - L_i^2 C_i^{22})^T P_2 \\ &\quad + P_2 (A_i^{22} - L_i^2 C_i^{22}) + A_i^{12T} A_i^{12}] e_i^2 + 2e_i^{1T} P_1 G_i^1 e_v, \end{aligned} \quad (39)$$

where  $e_v = v - \widehat{v}$ .

If  $K_i^1$  can be chosen such that  $P_1 G_i^1 = C_i^{11T} K_i^{1T}$ , then

$$\begin{aligned} e_i^{1T} P_1 G_i^1 \widehat{v} &= \|K_i^1 C_i^{11} e_i^1\| \rho_i = \|K_i^1 e_{\eta_i}\| \rho_i, \\ e_i^{1T} P_1 G_i^1 v &= (K_i^1 C_i^{11} e_i^1)^T v = (K_i^1 e_{\eta_i})^T v. \end{aligned} \quad (40)$$

Considering the following inequality:

$$e_i^{1T} P_1 G_i^1 v \leq \|K_i^1 e_{\eta_i}\| \|v\|, \quad (41)$$

and applying (35) and (36), (39) can be further manipulated as follows:

$$D^\alpha V_i \leq e_i^{1T} (-Q_i^1) e_i^1 + e_i^{2T} (-Q_i^2) e_i^2 - 2 \|K_i^1 e_{\eta_i}\| (\rho_i - \|v\|). \quad (42)$$

Let  $Q_i = \begin{bmatrix} Q_i^1 & 0 \\ 0 & Q_i^2 \end{bmatrix}$  and  $P = \begin{bmatrix} P_1 & 0 \\ 0 & P_2 \end{bmatrix}$ ,  $\lambda_{\min}(Q_i)$  denoted the minimum eigenvalue of  $Q_i$ , and  $\lambda_{\min}(P)$  and  $\lambda_{\max}(P)$  denoted the minimum and maximum eigenvalues of  $P$ . Then  $\lambda_{\min}(Q_i) > 0$ ,  $\lambda_{\min}(P) > 0$ , and  $\lambda_{\max}(P) > 0$ .

Choosing  $\rho_i$  large enough (this can be performed because  $v$  is bounded), one obtains

$$D^\alpha V_i \leq -\lambda_{\min}(Q_i) \|e_i\|^2. \quad (43)$$

And the Lyapunov function candidate is satisfied by

$$\lambda_{\min}(P) \|e_i\|^2 \leq V_i \leq \lambda_{\max}(P) \|e_i\|^2. \quad (44)$$

It follows from (43) and (44) that

$$D^\alpha V_i \leq -\frac{\lambda_{\min}(Q_i)}{\lambda_{\max}(P)} V_i. \quad (45)$$

There exists a nonnegative function  $M(t)$  such that

$$D^\alpha V_i + M(t) = -\frac{\lambda_{\min}(Q_i)}{\lambda_{\max}(P)} V_i. \quad (46)$$

Taking Laplace transform on both sides of (46) leads to

$$s^\alpha V_i(s) - s^{\alpha-1} V_i(0) + M(s) = -\frac{\lambda_{\min}(Q_i)}{\lambda_{\max}(P)} V_i(s), \quad (47)$$

where  $V_i(s) = \mathcal{L}\{V_i(t, e_i(t))\}$  and  $\mathcal{L}$  is the operator for Laplace transform. Based on (47),  $V_i$  can be expressed as follows:

$$V_i(s) = \frac{s^{\alpha-1} V_i(0) - M(s)}{s^\alpha + \lambda_{\min}(Q_i)/\lambda_{\max}(P)}. \quad (48)$$

From the existence and uniqueness theorem [9] for fractional-order differential equations and the inverse Laplace transform, the unique solution of (46) can be obtained as follows:

$$V_i(t) = V_i(0) E_\alpha \left( -\frac{\lambda_{\min}(Q_i)}{\lambda_{\max}(P)} t^\alpha \right) - M(t) * \left[ t^{\alpha-1} E_{\alpha,\alpha} \left( -\frac{\lambda_{\min}(Q_i)}{\lambda_{\max}(P)} t^\alpha \right) \right], \quad (49)$$

where  $*$  denotes the convolution operator.

Therefore,  $V_i(t) \leq V_i(0) E_\alpha(-\lambda_{\min}(Q_i)/\lambda_{\max}(P)t^\alpha)$  from the facts that both  $t^{\alpha-1}$  and  $E_{\alpha,\alpha}(-\lambda_{\min}(Q_i)/\lambda_{\max}(P)t^\alpha)$  are nonnegative. With the aid of (44), the estimation error  $e_i(t)$  satisfies the following inequality:

$$\|e_i(t)\| \leq \left[ \frac{V_i(0)}{\lambda_{\min}(P)} E_\alpha \left( -\frac{\lambda_{\min}(Q_i)}{\lambda_{\max}(P)} t^\alpha \right) \right]^{1/2}, \quad (50)$$

where  $V_i(0)/\lambda_{\min}(P) \geq 0$ .

Let  $m = V_i(0)/\lambda_{\min}(P) = V_i(0, e_i(0))/\lambda_{\min}(P) \geq 0$ , and then we have

$$\|e_i(t)\| \leq \left[ m E_\alpha \left( -\frac{\lambda_{\min}(Q_i)}{\lambda_{\max}(P)} t^\alpha \right) \right]^{1/2}, \quad (51)$$

where  $m = 0$  holds if and only if  $e_i(0) = 0$ . Because  $V(t, e_i)$  is locally Lipschitz with respect to  $e_i$  and  $V(0, e_i(0)) = 0$  if and only if  $e_i(0) = 0$ , and it follows that  $m = V_i(0, e_i(0))/\lambda_{\min}(P)$  is also Lipschitz with respect to  $e_i(0)$  and  $m(0) = 0$ . Therefore, the solution  $e_i(t)$  of the system formed by (28) and (22) is Mittag-Leffler stable.  $\square$

*Remark 18.* Theorem 17 implies that the state estimation errors  $e_i^1$  and  $e_i^2$  are bounded when  $E_\alpha(-\lambda_{\min}(Q_i)/\lambda_{\max}(P)t^\alpha)$  is bounded. The conclusion is the same as that for integer-order systems [1].

*Remark 19.* The third question in Section 2 has been addressed. To our knowledge the stability in the sense of Mittag-Leffler is first introduced here to study the state estimation error dynamics.

## 5. Fault Detection and Estimation of the Three-Cell Battery String

In this section, we apply the proposed method for fault detection and estimation of a three-cell battery string model reported in [1] and demonstrate its effectiveness in application. Then system (1) is now parameterized as follows:

$$\begin{aligned} A &= \begin{bmatrix} -1.6026 & 0 & 0 \\ 0 & -1.6026 & 0 \\ 0 & 0 & -1.6026 \end{bmatrix}, \\ B &= \begin{bmatrix} 0.1795 & 5.2484 & 0.0225 \\ 0.1795 & 5.2484 & 0.0225 \\ 0.1795 & 5.2484 & 0.0225 \end{bmatrix}, \\ C &= \begin{bmatrix} 1 & 0 & 0 \\ 0 & 1 & 0 \\ 0 & 0 & 1 \end{bmatrix}, \\ G &= \begin{bmatrix} 0.1 \\ 1 \\ 0.05 \end{bmatrix}, \\ F &= \begin{bmatrix} 3 & 0 & 0 \\ 0 & 3 & 0 \\ 0 & 0 & 3 \end{bmatrix}. \end{aligned} \quad (52)$$

A disturbance is selected as  $d(t) = 0.0151 \sin(5t)$ . It is assumed that  $f_1 = f_3 = 0$  for all the time. When  $t \in [0, T)$ ,  $f_2 = 0$  and when  $t \geq T$ ,  $f_2 = 0.2$ ; that is, fault  $f_2$  occurs at time  $T$ . Furthermore, a threshold is set as  $r_0 = 0.015$  and take  $T = 25$ s where  $s$  stands for "second."

Because there are three fault sources, system (1) has three formulations with each one corresponding to a particular fault. According to Lemma 5, nonsingular transform matrices are selected as

$$\begin{aligned} T_1 &= \begin{bmatrix} 1 & 0 & 0 \\ 0 & 1 & 0 \\ 0 & 0.05 & 1 \end{bmatrix}, \\ T_2 &= \begin{bmatrix} 1 & 0 & 0 \\ 0 & 1 & 0 \\ 0.5 & 0 & 1 \end{bmatrix}, \\ T_3 &= \begin{bmatrix} 0.1 & 0 & 1 \\ 1 & 0 & 0 \\ 0 & 1 & 0 \end{bmatrix} \end{aligned} \quad (53)$$

and  $S_i = T_i$ ,  $i = 1, 2, 3$ .

Obviously, for each  $i$ -th system, the second subsystem does not include  $i$ -th fault source  $f_i$  and their observers are designed as

$$\begin{aligned} D^\alpha \xi_1^2(t) &= -1.6026\xi_1^2(t) + 0.1705Z + 4.9860 \\ &\quad + 0.0214I - 0.15f_2 + 3f_3, \\ \eta_1^2(t) &= \xi_1^2(t); \\ D^\alpha \widehat{\xi}_1^2(t) &= -1.6026\widehat{\xi}_1^2(t) + 0.1705Z + 4.9860 \\ &\quad + 0.0214I + 0.6(\eta_1^2(t) - \widehat{\eta}_1^2(t)), \\ \widehat{\eta}_1^2(t) &= \widehat{\xi}_1^2(t), \\ D^\alpha \xi_2^2(t) &= -1.6026\xi_2^2(t) + 0.0897Z + 2.6242 \\ &\quad + 0.0113I - 1.5f_1 + 3f_3, \\ \eta_2^2(t) &= \xi_2^2(t); \\ D^\alpha \widehat{\xi}_2^2(t) &= -1.6026\widehat{\xi}_2^2(t) + 0.0897Z + 2.6242 \\ &\quad + 0.0113I + 0.3(\eta_2^2(t) - \widehat{\eta}_2^2(t)), \\ \widehat{\eta}_2^2(t) &= \widehat{\xi}_2^2(t), \\ D^\alpha \xi_3^2(t) &= -1.6026\xi_3^2(t) + 0.1616Z + 4.7236 \\ &\quad + 0.0203I + 3f_1 - 0.3f_2, \\ \eta_3^2(t) &= \xi_3^2(t); \\ D^\alpha \widehat{\xi}_3^2(t) &= -1.6026\widehat{\xi}_3^2(t) + 0.1616Z + 4.7236 \\ &\quad + 0.0203I + 0.6(\eta_3^2(t) - \widehat{\eta}_3^2(t)), \\ \widehat{\eta}_3^2(t) &= \widehat{\xi}_3^2(t), \end{aligned} \quad (54)$$

where  $L_1^2 = L_3^2 = 0.6$ ,  $L_2^2 = 0.3$ .

Then, the  $i$ -th fault-detection residual is designated as

$$r_i(t) = \|\eta_i^2(t) - \widehat{\eta}_i^2(t)\| = \|e_i^2(t)\|, \quad i = 1, 2, 3. \quad (55)$$

In what follows, we only show the first subsystem and its observer for  $i = 2$ . Let

$$\begin{aligned} \xi_2^1(t) &= \begin{bmatrix} \xi_{21}^1(t) \\ \xi_{22}^1(t) \end{bmatrix}, \\ \eta_2^1(t) &= \begin{bmatrix} \eta_{21}^1(t) \\ \eta_{22}^1(t) \end{bmatrix}, \end{aligned} \quad (56)$$

and then the subsystem and its sliding mode observer are as follows:

$$\begin{aligned} D^\alpha \xi_{21}^1(t) &= -1.6026\xi_{21}^1(t) + 0.1795Z + 5.2484 \\ &\quad + 0.0225I + 0.1d(t), \end{aligned}$$

$$\begin{aligned} D^\alpha \xi_{22}^1(t) &= -1.6026\xi_{22}^1(t) + 0.1795Z + 5.2484 \\ &\quad + 0.0225I + 3f_2 + d(t), \end{aligned} \quad (57)$$

$$\eta_{21}^1(t) = \xi_{21}^1(t),$$

$$\eta_{22}^1(t) = \xi_{22}^1(t), \quad (58)$$

and

$$\begin{aligned} D^\alpha \widehat{\xi}_{21}^1(t) &= -1.6026\widehat{\xi}_{21}^1(t) + 0.1795Z + 5.2484 \\ &\quad + 0.0225I + 0.1\widehat{d}(t) \\ &\quad + 3.6(\eta_{21}^1(t) - \widehat{\eta}_{21}^1(t)), \\ D^\alpha \widehat{\xi}_{22}^1(t) &= -1.6026\widehat{\xi}_{22}^1(t) + 0.1795Z + 5.2484 \\ &\quad + 0.0225I + 3\widehat{f}_2 + \widehat{d}(t) \\ &\quad + 3.5(\eta_{22}^1(t) - \widehat{\eta}_{22}^1(t)), \\ \widehat{\eta}_{21}^1(t) &= \widehat{\xi}_{21}^1(t), \\ \widehat{\eta}_{22}^1(t) &= \widehat{\xi}_{22}^1(t), \end{aligned} \quad (59)$$

where

$$\begin{aligned} \widehat{f}_2 &= \begin{cases} \rho \frac{h_1(t)}{h(t)}, & h(t) \neq 0; \\ 0, & h(t) = 0, \end{cases} \\ \widehat{d} &= \begin{cases} \rho \frac{h_2(t)}{h(t)}, & h(t) \neq 0; \\ 0, & h(t) = 0 \end{cases} \end{aligned} \quad (60)$$

and

$$\begin{aligned} h_1(t) &= 9(\xi_{21}^1 - \widehat{\xi}_{21}^1) + 4(\xi_{22}^1 - \widehat{\xi}_{22}^1), \\ h_2(t) &= 4(\xi_{21}^1 - \widehat{\xi}_{21}^1) + \left(0.3 + \frac{4}{3}\right)(\xi_{22}^1 - \widehat{\xi}_{22}^1), \\ h(t) &= \sqrt{h_1(t)^2 + h_2(t)^2}. \end{aligned} \quad (61)$$

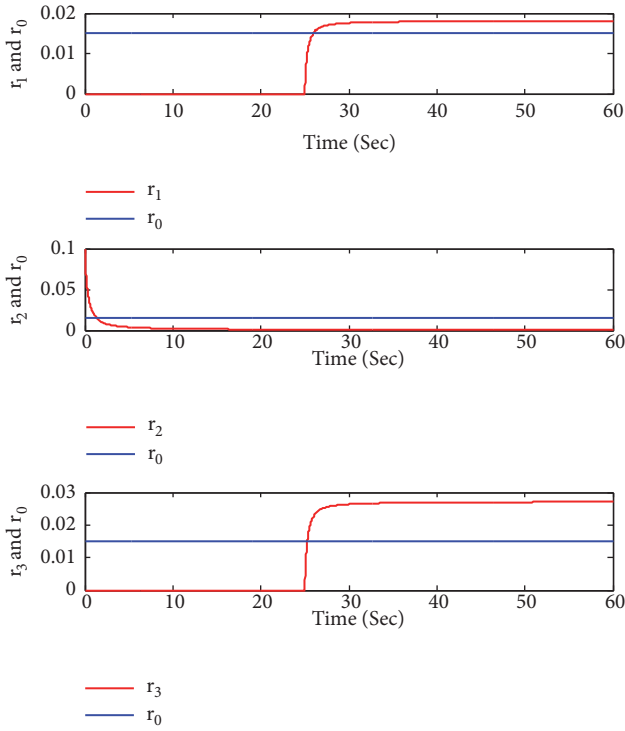


FIGURE 1: Fault detection and isolation when  $\rho = 0.25$ ,  $\alpha = 0.8$ .

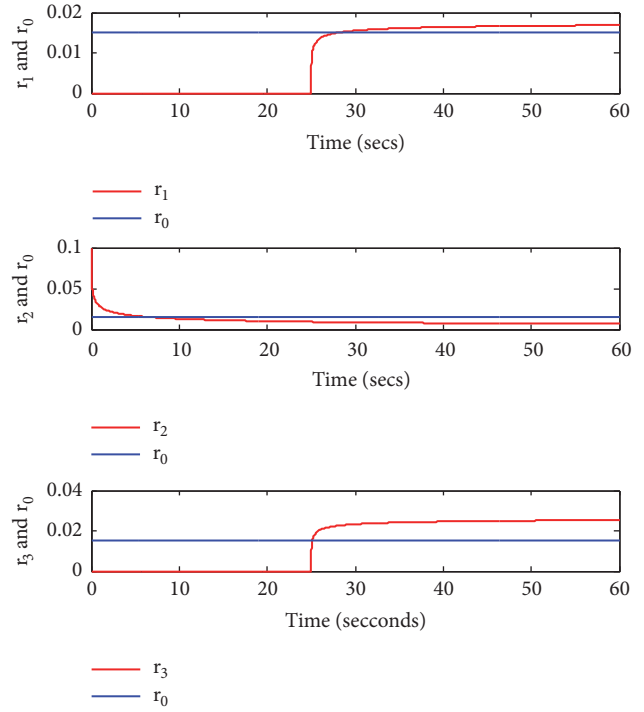


FIGURE 2: Fault detection and isolation when  $\rho = 100$ ,  $\alpha = 0.4$ .

To illustrate the performance of the above strategy, the Adams-Bashforth-Moulton predictor-corrector method is used to calculate the fractional system, and the detailed instructions of this algorithm are available in [47, 48] based on [49]. Next, the simulations are performed while parameter  $\rho$  and the commensurate order  $\alpha$  are changed.

Fault  $f_2(t)$  is caused by a change of internal resistance of the battery and occurs at time instant 25 seconds. Figures 1 and 2 show the evolution of fault-detection residuals  $r_i(t)$ ,  $i = 1, 2, 3$ , and the chosen threshold  $r_0$  where the horizontal bold lines are thresholds with  $\rho = 0.25, \alpha = 0.8$ , and  $\rho = 100, \alpha = 0.4$ . It can be seen indeed in the figures that  $f_2(t)$  is detected at 25s because  $r_1$  and  $r_3$  go beyond the threshold  $r_0$  after 25 seconds, and  $r_2$  is well below the threshold  $r_0$ . Moreover the evolution of fault-detection residuals  $r_1, r_2$ , and  $r_3$  is the same when parameters  $\rho$  and  $\alpha$  are changed.

Figures 3 and 4 show the evolution of the system states (terminal voltage) and their estimations with the fault estimate that is the second subsystem ( $i = 2$ ) with  $\rho = 0.25, \alpha = 0.8$  and  $\rho = 100, \alpha = 0.4$ . Although parameters  $\rho$  and  $\alpha$  are changed, it is noted that each state estimation error is Mittag-Leffler stable because the estimation curve is varying along its own state curve in a small bounded interval and the evolution of the curves has not been affected by the changing parameters. At time instant 25 seconds,  $\xi_{22}^1(t)$  and its estimation start to identify the isolated fault accurately in Figures 3 and 4.

To illustrate the advantages of our proposed method, the simulations are performed on the integer-order modeling of the three-cell battery string [1]. Figure 5 shows the evolution of state and its estimate with the fault estimate system by

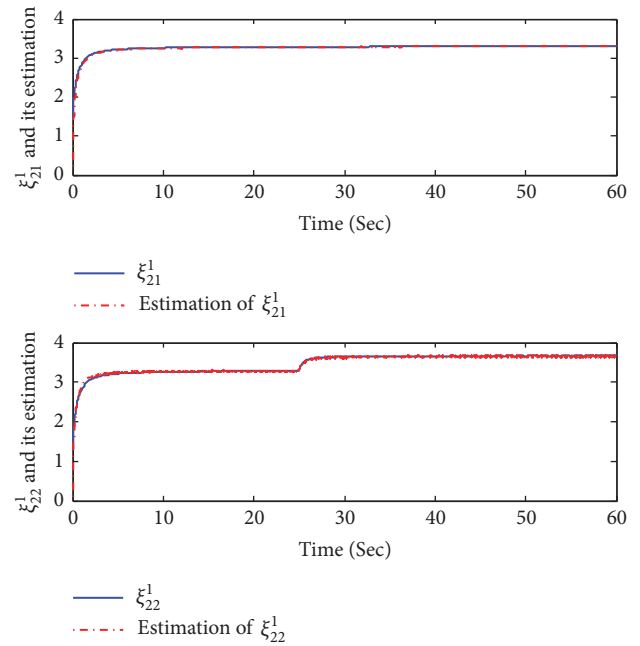


FIGURE 3: System state and estimate with the fault estimate when  $\rho = 0.25$ ,  $\alpha = 0.8$ .

applying the integer-order modeling in [1]. Compared with our proposed method, it can be found that the state and its estimation with the fault estimate start to identify the isolated fault at time instant 25 seconds. But at instant 50 seconds, dynamic curve of estimation with the fault estimate jumps again. The estimation value deviates from state value at the instant too. But the evolution of curves in Figures 3 and 4

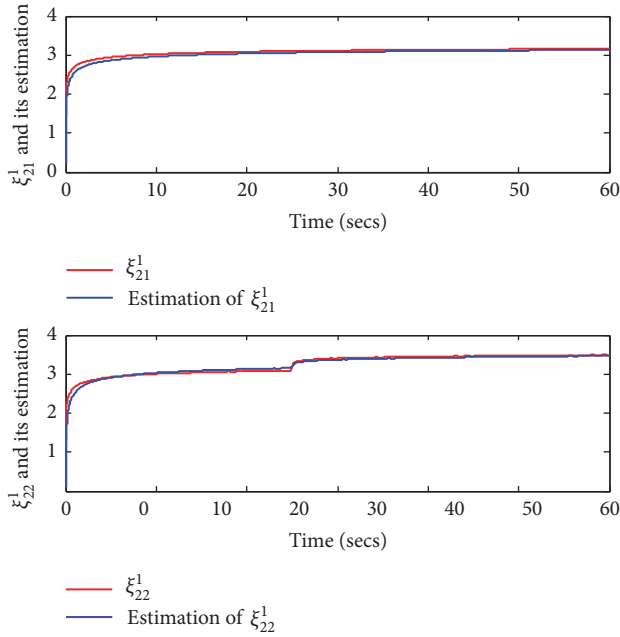


FIGURE 4: System state and estimate with the fault estimate when  $\rho = 100$ ,  $\alpha = 0.4$ .

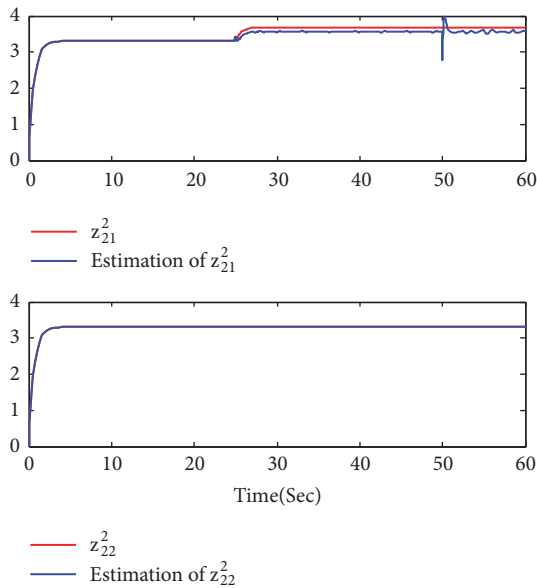


FIGURE 5: System state and estimate with the fault estimate of the integer-order modeling.

is changed smoothly except at time instant 25 seconds when fault  $f_2$  occurs. It is shown that our proposed method of fractional-order modeling has even better results than that of integer-order modeling.

## 6. Conclusions

Fault diagnosis and estimation problem have been studied for a fractional-order system with applications to Lithium-ion

battery cell. Sources of fault and system uncertainties are first separated into two subsystems through a transformation on the model of the system. A fractional-order Luenberger observer is designed to generate a fault-detection residual and faults are then easily detected and isolated. Secondly, a fractional-order sliding mode observer is constructed to provide an estimate of the isolated fault; hence, simultaneous fault detection, isolation, and estimation is accomplished. The effectiveness of the proposed strategy is demonstrated on a three-cell battery string. The proposed strategy is completely built on a new framework. Properties of fractional-order systems and Mittag-Leffler stability are used to describe the estimation error of observers by the Lyapunov directed method. The stability in the sense of Mittag-Leffler embodies properties of fractional calculus.

## Data Availability

The data supporting the conclusions of our manuscript are some open access articles that have been properly cited, and the readers can easily obtain these articles to verify the conclusions, replicate the analysis, and conduct secondary analyses. Therefore, we do not create a publicly available data repository.

## Conflicts of Interest

The authors declare that they have no conflicts of interest.

## Acknowledgments

This work was supported in part by the Natural Science Foundation of China under Grant 61873144 and Shandong Province under Grant ZR2017MF016 and in the other part by the Natural Science Fundamental Research Project of Jiangsu Colleges and Universities under Grant 17KJB120002, the Natural Science Foundation of Jiangsu Province under Grant BK20170291, and the National Natural Science Foundation of China under Grant 61703059.

## References

- [1] W. Chen, W.-T. Chen, M. Saif, M.-F. Li, and H. Wu, "Simultaneous fault isolation and estimation of lithium-ion batteries via synthesized design of Luenberger and learning observers," *IEEE Transactions on Control Systems Technology*, vol. 22, no. 1, pp. 290–298, 2014.
- [2] R. Razavi-Far, S. Chakrabarti, and M. Saif, "Multi-step-ahead prediction techniques for Lithium-ion batteries condition prognosis," in *Proceedings of the 2016 IEEE International Conference on Systems, Man, and Cybernetics (SMC)*, pp. 004675–004680, Budapest, Hungary, October 2016.
- [3] M. F. Samadi and M. Saif, "Identifiability analysis of an electrochemical model of li-ion battery," in *Proceedings of the 2016 American Control Conference, ACC 2016*, pp. 3107–3112, Boston, Mass, USA, July 2016.
- [4] M. F. Samadi and M. Saif, "Health monitoring of Li-ion batteries: A particle filtering approach," in *Proceedings of the 2015 IEEE*

- 24th International Symposium on Industrial Electronics (ISIE), pp. 831–836, Buzios, Rio de Janeiro, Brazil, June 2015.
- [5] M. F. Samadi and M. Saif, “State-Space Modeling and Observer Design of Li-Ion Batteries Using Takagi-Sugeno Fuzzy System,” *IEEE Transactions on Control Systems Technology*, vol. 25, no. 1, pp. 301–308, 2017.
  - [6] S. M. M. Alavi, M. F. Samadi, and M. Saif, “Diagnostics in lithium-ion batteries: Challenging issues and recent achievements,” in *Integration of Practice-Oriented Knowledge Technology: Trends and Prospectives*, pp. 277–291, Springer, Berlin, Germany, 2013.
  - [7] M. F. Samadi and M. Saif, “Integrated battery management system,” in *Integrated Systems: Innovations and Applications*, M. Fathi, Ed., pp. 173–193, Springer, Cham, Switzerland, 2015.
  - [8] T. Shen, J. Xin, and J. Huang, “Time-space fractional stochastic Ginzburg-Landau equation driven by gaussian white noise,” *Stochastic Analysis and Applications*, vol. 36, no. 1, pp. 103–113, 2018.
  - [9] I. Podlubny, *Fractional Differential Equations*, vol. 198 of *Mathematics in Science and Engineering*, Academic Press, San Diego, Calif, USA, 1999.
  - [10] R. L. Magin, *Fractional Calculus in Bioengineering*, Begell House, Redding, Calif, USA, 2006.
  - [11] N. Laskin, “Fractional market dynamics,” *Physica A: Statistical Mechanics and its Applications*, vol. 287, no. 3-4, pp. 482–492, 2000.
  - [12] K. M. Zhang, “On a sign-changing solution for some fractional differential equations,” *Boundary Value Problems*, vol. 2017, no. 59, 8 pages, 2017.
  - [13] J. Liu and Z. Zhao, “Multiple solutions for impulsive problems with non-autonomous perturbations,” *Applied Mathematics Letters*, vol. 64, pp. 143–149, 2017.
  - [14] Q. Feng and F. Meng, “Traveling wave solutions for fractional partial differential equations arising in mathematical physics by an improved fractional Jacobi elliptic equation method,” *Mathematical Methods in the Applied Sciences*, vol. 40, no. 10, pp. 3676–3686, 2017.
  - [15] A. M. El-Sayed, “Fractional-order diffusion-wave equation,” *International Journal of Theoretical Physics*, vol. 35, no. 2, pp. 311–322, 1996.
  - [16] Y. Guan, Z. Zhao, and X. Lin, “On the existence of positive solutions and negative solutions of singular fractional differential equations via global bifurcation techniques,” *Boundary Value Problems*, vol. 2016, no. 1, article 141, 2016.
  - [17] H. Liu and F. Meng, “Some new generalized Volterra-Fredholm type discrete fractional sum inequalities and their applications,” *Journal of Inequalities and Applications*, vol. 2016, no. 1, article 213, 2016.
  - [18] J. Sabatier, M. Aoun, A. Oustaloup, G. Grégoire, F. Ragot, and P. Roy, “Fractional system identification for lead acid battery state of charge estimation,” *Signal Processing*, vol. 86, no. 10, pp. 2645–2657, 2006.
  - [19] J. Sabatier, M. Cugnet, S. Laruelle et al., “A fractional order model for lead-acid battery crankability estimation,” *Communications in Nonlinear Science and Numerical Simulation*, vol. 15, no. 5, pp. 1308–1317, 2010.
  - [20] H. Wu, S. Yuan, and C. Yin, “A Lithium-Ion battery fractional order state space model and its time domain system identification,” in *Proceedings of the FISITA 2012 World Automotive Congress*, vol. 192 of *Lecture Notes in Electrical Engineering*, pp. 795–805, Springer Berlin Heidelberg, Berlin, Germany, 2013.
  - [21] C. Zou, L. Zhang, X. Hu, Z. Wang, T. Wik, and M. Pecht, “A review of fractional-order techniques applied to lithium-ion batteries, lead-acid batteries, and supercapacitors,” *Journal of Power Sources*, vol. 390, pp. 286–296, 2018.
  - [22] S. M. M. Alavi, C. R. Birkl, and D. A. Howey, “Time-domain fitting of battery electrochemical impedance models,” *Journal of Power Sources*, vol. 288, pp. 345–352, 2015.
  - [23] J. Zhang and J. Lee, “A review on prognostics and health monitoring of Li-ion battery,” *Journal of Power Sources*, vol. 196, no. 15, pp. 6007–6014, 2011.
  - [24] A. T. Stamps, C. E. Holland, R. E. White, and E. P. Gatzke, “Analysis of capacity fade in a lithium ion battery,” *Journal of Power Sources*, vol. 150, no. 1-2, pp. 229–239, 2005.
  - [25] K. W. E. Cheng, B. P. Divakar, H. Wu, K. Ding, and H. F. Ho, “Battery-management system (BMS) and SOC development for electrical vehicles,” *IEEE Transactions on Vehicular Technology*, vol. 60, no. 1, pp. 76–88, 2011.
  - [26] A. Sidhu, A. Izadian, and S. Anwar, “Adaptive nonlinear model-based fault diagnosis of li-ion batteries,” *IEEE Transactions on Industrial Electronics*, vol. 62, no. 2, pp. 1002–1011, 2015.
  - [27] M. U. Cuma and T. Koroglu, “A comprehensive review on estimation strategies used in hybrid and battery electric vehicles,” *Renewable & Sustainable Energy Reviews*, vol. 42, pp. 517–531, 2015.
  - [28] S. Dey and B. Ayalew, “A diagnostic scheme for detection, isolation and estimation of electrochemical faults in Lithium-Ion cells,” in *Proceedings of the ASME 2015 Dynamic Systems and Control Conference*, 10 pages, Columbus, Ohio, USA.
  - [29] S. Kong, M. Saif, and B. Liu, “Observer design for a class of nonlinear fractional-order systems with unknown input,” *Journal of The Franklin Institute*, vol. 354, no. 13, pp. 5503–5518, 2017.
  - [30] E. A. Boroujeni and H. R. Momeni, “Non-fragile nonlinear fractional order observer design for a class of nonlinear fractional order systems,” *Signal Processing*, vol. 92, no. 10, pp. 2365–2370, 2012.
  - [31] I. N’Doye, M. Darouach, H. Voos, and M. Zasadzinski, “Design of unknown input fractional-order observers for fractional-order systems,” *International Journal of Applied Mathematics and Computer Science*, vol. 23, no. 3, pp. 491–500, 2013.
  - [32] Y.-H. Lan and Y. Zhou, “Non-fragile observer-based robust control for a class of fractional-order nonlinear systems,” *Systems & Control Letters*, vol. 62, no. 12, pp. 1143–1150, 2013.
  - [33] P. Gong and W. Lan, “Adaptive robust tracking control for uncertain nonlinear fractional-order multi-agent systems with directed topologies,” *Automatica*, vol. 92, pp. 92–99, 2018.
  - [34] A. Aribi, C. Farges, M. Aoun, P. Melchior, S. Najjar, and M. N. Abdelkrim, “Fault detection based on fractional order models: Application to diagnosis of thermal systems,” *Communications in Nonlinear Science and Numerical Simulation*, vol. 19, no. 10, pp. 3679–3693, 2014.
  - [35] I. N’Doye and T.-M. Laleg-Kirati, “Fractional-order adaptive fault estimation for a class of nonlinear fractional-order systems,” in *Proceedings of the 2015 American Control Conference, ACC 2015*, pp. 3804–3809, Chicago, Ill, USA, July 2015.
  - [36] J. C. Trigeassou, N. Maamri, J. Sabatier, and A. Oustaloup, “A Lyapunov approach to the stability of fractional differential equations,” *Signal Processing*, vol. 91, no. 3, pp. 437–445, 2011.
  - [37] X. Lin, Z. Zhao, and Y. Guan, “Iterative Technology in a Singular Fractional Boundary Value Problem with  $q$ -Difference,” *Applied Mathematics*, vol. 07, no. 01, pp. 91–97, 2016.

- [38] J. C. Trigeassou, N. Maamri, J. Sabatier, and A. Oustaloup, "State variables and transients of fractional order differential systems," *Computers & Mathematics with Applications*, vol. 64, no. 10, pp. 3117–3140, 2012.
- [39] S. Kong, M. Saif, and H. Zhang, "Optimal filtering for Ito-stochastic continuous-time systems with multiple delayed measurements," *Institute of Electrical and Electronics Engineers Transactions on Automatic Control*, vol. 58, no. 7, pp. 1872–1877, 2013.
- [40] D. Wang, J. Zhang, and X. Wang, "Synchronization of uncertain fractional-order chaotic systems with disturbance based on a fractional terminal sliding mode controller," *Chinese Physics B*, vol. 22, no. 4, Article ID 040507, pp. 1–7, 2013.
- [41] M. Corless and J. Tu, "State and input estimation for a class of uncertain systems," *Automatica*, vol. 34, no. 6, pp. 757–764, 1998.
- [42] P. Kudva, N. Viswanadham, and A. Ramakrishna, "Observers for linear systems with unknown inputs," *IEEE Transactions on Automatic Control*, vol. 25, no. 1, pp. 113–115, 1980.
- [43] D. Matignon and B. Andréa-Novel, "Observer-based for fractional differential systems," in *Proceedings of the IEEE Conference on Decision and Control*, pp. 4967–4972, San Diego, Calif, USA, 1997.
- [44] Y. Li, Y. Chen, and I. Podlubny, "Mittag-Leffler stability of fractional order nonlinear dynamic systems," *Automatica*, vol. 45, no. 8, pp. 1965–1969, 2009.
- [45] J. M. Yu, H. Hu, S. B. Zhou, and X. R. Lin, "Generalized Mittag-Leffler stability of multi-variables fractional order nonlinear systems," *Automatica*, vol. 49, no. 6, pp. 1798–1803, 2013.
- [46] M. A. Duarte-Mermoud, N. Aguila-Camacho, J. A. Gallegos, and R. Castro-Linares, "Using general quadratic LYapunov functions to prove LYapunov uniform stability for fractional order systems," *Communications in Nonlinear Science and Numerical Simulation*, vol. 22, no. 1-3, pp. 650–659, 2015.
- [47] K. Diethelm, N. J. Ford, and A. D. Freed, "A predictor-corrector approach for the numerical solution of fractional differential equations," *Nonlinear Dynamics*, vol. 29, no. 1–4, pp. 3–22, 2002.
- [48] K. Diethelm, N. J. Ford, and A. D. Freed, "Detailed error analysis for a fractional Adams method," *Numerical Algorithms*, vol. 36, no. 1, pp. 31–52, 2004.
- [49] P. Ivo, *Fractional-Order Nonlinear Systems: Modeling, Analysis and Simulation*, Springer, Berlin, Germany, 2011.

## Research Article

# Bipartite Consensus for Multiagent Systems via Event-Based Control

Cui-Qin Ma <sup>1</sup> and Wei-Guo Sun<sup>2</sup>

<sup>1</sup>School of Mathematical Sciences, Qufu Normal University, Qufu 273165, Shandong, China

<sup>2</sup>Wucheng No. 2 Middle School, Wucheng 253300, Shandong, China

Correspondence should be addressed to Cui-Qin Ma; [cuiqinma@amss.ac.cn](mailto:cuiqinma@amss.ac.cn)

Received 5 September 2018; Accepted 25 September 2018; Published 24 October 2018

Guest Editor: Weihai Zhang

Copyright © 2018 Cui-Qin Ma and Wei-Guo Sun. This is an open access article distributed under the Creative Commons Attribution License, which permits unrestricted use, distribution, and reproduction in any medium, provided the original work is properly cited.

This paper studies bipartite consensus for first-order multiagent systems. To improve resource utilization, event-based protocols are considered for bipartite consensus. A new type of control gain is designed in the proposed protocols. By appropriate selection of control gains, the convergence rate of the closed-loop system can be adjusted. Firstly, for structural balance case, necessary and sufficient conditions are given on communication relations and consensus gains to achieve bipartite consensus. Secondly, for structural unbalance case, necessary and sufficient conditions are proposed to ensure the stabilizing of the system. It can be found that the system will not show Zeno behavior. Numerical simulations are used to demonstrate the theoretical results.

## 1. Introduction

Consensus problem is one of the hot topics in coordination of multiagent systems (MASs). In the last few years, research on consensus has received considerable attention [1–9]. Consensus means that agents can reach a common value through cooperative relations among agents. However, in real applications, not only cooperative but also competitive relations among agents exist. In these circumstances, bipartite consensus is studied [10–20]. Based on the cooperation and competition among agents, bipartite consensus can be achieved if agents agree upon a certain value with the same quantity and different signs. In [10], necessary and sufficient conditions for bipartite consensus of the single-integrator MASs are given. In [12], the communication condition is first reduced to be containing a spanning tree. In [14], the communication topology is extended to the time-varying case. In [15–20], bipartite consensus with measurement noise is considered.

It is worth pointing out that the above literature adopts a time-driven control pattern, where the state of the agents is monitored continuously and the control law updates are done at any moment. In practical implementation, the embedded

processors are often resource-limited and thus an event-based control fashion is more beneficial in MASs. For conventional consensus of MASs, an event-based control fashion was thoroughly studied [21–31]. In the pioneering work [21], an event-based feedback protocol was proposed. In [23], the event-based protocols for both fixed and switching topologies have been considered. In [25], the self-triggered protocol of MASs was taken into account. Then, in [28], a new event-based protocol for average consensus of MASs was proposed and continuous monitoring of agents' states was not required. The event-based consensus for general linear MASs can be found in [29–31]. Despite these productive results, works on bipartite consensus with event-based control strategy are still rare.

In this paper, we consider event-based bipartite consensus for first-order MASs. In contrast to [32, 33], a new function is introduced into the event-based protocol, such that the Laplacian-like event-based bipartite consensus protocols in [32, 33] are special cases of this paper. Due to the new function gain, the closed-loop system is time-varying. By use of state transition matrix, the closed-loop system is analyzed. For structural balance case, necessary and sufficient conditions are given on communication relations and consensus gains

to achieve bipartite consensus. For structural unbalance case, necessary and sufficient conditions are proposed to ensure the MAS stabilizing.

*Organization.* In Section 2, we give some basic concepts on signed graph and formulate the problem. In Section 3, we prove the main results. In Section 4, we show the validity of theoretical analysis through the simulation results. In Section 5, we conclude this paper and put forward further research directions.

*Notation.*  $R^{n \times m}$  represents all real matrices of  $n \times m$  order.  $\mathbf{0}$  denotes vector or matrix whose elements are 0.  $\mathbf{1}_n$  represents column vector whose elements are 1.  $\text{sgn}(\cdot)$  represents sign function.

## 2. Problem Formulation

The communication relations among  $N$  agents are expressed by the signed digraph  $\mathcal{G} = (\mathcal{V}, \mathcal{E}, \mathcal{A})$ , where  $\mathcal{V} = \{1, \dots, N\}$  is the node set and  $\mathcal{E}$  is the edge set.  $\mathcal{A} = (a_{ij}) \in R^{N \times N}$  is the weighted adjacency matrix of  $\mathcal{G}$ , where  $a_{ij} > 0$  and  $a_{ij} < 0$  represent competition relationship and cooperation relationship between  $i$  and  $j$ , respectively. Throughout this paper, we always assume that  $a_{ij} \neq 0 \iff (j, i) \in \mathcal{E}$ ,  $a_{ii} = 0$ , and  $a_{ij}a_{ji} \geq 0, \forall i, j \in \mathcal{V}$ .  $\mathcal{L} = \mathcal{C}_r - \mathcal{A}$  is the Laplacian of  $\mathcal{G}$ , where  $\mathcal{C}_r = \text{diag}(\sum_{p=1}^N |a_{1p}|, \dots, \sum_{p=1}^N |a_{Np}|)$ .  $\mathcal{G} = (\mathcal{V}, \mathcal{E}, \mathcal{A})$  is structurally balanced if  $\mathcal{V}$  can be divided into two subsets  $\mathcal{V}_1, \mathcal{V}_2, \mathcal{V}_1 \cup \mathcal{V}_2 = \mathcal{V}, \mathcal{V}_1 \cap \mathcal{V}_2 = \emptyset$ , satisfying  $a_{ij} \geq 0$  for  $\forall i, j \in \mathcal{V}_t (t \in \{1, 2\})$ , and  $a_{ij} \leq 0$  for  $\forall i \in \mathcal{V}_t, j \in \mathcal{V}_e (t \neq e \in \{1, 2\})$ .  $\mathcal{G}$  is structurally unbalanced otherwise.

Consider an MAS with  $N$  agents, whose dynamics obey the following equation:

$$\dot{x}_i(t) = u_i(t), \quad i = 1, \dots, N, \quad (1)$$

where  $x_i(t) \in R$  and  $u_i(t) \in R$  are the state and control input of the  $i$ th agent.

We use  $\mathcal{G} = (\mathcal{V}, \mathcal{E}, \mathcal{A})$  to express the communication relations among the  $N$  agents.

Considering the limit resources, people would like to reduce the frequency of control law updates. In this case, an event-based control law is more favorable. Our aim here is to provide an event-based control in order that all agents' states converge to values with the same modulus and different signs regardless of initial states.

To achieve this goal, we assume that each agent only updates its control law at discrete times indexed by  $t_0, t_1, \dots$ . We define the event-based control as follows:

$$u_i(t) = c(t) \sum_{j=1}^N |a_{ij}| \left[ \text{sgn}(a_{ij}) x_j(t_l) - x_i(t_l) \right], \quad (2)$$

$$\forall t \in [t_l, t_{l+1}),$$

where  $i = 1, \dots, N, l = 0, 1, \dots, c(t) > 0$  is a piecewise continuous function.

*Remark 1.* The control law will be actuated at discrete event times. A proper function  $c(t)$  will be designed to improve the convergence performance of the closed-loop system. In particular, when  $c(t) = 1$ , protocol (2) is reduced to event-based bipartite consensus protocols in [32, 33].

The state measurement error of the  $i$ th agent is denoted by  $\epsilon_i(t) = x_i(t_l) - x_i(t), i = 1, \dots, N, t \in [t_l, t_{l+1}), l = 0, 1, \dots$ . Let  $\Omega(t) = (\epsilon_1(t), \dots, \epsilon_N(t))^T$  and, hence,

$$\dot{X}(t) = -c(t) \mathcal{L}(X(t) + \Omega(t)), \quad (3)$$

where  $X(t) = (x_1(t), \dots, x_N(t))^T$ .

We introduce the following definition to characterize the behavior of (3).

*Definition 2.* System (1) is said to achieve bipartite consensus via event-based protocol  $\mathcal{U} = \{u_i, i = 1, \dots, N\}$ , if for system (1) with any given  $X(0) \in R^N$ , there exists  $f = (f_1, \dots, f_N)^T \in R^N (f_i \in \{\pm 1\}, i = 1, \dots, N)$  and  $\mu^* \in R$  such that  $\lim_{t \rightarrow \infty} \|X(t) - \mu^* f\| = 0$ , where  $\mu^* \in R$  depends on  $X(0)$  and the communication relations among agents.

We provide the following event triggering conditions:

$$|\epsilon_i(t)| \leq M e^{-\gamma t}, \quad i = 1, \dots, N, \quad (4)$$

where  $M > 0, 0 < \gamma < \min_{\lambda(L) \neq 0} \{\text{Re} \lambda(\mathcal{L})\}$ .

When the measurement error  $\epsilon_i(t)$  is over the threshold, the controller is triggered and updates itself. To analyze (3), we introduce assumptions as follows:

(T<sub>1</sub>)  $\mathcal{G} = (\mathcal{V}, \mathcal{E}, \mathcal{A})$  is structurally balanced.

(T<sub>2</sub>)  $\mathcal{G} = (\mathcal{V}, \mathcal{E}, \mathcal{A})$  contains a spanning tree.

(T<sub>3</sub>)  $\int_0^\infty c(s) ds = \infty$ .

The following lemma is highly related to the subsequent results.

**Lemma 3.** *If system (1) can achieve bipartite consensus via event-based protocol (2), then there exist  $f = (f_1, \dots, f_N)^T \in R^N, f_i \in \{\pm 1\}, i = 1, \dots, N$ , and  $\phi = (\phi_1, \dots, \phi_N)^T \in R^N$ , such that  $\lim_{t \rightarrow \infty} \Theta(t, 0) = f\phi^T$ , where  $\Theta(t, 0)$  is the state transition matrix of (3).*

*Proof.* The proof is omitted due to space limit.  $\square$

## 3. Main Results

The following result is the main result of this section.

**Theorem 4.** *System (1) can achieve bipartite consensus via event-based protocol (2) if and only if (T<sub>1</sub>), (T<sub>2</sub>), and (T<sub>3</sub>) hold.*

*Proof.*

*Sufficiency.* Assume  $\Theta(t, t_0)$  is the state transition matrix of (3). Then,  $\Theta(t, t_0) = e^{-\int_{t_0}^t c(s) ds \mathcal{L}}$ . Since (T<sub>1</sub>) and (T<sub>2</sub>) hold, Lemma 1 of [17] implies that  $\mathcal{L}$  has exactly one zero

eigenvalue and all nonzero eigenvalues are in the open right half plane. Thus, there exists  $Q$  satisfying

$$Q^{-1}\mathcal{L}Q = B = \text{diag}(0, B_2, \dots, B_w), \quad (5)$$

where  $B_i$  ( $i = 2, \dots, w$ ) is  $R_i \times R_i$  dimensional Jordan block with  $\zeta_i$  on its diagonal,  $R_2 + \dots + R_w = N - 1$ . Obviously,  $\zeta_2, \dots, \zeta_w$  are the eigenvalues of  $\mathcal{L}$ , and  $\text{Re}(\zeta_i) > 0$ ,  $i = 2, \dots, w$ . Combining this, we can get the state transition matrix:

$$\Theta(t, t_0) = Q \text{diag}\left(1, \Theta_{B_2^{\zeta_2}}(t, t_0), \dots, \Theta_{B_w^{\zeta_w}}(t, t_0)\right) Q^{-1}, \quad (6)$$

where  $\Theta_{B_k^{\zeta_k}}$ ,  $k = 2, \dots, w$ , is defined as in Lemma 3 of [17]. Thus, from  $(T_3)$ , we know that  $\lim_{t \rightarrow \infty} \Theta(t, t_0) = Q \text{diag}(1, 0, \dots, 0) Q^{-1}$ . By (3),  $X(t) = \Theta(t, 0)X(0) - X_\Omega$ , where  $X_\Omega = \int_0^t c(s)\Theta(t, s)\mathcal{L}\Omega(s)ds$ . By (6), one has

$$\begin{aligned} X_\Omega \\ = Q \int_0^t c(s) \text{diag}\left(1, \Theta_{B_2^{\zeta_2}}(t, s), \dots, \Theta_{B_w^{\zeta_w}}(t, s)\right) Q^{-1} \mathcal{L}\Omega(s) ds. \end{aligned} \quad (7)$$

Furthermore, by (5), one gets

$$Q^{-1}\mathcal{L}\Omega(s) = \text{diag}(0, B_2, \dots, B_w) Q^{-1}\Omega(s). \quad (8)$$

Assume  $Q^{-1} = (Q_{ij})$ . Then,  $Q^{-1}\Omega(s) = (\sum_{j=1}^N Q_{1j}\epsilon_j(s), \dots, \sum_{j=1}^N Q_{Nj}\epsilon_j(s))^T$ . This together with (8) gives

$$Q^{-1}\mathcal{L}\Omega(s) = (0, \Omega_2^*(s), \dots, \Omega_N^*(s))^T, \quad (9)$$

where  $\Omega_i^*(s)$  ( $i = 2, \dots, N$ ) is the linear combination of  $\zeta_2, \dots, \zeta_w$  and  $\sum_{j=1}^N Q_{kj}\epsilon_j(s)$ ,  $k = 1, \dots, N$ . Then, by (4), there must exist  $q^* > 0$ , such that

$$|\Omega_i^*(s)| \leq q^* e^{-\gamma s}, \quad i = 2, \dots, N. \quad (10)$$

Considering the specific form of  $\Theta_{B_i^{\zeta_i}}(t, s)$  ( $i = 2, \dots, w$ ) in Lemma 3 of [17], we get that  $X_\Omega = Q(0, \Lambda_2^\Omega(s), \dots, \Lambda_N^\Omega(s))^T$ , where  $\Lambda_p^\Omega(s)$  ( $p = 2, \dots, N$ ) is the linear combination of  $\int_0^t c(s)e^{-\zeta_i s} \int_s^t c(\tau)d\tau \left(\int_s^t c(\tau)d\tau\right)^m \Omega_q^*(s)ds$ ,  $m = 0, 1, \dots, R_i - 1$ ;  $i = 2, \dots, w$ ;  $q = 2, \dots, N$ .

By direct calculation, one obtains that

$$\begin{aligned} \lim_{t \rightarrow \infty} \int_0^t c(s) e^{-\zeta_i \int_s^t c(\tau)d\tau} \left(\int_s^t c(\tau) d\tau\right)^m e^{-\gamma s} ds \\ = \lim_{t \rightarrow \infty} \frac{m!}{\zeta_i^{m+1} e^{\gamma t}} = 0, \quad m = 0, 1, \dots, R_i - 1. \end{aligned} \quad (11)$$

This together with (10) leads to

$$\begin{aligned} \lim_{t \rightarrow \infty} \int_0^t c(s) e^{-\zeta_i \int_s^t c(\tau)d\tau} \left(\int_s^t c(\tau) d\tau\right)^m \Omega_q^*(s) ds = 0, \\ m = 0, 1, \dots, R_i - 1. \end{aligned} \quad (12)$$

Therefore,  $\lim_{t \rightarrow \infty} X_\Omega = 0$ , and thus  $\lim_{t \rightarrow \infty} X(t) = Q \text{diag}(1, 0, \dots, 0) Q^{-1} X(0) = Q_c Q_r^T X(0)$ , where  $Q_c$  is the first

column of  $Q$ ,  $Q_r^T$  is the first row of  $Q^{-1}$ , and  $Q_r^T Q_c = 1$ . By (5), one gets that  $\mathcal{L}Q_c = Q_r^T \mathcal{L} = 0$ . From  $(T_1)$ , we know that there exists  $f$  such that  $\mathcal{L}f = 0$ . Since the eigenspace corresponding to eigenvalue 0 is 1 dimensional,  $Q_c = m_0 f$ , where  $m_0 \neq 0$  is a constant. Denote  $\mu^* = m_0 Q_r^T X(0)$ . Then,  $\lim_{t \rightarrow \infty} X(t) = \mu^* f$  and  $\mu^*$  depends on  $X(0)$  and communication relations among agents. Therefore, Sufficiency holds.

*Necessity.* Assume by contradiction that  $(T_3)$  does not hold. Without loss of generality, let  $\int_0^\infty c(s)ds = \bar{c} > 0$ . Then,  $\lim_{t \rightarrow \infty} \Theta(t, 0) = e^{-\bar{c}\mathcal{L}}$ . It is an invertible matrix and thus  $\text{rank}(\lim_{t \rightarrow \infty} \Theta(t, 0)) = N$ . This contradicts Lemma 3. Therefore,  $(T_3)$  holds. Next, we prove that  $\mathcal{L}$  has exactly one zero eigenvalue. If 0 is not eigenvalue  $\mathcal{L}$ , then  $\lim_{t \rightarrow \infty} \Theta(t, 0) = 0$ . This implies that  $\lim_{t \rightarrow \infty} X(t)$  is independent of  $X(0)$ . It contradicts Definition 2. Thus, 0 is eigenvalue  $\mathcal{L}$ . If the geometric multiplicity of eigenvalue 0 is less than the algebraic multiplicity of 0, then by  $(T_3)$  and direct calculation, one has the notion that  $\lim_{t \rightarrow \infty} \Theta(t, 0)$  does not exist. It is a contradiction with Lemma 3. So, the geometric multiplicity equals the algebraic multiplicity of eigenvalue 0. Assume 0 is  $p$  dimensional and  $p > 1$ . Then, with abuse of notation,  $Q^{-1}\mathcal{L}Q = \text{diag}(\underbrace{0, \dots, 0}_p, B_{p+1}, \dots, B_w)$ . Hence,  $\lim_{t \rightarrow \infty} \Theta(t, 0) =$

$Q \text{diag}(\underbrace{1, \dots, 1}_p, \Theta_{B_{p+1}^{\zeta_{p+1}}}(t, 0), \dots, \Theta_{B_w^{\zeta_w}}(t, 0)) Q^{-1}$  and  $\text{rank}(\lim_{t \rightarrow \infty} \Theta(t, 0)) = p > 1$ . This contradicts Lemma 3. So,  $p = 1$ ; i.e.,  $\mathcal{L}$  has exactly one zero eigenvalue. With abuse of notation, (5) and (6) hold. Noticing Lemma 3, one gets  $Q \text{diag}(1, 0, 0, \dots, 0) Q^{-1} = f\phi^T$ . Therefore,  $Q_c = fm_1$ , where  $m_1 = \phi^T Q_c \neq 0$ . Since  $\mathcal{L}Q_c = 0$ ,  $\mathcal{L}f = 0$ . By the definition of Laplacian  $\mathcal{L}$ , for any  $q$ , one gets  $f_q \sum_{k \neq q} |a_{qk}| = f_k a_{qk}$ ,  $q = 1, \dots, N$ . Noticing  $f_q = \pm 1$ , one has  $f_q f_k a_{qk} = |a_{qk}| \geq 0$ . Let  $V_1 = \{q \mid f_q = 1\}$  and  $V_2 = \{q \mid f_q = -1\}$ ; then  $V_1 \cap V_2 = \emptyset$ ,  $V_1 \cup V_2 = V$ . If  $q \in \mathcal{V}_j$ ,  $j \in \{1, 2\}$ ,  $a_{qk} \geq 0, k \in \mathcal{V}_j$  or  $a_{qk} \leq 0, k \in \mathcal{V}_r, r \neq j, r \in \{1, 2\}$ . By definition,  $\mathcal{G}$  is structurally balanced; i.e.,  $(T_1)$  holds. From Lemma 1 of [17],  $\mathcal{G}$  has a spanning tree; i.e.,  $(T_2)$  holds.  $\square$

*Remark 5.* From (11), one obtains that the convergence rate of the closed-loop system is closely related to eigenvalues of  $\mathcal{L}$  and the rate of  $\int_0^t c(s)ds$  converging to infinity. It follows that, by appropriate selection of  $c(t)$ , the convergence rate of (3) can be adjusted.

From Theorem 4, we can see that structural balance is a necessary and sufficient condition to ensure bipartite consensus. When  $\mathcal{G}$  is structurally unbalanced, we investigate the evolution of the MAS:

$(T'_1)$   $\mathcal{G} = (\mathcal{V}, \mathcal{E}, \mathcal{A})$  is structurally unbalanced.

$(T'_2)$   $\mathcal{G} = (\mathcal{V}, \mathcal{E}, \mathcal{A})$  does not contain structurally balanced input solitary subgraphs.

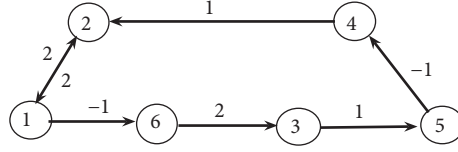
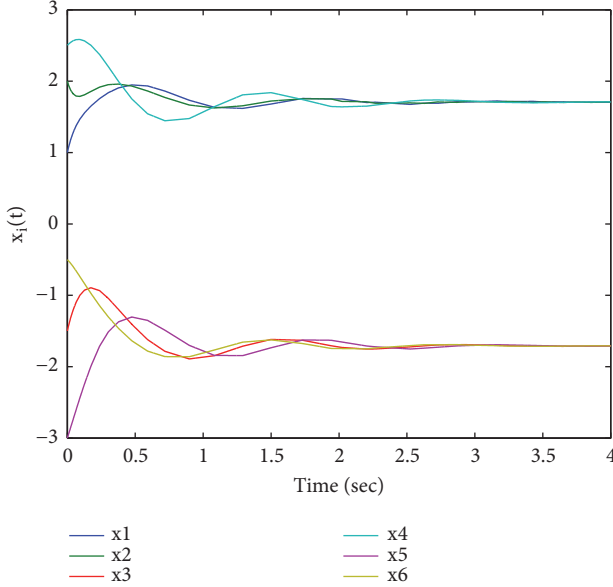
FIGURE 1: The communication relations  $\mathcal{G}_1$ .

FIGURE 2: Evolution of the states for six agents.

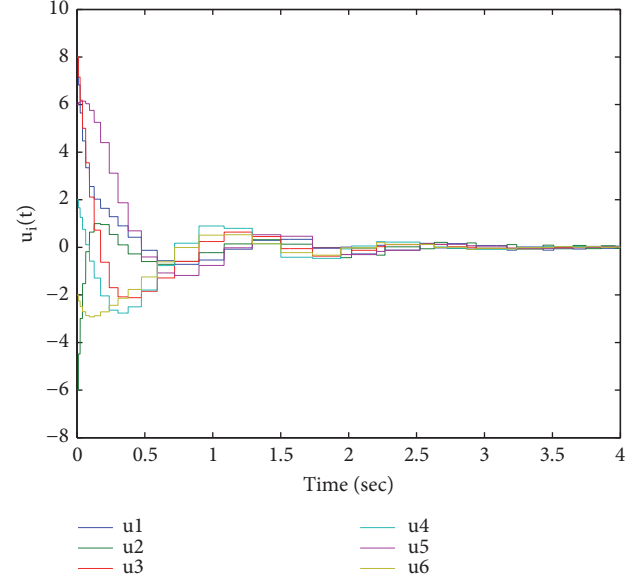


FIGURE 3: Evolution of control inputs for six agents.

An input solitary subgraph of  $\mathcal{G}$  indicates that agents of the subgraph cannot obtain information from other agents of  $\mathcal{G}$ .

**Theorem 6.** System (2) can be stabilizing via event-based protocol (2), i.e.,  $\lim_{t \rightarrow \infty} X(t) = 0$  if and only if  $(\mathbf{T}'_1)$ ,  $(\mathbf{T}'_2)$ , and  $(\mathbf{T}_3)$  hold.

*Proof.*

*Necessity.* The necessity is similar to the proof of Theorem 4.

*Sufficiency.* From  $(\mathbf{T}'_1)$ ,  $(\mathbf{T}'_2)$ , and Lemma 2 of [17], we can see that all eigenvalues of  $\mathcal{L}$  have positive real parts. Since  $(\mathbf{T}_3)$  holds, one has  $\lim_{t \rightarrow \infty} X(t) = 0$  by repeating the sufficiency proof of Theorem 4.  $\square$

#### 4. Numerical Simulation

*Example 1.* Six agents' communication relations are expressed by Figure 1, where  $\mathcal{G}_1 = (\mathcal{V}, \mathcal{E}_1, \mathcal{A}_1)$ ,  $\mathcal{V} = \{1, \dots, 6\}$ ,  $a_{12} = a_{21} = a_{36} = 2$ ,  $a_{45} = a_{61} = -1$ , and  $a_{24} = a_{53} = 1$ . Obviously,  $\mathcal{G}_1$  satisfies assumptions  $(\mathbf{T}_1)$  and  $(\mathbf{T}_2)$ . Laplacian  $\mathcal{L}_1$  has eigenvalues  $\lambda_1(\mathcal{L}_1) = 0$ ,  $\lambda_2(\mathcal{L}_1) = 4.5698$ ,  $\lambda_3(\mathcal{L}_1) = 0.6852 + 0.8449i$ ,  $\lambda_4(\mathcal{L}_1) = 0.6852 - 0.8449i$ ,  $\lambda_5(\mathcal{L}_1) = 2.0299 + 0.5637i$ , and  $\lambda_6(\mathcal{L}_1) = 2.0299 - 0.5637i$  ( $i^2 = -1$ ). It can be seen that 0 is a simple eigenvalue of  $\mathcal{L}_1$ , and  $\min_{\lambda(\mathcal{L}_1) \neq 0} \{\text{Re}\lambda(\mathcal{L}_1)\} = 0.6852$ . Agents' dynamics satisfy (1). Assume  $X(0) = (1, 2, -1.5, 2.5, -3, -0.5)$ . If we choose  $M = 1.5$ ,  $\gamma = 0.65$ , and  $c(t) = 1$  in (2), then  $c(t)$  satisfies  $(\mathbf{T}_3)$  and state trajectories are given in Figure 2. One can find that agents 1, 2, and 4

converge to 1.7 while agents 3, 5, and 6 converge to  $-1.7$ ; i.e., system (1) achieves bipartite consensus via event-based protocol (2). From Figure 3, we know that the inputs are constants between the event triggering time intervals. Furthermore, as shown in Figure 4, error norm of each agent converges to zero. This means that the MAS avoids the Zeno behavior.

*Example 2.* When communication relationship among the six agents is given by  $\mathcal{G}_2 = (\mathcal{V}, \mathcal{E}_2, \mathcal{A}_2)$  as shown in Figure 5, where  $a_{12} = a_{21} = a_{32} = a_{43} = a_{54} = 1$ ,  $a_{13} = a_{31} = -2$  and  $a_{65} = 2$ . Eigenvalues of Laplacian  $\mathcal{L}_2$  are  $\lambda_1(\mathcal{L}_2) = 0.7639$ ,  $\lambda_2(\mathcal{L}_2) = \lambda_3(\mathcal{L}_2) = \lambda_4(\mathcal{L}_2) = 1$ ,  $\lambda_5(\mathcal{L}_2) = 2$ , and  $\lambda_6(\mathcal{L}_2) = 5.2316$ , respectively.  $\mathcal{G}_2$  satisfies  $(\mathbf{T}'_1)$  and  $(\mathbf{T}'_2)$ . It is easy to know that  $\min_{\lambda(\mathcal{L}_2) \neq 0} \{\text{Re}\lambda(\mathcal{L}_2)\} = 0.7639$ . Let  $M = 1.2$ ,  $\gamma = 0.6$ , and  $c(t) = 1$ ; the state trajectories of the MAS can be obtained as shown in Figure 6. All states eventually converge to 0. This is consistent with Theorem 6. The evolution of control input and error norm are shown in Figures 7 and 8, respectively.

#### 5. Conclusion

In this paper, event-driven protocols are considered for bipartite consensus of MASs. Based on them, the number of controller updates is reduced. Under necessary and sufficient conditions on protocol gain and communication

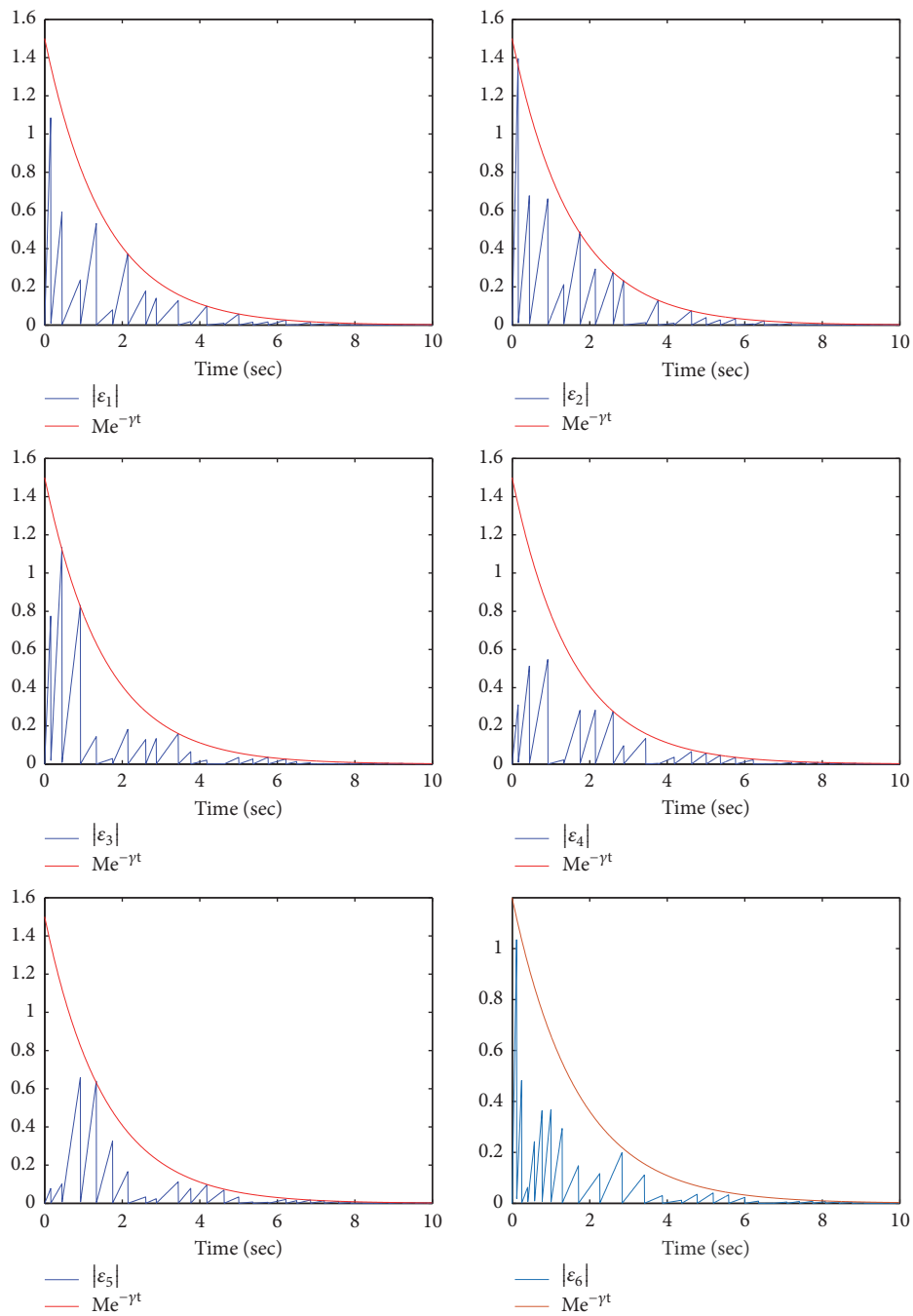


FIGURE 4: Six agents' error norms.

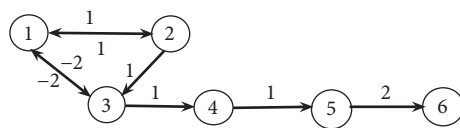
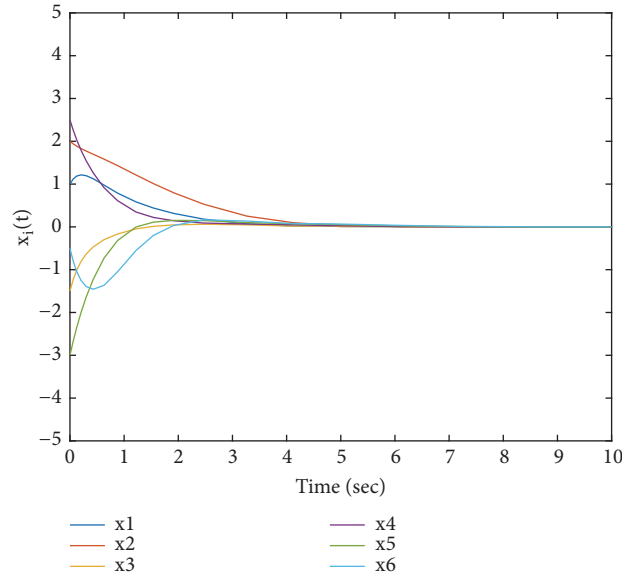
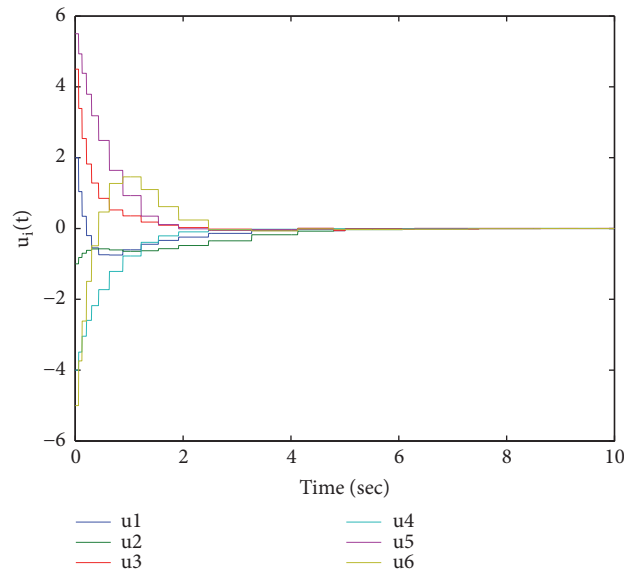


FIGURE 5: The communication relations  $\mathcal{G}_2$ .

FIGURE 6: Six agents' states under  $\mathcal{G}_2$ .FIGURE 7: Six agents' control inputs under  $\mathcal{G}_2$ .

topology, the MAS is shown to reach event-based bipartite consensus. When the graph is structurally unbalanced, the MAS is proved to be stabilizing. The further research is related to MASs with time-varying topology and time delays.

### Data Availability

The MatLab based models used to support the findings of this study are available from the corresponding author upon request.

### Conflicts of Interest

The authors declare that they have no conflicts of interest.

### Acknowledgments

This research was supported by Postgraduate Education Innovation Program of Shandong Province, under Grant no. SDYY16088, and the Young Teacher Capability Enhancement Program for Overseas Study, Qufu Normal University.

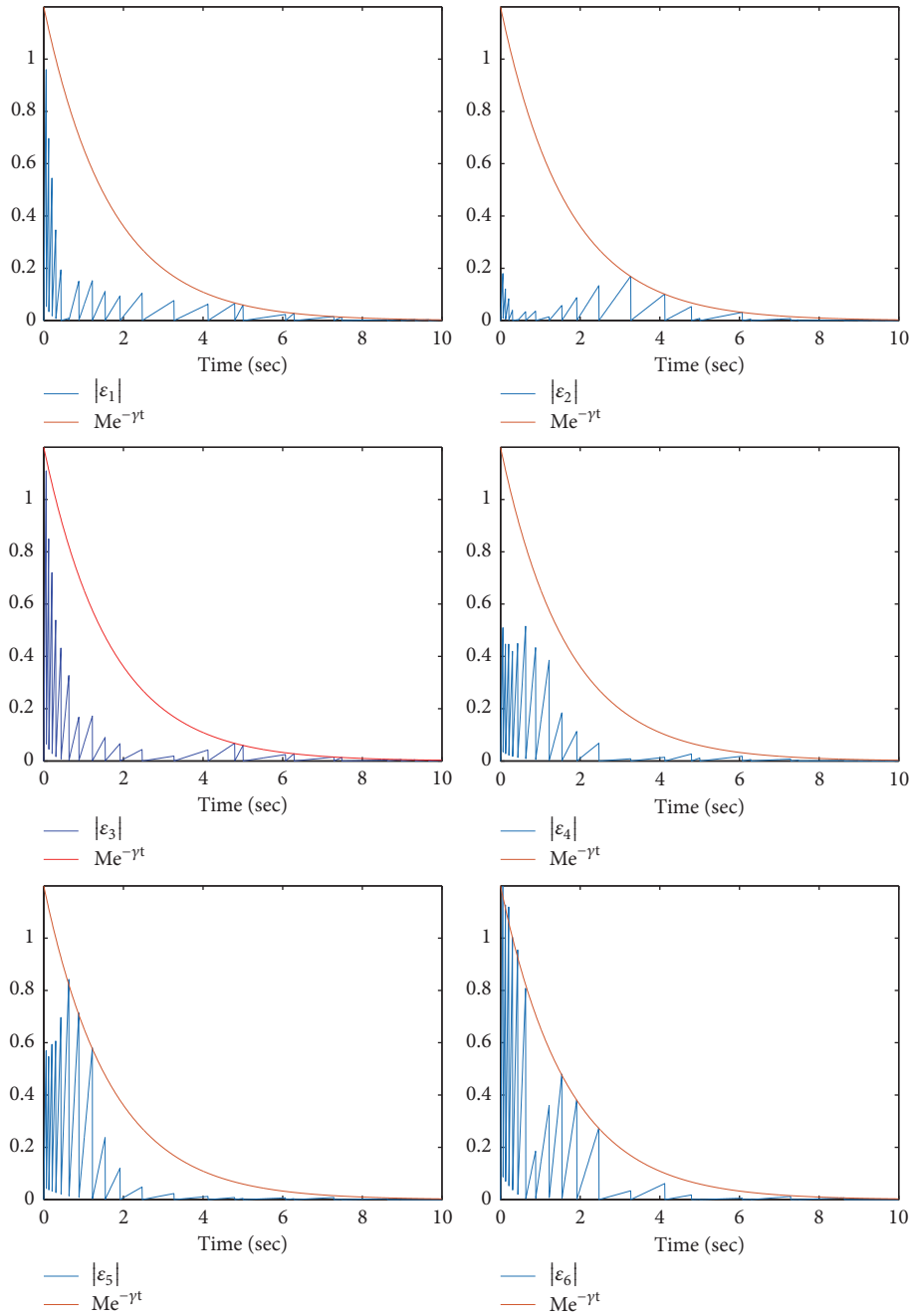


FIGURE 8: Six agents' error norms under  $\mathcal{G}_2$ .

**References**

[1] R. Olfati-Saber and R. M. Murray, "Consensus problems in networks of agents with switching topology and time-delays," *IEEE Transactions on Automatic Control*, vol. 49, no. 9, pp. 1520–1533, 2004.

[2] W. Ren and R. W. Beard, "Consensus seeking in multiagent systems under dynamically changing interaction topologies," *IEEE Transactions on Automatic Control*, vol. 50, no. 5, pp. 655–661, 2005.

[3] C. Q. Ma and J. F. Zhang, "Necessary and sufficient conditions for consensusability of linear multi-agent systems," *IEEE Transactions on Automatic Control*, vol. 55, no. 5, pp. 1263–1268, 2010.

[4] W. Sun, "Stabilization analysis of time-delay Hamiltonian systems in the presence of saturation," *Applied Mathematics and Computation*, vol. 217, no. 23, pp. 9625–9634, 2011.

[5] L. Gao, D. Wang, and G. Wang, "Further results on exponential stability for impulsive switched nonlinear time-delay systems with delayed impulse effects," *Applied Mathematics and Computation*, vol. 268, pp. 186–200, 2015.

- [6] C. Q. Ma, T. Li, and J. F. Zhang, "Consensus control for leader-following multi-agent systems with measurement noises," *Journal of Systems Science and Complexity*, vol. 23, no. 1, pp. 35–49, 2010.
- [7] H. Liu and F. Meng, "Interval oscillation criteria for second-order nonlinear forced differential equations involving variable exponent," *Advances in Difference Equations*, Paper No. 291, 14 pages, 2016.
- [8] J. Guo, L. Y. Wang, G. Yin, Y. Zhao, and J. F. Zhang, "Identification of Wiener systems with quantized inputs and binary-valued output observations," *Automatica*, vol. 78, pp. 280–286, 2017.
- [9] C. Q. Ma and J. F. Zhang, "On formability of linear continuous multi-agent systems," *Journal of Systems Science and Complexity*, vol. 25, no. 1, pp. 13–29, 2012.
- [10] C. Altafini, "Consensus problems on networks with antagonistic interactions," *IEEE Transactions on Automatic Control*, vol. 58, no. 4, pp. 935–946, 2013.
- [11] Z. Zheng, "Invariance of deficiency indices under perturbation for discrete Hamiltonian systems," *Journal of Difference Equations and Applications*, vol. 19, no. 8, pp. 1243–1250, 2013.
- [12] J. Hu and W. X. Zheng, "Emergent collective behaviors on cooperation networks," *Physics Letters A*, vol. 378, no. 26–27, pp. 1787–1796, 2014.
- [13] W. Sun and L. Peng, "Observer-based robust adaptive control for uncertain stochastic Hamiltonian systems with state and input delays," *Nonlinear Analysis: Modelling and Control*, vol. 19, no. 4, pp. 626–645, 2014.
- [14] A. V. Proskurnikov, A. S. Matveev, and M. Cao, "Opinion dynamics in social networks with hostile camps: consensus vs. polarization," *IEEE Transactions on Automatic Control*, vol. 61, no. 6, pp. 1524–1536, 2016.
- [15] C. Q. Ma and Z. Y. Qin, "Bipartite consensus on networks of agents with antagonistic interactions and measurement noises," *IET Control Theory & Applications*, vol. 10, no. 17, pp. 2306–2313, 2016.
- [16] L. Zhang and Z. Zheng, "Lyapunov type inequalities for the Riemann-Liouville fractional differential equations of higher order," *Advances in Difference Equations*, no. 270, 20 pages, 2017.
- [17] C. Q. Ma, Z. Y. Qin, and Y. B. Zhao, "Bipartite consensus of integrator multi-agent systems with measurement noise," *IET Control Theory & Applications*, vol. 11, no. 18, pp. 3313–3320, 2017.
- [18] Z. Zheng and Q. Kong, "Friedrichs extensions for singular Hamiltonian operators with intermediate deficiency indices," *Journal of Mathematical Analysis and Applications*, vol. 461, no. 2, pp. 1672–1685, 2018.
- [19] C. Q. Ma and L. Xie, "Necessary and sufficient conditions for leader-following bipartite consensus with measurement noise," *IEEE Transactions on Systems, Man, and Cybernetics: Systems*, pp. 1–6, 2018.
- [20] C. Q. Ma, W. Zhao, and Y. B. Zhao, "Bipartite linear  $\chi$ -consensus of double-integrator multi-agent systems with measurement noise," *Asian Journal of Control*, vol. 20, no. 1, pp. 577–584, 2018.
- [21] P. Tabuada, "Event-triggered real-time scheduling of stabilizing control tasks," *IEEE Transactions on Automatic Control*, vol. 52, no. 9, pp. 1680–1685, 2007.
- [22] J. Gu and F. Meng, "Some new nonlinear Volterra-Fredholm type dynamic integral inequalities on time scales," *Applied Mathematics and Computation*, vol. 245, pp. 235–242, 2014.
- [23] Z. Liu and Z. Chen, "Reaching consensus in networks of agents via event-triggered control," *Journal of Information and Computational Science*, vol. 8, no. 3, pp. 393–402, 2011.
- [24] W. Sun, Y. Wang, and R. Yang, "L2 disturbance attenuation for a class of time delay Hamiltonian systems," *Journal of Systems Science & Complexity*, vol. 24, no. 4, pp. 672–682, 2011.
- [25] D. V. Dimarogonas, E. Frazzoli, and K. H. Johansson, "Distributed event-triggered control for multi-agent systems," *IEEE Transactions on Automatic Control*, vol. 57, no. 5, pp. 1291–1297, 2012.
- [26] J. Guo, B. Mu, L. Y. Wang, G. Yin, and L. Xu, "Decision-based system identification and adaptive resource allocation," *IEEE Transactions on Automatic Control*, vol. 62, no. 5, pp. 2166–2179, 2017.
- [27] J. Cai and Z. Zheng, "Inverse spectral problems for discontinuous Sturm-Liouville problems of Atkinson type," *Applied Mathematics and Computation*, vol. 327, pp. 22–34, 2018.
- [28] G. S. Seyboth, D. V. Dimarogonas, and K. H. Johansson, "Event-based broadcasting for multi-agent average consensus," *Automatica*, vol. 49, no. 1, pp. 245–252, 2013.
- [29] Z. Zhang, F. Hao, L. Zhang, and L. Wang, "Consensus of linear multi-agent systems via event-triggered control," *International Journal of Control*, vol. 87, no. 6, pp. 1243–1251, 2014.
- [30] B. Wang, X. Meng, and T. Chen, "Event based pulse-modulated control of linear stochastic systems," *IEEE Transactions on Automatic Control*, vol. 59, no. 8, pp. 2144–2150, 2014.
- [31] D. Yang, W. Ren, X. Liu, and W. Chen, "Decentralized event-triggered consensus for linear multi-agent systems under general directed graphs," *Automatica*, vol. 69, pp. 242–249, 2016.
- [32] Y. Zhou and J. Hu, "Event-based bipartite consensus on signed networks," in *Proceedings of the 3rd Annual IEEE International Conference on Cyber Technology in Automation, Control, and Intelligent Systems, IEEE-CYBER 2013*, pp. 326–330, China, May 2013.
- [33] J. Zeng, F. Li, J. Qin, and W. X. Zheng, "Distributed event-triggered bipartite consensus for multiple agents over signed graph topology," in *Proceedings of the 2015 34th Chinese Control Conference (CCC)*, pp. 6930–6935, Hangzhou, China, July 2015.

## Research Article

# $H_\infty$ Control for Nonlinear Infinite Markov Jump Systems

Yueying Liu and Ting Hou 

College of Mathematics and Systems Science, Shandong University of Science and Technology, Qingdao 266590, China

Correspondence should be addressed to Ting Hou; ht\_math@sina.com

Received 6 July 2018; Revised 19 September 2018; Accepted 26 September 2018; Published 21 October 2018

Academic Editor: Xue-Jun Xie

Copyright © 2018 Yueying Liu and Ting Hou. This is an open access article distributed under the Creative Commons Attribution License, which permits unrestricted use, distribution, and reproduction in any medium, provided the original work is properly cited.

In this paper, we discuss the infinite horizon  $H_\infty$  control problem for a class of nonlinear stochastic systems with state, control, and disturbance dependent noise. The jumping parameters are modelled as an infinite-state Markov chain. Based on the solvability of a set of coupled Hamilton-Jacobi inequalities (HJIs), the exponential mean square  $H_\infty$  controller for the considered nonlinear stochastic systems is obtained. A numerical example is given to show the effectiveness of the proposed design method.

## 1. Introduction

During the past decades, as one of the most important robust control design,  $H_\infty$  control has been extensively studied in both theory and practical applications [1]. From the time-domain viewpoint,  $H_\infty$  control is to find a control law to eliminate the effect of external disturbance below a given level [2]. Due to the ability to model many real plants in practice, stochastic systems has gained much attention. In particular, stochastic  $H_\infty$  control was firstly investigated in [3] for Itô systems, where a stochastic bounded real lemma was established in the form of linear matrix inequalities. References [4, 5], respectively, studied  $H_\infty$  filtering and control for nonlinear stochastic systems via solving second-order nonlinear HJIs.

Stochastic systems with Markov jumps are powerful tool to describe physical systems which may encounter abrupt changes in their dynamics. In the theoretical study of stochastic Markov jump systems, stability and observability [6–11] and robust control [12–15] have been widely investigated. Recently, stable and control problems for nonlinear systems have become a hot research topic [16–22]. It should be pointed out that most of the aforementioned researches on Markov jump systems assume that Markov chain takes values in a finite set. However, Markov jump systems with infinite-state chains can be used to describe more plants in many real scenarios [23, 24]. Therefore, infinite Markov jump systems deserve our consideration. Recently, some papers

on stability [25–27] and control problems [28, 29] of linear infinite Markov jump systems have appeared. To be specific, infinite horizon  $H_2/H_\infty$  controller has been obtained by four coupled algebraic Riccati equations in [30]. Nevertheless, to the best of our knowledge,  $H_\infty$  control problem for a class of nonlinear stochastic systems with infinite Markov jumps is still unsolved, let alone the case of  $(x, u, v)$ -dependent noise. This situation motivates us to carry out the present research.

This paper is concerned with the infinite horizon  $H_\infty$  control problem for a class of nonlinear stochastic systems with infinite Markov jumps and  $(x, u, v)$ -dependent noise. The rest of the paper is organized as follows. Section 2 provides some useful definitions and lemmas. In Section 3, based on the generalized Itô-type formula and the technique of squares completion, an exponential mean square stable  $H_\infty$  controller is designed in terms of a set of coupled HJIs. And a numerical example is provided to illustrate the applicability of the proposed design approach. Conclusions are made in Section 4.

Next, we adopt the following notations.  $\mathcal{R}$  denotes the set of all real numbers and  $\mathcal{R}_+$  is the set of all nonnegative real numbers.  $\mathcal{R}^n$  and  $\mathcal{R}^{m \times n}$  stand for  $n$ -dimensional real vector space and the vector space of all  $m \times n$  matrices, respectively. For a matrix  $A$ ,  $A'$  represents the transpose and we denote  $A \geq 0$  ( $A > 0$ ) the positive semidefinite (definite) symmetric matrix. Also, we make use of the notation of  $\mathcal{S}_n$  and  $I_n$  for the set of all  $n \times n$  symmetric and identity matrices, respectively. The operator norm of  $\mathcal{R}^{m \times n}$  or the Euclidean norm of  $\mathcal{R}^n$  is

$\|\cdot\|$ . By  $l^2(\mathcal{R}_+; \mathcal{R}^m)$  we define the space of  $\mathcal{R}^m$ -valued, square integrable, and  $\mathcal{F}_t$ -measurable processes  $\zeta = \{\zeta(t, \omega) : \mathcal{R}_+ \times \Omega \rightarrow \mathcal{R}^m\}$  satisfying  $\|\zeta\|^2 = E \int_0^\infty \|\zeta(t)\|^2 dt < \infty$ . The class of functions  $V(x)$  which are twice continuously differential with respect to  $x \in \mathcal{U}$ , except possibly at the point  $x = 0$ , will be denoted by  $C^2(\mathcal{U})$ .  $\mathcal{D} := \{1, 2, \dots\}$ .

## 2. Preliminaries

Consider the following stochastic nonlinear system with infinite Markov jumps:

$$\begin{aligned} dx(t) &= [f_1(x(t), \eta_t) + g_1(x(t), \eta_t)u(t) \\ &\quad + h_1(x(t), \eta_t)v(t)] dt + [f_2(x(t), \eta_t) \\ &\quad + g_2(x(t), \eta_t)u(t) + h_2(x(t), \eta_t)v(t)] dw(t), \end{aligned} \quad (1)$$

$$z(t) = \begin{bmatrix} m(x(t), \eta_t) \\ u(t) \end{bmatrix},$$

$$x(0) = x_0 \in \mathcal{R}^n, \quad t \in \mathcal{R}_+,$$

where  $x(t) \in \mathcal{R}^n$ ,  $v(t) \in \mathcal{R}^{n_v}$ ,  $u(t) \in \mathcal{R}^{n_u}$ , and  $z(t) \in \mathcal{R}^{n_z}$  stand for the system state, exogenous disturbance, control input, and measurement output, respectively.  $w(t)$  is a standard one-dimensional Brownian motion on a probability space  $(\Omega, \mathcal{F}, \mathcal{P})$ . Assume that  $\mathcal{F}_t := \sigma(w(s), 0 \leq s \leq t) \vee \sigma(\eta(s), 0 \leq s \leq t) \vee \mathcal{N}$ , where  $\mathcal{N}$  denotes the totality of  $\mathcal{P}$ -null sets and the  $\sigma$ -algebras  $\sigma(w(s), 0 \leq s \leq t)$  and  $\sigma(\eta(s), 0 \leq s \leq t)$  are mutually independent. We denote  $\{\eta_t\}_{t \in \mathcal{R}_+}$  the right continuous, homogeneous Markov process on  $\Omega$  taking values in the countably infinite state space  $\mathcal{D}$  with generator  $Q = (q_{ij})_{i,j \in \mathcal{D}}$  given by

$$P(\eta_{t+s} = j \mid \eta_t = i) = \begin{cases} q_{ij}s + o(s), & i \neq j, \\ 1 + q_{ii}s + o(s), & i = j, \end{cases} \quad (2)$$

where  $s > 0$ ,  $\lim_{s \rightarrow 0} (o(s)/s) = 0$ ,  $q_{ij} \geq 0 (i, j \in \mathcal{D}, i \neq j)$  is the transition rate from mode  $i$  at time  $t$  to mode  $j$  at time  $t + s$  and  $q_{ii} = -\sum_{j \in \mathcal{D}, j \neq i} q_{ij} < \infty$  for all  $i \in \mathcal{D}$ . Suppose that  $f_1, g_1, h_1, f_2, g_2, h_2$ , and  $m$  satisfy the local Lipschitz condition and the linear growth condition for any  $i \in \mathcal{D}$ , which guarantee that system (1) has a unique strong solution [13, 31]. Moreover, assume  $f_1(0, i) = 0, f_2(0, i) = 0, i \in \mathcal{D}$ .

Denote  $\mathbb{E}_1^{m \times n}$  the Banach space of all sequences  $\{E \mid E = (E(1), E(2), \dots), E(i) \in \mathcal{R}^{m \times n}\}$  with the norm  $\|E\|_1 = \sum_{i=1}^\infty \|E(i)\| < \infty$ . Likewise, define another Banach space  $\mathbb{E}_\infty^{m \times n}$  with the norm  $\|E\|_\infty = \sup_{i \in \mathcal{D}} \|E(i)\|$ . Assume all coefficients of considered systems have a finite norm  $\|\cdot\|_\infty$ . If  $m = n$ ,  $\mathbb{E}_1^{m \times n}$  will be simplified as  $\mathbb{E}_1^n$  and so does  $\mathbb{E}_\infty^{m \times n}$ . When  $E(i) \in S_n$  and  $E(i) \geq 0, i \in \mathcal{D}$ ,  $\mathbb{E}_1^n(\mathbb{E}_\infty^n)$  is written as  $\mathbb{E}_1^{n+}$  (resp.,  $\mathbb{E}_\infty^{n+}$ ). For  $L, M \in \mathbb{E}_1^{n+}$ ,  $L \leq M$  implies that  $L(i) \leq M(i), i \in \mathcal{D}$ . Therefore, we have  $\|L\|_1 \leq \|M\|_1$ .

For each  $V \in C^2(\mathcal{R}^n \times \mathcal{D}; \mathcal{R})$ , an infinitesimal operator  $\mathcal{L}V : \mathcal{R}^n \times \mathcal{D} \rightarrow \mathcal{R}$  associated with system (1) is defined as follows [28, 31]:

$$\begin{aligned} \mathcal{L}V(x(t), i) &= \frac{\partial V(x(t), i)}{\partial x} [f_1(x(t), i) \\ &\quad + g_1(x(t), i)u(t) + h_1(x(t), i)v(t)] \\ &\quad + \sum_{j=1}^\infty q_{ij}V(x(t), j) + \frac{1}{2} \text{trace} \left\{ [f_2(x(t), i) \right. \\ &\quad + g_2(x(t), i)u(t) \\ &\quad + h_2(x(t), i)v(t)]' \frac{\partial^2 V(x(t), i)}{\partial x^2} \\ &\quad \cdot [f_2(x(t), i) + g_2(x(t), i)u(t) \\ &\quad \left. + h_2(x(t), i)v(t)] \right\}, \quad i \in \mathcal{D}. \end{aligned} \quad (3)$$

To study the infinite horizon nonlinear stochastic  $H_\infty$  control, the internal stability requirement is needed; thus we introduce the following definition.

*Definition 1* (see [13]). The unforced stochastic system with infinite Markov jumps,

$$dx(t) = f_1(x(t), \eta_t) dt + f_2(x(t), \eta_t) dw(t), \quad t \in \mathcal{R}_+, \quad (4)$$

is called exponentially mean square stable (EMSS) if there exist  $\alpha > 0$  and  $\beta \geq 1$  such that

$$E[\|x(t)\|^2] \leq \beta e^{-\alpha t} \|x_0\|^2 \quad (5)$$

for all  $t \in \mathcal{R}_+$ ,  $i \in \mathcal{D}$  and  $x_0 \in \mathcal{R}^n$ .

*Definition 2.* For a given  $\gamma > 0$ , the control  $u^*(t) \in l^2(\mathcal{R}_+; \mathcal{R}^{n_u})$  is said to be an infinite horizon  $H_\infty$  control of system (1), if

- (i)  $u^*(t)$  stabilizes system (1) internally; i.e. when  $v(t) = 0, u(t) = u^*(t)$ , the trajectory of system (1) with any initial value  $x(0) = x_0$  is EMSS
- (ii) For any nonzero  $v^*(t) \in l^2(\mathcal{R}_+; \mathcal{R}^{n_v})$  and zero initial state  $x_0 = 0$ , we always have

$$\|z(t)\|_{l^2(\mathcal{R}_+; \mathcal{R}^{n_z})} \leq \gamma \|v(t)\|_{l^2(\mathcal{R}_+; \mathcal{R}^{n_v})}. \quad (6)$$

*Remark 3.* If (6) holds, it is easy to verify that (6) is equivalent to  $\|L_\infty^{u^*}\| \leq \gamma$ , where the perturbation operator  $\|L_\infty^{u^*}\|$  is defined by  $L_\infty^{u^*} : l^2(\mathcal{R}_+; \mathcal{R}^{n_v}) \rightarrow l^2(\mathcal{R}_+; \mathcal{R}^{n_z})$  subject to system (1) with

$$\|L_\infty^{u^*}\| := \sup_{\substack{v(\cdot) \in l^2(\mathcal{R}_+; \mathcal{R}^{n_v}), v \neq 0 \\ \eta_0 \in \mathcal{D}, x_0 = 0}} \frac{\|z(t)\|_{l^2(\mathcal{R}_+; \mathcal{R}^{n_z})}}{\|v(t)\|_{l^2(\mathcal{R}_+; \mathcal{R}^{n_v})}}. \quad (7)$$

We provide some lemmas which are absolutely necessary to derive our main results.

**Lemma 4** (see [32]). For  $x, b \in \mathcal{R}^n$ ,  $A \in \mathcal{S}_n$ ,  $A^{-1}$  exists, we have

$$x'Ax + x'b + b'x = (x + A^{-1}b)'A(x + A^{-1}b) - b'A^{-1}b. \quad (8)$$

The following lemma generalizes Theorem 5.8 [31] and Corollary 3.2.3 [13] to the infinite Markov jump and nonlinear systems, respectively. Its proof can be easily shown by analogous arguments.

**Lemma 5.** Assume that there are a set of positive functions  $V(x, \eta_t) \in C^2(\mathcal{R}^n \times \mathcal{D}; \mathcal{R}^+)$  and positive constants  $c_1, c_2, c_3$  such that

$$c_1 \|x\|^2 \leq V(x, i) \leq c_2 \|x\|^2 \quad (9)$$

and

$$\mathcal{L}V(x, i) \leq -c_3 \|x\|^2 \quad (10)$$

for all  $x \in \mathcal{R}^n$  and  $i \in \mathcal{D}$ . Then system (4) is EMSS.

### 3. Infinite Horizon Nonlinear Stochastic $H_\infty$ Control

In this subsection, we attempt to obtain the sufficient condition for the infinite horizon nonlinear stochastic  $H_\infty$  control problem of system (1).

**Theorem 6.** For a given disturbance attenuation level  $\gamma > 0$ , if there exist a set of positive functions  $V(x, i) \in C^2(\mathcal{R}^n \times \mathcal{D}; \mathcal{R}^+)$ ,  $V(0, i) = 0$ , and  $\partial^2 V(x, i)/\partial x^2 \geq 0$  for all nonzero  $x \in \mathcal{R}^n$ ,  $i \in \mathcal{D}$  with the properties of

$$\begin{aligned} c_1 \|x\|^2 \leq V(x, i) \leq c_2 \|x\|^2, \\ -\|m(x, i)\|^2 \leq -c_3 \|x\|^2, \end{aligned} \quad (11)$$

for some positive constants  $c_1, c_2, c_3$  such that  $V(x, i)$  solves the coupled HJIs,

$$\begin{aligned} \Upsilon_i = & \frac{\partial V(x, i)'}{\partial x} f_1(x, i) + \frac{1}{2} f_2(x, i)' \frac{\partial^2 V(x, i)}{\partial x^2} f_2(x, i) \\ & + m(x, i)' m(x, i) + \sum_{j=1}^{\infty} q_{ij} V(x, j) \end{aligned}$$

$$\begin{aligned} E[V(x(T), \eta_T) - V(x_0, \eta_0) \mid \eta_0 = i] &= E \left\{ \int_0^T \mathcal{L}V(x, \eta_t) dt \mid \eta_0 = i \right\} \\ &= E \left\{ \int_0^T \left[ \frac{\partial V(x, \eta_t)'}{\partial x} (f_1(x, \eta_t) + g_1(x, \eta_t)u + h_1(x, \eta_t)v) + \sum_{j=1}^{\infty} q_{ij} V(x, j) \right. \right. \\ & \quad \left. \left. + \frac{1}{2} (f_2(x, \eta_t) + g_2(x, \eta_t)u + h_2(x, \eta_t)v)' \frac{\partial^2 V(x, \eta_t)}{\partial x^2} (f_2(x, \eta_t) + g_2(x, \eta_t)u + h_2(x, \eta_t)v) + \|m(x, \eta_t)\|^2 + \|u\|^2 \right. \right. \end{aligned}$$

$$\begin{aligned} & \left. - \frac{1}{4} \left[ f_2(x, i)' \frac{\partial^2 V(x, i)}{\partial x^2} h_2(x, i) \right. \right. \\ & \left. \left. + \frac{\partial V(x, i)'}{\partial x} h_1(x, i) \right] \left[ -\gamma^2 I \right. \right. \\ & \left. \left. + h_2(x, i)' \frac{\partial^2 V(x, i)}{\partial x^2} h_2(x, i) \right]^{-1} \right. \\ & \left. \cdot \left[ h_2(x, i)' \frac{\partial^2 V(x, i)}{\partial x^2} f_2(x, i) \right. \right. \\ & \left. \left. + h_1(x, i)' \frac{\partial V(x, i)'}{\partial x} \right] \right. \\ & \left. - \frac{1}{4} \left[ f_2(x, i)' \frac{\partial^2 V(x, i)}{\partial x^2} g_2(x, i) \right. \right. \\ & \left. \left. + \frac{\partial V(x, i)'}{\partial x} g_1(x, i) \right] \left[ I \right. \right. \\ & \left. \left. + g_2(x, i)' \frac{\partial^2 V(x, i)}{\partial x^2} g_2(x, i) \right]^{-1} \right. \\ & \left. \cdot \left[ g_2(x, i)' \frac{\partial^2 V(x, i)}{\partial x^2} f_2(x, i) \right. \right. \\ & \left. \left. + g_1(x, i)' \frac{\partial V(x, i)'}{\partial x} \right] \leq 0, \right. \\ & \left. -\gamma^2 I + h_2(x, i)' \frac{\partial^2 V(x, i)}{\partial x^2} h_2(x, i) < 0, \quad i \in \mathcal{D}, \right. \end{aligned} \quad (12)$$

then

$$\begin{aligned} u^*(x, i) = & -\frac{1}{2} \left[ I + g_2(x, i)' \frac{\partial^2 V(x, i)}{\partial x^2} g_2(x, i) \right]^{-1} \\ & \cdot \left[ g_2(x, i)' \frac{\partial^2 V(x, i)}{\partial x^2} f_2(x, i) \right. \\ & \left. + g_1(x, i)' \frac{\partial V(x, i)'}{\partial x} \right] \end{aligned} \quad (13)$$

is an infinite horizon  $H_\infty$  control of system (1).

*Proof.* We first verify that (6) holds. For any  $T > 0$  and initial state  $x_0 = 0, \eta_0 = i$ , note that the generalized Itô-type formula [28] and (3) yield

$$\begin{aligned}
& - \|z\|^2 - \gamma^2 \|v\|^2 + \gamma^2 \|v\|^2 \Big] dt \mid \eta_0 = i \Big\} \\
= & E \left\{ \int_0^T \left[ \Lambda_1(v, x, \eta_t) + \Lambda_2(x, \eta_t) + \Lambda_3(u, x, \eta_t) + \sum_{j=1}^{\infty} q_{ij} V(x, j) - \|z\|^2 + \gamma^2 \|v\|^2 \right. \right. \\
& \left. \left. + \frac{1}{2} \left( u' g_2(x, \eta_t)' \frac{\partial^2 V(x, \eta_t)}{\partial x^2} h_2(x, \eta_t) v + v' h_2(x, \eta_t)' \frac{\partial^2 V(x, \eta_t)}{\partial x^2} g_2(x, \eta_t) u \right) \right] dt \mid \eta_0 = i \right\}, \tag{14}
\end{aligned}$$

where

$$\begin{aligned}
\Lambda_1(v, x, \eta_t) &= v' \left( -\gamma^2 I + \frac{1}{2} \right. \\
&\quad \left. \cdot h_2(x, \eta_t)' \frac{\partial^2 V(x, \eta_t)}{\partial x^2} h_2(x, \eta_t) \right) v \\
&\quad + \frac{1}{2} \left( f_2(x, \eta_t)' \frac{\partial^2 V(x, \eta_t)}{\partial x^2} h_2(x, \eta_t) \right. \\
&\quad \left. + \frac{\partial V(x, \eta_t)'}{\partial x} h_1(x, \eta_t) \right) v + \frac{1}{2} \\
&\quad \cdot v' \left( h_2(x, \eta_t)' \frac{\partial^2 V(x, \eta_t)}{\partial x^2} f_2(x, \eta_t) \right. \\
&\quad \left. + h_1(x, \eta_t)' \frac{\partial V(x, \eta_t)}{\partial x} \right), \\
\Lambda_2(x, \eta_t) &= \frac{\partial V(x, \eta_t)'}{\partial x} f_1(x, \eta_t) + \frac{1}{2} \\
&\quad \cdot f_2(x, \eta_t)' \frac{\partial^2 V(x, \eta_t)}{\partial x^2} f_2(x, \eta_t) \\
&\quad + m(x, \eta_t)' m(x, \eta_t), \\
\Lambda_3(u, x, \eta_t) &= u' \left( I + \frac{1}{2} \right. \\
&\quad \left. \cdot g_2(x, \eta_t)' \frac{\partial^2 V(x, \eta_t)}{\partial x^2} g_2(x, \eta_t) \right) u \\
&\quad + \frac{1}{2} \left( f_2(x, \eta_t)' \frac{\partial^2 V(x, \eta_t)}{\partial x^2} g_2(x, \eta_t) \right.
\end{aligned}$$

$$\begin{aligned}
& \left. + \frac{\partial V(x, \eta_t)'}{\partial x} g_1(x, \eta_t) \right) u + \frac{1}{2} \\
& \cdot u' \left( g_2(x, \eta_t)' \frac{\partial^2 V(x, \eta_t)}{\partial x^2} f_2(x, \eta_t) \right. \\
& \left. + g_1(x, \eta_t)' \frac{\partial V(x, \eta_t)}{\partial x} \right). \tag{15}
\end{aligned}$$

Invoking  $\partial^2 V(x, i) / \partial x^2 \geq 0$ ,  $i \in \mathcal{D}$ , we deduce that

$$\begin{aligned}
& \frac{1}{2} \left( -u' g_2(x, \eta_t)' + v' h_2(x, \right. \\
& \left. \eta_t)' \right) \frac{\partial^2 V(x, \eta_t)}{\partial x^2} \left( -g_2(x, \eta_t) u + h_2(x, \eta_t) v \right) \\
& \geq 0, \tag{16}
\end{aligned}$$

which shows that

$$\begin{aligned}
& \frac{1}{2} \left( u' g_2(x, \eta_t)' \frac{\partial^2 V(x, \eta_t)}{\partial x^2} h_2(x, \eta_t) v \right. \\
& \left. + v' h_2(x, \eta_t)' \frac{\partial^2 V(x, \eta_t)}{\partial x^2} g_2(x, \eta_t) u \right) \\
& \leq \frac{1}{2} \left( u' g_2(x, \eta_t)' \frac{\partial^2 V(x, \eta_t)}{\partial x^2} g_2(x, \eta_t) u \right. \\
& \left. + v' h_2(x, \eta_t)' \frac{\partial^2 V(x, \eta_t)}{\partial x^2} h_2(x, \eta_t) v \right). \tag{17}
\end{aligned}$$

Hence,

$$\begin{aligned}
E [V(x(T), \eta_T) - V(x_0, \eta_0) \mid \eta_0 = i] &\leq E \left\{ \int_0^T \left[ \Lambda_1(v, x, \eta_t) + \Lambda_2(x, \eta_t) + \Lambda_3(u, x, \eta_t) + \sum_{j=1}^{\infty} q_{ij} V(x, j) - \|z\|^2 \right. \right. \\
&\quad \left. \left. + \gamma^2 \|v\|^2 + \frac{1}{2} \left( u' g_2(x, \eta_t)' \frac{\partial^2 V(x, \eta_t)}{\partial x^2} g_2(x, \eta_t) u + v' h_2(x, \eta_t)' \frac{\partial^2 V(x, \eta_t)}{\partial x^2} h_2(x, \eta_t) v \right) \right] dt \mid \eta_0 = i \right\} \tag{18} \\
&= E \left\{ \int_0^T \left[ \bar{\Lambda}_1(v, x, \eta_t) + \Lambda_2(x, \eta_t) + \bar{\Lambda}_3(u, x, \eta_t) + \sum_{j=1}^{\infty} q_{ij} V(x, j) - \|z\|^2 + \gamma^2 \|v\|^2 \right] dt \mid \eta_0 = i \right\},
\end{aligned}$$

where

$$\begin{aligned} \bar{\Lambda}_1(v, x, \eta_t) = & v' \left( -\gamma^2 I \right. \\ & \left. + h_2(x, \eta_t)' \frac{\partial^2 V(x, \eta_t)}{\partial x^2} h_2(x, \eta_t) \right) v \\ & + \frac{1}{2} \left( f_2(x, \eta_t)' \frac{\partial^2 V(x, \eta_t)}{\partial x^2} h_2(x, \eta_t) \right. \\ & \left. + \frac{\partial V(x, \eta_t)'}{\partial x} h_1(x, \eta_t) \right) v + \frac{1}{2} \\ & \cdot v' \left( h_2(x, \eta_t)' \frac{\partial^2 V(x, \eta_t)}{\partial x^2} f_2(x, \eta_t) \right. \\ & \left. + h_1(x, \eta_t)' \frac{\partial V(x, \eta_t)'}{\partial x} \right), \end{aligned} \quad (19)$$

$$\begin{aligned} \bar{\Lambda}_3(u, x, \eta_t) = & u' \left( I \right. \\ & \left. + g_2(x, \eta_t)' \frac{\partial^2 V(x, \eta_t)}{\partial x^2} g_2(x, \eta_t) \right) u \\ & + \frac{1}{2} \left( f_2(x, \eta_t)' \frac{\partial^2 V(x, \eta_t)}{\partial x^2} g_2(x, \eta_t) \right. \\ & \left. + \frac{\partial V(x, \eta_t)'}{\partial x} g_1(x, \eta_t) \right) u + \frac{1}{2} \\ & \cdot u' \left( g_2(x, \eta_t)' \frac{\partial^2 V(x, \eta_t)}{\partial x^2} f_2(x, \eta_t) \right. \\ & \left. + g_1(x, \eta_t)' \frac{\partial V(x, \eta_t)'}{\partial x} \right). \end{aligned}$$

Applying Lemma 4 to  $\bar{\Lambda}_1(v, x, \eta_t)$  and  $\bar{\Lambda}_3(u, x, \eta_t)$ , we conclude that

$$\begin{aligned} \bar{\Lambda}_1(v, x, \eta_t) = & (v + F_1)' \left( -\gamma^2 I \right. \\ & \left. + h_2(x, \eta_t)' \frac{\partial^2 V(x, \eta_t)}{\partial x^2} h_2(x, \eta_t) \right) (v + F_1), \\ & - \frac{1}{4} \left( f_2(x, \eta_t)' \frac{\partial^2 V(x, \eta_t)}{\partial x^2} h_2(x, \eta_t) \right. \\ & \left. + \frac{\partial V(x, \eta_t)'}{\partial x} h_1(x, \eta_t) \right) \cdot \left( -\gamma^2 I \right. \\ & \left. + h_2(x, \eta_t)' \frac{\partial^2 V(x, \eta_t)}{\partial x^2} h_2(x, \eta_t) \right)^{-1} \\ & \cdot \left( h_2(x, \eta_t)' \frac{\partial^2 V(x, \eta_t)}{\partial x^2} f_2(x, \eta_t) \right. \\ & \left. + h_1(x, \eta_t)' \frac{\partial V(x, \eta_t)'}{\partial x} \right), \end{aligned} \quad (20)$$

$$\begin{aligned} \bar{\Lambda}_3(u, x, \eta_t) = & (u + F_2)' \left( I \right. \\ & \left. + g_2(x, \eta_t)' \frac{\partial^2 V(x, \eta_t)}{\partial x^2} g_2(x, \eta_t) \right) (u + F_2) \\ & - \frac{1}{4} \left( f_2(x, \eta_t)' \frac{\partial^2 V(x, \eta_t)}{\partial x^2} g_2(x, \eta_t) \right. \\ & \left. + \frac{\partial V(x, \eta_t)'}{\partial x} g_1(x, \eta_t) \right) \cdot \left( I \right. \\ & \left. + g_2(x, \eta_t)' \frac{\partial^2 V(x, \eta_t)}{\partial x^2} g_2(x, \eta_t) \right)^{-1} \\ & \cdot \left( g_2(x, \eta_t)' \frac{\partial^2 V(x, \eta_t)}{\partial x^2} f_2(x, \eta_t) \right. \\ & \left. + g_1(x, \eta_t)' \frac{\partial V(x, \eta_t)'}{\partial x} \right), \end{aligned} \quad (21)$$

where

$$\begin{aligned} F_1 = & \frac{1}{2} \left[ -\gamma^2 I + h_2(x, \eta_t)' \frac{\partial^2 V(x, \eta_t)}{\partial x^2} h_2(x, \eta_t) \right]^{-1} \\ & \cdot \left[ h_2(x, \eta_t)' \frac{\partial^2 V(x, \eta_t)}{\partial x^2} f_2(x, \eta_t) \right. \\ & \left. + h_1(x, \eta_t)' \frac{\partial V(x, \eta_t)'}{\partial x} \right], \end{aligned} \quad (22)$$

$$\begin{aligned} F_2 = & \frac{1}{2} \left[ I + g_2(x, \eta_t)' \frac{\partial^2 V(x, \eta_t)}{\partial x^2} g_2(x, \eta_t) \right]^{-1} \\ & \cdot \left[ g_2(x, \eta_t)' \frac{\partial^2 V(x, \eta_t)}{\partial x^2} f_2(x, \eta_t) \right. \\ & \left. + g_1(x, \eta_t)' \frac{\partial V(x, \eta_t)'}{\partial x} \right]. \end{aligned} \quad (23)$$

Recalling (12) and substituting (20) and (21) into (18) yield that

$$\begin{aligned} E [V(x(T), \eta_T) - V(x_0, \eta_0) \mid \eta_0 = i] \\ \leq E \left\{ \int_0^T \left[ (v + F_1)' \right. \right. \\ \cdot \left( -\gamma^2 I + h_2(x, \eta_t)' \frac{\partial^2 V(x, \eta_t)}{\partial x^2} h_2(x, \eta_t) \right) \\ \cdot (v + F_1) + (u + F_2)' \\ \cdot \left( I + g_2(x, \eta_t)' \frac{\partial^2 V(x, \eta_t)}{\partial x^2} g_2(x, \eta_t) \right) (u + F_2) \\ \left. \left. - \|z\|^2 + \gamma^2 \|v\|^2 \right] dt \mid \eta_0 = i \right\}. \end{aligned} \quad (24)$$

In view of (12), for  $x_0 = 0$ , if we choose  $u = u^* = -F_2$ , then it follows from (24) that

$$E \left\{ \int_0^T \|z\|^2 dt \mid \eta_0 = i \right\} < \gamma^2 E \left\{ \int_0^T \|v\|^2 dt \mid \eta_0 = i \right\}. \quad (25)$$

Taking the limit for  $T \rightarrow \infty$  in the above, it is easy to show (6) by Definition 2.

Next, we remain to show that when  $v = 0$ ,  $u = u^*$ , the trajectory of system (1) with any initial value  $x(0) = x_0$  is EMSS. To this end, for  $i \in \mathcal{D}$ , let  $\mathcal{L}_{u^*}$  be the infinitesimal operator of system (1) with  $v = 0$ ,  $u = u^*$ ; then

$$\begin{aligned} \mathcal{L}_{u^*} V(x, i) \Big|_{v=0} &= \frac{\partial V(x, i)'}{\partial x} (f_1(x, i) + g_1(x, i) u^*) \\ &+ \sum_{j=1}^{\infty} q_{ij} V(x, j) + \frac{1}{2} (f_2(x, i) + g_2(x, i) \\ &\cdot u^*)' \frac{\partial^2 V(x, i)}{\partial x^2} (f_2(x, i) + g_2(x, i) u^*) \\ &= \frac{\partial V(x, i)'}{\partial x} f_1(x, i) + \frac{1}{2} f_2(x, i)' \frac{\partial^2 V(x, i)}{\partial x^2} f_2(x, i) \\ &+ \sum_{j=1}^{\infty} q_{ij} V(x, j) + \frac{\partial V(x, i)'}{\partial x} g_1(x, i) u^* + \frac{1}{2} \\ &\cdot f_2(x, i)' \frac{\partial^2 V(x, i)}{\partial x^2} g_2(x, i) u^* \\ &+ \frac{1}{2} (g_2(x, i) u^*)' \frac{\partial^2 V(x, i)}{\partial x^2} f_2(x, i) \\ &+ \frac{1}{2} (g_2(x, i) u^*)' \frac{\partial^2 V(x, i)}{\partial x^2} g_2(x, i) u^*, \\ &= \frac{\partial V(x, i)'}{\partial x} f_1(x, i) + \frac{1}{2} f_2(x, i)' \frac{\partial^2 V(x, i)}{\partial x^2} f_2(x, i) \\ &+ \sum_{j=1}^{\infty} q_{ij} V(x, j) + \Psi_{1i} + \Psi_{2i}, \end{aligned} \quad (26)$$

where

$$\begin{aligned} \Psi_{1i} &= \frac{\partial V(x, i)'}{\partial x} g_1(x, i) u^* + \frac{1}{2} f_2(x, i)' \\ &\frac{\partial^2 V(x, i)}{\partial x^2} g_2(x, i) u^* + \frac{1}{2} (g_2(x, i) \\ &\cdot u^*)' \frac{\partial^2 V(x, i)}{\partial x^2} f_2(x, i) = -\frac{1}{2} \\ &\cdot \frac{\partial V(x, i)'}{\partial x} g_1(x, i) \left[ I + g_2(x, i)' \frac{\partial^2 V(x, i)}{\partial x^2} g_2(x, i) \right]^{-1} \\ &\cdot \left[ g_2(x, i)' \frac{\partial^2 V(x, i)}{\partial x^2} f_2(x, i) \right. \\ &\left. + g_1(x, i)' \frac{\partial V(x, i)'}{\partial x} \right] - \frac{1}{4} f_2(x, i)' \end{aligned}$$

$$\begin{aligned} &i)' \frac{\partial^2 V(x, i)}{\partial x^2} g_2(x, i) \left[ I + g_2(x, i)' \frac{\partial^2 V(x, i)}{\partial x^2} g_2(x, i) \right]^{-1} \\ &\cdot \left[ g_2(x, i)' \frac{\partial^2 V(x, i)}{\partial x^2} f_2(x, i) + g_1(x, i)' \frac{\partial V(x, i)'}{\partial x} \right] \\ &- \frac{1}{4} \left[ f_2(x, i)' \frac{\partial^2 V(x, i)}{\partial x^2} g_2(x, i) + \frac{\partial V(x, i)'}{\partial x} g_1(x, i) \right] \\ &\cdot \left[ I \right. \\ &\left. + g_2(x, i)' \frac{\partial^2 V(x, i)}{\partial x^2} g_2(x, i) \right]^{-1} g_2(x, i) \\ &i)' \frac{\partial^2 V(x, i)}{\partial x^2} f_2(x, i), \end{aligned} \quad (27)$$

and

$$\begin{aligned} \Psi_{2i} &= \frac{1}{2} (g_2(x, i) u^*)' \frac{\partial^2 V(x, i)}{\partial x^2} g_2(x, i) u^* \\ &= \frac{1}{8} \left[ f_2(x, i)' \frac{\partial^2 V(x, i)}{\partial x^2} g_2(x, i) + \frac{\partial V(x, i)'}{\partial x} g_1(x, i) \right] \\ &\cdot \left[ I \right. \\ &\left. + g_2(x, i)' \frac{\partial^2 V(x, i)}{\partial x^2} g_2(x, i) \right]^{-1} \cdot g_2(x, i) \\ &i)' \frac{\partial^2 V(x, i)}{\partial x^2} g_2(x, i) \left[ I + g_2(x, i)' \frac{\partial^2 V(x, i)}{\partial x^2} g_2(x, i) \right]^{-1} \\ &\cdot \left[ g_2(x, i)' \frac{\partial^2 V(x, i)}{\partial x^2} f_2(x, i) + g_1(x, i)' \frac{\partial V(x, i)'}{\partial x} \right]. \end{aligned} \quad (28)$$

By direct calculations, one obtains that

$$\begin{aligned} \Psi_{1i} &= -\frac{1}{2} \left[ f_2(x, i)' \frac{\partial^2 V(x, i)}{\partial x^2} g_2(x, i) \right. \\ &\left. + \frac{\partial V(x, i)'}{\partial x} g_1(x, i) \right] \left[ I \right. \\ &\left. + g_2(x, i)' \frac{\partial^2 V(x, i)}{\partial x^2} g_2(x, i) \right]^{-1} \\ &\cdot \left[ g_2(x, i)' \frac{\partial^2 V(x, i)}{\partial x^2} f_2(x, i) \right. \\ &\left. + g_1(x, i)' \frac{\partial V(x, i)'}{\partial x} \right], \end{aligned} \quad (29)$$

and

$$\begin{aligned} \Psi_{2i} &\leq \frac{1}{8} \left[ f_2(x, i)' \frac{\partial^2 V(x, i)}{\partial x^2} g_2(x, i) \right. \\ &\left. + \frac{\partial V(x, i)'}{\partial x} g_1(x, i) \right] \left[ I \right. \end{aligned}$$

$$\begin{aligned}
 & + g_2(x, i)' \frac{\partial^2 V(x, i)}{\partial x^2} g_2(x, i) \Big]^{-1} \\
 & \cdot \left[ g_2(x, i)' \frac{\partial^2 V(x, i)}{\partial x^2} f_2(x, i) \right. \\
 & \left. + g_1(x, i)' \frac{\partial V(x, i)}{\partial x} \right] \cdot \\
 & - h_2(x, i)' \frac{\partial^2 V(x, i)}{\partial x^2} h_2(x, i) \Big]^{-1} \\
 & \cdot \left[ h_2(x, i)' \frac{\partial^2 V(x, i)}{\partial x^2} f_2(x, i) \right. \\
 & \left. + h_1(x, i)' \frac{\partial V(x, i)}{\partial x} \right] \leq -\|m(x, i)\|^2 \leq -c_3 \|x\|^2.
 \end{aligned} \tag{30}$$

Implementing (29) and (30) into (16) and taking into account (11) and (12), we have

$$\begin{aligned}
 \mathcal{L}_{u^*} V(x, i)|_{v=0} & \leq \frac{\partial V(x, i)'}{\partial x} f_1(x, i) + \frac{1}{2} \\
 & \cdot f_2(x, i)' \frac{\partial^2 V(x, i)}{\partial x^2} f_2(x, i) \\
 & + \sum_{j=1}^{\infty} q_{ij} V(x, j) - \frac{3}{8} \left[ f_2(x, i)' \frac{\partial^2 V(x, i)}{\partial x^2} g_2(x, i) \right. \\
 & \left. + \frac{\partial V(x, i)'}{\partial x} g_1(x, i) \right] \cdot \left[ I \right. \\
 & \left. + g_2(x, i)' \frac{\partial^2 V(x, i)}{\partial x^2} g_2(x, i) \right]^{-1} \\
 & \cdot \left[ g_2(x, i)' \frac{\partial^2 V(x, i)}{\partial x^2} f_2(x, i) \right. \\
 & \left. + g_1(x, i)' \frac{\partial V(x, i)}{\partial x} \right] \leq \frac{\partial V(x, i)'}{\partial x} f_1(x, i) + \frac{1}{2} \\
 & \cdot f_2(x, i)' \frac{\partial^2 V(x, i)}{\partial x^2} f_2(x, i) \\
 & + \sum_{j=1}^{\infty} q_{ij} V(x, j) - \frac{1}{4} \left[ f_2(x, i)' \frac{\partial^2 V(x, i)}{\partial x^2} g_2(x, i) \right. \\
 & \left. + \frac{\partial V(x, i)'}{\partial x} g_1(x, i) \right] \cdot \left[ I \right. \\
 & \left. + g_2(x, i)' \frac{\partial^2 V(x, i)}{\partial x^2} g_2(x, i) \right]^{-1} \\
 & \cdot \left[ g_2(x, i)' \frac{\partial^2 V(x, i)}{\partial x^2} f_2(x, i) \right. \\
 & \left. + g_1(x, i)' \frac{\partial V(x, i)}{\partial x} \right] \leq -m(x, i)' m(x, i) \\
 & - \frac{1}{4} \left[ f_2(x, i)' \frac{\partial^2 V(x, i)}{\partial x^2} h_2(x, i) \right. \\
 & \left. + \frac{\partial V(x, i)'}{\partial x} h_1(x, i) \right] \cdot \left[ \gamma^2 I \right.
 \end{aligned}$$

Based on Lemma 5, it results that system (1) with  $v = 0, u = u^*$  is EMSS. The proof is complete.  $\square$

*Remark 7.* It should be pointed that, in Theorem 6, if we take  $\Upsilon_i < 0$  in (12), system (1) is internally stable (globally asymptotically stable in probability) even without condition (11). Then the controller defined in (13) is still an  $H_{\infty}$  controller (globally asymptotically stable in probability).

Below, we will give an example to show the effectiveness of our above developed  $H_{\infty}$  design method.

*Example 8.* Consider a one-dimensional stochastic nonlinear system with infinite Markov jumps and the parameters as follows:

$$\begin{aligned}
 f_1(x, i) & = -\frac{2ix}{i+1}, \\
 g_1(x, i) & = \frac{1}{i+1}, \\
 h_1(x, i) & = \frac{1}{4}, \\
 f_2(x, i) & = \frac{x}{i+1}, \\
 g_2(x, i) & = 1, \\
 h_2(x, i) & = 1, \\
 m(x, i) & = \frac{ix}{2(i+1)}.
 \end{aligned} \tag{32}$$

Let  $\{\eta_t\}_{t \in \mathcal{D}_+}$  be a Poisson process with parameter  $\lambda > 0$ . It is obvious that  $\{\eta_t\}_{t \in \mathcal{D}_+}$  is a homogeneous Markov process with the countably infinite state space, and its infinitesimal matrix  $Q = (q_{ij})$  is given by  $-q_{ii} = q_{i, i+1} = \lambda$  and  $q_{ij} = 0, i \in \mathcal{D}, j \in \mathcal{D}/\{i, i+1\}$ .

Assume the disturbance attenuation level  $\gamma = \sqrt{2}$  and  $\lambda = 1$ . Then setting  $V(x, i) = ix^2/2(i+1)$ , we solve the coupled HJIs (12), it is easy to verify that the conditions of Theorem 6 are satisfied; thus, via Theorem 6, we have

$$\Upsilon_i = \frac{-15.5i^5 - 53.5i^4 - 30i^3 - 2.75i^2 + 8i + 2}{4(i+1)^2(i+2)(2i+1)} < 0. \tag{33}$$

So the  $H_{\infty}$  controller is

$$u^*(x, i) = -\frac{ix}{(i+1)(i+2)}. \tag{34}$$

With the initial conditions  $x_0 = 0.5$  and the exogenous disturbance  $v(t) = e^{-t} \sin t$ , Figure 1 shows the state response.

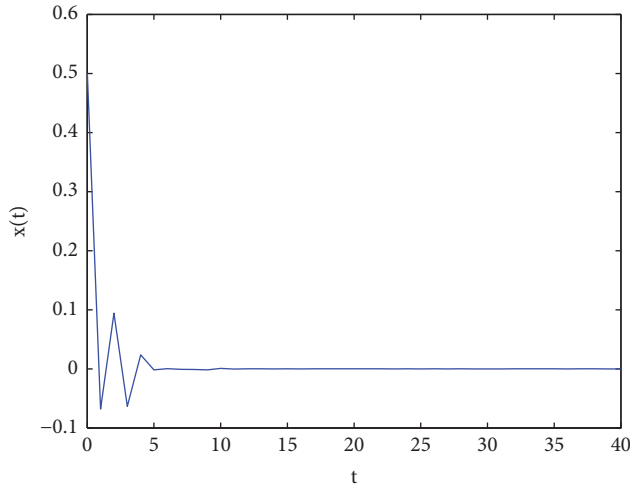


FIGURE 1: System state response in Example 8.

#### 4. Conclusion

For a class of nonlinear stochastic systems with infinite Markov jumps and  $(x, u, v)$ -dependent noise, a sufficient condition for infinite horizon  $H_\infty$  control problem has been obtained in terms of coupled HJIs, and the effectiveness of the proposed design method is demonstrated by a numerical example. There are some further research directions including the investigation on  $H_2/H_\infty$  control and  $H_\infty$  filter problems for nonlinear infinite Markov jump systems.

#### Data Availability

No data were used to support this study.

#### Conflicts of Interest

The authors declare that there are no conflicts of interest regarding the publication of this paper.

#### Acknowledgments

This work was supported by the National Natural Science Foundation of China (no. 61673013), the Natural Science Foundation of Shandong Province (no. ZR2016JL022), and the SDUST Research Fund (no. 2015TDJH105).

#### References

- [1] T. Basar and P. Bernhard,  *$H_\infty$ -Optimal Control and Related Minimax Design Problems: A Dynamic Game Approach*, Birkhäuser, Boston, Mass, USA, 2nd edition, 1995.
- [2] G. Zames, "Feedback and optimal sensitivity: model reference transformations, multiplicative seminorms, and approximate inverses," *IEEE Transactions on Automatic Control*, vol. 26, no. 2, pp. 301–320, 1981.
- [3] D. Hinrichsen and A. J. Pritchard, "Stochastic  $H_\infty$ ," *SIAM Journal on Control and Optimization*, vol. 36, no. 5, pp. 1504–1538, 1998.
- [4] W. Zhang, B. Chen, and C. Tseng, "Robust  $H_\infty$  filtering for nonlinear stochastic systems," *IEEE Transactions on Signal Processing*, vol. 53, no. 2, part 1, pp. 589–598, 2005.
- [5] W. Zhang and B. Chen, "State feedback  $H_\infty$  control for a class of nonlinear stochastic systems," *SIAM Journal on Control and Optimization*, vol. 44, no. 6, pp. 1973–1991, 2006.
- [6] Y. Fang and K. A. Loparo, "Stochastic stability of jump linear systems," *IEEE Transactions on Automatic Control*, vol. 47, no. 7, pp. 1204–1208, 2002.
- [7] N. Xiao, L. Xie, and M. Fu, "Stabilization of Markov jump linear systems using quantized state feedback," *Automatica*, vol. 46, no. 10, pp. 1696–1702, 2010.
- [8] C. Tan and W. H. Zhang, "On observability and detectability of continuous-time stochastic Markov jump systems," *Journal of Systems Science & Complexity*, vol. 28, no. 4, pp. 830–847, 2015.
- [9] Shaowei Zhou, Xiaoping Liu, Bing Chen, and Hongxia Liu, "Stability Analysis for a Class of Discrete-Time Nonhomogeneous Markov Jump Systems with Multiplicative Noises," *Complexity*, vol. 2018, Article ID 1586846, 9 pages, 2018.
- [10] J. Xiong, J. Lam, Z. Shu, and X. Mao, "Stability analysis of continuous-time switched systems with a random switching signal," *IEEE Transactions on Automatic Control*, vol. 59, no. 1, pp. 180–186, 2014.
- [11] L. Zhang, Y. Leng, and P. Colaneri, "Stability and stabilization of discrete-time semi-MARKov jump linear systems via semi-MARKov kernel approach," *Institute of Electrical and Electronics Engineers Transactions on Automatic Control*, vol. 61, no. 2, pp. 503–508, 2016.
- [12] V. Dragan, T. Morozan, and A. M. Stoica, *Mathematical Methods in Robust Control of Discrete-Time Linear Stochastic Systems*, Springer, New York, NY, USA, 2010.
- [13] V. Dragan, T. Morozan, and A.-M. Stoica, *Mathematical methods in robust control of linear stochastic systems*, Springer, New York, Second edition, 2013.
- [14] T. Hou, W. Zhang, and H. Ma, "Finite horizon  $H_2/H_\infty$  control for discrete-time stochastic systems with Markovian jumps and multiplicative noise," *IEEE Transactions on Automatic Control*, vol. 55, no. 5, pp. 1185–1191, 2010.
- [15] Y. Zhao and W. Zhang, "Observer-based controller design for singular stochastic Markov jump systems with state dependent noise," *Journal of Systems Science & Complexity*, vol. 29, no. 4, pp. 946–958, 2016.
- [16] Z. Wu, S. Wang, and M. Cui, "Tracking controller design for random nonlinear benchmark system," *Journal of The Franklin Institute*, vol. 354, no. 1, pp. 360–371, 2017.
- [17] Z. Wu, "Stability criteria of random nonlinear systems and their applications," *Institute of Electrical and Electronics Engineers Transactions on Automatic Control*, vol. 60, no. 4, pp. 1038–1049, 2015.
- [18] X. Xie and M. Jiang, "Output feedback stabilization of stochastic feedforward nonlinear time-delay systems with unknown output function," *International Journal of Robust and Nonlinear Control*, vol. 28, no. 1, pp. 266–280, 2018.
- [19] X. Xie, N. Duan, and C. Zhao, "A combined homogeneous domination and sign function approach to output-feedback stabilization of stochastic high-order nonlinear systems," *IEEE Transactions on Automatic Control*, vol. 59, no. 5, pp. 1303–1309, 2014.
- [20] M. Gao, L. Sheng, and W. Zhang, "Stochastic  $H_2/H_\infty$  control of nonlinear systems with time-delay and state-dependent noise," *Applied Mathematics and Computation*, vol. 266, pp. 429–440, 2015.

- [21] Mingyue Cui, Liangchao Geng, and Zhaojing Wu, "Random Modeling and Control of Nonlinear Active Suspension," *Mathematical Problems in Engineering*, vol. 2017, Article ID 4045796, 8 pages, 2017.
- [22] Y. Wang, Z. Pan, Y. Li, and W. Zhang, " $H_\infty$  control for nonlinear stochastic Markov systems with time-delay and multiplicative noise," *Journal of Systems Science & Complexity*, vol. 30, no. 6, pp. 1293–1315, 2017.
- [23] O. L. V. Costa and M. D. Fragoso, "Discrete-time LQ-optimal control problems for infinite Markov jump parameter systems," *IEEE Transactions on Automatic Control*, vol. 40, no. 12, pp. 2076–2088, 1995.
- [24] O. L. Costa and D. Z. Figueiredo, "Stochastic stability of jump discrete-time linear systems with Markov chain in a general Borel space," *IEEE Transactions on Automatic Control*, vol. 59, no. 1, pp. 223–227, 2014.
- [25] M. D. Fragoso and J. Baczynski, "Stochastic versus mean square stability in continuous time linear infinite Markov jump parameter systems," *Stochastic Analysis and Applications*, vol. 20, no. 2, pp. 347–356, 2002.
- [26] T. Hou and H. Ma, "Exponential stability for discrete-time infinite Markov jump systems," *IEEE Transactions on Automatic Control*, vol. 61, no. 12, pp. 4241–4246, 2016.
- [27] R. Song and Q. Zhu, "Stability of linear stochastic delay differential equations with infinite Markovian switchings," *International Journal of Robust and Nonlinear Control*, vol. 28, no. 3, pp. 825–837, 2018.
- [28] V. M. Ungureanu, "Optimal control for infinite dimensional stochastic differential equations with infinite Markov jumps and multiplicative noise," *Journal of Mathematical Analysis and Applications*, vol. 417, no. 2, pp. 694–718, 2014.
- [29] Y. Liu and T. Hou, "LQ optimal control for stochastic systems with infinite Markovian jumps," in *Proceedings of the 2017 Chinese Automation Congress (CAC)*, pp. 7107–7111, Jinan, October 2017.
- [30] Y. Liu, T. Hou, and X. Bai, "Infinite horizon  $H_2/H_\infty$  optimal control for discrete-time infinite Markov jump systems with  $(x,u,v)$ -dependent noise," in *36th Chinese Control Conference*, pp. 1955–1960, 2017.
- [31] X. Mao and C. Yuan, *Stochastic Differential Equations with Markovian Switching*, Imperial College Press, London, UK, 2006.
- [32] W. Zhang, B. Chen, H. Tang, L. Sheng, and M. Gao, "Some remarks on general nonlinear stochastic  $H_\infty$  control with state, control, and disturbance-dependent noise," *IEEE Transactions on Automatic Control*, vol. 59, no. 1, pp. 237–242, 2014.

## Research Article

# A New Robust Nonfragile Controller Design Scheme for a Class of Hybrid Systems through Piecewise Affine Models

Yunsai Chen <sup>1,2</sup>, Yongjie Pang,<sup>1</sup> Zhao Yang,<sup>3</sup> and Liang Ma<sup>3</sup>

<sup>1</sup>College of Shipbuilding Engineering, Harbin Engineering University, Harbin 150001, China

<sup>2</sup>Department of Technology, National Deep Sea Center, Qingdao 266237, China

<sup>3</sup>Qingdao National Laboratory for Marine Science and Technology, Scientific and Technology Infrastructure Department, Qingdao 266237, China

Correspondence should be addressed to Yunsai Chen; [cys@ndsc.org.cn](mailto:cys@ndsc.org.cn)

Received 19 July 2018; Revised 26 September 2018; Accepted 27 September 2018; Published 21 October 2018

Academic Editor: Leonardo Acho

Copyright © 2018 Yunsai Chen et al. This is an open access article distributed under the Creative Commons Attribution License, which permits unrestricted use, distribution, and reproduction in any medium, provided the original work is properly cited.

This paper investigates the robust  $\mathcal{H}_\infty$  nonfragile control problem for a class of discrete-time hybrid systems based on piecewise affine models. The objective is to develop an admissible piecewise affine nonfragile controller such that the resulting closed-loop system is asymptotically stable with robust  $\mathcal{H}_\infty$  performance  $\gamma$ . By employing a state-control augmentation methodology, some new sufficient conditions for the controller synthesis are formulated based on piecewise Lyapunov functions (PLFs). The controller gains can be obtained via solving a set of linear matrix inequalities. Simulation examples are finally presented to demonstrate the feasibility and effectiveness of the proposed approaches.

## 1. Introduction

Over the past few decades, hybrid systems have drawn tremendous attention from the control community, as they contain the competence to model the interaction between logic components and continuous dynamics [1–6]. Piecewise affine (PWA) systems are a rich class of hybrid systems, which can provide a useful modeling approach for the stability analysis and controller synthesis of hybrid systems [7–9]. In addition, the PWA models can approximate smooth nonlinear plants with arbitrary degrees of accuracy [10, 11].

In recent years, many valuable references on the systematic analysis and synthesis for the PWA systems have been published [12–22]. In [12], the stability of continuous-time PWA systems was analyzed by utilizing discontinuous piecewise Lyapunov functions (PLFs). On the basis of the idea in [12], some algorithms for stability and performance analysis of discrete-time PWA systems were proposed in [14] and the continuity of the PLFs was not required for the discrete-time case. The authors in [20] designed a static output-feedback controller for discrete-time PWA systems such that the resulting closed-loop system was asymptotically stable with

robust  $\mathcal{H}_\infty$  performance  $\gamma$ . The authors in [21] developed a reconfigurable control approach for continuous-time PWA systems with actuator and sensor faults, and the output tracking problem was investigated simultaneously. In [23], the problem of delay-dependent fixed-order memory piecewise affine  $\mathcal{H}_\infty$  output-feedback control for a class of nonlinear systems with time-varying delay was considered. The authors in [24] have proposed a novel system-augmentation approach to the delay-dependent reliable piecewise affine  $\mathcal{H}_\infty$  static output-feedback control for nonlinear systems with time-varying delay and sensor faults in the piecewise-Markovian-Lyapunov-functional-based framework.

On the other hand, since 1980s, the robust  $\mathcal{H}_\infty$  control problem has drawn much attention as it is robust against the system parameter uncertainties, unmodeled dynamics, and external disturbances [25, 26]. It is implicitly assumed in this control approach that the controllers are implemented precisely. In fact, controllers gains inevitably possess some degrees of errors or parameter variations due to physical limitations such as the inherent inaccuracy in analog systems, finite word length in arbitrary digital systems, and round-off errors in process of numerical computations [27].

Numbers of literatures have already shown that relatively small perturbations in the controller parameters can even result in instability of the closed-loop system [28–30]. For this case, it is realistic to synthesize a controller for a given uncertain system such that the controller is insensitive to some predefined admissible variations with respect to its gains. More recently, many efforts have been devoted to the nonfragile robust  $\mathcal{H}_\infty$  controller design problem [31–40]. For instance, a nonfragile  $\mathcal{H}_\infty$  controller with multiplicative gain perturbations was proposed for linear time invariant (LTI) systems in [31]. The author in [32] developed a decentralized robust state-feedback nonfragile control method for uncertain discrete-time large-scale systems with time-delays and controller gain variations. In [34], a nonfragile robust controller with parameter uncertainties was constructed for a class of nonlinear systems based on T-S fuzzy neural models. The authors in [40] considered the nonfragile robust  $\mathcal{H}_\infty$  control problem for fuzzy systems based on output information. In spite of the attractive features in piecewise affine systems, the authors in [41] proposed a state-feedback nonfragile robust controller design method for continuous-time PWA systems. The results in [41] were derived based on a common Lyapunov function (CLF), and the matrices  $B_i$  are not empowered to have uncertainties. To the best of the authors' knowledge, few attempts have been devoted to the robust nonfragile controller design for discrete-time piecewise affine systems based on PLFs, which inspires us for this study.

In this paper, we will consider the piecewise affine nonfragile control problem for a class of discrete-time hybrid systems based on piecewise affine models. Via employing a state-control augmentation approach, a new nonfragile controller synthesis method is proposed based on piecewise Lyapunov functions (PLFs), which removes the restrictive condition that the input matrices do not have uncertainties. This feature enables one to design the nonfragile controller for a broader class of industrial systems. It is shown that the resulting closed-loop PWA system is asymptotically stable with a prescribed disturbance attenuation level  $\gamma$ , and the controller gains can be acquired via solving a set of linear matrix inequalities (LMIs). Finally, two simulation examples are presented to show the effectiveness and amenability of the proposed approaches. The main contributions of this paper are listed as follows: (1) The controller is designed based on PLFs and piecewise affine models and the conservatism can be reduced. (2) A new robust piecewise affine nonfragile controller is designed to deal with the situations that perturbations exist in the controller gains. (3) The input matrices are empowered to have uncertainties, which is more applicable for some practical requirements.

The rest of this paper is organized as follows. The piecewise affine model description and nonfragile controller design are given in Section 2. The asymptotic stability analysis for resulting closed-loop system is shown in Section 3. Simulation examples are shown in Section 4 to verify the effectiveness of the proposed methods. Section 5 gives the conclusions.

*Notations.* The notations employed in this paper are standard. A real symmetric matrix  $A > 0$  ( $\geq 0$ ) indicates  $A$  being positive-definite (positive-semi-definite).  $\text{sym}\{X\}$  is the shorthand notation for  $X^T + X$ .

## 2. Problem Formulation

*2.1. Discrete-Time Piecewise Affine Systems.* A discrete-time piecewise affine system is shown as

$$\begin{aligned} x(t+1) &= (A_i + \Delta A_i)x(t) + a_i + \Delta a_i \\ &\quad + (B_i + \Delta B_i)u(t) + H_i w(t) \\ z(t) &= L_i x(t) + N_i u(t), \\ x(t) &\in \Sigma_i, \quad i \in \Pi := \{1, 2, \dots, \phi\} \end{aligned} \quad (1)$$

where  $x(t) \in \mathfrak{R}^n$  is the system state;  $u(t) \in \mathfrak{R}^m$  is the control input;  $z(t) \in \mathfrak{R}^p$  is the regulated output;  $w(t)$  is the external nonlinear disturbance belonging to  $l_2[0, \infty)$ ;  $\Sigma_i$  is a polyhedral partition from the state-space and  $\Pi$  is the index set of these polyhedral regions;  $\Delta A_i$ ,  $\Delta a_i$ , and  $\Delta B_i$  are the uncertainty terms of the  $i$ -th local affine model satisfying

$$[\Delta A_i \quad \Delta a_i \quad \Delta B_i] = W_{i1} \Delta_i(t) [M_{i1} \quad M_{i2} \quad M_{i3}], \quad i \in \Pi \quad (2)$$

with  $W_{i1}$ ,  $M_{i1}$ ,  $M_{i2}$ , and  $M_{i3}$  being known real constant matrices.  $\Delta_i(t)$  is unknown time-varying matrix satisfying

$$\Delta_i^T(t) \Delta_i(t) \leq \mathbf{I}. \quad (3)$$

*Remark 1.* The system model in (1) is in fact affine systems rather than linear systems as the offset term ( $a_i + \Delta a_i$ ) is involved. One can easily conclude that this type of models is more accurate for approximation to nonlinear systems [41].

Following the idea given in [20], define the region index  $\Pi = \Pi_0 \cup \Pi_1$ , where  $\Pi_1$  denotes the index set of subspaces without the origin and  $\Pi_0$  refers to the index set of subspaces containing the origin.

For future use, a new set  $\Omega$  is introduced to depict all possible region transitions

$$\Omega := \{(i, j) \mid x(t) \in \Sigma_i, x(t+1) \in \Sigma_j, i, j \in \Pi\}. \quad (4)$$

When  $(i, j) \in \Omega$  and  $i = j$ , the state is involved in the same region  $\Sigma_i$  at the time  $t$ . Otherwise, the state trajectories will jump from the region  $\Sigma_i$  to  $\Sigma_j$  at that time.

In this paper, it is assumed that each polyhedral regions  $\Sigma_i$  can be outer approximated by an ellipsoid  $\Psi_i$ , that is to say, there exist matrices  $Q_i$  and  $q_i$  such that

$$\Sigma_i \subseteq \Psi_i, \quad \Psi_i := \{x \mid \|Q_i x + q_i\| \leq 1\}. \quad (5)$$

When  $\Sigma_i$  are slab regions, the above covering is useful, and then the parameters  $Q_i$  and  $q_i$  are guaranteed to exist, and  $\Sigma_i \subseteq \Psi_i$  and  $\Psi_i \subseteq \Sigma_i$ . If the polyhedral regions  $\Sigma_i$  are slabs with

$$\Sigma_i = \{x \mid \alpha_i \leq x \leq \beta_i\}, \quad i \in \Pi, \quad (6)$$

where  $\alpha_i, \beta_i \in \mathfrak{R}$ ,  $\phi_i \in \mathfrak{R}^n$ , then each slab can be represented by a degenerate ellipsoid as in (6) with

$$\begin{aligned} Q_i &= \frac{2\phi_i^T}{\beta_i - \alpha_i}, \\ q_i &= \frac{\beta_i + \alpha_i}{\alpha_i - \beta_i}. \end{aligned} \quad (7)$$

For each ellipsoid region, we have the following relationship:

$$\begin{bmatrix} 1 \\ x(t) \end{bmatrix}^T \begin{bmatrix} q_i^T q_i - 1 & q_i^T Q_i \\ * & Q_i^T Q_i \end{bmatrix} \begin{bmatrix} 1 \\ x(t) \end{bmatrix} \leq 0, \quad i \in \Pi. \quad (8)$$

**2.2. Piecewise Affine Nonfragile Controller Design.** Borrowing the idea from [42], define  $\xi(t) = [x^T(t) \ u^T(t)]^T$ . As the inaccuracies or uncertainties inevitably involved in the controllers in many practical situations, for the piecewise affine system (1), a new nonfragile piecewise affine controller in differential form is designed as

$$u(t+1) = (K_i + \Delta K_i)\xi(t) + k_i + \Delta k_i, \quad (9)$$

where  $K_i \in \mathfrak{R}^{n_u \times (n_x + n_u)}$  and  $k_i \in \mathfrak{R}^{n_u}$  are the controller gains to be determined, and  $k_i = 0$  for  $i \in \Pi_0$ .  $\Delta K_i$  and  $\Delta k_i$  are unknown matrices standing for the gain perturbations satisfying

$$[\Delta K_i \ \Delta k_i] = W_{i2} \Delta_{ui}(t) [U_{i1} \ U_{i2}], \quad i \in \Pi, \quad (10)$$

where  $W_{i2}$ ,  $U_{i1}$ , and  $U_{i2}$  are known real constant matrices of appropriate dimensions. The real-valued matrix functions  $\Delta_{ui}(t)$  satisfy

$$\Delta_{ui}^T(t) \Delta_{ui}(t) \leq \mathbf{I}. \quad (11)$$

The parameter uncertainties in (1) and (9) are recognized to be admissible if (2)-(3) and (10)-(11) hold.

By applying the piecewise affine nonfragile controller (9) into system (1), the closed-loop system can be formulated as

$$\begin{aligned} \xi(t+1) &= (\mathcal{A}_i + \Delta \mathcal{A}_i)\xi(t) + a_i + \Delta a_i + \overline{H}_i w(t) \\ z(t) &= \overline{L}_i \xi(t), \\ x(t) &\in \Sigma_i, \end{aligned} \quad (12)$$

$i \in \Pi,$

where  $\mathcal{A}_i = \overline{A}_i + RK_i$ ,  $\Delta \mathcal{A}_i = \Delta \overline{A}_i + R\Delta K_i$ ,  $a_i = \overline{a}_i + Rk_i$ ,  $\Delta a_i = \Delta \overline{a}_i + R\Delta k_i$ , and

$$\begin{aligned} \overline{A}_i &= \begin{bmatrix} A_i & B_i \\ \mathbf{0} & \mathbf{0} \end{bmatrix}, \\ \Delta \overline{A}_i &= \begin{bmatrix} \Delta A_i & \Delta B_i \\ \mathbf{0} & \mathbf{0} \end{bmatrix}, \end{aligned}$$

$$\overline{a}_i = \begin{bmatrix} a_i \\ \mathbf{0} \end{bmatrix},$$

$$\Delta \overline{a}_i = \begin{bmatrix} \Delta a_i \\ \mathbf{0} \end{bmatrix},$$

$$R = \begin{bmatrix} \mathbf{0} \\ \mathbf{I}_{n_u} \end{bmatrix},$$

$$\overline{H}_i = \begin{bmatrix} H_i \\ \mathbf{0} \end{bmatrix},$$

$$\overline{L}_i = [L_i \ N_i].$$

(13)

Based on the augment vector  $\xi(t)$ , the following inequality implies (8) for each ellipsoid region,

$$\begin{bmatrix} 1 \\ \xi(t) \end{bmatrix}^T \begin{bmatrix} q_i^T q_i - 1 & q_i^T \overline{Q}_i \\ * & \overline{Q}_i^T \overline{Q}_i \end{bmatrix} \begin{bmatrix} 1 \\ \xi(t) \end{bmatrix} \leq 0, \quad i \in \Pi, \quad (14)$$

where  $\overline{Q}_i = [Q_i \ \mathbf{0}_{n_u \times n_u}]$ .

As practical control systems are always subject to external disturbance, thus, in this paper, we aim to synthesize an admissible piecewise affine nonfragile controller in the form of (9) such that the resulting closed-loop system is asymptotically stable with robust  $\mathcal{H}_\infty$  performance  $\gamma$  as

$$\|z\|_2 < \gamma \|w\|_2 \quad (15)$$

under zero initial conditions for all nonzero  $w(t) \in l_2[0, \infty]$ .

Before ending this section, the following lemmas will be employed to prove the main results in this paper.

**Lemma 2** (see [22]). *Real matrices  $Q > 0$ ,  $R$ ,  $\Delta(t)$ , and  $S$  are regular matrices with appropriate dimensions.  $\Delta(t)$  is time-varying satisfying  $\Delta^T(t)\Delta(t) \leq \mathbf{I}$ . The inequality*

$$Q + R\Delta(t)S + S^T\Delta^T(t)R^T < 0 \quad (16)$$

holds if and only if for some  $\varepsilon > 0$

$$Q + \varepsilon R^T R + \varepsilon^{-1} S^T S < 0. \quad (17)$$

### 3. Piecewise Affine Nonfragile Controller Analysis and Design

On the basis of piecewise Lyapunov functions (PLFs), some new approaches to robust  $\mathcal{H}_\infty$  piecewise affine nonfragile controller synthesis will be proposed in this section.

**Theorem 3.** For a given constant scalar  $\lambda$ , the closed-loop system (12) is asymptotically stable with disturbance attenuation level  $\gamma$  if there exist matrices  $0 < P_i = P_i^T \in \mathfrak{R}^{(n+m) \times (n+m)}$ ,  $\bar{K}_i \in \mathfrak{R}^{m \times (n+m)}$ ,  $\bar{k}_i \in \mathfrak{R}^m$ ,  $V_{i1} \in \mathfrak{R}^{n \times n}$ ,  $V_{i2} \in \mathfrak{R}^{m \times n}$ ,  $V_{i3} \in \mathfrak{R}^{m \times m}$ , and  $i \in \Pi$  and two sets of scalars  $\{r_{ij} < 0, i \in \Pi_1, (i, j) \in \Omega\}$ , and  $\{\varepsilon_i > 0, i \in \Pi\}$ , such that the following LMIs hold:

$$\begin{bmatrix} \Gamma_{ij1} + \varepsilon_{ij} \Theta_{i1}^T \Theta_{i1} & \Lambda_{i1}^{(1)} & \Lambda_{i1}^{(2)} \\ * & -\varepsilon_{ij} \mathbf{I} & \mathbf{0} \\ * & * & -\varepsilon_{ij} \mathbf{I} \end{bmatrix} < 0, \quad (18)$$

$$i \in \Pi_0, j \in \Pi, (i, j) \in \Omega,$$

$$\begin{bmatrix} \Gamma_{ij2} + \varepsilon_{ij} \Theta_{i2}^T \Theta_{i2} & \Lambda_{i2}^{(1)} & \Lambda_{i2}^{(2)} \\ * & -\varepsilon_{ij} \mathbf{I} & \mathbf{0} \\ * & * & -\varepsilon_{ij} \mathbf{I} \end{bmatrix} < 0, \quad (19)$$

$$i \in \Pi_1, j \in \Pi, (i, j) \in \Omega,$$

where

$$\Gamma_{ij1} = \begin{bmatrix} P_j - V_i - V_i^T & V_i \bar{A}_i + E \bar{K}_i & V_i \bar{H}_i \\ * & -P_i + \bar{L}_i^T \bar{L}_i & \mathbf{0} \\ * & * & -\gamma^2 \mathbf{I} \end{bmatrix},$$

$$\Theta_{i1} = \begin{bmatrix} \mathbf{0} & \mathbf{0} \\ \bar{M}_{i1}^T & U_{i1}^T \\ \mathbf{0} & \mathbf{0} \end{bmatrix},$$

$$\Lambda_{i1}^{(1)} = \begin{bmatrix} V_i \bar{W}_{i1} \\ \mathbf{0} \\ \mathbf{0} \end{bmatrix},$$

$$\Lambda_{i1}^{(2)} = \begin{bmatrix} V_i R W_{i2} \\ \mathbf{0} \\ \mathbf{0} \end{bmatrix},$$

$\Gamma_{ij2}$

$$= \begin{bmatrix} P_j - V_i - V_i^T & V_i \bar{a}_i + E \bar{k}_i & V_i \bar{A}_i + E \bar{K}_i & V_i \bar{H}_i \\ * & -r_{ij} (1 - q_i^T q_i) & r_{ij} q_i^T \bar{Q}_i & \mathbf{0} \\ * & * & -P_i + r_{ij} \bar{Q}_i^T \bar{Q}_i + \bar{L}_i^T \bar{L}_i & \mathbf{0} \\ * & * & * & -\gamma^2 \mathbf{I} \end{bmatrix},$$

$$\Theta_{i2} = \begin{bmatrix} \mathbf{0} & \mathbf{0} \\ M_{i2}^T & U_{i2}^T \\ \bar{M}_{i1}^T & U_{i1}^T \\ \mathbf{0} & \mathbf{0} \end{bmatrix},$$

$$\Lambda_{i2}^{(1)} = \begin{bmatrix} V_i \bar{W}_{i1} \\ \mathbf{0} \\ \mathbf{0} \\ \mathbf{0} \end{bmatrix},$$

$$\Lambda_{i2}^{(2)} = \begin{bmatrix} V_i R W_{i2} \\ \mathbf{0} \\ \mathbf{0} \\ \mathbf{0} \end{bmatrix},$$

$$V_i = \begin{bmatrix} V_{i1} & \lambda S V_{i2} \\ V_{i3} & V_{i2} \end{bmatrix},$$

$$E = \begin{bmatrix} \lambda S \\ \mathbf{I}_m \end{bmatrix},$$

$$\bar{A}_i = \begin{bmatrix} A_i & B_i \\ 0 & 0 \end{bmatrix},$$

$$\bar{a}_i = \begin{bmatrix} a_i \\ 0 \end{bmatrix},$$

$$\bar{H}_i = \begin{bmatrix} H_i \\ 0 \end{bmatrix},$$

$$\bar{W}_{i1} = \begin{bmatrix} W_{i1} \\ \mathbf{0} \end{bmatrix},$$

$$\bar{M}_{i1} = [M_{i1} \ M_{i3}],$$

(20)

and  $S \in \mathfrak{R}^{(n+m) \times m}$  is an arbitrary matrix.

Moreover, the controller gains for each subspace can be determined via

$$K_i = V_{i2}^{-1} \bar{K}_i, \quad (21)$$

$$k_i = V_{i2}^{-1} \bar{k}_i,$$

*Proof.* It is easy to see that condition (18) for  $i \in \Pi_0$  is a special case of condition (19) for  $i \in \Pi_1$ . Without loss of generality, in the following, the proof of the more complex case  $i \in \Pi_1$  is to be considered. Take the piecewise Lyapunov function as

$$V(t) = \xi^T(t) P_i \xi(t), \quad i \in \Pi. \quad (22)$$

It is also assumed that  $x(t+1) \in \Sigma_j$ . Then we have  $V(t+1) = \xi^T(t+1) P_j \xi(t+1)$ . The closed-loop system in (12) is asymptotically stable with robust  $\mathcal{H}_\infty$  performance  $\gamma$ , if the inequality

$$V(t+1) - V(t) + z^T(t) z(t) - \gamma^2 w^T(t) w(t) < 0 \quad (23)$$

holds.

By substituting (22) into (23), it yields that

$$\begin{aligned} & \xi^T(t+1) P_j \xi(t+1) - \xi^T(t) P_i \xi(t) + z^T(t) z(t) \\ & - \gamma^2 w^T(t) w(t) < 0, \quad (i, j) \in \Omega. \end{aligned} \quad (24)$$

Along the trajectories of closed-loop system (12), the following inequality implies (24) with  $(i, j) \in \Omega$ ,

$$\begin{aligned} & \begin{bmatrix} 1 \\ \xi(t) \\ w(t) \end{bmatrix}^T \left\{ \begin{bmatrix} a_i^T + \Delta a_i^T \\ \mathcal{A}_i^T + \Delta \mathcal{A}_i^T \\ \bar{H}_i^T \end{bmatrix} P_j(\star) + \begin{bmatrix} \mathbf{0} \\ \bar{\mathcal{L}}_i^T \\ \mathbf{0} \end{bmatrix} (\star) \right. \\ & \left. + \begin{bmatrix} \mathbf{0} & \mathbf{0} & \mathbf{0} \\ \star & -P_i & \mathbf{0} \\ \star & \star & -\gamma^2 \mathbf{I} \end{bmatrix} \right\} \begin{bmatrix} 1 \\ \xi(t) \\ w(t) \end{bmatrix} < 0. \end{aligned} \quad (25)$$

Noticing the state-space partition (14) and utilizing S-procedure, the following inequality implies (25) based on Schur complement:

$$\begin{aligned} & \begin{bmatrix} -P_j^{-1} & a_i + \Delta a_i & \mathcal{A}_i + \Delta \mathcal{A}_i & \bar{H}_i \\ \star & r_{ij}(q_i^T q_i - 1) & r_{ij} q_i^T \bar{Q}_i & \mathbf{0} \\ \star & \star & -P_i + r_{ij} \bar{Q}_i^T \bar{Q}_i + \bar{L}_i^T \bar{L}_i & \mathbf{0} \\ \star & \star & \star & -\gamma^2 \mathbf{I} \end{bmatrix} \\ & < 0, \quad i \in \Pi_1, (i, j) \in \Omega. \end{aligned} \quad (26)$$

It can be concluded that the Lyapunov matrices  $P_i$  and  $P_j$  are coupled with the system matrices. In order to facilitate

the controller design, we need to handle with the terms  $P_i$  and  $P_j^{-1}$ . To this end, for convenience in the controller synthesis, we make a congruence transformation to (26) by  $\text{diag}\{V_i, \mathbf{I}, \mathbf{I}, \mathbf{I}\}$  as

$$\begin{aligned} & \begin{bmatrix} -V_i P_j^{-1} V_i^T & V_i(a_i + \Delta a_i) & V_i(\mathcal{A}_i + \Delta \mathcal{A}_i) & V_i \bar{H}_i \\ \star & r_{ij}(q_i^T q_i - 1) & r_{ij} q_i^T \bar{Q}_i & \mathbf{0} \\ \star & \star & -P_i(\mu) + r_{ij} \bar{Q}_i^T \bar{Q}_i + \bar{L}_i^T \bar{L}_i & \mathbf{0} \\ \star & \star & \star & -\gamma^2 \mathbf{I} \end{bmatrix} \\ & < 0, \quad i \in \Pi_1, (i, j) \in \Omega. \end{aligned} \quad (27)$$

Notice that

$$\begin{aligned} P_j - V_i - V_i^T + V_i P_j^{-1} V_i^T &= (P_j - V_i) P_j^{-1} (P_j - V_i)^T \\ &\geq 0, \end{aligned} \quad (28)$$

which indicates that

$$-V_i P_j^{-1} V_i^T \leq P_j - V_i - V_i^T. \quad (29)$$

Based on (29), the following inequality implies (27):

$$\begin{aligned} & \begin{bmatrix} P_j - V_i - V_i^T & V_i(a_i + \Delta a_i) & V_i(\mathcal{A}_i + \Delta \mathcal{A}_i) & V_i \bar{H}_i \\ \star & r_{ij}(q_i^T q_i - 1) & r_{ij} q_i^T \bar{Q}_i & \mathbf{0} \\ \star & \star & -P_i(\mu) + r_{ij} \bar{Q}_i^T \bar{Q}_i + \bar{L}_i^T \bar{L}_i & \mathbf{0} \\ \star & \star & \star & -\gamma^2 \mathbf{I} \end{bmatrix} \\ & < 0, \quad i \in \Pi_1, (i, j) \in \Omega. \end{aligned} \quad (30)$$

Notice that the controller gains are not involved in the first row of the matrices  $\mathcal{A}_i$ ,  $\Delta \mathcal{A}_i$ ,  $a_i$ , and  $\Delta a_i$ . For numerical tractability, we specify  $V_i$  as

$$V_i = \begin{bmatrix} V_{i1} & \lambda S V_{i2} \\ V_{i3} & V_{i2} \end{bmatrix}, \quad i \in \mathcal{S}_1, \quad (31)$$

where  $\lambda$  and  $S$  are defined as in (20).

Based on the matrices defined as in (31), one has that

$$V_i R K_i = \begin{bmatrix} V_{i1} & \lambda S V_{i2} \\ V_{i3} & V_{i2} \end{bmatrix} \begin{bmatrix} \mathbf{0} \\ \mathbf{I}_{n_u} \end{bmatrix} K_i = E \bar{K}_i, \quad (32)$$

$$V_i R k_i = \begin{bmatrix} V_{i1} & \lambda S V_{i2} \\ V_{i3} & V_{i2} \end{bmatrix} \begin{bmatrix} \mathbf{0} \\ \mathbf{I}_{n_u} \end{bmatrix} k_i = E \bar{k}_i,$$

where  $R = [\lambda S^T \quad \mathbf{I}_{n_u}]^T$ ,  $\bar{K}_i = V_{i2} K_i$ ,  $\bar{k}_i = V_{i2} k_i$ .

Substitute (32) into (30), and use Lemma 2 to handle the uncertainty terms. Then the following inequality implies (30) for  $\varepsilon_i > 0$ ,  $i \in \Pi$ ,

$$\begin{aligned} & \begin{bmatrix} P_j - V_i - V_i^T & V_i \bar{a}_i + E \bar{k}_i & V_i \bar{\mathcal{A}}_i + R \bar{K}_i & V_i \bar{H}_i \\ \star & r_{ij}(q_i^T q_i - 1) & r_{ij} q_i^T \bar{Q}_i & \mathbf{0} \\ \star & \star & -P_i + r_{ij} \bar{Q}_i^T \bar{Q}_i + \bar{L}_i^T \bar{L}_i & \mathbf{0} \\ \star & \star & \star & -\gamma^2 \mathbf{I} \end{bmatrix} \\ & + \varepsilon_i^{-1} \begin{bmatrix} V_i \bar{W}_{i1} & V_i R W_{i2} \\ \mathbf{0} & \mathbf{0} \\ \mathbf{0} & \mathbf{0} \\ \mathbf{0} & \mathbf{0} \end{bmatrix} (\star) + \varepsilon_i \begin{bmatrix} \mathbf{0} & \mathbf{0} \\ M_{i2}^T & U_{i2}^T \\ \bar{M}_{i1}^T & U_{i1}^T \\ \mathbf{0} & \mathbf{0} \end{bmatrix} < 0 \end{aligned} \quad (33)$$

where

$$\bar{W}_{i1} = \begin{bmatrix} W_{i1} \\ \mathbf{0} \end{bmatrix}, \quad (34)$$

$$\bar{M}_{i1} = [M_{i1} \quad M_{i3}].$$

On the basis of Schur complement, it is easy to conclude that (19) implies (33). The proof is thus completed.  $\square$

*Remark 4.* Note that in most existing nonfragile controller synthesis references for PWA systems, the control input matrices are not empowered to have uncertainties, which is restrictive for the control system design. In addition, it is also difficult to design a nonfragile piecewise affine controller via the approach proposed in [16], as one needs to develop a singular value decomposition to the control input matrices. However, by employing a state-control augmentation strategy for the nonfragile piecewise affine controller design, then the controller gains and the control input matrices can be decoupled from each other. As the state-control augmentation methodology is exploited, the uncertainty terms  $\Delta K_i$  and  $\Delta k_i$  in the controller are decoupled from the system matrices. This feature makes it possible to design a piecewise affine nonfragile controller via convexification techniques in a uniform framework.

If the uncertainty terms, affine terms, and external disturbance do not exist, system (1) reduces to a nominal piecewise system as

$$x(t+1) = A_i x(t) + B_i u(t). \quad (35)$$

For system (35), a piecewise linear nonfragile controller in a differential form is designed as

$$u(t+1) = (K_i + \Delta K_i) \xi(t) \quad (36)$$

with  $\xi(t)$  and  $\Delta K_i$  defined as in (9).

Substituting the controller (36) into system (35), then the resulting closed-loop system is

$$\xi(t+1) = (\bar{A}_i + RK_i + R\Delta K_i) \xi(t) \quad (37)$$

where  $\bar{A}_i$  is denoted as in (13).

**Corollary 5.** For a given constant scalar  $\lambda$ , the closed-loop system (37) is asymptotically stable if there exist matrices  $0 < P_i = P_i^T \in \mathfrak{R}^{(n+m) \times (n+m)}$ ,  $\bar{K}_i \in \mathfrak{R}^{m \times (n+m)}$ ,  $V_{i1} \in \mathfrak{R}^{n \times n}$ ,  $V_{i2} \in \mathfrak{R}^{m \times n}$ ,  $V_{i3} \in \mathfrak{R}^{m \times m}$ , and  $i \in \Pi$  and a set of positive scalar  $\varepsilon_i > 0$ ,  $i \in \Pi$ , such that

$$\begin{bmatrix} P_j - V_i - V_i^T & V_i \bar{A}_i + E \bar{K}_i & V_i R W_{i2} \\ * & -P_i + \varepsilon_i U_{i1}^T U_{i1} & \mathbf{0} \\ * & * & -\varepsilon_i \mathbf{I} \end{bmatrix} < 0, \quad (38)$$

$$i \in \Pi.$$

Moreover, the controller gain can be obtained by  $K_i = V_{i2}^{-1} \bar{K}_i$ .

The derivation procedures are similar to that of Theorem 3. The proof is omitted.

*Remark 6.* Note that when the uncertainty terms in the form of (10) in the controller gains do not exist, that is to say,

$$W_{i2} = U_{i1} = U_{i2} = 0, \quad i \in \Pi, \quad (39)$$

then the piecewise affine nonfragile controller reduces to a regular piecewise affine state-feedback controller as

$$u(t+1) = K_i \xi(t) + k_i, \quad i \in \Pi, \quad (40)$$

where  $\xi(t) = [x^T(t) \ u^T(t)]^T$ .

## 4. Simulation

In this section, two simulation examples are shown to illustrate the effectiveness of the proposed approaches.

*Example 1.* Consider a discrete-time piecewise affine system in the form of (1) as follows:

$$\begin{aligned} x(t+1) &= (A_i + \Delta A_i) x(t) + a_i + \Delta a_i \\ &\quad + (B_i + \Delta B_i) u(t) + H_i w(t) \\ z(t) &= L_i x(t) + N_i u(t), \end{aligned} \quad (41)$$

$$x(t) \in \Sigma_i, \quad i \in \{1, 2, 3\},$$

and the system matrices are given as

$$A_1 = \begin{bmatrix} 1.2 & 0 \\ -0.1 & 0.4 \end{bmatrix},$$

$$A_2 = \begin{bmatrix} 0.5 & 0.1 \\ 0 & 1.1 \end{bmatrix},$$

$$A_3 = \begin{bmatrix} 1.1 & 0.3 \\ 0.1 & 0.2 \end{bmatrix},$$

$$a_1 = \begin{bmatrix} 0 \\ -0.45 \end{bmatrix},$$

$$a_2 = \begin{bmatrix} 0 \\ 0 \end{bmatrix},$$

$$a_3 = \begin{bmatrix} 0 \\ 0.45 \end{bmatrix},$$

$$B_1 = \begin{bmatrix} 1 \\ 0.5 \end{bmatrix},$$

$$B_2 = \begin{bmatrix} 1 \\ 1.5 \end{bmatrix},$$

$$B_3 = \begin{bmatrix} 0.9 \\ 1.2 \end{bmatrix},$$

$$H_1 = \begin{bmatrix} 0.8 \\ 0.5 \end{bmatrix},$$

$$\begin{aligned}
 H_2 &= \begin{bmatrix} 0.7 \\ 0.6 \end{bmatrix}, \\
 H_3 &= \begin{bmatrix} 0.4 \\ 0.4 \end{bmatrix}, \\
 L_1 &= [1 \ 0.3], \\
 L_2 &= [1.2 \ 0.5], \\
 L_3 &= [0.5 \ 1], \\
 N_1 &= 1, \\
 N_2 &= 0.8, \\
 N_3 &= 1.2, \\
 W_{11} &= \begin{bmatrix} 0.1 \\ 0.2 \end{bmatrix}, \\
 W_{21} &= \begin{bmatrix} 0.3 \\ 0.1 \end{bmatrix}, \\
 W_{31} &= \begin{bmatrix} 0.4 \\ 0.1 \end{bmatrix}, \\
 M_{11} &= [0.01 \ 0.01], \\
 M_{21} &= [0.01 \ 0.03], \\
 M_{31} &= [0.03 \ 0.02], \\
 M_{12} &= 0.1, \\
 M_{22} &= 0.2, \\
 M_{32} &= 0.05, \\
 M_{i3} &= 0.01,
 \end{aligned} \tag{42}$$

and the parameter uncertainties in controllers in terms of (10) are

$$\begin{aligned}
 W_{i2} &= 0.8, \\
 U_{i1} &= [0.8 \ 0.8 \ 0.8], \\
 U_{i2} &= 0.8,
 \end{aligned} \tag{43}$$

$i \in \{1, 2, 3\}.$

The decomposed regions are given as

$$\begin{aligned}
 \Sigma_1 &= \{x(t) \mid -\beta < x_1(t) \leq -\alpha\}, \\
 \Sigma_2 &= \{x(t) \mid -\alpha < x_1(t) \leq \alpha\}, \\
 \Sigma_3 &= \{x(t) \mid \alpha < x_1(t) \leq \beta\},
 \end{aligned} \tag{44}$$

where  $\alpha = 40$  and  $\beta = 400$ .

From the relationship in (7), we can obtain that  $\phi_i^T = [1 \ 0]$ , for  $i \in \Pi$ , and the parameters of the degenerate ellipsoids are

$$\begin{aligned}
 Q_1 &= \frac{2\phi_i^T}{\beta - \alpha}, \\
 q_1 &= \frac{\beta + \alpha}{\beta - \alpha}, \\
 Q_2 &= \frac{1}{d_1}, \\
 q_2 &= 0, \\
 Q_3 &= \frac{2\phi_i^T}{\beta - \alpha}, \\
 q_3 &= \frac{\beta + \alpha}{\alpha - \beta}.
 \end{aligned} \tag{45}$$

The objective is to design a piecewise affine nonfragile controller in the form of (9)-(10) such that the closed-loop system in (12) is asymptotically stable with a robust  $\mathcal{H}_\infty$  performance  $\gamma$ . Exploiting Theorem 3 with  $S = [1 \ 0]^T$  and  $\lambda = 1$ , the controller gains can be obtained as

$$\begin{aligned}
 K_1 &= [-1.3002 \ -0.1249 \ -1.2656], \\
 k_1 &= 0.2580, \\
 K_2 &= [-1.5930 \ -0.1369 \ -1.5294], \\
 k_2 &= 0, \\
 K_3 &= [-1.5756 \ -0.1317 \ -1.5052], \\
 k_3 &= -0.1308,
 \end{aligned} \tag{46}$$

with robust  $\mathcal{H}_\infty$  performance  $\gamma_{\min} = 1.4222$ .

It is worth pointing out that when  $k_i \equiv 0$ , the piecewise affine nonfragile controller (9) is characterized as a piecewise linear nonfragile controller given in (36). With  $\lambda = 1$ , Table 1 compares the robust performance between piecewise affine nonfragile controllers with piecewise linear nonfragile controllers with different matrix  $S$ .

It can be seen from Table 1 that the piecewise affine nonfragile controllers have a better robust  $\mathcal{H}_\infty$  performance than the piecewise linear nonfragile controllers.

To verify the effectiveness of the designed controllers, simulations are carried out. With  $S = [1 \ 0]^T$  and  $\lambda = 1$ , solving the LMIs in (18)-(19), we obtain the piecewise linear nonfragile controller gains as

$$\begin{aligned}
 K_1 &= [-1.3003 \ -0.1261 \ -1.2658], \\
 K_2 &= [-1.5903 \ -0.1367 \ -1.5266], \\
 K_3 &= [-1.5736 \ -0.1302 \ -1.5033].
 \end{aligned} \tag{47}$$

In this simulation example, the initial condition is  $x_0 = [2 \ -1.5]^T$ , and the external disturbance is  $w(t) = 120\pi^{-3.6t}$ .

TABLE 1: Comparison of robust  $\mathcal{H}_\infty$  performance for piecewise-affine/piecewise-linear nonfragile controllers.

Controller form	$S = \begin{bmatrix} 1 & 0 \end{bmatrix}^T$	$S = \begin{bmatrix} 1 & 1 \end{bmatrix}^T$	$S = \begin{bmatrix} 1 & -1 \end{bmatrix}^T$
piecewise affine controller	1.4222	1.6797	4.6871
piecewise linear controller	1.5924	1.7997	4.7362

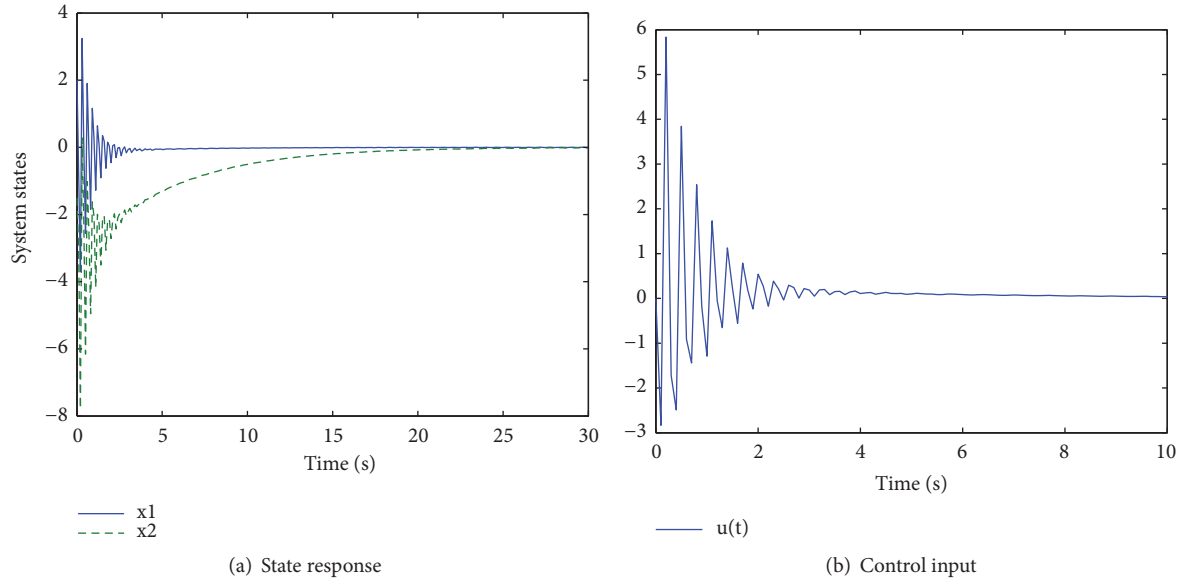


FIGURE 1: Simulation results in Example 1 by using piecewise affine nonfragile controller (9).

$\cos(4t)$ . By using the piecewise affine nonfragile controller in (9), the state response of the closed-loop system is demonstrated in Figure 1(a), and the control input is shown in Figure 1(b). It can be seen from Figure 1(a) that the curves of system states converge to the zero after 20s.

With the same initial conditions and external disturbance, use the piecewise linear nonfragile controller as in (36), and the time responses of the closed-loop system are demonstrated in Figures 2(a) and 2(b). Figure 2(a) shows that the curves of the closed-loop system states converge to the zero after 28s.

Compare Figure 1(a) with Figure 2(a), and one can conclude that the convergence rate of the closed-loop system states with using piecewise affine nonfragile controller is faster than those with using piecewise linear nonfragile controller.

Under zero initial conditions, Figure 3 presents the  $\mathcal{H}_\infty$  performance. The ratio  $\sqrt{\int_0^{t_f} z^T(t)z(t)dt} / \sqrt{\int_0^{t_f} w^T(t)w(t)dt}$  with using piecewise affine nonfragile controller is about 1.18, which is lower than  $\gamma_{\min} = 1.4222$ . The ratio  $\sqrt{\int_0^{t_f} z^T(t)z(t)dt} / \sqrt{\int_0^{t_f} w^T(t)w(t)dt}$  with using piecewise linear nonfragile controller is about 1.3, which is lower than  $\gamma_{\min} = 1.5924$ . It can also be seen that a better disturbance attenuation level can be obtained with the piecewise affine nonfragile controller.

In order to verify the advantages of piecewise affine nonfragile controller (9) over the piecewise affine state-feedback controller (40), another simulation is conducted.

Solve the LMIs in (18)-(19) with  $W_{i2} = 0$ ,  $U_{i1} = \begin{bmatrix} 0 & 0 & 0 \end{bmatrix}$ , and  $U_{i2} = 0$ ,  $i \in \{1, 2, 3\}$ . Feasible solutions can be obtained with  $\lambda = 1$  and  $S = \begin{bmatrix} 1 & 0 \end{bmatrix}^T$ , and the controller gains are

$$\begin{aligned}
 K_1 &= [-1.3202 \quad -0.1148 \quad -1.2689], \\
 k_1 &= 0.2038, \\
 K_2 &= [-1.4634 \quad -0.1183 \quad -1.3938], \\
 k_2 &= 0, \\
 K_3 &= [-1.4888 \quad -0.1168 \quad -1.4112], \\
 k_3 &= -0.1174.
 \end{aligned} \tag{48}$$

With the same initial conditions, disturbance, and parameter variations in the controller gains, apply controller (40) to system (41), and the trajectories of the closed-loop system states are shown in Figure 4. It can be seen from Figure 4 that the piecewise affine state-feedback controller (40) can not stabilize system (39) with parameter variations existing in the controller gains. From this case, we can see that the regular state-feedback controller can not deal with the situations that parameter variations exist in the controller gains.

This example clearly illustrates the advantages of the proposed piecewise affine nonfragile controller over the piecewise linear nonfragile controller and the piecewise affine state-feedback controller.

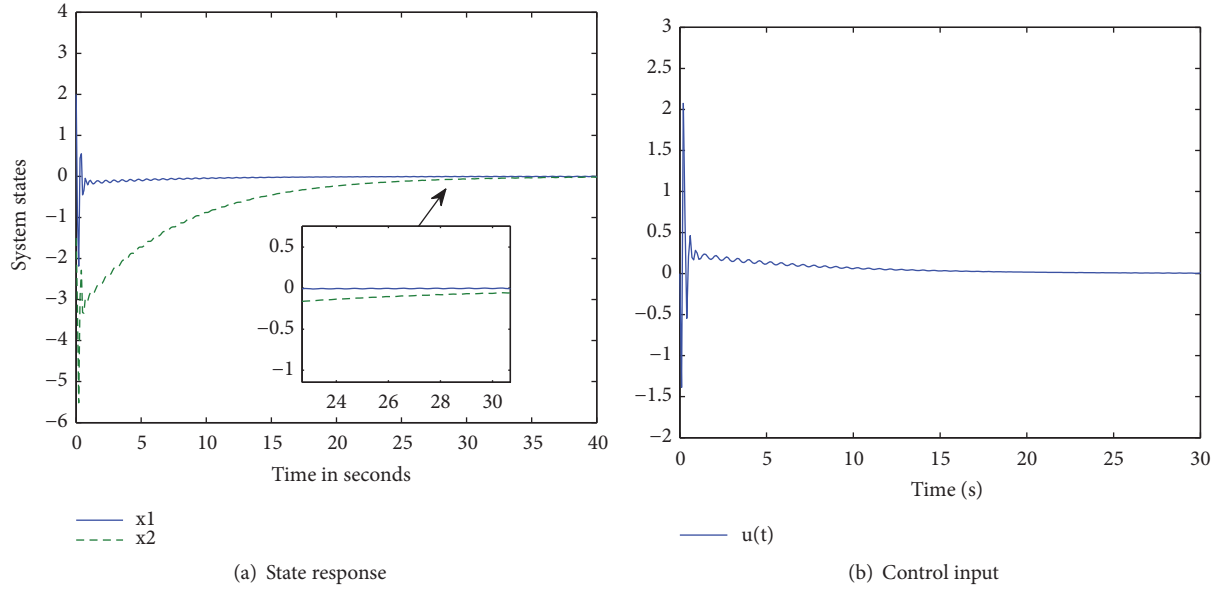


FIGURE 2: Simulation results in Example 1 by using piecewise linear nonfragile controller (36).

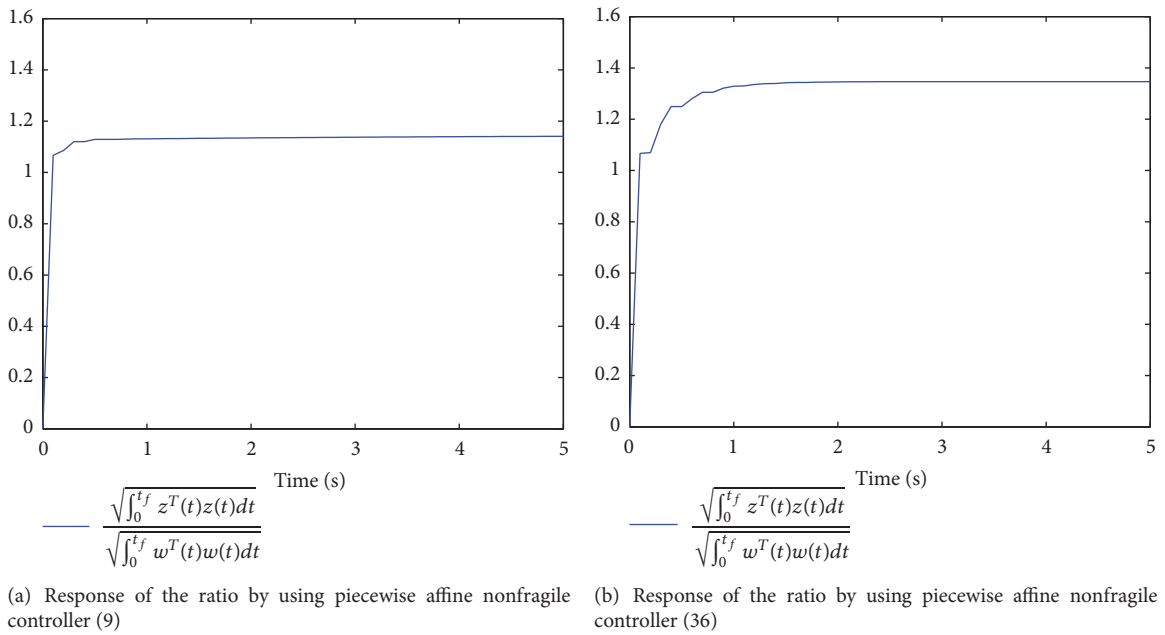


FIGURE 3: Response of the ratio  $\sqrt{\int_0^{t_f} z^T(t)z(t)dt} / \sqrt{\int_0^{t_f} w^T(t)w(t)dt}$  in Example 1.

*Example 2.* Consider another discrete-time Chua's circuit system represented by the piecewise affine model as

$$\begin{aligned}
 x(t+1) &= A_i x(t) + a_i + B_i u(t) + H_i w(t) \\
 z(t) &= L_i x(t) + N_i u(t), \quad (49) \\
 x(t) &\in \Sigma_i, \quad i \in \{1, 2, 3\}
 \end{aligned}$$

where the system matrices are

$$A_1 = \begin{bmatrix} 0.9955 & 0.0070 & 0 \\ 0.0007 & 0.9993 & -0.0011 \\ 0 & 0.0074 & 1 \end{bmatrix}, \quad a_1 = \begin{bmatrix} 0.0028 \\ 0 \\ 0 \end{bmatrix},$$

$$A_2 = \begin{bmatrix} 0.9983 & 0.0070 & 0 \\ 0.0007 & 0.9993 & -0.0011 \\ 0 & 0.0074 & 1 \end{bmatrix},$$

$$A_3 = \begin{bmatrix} 0.9955 & 0.0070 & 0 \\ 0.0007 & 0.9993 & -0.0011 \\ 0 & 0.0074 & 1 \end{bmatrix},$$

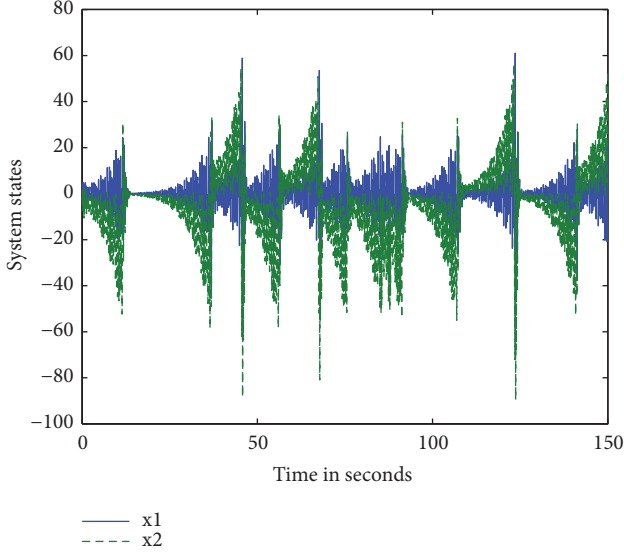


FIGURE 4: State responses in Example 1 by using piecewise affine state-feedback controller (40).

$$a_2 = \begin{bmatrix} 0 \\ 0 \\ 0 \end{bmatrix},$$

$$a_3 = \begin{bmatrix} -0.0028 \\ 0 \\ 0 \end{bmatrix},$$

$$B_1 = B_3 = \begin{bmatrix} -0.00998 \\ 0 \\ 0 \end{bmatrix},$$

$$B_2 = \begin{bmatrix} -0.00999 \\ 0 \\ 0 \end{bmatrix},$$

$$H_1 = H_3 = \begin{bmatrix} 0 \\ 2 \\ 0 \end{bmatrix},$$

$$H_2 = \begin{bmatrix} 0.5 \\ 0 \\ 0 \end{bmatrix},$$

$$L_1 = [1 \ 0 \ 0],$$

$$L_2 = [0.5 \ 0 \ 0],$$

$$L_3 = [1.5 \ 0 \ 0],$$

$$N_i = 0, \quad i \in \{1, 2, 3\}.$$

(50)

The decomposed regions are given as

$$\begin{aligned} \Sigma_1 &= \{x(t) \mid -\beta < x_1(t) \leq -\alpha\}, \\ \Sigma_2 &= \{x(t) \mid -\alpha < x_1(t) \leq \alpha\}, \\ \Sigma_3 &= \{x(t) \mid \alpha < x_1(t) \leq \beta\}, \end{aligned} \quad (51)$$

where  $\alpha = 1, \beta = 5$ .

From (7), we can obtain that  $\phi_i^T = [1 \ 0 \ 0]$ , for  $i \in \Pi$ , and the parameters of the degenerate ellipsoid are

$$\begin{aligned} Q_1 &= [0.5 \ 0 \ 0], \\ q_1 &= -1.5, \\ Q_2 &= [1 \ 0 \ 0], \\ q_2 &= 0, \\ Q_3 &= [0.5 \ 0 \ 0], \\ q_3 &= 1.5. \end{aligned} \quad (52)$$

It is assumed in this example that the perturbations existing in the controller gains are set as

$$\begin{aligned} M_{i2} &= 0.1, \\ U_{i1} &= [0.1 \ 0.1 \ 0.1 \ 0.1], \\ U_{i2} &= 0.3, \end{aligned} \quad (53)$$

$$i \in \{1, 2, 3\}.$$

As the controller gains contain parameter perturbations, we will design a piecewise affine nonfragile controller in (9) to guarantee that the closed-loop system is asymptotically stable with a robust  $\mathcal{H}_\infty$  performance  $\gamma$ . Exploiting Theorem 3 with  $S = [1 \ 0]^T$  and  $\lambda = 1$ , the controller gains can be obtained as

$$\begin{aligned} K_1 &= [-0.1688 \ -0.0053 \ -0.1464 \ 0.0017], \\ k_1 &= -4.7949 \times 10^{-4}, \\ K_2 &= [-0.0147 \ -0.0005 \ -0.0127 \ 0.0001], \\ k_2 &= 0, \\ K_3 &= [-0.0204 \ -0.0006 \ -0.0176 \ 0.0002], \\ k_3 &= 5.7296 \times 10^{-5}, \end{aligned} \quad (54)$$

with robust  $\mathcal{H}_\infty$  performance  $\gamma_{\min} = 0.2755$ .

To present the effectiveness of the designed controllers, simulations are carried out. With initial conditions  $x_0 = [3.5 \ 0 \ -3]^T$  and the external disturbance  $w(t) = 120\pi^{-3.6t} \cdot \cos(4t)$ , the state trajectories of the closed-loop system are demonstrated in Figure 5(a).

Solving the LMIs in (18)-(19) with  $W_{i2} = 0, U_{i1} = [0 \ 0 \ 0], U_{i2} = 0, i \in \{1, 2, 3\}$ , and  $\lambda = 1, S = [2 \ 2 \ 1]^T$ , then

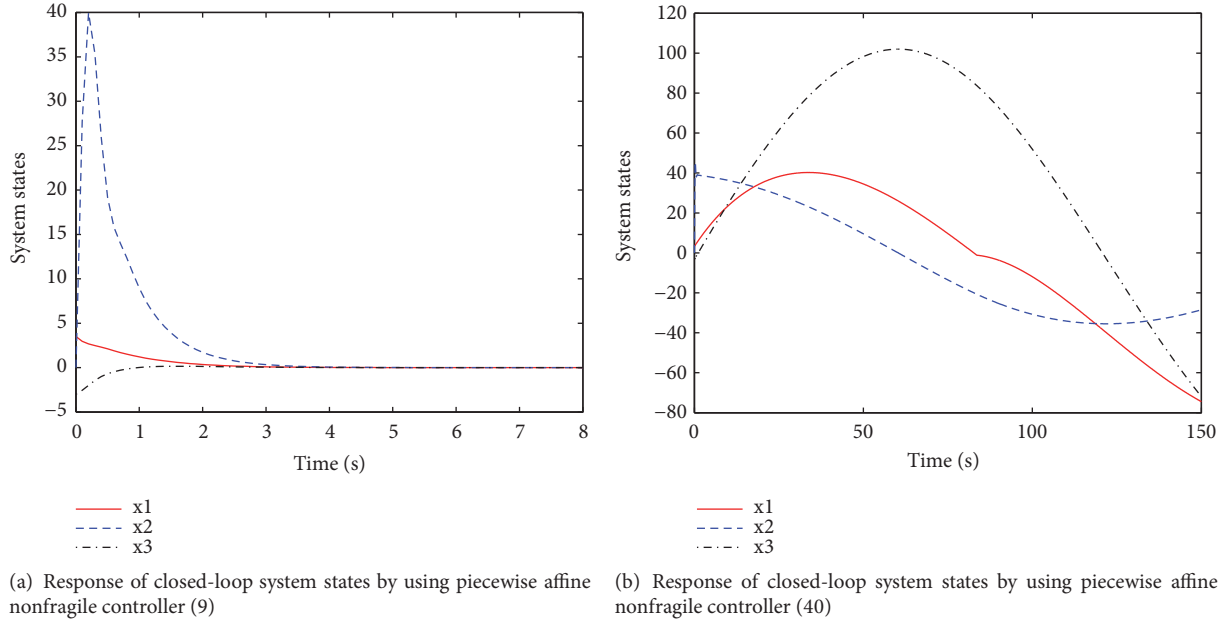


FIGURE 5: Response of the system states in Example 2.

the gains of the piecewise affine state-feedback controller (40) are

$$\begin{aligned}
 K_1 &= [-0.1407 \quad -0.0041 \quad -0.1471 \quad 0.0014], \\
 k_1 &= 1.3805 \times 10^{-6}, \\
 K_2 &= [-0.1688 \quad -0.0050 \quad -0.1772 \quad 0.0017], \\
 k_2 &= 0, \\
 K_3 &= [-0.1536 \quad -0.0045 \quad -0.1613 \quad 0.0015] \times 10^{-6}, \\
 k_3 &= 4.3196 \times 10^{-10}.
 \end{aligned} \tag{55}$$

With the same initial conditions and disturbance, we use controller (40) to system (49), and the closed-loop system states are demonstrated in Figure 5(b). It can be seen from Figure 5 that the piecewise affine state-feedback controller (40) can not stabilize system (49) with parameter variations existing in the controller gains.

## 5. Conclusion

In this paper, we have studied the nonfragile control problem for a class of discrete-time hybrid systems based on piecewise affine model. Based on PLFs, some new sufficient conditions for piecewise affine nonfragile controller synthesis are presented. By virtue of several convexification strategies, the controller gains can be attained via solving a set of linear matrix inequalities. Finally, simulation examples are carried out to demonstrate the advantages of the proposed methodologies.

## Data Availability

The data used to support the findings of this study are available from the corresponding author upon request.

## Conflicts of Interest

The authors declare that there are no conflicts of interest regarding the publication of this paper.

## Acknowledgments

This work is financially supported by the National Key Research and Development Program (Grants nos. 2017YFC0306804 and 2017YFC0305700) and State Key Laboratory of Ocean Engineering (Shanghai Jiao Tong University) (Grant no. 1715).

## References

- [1] A. Bemporad, G. Ferrari-Trecate, and M. Morari, "Observability and controllability of piecewise affine and hybrid systems," *IEEE Transactions on Automatic Control*, vol. 45, no. 10, pp. 1864–1876, 2000.
- [2] A. Bemporad and M. Morari, "Control of systems integrating logic, dynamics, and constraints," *Automatica*, vol. 35, no. 3, pp. 407–427, 1999.
- [3] A. N. Vargas, L. P. Sampaio, L. Acho, L. Zhang, and J. B. R. Do Val, "Optimal control of DC-DC buck converter via linear systems with inaccessible markovian jumping modes," *IEEE Transactions on Control Systems Technology*, vol. 24, no. 5, pp. 1820–1827, 2016.
- [4] L. Acho, J. Rodellar, C. Tutiví, and Y. Vidal, "Passive fault tolerant control strategy in controlled wind turbines," in *Proceeding*

- of the 3rd Conference on Control and Fault-Tolerant Systems (SysTol), pp. 636–641, Barcelona, Spain, 2016.
- [5] Y. L. Wei, M. Wang, and J. B. Qiu, “New approach to delay-dependent  $H_\infty$  filtering for discrete-time Markovian jump systems with time-varying delay and incomplete transition descriptions,” *IET Control Theory & Applications*, vol. 7, no. 5, pp. 684–696, 2013.
  - [6] Y. Wei, J. H. Park, H. R. Karimi, Y.-C. Tian, and H. Jung, “Improved stability and stabilization results for stochastic synchronization of continuous-time semi-markovian jump neural networks with time-varying delay,” *IEEE Transactions on Neural Networks and Learning Systems*, vol. 29, no. 6, pp. 2488–2501, 2017.
  - [7] D. Mignone, G. Ferrari-Trecate, and M. Morari, “Stability and stabilization of piecewise affine and hybrid systems: An LMI approach,” in *Proceedings of the 39th IEEE Conference on Decision and Control*, pp. 504–509, Australia, December 2000.
  - [8] X. Zhao, “Piecewise  $H_\infty$  static output feedback controller design for nonlinear systems based on T-S affine fuzzy models,” *Mathematical Problems in Engineering*, vol. 2015, Article ID 734934, 9 pages, 2015.
  - [9] Z. Zhou, M. Wang, and Q. Yin, “Robust H-infinity stabilization and resilient filtering for discrete-time constrained singular piecewise-affine systems,” *Mathematical Problems in Engineering*, vol. 2015, Article ID 878120, 16 pages, 2015.
  - [10] M. Johansson and A. Rantzer, “Computation of piecewise quadratic Lyapunov functions for hybrid systems,” *IEEE Transactions on Automatic Control*, vol. 43, no. 4, pp. 555–559, 1998.
  - [11] J. Qiu, Y. Wei, and L. Wu, “A novel approach to reliable control of piecewise affine systems with actuator faults,” *IEEE Transactions on Circuits and Systems II: Express Briefs*, vol. 64, no. 8, pp. 957–961, 2017.
  - [12] S. Pettersson and B. Lennartson, “Exponential stability of hybrid systems using piecewise quadratic Lyapunov functions resulting in LMIS,” *IFAC Proceedings Volumes*, vol. 32, no. 2, pp. 4810–4815, 1999.
  - [13] J. Imura, “Classification and stabilizability analysis of bimodal piecewise affine systems,” *International Journal of Robust and Nonlinear Control*, vol. 12, no. 10, pp. 897–926, 2002.
  - [14] G. Ferrari-Trecate, F. A. Cuzzola, D. Mignone, and M. Morari, “Analysis of discrete-time piecewise affine and hybrid systems,” *Automatica*, vol. 38, no. 12, pp. 2139–2146, 2002.
  - [15] Z. Tang, J. H. Park, Y. Wang, and J. Feng, “Distributed impulsive quasi-synchronization of Lure networks with proportional delay,” *IEEE Transactions on Cybernetics*, 2018.
  - [16] X. Yao, J. H. Park, H. Dong, L. Guo, and X. Lin, “Robust adaptive nonsingular terminal sliding mode control for automatic train operation,” *IEEE Transactions on Systems, Man, and Cybernetics: Systems*, pp. 1–10, 2017.
  - [17] X. Xie, N. Duan, and C. Zhao, “A combined homogeneous domination and sign function approach to output-feedback stabilization of stochastic high-order nonlinear systems,” *IEEE Transactions on Automatic Control*, vol. 59, no. 5, pp. 1303–1309, 2014.
  - [18] L. Xue, T. Zhang, W. Zhang, and X. Xie, “Global adaptive stabilization and tracking control for high-order stochastic nonlinear systems with time-varying delays,” *IEEE Transactions on Automatic Control*, vol. 63, no. 9, pp. 2928–2943, 2018.
  - [19] A. Hamadeh and J. Goncalves, “Reachability analysis of continuous-time piecewise affine systems,” *Automatica*, vol. 44, no. 12, pp. 3189–3194, 2008.
  - [20] J. Qiu, G. Feng, and H. Gao, “Approaches to robust  $H_\infty$  static output feedback control of discrete-time piecewise-affine systems with norm-bounded uncertainties,” *International Journal of Robust and Nonlinear Control*, vol. 21, no. 7, pp. 790–814, 2011.
  - [21] J. H. Richter, W. P. M. H. Heemels, N. van de Wouw, and J. Lunze, “Reconfigurable control of piecewise affine systems with actuator and sensor faults: stability and tracking,” *Automatica*, vol. 47, no. 4, pp. 678–691, 2011.
  - [22] Y. Wei, J. Qiu, P. Shi, and H.-K. Lam, “A New Design of  $h$ -Infinity Piecewise Filtering for Discrete-Time Nonlinear Time-Varying Delay Systems via T-S Fuzzy Affine Models,” *IEEE Transactions on Systems, Man, and Cybernetics: Systems*, vol. 47, no. 8, pp. 2034–2047, 2017.
  - [23] Y. Wei, J. Qiu, P. Shi, and M. Chadli, “Fixed-order piecewise-affine output feedback controller for fuzzy-affine-model-based nonlinear systems with time-varying delay,” *IEEE Transactions on Circuits and Systems I: Regular Papers*, vol. 64, no. 4, pp. 945–958, 2017.
  - [24] Y. Wei, J. Qiu, and H.-K. Lam, “A novel approach to reliable output feedback control of fuzzy-affine systems with time delays and sensor faults,” *IEEE Transactions on Fuzzy Systems*, vol. 25, no. 6, pp. 1808–1823, 2017.
  - [25] J. C. Doyle, K. Glover, P. P. Khargonekar, and B. A. Francis, “State-space solutions to standard  $H_2$  and  $H_\infty$  control problems,” *IEEE Transactions on Automatic Control*, vol. 34, no. 8, pp. 831–847, 1989.
  - [26] S. Liu, C. Xu, and L. Zhang, “Robust course keeping control of a fully submerged hydrofoil vessel without velocity measurement: an iterative learning approach,” *Mathematical Problems in Engineering*, vol. 2017, Article ID 7979438, 14 pages, 2017.
  - [27] L. H. Keel and S. P. Bhattacharyya, “Robust, fragile, or optimal?” *IEEE Transactions on Automatic Control*, vol. 42, no. 8, pp. 1098–1105, 1997.
  - [28] P. Dorato, “Non-fragile controller design: an overview,” in *Proceedings of the American Control Conference (ACC '98)*, vol. 5, pp. 2829–2831, June 1998.
  - [29] Y.-Q. Wu, H. Y. Su, R. Q. Lu, Z.-G. Wu, and Z. Shu, “Passivity-based non-fragile control for Markovian jump systems with aperiodic sampling,” *Systems & Control Letters*, vol. 84, pp. 35–43, 2015.
  - [30] H. Shen, F. Li, Z. Wu, J. H. Park, and V. Sreeram, “Fuzzy-model-based non-fragile control for nonlinear singularly perturbed systems with semi-markov jump parameters,” *IEEE Transactions on Fuzzy Systems*, pp. 1–1, 2018.
  - [31] G.-H. Yang and J. L. Wang, “Non-fragile  $H_\infty$  control for linear systems with multiplicative controller gain variations,” *Automatica*, vol. 37, no. 5, pp. 727–737, 2001.
  - [32] J. H. Park, “Robust non-fragile control for uncertain discrete-delay large-scale systems with a class of controller gain variations,” *Applied Mathematics and Computation*, vol. 149, no. 1, pp. 147–164, 2004.
  - [33] B. Zhang, S. Zhou, and T. Li, “A new approach to robust and non-fragile  $H_\infty$  control for uncertain fuzzy systems,” *Information Sciences*, vol. 177, no. 22, pp. 5118–5133, 2007.
  - [34] J. Yang, S. Zhong, and L. Xiong, “A descriptor system approach to non-fragile  $H_\infty$  control for uncertain fuzzy neutral systems,” *Fuzzy Sets and Systems*, vol. 160, no. 4, pp. 423–438, 2009.
  - [35] L. Li and Y. Jia, “Non-fragile dynamic output feedback control for linear systems with time-varying delay,” *IET Control Theory & Applications*, vol. 3, no. 8, pp. 995–1005, 2009.

- [36] R. Rakkiyappan, R. Sasirekha, S. Lakshmanan, and C. P. Lim, "Synchronization of discrete-time Markovian jump complex dynamical networks with random delays via non-fragile control," *Journal of The Franklin Institute*, vol. 353, no. 16, pp. 4300–4329, 2016.
- [37] N. Sakthivel, R. Rakkiyappan, and J. H. Park, "Non-fragile synchronization control for complex networks with additive time-varying delays," *Complexity*, vol. 21, no. 1, pp. 296–321, 2015.
- [38] Y. Yu, H. Dong, Z. Wang, W. Ren, and F. E. Alsaadic, "Design of non-fragile state estimators for discrete time-delayed neural networks with parameter uncertainties," *Neurocomputing*, vol. 182, pp. 18–24, 2016.
- [39] S. He, "Non-fragile passive controller design for nonlinear Markovian jumping systems via observer-based controls," *Neurocomputing*, vol. 147, pp. 350–357, 2015.
- [40] M. Kchaou, A. E. Hajjaji, and A. Toumi, "Non-fragile  $H_{\infty}$  output feedback control design for continuous-time fuzzy systems," *ISA Transactions*<sup>®</sup>, vol. 54, pp. 3–14, 2015.
- [41] N. Dadkhah and L. Rodrigues, "Non-fragile state-feedback control of uncertain piecewise-affine slab systems with input constraints: a convex optimisation approach," *IET Control Theory & Applications*, vol. 8, no. 8, pp. 626–632, 2014.
- [42] W. Ji, A. Wang, and J. Qiu, "A novel dynamic state feedback controller for discrete-time T-S fuzzy affine systems," in *Proceedings of the 2017 Seventh International Conference on Information Science and Technology (ICIST)*, pp. 1–7, Da Nang, Vietnam, April 2017.

## Research Article

# A New Stability Criterion for Neutral Stochastic Delay Differential Equations with Markovian Switching

Wei Hu <sup>1,2</sup>

<sup>1</sup>*School of Mathematics and Physics, Jiangsu University of Technology, Changzhou, 213001 Jiangsu, China*

<sup>2</sup>*School of Mathematical Sciences and Institute of Finance and Statistics, Nanjing Normal University, Nanjing, 210023 Jiangsu, China*

Correspondence should be addressed to Wei Hu; [huw@jst.edu.cn](mailto:huw@jst.edu.cn)

Received 22 July 2018; Accepted 25 September 2018; Published 14 October 2018

Academic Editor: Ju H. Park

Copyright © 2018 Wei Hu. This is an open access article distributed under the Creative Commons Attribution License, which permits unrestricted use, distribution, and reproduction in any medium, provided the original work is properly cited.

In this short paper, a new stability theorem for neutral stochastic delay differential equations with Markovian switching is investigated by applying stochastic analysis technique and Razumikhin stability approach. A novel criterion of the  $p$ th moment exponential stability is derived for the related systems. The feature of the criterion shows that the estimated upper bound for the diffusion operator of Lyapunov function is allowed to be indefinite, even if to be unbounded, which can loosen the constraints of the existing results. Last, an example is provided to illustrate the usefulness and significance of the theoretical results.

## 1. Introduction

As is well-known, the stability is very hot topic in deterministic or stochastic dynamic systems (for instance, see [1–37] and references therein). Recently, a class of stochastic hybrid systems (also known as stochastic systems with Markovian switching) has been used to model many practical systems where they may experience abrupt changes in their structure and parameters. In [38], the author explained that the Markovian switching systems had been emerging as a convenient mathematical framework for the formulation of various design problems in different fields such as target tracking, fault tolerant control, and manufacturing processes, which can be seen as the motivation of wide practical use of the theoretic results for hybrid systems. Owing to their widely real applications, stochastic systems with Markovian switching have received a great deal of attention and many interesting results have been reported in the literature. For example, [39] considered the stability of stochastic differential equations with infinite Markovian switchings and [40] studied the stability for stochastic differential equations with semi-Markovian switchings. The results of stochastic hybrid systems are applied in feedback controls and neural networks; please refer to [41–45] and the reference therein.

As an important class of hybrid stochastic system, neutral stochastic delay differential equations with Markovian switching (NSDDEwMS) have been applied in practice, such as traffic control, neural networks, and chemical process. Due to its wide applications, more and more researchers focus on this system. An important question for such a model is the stability analysis. Lyapunov-Razumikhin functions method and Lyapunov-Krasovskii functionals method are two effective methods that have been exploited for the stability analysis. For example, Mao in [46, 47] applied Razumikhin approach to derive the exponential stability criteria for neutral stochastic delay differential systems with Markovian switching. In [48–53], the authors considered the exponential stability by using Lyapunov-Krasovskii functionals method. Reference [54] applied some special techniques to study the exponential stability. Besides, Zhu in [55, 56] obtained several novel exponential stability criteria for some more complex systems with impulse control and Lévy noise. In addition, [57] considered the stability in distribution of neutral stochastic differential delay equations with Markovian switching and [58, 59] studied the almost sure stability for the same system.

Although the above exponential stability criteria can be used to judge the stability for many NSDDEwMS, nevertheless, these conditions in the above literature can be weakened

to cover a large collection of NSDDEwMS. In other words, there are some shortcomings in the former criteria. The main is that all the above criteria for exponential stability in the related literature imposed some strict conditions on the diffusion operator of Lyapunov functions. For example, [46, 47] required the estimated upper bound for the diffusion operator of Lyapunov functions to be negative constant numbers. Reference [48] needed that the estimated upper bound  $\lambda(t)$  must be a negative value function. Simply speaking, the former results all need that the upper bound  $\lambda(t)$  for the diffusion operator of the Lyapunov function is negative definite for all  $t$ . This restriction leads to the criteria having strong conservativeness in practice due to the fact that there are a large number of time-varying systems not satisfying the above conditions. As shown by an example in Section 4, the existing results and methods cannot be applied to analyse the stability for more general time-varying systems.

Motivated by the above discussion, in this short note, we focus on the exponential stability for NSDDEwMS. By using the notions such as uniformly stable function (USF), overshoot of the USF that dated from [60, 61] and then combining the stochastic analysis techniques, we obtain a novel stability criterion for NSDDEwMS. The feature of the criterion is that the coefficients of the estimated upper bound for the diffusion operator of Lyapunov functions can be allowed sign-changing as the time-varying, which can be used more widely than the existing results.

The rest of the paper is organized as follows. In Section 2, we introduce the model of NSDDEwMS and some preliminaries. The main result and its proof will be displayed in Section 3. An example is provided in Section 4. Finally, we conclude this paper with some general remarks in Section 5.

Throughout this short paper, let  $(\Omega, \mathcal{F}, \{\mathcal{F}_t\}_{t \geq 0}, \mathbb{P})$  be a complete probability space with a natural filtration  $\{\mathcal{F}_t\}_{t \geq 0}$  satisfying the usual condition (i.e., it is right continuous and  $\mathcal{F}_0$  contains all  $\mathbb{P}$ -null sets).  $|x|$  denotes the Euclidean norm of  $x$ . The symbol  $C([-\tau, 0], \mathbb{R}^n)$  denotes the family of continuous function  $\varphi$  from  $[-\tau, 0]$  to  $\mathbb{R}^n$  with the norm  $\|\varphi\| = \sup_{-\tau \leq \theta \leq 0} |\varphi(\theta)|$ . We use  $C_{\mathcal{F}_t}^p([-\tau, 0], \mathbb{R}^n)$  to denote the family of all  $\mathcal{F}_t$ -measurable,  $C([-\tau, 0], \mathbb{R}^n)$  valued random variables  $\varphi$  satisfying  $\sup_{-\tau \leq \theta \leq 0} \mathbb{E}|\varphi(\theta)|^p < \infty$ . We use  $\mathbb{E}[\cdot]$  to denote the expectation operator with respect to the probability measure  $\mathbb{P}$ . Let  $B_t = B(t) = (B_1(t), B_2(t), \dots, B_m(t))^T$  be an  $m$ -dimensional Brownian motion defined on a complete probability space.  $a \vee b = \max\{a, b\}$ .  $\mathbb{N}$  denotes the set of positive integers.

## 2. Preliminaries

Let  $\{r(t), t \geq 0\}$  be a right-continuous Markov chain on the probability space  $(\Omega, \mathcal{F}, \mathbb{P})$  taking values in a finite state space  $\mathcal{S} = \{1, 2, \dots, N\}$  with generator  $Q = (q_{ij})_{N \times N}$  given by

$$\begin{aligned} \mathbb{P}(r(t + \Delta t) = j \mid r(t) = i) \\ = \begin{cases} q_{ij}\Delta t + o(\Delta t), & \text{if } i \neq j \\ 1 + q_{ii}\Delta t + o(\Delta t), & \text{if } i = j \end{cases} \quad (1) \end{aligned}$$

where  $\Delta t > 0$ . Here  $q_{ij} \geq 0$  is the transition rate from  $i$  to  $j$  if  $i \neq j$  while  $q_{ii} = -\sum_{j \neq i} q_{ij} = -q_i$ .

In this short paper, we will consider the following neutral stochastic delay differential system with Markovian switching:

$$\begin{aligned} d[x(t) - u(t, x(t - \tau), r(t))] \\ = f(t, x(t), x(t - \tau), r(t)) dt \\ + g(t, x(t), x(t - \tau), r(t)) dB_t \end{aligned} \quad (2)$$

with the initial data  $x_0 = \phi = \{\phi(\theta), -\tau \leq \theta \leq 0\} \in C_{\mathcal{F}_0}^p([-\tau, 0], \mathbb{R}^n)$ . We assume that  $f, g$  satisfy the local Lipschitz condition and the linear growth condition. Additionally, we impose the following condition:

$$|u(t, x, i) - u(t, y, i)| \leq \kappa |x - y|, \quad \kappa \in (0, 1), \quad i \in \mathcal{S} \quad (3)$$

on  $u(\cdot)$  to guarantee the existence and uniqueness of solution  $x(t, \phi)$  for system (2) for all  $t \geq 0$ . We also assume that  $f(t, 0, 0, i) = 0$ ,  $g(t, 0, 0, i) = 0$ , and  $u(t, 0, i) = 0$ , which implies that the trivial solution of system (2) exists. In order to use Lyapunov's method to study the  $p$ th moment exponential stability, we need the following definitions.

*Definition 1.* The trivial solution of (2) is said to be  $p$ th moment exponentially stable if

$$\limsup_{t \rightarrow \infty} \frac{\ln \mathbb{E} |x(t, \phi)|^p}{t} < 0 \quad (4)$$

for all  $\phi \in C_{\mathcal{F}_0}^p([-\tau, 0], \mathbb{R}^n)$ . When  $p = 2$ , 2th moment exponential stability is usually called mean square exponentially stable.

*Definition 2.* The function  $V(t, x, i) : \mathbb{R}^+ \times \mathbb{R}^n \times \mathcal{S} \rightarrow \mathbb{R}^+$  belongs to class  $\Psi$  if it is a continuously twice differentiable with respect to  $x$  and once differentiable with respect to  $t$ .

Next, we need an operator  $\mathcal{L}V$  from  $\mathbb{R}^+ \times \mathbb{R}^n \times \mathbb{R}^n \times \mathcal{S}$  to  $\mathbb{R}$  by

$$\begin{aligned} \mathcal{L}V(t, x, y, i) = & V_t(t, x - u(t, y, i), i) + V_x(t, x \\ & - u(t, y, i), i) f(t, x, y, i) + \frac{1}{2} \text{trace} [g^T(t, x, y, i) \\ & \cdot V_{xx}(t, x - u(t, y, i), i) g(t, x, y, i)] \\ & + \sum_{j=1}^N q_{ij} V(t, x - u(t, y, i), j), \end{aligned} \quad (5)$$

where

$$\begin{aligned} V_x(t, x, i) &= \left( \frac{\partial V(t, x, i)}{\partial x_1}, \frac{\partial V(t, x, i)}{\partial x_2}, \dots, \frac{\partial V(t, x, i)}{\partial x_n} \right), \\ V_{xx}(t, x, i) &= \left( \frac{\partial^2 V(t, x, i)}{\partial x_i \partial x_j} \right)_{n \times n}, \\ V_t(t, x, i) &= \frac{\partial V(t, x, i)}{\partial t}. \end{aligned} \quad (6)$$

In order to overcome the difficult caused by the neutral item, we need the following inequality.

**Lemma 3.** Let  $p \geq 1$ . Then

$$\begin{aligned} (1 - \kappa)^{p-1} |x|^p - \kappa (1 - \kappa)^{p-1} |y|^p &\leq |x - u(t, y, i)|^p \\ &\leq (1 + \kappa)^{p-1} (|x|^p + \kappa |y|^p) \end{aligned} \quad (7)$$

holds for any  $(t, x, y, i) \in \mathbb{R}^+ \times \mathbb{R}^n \times \mathbb{R}^n \times \mathcal{S}$ .

The following lemma, which is important in the proof of the main result, can be found in Lemma 1 of [62].

**Lemma 4.** Let  $T^*$  be a constant. Let a function  $w : [-T^*, \infty) \rightarrow [0, \infty)$  admit a sequence  $\{v_i\}$  and positive constants  $\bar{v}_a$  and  $\bar{v}_b$ , such that  $v_0 = t_0$ ,  $v_{i+1} - v_i \in [\bar{v}_a, \bar{v}_b]$  for all  $i \geq 0$ .  $w$  is continuous on  $[v_i, v_{i+1})$  for all  $i \geq 0$  and the left limit  $\lim_{t \rightarrow v_i^-} w(t)$  exist. Assume that there exists a constant  $\rho \in (0, 1)$  such that  $w(t) \leq \rho \sup_{s \in [t-T^*, t]} w(s)$  holds for all  $t \geq t_0$ . Then

$$w(t) \leq e^{((\ln \rho)/T^*)(t-t_0)} \sup_{s \in [t_0-T^*, t_0]} w(s) \quad (8)$$

holds for all  $t \geq t_0$ .

The following definitions, which are dated from [60], are important in the proof of our main result.

**Definition 5.** A piecewise continuous function  $\mu$  is said to be a USF if the following linear time-varying equation is globally uniformly asymptotically stable:

$$dy(t) = \mu(t) y(t) dt, \quad \forall t \geq 0 \quad (9)$$

**Definition 6.** Let  $\mu(t)$  be a USF. Then the set

$$\Omega_\mu = \left\{ T > 0 : \sup_{t \geq 0} \left\{ \int_t^{t+T} \mu(s) ds \right\} < 0 \right\} \quad (10)$$

is said to be the uniform convergence set of  $\mu(t)$ . For any  $T \geq 0$ , the overshoot  $\varphi_\mu(T) := \varphi_\mu$  of  $\mu(t)$  is defined as follows:

$$\varphi_\mu = \sup_{t \geq 0} \left\{ \max_{\theta \in [0, T]} \left\{ \int_t^{t+\theta} \mu(s) ds \right\} \right\}. \quad (11)$$

### 3. Main Results

In this section, we will use stochastic analysis theory, Lyapunov's method, and Lemmas 3 and 4 to obtain a criterion for  $p$ th moment exponential stability of system (2). Our main result is the following.

**Theorem 7.** Let  $p, c_1, c_2, \kappa, \tau$  be all positive numbers, and  $\mu(t)$  is a USF. If there exist a function  $V \in \Psi$  and a constant  $T \in \Omega_\mu$  such that the following conditions hold for all  $t \geq 0$ ,

(1) for all  $x \in \mathbb{R}^n, i \in \mathcal{S}$ ,

$$c_1 |x|^p \leq V(t, x, i) \leq c_2 |x|^p, \quad (12)$$

(2) the following Razumikhin-type condition holds:

$$\mathbb{E} \mathcal{L}V(t, x(t), x(t-\tau), r(t))$$

$$\leq \mu(t) \mathbb{E}V(t, \bar{x}(t), r(t))$$

$$\text{if } \min_{i \in \mathcal{S}} \{\mathbb{E}V(t+\theta, x(t+\theta), i)\}$$

(13)

$$\leq q \max_{i \in \mathcal{S}} \{\mathbb{E}V(t, \bar{x}(t), i)\}$$

$$\forall \theta \in [-\tau, 0], \text{ where } q > \frac{c_2}{c_1} e^{\rho \mu} (1 - \kappa)^{-p}.$$

Then, system (2) is  $p$ th moment exponentially stable; here  $\bar{x}(t) \triangleq x(t) - u(t, x(t-\tau), r(t))$ .

*Proof.* First of all, we will prove the following fact: if  $q^{-1} \mathbb{E}V(t+\theta, x(t+\theta), r(t)) \leq \mathbb{E}V(t, \bar{x}(t), r(t))$  holds for all  $\theta \in [-\tau, 0]$  which implies  $\mathbb{E} \mathcal{L}V(t, x(t), x(t-\tau), r(t)) \leq \mu(t) \mathbb{E}V(t, \bar{x}(t), r(t))$ , then, for any  $t > T$ ,

$$\mathbb{E}V(t, \bar{x}(t), r(t))$$

$$\leq \max \left\{ \mathbb{E}V(t-T, \bar{x}(t-T), r(t-T)) e^{\int_{t-T}^t \mu(s) ds}, \right.$$

$$q^{-1} \sup_{s \in [t-T, t]} \sup_{\theta \in [-\tau, 0]} \mathbb{E}V(s+\theta, x(s+\theta), r(s+\theta))$$

(14)

$$\left. \cdot e^{\rho \mu} \right\}.$$

In order to prove inequality (14), we consider the following two cases:

(A):  $\sup_{\theta \in [-\tau, 0]} \mathbb{E}V(s+\theta, x(s+\theta), r(s+\theta)) \leq q \mathbb{E}V(s, \bar{x}(s), r(s))$  holds for all  $s \in [t-T, t]$ .

(B):  $\sup_{\theta \in [-\tau, 0]} \mathbb{E}V(s+\theta, x(s+\theta), r(s+\theta)) \leq q \mathbb{E}V(s, \bar{x}(s), r(s))$  does not hold for some  $s \in [t-T, t]$ .

For (A), we know that  $\mathbb{E} \mathcal{L}V(s, x(s), x(s-\tau), r(s)) \leq \mu(s) \mathbb{E}V(s, \bar{x}(s), r(s))$  holds for any  $s \in [t-T, t]$ . By using

Itô's formula and the standard stopping times technique, we obtain that

$$\begin{aligned} & \mathbb{E} \left( e^{-\int_{t-T}^t \mu(s) ds} V(t, \tilde{x}(t), r(t)) \right) = \mathbb{E} V(t-T, \tilde{x}(t-T), r(t-T)) \\ & + \mathbb{E} \int_{t-T}^t \left[ -\mu(s) e^{-\int_{t-T}^s \mu(v) dv} V(s, \tilde{x}(s), r(s)) \right. \\ & \left. + e^{-\int_{t-T}^s \mu(v) dv} \mathcal{L}V(s, x(s), x(s-\tau), r(s)) \right] ds \\ & \leq \mathbb{E} V(t-T, \tilde{x}(t-T), r(t-T)), \end{aligned} \quad (15)$$

which implies that  $\mathbb{E}V(t, \tilde{x}(t), r(t)) \leq \mathbb{E}V(t-T, \tilde{x}(t-T), r(t-T)) e^{\int_{t-T}^t \mu(s) ds}$ .

For (B), define  $t^* = \sup\{s \in [t-T, t] : \sup_{\theta \in [-\tau, 0]} \mathbb{E}V(s+\theta, x(s+\theta), r(s+\theta)) > q \mathbb{E}V(s, \tilde{x}(s), r(s))\}$ . Then  $t^* < t$  or  $t^* = t$ . If  $t^* < t$ , then, for all  $s \in [t^*, t]$ ,  $\sup_{\theta \in [-\tau, 0]} \mathbb{E}V(s+\theta, x(s+\theta), r(s+\theta)) \leq q \mathbb{E}V(s, \tilde{x}(s), r(s))$ . So according to the result of (A), we obtain that

$$\begin{aligned} \mathbb{E}V(t, \tilde{x}(t), r(t)) & \leq e^{\int_{t^*}^t \mu(s) ds} \mathbb{E}V(t^*, \tilde{x}(t^*), r(t^*)) \\ & = e^{\int_{t^*}^t \mu(s) ds} q^{-1} \sup_{\theta \in [-\tau, 0]} \mathbb{E}V(t^* \\ & + \theta, x(t^* + \theta), r(t^* + \theta)) \\ & \leq e^{\int_{t^*}^t \mu(s) ds} q^{-1} \sup_{s \in [t-T, t]} \sup_{\theta \in [-\tau, 0]} \mathbb{E}V(s \\ & + \theta, x(s + \theta), r(s + \theta)) \\ & \leq e^{\varrho_\mu} q^{-1} \sup_{s \in [t-T, t]} \sup_{\theta \in [-\tau, 0]} \mathbb{E}V(s \\ & + \theta, x(s + \theta), r(s + \theta)). \end{aligned} \quad (16)$$

If  $t^* = t$ , from the definition of  $t^*$ , we have

$$\begin{aligned} \mathbb{E}V(t, \tilde{x}(t), r(t)) & = \mathbb{E}V(t^*, \tilde{x}(t^*), r(t^*)) \\ & \leq q^{-1} \sup_{\theta \in [-\tau, 0]} \mathbb{E}V(t^* + \theta, x(t^* + \theta), r(t^* + \theta)) \\ & \leq e^{\varrho_\mu} q^{-1} \sup_{s \in [t-T, t]} \sup_{\theta \in [-\tau, 0]} \mathbb{E}V(s + \theta, x(s + \theta), r(s + \theta)). \end{aligned} \quad (17)$$

Combining the above three inequalities, we can see that inequality (14) holds.

Assume that  $q^{-1} \mathbb{E}V(t+\theta, x(t+\theta), r(t)) \leq \mathbb{E}V(t, \tilde{x}(t), r(t))$  holds for all  $\theta \in [-\tau, 0]$ , then  $q^{-1} \min_{i \in S} \{\mathbb{E}V(t+\theta, x(t+\theta), r(t), i)\} \leq q^{-1} \mathbb{E}V(t+\theta, x(t+\theta), r(t)) \leq \max_{i \in S} \{\mathbb{E}V(t, \tilde{x}(t), i)\}$  holds for all  $\theta \in [-\tau, 0]$ . According to condition (2), we know that  $\mathbb{E} \mathcal{L}V(t, x(t), x(t-\tau), r(t)) \leq$

$\mu(t) \mathbb{E}V(t, \tilde{x}(t), r(t))$ . Thus, from inequality (14), condition (1), and Lemma 3, we conclude that, for any  $t > T$ ,

$$\begin{aligned} & \mathbb{E}V(t, \tilde{x}(t), r(t)) \\ & \leq \max \left\{ \mathbb{E}V(t-T, \tilde{x}(t-T), r(t-T)) e^{\int_{t-T}^t \mu(s) ds}, \right. \\ & q^{-1} \sup_{s \in [t-T, t]} \sup_{\theta \in [-\tau, 0]} \mathbb{E}V(s+\theta, x(s+\theta), r(s+\theta)) \\ & \cdot e^{\varrho_\mu} \left. \right\} \leq \max \left\{ c_2 \mathbb{E} |\tilde{x}(t-T)|^p e^{\int_{t-T}^t \mu(s) ds}, \right. \\ & q^{-1} \sup_{s \in [t-T, t]} \sup_{\theta \in [-\tau, 0]} \mathbb{E}V(s+\theta, x(s+\theta), r(s+\theta)) \\ & \cdot e^{\varrho_\mu} \left. \right\} \leq \max \left\{ c_2 (1+\kappa)^{p-1} \right. \\ & \cdot (\mathbb{E} |x(t-T)|^p + \kappa \mathbb{E} |x(t-T-\tau)|^p) e^{\int_{t-T}^t \mu(s) ds}, \\ & q^{-1} \sup_{s \in [t-T, t]} \sup_{\theta \in [-\tau, 0]} \mathbb{E}V(s+\theta, x(s+\theta), r(s+\theta)) \\ & \cdot e^{\varrho_\mu} \left. \right\} \leq \max \left\{ \frac{c_2}{c_1} (1+\kappa)^p e^{\int_{t-T}^t \mu(s) ds}, q^{-1} e^{\varrho_\mu} \right\} \\ & \cdot \sup_{s \in [t-T, t]} \sup_{\theta \in [-\tau, 0]} \mathbb{E}V(s+\theta, \\ & x(s+\theta), r(s+\theta)). \end{aligned} \quad (18)$$

By condition (1), we can see that

$$\begin{aligned} \mathbb{E} |\tilde{x}(t)|^p & \leq \frac{c_2}{c_1} \max \left\{ \frac{c_2}{c_1} (1+\kappa)^p e^{\int_{t-T}^t \mu(s) ds}, q^{-1} e^{\varrho_\mu} \right\} \\ & \cdot \sup_{s \in [t-T, t]} \sup_{\theta \in [-\tau, 0]} \mathbb{E} |x(s+\theta)|^p \\ & := \eta \sup_{s \in [t-T, t]} \sup_{\theta \in [-\tau, 0]} \mathbb{E} |x(s+\theta)|^p. \end{aligned} \quad (19)$$

Using Lemma 3 again, we obtain that

$$\begin{aligned} & \mathbb{E} |x(t)|^p \\ & \leq \left[ \mathbb{E} |\tilde{x}(t)|^p + \kappa (1-\kappa)^{p-1} \mathbb{E} |x(t-\tau)|^p \right] (1-\kappa)^{1-p} \\ & = (1-\kappa)^{1-p} \mathbb{E} |\tilde{x}(t)|^p + \kappa \mathbb{E} |x(t-\tau)|^p \\ & \leq \left[ (1-\kappa)^{1-p} \eta + \kappa \right] \sup_{s \in [t-T, t]} \sup_{\theta \in [-\tau, 0]} \mathbb{E} |x(s+\theta)|^p. \end{aligned} \quad (20)$$

In order to use Lemma 4, we need to justify that  $(1-\kappa)^{1-p} \eta + \kappa < 1$ . In fact, on one hand, due to  $q > (c_2/c_1) e^{\varrho_\mu} (1-\kappa)^{-p}$ , there exists a constant  $\rho \in (0, 1)$  such that  $(c_2/c_1) q^{-1} e^{\varrho_\mu} (1-\kappa)^{1-p} \leq \rho - \kappa$ . On the other hand, due to  $\mu(t)$  being a USF and  $T \in \Omega_\mu$ , there exists a constant  $\rho_1 \in (0, 1)$  such that

$e^{\int_{t-T}^t \mu(s) ds} < (c_1/c_2)^2 ((1-\kappa)/(1+\kappa))^p ((\rho_1-\kappa)/(1-\kappa)) < 1$ .  
Thus

$$\begin{aligned} \mathbb{E} |x(t)|^p &\leq \left[ (1-\kappa)^{1-p} \eta + \kappa \right] \\ &\cdot \sup_{s \in [t-T, t]} \sup_{\theta \in [-\tau, 0]} \mathbb{E} |x(s+\theta)|^p = \left[ (1-\kappa)^{1-p} \frac{c_2}{c_1} \right. \\ &\cdot \max \left\{ \frac{c_2}{c_1} (1+\kappa)^p e^{\int_{t-T}^t \mu(s) ds}, q^{-1} e^{\varphi \mu} \right\} + \kappa \left. \right] \\ &\cdot \sup_{s \in [t-T, t]} \sup_{\theta \in [-\tau, 0]} \mathbb{E} |x(s+\theta)|^p \\ &\leq [\max \{ \rho_1 - \kappa, \rho - \kappa \} + \kappa] \\ &\cdot \sup_{s \in [t-T, t]} \sup_{\theta \in [-\tau, 0]} \mathbb{E} |x(s+\theta)|^p \\ &\leq \rho^* \sup_{s \in [t-T, t]} \sup_{\theta \in [-\tau, 0]} \mathbb{E} |x(s+\theta)|^p \\ &\leq \rho^* \sup_{s \in [t-T-\tau, t]} \mathbb{E} |x(s)|^p \end{aligned} \tag{21}$$

where  $\rho^* = \rho \vee \rho_1 \in (0, 1)$ . By Lemma 4, we derive that

$$\mathbb{E} |x(t)|^p \leq e^{((\ln \rho^*)/(T+\tau))(t-T)} \sup_{s \in [-\tau, T]} \mathbb{E} |x(s)|^p, \tag{22}$$

which implies that

$$\limsup_{t \rightarrow \infty} \frac{\ln \mathbb{E} |x(t)|^p}{t} = \frac{\ln \rho^*}{T + \tau} < 0. \tag{23}$$

In other words, we have proved that system (2) is  $p$ th moment exponentially stable.  $\square$

*Remark 8.* Here, by using stochastic analysis theory, some notions as uniformly stable function (USF), overshoot of the USF that dated from [60, 61], and some inequality techniques, we obtain a novel exponential stability criterion with respect to the related systems. The method we use here is rather different from the traditional Razumikhin approach. Thus, we provide a new method to investigate the stability analysis for neutral stochastic delayed differential equations with Markovian switchings. In the future, we can develop this approach to study the stability for impulsive neutral stochastic delayed differential equations.

*Remark 9.* If system (2) has no Markovian switching and  $\mu(t) \equiv \mu < 0$ , then  $e^{\varphi \mu} =$ ; the condition of Theorem 7  $q > (c_2/c_1)e^{\varphi \mu} (1-\kappa)^{-p}$  becomes  $q > (c_2/c_1)(1-\kappa)^{-p}$ , which is the same as the conditions in [46, 47]. If the model we considered has no Markovian switching, stochastic disturbance, and neutral item, then we can obtain the same result as Theorem 1 in [60]. Thus, our result is the generalization of Theorem 1 in [60] and the main results in [46, 47].

*Remark 10.* In Theorem 3.1 of [53], the condition (3.3) ensured that the coefficient of the estimated upper bound for the diffusion operator of Lyapunov function is a negative

value, and the condition of Theorem 3.1 in [48] required that the coefficient function of the estimated upper bound for the diffusion operator of Lyapunov function is a negative definite function, which are very conservative in the practice if the system is time-varying system. But our conditions allow this function to take values on  $\mathbb{R}$  and even allow it to be unbounded. Thus, our result can be used more widely and is less conservative than the existing results. See Example 1 for more details.

### 4. An Example

In this section, we will give an example to illustrate the validity and significance of our result.

*Example 1.* Now we will consider the following neutral-type stochastic delay differential system with Markovian switching:

$$\begin{aligned} d[x(t) - 0.2x(t-0.5)] \\ = f(t, x(t), x(t-0.5), r(t)) dt \\ + g(t, x(t), x(t-0.5), r(t)) dB_t, \end{aligned} \tag{24}$$

where

$$\begin{aligned} f(t, x(t), x(t-0.5), i) \\ = \begin{cases} \left( \frac{1}{16} t \cos t^2 - \frac{3}{2} \right) x(t-0.5) + \frac{1}{16} t \cos t^2 x(t), & i = 1, \\ \left( \frac{1}{8} t \cos t^2 - 1 \right) x(t-0.5), & i = 2, \end{cases} \end{aligned} \tag{25}$$

and

$$\begin{aligned} g(t, x(t), x(t-0.5), i) \\ = \begin{cases} (\tanh t) x(t-0.5), & i = 1, \\ e^{-tx^2(t-0.5)} x(t-0.5), & i = 2. \end{cases} \end{aligned} \tag{26}$$

$r(t)$  is a right-continuous Markov chain on the state space  $\mathcal{S} = \{1, 2\}$  with the generator

$$Q = \begin{bmatrix} -1 & 1 \\ 2 & -2 \end{bmatrix}. \tag{27}$$

Theorem 3.1 in [48] is void in determining the exponential stability for such a system. In fact, taking  $V(t, x, i) = |x|^2$  and  $c_1 = c_2 = 1$ , then, by Ito's formula,

$$\begin{aligned} \mathbb{E} \mathcal{L}V(t, x(t), x(t-0.5), 1) \\ \leq 2\mathbb{E} \left\{ (x(t) - 0.2x(t-0.5)) \right. \\ \cdot \left[ \left( \frac{1}{16} t \cos t^2 - \frac{3}{2} \right) x(t-0.5) + \frac{1}{16} t \cos t^2 x(t) \right] \left. \right\} \\ + \mathbb{E} |x(t-0.5)|^2 \leq \left( \frac{7}{40} t \cos t^2 - \frac{3}{4} \right) \mathbb{E} |x(t)|^2 \\ + \left( \frac{3}{40} t \cos t^2 - \frac{1}{20} \right) \mathbb{E} |x(t-0.5)|^2 \end{aligned} \tag{28}$$

and

$$\begin{aligned}
& \mathbb{E} \mathcal{L}V(t, x(t), x(t-0.5), 2) \\
& \leq 2\mathbb{E} \left[ (x(t) - 0.2x(t-0.5)) \left( \frac{1}{8}t \cos t^2 - 1 \right) \right. \\
& \quad \cdot x(t-0.5) \left. \right] + \mathbb{E} |x(t-0.5)|^2 \leq \left( \frac{1}{8}t \cos t^2 - 1 \right) \\
& \quad \cdot \mathbb{E} |x(t)|^2 + \left( \frac{1}{10}t \cos t^2 - \frac{2}{5} \right) \mathbb{E} |x(t-0.5)|^2.
\end{aligned} \tag{29}$$

Obviously, the conditions in Theorem 3.1 [48] do not hold. But we can judge the exponential stability for such system by using our result. Take  $V(t, x, i) = |x|^2$  and  $c_1 = c_2 = 1$ . By Ito's formula,

$$\begin{aligned}
& \mathbb{E} \mathcal{L}V(t, x(t), x(t-0.5), 1) \\
& \leq \left( \frac{1}{8}t \cos t^2 - 3 \right) \mathbb{E} |\bar{x}(t) x(t-0.5)| \\
& \quad + \frac{1}{8}t \cos t^2 \mathbb{E} |x(t) \bar{x}(t)| + \mathbb{E} |x(t-0.5)|^2 \\
& \leq \left[ \left( \frac{1}{8}t \cos t^2 - 3 \right) \frac{q+1}{2} + q \right] \mathbb{E} |\bar{x}(t)|^2 \\
& \quad + \frac{1}{8}t \cos t^2 \mathbb{E} |x(t) \bar{x}(t)| \\
& \leq \left[ \left( \frac{1}{8}t \cos t^2 - 3 \right) \frac{q+1}{2} + q \right] \mathbb{E} |\bar{x}(t)|^2 \\
& \quad + \frac{1}{8} \left( \frac{q+1}{2} \right) t \cos t^2 \mathbb{E} |\bar{x}(t)|^2 \\
& = \left[ \frac{1}{8}t \cos t^2 (q+1) - \frac{3(q+1)}{2} + q \right] \mathbb{E} |\bar{x}(t)|^2,
\end{aligned} \tag{30}$$

and

$$\begin{aligned}
& \mathbb{E} \mathcal{L}V(t, x(t), x(t-0.5), 2) \\
& \leq \left( \frac{1}{8}t \cos t^2 - 1 \right) \mathbb{E} |\bar{x}(t)|^2 \\
& \quad + \left( \frac{1}{8}t \cos t^2 - 1 \right) \mathbb{E} |x(t-0.5)|^2 \\
& \quad + \mathbb{E} |x(t-0.5)|^2 \\
& \leq \left[ \left( \frac{1}{4}t \cos t^2 - 2 \right) \frac{q+1}{2} + q \right] \mathbb{E} |\bar{x}(t)|^2 \\
& = \left( \frac{1}{8}t \cos t^2 (q+1) + q \right) \mathbb{E} |\bar{x}(t)|^2.
\end{aligned} \tag{31}$$

Choosing  $q = 3$ , then  $\mathbb{E} \mathcal{L}V(t, x(t), x(t-0.5), r(t)) \leq \mu(t) \mathbb{E} V(t, \bar{x}(t), r(t))$ , where  $\mu(t) = (1/2)t \cos t^2 - 1$ . Here,

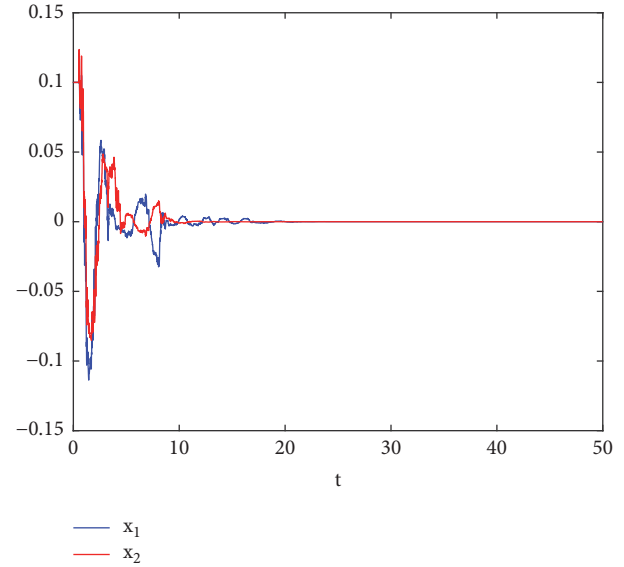


FIGURE 1: The state response of Example 1.

$\mu(t)$  is an unbounded function, taking values in  $\mathbb{R}$ , so we cannot use any former results to judge the mean-square exponential stability for such system. But, from our result, we can determine its stability. In fact, taking  $T = 1$ , then  $\int_t^{t+1} \mu(s) ds = -1/2 < 0$  holds for all  $t \geq 0$ . Thus  $T \in \Omega_\mu$ . Additionally,  $e^{\varrho\mu} \leq e^{0.5}$ , and  $q^{-1} e^{\varrho\mu} (1-k)^{-P} \leq 3^{-1} \times e^{0.5} \times 0.8^{-2} < 1$ . By Theorem 7, the system is mean square exponentially stable. See Figure 1.

## 5. Conclusion

In this paper, we investigate the stability criterion for neutral stochastic delay differential equations with Markovian switching. By using stochastic analysis technique and Razumikhin approach, we overcome the difficulty caused by the neutral item for the related system. Finally, we derive a new and novel Razumikhin exponential stability criterion. The feature of the result is that the estimated upper bound for the diffusion operator of Lyapunov function is allowed to take values on  $\mathbb{R}$ , even if it is allowed to be unbounded. The criterion can reduce some restrictiveness of the related results that are existing in the previous literature. An example is provided to show the superiority of the new exponential stability criterion.

## Data Availability

No data were used to support this study.

## Conflicts of Interest

The author declares that they have no conflicts of interest.

## Acknowledgments

This work was supported by the China Postdoctoral Science Foundation (2018M632325).

## References

- [1] X. Zheng, Y. Shang, and X. Peng, "Orbital stability of periodic traveling wave solutions to the generalized Zakharov equations," *Acta Mathematica Scientia*, vol. 37, no. 4, pp. 998–1018, 2017.
- [2] Y. Guo, "Mean square exponential stability of stochastic delay cellular neural networks," *Electronic Journal of Qualitative Theory of Differential Equations*, no. 34, pp. 1–10, 2013.
- [3] Q. Zhu and H. Wang, "Output feedback stabilization of stochastic feedforward systems with unknown control coefficients and unknown output function," *Automatica*, vol. 87, pp. 166–175, 2018.
- [4] H. Wang and Q. Zhu, "Finite-time stabilization of high-order stochastic nonlinear systems in strict-feedback form," *Automatica*, vol. 54, pp. 284–291, 2015.
- [5] G. Wang, "Existence-stability theorems for strong vector set-valued equilibrium problems in reflexive Banach spaces," *Journal of Inequalities and Applications*, vol. 239, pp. 1–14, 2015.
- [6] Y. Bai and X. Mu, "Global asymptotic stability of a generalized SIRS epidemic model with transfer from infectious to susceptible," *Journal of Applied Analysis and Computation*, vol. 8, no. 2, pp. 402–412, 2018.
- [7] Q. Zhu, S. Song, and T. Tang, "Mean square exponential stability of stochastic nonlinear delay systems," *International Journal of Control*, vol. 90, no. 11, pp. 2384–2393, 2017.
- [8] Y. Guo, "Global asymptotic stability analysis for integro-differential systems modeling neural networks with delays," *Zeitschrift für Angewandte Mathematik und Physik*, vol. 61, no. 6, pp. 971–978, 2010.
- [9] L. Gao, D. Wang, and G. Wang, "Further results on exponential stability for impulsive switched nonlinear time-delay systems with delayed impulse effects," *Applied Mathematics and Computation*, vol. 268, pp. 186–200, 2015.
- [10] Y. Guo, "Exponential stability analysis of travelling waves solutions for nonlinear delayed cellular neural networks," *Dynamical Systems*, vol. 32, no. 4, pp. 490–503, 2017.
- [11] Y. Li, Y. Sun, and F. Meng, "New criteria for exponential stability of switched time-varying systems with delays and nonlinear disturbances," *Nonlinear Analysis: Hybrid Systems*, vol. 26, pp. 284–291, 2017.
- [12] B. Wang and Q. Zhu, "Stability analysis of Markov switched stochastic differential equations with both stable and unstable subsystems," *Systems & Control Letters*, vol. 105, pp. 55–61, 2017.
- [13] L. G. Wang, K. P. Xu, and Q. W. Liu, "On the stability of a mixed functional equation deriving from additive, quadratic and cubic mappings," *Acta Mathematica Sinica*, vol. 30, no. 6, pp. 1033–1049, 2014.
- [14] Q. Zhu, S. Song, and P. Shi, "Effect of noise on the solutions of non-linear delay systems," *IET Control Theory & Applications*, vol. 12, no. 13, pp. 1822–1829, 2018.
- [15] G. Liu, S. Xu, Y. Wei, Z. Qi, and Z. Zhang, "New insight into reachable set estimation for uncertain singular time-delay systems," *Applied Mathematics and Computation*, vol. 320, pp. 769–780, 2018.
- [16] W. Sun, Y. Wang, and R. Yang, "L2 disturbance attenuation for a class of time delay Hamiltonian systems," *Journal of Systems Science & Complexity*, vol. 24, no. 4, pp. 672–682, 2011.
- [17] Q. Zhu, "Asymptotic stability in the pth moment for stochastic differential equations with Lévy noise," *Journal of Mathematical Analysis and Applications*, vol. 416, no. 1, pp. 126–142, 2014.
- [18] Y. Guo, "Global stability analysis for a class of Cohen-Grossberg neural network models," *Bulletin of the Korean Mathematical Society*, vol. 49, no. 6, pp. 1193–1198, 2012.
- [19] J. Hu and A. Xu, "On stability of F-Gorenstein flat categories," *Algebra Colloquium*, vol. 23, no. 2, pp. 251–262, 2016.
- [20] W. W. Sun, "Stabilization analysis of time-delay Hamiltonian systems in the presence of saturation," *Applied Mathematics and Computation*, vol. 217, no. 23, pp. 9625–9634, 2011.
- [21] H. Wang and Q. Zhu, "Global Stabilization of Stochastic Nonlinear Systems via C 1 and C  $\infty$  Controllers," *Institute of Electrical and Electronics Engineers Transactions on Automatic Control*, vol. 62, no. 11, pp. 5880–5887, 2017.
- [22] Y. Guo, "Mean square global asymptotic stability of stochastic recurrent neural networks with distributed delays," *Applied Mathematics and Computation*, vol. 215, no. 2, pp. 791–795, 2009.
- [23] Q. Zhu, "Stability analysis of stochastic delay differential equations with Lévy noise," *Systems & Control Letters*, vol. 118, pp. 62–68, 2018.
- [24] W. Sun and L. Peng, "Observer-based robust adaptive control for uncertain stochastic Hamiltonian systems with state and input delays," *Lithuanian Association of Nonlinear Analysts. Nonlinear Analysis: Modelling and Control*, vol. 19, no. 4, pp. 626–645, 2014.
- [25] W. Qi, Y. Kao, X. Gao, and Y. Wei, "Controller design for time-delay system with stochastic disturbance and actuator saturation via a new criterion," *Applied Mathematics and Computation*, vol. 320, pp. 535–546, 2018.
- [26] L. G. Wang and B. Liu, "Fuzzy stability of a functional equation deriving from additive, quadratic, cubic and quartic functions," *Acta Mathematica Sinica*, vol. 55, no. 5, pp. 841–854, 2012.
- [27] Q. Zhu and B. Song, "Exponential stability of impulsive nonlinear stochastic differential equations with mixed delays," *Nonlinear Analysis: Real World Applications*, vol. 12, no. 5, pp. 2851–2860, 2011.
- [28] F. Li and Y. Bao, "Uniform stability of the solution for a memory-type elasticity system with nonhomogeneous boundary control condition," *Journal of Dynamical and Control Systems*, vol. 23, no. 2, pp. 301–315, 2017.
- [29] Y.-H. Feng and C.-M. Liu, "Stability of steady-state solutions to Navier-Stokes-Poisson systems," *Journal of Mathematical Analysis and Applications*, vol. 462, no. 2, pp. 1679–1694, 2018.
- [30] X. Zheng, Y. Shang, and X. Peng, "Orbital stability of solitary waves of the coupled Klein-Gordon-Zakharov equations," *Mathematical Methods in the Applied Sciences*, vol. 40, no. 7, pp. 2623–2633, 2017.
- [31] T. Li and Y. F. Yang, "Stability of large steady-state solutions to non-isentropic Euler-Maxwell systems," *Journal of Nanjing Normal University*, vol. 40, no. 4, pp. 26–35, 2017.
- [32] Y. Guo, "Globally robust stability analysis for stochastic Cohen-Grossberg neural networks with impulse and time-varying delays," *Ukrainian Mathematical Journal*, vol. 69, no. 8, pp. 1049–1060, 2017.
- [33] Q. Zhu, J. Cao, and R. Rakkiyappan, "Exponential input-to-state stability of stochastic Cohen-Grossberg neural networks with mixed delays," *Nonlinear Dynamics*, vol. 79, no. 2, pp. 1085–1098, 2015.
- [34] L. G. Wang and B. Liu, "The Hyers-Ulam stability of a functional equation deriving from quadratic and cubic functions in quasi- $\beta$ -normed spaces," *Acta Mathematica Sinica*, vol. 26, no. 12, pp. 2335–2348, 2010.

- [35] M. Li and J. Wang, "Exploring delayed Mittag-Leffler type matrix functions to study finite time stability of fractional delay differential equations," *Applied Mathematics and Computation*, vol. 324, pp. 254–265, 2018.
- [36] Y. Guo, "Nontrivial periodic solutions of nonlinear functional differential systems with feedback control," *Turkish Journal of Mathematics*, vol. 34, no. 1, pp. 35–44, 2010.
- [37] L. Li, F. Meng, and P. Ju, "Some new integral inequalities and their applications in studying the stability of nonlinear integro-differential equations with time delay," *Journal of Mathematical Analysis and Applications*, vol. 377, no. 2, pp. 853–862, 2011.
- [38] M. Mariton, *Jump Linear Systems in Automatica Control*, Marcel Dekker, 1990.
- [39] R. Song and Q. Zhu, "Stability of linear stochastic delay differential equations with infinite Markovian switchings," *International Journal of Robust and Nonlinear Control*, vol. 28, no. 3, pp. 825–837, 2018.
- [40] B. Wang and Q. Zhu, "Stability analysis of semi-Markov switched stochastic systems," *Automatica*, vol. 94, pp. 72–80, 2018.
- [41] Q. X. Zhu and Q. Y. Zhang, "Pth moment exponential stabilisation of hybrid stochastic differential equations by feedback controls based on discrete-time state observations with a time delay," *IET Control Theory & Applications*, vol. 11, no. 12, pp. 1992–2003, 2017.
- [42] Q. Zhu, R. Rakkiyappan, and A. Chandrasekar, "Stochastic stability of Markovian jump BAM neural networks with leakage delays and impulse control," *Neurocomputing*, vol. 136, pp. 136–151, 2014.
- [43] Q. Zhu and J. Cao, "Stability of Markovian jump neural networks with impulse control and time varying delays," *Nonlinear Analysis: Real World Applications*, vol. 13, no. 5, pp. 2259–2270, 2012.
- [44] Y. Liu, J. H. Park, B. Guo, F. Fang, and F. Zhou, "Event-triggered dissipative synchronization for Markovian jump neural networks with general transition probabilities," *International Journal of Robust and Nonlinear Control*, vol. 28, no. 13, pp. 3893–3908, 2018.
- [45] R. Zhang, D. Zeng, J. H. Park, Y. Liu, and S. Zhong, "A new approach to stochastic stability of markovian neural networks with generalized transition rates," *IEEE Transactions on Neural Networks and Learning Systems*, pp. 1–12, 2018.
- [46] X. Mao, "Exponential stability in mean square of neutral stochastic differential-functional equations," *Systems & Control Letters*, vol. 26, no. 4, pp. 245–251, 1995.
- [47] X. Mao, "Razumikhin-type theorems on exponential stability of neutral stochastic functional-differential equations," *SIAM Journal on Mathematical Analysis*, vol. 28, no. 2, pp. 389–401, 1997.
- [48] H. Chen, P. Shi, and C.-C. Lim, "Stability analysis for neutral stochastic delay systems with Markovian switching," *Systems & Control Letters*, vol. 110, pp. 38–48, 2017.
- [49] Q. Zhu and J. Cao, "pth moment exponential synchronization for stochastic delayed Cohen-Grossberg neural networks with Markovian switching," *Nonlinear Dynamics*, vol. 67, no. 1, pp. 829–845, 2012.
- [50] Y. Chen, W. X. Zheng, and A. Xue, "A new result on stability analysis for stochastic neutral systems," *Automatica*, vol. 46, no. 12, pp. 2100–2104, 2010.
- [51] L. Shaikhet, "Some new aspects of Lyapunov-type theorems for stochastic differential equations of neutral type," *SIAM Journal on Control and Optimization*, vol. 48, no. 7, pp. 4481–4499, 2010.
- [52] Q. Zhu and J. Cao, "Stability analysis of markovian jump stochastic BAM neural networks with impulse control and mixed time delays," *IEEE Transactions on Neural Networks and Learning Systems*, vol. 23, no. 3, pp. 467–479, 2012.
- [53] Y. Xu and Z. He, "Exponential stability of neutral stochastic delay differential equations with Markovian switching," *Applied Mathematics Letters*, vol. 52, pp. 64–73, 2016.
- [54] K. Liu and X. Xia, "On the exponential stability in mean square of neutral stochastic functional differential equations," *Systems & Control Letters*, vol. 37, no. 4, pp. 207–215, 1999.
- [55] Q. Zhu, "Razumikhin-type theorem for stochastic functional differential equations with Lévy noise and Markov switching," *International Journal of Control*, vol. 90, no. 8, pp. 1703–1712, 2017.
- [56] Q. Zhu, "pth moment exponential stability of impulsive stochastic functional differential equations with Markovian switching," *Journal of The Franklin Institute*, vol. 351, no. 7, pp. 3965–3986, 2014.
- [57] J. Bao, Z. Hou, and C. Yuan, "Stability in distribution of neutral stochastic differential delay equations with Markovian switching," *Statistics & Probability Letters*, vol. 79, no. 15, pp. 1663–1673, 2009.
- [58] X. Li and X. Mao, "A note on almost sure asymptotic stability of neutral stochastic delay differential equations with Markovian switching," *Automatica*, vol. 48, no. 9, pp. 2329–2334, 2012.
- [59] X. Mao, Y. Shen, and C. Yuan, "Almost surely asymptotic stability of neutral stochastic differential delay equations with Markovian switching," *Stochastic Processes and Their Applications*, vol. 118, no. 8, pp. 1385–1406, 2008.
- [60] B. Zhou and A. V. Egorov, "Razumikhin and Krasovskii stability theorems for time-varying time-delay systems," *Automatica*, vol. 71, pp. 281–291, 2016.
- [61] B. Zhou and W. Luo, "Improved Razumikhin and Krasovskii stability criteria for time-varying stochastic time-delay systems," *Automatica*, vol. 89, pp. 382–391, 2018.
- [62] F. Mazenc, M. Malisoff, and S.-I. Niculescu, "Stability analysis for systems with time-varying delay: Trajectory based approach," in *Proceedings of the 54th IEEE Conference on Decision and Control (CDC '15)*, pp. 1811–1816, Osaka, Japan, December 2015.

## Research Article

# A Novel Nonlinear Fault Tolerant Control for Manipulator under Actuator Fault

Jing Zhao <sup>1,2</sup>, Sen Jiang,<sup>1</sup> Fei Xie <sup>2,3</sup>, Zhen He <sup>4</sup> and Jian Fu <sup>5</sup>

<sup>1</sup>Jiangsu Engineering Laboratory for Internet of Things and Intelligent Robots, Nanjing University of Posts and Telecommunications, Nanjing 210023, China

<sup>2</sup>Jiangsu Key Laboratory of 3D Printing Equipment and Manufacturing, Nanjing Normal University, Nanjing 210023, China

<sup>3</sup>Nanjing Institute of Intelligent High-end Equipment Industry Limited Company, Nanjing 210042, China

<sup>4</sup>School of Automation, Nanjing University of Aeronautics and Astronautics, Nanjing 210016, China

<sup>5</sup>College of Energy and Power Engineering, Nanjing University of Science and Technology, Nanjing 210094, China

Correspondence should be addressed to Fei Xie; xiefei@njnu.edu.cn

Received 2 June 2018; Revised 29 August 2018; Accepted 9 September 2018; Published 14 October 2018

Academic Editor: Xue-Jun Xie

Copyright © 2018 Jing Zhao et al. This is an open access article distributed under the Creative Commons Attribution License, which permits unrestricted use, distribution, and reproduction in any medium, provided the original work is properly cited.

A fault tolerant control (FTC) scheme based on adaptive sliding mode control technique is proposed for manipulator with actuator fault. Firstly, the dynamic model of manipulator is introduced and its actuator faulty model is established. Secondly, a fault tolerant controller is designed, in which both the parameters of actuator fault and external disturbance are estimated and updated by online adaptive technology. Finally, taking a two-joint manipulator as example, simulation results show that the proposed fault tolerant control scheme is effective in tolerating actuator fault; meanwhile it has strong robustness for external disturbance.

## 1. Introduction

With the rapid development of modern science technology, manipulator has emerged as an important area of research, and more manipulators are applied in our life to reduce the burden of work. In [1, 2] two cleaning robots are designed to help people complete household cleaning tasks better. Besides, some tasks cannot be completed by a single manipulator, but two more cooperating manipulators are required. Thus, a control method of dual manipulators is proposed to replace the human workers to assemble and grasp objects [3, 4]. Reference [5] addressed a decentralized controller with constrained error variable and a radial basis function network for space manipulator. Besides the above application, manipulator also plays an important role in dangerous environment where people can not directly participate. In outer space, nobody can stay much long. Therefore, an advanced mechanical arm system is needed to perform some exploratory and experimental tasks, especially extravehicular mission, such as space assembly, spacecraft maintenance, satellite interaction, and outer space exploration. Thus, it greatly reduces the risks of the astronauts going out of the

cabin and improves the efficiency and safety of space mission [6]. In recent years, many researchers have done a great deal of products on manipulators. The American space robot remote service system and the lightweight modular space manipulator system developed by German and Canadian giant robotic arm have been successfully launched following the rocket and completed the task. What is more, there are also some other space manipulators serving in International Space Station, including Dextre, SSRMS, and ERA [7–9].

In the current industrial application, manipulator has become increasingly important [10], therefore, the stability and reliability of manipulator system are crucial factors [11–15]. Sophisticated and dangerous work such as welding and space tasks that require high precision are assigned to robots. The robotic manipulator is a typical complex underactuated system with redundancy, multivariate, highly nonlinearities and coupling. On the one hand, as friction coefficient between joints always changes over time, and external disturbance is uncertain [16], fault may occur in manipulator. In particular, in dangerous environment, fault may occur more easily, such as hard environment conditions, particle radiation, electromagnetic interference [17], and

low temperature; consequently the performance will greatly decrease, even leading mission to fail. On the other hand, artificial repair is nearly impossible in outer space. In conclusion manipulator is needed to tolerate fault and continue the given operation task. Consequently, fault tolerant control is vital in security assurance for manipulator. FTC technique also applies on UAV team, cooperative control, distributed control, mobile wireless, networks, and communications [18]. The performance of feedback control system depends on actuators, sensors, and data acquisition/interface components. Faulty components will lead to the deterioration of the overall system stability, which has been a safety problem in control system [19]. At present, there have been a large number of FTC schemes. In the FTC literature, different approaches have been reported, such as robust FTC presented in [20], adaptive FTC designed in [21, 22], nonlinear FTC proposed in [23], and sliding mode FTC proposed in [24, 25]. However, there are not many FTC schemes for manipulator. In [26] a novel finite time FTC based on adaptive neural network nonsingular fast terminal sliding mode is addressed for uncertain robot manipulators with actuator faults, and it is verified that the system possesses strong robustness, no singularity, less chattering, and fast finite time convergence by simulation [27–33]. In [34] a robust LQR/LQI FTC method is developed for a 2DOF unmanned bicycle robot with actuator fault. Different from [26], [34, 35] proposed a decentralized FTC for reconfigurable manipulator with sensor fault.

Compared with the above-mentioned methods, sliding mode control (SMC) has attractive advantages of efficient characteristics thanks to its insensibility to matched uncertainties and disturbances [36]. Therefore, SMC is adopted to design the fault tolerant controller in this paper. However, chattering of the sliding mode control signal has become the major issue to its actual applications, which can lead to the deterioration of the overall system. In order to solve such problem, a novel sliding mode control technology, dynamic sliding mode control, is designed [37]. In FTC method, observers are usually designed to estimate disturbances and fault information; for example, in [38] a fault diagnosis via higher order sliding mode observers is proposed for manipulator system; different from [39, 40], observers are not considered in this paper, in which, the proposed controller is much easier to realize in practical application.

The main theoretical contributions of this paper can be briefly outlined as follows.

- (1) Compared with the design of traditional sliding surface, the novel dynamic sliding mode controller proposed in this paper can reduce the chattering effectively.
- (2) In comparison with traditional method to handle unknown system parameters and disturbances, adaptive algorithm is adopted to update parameters online; it is not necessary to obtain the accurate value of disturbances.
- (3) In comparison with the conventional FTC method, there is no need to design a fault diagnosis and detection observer, and the unknown fault can be estimated by the proposed adaptive algorithm.

The rest of this paper is organized as follows. In Section 2, the dynamic model of space manipulator and its actuator fault model are introduced. Then a fault tolerant controller is designed, in which parameters of actuator fault and external disturbance are estimated and updated by online adaptive method in Section 3. Finally, simulation results demonstrate the proposed fault tolerant controller is able to tolerate actuator fault, as well as the strong robustness for external disturbance.

## 2. Mathematic Model

*2.1. Dynamic model.* An articular robot system is a typical redundant, multivariable nonlinear complex dynamic coupling system [39]. When dealing with manipulator, we usually adopt its simplified model as follows due to the extreme complexity of its general dynamic model manipulator:

$$H(q)\ddot{q} + C(q, \dot{q})\dot{q} + G(q) + F(\dot{q}) = \tau + \tau_d \quad (1)$$

where  $q \in \mathbb{R}^n$ ,  $\dot{q} \in \mathbb{R}^n$ ,  $\ddot{q} \in \mathbb{R}^n$  represent joint position, velocity, and acceleration vector, respectively; here position refers to joint angle.  $H(q) \in \mathbb{R}^{n \times n}$  denotes symmetric positive definite inertia matrix.  $C(q, \dot{q}) \in \mathbb{R}^{n \times n}$  represents Coriolis force and centrifugal force matrix.  $G(q) \in \mathbb{R}^n$  denotes gravity torque vector.  $F(\dot{q}) \in \mathbb{R}^n$  is friction torque vector.  $\tau_d \in \mathbb{R}^n$  denotes external disturbance and model parameter uncertainties torque vector.  $\tau \in \mathbb{R}^n$  denotes control torque vector.

The above manipulator system (1) has the following property which is beneficial in subsequent controller design.

*Property.*  $\dot{H}(q) - 2C(q, \dot{q})$  is a skew symmetric matrix [41]; i.e.,  $\Gamma^T(\dot{H}(q) - 2C(q, \dot{q}))\Gamma = 0, \forall \Gamma \in \mathbb{R}^n$ .

*2.2. Fault Model.* Instead of locked-joint fault, loss of effectiveness considered in this paper means the free-swinging fault; that is, fault joint swings freely without constraints. On the contrary, locked-joint fault means that fault joint is locked at its current position and cannot move any more. The move of manipulator system depends on the rotation of motor, which ranges from 0 degree to 300 degree. The free-swinging fault here that may be caused by a hardware or software fault in a manipulator can lead to the loss of torque (or force) on a joint [42]. Then the free-swinging fault model is established as follows:

$$H(q)\ddot{q} + C(q, \dot{q})\dot{q} + G(q) + F(\dot{q}) = \tau_f + \tau_d \quad (2)$$

where  $\tau_f = E\tau$ ,  $E = \text{diag}\{e_i\}$ ,  $i = 1, 2, \dots, n$ , and  $e_i \in (0, 1)$  represents actuator loss of effectiveness factor which refers to the free-swinging fault in this paper, and the proposed FTC of manipulator is mainly designed under such case. When  $e_i = 1$ , the  $i_{th}$  joint is normal without fault; when  $e_i = 0$ , the  $i_{th}$  joint is with lock in place that means that the joint is locked at its current position, which is not considered in this paper. Define  $\Delta E(t) = I - E = \text{diag}\{1 - e_i(t)\}$ , where  $I$  is the identity matrix and  $\|\Delta E(t)\| = 1 - \min\{e_i(t)\}$ ; then system (2) can be transformed as

$$H\ddot{q} = \tau - \Delta E(t)\tau + \tau_d + g(q, \dot{q}) \quad (3)$$

where  $g(q, \dot{q}) = -C(q, \dot{q})\dot{q} - G(q) - F(\dot{q})$ . For convenience, define  $H \triangleq H(q)$ ,  $C \triangleq C(q, \dot{q})$ ,  $G \triangleq G(q)$ ,  $F \triangleq F(\dot{q})$ , and  $g \triangleq g(q, \dot{q})$ .

### 3. Fault Tolerant Controller Design

**3.1. Problem Statement.** In this paper, we are absorbed in investigating an FTC method for manipulator with actuator fault. The trajectory tracking problem of fault system (2) is considered. The control objective can be described as that for a manipulator control system with actuator fault, an FTC method is proposed to ensure that the closed-loop system is stable, i.e., when  $t \rightarrow \infty$ ,  $q \rightarrow q_d$ , where  $q_d$  denotes the desired position signal. For this purpose, an FTC method based on adaptive dynamic sliding mode technology is proposed. Firstly, an assumption is given as follows.

*Assumption 1.* The external disturbance  $\tau_d$  is assumed to be norm-bounded.

$$\|\tau_d\| \leq K \quad (4)$$

where  $K$  is an unknown positive constant and  $\|\cdot\|$  represents  $L_\infty$  norm in this paper.

**3.2. Controller Design.** As mentioned in the above section, the desired position signal is defined as  $q_d$ , so the tracking error is  $z = q - q_d$ . Then the conventional sliding mode surface is selected as

$$S = \dot{z} + lz \quad (5)$$

where  $l \in \mathbb{R}^{n \times n}$  is a positive matrix; further,

$$\dot{S} = \ddot{z} + l\dot{z} = \ddot{q} - \ddot{q}_d + l(\dot{q} - \dot{q}_d). \quad (6)$$

Next, the dynamic sliding mode surface is selected as

$$J = S + \chi \quad (7)$$

where  $\chi$  can be considered as the error between  $J$  and  $S$  and its derivative of time is  $\dot{\chi} = \rho_1 \|S\|^{0.5} \text{sgn}(S) - \rho_2 \|J\|^{0.5} \text{sgn}(J)$ , where  $\text{sgn}(S) = [\text{sgn}(S_1), \text{sgn}(S_2), \dots, \text{sgn}(S_n)]^T$ ,  $\text{sgn}(J) = [\text{sgn}(J_1), \text{sgn}(J_2), \dots, \text{sgn}(J_n)]^T$ ,  $\rho_1$  is the sliding mode gain of conventional sliding mode surface  $S$ , and  $\rho_2$  is the sliding mode gain of dynamic sliding mode surface  $J$ . They are two positive constants satisfying  $\rho_1 > 0$ ,  $\rho_2 > 0$ ,  $\rho_1 \neq \rho_2$ , and for more details please refer to Remark 6.

**Theorem 2.** *Considering manipulator system with free-swinging fault and external disturbance (2) under Assumption 1, a fault tolerant control input based on adaptive sliding mode controller (8) and adaptive law (9) can guarantee asymptotic output tracking of manipulator control system in both cases of no fault and fault, which guarantees the boundedness of all the closed-loop signals and asymptotic output tracking.*

$$\tau = -g - Hf - CJ - \phi \text{sgn}(J) - \widehat{K} \text{sgn}(J) \quad (8)$$

$$\dot{\widehat{K}} = \mu \sum_{i=1}^n |J_i| \quad (9)$$

where  $\widehat{K}$  is the estimated value of  $K$ ,  $\varepsilon$  is a positive constant,  $f = -\dot{q}_d + l(\dot{q} - \dot{q}_d) + \dot{\chi}$ ,  $\phi = (b/(1-b))[\|g + Hf + CJ\| + \widehat{K} \text{sgn}(J) + \varepsilon]$ , and  $b = \|\Delta E\|$ . To satisfy the stability of the system, achieve a good tracking effectiveness, and estimate the value of disturbances, (9) is obtained to put an integral action in the definition of (8).

*Proof.* Define a Lyapunov function as follows:

$$V = \frac{1}{2} J^T H J + \frac{1}{2\mu} \widehat{K}^2 \quad (10)$$

where  $\widehat{K}$  denotes the estimated error of disturbance; that is,  $\widehat{K} = K - \widehat{K}$  and  $\mu$  is a positive constant. The time derivative of  $V$  is obtained.

$$\begin{aligned} \dot{V} &= \frac{1}{2} J^T \dot{H} J + J^T H \dot{J} - \frac{1}{\mu} \widehat{K} \dot{\widehat{K}} \\ &= \frac{1}{2} J^T (\dot{H} - 2C) J + J^T C J + J^T H \dot{J} - \frac{1}{\mu} \widehat{K} \dot{\widehat{K}} \\ &= J^T (CJ + H\dot{J}) - \frac{1}{\mu} \widehat{K} \dot{\widehat{K}} \\ &= J^T (CJ + H\dot{q} + Hf) - \frac{1}{\mu} \widehat{K} \dot{\widehat{K}} \end{aligned} \quad (11)$$

Substituting (3) into the above equation, one can obtain the following.

$$\dot{V} = J^T (CJ + \tau - \Delta E(t) \tau + \tau_d + g + Hf) - \frac{1}{\mu} \widehat{K} \dot{\widehat{K}} \quad (12)$$

Applying controller (8) and adaptive law (9) into the above equation, one can obtain

$$\begin{aligned} \dot{V} &= J^T [-\Delta E(t) \tau - \phi \text{sgn}(J) - \widehat{K} \text{sgn}(J) + \tau_d] \\ &\quad - \frac{1}{\mu} \widehat{K} \dot{\widehat{K}} \\ &= J^T [-\Delta E(t) \tau - \phi \text{sgn}(J)] - \widehat{K} J^T \text{sgn}(J) + J^T \tau_d \\ &\quad - \frac{1}{\mu} \widehat{K} \dot{\widehat{K}} \\ &\leq J^T [-\Delta E(t) \tau - \phi \text{sgn}(J)] - \widehat{K} \sum_{i=1}^n |J_i| + K \sum_{i=1}^n |J_i| \\ &\quad - \frac{1}{\mu} \widehat{K} \dot{\widehat{K}} \\ &= J^T [-\Delta E(t) \tau - \phi \text{sgn}(J)] + \widehat{K} \left( \sum_{i=1}^n |J_i| - \frac{1}{\mu} \dot{\widehat{K}} \right) \end{aligned} \quad (13)$$

Further simplify

$$\begin{aligned}
\dot{V} &= J^T [-\Delta E(t)\tau - \phi \text{sgn}(J)] \\
&= J^T \Delta E(t) [g + Hf + CJ + \phi \text{sgn}(J) + \widehat{K} \text{sgn}(J)] \\
&\quad - J^T \phi \text{sgn}(J) \\
&\leq b \|J\| [\|g + Hf + CJ\| + \widehat{K} \text{sgn}(J)] + b\phi \sum_{i=1}^n |J_i| \\
&\quad - \phi \sum_{i=1}^n |J_i| \\
&\leq b \sum_{i=1}^n |J_i| [\|g + Hf + CJ\| + \widehat{K} \text{sgn}(J)] \\
&\quad - \phi (1-b) \sum_{i=1}^n |J_i| = -b\epsilon \sum_{i=1}^n |J_i| \leq 0
\end{aligned} \tag{14}$$

and, thus, the stability of the closed-loop system is verified.  $\square$

*Remark 3.* In practical application, the smallest valuable of actuator fault  $\min\{e_i(t)\}$  is usually unknown; therefore it is necessary to design an adaptive law to estimate fault information. To solve this problem, an adaptive fault tolerant controller will be designed in the following, in which adaptive scheme is adopted to estimate both the actuator fault and external disturbance.

When dealing with the faulty term, define  $b = \|\Delta E(t)\|$ ,  $\xi = 1/(1-b)$ , and then adaptive algorithm is adopted to estimate  $\xi$ , which can compensate for the existent fault. Regarding the disturbance, based on Assumption 1,  $\widehat{K}$  is used to compensate for the existent disturbance by adaptive technique.

**Theorem 4.** *Based on Theorem 2, considering manipulator system with free-swinging fault and external disturbance (2) under Assumption 1, the minimum boundary value of actuator fault  $\min\{e_i(t)\}$  is unknown, and an FTC input based on adaptive sliding mode controller (15) and adaptive laws (16)-(17) can guarantee asymptotic output tracking of manipulator control system in both cases, i.e., no fault and fault, which guarantees the boundedness of all the closed-loop signals and asymptotic output tracking.*

$$\tau = -g - Hf - CJ - \gamma(t) \text{sgn}(J) - \widehat{K} \text{sgn}(J) \tag{15}$$

$$\dot{\widehat{K}} = \mu \sum_{i=1}^n |J_i| \tag{16}$$

$$\dot{\widehat{\xi}} = \beta \delta \sum_{i=1}^n |J_i| \tag{17}$$

where  $\widehat{K}$  is the estimated value of  $K$ ,  $\delta = \|g + Hf + CJ\| + \widehat{K} + \epsilon$ , and  $\epsilon$  is a positive constant.  $\gamma(t) = -\delta + \widehat{\xi}\delta$ , and  $\widehat{\xi}$  is the estimated value of  $\xi$ .

*Proof.* In order to prove the stability of the overall system, the Lyapunov function is selected as

$$V = V_1 + V_2 + V_3 \tag{18}$$

where  $V_1, V_2, V_3$  represent three Lyapunov functions which will be elaborated in the following 3 steps; further,

$$\dot{V} = \dot{V}_1 + \dot{V}_2 + \dot{V}_3. \tag{19}$$

The process of proof is divided into three steps.

*Step 1* (adaptive law analysis). To obtain the adaptive laws of fault and disturbance, the Lyapunov function is chosen as

$$V_1 = \frac{1}{2} J^T H J + \frac{1}{2\mu} \widehat{K}^2 + \frac{1-b}{2\beta} \widehat{\xi}^2 \tag{20}$$

where  $\widehat{K}$  denotes the estimated error of disturbance,  $\widehat{\xi}$  denotes the estimated error of fault,  $\widehat{K} = K - \widehat{K}$ ,  $\widehat{\xi} = \xi - \widehat{\xi}$ , and  $\mu$  and  $\beta$  are both positive constants. The time derivative of  $V_1$  is obtained.

$$\begin{aligned}
\dot{V}_1 &= \frac{1}{2} J^T \dot{H} J + J^T H \dot{J} - \frac{1}{\mu} \widehat{K} \dot{\widehat{K}} - \frac{1-b}{\beta} \widehat{\xi} \dot{\widehat{\xi}} \\
&= \frac{1}{2} J^T (\dot{H} - 2C) J + J^T C J + J^T H \dot{J} - \frac{1}{\mu} \widehat{K} \dot{\widehat{K}} \\
&\quad - \frac{1-b}{\beta} \widehat{\xi} \dot{\widehat{\xi}} \\
&= J^T (CJ + H\dot{q} + Hf) - \frac{1}{\mu} \widehat{K} \dot{\widehat{K}} - \frac{1-b}{\beta} \widehat{\xi} \dot{\widehat{\xi}}
\end{aligned} \tag{21}$$

Substituting (3) into the above equation, one obtains the following.

$$\begin{aligned}
\dot{V}_1 &= J^T (CJ + \tau - \Delta E(t)\tau + \tau_d + g + Hf) - \frac{1}{\mu} \widehat{K} \dot{\widehat{K}} \\
&\quad - \frac{1-b}{\beta} \widehat{\xi} \dot{\widehat{\xi}}
\end{aligned} \tag{22}$$

Applying controller (15) into the above equation yields the following.

$$\begin{aligned}
\dot{V}_1 &= J^T [-\Delta E(t)\tau - \gamma(t) \text{sgn}(J) - \widehat{K} \text{sgn}(J) + \tau_d] \\
&\quad - \frac{1}{\mu} \widehat{K} \dot{\widehat{K}} - \frac{1-b}{\beta} \widehat{\xi} \dot{\widehat{\xi}} \\
&= J^T [-\Delta E(t)\tau - \gamma(t) \text{sgn}(J)] + \widehat{K} \sum_{i=1}^n |J_i| \\
&\quad - \frac{1}{\mu} \widehat{K} \dot{\widehat{K}} - \frac{1-b}{\beta} \widehat{\xi} \dot{\widehat{\xi}} \\
&= J^T [-\Delta E(t)\tau - \gamma(t) \text{sgn}(J)] \\
&\quad + \widehat{K} \left( \sum_{i=1}^n |J_i| - \frac{1}{\mu} \dot{\widehat{K}} \right) - \frac{1-b}{\beta} \widehat{\xi} \dot{\widehat{\xi}}
\end{aligned} \tag{23}$$

Substituting adaptive law (16) into the above equation yields the following.

$$\begin{aligned}
\dot{V}_1 &\leq J^T \left[ -\Delta E(t) \tau - \gamma(t) \operatorname{sgn}(J) \right] - \frac{1-b}{\beta} \dot{\xi} \hat{\xi} \\
&= -\gamma(t) \sum_{i=1}^n |J_i| - \frac{1-b}{\beta} \dot{\xi} \hat{\xi} + J^T \\
&\quad \Delta E(t) \left[ g + Hf + CJ + \gamma(t) \operatorname{sgn}(J) + \widehat{K} \operatorname{sgn}(J) \right] \\
&\leq (1-\widehat{\xi}) \delta \sum_{i=1}^n |J_i| - \frac{1-b}{\beta} \dot{\xi} \hat{\xi} \\
&\quad + b \|J^T\| \left[ \|g + Hf + CJ\| + \gamma(t) + \widehat{K} \right] \\
&\leq (1-\widehat{\xi}) \delta \sum_{i=1}^n |J_i| - \frac{1-b}{\beta} \dot{\xi} \hat{\xi} + b \sum_{i=1}^n |J_i| (-\varepsilon + \widehat{\xi} \delta) \\
&= (1-\widehat{\xi} + b\widehat{\xi}) \delta \sum_{i=1}^n |J_i| - \frac{1-b}{\beta} \dot{\xi} \hat{\xi} - \varepsilon b \sum_{i=1}^n |J_i| \\
&= (1-b) (\xi - \widehat{\xi}) \delta \sum_{i=1}^n |J_i| - \frac{1-b}{\beta} \dot{\xi} \hat{\xi} - \varepsilon b \sum_{i=1}^n |J_i| \\
&= (1-b) \widehat{\xi} \left( \delta \sum_{i=1}^n |J_i| - \frac{1}{\beta} \dot{\xi} \hat{\xi} \right) - \varepsilon b \sum_{i=1}^n |J_i|
\end{aligned} \tag{24}$$

As a result, applying adaptive law (17) into the above equation, one can obtain the following.

$$\dot{V}_1 = -\varepsilon b \sum_{i=1}^n |J_i| \leq 0 \tag{25}$$

*Step 2* (reach time analysis). Before analysis, a lemma is proposed as follows to obtain the convergence time.

**Lemma 5.** *The dynamic sliding mode function  $J$  exists and can converge within finite time  $t_J$ ; please see [43] for more details.*

*After time  $t_J$ , the surface  $J = 0$ ; from (7), one can obtain the following.*

$$\dot{S} = -\dot{\chi} = -\rho_1 \|S\|^{0.5} \operatorname{sgn}(S) \tag{26}$$

*Further, a Lyapunov function is selected as follows to obtain the convergence time of system.*

$$V_2 = \frac{1}{2} S^T S \tag{27}$$

*Further,*

$$\dot{V}_2 = S^T \dot{S} = S^T \left( -\rho_1 \|S\|^{0.5} \operatorname{sgn}(S) \right) \leq -\rho_1 \|S\|^{1.5} \leq 0. \tag{28}$$

*To solve the above differential equation, the following equation can be obtained by (27).*

$$V_2 = \frac{1}{2} \|S\|^2 \tag{29}$$

*Further,*

$$\|S\| = |2V_2|^{1/2} \tag{30}$$

*Substituting (30) to (28) yields the following.*

$$\dot{V}_2 \leq -\rho_1 |2V_2|^{3/4}. \tag{31}$$

*Thus*

$$\begin{aligned}
V_2^{-3/4} dV_2 &\leq -2^{3/4} \rho_1 dt \int_{t_J}^t V_2^{-3/4} dV_2 \\
&\leq \int_{t_J}^t -2^{3/4} \rho_1 dt \left[ V_2(t)^{1/4} - V_2(t_J)^{1/4} \right] \\
&\leq -2^{3/4} \rho_1 (t - t_J).
\end{aligned} \tag{32}$$

*As time  $t$  reaches  $t_S$ , the conventional sliding mode surface  $S$  will converge to zero; i.e., when  $t = t_S$ ,  $S = 0$ ; that is,  $V_2(t) = V_2(t_S)$ ; thus*

$$-4V_2(t_J)^{1/4} \leq -2^{3/4} \rho_1 (t_S - t_J) \tag{33}$$

*Thus, one can obtain the following.*

$$t_S \leq \frac{4V_2(t_J)^{1/4} + 2^{3/4} \rho_1 t_J}{2^{3/4} \rho_1} \tag{34}$$

*Consequently, sliding mode surface  $S$  will converge to zero within finite time.*

$$t_S \leq \frac{4V_2(t_J)^{1/4} + 2^{3/4} \rho_1 t_J}{2^{3/4} \rho_1} \tag{35}$$

*Now, it is verified that conventional sliding mode surface  $S$  and dynamic sliding mode surface  $J$  can both converge to zero within finite time, and dynamic surface converges faster than conventional surface; i.e.,  $\lim_{t \geq t_J} (J/S) = 0$ . As  $t \rightarrow t_S$  is reached,  $S = 0$ ; substituting this into (5), one can obtain the following.*

$$\dot{z} = -lz \tag{36}$$

*Step 3* (tracking error analysis). To prove the convergence of the tracking error  $z$ , the Lyapunov function is defined as follows.

$$V_3 = \frac{1}{2} z^T z \tag{37}$$

*Thus*

$$\dot{V}_3 = z^T \dot{z} \leq -l \|z\|^2 \leq 0 \tag{38}$$

and, therefore, tracking error  $z$  is convergent, which means that when  $t \rightarrow \infty$ ,  $q \rightarrow q_d$ ,  $z \rightarrow 0$ . Therefore, according to the above three steps, it is easy to be seen that  $\dot{V} < 0$  in (19), which means that the overall system can be stable with the proposed controller. The proof is completed.  $\square$

*Remark 5.* Practically, due to the hysteresis of nonlinear and switching,  $\|J\|$  cannot converge to zero accurately within a finite time; therefore, the adaptive parameters  $\hat{K}$  and  $\hat{\xi}$  of the estimated values for  $K$  and  $\xi$  may increase boundlessly. In the other words,  $\hat{K}$  and  $\hat{\xi}$  obtained by the proposed adaptive algorithm will be not accurate, which may increase towards infinity. In practical engineering, it is difficult to apply (16)-(17) directly. Consequently, to solve such a problem, dead zone technique is used [44] and adaptive laws (16) and (17) are modified as

$$\dot{\hat{K}} = \begin{cases} \mu \sum_{i=1}^n |J_i|, & |J_i| \geq \lambda_1 \\ 0, & |J_i| < \lambda_1 \end{cases} \quad (39)$$

$$\dot{\hat{\xi}} = \begin{cases} \beta \delta \sum_{i=1}^n |J_i|, & |J_i| \geq \lambda_2 \\ 0, & |J_i| < \lambda_2 \end{cases} \quad (40)$$

where  $\lambda_1$  and  $\lambda_2$  are both small positive constants.

*Remark 6.* The dynamic sliding function  $J$  reaches and remains on the sliding surface  $J = 0$  before the conventional sliding function  $S$  gets to the sliding surface  $S = 0$  if and only if  $\rho_1, \rho_2$  satisfy [45]

$$|J(0)| \leq \left( \frac{\rho_2}{\rho_1} \right)^2 |S(0)|. \quad (41)$$

## 4. Simulation

In order to verify the validity of control method proposed in this paper, we applied it to two-joint manipulator model. In this section, four cases with considering signal fault and double joints faults, respectively, will be simulated to present the tracking effectiveness of manipulator.

### 4.1. Simulation Cases

*Case 1.* Link 1 and link 2 are both healthy without fault; i.e.,  $E = I$ , where  $I$  is the identity matrix.

*Case 2.* Link 1 is healthy, and actuator fault occurs in link 2 at 10s; i.e.,

$$e_1 = 1$$

$$e_2 = \begin{cases} 1, & t < 10s \\ 0.2, & t \geq 10s. \end{cases} \quad (42)$$

*Case 3.* Actuator fault occurs in link 1 at 10s, and link 2 is healthy; i.e.,

$$e_1 = \begin{cases} 1, & t < 10s \\ 0.6, & t \geq 10s. \end{cases} \quad (43)$$

$$e_2 = 1$$

*Case 4.* Actuator fault occurs in link 1 and link 2 at 10s; i.e.,

$$e_1 = \begin{cases} 1, & t < 10s \\ 0.6, & t \geq 10s \end{cases} \quad (44)$$

$$e_2 = \begin{cases} 1, & t < 10s \\ 0.2, & t \geq 10s. \end{cases}$$

*Simulation Parameters.* The parameters of simulation are designed as follows.

$$H(q) = \begin{bmatrix} 3.66 + 1.74 \cos q_2 & 0.76 + 0.87 \cos q_2 \\ 0.76 + 0.87 \cos q_2 & 0.76 \end{bmatrix}$$

$$G(q) = \begin{bmatrix} 3.04g \cos q_1 + 0.87g \cos(q_1 + q_2) \\ 0.87g \cos(q_1 + q_2) \end{bmatrix} \quad (45)$$

$$\tau_d = \begin{bmatrix} 0.2 \sin \dot{q}_1 \\ 0.2 \sin \dot{q}_2 \end{bmatrix}$$

The initial state of manipulator system is selected as  $q_0 = (0, 0)^T \text{rad/s}$ ,  $\dot{q}_0 = (0, 0)^T \text{rad/s}$ .

Tracked objective trajectory is  $q_{d1} = 0.7 \sin(\pi t) \text{rad}$ ,  $q_{d2} = \sin(\pi t) \text{rad}$ , respectively.

To make the overall system stable, equipped with strong robustness and fault tolerance, the parameters of the proposed controller are selected as  $\varepsilon = 1$ , and the learning gains of adaptive laws are adopted as  $\mu = 0.5$ ,  $\beta = 0.1$ . To realize fast convergence of the sliding mode surface, sliding mode parameters are designed as  $l = \text{diag}\{0.001, 0.001\}$ ,  $\rho_1 = 0.3$ ,  $\rho_2 = 5$   $\lambda_1 = \lambda_2 = 0.05$ .

*Simulation Results and Analysis.* In the simulation, according to the designed control law (15) and adaptive laws (39), (40), the time of fault tolerance in each case is shown in Table 1, and the corresponding simulation results are depicted in Figures 1–8, which show time responses of link position tracking, velocity tracking.

Figure 1 shows the tracking responses in Case 1. From Figure 1, we can see that the position and speed signal of link 1 can track the corresponding desired signal within 5s. Meanwhile, Figure 1 shows that tracking trajectories of position and speed of link 2 between actual signal and desired signal can converge to zero in 5s and then reach stability. From Figure 5, it is easy to be seen that the control torque can converge within 4 seconds without actuator fault in this case.

Figure 2 depicts the time responses of trajectory tracking in Case 2. From Figure 2, it can be easily seen that the position and speed tracking errors of link 1 between actual signal and desired signal can converge to zero in 5s without actuator fault. Also, Figure 2 shows that tracking error of two links can converge to zero in 5s; after actuator fault occurs in link 2 at 10s, system can rapidly deal with the fault and realize trajectory tracking within 5 seconds. From Figure 6, we can see that when actuator fault occurs in link 2, the control

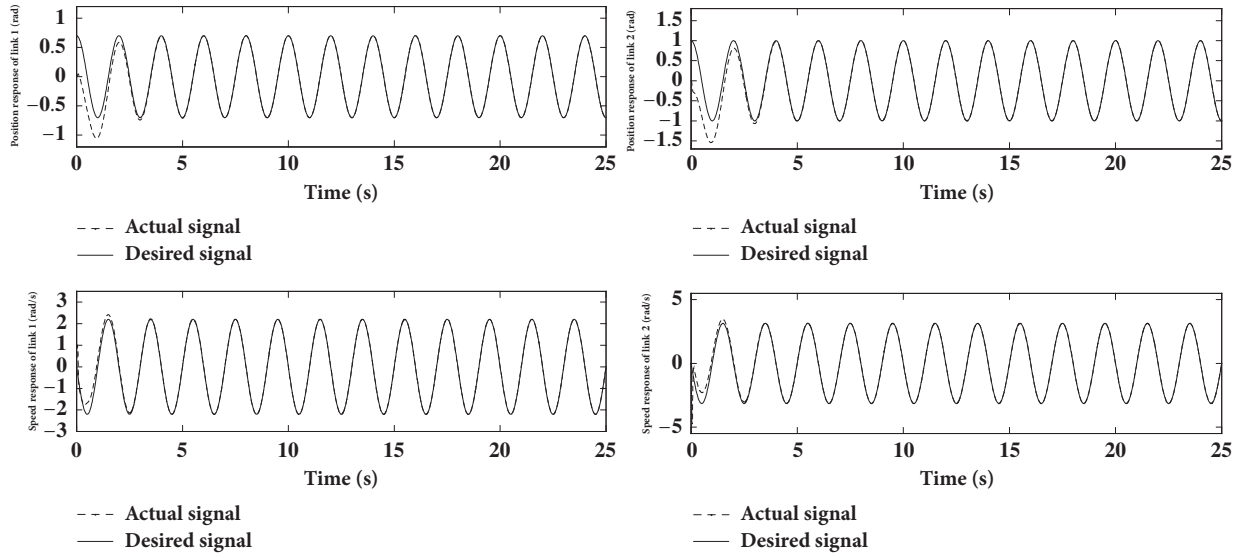


FIGURE 1: Tracking responses of links 1 and 2 in Case 1.

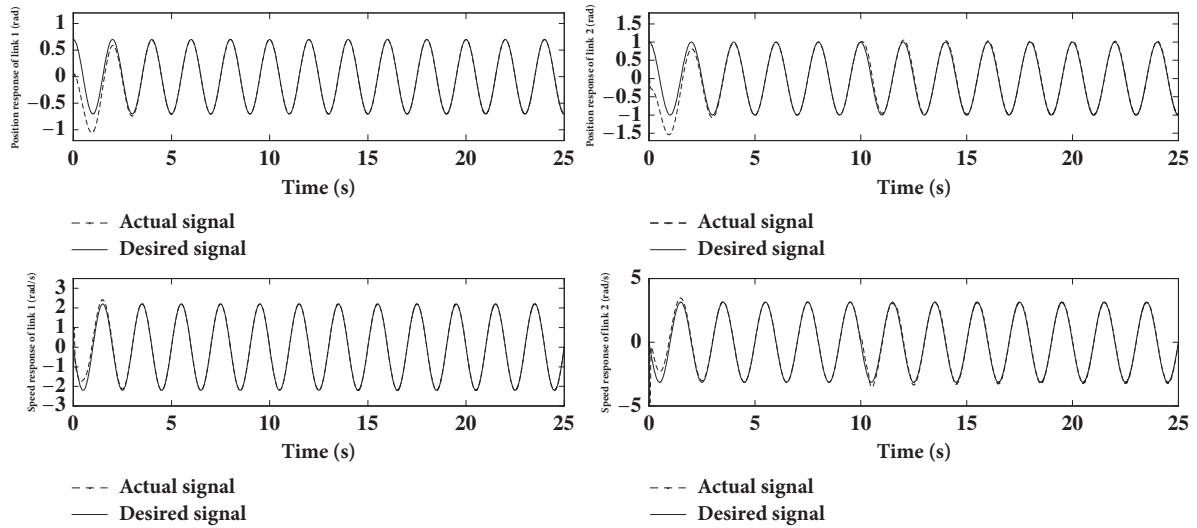


FIGURE 2: Tracking responses of links 1 and 2 in Case 2.

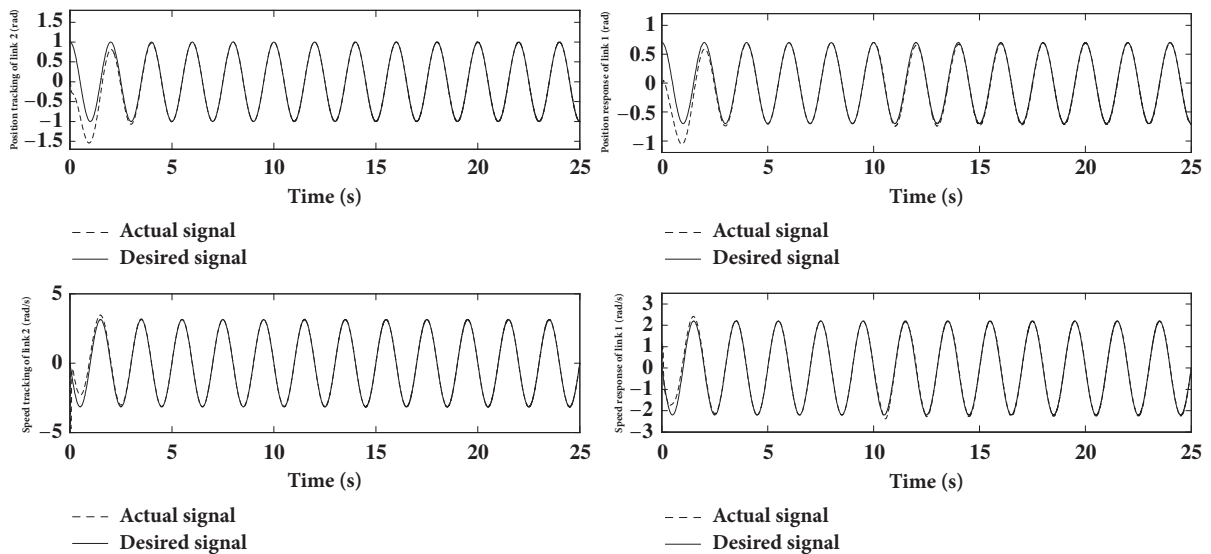


FIGURE 3: Tracking responses of links 1 and 2 in Case 3.

TABLE 1: Time of fault tolerance.

CASES	Position tracking of link1(s)	Speed tracking of link1(s)	Control torque of link1(s)	Position tracking of link2(s)	Speed tracking of link2(s)	Control torque of link2(s)
1	/	/	/	/	/	/
2	/	/	/	5	5	3
3	7	7	3	/	/	/
4	7	7	3	5	5	3

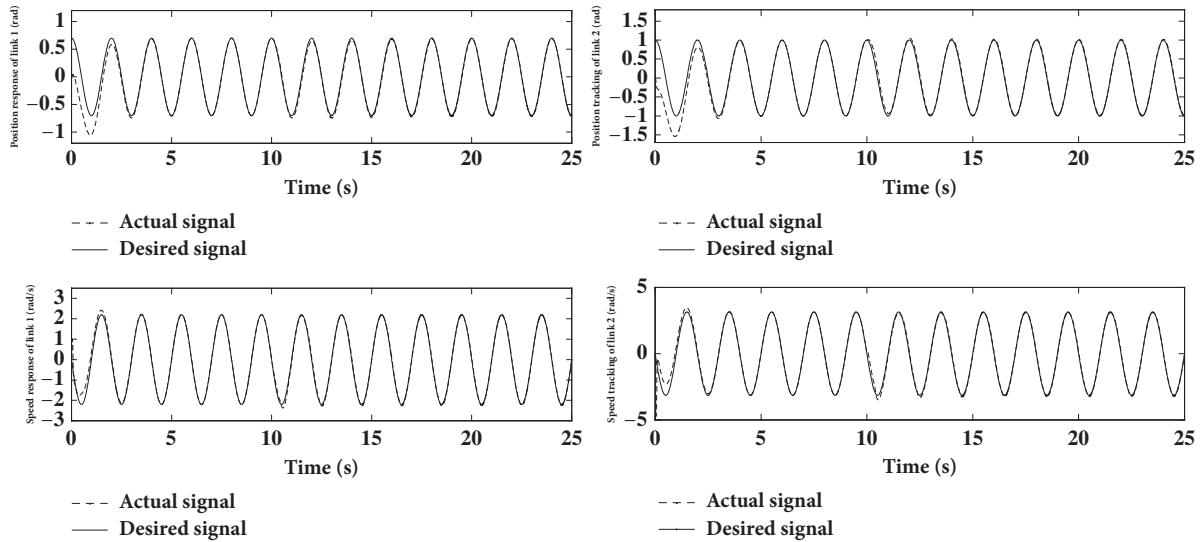


FIGURE 4: Tracking responses of links 1 and 2 in Case 4.

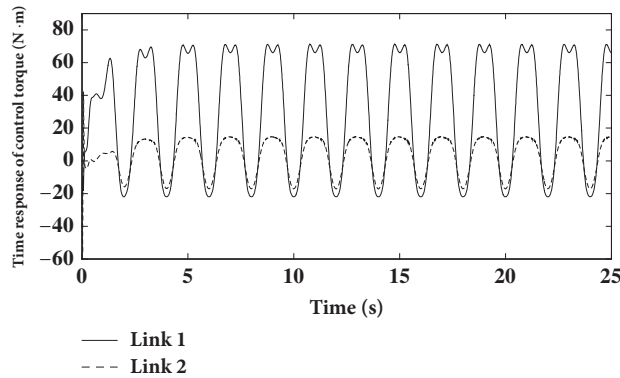


FIGURE 5: Time responses of control torque in Case 1.

torque of link 2 can handle the fault within 3 seconds, but a little chattering phenomenon appears.

The tracking responses in Case 3 are shown in Figure 3, from which, it can be easily seen that link position can deal with fault by itself and basically track the desired position signal in 7s when actuator fault appears in link 1 at 10s. Compared with other cases, the error between actual signal and desired signal is a little high, but is still in an acceptable range. Figure 3 also provides the actual speed of link 1 with actuator fault being able to track expected signal within 7s. From Figure 3 we can, respectively, see position and speed of link 2 with no fault being able to easily realize the trajectory

tracking in 5s. Figure 7 shows the time response of control torque, from which we can see that the amplitude of link 1 increases and control torque can reconverge within 3 seconds.

Figure 4 provides the trajectory tracking responses of two links in this case. The tracking response of link 1 is shown in Figure 4, from which, it is easy to see that when actuator of link 1 failed at 10s, position signal and speed signal of link 1 can deal with fault and basically track the desired signals in 7 seconds. Although there exists a certain error in both position and speed tracking, the error is acceptable in programming. Figure 4 also depicts the tracking response of link 2, from which, we can see that it takes 5 seconds for position and

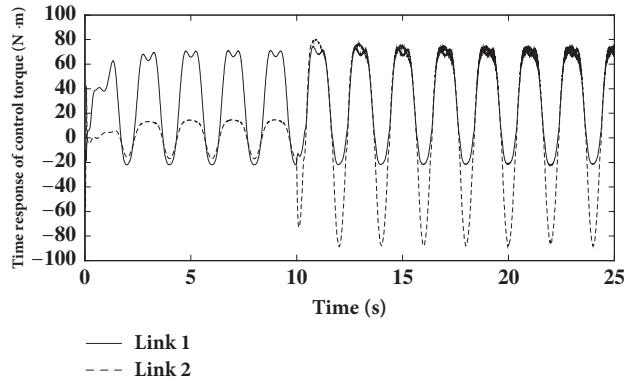


FIGURE 6: Time responses of control torque in Case 2.

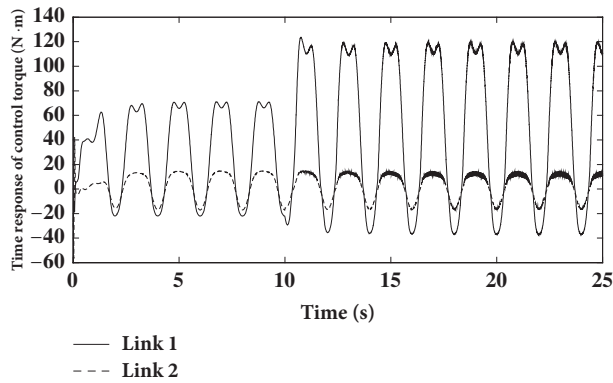


FIGURE 7: Time responses of control torque in Case 3.

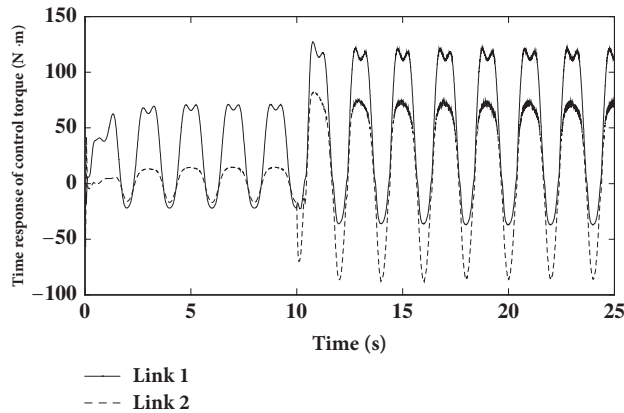


FIGURE 8: Time responses of control torque in Case 4.

speed signal to track the corresponding desired signals when actuator fault occurs in link 2 at 10s. Figure 8 depicts the time response of control torque in this case, from which it can be easily seen that the amplitudes of 2 links increase, and control torque can reconverge within 3 seconds but a little chattering phenomenon appears.

From Table 1 and Figures 1–8, we can see that when both actuators are healthy without fault, the overall system can realize trajectory tracking within 5 seconds; when actuator fault occurs in link 2, tracking responses of link 2 can reconverge to desired signal within 5 seconds; when actuator

fault occurs in link 1, tracking responses of link 1 can reconverge to desired signal within 7 seconds; when actuator fault occurs in two links, tracking responses of links 1 and 2 can reconverge to desired signal within 7 and 5 seconds, respectively. Therefore, the trajectory tracking effectiveness of the FTC method proposed in this paper is verified.

### 5. Conclusions

In this paper, a novel FTC scheme based on adaptive sliding mode method is investigated for manipulator with actuator

fault and external disturbance. Firstly the general dynamic model of space manipulator is introduced and further its actuator faulty model is established. Secondly, an adaptive fault tolerant controller is designed for manipulator with actuator fault. Parameters of fault and disturbance are estimated and updated by online adaptive method. Finally the proposed controller is applied to two-joint manipulator; from the simulation results it is shown that the controller proposed in this paper can not only realize a good trajectory tracking, but also tolerate actuator fault and present strong robustness for external disturbance, while effectively reducing the chattering phenomenon of sliding mode control.

## Data Availability

The data supporting the conclusions of our manuscript are some open access articles that have been properly cited, and the readers can easily obtain these articles to verify the conclusions, replicate the analysis, and conduct secondary analyses. Therefore, we did not create a publicly available data repository.

## Conflicts of Interest

The authors declare that they have no conflicts of interest.

## Acknowledgments

This work is supported by National Nature Science Foundation (under Grant 61601228, 61403210, and 61603191), Natural Science Foundation of Jiangsu (BK20161021), the Open Program of Jiangsu Key Laboratory of 3D Printing Equipment and Manufacturing (BM2013006), Item number 3DL201607, and the National Key Research and Development Program of China (Grant No. 2017YFB1103200).

## References

- [1] D. Zhao, S. Li, and Q. Zhu, "A new TSMC prototype robust nonlinear task space control of a 6 DOF parallel robotic manipulator," *International Journal of Control, Automation, and Systems*, vol. 8, no. 6, pp. 1189–1197, 2010.
- [2] Y. Tanise, K. Taniguchi, S. Yamazaki, M. Kamata, Y. Yamada, and T. Nakamura, "Development of an air duct cleaning robot for housing based on peristaltic crawling motion," in *Proceedings of the 2017 IEEE International Conference on Advanced Intelligent Mechatronics, AIM 2017*, pp. 1267–1272, Germany, July 2017.
- [3] A. S. Al-Yahmadi, J. Abdo, and T. C. Hsia, "Modeling and control of two manipulators handling a flexible object," *Journal of The Franklin Institute*, vol. 344, no. 5, pp. 349–361, 2007.
- [4] Buren, G. Sun, and R. Hu, "Flexible force control on robot arm for spacecraft assembly," *Spacecraft Environment Engineering*, vol. 465, no. 21, pp. 147–152, 2014.
- [5] L. A. Tuan, Y. H. Joo, P. X. Duong et al., "Parameter estimator integrated-sliding mode control of dual arm robots," *International Journal of Control Automation & Systems*, vol. 15, no. 6, pp. 2754–2763, 2017.
- [6] Y. Xu, H. Sun, Q. Jia et al., "Control of space robotic manipulators with faults," *Mechanical Science & Technology*, vol. 25, no. 12, pp. 1503–1423, 2006.
- [7] E. Coleshill, L. Oshinowo, R. Rembala, B. Bina, D. Rey, and S. Sindelar, "Dextre: improving maintenance operations on the International Space Station," *Acta Astronautica*, vol. 64, no. 9–10, pp. 869–874, 2009.
- [8] S. B. Nokleby, "Singularity analysis of the canadarm," *Mechanism & Machine Theory*, vol. 42, no. 4, pp. 442–454, 2007.
- [9] R. Boumans and C. Heemskerk, "The European Robotic Arm for the International Space Station," *Robotics and Autonomous Systems*, vol. 23, no. 1–2, pp. 17–27, 1998.
- [10] I. Duleba and M. Opalka, "A comparison of Jacobian-based methods of inverse kinematics for serial robot manipulators," *International Journal of Applied Mathematics & Computer Science*, vol. 23, pp. 373–382, 2013.
- [11] Y. Guo, "Globally robust stability analysis for stochastic Cohen-Grossberg neural networks with impulse and time-varying delays," *Ukrainian Mathematical Journal*, vol. 69, no. 8, pp. 1220–1233, 2017.
- [12] W. Liu, J. Cui, and J. Xin, "A block-centered finite difference method for an unsteady asymptotic coupled model in fractured media aquifer system," *Journal of Computational and Applied Mathematics*, vol. 337, pp. 319–340, 2018.
- [13] X. Zheng, Y. Shang, and X. Peng, "Orbital stability of solitary waves of the coupled Klein-Gordon-Zakharov equations," *Mathematical Methods in the Applied Sciences*, vol. 40, no. 7, pp. 2623–2633, 2017.
- [14] X. Zheng, Y. Shang, and X. Peng, "Orbital stability of periodic traveling wave solutions to the generalized Zakharov equations," *Acta Mathematica Scientia*, vol. 37, no. 4, pp. 1–21, 2017.
- [15] L. Gao, D. Wang, and G. Wang, "Further results on exponential stability for impulsive switched nonlinear time-delay systems with delayed impulse effects," *Applied Mathematics and Computation*, vol. 268, pp. 186–200, 2015.
- [16] W. W. Sun, "Stabilization analysis of time-delay Hamiltonian systems in the presence of saturation," *Applied Mathematics and Computation*, vol. 217, no. 23, pp. 9625–9634, 2011.
- [17] W. Sun, Y. Wang, and R. Yang, "L2 disturbance attenuation for a class of time delay Hamiltonian systems," *Journal of Systems Science & Complexity*, vol. 24, no. 4, pp. 672–682, 2011.
- [18] Z. Cen, H. Noura, and Y. A. Younes, "Systematic fault tolerant control based on adaptive Thau observer estimation for quadrotor UAVs," *International Journal of Applied Mathematics and Computer Science*, vol. 25, no. 1, pp. 159–174, 2015.
- [19] M. Bonf, P. Castaldi, N. Mimmo et al., "Active fault tolerant control of nonlinear systems: the cart-pole example," *International journal of applied mathematics & computer science*, vol. 21, no. 3, pp. 441–445, 2011.
- [20] M. Z. Gao, G. P. Cai, and N. Ying, "Robust adaptive fault-tolerant  $H_8$  control of re-entry vehicle considering actuator and sensor faults based on trajectory optimization," *International Journal of Control Automation & Systems*, vol. 14, no. 1, pp. 198–210, 2016.
- [21] C. Yang, T. Teng, B. Xu et al., "Global adaptive tracking control of robot manipulators using neural networks with finite-time learning convergence," *International Journal of Control Automation & Systems*, vol. 11, pp. 1–9, 2017.
- [22] Z. Yu, F. Wang, and L. Liu, "An adaptive fault-tolerant robust controller with fault diagnosis for submarine's vertical movement," *International Journal of Control, Automation, and Systems*, vol. 13, no. 6, pp. 1337–1345, 2015.

- [23] L. Li, Y. Yang, S. X. Ding, Y. Zhang, and S. Zhai, "On fault-tolerant control configurations for a class of nonlinear systems," *Journal of The Franklin Institute*, vol. 352, no. 4, pp. 1397–1416, 2015.
- [24] P. Yang, R. Guo, X. Pan et al., "Study on the sliding mode fault tolerant predictive control based on multi agent particle swarm optimization," *International Journal of Control Automation & Systems*, vol. 3, pp. 1–9, 2017.
- [25] J. Yang, F. Zhu, X. Wang, and X. Bu, "Robust sliding-mode observer-based sensor fault estimation, actuator fault detection and isolation for uncertain nonlinear systems," *International Journal of Control, Automation, and Systems*, vol. 13, no. 5, pp. 1037–1046, 2015.
- [26] M. Van, S. S. Ge, and H. Ren, "Finite time fault tolerant control for robot manipulators using time delay estimation and continuous nonsingular fast terminal sliding mode control," *IEEE Transactions on Cybernetics*, 2016.
- [27] Y. Guo, "Nontrivial periodic solutions of nonlinear functional differential systems with feedback control," *Turkish Journal of Mathematics*, vol. 34, no. 1, pp. 35–44, 2010.
- [28] S. Liu, J. Wang, Y. Zhou, and M. Feckan, "Iterative learning control with pulse compensation for fractional differential systems," *Mathematica Slovaca*, vol. 68, no. 3, pp. 563–574, 2018.
- [29] C. Ma, T. Li, and J. Zhang, "Consensus control for leader-following multi-agent systems with measurement noises," *Journal of Systems Science and Complexity*, vol. 23, no. 1, pp. 35–49, 2010.
- [30] G. Wang, "Existence-stability theorems for strong vector set-valued equilibrium problems in reflexive Banach spaces," *Journal of Inequalities and Applications*, vol. 239, pp. 1–14, 2015.
- [31] Y. Guo, "Global stability analysis for a class of Cohen-Grossberg neural network models," *Bulletin of the Korean Mathematical Society*, vol. 49, no. 6, pp. 1193–1198, 2012.
- [32] L. Li, F. Meng, and P. Ju, "Some new integral inequalities and their applications in studying the stability of nonlinear integro-differential equations with time delay," *Journal of Mathematical Analysis and Applications*, vol. 377, no. 2, pp. 853–862, 2011.
- [33] F. Li and Y. Bao, "Uniform stability of the solution for a memory-type elasticity system with nonhomogeneous boundary control condition," *Journal of Dynamical and Control Systems*, vol. 23, no. 2, pp. 301–315, 2017.
- [34] A. Owczarkowski and D. Horla, "Robust LQR and LQI control with actuator failure of a 2DOF unmanned bicycle robot stabilized by an inertial wheel," *International Journal of Applied Mathematics and Computer Science*, vol. 26, no. 2, pp. 325–334, 2016.
- [35] D. Y. Li and L. Y. Chun, "Sensor fault identification and decentralized fault-tolerant control of reconfigurable manipulator based on sliding mode observer," in *Proceedings of the 2012 International Conference on Control Engineering and Communication Technology, ICCECT 2012*, pp. 137–140, China, December 2012.
- [36] A. Ferreira de Loza, J. Cieslak, D. Henry, A. Zolghadri, and L. M. Fridman, "Output tracking of systems subjected to perturbations and a class of actuator faults based on HOSM observation and identification," *Automatica*, vol. 59, pp. 200–205, 2015.
- [37] Y. Feng, X. Yu, and Z. Man, "Non-singular terminal sliding mode control of rigid manipulators," *Automatica*, vol. 38, no. 12, pp. 2159–2167, 2002.
- [38] L. M. Capisani, A. Ferrara, A. Ferreira De Loza, and L. M. Fridman, "Manipulator fault diagnosis via higher order sliding-mode observers," *IEEE Transactions on Industrial Electronics*, vol. 59, no. 10, pp. 3979–3986, 2012.
- [39] A. Yarza, V. Santibanez, and J. Moreno-Valenzuela, "An adaptive output feedback motion tracking controller for robot manipulators: uniform global asymptotic stability and experimentation," *International Journal of Applied Mathematics and Computer Science*, vol. 23, no. 3, pp. 599–611, 2013.
- [40] W. Sun and L. Peng, "Observer-based robust adaptive control for uncertain stochastic Hamiltonian systems with state and input delays," *Lithuanian Association of Nonlinear Analysts. Nonlinear Analysis: Modelling and Control*, vol. 19, no. 4, pp. 626–645, 2014.
- [41] Q. L. Hu, L. Xu, and A. H. Zhang, "Adaptive backstepping trajectory tracking control of robot manipulator," *Journal of The Franklin Institute*, vol. 349, no. 3, pp. 1087–1105, 2012.
- [42] J.-H. Shin and J.-J. Lee, "Fault Detection And Robust Fault Recovery Control for Robot Manipulators with Actuator Failures," in *Proceedings of the 1999 IEEE International Conference on Robotics and Automation, ICRA99*, vol. 2, pp. 861–866, May 1999.
- [43] J. K. Liu, *Sliding Mode Control Design and MATLAB Simulation: The Basic Theory and Design Method*, Tsinghua University Press, 2005.
- [44] S. Mondal and C. Mahanta, "Adaptive second order terminal sliding mode controller for robotic manipulators," *Journal of The Franklin Institute*, vol. 351, no. 4, pp. 2356–2377, 2014.
- [45] A. J. Koshkouei, K. J. Burnham, and A. S. I. Zinober, "Dynamic sliding mode control design," *IEE Proceedings - Control Theory and Applications*, vol. 152, no. 4, pp. 392–396, 2005.

## Research Article

# Finite-Time Stabilization for Stochastic Inertial Neural Networks with Time-Delay via Nonlinear Delay Controller

Deyi Li,<sup>1,2</sup> Yuanyuan Wang,<sup>1,2</sup> Guici Chen ,<sup>1,2</sup> and Shasha Zhu<sup>1,2</sup>

<sup>1</sup>College of Science, Wuhan University of Science and Technology, Wuhan 430065, China

<sup>2</sup>Hubei Province Key Laboratory of System Science in Metallurgical Process, Wuhan University of Science and Technology, Wuhan 430065, China

Correspondence should be addressed to Guici Chen; [gcichen@163.com](mailto:gcichen@163.com)

Received 13 August 2018; Accepted 24 September 2018; Published 9 October 2018

Academic Editor: Xue-Jun Xie

Copyright © 2018 Deyi Li et al. This is an open access article distributed under the Creative Commons Attribution License, which permits unrestricted use, distribution, and reproduction in any medium, provided the original work is properly cited.

This paper pays close attention to the problem of finite-time stabilization related to stochastic inertial neural networks with or without time-delay. By establishing proper Lyapunov-Krasovskii functional and making use of matrix inequalities, some sufficient conditions on finite-time stabilization are obtained and the stochastic settling-time function is also estimated. Furthermore, in order to achieve the finite-time stabilization, both delayed and nondelayed nonlinear feedback controllers are designed, respectively, in terms of solutions to a set of linear matrix inequalities (LMIs). Finally, a numerical example is provided to demonstrate the correction of the theoretical results and the effectiveness of the proposed control design method.

## 1. Introduction

In recent years, more and more scholars have been attracted by neural networks due to their successful applications in associative memory [1, 2], pattern recognition [3], signal processing, optimization problems, and so forth [4]. These applications always rely on the dynamic behaviors of neural networks. Therefore, the investigation of dynamic trajectories is necessary for applied designation of neural networks. Hence, a large number of studies on stability [5–8], stabilization [9, 10], passivity [11], dissipativity [12, 13], synchronization [14, 15], and state estimation [16, 17] for neural networks have been reported.

On the other hand, many researchers have studied Hopfield neural networks [18], cell neural networks, recurrent neural networks [9, 19], Cohen-Grossberg neural networks, bidirectional associative memory neural networks, and Lotka-Volterra neural networks, as well as inertial neural networks [12, 14, 15, 20], which are more intricate than all kinds of prementioned neural networks with the standard resistor-capacitor variety [21]. The inertial term is taken as a critical tool to bring complex bifurcation behavior and chaos.

It has been confirmed that stochastic disturbances, which are unavoidable in actual applications of artificial neural

networks, are probably one of the main sources leading to undesirable behaviors of dynamical systems, especially when a neural network is implemented for applications. Therefore, it is of great significance to study the stability and stabilization problems of neural networks with stochastic disturbances [22–24]. However, to the best of authors' knowledge, most of the researchers have either investigated the stability for stochastic neural networks with time-delay [25–28] or studied the stability for inertial neural networks with time-delay [20]. There are rare literatures that considered the finite-time stabilization for stochastic inertial neural networks with time-delay.

Inspired by the above comprehensive analysis, in this paper, we are devoted to investigating the finite-time stabilization for stochastic inertial neural networks with time-delay. First, by utilizing an appropriate variable substitution, a stochastic inertial neural network can be transformed into a first-order stochastic differential system. Then, some sufficient conditions on finite-time stability in probability are derived by means of establishing an appropriate Lyapunov function and applying inequality techniques. Moreover, the stochastic settling-time function is also given.

## 2. Problem Formulation and Preliminaries

**2.1. Systems Description.** Firstly, the inertial neural networks (INNs) without time-delay are considered, which is described as follows:

$$\begin{aligned} \frac{d^2 x_i(t)}{dt^2} = & -a_i \frac{dx_i(t)}{dt} - b_i x_i(t) + \sum_{j=1}^n c_{ij} f_j(x_j(t)) \\ & + I_i(t), \quad i = 1, 2, \dots, n \end{aligned} \quad (1)$$

where  $x_i(t)$  is the state of the  $i$ -th neuron; the second derivative  $d^2 x_i(t)/dt^2$  is the inertial term of INNs (1).  $a_i > 0$ ,  $b_i > 0$  are constants.  $c_{ij}$  denotes the connection weight between the  $i$ -th neuron and the  $j$ -th neuron.  $f_j(\cdot)$  stands for activation function of the  $j$ -th neuron with  $f_j(0) = 0$  ( $j = 1, 2, \dots, n$ ).  $I_i(t)$  is the external input on the  $i$ -th neuron.

The initial conditions of INNs (1) are

$$\begin{aligned} x_i(0) &= \varphi_i(0), \\ \frac{dx_i(0)}{dt} &= \psi_i(0), \\ i &= 1, 2, \dots, n, \end{aligned} \quad (2)$$

where  $\varphi_i(0)$  and  $\psi_i(0)$  are real-valued continuous functions.

Suppose that the external input  $I_i(t)$  is subject to the environmental noise and is described by  $I_i(t) = u_i(t) + \beta_i(t, x_i(t))\dot{\omega}_i(t)$ , where  $u_i(t)$  is known as the control input and  $\omega_i(t)$  is a one-dimensional white noise, which is also called Brown motion defined on a complete probability space  $(\Omega, \mathcal{F}, P)$  and satisfied with

$$\begin{aligned} \mathbb{E}[\omega_i(t)] &= 0, \\ \mathbb{E}[\omega_i^2(t)] &= dt, \\ \mathbb{E}[\omega_i(t)\omega_j(t)] &= 0 \quad (i \neq j), \end{aligned} \quad (3)$$

and  $\beta_i(t, x_i(t))$  is the intensity function of the noise.

Then INNs (1) can be written the following stochastic inertial neural networks (SINNs):

$$\begin{aligned} \frac{d^2 x_i(t)}{dt^2} = & -a_i \frac{dx_i(t)}{dt} - b_i x_i(t) + \sum_{j=1}^n c_{ij} f_j(x_j(t)) \\ & + u_i(t) + \beta_i(t, x_i(t))\dot{\omega}_i(t). \end{aligned} \quad (4)$$

**2.2. Problems Formulation.** In general, making use of the variable transformation,

$$y_i(t) = \frac{dx_i(t)}{dt} + \xi_i x_i(t), \quad i = 1, 2, \dots, n, \quad (5)$$

then the SINNs (4) can be rewritten as

$$\begin{aligned} dx_i(t) &= [-\xi_i x_i(t) + y_i(t)] dt, \\ dy_i(t) & \end{aligned}$$

$$\begin{aligned} = & \left[ -\tilde{a}_i y_i(t) - \tilde{b}_i x_i(t) + \sum_{j=1}^n c_{ij} f_j(x_j(t)) + u_i(t) \right] dt \\ & + \beta_i(t, x_i(t)) d\omega_i(t), \end{aligned} \quad (6)$$

and the initial conditions are given as

$$\begin{aligned} x_i(0) &= \varphi_i(0), \\ y_i(0) &= -\xi_i(0)\varphi_i(0) + \psi_i(0), \\ i &= 1, 2, \dots, n, \end{aligned} \quad (7)$$

where  $\tilde{a}_i = a_i - \xi_i$ ,  $\tilde{b}_i = b_i + \xi_i(\xi_i - a_i)$ .

Moreover, the controller  $v_i(t)$  is considered; we have the following SINNs:

$$\begin{aligned} dx_i(t) &= [-\xi_i x_i(t) + y_i(t) + v_i(t)] dt, \\ dy_i(t) &= \left[ -\tilde{a}_i y_i(t) - \tilde{b}_i x_i(t) + \sum_{j=1}^n c_{ij} f_j(x_j(t)) + u_i(t) \right] dt \\ & + \beta_i(t, x_i(t)) d\omega_i(t), \\ i &= 1, 2, \dots, n. \end{aligned} \quad (8)$$

Denote

$$\begin{aligned} x(t) &= (x_1(t), x_2(t), \dots, x_n(t))^T, \\ y(t) &= (y_1(t), y_2(t), \dots, y_n(t))^T, \\ \Xi &= \text{diag}\{\xi_1, \xi_2, \dots, \xi_n\}, \\ v(t) &= (v_1(t), v_2(t), \dots, v_n(t))^T, \\ A &= \text{diag}\{\tilde{a}_1, \tilde{a}_2, \dots, \tilde{a}_n\}, \\ B &= \text{diag}\{\tilde{b}_1, \tilde{b}_2, \dots, \tilde{b}_n\}, \\ C &= (c_{ij})_{n \times n}, \\ \beta(t, x(t)) & \end{aligned} \quad (9)$$

$$= (\beta_1(t, x_1(t)), \beta_2(t, x_2(t)), \dots, \beta_n(t, x_n(t)))^T,$$

$$\omega(t) = (\omega_1(t), \omega_2(t), \dots, \omega_n(t)),$$

$$u(t) = (u_1(t), u_2(t), \dots, u_n(t))^T.$$

Thus, the SINNs (8) can be written in vector form as

$$\begin{aligned} dx(t) &= [-\Xi x(t) + y(t) + v(t)] dt, \\ dy(t) &= [-Ay(t) - Bx(t) + Cf(x(t)) + u(t)] dt \\ & + \beta(t, x(t)) d\omega(t). \end{aligned} \quad (10)$$

The control inputs to be designed are of the following form:

$$\begin{aligned} v(t) &= -K_1 x(t) - K_2 \text{sign}(x(t)) |x(t)|^\mu, \\ u(t) &= -K_3 y(t) - K_4 \text{sign}(y(t)) |y(t)|^\mu, \end{aligned} \quad (11)$$

where  $\text{sign}(x(t)) = (\text{sign}(x_1(t)), \text{sign}(x_2(t)), \dots, \text{sign}(x_n(t)))^T$ ,  $\text{sign}(y(t)) = (\text{sign}(y_1(t)), \text{sign}(y_2(t)), \dots, \text{sign}(y_n(t)))^T$ , and  $K_1, K_2, K_3, K_4$  are the control gain matrices to be determined.  $\mu$  is a positive constant with  $0 < \mu < 1$ .

*Remark 1.* There are three cases for the value of  $\mu$ . If  $0 < \mu < 1$ , the controllers  $u(t), v(t)$  are continuous functions with respect to  $x$  and  $y$ , respectively, which bring about the continuity of SINNs (10) with respect to the systems state [29, 30], but the local Lipschitz condition is dissatisfied. If  $\mu = 0$ ,  $u(t), v(t)$  turn to be discontinuous ones, which have been studied in [31, 32]. If  $\mu = 1$ , then they become the typical stabilization issues which only can realize an asymptotical stabilization in infinite time [33, 34] due to the local Lipschitz conditions.

*Remark 2.* In fact, the control gain matrices  $K_1, K_2, K_3, K_4$  in the controllers  $v(t)$  and  $u(t)$  play different roles in ensuring the finite-time stability of the SINNs (10) with (11), where  $K_1$  and  $K_3$  are used to guarantee the Lyapunov stability of the SINNs (10). And the convergence to zero of the SINNs (10) is determined by  $K_2$  and  $K_4$ .

To achieve our main results, some assumptions, lemmas, and definitions are necessary to introduce firstly.

*Assumption 3.* The nonlinear activation function  $f$  satisfies  $f(0) = 0$ , and there exist some constants  $m_{1i}^-, m_{1i}^+ (i = 1, 2, \dots, n)$ , such that

$$M_1^- \leq \frac{f(x_1) - f(x_2)}{x_1 - x_2} \leq M_1^+ \quad (12)$$

hold for all  $x_1, x_2 \in \mathbb{R}$  and  $x_1 \neq x_2$ , where  $M_1^- = \text{diag}\{m_{11}^-, m_{12}^-, \dots, m_{1n}^-\}$ ,  $M_1^+ = \text{diag}\{m_{11}^+, m_{12}^+, \dots, m_{1n}^+\}$ .

*Remark 4.* If we choose  $m_{1i} = \max\{|m_{1i}^-|, |m_{1i}^+|\}$ , the inequalities in Assumption 3 can be written as

$$\left| \frac{f(x_1) - f(x_2)}{x_1 - x_2} \right| \leq M_1, \quad (13)$$

where  $M_1 = \text{diag}\{m_{11}, m_{12}, \dots, m_{1n}\}$ , which has been considered.

*Assumption 5.* The intensity function  $\beta(t, x(t))$  is a continuous function and is supposed to satisfy that

$$\text{trace} [\beta^T(t, x(t)) \beta(t, x(t))] \leq x^T(t) M_2^T M_2 x(t), \quad (14)$$

where  $M_2$  is a known matrix with appropriate dimensions.

*Definition 6.* The SINNs (10) are said to be finite-time stabilizable by the controller (11); that is, the SINNs (10) are

finite-time stable if, for any initial state  $x(0), y(0)$ , there exists a finite-time function  $T_0$  such that

$$\mathbb{E} \|x(t)\| = \mathbb{E} \|y(t)\| = 0, \quad \forall t \geq T_0, \quad (15)$$

where  $T_0 = T_0(x(0), y(0), \omega) = \inf\{T \geq 0 : x(t) = y(t) = 0, \forall t \geq T\}$  is called the stochastic settling time function satisfying  $E[T_0] < \infty$ .

**Lemma 7** (see [35]). *Suppose that SINNs (10) admit a unique solution. If there exist a  $C^2$  function  $V: \mathbb{R}^n \rightarrow \mathbb{R}_+$ ,  $\mathcal{K}_\infty$  class functions  $\mu_1$  and  $\mu_2$ , and positive real constant  $\eta > 0$  and  $0 < \gamma < 1$ , such that for all  $x \in \mathbb{R}^n$  and  $t \geq 0$ ,*

$$\begin{aligned} \mu_1(|x|) &\leq V(x) \leq \mu_2(|x|), \\ \mathcal{L}V(x) &\leq -\eta(V(x))^\gamma, \end{aligned} \quad (16)$$

*then the origin of SINNs (10) are stochastically finite-time stable, and  $\mathbb{E}[T_0] < \mathbb{E}(V(x_0))^{1-\gamma}/\eta(1-\gamma)$ .*

**Lemma 8** (see [9]). *If  $a_1, a_2, \dots, a_n$  are positive number and  $0 < r < p$ , then*

$$\left( \sum_{i=1}^n a_i^p \right)^{1/p} \leq \left( \sum_{i=1}^n a_i^r \right)^{1/r}. \quad (17)$$

### 3. Main Results

#### 3.1. Finite-Time Stabilization Feedback Controller Design without Time-Delay

**Theorem 9.** *The controlled systems (10) with (11) are finite-time stable, if there exist some positive-definite matrices  $P_1, P_2, M_3 \in \mathbb{R}^{n \times n}$  and some known constant matrices  $M_1, M_2$  with compatible dimensions, such that*

$$\begin{pmatrix} \Theta_{11} & \Theta_{12} \\ * & \Theta_{22} \end{pmatrix} < 0, \quad (18)$$

*Moreover, the upper bound of the stochastic settling time for stabilization can be estimated as  $\mathbb{E}\{T_0\} \leq (\lambda_2(E\|x(0)\|^{1-\mu} + E\|y(0)\|^{1-\mu}))/\lambda_1(1-\mu)$ , where*

$$\begin{aligned} \Theta_{11} &= -P_1 \Xi - \Xi^T P_1 - P_1 K_1 - K_1^T P_1 + M_1^T M_3^{-1} M_1 \\ &\quad + M_2^T P_2 M_2, \\ \Theta_{12} &= P_1 - B^T P_2, \\ \Theta_{22} &= -P_2 A - A^T P_2 - P_2 K_3 - K_3^T P_2 + P_2 C M_3 C^T P_2, \\ \lambda_1 &= \min\{\lambda_{\min}(P_1 K_2), \lambda_{\min}(P_2 K_4)\}, \\ \lambda_2 &= \max\{\lambda_{\max}(P_1), \lambda_{\max}(P_2)\}. \end{aligned} \quad (19)$$

*Proof.* Taking controller (11) into SINNs (10), it follows that

$$\begin{aligned} dx(t) &= [-(\Xi + K_1)x(t) + y(t) \\ &\quad - K_2 \text{sign}|x(t)|^\mu] dt, \\ dy(t) &= [-(A + K_3)y(t) - Bx(t) + Cf(x(t)) \\ &\quad - K_4 \text{sign}(y(t))|y(t)|^\mu] dt + \beta(t, x(t)) d\omega(t). \end{aligned} \quad (20)$$

Next, we will prove that system (20) is finite-time stable in the sense of Definition 6.

Construct a Lyapunov function as

$$V(t) = x^T(t)P_1x(t) + y^T(t)P_2y(t), \quad (21)$$

where  $P_1$  and  $P_2$  are positive definite matrices. Then, calculate the time derivative of  $V(t)$  along the trajectories of systems (20); we get

$$dV(t) = \mathcal{L}V(t) dt + 2y^T(t)P_2\beta(t, x(t)) d\omega(t), \quad (22)$$

where

$$\begin{aligned} \mathcal{L}V(t) &= 2x^T(t)P_1[-(\Xi + K_1)x(t) + y(t) \\ &\quad - K_2 \text{sign}(x(t))|x(t)|^\mu] + 2y^T(t) \\ &\quad \cdot P_2[-(A + K_3)y(t) - Bx(t) + Cf(x(t)) \\ &\quad - K_4 \text{sign}(y(t))|y(t)|^\mu] \\ &\quad + \text{trace}[\beta^T(t, x(t))P_2\beta(t, x(t))] = -2x^T(t)P_1(\Xi \\ &\quad + K_1)x(t) + 2x^T(t)P_1y(t) - 2y^T(t)P_2Bx(t) \\ &\quad - 2x^T(t)P_1K_2 \text{sign}(x(t))|x(t)|^\mu - 2y^T(t)P_2K_4 \\ &\quad \cdot \text{sign}(y(t))|y(t)|^\mu - 2y^T(t)P_2(A + K_3)y(t) \\ &\quad + 2Y^TP_2Cf(x(t)) \\ &\quad + \text{trace}[\beta^T(t, x(t))P_2\beta(t, x(t))]. \end{aligned} \quad (23)$$

From (13), we have

$$\begin{aligned} 2y^T(t)P_2Cf(x(t)) &= y^T(t)P_2Cf(x(t)) \\ &\quad + f^T(x(t))C^TP_2y(t) \\ &\leq y^T(t)P_2CM_3C^TP_2y(t) \\ &\quad + f^T(x(t))M_3^{-1}f(x(t)) \\ &\leq y^T(t)P_2CM_3C^TP_2y(t) \\ &\quad + x^T(t)M_1^TM_3^{-1}M_1x(t). \end{aligned} \quad (24)$$

From (14), we have

$$\begin{aligned} \text{trace}[\beta^T(t, x(t))P_2\beta(t, x(t))] \\ \leq x^T(t)M_2^TP_2M_2x(t). \end{aligned} \quad (25)$$

Combining (23)-(25) and condition (18), one can follow that

$$\begin{aligned} \mathcal{L}V(t) &\leq x^T(t) \\ &\quad \cdot [-2P_1(\Xi + K_1) + M_1^TM_3^{-1}M_1 + M_2^TP_2M_2]x(t) \\ &\quad + 2x^T(t)[P_1 - B^TP_2]y(t) + y^T(t) \\ &\quad \cdot [-2P_2(A + K_3) + P_2CM_3C^TP_2]y(t) - 2x^T(t) \\ &\quad \cdot P_1K_2 \text{sign}(x(t))|x(t)|^\mu - 2y^T(t)P_2K_4 \\ &\quad \cdot \text{sign}(y(t))|y(t)|^\mu \\ &\leq (x^T(t) \ y^T(t)) \begin{pmatrix} \Theta_{11} & \Theta_{12} \\ * & \Theta_{22} \end{pmatrix} \begin{pmatrix} x(t) \\ y(t) \end{pmatrix} - 2x^T(t) \\ &\quad \cdot P_1K_2 \text{sign}(x(t))|x(t)|^\mu - 2y^T(t)P_2K_4 \\ &\quad \cdot \text{sign}(y(t))|y(t)|^\mu \leq -2x^T(t)P_1K_2 \text{sign}(x(t)) \\ &\quad \cdot |x(t)|^\mu - 2y^T(t)P_2K_4 \text{sign}(y(t))|y(t)|^\mu \\ &\leq -\lambda_{\min}(P_1K_2 + K_2^TP_1) \sum_{i=1}^n |x_i(t)|^{\mu+1} \\ &\quad - \lambda_{\min}(P_2K_4 + K_4^TP_2) \sum_{i=1}^n |y_i(t)|^{\mu+1}. \end{aligned} \quad (26)$$

Due to  $0 < \mu < 1$ , together with Lemma 8, one has

$$\left( \sum_{i=1}^n |x_i(t)|^{\mu+1} \right)^{1/(\mu+1)} \geq \left( \sum_{i=1}^n |x_i(t)|^2 \right)^{1/2}, \quad (27)$$

and then

$$\begin{aligned} \sum_{i=1}^n |x_i(t)|^{\mu+1} &\geq \left( \sum_{i=1}^n |x_i(t)|^2 \right)^{(\mu+1)/2} \\ &= [x^T(t)x(t)]^{(\mu+1)/2}. \end{aligned} \quad (28)$$

Similarly, we have

$$\begin{aligned} \sum_{i=1}^n |y_i(t)|^{\mu+1} &\geq \left( \sum_{i=1}^n |y_i(t)|^2 \right)^{(\mu+1)/2} \\ &= [y^T(t)y(t)]^{(\mu+1)/2}. \end{aligned} \quad (29)$$

So, we have

$$\begin{aligned} \mathcal{L}V(t) \\ \leq -\lambda_{\min}(P_1K_2 + K_2^TP_1) [x^T(t)x(t)]^{(\mu+1)/2} \\ - \lambda_{\min}(P_2K_4 + K_4^TP_2) [y^T(t)y(t)]^{(\mu+1)/2}. \end{aligned} \quad (30)$$

Now, taking the expectations on both sides of (22), and letting  $\lambda_1 = \min\{\lambda_{\min}(P_1K_2), \lambda_{\min}(P_2K_4)\}$ ,  $\lambda_2 = \max\{\lambda_{\max}(P_1), \lambda_{\max}(P_2)\}$ , we can get

$$\begin{aligned} & \mathbb{E}\{dV(t)\} \\ & \leq -2\lambda_1 \mathbb{E}\left\{\left[x^T(t)x(t)\right]^{(\mu+1)/2} + \left[y^T(t)y(t)\right]^{(\mu+1)/2}\right\} \\ & \leq -2\lambda_1 \lambda_2^{-(\mu+1)/2} \mathbb{E}\{V(t)^{(\mu+1)/2}\}, \\ & \mathbb{E}\{V^{(\mu+1)/2}(0)\} = (\mathbb{E}\{V(0)\})^{(\mu+1)/2}. \end{aligned} \quad (31)$$

From Lemma 7, we get that the controlled systems (20) are finite-time stable, and the upper bounded stochastic settling time can be estimated by

$$\begin{aligned} \mathbb{E}\{T_0\} &= \frac{\lambda_2^{(\mu+1)/2} \mathbb{E}[V(0)]^{(1-\mu)/2}}{2\lambda_1((1-\mu)/2)} \\ &\leq \frac{\lambda_2^{(\mu+1)/2} \lambda_2^{(1-\mu)/2} (\mathbb{E}\|x(0)\|_2^{1-\mu} + \mathbb{E}\|y(0)\|_2^{1-\mu})}{\lambda_1(1-\mu)} \\ &= \frac{\lambda_2 (\mathbb{E}\|x(0)\|_2^{1-\mu} + \mathbb{E}\|y(0)\|_2^{1-\mu})}{\lambda_1(1-\mu)}. \end{aligned} \quad (32)$$

This completes the proof.  $\square$

Summing up the above analysis, some sufficient conditions on finite-time stability for the SINNs (10) with (11) are obtained. In the following, we mainly focus on the design of finite-time stabilizing controllers by transforming the sufficient conditions into solvable linear matrix inequalities.

**Theorem 10.** *If there exist some positive definite matrices  $X_1, X_2, M_3$ , matrices  $Y_1, Y_2$  with appropriate dimensions, for fixed control gain matrices  $K_2$  and  $K_4$ , such that*

$$\begin{pmatrix} \Phi_{11} & \Phi_{12} & X_1 M_1^T & X_1 M_2^T & 0 \\ * & \Phi_{22} & 0 & 0 & CM_3 \\ * & * & -M_3 & 0 & 0 \\ * & * & * & -X_2 & 0 \\ * & * & * & * & -M_3 \end{pmatrix} < 0, \quad (33)$$

where

$$\begin{aligned} \Phi_{11} &= -\Xi X_1 - X_1 \Xi^T - Y_1 - Y_1^T, \\ \Phi_{12} &= X_2 - X_1 B^T, \\ \Phi_{22} &= -AX_2 - X_2 A^T - Y_2 - Y_2^T, \end{aligned} \quad (34)$$

then the finite-time stabilization problem is solvable for the stochastic inertial neural networks (4) and the control gain matrices  $K_1 = Y_1 X_1^{-1}$ ,  $K_3 = Y_2 X_2^{-1}$ .

*Proof.* Setting  $P_1^{-1} = X_1$ ,  $P_2^{-1} = X_2$ ,  $K_1 X_1 = Y_1$ ,  $K_3 X_2 = Y_2$ , (18) can be written as

$$\begin{pmatrix} \Theta_{111} & \Theta_{112} \\ * & \Theta_{122} \end{pmatrix} < 0, \quad (35)$$

where

$$\begin{aligned} \Theta_{111} &= -X_1^{-1} \Xi - \Xi^T X_1^{-1} - X_1^{-1} K_1 - K_1^T X_1^{-1} \\ &\quad + M_1^T M_3^{-1} M_1 + M_2^T X_2^{-1} M_2, \\ \Theta_{112} &= X_1^{-1} - B^T X_2^{-1}, \\ \Theta_{122} &= -X_2^{-1} A - A^T X_2^{-1} - X_2^{-1} K_3 - K_3^T X_2^{-1} \\ &\quad + X_2^{-1} C M_3 C^T X_2^{-1}. \end{aligned} \quad (36)$$

Then, left- and right-multiplying inequality (35) by the block-diagonal matrix  $\text{diag}\{X_1, I\}$ , which follows

$$\begin{pmatrix} X_1 & 0 \\ 0 & I \end{pmatrix} \begin{pmatrix} \Theta_{111} & \Theta_{112} \\ * & \Theta_{122} \end{pmatrix} \begin{pmatrix} X_1 & 0 \\ 0 & I \end{pmatrix} = \begin{pmatrix} \Theta_{211} & \Theta_{212} \\ * & \Theta_{222} \end{pmatrix} < 0, \quad (37)$$

where

$$\begin{aligned} \Theta_{211} &= -\Xi X_1 - X_1 \Xi^T - K_1 X_1 - X_1 K_1^T \\ &\quad + X_1 M_1^T M_3^{-1} M_1 X_1 + X_1 M_2^T X_2^{-1} M_2 X_1, \\ \Theta_{212} &= I - X_1 B^T X_2^{-1}, \\ \Theta_{222} &= -X_2^{-1} A - A^T X_2^{-1} - X_2^{-1} K_3 - K_3^T X_2^{-1} \\ &\quad + X_2^{-1} C M_3 C^T X_2^{-1}, \end{aligned} \quad (38)$$

and left- and right-multiplying inequality (37) by the block-diagonal matrix  $\text{diag}\{I, X_1\}$ , we can obtain

$$\begin{pmatrix} I & 0 \\ 0 & X_1 \end{pmatrix} \begin{pmatrix} \Theta_{211} & \Theta_{212} \\ * & \Theta_{222} \end{pmatrix} \begin{pmatrix} I & 0 \\ 0 & X_1 \end{pmatrix} = \begin{pmatrix} \Theta_{311} & \Theta_{312} \\ * & \Theta_{322} \end{pmatrix} < 0, \quad (39)$$

where

$$\begin{aligned} \Theta_{311} &= -\Xi X_1 - X_1 \Xi^T - K_1 X_1 - X_1 K_1^T \\ &\quad + X_1 M_1^T M_3^{-1} M_1 X_1 + X_1 M_2^T X_2^{-1} M_2 X_1, \\ \Theta_{312} &= X_2 - X_1 B^T, \\ \Theta_{322} &= -AX_2 - X_2 A^T - K_3 X_2 - X_2 K_3^T + CM_3 C^T, \end{aligned} \quad (40)$$

By Schur complement, (33) implies the above inequality (39) holds. This completes the proof.  $\square$

**3.2. Finite-Time Stabilization Feedback Controller Design with Time-Delay.** In the above section, we discussed the finite-time stabilization for stochastic inertial neural networks without time-delay. However, when designing a neural network or implementing it, the occurrence of time-delay is unavoidable. It may cause instability and oscillation [36–38]. Therefore, in order to reduce the conservatism, in this section, we will study the finite-time stabilization for stochastic inertial neural networks with time-delay.

Consider the following SINNs with time-delay,

$$\begin{aligned} \frac{d^2 x_i(t)}{dt^2} &= -a_i \frac{dx_i(t)}{dt} - b_i x_i(t) \\ &+ \sum_{j=1}^n c_{ij} f_j(x_j(t)) + \sum_{j=1}^n c_{ij} f_j(x_j(t)) \\ &+ \sum_{j=1}^n d_{ij} f_j(x_j(t-h_j(t))) + u_i(t) \\ &+ \beta_i(t, x_i(t)) \dot{w}_i(t), \end{aligned} \quad (41)$$

where  $h_j(t)$  is the time-varying delay of  $j$ -th neuron with  $0 \leq h_j(t) \leq h$ .

Denote

$$\begin{aligned} D &= (d_{ij})_{n \times n}, \\ h(t) &= (h_1(t), h_2(t), \dots, h_n(t))^T. \end{aligned} \quad (42)$$

Then we have

$$\begin{aligned} dx(t) &= [-\Xi x(t) + y(t) + v(t)] dt, \\ dy(t) &= [-Ay(t) - Bx(t) + Cf(x(t)) \\ &+ Df(x(t-h(t))) + u(t)] dt \\ &+ \beta(t, x(t)) dw(t). \end{aligned} \quad (43)$$

The nonlinear delay-feedback controller is designed as the following form:

$$\begin{aligned} v(t) &= -K_1 x(t) - K_2 \text{sign}(x(t)) |x(t)|^\mu, \\ u(t) &= -K_3 y(t) - K_4 \text{sign}(y(t)) |y(t)|^\mu \\ &- DM_1 \text{sign}(x(t)) |x(t-h(t))|, \end{aligned} \quad (44)$$

where  $K_1, K_2, K_3, K_4$  are gain matrices to be determined, and  $M_1 = \text{diag}\{m_{11}, m_{12}, \dots, m_{1n}\}$ ,  $m_{1i} = \max\{|m_{1i}^-|, |m_{1i}^+|\}$ .

**Theorem 11.** *The SINNs with time-delay (43) with (44) are finite-time stable, if there exist some positive-definite matrices  $P_1, P_2 \in \mathbb{R}^{n \times n}$  such that*

$$\begin{pmatrix} \Theta_{11} & \Theta_{12} \\ * & \Theta_{22} \end{pmatrix} < 0, \quad (45)$$

where

$$\begin{aligned} \Theta_{11} &= -P_1 \Xi - \Xi^T P_1 - P_1 K_1 - K_1^T P_1 + M_1^T M_3^{-1} M_1 \\ &+ M_2^T P_2 M_2, \\ \Theta_{12} &= P_1 - B^T P_2, \end{aligned} \quad (46)$$

$$\Theta_{22} = -P_2 A - A^T P_2 - P_2 K_3 - K_3^T P_2 + P_2 C M_3 C^T P_2.$$

Moreover, the upper bound of the stochastic setting time for stabilization can be estimated as  $\mathbb{E}\{T_0\} \leq (\lambda_2(\mathbb{E}\{\|x(0)\|\}^{1-\mu} + \mathbb{E}\{\|y(0)\|\}^{1-\mu}))/\lambda_1(1-\mu)$  with  $\lambda_1 = \min\{\lambda_{\min}(P_1 K_2), \lambda_{\min}(P_2 K_4)\}$  and  $\lambda_2 = \max\{\lambda_{\max}(P_1), \lambda_{\max}(P_2)\}$ .

*Proof.* Construct a Lyapunov function:

$$V(t) = x^T(t) P_1 x(t) + y^T(t) P_2 y(t). \quad (47)$$

Calculating the Itô differential of  $V(t)$  along with (43), we can obtain

$$\begin{aligned} \mathcal{L}V(t) &= 2x^T(t) P_1 [- (\Xi + K_1) x(t) + y(t) \\ &- K_2 \text{sign}(x(t)) |x(t)|^\mu] + 2y^T(t) \\ &\cdot P_2 [- (A + K_3) y(t) - Bx(t) + Cf(x(t)) \\ &- K_4 \text{sign}(y(t)) |y(t)|^\mu] \\ &+ \text{trace} [\beta^T(t, x(t)) P_2 \beta(t, x(t))] = -2x^T(t) \\ &\cdot P_1 (\Xi + K_1) x(t) + 2x^T(t) P_1 y(t) - 2y^T(t) \\ &\cdot P_2 Bx(t) - 2x^T(t) P_1 K_2 \text{sign}(x(t)) |x(t)|^\mu \\ &- 2y^T(t) P_2 K_4 \text{sign}(y(t)) |y(t)|^\mu - 2y^T(t) P_2 (A \\ &+ K_3) y(t) + 2Y^T P_2 Cf(x(t)) + 2y^T P_2 D \\ &\times [|f(x(t-h(t)))| \\ &- M_1 \text{sign}(x(t)) |x(t-h(t))|] \\ &+ \text{trace} [\beta^T(t, x(t)) P_2 \beta(t, x(t))] \leq -2x^T(t) \\ &\cdot P_1 (\Xi + K_1) x(t) + 2x^T(t) P_1 y(t) - 2y^T(t) \\ &\cdot P_2 Bx(t) - 2x^T(t) P_1 K_2 \text{sign}(x(t)) |x(t)|^\mu \\ &- 2y^T(t) P_2 K_4 \text{sign}(y(t)) |y(t)|^\mu - 2y^T(t) P_2 (A \\ &+ K_3) y(t) + 2Y^T P_2 Cf(x(t)) \\ &+ \text{trace} [\beta^T(t, x(t)) P_2 \beta(t, x(t))]. \end{aligned} \quad (48)$$

We can see that the right of inequality (48) equals (23). Hence, the rest of the proof is the same as that of Theorem 9 and it is omitted here.  $\square$

Similar to the proof of Theorem 10, we have the following result.

**Theorem 12.** *If there exist some positive definite matrices  $X_1, X_2$ , matrices  $Y_1, Y_2$  with appropriate dimensions, for fixed control gain matrices  $K_2$  and  $K_4$ , such that*

$$\begin{pmatrix} \Phi_{11} & \Phi_{12} & X_1 M_1^T & X_1 M_2^T & 0 \\ * & \Phi_{22} & 0 & 0 & C M_3 \\ * & * & -M_3 & 0 & 0 \\ * & * & * & -X_2 & 0 \\ * & * & * & * & -M_3 \end{pmatrix} < 0, \quad (49)$$

where

$$\begin{aligned}\Phi_{11} &= -\Xi X_1 - X_1 \Xi^T - Y_1 - Y_1^T, \\ \Phi_{12} &= X_2 - X_1 B^T, \\ \Phi_{22} &= -A X_2 - X_2 A^T - Y_2 - Y_2^T,\end{aligned}\quad (50)$$

then the finite-time stabilization problem is solvable for the stochastic inertial neural networks (41) and the control gain matrices  $K_1 = Y_1 X_1^{-1}$ ,  $K_3 = Y_2 X_2^{-1}$ .

#### 4. Illustrative Example

Consider the following stochastic inertial neural networks with time-delay:

$$\begin{aligned}\frac{d^2 x_i(t)}{dt^2} &= -a_i \frac{dx_i(t)}{dt} - b_i x_i(t) + \sum_{j=1}^n c_{ij} f_j(x_j(t)) \\ &+ \sum_{j=1}^n c_{ij} f_j(x_j(t)) \\ &+ \sum_{j=1}^n d_{ij} f_j(x_j(t - h_j(t))) \\ &+ \beta_i(t, x_i(t)) \dot{\omega}_i(t),\end{aligned}\quad (51)$$

which are equivalent to the following vector form:

$$\begin{aligned}dx(t) &= [-\Xi x(t) + y(t) + v(t)] dt, \\ dy(t) &= [-A y(t) - B x(t) + C f(x(t)) \\ &+ D f(x(t - h(t))) + u(t)] dt \\ &+ \beta(t, x(t)) d\omega(t),\end{aligned}\quad (52)$$

where

$$\begin{aligned}\Xi &= \begin{pmatrix} 1 & 0 \\ 0 & 3 \end{pmatrix}, \\ A &= \begin{pmatrix} 2 & 0 \\ 0 & 3 \end{pmatrix}, \\ B &= \begin{pmatrix} 4 & 0 \\ 0 & 6 \end{pmatrix}, \\ C &= \begin{pmatrix} 2 & -5 \\ -1 & -3 \end{pmatrix}, \\ D &= \begin{pmatrix} 1 & -1 \\ -1 & -2 \end{pmatrix}, \\ \beta(t, x(t)) &= \begin{pmatrix} \sin(x_1 + x_2) & 0 \\ 0 & 2 \cos 2(x_1 - x_2) \end{pmatrix}, \\ f(x(t)) &= \begin{pmatrix} \tanh(x_1) \\ \tanh(x_2) \end{pmatrix}, \\ h(t) &= \begin{pmatrix} 0.25 \sin(t) + 0.75 \\ 0.25 \sin(t) + 0.75 \end{pmatrix},\end{aligned}$$

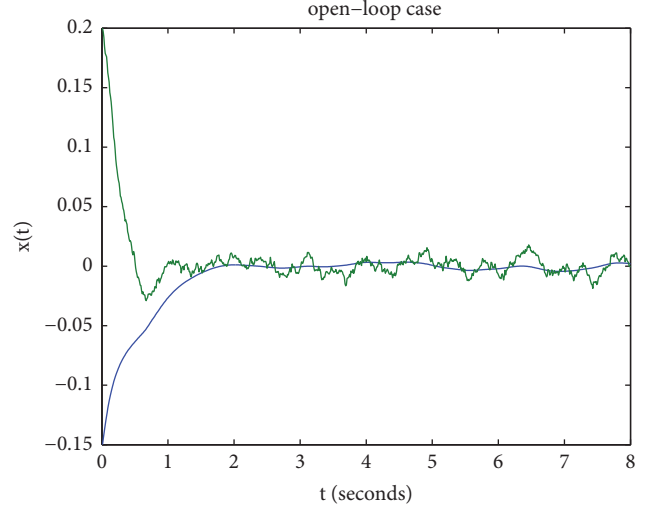


FIGURE 1: The state trajectories for open-loop SINNs (52) with initial condition  $x(0) = (-0.15, 0.2)^T$ ,  $y(0) = (0.3, 0.3)^T$ .

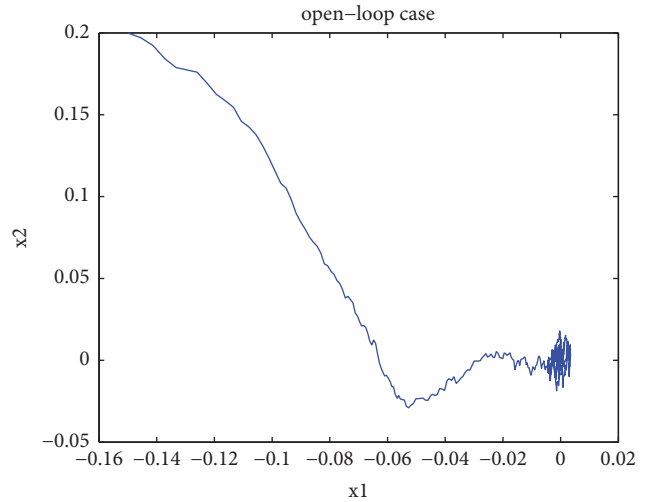


FIGURE 2: The phrase trajectories for open-loop SINNs (52) with initial condition  $x(0) = (-0.15, 0.2)^T$ ,  $y(0) = (0.3, 0.3)^T$ .

$$\begin{aligned}M_1 &= \begin{pmatrix} 1 & 0 \\ 0 & 1 \end{pmatrix}, \\ M_2 &= \begin{pmatrix} 1 & 1 \\ 2 & -2 \end{pmatrix}.\end{aligned}\quad (53)$$

Setting the initial values  $x(0) = (-0.15, 0.2)^T$ ,  $y(0) = (0.3, 0.3)^T$ , the state trajectories and phrase trajectories of the open-loop system are shown in Figures 1 and 2, respectively. Moreover, take 10 sets of numbers randomly as the initial values of  $x(0)$  and  $y(0)$  and satisfy  $x(0) \in (-1, 1)$ ,  $y(0) \in (-3, 3)$ . Then the corresponding state trajectories and phrase trajectories of the open-loop system are shown in Figures 3 and 4, respectively. Obviously, the stochastic inertial neural networks with time-delay (51) are not finite-time stabilization.

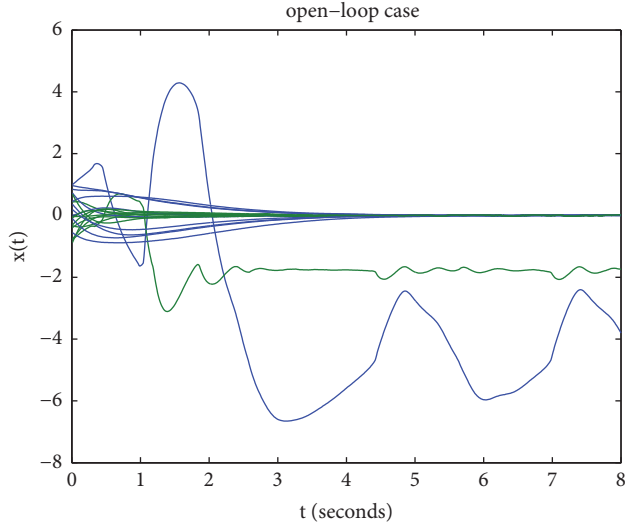


FIGURE 3: The state trajectories for open-loop SINNs (52) with 10 different initial conditions  $x(0) \in (-1, 1)$ ,  $y(0) \in (-3, 3)$ .

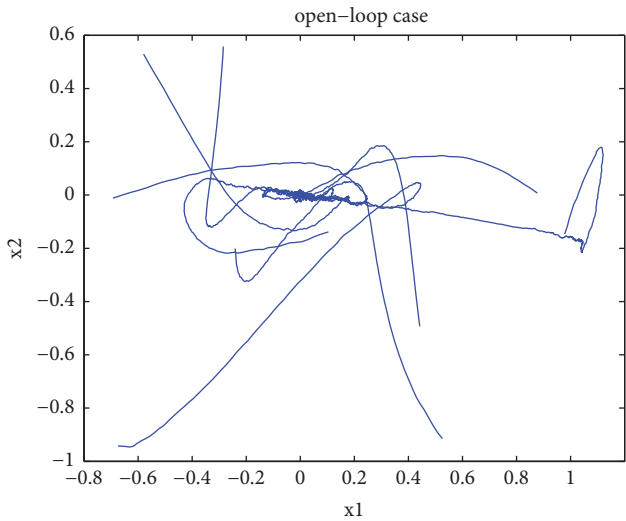


FIGURE 4: The phrase trajectories for open-loop SINNs (52) with 10 different initial conditions  $x(0) \in (-1, 1)$ ,  $y(0) \in (-3, 3)$ .

Hence, we need to design the delay-feedback controller as (44) for system (51), where the parameter  $\mu$  is chosen as 0.6, and the initial values  $x(0) = (-1, 1)^T$ ,  $y(0) = (3, -3)^T$ ,  $K_2 = \begin{pmatrix} 5 & 2 \\ 2 & 1 \end{pmatrix}$ ,  $K_4 = \begin{pmatrix} 3 & 2 \\ 2 & 4 \end{pmatrix}$ . The solution of (49) is derived by resorting to Matlab LMI Control Toolbox:

$$X_1 = \begin{pmatrix} 0.0793 & 0.0242 \\ 0.0242 & 0.0712 \end{pmatrix},$$

$$X_2 = \begin{pmatrix} 0.5705 & 0.0492 \\ 0.0492 & 0.6263 \end{pmatrix},$$

$$M_3 = \begin{pmatrix} 0.2766 & 0.0585 \\ 0.0585 & 0.0399 \end{pmatrix},$$

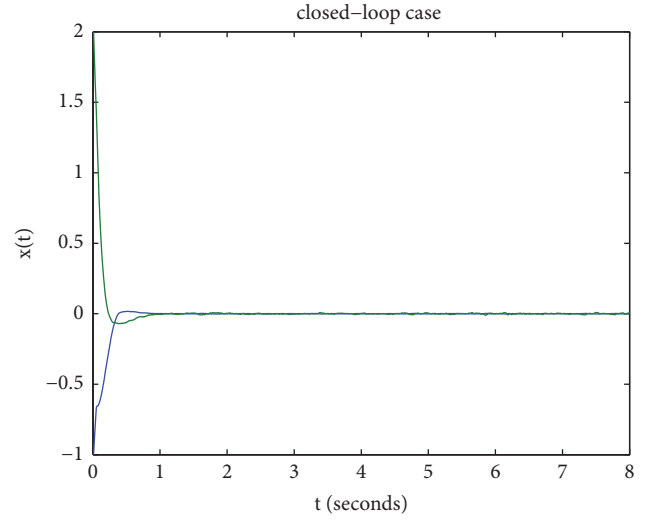


FIGURE 5: The state trajectories for closed-loop SINNs (52) with initial condition  $x(0) = (-1, 1)^T$ ,  $y(0) = (-3, 3)^T$ .

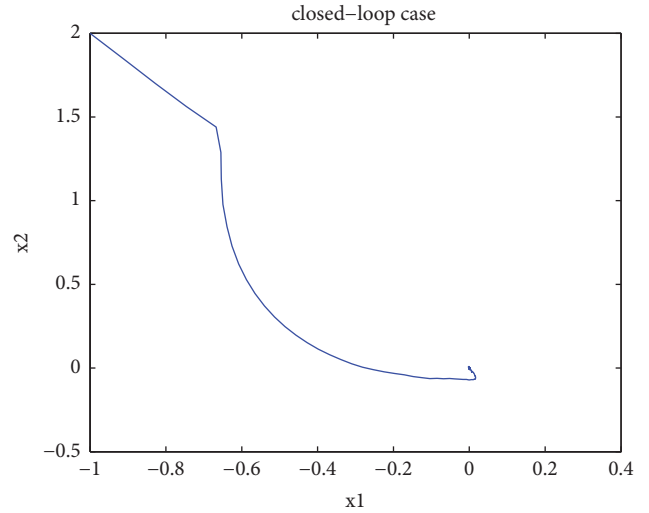


FIGURE 6: The phrase trajectories for closed-loop SINNs (52) with initial condition  $x(0) = (-1, 1)^T$ ,  $y(0) = (-3, 3)^T$ .

$$Y_1 = \begin{pmatrix} 0.3609 & -9.9199 \\ 9.8791 & 0.2501 \end{pmatrix},$$

$$Y_2 = \begin{pmatrix} -0.5432 & -5.9469 \\ 5.4102 & -1.0974 \end{pmatrix},$$

$$K_1 = \begin{pmatrix} 52.5297 & 152.1518 \\ 137.7642 & -43.3383 \end{pmatrix},$$

$$K_3 = \begin{pmatrix} -0.1341 & -9.4851 \\ 9.6993 & -2.5141 \end{pmatrix}.$$

(54)

We can get  $P_1 = \begin{pmatrix} 14.0697 & -4.7821 \\ -4.7821 & 15.6703 \end{pmatrix}$ ,  $P_2 = \begin{pmatrix} 1.7648 & -0.1386 \\ -0.1386 & 1.6076 \end{pmatrix}$ ,  $T_0 \leq 3.2211$ . The state trajectories and phrase trajectories of close-loop system are shown in Figures 5 and 6, respectively.

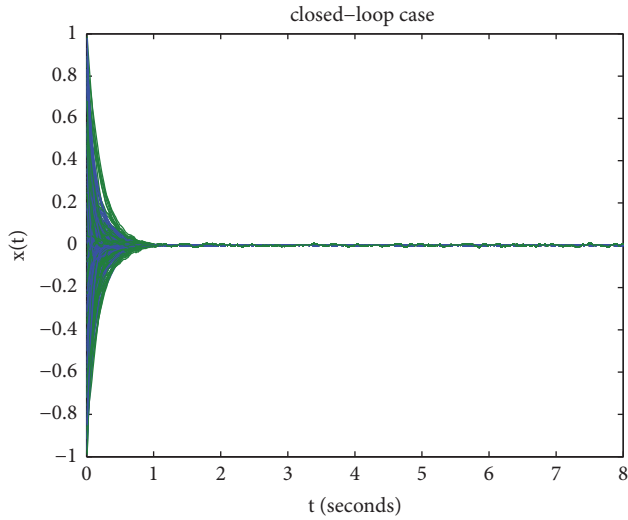


FIGURE 7: The state trajectories for closed-loop SINNs (52) with 100 different initial conditions  $x(0) \in (-1, 1)$ ,  $y(0) \in (-3, 3)$ .

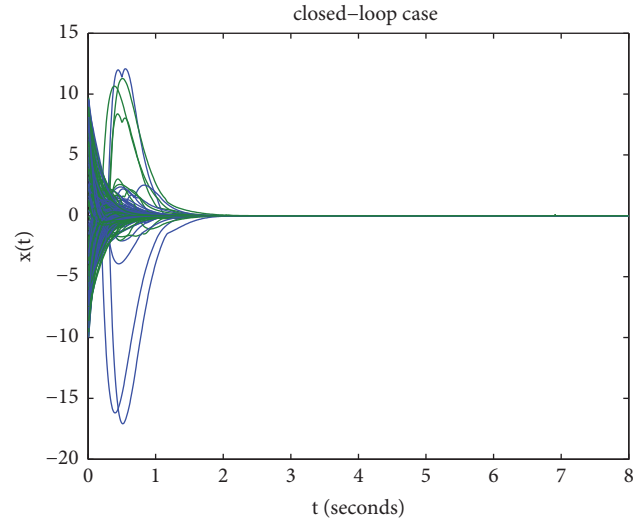


FIGURE 9: The state trajectories for closed-loop SINNs (52) with 100 different initial conditions  $x(0) \in (-10, 10)$ ,  $y(0) \in (-30, 30)$ .

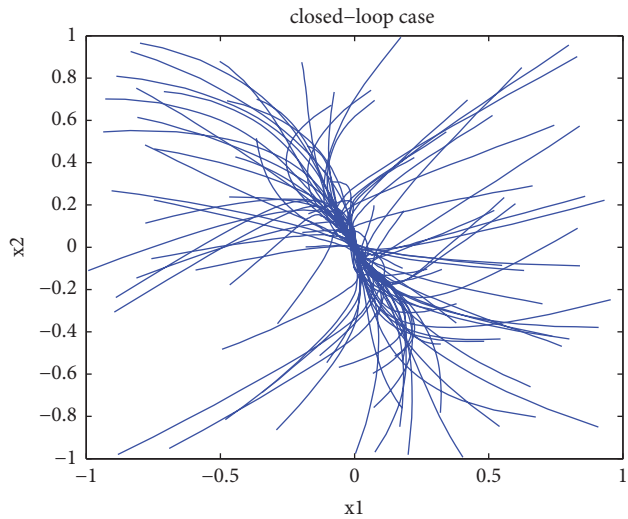


FIGURE 8: The phase trajectories for closed-loop SINNs (52) with 100 different initial conditions  $x(0) \in (-1, 1)$ ,  $y(0) \in (-3, 3)$ .

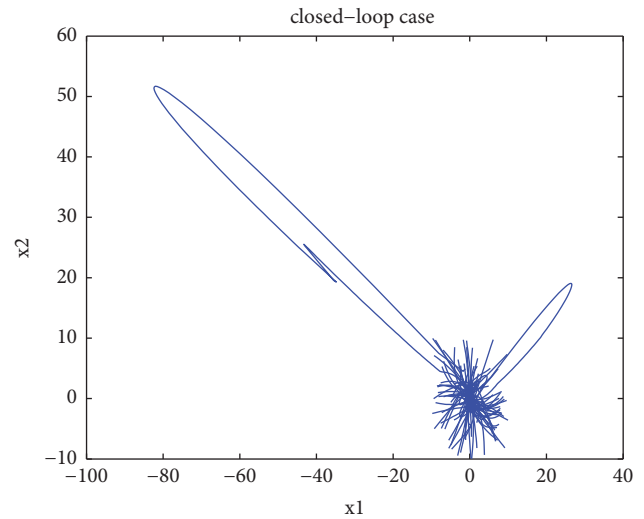


FIGURE 10: The phase trajectories for closed-loop SINNs (52) with 100 different initial conditions  $x(0) \in (-10, 10)$ ,  $y(0) \in (-30, 30)$ .

In order to make the result of the simulation more convincing, we take 100 sets of numbers randomly as the initial values of  $x(0)$  and  $y(0)$  and satisfy  $x(0) \in (-1, 1)$ ,  $y(0) \in (-3, 3)$ . Then the corresponding state trajectories are shown in Figure 7 and the corresponding phase trajectories are shown in Figure 8. Obviously, the stochastic inertial neural networks with time-delay (51) are finite-time stabilization. Moreover, when  $x(0) \in (-10, 10)$ ,  $y(0) \in (-30, 30)$ , we have state trajectories in Figure 9 and phase trajectories in Figure 10, which also figure out that the stochastic inertial neural networks with time-delay (51) are finite-time stabilization.

### 5. Conclusions

In this work, by constructing a proper Lyapunov function, the finite-time stabilization problem has been addressed for

stochastic inertial neural networks with or without time-delay. Provided that a set of LMIs are feasible, a suitable delayed or nondelayed nonlinear feedback controller can be designed such that finite-time stability in probability can be ensured for the system under study. An example has been given to demonstrate the correctness of the theoretical results and the effectiveness of the proposed methods.

### Data Availability

No data were used to support this study.

### Conflicts of Interest

The authors declare no conflicts of interest.

## Acknowledgments

This work was supported by the Nation Natural Science Foundation of China under Grants 61473213 and 61671338.

## References

- [1] S. G. Hu, Y. Liu, Z. Liu et al., "Associative memory realized by a reconfigurable memristive Hopfield neural network," *Nature Communications*, vol. 6, article no. 8522, 2015.
- [2] J. Yang, L. Wang, Y. Wang, and T. Guo, "A novel memristive Hopfield neural network with application in associative memory," *Neurocomputing*, vol. 227, pp. 142–148, 2017.
- [3] J. F. Durodola, N. Li, S. Ramachandra, and A. N. Thite, "A pattern recognition artificial neural network method for random fatigue loading life prediction," *International Journal of Fatigue*, vol. 99, pp. 55–67, 2017.
- [4] X.-M. Zhang, Q.-L. Han, X. Ge, and D. Ding, "An overview of recent developments in Lyapunov-Krasovskii functionals and stability criteria for recurrent neural networks with time-varying delays," *Neurocomputing*, 2018.
- [5] S. Xu and J. Lam, "A new approach to exponential stability analysis of neural networks with time-varying delays," *Neural Networks*, vol. 19, no. 1, pp. 76–83, 2006.
- [6] X.-M. Zhang and Q.-L. Han, "Global asymptotic stability for a class of generalized neural networks with interval time-varying delay," *IEEE Trans. Neural Netw.*, vol. 22, pp. 1180–1192, 2011.
- [7] S.-P. Xiao, H.-H. Lian, H.-B. Zeng, G. Chen, and W.-H. Zheng, "Analysis on robust passivity of uncertain neural networks with time-varying delays via free-matrix-based integral inequality," *International Journal of Control, Automation, and Systems*, vol. 15, no. 5, pp. 2385–2394, 2017.
- [8] X.-M. Zhang and Q.-L. Han, "Global asymptotic stability analysis for delayed neural networks using a matrix-based quadratic convex approach," *Neural Networks*, vol. 54, pp. 57–69, 2014.
- [9] G. Chen, H. Wang, and Y. Yang, "Finite-time stabilization for stochastic delayed recurrent neural networks via nonlinear delay-feedback controller," in *Proceedings of the 2017 Chinese Automation Congress (CAC)*, pp. 1411–1416, Jinan, October 2017.
- [10] Y. Wei, J. H. Park, H. R. Karimi, Y.-C. Tian, and H. Jung, "Improved Stability and Stabilization Results for Stochastic Synchronization of Continuous-Time Semi-Markovian Jump Neural Networks With Time-Varying Delay," *IEEE Transactions on Neural Networks and Learning Systems*, 2017.
- [11] S. Zhu, Y. Shen, and G. Chen, "Exponential passivity of neural networks with time-varying delay and uncertainty," *Physics Letters A*, vol. 375, no. 2, pp. 136–142, 2010.
- [12] Z. Tu, J. Cao, and T. Hayat, "Matrix measure based dissipativity analysis for inertial delayed uncertain neural networks," *Neural Networks*, vol. 75, pp. 47–55, 2016.
- [13] J. Wang, X.-M. Zhang, and Q.-L. Han, "Event-triggered generalized dissipativity filtering for neural networks with time-varying delays," *IEEE Transactions on Neural Networks and Learning Systems*, vol. 27, no. 1, pp. 77–88, 2015.
- [14] D. Huang, M. Jiang, and J. Jian, "Finite-time synchronization of inertial memristive neural networks with time-varying delays via sampled-date control," *Neurocomputing*, vol. 266, pp. 527–539, 2017.
- [15] N. Cui, H. Jiang, C. Hu, and A. Abdurahman, "Finite-time synchronization of inertial neural networks," *Journal of the Association of Arab Universities for Basic and Applied Sciences*, vol. 24, no. 1, pp. 300–309, 2018.
- [16] X. Zhang and Q. Han, "State estimation for static neural networks with time-varying delays based on an improved reciprocally convex inequality," *IEEE Transactions on Neural Networks and Learning Systems*, pp. 1–6, 2017.
- [17] C. Lu, X. Zhang, M. Wu, Q. Han, and Y. He, "Energy-to-Peak State Estimation for Static Neural Networks With Interval Time-Varying Delays," *IEEE Transactions on Cybernetics*, vol. 48, no. 10, pp. 2823–2835, 2018.
- [18] S. Zhang, Y. Yu, and Q. Wang, "Stability analysis of fractional-order Hopfield neural networks with discontinuous activation functions," *Neurocomputing*, vol. 171, pp. 1075–1084, 2016.
- [19] R. J. Williams and D. Zipser, "A learning algorithm for continually running fully recurrent neural networks," *Neural Computation*, vol. 1, no. 2, pp. 270–280, 1989.
- [20] Z. Tu, J. Cao, and T. Hayat, "Global exponential stability in Lagrange sense for inertial neural networks with time-varying delays," *Neurocomputing*, vol. 171, pp. 524–531, 2016.
- [21] K. L. Babcock and R. M. Westervelt, "Stability and dynamics of simple electronic neural networks with added inertia," *Physica D: Nonlinear Phenomena*, vol. 23, no. 1-3, pp. 464–469, 1986.
- [22] R. Sakthivel, R. Samidurai, and S. . Anthoni, "Exponential stability for stochastic neural networks of neural type with impulsive effects," *Modern Physics Letters B. Condensed Matter Physics, Statistical Physics, Applied Physics*, vol. 24, no. 11, pp. 1099–1110, 2010.
- [23] F. Wang, Y. Chen, and M. Liu, "pth moment exponential stability of stochastic memristor-based bidirectional associative memory (BAM) neural networks with time delays," *Neural Networks*, vol. 98, pp. 192–202, 2018.
- [24] Q. Zhu, C. Huang, and X. Yang, "Exponential stability for stochastic jumping BAM neural networks with time-varying and distributed delays," *Nonlinear Analysis: Hybrid Systems*, vol. 5, no. 1, pp. 52–77, 2011.
- [25] Z. Meng and Z. Xiang, "Stability analysis of stochastic memristor-based recurrent neural networks with mixed time-varying delays," *Neural Computing and Applications*, pp. 1–13, 2016.
- [26] J. L. Yin, S. Khoo, Z. H. Man, and X. H. Yu, "Finite-time stability and instability of stochastic nonlinear systems," *Automatica*, vol. 47, no. 12, pp. 2671–2677, 2011.
- [27] X. Song and X. Yan, "Linear quadratic Gaussian control for linear time-delay systems," *IET Control Theory & Applications*, vol. 8, no. 6, pp. 375–383, 2014.
- [28] X. Yan, X. Song, and X. Wang, "Global output-feedback stabilization for nonlinear time-delay systems with unknown control coefficients," *International Journal of Control, Automation, and Systems*, vol. 16, no. 4, pp. 1550–1557, 2018.
- [29] X. Liu, N. Jiang, J. Cao, S. Wang, and Z. Wang, "Finite-time stochastic stabilization for BAM neural networks with uncertainties," *Journal of The Franklin Institute*, vol. 350, no. 8, pp. 2109–2123, 2013.
- [30] F. Xiao, L. Wang, J. Chen, and Y. Gao, "Finite-time formation control for multi-agent systems," *Automatica*, vol. 45, no. 11, pp. 2605–2611, 2009.
- [31] J. Cortés, "Finite-time convergent gradient flows with applications to network consensus," *Automatica*, vol. 42, no. 11, pp. 1993–2000, 2006.
- [32] G. Chen, F. L. Lewis, and L. Xie, "Finite-time distributed consensus via binary control protocols," *Automatica*, vol. 47, no. 9, pp. 1962–1968, 2011.

- [33] J. Lu, D. W. C. Ho, and Z. Wang, "Pinning stabilization of linearly coupled stochastic neural networks via minimum number of controllers," *IEEE Transactions on Neural Networks and Learning Systems*, vol. 20, no. 10, pp. 1617–1629, 2009.
- [34] X. Li, "New results on global exponential stabilization of impulsive functional differential equations with infinite delays or finite delays," *Nonlinear Analysis: Real World Applications*, vol. 11, no. 5, pp. 4194–4201, 2010.
- [35] J. Yin and S. Khoo, "Comments on finite-time stability theorem of stochastic nonlinear systems," *Automatica*, vol. 47, no. 7, pp. 1542–1543, 2011.
- [36] B. Zhang, Q. Han, X. Zhang, and Yu. X., "Sliding mode control with mixed current and delayed states for offshore steel jacket platform," *IEEE Trans. Control Syst. Technol.*, vol. 22, pp. 1769–1783, 2014.
- [37] B.-L. Zhang, Q.-L. Han, and X.-M. Zhang, "Recent advances in vibration control of offshore platforms," *Nonlinear Dynamics*, vol. 89, no. 2, pp. 755–771, 2017.
- [38] S. Xiao, L. Xu, H. Zeng, and K. L. Teo, "Improved Stability Criteria for Discrete-time Delay Systems via Novel Summation Inequalities," *International Journal of Control, Automation, and Systems*, vol. 16, no. 4, pp. 1592–1602, 2018.

## Research Article

# Predefined-Time Consensus of Nonlinear First-Order Systems Using a Time Base Generator

J. Armando Colunga <sup>1</sup>, Carlos R. Vázquez <sup>2</sup>,  
Héctor M. Becerra <sup>1</sup> and David Gómez-Gutiérrez <sup>2,3</sup>

<sup>1</sup>Centro de Investigación en Matemáticas (CIMAT), A.C., Computer Science Department, GTO, Mexico

<sup>2</sup>Tecnologico de Monterrey, Escuela de Ingeniería y Ciencias, Zapopan, Mexico

<sup>3</sup>Intel Tecnología de México, Multi-Agent Autonomous Systems Lab, Intel Labs, Zapopan, Mexico

Correspondence should be addressed to Héctor M. Becerra; [hector.becerra@cimat.mx](mailto:hector.becerra@cimat.mx)

Received 16 June 2018; Revised 11 September 2018; Accepted 17 September 2018; Published 9 October 2018

Academic Editor: Ju H. Park

Copyright © 2018 J. Armando Colunga et al. This is an open access article distributed under the Creative Commons Attribution License, which permits unrestricted use, distribution, and reproduction in any medium, provided the original work is properly cited.

This paper proposes a couple of consensus algorithms for multiagent systems in which agents have first-order nonlinear dynamics, reaching the consensus state at a predefined time independently of the initial conditions. The proposed consensus protocols are based on the so-called time base generators (TBGs), which are time-dependent functions used to build time-varying control laws. Predefined-time convergence to the consensus is proved for connected undirected communication topologies and directed topologies having a spanning tree. Furthermore, one of the proposed protocols is based on the super-twisting controller, providing robustness against disturbances while maintaining the predefined-time convergence property. The performance of the proposed methods is illustrated in simulations, and it is compared with finite-time, fixed-time, and predefined-time consensus protocols. It is shown that the proposed TBG protocols represent an advantage not only in the possibility to define a settling time but also in providing smoother and smaller control actions than existing finite-time, fixed-time, and predefined-time consensus.

## 1. Introduction

Recent years have seen an increasing interest in algorithms allowing a group of systems to reach a common value for its internal state through local interaction. This problem has been addressed, from different viewpoints, in the consensus of multiagent systems (MASs) [1, 2] and in the synchronization of complex dynamical networks [3–5]. On the one hand, consensus protocols have been applied to flocking [6], formation control [7, 8], and distributed resource allocation [9, 10]. On the other hand, the results on synchronization of complex dynamical networks have been applied to neuroscience [3], power-grids [3], and the chaotic synchronization for secure communication in swarms [11].

Several works have been published proposing consensus and synchronization algorithms for different types of systems, considering static [12–14] and dynamic networks [4, 5]. Regarding first-order agents, the standard protocol (the input

of an agent is a linear combination of the errors between the agent's state and those of its neighbors) achieves consensus if the graph topology is strongly connected [15, 16]. This algorithm achieves consensus also for dynamic topologies, switching among connected graphs [15, 17]. For directed graphs topologies, a common requirement is that the graph contains a spanning-tree (e.g., [18]). All these algorithms are based on linear protocols and achieve consensus in an asymptotic fashion, where convergence rate is a function of the algebraic connectivity of the graph.

With the aim of developing consensus protocols satisfying real-time constraints, finite-time consensus has received a great deal of attention. The main focus has been in defining nonlinear protocols evaluated either on each of the neighbors' errors or on the sum of the neighbors' errors. For finite-time convergence, binary protocols based on the  $\text{sign}(\bullet)$  function have been proposed to achieve consensus to the average value [19, 20], the average-min-max value [21], the

median value [22], and the maximum or minimum value [23] of the agent's initial conditions. Continuous finite-time protocols, based on the  $|\cdot|^{\alpha}\text{sign}(\cdot)$  function, with  $0 < \alpha < 1$ , have been introduced in [12, 24]. Some algorithms have been extended to achieve finite-time consensus for strongly connected dynamic topologies [20, 25]. Fixed-time protocols have also been proposed in [26, 27]. In these, there exists a bound for the convergence time that is independent of the initial conditions [28, 29]. The protocols are mainly based on functions of the form  $|\cdot|^p\text{sign}(\cdot) + |\cdot|^q\text{sign}(\cdot)$ , with  $0 < q < 1 < p$ .

The methods mentioned above cannot be used in applications where real-time constraints have to be accomplished, since in both finite-time and fixed-time consensus, the relationship between the protocol parameters and the convergence time is not straightforward. Thus it is difficult to define the convergence time bound as a function of the protocol parameters. Moreover, the convergence time bound is often overestimated.

To address the consensus design problem with real-time constraints, predefined-time convergence has to be investigated. In this, the time at which consensus is achieved is predefined a priori as a parameter of the consensus protocol, being independent of the initial conditions. Few works have addressed the predefined-time consensus problem. In [30, 31], linear protocols that use time-varying control gains were proposed for reaching network consensus at a preset time. By using a motion planning strategy, predefined-time consensus protocols based on a time-varying sampling sequence convergent to a specified settling time are proposed in [32, 33]. Preliminary versions of a couple of predefined-time protocols were proposed in [34], taking advantage of time base generators (TBGs), which are parametric time signals that converge to zero in a specified time [35], and can be tracked using feedback controllers.

In this work, a couple of consensus algorithms based on TBGs are proposed as an extension to [34]. One algorithm is based on a linear-feedback, and the other is based on the super-twisting controller for the tracking of the TBG signal. The proposed approach can be applied to systems in which agents belong to the class of first-order controllable linear systems and nonlinear systems that can be linearized by state feedback [36]. Comparisons between the proposed protocols and finite-time, fixed-time, and predefined-time protocols are provided through simulations, showing the advantages of the proposed approach. In contrast with works on predefined-time consensus [30–32], the contribution of this paper is threefold: First, the proposed controllers yield smoother auxiliary control signals (without considering the linearization terms) with smaller magnitudes. Second, there are no parameters in the proposed consensus protocols depending on the algebraic connectivity of the graph considered. Third, a super-twisting controller is presented to deal with perturbed dynamics in the network's agents. With respect to our preliminary conference version [34], two main extensions are reported herein: (1) the new linear-feedback protocol drives the agents towards the initial conditions average (for undirected graphs) or the weighted sum of the initial conditions (for directed graphs), whereas in our previous work the consensus value was artificially specified;

(2) convergence to the consensus value in predefined time is demonstrated even if uncertainty in the knowledge of the initial state is introduced in the controller, at difference of our previous results, where it was assumed that the initial state was perfectly known.

It is known that second-order systems can represent a broader class of real systems than first-order systems. However, the last class of systems has also broad applicability, for instance, in robotics for kinematic control of holonomic robots. We are very interested in generalizing our results even for systems of a higher order than two, taking into account existing results like the ones in [37, 38].

The rest of this paper is organized as follows. Section 2 introduces some background in algebraic graph theory, defines the class of systems for which the proposed method is applicable, and formulates the problem to be solved in this paper. Section 3 presents the proposed consensus protocols: a linear-feedback and a super-twisting controller for the tracking of the TBG signal. Section 4 presents simulation results and a comparison of the proposed controllers with existing approaches. Section 5 provides conclusions.

## 2. Preliminaries and Problem Definition

**2.1. Algebraic Graph Theory.** Agents' communication is represented by a graph  $\mathcal{G} = (\mathbf{V}, \mathbf{E}, \mathbf{A})$ , which consists of a set of vertices (nodes or agents in this work)  $\mathbf{V} = \{1, \dots, N\}$ , a set of edges  $\mathbf{E} \subseteq \mathbf{V} \times \mathbf{V}$ , and a weighted adjacency matrix  $\mathbf{A} = [a_{ij}]$  with nonnegative adjacency elements  $a_{ij}$ , i.e.,  $a_{ij} > 0$  iff  $(i, j) \in \mathbf{E}$ . The set of neighbors of agent  $i$  is denoted by  $\mathbf{N}_i = \{j \in \mathbf{V} : (j, i) \in \mathbf{E}\}$ .

*Definition 1* (see [39, 40]). A graph  $\mathcal{G}$  is called *directed* if there is an entry of  $\mathbf{A}$  that fulfills  $a_{ij} > 0$ ; i.e.,  $(i, j) \in \mathbf{E}$  represents that agent  $j$  receives the information of the state value  $x_i$  of the agent  $i$ ; otherwise,  $a_{ij} = 0$ , i.e.,  $(j, i) \notin \mathbf{E}$ . A graph  $\mathcal{G}$  is called *undirected* if the pairs of nodes are not ordered  $a_{ij} = a_{ji} > 0$ ; otherwise,  $a_{ij} = a_{ji} = 0$ , i.e.,  $(i, j), (j, i) \notin \mathbf{E}$ .

*Definition 2* (see [39, 40]). A directed path (respectively, undirected path) from nodes  $v_j$  to  $v_i$  is a sequence of distinct edges of the form  $(v_i, v_{i_1}), (v_{i_1}, v_{i_2}), \dots, (v_{i_{k-1}}, v_j)$  in a directed graph (respectively, undirected graph). A graph is strongly connected (respectively, connected) if there exists a directed path (respectively, undirected path) between any two distinct vertices  $v_i$  and  $v_j$  in  $\mathcal{G}$ .

*Definition 3* (see [16, 18]). A directed graph  $\mathcal{G}$  has a directed spanning tree if there exists a node  $v_i$  (a root) such that all other nodes can be linked to  $v_i$  via a directed path.

If an undirected graph has a directed spanning tree, then the graph is connected. A strongly connected directed graph contains at least one directed spanning tree [16, 18].

*Definition 4* (see [16]). Let  $\mathcal{G}$  be a graph on  $N$  vertices labelled as  $1, \dots, N$ . The *Laplacian matrix* of  $\mathcal{G}$  is defined as the  $N \times N$  matrix  $\mathbf{L} = [l_{ij}]$ , where

$$l_{ij} = \begin{cases} -a_{ij}, & \text{if } i \neq j, \\ \sum_{k=1, k \neq i}^N a_{ik}, & \text{if } i = j. \end{cases} \quad (1)$$

In this work, we will propose and analyze consensus protocols for two kinds of networks: connected undirected graphs and directed graphs with a directed spanning tree [2, 16, 18].

**Lemma 5** ([2, 16, 18]).  $\mathbf{L}$  has at most one zero eigenvalue  $\lambda_1(\mathbf{L})$  with  $\mathbf{1}_N$  as the corresponding right eigenvector, where  $\mathbf{1}_N$  denotes a column vector with all entries equal to one, i.e.,  $\lambda_1(\mathbf{L}) = 0$ ,  $\text{Re}(\lambda_i(\mathbf{L})) > 0$ ,  $\forall i = \{2, \dots, N\}$  and  $\mathbf{L}\mathbf{1}_N = \mathbf{0}_N$ . Furthermore, if the graph is undirected and connected,  $\mathbf{L}$  has a left eigenvector  $\boldsymbol{\gamma}$  that satisfies  $\boldsymbol{\gamma}^T \mathbf{L} = \mathbf{0}_N^T$  and  $\boldsymbol{\gamma} = \mathbf{1}_N$ , where  $\mathbf{0}_N$  represents a column vector of zeros. If the graph is directed and has a spanning tree then  $\boldsymbol{\gamma}^T \mathbf{L} = \mathbf{0}_N^T$  and  $\boldsymbol{\gamma}^T \mathbf{1}_N = 1$ .

Finally, let us introduce a matrix transformation that will be useful later on. Let  $\mathbf{J} \in \mathbb{C}^{N \times N}$  be the Jordan form associated with  $\mathbf{L}$ . Then, there exists a nonsingular matrix  $\mathbf{S} \in \mathbb{C}^{N \times N}$  such that

$$\mathbf{S}^{-1} \mathbf{L} \mathbf{S} = \mathbf{J} = \begin{bmatrix} 0 & \mathbf{0}_{N-1}^T \\ \mathbf{0}_{N-1} & \hat{\mathbf{J}} \end{bmatrix} \quad (2)$$

where  $\hat{\mathbf{J}} \in \mathbb{C}^{(N-1) \times (N-1)}$  is the Jordan matrix associated with the nonzero eigenvalues of  $\mathbf{L}$  [39, 41] and  $\mathbf{0}_{N-1}$  represents a column vector of zeros of size  $N - 1$ .

**2.2. Problem Definition.** In this paper, we will consider a set of  $N$  agents connected through a network, which are modeled as first-order nonlinear systems as follows

$$\dot{x}_i(t) = f_i(x_i) + g_i(x_i)u_i(t) + \rho_i(t), \quad i \in \{1, \dots, N\} \quad (3)$$

Where, for the agent  $i$ ,  $x_i(t) \in \mathbb{R}$  is the system's state,  $u_i(t) \in \mathbb{R}$  is the control input,  $f_i(x_i)$  and  $g_i(x_i)$  are smooth nonlinear functions, and  $\rho_i(t) \in \mathbb{R}$  is a bounded disturbance. In order to represent the multiagent system (MAS) dynamics, denote  $\mathbf{x} = [x_1, \dots, x_N]^T$ ,  $\mathbf{u} = [u_1, \dots, u_N]^T$ ,  $\mathbf{f} = [f_1, \dots, f_N]^T$ ,  $\mathbf{g} = [g_1, \dots, g_N]^T$ , and  $\boldsymbol{\rho} = [\rho_1, \dots, \rho_N]^T \in \mathbb{R}^N$ . Then, the complete dynamics (3) can be written as

$$\dot{\mathbf{x}}(t) = \mathbf{f}(\mathbf{x}) + \mathbf{g}(\mathbf{x})\mathbf{u}(t) + \boldsymbol{\rho}(t). \quad (4)$$

Let us propose a linearizing control law of the form  $u_i = (-f_i(x_i) + v_i)/g_i(x_i)$  for each agent (3), where  $v_i$  is an auxiliary control input and it is assumed that  $g_i(x_i) \neq 0$ , i.e., the relative degree is well defined [36] and the agent is controllable. The closed-loop dynamics for the  $i$ -th agent are now linear and given by

$$\dot{x}_i(t) = v_i(t) + \rho_i(t), \quad i \in \{1, \dots, N\}. \quad (5)$$

The complete closed-loop dynamics for all the agents can be written as

$$\dot{\mathbf{x}}(t) = \mathbf{v}(t) + \boldsymbol{\rho}(t) \quad (6)$$

where  $\mathbf{v} = [v_1, \dots, v_N]^T \in \mathbb{R}^N$ .

In a MAS, the consensus error of agent  $i$  with respect to its neighbors is defined as [2]

$$e_i(t) = \sum_{j \in \mathcal{N}_i} a_{ij} (x_j(t) - x_i(t)), \quad i \in \{1, \dots, N\}. \quad (7)$$

The consensus error for the complete MAS can be expressed in a compact form as [2]

$$\mathbf{e}(t) = [e_1(t), \dots, e_N(t)]^T = -\mathbf{L}\mathbf{x}(t). \quad (8)$$

**Problem statement:** given a MAS with agents modeled as first-order nonlinear systems (3) and with an associated graph  $\mathcal{G}$ , design a consensus protocol for each agent in the form  $u_i = \gamma(e_i, x_i, t)$ , such that the state of all the agents reaches a consensus value  $x^*$  in a predefined time  $t_f$  from any initial state  $\mathbf{x}(0)$ , i.e.,  $x_i(t) \rightarrow x^*$ ,  $\forall i = \{1, \dots, N\}$ , as  $t \rightarrow t_f$ . Therefore, the consensus error (8) converges to zero at time  $t_f$ .

**Remark 6.** The consensus problem in MASs is closely related to the synchronization problem in complex dynamical networks, but they have been addressed from different viewpoints [42]. In fact, the consensus problem can be posed as a complete-synchronization problem. In the former, the analysis is often based on the matrix Laplacian approach [2] and the agents have simple dynamics such as single integrator dynamics, a chain of integrators, or linear systems. The recent focus has been on defining finite-time, fixed-time, and predefined-time protocols for fixed and dynamic networks. In the synchronization problem in complex networks the analysis is often based in the Master stability function formalism [3, 42] and addresses interconnected systems with complex dynamics, for instance, chaotic attractors. Although recently some works have addressed synchronization in dynamic networks, e.g., Markov jump topologies [4, 5], most of the work has been focused on static topologies. For further details on the synchronization problem, we refer the reader to [3].

**2.3. Time Base Generator (TBG).** Time base generators are parametric functions of time, particularly designed to stabilize a system in such a way that its state describes a convenient transient profile. TBGs have been previously used to achieve predefined-time convergence of first and higher order dynamics for single systems in [35]. For the case of single first-order systems, TBGs have been used for the control of robots at kinematic level [43].

A *time base generator (TBG)* is a continuous and differentiable time-dependent polynomial function  $h(t)$  described as [35]

$$h(t) = \begin{cases} \boldsymbol{\tau}(t) \cdot \mathcal{C} & \text{if } t \in [0, t_f] \\ 0 & \text{otherwise} \end{cases} \quad (9)$$

where  $\boldsymbol{\tau}(t) = [t^r \ t^{r-1} \ \dots \ t \ 1]$  is the time basis vector and  $\mathcal{C}$  is a vector of coefficients of proper dimensions. For first-order systems, it is required to compute a TBG fulfilling the following conditions at initial time and final time  $t_f$ ,

$$h(t) = \begin{cases} 1, & \text{if } t = 0 \\ 0, & \text{if } t \geq t_f \end{cases} \quad (10)$$

$$\dot{h}(t) = 0, \quad \text{if } t = 0 \text{ or } t \geq t_f.$$

In [35], a couple of procedures for calculating the coefficients  $\mathcal{C}$ , fulfilling the required constraints, have been introduced. In particular, when a high degree polynomial is used, an optimization procedure can be applied to find the best coefficients.

### 3. Consensus Protocols Using the TBG

In this section, we present consensus protocols that take advantage of the TBG to enforce convergence of a MAS in predefined time. In the first two subsections, we present results for unperturbed systems, i.e., for  $\rho = \mathbf{0}_N$ , while in Section 3.3 we consider perturbed systems.

*3.1. Previous Results.* In [34], a consensus protocol was proposed for the MAS (4) by introducing a time-varying control gain in order to drive the system to a neighborhood about a given consensus value  $x^*$  in a predefined time  $t_f$ , from any initial state  $\mathbf{x}(0)$ . Consequently, the consensus error (8) converges to a neighborhood about the origin at  $t_f$ . Such consensus protocol is similar in nature to those in [30, 31].

In the same preliminary work [34], we have proposed the following open-loop controller to enforce predefined-time convergence to a desired consensus value  $\bar{x}$ , provided that the MAS (4) is not perturbed and the initial state is known,

$$u_i(t) = \frac{1}{g_i(x_i)} (-f_i(x_i) + v_i), \quad i \in \{1, \dots, N\} \quad (11)$$

$$v_i = \dot{h}(t)(x_i(0) - \bar{x})$$

where  $h(t)$  fulfills (10). In that work, it was demonstrated that consensus to  $\bar{x}$  is achieved in time  $t_f$  and the resulting consensus error trajectory in the interval  $t \in [0, t_f]$  is given by

$$\widehat{\mathbf{e}}(t) = h(t) \mathbf{e}_0 = -h(t) \mathbf{L} \mathbf{x}_0 \quad (12)$$

where  $\mathbf{e}(0) = \mathbf{e}_0 = [e_1(0), \dots, e_N(0)]^T$  is the consensus error vector (8) at the initial condition  $\mathbf{x}(0) = \mathbf{x}_0 = [x_1(0), \dots, x_N(0)]^T$ .

To provide closed-loop stability of the tracking error, a different protocol was proposed in [34] to address the predefined-time consensus problem as a trajectory tracking problem, where the reference trajectory depends on the TBG. Such protocol is described as follows,

$$u_i(t) = \frac{1}{g_i(x_i)} (-f_i(x_i) + v_i), \quad i \in \{1, \dots, N\} \quad (13)$$

$$v_i = \dot{h}(t)(x_i(0) - \bar{x}) + k_f(e_i(t) - h(t)e_i(0)).$$

This protocol guarantees stability during the transient behavior and also after the settling time, i.e., for any  $t \geq t_f$ . The controller for each agent in (13) consists of two terms: the first one is a feed-forward term that yields the evolution of each agent's error from the initial value  $e_i(0)$  to the origin at time  $t_f$ , following a transient profile defined by the TBG as  $\widehat{e}_i(t) = h(t)e_i(0)$ ; the second term is a feedback term that corrects any deviation of  $e_i(t)$  from the transient profile  $\widehat{e}_i(t)$ , providing global stability of the error dynamics.

*3.2. Consensus Based on the Error Feedback.* In the conference paper [34], whose main results were summarized above, consensus protocols were proposed achieving predefined-time convergence to a consensus value  $\bar{x}$ , which must be specified in the control law. Moreover, it was assumed that the initial state is accurately known since this value is used in the protocols.

Nevertheless, in most of the protocols proposed in the literature, the consensus value is a quantity that inherently results from the initial states and the connectivity of the graph model [15]. The consensus value may represent important information to be recovered, as in a network of sensors. For this reason, in this paper, we propose a new consensus protocol that yields predefined-time convergence of the unperturbed MAS (4) without the need of specifying a consensus value. Moreover, we consider uncertainties in the knowledge of the initial conditions.

In the sequel, consider that the consensus protocol has an estimate of the initial state, denoted as  $\widehat{\mathbf{x}}_0 = [\widehat{x}_1(0), \dots, \widehat{x}_N(0)]^T$ , instead of the real initial state  $\mathbf{x}_0$ . In this way,

$$\widehat{\mathbf{x}}_0 = \mathbf{x}_0 + \mathbf{d} \quad (14)$$

where  $\mathbf{d} = [d_1, \dots, d_N]^T$  is a vector of uncertainty in the initial state. From (14), the uncertain initial consensus error can be computed as

$$\widehat{\mathbf{e}}_0 = [\widehat{e}_1(t), \dots, \widehat{e}_N(t)]^T = -\mathbf{L} \widehat{\mathbf{x}}_0. \quad (15)$$

The following theorem introduces one of the main results of this paper, a feedback-based consensus protocol able to achieve consensus without the need of specifying the consensus value and able to track the trajectories given by the TBG when there is uncertainty in the initial state  $\widehat{\mathbf{x}}_0$  introduced in the controller.

**Theorem 7.** *Consider a MAS with a connected undirected communication topology or directed topology having a spanning tree modeled as in (4). Let  $k_f \in \mathbb{R}^+$  be a constant state-feedback gain. Then, the time-varying feedback control law*

$$u_i(t) = \frac{1}{g_i(x_i)} (-f_i(x_i) + v_i), \quad i \in \{1, \dots, N\} \quad (16)$$

$$v_i = -\dot{h}(t)\widehat{e}_i(0) + k_f(e_i(t) - h(t)\widehat{e}_i(0)),$$

with  $h(t)$  as in (10) and  $\widehat{e}_i(0)$  computed from the initial state estimate  $\widehat{\mathbf{x}}_0$ , provides global asymptotic stability of the tracking error  $\boldsymbol{\xi}(t) = \mathbf{e}(t) - h(t)\widehat{\mathbf{e}}_0$ . Therefore, assuming  $\rho(t) = \mathbf{0}_N$ , predefined-time convergence of the MAS (4) to a consensus value  $x^*$  is achieved at  $t_f$  from any initial state  $\mathbf{x}_0$ .

*Proof.* First, let us demonstrate the stability of the tracking error. The dynamics (3) with  $\rho_i(t) = 0, \forall i = \{1, \dots, N\}$ , under the control action (16), can be written in vector notation as

$$\dot{\mathbf{x}}(t) = -\dot{h}(t)\widehat{\mathbf{e}}_0 + k_f(\mathbf{e}(t) - h(t)\widehat{\mathbf{e}}_0). \quad (17)$$

Computing  $\dot{e}(t)$  from (8) and using the linearized dynamics (17), we have

$$\begin{aligned}\dot{\xi}(t) &= \dot{e}(t) - \dot{h}(t)\widehat{e}_0 = -L\dot{x}(t) - \dot{h}(t)\widehat{e}_0 \\ &= -L\dot{x}(t) + \dot{h}(t)L\widehat{x}_0 \\ &= -\dot{h}(t)L^2\widehat{x}_0 - k_f L\xi(t) + \dot{h}(t)L\widehat{x}_0 \\ &= -k_f L\xi(t) + \dot{h}(t)L(\widehat{x}_0 - L\widehat{x}_0).\end{aligned}\quad (18)$$

By using  $h(0) = 1$ , the initial tracking error is computed as

$$\begin{aligned}\xi(0) &= e_0 - h(0)\widehat{e}_0 = -Lx_0 + L(x_0 + d) = Ld \\ &= SJS^{-1}d,\end{aligned}\quad (19)$$

with  $L = SJS^{-1}$ , where  $J \in \mathbb{C}^{N \times N}$  is the Jordan form associated with  $L$  and  $S \in \mathbb{C}^{N \times N}$  is a nonsingular matrix [39].

Let  $\zeta(t) = S^{-1}\xi(t)$ , then  $\zeta(0) = JS^{-1}d$ , and according to (2), it follows that the first entry of  $\zeta(0)$  is null, i.e.,  $\zeta_1(0) = 0$ . Now, taking the time derivative of  $\zeta(t)$  and using (18), we have

$$\begin{aligned}\dot{\zeta}(t) &\triangleq [\dot{\zeta}_1(t), \dots, \dot{\zeta}_N(t)]^T = S^{-1}\dot{\xi}(t) \\ &= S^{-1}(-k_f L\xi(t) + \dot{h}(t)L(\widehat{x}_0 - L\widehat{x}_0)) \\ &= -k_f S^{-1}(SJS^{-1})S\zeta(t) \\ &\quad + \dot{h}(t)S^{-1}(SJS^{-1})(\widehat{x}_0 - (SJS^{-1})\widehat{x}_0) \\ &= -k_f J\zeta(t) + \dot{h}(t)J(S^{-1} - JS^{-1})\widehat{x}_0.\end{aligned}\quad (20)$$

Let  $\phi(t) = [\zeta_2(t), \dots, \zeta_N(t)]^T$ , and  $S^{-1} = \begin{bmatrix} r \\ Y \end{bmatrix}$ , where  $r \in \mathbb{R}^{1 \times N}$  and  $Y \in \mathbb{C}^{(N-1) \times N}$ . Then, we can verify that (20) can be written as

$$\begin{aligned}\dot{\zeta}_1(t) &= 0 \\ \dot{\phi}(t) &= -k_f \widehat{J}\phi(t) + F(t)\end{aligned}\quad (21)$$

where  $F(t) = \dot{h}(t)\widehat{J}(Y - \widehat{J}Y)\widehat{x}(0)$  and  $\widehat{J} \in \mathbb{C}^{(N-1) \times (N-1)}$  is the Jordan matrix associated with  $L$  for  $\{\lambda_2, \dots, \lambda_N\}$ ,  $\text{Re}(\lambda_i(L)) > 0$ ,  $\forall i = \{2, \dots, N\}$ .

It can be shown that the solutions of the differential equations (21) are the following [44]:

$$\begin{aligned}\zeta_1(t) &= \zeta_1(0) = 0 \\ \phi(t) &= e^{-k_f \widehat{J}t} \left( \phi(0) + \int_0^t e^{k_f \widehat{J}s} F(s) ds \right), \\ &\quad t \in [0, t_f]\end{aligned}\quad (22)$$

where  $e^{-k_f \widehat{J}t} \in \mathbb{C}^{(N-1) \times (N-1)}$  is the exponential matrix. Then, it follows that

$$\lim_{t \rightarrow +\infty} \phi(t) = \lim_{t \rightarrow +\infty} [\zeta_2(t), \dots, \zeta_N(t)]^T = \mathbf{0}_{N-1}, \quad (23)$$

since the integral is a finite value due to  $\dot{h}(t) = 0$ ,  $\forall t \geq t_f$ , and  $-k_f \widehat{J}$  has eigenvalues with negative real parts [18, 45]. Notice that the convergence speed is determined by the dominant eigenvalue  $\lambda_2$  of  $L$  ([15]) and the control gain  $k_f$ .

Since  $\lim_{t \rightarrow +\infty} \zeta_i(t) = 0$ ,  $\forall i \in \{1, \dots, N\}$ , then

$$\begin{aligned}\lim_{t \rightarrow +\infty} \xi(t) &= S \lim_{t \rightarrow +\infty} \zeta(t) \\ &= S \lim_{t \rightarrow +\infty} [\zeta_1(t), \dots, \zeta_N(t)]^T \\ &= S[0, \dots, 0]^T = \mathbf{0}_N.\end{aligned}\quad (24)$$

Therefore, the tracking error converges to the origin. In fact, from (21) it can be seen that the tracking error is globally asymptotically stable, since the real part of the eigenvalues of  $-k_f \widehat{J}$  is negative,  $\zeta_1(t) = 0$ , and  $F(t)$  can be seen as a disturbance that becomes null for  $t \geq t_f$ . The stability of the tracking error implies that  $e(t)$  follows  $h(t)\widehat{e}_0$ ; thus  $e(t)$  converges to the origin at the predefined-time  $t_f$ . Any small final error in time  $t \geq t_f$  is corrected by the control input  $u_i = (1/g_i(x_i))(-f_i(x_i) + k_f e_i(t))$ , which is applied to each agent for  $t \geq t_f$ .

By using the property  $L\mathbf{1}_N = \mathbf{0}_N$  (in accordance to Lemma 5), the converge of the consensus error (8) to the origin implies

$$x(t) \rightarrow x(t_f) = x^* \mathbf{1}_N \quad \text{as } t \rightarrow t_f, \quad (25)$$

i.e.,

$$x_i(t) \rightarrow x^* \quad \text{as } t \rightarrow t_f, \quad \forall i = \{1, \dots, N\}. \quad (26)$$

That is, the system (4) achieves predefined-time convergence to a consensus value  $x^*$  at  $t_f$  using the consensus protocol (16).

Now, let us compute the final consensus value. First, define  $y(t) = \gamma^T x(t)$ , where  $\gamma$  is defined in Lemma 5. For the two types of considered graphs,  $y(t)$  is an invariant quantity, since

$$\begin{aligned}\dot{y}(t) &= \gamma^T \dot{x}(t) = \gamma^T (-\dot{h}(t)\widehat{e}_0 + k_f (e(t) - h(t)\widehat{e}_0)) \\ &= \gamma^T L(\dot{h}(t)\widehat{x}_0 - k_f (x(t) - h(t)\widehat{x}_0)) = 0, \\ &\quad \forall x(t)\end{aligned}\quad (27)$$

where  $\gamma^T L = \mathbf{0}_N^T$  by Lemma 5. Thus,

$$\lim_{t \rightarrow t_f} y(t) = y(0) = \gamma^T x(0) \quad (28)$$

Moreover, from (25) it follows that

$$\lim_{t \rightarrow t_f} y(t) = \gamma^T \lim_{t \rightarrow t_f} x(t) = \gamma^T (x^* \mathbf{1}_N). \quad (29)$$

Then, for a connected undirected graph and by Lemma 5 ( $\gamma = \mathbf{1}_N$ ), it is obtained that

$$\begin{aligned}\gamma^T x^* \mathbf{1}_N &= \gamma^T x_0, \\ x^* (\mathbf{1}_N)^T \mathbf{1}_N &= (\mathbf{1}_N)^T x_0,\end{aligned}\quad (30)$$

and solving for  $x^*$ , one has

$$x^* = \frac{\sum_{i=1}^N x_i(0)}{N} = \text{Ave}(\mathbf{x}_0). \quad (31)$$

Hence, the consensus value  $x^*$  is the average of the initial state  $\mathbf{x}_0$  for connected undirected graphs. Now, for a directed graph with a directed spanning tree and by Lemma 5 ( $\mathbf{y}^T \mathbf{1}_N = 1$ ), it results in

$$x^* = \frac{\mathbf{y}^T \mathbf{x}_0}{\mathbf{y}^T \mathbf{1}_N} = \mathbf{y}^T \mathbf{x}_0. \quad (32)$$

Therefore, the consensus value is given by (32) for a directed graph with a directed spanning tree.

Thus, system (4) with  $\boldsymbol{\rho}(t) = \mathbf{0}_N$  achieves predefined-time convergence to a consensus value  $x^*$  at  $t_f$  in the presence of uncertainty in the initial state  $\mathbf{x}_0$  using the consensus protocol (16).  $\square$

*Remark 8.* It is worth noting that, in contrast to the use of the consensus protocol (13), the feed-forward term of  $v_i$  in (16) is not sufficient to drive the consensus error trajectory to the TBG reference trajectory  $\hat{\mathbf{e}}(t) = h(t)\hat{\mathbf{e}}_0$  even for  $\mathbf{d} = \mathbf{0}_N$ ; consequently, system (4) under the first term of (16) does not reach predefined-time convergence to a consensus value  $x^*$  at  $t_f$ . In such a case, the final state is given by  $\mathbf{x}(t_f) = (\mathbf{I}_N - \mathbf{L})\mathbf{x}_0 - \mathbf{L}\mathbf{d}$ , where  $\mathbf{I}_N$  denotes the identity matrix of size  $N$ . Therefore, the use of the feedback term in (16) is required in any case.

It can be seen that the consensus protocol (16) can solve the problem of predefined-time consensus stated in Section 2.2 by tracking the trajectories given by the TBG even when considering uncertainty  $\mathbf{d}$  in the initial state. In this sense, the compensation term for tracking must guarantee reaching the TBG trajectories before the desired convergence time  $t_f$ . This means that the tracking control gain  $k_f$  must be higher for a larger uncertainty in the initial state. Then, there is a limit on the values of  $\mathbf{d}$  that can be managed by the consensus protocol.

*Remark 9.* Theorem 7 represents a novel contribution on consensus for nonlinear MAS: First, the predefined-time consensus is solved for nonlinear first-order systems. Second, the auxiliary control inputs  $v_i(t)$  in (16) are smooth signals even at  $t = 0$ , which is not the case of other approaches reported in the literature. Third, the proposed consensus protocols do not have parameters depending on the algebraic connectivity of the graph considered. Finally, the stability analysis is performed by using standard techniques for linear systems (upon feedback linearization of the original systems), while most of the works regarding finite-time and fixed-time and even the few existing works on predefined-time convergence adopt more sophisticated techniques such as homogeneity theory and Lyapunov functions.

*Remark 10.* The result introduced by Theorem 7, compared to our previous conference work [34], is twofold: (1) a new consensus protocol is proposed, achieving predefined-time

convergence of the unperturbed MAS (4) without the need of specifying a consensus value; (2) the effect of considering uncertainty in the knowledge of the initial conditions is analyzed, demonstrating that convergence to a consensus value can still be achieved.

**3.3. Robust Predefined-Time Consensus.** In the previous consensus protocol, we have considered unperturbed dynamics (i.e.,  $\boldsymbol{\rho}(t) = \mathbf{0}_N$ ). To effectively deal with disturbances, a robust protocol is introduced in this section, by combining the super-twisting controller (STC), which can compensate for matched uncertainties/disturbances [46], with the TBG, leading to a robust predefined-time controller.

In this scheme, it is assumed that there exists a leader  $x_l(t) \in \mathbb{R}$  in the network system, whose dynamics can be modeled as in [47] by

$$\dot{x}_l(t) = u_l(t) \quad (33)$$

where  $u_l(t) \in \mathbb{R}$  is the leader's control input. In this case,  $N$  agents are now the followers with dynamics (3). The consensus error for each follower is defined as [47]

$$e_i^f(t) = \sum_{j \in \mathcal{N}_i} a_{ij} (x_j(t) - x_i(t)) - b_i (x_i(t) - x_l(t)) \quad (34)$$

where  $b_i \in \mathbb{R}$  represents the leader's adjacency with  $b_i > 0$  if agent  $i$  is a neighbor of the leader; otherwise  $b_i = 0$ ,  $\forall i = \{1, \dots, N\}$ .

The tracking error is given by

$$\xi_i(t) = e_i^f(t) - h(t)\hat{\mathbf{e}}_i(0) \quad (35)$$

where  $h(t)\hat{\mathbf{e}}_i(0)$  is the TBG reference trajectory for the  $i$ -th and  $\hat{\mathbf{e}}_i(0)$  is computed from the initial state estimate  $\hat{\mathbf{x}}_0$  as in (15). The tracking error will be used as the sliding surface; thus

$$s_i(t) = \xi_i(t) = e_i^f(t) - h(t)\hat{\mathbf{e}}_i(0). \quad (36)$$

**Theorem 11.** Consider a MAS modeled as in (4) with a leader (33). For each agent  $i$ , define  $\beta_i = (\sum_{j \in \mathcal{N}_i} a_{ij} + b_i)$  and the sliding surface (36). Consider a function  $h(t)$  as in (10). There exist gains  $k_1 > 0$  and  $k_2 > \varrho(M)$ , for some function  $\varrho(\bullet)$  and a constant  $M > 0$ , such that the following nonlinear controller defined for each agent

$$\begin{aligned} u_i(t) &= (\beta_i g_i)^{-1} (\bar{v}_i + v_i), \quad i \in \{1, \dots, N\} \\ \bar{v}_i &= b_i u_l + \sum_{j \in \mathcal{N}_i} a_{ij} (f_j + g_j u_j) - \beta_i f_i - \dot{h}(t)\hat{\mathbf{e}}_i(0) \\ v_i &= k_1 |s_i|^{1/2} \text{sign}(s_i) - w_i \\ \dot{w}_i &= -k_2 \text{sign}(s_i) \end{aligned} \quad (37)$$

achieves predefined-time convergence to the leader's state  $x_l$  at  $t_f$ , allowing  $\rho_i(t) \neq 0$ , from any initial state  $x_i(0)$ .

*Proof.* First, taking the time derivative of the tracking error (35) and using the dynamics of the followers (3) and the leader (33), it is obtained that

$$\begin{aligned}
 \dot{\xi}_i(t) &= \dot{e}_i^f(t) - \dot{h}(t) \hat{e}_i(0) \\
 &= \sum_{j \in N_i} a_{ij} (\dot{x}_j(t) - \dot{x}_i(t)) - b_i (\dot{x}_i(t) - \dot{x}_i(t)) \\
 &\quad - \dot{h}(t) \hat{e}_i(0) \\
 &= -\beta_i (f_i + g_i u_i) + \sum_{j \in N_i} a_{ij} (f_j + g_j u_j) + b_i u_i \\
 &\quad - \beta_i \rho_i + \sum_{j \in N_i} a_{ij} \rho_j - \dot{h}(t) \hat{e}_i(0).
 \end{aligned} \tag{38}$$

Now, using (38) and plugging the control law (37) in the time derivative of the sliding surface (36), it results in

$$\begin{aligned}
 \dot{s}_i &= \dot{\xi}_i(t) = -k_1 |s_i|^{1/2} \text{sign}(s_i) + w_i + \rho_{d_i} \\
 \dot{w}_i &= -k_2 \text{sign}(s_i),
 \end{aligned} \tag{39}$$

where  $\rho_{d_i} = \sum_{j \in N_i} a_{ij} \rho_j - \beta_i \rho_i$ . Let  $z_i = w_i + \rho_{d_i}$ ; then the previous expression can be rewritten as

$$\begin{aligned}
 \dot{s}_i &= -k_1 |s_i|^{1/2} \text{sign}(s_i) + z_i \\
 \dot{z}_i &= -k_2 \text{sign}(s_i) + \dot{\rho}_{d_i}.
 \end{aligned} \tag{40}$$

It has been proven in [46] that, for a bounded continuously differentiable disturbance, i.e., if  $|\rho_{d_i}| < L$  and  $|\dot{\rho}_{d_i}| < M$  for some constants  $L > 0$ ,  $M > 0$ , the second-order dynamics (40) converge globally to the origin ( $s_i = 0, z_i = 0$ ) in finite time in spite of the disturbance, if adequate positive control gains  $k_1 > 0$  and  $k_2 > \varrho(M)$  are used. Moreover, the remaining dynamics of the tracking error system are constrained to the sliding surface, such that  $s_i = \dot{s}_i = 0$ , meaning that each agent  $e_i^f(t)$  follows  $h(t) \hat{e}_i(0)$ . Consequently, the consensus error converges to zero in the predefined-time  $t_f$  and the consensus value is given by the leader's state  $x_l$  [47].  $\square$

*Remark 12.* To the best of our knowledge, the only works that propose predefined-time consensus protocols by other authors are [30–32]. The consensus control law (37) has the advantage, over those protocols, of providing robustness against large matched perturbations.

Some important issues to be considered during real-world applications of the proposed distributed control protocols are threefold: First, all the clocks of the agents in the network must be synchronized to achieve predefined-time convergence. Second, physical constraints of the systems must be taken into account to set  $t_f$ , considering that a small  $t_f$  will result in large control inputs. Thus the maximum allowable input of each agent must be taken into consideration to set  $t_f$ . Third, we are currently assuming no time delay in the agent's communication; however, time delays may exist in some systems and may affect the convergence to the consensus.

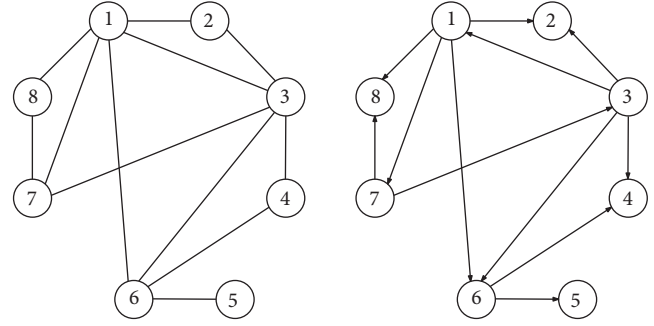


FIGURE 1: Communication graphs. Left: undirected graph  $\mathcal{G}_1$ . Right: directed graph  $\mathcal{G}_2$ .

## 4. Simulation Results

In this section, simulation results are shown to illustrate the advantages of the proposed protocols. All the simulations consider a MAS of 8 agents, described by (3) with  $f_i(x_i) = x_i^2$  for agents 1 to 4,  $f_i(x_i) = \sin(x_i)$  for agents 5 to 8, and  $g_i(x_i) = 5$  for all the 8 agents. The convergence time is preset to  $t_f = 5$  seconds. For this, the TBG is described by the function  $h(t) = 2(t/t_f)^3 - 3(t/t_f)^2 + 1$ , which fulfills (9), i.e.,  $h(0) = 1$ ,  $h(5) = 0$ , and  $\dot{h}(0) = \dot{h}(5) = 0$ . Both proposed distributed control laws are implemented as defined in (16) and (37). The implementation essentially requires the computation of the TBG reference and its time derivative, which means to evaluate the functions  $h(t)$  and  $\dot{h}(t)$  at each iteration and compute the consensus error for each agent depending on the neighbors state as given by (7).

We use the communication topologies shown in Figure 1 (obtained from [30]), denoted as  $\mathcal{G}_1$  and  $\mathcal{G}_2$ , where  $\mathcal{G}_1$  is a connected undirected graph and  $\mathcal{G}_2$  is a directed graph having a directed spanning tree. The simulations were implemented in MATLAB using the Euler forward method to approximate the time derivatives with a time step of 0.1 ms.

The initial states of the eight agents are  $\mathbf{x}_0 = [-0.61, 3.52, -1.07, 0.73, 1.48, 0.19, 1.97, 0.72]^T$ . The uncertainties in the initial states are set to be  $\mathbf{d} = [0.22, 0.15, -0.39, 0.27, 0.34, 0.21, -0.36, -0.09]^T$ .

**4.1. Simulation of the Consensus Protocol Based on the Error Feedback.** This subsection is devoted to showing the performance of the TBG protocol (16). Figures 2 and 3 show the transient behavior of the MAS under (16) with  $k_f = 100$ , for  $\mathcal{G}_1$  and  $\mathcal{G}_2$ , respectively. For the case shown in Figure 2, perfect knowledge of the initial conditions is assumed, while in Figure 3, there exists uncertainty in the initial condition knowledge, given by  $\mathbf{d}$ . In both cases the agent's state (top graphs in the figures) reaches consensus at the predefined 5 seconds.

It can be seen in Figure 2 (middle) that the auxiliary control inputs  $v_i(t)$  generated by the control protocol (16) are smooth signals even at  $t = 0$ . This is due to the properties of the TBG, which yields that each  $v_i$  starts at zero and returns to zero at time  $t_f$ . This is not the case for the control inputs  $u_i$ , since they include the nonlinearities that must be cancelled.

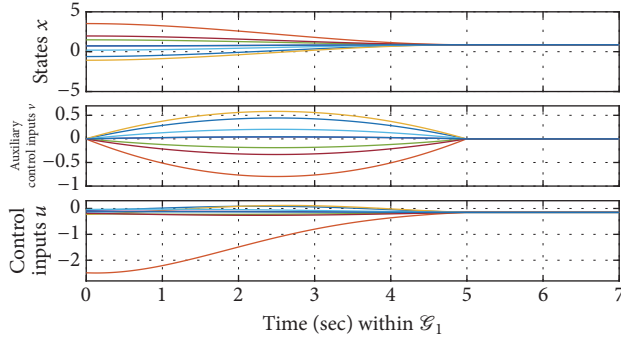


FIGURE 2: Predefined-time TBG-tracking controller (16) for  $\mathcal{S}_1$ . The convergence time is preset to 5 sec., and the consensus value is  $\sum_{i=1}^N x_i(0)/N = 0.8676$ .

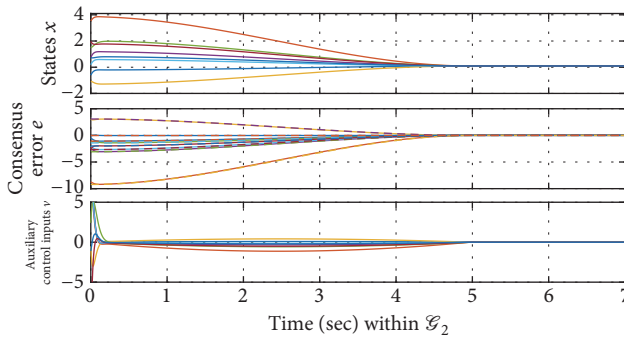


FIGURE 3: Predefined-time TBG-tracking controller (16) for  $\mathcal{S}_2$  and uncertainty in the initial state. In the error trajectories, the continuous lines represent the evolution of the errors whereas the TBG reference is drawn with dash line. The convergence time is preset to 5 sec., and the consensus value is  $\gamma^T x_0 = 0.0946$ .

In the case where the uncertainty  $\mathbf{d}$  in the initial state is considered (Figure 3), the second term of  $v_i$  in (16) is not initially null to compensate the deviation from the reference given by the TBG. It can be seen in Figure 3 (middle and bottom) that the consensus errors do not initiate over the references and consequently the auxiliary controls are not null at  $t = 0$ .

**4.2. Comparison with Others Approaches.** In this subsection, first, we compare the proposed control law (16) with other predefined-time control protocols [30–32]. As described in Section 1, to the authors' knowledge, these are the existing approaches that solve the problem of predefined-time convergence. Each one of these works refers to their proposal with a different adjective: preset-time consensus [30], prescribed-time consensus [31], and specified-time consensus [32]. We can see in Figures 4–6 that consensus is achieved by using any of these approaches. We have to say that the control protocols of [30, 31] are very similar; both of them are based on the use of a time-varying control gain. Between their similarities, we can see in Figures 4 and 5 the large initial value of the auxiliary control inputs. This is also the case for the specified-time consensus [32] of Figure 6. Notice that the auxiliary control inputs of the TBG-based controller, shown

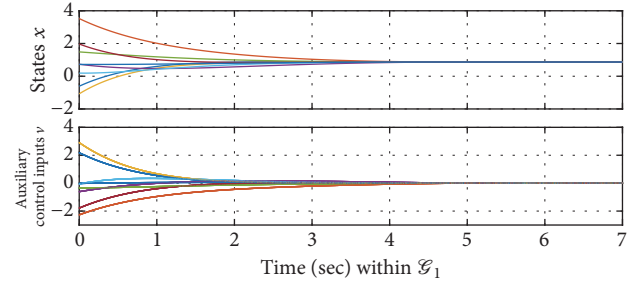


FIGURE 4: Preset-time controller [30] for  $\mathcal{S}_1$ . The convergence time is preset to 5 sec., and the consensus value is  $\sum_{i=1}^N x_i(0)/N = 0.8676$ .

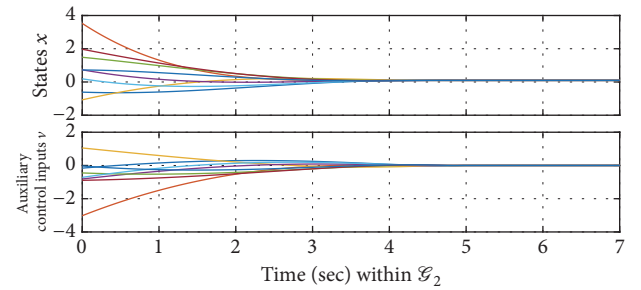


FIGURE 5: Prescribed-time controller [31] for  $\mathcal{S}_2$ . The convergence time is preset to 5 sec., and the consensus value is 0.0946.

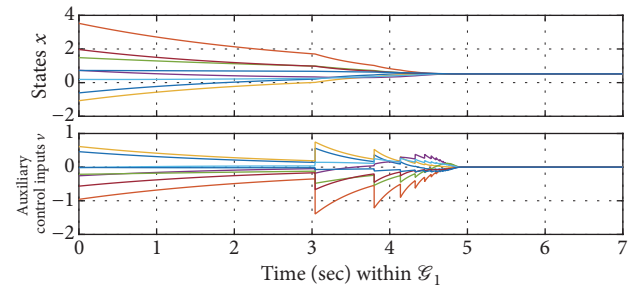


FIGURE 6: Specified-time controller [32] for  $\mathcal{S}_1$ . The convergence time is preset to 5 sec., and the consensus value is 0.5196.

in Figure 2, started in zero and were smoother and of lower magnitude compared to the large initial auxiliary control effort of the other predefined-time consensus approaches.

Additionally, we can see that the specified-time consensus protocol in Figure 6 generates discontinuities in the auxiliary inputs along the time, according to its planned switching strategy. Moreover, although this consensus approach was tested on the undirected graph  $\mathcal{S}_1$ , the consensus value is not the average of the initial state as one could expect.

Following the comparison, we evaluate the TBG controller (16) and different finite-time, fixed-time, and predefined-time consensus protocols reported in the literature, by applying the protocols to the MAS with the communication topologies  $\mathcal{S}_1$  and  $\mathcal{S}_2$ . In particular, the protocols in [20, 48] ensure finite-time convergence, and the one proposed in [27] guarantees fixed-time convergence. The predefined-time protocols [30–32] and the proposed

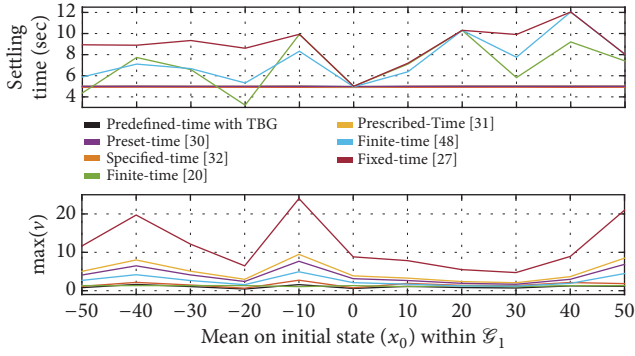


FIGURE 7: Comparison of the TBG-tracking controller (16) with other approaches for  $\mathcal{S}_1$ . Top: settling time as a function of the initial condition  $\mathbf{x}_0$ . Bottom: maximum value of the auxiliary control input as a function of the initial condition  $\mathbf{x}_0$ .

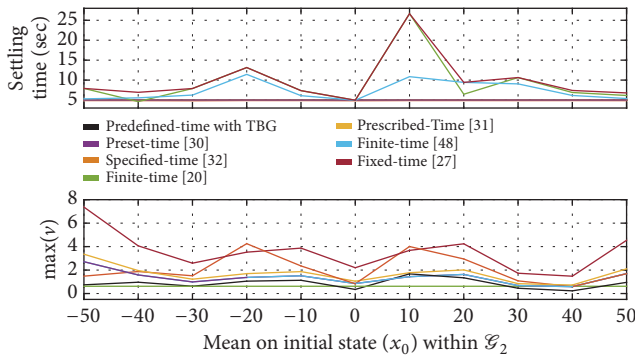


FIGURE 8: Comparison of the TBG-tracking controller (16) with other approaches for  $\mathcal{S}_2$ . Top: settling time as a function of the initial condition  $\mathbf{x}_0$ . Bottom: maximum value of the auxiliary control input as a function of the initial condition  $\mathbf{x}_0$ .

TBG-tracking controller (16) achieve predefined-time convergence. The finite-time and fixed-time controllers were tuned to achieve a similar convergence time around the 5 seconds of predefined time, from the initial condition  $\mathbf{x}_0$ . Then, several simulations were performed for different initial states of the form  $\alpha\mathbf{x}_0$ , where  $\alpha$  was varying in such a way that the mean of  $\alpha\mathbf{x}_0$  ranges from  $-50$  to  $50$ . The same control gains were used in all the experiments. Finally, for every experiment, the convergence time of the system, defined as the time at which  $\|\mathbf{e}\| < 1 \times 10^{-4}$ , was measured; similarly, the maximum absolute value of the auxiliary control input  $\mathbf{v}$  was recorded.

The results are shown in Figures 7 and 8, where it can be observed that the proposed TBG-based control (16) and the other predefined-time controllers [30–32] are able to maintain the same convergence time for all the initial conditions. Furthermore, note that the maximum auxiliary control efforts were lower for both the TBG-based control and the finite-time control [20]. The last control law is of the form  $k \text{sign}(\bullet)$ . In particular, the consensus protocols [30, 31] explicitly include a parameter that must be set accordingly to an eigenvalue of the Laplacian matrix, which depends on the connectivity of the graph considered. This is not the case

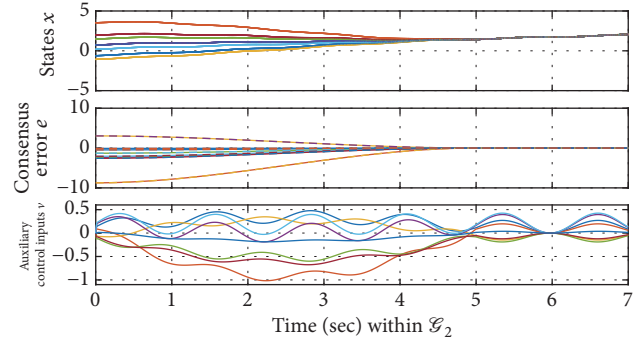


FIGURE 9: Predefined-time TBG-tracking controller (16), which is not robust for perturbed dynamics and  $\mathcal{S}_2$ .

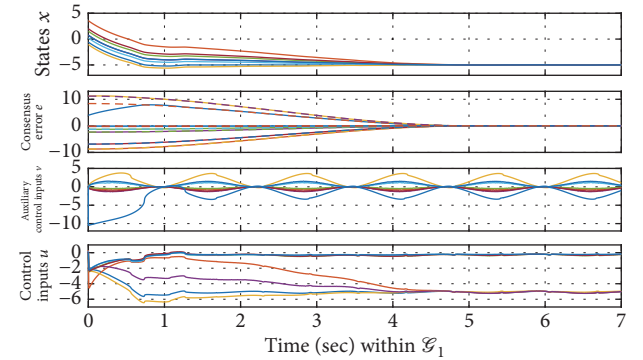


FIGURE 10: Robust predefined-time TBG controller (37) for perturbed systems and  $\mathcal{S}_1$ . In the error trajectories, the continuous lines represent the evolution of the errors whereas the TBG reference is drawn with dash line. The convergence time is preset to 5 sec.

for the proposed control protocols. Therefore, the simulations show that the proposed TBG protocol (16) represents an advantage not only in the possibility to define a settling time but also in providing smooth and efficient control actions.

**4.3. Robust Predefined-Time Consensus.** All the previous simulations considered ideal dynamics in (3), i.e.,  $\rho_i(t) = 0$  for all the agents. In fact, the TBG-tracking controller (16) is not able to deal with matched bounded disturbances. For instance, Figure 9 shows the MAS with the topology  $\mathcal{S}_2$  under this protocol and matching perturbations  $\rho_i(t) = \alpha_i(1 + 1 \sin(5t))$ , with  $\alpha_i$  randomly selected in  $(0, 0.5)$ . It can be observed that the state of the MAS does not establish in a consensus value due to the perturbation. A similar behavior can be obtained with the other existing predefined-time consensus protocols [30–32].

In order to deal with the described matching perturbations  $\rho_i(t) = \alpha_i(1 + 1 \sin(5t))$ , the proposed robust predefined-time TBG controller (37) has to be used. For this, a leader is defined with dynamics (33), having communication only with the first follower agent, i.e.,  $b_1 = 1$  and  $b_i = 0, \forall i = \{2, \dots, 8\}$ . The gains of the robust controller (37) were set as  $k_1 = 5$  and  $k_2 = 5$ ; and the leader's state was maintained constant and equal to  $x_l(t) = -5$  by setting its control input as  $u_l = 0$ . Figures 10 and 11 show the results obtained when the

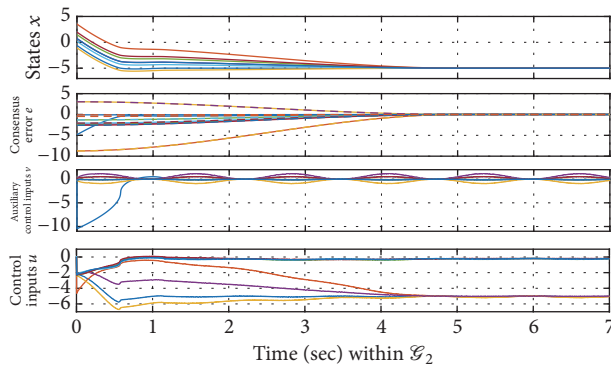


FIGURE 11: Robust predefined-time TBG controller (37) for perturbed systems and  $\mathcal{E}_2$ . In the error trajectories, the continuous lines represent the evolution of the errors whereas the TBG reference is drawn with dash line. The convergence time is preset to 5 sec.

communication between the followers is described by  $\mathcal{E}_1$  and  $\mathcal{E}_2$ , respectively. Notice that the error trajectories are driven to zero in the predefined time  $t_f = 5$ , while the control input keeps oscillating after  $t_f$  in order to reject the disturbance  $\rho(t)$ .

## 5. Conclusions

In this paper, a couple of predefined-time consensus protocols for first-order nonlinear MAS under both undirected and directed communication topologies have been proposed. In these protocols, the convergence time to achieve consensus can be set by the user, and it is independent of the initial state conditions. For this, the TBG (time base generator) is combined with feedback controllers to achieve closed-loop stability and robustness. In particular, one protocol uses the super-twisting controller to deal with perturbations. The performance of the proposed controllers has been compared with existing finite-time, fixed-time, and predefined-time controllers through simulations. The results have shown that the proposed protocols achieve consensus in the predefined time, independently of the initial conditions, and exhibit closed-loop stability. Moreover, a benefit of the proposed controllers is that they yield smoother control signals with smaller magnitude than the existing approaches reported in the literature. Furthermore, the proposed schemes can reach predefined-time consensus even when there exists uncertainty in the knowledge of the initial conditions, and the super-twisting protocol is robust against matching perturbations.

Future works will focus on extending the results presented in this paper to the case of high-order nonlinear MAS, as well as in considering the predefined-time consensus problem in Markovian jump topologies [4, 5].

## Data Availability

The paper is a theoretical result on consensus with predefined-time convergence. All proofs are presented, and simulations are provided to illustrate the result. In the

authors' opinion, there is no need to provide the numerical experiments; simulations can be provided and made available under request.

## Conflicts of Interest

The authors declare that there are no conflicts of interest regarding the publication of this manuscript.

## Acknowledgments

The first two authors were supported in part by Conacyt [grant No. 220796]. The authors would also like to acknowledge the partial support of Intel Corporation for the development of this work.

## References

- [1] F. Jiang and L. Wang, "Finite-time information consensus for multi-agent systems with fixed and switching topologies," *Physica D: Nonlinear Phenomena*, vol. 238, no. 16, pp. 1550–1560, 2009.
- [2] R. Olfati-Saber and R. M. Murray, "Consensus problems in networks of agents with switching topology and time-delays," *IEEE Transactions on Automatic Control*, vol. 49, no. 9, pp. 1520–1533, 2004.
- [3] A. Arenas, A. D. Guilera, J. Kurths, Y. Moreno, and C. Zhou, "Synchronization in complex networks," *Physics Reports*, vol. 469, no. 3, pp. 93–153, 2008.
- [4] H. Shen, J. H. Park, Z.-G. Wu, and Z. Zhang, "Finite-time  $H_\infty$  synchronization for complex networks with semi-Markov jump topology," *Communications in Nonlinear Science and Numerical Simulation*, vol. 24, no. 1–3, pp. 40–51, 2015.
- [5] H. Shen, S. Huo, J. Cao, and T. Huang, "Generalized state estimation for Markovian coupled networks under round-robin protocol and redundant channels," *IEEE Transactions on Cybernetics*, pp. 1–10, 2018.
- [6] R. Olfati-Saber, "Flocking for multi-agent dynamic systems: algorithms and theory," *IEEE Transactions on Automatic Control*, vol. 51, no. 3, pp. 401–420, 2006.
- [7] K.-K. Oh, M.-C. Park, and H.-S. Ahn, "A survey of multi-agent formation control," *Automatica*, vol. 53, pp. 424–440, 2015.
- [8] W. Ren, "Distributed attitude alignment in spacecraft formation flying," *International Journal of Adaptive Control and Signal Processing*, vol. 21, no. 2–3, pp. 95–113, 2007.
- [9] Y. Xu, G. Yan, K. Cai, and Z. Lin, "Fast centralized integer resource allocation algorithm and its distributed extension over digraphs," *Neurocomputing*, vol. 270, pp. 91–100, 2017.
- [10] Y. Xu, T. Han, K. Cai, Z. Lin, G. Yan, and M. Fu, "A distributed algorithm for resource allocation over dynamic digraphs," *IEEE Transactions on Signal Processing*, vol. 65, no. 10, pp. 2600–2612, 2017.
- [11] D. Gómez-Gutiérrez and R. De La Guardia, "Chaotic-based synchronization for secure network communications, US Patent 9438422B2," 2016.
- [12] L. Wang and F. Xiao, "Finite-time consensus problems for networks of dynamic agents," *IEEE Transactions on Automatic Control*, vol. 55, no. 4, pp. 950–955, 2010.
- [13] Z. Zuo and L. Tie, "A new class of finite-time nonlinear consensus protocols for multi-agent systems," *International Journal of Control*, vol. 87, no. 2, pp. 363–370, 2014.

- [14] D. Gómez-Gutiérrez, J. Ruiz-León, S. Celikovsky, and J. D. Sánchez-Torres, "A finite-time consensus algorithm with simple structure for fixed networks," *Computación y Sistemas*, vol. 22, no. 2, 2018.
- [15] R. Olfati-Saber, J. A. Fax, and R. M. Murray, "Consensus and cooperation in networked multi-agent systems," *Proceedings of the IEEE*, vol. 95, no. 1, pp. 215–233, 2007.
- [16] W. Ren and R. W. Beard, *Distributed Consensus in Multi-Vehicle Cooperative Control*, Springer, 2008.
- [17] K. Cai and H. Ishii, "Average consensus on arbitrary strongly connected digraphs with time-varying topologies," *Institute of Electrical and Electronics Engineers Transactions on Automatic Control*, vol. 59, no. 4, pp. 1066–1071, 2014.
- [18] Z. Li and Z. Duan, *Cooperative Control of Multi-Agent Systems: A Consensus Region Approach*, CRC Press, Boca Raton, Fla, USA, 2014.
- [19] H. Sayyaadi and M. R. Doostmohammadian, "Finite-time consensus in directed switching network topologies and time-delayed communications," *Scientia Iranica*, vol. 18, no. 1, pp. 75–85, 2011.
- [20] M. Franceschelli, A. Giua, A. Pisano, and E. Usai, "Finite-time consensus for switching network topologies with disturbances," *Nonlinear Analysis: Hybrid Systems*, vol. 10, pp. 83–93, 2013.
- [21] J. Cortés, "Finite-time convergent gradient flows with applications to network consensus," *Automatica*, vol. 42, no. 11, pp. 1993–2000, 2006.
- [22] M. Franceschelli, A. Giua, and A. Pisano, "Finite-time consensus on the median value with robustness properties," *Institute of Electrical and Electronics Engineers Transactions on Automatic Control*, vol. 62, no. 4, pp. 1652–1667, 2017.
- [23] B. Liu, W. Lu, and T. Chen, "Consensus in continuous-time multiagent systems under discontinuous nonlinear protocols," *IEEE Transactions on Neural Networks and Learning Systems*, vol. 26, no. 2, pp. 290–301, 2015.
- [24] Y.-K. Zhu, X.-P. Guan, and X.-Y. Luo, "Finite-time consensus for multi-agent systems via nonlinear control protocols," *International Journal of Automation and Computing*, vol. 10, no. 5, pp. 455–462, 2013.
- [25] Y. Shang, "Finite-time consensus for multi-agent systems with fixed topologies," *International Journal of Systems Science*, vol. 43, no. 3, pp. 499–506, 2012.
- [26] S. E. Parsegov, A. E. Polyakov, and P. S. Shcherbakov, "Fixed-time consensus algorithm for multi-agent systems with integrator dynamics," in *Proceedings of the 4th IFAC Workshop on Distributed Estimation and Control in Networked Systems, NecSys 2013*, pp. 110–115, September 2013.
- [27] Z. Zuo, Q. L. Han, B. Ning, X. Ge, and X. M. Zhang, "An overview of recent advances in fixed-time cooperative control of multiagent systems," *IEEE Transactions on Industrial Informatics*, vol. 14, no. 6, pp. 2322–2334, 2018.
- [28] E. Cruz-Zavala, J. A. Moreno, and L. Fridman, "Uniform Second-Order Sliding Mode Observer for mechanical systems," in *Proceedings of the 2010 11th International Workshop on Variable Structure Systems, VSS 2010*, pp. 14–19, Mexico, June 2010.
- [29] A. Polyakov, "Nonlinear feedback design for fixed-time stabilization of linear control systems," *IEEE Transactions on Automatic Control*, vol. 57, no. 8, pp. 2106–2110, 2012.
- [30] C. Yong, X. Guangming, and L. Huiyang, "Reaching consensus at a preset time: single-integrator dynamics case," in *Proceedings of the 31st Chinese Control Conference (CCC)*, pp. 6220–6225, IEEE, 2012.
- [31] Y. Wang, Y. Song, D. J. Hill, and M. Krstic, "Prescribed-time consensus and containment control of networked multiagent systems," *IEEE Transactions on Cybernetics*, 2018.
- [32] Y. Zhao and Y. Liu, "Specified-time consensus for multi-agent systems," in *Proceedings of the 2017 Chinese Automation Congress (CAC)*, pp. 732–737, Jinan, October 2017.
- [33] Y. Liu, Y. Zhao, W. Ren, and G. Chen, "Appointed-time consensus: accurate and practical designs," *Automatica*, vol. 89, pp. 425–429, 2018.
- [34] J. A. Colunga, C. R. Vázquez, H. M. Becerra, and D. Gómez-Gutiérrez, "Predefined-time consensus using a time base generator (TBG)," in *Proceedings of the IFAC Second Conference on Modelling, Identification and Control of Nonlinear Systems (MICNON)*, vol. 51, pp. 246–253, 2018.
- [35] H. M. Becerra, C. R. Vazquez, G. Arechavaleta, and J. Delfin, "Predefined-time convergence control for high-order integrator systems using time base generators," *IEEE Transactions on Control Systems Technology*, vol. 26, no. 5, pp. 1866–1873, 2018.
- [36] H. K. Khalil and J. W. Grizzle, *Nonlinear Systems*, vol. 3, Prentice Hall, New Jersey, NJ, USA, 2002.
- [37] Q. Ma, S. Xu, F. L. Lewis, B. Zhang, and Y. Zou, "Cooperative output regulation of singular heterogeneous multiagent systems," *IEEE Transactions on Cybernetics*, vol. 46, no. 6, pp. 1471–1475, 2016.
- [38] Q. Ma, "Cooperative control of multi-agent systems with unknown control directions," *Applied Mathematics and Computation*, vol. 292, pp. 240–252, 2017.
- [39] A. H. Roger and R. J. Charles, *Matrix Analysis*, Cambridge University Press, New York, NY, USA, 2nd edition, 2013.
- [40] W. Yu, G. Wen, G. Chen, and J. Cao, *Distributed Cooperative Control of Multi-agent Systems*, John Wiley and Sons, 2016.
- [41] Z. Li and Z. Duan, "Distributed consensus protocol design for general linear multi-agent systems: a consensus region approach," *IET Control Theory & Applications*, vol. 8, no. 18, pp. 2145–2161, 2014.
- [42] Z. Li, Z. Duan, G. Chen, and L. Huang, "Consensus of multiagent systems and synchronization of complex networks: a unified viewpoint," *IEEE Transactions on Circuits and Systems I: Regular Papers*, vol. 57, no. 1, pp. 213–224, 2010.
- [43] G. Jarquín, G. Arechavaleta, and V. Parra-Vega, "Time parametrization of prioritized inverse kinematics based on terminal attractors," in *Proceedings of the 2011 IEEE/RSJ International Conference on Intelligent Robots and Systems: Celebrating 50 Years of Robotics, IROS'11*, pp. 1612–1617, USA, September 2011.
- [44] M. Braun, *Differential Equations and Their Applications: An Introduction to Applied Mathematics*, vol. 11, Springer Science and Business Media, Third edition, 1983.
- [45] H. K. Khalil and J. Grizzle, *Nonlinear systems*, vol. 3, Prentice hall, Upper Saddle River, New Jersey, NJ, USA, 2002.
- [46] J. A. Moreno and M. Osorio, "Strict Lyapunov functions for the super-twisting algorithm," *IEEE Transactions on Automatic Control*, vol. 57, no. 4, pp. 1035–1040, 2012.
- [47] S. Mondal, R. Su, and L. Xie, "Heterogeneous consensus of higher-order multi-agent systems with mismatched uncertainties using sliding mode control," *International Journal of Robust and Nonlinear Control*, vol. 27, no. 13, pp. 2303–2320, 2017.
- [48] Y. Cao and W. Ren, "Finite-time consensus for multi-agent networks with unknown inherent nonlinear dynamics," *Automatica*, vol. 50, no. 10, pp. 2648–2656, 2014.

## Research Article

# On Leaderless and Leader-Following Consensus for Heterogeneous Nonlinear Multiagent Systems via Discontinuous Distributed Control Protocol

Fei Wang <sup>1</sup> and Yongqing Yang<sup>2</sup>

<sup>1</sup>*School of Mathematical Sciences, Qufu Normal University, Qufu 273165, Shandong Province, China*

<sup>2</sup>*School of Science, Jiangnan University, Wuxi 214122, Jiangsu Province, China*

Correspondence should be addressed to Fei Wang; [fei\\_9206@163.com](mailto:fei_9206@163.com)

Received 14 July 2018; Revised 6 September 2018; Accepted 16 September 2018; Published 4 October 2018

Academic Editor: Ju H. Park

Copyright © 2018 Fei Wang and Yongqing Yang. This is an open access article distributed under the Creative Commons Attribution License, which permits unrestricted use, distribution, and reproduction in any medium, provided the original work is properly cited.

This paper is concerned with consensus of heterogeneous nonlinear multiagent systems via distributed control. Both the cases of leaderless and leader-following are systematically investigated. Different from some existing results, completed consensus can be reached in this paper among heterogeneous multiagent network instead of bounded-consensus. First, a novel distributed control protocol is proposed, and some general consensus criteria are derived for multiagent systems without leader. Second, a leader with unknown but bounded input for the heterogeneous multiagent network is considered; aperiodically intermittent communications among followers are considered to avoid channel blocking in this case. Finally, two simulation examples are presented to verify the effectiveness of the main results.

## 1. Introduction

In recent years, distributed coordinated control of multiagent systems has been widely studied due to its easy implementation, strong robustness, and high self-organizability. There were many applications of multiagent systems in the field of robotic systems, UAVs (unmanned air vehicles), wireless sensor networks, and so on [1–4]. As a hot topic of multiagent systems, consensus has attracted great attention in systems and control theory. Many papers have been concerned with consensus problem of multiagent systems, in which, consensus can be reached among multiagent systems via sufficient local information exchanges between agents and their neighbors; one can see [5–11] and references therein.

There were two kinds of consensus named leaderless consensus and leader-following consensus, respectively. It is called leaderless consensus problem if there is no specified leader in the multiagent systems; it is called leader-following consensus problem otherwise. Both leaderless consensus and leader-following consensus have gotten many results recently. For example, distributed leaderless consensus algorithms for networked Euler-Lagrange systems have been investigated

in [12]. Reference [13] has studied leaderless consensus problem of a group of mobile agents interconnected by a star-like topology. On the other hand, leader-following consensus of multiagent systems has been considered in [14], in which both fixed and switching topologies have been considered. Based on  $M$ -matrix strategies, pinning-controlled leader-following consensus in multiagent systems has been discussed in [15]. More results about leaderless consensus or leader-following consensus can be seen in [16–20] and references therein. In general, the leader-following consensus problem could be translated into the stability problem of error systems. There were many theoretical tools and results about the analysis of the stability of dynamical systems [21–24]. To deal with the leaderless consensus problem, a virtual leader is often introduced or some matrix analysis techniques are used.

Note that the majority of above publications were concerned with identical systems. However, heterogeneous dynamic networks widely existed in real world, in which, each agent may have different parameters. A heterogeneous multiagent network cannot force consensus by static linear controllers. Thus, more results about heterogeneous dynamic networks were concerned with quasi-consensus (also named

bounded-consensus). For example, [25] investigates the bounded-consensus problem for cooperative heterogeneous agents with nonlinear dynamics in a directed communication network. Quasi-synchronization of heterogeneous dynamic networks via distributed impulsive control have been studied in [26]. More recently, quasi-synchronization is investigated for heterogeneous complex networks with switching sequentially disconnected topology in [27]. To the best of our knowledge, few literature works have appeared concerning the problems of complete consensus among heterogeneous multiagent systems, which provides the motivation of the current study. Note that nonlinearity is inescapable in real world systems [28–30]. The dynamics analysis of nonlinear systems has gotten many results [31–36], even to the nonlinear fractional order systems [37, 38]. Thus, nonlinear multiagent systems would be considered in this paper.

In this paper, we investigated both leaderless and leader-following consensus in a heterogenous network environment. The contributions of this paper are as follows: First, based a novel discontinuous distributed control protocol, the leaderless consensus has been reached under some simple conditions. Then, under the analysis method, the leader-following consensus also has been studied, in which case, the communication among followers is aperiodically intermittent. Most of the existing results about consensus for the heterogeneous multiagent systems have adopted the adaptive strategy; one can see [39–42] and references therein. Compared with some existing results, the control protocol in this paper is static, which may be easier to implement.

The rest of the paper is organized as follows: In Section 2, we introduce some definitions and some lemmas which are necessary for presenting our results in the following. The main results about leaderless consensus and leader-following consensus of heterogenous multiagents are presented in Section 3. Then, some examples are given to demonstrate the effectiveness of our results in Section 4. Conclusions are finally drawn in Section 5.

*Notations.* In this paper,  $\mathbb{R}^n$  denotes the set of all  $n$ -dimensional column vectors. Let  $I_n$  be  $n$ -dimensional identity matrix. For any  $x \in \mathbb{R}^n$ ,  $\|x\|_1 = \sum_{i=1}^n |x_i|$ ,  $\|x\| = \sqrt{\sum_{i=1}^n x_i^2}$ ,  $\text{sign}(x) = [\text{sign}(x_1), \text{sign}(x_2), \dots, \text{sign}(x_n)]^T \in \mathbb{R}^n$ , where  $\text{sign}(x_i) = 1$  when  $x_i > 0$ ,  $\text{sign}(x_i) = -1$  when  $x_i < 0$ ; otherwise  $\text{sign}(x_i) = 0$ . For a square matrix  $A \in \mathbb{R}^{m \times n}$ , let  $\|A\| = \sqrt{\sum_{i=1}^m \sum_{j=1}^n a_{ij}^2}$ ,  $A^T$  be its transpose, and  $\lambda_{\max}(A)$  and  $\lambda_{\min}(A)$  be the maximum and minimum eigenvalues of  $A$ , respectively.  $\otimes$  denotes Kronecker product.

## 2. Preliminaries

Considering the following heterogeneous multiagent system consisting of  $N$  agents, the dynamical behavior of  $i$ th agent is described as

$$\dot{x}_i(t) = A_i x_i(t) + B_i f(x_i(t)) + u_i(t), \quad (1)$$

where  $x_i(t) \in \mathbb{R}^n$  denotes the state of  $i$ th agent,  $f(x_i(t)) = [f_1(x_i(t)), f_2(x_i(t)), \dots, f_n(x_i(t))]^T \in \mathbb{R}^n$  is a nonlinear

function,  $u_i(t)$  is control input would be given later, and  $A_i$  and  $B_i$  are constant matrix.

Throughout this paper, the following assumption of nonlinear function  $f(\cdot)$  should be satisfied for the system.

*Assumption 1.* For the nonlinear function  $f(\cdot)$ , there exist constants  $l_{ij}^f \geq 0$ ,  $i, j = 1, 2, \dots, n$ , such that, for any  $x, y \in \mathbb{R}^n$ ,

$$|f_i(x) - f_i(y)| \leq \sum_{j=1}^n l_{ij}^f |x_j - y_j|. \quad (2)$$

*Remark 2.* Let  $L_f = (l_{ij}^f)_{n \times n}$ . Then, for any diagonal matrices  $\Lambda_f > 0$ , this assumption implies that  $(x - y)^T L_f^T \Lambda_f L_f (x - y) \geq (f(x) - f(y))^T \Lambda_f (f(x) - f(y))$ . And note that a lot of systems can be satisfied, such as Chua's circuit and some chaotic neural networks.

To get our main results, some preliminaries of graph would be given. Let  $\mathcal{G} = \{\Delta, E, W\}$  be a undirected graph of order  $N$ , where  $\Delta = \{v_1, v_2, \dots, v_N\}$ ,  $E \subseteq \Delta \times \Delta$  denote the set of nodes and edges, respectively. For any  $i$ ,  $a_{ii} = 0$ .  $e_{ij} = (v_i, v_j) \in E$  is an edge from  $i$  to  $j$ , where  $i \neq j$ , which means that  $v_j$  can receive message from  $v_i$ .  $v_i$  is a neighbor of  $v_j$  if  $e_{ij} \in E$ . The set of all neighbors of  $v_i$  can be denoted as  $\mathcal{N}_i = \{v_j : e_{ij} \in E, j = 1, 2, \dots, N\}$ .  $A = \{a_{ij}\} \in \mathbb{R}^{N \times N}$  denotes weighted adjacency matrix, where  $a_{ij}$  is weight which is satisfied  $a_{ij} = a_{ji} \neq 0$  if  $e_{ij} \in E$  and  $a_{ij} = 0$  otherwise. We assume  $a_{ii} = 0$  for all  $i = 1, 2, \dots, N$ .

*Assumption 3.* The topological structure is undirected in this paper, and the undirected communication graph is connected.

## 3. Main Results

*3.1. Leaderless Consensus of Heterogeneous Multiagent System.* This subsection considers the leaderless case; without loss of generality, define the state error as  $e_i(t) = x_{i+1}(t) - x_1(t)$ , for  $i = 1, 2, \dots, N - 1$ ; then, one has

$$\begin{aligned} \dot{e}_i(t) &= A_{i+1} x_{i+1}(t) - A_1 x_1(t) + B_{i+1} f(x_{i+1}(t)) \\ &\quad - B_1 f(x_1(t)) + u_{i+1}(t) - u_1(t). \end{aligned} \quad (3)$$

In this case,  $u_i(t)$  is designed as

$$u_i(t) = -c \sum_{j=1}^N l_{ij} x_j(t) - c \hat{d}_i \text{sign}(x_i(t) - x_1(t)), \quad (4)$$

where the Laplacian matrix  $L = (l_{ij})_{N \times N}$  is associated with the adjacency matrix  $\mathcal{A} = (a_{ij})_{N \times N}$  defined by the following.

$$l_{ij} = \begin{cases} -a_{ij} & \text{for } i \neq j \\ \sum_{j=1, j \neq i}^N a_{ij} & \text{for } i = j \end{cases} \quad (5)$$

By some simple derivations, one can get the following error dynamic equation for  $i = 1, 2, \dots, N-1$ :

$$\begin{aligned} \dot{e}_i(t) &= A_{i+1}e_i(t) + B_{i+1}h(e_i(t)) + w_{i+1}(x_1(t)) \\ &\quad - c \sum_{j=1}^N (l_{i+1,j} - l_{1j}) x_j(t) - c\hat{d}_{i+1} \text{sign}(e_i(t)), \end{aligned} \quad (6)$$

where  $h(e_i(t)) = f(x_{i+1}(t)) - f(x_1(t))$ ,  $w_i(x_1(t)) = (A_i - A_1)x_1(t) + (B_i - B_1)f(x_1(t))$ . Let  $\hat{L} = (\hat{l}_{ij})_{N \times N}$  and  $\hat{l}_{ij} = l_{i+1,j+1} - l_{1,j+1}$  for  $i, j = 1, 2, \dots, N-1$ ; one has  $\sum_{j=1}^{N-1} \hat{l}_{ij} = l_{11} - l_{i+1,1}$  for  $i = 1, 2, \dots, N-1$ ; then, we have  $\sum_{j=1}^N (l_{i+1,j} - l_{1j})x_j(t) = \sum_{j=1}^{N-1} \hat{l}_{ij}e_j(t)$  and thus the error equation can be rewritten as

$$\begin{aligned} \dot{e}_i(t) &= A_{i+1}e_i(t) + B_{i+1}h(e_i(t)) + w_{i+1}(x_1(t)) \\ &\quad - c \sum_{j=1}^{N-1} \hat{l}_{ij}e_j(t) - c\hat{d}_{i+1} \text{sign}(e_i(t)). \end{aligned} \quad (7)$$

The following assumption needs to be satisfied in this subsection.

*Assumption 4.* The  $x_1(t)$  is bounded; i.e., for any initial  $x_1(t_0)$ , there exists  $T$ , such that  $\|x_1(t)\| \leq \delta$ ,  $t \geq T$ , where  $\delta$  is a positive constant. Furthermore, with Assumption 1, one has that  $w_i(x_1(t))$  is also bounded; i.e.,  $\|w_i(x_1(t))\| \leq \varepsilon_i$ ,  $t \geq T$ , where  $\varepsilon_i$  is a positive constant.

**Theorem 5.** Under Assumptions 1, 3, and 4, the leaderless consensus of the heterogeneous multiagent system could be achieved if there exist positive definite diagonal matrix  $P$  and constants  $\alpha > 0$ ,  $\beta > 0$  such that

$$\hat{d}_{i+1} \geq \frac{\|P\|(\varepsilon_{i+1})}{c\lambda_{\min}(P)}; \quad (8)$$

$$\begin{bmatrix} PA_{i+1} + A_{i+1}^T P + L_f^T \Lambda_f L_f & PB_{i+1} \\ PB_{i+1} & -\Lambda_f \end{bmatrix} < \begin{bmatrix} \alpha P & 0 \\ 0 & 0 \end{bmatrix}; \quad (9)$$

$$(\alpha + \beta)I_{N-1} < 2c\hat{L}; \quad (10)$$

for  $i = 1, 2, \dots, N-1$ , where matrices  $\Lambda_f$  and  $L_f$  have been mentioned in Remark 2.

*Proof.* Choose a Lyapunov function as  $V(t) = (1/2) \sum_{i=1}^{N-1} e_i^T(t) P e_i(t)$ ; taking the time derivative of  $V(t)$  along the trajectories of (7), one obtains the following.

$$\begin{aligned} \dot{V}(t) &= \sum_{i=1}^{N-1} e_i^T(t) P \dot{e}_i(t) = \sum_{i=1}^{N-1} e_i^T(t) P \left\{ A_{i+1}e_i(t) \right. \\ &\quad + B_{i+1}h(e_i(t)) + w_{i+1}(x_1(t)) - c \sum_{j=1}^{N-1} \hat{l}_{ij}e_j(t) \\ &\quad \left. - c\hat{d}_{i+1} \text{sign}(e_i(t)) \right\} \leq \frac{1}{2} \end{aligned}$$

$$\cdot \sum_{i=1}^{N-1} e_i^T(t) (PA_{i+1} + A_{i+1}^T P) e_i(t)$$

$$\begin{aligned} &+ \sum_{i=1}^{N-1} e_i^T(t) PB_{i+1}h(e_i(t)) \\ &+ \sum_{i=1}^{N-1} e_i^T(t) Pw_{i+1}(x_1(t)) - c \sum_{i=1}^{N-1} e_i^T(t) P \sum_{j=1}^{N-1} \hat{l}_{ij}e_j(t) \\ &- c \sum_{i=1}^{N-1} \hat{d}_{i+1} e_i^T(t) P \text{sign}(e_i(t)) \end{aligned} \quad (11)$$

Based on Cauchy inequality (i.e.,  $(\sum_{i=1}^n a_k b_k)^2 \leq \sum_{i=1}^n a_k^2 \sum_{i=1}^n b_k^2$ ) and the definition of the function  $\text{sign}(\cdot)$ , noting that  $P$  is a positive definite diagonal matrix, it is easy to get

$$\begin{aligned} -c\hat{d}_{i+1} e_i^T(t) P \text{sign}(e_i(t)) &= -c\hat{d}_{i+1} \sum_{j=1}^n p_j |e_{ij}(t)| \\ &\leq -c\hat{d}_{i+1} \lambda_{\min}(P) \|e_i(t)\|_1 \end{aligned} \quad (12)$$

$$\leq -c\hat{d}_{i+1} \lambda_{\min}(P) \|e_i(t)\|,$$

$$e_i^T(t) Pw_{i+1}(x_1(t)) \leq \varepsilon_{i+1} \|P\| \|e_i(t)\|.$$

According to Remark 2 and (12), we have

$$\begin{aligned} \dot{V}(t) &\leq \frac{1}{2} \\ &\cdot \sum_{i=1}^{N-1} e_i^T(t) (PA_{i+1} + A_{i+1}^T P + L_f^T \Lambda_f L_f) e_i(t) - \frac{1}{2} \\ &\cdot \sum_{i=1}^{N-1} h^T(e_i(t)) \Lambda_f h(e_i(t)) \\ &+ \sum_{i=1}^{N-1} e_i^T(t) PB_{i+1}h(e_i(t)) \\ &+ \sum_{i=1}^{N-1} \left( \varepsilon_{i+1} - c\hat{d}_{i+1} \frac{\lambda_{\min}(P)}{\|P\|} \right) \|P\| \|e_i(t)\| - ce^T(t) \end{aligned} \quad (13)$$

$$\cdot (\hat{L} \otimes P) e(t) = \frac{1}{2} \sum_{i=1}^{N-1} [e_i^T(t), h^T(e_i(t))]$$

$$\cdot \begin{bmatrix} PA_{i+1} + A_{i+1}^T P + L_f^T \Lambda_f L_f & PB_{i+1} \\ PB_{i+1} & -\Lambda_f \end{bmatrix} \begin{bmatrix} e_i(t) \\ h(e_i(t)) \end{bmatrix}$$

$$+ \sum_{i=1}^{N-1} \left( \varepsilon_{i+1} - c\hat{d}_{i+1} \frac{\lambda_{\min}(P)}{\|P\|} \right) \|P\| \|e_i(t)\| - ce^T(t)$$

$$\cdot (\hat{L} \otimes P) e(t),$$

where  $e(t) = [e_1^T(t), e_2^T(t), \dots, e_{N-1}^T(t)]^T$ . Then, according to (8), (9), and (10), we have

$$\dot{V}(t) \leq e^T(t) \left( \left( \frac{\alpha}{2} I_{N-1} - c\hat{L} \right) \otimes P \right) e(t) \leq -\beta V(t). \quad (14)$$

This completes the proof.  $\square$

3.2. *Leader-Following Consensus with Aperiodically Intermittent Communication.* The leader with unknown input is described as

$$\dot{x}_0(t) = A_0 x_0(t) + B_0 f(x_0(t)) + u_0(t), \quad (15)$$

where  $u_0(t)$  is unknown input.  $u_i(t)$  in this case is designed as

$$u_i(t) = \begin{cases} -c \sum_{j=1}^N l_{ij} x_j(t) - cd_i (x_i(t) - x_0(t)) - c\hat{d}_i \text{sign}(x_i(t) - x_0(t)) & \text{for } t \in [t_k, s_k] \\ -c\hat{d}_i \text{sign}(x_i(t) - x_0(t)) & \text{for } t \in (s_k, t_{k+1}) \end{cases} \quad (16)$$

where  $0 = t_0 \leq s_0 \leq t_1 \leq s_1 \leq \dots \leq t_k \leq s_k \leq t_{k+1} \leq \dots$ ; time interval  $[t_k, s_k]$  is called the communication time, i.e., every agent can interact with its neighbors in this time interval, while  $(s_k, t_{k+1})$  is called rest time, in which, every agent can communicate only with

leader but not its neighbors. Denote by  $c_k = s_k - t_k$  and  $r_k = t_{k+1} - s_k$  the communication width and the rest width, respectively. Let error signal  $e_i(t) = x_i(t) - s(t)$ ; by some simple derivation, one can get the following error dynamic equation:

$$\dot{e}_i(t) = \begin{cases} A_i e_i(t) + B_i g(e_i(t)) + w_i(s(t)) - u_0(t) - c \sum_{j=1}^N l_{ij} e_j(t) - cd_i (g_i(t)) - c\hat{d}_i \text{sign}(e_i(t)) & \text{for } t \in [t_k, s_k] \\ A_i e_i(t) + B_i g(e_i(t)) + w_i(s(t)) - u_0(t) - c\hat{d}_i \text{sign}(e_i(t)) & \text{for } t \in (s_k, t_{k+1}) \end{cases} \quad (17)$$

where  $g(e_i(t)) = f(x_i(t)) - f(s(t))$ ,  $w_i(s(t)) = (A_i - A_0)s(t) + (B_i - B_0)f(s(t))$ .

*Assumption 6.* The  $s(t)$  is bounded; i.e., for any initial  $s(t_0)$ , there exists  $T$ , such that  $\|s(t)\| \leq \delta$ ,  $t \geq T$ , where  $\delta$  is a positive constant. That is,  $s(t)$  also could be an equilibrium point, a periodic orbit, or even a chaotic orbit throughout this paper. Furthermore, with Assumption 1, one has that  $w_i(s(t))$  is also bounded; i.e.,  $\|w_i(s(t))\| \leq \varepsilon_i$ ,  $t \geq T$ , where  $\varepsilon_i$  is a positive constant.

*Assumption 7.* The unknown input of leader  $u_0(t)$  in this paper is assumed bounded; let  $\|u_0(t)\| \leq \varepsilon_0$ .

*Remark 8.* There were many results about heterogeneous dynamic networks recently [1]; however, most of which have investigated quasi-synchronization or bounded-consensus of them. This paper would study the complete consensus for a heterogeneous multiagent network; furthermore, the leader in this paper has an unknown but bounded input, which has not been seen yet. The results in this paper can be applied for tracking an unknown target by a heterogeneous multiagent network. Note that communications among agents and their neighbors are aperiodic intermittent, which could prevent blocking the communication channel.

**Theorem 9.** *Under Assumptions 1, 3, 6, and 7, consensus of the heterogeneous multiagent system could be achieved if there exist positive definite diagonal matrix  $P$  and constants  $\alpha > 0$ ,  $\beta > 0$  such that*

$$\hat{d}_i \geq \frac{\|P\|(\varepsilon_0 + \varepsilon_i)}{c\lambda_{\min}(P)}; \quad (18)$$

$$\begin{bmatrix} PA_i + A_i^T P + L_f^T \Lambda_f L_f & PB_i \\ PB_i & -\Lambda_f \end{bmatrix} < \begin{bmatrix} \alpha P & 0 \\ 0 & 0 \end{bmatrix}; \quad (19)$$

$$(\alpha + \beta) I_N < 2c(L + D); \quad (20)$$

$$\lim_{k \rightarrow +\infty} \sum_{m=0}^{k-1} (\beta c_m - \alpha r_m) = +\infty; \quad (21)$$

where  $D = \text{diag}\{d_1, d_2, \dots, d_N\}$  and  $c_k = s_k - t_k$ ,  $r_k = t_{k+1} - s_k$ ,  $k = 0, 1, 2, \dots$ , matrices  $\Lambda_f$  and  $L_f$  have been mentioned in Remark 2.

*Proof.* Choose a Lyapunov function as  $V(t) = (1/2) \sum_{i=1}^N e_i^T(t) P e_i(t)$ ; for  $t \in [t_k, s_k]$ ,  $k = 0, 1, 2, \dots$ , taking the time derivative of  $V(t)$  along the trajectories of (17), one obtains the following.

$$\begin{aligned} \dot{V}(t) &= \sum_{i=1}^N e_i^T(t) P \dot{e}_i(t) = \sum_{i=1}^N e_i^T(t) P \left\{ A_i e_i(t) \right. \\ &\quad + B_i g(e_i(t)) + w_i(s(t)) - u_0(t) - c \sum_{j=1}^N l_{ij} e_j(t) \\ &\quad \left. - cd_i (g_i(t)) - c\hat{d}_i \text{sign}(e_i(t)) \right\} = \frac{1}{2} \\ &\quad \cdot \sum_{i=1}^N e_i^T(t) (PA_i + A_i^T P) e_i(t) \\ &\quad + \sum_{i=1}^N e_i^T(t) PB_i g(e_i(t)) + \sum_{i=1}^N e_i^T(t) P w_i(s(t)) \\ &\quad + \sum_{i=1}^N e_i^T(t) P u_0(t) - c \sum_{i=1}^N \hat{d}_i e_i^T(t) P \text{sign}(e_i(t)) \\ &\quad - c \sum_{i=1}^N e_i^T(t) P \sum_{j=1}^N l_{ij} e_j(t) - cd_i \sum_{i=1}^N e_i^T(t) P e_i(t) \end{aligned} \quad (22)$$

Similar to the proof of Theorem 5, one has

$$\begin{aligned} e_i^T(t) P w_i(s(t)) &\leq \varepsilon_i \|P\| \|e_i(t)\|, \\ e_i^T(t) P u_0(t) &\leq \varepsilon_0 \|P\| \|e_i(t)\| \\ -\widehat{c} \widehat{d}_i e_i^T(t) P \operatorname{sign}(e_i(t)) &\leq -\widehat{c} \widehat{d}_i \lambda_{\min}(P) \|e_i(t)\|. \end{aligned} \quad (23)$$

Then, from (23), (18), (19), and (20) and Remark 2, we have

$$\dot{V}(t) \leq -\beta V(t), \quad t \in [t_k, s_k]. \quad (24)$$

On the other hand, when  $t \in (s_k, t_{k+1})$ ,  $k = 0, 1, 2, \dots$ , taking the time derivative of  $V(t)$  along the trajectories of (17), similarly, one can obtain

$$\dot{V}(t) \leq \alpha V(t), \quad t \in (s_k, t_{k+1}). \quad (25)$$

Now, we estimate  $V(t)$  based on the above two inequations.

For  $t \in [t_0, s_0]$ , it is easy to get  $V(t) \leq V(t_0)e^{-\beta(t-t_0)}$  and  $V(s_0) \leq V(t_0)e^{-\beta c_0}$ .

For  $t \in (s_0, t_1)$ , it is easy to get  $V(t) \leq V(s_0)e^{\alpha(t-s_0)} \leq V(t_0)e^{-\beta c_0 + \alpha(t-s_0)}$  and  $V(t_1) \leq V(t_0)e^{-\beta c_0 + \alpha r_0}$ .

For  $t \in [t_1, s_1]$ , one has  $V(t) \leq V(t_1)e^{-\beta(t-t_1)} \leq V(t_0)e^{-\beta c_0 + \alpha r_0 - \beta(t-t_1)}$  and  $V(s_1) \leq V(t_0)e^{-\beta(c_0+c_1) + \alpha r_0}$ .

For  $t \in (s_1, t_2)$ , one has  $V(t) \leq V(s_1)e^{\alpha(t-s_1)} \leq V(t_0)e^{-\beta(c_0+c_1) + \alpha r_0 + \alpha(t-s_1)}$  and  $V(t_2) \leq V(t_0)e^{-\beta(c_0+c_1) + \alpha(r_0+r_1)}$ .

Generally, when  $t \in [t_k, s_k]$ ,

$$\begin{aligned} V(t) &\leq V(t_0) e^{-\beta \sum_{m=0}^{k-1} c_m + \alpha \sum_{m=0}^{k-1} r_m - \beta(t-t_k)} \\ &\leq V(t_0) e^{-\sum_{m=0}^{k-1} (\beta c_m - \alpha r_m)}, \end{aligned} \quad (26)$$

and when  $t \in (s_k, t_{k+1})$ ,

$$\begin{aligned} V(t) &\leq V(t_0) e^{-\beta \sum_{m=0}^k c_m + \alpha \sum_{m=0}^{k-1} r_m - \alpha(t-s_k)} \\ &\leq V(t_0) e^{-\sum_{m=0}^{k-1} (\beta c_m - \alpha r_m) - (\alpha + \beta)c_k} \\ &\leq V(t_0) e^{-\sum_{m=0}^{k-1} (\beta c_m - \alpha r_m)}. \end{aligned} \quad (27)$$

Thus, for any  $t > 0$ , we have  $V(t) \leq V(t_0)e^{-\sum_{m=0}^{k-1} (\beta c_m - \alpha r_m)}$ , combined with (21),  $\lim_{t \rightarrow +\infty} V(t) = 0$ , which implies that  $\lim_{t \rightarrow +\infty} \|e_i(t)\| = 0$ ; i.e., the consensus could be achieved; this completes our proof.  $\square$

Note that condition (21) in Theorem 5 is difficult to check due to its infinity. The following results could be checked easily based on a higher request for the intermittent communication.

**Corollary 10.** *Under Assumptions 1, 3, 6, and 7, consensus of the heterogeneous multiagent system could be achieved if there exist positive definite diagonal matrix  $P$  and constants  $\alpha > 0$ ,  $\beta > 0$  such that (18)-(20) and the following condition holds:*

$$\frac{\check{c}}{\widehat{T}} > \frac{\alpha}{\alpha + \beta}, \quad (28)$$

where  $\check{c} = \min\{c_1, c_2, \dots\}$ ,  $\widehat{T} = \min\{t_1 - t_0, t_2 - t_1, \dots\}$ .

*Proof.* It is obviously that (29) implies (21) based on the definition of notations  $\check{c}$  and  $\widehat{T}$ . Consequently, the result can be obtained.  $\square$

The periodically intermittent communication is obviously a special case of Theorem 5; in periodical case, let  $T \equiv t_{k+1} - t_k$ , and  $\widehat{c} \equiv s_k - t_k$  for any  $k = 0, 1, 2, \dots$ ; the following corollary could be obtained naturally.

**Corollary 11.** *Under Assumptions 1, 3, 6, and 7, consensus of the heterogeneous multiagent system could be achieved if there exist positive definite diagonal matrix  $P$  and constants  $\alpha > 0$ ,  $\beta > 0$  such that (18)-(20) and the following condition holds:*

$$\frac{\widehat{c}}{T} > \frac{\alpha}{\alpha + \beta}. \quad (29)$$

## 4. Numerical Simulations

In this section, two examples are given to check our theorem results above.

**4.1. Leaderless Consensus.** In this subsection, we have a multiagent system consisting of four heterogeneous agents. The Laplacian matrix  $L$  is given as

$$L = \begin{bmatrix} 2 & -1 & -1 & 0 \\ -1 & 3 & -1 & -1 \\ -1 & -1 & 3 & -1 \\ 0 & -1 & -1 & 2 \end{bmatrix}. \quad (30)$$

In this example, let  $n = 3$ ,  $x_i(t) = [x_{i1}(t), x_{i2}(t), x_{i3}(t)]^T$ ,  $f_j(x_{ij}(t)) = 0.5(|x_{ij}(t) + 1| - |x_{ij}(t) - 1|)$ ,  $i = 1, 2, 3, 4$ . The matrices  $A_i$  and  $B_i$  are given as

$$A_1 = \begin{bmatrix} -1 & 0 & 0 \\ 0 & -1 & 0 \\ 0 & 0 & -1 \end{bmatrix},$$

$$A_2 = \begin{bmatrix} -0.2 & 0 & 0 \\ 0 & -0.2 & 0 \\ 0 & 0 & -0.2 \end{bmatrix},$$

$$A_3 = \begin{bmatrix} -0.1 & 0 & 0 \\ 0 & -1 & 0 \\ 0 & 0 & -1 \end{bmatrix},$$

$$A_4 = \begin{bmatrix} -2 & 0 & 0 \\ 0 & -2 & 0 \\ 0 & 0 & -2 \end{bmatrix},$$

$$B_1 = \begin{bmatrix} 1.25 & -3.2 & -3.2 \\ -3.2 & 1.1 & -4.4 \\ -3.2 & 4.4 & 1 \end{bmatrix},$$

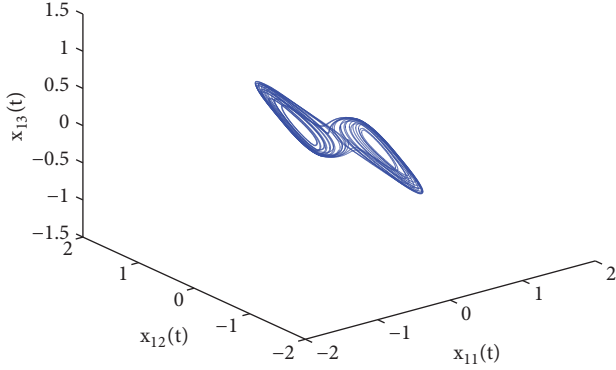


FIGURE 1: Trajectory of the  $[x_{11}(t), x_{12}(t), x_{13}(t)]$  with initial values  $[0.1, 0.1, 0.1]$ .

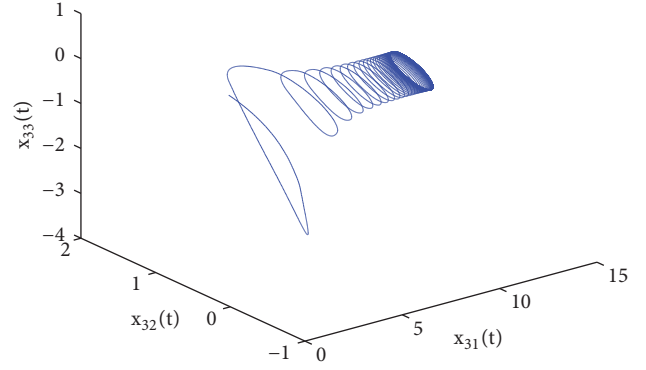


FIGURE 3: Trajectory of the  $[x_{31}(t), x_{32}(t), x_{33}(t)]$  with initial values  $[6, -2, 12]$ .

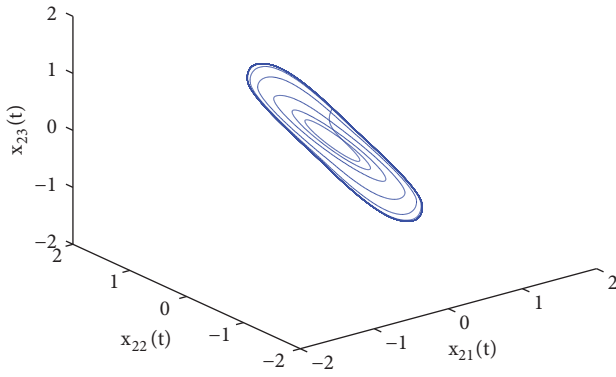


FIGURE 2: Trajectory of the  $[x_{21}(t), x_{22}(t), x_{23}(t)]$  with initial values  $[4, -6, 8]$ .

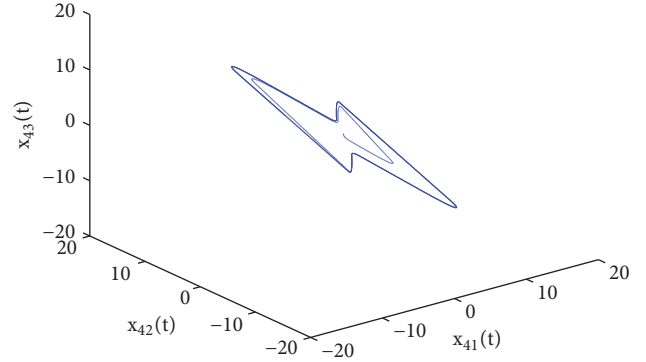


FIGURE 4: Trajectory of the  $[x_{41}(t), x_{42}(t), x_{43}(t)]$  with initial values  $[2, -4, 10]$ .

$$\begin{aligned}
 B_2 &= \begin{bmatrix} 1.25 & 3 & -3.2 \\ -3.2 & 1.1 & -4.4 \\ -3.2 & 4.4 & 1 \end{bmatrix}, \\
 B_3 &= \begin{bmatrix} 1.5 & -2.2 & -3 \\ -3.2 & 1 & -4.4 \\ -3.2 & 4.4 & 1 \end{bmatrix}, \\
 B_4 &= \begin{bmatrix} -1.25 & -3.2 & -3 \\ -3.2 & 1 & -4.4 \\ -1 & 4.4 & 1 \end{bmatrix}.
 \end{aligned}
 \tag{31}$$

Without control, the trajectories of these four agents are shown as Figures 1–4 with corresponding initial values. It is obviously that they have different dynamics, the first agent has a chaotic behavior, the second agent may have a convergent trajectory, the third agent has a periodic orbit, etc. According to the simulation, we have  $\varepsilon_2 = 5.7084$ ,  $\varepsilon_3 = 2.5655$ ,  $\varepsilon_4 = 7.6434$ , and based on the analysis of Section 3.1, the  $\hat{L}$  could be obtained as

$$\hat{L} = \begin{bmatrix} 4 & 0 & -1 \\ 0 & 4 & -1 \\ 0 & 0 & 2 \end{bmatrix}. \tag{32}$$

In order to reach consensus for the heterogeneous multiagent system, let  $c = 10$ . The  $L_f$  can be selected as  $I_3$ . To solve (9) and (10), we set  $\alpha = 20$ ; then, by using MATLAB LMI Toolbox one has  $\beta = 9.8989$  and  $P = 0.3136I_3$ . By some simple computations about (8),  $\hat{d}_i$  can be selected as  $\hat{d}_1 = 0.6$ ,  $\hat{d}_2 = 0.3$ ,  $\hat{d}_3 = 0.8$ . Then, all conditions of Theorem 5 can be satisfied. Figures 5 and 6 give the simulations for the state variables  $x_{ij}(t)$  and error variables  $e_{ij}(t) = x_{i+1,j}(t) - x_{1j}(t)$ , respectively.

**4.2. Leader-Following Consensus.** In this example, the coefficient matrices  $A$ ,  $B$ ,  $A_i$ ,  $B_i$  are given as

$$\begin{aligned}
 A &= \begin{bmatrix} -2.5 & 10 & 0 \\ 1 & -1 & 1 \\ 0 & -18 & 0 \end{bmatrix}, \\
 A_1 &= \begin{bmatrix} -2.5 & 10 & 0 \\ 1 & -1 & 1 \\ 0 & -18 & -0.5 \end{bmatrix},
 \end{aligned}$$

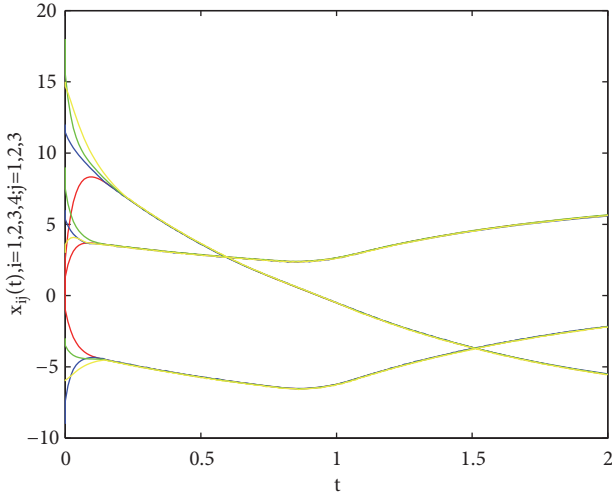


FIGURE 5: Time evolution of state variables of four heterogeneous agents with control.

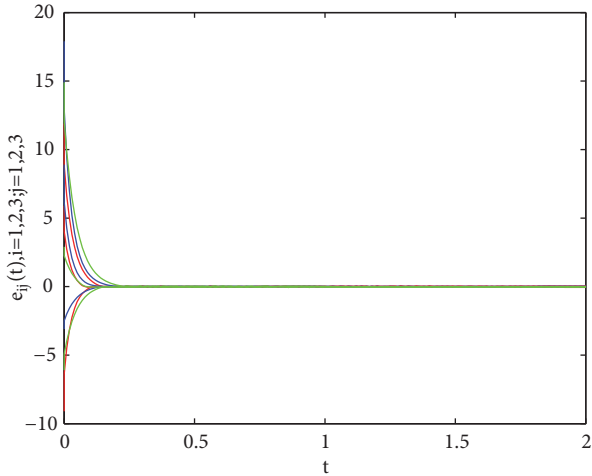


FIGURE 6: Time evolution of error variables  $e_i(t)$  with control.

$$A_2 = \begin{bmatrix} -2.5 & 10 & 0 \\ 1 & 1 & 1 \\ 0 & -18 & 0.3 \end{bmatrix},$$

$$A_3 = \begin{bmatrix} -2.6 & 10 & 0 \\ 1 & -0.9 & 1 \\ 0 & -23 & 0 \end{bmatrix},$$

$$B = \begin{bmatrix} \frac{35}{6} & 0 & 0 \\ 0 & 0 & 0 \\ 0 & 0 & 0 \end{bmatrix},$$

$$B_2 = \begin{bmatrix} \frac{35}{6} & 0 & 0 \\ 0 & 0 & 0 \\ 0 & 0 & 0 \end{bmatrix},$$

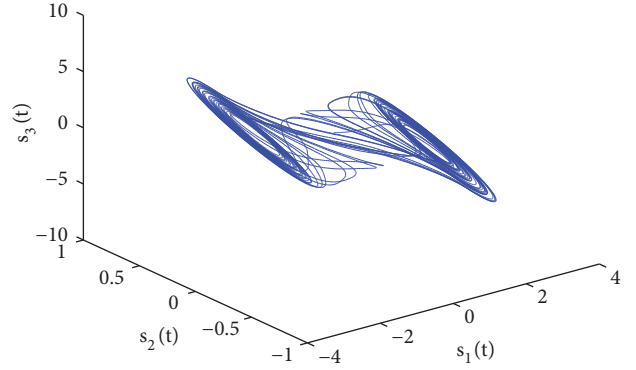


FIGURE 7: Trajectory of the  $[s_1(t), s_2(t), s_3(t)]$  with initial values  $[0.1, 0.1, 0.1]$ .

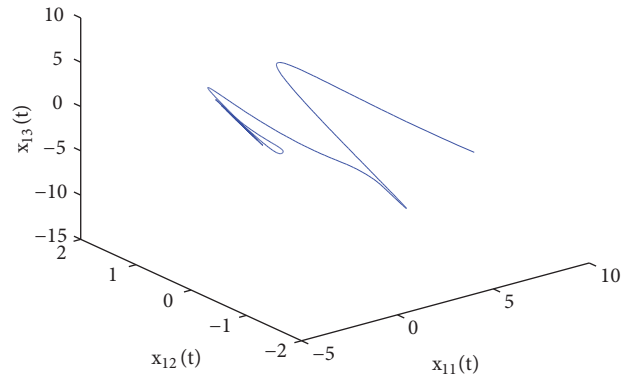


FIGURE 8: Trajectory of the  $[x_{11}(t), x_{12}(t), x_{13}(t)]$  with initial values  $[4, -2, 1]$ .

$$B_3 = \begin{bmatrix} \frac{29}{6} & 0 & 0 \\ 0 & 0 & 0 \\ 0.1 & 0 & 0 \end{bmatrix},$$

$$B_4 = \begin{bmatrix} \frac{35}{6} & 0 & 0 \\ 0 & 0 & 0 \\ 0 & 0 & 0 \end{bmatrix}.$$

(33)

Meanwhile, let  $n = 3$ ,  $x_i(t) = [x_{i1}(t), x_{i2}(t), x_{i3}(t)]^T$ ,  $f_j(x_{ij}(t)) = 0.5(|x_{ij}(t) + 1| - |x_{ij}(t) - 1|)$ ,  $i = 1, 2, 3$ ,  $j = 1, 2, 3$ . Without control, the different trajectories of the leader and three followers are shown as Figures 7–10 with corresponding initial values. According to the simulation, we have  $\varepsilon_1 = 3.1291$ ,  $\varepsilon_2 = 2.0604$ ,  $\varepsilon_3 = 4.0596$ . Assume that the network is connected and the Laplacian matrix  $L$  is

$$L = \begin{bmatrix} 1 & -1 & 0 \\ -1 & 2 & -1 \\ 0 & -1 & 1 \end{bmatrix}. \quad (34)$$

Let  $D = \text{diag}\{2, 4, 6\}$  and  $u_0(t) = 1.1 \sin(t)$ . Then, choosing  $\alpha = 30$ ,  $c = 20$  and solving (19) and (20) yield  $\beta =$

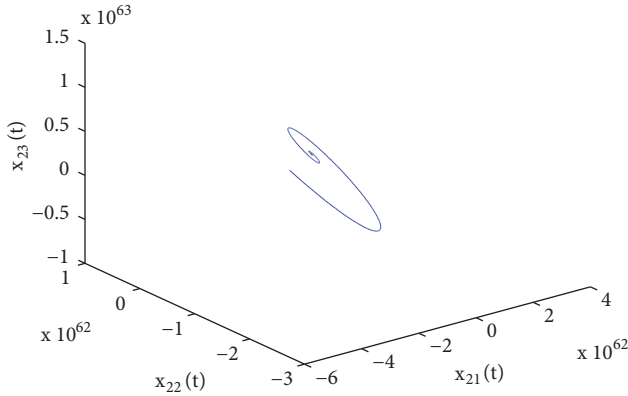


FIGURE 9: Trajectory of the  $[x_{21}(t), x_{22}(t), x_{23}(t)]$  with initial values  $[3, 2, -1]$ .

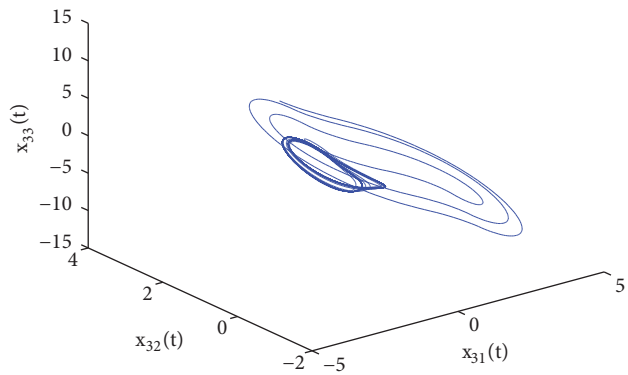


FIGURE 10: Trajectory of the  $[x_{31}(t), x_{32}(t), x_{33}(t)]$  with initial values  $[-1, 2, 5]$ .

31.7071 and  $P = 0.0048I_3$ . From (18), one can let  $\hat{d}_1 = 0.25$ ,  $\hat{d}_2 = 0.36$ ,  $\hat{d}_3 = 0.37$ . For the sake of convenience, in this simulation, the period intermittent strategy will be considered. By Corollary 11, one can choose  $\hat{c}/T = 0.7$ . Thus, one can conclude that the leader-follower consensus can be achieved according to Corollary 11. Figures 11 and 12 give the simulations for the state variables  $x_{ij}(t)$ ,  $s_j(t)$  and error variables  $e_{ij}(t) = x_{ij}(t) - s_j(t)$ , respectively.

## 5. Conclusion

The leaderless consensus and leader-follower consensus of heterogeneous multiagent network have been studied in this paper. By utilizing a discontinuous communication protocol, leaderless consensus criterions formed as LMIs have been derived at first. Then, an unknown leader has been considered; under our discontinuous control protocol, the consensus could be obtained based on some conditions. The results in this paper could be applied to tracking control problem for an unknown target. In the leader-follower case, the communication among followers was aperiodically intermittent, which could prevent blocking the ways of signal transmission. Finally, simulation results have also been given to check the obtained theory results. Noting that this paper just considered an undirected topology of the network, future

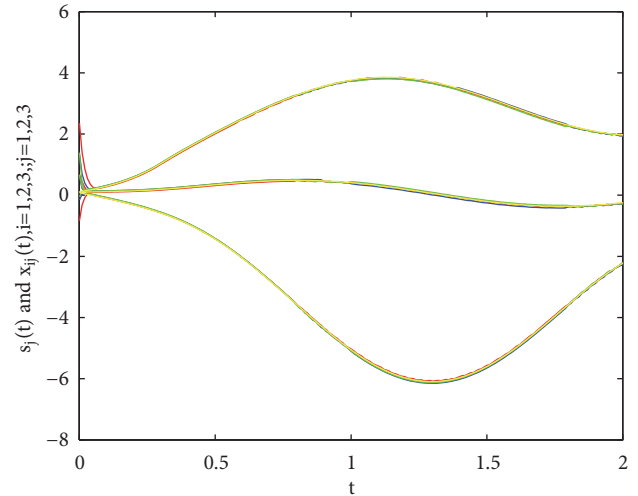


FIGURE 11: Time evolution of state variables of leader and three followers with control.

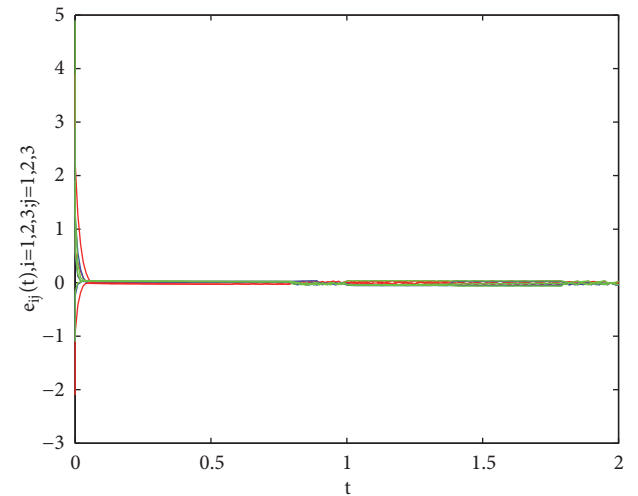


FIGURE 12: Time evolution of error variables  $e_i(t)$  with control.

works include the study of directed structure and even switching topologies, which are more suitable to the real world. Time-delays are also inescapable in real world systems [16, 43–45]; however, this paper has not considered the time-delay, which would be a significant topic in our future work.

## Data Availability

No data have been used to support this study.

## Disclosure

The numerical simulation part was performed using the MATLAB software.

## Conflicts of Interest

The authors declare that they have no conflicts of interest.

## Acknowledgments

This work was jointly supported by the Natural Science Foundation of Jiangsu Province of China under Grant No. BK20161126.

## References

- [1] J. Kim, H. Shim, H. Kim, M. Jung, I. Choi, and J. Kim, "A cooperative multi-agent system and its real time application to robot soccer," in *Proceedings of the International Conference on Robotics and Automation*, pp. 638–643, Albuquerque, NM, USA.
- [2] E. L. Karfopoulos and N. D. Hatzigiorgiou, "A multi-agent system for controlled charging of a large population of electric vehicles," *IEEE Transactions on Power Systems*, vol. 28, no. 2, pp. 1196–1204, 2013.
- [3] J. Wu, S. Yuan, S. Ji, G. Zhou, Y. Wang, and Z. Wang, "Multi-agent system design and evaluation for collaborative wireless sensor network in large structure health monitoring," *Expert Systems with Applications*, vol. 37, no. 3, pp. 2028–2036, 2010.
- [4] R. Olfati-Saber, "Flocking for multi-agent dynamic systems: algorithms and theory," *IEEE Transactions on Automatic Control*, vol. 51, no. 3, pp. 401–420, 2006.
- [5] W. Yu, G. Chen, and M. Cao, "Some necessary and sufficient conditions for second-order consensus in multi-agent dynamical systems," *Automatica*, vol. 46, no. 6, pp. 1089–1095, 2010.
- [6] Z. Li, W. Ren, X. Liu, and M. Fu, "Consensus of multi-agent systems with general linear and Lipschitz nonlinear dynamics using distributed adaptive protocols," *IEEE Transactions on Automatic Control*, vol. 58, no. 7, pp. 1786–1791, 2013.
- [7] W. Yu, W. X. Zheng, G. Chen, W. Ren, and J. Cao, "Second-order consensus in multi-agent dynamical systems with sampled position data," *Automatica*, vol. 47, no. 7, pp. 1496–1503, 2011.
- [8] Z. Li, W. Ren, X. Liu, and L. Xie, "Distributed consensus of linear multi-agent systems with adaptive dynamic protocols," *Automatica*, vol. 49, no. 7, pp. 1986–1995, 2013.
- [9] C. Ma, T. Li, and J. Zhang, "Consensus control for leader-following multi-agent systems with measurement noises," *Journal of Systems Science and Complexity*, vol. 23, no. 1, pp. 35–49, 2010.
- [10] G. Wen, W. Yu, Y. Xia, X. Yu, and J. Hu, "Distributed tracking of nonlinear multiagent systems under directed switching topology: An observer-based protocol," *IEEE Transactions on Systems, Man, and Cybernetics: Systems*, vol. 47, no. 5, pp. 869–881, 2017.
- [11] G. Wen, Z. Duan, G. Chen, and W. Yu, "Consensus tracking of multi-agent systems with Lipschitz-type node dynamics and switching topologies," *IEEE Transactions on Circuits and Systems I: Regular Papers*, vol. 61, no. 2, pp. 499–511, 2014.
- [12] W. Ren, "Distributed leaderless consensus algorithms for networked Euler-Lagrange systems," *International Journal of Control*, vol. 82, no. 11, pp. 2137–2149, 2009.
- [13] J. Hu, Y. Hong, and G. Feng, "Distributed dynamic control for leaderless multi-agent consensus with star-like topology," *Asian Journal of Control*, vol. 10, no. 2, pp. 233–237, 2008.
- [14] W. Ni and D. Cheng, "Leader-following consensus of multi-agent systems under fixed and switching topologies," *Systems & Control Letters*, vol. 59, no. 3–4, pp. 209–217, 2010.
- [15] Q. Song, F. Liu, J. Cao, and W. Yu, "M-matrix strategies for pinning-controlled leader-following consensus in multiagent systems with nonlinear dynamics," *IEEE Transactions on Cybernetics*, vol. 43, no. 6, pp. 1688–1697, 2013.
- [16] Z. Meng, W. Ren, Y. Cao, and Z. You, "Leaderless and leader-following consensus with communication and input delays under a directed network topology," *IEEE Transactions on Systems, Man, and Cybernetics, Part B: Cybernetics*, vol. 41, no. 1, pp. 75–88, 2011.
- [17] J. M. Kim, J. B. Park, and Y. H. Choi, "Leaderless and leader-following consensus for heterogeneous multi-agent systems with random link failures," *IET Control Theory & Applications*, vol. 8, no. 1, pp. 51–60, 2014.
- [18] Z. Qiu, L. Xie, and Y. Hong, "Quantized leaderless and leader-following consensus of high-order multi-agent systems with limited data rate," *Institute of Electrical and Electronics Engineers Transactions on Automatic Control*, vol. 61, no. 9, pp. 2432–2447, 2016.
- [19] H. Du, G. Wen, G. Chen, J. Cao, and F. E. Alsaadi, "A distributed finite-time consensus algorithm for higher-order leaderless and leader-following multiagent systems," *IEEE Transactions on Systems, Man, and Cybernetics: Systems*, vol. 99, pp. 1–10, 2017.
- [20] J. Wang, L. Su, H. Shen, Z.-G. Wu, and J. H. Park, "Mixed H $\infty$ /passive sampled-data synchronization control of complex dynamical networks with distributed coupling delay," *Journal of The Franklin Institute*, vol. 354, no. 3, pp. 1302–1320, 2017.
- [21] M. Li and J. Wang, "Exploring delayed Mittag-Leffler type matrix functions to study finite time stability of fractional delay differential equations," *Applied Mathematics and Computation*, vol. 324, pp. 254–265, 2018.
- [22] Y. Guo, "Global stability analysis for a class of Cohen-Grossberg neural network models," *Bulletin of the Korean Mathematical Society*, vol. 49, no. 6, pp. 1193–1198, 2012.
- [23] Y. Guo, "Global asymptotic stability analysis for integro-differential systems modeling neural networks with delays," *Zeitschrift für Angewandte Mathematik und Physik*, vol. 61, no. 6, pp. 971–978, 2010.
- [24] W. W. Sun, "Stabilization analysis of time-delay Hamiltonian systems in the presence of saturation," *Applied Mathematics and Computation*, vol. 217, no. 23, pp. 9625–9634, 2011.
- [25] L. Wang, W.-J. Feng, M. Z. Chen, and Q.-G. Wang, "Global bounded consensus in heterogeneous multi-agent systems with directed communication graph," *IET Control Theory & Applications*, vol. 9, no. 1, pp. 147–152, 2015.
- [26] W. He, F. Qian, J. Lam, G. Chen, Q.-L. Han, and J. Kurths, "Quasi-synchronization of heterogeneous dynamic networks via distributed impulsive control: error estimation, optimization and design," *Automatica*, vol. 62, pp. 249–262, 2015.
- [27] J. Fan, Z. Wang, and G. Jiang, "Quasi-synchronization of heterogeneous complex networks with switching sequentially disconnected topology," *Neurocomputing*, vol. 237, pp. 342–349, 2017.
- [28] L. Liu, F. Sun, X. Zhang, and Y. Wu, "Bifurcation analysis for a singular differential system with two parameters via topological degree theory," *Nonlinear Analysis: Modelling and Control*, vol. 22, no. 1, pp. 31–50, 2017.
- [29] L. Gao, D. Wang, and G. Wang, "Further results on exponential stability for impulsive switched nonlinear time-delay systems with delayed impulse effects," *Applied Mathematics and Computation*, vol. 268, pp. 186–200, 2015.
- [30] L. Li, F. Meng, and P. Ju, "Some new integral inequalities and their applications in studying the stability of nonlinear integro-differential equations with time delay," *Journal of Mathematical Analysis and Applications*, vol. 377, no. 2, pp. 853–862, 2011.

- [31] Y. Guo, "Globally robust stability analysis for stochastic Cohen-Grossberg neural networks with impulse and time-varying delays," *Ukrainian Mathematical Journal*, vol. 69, no. 8, pp. 1049–1060, 2017.
- [32] Y. Bai and X. Mu, "Global asymptotic stability of a generalized SIRS epidemic model with transfer from infectious to susceptible," *Journal of Applied Analysis and Computation*, vol. 8, no. 2, pp. 402–412, 2018.
- [33] Y. Guo, "Nontrivial periodic solutions of nonlinear functional differential systems with feedback control," *Turkish Journal of Mathematics*, vol. 34, no. 1, pp. 35–44, 2010.
- [34] Y. Li, Y. Sun, and F. Meng, "New criteria for exponential stability of switched time-varying systems with delays and nonlinear disturbances," *Nonlinear Analysis: Hybrid Systems*, vol. 26, pp. 284–291, 2017.
- [35] M. Han, L. Sheng, and X. Zhang, "Bifurcation theory for finitely smooth planar autonomous differential systems," *Journal of Differential Equations*, vol. 264, no. 5, pp. 3596–3618, 2018.
- [36] J. Wang, K. Liang, X. Huang, Z. Wang, and H. Shen, "Dissipative fault-tolerant control for nonlinear singular perturbed systems with Markov jumping parameters based on slow state feedback," *Applied Mathematics and Computation*, vol. 328, pp. 247–262, 2018.
- [37] Y. Guo, "Nontrivial solutions for boundary-value problems of nonlinear fractional differential equations," *Bulletin of the Korean Mathematical Society*, vol. 47, no. 1, pp. 81–87, 2010.
- [38] Y. Guo, "Solvability of boundary-value problems for nonlinear fractional differential equations," *Ukrainian Mathematical Journal*, vol. 62, no. 9, pp. 1409–1419, 2011.
- [39] M. Guo, D. Xu, and L. Liu, "Cooperative output regulation of heterogeneous nonlinear multi-agent systems with unknown control directions," *Institute of Electrical and Electronics Engineers Transactions on Automatic Control*, vol. 62, no. 6, pp. 3039–3045, 2017.
- [40] S. Li, M. J. Er, and J. Zhang, "Distributed Adaptive Fuzzy Control for Output Consensus of Heterogeneous Stochastic Nonlinear Multi-Agent Systems," *IEEE Transactions on Fuzzy Systems*, vol. 26, no. 3, pp. 1138–1152, 2018.
- [41] Y. Zhang and S. Li, "Adaptive near-optimal consensus of high-order nonlinear multi-agent systems with heterogeneity," *Automatica*, vol. 85, pp. 426–432, 2017.
- [42] S. Zuo, Y. Song, F. L. Lewis, and A. Davoudi, "Adaptive output containment control of heterogeneous multi-agent systems with unknown leaders," *Automatica*, vol. 92, pp. 235–239, 2018.
- [43] G. Liu, S. Xu, Y. Wei, Z. Qi, and Z. Zhang, "New insight into reachable set estimation for uncertain singular time-delay systems," *Applied Mathematics and Computation*, vol. 320, pp. 769–780, 2018.
- [44] W. Sun, Y. Wang, and R. Yang, "L2 disturbance attenuation for a class of time delay Hamiltonian systems," *Journal of Systems Science & Complexity*, vol. 24, no. 4, pp. 672–682, 2011.
- [45] W. Sun and L. Peng, "Observer-based robust adaptive control for uncertain stochastic Hamiltonian systems with state and input delays," *Lithuanian Association of Nonlinear Analysts. Nonlinear Analysis: Modelling and Control*, vol. 19, no. 4, pp. 626–645, 2014.

## Research Article

# $H_\infty$ Robust Tracking Control of Stochastic T-S Fuzzy Systems with Poisson Jumps

Xiangyun Lin <sup>1</sup>, Weihai Zhang <sup>2</sup> and Bor-Sen Chen <sup>3,4</sup>

<sup>1</sup>College of Mathematics and Systems, Shandong University of Science and Technology, Qingdao 266590, China

<sup>2</sup>College of Electrical Engineering and Automation, Shandong University of Science and Technology, Qingdao 266590, China

<sup>3</sup>Department of Electrical Engineering, National Tsing Hua University, Hsinchu 30013, Taiwan

<sup>4</sup>Department of Electrical Engineering, Yuan Ze University, Chung-Li 32003, Taiwan

Correspondence should be addressed to Xiangyun Lin; lxy9393@sina.com

Received 29 July 2018; Accepted 17 September 2018; Published 2 October 2018

Academic Editor: Peter Liu

Copyright © 2018 Xiangyun Lin et al. This is an open access article distributed under the Creative Commons Attribution License, which permits unrestricted use, distribution, and reproduction in any medium, provided the original work is properly cited.

A robust adaptive  $H_\infty$  tracking control design for nonlinear stochastic systems with both Brownian motion and Poisson jumps is proposed, which is based on Takagi–Sugeno (T-S) type fuzzy techniques. Because the state of to-be-controlled systems cannot be known exactly, to overcome this difficulty, the state estimation systems and error estimation systems are introduced to obtain an augmented system. By using the fuzzy systems to approximate the nonlinear systems, an adaptive fuzzy control is employed to achieve the desired  $H_\infty$  tracking performance for stochastic systems with exogenous disturbance. A simulation example is presented to illustrate the tracking performance of the proposed design method.

## 1. Introduction

Adaptive control theory is a powerful methodology which has been widely applied to design feedback control for systems with parametric uncertainties or for plants with unknown structure or changing operating conditions [1, 2]. Because there are uncertainties in the systems, the laws of adaptive control design schemes no more depend on the fixed description of input-output relationships but are related to the estimation of the system's state or output and those estimating errors [3–6].

The robust  $H_\infty$  tracking control theory is a powerful methodology to design feedback controllers where the system parametric uncertainties are seen as the exogenous disturbance [7–9]. This methodology is widely applied in networked control systems [10], mobile robots [11], etc. The objective of the robust  $H_\infty$  tracking control design is to construct an adaptive controller which guarantees the  $H_\infty$  tracking control performance. Based on the system's structure, the robust  $H_\infty$  tracking control designing methods include linear  $H_\infty$  control and nonlinear  $H_\infty$  control. Linear  $H_\infty$  control design problems are based on solving a kind of algebra Riccati inequalities which can be solved by the

LMI's method. And the nonlinear  $H_\infty$  control design involves solving a nonlinear Hamilton-Jacobi inequality (HJI) [12]. However, it is very difficult to solve the Hamilton-Jacobi equalities or inequalities [13, 14]. In practice, to overcome this difficulty, the fuzzy methods have been applied to the  $H_\infty$  robust control design of nonlinear systems where the Takagi–Sugeno (T-S) type fuzzy is widely used [15–17].

Stochastic systems are applied in economics [18], biology [19], and natural science to describe the randomness in models [20–23]. Based on the distribution properties of the inserted random variables, stochastic systems include Itô-type systems driven by Brownian motion [24, 25], systems driven by Markovian jumps [26], systems driven by Poisson jumps or Lévy process [27], and their compound forms [28–30]. The linear stochastic  $H_\infty$  theory has been developed since 1990s via the linear matrix inequalities (LMI) approach [31]. The nonlinear stochastic  $H_\infty$  problems are solved by means of Hamilton-Jacobi equations [25]. In practice, there exist sudden shifts in the systems. In order to describe such phenomenon, Poisson jumps are inserted in the model, so the stochastic systems are driven not only by Brownian motion but also by Poisson jumps or Lévy process [27, 28]. The main complication in the  $H_\infty$  tracking control design problem

studied here is due to the presence of both deterministic, stochastic perturbations and Poisson jumps terms in the system. Nonlinear  $H_\infty$  tracking theory and fuzzy control design are combined together to construct the adaptive fuzzy-based controller which guarantees the  $H_\infty$  tracking control performance.

This paper is organized as follows: In Section 2, some lemmas about stochastic differential equations with Poisson jumps are reviewed, which will be used in the latter theoretical analysis and deductions. In Section 3, the theories of  $H_\infty$  tracking control are extended to the case of linear stochastic systems with Poisson jumps. In Section 4, the  $H_\infty$  tracking control design methods based on the Takagi–Sugeno type fuzzy techniques are applied to the nonlinear stochastic systems with Poisson jumps, and the  $H_\infty$  tracking controller is obtained. In Section 5, the air-to-air missile pursuit systems are presented to show the effectiveness of the proposed method.

*Notation.* For convenience, we adopt the following notations:  $\mathbb{R}^{m \times n}$ : the set of all real  $m \times n$  matrices.  $\mathbb{R}^n$ : the set of all  $n$ -dimensional real vectors.  $A > 0$  ( $A \geq 0$ ): the positive definite (semidefinite) matrix  $A$ .  $A^T$ : the transpose of matrix  $A$ .  $I$ : the identity matrix with proper order.  $\mathbb{E}[\xi]$ : the expectation of random variable  $\xi$ .  $\|x\|$ : the Euclidean norm of vector  $x \in \mathbb{R}^n$ .

## 2. Preliminaries

Let  $(\Omega, \mathcal{F}, \mathbb{F}, \Pr)$  be a complete probability space where  $\mathbb{F} = \{\mathcal{F}_t : t \geq 0\}$  is a filtration generated by Brownian motion (Wiener process)  $\{W(t), t \geq 0\}$  and Poisson process  $\{N(t), t \geq 0\}$  which are two mutually independent stochastic processes:

- (i)  $W(t)$  is a  $d$ -dimensional standard Brownian motion with  $E[W(t)] = 0$  and  $E[W(t)W(t)^T] = I_d$ ;
- (ii)  $N(t)$  is a Poisson jump process with rate  $\lambda > 0$  and  $\mathbb{E}[N(t)] = \lambda t$ .

Let

$$\mathcal{F}_t = \sigma(N(s) : s \leq t) \vee \sigma(W(s) : s \leq t) \vee \mathcal{N}, \quad (1)$$

where  $\mathcal{N}$  denotes the totality of  $P$ -null sets. Then the filtration  $\mathbb{F} = \{\mathcal{F}_t\}_{t \geq 0}$ . We firstly review some basic theories of stochastic differential equations driven by both Brownian motion and Poisson jumps:

$$\begin{aligned} dx(t) &= f(t, x(t)) dt + \sigma(t, x(t)) dW(t) \\ &\quad + \gamma(t, x(t)) dN(t), \end{aligned} \quad (2)$$

$$x(0) = x_0 \in \mathbb{R}^n.$$

**Lemma 1.** Let  $f(t, x), \sigma(t, x), \gamma(t, x)$  be  $\mathbb{R}^n$ -valued functions on  $[0, T] \times \mathbb{R}^n$  and, for some positive constant  $K$ , satisfy the Lipschitz condition

$$\begin{aligned} |f(t, x) - f(t, y)| + |\sigma(t, x) - \sigma(t, y)| \\ + |\gamma(t, x) - \gamma(t, y)| \leq K \|x - y\|, \end{aligned} \quad (3)$$

and linear growth condition

$$|f(t, x)| + |\sigma(t, x)| + |\gamma(t, x)| \leq K \|x\| \quad (4)$$

for all  $x, y \in \mathbb{R}^n, t \in [0, T]$ . Then the stochastic differential equation (2) has a unique adapted solution with right continuation and left limitation.

Under the conditions of Lemma 1, we then review the Itô's formula of (2) (see [32], Chapter 4, Rule 4.24).

**Lemma 2.** Let  $V(t, x)$  be twice continuously differentiable in  $x$  and once in  $t$ ;  $x(t)$  is the solution of stochastic differential equation (2). Then

$$\begin{aligned} dV(t, x(t)) &= \left[ V_t(t, x(t)) + V_x^T(t, x(t)) f(t, x(t)) \right. \\ &\quad \left. + \frac{1}{2} \sigma^T(t, x(t)) V_{xx}(t, x(t)) \sigma(t, x(t)) \right] dt \\ &\quad + V_x(t, x(t)) \sigma(t, x(t)) dW(t) \\ &\quad + [V(t, x(t) + \gamma(t, x(t))) - V(t, x(t))] dN(t). \end{aligned} \quad (5)$$

The following lemma is a kind of martingale inequality; see Proposition 7.15 in [33].

**Lemma 3.** For a finite  $T_f > 0$ , let  $\{X_t\}_{0 \leq t \leq T_f}$  be a submartingale (or martingale, or supermartingale) with respect to filtrations  $\mathbb{F} = \{\mathcal{F}_t\}_{0 \leq t \leq T_f}$ . Then for any  $r > 0$ , there exists

$$\Pr \left\{ \sup_{0 \leq t \leq T_f} |X_t| \geq r \right\} \leq \frac{3}{r} \sup_{0 \leq t \leq T_f} \mathbb{E} |X_t|. \quad (6)$$

*Remark 4.* Because Brownian motion  $W(t)$  is a martingale with respect to filtration  $\mathbb{F}$ , and Poisson process  $N(t)$  is a submartingale, by Lemma 3, for every finite  $T_f > 0$ , there exist

$$\begin{aligned} \Pr \left\{ \sup_{0 \leq t \leq T_f} |W(t)| \geq r \right\} &\leq \frac{3}{r} \sup_{0 \leq t \leq T_f} \mathbb{E} |W(t)| \\ &= \frac{3}{r} \sup_{0 \leq t \leq T_f} \sqrt{\frac{2t}{\pi}} = \frac{3}{r} \sqrt{\frac{2T_f}{\pi}}, \end{aligned} \quad (7)$$

and

$$\begin{aligned} \Pr \left\{ \sup_{0 \leq t \leq T_f} |N(t)| \geq r \right\} &\leq \frac{3}{r} \sup_{0 \leq t \leq T_f} \mathbb{E} |N(t)| = \frac{3}{r} \sup_{0 \leq t \leq T_f} \lambda t \\ &= \frac{3\lambda T_f}{r}, \end{aligned} \quad (8)$$

or equivalently,

$$\Pr \left\{ \sup_{0 \leq t \leq T_f} |W(t)| < r \right\} \geq 1 - \frac{3}{r} \sqrt{\frac{2T_f}{\pi}}, \quad (9)$$

and

$$\Pr \left\{ \sup_{0 \leq t \leq T_f} |N(t)| < r \right\} \geq 1 - \frac{3\lambda T_f}{r}. \quad (10)$$

Therefore, when  $r$  is large enough,  $|W(t)|$  and  $N(t)$  have upper bound with probability  $p_1(r) = 1 - (3/r)\sqrt{2T_f/\pi}$  and  $p_2(r) = 1 - 3\lambda T_f/r$ , respectively. Furthermore,  $p_1(r) \rightarrow 1$  and  $p_2(r) \rightarrow 1$  when  $r \rightarrow +\infty$ .

### 3. $H_\infty$ Robust Tracking Control of Linear Systems

Consider the linear control system with the following forms:

$$\begin{aligned} dx(t) &= [Ax(t) + Bu(t) + Ew(t)] dt \\ &+ [A_1x(t) + E_1w(t)] dW_1(t) \\ &+ [A_2x(t) + E_2w(t)] dN_1(t), \end{aligned} \quad (11)$$

$$y(t) = Cx(t) + v,$$

where  $A \in \mathbb{R}^{n \times n}$ ,  $B \in \mathbb{R}^{n \times n_u}$ ,  $E, E_1, E_2 \in \mathbb{R}^{n \times n_w}$ ,  $C \in \mathbb{R}^{n_y \times n}$ , and  $D \in \mathbb{R}^{n_y \times n_v}$  are the system's coefficient matrices;  $x(t) \in \mathbb{R}^n$  is the state,  $y(t) \in \mathbb{R}^{n_y}$  is the measurement,  $w(t) \in \mathbb{R}^{n_w}$  and  $v(t) \in \mathbb{R}^{n_v}$  are the exogenous disturbances; and  $W_1(t)$  is the standard 1-dimensional Wiener process and  $N_1(t)$  is the Poisson process with Poisson intensity  $\lambda > 0$ .

Now, we review the basic theory of stochastic differential equations driven by both martingale and Poisson jumps. In order to design the tracking control of system (11), a reference model is suggested as follows:

$$dx_r(t) = [A_r x_r(t) + r(t)] dt, \quad (12)$$

where  $x_r(t) \in \mathbb{R}^n$  is the desired reference state to be tracked by  $x(t)$ ,  $A_r \in \mathbb{R}^{n \times n}$  is a specified asymptotically stable matrix, and  $r(t)$  is a bounded reference input at the steady state,  $x_r(t) = -A_r^{-1}r(t)$ . In practice,  $r(t)$  and  $A_r$  are given by user or designer to specify the transient and the steady state of reference signal  $x_r(t)$  to be tracked.

Denote the tracking errors as

$$e_r(t) = x(t) - x_r(t). \quad (13)$$

For the tracking error  $e_r(t)$ , we consider the  $H_\infty$  robust tracking performance as follows:

$$\frac{\int_0^{t_f} \mathbb{E} \{ e_r^T(t) Q e_r(t) \} dt}{\int_0^{t_f} \mathbb{E} [\bar{w}^T(t) \bar{w}(t)] dt} \leq \rho^2. \quad (14)$$

Here  $Q$  is a positive definite matrix,  $t_f > 0$  is the terminal time of control, and  $\bar{w}(t) = [v(t)^T w(t)^T r(t)^T]^T$ . The physical meaning of (14) is that the effect of any  $\bar{w}$  on tracking error  $e_r(t)$  must be attenuated below a desired level  $\rho > 0$  from the viewpoint of energy. The following observer is proposed to deal with the state estimation of linear system (11):

$$\begin{aligned} d\hat{x}(t) &= [A\hat{x}(t) + Bu(t) + L(y(t) - \hat{y}(t))] dt, \\ \hat{y}(t) &= C\hat{x}(t). \end{aligned} \quad (15)$$

Denote the estimation errors as

$$e(t) = x(t) - \hat{x}(t). \quad (16)$$

Combining (11) and (15), we get

$$\begin{aligned} de(t) &= [(A - LC)e(t) - Lv(t)] dt \\ &+ [A_1x(t) + w(t)] dW_1(t) \\ &+ [A_2x(t) + w(t)] dN_1(t). \end{aligned} \quad (17)$$

Suppose the controller  $u(t)$  has the form as

$$u(t) = K[\hat{x}(t) - x_r(t)]. \quad (18)$$

The performance (14) considering control effort is revised as

$$\frac{\int_0^{t_f} \mathbb{E} \{ e_r^T(t) Q e_r(t) + u^T(t) R u(t) \} dt}{\int_0^{t_f} \mathbb{E} [\bar{w}^T(t) \bar{w}(t)] dt} \leq \rho^2, \quad (19)$$

where  $R$  is a positive definite matrix. Let  $\tilde{x} = [e^T, x^T, x_r^T]^T$  and substitute (18) into (11); then system (11) and (17) can be augmented as the following form

$$\begin{aligned} d\tilde{x}(t) &= [\tilde{A}\tilde{x}(t) + \tilde{E}\tilde{w}(t)] dt \\ &+ [\tilde{A}_1\tilde{x}(t) + \tilde{E}_1\tilde{w}(t)] dW_1(t) \\ &+ [\tilde{A}_2\tilde{x}(t) + \tilde{E}_2\tilde{w}(t)] dN_1(t), \end{aligned} \quad (20)$$

and the  $H_\infty$  performance of (19) equals

$$\int_0^{t_f} \tilde{x}^T(t) \tilde{Q} \tilde{x}(t) dt \leq \rho^2 \int_0^{t_f} \tilde{w}^T(t) \tilde{w}(t) dt \quad (21)$$

where

$$\tilde{A} = \begin{bmatrix} A - LC & 0 & 0 \\ -BK & A + BK & -BK \\ 0 & 0 & A_r \end{bmatrix},$$

$$\tilde{A}_1 = \begin{bmatrix} 0 & A_1 & 0 \\ 0 & A_1 & 0 \\ 0 & 0 & 0 \end{bmatrix},$$

$$\tilde{A}_2 = \begin{bmatrix} 0 & A_2 & 0 \\ 0 & A_2 & 0 \\ 0 & 0 & 0 \end{bmatrix},$$

$$\begin{aligned}\tilde{E} &= \begin{bmatrix} -L & E & 0 \\ 0 & E & 0 \\ 0 & 0 & I \end{bmatrix}, \\ \tilde{E}_1 &= \begin{bmatrix} 0 & E_1 & 0 \\ 0 & E_1 & 0 \\ 0 & 0 & 0 \end{bmatrix}, \\ \tilde{E}_2 &= \begin{bmatrix} 0 & E_2 & 0 \\ 0 & E_2 & 0 \\ 0 & 0 & 0 \end{bmatrix}, \\ \tilde{Q} &= \begin{bmatrix} K^T RK & -K^T RK & K^T RK \\ -K^T RK & K^T RK + Q & -K^T RK - Q \\ K^T RK & -K^T RK - Q & K^T RK + Q \end{bmatrix}.\end{aligned}\quad (22)$$

In order to achieve the  $H_\infty$  tracking performance (19) with a prescribed attenuation level  $\rho$ , an auxiliary symmetric positive definite matrix  $\tilde{P}$  is suggested. The matrices of  $\tilde{A}$  and  $\tilde{E}$  include the to-be-designed matrices  $K$  and  $L$ . If the initial state  $x(0)$ ,  $x_r(0)$  and the estimation error  $e(0)$  are also considered, the performance of (19) can be described as follows.

$$\begin{aligned}& \int_0^{t_f} \mathbb{E} \{ e_r^T(t) Q e_r(t) + u^T(t) R u(t) \} dt \\ & \leq \tilde{x}(0)^T \tilde{P} \tilde{x}(0) + \rho^2 \int_0^{t_f} \mathbb{E} [ \tilde{w}^T(t) \tilde{w}(t) ] dt\end{aligned}\quad (23)$$

**Theorem 5.** Suppose  $\tilde{P} \in \mathcal{S}_+^{3n}(\mathbb{R})$ ,  $K \in \mathbb{R}^{n_u \times n}$ ,  $L \in \mathbb{R}^{n_y \times n}$ , constitute the solution of the following Riccati matrix inequality:

$$\tilde{\mathcal{H}}(\tilde{P}) \leq 0, \quad (24)$$

$$\rho^2 I - \tilde{E}_1^T \tilde{P} \tilde{E}_1 - \lambda \tilde{E}_2^T \tilde{P} \tilde{E}_2 > 0 \quad (25)$$

where

$$\begin{aligned}\tilde{\mathcal{H}}(\tilde{P}) &= \tilde{A}^T \tilde{P} + \tilde{P} \tilde{A} + \tilde{A}_1^T \tilde{P} \tilde{A}_1 + \lambda \tilde{A}_2^T \tilde{P} \tilde{A}_2 + \tilde{Q} \\ &+ (\tilde{P} \tilde{E} + \tilde{A}_1^T \tilde{P} \tilde{E}_1 + \lambda \tilde{A}_2^T \tilde{P} \tilde{E}_2) \\ &\times (\rho^2 I - \tilde{E}_1^T \tilde{P} \tilde{E}_1 - \lambda \tilde{E}_2^T \tilde{P} \tilde{E}_2)^{-1} \\ &\cdot (\tilde{P} \tilde{E} + \tilde{A}_1^T \tilde{P} \tilde{E}_1 + \lambda \tilde{A}_2^T \tilde{P} \tilde{E}_2)^T.\end{aligned}\quad (26)$$

Then the  $H_\infty$  tracking control performance in (24) is guaranteed for a prescribed  $\rho^2$ .

*Proof.* Let  $\tilde{V}(\tilde{x}) = \tilde{x}^T \tilde{P} \tilde{x}$ ,  $\tilde{x} \in \mathbb{R}^{3n}$ . By Itô formula, we get

$$\begin{aligned}\tilde{V}(\tilde{x}(t_f)) - \tilde{V}(\tilde{x}(0)) &= \int_0^{t_f} \{ \tilde{x}^T(t) \\ &\cdot [\tilde{A}^T \tilde{P} + \tilde{P} \tilde{A} + \tilde{A}_1^T \tilde{P} \tilde{A}_1 + \lambda \tilde{A}_2^T \tilde{P} \tilde{A}_2] \tilde{x}(t) + 2 \tilde{x}^T(t) \\ &\cdot [\tilde{P} \tilde{E} + \tilde{A}_1^T \tilde{P} \tilde{E}_1 + \lambda \tilde{A}_2^T \tilde{P} \tilde{E}_2] \tilde{w}(t) \\ &+ \tilde{w}^T [\tilde{E}_1^T \tilde{P} \tilde{E}_1 + \lambda \tilde{E}_2^T \tilde{P} \tilde{E}_2] \tilde{w} \} dt + 2 \int_0^{t_f} \tilde{x}^T(t) \\ &\cdot \tilde{P} [\tilde{A}_1 \tilde{x}(t) + \tilde{E}_1 \tilde{w}(t)] dW_1(t) \\ &+ 2 \int_0^{t_f} \tilde{x}^T(t) \tilde{P} [\tilde{A}_2 \tilde{x}(t) + \tilde{E}_2 \tilde{w}(t)] d\tilde{N}_1(t).\end{aligned}\quad (27)$$

Taking expectation on the both sides, we obtain

$$\begin{aligned}\mathbb{E} [\tilde{V}(\tilde{x}(t_f))] &= \tilde{V}(\tilde{x}(0)) + \int_0^{t_f} \mathbb{E} \{ \tilde{x}^T(t) \\ &\cdot [\tilde{A}^T \tilde{P} + \tilde{P} \tilde{A} + \tilde{A}_1^T \tilde{P} \tilde{A}_1 + \lambda \tilde{A}_2^T \tilde{P} \tilde{A}_2] \tilde{x}(t) + 2 \tilde{x}^T(t) \\ &\cdot [\tilde{P} \tilde{E} + \tilde{A}_1^T \tilde{P} \tilde{E}_1 + \lambda \tilde{A}_2^T \tilde{P} \tilde{E}_2] \tilde{w}(t) \\ &+ \tilde{w}^T [\tilde{E}_1^T \tilde{P} \tilde{E}_1 + \lambda \tilde{E}_2^T \tilde{P} \tilde{E}_2] \tilde{w} \} dt.\end{aligned}\quad (28)$$

Thus, we have

$$\begin{aligned}& \int_0^{t_f} \mathbb{E} [ \tilde{x}^T(t) \tilde{Q} \tilde{x}(t) ] dt = \tilde{V}(\tilde{x}(0)) - \mathbb{E} [ \tilde{V}(\tilde{x}(t_f)) ] \\ &+ \int_0^{t_f} \mathbb{E} \{ \tilde{x}^T(t) \\ &\cdot [\tilde{A}^T \tilde{P} + \tilde{P} \tilde{A} + \tilde{A}_1^T \tilde{P} \tilde{A}_1 + \lambda \tilde{A}_2^T \tilde{P} \tilde{A}_2 + \tilde{Q}] \tilde{x}(t) \\ &+ 2 \tilde{x}^T(t) [\tilde{P} \tilde{E} + \tilde{A}_1^T \tilde{P} \tilde{E}_1 + \lambda \tilde{A}_2^T \tilde{P} \tilde{E}_2] \tilde{w}(t) \\ &- \tilde{w}^T [\rho^2 I - \tilde{E}_1^T \tilde{P} \tilde{E}_1 - \lambda \tilde{E}_2^T \tilde{P} \tilde{E}_2] \tilde{w} + \rho^2 \tilde{w}^T(t) \\ &\cdot \tilde{w}(t) \} dt.\end{aligned}\quad (29)$$

Completing the square for  $\tilde{w}$ , we have

$$\begin{aligned}& \int_0^{t_f} \mathbb{E} [ \tilde{x}^T(t) \tilde{Q} \tilde{x}(t) ] dt \\ &= \tilde{V}(\tilde{x}(0)) + \rho^2 \int_0^{t_f} \mathbb{E} [ \tilde{w}^T(t) \tilde{w}(t) ] dt \\ &+ \int_0^{t_f} \mathbb{E} \{ \tilde{x}^T(t) \tilde{\mathcal{H}}(\tilde{P}) \tilde{x}(t) \} dt \\ &- \mathbb{E} [ \tilde{V}(\tilde{x}(t_f)) ] \\ &- \int_0^{t_f} \mathbb{E} [ \| \tilde{w}(t) - \tilde{M}^{-1} \tilde{M}_1^T \tilde{x}(t) \|_{\tilde{R}}^2 ] dt\end{aligned}\quad (30)$$

where  $\tilde{M} = \rho^2 I - \tilde{E}_1^T \tilde{P} \tilde{E}_1 - \lambda \tilde{E}_2^T \tilde{P} \tilde{E}_2$  and  $\tilde{M}_1 = \tilde{P} \tilde{E} + \tilde{A}_1^T \tilde{P} \tilde{E}_1 + \lambda \tilde{A}_2^T \tilde{P} \tilde{E}_2$ . Together with (24), inequality (24) is proved. This ends the proof.  $\square$

In order to find a solution for matrix inequality (24), suppose  $\tilde{P}$  has the following block form

$$\tilde{P} = \begin{bmatrix} P_{11} & 0 & 0 \\ 0 & P_{22} & 0 \\ 0 & 0 & P_{33} \end{bmatrix}, \quad (31)$$

and then

$$\mathcal{H}(\tilde{P}) = \begin{bmatrix} \tilde{\mathcal{H}}_{11} & \tilde{\mathcal{H}}_{12} & \tilde{\mathcal{H}}_{13} \\ * & \tilde{\mathcal{H}}_{22} & \tilde{\mathcal{H}}_{23} \\ * & * & \tilde{\mathcal{H}}_{33} \end{bmatrix}, \quad (32)$$

where

$$\begin{aligned} \tilde{\mathcal{H}}_{11} &= A^T P_{11} + P_{11} A - C^T L^T P_{11} - P_{11} L C + K^T R K \\ &\quad + \frac{1}{\rho^2} P_{11} L L^T P_{11} + P_{11} E M^{-1} E^T P_{11}, \\ \tilde{\mathcal{H}}_{12} &= -K^T B^T P_{22} + P_{11} E M^{-1} [E^T P_{22} \\ &\quad + E_1^T (P_{11} + P_{22}) A_1 + \lambda E_2^T (P_{11} + P_{22}) A_2] \\ &\quad - K^T R K, \\ \tilde{\mathcal{H}}_{13} &= K^T R K, \\ \tilde{\mathcal{H}}_{22} &= (A^T + K^T B^T) P_{22} + P_{22} (A + B K) + Q \\ &\quad + K^T R K + A_1^T (P_{11} + P_{22}) A_1 + \lambda A_2^T (P_{11} + P_{22}) \\ &\quad \cdot A_2 + [P_{22} E + A_1^T (P_{11} + P_{22}) E_1 \\ &\quad + \lambda A_2^T (P_{11} + P_{22}) E_2] M^{-1} [E^T P_{22} \\ &\quad + E_1^T (P_{11} + P_{22}) A_1 + \lambda E_2^T (P_{11} + P_{22}) A_2], \\ \tilde{\mathcal{H}}_{23} &= -P_{22} B K - K^T R K - Q, \\ \tilde{\mathcal{H}}_{33} &= A_r^T P_{33} + P_{33} A_r + Q + K^T R K + \frac{1}{\rho^2} P_{33} P_{33}, \end{aligned} \quad (33)$$

and

$$M = \rho^2 I - E_1^T (P_{11} + P_{22}) E_1 - \lambda E_2^T (P_{11} + P_{22}) E_2. \quad (34)$$

Because

$$\begin{aligned} \tilde{\mathcal{H}}_{11} &= A^T P_{11} + P_{11} A + K^T R K + P_{11} E M^{-1} E^T P_{11} \\ &\quad - \rho^2 C^T C \\ &\quad + \frac{1}{\rho^2} (P_{11} L - \rho^2 C^T) (P_{11} L - \rho^2 C^T)^T, \end{aligned} \quad (35)$$

and

$$\begin{aligned} \tilde{\mathcal{H}}_{22} &= A^T P_{22} + P_{22} A - P_{22} B R^{-1} B^T P_{22} + Q + A_1^T (P_{11} \\ &\quad + P_{22}) A_1 + \lambda A_2^T (P_{11} + P_{22}) A_2 + [P_{22} E \\ &\quad + A_1^T (P_{11} + P_{22}) E_1 + \lambda A_2^T (P_{11} + P_{22}) E_2] \\ &\quad \cdot M^{-1} [E^T P_{22} + E_1^T (P_{11} + P_{22}) A_1 \\ &\quad + \lambda E_2^T (P_{11} + P_{22}) A_2] + (K + R^{-1} B^T P_{22})^T R (K \\ &\quad + R^{-1} B^T P_{22}), \end{aligned} \quad (36)$$

we take  $L = \rho^2 P_{11}^{-1} C^T$  and  $K = -R^{-1} B^T P_{22}$ . Then

$$\begin{aligned} \tilde{\mathcal{H}}_{11} &= A^T P_{11} + P_{11} A + P_{22} B R^{-1} B^T P_{22} - \rho^2 C^T C \\ &\quad + P_{11} E M^{-1} E^T P_{11}, \\ \tilde{\mathcal{H}}_{12} &= P_{11} E M^{-1} [E^T P_{22} + E_1^T (P_{11} + P_{22}) A_1 \\ &\quad + \lambda E_2^T (P_{11} + P_{22}) A_2], \\ \tilde{\mathcal{H}}_{13} &= P_{22} B R^{-1} B^T P_{22}, \\ \tilde{\mathcal{H}}_{22} &= A^T P_{22} + P_{22} A - P_{22} B R^{-1} B^T P_{22} + Q + A_1^T (P_{11} \\ &\quad + P_{22}) A_1 + \lambda A_2^T (P_{11} + P_{22}) A_2 + [P_{22} E \\ &\quad + A_1^T (P_{11} + P_{22}) E_1 + \lambda A_2^T (P_{11} + P_{22}) E_2] M^{-1} \\ &\quad \times [E^T P_{22} + E_1^T (P_{11} + P_{22}) A_1 \\ &\quad + \lambda E_2^T (P_{11} + P_{22}) A_2], \\ \tilde{\mathcal{H}}_{23} &= -Q, \\ \tilde{\mathcal{H}}_{33} &= A_r^T P_{33} + P_{33} A_r + Q + P_{22} B R^{-1} B^T P_{22} + \frac{1}{\rho^2} \\ &\quad \cdot P_{33} P_{33}. \end{aligned} \quad (37)$$

**Proposition 6.** Suppose  $P_{11} \in \mathcal{S}_+(\mathbb{R})$ ,  $P_{22} \in \mathcal{S}_+(\mathbb{R})$ , and  $P_{33} \in \mathcal{S}_+(\mathbb{R})$  are the solution of the following block matrix inequality:

$$H := \begin{bmatrix} H_{11} & 0 & 0 & P_{11} E & 0 & P_{22} B \\ * & H_{22} & -Q & H_{24} & 0 & 0 \\ * & * & H_{33} & 0 & P_{33} & 0 \\ * & * & * & -M & 0 & 0 \\ * & * & * & * & -\rho^2 I & 0 \\ * & * & * & * & * & -R \end{bmatrix} \leq 0, \quad (38)$$

and

$$M < 0, \quad (39)$$

where

$$\begin{aligned}
H_{11} &= A^T P_{11} + P_{11} A - \rho^2 C^T C, \\
H_{22} &= A^T P_{22} + P_{22} A - P_{22} B R^{-1} B^T P_{22} + Q, \\
H_{23} &= -Q, \\
H_{24} &= P_{22} E + A_1^T (P_{11} + P_{22}) E_1 \\
&\quad + \lambda A_2^T (P_{11} + P_{22}) E_2, \\
H_{33} &= A_r^T P_{33} + P_{33} A_r + Q.
\end{aligned} \tag{40}$$

Then  $\tilde{P}$  with form of (31),  $L = \rho^2 P_{11}^{-1} C^T$  and  $K = -R^{-1} B^T P_{22}$  are the solutions of (24) and (25). Moreover, the  $H_\infty$  tracking control performance in (24) is guaranteed for a prescribed  $\rho^2$ .

*Proof.* Applying the well-known Schur definiteness criterion to symmetric block matrix  $H$ , together with  $L = \rho^2 P_{11}^{-1} C^T$  and  $K = -R^{-1} B^T P_{22}$ , it is easy to see that (38) is equivalent to (24). As far as the  $H_\infty$  tracking control performance in (24) is guaranteed, it can be directly obtained by Theorem 5.  $\square$

*Remark 7.* In equation (32) and (37), if there exists  $P_{11} > 0$  such that  $\tilde{\mathcal{H}}_{11} \leq 0$ , this implies

$$A^T P_{11} + P_{11} A - C^T L^T P_{11} - P_{11} L C \leq 0, \tag{41}$$

i.e.,

$$(A - LC)^T P_{11} + P_{11} (A - LC) \leq 0. \tag{42}$$

Thus, the following system

$$d\bar{e}(t) = (A - LC) \bar{e}(t) dt \tag{43}$$

is stable. Furthermore, if there exists  $P_{11} > 0$  such that  $\tilde{\mathcal{H}}_{11} < 0$ , this implies

$$(A - LC)^T P_{11} + P_{11} (A - LC) < 0. \tag{44}$$

Therefore, system (43) is asymptotically stable; i.e.,  $A - LC$  is stable. In this paper, the estimation error system (17) can be seen as the extension of (43) where (17) presents the differences between  $\hat{x}(t)$  and  $x(t)$ . Furthermore, in (38),  $H_{11} < 0$ ; i.e.,

$$A^T P_{11} + P_{11} A - \rho^2 C^T C < 0, \tag{45}$$

and if  $C = 0$ , then  $A$  is stable. However, in general,  $C \neq 0$ ; the matrix  $A$  is not necessarily stable.

#### 4. Nonlinear Systems and Corresponding Fuzzy Systems

For nonlinear system as in the following forms

$$\begin{aligned}
dx(t) &= [f(x(t)) + g(x(t))u(t) + E(x)w(t)] dt \\
&\quad + [f_1(x(t)) + E_1(x)w(t)] dW_1(t) \\
&\quad + [f_2(x(t)) + E_2(x)w(t)] dN_1(t), \\
y(t) &= m(x(t)) + v, \quad i = 1, 2, \dots, r,
\end{aligned} \tag{46}$$

the reference model is suggested as follows:

$$dx_r(t) = [f_r(x_r(t)) + r(t)] dt. \tag{47}$$

The observer is proposed to deal with the state estimation of system (46)

$$\begin{aligned}
d\hat{x}(t) &= [f(\hat{x}(t)) + g(\hat{x}(t))u(t) \\
&\quad + L(\hat{x})(y(t) - \hat{y}(t))] dt, \quad \hat{y}(t) = m(\hat{x}(t)).
\end{aligned} \tag{48}$$

Let

$$e(t) = x(t) - \hat{x}(t), \tag{49}$$

and denote  $\tilde{x} = [e^T, x^T, x_r^T]^T$ ,  $\tilde{w} = [v^T, w^T, r^T]^T$ . Design the control  $u$  with form of

$$u(t) = K(\tilde{x}(t)) [\tilde{x}(t) - x_r(t)], \tag{50}$$

and then

$$\begin{aligned}
d\tilde{x}(t) &= [\tilde{f}(\tilde{x}(t)) + \tilde{E}(\tilde{x}(t))\tilde{w}(t)] dt \\
&\quad + [\tilde{f}_1(\tilde{x}(t)) + \tilde{E}_1(\tilde{x}(t))\tilde{w}(t)] dW_1(t) \\
&\quad + [\tilde{f}_2(\tilde{x}(t)) + \tilde{E}_2(\tilde{x}(t))\tilde{w}(t)] dN_1(t),
\end{aligned} \tag{51}$$

where

$$\begin{aligned}
\tilde{f}(\tilde{x}) &= [(f(x) - f(\hat{x})) \\
&\quad + (g(x) - g(\hat{x}))K(\hat{x})(\hat{x} - x_r) \\
&\quad - L(\hat{x})(m(x) - m(\hat{x}))]^T, (f(x) \\
&\quad + g(x)K(\hat{x})(\hat{x} - x_r))^T, f_r(x_r)^T]^T, \\
\tilde{f}_1(\tilde{x}) &= [f_1(x)^T, f_1(x)^T, 0^T]^T, \\
\tilde{f}_2(\tilde{x}) &= [f_2(x)^T, f_2(x)^T, 0^T]^T, \\
\tilde{E}(\tilde{x}) &= \begin{bmatrix} -L(\hat{x}) & E(x) & 0 \\ 0 & E(x) & 0 \\ 0 & 0 & I \end{bmatrix}, \\
\tilde{E}_1(\tilde{x}) &= \begin{bmatrix} 0 & E_1(x) & 0 \\ 0 & E_1(x) & 0 \\ 0 & 0 & 0 \end{bmatrix}, \\
\tilde{E}_2(\tilde{x}) &= \begin{bmatrix} 0 & E_2(x) & 0 \\ 0 & E_2(x) & 0 \\ 0 & 0 & 0 \end{bmatrix}.
\end{aligned} \tag{52}$$

For a positive function  $\tilde{l}(\tilde{x})$ , an auxiliary positive function  $\tilde{V}$  is suggested. The  $H_\infty$  tracking performance considering the initial condition is given by

$$\begin{aligned}
\int_0^{t_f} \mathbb{E} [\tilde{l}(\tilde{x}(t))] dt \leq \tilde{V}(\tilde{x}(0)) \\
+ \rho^2 \int_0^{t_f} \mathbb{E} [\tilde{w}^T(t)\tilde{w}(t)] dt.
\end{aligned} \tag{53}$$

**Theorem 8.** Suppose  $\tilde{V} : \mathbb{R}^{3n} \rightarrow \mathbb{R}_+$ ,  $K(\tilde{x})$ ,  $L(\tilde{x})$  constitute the solution of the following Hamilton-Jacobi inequality:

$$\tilde{\mathcal{H}}_1(\tilde{V})(\tilde{x}) \leq 0, \quad (54)$$

$$\rho^2 I - \frac{1}{2} \tilde{E}_1^T \tilde{V}_{\tilde{x}\tilde{x}} \tilde{E}_1 - \frac{\lambda}{2} \tilde{E}_2^T S \tilde{E}_2 > 0, \quad (55)$$

where (variable  $\tilde{x}$  is omitted)

$$\begin{aligned} \tilde{\mathcal{H}}_1(\tilde{V})(\tilde{x}) := & \tilde{V}_{\tilde{x}}^T (\tilde{f} + \lambda \tilde{f}_2) + \frac{1}{2} \tilde{f}_1^T \tilde{V}_{\tilde{x}\tilde{x}} \tilde{f}_1 + \frac{\lambda}{2} \tilde{f}_2^T S \tilde{f}_2 \\ & + \tilde{l} + \frac{1}{4} (\tilde{V}_{\tilde{x}}^T \tilde{E} + \tilde{f}_1^T \tilde{V}_{\tilde{x}\tilde{x}} \tilde{E}_1 + \lambda \tilde{V}_{\tilde{x}}^T \tilde{E}_2 + \lambda \tilde{f}_2^T S \tilde{E}_2) \\ & \times \left( \rho^2 I - \frac{1}{2} \tilde{E}_1^T \tilde{V}_{\tilde{x}\tilde{x}} \tilde{E}_1 - \frac{\lambda}{2} \tilde{E}_2^T S \tilde{E}_2 \right)^{-1} \\ & \cdot (\tilde{V}_{\tilde{x}}^T \tilde{E} + \tilde{f}_1^T \tilde{V}_{\tilde{x}\tilde{x}} \tilde{E}_1 + \lambda \tilde{V}_{\tilde{x}}^T \tilde{E}_2 + \lambda \tilde{f}_2^T S \tilde{E}_2)^T, \end{aligned} \quad (56)$$

and  $S \in \mathcal{S}_+(\mathbb{R})$  is a fixed positive definite matrix with

$$\tilde{V}_{\tilde{x}\tilde{x}}(\tilde{x}) \leq S. \quad (57)$$

Then the  $H_\infty$  tracking control performance in (53) is guaranteed for a prescribed  $\rho^2 > 0$ .

*Proof.* Applying Itô's formula to  $\tilde{V}(\tilde{x}(t))$ , there exist

$$\begin{aligned} & \int_0^{t_f} \mathbb{E} [\tilde{l}(\tilde{x}(t))] dt \\ & = \tilde{V}(\tilde{x}_0) - \mathbb{E} [\tilde{V}(\tilde{x}_{t_f})] \\ & \quad + \rho^2 \int_0^{t_f} \mathbb{E} [\tilde{w}^T(t) \tilde{w}(t)] dt \\ & \quad + \int_0^{t_f} \mathbb{E} [\tilde{\mathcal{H}}_1(\tilde{V})(\tilde{x}(t)) - \|\tilde{w}(t) - \xi(t)\|_{\Xi}^2] dt, \end{aligned} \quad (58)$$

where

$$\begin{aligned} \Xi = & \rho^2 I - \frac{1}{2} \tilde{E}_1^T (\tilde{x}(t)) \tilde{V}_{\tilde{x}\tilde{x}} (\tilde{x}(t)) \tilde{E}_1 (\tilde{x}(t)) - \frac{\lambda}{2} \\ & \cdot \tilde{E}_2^T (\tilde{x}(t)) S \tilde{E}_2 (\tilde{x}(t)) \\ \xi(t) = & \frac{1}{2} \Xi^{-1} [\tilde{V}_{\tilde{x}}^T (\tilde{x}(t)) \tilde{E} (\tilde{x}(t)) \\ & + \tilde{f}_1^T (\tilde{x}(t)) \tilde{V}_{\tilde{x}\tilde{x}} (\tilde{x}(t)) \tilde{E}_1 (\tilde{x}(t)) \\ & + \lambda \tilde{V}_{\tilde{x}}^T (\tilde{x}(t)) \tilde{E}_2 (\tilde{x}(t)) + \lambda \tilde{f}_2^T (\tilde{x}(t)) S \tilde{E}_2 (\tilde{x}(t))]^T. \end{aligned} \quad (59)$$

Keeping in mind that  $\tilde{V}$  is positive and applying (54), we prove that

$$\int_0^{t_f} \mathbb{E} [\tilde{l}(\tilde{x}(t))] dt \leq \rho^2 \int_0^{t_f} \mathbb{E} [\tilde{w}^T(t) \tilde{w}(t)] dt. \quad (60)$$

This ends the proof.  $\square$

The nonlinear system (46), (47), (48), (50), and (51) can be described by T-S fuzzy model as follows.

*Model Rule i*

IF  $\zeta(t)$  is  $M_{i1}$ , and  $\dots$  and  $\zeta_p(t)$  is  $M_{ip}$ , THEN

$$\begin{aligned} dx(t) = & [A^{(i)} x(t) + B^{(i)} u(t) + w(t)] dt \\ & + [A_1^{(i)} x(t) + w(t)] dW_1(t) \\ & + [A_2^{(i)} x(t) + w(t)] dN_1(t), \end{aligned} \quad (61)$$

$$y(t) = C^{(i)} x(t) + v, \quad i = 1, 2, \dots, r.$$

Corresponding reference model is suggested as follows:

$$dx_r(t) = [A_r^{(i)} x_r(t) + r(t)] dt, \quad (62)$$

where  $\zeta(t) = (\zeta_1(t), \dots, \zeta_p(t))$  are the premise variables,  $M_{ij}$  is the fuzzy set, and  $r$  is the number of model rules.

The following observer is proposed to deal with the state estimation of fuzzy system (61)

$$\begin{aligned} d\hat{x}(t) = & [A^{(i)} \hat{x}(t) + B^{(i)} u(t) + L^{(i)} (y(t) - \hat{y}(t))] dt, \\ \hat{y}(t) = & C^{(i)} \hat{x}(t). \end{aligned} \quad (63)$$

Then the controller  $u(t)$  has the form as

$$u(t) = K^{(i)} [\hat{x}(t) - x_r(t)]. \quad (64)$$

Let  $\tilde{M}_{ij}(\zeta_j(t))$  be the grade of membership of  $\zeta_j(t)$  in  $M_{ij}$ ; then the membership function of  $\zeta(t)$  for the  $i$ 'th rule is

$$\mu_i(\zeta(t)) = \tilde{M}_{i1} \tilde{M}_{i2} \dots \tilde{M}_{ip} \geq 0, \quad (65)$$

with  $\sum_{i=1}^r \mu_i(\zeta(t)) > 0$ . The standard membership function is defined by

$$h_i(\zeta(t)) = \frac{\mu_i(\zeta(t))}{\sum_{i=1}^r \mu_i(\zeta(t))}. \quad (66)$$

Then the fuzzy system is inferred as

$$\begin{aligned} dx(t) = & \sum_{i=1}^r h_i(\zeta(t)) \{ [A^{(i)} x(t) + B^{(i)} u(t) + w(t)] dt \\ & + [A_1^{(i)} x(t) + w(t)] dW_1(t) \\ & + [A_2^{(i)} x(t) + w(t)] dN_1(t) \}, \end{aligned} \quad (67)$$

$$y(t) = \sum_{i=1}^r h_i(\zeta(t)) \{ C^{(i)} x(t) + v \},$$

and

$$\begin{aligned} d\hat{x}(t) = & \sum_{i=1}^r h_i(\zeta(t)) \\ & \cdot \{ [A^{(i)} \hat{x}(t) + B^{(i)} u(t) + L^{(i)} (y(t) - \hat{y}(t))] dt \}, \end{aligned} \quad (68)$$

$$\hat{y}(t) = \sum_{i=1}^r h_i(\zeta(t)) \{ C^{(i)} \hat{x}(t) \},$$

with estimation errors

$$\begin{aligned}
 de(t) &= \sum_{i=1}^r h_i(\zeta(t)) \\
 &\cdot \left\{ \left[ A^{(i)} e(t) - L^{(i)} (y(t) - \hat{y}(t)) + w(t) \right] dt \right. \\
 &+ \left[ A_1^{(i)} x(t) + w(t) \right] dW_1(t) \\
 &+ \left. \left[ A_2^{(i)} x(t) + w(t) \right] dN_1(t) \right\}. \quad (69)
 \end{aligned}$$

Then the controller  $u(t)$  has the form as

$$u(t) = \sum_{i=1}^r h_i(\zeta(t)) \left\{ K^{(i)} [\hat{x}(t) - x_r(t)] \right\}. \quad (70)$$

and

$$\begin{aligned}
 l(e_r(t), u(t)) \\
 = \sum_{i=1}^r h_i(\zeta(t)) \left\{ e_r^T(t) Q^{(i)} e_r(t) + u^T(t) R^{(i)} u(t) \right\}. \quad (71)
 \end{aligned}$$

## 5. Simulation Examples

As the application of tracking system, the air-to-air missile pursuit systems are discussed, which are used to shot down escaping target such as aircraft, fighter, or missile [34, 35]. The relative dynamic motion between a homing-missile and the escaping target is described by the following system driven by both Wiener process and Poisson process.

$$\begin{aligned}
 dx_1(t) &= x_2(t) dt + c_1 x_2(t) dW(t), \\
 dx_2(t) &= \left[ \frac{x_3^2(t)}{x_1(t)} + u_1(t) + v_1(t) \right] dt \\
 &+ \left[ c_2 \frac{x_3^2(t)}{x_1(t)} + v_1(t) \right] dW(t), \\
 dx_3(t) &= \left[ -\frac{x_2(t) x_3(t)}{x_1(t)} + u_2(t) + v_2(t) \right] dt \\
 &+ \left[ c_3 \frac{x_2(t) x_3(t)}{x_1(t)} + v_2(t) \right] dW(t) \\
 &+ \left[ c_4 \frac{x_3(t)}{x_1(t)} + v_2(t) \right] dN(t), \\
 y(t) &= \begin{bmatrix} x_1(t) \\ x_3(t) \end{bmatrix}, \quad x(0) = x_0 \in D, \quad t \in [0, t_f].
 \end{aligned} \quad (72)$$

Here  $x(t) = (x_1(t), x_2(t), x_3(t))^T$  is the system state which describes the trajectory of missile, concretely;  $x_1(t)$  is the relative distance between the missile and target; see Figure 1;  $x_2(t)$  is the radial relative velocity;  $x_3(t)$  is the tangential relative velocity; see Figure 2; and  $u(t) = (u_1(t), u_2(t))^T$  is the input control with  $u_1$  and  $u_2$  being the missiles acceleration components along the  $x_1$  and  $x_2$  axes.  $W(t)$  denotes the

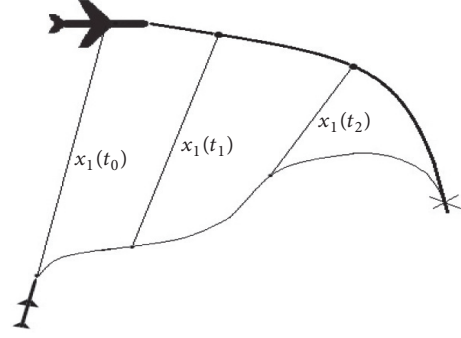


FIGURE 1: Pursuit guidance course at time  $t_0 < t_1 < t_2 < t_f$ .

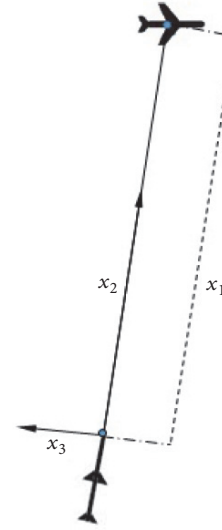


FIGURE 2: The geometric relationship between the target and missile.

continuous noise of the system such as the air friction caused by air resistance and the inner thermal noise caused by missile operating system. Poisson process  $N(t)$  denotes the sudden discrete noise of the system such as directional trimming, or deceptive behavior of the missile to avoid being shot down by shooting out gas from two side jets.  $y(t)$  is the measurement and  $t_f$  is the fighting time which denotes the missile's effective working time, and  $C = [1 \ 0 \ 1]^T$ .

Take  $t_f = 25(\text{sec})$ ,  $x_1(0) = 7875(\text{m})$ ,  $x_2(0) = -343(\text{m/s})$ ,  $x_3(0) = -10(\text{rad/s})$ ,  $c_1 = c_2 = c_3 = 0.11$ ,  $c_4 = 0.3$ ,  $Q = \text{diag}(0, 1, 1) \times 10^{-2}$ ,  $R = I_2$ , and the density of Poisson jump  $N(t)$  is 0.02; i.e.,  $\lambda = 0.02$ ,  $\rho^2 = 0.49$ , and

$$\begin{aligned}
 E = E_1 &= \begin{bmatrix} 0 & 0 \\ 1 & 0 \\ 0 & 1 \end{bmatrix} \times 10^{-3}, \\
 E_2 &= \begin{bmatrix} 0 & 0 \\ 0 & 0 \\ 0 & 1 \end{bmatrix} \times 10^{-3}. \quad (73)
 \end{aligned}$$

Let  $r(t)$  the trajectory of the target's motion which is embedded in a reference model as follows:

$$\begin{aligned} dx_r &= [A_r x_r + r(t)] dt, \\ x_r(0) &= x_0, \end{aligned} \quad (74)$$

where  $A_r = -I_3$  which implies the steady state  $x_r(t) = r(t)$ . Let  $r(t)$  be the reference trajectories with

$$r(t) = \begin{bmatrix} t^2 - 362.6t + 7987.6 \\ 1.3t^2 - 24.1t - 274.4 \\ -0.9t^2 + 0.0149t - 0.0509 \end{bmatrix}, \quad (75)$$

$$t \in [0, 25],$$

$$\begin{aligned} d\hat{x}_1(t) &= [\hat{x}_2(t) + L_1(y(t) - \hat{y}(t))] dt, \\ d\hat{x}_2(t) &= \frac{\hat{x}_3^2(t)}{\hat{x}_1(t)} dt, \\ d\hat{x}_3(t) &= -\frac{\hat{x}_2(t)\hat{x}_3(t)}{\hat{x}_1(t)} dt, \\ \hat{y}(t) &= \hat{x}_1(t), \quad t \in [0, t_f]. \end{aligned} \quad (76)$$

Choose the fuzzy variable  $\zeta = x_3/x_1$  and the fuzzy rules as follows:

*Rule 1* ( $\zeta$  about  $-0.45$ ).

$$\begin{aligned} A^{(1)} &= \begin{bmatrix} 0 & 1 & 0 \\ 0 & 0 & -0.45 \\ 0 & 0.45 & 0 \end{bmatrix}, \\ A_1^{(1)} &= \begin{bmatrix} 0 & 0.3 & 0 \\ 0 & 0 & -0.135 \\ 0 & 0.135 & 0 \end{bmatrix}, \\ A_2^{(1)} &= \begin{bmatrix} 0 & 0 & 0 \\ 0 & 0 & 0 \\ 0 & 0.135 & 0 \end{bmatrix}, \\ P_1^{(1)} &= \begin{bmatrix} 0.3564 & -1.584 & -0.792 \\ -1.584 & 7.4571 & 1.76 \\ -0.792 & 1.76 & 9.2171 \end{bmatrix}, \\ P_2^{(1)} &= \begin{bmatrix} 0 & 0 & 0 \\ 0 & 0.43 & 0 \\ 0 & 0 & 0.43 \end{bmatrix}, \\ P_3^{(1)} &= \begin{bmatrix} 0.49 & 0 & 0 \\ 0 & 0.49 & 0 \\ 0 & 0 & 0.49 \end{bmatrix} \end{aligned} \quad (77)$$

*Rule 2* ( $\zeta$  about  $-0.3$ ).

$$\begin{aligned} A^{(2)} &= \begin{bmatrix} 0 & 1 & 0 \\ 0 & 0 & -0.3 \\ 0 & 0.3 & 0 \end{bmatrix}, \\ A_1^{(2)} &= \begin{bmatrix} 0 & 0.3 & 0 \\ 0 & 0 & -0.09 \\ 0 & 0.09 & 0 \end{bmatrix}, \\ A_2^{(2)} &= \begin{bmatrix} 0 & 0 & 0 \\ 0 & 0 & 0 \\ 0 & -0.09 & 0 \end{bmatrix}, \\ P_1^{(2)} &= \begin{bmatrix} 0.2376 & -1.584 & -0.792 \\ -1.584 & 11.1857 & 2.64 \\ -0.792 & 2.64 & 13.8257 \end{bmatrix}, \\ P_2^{(2)} &= \begin{bmatrix} 0 & 0 & 0 \\ 0 & 0.35 & 0 \\ 0 & 0 & 0.35 \end{bmatrix}, \\ P_3^{(2)} &= \begin{bmatrix} 0.49 & 0 & 0 \\ 0 & 0.49 & 0 \\ 0 & 0 & 0.49 \end{bmatrix} \end{aligned} \quad (78)$$

*Rule 3* ( $\zeta$  about  $-0.15$ ).

$$\begin{aligned} A^{(3)} &= \begin{bmatrix} 0 & 1 & 0 \\ 0 & 0 & -0.15 \\ 0 & 0.15 & 0 \end{bmatrix}, \\ A_1^{(3)} &= \begin{bmatrix} 0 & 0.3 & 0 \\ 0 & 0 & -0.045 \\ 0 & 0.045 & 0 \end{bmatrix}, \\ A_2^{(3)} &= \begin{bmatrix} 0 & 0 & 0 \\ 0 & 0 & 0 \\ 0 & -0.045 & 0 \end{bmatrix}, \\ P_1^{(3)} &= \begin{bmatrix} 0.1188 & -1.584 & -0.792 \\ -1.584 & 22.3714 & 5.28 \\ -0.792 & 5.28 & 27.6514 \end{bmatrix}, \\ P_2^{(3)} &= \begin{bmatrix} 0 & 0 & 0 \\ 0 & 0.25 & 0 \\ 0 & 0 & 0.25 \end{bmatrix}, \\ P_3^{(3)} &= \begin{bmatrix} 0.49 & 0 & 0 \\ 0 & 0.49 & 0 \\ 0 & 0 & 0.49 \end{bmatrix} \end{aligned} \quad (79)$$

Rule 4 ( $\zeta$  about  $-0.07$ ).

$$A^{(4)} = \begin{bmatrix} 0 & 1 & 0 \\ 0 & 0 & -0.07 \\ 0 & 0.07 & 0 \end{bmatrix},$$

$$A_1^{(4)} = \begin{bmatrix} 0 & 0.3 & 0 \\ 0 & 0 & -0.021 \\ 0 & 0.021 & 0 \end{bmatrix}$$

$$A_2^{(4)} = \begin{bmatrix} 0 & 0 & 0 \\ 0 & 0 & 0 \\ 0 & -0.021 & 0 \end{bmatrix},$$

$$P_1^{(4)} = \begin{bmatrix} 0.055468 & -1.5848 & -0.7924 \\ -1.5848 & 47.9628 & 11.32 \\ -0.7924 & 11.32 & 59.2828 \end{bmatrix},$$

$$P_2^{(4)} = \begin{bmatrix} 0 & 0 & 0 \\ 0 & 0.17 & 0 \\ 0 & 0 & 0.17 \end{bmatrix},$$

$$P_3^{(4)} = \begin{bmatrix} 0.49 & 0 & 0 \\ 0 & 0.49 & 0 \\ 0 & 0 & 0.49 \end{bmatrix}$$

Rule 5 ( $\zeta$  about  $-0.04$ ).

$$A^{(5)} = \begin{bmatrix} 0 & 1 & 0 \\ 0 & 0 & -0.04 \\ 0 & 0.04 & 0 \end{bmatrix},$$

$$A_1^{(5)} = \begin{bmatrix} 0 & 0.3 & 0 \\ 0 & 0 & -0.012 \\ 0 & 0.012 & 0 \end{bmatrix}$$

$$A_2^{(5)} = \begin{bmatrix} 0 & 0 & 0 \\ 0 & 0 & 0 \\ 0 & -0.012 & 0 \end{bmatrix}$$

$$P_1^{(5)} = \begin{bmatrix} 0.031712 & -1.5856 & -0.7928 \\ -1.5856 & 83.9773 & 19.82 \\ -0.7928 & 19.82 & 103.7973 \end{bmatrix},$$

$$P_2^{(5)} = \begin{bmatrix} 0 & 0 & 0 \\ 0 & 0.13 & 0 \\ 0 & 0 & 0.13 \end{bmatrix},$$

$$P_3^{(5)} = \begin{bmatrix} 0.49 & 0 & 0 \\ 0 & 0.49 & 0 \\ 0 & 0 & 0.49 \end{bmatrix}$$

Rule 6 ( $\zeta$  about  $-0.012$ ).

$$A^{(6)} = \begin{bmatrix} 0 & 1 & 0 \\ 0 & 0 & -0.012 \\ 0 & 0.012 & 0 \end{bmatrix}$$

$$A_1^{(6)} = \begin{bmatrix} 0 & 0.3 & 0 \\ 0 & 0 & -0.0036 \\ 0 & 0.0036 & 0 \end{bmatrix},$$

$$A_2^{(6)} = \begin{bmatrix} 0 & 0 & 0 \\ 0 & 0 & 0 \\ 0 & -0.0036 & 0 \end{bmatrix}$$

$$P_1^{(6)} = \begin{bmatrix} 0.0095126 & -1.5854 & -0.79272 \\ -1.5854 & 279.8962 & 66.06 \\ -0.79272 & 66.06 & 345.9562 \end{bmatrix},$$

$$P_2^{(6)} = \begin{bmatrix} 0 & 0 & 0 \\ 0 & 0.07 & 0 \\ 0 & 0 & 0.07 \end{bmatrix},$$

$$P_3^{(6)} = \begin{bmatrix} 0.49 & 0 & 0 \\ 0 & 0.49 & 0 \\ 0 & 0 & 0.49 \end{bmatrix}$$

(80)

(82)

Rule 7 ( $\zeta$  about  $-0.008$ ).

$$A^{(7)} = \begin{bmatrix} 0 & 1 & 0 \\ 0 & 0 & -0.008 \\ 0 & 0.008 & 0 \end{bmatrix}$$

$$A_1^{(7)} = \begin{bmatrix} 0 & 0.3 & 0 \\ 0 & 0 & -0.0024 \\ 0 & 0.0024 & 0 \end{bmatrix},$$

$$A_2^{(7)} = \begin{bmatrix} 0 & 0 & 0 \\ 0 & 0 & 0 \\ 0 & 0.0024 & 0 \end{bmatrix}$$

$$P_1^{(7)} = \begin{bmatrix} 0.0063424 & -1.5856 & -0.7928 \\ -1.5856 & 419.8867 & 99.1 \\ -0.7928 & 99.1 & 518.9867 \end{bmatrix},$$

$$P_2^{(7)} = \begin{bmatrix} 0 & 0 & 0 \\ 0 & 0.06 & 0 \\ 0 & 0 & 0.06 \end{bmatrix},$$

$$P_3^{(7)} = \begin{bmatrix} 0.49 & 0 & 0 \\ 0 & 0.49 & 0 \\ 0 & 0 & 0.49 \end{bmatrix}.$$

(81)

(83)

*Remark 9.* We find that, in the fuzzy rules, the coefficients of  $A^{(i)}$  have the form with

$$A = \begin{bmatrix} 0 & 1 & 0 \\ 0 & 0 & -b \\ 0 & b & 0 \end{bmatrix}, \quad (84)$$

where  $b > 0$ . For every rule  $i$ ,  $P_{11}$ ,  $P_{22}$ , and  $P_{33}$  are solved by the following steps:

*Step 1.* Solve  $P_{11}^* > 0$  such that

$$P_{11}^* = \arg \max_{P_{11} > 0} \alpha \quad (85)$$

subject to

$$A^T P_{11} + P_{11} A - \rho^2 C^T C \leq -\alpha I, \quad (86)$$

$$\alpha > 0. \quad (87)$$

The above optimal  $P_{11}^*$  could be solved by increasing  $\alpha$  until  $P_{11}$  cannot be found in LMIs (86) and (87).

*Step 2.* Fix  $P_{11} = P_{11}^*$  solved by Step 1. Suppose  $P_{22}$  has the form of

$$P_{22} = \begin{bmatrix} 0 & 0 & 0 \\ 0 & p & q \\ 0 & q & p \end{bmatrix}, \quad (88)$$

where  $p > 0, q \geq 0$ . Solve  $p, q$  such that

$$\bar{\mathcal{H}}_2 := \begin{bmatrix} \bar{\mathcal{H}}_{11} & \bar{\mathcal{H}}_{12} \\ * & \bar{\mathcal{H}}_{22} \end{bmatrix} \leq 0, \quad (89)$$

where  $\bar{\mathcal{H}}_{ij}$  is determined by (37),  $i, j = 1, 2$ . Under the conditions of  $p > 0, p^2 > q^2$ , for a fixed  $q$ ,  $P_{22}$  can be solved by increasing  $p$  until matrix inequality (89) can be true.

*Step 3.* Fix  $P_{11}$  and  $P_{22}$  which are determined by Steps 1 and 2. The positive definite matrix  $P_{33} > 0$  can be obtained by solving the LMIs (38) in which  $P_{11}$  and  $P_{22}$  are fixed matrices.

The weighted function  $h_i(\zeta)$  is given by

$$h_1(\zeta) = \begin{cases} 1 - \frac{\zeta - \zeta_1}{\zeta_2 - \zeta_1}, & \zeta_1 \leq \zeta < \zeta_2 \\ 1, & \zeta < \zeta_1 \\ 0, & \text{others} \end{cases} \quad (90)$$

$$h_i(\zeta) = \begin{cases} 1 - \frac{\zeta - \zeta_i}{\zeta_{i+1} - \zeta_i}, & \zeta_i \leq \zeta < \zeta_{i+1} \\ 1 - \frac{\zeta_i - \zeta}{\zeta_i - \zeta_{i-1}}, & \zeta_{i-1} \leq \zeta < \zeta_i \\ 0, & \text{others} \end{cases} \quad (91)$$

$$h_7(\zeta) = \begin{cases} 1 - \frac{\zeta - \zeta_6}{\zeta_7 - \zeta_6}, & \zeta_6 \leq \zeta < \zeta_7 \\ 1, & \zeta_7 \leq \zeta \\ 0, & \text{others} \end{cases} \quad (92)$$

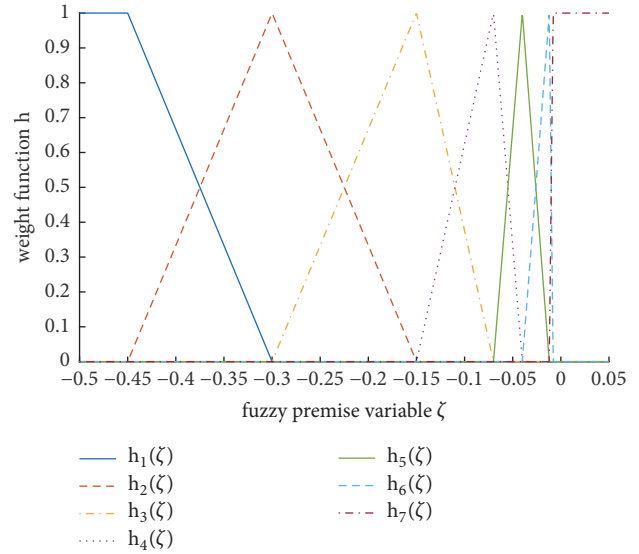


FIGURE 3: Fuzzy rules based on weighted functions  $h_i(\zeta)$  defined by (90)–(92).

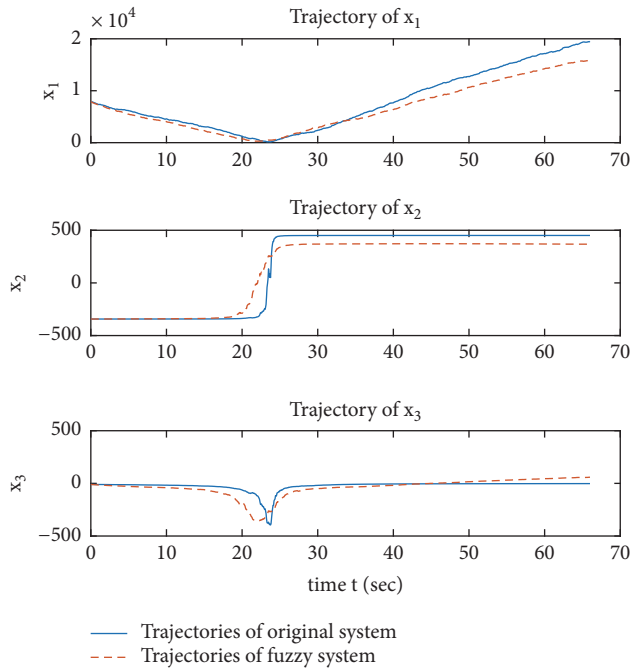


FIGURE 4: The sample trajectories of the fuzzy system (67) with coefficient matrices provided by Rules 1–7 and the original system (72).

where  $\zeta_1 = -0.45, \zeta_2 = -0.07, \zeta_3 = -0.012, \zeta_4 = -0.008, i = 2, 3, 4, 5, 6$ . Figure 3 shows the profiles of  $h_i(\zeta), i = 1, 2, \dots, 7$ .

Figure 4 shows the sample trajectories of the original system (72) and the corresponding fuzzy system (67) with  $u = 0$  and  $v = 0$ . This illustrates that the T-S fuzzy method can be used to approximate the stochastic nonlinear systems via the fuzzy systems with proper coefficients given by Rule  $i, i = 1, 2, \dots, 7$ .

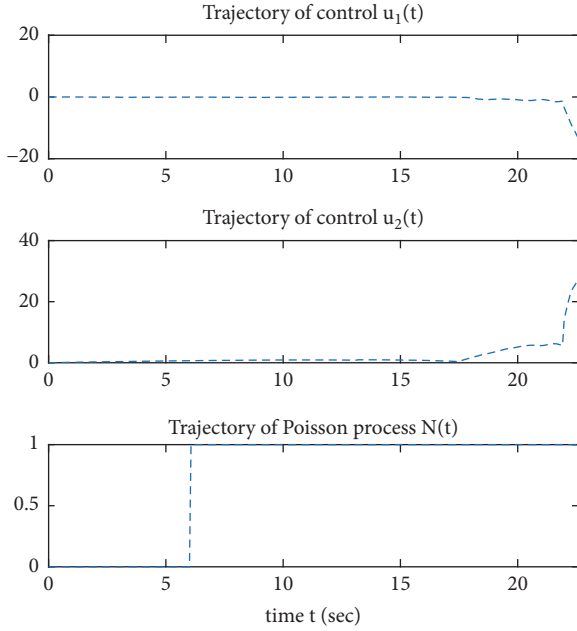


FIGURE 5: The sample trajectories of fuzzy control  $u_1(t)$ ,  $u_2(t)$  for fuzzy system (67) with coefficient matrices provided by Rules 1–7 corresponding to nonlinear system (72) under Poisson process.

By (70), the  $H_\infty$  tracking fuzzy control  $u(t) = [u_1(t), u_2(t)]^T$  is obtained by

$$u(t) = \sum_{i=1}^7 h_i(\zeta(t)) \{K^{(i)} [\hat{x}(t) - x_r(t)]\}. \quad (93)$$

Here  $K^{(i)} = -P_{22}^{(i)}$ ,  $i = 1, 2, \dots, 7$ . Figure 5 illustrates the sample trajectories of fuzzy control  $u(t)$  for system (72) with Poisson process. It shows that the values of control change violently when Poisson jumps occur.

Figures 6, 7, and 8 show the sample trajectories of the components of the state  $x(t)$ , the reference  $x_r(t)$ , and the estimation state  $\hat{x}(t)$ . These show that, under the proposed  $H_\infty$  tracking fuzzy control (93), the state  $x(t)$  and its estimation  $\hat{x}(t)$  of fuzzy system (67) with coefficient matrices provided by Rules 1–7 corresponding to (72) take values around the reference trajectory  $x_r(t)$ . Figure 9 shows the estimation error  $|e(t)|^2 = |x(t) - \hat{x}(t)|^2$  which illustrates the performance difference between the state estimation  $\hat{x}(t)$  and the state  $x(t)$ . The four figures confirm that the control defined by (93) can achieve the desired performance (53) with  $\tilde{l}(\hat{x}(t)) = l(e_r(t), u(t))$ , where  $l(e_r(t), u(t))$  is defined by (71).

Now, we compare our results with that in [35]. In [35], the guidance law uses the information for the target acceleration bound, and the guidance command is derived based on the nonlinear planar engagement kinematics. In our guidance law design, we consider the nonlinear model of the system with fuzzy method. Some comparisons are given as follows:

(1) In the control algorithm of [35], the sliding mode control scheme is used to obtain the guidance law. In our control design, an adaptive fuzzy scheme is employed to

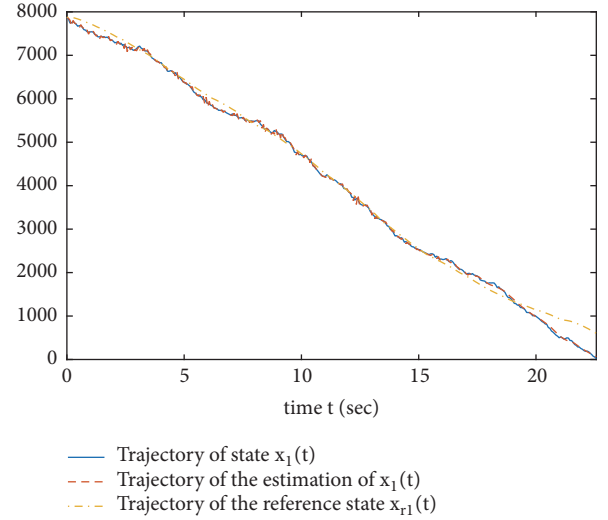


FIGURE 6: The sample trajectories of  $x_1(t)$  and  $x_{r1}(t)$  of fuzzy system (67) with coefficient matrices provided by Rules 1–7 under fuzzy control (93) corresponding to nonlinear system (72).

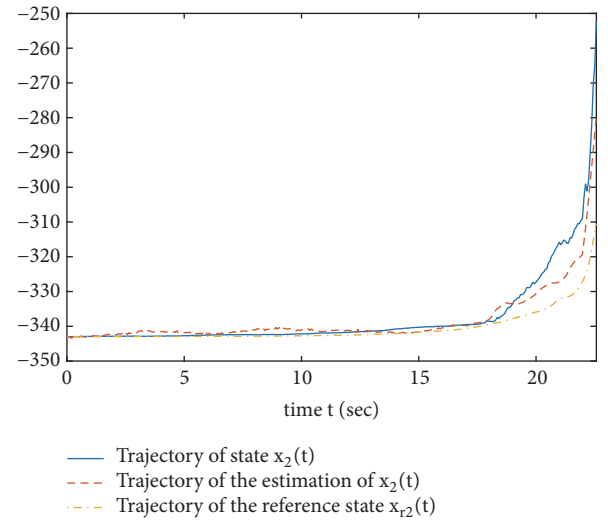


FIGURE 7: Trajectories of  $x_2(t)$  and  $x_{r2}(t)$  of fuzzy system (67) with coefficient matrices provided by Rules 1–7 under fuzzy control (93) corresponding to nonlinear system (72).

cancel the exogenous disturbance  $v(t)$  in the stochastic system with Brownian motion and Poisson jumps.

(2) The controller obtained in [35] is based on solving a nonlinear function  $V(x)$ . In our paper, the robust tracking controller is given with fuzzy forms in (70) which is only based on the locally linear approximation.

(3) The controller in [35] depends on the sliding surface and the state. Our controller  $u(t)$  in (70) depends on the difference between the state  $x(t)$  and the reference trajectory  $x_r(t)$  and the estimation errors  $e(t)$ .

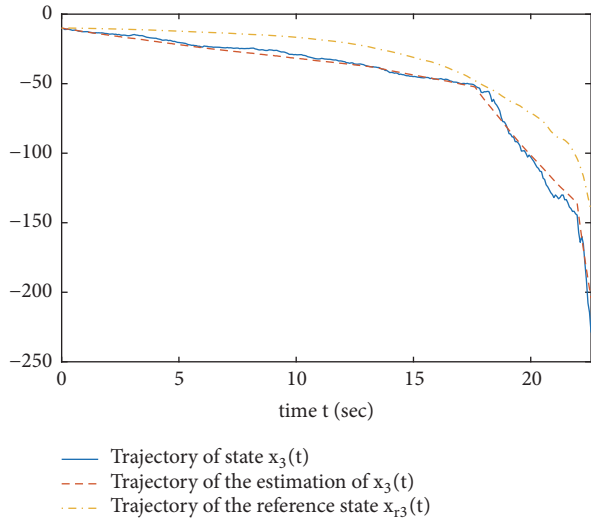


FIGURE 8: Trajectories of  $x_3(t)$  and  $x_{r3}(t)$  of fuzzy system (67) with coefficient matrices provided by Rules 1–7 under fuzzy control (93) corresponding to nonlinear system (72).

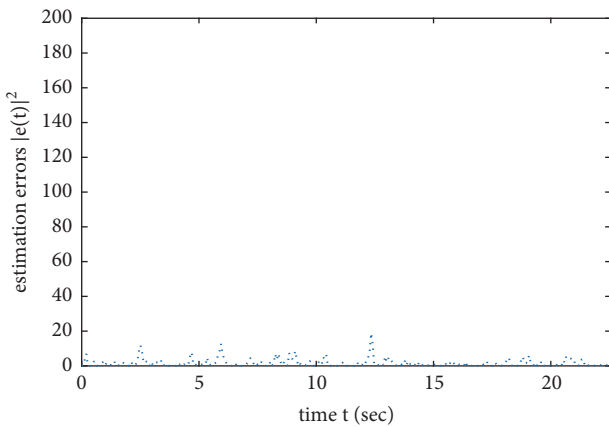


FIGURE 9: The estimation errors  $|e(t)|^2$  of fuzzy system (67) with coefficient matrices provided by Rules 1–7 under fuzzy control (93) corresponding to nonlinear system (72).

## 6. Conclusion

The  $H_\infty$  tracking control technique combining with adaptive control algorithm and T-S fuzzy method has been studied to design the  $H_\infty$  tracking control to achieve the desired performance for nonlinear stochastic systems driven by both Brownian motion and Poisson jumps. By using adaptive fuzzy control algorithms, the corresponding adaptive fuzzy control laws are derived, which have been employed to treat the  $H_\infty$  design problem. A real-world example is used to show the effectiveness of the proposed method. Simulation results illustrate that the proposed adaptive T-S fuzzy control algorithms are practically useful to achieve the  $H_\infty$  tracking performance.

## Data Availability

No data were used to support this study.

## Conflicts of Interest

The authors declare that they have no conflicts of interest.

## Acknowledgments

This work was supported by the National Natural Science Foundation of China (No. 61573227), the Research Fund for the Taishan Scholar Project of Shandong Province of China, the Natural Science Foundation of Shandong Province of China (No. ZR2016FM48, ZR2015FM014), SDUST Research Fund (No. 2015TDJH105), and the Ministry of Science and Technology of Taiwan under the contract No. MOST-106-2221-E-007-010-MY2.

## References

- [1] R. Marino and P. Tomei, “Global adaptive output-feedback control of nonlinear systems. I. Linear parameterization,” *Institute of Electrical and Electronics Engineers Transactions on Automatic Control*, vol. 38, no. 1, pp. 17–32, 1993.
- [2] M. KrsticH, I. Kanellakopoulos, and P. V. KokotovicH, *Nonlinear and Adaptive Control Design*, Wiley, New York, NY, USA, 1995.
- [3] H. K. Khalil, “Adaptive output feedback control of nonlinear systems represented by input-output models,” *IEEE Transactions on Automatic Control*, vol. 41, no. 2, pp. 177–188, 1996.
- [4] P. A. Ioannou and J. Sun, *Robust adaptive control*, Prentice-Hall, Englewood Cliffs, NJ, 1996.
- [5] A. Tewari, *Adaptive Aeroservoelastic Control*, John Wiley & Sons, West Sussex, UK, 2016.
- [6] G. Li and M. Chen, “Infinite horizon linear quadratic optimal control for stochastic difference time-delay systems,” *Advances in Difference Equations*, vol. 2015, article 14, 2015.
- [7] B. S. Chen, Ch. Hs. Lee, and Y. Ch. Chang, “ $H_\infty$  tracking design of uncertainty nonlinear SISO systems: adaptive fuzzy approach,” *IEEE Transactions on Fuzzy Systems*, vol. 4, no. 1, pp. 32–43, 1996.
- [8] Z. Yan, G. Zhang, J. Wang, and W. Zhang, “State and output feedback finite-time guaranteed cost control of linear itô stochastic systems,” *Journal of Systems Science & Complexity*, vol. 28, no. 4, pp. 813–829, 2015.
- [9] Y. Jing, Y. Liu, and S. Zhou, “Prescribed performance finite-time tracking control for uncertain nonlinear systems,” *Journal of Systems Science & Complexity*, vol. 31, pp. 1–15, 2018.
- [10] R. Postoyan, N. van de Wouw, D. Nešić, and W. P. Heemels, “Tracking control for nonlinear networked control systems,” *IEEE Transactions on Automatic Control*, vol. 59, no. 6, pp. 1539–1554, 2014.
- [11] Z. P. Jiang and H. Nijmeijer, “Tracking control of mobile robots: a case study in backstepping,” *Automatica*, vol. 33, no. 7, pp. 1393–1399, 1997.
- [12] Y.-C. Chang, “Robust tracking control for nonlinear MIMO systems via fuzzy approaches,” *Automatica*, vol. 36, no. 10, pp. 1535–1545, 2000.
- [13] H. H. Dong, B. Y. Guo, and B. S. Yin, “Generalized fractional supertrace identity for Hamiltonian structure of NLS–MKdV hierarchy with self-consistent sources,” *Analysis and Mathematical Physics*, vol. 6, no. 2, pp. 199–209, 2016.
- [14] F. Liu, Z. Wang, and F. Wang, “Hamiltonian systems with positive topological entropy and conjugate points,” *Journal of*

- Applied Analysis and Computation*, vol. 5, no. 3, pp. 527–533, 2015.
- [15] C.-S. Tseng, B.-S. Chen, and H.-J. Uang, “Fuzzy tracking control design for nonlinear dynamic systems via T-S fuzzy model,” *IEEE Transactions on Fuzzy Systems*, vol. 9, no. 3, pp. 381–392, 2001.
- [16] F. Wang, B. Chen, C. Lin, J. Zhang, and X. Meng, “Adaptive neural network finite-time output feedback control of quantized nonlinear systems,” *IEEE Transactions on Cybernetics*, vol. 48, no. 6, pp. 1839–1848, 2018.
- [17] W. Lv and F. Wang, “Adaptive tracking control for a class of uncertain nonlinear systems with infinite number of actuator failures using neural networks,” *Advances in Difference Equations*, Paper No. 374, 16 pages, 2017.
- [18] X. Lin, W. Zhang, and X. Wang, “The output feedback  $H_{\infty}$  control design for the linear stochastic system driven by both Brownian motion and Poisson jumps: A nonlinear matrix inequality approach,” *Asian Journal of Control*, vol. 15, no. 4, pp. 1139–1148, 2013.
- [19] X. Z. Meng, S. N. Zhao, T. Feng, and T. H. Zhang, “Dynamics of a novel nonlinear stochastic SIS epidemic model with double epidemic hypothesis,” *Journal of Mathematical Analysis and Applications*, vol. 433, no. 1, pp. 227–242, 2016.
- [20] X. Li, X. Lin, and Y. Lin, “Lyapunov-type conditions and stochastic differential equations driven by  $G$ -Brownian motion,” *Journal of Mathematical Analysis and Applications*, vol. 439, no. 1, pp. 235–255, 2016.
- [21] C. Tan and W. H. Zhang, “On observability and detectability of continuous-time stochastic Markov jump systems,” *Journal of Systems Science & Complexity*, vol. 28, no. 4, pp. 830–847, 2015.
- [22] X. Liu, Y. Li, and W. Zhang, “Stochastic linear quadratic optimal control with constraint for discrete-time systems,” *Applied Mathematics and Computation*, vol. 228, pp. 264–270, 2014.
- [23] Z. Yan and W. Zhang, “Finite-Time Stability and Stabilization of Itô-Type Stochastic Singular Systems,” *Abstract and Applied Analysis*, vol. 2014, Article ID 263045, 10 pages, 2014.
- [24] W. Zhang, L. Xie, and B.-S. Chen, *Stochastic  $H_2/H_{\infty}$  control: A Nash game approach*, Taylor and Francis, London, UK, 2017.
- [25] W. Zhang and B. Chen, “State feedback  $H_{\infty}$  control for a class of nonlinear stochastic systems,” *SIAM Journal on Control and Optimization*, vol. 44, no. 6, pp. 1973–1991, 2006.
- [26] Y. Cao and J. Lam, “Robust  $H_{\infty}$  control of uncertain Markovian jump systems with time delay,” *IEEE Transactions on Automatic Control*, vol. 45, no. 1, pp. 77–83, 2000.
- [27] B.-S. Chen and C.-F. Wu, “Robust scheduling filter design for a class of nonlinear stochastic Poisson signal systems,” *IEEE Transactions on Signal Processing*, vol. 63, no. 23, pp. 6245–6257, 2015.
- [28] X. Lin and R. Zhang, “ $H_{\infty}$  control for stochastic systems with Poisson jumps,” *Journal of Systems Science and Complexity*, vol. 24, no. 4, pp. 683–700, 2011.
- [29] J. Chen, T. Zhang, Z. Zhang, C. Lin, and B. Chen, “Stability and output feedback control for singular Markovian jump delayed systems,” *Mathematical Control and Related Fields*, vol. 8, no. 2, pp. 475–490, 2018.
- [30] S. Jiao, H. Shen, Y. Wei, X. Huang, and Z. Wang, “Further results on dissipativity and stability analysis of Markov jump generalized neural networks with time-varying interval delays,” *Applied Mathematics and Computation*, vol. 336, pp. 338–350, 2018.
- [31] D. Hinrichsen and A. J. Pritchard, “Stochastic  $H_{\infty}$ ,” *SIAM Journal on Control and Optimization*, vol. 36, no. 5, pp. 1504–1538, 1998.
- [32] F. B. Hanson, *Applied Stochastic Processes and Control for Jump-Diffusions*, vol. 13 of *Advances in Design and Control*, SIAM, Philadelphia, Pa, USA, 2007.
- [33] O. Kallenberg, *Foundations of modern probability*, Probability and its Applications, Springer-Verlag, New York, NY, USA, 2nd edition, 2002.
- [34] H.-J. Uang and B.-S. Chen, “Robust adaptive optimal tracking design for uncertain missile systems: a fuzzy approach,” *Fuzzy Sets and Systems*, vol. 126, no. 1, pp. 63–87, 2002.
- [35] J. Moon, K. Kim, and Y. Kim, “Design of missile guidance law via variable structure control,” *Journal of Guidance, Control, and Dynamics*, vol. 24, no. 4, pp. 659–664, 2001.

## Research Article

# Global Output Feedback Stabilization of Nonlinear Systems with a Time-Varying Power and Unknown Output Function

Chao Guo<sup>1</sup> and Kemei Zhang<sup>2</sup> 

<sup>1</sup>Institute of Automation, Qufu Normal University, Shandong Province 273165, China

<sup>2</sup>School of Mathematics Sciences, Qufu Normal University, Shandong Province 273165, China

Correspondence should be addressed to Kemei Zhang; zhkm90@126.com

Received 24 June 2018; Accepted 10 September 2018; Published 27 September 2018

Guest Editor: Weihai Zhang

Copyright © 2018 Chao Guo and Kemei Zhang. This is an open access article distributed under the Creative Commons Attribution License, which permits unrestricted use, distribution, and reproduction in any medium, provided the original work is properly cited.

This paper studies the problem of global output feedback stabilization for a class of nonlinear systems with a time-varying power and unknown output function. For nonlinear systems with a time-varying power and unknown continuous output function, by constructing a new nonlinear reduced-order observer together with adding a power integrator method, a new function to determine the maximal open sector  $\Omega$  of output function is given. As long as output function belongs to any closed sector included in  $\Omega$ , it is shown that the equilibrium point of the closed-loop system can be guaranteed globally uniformly asymptotically stable by an output feedback controller.

## 1. Introduction

Consider nonlinear systems with the unknown output function

$$\begin{aligned} \dot{x}_i(t) &= [x_{i+1}(t)]^{p(t)} + \phi_i(t, x_1(t), \dots, x_i(t)), \\ & \quad i = 1, \dots, n-1, \\ \dot{x}_n(t) &= [u(t)]^{p(t)} + \phi_n(t, x_1(t), \dots, x_n(t)), \\ y(t) &= h(x_1(t)), \end{aligned} \quad (1)$$

where  $x = (x_1, \dots, x_n)^\top \in \mathbb{R}^n$ ,  $u \in \mathbb{R}$ , and  $y \in \mathbb{R}$  are the unmeasurable state, control input, and output, respectively. For a real constant  $\varrho > 0$ ,  $[\cdot]^\varrho$  is defined as  $[\cdot]^\varrho = \text{sgn}(\cdot) \cdot |\cdot|^\varrho$ . The time-varying power  $p(t) : \mathbb{R}^+ \rightarrow \mathbb{R}^+$  is a continuous bounded function satisfying  $1 \leq \underline{p} \leq p(t) \leq \bar{p}$  with two constants  $\underline{p}$  and  $\bar{p}$ . For  $i = 1, \dots, n$ ,  $\phi_i(\cdot) : \mathbb{R}^+ \times \mathbb{R}^i \rightarrow \mathbb{R}$  are continuous in the first argument and locally Lipschitz with respect to the rest variables with  $\phi_i(t, 0) = 0$ . Output function  $h(\cdot)$  is an unknown continuous function with  $h(0) = 0$ .

Over the past decade, with the help of adding a power integrator method, homogeneous domination method, and recursive observer design, there exist some interesting results on state/output feedback design of high-order nonlinear systems, whose powers are known constant ratios of odd integers; see [1–16] and the references therein.

In recent years, some interesting results have been achieved on output feedback design of nonlinear systems with known constant powers and unknown output function. For the nonlinear systems (1) with  $p(t) = 1$ , when  $h(\cdot)$  is a continuous differentiable function and its derivative with known upper and lower bounds, global output feedback stabilization and finite-time output feedback stabilization have been achieved in [17–19] and [20], respectively. When the derivative of  $h(\cdot)$  is with unknown upper bound, [21] achieved semi-global output feedback control. Furthermore, when  $h(\cdot)$  is extended to be only a continuous function, with the help of the given maximal sector region of output function, [22] achieved output feedback stabilization. Lately, in [23], a new design and analysis method for high-order nonlinear systems with unknown continuous output function was proposed based on adding

a power integrator method and homogeneous domination method.

According to some practice [24–26], it is well-known that the timely deteriorated performance of system often results in different running data, which usually identify the powers of system. Therefore, the powers of system are usually not fixed and can be varying with a suitable bound even in the same working condition. For example, as a practical second-order dynamic model of reduced-order boiler-turbine unit, two typical different powers  $p(t) = 1.072$  and  $p(t) = 1.031$  have been identified in [25] and [26], respectively. For nonlinear systems with a time-varying power, [27, 28] achieved global state feedback stabilization based on interval homogeneous domination approach. As far as we know, [29] is the first paper to study the output feedback stabilization of nonlinear systems (1) with  $h(x_1) = x_1$  by the revamped method of adding a power integrator together with the recursive nonlinear observer design. Naturally, an interesting problem is put forward: *For more general nonlinear systems (1) with  $h(x_1)$  being an unknown continuous function, can we design an output feedback controller?*

In this paper, we make an attempt to handle this problem. Some essential technical difficulties in control design will be inevitably produced: (i) Compared with [29], since output function is unknown, we construct a new nonlinear reduced-order observer without using the unmeasurable state  $x_1$ . (ii) Compared with [23], a new function to determine the maximal open sector  $\Omega$  of output function is given since the power of system is time-varying. As long as output function belongs to any closed sector included in  $\Omega$ , the equilibrium point of the closed-loop system is globally uniformly asymptotically stable under the constructed output feedback controller.

This paper is organized as follows. Section 2 gives some preliminaries. The design and analysis of output feedback controller are given in Section 3, following a simulation example in Section 4. Section 5 concludes this paper.

## 2. Mathematical Preliminaries

Some notations, definitions, and lemmas are to be used throughout this paper.

In this paper, the argument of function will be omitted whenever no confusion can arise from the context.  $R$ ,  $R^+$ , and  $R^n$  denote the set of real numbers, the set of all nonnegative real numbers, and the real  $n$ -dimensional space. For constant  $\beta_i$ ,  $i = 1, \dots, n$ , let  $\beta_{i\sim j} = \prod_{k=i}^j \beta_k$ ,  $1 \leq i < j \leq n$ , and  $\beta_{i\sim i} = \beta_i$ ,  $\beta_{i\sim(i-1)} = 1$ ,  $\beta_{0\sim i} = 0$ . For integers  $a, b$  and constant  $\Lambda_i$ ,  $\sum_{i=a}^b \Lambda_i = 0$  when  $a > b$ .

**Definition 1** (see [30]). A function  $h(\cdot) : R \rightarrow R$  is said to belong to the sector  $[\rho_1, \rho_2]$  if  $(h(s) - \rho_1 s)(h(s) - \rho_2 s) \leq 0$ , where  $\rho_1$  and  $\rho_2$  are constants with  $\rho_1 < \rho_2$ . If the inequality is strict, we write the sector as  $(\rho_1, \rho_2)$ .

The following lemmas will serve as the basis for the development of output feedback controller. Lemmas 2–5 are used to enlarge inequalities. Lemmas 6 and 7 are Lyapunov

stability theorem for the global uniformly asymptotically stable of the closed-loop system.

**Lemma 2** (see [31]). Let  $p(t)$  be a real-valued function of  $t \in R^+$  satisfying  $0 < p(t) < +\infty$ . For any  $x_i \in R$ ,  $i = 1, \dots, n$ ,

$$\begin{aligned} & (|x_1| + \dots + |x_n|)^{p(t)} \\ & \leq \max\{n^{p(t)-1}, 1\} (|x_1|^{p(t)} + \dots + |x_n|^{p(t)}). \end{aligned} \quad (2)$$

**Lemma 3** (see [32]). Let  $p(t), q(t)$  be positive real-valued functions of  $t \in R^+$  and  $\gamma(x, y)$  be a positive real-valued function of  $x, y \in R$ . For any  $x, y \in R$ ,

$$\begin{aligned} & |x|^{p(t)} |y|^{q(t)} \\ & \leq \frac{p(t)}{p(t) + q(t)} \gamma(x, y) |x|^{p(t)+q(t)} \\ & \quad + \frac{q(t)}{p(t) + q(t)} \gamma^{-p(t)/q(t)}(x, y) |y|^{p(t)+q(t)}. \end{aligned} \quad (3)$$

**Lemma 4** (see [33]). Let  $p(t)$  be a real-valued function of  $t \in R^+$  satisfying  $p(t) \geq 1$ . For any  $x, y \in R$ ,

$$\begin{aligned} & \left| [x]^{p(t)} - [y]^{p(t)} \right| \\ & \leq p(t) \left( 2^{p(t)-3} + 1 \right) \left( |x - y|^{p(t)} + |x - y| |y|^{p(t)-1} \right), \end{aligned} \quad (4)$$

where  $|y|^{p(t)-1} := 0$  if  $y = 0$  and  $p(t) = 1$ .

**Lemma 5** (see [33]). Let  $p(t)$  be a real-valued function of  $t \in R^+$  satisfying  $p(t) \geq 1$ . For any  $x, y \in R$ ,

$$-(x - y) \left( [x]^{p(t)} - [y]^{p(t)} \right) \leq -2^{1-p(t)} |x - y|^{p(t)+1}. \quad (5)$$

**Lemma 6** (see [30]). Let  $V : R^n \rightarrow R$  be a continuous positive definite and radially unbounded function defined on  $R^n$ ; then there exist class  $\mathcal{K}_\infty$  functions  $\pi_1$  and  $\pi_2$  defined on  $[0, +\infty)$  such that  $\pi_1(\|x\|) \leq V(x) \leq \pi_2(\|x\|)$  for all  $x \in R^n$ .

**Lemma 7** (see [30]). For the nonautonomous system  $\dot{x} = f(t, x)$ , let  $x = 0$  be an equilibrium point of system and  $V : R^+ \times R^n \rightarrow R^+$  be a continuously differentiable function such that  $W_1(x) \leq V(t, x) \leq W_2(x)$  and  $\partial V / \partial t + (\partial V / \partial x) f(t, x) \leq -W_3(x)$  hold for any  $t \geq 0$  and  $x \in R^n$ , where  $W_1(x), W_2(x), W_3(x)$  are continuous positive definite functions on  $R^n$  and  $W_1(x)$  is radially unbounded. Then  $x = 0$  is globally uniformly asymptotically stable.

## 3. Output Feedback Controller Design and Stability Analysis

**3.1. Control Objective of This Paper.** The objective of this paper is to construct an output feedback controller for system (1) such that the equilibrium point of the closed-loop system is globally uniformly asymptotically stable when the maximal open sector of output function is given.

*Assumption 8.* There is a known constant  $c \geq 0$  such that for  $i = 1, \dots, n$ ,

$$\begin{aligned} & |\phi_i(t, x) - \phi_i(t, y)| \\ & \leq c \sum_{j=1}^N \left( \sum_{k=1}^i \left( |x_k - y_k|^{a_{k,j}(t)} \sum_{q=1}^i \left( |x_q|^{b_{k,j}(t)} + |y_q|^{b_{k,j}(t)} \right) \right) \right), \end{aligned} \quad (6)$$

for all  $x, y \in R^n$ , where  $N$  is an arbitrary positive integer and the real-valued functions  $a_{k,j}(t)$  and  $b_{k,j}(t)$  satisfy the following relations:

$$\begin{aligned} & a_{k,j}(t) + b_{k,j}(t) = p(t), \\ & \underline{a}_{k,j} \leq a_{k,j}(t) \leq \bar{a}_{k,j}, \quad \underline{b}_{k,j} \leq b_{k,j}(t) \leq \bar{b}_{k,j}, \end{aligned} \quad (7)$$

for all  $j = 1, \dots, N$  and  $k = 1, \dots, i$ , with  $0 < \underline{a}_{k,j} \leq \bar{a}_{k,j}$  and  $0 < \underline{b}_{k,j} \leq \bar{b}_{k,j}$ . By Lemma 3 and Assumption 8, there exists a constant  $\bar{c} \geq 0$  such that

$$\begin{aligned} & |\phi_i(t, x_1, \dots, x_i)| \leq \bar{c} \left( |x_1|^{p(t)} + \dots + |x_i|^{p(t)} \right), \\ & i = 1, \dots, n. \end{aligned} \quad (8)$$

*Remark 9.* As far as we know, under Assumption 8, [29] is the first paper to study output feedback stabilization of nonlinear system (1) with  $h(x_1) = x_1$ . In this paper, we will consider system (1) with  $h(x_1)$  being an unknown continuous function.

### 3.2. State Feedback Controller Design of System (1)

*Step 1.* Taking  $\xi_1 = x_1$ ,  $V_1(x_1) = (1/2)x_1^2$ , it follows from (1) and (8) that

$$\begin{aligned} \dot{V}_1 &= x_1 [x_2]^{p(t)} + x_1 \phi_1 \\ &\leq x_1 \left( [x_2]^{p(t)} - [x_2^*]^{p(t)} \right) + x_1 [x_2^*]^{p(t)} \\ &\quad + \bar{c} |x_1|^{p(t)+1}. \end{aligned} \quad (9)$$

Choose the virtual controller  $x_2^* = -\beta_1 x_1$  with  $\beta_1 = (r_{1,1} + \bar{c})^{1/p}$ , where  $r_{1,1} \geq 1$  is a constant to be designed. Due to  $(r_{1,1} + \bar{c})^{p(t)/p} \geq (r_{1,1} + \bar{c})$ , (9) becomes

$$\dot{V}_1 \leq -r_{1,1} |\xi_1|^{p(t)+1} + \xi_1 \left( [x_2]^{p(t)} - [x_2^*]^{p(t)} \right). \quad (10)$$

*Inductive Step.* Suppose that at step  $k-1$  ( $k \geq 2$ ), there is a positive definite and radially unbounded Lyapunov function  $V_{k-1}(\xi_1, \dots, \xi_{k-1}) = V_{k-2}(\xi_1, \dots, \xi_{k-2}) + (1/2)\xi_{k-1}^2$  and a set of virtual controllers  $x_2^*, \dots, x_k^*$  defined by

$$\begin{aligned} & \xi_1 = x_1, \\ & x_i^* = -\beta_{i-1} \xi_{i-1}, \\ & \xi_i = x_i - x_i^*, \\ & i = 2, \dots, k, \end{aligned} \quad (11)$$

such that

$$\begin{aligned} \dot{V}_{k-1} &\leq -\sum_{i=1}^{k-2} \left( r_{i,i} - \bar{r}_{i+1,1} - \sum_{j=i+1}^{k-1} \bar{r}_{j,i} \right) |\xi_i|^{p(t)+1} \\ &\quad - r_{k-1,k-1} |\xi_{k-1}|^{p(t)+1} \\ &\quad + \xi_{k-1} \left( [x_k]^{p(t)} - [x_k^*]^{p(t)} \right), \end{aligned} \quad (12)$$

where  $\bar{r}_{i+1,1}, \bar{r}_{j,i}$ ,  $j = i+1, \dots, k-1$ ,  $i = 1, \dots, k-2$ , are positive constants,  $r_{1,1}, \dots, r_{k-1,k-1} \geq 1$  are constants to be designed, and  $\beta_1, \dots, \beta_{k-1}$  are positive constants dependent on  $r_{1,1}, \dots, r_{k-1,k-1}$ . In what follows, we will show that (12) still holds at step  $k$ .

By (11), one has  $x_k^* = -\sum_{i=1}^{k-1} \beta_{i \sim (k-1)} x_i$ , which together with (1) lead to

$$\dot{\xi}_k = [x_{k+1}]^{p(t)} + \phi_k + \sum_{i=1}^{k-1} \beta_{i \sim (k-1)} \left( [x_{i+1}]^{p(t)} + \phi_i \right). \quad (13)$$

Constructing  $V_k(\xi_1, \dots, \xi_k) = V_{k-1}(\xi_1, \dots, \xi_{k-1}) + (1/2)\xi_k^2$ , it follows from (12) and (13) that

$$\begin{aligned} \dot{V}_k &\leq -\sum_{i=1}^{k-2} \left( r_{i,i} - \bar{r}_{i+1,1} - \sum_{j=i+1}^{k-1} \bar{r}_{j,i} \right) |\xi_i|^{p(t)+1} \\ &\quad - r_{k-1,k-1} |\xi_{k-1}|^{p(t)+1} + \xi_{k-1} \left( [x_k]^{p(t)} - [x_k^*]^{p(t)} \right) \\ &\quad + \xi_k \left( [x_{k+1}]^{p(t)} + \phi_k \right. \\ &\quad \left. + \sum_{i=1}^{k-1} \beta_{i \sim (k-1)} \left( [x_{i+1}]^{p(t)} + \phi_i \right) \right). \end{aligned} \quad (14)$$

By (8), (11), and Lemmas 2–4, we derive

$$\begin{aligned} & \xi_{k-1} \left( [x_k]^{p(t)} - [x_k^*]^{p(t)} \right) \\ & \leq |\xi_{k-1}| \cdot \bar{p} \left( 2^{\bar{p}-3} + 1 \right) \left( |\xi_k|^{p(t)} + |\xi_k| |x_k^*|^{p(t)-1} \right) \\ & \leq \bar{r}_{k,1} |\xi_{k-1}|^{p(t)+1} + \lambda_{k,1} |\xi_k|^{p(t)+1}, \\ & \xi_k \left( \phi_k + \sum_{i=1}^{k-1} \beta_{i \sim (k-1)} \left( [x_{i+1}]^{p(t)} + \phi_i \right) \right) \\ & \leq |\xi_k| \left( \bar{\beta}_1 |\xi_1|^{p(t)} + \bar{\beta}_2 |x_2|^{p(t)} + \dots + \bar{\beta}_k |x_k|^{p(t)} \right) \\ & \leq \sum_{i=1}^{k-1} \bar{r}_{k,i} |\xi_i|^{p(t)+1} + \lambda_{k,2} |\xi_k|^{p(t)+1}, \end{aligned} \quad (15)$$

where  $\bar{\beta}_i = \beta_{(i-1) \sim (k-1)} + \bar{c} \left( 1 + \sum_{j=i}^{k-1} \beta_{j \sim (k-1)} \right)$ ,  $\bar{r}_{k,1}, \bar{r}_{k,2}, \dots, \bar{r}_{k,k-1}$  are positive constants, and  $\lambda_{k,1}$  and  $\lambda_{k,2}$  are positive constants

dependent on  $\bar{r}_{k,1}$  and  $\bar{r}_{k,1}, \dots, \bar{r}_{k,k-1}$ , respectively. Substituting (15) and (16) into (14) leads to

$$\begin{aligned} \dot{V}_k \leq & -\sum_{i=1}^{k-1} \left( r_{i,i} - \bar{r}_{i+1,1} - \sum_{j=i+1}^k \bar{r}_{j,i} \right) |\xi_i|^{p(t)+1} \\ & + \xi_k \left( [x_{k+1}]^{p(t)} - [x_{k+1}^*]^{p(t)} \right) + \xi_k [x_{k+1}^*]^{p(t)} \\ & + (\lambda_{k,1} + \lambda_{k,2}) |\xi_k|^{p(t)+1}. \end{aligned} \quad (17)$$

Choose the virtual controller  $x_{k+1}^* = -\beta_k \xi_k$  with  $\beta_k = (r_{k,k} + \lambda_{k,1} + \lambda_{k,2})^{1/p}$ , where  $r_{k,k} \geq 1$  is a constant to be designed. Due to  $(r_{k,k} + \lambda_{k,1} + \lambda_{k,2})^{p(t)/p} \geq (r_{k,k} + \lambda_{k,1} + \lambda_{k,2})$ , (17) becomes

$$\begin{aligned} \dot{V}_k \leq & -\sum_{i=1}^{k-1} \left( r_{i,i} - \bar{r}_{i+1,1} - \sum_{j=i+1}^k \bar{r}_{j,i} \right) |\xi_i|^{p(t)+1} \\ & - r_{k,k} |\xi_k|^{p(t)+1} + \xi_k \left( [x_{k+1}]^{p(t)} - [x_{k+1}^*]^{p(t)} \right). \end{aligned} \quad (18)$$

This completes the inductive step.

*Step n.* The Lyapunov function  $V_n(\xi) = V_{n-1}(\xi_1, \dots, \xi_{n-1}) + (1/2)\xi_n^2 = \sum_{i=1}^n (1/2)\xi_i^2$  and a positive constant  $\lambda$  give

$$\begin{aligned} \dot{V}_n \leq & -\sum_{i=1}^{n-1} \left( r_{i,i} - \bar{r}_{i+1,1} - \sum_{j=i+1}^n \bar{r}_{j,i} \right) |\xi_i|^{p(t)+1} \\ & + \lambda |\xi_n|^{p(t)+1} + \xi_n \left( [u]^{p(t)} - [x_{n+1}^*]^{p(t)} \right) \\ & + \xi_n [x_{n+1}^*]^{p(t)}, \end{aligned} \quad (19)$$

where  $\xi_i$  is defined as in (11) for  $i = 1, \dots, n$ . Choose virtual controller  $x_{n+1}^* = -\beta_n \xi_n$  with  $\beta_n = (r_{n,n} + \lambda)^{1/p}$ , where  $r_{n,n} \geq 1$  is a constant to be designed. Due to  $(r_{n,n} + \lambda)^{p(t)/p} \geq (r_{n,n} + \lambda)$ , (19) becomes

$$\begin{aligned} \dot{V}_n \leq & -\sum_{i=1}^{n-1} \left( r_{i,i} - \bar{r}_{i+1,1} - \sum_{j=i+1}^n \bar{r}_{j,i} \right) |\xi_i|^{p(t)+1} \\ & - r_{n,n} |\xi_n|^{p(t)+1} + \xi_n \left( [u]^{p(t)} - [x_{n+1}^*]^{p(t)} \right). \end{aligned} \quad (20)$$

**3.3. Output Feedback Controller Design of System (1).** For system (1), since output function is unknown, the state  $x_1$  is exactly unknown. We construct the output-driven nonlinear reduced-order observer

$$\begin{aligned} \dot{\hat{z}}_i &= -l_i \left( [\hat{x}_i]^{p(t)} + \hat{\phi}_{i-1} \right), \\ \hat{x}_i &= \hat{z}_i + l_i \hat{x}_{i-1}, \quad i = 2, \dots, n, \end{aligned} \quad (21)$$

where  $\hat{x}_1 = y$ ,  $\hat{\phi}_{i-1} := \phi_{i-1}(t, \hat{x}_1, \dots, \hat{x}_{i-1})$ ,  $i = 2, \dots, n$ , and the observer gains  $l_i \geq 1$ ,  $i = 2, \dots, n$ , are constants to be determined.

*Remark 10.* Compared with the observer in [29], since the unknown output function  $h(\cdot)$  causes  $x_1$  to be exactly

unknown, a new output-driven nonlinear reduced-order observer (21) is designed without using  $x_1$  but  $y$  to rebuild unmeasured states. Moreover, not all but the first  $n - 1$  nonlinearities are used in the design of observer. For a second-order system Example 4.1 in [29], we can design an observer without using nonlinearity; see the simulation example in this paper for the details.

Based on  $x_{n+1}^* = -\beta_n \xi_n = -\sum_{i=1}^n \beta_{i-n} x_i$ , an output feedback controller is designed as

$$u = -\sum_{i=1}^n \beta_{i-n} \hat{x}_i = -\beta_{1-n} y - \sum_{i=2}^n \beta_{i-n} \hat{x}_i. \quad (22)$$

Define the error

$$e_i = z_i - \hat{z}_i, \quad z_i = x_i - l_i x_{i-1}, \quad i = 2, \dots, n. \quad (23)$$

By (1), (21), and (23), one has

$$\begin{aligned} \dot{e}_i &= -l_i \left( [x_i]^{p(t)} - [\hat{x}_i]^{p(t)} \right) + [x_{i+1}]^{p(t)} + \phi_i \\ &\quad - l_i \left( \phi_{i-1} - \hat{\phi}_{i-1} \right), \quad i = 2, \dots, n-1, \\ \dot{e}_n &= -l_n \left( [x_n]^{p(t)} - [\hat{x}_n]^{p(t)} \right) + [u]^{p(t)} + \phi_n \\ &\quad - l_n \left( \phi_{n-1} - \hat{\phi}_{n-1} \right). \end{aligned} \quad (24)$$

For the Lyapunov function  $U(e) = \sum_{i=2}^n (1/2)e_i^2$ , it follows from (21), (23), and (24) that

$$\begin{aligned} \dot{U} &= -\sum_{i=2}^n l_i e_i \left( [z_i + l_i x_{i-1}]^{p(t)} - [\hat{z}_i + l_i x_{i-1}]^{p(t)} \right) \\ &\quad - \sum_{i=2}^n l_i e_i \left( [\hat{z}_i + l_i x_{i-1}]^{p(t)} - [\hat{z}_i + l_i \hat{x}_{i-1}]^{p(t)} \right) \\ &\quad + \sum_{i=2}^{n-1} e_i [x_{i+1}]^{p(t)} + e_n [u]^{p(t)} + \sum_{i=2}^n e_i \phi_i \\ &\quad - \sum_{i=2}^n l_i e_i \left( \phi_{i-1} - \hat{\phi}_{i-1} \right). \end{aligned} \quad (25)$$

By (23), Lemma 5, and the fact that  $1 \leq \underline{p} \leq p(t) \leq \bar{p}$ , we obtain for  $i = 2, \dots, n$ ,

$$\begin{aligned} & -l_i e_i \left( [z_i + l_i x_{i-1}]^{p(t)} - [\hat{z}_i + l_i x_{i-1}]^{p(t)} \right) \\ &= -l_i \left( (z_i + l_i x_{i-1}) - (\hat{z}_i + l_i x_{i-1}) \right) \\ &\quad \cdot \left( [z_i + l_i x_{i-1}]^{p(t)} - [\hat{z}_i + l_i x_{i-1}]^{p(t)} \right) \\ &\leq -2^{1-\bar{p}} l_i |e_i|^{p(t)+1}. \end{aligned} \quad (26)$$

Next, we give the estimate of the others on the right-hand side of (25) by Propositions 11–14, whose proofs are included in the Appendix.

**Proposition 11.** *There is a positive constant  $b_1$ , and positive constants  $c_{1,i}, i = 2, \dots, n$ , dependent on  $b_1$  such that*

$$\begin{aligned} & \sum_{i=2}^{n-1} e_i [x_{i+1}]^{p(t)} + \sum_{i=2}^n e_i \phi_i \\ & \leq b_1 \sum_{i=1}^n |\xi_i|^{p(t)+1} + \sum_{i=2}^n c_{1,i} |e_i|^{p(t)+1}. \end{aligned} \quad (27)$$

**Proposition 12.** *There is a positive constant  $b_2$ , a positive constant  $\alpha_n$  dependent on  $b_2$ , and positive constants  $\alpha_i, i = 1, \dots, n-1$ , dependent on  $b_2, l_{i+1}, \dots, l_n$  such that*

$$\begin{aligned} & - \sum_{i=2}^n l_i e_i \left( [\tilde{z}_i + l_i x_{i-1}]^{p(t)} - [\tilde{z}_i + l_i \hat{x}_{i-1}]^{p(t)} \right) \\ & \leq b_2 \sum_{i=1}^n |\xi_i|^{p(t)+1} + \alpha_n |e_n|^{p(t)+1} \\ & \quad + \sum_{i=2}^{n-1} \alpha_i (l_{i+1}, \dots, l_n) |e_i|^{p(t)+1} \\ & \quad + \alpha_1 (l_2, \dots, l_n) |x_1 - \hat{x}_1|^{p(t)+1}. \end{aligned} \quad (28)$$

**Proposition 13.** *There is a positive constant  $b_3$ , a positive constant  $\gamma_n$  dependent on  $b_3$ , and positive constants  $\gamma_i, i = 1, \dots, n-1$ , dependent on  $b_3, l_{i+1}, \dots, l_n$  such that*

$$\begin{aligned} & - \sum_{i=2}^n l_i e_i (\phi_{i-1} - \hat{\phi}_{i-1}) \\ & \leq b_3 \sum_{i=1}^n |\xi_i|^{p(t)+1} + \gamma_n |e_n|^{p(t)+1} \\ & \quad + \sum_{i=2}^{n-1} \gamma_i (l_{i+1}, \dots, l_n) |e_i|^{p(t)+1} \\ & \quad + \gamma_1 (l_2, \dots, l_n) |x_1 - \hat{x}_1|^{p(t)+1}. \end{aligned} \quad (29)$$

**Proposition 14.** *There is a positive constant  $b_4$ , a positive constant  $\sigma_n$  dependent on  $b_4$ , and positive constants  $\sigma_i, i = 1, \dots, n-1$ , dependent on  $l_{i+1}, \dots, l_n$  such that*

$$\begin{aligned} e_n [u]^{p(t)} & \leq b_4 |\xi_n|^{p(t)+1} + \sigma_n |e_n|^{p(t)+1} \\ & \quad + \sum_{i=2}^{n-1} \sigma_i (l_{i+1}, \dots, l_n) |e_i|^{p(t)+1} \\ & \quad + \sigma_1 (l_2, \dots, l_n) |x_1 - \hat{x}_1|^{p(t)+1}. \end{aligned} \quad (30)$$

To estimate the term  $\xi_n ([u]^{p(t)} - [x_{n+1}^*]^{p(t)})$  in (20), we give the following proposition whose proof is also included in the Appendix.

**Proposition 15.** *There is a positive constant  $b_5$ , a positive constant  $\omega_n$  dependent on  $b_5$ , and positive constants  $\omega_i, i = 1, \dots, n-1$ , dependent on  $b_5, l_{i+1}, \dots, l_n$  such that*

$$\begin{aligned} & \xi_n \left( [u]^{p(t)} - [x_{n+1}^*]^{p(t)} \right) \\ & \leq b_5 |\xi_n|^{p(t)+1} + \omega_n |e_n|^{p(t)+1} \\ & \quad + \sum_{i=2}^{n-1} \omega_i (l_{i+1}, \dots, l_n) |e_i|^{p(t)+1} \\ & \quad + \omega_1 (l_2, \dots, l_n) |x_1 - \hat{x}_1|^{p(t)+1}. \end{aligned} \quad (31)$$

Define  $T(\xi, e) = V_n(\xi) + U(e) = \sum_{i=1}^n (1/2)\xi_i^2 + \sum_{i=2}^n (1/2)e_i^2$ . By (20), (25), (26), and Propositions 11–15, one obtains

$$\begin{aligned} \dot{T} & \leq - \sum_{i=1}^{n-1} \left( r_{i,i} - \tilde{r}_{i+1,i} - \sum_{j=i+1}^n \tilde{r}_{j,i} - (b_1 + b_2 + b_3) \right) \\ & \quad \cdot |\xi_i|^{p(t)+1} - (r_{n,n} - (b_1 + b_2 + b_3 + b_4 + b_5)) \\ & \quad \cdot |\xi_n|^{p(t)+1} - (2^{1-\bar{p}} l_n - \theta_n) |e_n|^{p(t)+1} \\ & \quad - \sum_{i=2}^{n-1} (2^{1-\bar{p}} l_i - \theta_i (l_{i+1}, \dots, l_n)) |e_i|^{p(t)+1} \\ & \quad + \theta_1 (l_2, \dots, l_n) |x_1 - \hat{x}_1|^{p(t)+1}, \end{aligned} \quad (32)$$

where  $\theta_i = \alpha_i + \gamma_i + \sigma_i + \omega_i + c_{1,i}$  with  $c_{1,1} = 0, i = 1, \dots, n$ , it is easy to see that  $\theta_n$  is a positive constant, and  $\theta_i, i = 1, \dots, n-1$ , are positive constants dependent on  $l_{i+1}, \dots, l_n$ . For some positive constants  $b_0, \tilde{b}_1, \dots, \tilde{b}_n$ , design  $r_{1,1}, \dots, r_{n,n}$  such that

$$\begin{aligned} r_{1,1} & \geq \max \left\{ \tilde{r}_{2,1} + \sum_{j=2}^n \tilde{r}_{j,1} + b_1 + b_2 + b_3 + b_0 + \tilde{b}_1, 1 \right\}, \\ r_{i,i} & \geq \max \left\{ \tilde{r}_{i+1,i} + \sum_{j=i+1}^n \tilde{r}_{j,i} + b_1 + b_2 + b_3 + \tilde{b}_i, 1 \right\}, \\ & \quad i = 2, \dots, n-1, \end{aligned} \quad (33)$$

$$r_{n,n} \geq \max \{ b_1 + b_2 + b_3 + b_4 + b_5 + \tilde{b}_n, 1 \},$$

and for some positive constants  $\tilde{d}_2, \dots, \tilde{d}_n$ , choose  $l_2, \dots, l_n$  as

$$\begin{aligned} l_n & \geq \max \{ 2^{\bar{p}-1} (\tilde{d}_n + \theta_n), 1 \}, \\ l_i & \geq \max \{ 2^{\bar{p}-1} (\tilde{d}_i + \theta_i (l_{i+1}, \dots, l_n)), 1 \}, \\ & \quad i = n-1, \dots, 2. \end{aligned} \quad (34)$$

By (33) and (34), (32) becomes

$$\begin{aligned} \dot{T} \leq & -b_0 |\xi_1|^{p(t)+1} - \sum_{i=1}^n \tilde{b}_i |\xi_i|^{p(t)+1} - \sum_{i=2}^n \tilde{d}_i |e_i|^{p(t)+1} \\ & + \theta_1 (l_2, \dots, l_n) |x_1 - \hat{x}_1|^{p(t)+1}. \end{aligned} \quad (35)$$

### 3.4. Stability and Convergence Analysis

**Theorem 16.** *If Assumption 8 holds for system (1), there is a maximal open sector  $\Omega = (1 - \bar{\rho}, 1 + \bar{\rho})$  with  $\bar{\rho}$  being a positive constant, as long as the unknown output function  $h(\cdot)$  belongs to any closed sector included in  $\Omega$ , under the output feedback controller (21) and (22):*

(i) *the solutions of the closed-loop system (1), (21), (22) are well-defined on  $[0, +\infty)$ ,*

(ii) *the equilibrium point  $x = 0$  is globally uniformly asymptotically stable.*

*Proof.* (i) We firstly give the choice of  $r_{1,1}, \dots, r_{n,n}, \beta_1, \dots, \beta_n$ . At Step 1, for any given  $\tilde{r}_{2,1}, \tilde{r}_{2,1}, \dots, \tilde{r}_{n,1}, b_1, b_2, b_3, b_0, \tilde{b}_1$ , by (33), we can choose  $r_{1,1}$ ; then  $\beta_1$  can be calculated. At step 2, for any given  $\tilde{r}_{3,1}, \tilde{r}_{3,2}, \dots, \tilde{r}_{n,2}, b_1, b_2, b_3, \tilde{b}_2$ , by (33), we can choose  $r_{2,2}$ ; then  $\beta_2$  can be calculated when  $\lambda_{2,1}, \lambda_{2,2}$  have been obtained by (15) and (16). One by one, at Step n, for any given  $b_1, b_2, b_3, b_4, b_5, \tilde{b}_n$ , by (33), we can choose  $r_{n,n}$ ; then  $\beta_n$  can be calculated.

Secondly, we give the choice of  $l_n, \dots, l_2$ . For the given  $b_1, b_2, b_3, b_4, b_5$ , we can get  $c_{1,n}, \alpha_n, \gamma_n, \sigma_n, \omega_n$ . Then for any given  $\tilde{d}_n$ , by (34), we can choose  $l_n$ . Next, for the given  $b_1, b_2, b_3, b_5$ , one get  $c_{1,n-1}, \alpha_{n-1}(l_n), \gamma_{n-1}(l_n), \sigma_{n-1}(l_n), \omega_{n-1}(l_n)$ . Then for any given  $\tilde{d}_{n-1}, l_{n-1}$  can be chosen by (34). In turn, we can get  $l_{n-2}, \dots, l_2$ .

Finally, we give the sector of output function. Denote  $\kappa = (\tilde{r}_{2,1}, \dots, \tilde{r}_{n,1}, \tilde{r}_{2,1}, \dots, \tilde{r}_{n,1}, \dots, \tilde{r}_{n,n-2}, \tilde{r}_{n,n-1}, b_1, \dots, b_5, b_0, \tilde{b}_1, \dots, \tilde{b}_n, \tilde{d}_2, \dots, \tilde{d}_n)$ ,  $\Omega_l = \{l = (l_2, \dots, l_n) \mid r_{1,1} \geq \max\{\tilde{r}_{2,1} + \sum_{j=2}^n \tilde{r}_{j,1} + b_1 + b_2 + b_3 + b_0 + \tilde{b}_1, 1\}, r_{i,i} \geq \max\{\tilde{r}_{i+1,1} + \sum_{j=i+1}^n \tilde{r}_{j,i} + b_1 + b_2 + b_3 + \tilde{b}_i, 1\}, i = 2, \dots, n-1, r_{n,n} \geq \max\{b_1 + b_2 + b_3 + b_4 + b_5 + \tilde{b}_n, 1\}, l_n \geq \max\{2^{\bar{p}-1}(\tilde{d}_n + \theta_n), 1\}, l_i \geq \max\{2^{\bar{p}-1}(\tilde{d}_i + \theta_i(l_{i+1}, \dots, l_n)), 1\}, i = n-1, \dots, 2\}$ , and

$$\begin{aligned} \rho = \rho(l_2, \dots, l_n) = \min & \left\{ \left( \frac{b_0}{2\theta_1(l_2, \dots, l_n)} \right)^{1/(\bar{p}+1)}, \right. \\ & \left. \left( \frac{b_0}{2\theta_1(l_2, \dots, l_n)} \right)^{1/(\underline{p}+1)} \right\}. \end{aligned} \quad (36)$$

In fact, one can determine the supremum of  $\rho$ ; that is, select constant

$$\bar{\rho} = \sup_{\kappa \in R^+, l \in \Omega_l} \rho(l_2, \dots, l_n), \quad (37)$$

as the supremum of  $\rho$ . Hence, the maximal open sector of output function is  $\Omega = (1 - \bar{\rho}, 1 + \bar{\rho})$ . When output function

$h(x_1)$  in (1) belongs to any closed sector  $[1 - \bar{\rho} + \epsilon, 1 + \bar{\rho} - \epsilon] \subset \Omega$  with  $0 < \epsilon < \bar{\rho}$ , by Definition 1,

$$\begin{aligned} & (h(x_1) - (1 - \bar{\rho} + \epsilon)x_1)(h(x_1) - (1 + \bar{\rho} - \epsilon)x_1) \\ & \leq 0 \implies \\ & (h(x_1) - (1 + \bar{\rho} - \epsilon)x_1)x_1 \leq 0 \\ & \leq (h(x_1) - (1 - \bar{\rho} + \epsilon)x_1)x_1 \implies \\ & (1 - \bar{\rho} + \epsilon)x_1^2 \leq h(x_1)x_1 \leq (1 + \bar{\rho} - \epsilon)x_1^2 \implies \\ & -(\bar{\rho} - \epsilon)x_1^2 \leq (h(x_1) - x_1)x_1 \leq (\bar{\rho} - \epsilon)x_1^2 \implies \\ & |x_1 - h(x_1)| \leq (\bar{\rho} - \epsilon)|x_1|, \end{aligned} \quad (38)$$

from which one has

$$\begin{aligned} |x_1 - \hat{x}_1|^{p(t)+1} & = |\xi_1 - h(\xi_1)|^{p(t)+1} \\ & \leq (\bar{\rho} - \epsilon)^{p(t)+1} |\xi_1|^{p(t)+1}. \end{aligned} \quad (39)$$

With the help of  $\underline{p} + 1 \leq p(t) + 1 \leq \bar{p} + 1$ , (36), and (37), we derive

$$(\bar{\rho} - \epsilon)^{p(t)+1} < \rho^{p(t)+1} \leq \rho^{\bar{p}+1} + \rho^{\underline{p}+1} \leq \frac{b_0}{\theta_1(l_2, \dots, l_n)}. \quad (40)$$

From (39) and (40), (35) becomes

$$\dot{T} \leq -\sum_{i=1}^n \tilde{b}_i |\xi_i|^{p(t)+1} - \sum_{i=2}^n \tilde{d}_i |e_i|^{p(t)+1}. \quad (41)$$

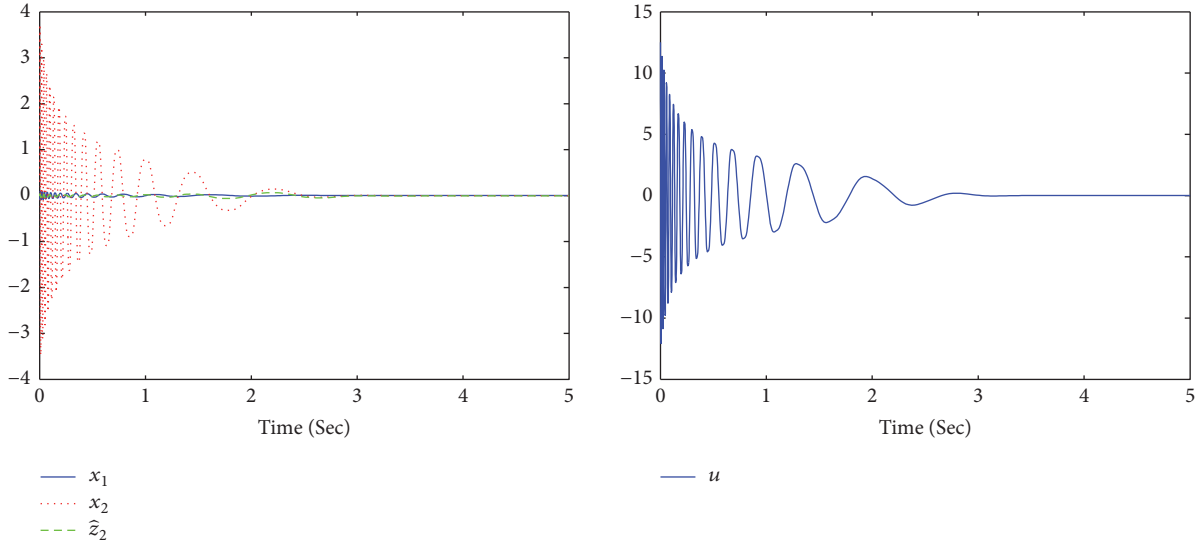
Motivated by [29], with the help of  $\underline{p} + p(t) + 1 \leq \underline{p} + \bar{p} + 1 \leq p(t) + 1 + \bar{p}$ , one obtains

$$\begin{aligned} |\xi_i|^{p+\bar{p}+1} & \leq |\xi_i|^{p(t)+1} (|\xi_i|^{\underline{p}} + |\xi_i|^{\bar{p}}) \implies \\ |\xi_i|^{p(t)+1} & \geq \frac{|\xi_i|^{\bar{p}+1}}{1 + |\xi_i|^{\bar{p}-\underline{p}}}, \\ & i = 1, \dots, n, \\ |e_i|^{p+\bar{p}+1} & \leq |e_i|^{p(t)+1} (|e_i|^{\underline{p}} + |e_i|^{\bar{p}}) \implies \\ |e_i|^{p(t)+1} & \geq \frac{|e_i|^{\bar{p}+1}}{1 + |e_i|^{\bar{p}-\underline{p}}}, \\ & i = 2, \dots, n, \end{aligned} \quad (42)$$

from which (41) becomes

$$\dot{T} \leq -\left( \sum_{i=1}^n \frac{\tilde{b}_i |\xi_i|^{\bar{p}+1}}{1 + |\xi_i|^{\bar{p}-\underline{p}}} + \sum_{i=2}^n \frac{\tilde{d}_i |e_i|^{\bar{p}+1}}{1 + |e_i|^{\bar{p}-\underline{p}}} \right) =: -W(\xi, e). \quad (43)$$

It is easy to see that  $W(\xi, e)$  is a continuous and positive function with respect to  $(\xi, e)$ .


 FIGURE 1: The responses of the closed-loop system (46), (47) with  $h(x_1) = x_1$ .

By the transformations (11), system (1) can be transformed into a  $\xi$ -system:

$$\dot{\xi}_i(t) = f_i(t, \xi(t), u(t)), \quad i = 1, \dots, n, \quad (44)$$

where  $f_i(\cdot)$  is a continuous function with  $f_i(t, 0) = 0$ . Denote  $\bar{\omega} = (\xi_1, \dots, \xi_n, e_2, \dots, e_n)^\top$ , by the existence and continuation of the solution, the solution  $\bar{\omega}(t)$  of  $\bar{\omega}$ -system (24), (44) is defined on  $[0, t_m)$  with  $0 < t_m \leq +\infty$ .

Due to  $T(\bar{\omega}) = \sum_{i=1}^n (1/2)\xi_i^2 + \sum_{i=2}^n (1/2)e_i^2$ , it is obvious that  $T(\bar{\omega})$  is a continuously differentiable, positive definite, and radially unbounded function. By Lemma 6, there are class  $\mathcal{K}_\infty$  functions  $\pi_1(\cdot)$  and  $\pi_2(\cdot)$  such that

$$\pi_1(\|\bar{\omega}\|) \leq T(\bar{\omega}) \leq \pi_2(\|\bar{\omega}\|), \quad \forall \bar{\omega} \in R^{2n-1}. \quad (45)$$

Since  $\pi_1(\cdot)$  is a class  $\mathcal{K}_\infty$  function, then for any  $\varepsilon > 0$ , one can always find a  $\delta = \delta(\varepsilon)$  with  $\delta > \varepsilon > 0$  such that  $\pi_2(\varepsilon) \leq \pi_1(\delta)$ . If  $\|\bar{\omega}(0)\| < \varepsilon$ , by (43) and (45),  $\pi_1(\|\bar{\omega}(t)\|) \leq T(\bar{\omega}(t)) \leq T(\bar{\omega}(0)) \leq \pi_2(\|\bar{\omega}(0)\|) \leq \pi_2(\varepsilon) \leq \pi_1(\delta)$  for all  $t \in [0, t_m)$ , which means that  $\|\bar{\omega}(t)\| \leq \delta$  for all  $t \in [0, t_m)$ . Hence,  $t_m$  is not an escape time; that is,  $\bar{\omega}(t)$  is well-defined on  $[0, +\infty)$ , so is  $x(t)$ .

(ii) Since  $t_m = +\infty$ , from (43), (45), and Lemma 7, we know that the equilibrium point  $\bar{\omega} = 0$  of  $\bar{\omega}$ -system (24), (44) is globally uniformly asymptotically stable. By the continuity of  $x_i^*(\xi_{i-1})$  on  $\xi_{i-1}$  and  $x_i^*(0) = 0$ , it is easy to recursively prove that the equilibrium point  $x = 0$  of the closed-loop system (1), (21), (22) is globally uniformly asymptotically stable.  $\square$

*Remark 17.* Since the power of system is time-varying, a new function (36) is given to acquire its supremum, which is used to determine the maximal open sector of output function. Moreover, a rigorous analysis is given to establish the stability of the closed-loop system.

## 4. Simulation Example

Consider the second-order nonlinear system in [29]

$$\begin{aligned} \dot{x}_1 &= [x_2]^{2+\cos(t)}, \\ \dot{x}_2 &= [u]^{2+\cos(t)} + x_1^{1/3} |x_2|^{\cos(t)+5/3}, \\ y &= h(x_1). \end{aligned} \quad (46)$$

As discussed in [29], Assumption 8 holds and  $\underline{p} = 1$ ,  $\bar{p} = 3$ . Following the design process as in Section 3 in this paper, we can design output feedback controller without using the nonlinearity  $x_1^{1/3} |x_2|^{\cos(t)+5/3}$ ,

$$\begin{aligned} \dot{\hat{z}}_2 &= -l_2 [\hat{x}_2]^{p(t)}, \quad \hat{x}_2 = \hat{z}_2 + l_2 y, \\ u &= -\beta_1 \beta_2 y - \beta_2 \hat{x}_2. \end{aligned} \quad (47)$$

Choose  $\kappa = (\tilde{r}_{2,1}, \tilde{r}_{2,1}, b_1, b_2, b_4, b_5, b_0, \tilde{b}_1, \tilde{b}_2, \tilde{d}_2) = (0.1, 0.1, 0.1, 0.1, 0.1, 0.1, 0.4, 0.1, 0.1, 0.4)$ . By choosing  $r_{1,1} = 1$ ,  $r_{2,2} = 1$ , we obtain  $\beta_1 = 1$ ,  $\beta_2 = 9.63$ , and choose  $l = l_2 = 12$ .

When  $h(x_1) = x_1$  as in [29], it means that we do not need to give the sector of the output function. In simulation, under the output feedback controller (47), by selecting the initial conditions  $x_1(0) = -0.1$ ,  $x_2(0) = 0.3$ ,  $\hat{z}_2(0) = 0$ , Figure 1 demonstrates the effectiveness of control scheme.

When  $h(x_1) \neq x_1$ , the design method in [29] is inapplicable. Following the design process as in Section 3 in this paper, we can get a sector of output function, that is,  $[1 - \rho, 1 + \rho]$  with  $\rho = \rho(l_2) = \min\{(b_0/2\theta_1(l_2))^{1/(\bar{p}+1)}, (b_0/2\theta_1(l_2))^{1/(\underline{p}+1)}\} = 0.0131$ . In simulation, we choose  $h(x_1) = x_1 + 0.01|x_1|$  which is only continuous but not differentiable;  $h(x_1)$  belongs to sector  $[0.9869, 1.0131]$  obviously. By selecting the initial conditions  $x_1(0) = 0.1$ ,  $x_2(0) = -0.3$ ,  $\hat{z}_2(0) = 0.01$ , Figure 2 illustrates the validity of control scheme.

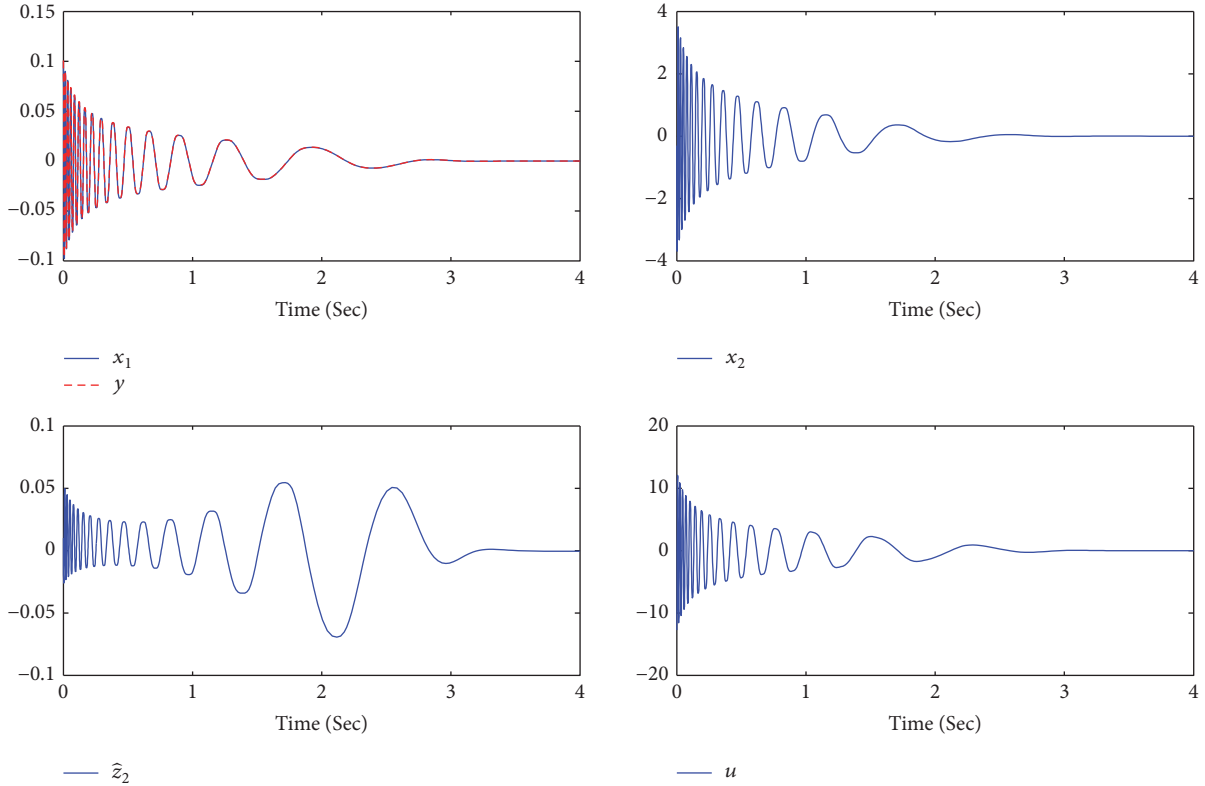


FIGURE 2: The responses of the closed-loop system (46), (47) with  $h(x_1) = x_1 + 0.01|x_1|$ .

## 5. Conclusions

In this paper, output feedback stabilization of nonlinear systems with a time-varying power and unknown continuous output function is studied. By constructing a new nonlinear reduced-order observer together with adding a power integrator method, a new function to determine the maximal open sector  $\Omega$  of output function is given. As long as output function belongs to any closed sector included in  $\Omega$ , an output feedback controller is constructed to guarantee that the equilibrium point of the closed-loop system is globally uniformly asymptotically stable.

For the future work, an interesting problem is for more general nonlinear systems with time-varying powers, that is, nonlinear systems with different time-varying powers or under the weaker condition on nonlinearities, can we design a stable output feedback controller?

## Appendix

*Proof of Proposition 11.* By (8), (11), and Lemmas 2 and 3, we obtain

$$\begin{aligned} & \sum_{i=2}^{n-1} e_i [x_{i+1}]^{p(t)} + \sum_{i=2}^n e_i \phi_i \\ & \leq \sum_{i=2}^{n-1} |e_i| |x_{i+1}|^{p(t)} \end{aligned}$$

$$\begin{aligned} & + \sum_{i=2}^n \bar{c} |e_i| \left( |x_1|^{p(t)} + \cdots + |x_i|^{p(t)} \right) \\ & \leq b_1 \sum_{i=1}^n |\xi_i|^{p(t)+1} + \sum_{i=2}^n c_{1,i} |e_i|^{p(t)+1}, \end{aligned} \quad (\text{A.1})$$

where  $b_1 > 0$  is a constant, and  $c_{1,i} > 0, i = 2, \dots, n$ , are constants dependent on  $b_1$ .  $\square$

*Proof of Proposition 12.* By (11), (21), and (23), one has for  $i = 2, \dots, n$ ,

$$\begin{aligned} x_i - \hat{x}_i &= e_i + l_i (x_{i-1} - \hat{x}_{i-1}) \\ &= e_i + \sum_{j=2}^{i-1} l_{(j+1) \sim i} e_j + l_{2 \sim i} (x_1 - \hat{x}_1), \end{aligned} \quad (\text{A.2})$$

$$\hat{z}_i + l_i x_{i-1} = x_i - e_i = \xi_i - \beta_{i-1} \xi_{i-1} - e_i, \quad (\text{A.3})$$

from which, by Lemmas 2–4, we derive

$$\begin{aligned} & -l_i e_i \left( [\hat{z}_i + l_i x_{i-1}]^{p(t)} - [\hat{z}_i + l_i \hat{x}_{i-1}]^{p(t)} \right) \leq l_i |e_i| \\ & \quad \cdot \bar{p} (2^{\bar{p}-3} + 1) \left( |l_i (x_{i-1} - \hat{x}_{i-1})|^{p(t)} \right) \\ & \quad + |l_i (x_{i-1} - \hat{x}_{i-1})| |\hat{z}_i + l_i x_{i-1}|^{p(t)-1} \leq l_i |e_i| \\ & \quad \cdot \bar{p} (2^{\bar{p}-3} + 1) \left( |l_i e_{i-1} + l_{(i-1) \sim i} e_{i-2} + \cdots + l_{3 \sim i} e_2 \right. \end{aligned}$$

$$\begin{aligned}
 & + l_{2\sim i} (x_1 - \hat{x}_1)^{p(t)} + |l_i e_{i-1} + l_{(i-1)\sim i} e_{i-2} + \dots \\
 & + l_{3\sim i} e_2 + l_{2\sim i} (x_1 - \hat{x}_1)| |\xi_i - \beta_{i-1} \xi_{i-1} - e_i|^{p(t)-1} \\
 & \leq \frac{b_2}{2} (|\xi_{i-1}|^{p(t)+1} + |\xi_i|^{p(t)+1}) + c_{2,i} |e_i|^{p(t)+1} \\
 & + \sum_{j=2}^{i-1} \alpha_{i,j} (l_{j+1}, \dots, l_i) |e_j|^{p(t)+1} + \alpha_{i,1} (l_2, \dots, l_i) |x_1 \\
 & - \hat{x}_1|^{p(t)+1}, \\
 & \hspace{15em} + \sum_{j=2}^{n-1} \alpha_j (l_{j+1}, \dots, l_n) |e_j|^{p(t)+1} \\
 & + \alpha_1 (l_2, \dots, l_n) |x_1 - \hat{x}_1|^{p(t)+1}, \tag{A.5}
 \end{aligned}$$

where  $\alpha_j = \sum_{i=j+1}^n \alpha_{i,j} (l_{j+1}, \dots, l_i) + c_{2,j}$  with  $c_{2,1} = 0$ ,  $j = 1, \dots, n$ , that is,  $\alpha_n > 0$  is a constant dependent on  $b_2$ , and  $\alpha_j > 0$ ,  $j = 1, \dots, n-1$ , are constants dependent on  $b_2, l_{j+1}, \dots, l_n$ .  $\square$

*Proof of Proposition 13.* By (A.2), Assumption 8, and Lemmas 2 and 3, one has

$$\begin{aligned}
 |\phi_1(t, x_1) - \phi_1(t, \hat{x}_1)| & \leq c \sum_{j=1}^N (|x_1 - \hat{x}_1|^{a_{1,j}(t)} \\
 & \cdot (|x_1|^{b_{1,j}(t)} + |x_1 - (x_1 - \hat{x}_1)|^{b_{1,j}(t)})) \\
 & \leq \hat{c} \sum_{j=1}^N (|x_1 - \hat{x}_1|^{a_{1,j}(t)} |x_1|^{b_{1,j}(t)} + |x_1 - \hat{x}_1|^{p(t)}), \tag{A.6}
 \end{aligned}$$

and for  $i = 2, \dots, n$ ,

where  $e_1 = 0$ ,  $b_2 > 0$  is a constant,  $c_{2,i} > 0$  is a constant dependent on  $b_2$ , and  $\alpha_{i,j} > 0$ ,  $j = 1, \dots, i-1$ , are constants dependent on  $b_2, l_{j+1}, \dots, l_i$ . From (A.4), it follows that

$$\begin{aligned}
 & - \sum_{i=2}^n l_i e_i (|\tilde{z}_i + l_i x_{i-1}|)^{p(t)} \\
 & \leq b_2 \sum_{i=1}^n |\xi_i|^{p(t)+1} + \alpha_n |e_n|^{p(t)+1}
 \end{aligned}$$

$$\begin{aligned}
 |\phi_i(t, x_1, \dots, x_i) - \phi_i(t, \hat{x}_1, \dots, \hat{x}_i)| & \leq c \sum_{j=1}^N \left( \sum_{k=1}^i (|x_k - \hat{x}_k|^{a_{k,j}(t)} \sum_{q=1}^i (|x_q|^{b_{k,j}(t)} + |\hat{x}_q|^{b_{k,j}(t)})) \right) \leq c \sum_{j=1}^N (|x_1 - \hat{x}_1|^{a_{1,j}(t)} \\
 & \cdot (|x_1|^{b_{1,j}(t)} + |x_1 - (x_1 - \hat{x}_1)|^{b_{1,j}(t)}) + |x_1 - \hat{x}_1|^{a_{1,j}(t)} \sum_{q=2}^i (|x_q|^{b_{1,j}(t)} \\
 & + |x_q - (e_q + l_q e_{q-1} + l_{(q-1)\sim q} e_{q-2} + \dots + l_{3\sim q} e_2 + l_{2\sim q} (x_1 - \hat{x}_1))|^{b_{1,j}(t)}) \\
 & + \sum_{k=2}^i \left( |e_k + l_k e_{k-1} + l_{(k-1)\sim k} e_{k-2} + \dots + l_{3\sim k} e_2 + l_{2\sim k} (x_1 - \hat{x}_1)|^{a_{k,j}(t)} (|x_1|^{b_{k,j}(t)} + |x_1 - (x_1 - \hat{x}_1)|^{b_{k,j}(t)}) \right) \\
 & + |e_k + l_k e_{k-1} + l_{(k-1)\sim k} e_{k-2} + \dots + l_{3\sim k} e_2 + l_{2\sim k} (x_1 - \hat{x}_1)|^{a_{k,j}(t)} \\
 & \cdot \sum_{q=2}^i (|x_q|^{b_{k,j}(t)} + |x_q - (e_q + l_q e_{q-1} + l_{(q-1)\sim q} e_{q-2} + \dots + l_{3\sim q} e_2 + l_{2\sim q} (x_1 - \hat{x}_1))|^{b_{k,j}(t)}) \Big) \leq \hat{c} \sum_{j=1}^N (|x_1 - \hat{x}_1|^{a_{1,j}(t)} \\
 & \cdot \sum_{q=1}^i |x_q|^{b_{1,j}(t)} + \bar{\gamma}_{i,i} |e_i|^{p(t)} + \sum_{k=2}^{i-1} \bar{\gamma}_{i,k} (l_{k+1}, \dots, l_i) |e_k|^{p(t)} + \bar{\gamma}_{i,1} (l_2, \dots, l_i) |x_1 - \hat{x}_1|^{p(t)} \\
 & + \sum_{k=2}^i \left( |e_k + l_k e_{k-1} + l_{(k-1)\sim k} e_{k-2} + \dots + l_{3\sim k} e_2 + l_{2\sim k} (x_1 - \hat{x}_1)|^{a_{k,j}(t)} \sum_{q=1}^i |x_q|^{b_{k,j}(t)} \right) \Big), \tag{A.7}
 \end{aligned}$$

where  $\hat{c} > 0$  is a constant,  $\bar{\gamma}_{i,i}$  is a positive constant, and  $\bar{\gamma}_{i,k}, k = 1, \dots, i - 1$ , are positive constants dependent on  $l_{k+1}, \dots, l_i$ . From (11), (A.6), (A.7), and Lemmas 2 and 3, it follows that for  $i = 2, \dots, n$ ,

$$\begin{aligned}
 & -l_i e_i (\phi_{i-1} - \hat{\phi}_{i-1}) \\
 & \leq l_i |e_i| |\phi_{i-1}(t, x_1, \dots, x_{i-1}) - \phi_{i-1}(t, \hat{x}_1, \dots, \hat{x}_{i-1})| \\
 & \leq \frac{b_3}{n} \sum_{j=1}^{i-1} |\xi_j|^{p(t)+1} + c_{3,i} |e_i|^{p(t)+1} \\
 & + \sum_{j=2}^{i-1} \gamma_{i,j} (l_{j+1}, \dots, l_i) |e_j|^{p(t)+1} \\
 & + \gamma_{i,1} (l_2, \dots, l_i) |x_1 - \hat{x}_1|^{p(t)+1},
 \end{aligned} \tag{A.8}$$

where  $b_3 > 0$  is a constant,  $c_{3,i} > 0$  is a constant dependent on  $b_3$ , and  $\gamma_{i,j} > 0, j = 1, \dots, i - 1$ , are constants dependent on  $b_3, l_{j+1}, \dots, l_i$ . Similar to (A.6), it follows from (A.8) that

$$\begin{aligned}
 & -\sum_{i=2}^n l_i e_i (\phi_{i-1} - \hat{\phi}_{i-1}) \\
 & \leq b_3 \sum_{i=1}^n |\xi_i|^{p(t)+1} + \gamma_n |e_n|^{p(t)+1} \\
 & + \sum_{j=2}^{n-1} \gamma_j (l_{j+1}, \dots, l_n) |e_j|^{p(t)+1} \\
 & + \gamma_1 (l_2, \dots, l_n) |x_1 - \hat{x}_1|^{p(t)+1},
 \end{aligned} \tag{A.9}$$

where  $\gamma_j = \sum_{i=j+1}^n \gamma_{i,j} (l_{j+1}, \dots, l_i) + c_{3,j}$  with  $c_{2,1} = 0, j = 1, \dots, n$ , that is,  $\gamma_n > 0$  is a constant dependent on  $b_3$ , and  $\gamma_j > 0, j = 1, \dots, n - 1$ , are constants dependent on  $b_3, l_{j+1}, \dots, l_n$ .  $\square$

*Proof of Proposition 14.* By (11), (22), and (A.2), one has

$$\begin{aligned}
 u & = \sum_{i=1}^n \beta_{i-n} (x_i - \hat{x}_i) - \sum_{i=1}^n \beta_{i-n} x_i \\
 & = -\beta_n \xi_n + \bar{\sigma}_1 (l_2, \dots, l_n) (x_1 - \hat{x}_1) \\
 & + \sum_{i=2}^{n-1} \bar{\sigma}_i (l_{i+1}, \dots, l_n) e_i + \bar{\sigma}_n e_n,
 \end{aligned} \tag{A.10}$$

where  $\bar{\sigma}_i = \sum_{j=i}^n \beta_{j-n} l_{(i+1) \sim j}, i = 1, \dots, n$ , that is,  $\bar{\sigma}_n$  is a positive constant, and  $\bar{\sigma}_i, i = 1, \dots, n - 1$ , are positive constants dependent on  $l_{i+1}, \dots, l_n$ . By (A.10) and Lemmas 2 and 3, we derive

$$\begin{aligned}
 e_n [u]^{p(t)} & \leq |e_n| |u|^{p(t)} \\
 & \leq b_4 |\xi_n|^{p(t)+1} + \sigma_n |e_n|^{p(t)+1} \\
 & + \sum_{i=2}^{n-1} \sigma_i (l_{i+1}, \dots, l_n) |e_i|^{p(t)+1} \\
 & + \sigma_1 (l_2, \dots, l_n) |x_1 - \hat{x}_1|^{p(t)+1},
 \end{aligned} \tag{A.11}$$

where  $b_4 > 0$  is a constant,  $\sigma_n > 0$  is a constant dependent on  $b_4$ , and  $\sigma_i > 0, i = 1, \dots, n - 1$ , are constants dependent on  $l_{i+1}, \dots, l_n$ .  $\square$

*Proof of Proposition 15.* By  $x_{n+1}^* = \beta_n \xi_n$  and (A.10), one has

$$\begin{aligned}
 u - x_{n+1}^* & = \bar{\sigma}_1 (l_2, \dots, l_n) (x_1 - \hat{x}_1) \\
 & + \sum_{i=2}^{n-1} \bar{\sigma}_i (l_{i+1}, \dots, l_n) e_i + \bar{\sigma}_n e_n,
 \end{aligned} \tag{A.12}$$

from which, by Lemmas 2–4, we derive

$$\begin{aligned}
 \xi_n \left( [u]^{p(t)} - [x_{n+1}^*]^{p(t)} \right) & \leq |\xi_n| \cdot \bar{p} (2^{\bar{p}-3} + 1) \\
 & \cdot \left( |u - x_{n+1}^*|^{p(t)} + |u - x_{n+1}^*| |x_{n+1}^*|^{p(t)-1} \right) \\
 & \leq b_5 |\xi_n|^{p(t)+1} + \omega_n |e_n|^{p(t)+1} \\
 & + \sum_{i=2}^{n-1} \omega_i (l_{i+1}, \dots, l_n) |e_i|^{p(t)+1} + \omega_1 (l_2, \dots, l_n) \\
 & \cdot |x_1 - \hat{x}_1|^{p(t)+1},
 \end{aligned} \tag{A.13}$$

where  $b_5 > 0$  is a constant,  $\omega_n > 0$  is a constant dependent on  $b_5$ , and  $\omega_i > 0, i = 1, \dots, n - 1$ , are constants dependent on  $b_5, l_{i+1}, \dots, l_n$ .  $\square$

### Data Availability

The data supporting the conclusions of the manuscript are some open access articles that have been properly cited, and the readers can easily obtain these articles to verify the conclusions, replicate the analysis, and conduct secondary analyses. Therefore, we do not create a publicly available data repository.

### Conflicts of Interest

The authors declare that they have no competing interests.

### Acknowledgments

This work was supported by the Taishan Scholar Project of Shandong Province of China (No. ts201712040), National Natural Science Foundation of China (No. 61673242), and Shandong Provincial Natural Science Foundation of China (No. ZR2016FM10).

## References

- [1] W. Lin and C.-J. Qian, "Adding one power integrator: a tool for global stabilization of high-order lower-triangular systems," *Systems & Control Letters*, vol. 39, no. 5, pp. 339–351, 2000.
- [2] W. Lin, C.-J. Qian, and X.-Q. Huang, "Disturbance attenuation of a class of non-linear systems via output feedback," *International Journal of Robust and Nonlinear Control*, vol. 13, no. 15, pp. 1359–1369, 2003.
- [3] B. Yang and W. Lin, "Homogeneous observers, iterative design, and global stabilization of high-order nonlinear systems by smooth output feedback," *Institute of Electrical and Electronics Engineers Transactions on Automatic Control*, vol. 49, no. 7, pp. 1069–1080, 2004.
- [4] J. Polendo and C.-J. Qian, "A generalized homogeneous domination approach for global stabilization of inherently nonlinear systems via output feedback," *International Journal of Robust and Nonlinear Control*, vol. 17, no. 7, pp. 605–629, 2007.
- [5] X.-J. Xie and X.-H. Zhang, "Further results on global state feedback stabilization of nonlinear high-order feedforward systems," *ISA Transactions*, vol. 53, no. 2, pp. 341–346, 2014.
- [6] X.-H. Zhang and X.-J. Xie, "Global state feedback stabilisation of nonlinear systems with high-order and low-order nonlinearities," *International Journal of Control*, vol. 87, no. 3, pp. 642–652, 2014.
- [7] X.-J. Xie, N. Duan, and C.-R. Zhao, "A combined homogeneous domination and sign function approach to output-feedback stabilization of stochastic high-order nonlinear systems," *IEEE Transactions on Automatic Control*, vol. 59, no. 5, pp. 1303–1309, 2014.
- [8] Z.-Q. Zhang, S.-Y. Xu, and B.-Y. Zhang, "Asymptotic tracking control of uncertain nonlinear systems with unknown actuator nonlinearity," *IEEE Transactions on Automatic Control*, vol. 59, no. 5, pp. 1336–1341, 2014.
- [9] X.-H. Zhang, X.-J. Xie, and Y.-X. Huang, "Global state feedback stabilization of high-order nonlinear systems with multiple time-varying delays," *Journal of The Franklin Institute*, vol. 352, no. 1, pp. 271–290, 2015.
- [10] Z.-Y. Sun, L.-R. Xue, and K.-M. Zhang, "A new approach to finite-time adaptive stabilization of high-order uncertain nonlinear system," *Automatica*, vol. 58, no. 8, pp. 60–66, 2015.
- [11] K.-M. Zhang and X.-H. Zhang, "Finite-time stabilisation for high-order nonlinear systems with low-order and high-order nonlinearities," *International Journal of Control*, vol. 88, no. 8, pp. 1576–1585, 2015.
- [12] X.-H. Zhang, K.-M. Zhang, and M.-M. Jiang, "Global output feedback stabilisation of high-order nonlinear systems with low-order and high-order nonlinearities," *International Journal of Control*, vol. 88, no. 11, pp. 2194–2210, 2015.
- [13] Z.-Y. Sun, T. Li, and S.-H. Yang, "A unified time-varying feedback approach and its applications in adaptive stabilization of high-order uncertain nonlinear systems," *Automatica*, vol. 70, no. 8, pp. 249–257, 2016.
- [14] X.-H. Zhang, K.-M. Zhang, and X.-J. Xie, "Finite-time output feedback stabilization of nonlinear high-order feedforward systems," *International Journal of Robust and Nonlinear Control*, vol. 26, no. 8, pp. 1794–1814, 2016.
- [15] Z.-Y. Sun, C.-H. Zhang, and Z. Wang, "Adaptive disturbance attenuation for generalized high-order uncertain nonlinear systems," *Automatica*, vol. 80, pp. 102–109, 2017.
- [16] Z.-Y. Sun, M.-M. Yun, and T. Li, "A new approach to fast global finite-time stabilization of high-order nonlinear system," *Automatica*, vol. 81, pp. 455–463, 2017.
- [17] J.-Y. Zhai and C.-J. Qian, "Global control of nonlinear systems with uncertain output function using homogeneous domination approach," *International Journal of Robust and Nonlinear Control*, vol. 22, no. 14, pp. 1543–1561, 2012.
- [18] W.-Q. Ai, J.-Y. Zhai, and S.-M. Fei, "Universal adaptive regulation for a class of nonlinear systems with unknown time delays and output function via output feedback," *Journal of The Franklin Institute*, vol. 350, no. 10, pp. 3168–3187, 2013.
- [19] M.-M. Jiang, P. Wang, and X.-J. Xie, "Global output feedback stabilisation of nonlinear time-delay systems with unknown output function," *International Journal of Systems Science*, vol. 48, no. 12, pp. 2554–2564, 2017.
- [20] J.-Y. Zhai, "Global finite-time output feedback stabilisation for a class of uncertain nontriangular nonlinear systems," *International Journal of Systems Science*, vol. 45, no. 3, pp. 637–646, 2014.
- [21] X.-J. Xie, Z.-J. Li, and K.-M. Zhang, "Semi-global output feedback control for nonlinear systems with uncertain time-delay and output function," *International Journal of Robust and Nonlinear Control*, vol. 27, no. 15, pp. 2549–2566, 2017.
- [22] Z.-J. Li, X.-J. Xie, and K.-M. Zhang, "Output feedback stabilisation for nonlinear systems with unknown output function and control coefficients and its application," *International Journal of Control*, vol. 90, no. 5, pp. 1027–1036, 2017.
- [23] M.-M. Jiang, X.-J. Xie, and K.-M. Zhang, "Finite-time output feedback stabilization of high-order uncertain nonlinear systems," *International Journal of Control*, vol. 91, no. 6, pp. 1338–1349, 2018.
- [24] C.-L. Rui, M. Reyhanoglu, I. Kolmanovskiy, S. Cho, and N.-H. McClamroch, "Nonsmooth stabilization of an underactuated unstable two degrees of freedom mechanical system," in *Proceedings of the 1997 36th IEEE Conference on Decision and Control*, vol. 4, pp. 3998–4003, San Diego, Calif, USA, December 1997.
- [25] J.-Z. Liu, S. Yan, D.-L. Zeng, Y. Hu, and Y. Lv, "A dynamic model used for controller design of a coal fired once-through boiler-turbine unit," *Energy*, vol. 93, pp. 2069–2078, 2015.
- [26] Z.-G. Su, C.-J. Qian, and J. Shen, "Interval homogeneity-based control for a class of nonlinear systems with unknown power drifts," *Institute of Electrical and Electronics Engineers Transactions on Automatic Control*, vol. 62, no. 3, pp. 1445–1450, 2017.
- [27] C.-C. Chen, C.-J. Qian, Y.-W. Liang, and S.-H. Li, "Interval homogeneous domination approach for global stabilization of nonlinear systems with time-varying powers," in *Proceedings of the 55th IEEE Conference on Decision and Control, CDC 2016*, pp. 7258–7263, USA, December 2016.
- [28] C.-C. Chen and S. S.-D. Xu, "Global Stabilization for a Class of Genuinely Nonlinear Systems with a Time-Varying Power: An Interval Homogeneous Domination Approach," *IEEE Access*, vol. 6, pp. 11255–11264, 2018.
- [29] C.-C. Chen, C.-J. Qian, X.-Z. Lin, Z.-Y. Sun, and Y.-W. Liang, "Smooth output feedback stabilization for a class of nonlinear systems with time-varying powers," *International Journal of Robust and Nonlinear Control*, vol. 27, no. 18, pp. 5113–5128, 2017.
- [30] H.-K. Khalil, *Nonlinear Systems*, Prentice-Hall, New Jersey, NJ, USA, 2002.
- [31] G. Hardy, J. Littlewood, and G. Polya, *Inequalities*, Cambridge University Press, Cambridge, UK, 2nd edition, 1988.

- [32] Z.-Y. Sun, X.-H. Zhang, and X.-J. Xie, "Continuous global stabilisation of high-order time-delay nonlinear systems," *International Journal of Control*, vol. 86, no. 6, pp. 994–1007, 2013.
- [33] Z.-Y. Sun, X.-H. Zhang, and X.-J. Xie, "Global continuous output-feedback stabilization for a class of high-order nonlinear systems with multiple time delays," *Journal of The Franklin Institute*, vol. 351, no. 8, pp. 4334–4356, 2014.

## Research Article

# Unbiased Minimum Variance Estimation for Discrete-Time Systems with Measurement Delay and Unknown Measurement Disturbance

Yu Guan<sup>1</sup> and Xinmin Song <sup>2</sup>

<sup>1</sup>*School of Information Science and Engineering, Shandong Normal University, Jinan 250014, China*

<sup>2</sup>*School of Information Science and Engineering and Institute of Data Science and Technology, Shandong Normal University, Jinan 250014, China*

Correspondence should be addressed to Xinmin Song; [xinminsong@sina.com](mailto:xinminsong@sina.com)

Received 16 August 2018; Accepted 9 September 2018; Published 25 September 2018

Academic Editor: Xue-Jun Xie

Copyright © 2018 Yu Guan and Xinmin Song. This is an open access article distributed under the Creative Commons Attribution License, which permits unrestricted use, distribution, and reproduction in any medium, provided the original work is properly cited.

This paper addresses the state estimation problem for stochastic systems with unknown measurement disturbances whose any prior information is unknown and measurement delay resulting from the inherent limited bandwidth. For such complex systems, the Kalman-like one-step predictor independent of unknown measurement disturbances is designed based on the linear unbiased minimum variance criterion and the reorganized innovation analysis approach. One simulation example shows the effectiveness of the proposed algorithms.

## 1. Introduction

In recent years, networked control systems have attracted much attention and much work has been done due to the wide applications in communication systems [1, 2], fault detection [3, 4], and sensor [5]. However, these networks are usually unreliable and may lead to measurement delays due to inherent limited bandwidth. According to different kinds of time delay, many results have sprung up, such as control input delay [6, 7], state-dependent delay [8], state-independent delay [9–11], output delay [12, 13], communication delay [14], distributed-delay [15–17], and time-varying delay [18, 19]. In addition, the unknown disturbances in system modeling or external environment are ubiquitous feature in the piratical systems. The measurement delays and unknown observation disturbances can influence the performance or even results in systems instability. For these reasons, it is not surprising that the study of the state estimation problem for systems with time-delays and unknown observation disturbances has been an enthusiasm for a large number of scholars.

The early work on the discrete-time systems with time delay has been investigated by system augmentation [20]

or partial difference Riccati equation approach [21]. In [21], the partial difference Riccati equation approach is used to settle the measurement delay problem for linear systems. In order to lessen the computational cost (compared with state augmentation approach and partial difference Riccati equation approach), [22] proposes the reorganized innovation approach, by calculating two standard Riccati difference equations of the same dimension as the original system; the authors solve the finite horizon estimation problem for measurement delayed systems. In [23], the linear minimum mean square estimation filter for systems with measurement delay is calculated in terms of two Riccati difference equations and one Lyapunov difference equation. It should be pointed that all the aforementioned estimators do not consider the disturbance in observation.

In practice, the unknown disturbances in system modeling or external environment are another ubiquitous feature [24–26]. The early works on unbiased minimum variance problems with observation disturbances can be traced back to [27]. For these unknown disturbances without any prior knowledge, unbiased minimum variance filter instead of Kalman filter is more effective in tracing the true state.

Reference [28] obtains a more general unbiased estimator using the approach in [27] and presents the convergence analysis of the estimator. In [29], the authors consider global optimality of unbiased estimator based on [27, 28]. In [30], the authors consider event-based state estimation of linear dynamic systems with unknown inputs. Different from the aforementioned methods about linear discrete-time systems with observation disturbance, [31, 32] solve the state estimation with partially observed inputs problem without adding unbiased constraint. However, [28–33] only consider the state estimation problem of the state equation with unknown input. It should be pointed that measurement disturbances are ubiquitous feature in practical systems and the estimation problems for discrete-time systems with unknown measurement disturbance are also important. Motivated by the preceding works about measurement delay and unknown measurement disturbance, we study linear unbiased estimation for discrete-time systems with measurement delay and unknown measurement disturbance in this paper. By employing the linear unbiased minimum variance approach and the reorganized innovation analysis approach, one Kalman-like one-step ahead predictor is derived in terms of two Riccati difference equations of the same dimension with the state model, which may reduce the computation when delay is large, compared with the classic state augmentation approach [20] and partial difference Riccati equation approach [21, 34]. Further, just like the stability of the classical Kalman filter [35] and the mean square stability analysis [36], we develop a parallel to obtain the stability properties of the proposed unbiased estimator under standard conditions.

The organization of this paper is as follows. In Section 2, we present the problem statement, some assumptions and remarks. In Section 3, we deduce the state estimation according to the reorganized innovation analysis approach, then we obtain the finite and infinite horizon filter based on the linear unbiased minimum variance criterion, respectively. In Section 4, a numerical example is given to illustrate the effectiveness of the proposed approach. In Section 5, we provide some concluding remarks.

*Notation.* Throughout this paper, the superscripts “ $-1$ ” and “ $T$ ” represent the inverse and transpose of a matrix.  $\mathcal{R}^n$  denotes the  $n$ -dimensional Euclidean space.  $\mathcal{R}^{n \times m}$  is the set of all  $n \times m$  real matrices.  $\delta_{ij} = 0$  for  $i \neq j$  and  $\delta_{ii} = 1$ .  $\mathcal{L}\{\{y(s)\}_{s=0}^k\}$  denotes the linear subspace spanned by the measurement sequence  $\{y(0), \dots, y(k)\}$ .  $\lambda_i(X)$  denotes the  $i$ th eigenvalue of a square matrix  $X$ . Furthermore, the mathematical expectation operator is denoted by  $E$ .

## 2. Problems Statement and Preliminary

Consider the following linear system:

$$x(k+1) = Ax(k) + n(k) \quad (1)$$

$$y_0(k) = B_0x(k) + C_0u_0(k) + v_0(k) \quad (2)$$

$$y_1(k) = B_1x(k-d) + C_1u_1(k) + v_1(k), \quad k \geq d \quad (3)$$

where  $x(k) \in \mathcal{R}^n$ ,  $y_0(k) \in \mathcal{R}^{m_0}$ , and  $y_1(k) \in \mathcal{R}^{m_1}$  are the state, current, and delayed measurement, respectively.  $n(k)$  is the process noise,  $v_0(k)$  and  $v_1(k)$  are the measurement noises.  $u_0(k) \in \mathcal{R}^{p_0}$  and  $u_1(k) \in \mathcal{R}^{p_1}$  are the unknown measurement disturbances without any prior knowledge. For simplicity of presentation, we assume that  $A$ ,  $B_0$ ,  $B_1$ ,  $C_0$ , and  $C_1$  are constant matrices with suitable dimensions even though the later development and results can be easily adapted to the time-varying case.

*Assumption 1.*  $n(k)$ ,  $v_0(k)$ , and  $v_1(k)$  are uncorrelated white noises of zero mean and covariance as

$$\begin{aligned} E\{n(k)n^T(j)\} &= Q\delta_{kj}, \\ E\{v_0(k)v_0^T(j)\} &= R_0\delta_{kj}, \\ E\{v_1(k)v_1^T(j)\} &= R_1\delta_{kj} \end{aligned} \quad (4)$$

*Assumption 2.* The initial state  $x(0)$  is uncorrelated with  $n(k)$ ,  $v_0(k)$ , and  $v_1(k)$  and satisfies

$$\begin{aligned} E\{x(0)\} &= \mu_0, \\ E\{[x(0) - \mu_0][x(0) - \mu_0]^T\} &= P_0 \end{aligned} \quad (5)$$

*Assumption 3.*  $\text{rank}[C_0] = p_0 < m_0$ ;  $\text{rank}[C_1] = p_1 < m_1$ .

To the estimation problems of stochastic systems, Assumptions 1 and 2 are general. Assumption 3 guarantees the existence of the following predictors designed.

For convenience, the measurement  $y(k)$  can be rewritten as follows:

$$y(k) = \begin{cases} y_0(k), & 0 \leq k < d \\ \begin{bmatrix} y_0(k) \\ y_1(k) \end{bmatrix}, & k \geq d \end{cases} \quad (6)$$

*Problem.* For the given measurements  $\{y(k)\}_{k=0}^M$ , our aim is to design a minimum variance unbiased Kalman-like one-step predictor  $\hat{x}(k+1)$ . Further, we will consider the infinite horizon predictor design  $\hat{x}(k+1)$ .

*Remark 4.* As for time delay systems, we can settle the estimation problem by using the state augmentation approach or partial difference Riccati equation approach. However the augmented approach or partial difference Riccati equation approach may bring expensive computational cost when the delay  $d$  is large [22]. In the following, we will deduce the estimation problem based on the reorganized innovation approach and linear minimum variance unbiased criterion instead of the augmented approach.

## 3. Main Results

*3.1. Finite Horizon Estimation.* We note that  $y_1(k)$  is an additional measurement of the state  $x(k-d)$  which is obtained at time instant  $k$  with time delay  $d$ , so the measurement

$y(k)$  consists of time delay when  $k \geq d$ . Apparently, the linear space  $\mathcal{L}\{\{y(s)\}_{s=0}^k\}$  contains the same information as  $\mathcal{L}\{\{Y_1(s)\}_{s=0}^{k-d}, \{Y_0(s)\}_{s=k-d+1}^k\}$ , where the new observations  $Y_1(s)$  and  $Y_0(s)$  are provided as follows:

$$Y_1(s) = \begin{bmatrix} y_0(s) \\ y_1(s+d) \end{bmatrix}, \quad 0 \leq s \leq k-d \quad (7)$$

$$Y_0(s) = y_0(s), \quad k-d < s \leq k \quad (8)$$

Obviously,  $Y_1(s)$  and  $Y_0(s)$  satisfy

$$Y_1(s) = Bx(s) + CU(s) + V(s) \quad (9)$$

$$Y_0(s) = B_0x(s) + C_1u_0(s) + V_0(s) \quad (10)$$

where

$$\begin{aligned} B &= \begin{bmatrix} B_0 \\ B_1 \end{bmatrix}, \\ C &= \begin{bmatrix} C_0 & 0 \\ 0 & C_1 \end{bmatrix}, \\ U(s) &= \begin{bmatrix} u_0(s) \\ u_1(s+d) \end{bmatrix}, \\ V(s) &= \begin{bmatrix} v_0(s) \\ v_1(s+d) \end{bmatrix}, \\ V_0(s) &= v_0(s) \end{aligned} \quad (11)$$

It is obvious that the new measurements  $Y_0(s)$  and  $Y_1(s)$  are delay-free and the associated measurement noises  $V_0(s)$  and  $V(s)$  are white noises with zero mean and covariance matrices  $R_{V_0(s)} = R_0$ ,  $R_{V(s)} = R = \text{diag}\{R_0, R_1\}$ .

**Theorem 5.** When  $k \geq d$ , based on linear minimum variance unbiased criterion, we produce a recursive state estimator decoupling with the disturbance for system (1), (7), and (8) in the Kalman-like form:

$$\begin{aligned} \hat{x}(s+1, 0) &= A\hat{x}(s, 0) \\ &+ K_0(s) [Y_0(s) - B_0\hat{x}(s, 0)], \\ &k-d < s < k \end{aligned} \quad (12)$$

$$\hat{x}(k-d+1, 0) = \hat{x}(k-d+1, 1)$$

where

$$\begin{aligned} K_0(s) &= [G_0(s) - \Lambda_0^T(s) C_0^T] D_0^{-1}(s) \\ D_0(s) &= B_0 P_0(s) B_0^T + R_0 \\ G_0(s) &= A P_0(s) B_0^T \\ \Lambda_0^T(s) &= [C_0^T D_0^{-1}(s) C_0]^{-1} C_0^T D_0^{-1}(s) G_0^T(s) \end{aligned} \quad (13)$$

The prediction error covariance matrix  $P_0(s+1)$  is computed by

$$\begin{aligned} P_0(s+1) &= K_0(s) D_0(s) K_0^T(s) - G_0(s) K_0^T(s) \\ &- K_0(s) G_0^T(s) + A P_0(s) A^T + Q \end{aligned} \quad (14)$$

$$P_0(k-d+1) = P_1(k-d+1) \quad (15)$$

As for  $\hat{x}(k-d+1, 1)$  and  $P_1(k-d+1)$ , they are obtained by

$$\begin{aligned} \hat{x}(s+1, 1) &= A\hat{x}(s, 1) + K_1(s) [Y_1(s) - B\hat{x}(s, 1)], \\ &0 \leq s \leq k-d \end{aligned} \quad (16)$$

$$\hat{x}(0, 1) = \mu_0, \quad (17)$$

where

$$K_1(s) = [G_1(s) - \Lambda_1^T(s) C^T] D_1^{-1}(s) \quad (18)$$

$$D_1(s) = B P_1(s) B^T + R \quad (19)$$

$$G_1(s) = A P_1(s) B^T \quad (20)$$

$$\Lambda_1^T(s) = [C^T D_1^{-1}(s) C]^{-1} C^T D_1^{-1}(s) G_1^T(s) \quad (21)$$

The prediction error covariance matrix  $P_1(s+1)$  is computed by

$$\begin{aligned} P_1(s+1) &= K_1(s) D_1(s) K_1^T(s) - G_1(s) K_1^T(s) \\ &- K_1(s) G_1^T(s) + A P_1(s) A^T + Q \end{aligned} \quad (22)$$

$$P_1(0) = P_0. \quad (23)$$

*Proof.* When  $0 < s \leq k-d$ , from (1) and (16), we have the prediction error equation as follows:

$$\begin{aligned} \tilde{x}(s+1, 1) &= x(s+1) - \hat{x}(s+1, 1) \\ &= Ax(s) + n(s) - A\hat{x}(s, 1) \\ &- K_1(s) [Y_1(s) - B\hat{x}(s, 1)] \\ &= [A - K_1(s) B] \tilde{x}(s, 1) + n(s) \\ &- K_1(s) V(s) - K_1(s) CU(s) \end{aligned} \quad (24)$$

Assume  $\hat{x}(s, 1)$  to be unbiased; in order to guarantee that  $\hat{x}(s+1, 1)$  be an unbiased estimate of  $x(s+1)$ , we must have  $E[\tilde{x}(s+1, 1)] = 0$ , then we have

$$K_1(s) C = 0 \quad (25)$$

Substituting (25) into (24), (24) can be rewritten as

$$\begin{aligned} \tilde{x}(s+1, 1) &= [A - K_1(s) B] \tilde{x}(s, 1) + n(s) \\ &- K_1(s) V(s) \end{aligned} \quad (26)$$

From (26), the prediction error covariance matrix  $P_1(s+1)$  is computed by

$$\begin{aligned} P_1(s+1) &= E[\tilde{x}(s+1,1)\tilde{x}^T(s+1,1)] \\ &= [A - K_1(s)B]P_1(s)[A - K_1(s)B]^T + Q \\ &\quad + K_1(s)RK_1^T(s) \\ &= K_1(s)D_1(s)K_1^T(s) - G_1(s)K_1^T(s) \\ &\quad - K_1(s)G_1^T(s) + AP_1(s)A^T + Q \end{aligned} \quad (27)$$

where  $D_1(s)$  and  $G_1(s)$  are given by (19) and (20). In order to minimize the estimation error variance (27) under the constraint (25), we introduce an auxiliary equation

$$\begin{aligned} J(s) &= tr\{P_1(s+1)\} + tr\{K_1(s)C\Lambda(s)\} \\ &\quad + tr\{\Lambda^T(s)C^TK_1^T(s)\} \end{aligned} \quad (28)$$

where  $\Lambda(s)$  is the Lagrange multipliers. Taking the derivatives with respect to  $K_1(s)$  equal to zero yields

$$K_1(s)D_1(s) + \Lambda(s)C^T - G_1(s) = 0 \quad (29)$$

Combining (25) and (29) gives the matrix equation

$$\begin{bmatrix} D_1(s) & C \\ C^T & 0 \end{bmatrix} \begin{bmatrix} K_1^T(s) \\ \Lambda(s) \end{bmatrix} = \begin{bmatrix} G_1^T(s) \\ 0 \end{bmatrix} \quad (30)$$

Equation (30) has a unique solution if and only if the coefficients is nonsingular. Due to Assumption 3 and the fact that  $D_1(s)$  is nonsingular, the coefficient matrix of (30) is nonsingular. Obviously, premultiplying left- and right-hand sides of (30) by the inverse of coefficient matrix yields (19) and (21). When  $k-d < s \leq k$ , the proof is similar to the case  $0 \leq s \leq k-d$ , so we omit it here.  $\square$

*Remark 6.* The system dimension will get more and more higher with the increase of time delay  $d$ ; thus, computational complexity will get higher when using the classical state augmentation approach. But when we adopt the reorganized innovation analysis approach, we only need to solve two Riccati equations which have the same order of the state equation, so it can greatly reduce the computational complexity compared with the classical augmentation approach when time delay  $d$  is large.

**3.2. Infinite Horizon Estimation.** In this subsection, we consider the steady unbiased estimator design. First, let us present the lemma below as the initial step for the convergence analysis.

**Lemma 7.** *If there exist  $K \in R^{n \times (m_0+m_1)}$  such that*

$$\begin{aligned} KC &= 0, \\ \lambda_i[A - KB] &< 1 \end{aligned} \quad (31)$$

for  $i = 1, 2, \dots, n$ , then the sequence  $\{P_1(s+1)\}$  abided by (22) is bounded for any  $s$  given any initial condition  $0 \leq \{P_1(0)\} \leq \infty$ .

*Proof.* Let us consider a suboptimal unbiased filter as follows:

$$\begin{aligned} \hat{x}^{sub}(s+1,1) &= A\hat{x}(s,1) + K^{sub}[Y_1(s) - B\hat{x}(s,1)], \\ &0 \leq s \leq k-d \end{aligned} \quad (32)$$

where  $K^{sub}C = 0$ ,  $\lambda_i[A - K^{sub}B] < 1$ . Then the following state estimation error  $\tilde{x}^{sub}(s+1,1) = x(s+1) - \hat{x}^{sub}(s+1,1)$  is given by

$$\begin{aligned} \tilde{x}^{sub}(s+1,1) &= [A - K^{sub}B]\tilde{x}^{sub}(s,1) + n(s) \\ &\quad - K^{sub}V(s) \end{aligned} \quad (33)$$

with the associated covariance matrix  $P_1^{sub}(s+1)$  being given by

$$\begin{aligned} P_1^{sub}(s+1) &= [A - K^{sub}B]P_1^{sub}(s)[A - K^{sub}B]^T \\ &\quad + Q + K^{sub}RK^{subT} \end{aligned} \quad (34)$$

Thus  $P_1^{sub}(s+1)$  is bounded for any nonnegative initial condition due to the fact that  $\lambda_i[A - K^{sub}B] < 1$ . Comparing the above suboptimal estimator to the designed optimal estimator, the optimality tell us that  $P_1(s+1) \leq P_1^{sub}(s+1)$  for the same initial value. This proves the boundedness of  $P_1^{sub}(s+1)$ .  $\square$

**Theorem 8.** *If there exist  $K \in R^{n \times (m_0+m_1)}$  such that  $KC = 0$ ,  $\lambda_i[A - KB] < 1$ , and  $A, Q^{1/2}$  is stabilizable, then  $\{P_1(s+1)\}$  abided by (22) converges to a unique fixed point  $P_1$  for any initial condition, where  $P_1$  is computed by*

$$P_1 = K_1D_1K_1^T - G_1K_1^T - K_1G_1^T + AP_1A^T + Q \quad (35)$$

and

$$K_1 = [G_1 - \Lambda_1^TC^T]D_1^{-1} \quad (36)$$

$$D_1 = BP_1B^T + R \quad (37)$$

$$G_1 = AP_1B^T \quad (38)$$

$$\Lambda_1^T = [C^TD_1^{-1}C]^{-1}C^TD_1^{-1}G_1^T. \quad (39)$$

When  $0 < s \leq k-d$ , we have the state predictor as follows:

$$\hat{x}(s+1,1) = A\hat{x}(s,1) + K_1[Y_1(s) - B\hat{x}(s,1)] \quad (40)$$

$$\hat{x}(0,1) = \mu_0 \quad (41)$$

When  $k-d < s \leq k$ , the state predictor is as follows:

$$\begin{aligned} \hat{x}(s+1,0) &= A\hat{x}(s,0) \\ &\quad + K_0(s)[Y_0(s) - B_0\hat{x}(s,0)] \end{aligned} \quad (42)$$

$$\hat{x}(k-d+1,0) = \hat{x}(k-d+1,1), \quad (43)$$

where

$$\begin{aligned} K_0(s) &= [D_0^{-1}(s) (G_0^T(s) - C_0 \Lambda_0^T(s))]^T \\ D_0(s) &= B_0 P_0(s) B_0^T + R_0 \\ G_0(s) &= A P_0(s) B_0^T \\ \Lambda_0^T(s) &= [C_0^T D_0^{-1}(s) C_0]^{-1} C_0^T D_0^{-1}(s) G_0^T(s) \end{aligned} \quad (44)$$

The prediction error covariance matrix  $P_0(s+1)$  is computed by

$$\begin{aligned} P_0(s+1) &= K_0(s) D_0(s) K_0^T(s) - G_0(s) K_0^T(s) \\ &\quad - K_0(s) G_0^T(s) + A P_0(s) A^T + Q \end{aligned} \quad (45)$$

$$P_0(k-d+1) = P_1. \quad (46)$$

*Proof.* By simple calculation, the Riccati equation in (22) can be formulated as

$$\begin{aligned} P_1(s+1) &= [A - K_1(s) B] P_1(s) [A - K_1(s) B]^T + Q \\ &\quad + K_1(s) R K_1^T(s). \end{aligned} \quad (47)$$

Then according to [35, 37] and Lemma 7, the convergence analysis can be readily obtained and we omitted here.  $\square$

*Remark 9.* Under the condition that  $KC = 0$ ,  $\lambda_i[A - KB] < 1$ , and  $A, Q^{1/2}$  is stabilizable, we have obtained the steady-state filter (40). This is important when one desires to replace the time-varying filter with the corresponding steady-state version to reduce estimator complexity. On the other hand, the filter in (42) only iterates  $d - 1$  steps; hence we can implement the estimator in finite horizon on the basis of the steady-state filter (40).

## 4. Numerical Example

In this section, we present a numerical example to manifest the proposed approach about linear optimal estimation. Consider the linear discrete-time system with measurement delay and unknown observation disturbance

$$\begin{aligned} x(k+1) &= \begin{bmatrix} 0.78 & 0.40 \\ 0.30 & 0.60 \end{bmatrix} x(k) + n(k), \\ y_0(k) &= \begin{bmatrix} 1 & 2 \\ 2 & 1 \end{bmatrix} x(k) + \begin{bmatrix} 1 \\ 1 \end{bmatrix} u_0(k) + v_0(k), \\ y_1(k) &= \begin{bmatrix} 2 & 1 \\ 1 & 2 \end{bmatrix} x(k-10) + \begin{bmatrix} 1 & 0 \\ 0 & 1 \end{bmatrix} u_1(k) \\ &\quad + v_1(k), \end{aligned} \quad (48)$$

where  $x(0) = \begin{bmatrix} -2 \\ 2 \end{bmatrix}$ ,  $\hat{x}(0,1) = \begin{bmatrix} 0 \\ 0 \end{bmatrix}$ ,  $Q = \begin{bmatrix} 1 & 0 \\ 0 & 1 \end{bmatrix}$ ,  $u_0(k) = 0.2$ ,  $u_1(k) = \begin{bmatrix} 0.25 \\ 0.3 \end{bmatrix}$ ,  $R_0 = R_1 = I_{2 \times 2}$ ,  $n(k)$ ,  $v_0(k)$ , and  $v_1(k)$  are white noises with zero mean and covariances  $Q$ ,  $R_1$  and  $R_2$ , respectively.

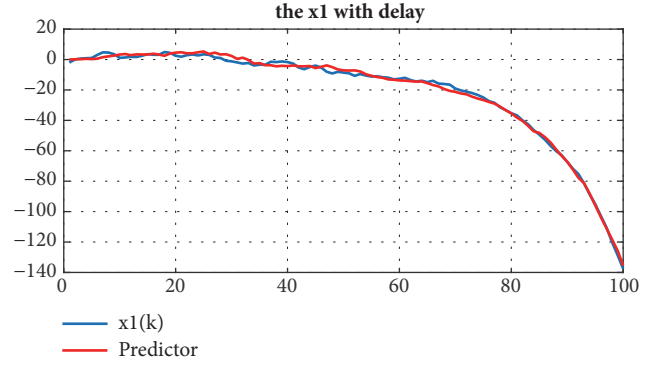


FIGURE 1: The first state component  $x_1(k)$  and the filter  $\hat{x}_1(k)$  for two channels.

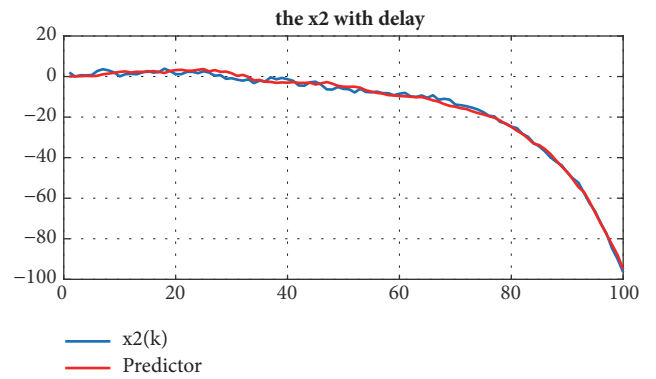


FIGURE 2: The second state component  $x_2(k)$  and the predictor  $\hat{x}_2(k)$  for two channels.

According to Theorem 5, the simulation results are given in Figures 1 and 2, respectively. From the simulation results, we observe that the estimator can track the true state  $x(k)$  well, which proves that our proposed approach in this paper is effective. According to Theorem 8, we obtain the following steady estimator:

$$\begin{aligned} \hat{x}(s+1, 1) &= A \hat{x}(s, 1) + K_1 [Y_1(s) - B \hat{x}(s, 1)] \\ \hat{x}(0, 1) &= \mu_0, \end{aligned} \quad (49)$$

where

$$P = \begin{bmatrix} 10.7546 & 7.0447 \\ 7.0447 & 6.1737 \end{bmatrix}. \quad (50)$$

## 5. Conclusion

In this paper, we have proposed a linear minimum unbiased predictor for discrete-time systems with measurement delay and unknown measurement disturbance. Firstly, we have used the reorganized innovation analysis approach to deal with the measurement delay. In this way, one has avoided the giant computation brought by the augmentation approach or partial difference Riccati equation approach. Then based on the linear unbiased minimum variance criterion, we have

calculated the minimum variance unbiased predictor, which is designed by calculating two Riccati equations with the same dimension as the state model. The future study direction is to consider the linear unbiased estimation for discrete-time systems with packet dropping and unknown disturbance, where the unknown disturbance appears in both the state equation and the measurement equation.

## Data Availability

The simulation data are available from the corresponding author on reasonable request. Except for simulation data, no data is used to support this study.

## Conflicts of Interest

The authors declare that they have no conflicts of interest.

## Acknowledgments

This work was supported in part by the National Science Foundation of Shandong Province (ZR2016FM17) and the Chinese Postdoctoral Science Foundation (2017M612336).

## References

- [1] T. Zhang, W. Chen, Z. Han, and Z. Cao, "A cross-layer perspective on energy harvesting-aided green communications over fading channels," *IEEE Transactions on Vehicular Technology*, vol. 64, no. 4, pp. 1519–1534, 2015.
- [2] S. Zhang, J. Zhang, and H. C. So, "Mean square deviation analysis of LMS and NLMS algorithms with white reference inputs," *Signal Processing*, vol. 131, pp. 20–26, 2017.
- [3] Y. Li, H. R. Karimi, Q. Zhang, D. Zhao, and Y. Li, "Fault detection for linear discrete time-varying systems subject to random sensor delay: a riccati equation approach," *IEEE Transactions on Circuits and Systems I: Regular Papers*, vol. 65, no. 5, pp. 1707–1716, 2018.
- [4] Y. Ren, A. Wang, and H. Wang, "Fault diagnosis and tolerant control for discrete stochastic distribution collaborative control systems," *IEEE Transactions on Systems, Man, and Cybernetics: Systems*, vol. 45, no. 3, pp. 462–471, 2015.
- [5] M. Yadegar, F. Karami, and J. H. Nobari, "A new control structure to reduce time delay of tracking sensors by applying an angular position sensor," *ISA Transactions*, vol. 63, pp. 133–139, 2016.
- [6] G. Meinsma and L. Mirkin, " $H_\infty$  control of systems with multiple I/O delays via decomposition to adobe problems," *IEEE Transactions on Automatic Control*, vol. 50, no. 2, pp. 199–211, 2005.
- [7] X. Tan, J. Cao, X. Li, and A. Alsaedi, "Leader-following mean square consensus of stochastic multi-agent systems with input delay via event-triggered control," *IET Control Theory & Applications*, vol. 12, no. 2, pp. 299–309, 2018.
- [8] X. Li and J. Wu, "Sufficient stability conditions of nonlinear differential systems under impulsive control with state-dependent delay," *IEEE Transactions on Automatic Control*, vol. 63, no. 1, pp. 306–311, 2018.
- [9] X. Yan and X. Song, "Global practical tracking by output feedback for nonlinear systems with unknown growth rate and time delay," *The Scientific World Journal*, vol. 2014, Article ID 713081, 7 pages, 2014.
- [10] X. Yan, X. Song, and X. Wang, "Global output-feedback stabilization for nonlinear time-delay systems with unknown control coefficients," *International Journal of Control, Automation, and Systems*, vol. 16, no. 4, pp. 1550–1557, 2018.
- [11] K. Zhang, C.-R. Zhao, and X.-J. Xie, "Global output feedback stabilisation of stochastic high-order feedforward nonlinear systems with time-delay," *International Journal of Control*, vol. 88, no. 12, pp. 2477–2487, 2015.
- [12] Z. Duan, X. Song, and M. Qin, "Limited memory optimal filter for discrete-time systems with measurement delay," *Aerospace Science and Technology*, vol. 68, pp. 422–430, 2017.
- [13] X. Song, J. H. Park, and X. Yan, "Linear estimation for measurement-delay systems with periodic coefficients and multiplicative noise," *IEEE Transactions on Automatic Control*, vol. 62, no. 8, pp. 4124–4130, 2017.
- [14] Z. Wang, H. Zhang, X. Song, and H. Zhang, "Consensus problems for discrete-time agents with communication delay," *International Journal of Control, Automation, and Systems*, vol. 15, no. 4, pp. 1515–1523, 2017.
- [15] W. Hou, Z. Wu, M. Fu, and H. Zhang, "Constrained consensus of discrete-time multi-agent systems with time delay," *International Journal of Systems Science*, vol. 49, no. 5, pp. 947–953, 2018.
- [16] L. Chao, "Hybrid delayed synchronizations of complex chaotic systems in modulus-phase spaces and its application," *Journal of Computational and Nonlinear Dynamics*, vol. 11, no. 4, Article ID 041010, 8 pages, 2016.
- [17] B. Y. Zhang, J. Lam, and S. Y. Xu, "Stability analysis of distributed delay neural networks based on relaxed Lyapunov-Krasovskii Functionals," *IEEE Transactions on Neural Networks and Learning Systems*, vol. 26, no. 7, pp. 1480–1492, 2015.
- [18] F. Gao, F. Yuan, and Y. Wu, "Global stabilisation of high-order non-linear systems with time-varying delays," *IET Control Theory & Applications*, vol. 7, no. 13, pp. 1737–1744, 2013.
- [19] F. Gao, Y. Wu, and F. Yuan, "Global output feedback stabilisation of high-order nonlinear systems with multiple time-varying delays," *International Journal of Systems Science*, vol. 47, no. 10, pp. 2382–2392, 2016.
- [20] L. Xiao, A. Hassibi, and J. P. How, "Control with random communication delays via a discrete-time jump system approach," in *Proceedings of the American Control Conference*, vol. 3, pp. 2199–2204, Chicago, Ill, USA, June 2000.
- [21] I. Y. Song, D. Y. Kim, V. Shin, and M. Jeon, "Receding horizon filtering for discrete-time linear systems with state and observation delays," *IET Radar, Sonar & Navigation*, vol. 6, no. 4, pp. 263–271, 2012.
- [22] H. Zhang, L. Xie, D. Zhang, and Y. C. Soh, "A reorganized innovation approach to linear estimation," *IEEE Transactions on Automatic Control*, vol. 49, no. 10, pp. 1810–1814, 2004.
- [23] X. Song and J. H. Park, "Linear optimal estimation for discrete-time measurement delay systems with multichannel multiplicative noise," *IEEE Transactions on Circuits and Systems II: Express Briefs*, vol. 64, no. 2, pp. 156–160, 2017.
- [24] C.-R. Zhao, X.-J. Xie, and N. Duan, "Adaptive state-feedback stabilization for high-order stochastic nonlinear systems driven by noise of unknown covariance," *Mathematical Problems in Engineering*, vol. 2012, Article ID 246579, 13 pages, 2012.
- [25] X. Xie and M. Jiang, "Output feedback stabilization of stochastic feedforward nonlinear time-delay systems with unknown output function," *International Journal of Robust and Nonlinear Control*, vol. 28, no. 1, pp. 266–280, 2018.

- [26] N. Duan, H. Min, and X. Qin, "Adaptive stabilization of stochastic nonlinear systems disturbed by unknown time delay and covariance noise," *Mathematical Problems in Engineering*, vol. 2017, Article ID 8084529, 9 pages, 2017.
- [27] P. K. Kitanidis, "Unbiased minimum-variance linear state estimation," *Automatica*, vol. 23, no. 6, pp. 775–778, 1987.
- [28] M. Darouach and M. Zasadzinski, "Unbiased minimum variance estimation for systems with unknown exogenous inputs," *Automatica*, vol. 33, no. 4, pp. 717–719, 1997.
- [29] W. S. Kerwin and J. L. Prince, "On the optimality of recursive unbiased state estimation with unknown inputs," *Automatica*, vol. 36, no. 9, pp. 1381–1383, 2000.
- [30] D. Shi, T. Chen, and M. Darouach, "Event-based state estimation of linear dynamic systems with unknown exogenous inputs," *Automatica*, vol. 69, pp. 275–288, 2016.
- [31] B. Li, "State estimation with partially observed inputs: a unified Kalman filtering approach," *Automatica*, vol. 49, no. 3, pp. 816–820, 2013.
- [32] J. Su, B. Li, and W.-H. Chen, "On existence, optimality and asymptotic stability of the Kalman filter with partially observed inputs," *Automatica*, vol. 53, pp. 149–154, 2015.
- [33] Y. Li, "State estimation for stochastic discrete-time systems with multiplicative noises and unknown inputs over fading channels," *Applied Mathematics Computation*, vol. 320, pp. 116–130, 2018.
- [34] X. Song and X. Yan, "Linear quadratic Gaussian control for linear time-delay systems," *IET Control Theory & Applications*, vol. 8, no. 6, pp. 375–383, 2014.
- [35] B. Anderson and J. Moore, *Optimal Filtering*, Prentice Hall, 1979.
- [36] H. Zhang, X. Song, and L. Shi, "Convergence and mean square stability of suboptimal estimator for systems with measurement packet dropping," *IEEE Transactions on Automatic Control*, vol. 57, no. 5, pp. 1248–1253, 2012.
- [37] H. Fang and R. A. de Callafon, "On the asymptotic stability of minimum-variance unbiased input and state estimation," *Automatica*, vol. 48, no. 12, pp. 3183–3186, 2012.

## Research Article

# Trajectory Design and Tracking Control for Nonlinear Underactuated Wheeled Inverted Pendulum

Shuli Gong <sup>1</sup>, Ancai Zhang <sup>2,3,4</sup>, Jinhua She <sup>3,5</sup>, Xinghui Zhang <sup>2,4</sup> and Yuanyuan Liu<sup>1</sup>

<sup>1</sup>School of Mathematics and Statistics, Linyi University, Linyi, Shandong 276005, China

<sup>2</sup>School of Automation and Electrical Engineering, Linyi University, Linyi, Shandong 276005, China

<sup>3</sup>School of Engineering, Tokyo University of Technology, Hachioji, Tokyo 192-0982, Japan

<sup>4</sup>Key Laboratory of Complex Systems and Intelligent Computing in Universities of Shandong, Linyi, Shandong 276000, China

<sup>5</sup>School of Automation, China University of Geosciences, Wuhan, Hubei 430074, China

Correspondence should be addressed to Ancai Zhang; zhangancai23@hotmail.com

Received 4 July 2018; Accepted 3 September 2018; Published 24 September 2018

Academic Editor: Ju H. Park

Copyright © 2018 Shuli Gong et al. This is an open access article distributed under the Creative Commons Attribution License, which permits unrestricted use, distribution, and reproduction in any medium, provided the original work is properly cited.

An underactuated wheeled inverted pendulum (UWIP) is a nonlinear mechanical system that has two degrees of freedom and has only one control input. The motion planning problem for this nonlinear system is difficult to solve because of the existence of an uncontrollable manifold in the configuration space. In this paper, we present a method of designing motion trajectory for this underactuated system. The design of trajectory is based on the dynamic properties of the UWIP system. Furthermore, the tracking control of the UWIP for the constructed trajectory is also studied. A tracking control law is designed by using quadratic optimal control theory. Numerical simulation results verify the effectiveness of the presented theoretical results.

## 1. Introduction

There are many complex dynamic systems in nature. The nonlinear system is an important type of natural system. Since this kind of system can more accurately reflect the essential characteristics of natural systems, they have been attracting more and more attention in the past few decades. Researchers have carried out intensively study on the dynamic analysis and control problem for the nonlinear systems [1–8].

Recently, the control of the nonlinear underactuated mechanical system (UMS) is a hot issue in the engineering area. A UMS has fewer actuators than degrees of freedom (DOF) [9]. There are many examples of the UMS in our daily life. Those include a surface vessel [10], a VTOL aircraft [11], a bridge crane [12], an underwater vehicle [13], and a helicopter [14]. The reduction of actuators makes the UMS have light weight, low energy consumption, flexible movement, and other features. It has wide application prospects in many fields.

However, the control problems presented by the UMS are not easy to solve because of the following two reasons. First, the UMS usually has complex nonlinear dynamics and does

not be strict feedback linearized [15]. Second, the UMS has nonholonomic constraints due to the reduction of actuators [16]. This means that the state variables of UMS are located in an uncontrollable manifold in the configuration space. The control of the UMS is a challenging problem in the nonlinear control area.

In order to conveniently study the control theory of the UMS, some experimental models of the UMS have been built in a lab environment (e.g., Acrobot [17], Furuta pendulum [18], Beam-ball [19], and TORA [20]). Based on these models, many nonlinear control methods have been developed, for example, an equivalent input disturbance (EID) method in [21], an energy-based and nonsmooth Lyapunov function method in [22], a reduced-order control method in [23], and a PID passivity-based method in [24].

An underactuated wheeled inverted pendulum (UWIP) is a recent presented lab model of the UMS [25]. This mechanical system has a wheel and an inverted pendulum (see Figure 1). An actuator drives the wheel to move in a horizontal plane. And the inverted pendulum can freely rotate in a vertical plane. The UWIP is a 2-DOF complex nonlinear system that is not strict feedback linearizable. It

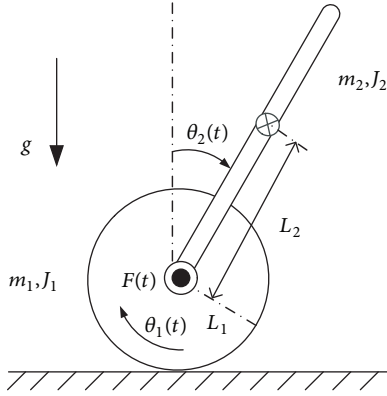


FIGURE 1: Underactuated wheeled inverted pendulum (UWIP).

has a second-order nonholonomic constraint and has an uncontrollable passive DOF. All these make the motion control of the UWIP system be difficult to solve. So far, there are no research results about the motion planning of the system. This inspires the study in this paper. We solve this difficult problem in this study. First, the dynamic properties of the UWIP system are analyzed. Based on these properties, a method of constructing a motion trajectory for this mechanical system is developed. The trajectory starts from the straight-down equilibrium point and ends at the straight-up equilibrium point. After that, a tracking control law is designed to quickly track the constructed trajectory. This enables the stabilizing control of the UWIP between two equilibrium points to be achieved along a reference trajectory. Compared to a local stabilizing control method for the UWIP in [25], our presented strategy uses a single control law to achieve the stabilizing control of the UWIP in its whole motion space. Moreover, we can predict the movement process and transient characteristics of the UWIP in advance. It is very useful to guarantee the operation of the control system to be safe. The validity of the theoretical results is demonstrated by numerical simulation experiment.

## 2. Model of Underactuated Wheeled Inverted Pendulum

The model of the UWIP is shown in Figure 1, where  $m_1$ ,  $J_1$ ,  $L_1$ , and  $\theta_1(t)$  are the mass, the moment of inertia, the radius, and the rotational angle of the wheel, respectively;  $m_2$ ,  $J_2$ ,  $L_2$ , and  $\theta_2(t)$  are the mass, the moment of inertia, the distance from the endpoint to the center of mass, and the rotational angle of the pendulum, respectively;  $F(t)$  is the input torque applied on the wheel;  $g = 9.80665 \text{ m/s}^2$  is the gravitational acceleration.

It follows from the derivations in [25] that the kinetic and potential energy of the UWIP system is

$$\begin{aligned} K(\boldsymbol{\theta}, \dot{\boldsymbol{\theta}}) &= \frac{1}{2} \dot{\boldsymbol{\theta}}(t)^\top D(\theta_2) \dot{\boldsymbol{\theta}}(t), \\ P(\boldsymbol{\theta}) &= \alpha_4 \cos \theta_2(t), \end{aligned} \quad (1)$$

where  $\boldsymbol{\theta}(t) = [\theta_1(t), \theta_2(t)]^\top$ ,  $\dot{\boldsymbol{\theta}}(t) = d\boldsymbol{\theta}(t)/dt$ ,

$$\begin{aligned} D(\theta_2) &= \begin{bmatrix} \alpha_1 & \alpha_2 \cos \theta_2(t) \\ \alpha_2 \cos \theta_2(t) & \alpha_3 \end{bmatrix}, \\ \alpha_1 &= (m_1 + m_2) L_1^2 + J_1, \\ \alpha_2 &= m_2 L_1 L_2, \\ \alpha_3 &= m_2 L_2^2 + J_2, \\ \alpha_4 &= m_2 L_2 g. \end{aligned} \quad (2)$$

The Euler-Lagrange motion equations of the system are

$$\begin{aligned} \frac{d}{dt} \left[ \frac{\partial L(\boldsymbol{\theta}, \dot{\boldsymbol{\theta}})}{\partial \dot{\theta}_1} \right] - \frac{\partial L(\boldsymbol{\theta}, \dot{\boldsymbol{\theta}})}{\partial \theta_1} &= F(t), \\ \frac{d}{dt} \left[ \frac{\partial L(\boldsymbol{\theta}, \dot{\boldsymbol{\theta}})}{\partial \dot{\theta}_2} \right] - \frac{\partial L(\boldsymbol{\theta}, \dot{\boldsymbol{\theta}})}{\partial \theta_2} &= 0, \end{aligned} \quad (3)$$

where  $L(\boldsymbol{\theta}, \dot{\boldsymbol{\theta}}) = K(\boldsymbol{\theta}, \dot{\boldsymbol{\theta}}) - P(\boldsymbol{\theta})$  is the Lagrangian of the system. Equation (3) is equivalent to

$$D(\theta_2) \begin{bmatrix} \ddot{\theta}_1(t) \\ \ddot{\theta}_2(t) \end{bmatrix} + \begin{bmatrix} -\alpha_2 \dot{\theta}_2^2(t) \sin \theta_2(t) \\ -\alpha_4 \sin \theta_2(t) \end{bmatrix} = \begin{bmatrix} F(t) \\ 0 \end{bmatrix}. \quad (4)$$

The state variables of (4) are selected to be

$$\begin{aligned} x_1(t) &= \theta_1(t), \\ x_2(t) &= \theta_2(t), \\ x_3(t) &= \dot{\theta}_1(t), \\ x_4(t) &= \dot{\theta}_2(t). \end{aligned} \quad (5)$$

This gives the state-space form of (4) as

$$\begin{aligned} \dot{x}_1(t) &= x_3(t), \\ \dot{x}_2(t) &= x_4(t), \\ \begin{bmatrix} \dot{x}_3(t) \\ \dot{x}_4(t) \end{bmatrix} &= D^{-1}(x_2) \begin{bmatrix} \alpha_2 x_4^2(t) \sin x_2(t) + F(t) \\ \alpha_4 \sin x_2(t) \end{bmatrix}. \end{aligned} \quad (6)$$

## 3. Dynamic Properties of the UWIP System

The UWIP system (6) has the following dynamic properties.

**Theorem 1.** *If the control law for (6) is designed to be*

$$F(t) = -\mu x_3(t), \quad \mu > 0, \quad (7)$$

*then the closed-loop control system has two equilibrium points*

$$\begin{aligned} \mathbf{x}_U^* &= [x_1^*, 0, 0, 0]^\top, \\ \mathbf{x}_D^* &= [x_1^*, \pi, 0, 0]^\top, \end{aligned} \quad (8)$$

*where  $\mu$  and  $x_1^*$  are constants. Moreover,  $\mathbf{x}_D^*$  is a stable equilibrium point while  $\mathbf{x}_U^*$  is not.*

*Proof.* Substituting (7) into (6) yields the closed-loop control system

$$\begin{bmatrix} \dot{x}_1(t) \\ \dot{x}_2(t) \\ \dot{x}_3(t) \\ \dot{x}_4(t) \end{bmatrix} = \begin{bmatrix} x_3(t) \\ x_4(t) \\ D^{-1}(x_2) \begin{bmatrix} \alpha_2 x_4^2(t) \sin x_2(t) - \mu x_3(t) \\ \alpha_4 \sin x_2(t) \end{bmatrix} \end{bmatrix} \quad (9)$$

The equilibrium points of the system (9) satisfy

$$\begin{aligned} x_3(t) &= 0, \\ x_4(t) &= 0, \\ \begin{bmatrix} \alpha_2 x_4^2(t) \sin x_2(t) - \mu x_3(t) \\ \alpha_4 \sin x_2(t) \end{bmatrix} &= \begin{bmatrix} 0 \\ 0 \end{bmatrix}. \end{aligned} \quad (10)$$

It follows from (5) and (10) that  $x_3(t) = x_4(t) = 0$ ,  $x_1(t) = x_1^*$ , and  $\sin x_2(t) = 0$ . By considering the fact that  $x_2(t) = \theta_2(t)$  is a cyclic variable with a period  $2\pi$ , it is easy to get  $x_2(t) = 0$  or  $\pi$  from  $\sin x_2(t) = 0$ . So, the equilibrium points of the closed-loop control system are  $\mathbf{x}_U^*$  and  $\mathbf{x}_D^*$ .

In order to determine the stability of the equilibrium points  $\mathbf{x}_U^*$  and  $\mathbf{x}_D^*$ , we approximately linearize the nonlinear system (9) around them. It gives the following two approximate linearization matrices:

$$\begin{aligned} A_U^* &= \begin{bmatrix} 0 & 0 & 1 & 0 \\ 0 & 0 & 0 & 1 \\ 0 & -\frac{\alpha_2 \alpha_4}{\alpha_1 \alpha_3 - \alpha_2^2} & -\frac{\mu \alpha_3}{\alpha_1 \alpha_3 - \alpha_2^2} & 0 \\ 0 & \frac{\alpha_1 \alpha_4}{\alpha_1 \alpha_3 - \alpha_2^2} & \frac{\mu \alpha_2}{\alpha_1 \alpha_3 - \alpha_2^2} & 0 \end{bmatrix}, \\ A_D^* &= \begin{bmatrix} 0 & 0 & 1 & 0 \\ 0 & 0 & 0 & 1 \\ 0 & -\frac{\alpha_2 \alpha_4}{\alpha_1 \alpha_3 - \alpha_2^2} & -\frac{\mu \alpha_3}{\alpha_1 \alpha_3 - \alpha_2^2} & 0 \\ 0 & \frac{\alpha_1 \alpha_4}{\alpha_1 \alpha_3 - \alpha_2^2} & \frac{\mu \alpha_2}{\alpha_1 \alpha_3 - \alpha_2^2} & 0 \end{bmatrix}. \end{aligned} \quad (11)$$

Both  $A_U^*$  and  $A_D^*$  have the same form

$$A^* = \begin{bmatrix} 0 & 0 & 1 & 0 \\ 0 & 0 & 0 & 1 \\ 0 & A_{32} & A_{33} & 0 \\ 0 & A_{42} & A_{43} & 0 \end{bmatrix}, \quad (12)$$

where  $A_{ij}$  ( $i = 3, 4$ ,  $j = 2, 3$ ) are constants. The characteristic polynomial of the matrix  $A^*$  is

$$\begin{aligned} |sI_4 - A^*| \\ = s \left[ s^3 - A_{33}s^2 - A_{42}s + A_{42}A_{33} - A_{32}A_{43} \right], \end{aligned} \quad (13)$$

where  $s$  is a variable symbol and  $I_4$  is a  $4 \times 4$  identity matrix. By using Routh-Hurwitz stability criterion [26], it is not difficult to obtain the stability conditions for  $A^*$  as

$$\begin{aligned} A_{33} &< 0, \\ A_{32}A_{43} &> 0, \\ A_{42}A_{33} - A_{32}A_{43} &> 0. \end{aligned} \quad (14)$$

Since  $\alpha_i > 0$  ( $i = 1, 2, 3, 4$ ) and  $\alpha_1 \alpha_3 - \alpha_2^2 > 0$ , a simple verification gives that  $A_D^*$  satisfies (14) and  $A_U^*$  does not. So, the equilibrium point  $\mathbf{x}_D^*$  is stable and  $\mathbf{x}_U^*$  is unstable. The proof is completed.  $\square$

**Theorem 2.** *The closed-loop control system (6) and (7) asymptotically converges to the equilibrium point  $\mathbf{x}_D^*$  if the initial condition  $\mathbf{x}_0^*$  is different from  $\mathbf{x}_U^*$ .*

*Proof.* For the closed-loop control system (6) and (7), a Lyapunov function is designed to be

$$\begin{aligned} V(\mathbf{x}) &= \frac{1}{2} [x_3, x_4] \begin{bmatrix} \alpha_1 & \alpha_2 \cos x_2 \\ \alpha_2 \cos x_2 & \alpha_3 \end{bmatrix} \begin{bmatrix} x_3 \\ x_4 \end{bmatrix} \\ &+ \alpha_4 (1 + \cos x_2). \end{aligned} \quad (15)$$

Then, we get

$$\begin{aligned} \frac{dV(\mathbf{x})}{dt} &= [x_3, x_4] \begin{bmatrix} \alpha_1 & \alpha_2 \cos x_2 \\ \alpha_2 \cos x_2 & \alpha_3 \end{bmatrix} \begin{bmatrix} \dot{x}_3 \\ \dot{x}_4 \end{bmatrix} \\ &+ \frac{1}{2} [x_3, x_4] \begin{bmatrix} 0 & -\alpha_2 x_4 \sin x_2 \\ -\alpha_2 x_4 \sin x_2 & 0 \end{bmatrix} \begin{bmatrix} x_3 \\ x_4 \end{bmatrix} \\ &- \alpha_4 x_4 \sin x_2 \\ &= [x_3, x_4] \begin{bmatrix} \alpha_2 x_4^2 \sin x_2 - \mu x_3 \\ \alpha_4 \sin x_2 \end{bmatrix} \\ &- (\alpha_2 x_3 x_4 + \alpha_4) x_4 \sin x_2 = -\mu x_3^2(t) \leq 0. \end{aligned} \quad (16)$$

Letting  $\dot{V}(\mathbf{x}) = 0$  gives  $x_3(t) = 0$ . Combining  $x_3(t) = 0$  and the third equation of (4) yields

$$(\alpha_3 x_4^2(t) - \alpha_4 \cos x_2(t)) \sin x_2(t) = 0. \quad (17)$$

In addition,  $\dot{V}(\mathbf{x}) = 0$  means that  $V(\mathbf{x}) = C$  is a constant. It follows from  $x_3(t) = 0$  and  $V(\mathbf{x}) = C$  that

$$\alpha_3 x_4^2(t) + \alpha_4 \cos x_2(t) = C - \alpha_4. \quad (18)$$

Note that (17) means

$$\alpha_3 x_4^2(t) - \alpha_4 \cos x_2(t) = 0 \quad (19)$$

or

$$\sin x_2(t) = 0. \quad (20)$$

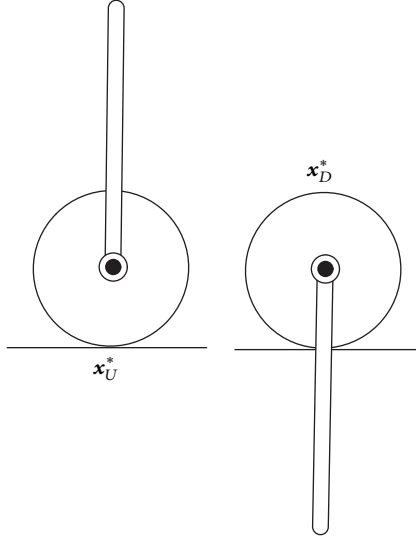


FIGURE 2: Physical models of  $\mathbf{x}_U^*$  and  $\mathbf{x}_D^*$ .

Combining (18) and (19) yields that  $x_2(t)$  is a constant. The second equation of (6) gives  $x_4(t) = 0$ . From (19), we get  $\cos x_2(t) = 0$ . Furthermore, it follows from  $x_3(t) = x_4(t) = 0$  and (6) that  $\sin x_2(t) = 0$ . It is in conflict with  $\cos x_2(t) = 0$ . So, (19) does not hold.

The above analysis results tell us that  $x_3(t) = x_4(t) = 0$  and  $\sin x_2(t) = 0$  from  $\dot{V}(\mathbf{x}) = 0$ . By using LaSalle's theorem [15], we know that the closed-loop control system (6) and (7) asymptotically converges to the largest invariant set in

$$\begin{aligned} \Omega &= \{\mathbf{x}(t) \mid x_3(t) = x_4(t) = 0, \sin x_2(t) = 0\} \\ &= \{\mathbf{x}_D^*, \mathbf{x}_U^*\}. \end{aligned} \quad (21)$$

Since  $\mathbf{x}_U^*$  is an unstable equilibrium point of the closed-loop system (6) and (7), the system asymptotically converges to  $\mathbf{x}_D^*$  when  $\mathbf{x}_0^* \neq \mathbf{x}_U^*$ . The proof is completed.  $\square$

*Remark 3.* The point  $\mathbf{x}_U^*$  means that the pendulum of the UWIP is stabilized at the straight-up position while the wheel does not spin. Similarly, the meaning of  $\mathbf{x}_D^*$  is that the pendulum is stabilized at the straight-down position while the wheel does not spin. The physical models of  $\mathbf{x}_U^*$  and  $\mathbf{x}_D^*$  are shown in Figure 2. Note that  $x_3(t) = \dot{\theta}_1(t)$  is the velocity variable of the wheel. So, the control law  $F(t)$  designed in (7) can be considered as a virtual friction torque for the UWIP system. Under the operation of this torque, the UWIP asymptotically converges to  $\mathbf{x}_D^*$  from any initial position  $\mathbf{x}_0^* \neq \mathbf{x}_U^*$ . This property will be used to design a trajectory for the UWIP in its whole motion space below.

#### 4. Design of Motion Trajectory

In this section, a motion trajectory of the UWIP between the equilibrium points  $\mathbf{x}_D^*$  and  $\mathbf{x}_U^*$  is designed. The design process of the trajectory has the following three steps.

*Step 1.* The initial condition of the closed-loop system (6) and (7) is selected to be

$$\mathbf{x}_0^* = [x_1^*, 0, \omega, 0]^\top, \quad (22)$$

where  $\omega > 0$  is a very small constant. The physical meaning for (22) is that the UWIP starts to move from the position  $\mathbf{x}_U^*$  with a small velocity in the wheel. Since  $\mathbf{x}_0^* \neq \mathbf{x}_U^*$ , it follows from the Theorem 2 that the UWIP asymptotically converges to the equilibrium point  $\mathbf{x}_D^*$ . This motion trajectory and its accompanied control input are denoted to be

$$\begin{aligned} \mathbf{x}_D(t) &= [x_{D1}(t), x_{D2}(t), x_{D3}(t), x_{D4}(t)]^\top, \\ F_D(t) &= -\mu x_{D3}(t), \quad t \in [0, T], \end{aligned} \quad (23)$$

where  $T$  is the stabilization time that is defined to be

$$\|\mathbf{x}_D(t) - \mathbf{x}_D^*\|_2 \leq 0.05, \quad t \geq T. \quad (24)$$

Equation (24) means that  $\mathbf{x}_D(t) = \mathbf{x}_D^*$  approximately holds when  $t \geq T$ .

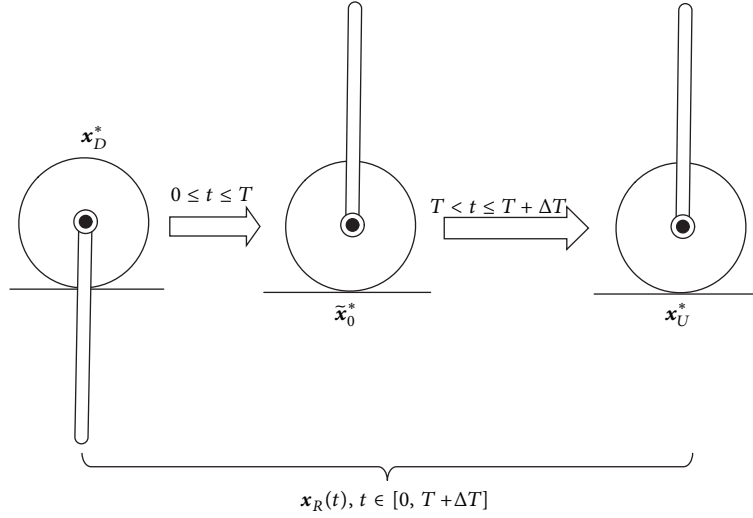
*Step 2.* Based on  $\mathbf{x}_D(t)$  and  $F_D(t)$ , we construct

$$\begin{aligned} \mathbf{x}_U(t) &= [x_{U1}(t), x_{U2}(t), x_{U3}(t), x_{U4}(t)]^\top, \\ x_{U1}(t) &= x_{D1}(T-t), \\ x_{U2}(t) &= x_{D2}(T-t), \\ x_{U3}(t) &= -x_{D3}(T-t), \\ x_{U4}(t) &= -x_{D4}(T-t), \\ F_U(t) &= F_D(T-t), \quad t \in [0, T]. \end{aligned} \quad (25)$$

Note that  $x_{D1}(t)$  and  $x_{D2}(t)$  are the position variables, and  $x_{D3}(t)$  and  $x_{D4}(t)$  are the velocity variables of the UWIP system. Thus,  $\mathbf{x}_U(t)$  is a reverse trajectory of  $\mathbf{x}_D(t)$  during  $t \in [0, T]$ . And the initial and final positions of  $\mathbf{x}_U(t)$  are

$$\begin{aligned} \mathbf{x}_U(0) &= [x_{D1}(T), x_{D2}(T), -x_{D3}(T), -x_{D4}(T)]^\top \\ &\approx \mathbf{x}_D^*, \end{aligned} \quad (26)$$

$$\begin{aligned} \mathbf{x}_U(T) &= [x_{D1}(0), x_{D2}(0), -x_{D3}(0), -x_{D4}(0)]^\top \\ &= [x_1^*, 0, -\omega, 0]^\top \triangleq \tilde{\mathbf{x}}_0^*. \end{aligned}$$


 FIGURE 3: The diagram of the trajectory  $\mathbf{x}_R(t)$ .

Let  $v = T - t$ . Since  $\mathbf{x}_D(t)$  and  $F_D(t)$  satisfy (6), we get

$$\begin{aligned} \frac{dx_{U1}(t)}{dt} &= \frac{dx_{U1}(t)}{dv} \frac{dv}{dt} = -\frac{dx_{D1}(v)}{dv} = -x_{D3}(v) \\ &= x_{U3}(t), \end{aligned}$$

$$\begin{aligned} \frac{dx_{U2}(t)}{dt} &= \frac{dx_{U2}(t)}{dv} \frac{dv}{dt} = -\frac{dx_{D2}(v)}{dv} = -x_{D4}(v) \\ &= x_{U4}(t), \end{aligned}$$

$$\begin{aligned} \begin{bmatrix} \frac{dx_{U3}(t)}{dt} \\ \frac{dx_{U4}(t)}{dt} \end{bmatrix} &= \begin{bmatrix} \frac{dx_{U3}(t)}{dv} \frac{dv}{dt} \\ \frac{dx_{U4}(t)}{dv} \frac{dv}{dt} \end{bmatrix} = \begin{bmatrix} \frac{dx_{D3}(v)}{dv} \\ \frac{dx_{D4}(v)}{dv} \end{bmatrix} \\ &= D^{-1}(x_{D2}(v)) \begin{bmatrix} \alpha_2 x_{D4}^2(v) \sin x_{D2}(v) + F_D(v) \\ \alpha_4 \sin x_{D2}(v) \end{bmatrix} \\ &= D^{-1}(x_{U2}(t)) \begin{bmatrix} \alpha_2 x_{U4}^2(t) \sin x_{U2}(t) + F_U(t) \\ \alpha_4 \sin x_{U2}(t) \end{bmatrix}. \end{aligned} \quad (27)$$

This means that  $\mathbf{x}_U(t)$  and  $F_U(t)$  satisfy (6).

*Step 3.* Since the constant  $\omega$  is very small,  $\tilde{\mathbf{x}}_0^*$  is very close to the equilibrium point  $\mathbf{x}_U^*$ . It enables us to introduce a time period  $\Delta T$  and to define

$$\begin{aligned} \mathbf{x}_R(t) &= [x_{R1}(t), x_{R2}(t), x_{R3}(t), x_{R4}(t)]^T, \\ \mathbf{x}_R(t) &= \begin{cases} \mathbf{x}_U(t), & t \in [0, T], \\ \mathbf{x}_U^*, & t \in (T, T + \Delta T], \end{cases} \\ F_R(t) &= \begin{cases} F_U(t), & t \in [0, T], \\ 0, & t \in (T, T + \Delta T]. \end{cases} \end{aligned} \quad (28)$$

The diagram of the trajectory  $\mathbf{x}_R(t)$  is shown in Figure 3. Note that  $\mathbf{x}_R(t)$  is a motion trajectory of the UWIP between the equilibrium points  $\mathbf{x}_D^*$  and  $\mathbf{x}_U^*$ . By comparing  $\mathbf{x}_U(T)$  to  $\mathbf{x}_U^*$ , we find that the element  $x_{R3}(t)$  in  $\mathbf{x}_R(t)$  suffers from a very small step change at  $t = T$ . Furthermore, it is not difficult to verify that  $\mathbf{x}_R(t)$  and  $F_R(t)$  also satisfy (6) because  $\mathbf{x}_U(t)$  and  $F_U(t)$  satisfy (6).

## 5. Design of Tracking Control Law

The design of tracking control law for the trajectory  $\mathbf{x}_R(t)$  is concerned in this section. Denote the error variables to be

$$\begin{aligned} \mathbf{e}(t) &= [e_1(t), e_2(t), e_3(t), e_4(t)]^T, \\ e_1(t) &= x_1(t) - x_{R1}(t), \\ e_2(t) &= x_2(t) - x_{R2}(t), \\ e_3(t) &= x_3(t) - x_{R3}(t), \\ e_4(t) &= x_4(t) - x_{R4}(t), \\ \tau(t) &= F(t) - F_R(t). \end{aligned} \quad (29)$$

From (6), we get the nonlinear error dynamic equations as

$$\begin{bmatrix} \dot{e}_1(t) \\ \dot{e}_2(t) \\ \dot{e}_3(t) \\ \dot{e}_4(t) \end{bmatrix} = \begin{bmatrix} e_3(t) \\ e_4(t) \\ f_1(\mathbf{e}) \\ f_2(\mathbf{e}) \end{bmatrix} + \begin{bmatrix} 0 \\ 0 \\ g_1(\mathbf{e}) \\ g_2(\mathbf{e}) \end{bmatrix} \tau(t), \quad (30)$$

where

$$\begin{aligned} \begin{bmatrix} f_1(\mathbf{e}) \\ f_2(\mathbf{e}) \end{bmatrix} &= \Phi^{-1}(e_2)(\phi_1(e_2) + \phi_2(\mathbf{e})), \\ \begin{bmatrix} g_1(\mathbf{e}) \\ g_2(\mathbf{e}) \end{bmatrix} &= \Phi^{-1}(e_2) \begin{bmatrix} 1 \\ 0 \end{bmatrix}, \\ \phi_1(e_2) &= \begin{bmatrix} -\alpha_2 \dot{x}_{R4} (\cos(e_2 + x_{R2}) - \cos x_{R2}) \\ -\alpha_2 \dot{x}_{R3} (\cos(e_2 + x_{R2}) - \cos x_{R2}) \end{bmatrix}, \end{aligned} \quad (31)$$

$$\begin{aligned} \phi_2(\mathbf{e}) &= \begin{bmatrix} \alpha_2 ((e_4 + x_{R4})^2 \sin(e_2 + x_{R2}) - x_{R4}^2 \sin x_{R2}) \\ \alpha_4 (\sin(e_2 + x_{R2}) - \sin x_{R2}) \end{bmatrix}, \\ \Phi(e_2) &= \begin{bmatrix} \alpha_1 & \alpha_2 \cos(e_2 + x_{R2}) \\ \alpha_2 \cos(e_2 + x_{R2}) & \alpha_3 \end{bmatrix}. \end{aligned}$$

In order to make the UWIP track the trajectory  $\mathbf{x}_R(t)$ , we need to design a stabilizing control law  $\tau(t)$  for (30) such that  $\mathbf{e}(t)$  converges to the origin quickly.

Note that (30) is a complex nonlinear control system for  $\mathbf{e}(t)$ . An approximate linearization method is used to design the stabilizing control law here. Linearizing (30) around  $\mathbf{e}(t) = 0$  gives the following linear approximation model:

$$\dot{\mathbf{e}}(t) = A(t)\mathbf{e}(t) + B(t)\tau(t), \quad (32)$$

where

$$\begin{aligned} A(t) &= \begin{bmatrix} 0 & 0 & 1 & 0 \\ 0 & 0 & 0 & 1 \\ 0 & \Psi_1(t) & \Psi_2(t) & 0 \\ 0 & \Psi_3(t) & \Psi_4(t) & 0 \end{bmatrix}, \\ B(t) &= \begin{bmatrix} 0 \\ 0 \\ \Psi_5(t) \\ \Psi_6(t) \end{bmatrix}, \\ \Psi_1(t) &= \frac{\alpha_2 \alpha_3 \phi_1(t) - \alpha_2 \cos x_{R2}(t) \phi_2(t)}{\alpha_1 \alpha_3 - \alpha_2^2 \cos^2 x_{R2}(t)}, \\ \Psi_2(t) &= \frac{2\alpha_2 \alpha_3 x_{R4}(t) \sin x_{R2}(t)}{\alpha_1 \alpha_3 - \alpha_2^2 \cos^2 x_{R2}(t)}, \\ \Psi_3(t) &= \frac{-\alpha_2^2 \cos x_{R2}(t) \phi_1(t) + \alpha_1 \phi_2(t)}{\alpha_1 \alpha_3 - \alpha_2^2 \cos^2 x_{R2}(t)}, \\ \Psi_4(t) &= -\frac{2\alpha_2^2 x_{R4}(t) \sin x_{R2}(t) \cos x_{R2}(t)}{\alpha_1 \alpha_3 - \alpha_2^2 \cos^2 x_{R2}(t)}, \end{aligned}$$

$$\begin{aligned} \Psi_5(t) &= \frac{\alpha_3}{\alpha_1 \alpha_3 - \alpha_2^2 \cos^2 x_{R2}(t)}, \\ \Psi_6(t) &= -\frac{\alpha_2 \cos x_{R2}(t)}{\alpha_1 \alpha_3 - \alpha_2^2 \cos^2 x_{R2}(t)}, \\ \phi_1(t) &= \dot{x}_{R4}(t) \sin x_{R2}(t) + x_{R4}^2(t) \cos x_{R2}(t), \\ \phi_2(t) &= \alpha_2 \dot{x}_{R3}(t) \sin x_{R2}(t) + \alpha_4 \cos x_{R2}(t). \end{aligned} \quad (33)$$

Assume that  $(A(t), B(t))$  is controllable. So, the time-variant Riccati matrix equation

$$\begin{aligned} \dot{P}(t) + A^T(t)P(t) + P(t)A(t) \\ - P(t)B(t)R^{-1}B^T(t)P(t) + Q = 0 \end{aligned} \quad (34)$$

has a positive definite solution  $P(t)$ , where  $Q \in \mathbb{R}^{4 \times 4}$  is a positive definite matrix and  $R$  is a positive constant. Based on the quadratic optimal control theory, the control law

$$\tau(t) = -R^{-1}B^T(t)P(t) \quad (35)$$

stabilizes the error dynamic equation (32) at the origin quickly. As a result, the control law  $F(t) = \tau(t) + F_R(t)$  enables the UWIP quickly to track the trajectory  $\mathbf{x}_R(t)$ . This guarantees the control objective of swing the UWIP up from  $\mathbf{x}_D^*$  and stabilizing it at  $\mathbf{x}_U^*$  to be achieved.

## 6. Numerical Example

This section presents a numerical example to verify the validity of the above theoretical analysis results.

The physical parameters of the UWIP in [25] were chosen for simulations

$$\begin{aligned} m_1 &= 1 \text{ kg}, \\ m_2 &= 2 \text{ kg}, \\ L_1 &= 0.1 \text{ m}, \\ L_2 &= 0.2 \text{ m}, \\ J_1 &= 0.01 \text{ kg} \cdot \text{m}^2, \\ J_2 &= 0.0267 \text{ kg} \cdot \text{m}^2. \end{aligned} \quad (36)$$

And the parameters in (7) and (22) were selected to be

$$\begin{aligned} \mu &= 0.25, \\ \mathbf{x}_1^* &= 0, \\ \omega &= 0.001. \end{aligned} \quad (37)$$

The sampling period for simulations was chosen to be 0.001 s. From the design process in Step 1 of Section 4, we got the trajectory  $\mathbf{x}_D(t)$  (see Figure 4). The simulation result shows that the UWIP starts to move from the position  $\mathbf{x}_0^*$  in (22) and is stabilized at the position  $\mathbf{x}_D^*$  in (8). The stabilizing

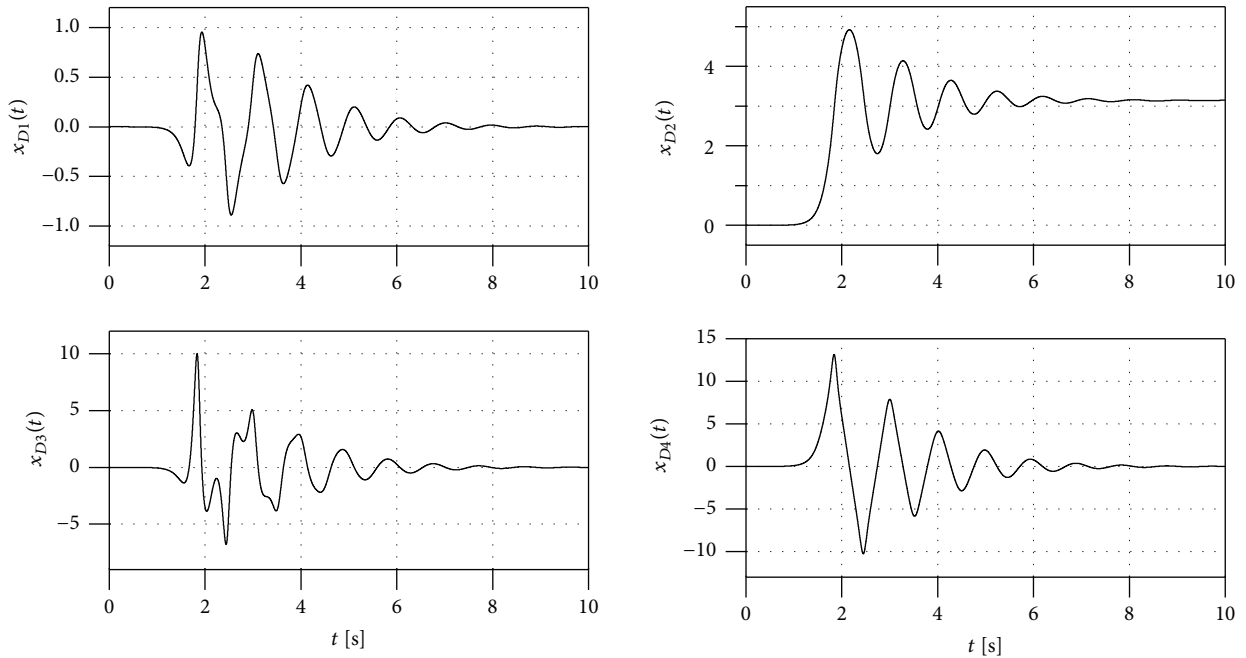


FIGURE 4: Simulation result of the trajectory  $\mathbf{x}_D(t)$ .

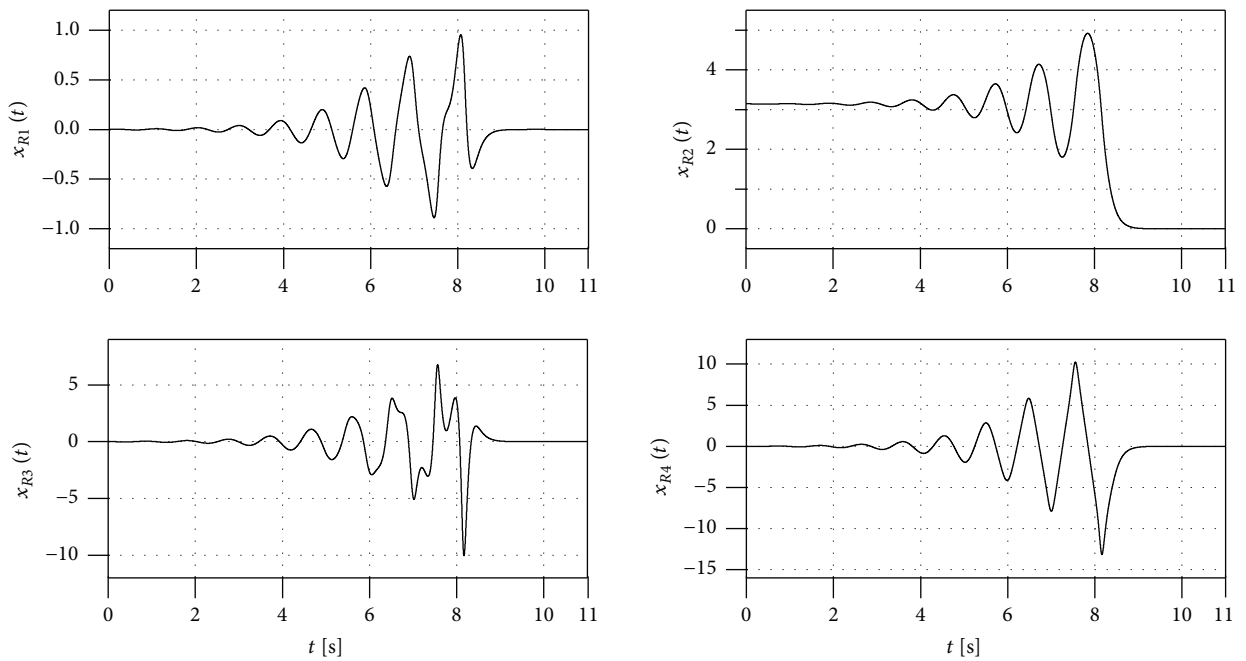


FIGURE 5: Time response of the trajectory  $\mathbf{x}_R(t)$ .

motion process of the UWIP is smooth. And the stabilization time is  $T = 10$  s. This demonstrates the effectiveness of the Theorem 2.

The time period  $\Delta T$  in (28) was taken to be 1 s. From the design process in Steps 2 and 3 of Section 4, the trajectory  $\mathbf{x}_R(t)$  was obtained in Figure 5 based on  $\mathbf{x}_D(t)$ , (25), and (28). The simulation results in Figure 5 show that  $\mathbf{x}_R(t)$  is a motion trajectory of the UWIP from  $\mathbf{x}_D^*$  to  $\mathbf{x}_U^*$ . To design a control law

of tracking this trajectory, the parameters in (34) were chosen to be  $Q = 0.5I_4$  and  $R = 5$ . And the MATLAB function *LQR* was used to solve (34). The tracking control results for the desired trajectory  $\mathbf{x}_R(t)$  are shown in Figure 6. Note that the UWIP quickly and exactly tracks the  $\mathbf{x}_R(t)$  by the operation of our designed tracking control law. As a result, the stabilizing control of the UWIP from  $\mathbf{x}_D^*$  to  $\mathbf{x}_U^*$  is achieved along the trajectory  $\mathbf{x}_R(t)$ .

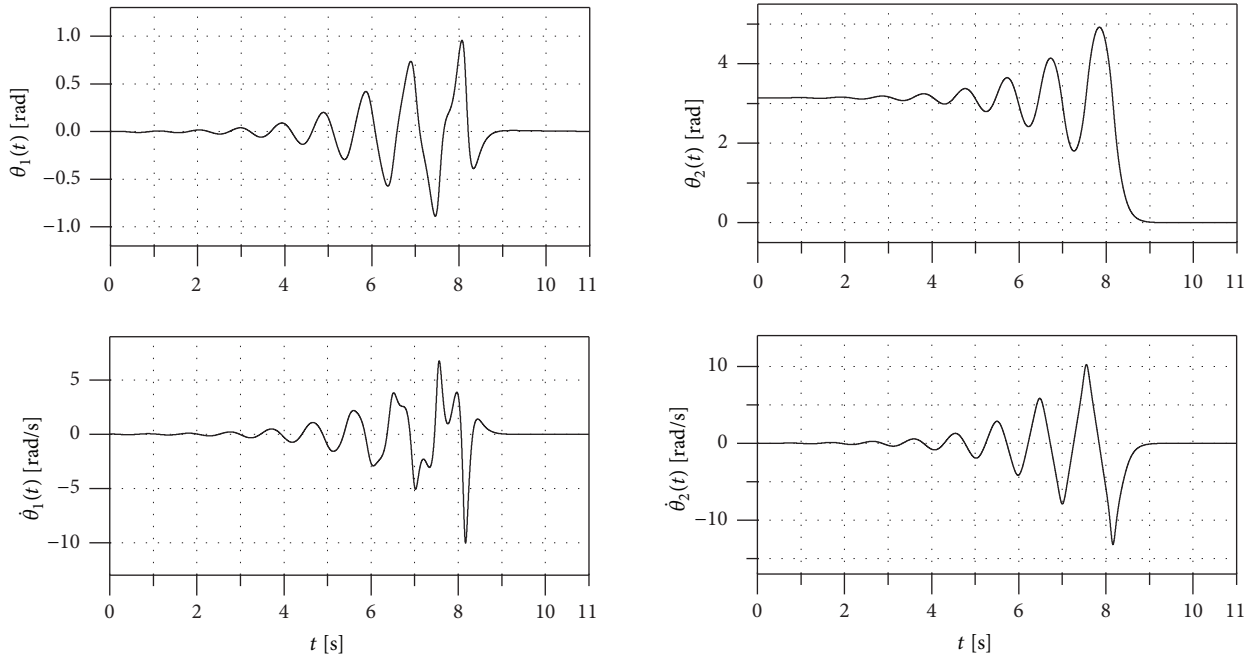


FIGURE 6: Tracking control of the UWIP for the trajectory  $\mathbf{x}_R(t)$ .

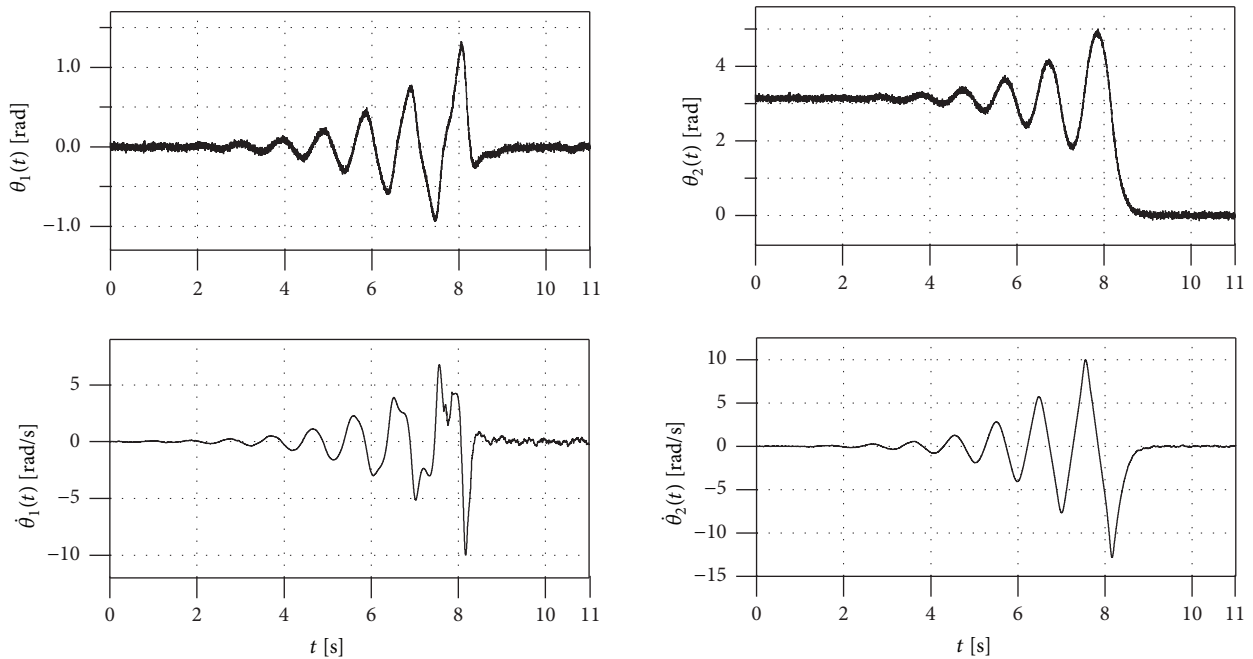


FIGURE 7: Simulation results of tracking  $\mathbf{x}_R(t)$  when considering parameter uncertainties, external disturbances, and input saturation.

In order to show the applicability of the presented strategy under realistic conditions, its robustness needs to be verified. To do that, we took the parameter  $J_1$  to be 5% smaller and  $J_2$  to be 5% larger than their nominal values, added white noise disturbances to the measured variable (peak value:  $\pm 0.1$ ), and set the saturation range of input to be  $[-3.5, 3]$ . Simulation results show that our developed method is still effective in that case (see Figure 7).

## 7. Conclusion

This paper addressed the trajectory design and tracking control problems for an underactuated wheeled inverted pendulum (UWIP). A new motion planning strategy was developed for this underactuated system. First, the dynamic properties of the UWIP system were analyzed. And then, the analysis properties were used to construct a trajectory of the

UWIP between two equilibrium points. After that, a control law was designed to make the UWIP track the constructed trajectory. This ensured the motion control of the UWIP between two equilibrium points to be achieved. Finally, numerical simulation results demonstrated the validity of our theoretical results. In the future, we will further explore how to extend the main idea of our presented method to the control of other nonlinear systems.

## Data Availability

The simulation data used to support the findings of this study are available from the corresponding author upon request.

## Conflicts of Interest

The authors declare that there are no conflicts of interest regarding the publication of this article.

## Acknowledgments

This work was supported in part by National Natural Science Foundation of China under Grants nos. 61773193, 61703194, and 61873348, by the program of JSPS (Japan Society for the Promotion of Science) International Research Fellows under Grant no. 17F17791, and by the project of Young Teacher Growth Program of Shandong Province.

## References

- [1] X. Hao, L. Liu, and Y. Wu, "Existence and multiplicity results for nonlinear periodic boundary value problems," *Nonlinear Analysis: Theory, Methods & Applications*, vol. 72, no. 9-10, pp. 3635–3642, 2010.
- [2] Y. Han, X. Zhang, L. Liu, and Y. Wu, "Multiple Positive Solutions of Singular Nonlinear Sturm-Liouville Problems with Carathéodory Perturbed Term," *Journal of Applied Mathematics*, vol. 2012, Article ID 160891, 23 pages, 2012.
- [3] X. Hao, L. Liu, and Y. Wu, "Positive solutions for nonlinear fractional semipositone differential equation with nonlocal boundary conditions," *Journal of Nonlinear Sciences and Applications. JNSA*, vol. 9, no. 6, pp. 3992–4002, 2016.
- [4] B. Zhu, L. Liu, and Y. Wu, "Local and global existence of mild solutions for a class of nonlinear fractional reaction-diffusion equations with delay," *Applied Mathematics Letters*, vol. 61, pp. 73–79, 2016.
- [5] W. Qi, J. H. Park, J. Cheng, Y. Kao, and X. Gao, "Anti-windup design for stochastic Markovian switching systems with mode-dependent time-varying delays and saturation nonlinearity," *Nonlinear Analysis: Hybrid Systems*, vol. 26, pp. 201–211, 2017.
- [6] L. Liu, H. Li, C. Liu, and Y. Wu, "Existence and uniqueness of positive solutions for singular fractional differential systems with coupled integral boundary conditions," *The Journal of Nonlinear Science and its Applications*, vol. 10, no. 1, pp. 243–262, 2017.
- [7] Y. Sun, L. Liu, and Y. Wu, "The existence and uniqueness of positive monotone solutions for a class of nonlinear Schrödinger equations on infinite domains," *Journal of Computational and Applied Mathematics*, vol. 321, pp. 478–486, 2017.
- [8] W. Qi, G. Zong, and H. R. Karim, "Observer-Based Adaptive SMC for Nonlinear Uncertain Singular Semi-Markov Jump Systems With Applications to DC Motor," *IEEE Transactions on Circuits and Systems I: Regular Papers*, vol. 65, no. 9, pp. 2951–2960, 2018.
- [9] A. Zhang, X. Lai, M. Wu, and J. She, "Stabilization of underactuated two-link gymnast robot by using trajectory tracking strategy," *Applied Mathematics and Computation*, vol. 253, pp. 193–204, 2015.
- [10] W. Dong and Y. Guo, "Global time-varying stabilization of underactuated surface vessel," *IEEE Transactions on Automatic Control*, vol. 50, no. 6, pp. 859–864, 2005.
- [11] X. Wang, J. Liu, and K. Cai, "Tracking control for a velocity-sensorless VTOL aircraft with delayed outputs," *Automatica*, vol. 45, no. 12, pp. 2876–2882, 2009.
- [12] N. Sun and Y. Fang, "Nonlinear tracking control of underactuated cranes with load transferring and lowering: theory and experimentation," *Automatica*, vol. 50, no. 9, pp. 2350–2357, 2014.
- [13] D. A. Mercado Ravell, M. M. Maia, and F. J. Diez, "Modeling and control of unmanned aerial/underwater vehicles using hybrid control," *Control Engineering Practice*, vol. 76, pp. 112–122, 2018.
- [14] I. Meza, L. Aguilar, A. Shiriaev, L. Freidovich, and Y. Orlov, "Periodic motion planning and nonlinear  $H_\infty$  tracking control of a 3-DOF underactuated helicopter," *International Journal of Systems Science*, vol. 42, no. 5, pp. 829–838, 2011.
- [15] H. Khalil, *Nonlinear Systems*, Prentice-Hall, New Jersey, NJ, USA, 3rd edition, 2002.
- [16] G. Oriolo and Y. Nakamura, "Control of mechanical systems with second-order nonholonomic constraints: Underactuated manipulators," in *Proceedings of the 30th IEEE Conference on Decision and Control (Part 1 of 3)*, pp. 2398–2403, December 1991.
- [17] X. Xin and M. Kaneda, "Analysis of the energy-based swing-up control of the Acrobot," *International Journal of Robust and Nonlinear Control*, vol. 17, no. 16, pp. 1503–1524, 2007.
- [18] M. Ramírez-Neria, H. Sira-Ramírez, R. Garrido-Moctezuma, and A. Luviano-Juárez, "Linear active disturbance rejection control of underactuated systems: the case of the Furuta pendulum," *ISA Transactions*, vol. 53, no. 4, pp. 920–928, 2014.
- [19] M. K. Choudhary and G. Naresh Kumar, "ESO based LQR controller for ball and beam system," *IFAC-PapersOnLine*, vol. 49, no. 1, pp. 607–610, 2016.
- [20] F. Celani, "Output regulation for the TORA benchmark via rotational position feedback," *Automatica*, vol. 47, no. 3, pp. 584–590, 2011.
- [21] J. She, A. Zhang, X. Lai, and M. Wu, "Global stabilization of 2-DOF underactuated mechanical systems—an equivlent-input-disturbance approach," *Nonlinear Dynamics*, vol. 69, no. 1-2, pp. 495–509, 2012.
- [22] X. Lai, J. She, S. X. Yang, and M. Wu, "Comprehensive unified control strategy for underactuated two-link manipulators," *IEEE Transactions on Systems, Man, and Cybernetics, Part B: Cybernetics*, vol. 39, no. 2, pp. 389–398, 2009.
- [23] X. Xin and Y. Liu, "Reduced-order stable controllers for two-link underactuated planar robots," *Automatica*, vol. 49, no. 7, pp. 2176–2183, 2013.
- [24] J. G. Romero, A. Donaire, R. Ortega, and P. Borja, "Global Stabilisation of Underactuated Mechanical Systems via PID Passivity-Based Control," *IFAC-PapersOnLine*, vol. 50, no. 1, pp. 9577–9582, 2017.

- [25] Y. Ge, A. Zhang, J. Huo, S. Duan, L. Wang, and J. Kang, "Modeling and stabilizing control of wheeled acrobatic robot," *Application in Automation*, vol. 2017, no. 3, pp. 101–103, 2017.
- [26] J. Huang, *Automatic Control Principles and Applications*, Higher education press, Beijing, China, 2nd edition, 2009.

## Research Article

# A Nonhomogeneous Multivariable Grey Prediction NMGM Modeling Mechanism and Its Application

Haixia Wang <sup>1</sup> and Lingdi Zhao <sup>1,2</sup>

<sup>1</sup>School of Economics, Ocean University of China, Qingdao, Shandong 266100, China

<sup>2</sup>Marine Development Studies Institute of OUC, Key Research Institute in Universities, Qingdao, Shandong 266100, China

Correspondence should be addressed to Lingdi Zhao; [lingdizhao512@163.com](mailto:lingdizhao512@163.com)

Received 18 July 2018; Accepted 4 September 2018; Published 24 September 2018

Guest Editor: Weihai Zhang

Copyright © 2018 Haixia Wang and Lingdi Zhao. This is an open access article distributed under the Creative Commons Attribution License, which permits unrestricted use, distribution, and reproduction in any medium, provided the original work is properly cited.

The purpose of this paper is to explore modeling mechanism of a nonhomogeneous multivariable grey prediction NMGM(1,  $m$ ,  $k^\alpha$ ) model and its application. Although multi-variable grey prediction MGM(1,  $m$ ) model has been employed in many fields, its prediction results are not always satisfactory. Traditional MGM(1,  $m$ ) model is constructed on the hypothesis that original data sequences are in accord with homogeneous index trend; however, the nonhomogeneous index data sequences are the most common data existing in all systems, and how to handle multivariable nonhomogeneous index data sequences is an urgent problem. This paper proposes a novel nonhomogeneous multivariable grey prediction model termed NMGM(1,  $m$ ,  $k^\alpha$ ) to deal with those data sequences that are not in accord with homogeneous index trend. Based on grey prediction theory, by least square method and solutions of differential equations, the modeling mechanism and time response function of the proposed model are expounded. A case study demonstrates that the novel model provides preferable prediction performance compared with traditional MGM(1,  $m$ ) model. This work is an extension of the multivariable grey prediction model and enriches the study of grey prediction theory.

## 1. Introduction

Grey system theory (GST), with the superiority of dealing with uncertain problems that have partially unknown parameters, has been developed greatly since it was applied to system theory [1]. Traditional system analysis theory such as the qualitative theory of dynamic systems [2–18] is built on the assumption of acknowledging the system structure. However, with the rapid development of science and technology, it is impossible to completely master system structure as the system is becoming more complex and uncertain. Grey system theory has been adopted to various aspects of fields including systems analysis, forecasting, and decision-making due to its advantages in tackling semicomplex uncertainty problems.

Forecasting a future development is always of significant importance in energy [19], science and technology [20], and some other fields. A large number of studies on forecasting models and applications have been reported, such as garch-types models needing plenty of data, and sample size would limit the predictive accuracy of those methods

[21]. Nevertheless, searching enough effective data is almost impossible either in physical system or in generalized system. Grey prediction models show excellent ability in dealing with small data problems since they were proposed by Professor Deng [22].

Grey forecasting models can be divided into two categories according to the number of variables, single-variable grey forecasting models where GM(1, 1) is the core [23–26] and multivariable grey forecasting models, represented by GM(1,  $n$ ) [27–29] and MGM(1,  $m$ ) [30]. Zeng et al. [27] pointed out that there were some structure deficiencies in GM(1,  $n$ ), which may lead to greater errors. The MGM(1,  $m$ ) model can reflect mutual relationship among systematic variables and performed better prediction accuracy compared with single variable prediction models. Compared to signal grey prediction models, multivariable grey prediction model MGM(1,  $m$ ) is a distinct grey model being adequate for considering the mutual interactions of multiple variables in a system, and it is of vital importance in simulating and forecasting the multivariable data sequences.

The nonhomogeneous index data sequences are the most common data existing in all systems, Cui et al. [31] put forward a novel NGM(1, 1,  $k$ ) model in order to solve the nonhomogeneous index function and established the foundation of our study. This grey model (NGM) is a novel tool to tackle the nonhomogeneous data sequence, which attracted considerable interest of research [32]. How to handle multivariable nonhomogeneous data sequences is an urgent problem; this paper expounds a novel nonhomogeneous multivariable grey prediction model termed NMGM(1,  $m$ ,  $k^\alpha$ ) to tackle the multivariable nonhomogeneous index data sequences.

In recent years, great attention has been devoted to optimizing and expanding applications of MGM(1,  $m$ ) model [33–38]. Xiong et al. [33] provided background values to improve the original MGM model, which can be used to eliminate the random fluctuations and errors of the observational data. Guo et al. [37] constructed SMGM through coupling self-memory principle of dynamic system to MGM; the example showed that SMGM had superior predictive performance over other traditional grey prediction models. Karaaslan and Özden [38] analyzed Turkey's ratings credit by multivariable grey prediction model and expanded the application scope of multivariable grey prediction model. Those studies illustrated that multivariable grey prediction model is widely used in many fields.

Through analyzing the existing research on MGM(1,  $m$ ) model, we find that most of scholars optimized the model from the view of modeling parameters to better fit data sequences with index law rather than optimizing the model from modeling structure of MGM(1,  $m$ ) model. Traditional MGM(1,  $m$ ) model was constructed on the hypothesis that data sequences are suitable for grey exponential law resulted from accumulated generation operation. The simulated original data sequences are usually in the form of

$$\widehat{X}^{(0)}(k) = e^{Bk} A, \quad k \geq 2. \quad (1)$$

However, in multivariable system analysis, there are only a few data with characteristic of this hypothesis but more for other hypotheses that original data sequences are in accord with nonhomogeneous index trend. Therefore, it is necessary to propose a novel multivariable grey prediction model that is proper for data sequences that are not in accord with homogeneous index trend. This paper presents the novel model NMGM(1,  $m$ ,  $k^\alpha$ ) to handle the nonhomogeneous index data sequences in the form of

$$\widehat{X}^{(0)}(k) = e^{Bk} A + C, \quad k \geq 2. \quad (2)$$

By least square method and differential equations, we obtain parameters identification values and time response function of the novel model. The prediction accuracy is theoretically analyzed and a case study is presented to illustrate the effectiveness of the proposed model. The remainder of this paper is organized as follows. A novel nonhomogeneous multivariable grey prediction model and its modeling mechanism are presented in Section 2. The precision analysis and a case study are adopted to demonstrate the effectiveness and practicality of the novel model in Section 3. Our conclusions and future work are given in Section 4.

## 2. Grey NMGM(1, $m$ , $k^\alpha$ ) Model

Multivariable grey prediction model is one of the frequently used grey forecasting models. In this section, we present the modeling mechanism and time response function of the novel model NMGM(1,  $m$ ,  $k^\alpha$ ). The constructing process of NMGM(1,  $m$ ,  $k^\alpha$ ) is presented below.

*Definition 1.* Assume that  $X^{(0)} = (X_1^{(0)}, X_2^{(0)}, \dots, X_m^{(0)})^T$  is a nonnegative original data matrix and the original nonnegative data vector  $X_j^{(0)}$  is

$$X_j^{(0)} = (x_j^{(0)}(1), x_j^{(0)}(2), \dots, x_j^{(0)}(n)), \quad j = 1, 2, \dots, m. \quad (3)$$

The data matrix  $X^{(1)} = (X_1^{(1)}, X_2^{(1)}, \dots, X_m^{(1)})^T$  is called the first-order accumulated generation vector, where

$$X_j^{(1)} = (x_j^{(1)}(1), x_j^{(1)}(2), \dots, x_j^{(1)}(n)), \quad j = 1, 2, \dots, m \quad (4)$$

and

$$x_j^{(1)}(k) = \sum_{i=1}^k x_j^{(0)}(i), \quad k = 1, 2, \dots, n. \quad (5)$$

The adjacent neighbour average sequence is  $Z^{(1)} = (Z_1^{(1)}, Z_2^{(1)}, \dots, Z_m^{(1)})^T$  and

$$Z_j^{(1)} = (z_j^{(1)}(1), z_j^{(1)}(2), \dots, z_j^{(1)}(n)), \quad j = 1, 2, \dots, m, \quad (6)$$

where

$$z_j^{(1)}(k) = 0.5 (x_j^{(1)}(k) + x_j^{(1)}(k-1)), \quad k = 2, 3, \dots, n. \quad (7)$$

The original form of nonhomogeneous multivariable grey prediction model abbreviated NMGM(1,  $m$ ,  $k^\alpha$ ) is defined as follows:

$$\begin{aligned} \frac{dx_1^{(1)}(t)}{dt} &= a_{11}x_1^{(1)}(t) + a_{12}x_2^{(1)}(t) + \dots + a_{1m}x_m^{(1)}(t) \\ &\quad + b_1t^\alpha, \\ \frac{dx_2^{(1)}(t)}{dt} &= a_{21}x_1^{(1)}(t) + a_{22}x_2^{(1)}(t) + \dots + a_{2m}x_m^{(1)}(t) \\ &\quad + b_2t^\alpha, \\ &\quad \vdots \\ \frac{dx_m^{(1)}(t)}{dt} &= a_{m1}x_1^{(1)}(t) + a_{m2}x_2^{(1)}(t) + \dots + a_{mm}x_m^{(1)}(t) \\ &\quad + b_mt^\alpha, \end{aligned} \quad (8)$$

where  $\alpha \geq 0$ . We denote the notation

$$A = \begin{pmatrix} a_{11} & a_{12} & \cdots & a_{1m} \\ a_{21} & a_{22} & \cdots & a_{2m} \\ \vdots & \vdots & \ddots & \vdots \\ a_{m1} & a_{m2} & \cdots & a_{mm} \end{pmatrix} \text{ and} \quad (9)$$

$$B = \begin{pmatrix} b_1 \\ \vdots \\ b_m \end{pmatrix}.$$

For the convenience of the reader, (8) can be written in matrix, which is

$$\frac{dX^{(1)}(t)}{dt} = AX^{(1)}(t) + Bt^\alpha. \quad (10)$$

*Definition 2.* Assume that  $X^{(0)}$  is nonnegative original data matrix,  $X^{(1)}$  is the first-order accumulated generation sequences, and  $Z^{(1)}$  is adjacent neighbour average sequences. The differential equation

$$\frac{dX^{(1)}(t)}{dt} = AZ^{(1)}(t) + Bt^\alpha \quad (11)$$

is said to be basic form of nonhomogeneous multivariable grey prediction model abbreviated as NMGM(1,  $m, k^\alpha$ ). The differential equation

$$\frac{dX^{(1)}(t)}{dt} = AX^{(1)}(t) + Bt^\alpha \quad (12)$$

is said to be whitening differential equation of grey NMGM(1,  $m, k^\alpha$ ) model. The discrete form of NMGM(1,  $m, k^\alpha$ ) model is

$$x_j^{(0)}(k) = \sum_{l=1}^m a_{jl} z_l^{(1)}(k) + b_j k^\alpha, \quad (13)$$

$$j = 1, 2, \dots, m, \quad k = 1, 2, \dots, n.$$

The novel model NMGM(1,  $m, k^\alpha$ ) contains a nonlinear correction term  $Bk^\alpha$ , and  $Bk^\alpha$  is said to be time term of the model. The restored values of original data sequences can be adjusted through their coefficients  $Bk^\alpha$ , which is more suitable for time series prediction. It is easy to see that MGM(1,  $m$ ) model is a special case of NMGM(1,  $m, k^\alpha$ ) model when  $\alpha = 0$ .

In the following, we illustrate the modeling mechanism of NMGM(1,  $m, k^\alpha$ ) model.

**Theorem 3.** Assume that  $X^{(0)}$  is nonnegative original data matrix,  $X^{(1)}$  is first-order accumulated generation sequences, and  $Z^{(1)}$  is adjacent neighbour average sequences. If  $a_j = (a_{j1}, \dots, a_{jm}, b_j)^T$ , then

$$(\hat{a}_1, \hat{a}_2, \dots, \hat{a}_m) = (P^T P)^{-1} P^T (Q_1, Q_2, \dots, Q_m), \quad (14)$$

where

$$P = \begin{pmatrix} z_1^{(1)}(2) & z_2^{(1)}(2) & \cdots & z_m^{(1)}(2) & 2^\alpha \\ z_1^{(1)}(3) & z_2^{(1)}(3) & \cdots & z_m^{(1)}(3) & 3^\alpha \\ \vdots & \vdots & \ddots & \vdots & \vdots \\ z_1^{(1)}(n) & z_2^{(1)}(n) & \cdots & z_m^{(1)}(n) & n^\alpha \end{pmatrix} \quad (15)$$

and

$$Q_j = (x_j^{(0)}(2), x_j^{(0)}(3), \dots, x_j^{(0)}(n))^T, \quad (16)$$

$$j = 1, 2, \dots, m.$$

*Proof.* Substituting all data values into the discrete form of the model, we obtain

$$x_1^{(0)}(k) = a_{11} z_1^{(1)}(k) + a_{12} z_2^{(1)}(k) + \cdots + a_{1m} z_m^{(1)}(k) + b_1 k^\alpha,$$

$$x_2^{(0)}(k) = a_{21} z_1^{(1)}(k) + a_{22} z_2^{(1)}(k) + \cdots + a_{2m} z_m^{(1)}(k) + b_2 k^\alpha, \quad (17)$$

$$\vdots$$

$$x_m^{(0)}(k) = a_{m1} z_1^{(1)}(k) + a_{m2} z_2^{(1)}(k) + \cdots + a_{mm} z_m^{(1)}(k) + b_m k^\alpha.$$

For one of the fixed equations  $j$ , setting  $k = 2, 3, \dots, n$ , we have

$$x_j^{(0)}(2) = a_{j1} z_1^{(1)}(2) + a_{j2} z_2^{(1)}(2) + \cdots + a_{jm} z_m^{(1)}(2) + 2^\alpha b_j,$$

$$x_j^{(0)}(3) = a_{j1} z_1^{(1)}(3) + a_{j2} z_2^{(1)}(3) + \cdots + a_{jm} z_m^{(1)}(3) + 3^\alpha b_j, \quad (18)$$

$$\vdots$$

$$x_j^{(0)}(n) = a_{j1} z_1^{(1)}(n) + a_{j2} z_2^{(1)}(n) + \cdots + a_{jm} z_m^{(1)}(n) + n^\alpha b_j.$$

The matrix form of the above equations is  $Q_j = Pa_j$ ,  $j = 1, 2, \dots, m$ .

In order to get parameters vector  $\hat{a}_j = (\hat{a}_{j1}, \dots, \hat{a}_{jm}, \hat{b}_j)^T$  ( $j = 1, 2, \dots, m$ ), substituting  $\sum_{l=1}^m a_{jl} z_l^{(1)}(k) + b_j k^\alpha$  with  $\sum_{l=1}^m \hat{a}_{jl} z_l^{(1)}(k) + \hat{b}_j k^\alpha$  ( $k = 2, 3, \dots, n, j = 1, 2, \dots, m$ ), we obtain the error sequence  $\epsilon_j = Q_j - P\hat{a}_j$ . Let

$$S_j = \epsilon_j^T \epsilon_j = (Q_j - P\hat{a}_j)^T (Q_j - P\hat{a}_j)$$

$$= \sum_{k=2}^n \left[ x_j^{(0)}(k) - \sum_{l=1}^m \hat{a}_{jl} z_l^{(1)}(k) - \hat{b}_j k^\alpha \right]^2. \quad (19)$$

Then the parameters vector  $\hat{a}_j = (\hat{a}_{j1}, \dots, \hat{a}_{jm}, \hat{b}_j)^T$  making  $S_j$  minimum should satisfy

$$\begin{aligned} \frac{\partial S_j}{\partial \hat{a}_{j1}} &= \sum_{k=2}^n \left[ \hat{b}_j k^\alpha + \sum_{l=1}^m \hat{a}_{jl} z_l^{(1)}(k) - x_j^{(0)}(k) \right] z_1^{(1)}(k) \\ &= 0, \\ \frac{\partial S_j}{\partial \hat{a}_{j2}} &= \sum_{k=2}^n \left[ \hat{b}_j k^\alpha + \sum_{l=1}^m \hat{a}_{jl} z_l^{(1)}(k) - x_j^{(0)}(k) \right] z_2^{(1)}(k) \\ &= 0, \\ &\vdots \\ \frac{\partial S_j}{\partial \hat{b}_j} &= \sum_{k=2}^n \left[ \hat{b}_j k^\alpha + \sum_{l=1}^m \hat{a}_{jl} z_l^{(1)}(k) - x_j^{(0)}(k) \right] k^\alpha = 0. \end{aligned} \quad (20)$$

Hence, we deduce that

$$\begin{aligned} &\begin{pmatrix} \sum_{k=2}^n (z_1^{(1)}(k))^2 & \dots & \sum_{k=2}^n k^\alpha z_1^{(1)}(k) \\ \vdots & \ddots & \vdots \\ \sum_{k=2}^n k^\alpha z_1^{(1)}(k) & \dots & \sum_{k=2}^n k^{2\alpha} \end{pmatrix} \begin{pmatrix} \hat{a}_{j1} \\ \vdots \\ \hat{a}_{jm} \\ \hat{b}_j \end{pmatrix} \\ &= \begin{pmatrix} z_1^{(1)}(2) & \dots & z_1^{(1)}(n) \\ \vdots & \ddots & \vdots \\ z_m^{(1)}(2) & \dots & z_m^{(1)}(n) \\ 2^\alpha & \dots & n^\alpha \end{pmatrix} \begin{pmatrix} x_j^{(0)}(2) \\ \vdots \\ x_j^{(0)}(n) \end{pmatrix}. \end{aligned} \quad (21)$$

Thus, we obtain the desired solution

$$\hat{a}_j = (P^T P)^{-1} P^T Q_j, \quad (22)$$

where  $P$  and  $Q_j$  are defined in Theorem 3. We can get the results of  $\hat{A}$  and  $\hat{B}$  by letting  $j = 1, 2, \dots, m$ .

The NMGM(1,  $m, k^\alpha$ ) model reduces to MGM(1,  $m$ ) when  $\alpha = 0$ , and NMGM(1,  $m, k^\alpha$ ) model becomes NMGM(1,  $m, k$ ) model when  $\alpha = 1$ . In the following, we give the time response function of MGM(1,  $m$ ), NMGM(1,  $m, k$ ), and NMGM(1,  $m, k^\alpha$ ), respectively.  $\square$

**Theorem 4.** Suppose that  $X^{(0)}$  is nonnegative original data matrix,  $X^{(1)}$  is first-order accumulated generation sequences and  $Z^{(1)}$  is adjacent neighbour average sequences. The parameters  $A$  and  $B$  are obtained by Theorem 3. Then

(1) The time response function of MGM(1,  $m$ ) model is

$$\hat{X}^{(1)}(k) = e^{A(k-1)} (X^{(1)}(1) + A^{-1}B) - A^{-1}B, \quad k \geq 2. \quad (23)$$

(2) The inverse accumulated generation is

$$\hat{X}^{(0)}(k) = \hat{X}^{(1)}(k) - \hat{X}^{(1)}(k-1), \quad k \geq 2. \quad (24)$$

**Theorem 5.** Assume that  $X^{(0)}$ ,  $X^{(1)}$ , and  $Z^{(1)}$  are defined as Theorem 4. The parameters  $A$  and  $B$  are obtained by Theorem 3. Then

(1) The time response sequence of discrete NMGM(1,  $m, k$ ) model is

$$\begin{aligned} \hat{X}^{(1)}(k) &= (x_1^{(1)}(k), x_2^{(1)}(k), \dots, x_m^{(1)}(k))^T \\ &= e^{A(k-1)} (X^{(0)}(1) + A^{-1}B + (A^{-1})^2 B) \\ &\quad - (A^{-1}Bk + (A^{-1})^2 B), \quad k \geq 2. \end{aligned} \quad (25)$$

(2) The inverse accumulated generation is

$$\hat{X}^{(0)}(k) = \hat{X}^{(1)}(k) - \hat{X}^{(1)}(k-1), \quad k \geq 2. \quad (26)$$

*Proof.* (1) Multiplying the whitening differential equation of NMGM(1,  $m, k$ ) model by  $e^{-At}$  we have

$$e^{-At} \frac{dX^{(1)}(t)}{dt} - e^{-At} AX^{(1)}(t) = e^{-At} Bt, \quad (27)$$

which is equivalent to

$$\frac{d(e^{-At} X^{(1)}(t))}{dt} = e^{-At} Bt. \quad (28)$$

Integrating the above equation from  $t_0$  to  $t$ , we get

$$\begin{aligned} &e^{-At} X^{(1)}(t) - e^{-At_0} X^{(1)}(t_0) \\ &= -e^{-At} A^{-1}Bt - e^{-At} (A^{-1})^2 B + e^{-At_0} A^{-1}Bt_0 \\ &\quad + e^{-At_0} (A^{-1})^2 B. \end{aligned} \quad (29)$$

Multiplying the equation by  $e^{At}$ , we obtain

$$\begin{aligned} X^{(1)}(t) &= e^{A(t-t_0)} (X^{(0)}(t_0) + A^{-1}Bt_0 + (A^{-1})^2 B) \\ &\quad - (A^{-1}Bt + (A^{-1})^2 B). \end{aligned} \quad (30)$$

Set  $t_0 = 1$  and  $t = k$ . We get time response function of discrete NMGM(1,  $m, k$ ) model

$$\begin{aligned} \hat{X}^{(1)}(k) &= (x_1^{(1)}(k), x_2^{(1)}(k), \dots, x_m^{(1)}(k))^T \\ &= e^{A(k-1)} (X^{(0)}(1) + A^{-1}B + (A^{-1})^2 B) \\ &\quad - (A^{-1}Bk + (A^{-1})^2 B), \quad k \geq 2. \end{aligned} \quad (31)$$

(2) The restored data is easy to obtain by the definition of first-order accumulated data sequences and so is omitted.  $\square$

**Theorem 6.** Assume that  $X^{(0)}$ ,  $X^{(1)}$ , and  $Z^{(1)}$  are defined as Theorem 4. The parameters  $A$  and  $B$  are obtained by Theorem 3. The time response function of NMGM(1,  $m, k^\alpha$ ) model is

$$\hat{X}^{(1)}(t) = e^{At} \left( \int t^\alpha e^{-At} dt \right) B. \quad (32)$$

TABLE 1: The original data of  $X_1$  and  $X_2$  (unit: yuan).

Variable	Time						
	$k = 1$	$k = 2$	$k = 3$	$k = 4$	$k = 5$	$k = 6$	$k = 7$
$X_1^{(0)}$	7375	8178	9262	10482	12319	14084	16378
$X_2^{(0)}$	3785	3996	4239	4754	5276	5813	6561

### 3. Precision Analysis

In this part, we compare the precision of MGM(1,  $m$ ) and NMGM(1,  $m, k$ ) model to illustrate the practicality of our results.

**3.1. Theoretical Analysis.** The predictive performance is of great importance in multivariable grey prediction when constructing a new model. Though many scholars conducted much research to improve the precision of MGM(1,  $m$ ) model and obtained some progress, their findings are not always satisfactory. Most researchers investigated MGM(1,  $m$ ) model based on the hypothesis that original data sequences are in accord with homogeneous sequences. The time response function of MGM(1,  $m$ ) model indicates that the restored data of MGM(1,  $m$ ) model is

$$\begin{aligned} \widehat{X}^{(0)}(k) &= \widehat{X}^{(1)}(k) - \widehat{X}^{(1)}(k-1) \\ &= e^{A(k-2)}(e^A - I)(X^{(1)}(1) + A^{-1}B), \end{aligned} \quad (33)$$

$k \geq 2,$

where  $I$  is unit matrix. Similarly, we obtain the restored values of NMGM(1,  $m, k$ ) model

$$\begin{aligned} \widehat{X}^{(0)}(k) &= \widehat{X}^{(1)}(k) - \widehat{X}^{(1)}(k-1) \\ &= e^{A(k-2)}(e^A - I)(X^{(0)}(1) + A^{-1}B + (A^{-1})^2B) \\ &\quad - A^{-1}B, \quad k \geq 2. \end{aligned} \quad (34)$$

Compared with restored data functions of MGM and NMGM model, we find that the restored function of MGM(1,  $m$ ) model is a data sequence with pure exponential growth law. The simulation and prediction function of NMGM(1,  $m, k$ ) model is in accordance with nonhomogeneous grey exponential law.

To demonstrate the practicability and maneuverability of nonhomogeneous multivariable grey prediction NMGM model, a case study is employed to compare the predictive performance of MGM and NMGM model.

**3.2. Case Study.** Per-capita net income of rural households and per-capita disposable income of urban residents are considered to be two important indicators that can reflect people's living standard and economic level. Therefore, it is necessary and helpful to control the variation trend of per-capita income. However, making such a prediction is challenging because per-capita net income of rural households and per-capita disposable income of urban residents are influenced by many factors. Grey prediction model is fairly

appropriate for this problem and shows excellent ability in solving such problems [39, 40]. Zhao et al. [39] forecasted per-capita annual net income of rural households in China by optimized grey GM(1, 1) model, which demonstrated that grey prediction model can be used effectively. In the following, the per-capita net income of rural households and per-capita disposable income of urban residents of Jiangsu province are forecasted by multivariable grey prediction model.

Jiangsu is a representative province of urban development in China, which enters into a new phase of economic development and undergoes a rapid development. Per-capita net income of rural households and per-capita disposable income of urban residents from 2001 to 2013 in Jiangsu province are chosen [41], which are obtained from Jiangsu Province Statistical Yearbook. The average annual growth rate of per-capita net income of rural households is 13.7%, and the average annual growth rate of per-capita disposable income of urban residents is only 11.25%. The per-capita net income of rural households and per-capita disposable income of urban residents are all affected by some certain factors, and there exist interaction and interrelation between them. The data set 2001–2013 is stable, which is suitable for constructing grey prediction model.

The data is divided into two groups: the data set 2001–2007 are used as original data while those 2008–2013 as test. Assume that 2001 is  $k = 1$  and so on as shown in Table 1. The input data sequence is the per-capita net income of rural households and per-capita disposable income of urban residents from 2001 to 2007 of Jiangsu province; then parameters of MGM and NMGM model can be determined. On the basis of this, the forecasting results of 2008–2013 can be calculated by Theorems 4 and 5.

In the following, we construct MGM(1,  $m$ ) model and NMGM(1,  $m, k$ ) model to compare the prediction accuracy. Let  $X_1$  be the per-capita disposable income of urban residents and  $X_2$  be the per-capita net income of rural households.

By traditional MGM(1,  $m$ ) model, we construct MGM(1, 2) model

$$\begin{aligned} \frac{dx_1^{(1)}(k)}{dk} &= 0.2732x_1^{(1)}(k) - 0.3044x_2^{(1)}(k) \\ &\quad + 6772.164, \\ \frac{dx_2^{(1)}(k)}{dk} &= 0.08618x_1^{(1)}(k) - 0.096x_2^{(1)}(k) \\ &\quad + 3526.2495. \end{aligned} \quad (35)$$

By NMGM(1,  $m, k$ ) proposed in this paper, we construct NMGM(1, 2,  $k$ ) model

TABLE 2: The actual and prediction values of  $X_1$  and  $X_2$  (unit: yuan).

Time	Actual values		MGM		NMGM	
	$X_1^{(0)}$	$X_2^{(0)}$	$\widehat{X}_1^{(0)}$	$\widehat{X}_2^{(0)}$	$\widehat{X}_1^{(0)}$	$\widehat{X}_2^{(0)}$
$k = 8$	18680	7357	19011.8	7385.7	10547.9	4025.6
$k = 9$	20965	8108	22235.2	8402.1	20863.7	7974.6
$k = 10$	23217	8980	26083.5	9615.7	24427.2	9100
$k = 11$	26341	10805	30677.9	11064.5	28672.5	10441.5
$k = 12$	29677	12202	36163.4	12794.3	33730	12039
$k = 13$	32538	13598	42712.4	14859.5	39755.1	13942.7

TABLE 3: The relative errors of MGM and NMGM (unit: %).

Time	$X_1$		$X_2$	
	MGM	NMGM	MGM	NMGM
$k = 8$	1.78	4.32	0.39	4.44
$k = 9$	6.06	0.48	3.62	1.65
$k = 10$	12.34	5.2	7.07	1.34
$k = 11$	16.46	8.8	2.4	3.36
$k = 12$	21.86	12.01	4.85	1.33
$k = 13$	31.27	22.18	9.27	2.53
MRE	14.96	8.83	4.6	2.44

$$\begin{aligned} \frac{dx_1^{(1)}(k)}{dk} &= 3.7136x_1^{(1)}(k) - 11.2009x_2^{(1)}(k) \\ &\quad + 15103.6306k, \\ \frac{dx_2^{(1)}(k)}{dk} &= 1.8827x_1^{(1)}(k) - 5.7843x_2^{(1)}(k) \\ &\quad + 7878.2759k. \end{aligned} \quad (36)$$

Actual values and prediction values of MGM(1,  $m$ ) and NMGM(1,  $m, k$ ) model are presented in Table 2. As can be seen from Table 2, the prediction values of NMGM(1, 2,  $k$ ) are more close to actual values compared with MGM(1, 2) prediction values.

To analyze reliability of the model, the accuracy of models should be tested. Two criteria are employed to measure the model, including relative error (RE) and mean relative error (MRE), by which we can investigate the effectiveness of the proposed model, where

$$\begin{aligned} \text{RE} &= \left| \frac{x_i(k) - \widehat{x}_i(k)}{x_i(k)} \right| \times 100\%, \\ \text{MRE} &= \frac{1}{n} \sum_{k=1}^n \left| \frac{x_i(k) - \widehat{x}_i(k)}{x_i(k)} \right| \times 100\%. \end{aligned} \quad (37)$$

The relative errors of per-capita disposable income of urban residents and per-capita net income of rural households predicted by MGM(1, 2) and NMGM(1, 2,  $k$ ) model are listed in Table 3. The mean relative error (MRE) indicates that NMGM(1, 2,  $k$ ) model is more accurate than traditional MGM(1, 2) model. From the comparative analysis, we know that NMGM(1,  $m, k$ ) model can better follow the tendency of per-capita disposable income of urban residents and per-capita net income of rural households. The case study shows

that the novel nonhomogeneous NMGM(1,  $m, k^\alpha$ ) model has certain advantages compared with traditional multiple grey prediction model.

#### 4. Conclusions and Future Research

Forecasting a future development is always an important issue in system analysis; however, because of the limitation of information and knowledge, only part of system structure could be fully realized. Grey forecasting models demonstrated its superiority in dealing with problems that partial information known and partial information unknown.

This paper put forward a novel model named NMGM(1,  $m, k^\alpha$ ) to tackle the nonhomogeneous multivariable data sequences, and the novel model makes up the deficiency of traditional MGM(1,  $m$ ) model. By least square method and differential equations, we present the modeling mechanism and time response function of the proposed model. The case study shows that the improved model is more accurately than traditional MGM(1,  $m$ ) model.

The proposed NMGM(1,  $m, k^\alpha$ ) model is fairly appropriate for the systems that are affected by other relative factors and their characteristic values are not in accordance with exponential law completely, and the novel NMGM(1,  $m, k^\alpha$ ) model can improve the adaptability of the traditional grey model.

There are also some problems needed to be solved in our future work, such as the optimization of background value, properties of novel model, finding the best  $\alpha$  for some specific cases, and integrating other kinds of optimization techniques with the novel model in order to further improve the prediction accuracy. This work is an extension of the multivariable grey prediction MGM(1,  $m$ ) model and a

great contribution to the development of multivariable grey prediction theory.

### Data Availability

The data used to support the findings of this study are from Jiangsu Province Statistical Yearbook and the data are included within the article.

### Conflicts of Interest

The authors declare that they have no conflicts of interest.

### Acknowledgments

This research is supported by National Natural Science Foundation of China (Grant no. 71473233).

### References

- [1] S. F. Liu, J. Forrest, and Y. J. Yang, "Advances in grey systems research," *The Journal of Grey System*, vol. 25, no. 2, pp. 1–18, 2013.
- [2] P. Wang and X. Liu, "Rapid convergence for telegraph systems with periodic boundary conditions," *Journal of Function Spaces*, vol. 2017, Article ID 1982568, 10 pages, 2017.
- [3] T. Li and Y. V. Rogovchenko, "Oscillation criteria for second-order superlinear Emden-Fowler neutral differential equations," *Monatshefte für Mathematik*, vol. 184, no. 3, pp. 489–500, 2017.
- [4] T. Li and Y. V. Rogovchenko, "On asymptotic behavior of solutions to higher-order sublinear Emden-Fowler delay differential equations," *Applied Mathematics Letters*, vol. 67, pp. 53–59, 2017.
- [5] T. Li and Y. V. Rogovchenko, "Oscillation criteria for even-order neutral differential equations," *Applied Mathematics Letters*, vol. 61, pp. 35–41, 2016.
- [6] M. Bohner, T. S. Hassan, and T. Li, "Fite-Hille-Wintner-type oscillation criteria for second-order half-linear dynamic equations with deviating arguments," *Indagationes Mathematicae*, vol. 29, no. 2, pp. 548–560, 2018.
- [7] R. Shah and T. Li, "The thermal and laminar boundary layer flow over prolate and oblate spheroids," *International Journal of Heat and Mass Transfer*, vol. 121, pp. 607–619, 2018.
- [8] Q. Feng and F. Meng, "Explicit solutions for space-time fractional partial differential equations in mathematical physics by a new generalized fractional Jacobi elliptic equation-based sub-equation method," *Optik - International Journal for Light and Electron Optics*, vol. 127, no. 19, pp. 7450–7458, 2016.
- [9] Q. Feng and F. Meng, "Traveling wave solutions for fractional partial differential equations arising in mathematical physics by an improved fractional Jacobi elliptic equation method," *Mathematical Methods in the Applied Sciences*, vol. 40, no. 10, pp. 3676–3686, 2017.
- [10] J. Shao, Z. Zheng, and F. Meng, "Oscillation criteria for fractional differential equations with mixed nonlinearities," *Advances in Difference Equations*, vol. 2013, no. 1, pp. 1–9, 2013.
- [11] R. Xu, "Oscillation criteria for nonlinear fractional differential equations," *Journal of Applied Mathematics*, vol. 169, Article ID 971357, pp. 1–7, 2013.
- [12] F. Meng and Y. Huang, "Interval oscillation criteria for a forced second-order nonlinear differential equations with damping," *Applied Mathematics and Computation*, vol. 218, no. 5, pp. 1857–1861, 2011.
- [13] G. E. Chatzarakis and T. X. Li, "Oscillation criteria for delay and advanced differential equations with nonmonotone arguments," *Complexity*, vol. 2018, Article ID 8237634, 18 pages, 2018.
- [14] R. Xu and F. Meng, "New Kamenev-type oscillation criteria for second order neutral nonlinear differential equations," *Applied Mathematics and Computation*, vol. 188, no. 2, pp. 1364–1370, 2007.
- [15] F. Meng and R. Xu, "Oscillation criteria for certain even order quasi-linear neutral differential equations with deviating arguments," *Applied Mathematics and Computation*, vol. 190, no. 1, pp. 458–464, 2007.
- [16] L. H. Liu and Y. Z. Bai, "New oscillation criteria for second-order nonlinear neutral delay differential equations," *Journal of Computational and Applied Mathematics*, vol. 231, no. 2, pp. 657–663, 2009.
- [17] H. Liu, F. Meng, and P. Liu, "Oscillation and asymptotic analysis on a new generalized Emden-Fowler equation," *Applied Mathematics and Computation*, vol. 219, no. 5, pp. 2739–2748, 2012.
- [18] R. Xu and F. Meng, "Oscillation criteria for second order quasi-linear neutral delay differential equations," *Applied Mathematics and Computation*, vol. 192, no. 1, pp. 216–222, 2007.
- [19] N. Xu, Y. Dang, and Y. Gong, "Novel grey prediction model with nonlinear optimized time response method for forecasting of electricity consumption in China," *Energy*, vol. 118, pp. 473–480, 2017.
- [20] K. D. Yin, S. Y. Li, and X. M. Li, "Research on China's strategic emerging marine industry based on a new GRA model," *The Journal of Grey System*, vol. 28, no. 4, pp. 1–14, 2016.
- [21] H. Y. Kim and C. H. Won, "Forecasting the volatility of stock price index: A hybrid model integrating LSTM with multiple GARCH-type models," *Expert Systems with Applications*, vol. 103, pp. 25–37, 2018.
- [22] J. L. Deng, "Introduction to grey system theory," *The Journal of Grey System*, vol. 1, no. 1, pp. 1–24, 1989.
- [23] C.-N. Wang, H.-K. Nguyen, and R.-Y. Liao, "Partner selection in supply chain of vietnam's textile and apparel industry: the application of a hybrid DEA and GM (1,1) approach," *Mathematical Problems in Engineering*, vol. 2017, Article ID 7826840, 16 pages, 2017.
- [24] F. Ren and L. Gu, "Study on transition of primary energy structure and carbon emission reduction targets in China based on Markov chain model and GM (1, 1)," *Mathematical Problems in Engineering*, vol. 2016, Article ID 4912935, 8 pages, 2016.
- [25] C. Yuan, S. Liu, and Z. Fang, "Comparison of China's primary energy consumption forecasting by using ARIMA (the autoregressive integrated moving average) model and GM(1,1) model," *Energy*, vol. 100, pp. 384–390, 2016.
- [26] T. X. Yao, S. F. Liu, and N. M. Xie, "On the properties of small sample of GM(1, 1) model," *Applied Mathematical Modelling*, vol. 33, no. 4, pp. 1894–1903, 2009.
- [27] B. Zeng, C. Luo, S. Liu, Y. Bai, and C. Li, "Development of an optimization method for the GM(1,N) model," *Engineering Applications of Artificial Intelligence*, vol. 55, pp. 353–362, 2016.
- [28] T.-L. Tien, "A research on the grey prediction model GM(1, n)," *Applied Mathematics and Computation*, vol. 218, no. 9, pp. 4903–4916, 2012.

- [29] Z.-X. Wang, "A GM(1,N)-based economic cybernetics model for the high-tech industries in China," *Kybernetes*, vol. 43, no. 5, pp. 672–685, 2014.
- [30] J. Zhai, J. M. Sheng, and Y. J. Feng, "The grey model MGM(1, n) and its application," *System Engineering Theory and Practice*, vol. 17, no. 5, pp. 109–113, 1997.
- [31] J. Cui, S.-F. Liu, B. Zeng, and N.-M. Xie, "A novel grey forecasting model and its optimization," *Applied Mathematical Modelling*, vol. 37, no. 6, pp. 4399–4406, 2013.
- [32] X. Ma, Y.-S. Hu, and Z.-B. Liu, "A novel kernel regularized nonhomogeneous grey model and its applications," *Communications in Nonlinear Science and Numerical Simulation*, vol. 48, pp. 51–62, 2017.
- [33] P. P. Xiong, Y. G. Dang, X. H. Wu, and X. M. Li, "Combined model based on optimized multi-variable grey model and multiple linear regression," *Journal of Systems Engineering and Electronics*, vol. 22, no. 4, pp. 615–620, 2011.
- [34] Y. Han, S.-G. Xu, and C.-W. Yu, "Multi-variable grey model (MGM (1, n, q)) based on genetic algorithm and its application in urban water consumption simulation," *Journal of System Simulation*, vol. 20, no. 17, pp. 4533–4536, 2008.
- [35] S. Li, X. Yang, and R. Li, "Forecasting China's coal power installed capacity: a comparison of MGM, ARIMA, GM-ARIMA, and NMGM models," *Sustainability*, vol. 10, no. 2, p. 506, 2018.
- [36] J. Wang, S. Liu, J. Shao, M. Long, J. Wang, and Y. Tang, "Study on dual pre-warning of transmission line icing based on improved residual MGM-Markov theory," *IEEE Transactions on Electrical and Electronic Engineering*, vol. 13, no. 4, pp. 561–569, 2018.
- [37] X. J. Guo, S. F. Liu, L. F. Wu, Y. B. Gao, and Y. J. Yang, "A multi-variable grey model with a self-memory component and its application on engineering prediction," *Engineering Applications of Artificial Intelligence*, vol. 42, pp. 82–93, 2015.
- [38] A. Karaaslan and K. Ö. Özden, "Forecasting turkey's credit ratings with multivariate grey model and grey relational analysis," *The Journal of Quantitative Economics*, vol. 15, no. 3, pp. 583–610, 2017.
- [39] Z. Zhao, J. Wang, J. Zhao, and Z. Su, "Using a Grey model optimized by Differential Evolution algorithm to forecast the per capita annual net income of rural households in China," *Omega International Journal of Management Science*, vol. 40, no. 5, pp. 525–532, 2012.
- [40] Z. Y. Meng, C. Y. Xu, and H. X. Lan, "Fuzzy GM(1, 1) model based per capital income predicted of farmers in the world natural and cultural heritage area: take Leshan city for an example," in *Proceedings of the Eleventh International Conference on Management Science and Engineering Management*, pp. 1007–1018, 2017.
- [41] P. P. Xiong, *The Optimization Method Research on Grey MGM(1, m) and Verhulst Model*, Nanjing University of Aeronautics and Astronautics, Nanjing, China, 2012.

## Research Article

# Adaptive Fuzzy Command Filtered Control for Chua's Chaotic System

Lin Wang <sup>1</sup>, Hui Wei <sup>1</sup> and Chunzhi Yang<sup>2</sup>

<sup>1</sup>*School of Mathematics and Big Data, Anhui University of Science and Technology, Huainan 232001, China*

<sup>2</sup>*Department of Applied Mathematics, Huainan Normal University, Huainan 232038, China*

Correspondence should be addressed to Hui Wei; [austweihui@sina.com](mailto:austweihui@sina.com)

Received 1 July 2018; Accepted 4 September 2018; Published 20 September 2018

Academic Editor: Xue-Jun Xie

Copyright © 2018 Lin Wang et al. This is an open access article distributed under the Creative Commons Attribution License, which permits unrestricted use, distribution, and reproduction in any medium, provided the original work is properly cited.

In this paper, we propose the command filtered adaptive fuzzy backstepping control (AFBC) approach for Chua's chaotic system with external disturbance. Based on two proposed first-order command filters, the convergence of tracking errors as well as the problem of "explosion of complexity" in traditional backstepping design procedure is solved. In the command filtered AFBC design, we do not need to calculate the complicated partial derivatives of the virtual control inputs. Fuzzy logic systems (FLSs) are used to identify the system uncertainties in real time. Based on Lyapunov stability criterion, the proposed controller can guarantee that all signals in the closed-loop system keep bounded, and the tracking errors converge to a small region eventually. Finally, simulation studies have been provided to verify the effectiveness of the proposed method.

## 1. Introduction

It is well known that adaptive backstepping control (ABC) is an effective technique for controlling nonlinear systems in parameter strict-feedback form [1]. For ABC of strict-feedback nonlinear systems without system uncertainties and external disturbances, this issue has been studied by using many control approaches [2–4]. Based on the sliding mode filters, [5, 6] estimated the command derivatives in the design of ABC. Linear filters for derivative generation were considered in [7]. Then, Farrell et al. in [8] introduced a command filtered backstepping control (CFBC) method, in which some new approaches were given to indicate that the virtual tracking errors between the signals of the command filtered and standard ABC methods were of  $\mathcal{O}(1/W)$ , where  $W$  represented the frequency of the command filter. Up to now, many command filter control methods have been reported [9–11]. The above literature only addressed the nonadaptive case for nonlinear feedback systems. Design of ABC with complicated situations was given in, for instance, [12–20]. It should be mentioned that the dimension of the input variables of the estimated system must be extended to include the reference trajectory and its first derivatives. However, the aforementioned works studied the approximation problem of

the command derivatives, but the resulting implementation does not achieve the theoretical guarantees of the ABC design. That is to say, new approaches are expected to solve this problem.

It has been shown that modeling of plant systems is badly affected by system uncertainties, i.e., parameter uncertainties, modeling errors, external disturbances, etc. This strongly motivates the study to design a robust, flexible, and effective controller, which can suppress complexities that demean the exhibition of the plants [21–37]. For backstepping control of nonlinear systems subject to system uncertainties, some control methods have been proposed, for example, in [38–43]. On the other hand, to tackle system uncertainties, scientists and researchers have proposed a lot of intelligent methods such as fuzzy logic systems (FLSs), neural networks, and neurofuzzy systems. In these methods, FLSs have been shown to be most successful and popular [44–48]. Following later advancement in intelligent control techniques, adaptive fuzzy controllers were developed such as fuzzy gain scheduled PID controller, fuzzy model reference adaptive controller, and self-organizing fuzzy controller. Adaptive fuzzy backstepping control (AFBC) methods also have been reported recently, for example, in [2, 4, 38, 45, 49, 50]. In [4], AFBC has been established for fractional-order strict-feedback systems. In [45],

AFBC has been given for uncertain nonlinear systems with input saturation. Wang et al. introduced a command filtered AFBC approach for uncertain nonlinear systems, where the ‘‘explosion of complexity’’ problem in backstepping design and chattering phenomenon were solved [49]. However, in their work, external disturbance was not considered, and a complicated second-order filter was used in the controller design.

Motivated by above discussion, this paper will investigate the control uncertain Chua’s chaotic system with external disturbance by means of command filtered AFBC. Combining the ABC method and command filter, a robust command filter AFBC is established. The proposed method can guarantee that all signals in the closed-loop system remain bounded, and the tracking errors converge to a small neighborhood of the origin eventually. The main contributions of this paper can be summarized as follows.

(1) The proposed command filter AFBC method works well even in the presence of full unknown system structure and external disturbance. A simple first-order filter has been introduced. Compared with the filter introduced in [49], our method is simpler and easier to be established. The proposed command filter guarantees that the commanded tracking error as well as its first derivative satisfies our control objective.

(2) By using the proposed command filter, the conventional ‘‘explosion of complexity’’ problem can be avoided. That is to say, the complicated calculation of partial derivative of the virtual control input is unnecessary. Our controller and adaptation laws are more concise compared with dynamic surface control approach, for example, in [51, 52].

The structure of this paper is arranged as follows. Section 2 gives the description of FLSs. The description of the problem and the controller design as well as the stability analysis are included in Section 3. The simulation results are indicated in Section 4. Finally, Section 5 gives a brief conclusion of this paper.

## 2. Description of FLS

A FLS contains four parts, i.e., the knowledge base, fuzzifier, fuzzy inference engine basing on the fuzzy rules, and defuzzifier. The  $j$ -th fuzzy rule is written as

$$\mathcal{R}^{(j)}: \text{if } x_1 \text{ is } E_1^j, x_2 \text{ is } E_2^j, \dots, x_n \text{ is } E_n^j, \text{ then } \hat{f}(\mathbf{x}(t)) \text{ is } C^j \quad (j = 1, 2, \dots, N)$$

where  $\mathbf{x}(t) = [x_1(t), x_2(t), \dots, x_n(t)]^T \in \mathbb{R}^n$  and  $\hat{f}(\mathbf{x}(t)) \in \mathbb{R}$  are, respectively, the input and the output of fuzzy logic systems.  $E_i^j$  and  $C^j$  ( $i = 1, 2, \dots, n$ ) are fuzzy sets belonging to  $\mathbb{R}$ . The output of fuzzy logic systems can be expressed by

$$\hat{f}(\mathbf{x}(t)) = \frac{\sum_{j=1}^N \theta_j(t) \left[ \prod_{i=1}^n \mu_{E_i^j}(x_i(t)) \right]}{\sum_{j=1}^N \left[ \prod_{i=1}^n \mu_{E_i^j}(x_i(t)) \right]}, \quad (1)$$

where  $\theta_j(t)$  is a value where fuzzy membership function  $\mu_{C^j}$  is maximum. Generally, we can consider that  $\mu_{C^j}(\theta_j(t)) = 1$ , and fuzzy basic function is  $\varphi_j(\mathbf{x}(t)) = \prod_{i=1}^n \mu_{E_i^j}(x_i(t)) / \sum_{j=1}^N \left[ \prod_{i=1}^n \mu_{E_i^j}(x_i(t)) \right]$ . Let  $\boldsymbol{\varphi}(\mathbf{x}(t)) = [\varphi_1(\mathbf{x}(t)), \varphi_2(\mathbf{x}(t)), \dots, \varphi_N(\mathbf{x}(t))]^T$ ,  $\boldsymbol{\theta}(t) = [\theta_1(t), \theta_2(t), \dots, \theta_N(t)]^T$ , and then output of fuzzy logic systems can be written as

$$\hat{f}(\mathbf{x}(t)) = \boldsymbol{\theta}^T(t) \boldsymbol{\varphi}(\mathbf{x}(t)). \quad (2)$$

**Lemma 1.** Suppose that  $h(\mathbf{x})$  is a continuous function defined on compact set  $\Omega$ ; for any constants  $\varepsilon > 0$ , there exists a fuzzy logic system approximating function  $\hat{f}(\mathbf{x})$  forming (2) such that

$$\sup_{\Omega} \left| h(\mathbf{x}(t)) - \hat{\boldsymbol{\theta}}^T(t) \boldsymbol{\varphi}(\mathbf{x}(t)) \right| \leq \varepsilon, \quad (3)$$

where  $\hat{\boldsymbol{\theta}}(t)$  is an estimator of optimal vector  $\boldsymbol{\theta}^*$ .

## 3. Main Results

**3.1. Problem Description.** The controlled Chua’s system is described as

$$\begin{aligned} \dot{x}_1(t) &= \alpha x_2(t) - \alpha x_1(t) - f(x_1(t)) + g_1(x_1(t)), \\ \dot{x}_2(t) &= x_3(t) + x_1(t) - x_2(t) + g_2(\bar{\mathbf{x}}_2(t)), \\ \dot{x}_3(t) &= \beta x_2(t) - \gamma x_3(t) + g_3(\mathbf{x}(t)) + d(t) + u(t), \\ y(t) &= x_1(t), \end{aligned} \quad (4)$$

with

$$f(x_1(t)) = ax_1(t) + b(|x_1(t) + 1| - |x_1(t) - 1|) \quad (5)$$

where  $\alpha, \beta, \gamma, a$ , and  $b$  are system parameters,  $y \in \mathcal{R}$  represents the system output,  $g_1(x_1(t))$ ,  $g_2(\bar{\mathbf{x}}_2(t))$ , and  $g_3(\mathbf{x}(t))$  are the system uncertainties with  $\bar{\mathbf{x}}_2(t) = [x_1(t), x_2(t)]^T \in \mathcal{R}^2$ ,  $\mathbf{x}(t) = [x_1(t), x_2(t), x_3(t)]^T \in \mathcal{R}^3$ ,  $d(t) \in \mathcal{R}$  is an unknown external disturbance, and  $u(t) \in \mathcal{R}$  denotes the control input.

Define the output tracking error  $e_1(t) = x_1(t) - x_1^c(t)$  where  $x_1^c(t) \in \mathcal{R}$  is a known smooth enough referenced signal. The paper aims to design a proper controller  $u(t)$  such that the tracking error  $e_1(t)$  tends to an arbitrary small region.

**3.2. Controller Design.** To meet the control objective, a robust command filtered backstepping controller that contains three steps will be constructed.

**Step 1.** Consider the first dynamical equation in system (4):

$$\dot{x}_1(t) = \alpha x_2(t) + \Delta g_1(x_1(t)), \quad (6)$$

where  $\Delta g_1(x_1(t)) = -\alpha x_1(t) - f(x_1(t)) + g_1(x_1(t))$  is an unknown nonlinear function. Thus,  $\Delta g_1(x_1(t))$  can be approximated through FLS (2) as

$$\begin{aligned} \Delta g_1(x_1(t)) &= \boldsymbol{\theta}_1^T(t) \boldsymbol{\varphi}_1(x_1(t)) \\ &= \boldsymbol{\theta}_1^{*T} \boldsymbol{\varphi}_1(x_1(t)) + \varepsilon_1(t) \end{aligned} \quad (7)$$

where  $\theta_1^{*T}$  represents the optimal fuzzy parameter and  $\varepsilon_1(t)$  is the optimal approximation error. Then, the virtual input can be designed as

$$z_2(t) = -\frac{1}{\alpha} \left[ k_1 e_1(t) + \theta_1^T(t) \varphi_1(x_1(t)) + \widehat{\varepsilon}_1(t) \arctan\left(\frac{\bar{e}_1(t)}{\lambda_1}\right) - \dot{x}_1^c(t) \right] \quad (8)$$

where  $\widehat{\varepsilon}_1(t)$  is the estimation of the upper bound of the fuzzy approximation error  $\varepsilon_1(t)$ ,  $k_1$  and  $\lambda_1$  are two positive design parameters, and  $\bar{e}_1(t)$  is the compensated tracking error that will be defined later. Then, it follows from (6), (7), and (8) that

$$\begin{aligned} \dot{e}_1(t) &= \alpha x_2(t) + \Delta g_1(x_1(t)) - \dot{x}_1^c(t) \\ &= \alpha(x_2(t) - z_2(t)) + \Delta g_1(x_1(t)) - \dot{x}_1^c(t) \\ &\quad + \alpha z_2(t) \\ &= -k_1 e_1(t) + \alpha(x_2(t) - z_2(t)) + \theta_1^{*T} \varphi_1(x_1(t)) \\ &\quad + \varepsilon_1(t) - \theta_1^T(t) \varphi_1(x_1(t)) \\ &\quad - \widehat{\varepsilon}_1(t) \arctan\left(\frac{\bar{e}_1(t)}{\lambda_1}\right) \\ &= -k_1 e_1(t) + \alpha(x_2^c(t) - z_2(t)) \\ &\quad - \bar{\theta}_1^T(t) \varphi_1(x_1(t)) + \varepsilon_1(t) \\ &\quad - \widehat{\varepsilon}_1(t) \arctan\left(\frac{\bar{e}_1(t)}{\lambda_1}\right) + \alpha e_2(t) \end{aligned} \quad (9)$$

where  $\bar{\theta}_1^T(t) = \theta_1^T(t) - \theta_1^{*T}$  is the fuzzy parameter estimation error,  $e_2(t) = x_2(t) - x_2^c(t)$  is the command filtered tracking error, and  $x_2^c$  will be given later. The compensated tracking error signal can be defined as

$$\bar{e}_1(t) = e_1(t) - \zeta_1(t) \quad (10)$$

where  $\zeta_1(t)$  is an added term which is the solution of the following filter:

$$\dot{\zeta}_1(t) = -k_1 \zeta_1(t) + \alpha(x_2^c(t) - z_2(t)) + \alpha \zeta_2(t) \quad (11)$$

where  $\zeta_2(t)$  will be given in Step 2 and  $x_2^c(t)$  is obtained by the filter

$$\dot{x}_2^c(t) = -\omega_2(x_2^c(t) - z_2(t)) \quad (12)$$

with  $\omega_2 > 0$  being a design parameter. The initial condition for  $x_2^c(t)$  is  $x_2^c(0) = 0$ . Thus, adaptation laws for  $\theta_1(t)$  and  $\widehat{\varepsilon}_1(t)$  are designed as

$$\dot{\theta}_1(t) = c_{11} \bar{e}_1(t) \varphi_1(x_1(t)) - c_{11} c_{12} \theta_1(t) \quad (13)$$

and

$$\dot{\widehat{\varepsilon}}_1(t) = c_{41} \bar{e}_1(t) \tanh\left(\frac{\bar{e}_1(t)}{\lambda_1}\right) - c_{41} c_{42} \widehat{\varepsilon}_1(t), \quad (14)$$

respectively, where  $c_{11}$ ,  $c_{12}$ ,  $c_{41}$ , and  $c_{42}$  are all positive design parameters.

*Step 2.* It follows from (4) that

$$\dot{x}_2(t) = x_3(t) + \Delta g_2(\bar{x}_2(t)) \quad (15)$$

where  $\Delta g_2(\bar{x}_2(t)) = x_1(t) - x_2(t) + g_2(\bar{x}_2(t))$  is an unknown nonlinear function, which can be approximated through FLS (2) by

$$\begin{aligned} \Delta g_2(\bar{x}_2(t)) &= \theta_2^T(t) \varphi_2(\bar{x}_2(t)) \\ &= \theta_2^{*T} \varphi_2(\bar{x}_2(t)) + \varepsilon_2(t). \end{aligned} \quad (16)$$

The virtual tracking errors, similar to that in Step 1, are defined as

$$\begin{aligned} e_2(t) &= x_2(t) - x_2^c(t), \\ \bar{e}_2(t) &= e_2(t) - \zeta_2(t), \end{aligned} \quad (17)$$

with

$$\dot{\zeta}_2(t) = -k_2 \zeta_2(t) + x_3^c(t) - z_3(t) + \zeta_3(t) \quad (18)$$

where  $\zeta_2(0) = 0$ ,  $\zeta_3(t)$  will be given in Step 3,

$$\dot{x}_3^c(t) = -\omega_3(x_3^c(t) - z_3(t)), \quad (19)$$

$z_3(t)$  is the virtual control input designed as

$$\begin{aligned} z_3(t) &= -k_2 e_2(t) - \theta_2^T(t) \varphi_2(\bar{x}_2(t)) \\ &\quad - \widehat{\varepsilon}_2(t) \arctan\left(\frac{\bar{e}_2(t)}{\lambda_2}\right) + x_2^c(t) - \alpha \bar{e}_1(t) \end{aligned} \quad (20)$$

with  $k_2$  and  $\lambda_2$  being positive design parameters. Adaptation laws for  $\theta_2(t)$  and  $\widehat{\varepsilon}_2(t)$  can be given as

$$\dot{\theta}_2(t) = c_{21} \bar{e}_2(t) \varphi_2(\bar{x}_2(t)) - c_{21} c_{22} \theta_2(t) \quad (21)$$

and

$$\dot{\widehat{\varepsilon}}_2(t) = c_{51} \bar{e}_2(t) \tanh\left(\frac{\bar{e}_2(t)}{\lambda_1}\right) - c_{51} c_{52} \widehat{\varepsilon}_2(t) \quad (22)$$

where  $c_{21}$ ,  $c_{22}$ ,  $c_{51}$ , and  $c_{52}$  are all positive design parameters. Based on above discussion, we have

$$\begin{aligned} \dot{e}_2(t) &= x_3(t) + \Delta g_2(\bar{x}_2(t)) - \dot{x}_2^c(t) \\ &= x_3(t) - z_3(t) + \Delta g_3(\bar{x}_2(t)) - \dot{x}_2^c(t) + z_3(t) \\ &= -k_2 e_2(t) + x_3(t) - z_3(t) + \theta_2^{*T} \varphi_2(\bar{x}_2(t)) \\ &\quad + \varepsilon_2(t) - \theta_2^T(t) \varphi_2(\bar{x}_2(t)) \\ &\quad - \widehat{\varepsilon}_2(t) \arctan\left(\frac{\bar{e}_2(t)}{\lambda_2}\right) - \alpha \bar{e}_1(t) \\ &= -k_2 e_2(t) + x_3^c(t) - z_3(t) - \bar{\theta}_2^T(t) \varphi_2(\bar{x}_2(t)) \\ &\quad + \varepsilon_2(t) - \widehat{\varepsilon}_2(t) \arctan\left(\frac{\bar{e}_2(t)}{\lambda_2}\right) - \alpha \bar{e}_1(t) \\ &\quad + e_3(t). \end{aligned} \quad (23)$$

Step 3. According to (4), we have

$$\dot{x}_3(t) = \Delta g_3(\mathbf{x}(t)) + d(t) + u(t) \quad (24)$$

with  $\Delta g_3(\mathbf{x}(t)) = \beta x_2(t) - \gamma x_3(t) + g_3(\mathbf{x}(t))$  being an unknown nonlinear function that can be approximated by

$$\Delta g_3(\bar{\mathbf{x}}(t)) = \boldsymbol{\theta}_3^T(t) \boldsymbol{\varphi}_3(\bar{\mathbf{x}}(t)) = \boldsymbol{\theta}_3^{*T} \boldsymbol{\varphi}_3(\bar{\mathbf{x}}(t)) + \varepsilon_3(t). \quad (25)$$

The control input is designed as

$$\begin{aligned} u(t) = & -k_3 e_3(t) - \boldsymbol{\theta}_3^T(t) \boldsymbol{\varphi}_3(\bar{\mathbf{x}}(t)) \\ & - \left( \hat{\varepsilon}_2(t) + \hat{d}(t) \right) \arctan\left(\frac{\tilde{e}_3(t)}{\lambda_3}\right) + \dot{x}_3^c(t) \\ & - e_2(t) \end{aligned} \quad (26)$$

where  $k_3, \lambda_3$  are two positive design parameters and  $\hat{d}(t)$  is the estimation of external disturbance  $d(t)$ . The compensated tracking errors are defined by

$$\begin{aligned} e_3(t) &= x_3(t) - x_3^c(t), \\ \tilde{e}_3(t) &= e_3(t) - \zeta_3(t), \end{aligned} \quad (27)$$

where

$$\dot{\zeta}_3(t) = -k_3 \zeta_3(t) - \zeta_2(t). \quad (28)$$

We design the following adaptation laws:

$$\dot{\boldsymbol{\theta}}_3(t) = c_{31} \tilde{e}_3(t) \boldsymbol{\varphi}_2(\bar{\mathbf{x}}(t)) - c_{31} c_{32} \boldsymbol{\theta}_3(t), \quad (29)$$

$$\dot{\hat{\varepsilon}}_3(t) = c_{61} \tilde{e}_3(t) \tanh\left(\frac{\tilde{e}_3(t)}{\lambda_3}\right) - c_{61} c_{62} \hat{\varepsilon}_3(t) \quad (30)$$

and

$$\dot{\hat{d}}(t) = c_{71} \tilde{e}_3(t) \tanh\left(\frac{\tilde{e}_3(t)}{\lambda_3}\right) - c_{71} c_{72} \hat{d}(t) \quad (31)$$

where  $c_{31}, c_{32}, c_{61}, c_{62}, c_{71}$ , and  $c_{72}$  are all positive design parameters. Thus,

$$\begin{aligned} \dot{e}_3(t) &= \Delta g_3(\bar{\mathbf{x}}(t)) - \dot{x}_3^c(t) + d(t) + u(t) \\ &= -k_3 e_3(t) + \boldsymbol{\theta}_3^{*T} \boldsymbol{\varphi}_3(\bar{\mathbf{x}}(t)) + \varepsilon_3(t) + d(t) \\ &\quad - \hat{d}(t) \arctan\left(\frac{\tilde{e}_3(t)}{\lambda_3}\right) - \boldsymbol{\theta}_3^T(t) \boldsymbol{\varphi}_3(\bar{\mathbf{x}}(t)) \\ &\quad - \hat{\varepsilon}_3(t) \arctan\left(\frac{\tilde{e}_3(t)}{\lambda_3}\right) - e_2(t) \\ &= -k_3 e_3(t) - \tilde{\boldsymbol{\theta}}_3^T(t) \boldsymbol{\varphi}_3(\bar{\mathbf{x}}(t)) + \varepsilon_3(t) + d(t) \\ &\quad - \hat{d}(t) \arctan\left(\frac{\tilde{e}_3(t)}{\lambda_3}\right) \\ &\quad - \hat{\varepsilon}_3(t) \arctan\left(\frac{\tilde{e}_3(t)}{\lambda_3}\right) - e_2(t). \end{aligned} \quad (32)$$

Here  $\tilde{d}(t) = \hat{d}(t) - d(t)$  is the estimation error of  $d(t)$ .

To proceed, we need the following assumption and lemma.

*Assumption 2.* The external disturbance and the fuzzy approximate errors are bounded; i.e., there exist some positive constants  $d^*$  and  $\varepsilon_i^*$  such that  $|d(t)| \leq d^*$  and  $\varepsilon_i(t) \leq \varepsilon_i^*$ .

**Lemma 3** (see [49]). *Suppose that  $\lambda > 0$ ; then it holds that*

$$|y| - y \tanh\left(\frac{y}{\lambda}\right) \leq \kappa \lambda \quad (33)$$

where  $\kappa = 0.2785$  is a constant.

**3.3. Stability Analysis.** According to the above analysis, the dynamical equations for the tracking errors are obtained as

$$\begin{aligned} \dot{\tilde{e}}_1(t) &= \dot{e}_1(t) - \dot{\zeta}_1(t) \\ &= -k_1 e_1(t) + \alpha(x_2^c(t) - z_2(t)) \\ &\quad - \tilde{\boldsymbol{\theta}}_1^T(t) \boldsymbol{\varphi}_1(x_1(t)) + \varepsilon_1(t) \\ &\quad - \hat{\varepsilon}_1(t) \arctan\left(\frac{\tilde{e}_1(t)}{\lambda_1}\right) + \alpha e_2(t) - \dot{\zeta}_1(t) \\ &= -k_1 e_1(t) - \tilde{\boldsymbol{\theta}}_1^T(t) \boldsymbol{\varphi}_1(x_1(t)) + \varepsilon_1(t) \\ &\quad - k_1 \zeta_1(t) - \hat{\varepsilon}_1(t) \arctan\left(\frac{\tilde{e}_1(t)}{\lambda_1}\right) + \alpha e_2(t) \\ &\quad - \alpha \zeta_2(t) \\ &= -k_1 \tilde{e}_1(t) + \alpha \tilde{e}_2(t) - \tilde{\boldsymbol{\theta}}_1^T(t) \boldsymbol{\varphi}_1(x_1(t)) + \varepsilon_1(t) \\ &\quad - \hat{\varepsilon}_1(t) \arctan\left(\frac{\tilde{e}_1(t)}{\lambda_1}\right), \\ \dot{\tilde{e}}_2(t) &= \dot{e}_2(t) - \dot{\zeta}_2(t) \\ &= -k_2 e_2(t) + x_3^c(t) - z_3(t) - \tilde{\boldsymbol{\theta}}_2^T(t) \boldsymbol{\varphi}_2(\bar{\mathbf{x}}_2(t)) \\ &\quad + e_2(t) - \hat{\varepsilon}_2(t) \arctan\left(\frac{\tilde{e}_2(t)}{\lambda_2}\right) - \alpha \tilde{e}_1(t) \\ &\quad + e_3(t) - \dot{\zeta}_2(t) \\ &= -k_2 e_2(t) - \tilde{\boldsymbol{\theta}}_2^T(t) \boldsymbol{\varphi}_2(\bar{\mathbf{x}}_2(t)) + \varepsilon_2(t) - \zeta_3(t) \\ &\quad - \hat{\varepsilon}_2(t) \arctan\left(\frac{\tilde{e}_2(t)}{\lambda_2}\right) - \alpha \tilde{e}_1(t) + e_3(t) \\ &\quad - k_2 \zeta_2(t) \\ &= -k_2 \tilde{e}_2(t) - \tilde{\boldsymbol{\theta}}_2^T(t) \boldsymbol{\varphi}_2(\bar{\mathbf{x}}_2(t)) + \varepsilon_2(t) + \tilde{e}_3(t) \\ &\quad - \hat{\varepsilon}_2(t) \arctan\left(\frac{\tilde{e}_2(t)}{\lambda_2}\right) - \alpha \tilde{e}_1(t), \end{aligned} \quad (34)$$

$$\begin{aligned} \dot{\tilde{e}}_2(t) &= \dot{e}_2(t) - \dot{\zeta}_2(t) \\ &= -k_2 e_2(t) + x_3^c(t) - z_3(t) - \tilde{\boldsymbol{\theta}}_2^T(t) \boldsymbol{\varphi}_2(\bar{\mathbf{x}}_2(t)) \\ &\quad + e_2(t) - \hat{\varepsilon}_2(t) \arctan\left(\frac{\tilde{e}_2(t)}{\lambda_2}\right) - \alpha \tilde{e}_1(t) \\ &\quad + e_3(t) - \dot{\zeta}_2(t) \\ &= -k_2 e_2(t) - \tilde{\boldsymbol{\theta}}_2^T(t) \boldsymbol{\varphi}_2(\bar{\mathbf{x}}_2(t)) + \varepsilon_2(t) - \zeta_3(t) \\ &\quad - \hat{\varepsilon}_2(t) \arctan\left(\frac{\tilde{e}_2(t)}{\lambda_2}\right) - \alpha \tilde{e}_1(t) + e_3(t) \\ &\quad - k_2 \zeta_2(t) \\ &= -k_2 \tilde{e}_2(t) - \tilde{\boldsymbol{\theta}}_2^T(t) \boldsymbol{\varphi}_2(\bar{\mathbf{x}}_2(t)) + \varepsilon_2(t) + \tilde{e}_3(t) \\ &\quad - \hat{\varepsilon}_2(t) \arctan\left(\frac{\tilde{e}_2(t)}{\lambda_2}\right) - \alpha \tilde{e}_1(t), \end{aligned} \quad (35)$$

$$\begin{aligned}
 \dot{\tilde{e}}_3(t) &= \dot{e}_3(t) - \dot{\zeta}_3(t) \\
 &= -k_3 e_3(t) - \tilde{\theta}_3^T(t) \boldsymbol{\varphi}_3(\bar{\mathbf{x}}(t)) + \varepsilon_3(t) \\
 &\quad - \hat{d}(t) \arctan\left(\frac{\tilde{e}_3(t)}{\lambda_3}\right) - \dot{\zeta}_3(t) - e_2(t) \\
 &\quad - \tilde{e}_3(t) \arctan\left(\frac{\tilde{e}_3(t)}{\lambda_3}\right) + d(t) \\
 &= -k_3 \tilde{e}_3(t) - \tilde{\theta}_3^T(t) \boldsymbol{\varphi}_3(\bar{\mathbf{x}}(t)) + \varepsilon_3(t) + d(t) \\
 &\quad - \hat{d}(t) \arctan\left(\frac{\tilde{e}_3(t)}{\lambda_3}\right) - \tilde{e}_2(t) \\
 &\quad - \tilde{e}_3(t) \arctan\left(\frac{\tilde{e}_3(t)}{\lambda_3}\right).
 \end{aligned} \tag{36}$$

**Remark 4.** In this paper, to cancel the effect of the signals  $x_i^c(t) - z_i(t)$ ,  $i = 1, 2, 3$ , three filters, i.e., (11), (18), and (28) have been introduced. It should be pointed out that the proposed filters can guarantee the boundedness of the added signals  $\zeta_1(t)$ ,  $\zeta_2(t)$ ,  $\zeta_3(t)$ . The stability analysis for these signals is presented in Theorem 5.

**Theorem 5.** *If the input signals  $x_i^c(t) - z_i(t)$ ,  $i = 1, 2, 3$ , satisfy  $|x_i^c(t) - z_i(t)| \leq B$  where  $B$  is a positive constant, then the filters defined as (11), (18), and (28) have state variables bounded by*

$$\|\zeta(t)\| \leq \frac{A}{2\underline{k}} (1 - e^{-2\underline{k}t}) \tag{37}$$

where  $\zeta(t) = [\zeta_1(t), \zeta_2(t), \zeta_3(t)]^T \in \mathcal{R}^3$ ,  $\underline{k} = (1/2)\min\{k_1, k_2, k_3\}$ , and  $A = B + \alpha$ .

*Proof.* The Lyapunov function candidate is chosen as  $V_1(t) = (1/2)\|\zeta(t)\|^2$ . According to (11), (18), and (28), the derivative of  $V_1(t)$  with respect to time can be given as

$$\begin{aligned}
 \dot{V}_1(t) &= \sum_{i=1}^3 \zeta_i(t) \dot{\zeta}_i(t) \\
 &= -\sum_{i=1}^3 k_i \zeta_i^2(t) + \alpha \zeta_1(t) (x_2^c(t) - z_2(t)) \\
 &\quad + \zeta_2(t) (x_3^c(t) - z_3(t)) \\
 &\leq -2\underline{k} \|\zeta(t)\|^2 + A \|\zeta(t)\| \\
 &\leq -4\underline{k} V_1(t) + \sqrt{2A} \sqrt{V_1(t)}.
 \end{aligned} \tag{38}$$

Thus, (38) implies that (37) holds.  $\square$

The main results of this section are included in the following theorem.

**Theorem 6.** *Consider system (4) under Assumption 2. The virtual control inputs are chosen as (8) and (20). The filters are given as (11), (12), (18), (19), and (28). The fuzzy parameters are updated by (13), (21), and (29). The estimation of the fuzzy*

*approximation errors is updated by (14), (22), and (30). The estimation of  $d(t)$  is given as (31). Then, the control input (26) guarantees that the tracking errors  $\tilde{e}_1(t)$ ,  $\tilde{e}_2(t)$ , and  $\tilde{e}_3(t)$  converge to a small region of zero if proper design parameters are chosen.*

*Proof.* Let the Lyapunov function candidate be

$$\begin{aligned}
 V(t) &= \frac{1}{2} \sum_{i=1}^3 \tilde{e}_i^2(t) + \sum_{i=1}^3 \frac{1}{2c_{i1}} \tilde{\theta}_i^T(t) \tilde{\theta}_i(t) \\
 &\quad + \sum_{i=1}^3 \frac{1}{2c_{i+3,1}} \tilde{e}_i^2(t) + \frac{1}{2c_{71}} \tilde{d}^2(t)
 \end{aligned} \tag{39}$$

where  $\tilde{e}_i(t) = \hat{e}_i(t) - \varepsilon_i^*$ ,  $\tilde{d}(t) = \hat{d}(t) - d^*$  are estimation errors. It follows from (34), (35), (36), Assumption 2, and Lemma 3 that

$$\begin{aligned}
 \sum_{i=1}^3 \tilde{e}_i(t) \dot{\tilde{e}}_i(t) &= \sum_{i=1}^3 \tilde{e}_i(t) \left[ \varepsilon_i(t) - \hat{e}_i(t) \arctan\left(\frac{\tilde{e}_i(t)}{\lambda_i}\right) \right] \\
 &\quad - \tilde{e}_1(t) \tilde{\theta}_1^T(t) \boldsymbol{\varphi}_1(x_1(t)) - \tilde{e}_2(t) \tilde{\theta}_2^T(t) \boldsymbol{\varphi}_2(\bar{\mathbf{x}}_2(t)) \\
 &\quad - \tilde{e}_3(t) \tilde{\theta}_3^T(t) \boldsymbol{\varphi}_3(\bar{\mathbf{x}}(t)) - \sum_{i=1}^3 k_i \tilde{e}_i^2(t) + \tilde{e}_3(t) \left[ d(t) \right. \\
 &\quad \left. - \hat{d}(t) \arctan\left(\frac{\tilde{e}_3(t)}{\lambda_3}\right) \right] \leq \sum_{i=1}^3 \left[ |\tilde{e}_i(t)| \varepsilon_i^* \right. \\
 &\quad \left. - \tilde{e}_i(t) \hat{e}_i(t) \arctan\left(\frac{\tilde{e}_i(t)}{\lambda_i}\right) \right] - \tilde{e}_1(t) \tilde{\theta}_1^T(t) \\
 &\quad \cdot \boldsymbol{\varphi}_1(x_1(t)) - \tilde{e}_2(t) \tilde{\theta}_2^T(t) \boldsymbol{\varphi}_2(\bar{\mathbf{x}}_2(t)) - \tilde{e}_3(t) \tilde{\theta}_3^T(t) \\
 &\quad \cdot \boldsymbol{\varphi}_3(\bar{\mathbf{x}}(t)) - \sum_{i=1}^3 k_i \tilde{e}_i^2(t) + |\tilde{e}_3(t)| d^* - \tilde{e}_3(t) \hat{d}(t) \\
 &\quad \cdot \arctan\left(\frac{\tilde{e}_3(t)}{\lambda_3}\right) = \sum_{i=1}^3 \left[ |\tilde{e}_i(t)| \varepsilon_i^* \right. \\
 &\quad \left. - \tilde{e}_i(t) \hat{e}_i(t) \arctan\left(\frac{\tilde{e}_i(t)}{\lambda_i}\right) \right] \\
 &\quad - \tilde{e}_i(t) \varepsilon_i^* \arctan\left(\frac{\tilde{e}_i(t)}{\lambda_i}\right) \Big] - \tilde{e}_2(t) \tilde{\theta}_2^T(t) \boldsymbol{\varphi}_2(\bar{\mathbf{x}}_2(t)) \\
 &\quad - \tilde{e}_3(t) \tilde{\theta}_3^T(t) \boldsymbol{\varphi}_3(\bar{\mathbf{x}}(t)) - \tilde{e}_1(t) \tilde{\theta}_1^T(t) \boldsymbol{\varphi}_1(x_1(t)) \\
 &\quad + |\tilde{e}_3(t)| d^* - \tilde{e}_3(t) \hat{d}(t) \arctan\left(\frac{\tilde{e}_3(t)}{\lambda_3}\right) \\
 &\quad + \sum_{i=1}^3 \tilde{e}_i(t) \varepsilon_i^* \arctan\left(\frac{\tilde{e}_i(t)}{\lambda_i}\right) - \sum_{i=1}^3 k_i \tilde{e}_i^2(t) \\
 &\quad - \tilde{e}_3(t) d^* \arctan\left(\frac{\tilde{e}_3(t)}{\lambda_3}\right)
 \end{aligned}$$

$$\begin{aligned}
& + \tilde{\varepsilon}_3(t) d^* \arctan\left(\frac{\tilde{\varepsilon}_3(t)}{\lambda_3}\right) \\
& \leq \sum_{i=1}^3 \left[ -\tilde{\varepsilon}_i(t) \hat{\varepsilon}_i(t) \arctan\left(\frac{\tilde{\varepsilon}_i(t)}{\lambda_i}\right) \right. \\
& \quad \left. + \tilde{\varepsilon}_i(t) \varepsilon_i^* \arctan\left(\frac{\tilde{\varepsilon}_i(t)}{\lambda_i}\right) \right] - \sum_{i=1}^3 k_i \tilde{\varepsilon}_i^2(t) - \tilde{\varepsilon}_2(t) \\
& \quad \cdot \tilde{\theta}_2^T(t) \boldsymbol{\varphi}_2(\bar{\mathbf{x}}_2(t)) - \tilde{\varepsilon}_3(t) \tilde{\theta}_3^T(t) \boldsymbol{\varphi}_3(\bar{\mathbf{x}}(t)) - \tilde{\varepsilon}_1(t) \\
& \quad \cdot \tilde{\theta}_1^T(t) \boldsymbol{\varphi}_1(x_1(t)) - \tilde{\varepsilon}_3(t) \tilde{d}(t) \arctan\left(\frac{\tilde{\varepsilon}_3(t)}{\lambda_3}\right) \\
& \quad + \kappa \sum_{i=1}^3 \lambda_i \varepsilon_i^* + \kappa \lambda_3 d^* + \tilde{\varepsilon}_3(t) d^* \arctan\left(\frac{\tilde{\varepsilon}_3(t)}{\lambda_3}\right) \\
& = -\sum_{i=1}^3 \tilde{\varepsilon}_i(t) \tilde{\varepsilon}_i(t) \arctan\left(\frac{\tilde{\varepsilon}_i(t)}{\lambda_i}\right) - \sum_{i=1}^3 k_i \tilde{\varepsilon}_i^2(t) \\
& \quad - \tilde{\varepsilon}_3(t) \tilde{d}(t) \arctan\left(\frac{\tilde{\varepsilon}_3(t)}{\lambda_3}\right) - \tilde{\varepsilon}_2(t) \tilde{\theta}_2^T(t) \\
& \quad \cdot \boldsymbol{\varphi}_2(\bar{\mathbf{x}}_2(t)) - \tilde{\varepsilon}_3(t) \tilde{\theta}_3^T(t) \boldsymbol{\varphi}_3(\bar{\mathbf{x}}(t)) - \tilde{\varepsilon}_1(t) \tilde{\theta}_1^T(t) \\
& \quad \cdot \boldsymbol{\varphi}_1(x_1(t)) + \kappa \lambda_3 d^* + \kappa \sum_{i=1}^3 \lambda_i \varepsilon_i^*. \tag{40}
\end{aligned}$$

By using the adaptations laws (13), (14), (21), (22), (29), (30), and (31), we have

$$\begin{aligned}
\sum_{i=1}^3 \frac{1}{c_{i1}} \tilde{\theta}_i^T(t) \dot{\tilde{\theta}}_i(t) & = \sum_{i=1}^3 \frac{1}{c_{i1}} \tilde{\theta}_i^T(t) \dot{\theta}_i(t) \\
& = \tilde{\varepsilon}_2(t) \tilde{\theta}_2^T(t) \boldsymbol{\varphi}_2(\bar{\mathbf{x}}_2(t)) + \tilde{\varepsilon}_3(t) \tilde{\theta}_3^T(t) \boldsymbol{\varphi}_3(\bar{\mathbf{x}}(t)) \\
& \quad + \tilde{\varepsilon}_1(t) \tilde{\theta}_1^T(t) \boldsymbol{\varphi}_1(x_1(t)) - \sum_{i=1}^3 c_{i2} \tilde{\theta}_i^T(t) \dot{\theta}_i(t) \\
& = \tilde{\varepsilon}_2(t) \tilde{\theta}_2^T(t) \boldsymbol{\varphi}_2(\bar{\mathbf{x}}_2(t)) + \tilde{\varepsilon}_3(t) \tilde{\theta}_3^T(t) \boldsymbol{\varphi}_3(\bar{\mathbf{x}}(t)) \\
& \quad + \tilde{\varepsilon}_1(t) \tilde{\theta}_1^T(t) \boldsymbol{\varphi}_1(x_1(t)) \\
& \quad - \sum_{i=1}^3 c_{i2} \tilde{\theta}_i^T(t) (\tilde{\theta}_i(t) + \theta_i^*) \\
& \leq \tilde{\varepsilon}_2(t) \tilde{\theta}_2^T(t) \boldsymbol{\varphi}_2(\bar{\mathbf{x}}_2(t)) + \tilde{\varepsilon}_3(t) \tilde{\theta}_3^T(t) \boldsymbol{\varphi}_3(\bar{\mathbf{x}}(t)) \\
& \quad + \tilde{\varepsilon}_1(t) \tilde{\theta}_1^T(t) \boldsymbol{\varphi}_1(x_1(t)) - \sum_{i=1}^3 \frac{c_{i2}}{2} \tilde{\theta}_i^T(t) \tilde{\theta}_i(t) \\
& \quad + \sum_{i=1}^3 \frac{c_{i2}}{2} \theta_i^{*T} \theta_i^*, \tag{41}
\end{aligned}$$

$$\begin{aligned}
\sum_{i=1}^3 \frac{1}{2c_{i+3,1}} \tilde{\varepsilon}_i(t) \dot{\tilde{\varepsilon}}_i(t) & = \sum_{i=1}^3 \frac{1}{2c_{i+3,1}} \tilde{\varepsilon}_i(t) \dot{\varepsilon}_i(t) \\
& = \sum_{i=1}^3 \tilde{\varepsilon}_i(t) \left[ \tilde{\varepsilon}_i(t) \tanh\left(\frac{\tilde{\varepsilon}_i(t)}{\lambda_i}\right) - c_{i+3,2} \tilde{\varepsilon}_i(t) \right] \\
& = \sum_{i=1}^3 \tilde{\varepsilon}_i(t) \tilde{\varepsilon}_i(t) \tanh\left(\frac{\tilde{\varepsilon}_i(t)}{\lambda_i}\right) \\
& \quad - \sum_{i=1}^3 c_{i+3,2} \tilde{\varepsilon}_i(t) (\tilde{\varepsilon}_i(t) + \varepsilon_i^*) \\
& \leq \sum_{i=1}^3 \tilde{\varepsilon}_i(t) \tilde{\varepsilon}_i(t) \tanh\left(\frac{\tilde{\varepsilon}_i(t)}{\lambda_i}\right) - \sum_{i=1}^3 \frac{c_{i+3,2}}{2} \tilde{\varepsilon}_i^2(t) \\
& \quad + \sum_{i=1}^3 \frac{c_{i+3,2}}{2} \varepsilon_i^{*2}, \\
\frac{1}{c_{71}} \tilde{d}(t) \dot{\tilde{d}}(t) & = \tilde{d}(t) \tilde{\varepsilon}_3(t) \tanh\left(\frac{\tilde{\varepsilon}_3(t)}{\lambda_3}\right) - c_{72} \tilde{d}(t) (\tilde{d}(t) + d^*) \\
& \leq \tilde{d}(t) \tilde{\varepsilon}_3(t) \tanh\left(\frac{\tilde{\varepsilon}_3(t)}{\lambda_3}\right) - \frac{c_{72}}{2} \tilde{d}^2(t) + \frac{c_{72}}{2} d^{*2}. \tag{42}
\end{aligned}$$

According to (40), (41), (42), and (43), the derivative of Lyapunov function (39) can be obtained as

$$\begin{aligned}
\dot{V}(t) & \leq -\sum_{i=1}^3 k_i \tilde{\varepsilon}_i^2(t) + \kappa \lambda_3 d^* + \kappa \sum_{i=1}^3 \lambda_i \varepsilon_i^* \\
& \quad - \sum_{i=1}^3 \frac{c_{i+3,2}}{2} \tilde{\varepsilon}_i^2(t) + \sum_{i=1}^3 \frac{c_{i+3,2}}{2} \varepsilon_i^{*2} \\
& \quad - \sum_{i=1}^3 \frac{c_{i2}}{2} \tilde{\theta}_i^T(t) \tilde{\theta}_i(t) + \sum_{i=1}^3 \frac{c_{i2}}{2} \theta_i^{*T} \theta_i^* - \frac{c_{72}}{2} \tilde{d}^2(t) \\
& \quad + \frac{c_{72}}{2} d^{*2} \\
& = -\sum_{i=1}^3 k_i \tilde{\varepsilon}_i^2(t) - \sum_{i=1}^3 \frac{c_{i+3,2}}{2} \tilde{\varepsilon}_i^2(t) \\
& \quad - \sum_{i=1}^3 \frac{c_{i2}}{2} \tilde{\theta}_i^T(t) \tilde{\theta}_i(t) - \frac{c_{72}}{2} \tilde{d}^2(t) + \kappa \lambda_3 d^* \\
& \quad + \kappa \sum_{i=1}^3 \lambda_i \varepsilon_i^* + \sum_{i=1}^3 \frac{c_{i+3,2}}{2} \varepsilon_i^{*2} + \sum_{i=1}^3 \frac{c_{i2}}{2} \theta_i^{*T} \theta_i^* \\
& \quad + \frac{c_{72}}{2} d^{*2} \\
& \leq -\frac{C_1}{2} \sum_{i=1}^3 \tilde{\varepsilon}_i^2(t) - C_2 \sum_{i=1}^3 \frac{1}{2c_{i1}} \tilde{\theta}_i^T(t) \tilde{\theta}_i(t) \\
& \quad - C_3 \sum_{i=1}^3 \frac{1}{2c_{i+3,1}} \tilde{\varepsilon}_i^2(t) - \frac{C_4}{2c_{71}} \tilde{d}^2(t) + C_5 \tag{44}
\end{aligned}$$

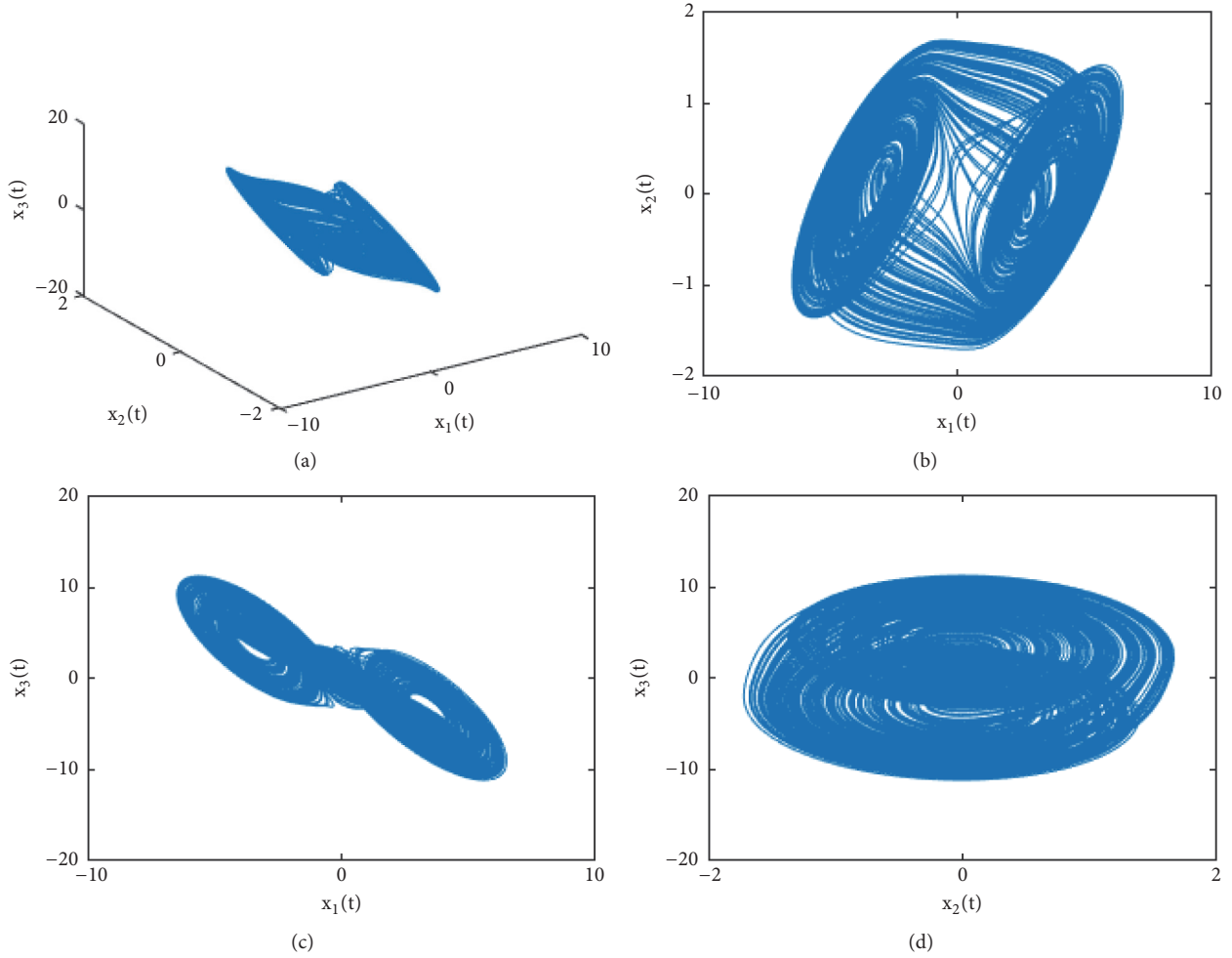


FIGURE 1: Dynamical behavior of system (4) in (a)  $x_1 - x_2 - x_3$ , (b)  $x_1 - x_2$  plane, (c)  $x_1 - x_3$  plane, and (d)  $x_2 - x_3$  plane.

where  $C_1 = 2 \min\{k_1, k_2, k_3\}$ ,  $C_2 = \min\{c_{11}c_{12}, c_{21}c_{22}, c_{31}c_{32}\}$ ,  $C_3 = \min\{c_{41}c_{42}, c_{51}c_{52}, c_{61}c_{62}\}$ ,  $C_4 = c_{71}c_{72}$ , and  $C_5 = \kappa\lambda_3 d^* + \kappa \sum_{i=1}^3 \lambda_i \varepsilon_i^* + \sum_{i=1}^3 (c_{i+3,2}/2) \varepsilon_i^{*2} + \sum_{i=1}^3 (c_{i2}/2) \theta_i^{*T} \theta_i^* + c_{72}/2$  are positive constants.

According to (44) one knows that when  $t \rightarrow \infty$ ,  $(1/2) \sum_{i=1}^3 \tilde{e}_i^2(t) \leq C_5/C_1$ ,  $\sum_{i=1}^3 (1/2c_{i1}) \tilde{\theta}_i^T(t) \tilde{\theta}_i(t) \leq C_5/C_2$ ,  $\sum_{i=1}^3 (1/2c_{i+3,1}) \tilde{e}_i^2(t) \leq C_5/C_3$ , and  $(1/2c_{71}) \tilde{d}^2(t) \leq C_5/C_4$ . That is to say, all signals in the closed-loop system will keep bounded. The tracking errors  $\tilde{e}_1(t)$ ,  $\tilde{e}_2(t)$ , and  $\tilde{e}_3(t)$  will eventually converge to a small region of zero if proper design parameters are chosen (small  $C_5$  and large  $C_1$ ).  $\square$

#### 4. Simulation Example

Let the system parameters be  $\alpha = 11.25$ ,  $\beta = 18.6$ ,  $\gamma = 0$ ,  $a = -0.68$ ,  $b = -0.545$ , and the initial condition be  $\mathbf{x}(0) = [1.5, -1, 0.5]^T$ . Then, the uncontrolled system (4) (i.e.,  $g_i(\cdot) \equiv d(t) \equiv u(t) \equiv 0$ ,  $i = 1, 2, 3$ ) shows complicated behavior, which is depicted in Figure 1.

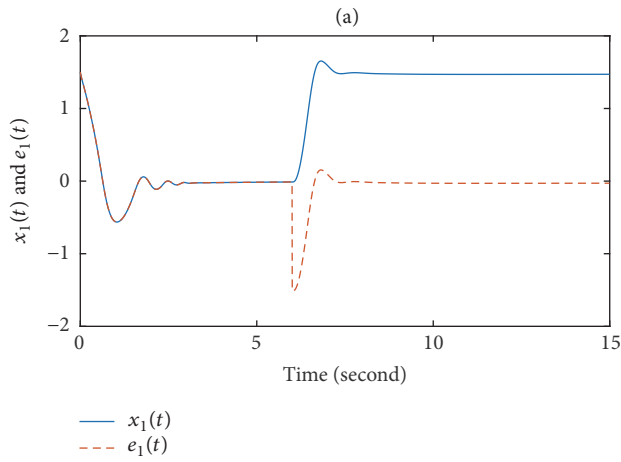
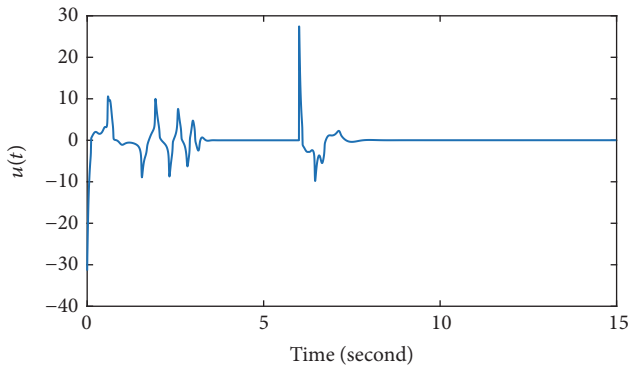
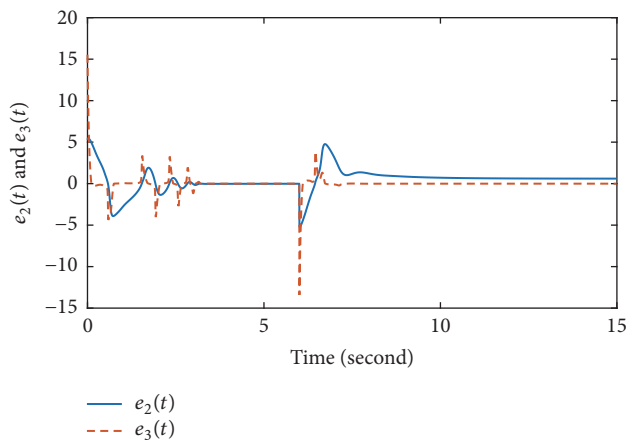
In simulation, the system uncertainties are chosen as  $g_1(x_1(t)) = \sin(x_1(t))$ ,  $g_2(\bar{\mathbf{x}}_2(t)) = \sin\sqrt{x_1^2(t) + x_2^2(t)}$ , and

$g_3(\mathbf{x}(t)) = \cos\sqrt{x_1^2(t) + x_2^2(t) + x_3^2(t)}$ . The disturbance is selected as  $d(t) = 0.2 \sin t + 0.1 \cos t$ . The referenced signal  $x_1^c(t)$  is defined by

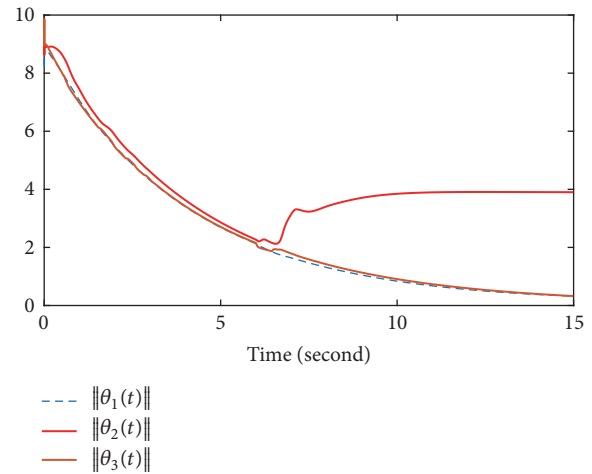
$$x_1^c(t) = \begin{cases} 0 & t \in [0, 6], \\ 1.5 & t > 6. \end{cases} \quad (45)$$

There are three FLSs used. For the first FLS, the input variable is  $x_1(t)$ , and we define 5 Gaussian membership function distributed on interval  $[-5, 5]$ . For the second one, the input variables are  $x_1(t)$  and  $x_2(t)$ . For each input, we define 5 Gaussian membership functions distributed on interval  $[-5, 5]$ . For the last one, the input variables are  $x_1(t)$ ,  $x_2(t)$ , and  $x_3(t)$ . For inputs  $x_1(t)$  and  $x_2(t)$ , we define 5 Gaussian membership functions distributed on interval  $[-5, 5]$ , and for input  $x_3(t)$ , we define 5 Gaussian membership functions distributed on interval  $[-10, 10]$ . The initial conditions for FLSs are  $\theta_1(0) = \mathbf{0}_{5 \times 1}$ ,  $\theta_2(0) = \mathbf{0}_{25 \times 1}$ , and  $\theta_3(0) = \mathbf{0}_{125 \times 1}$ .

The simulation results are presented in Figures 2–5. It has been shown that in Figure 2, the state  $x_1(t)$  tracks the referenced signal  $x_1^c(t) = 0$  for  $t \leq 5$  in about 2.5 seconds and tends to  $x_1^c(t) = 1.5$  for  $t > 5$  in a short time. The

FIGURE 2:  $x_1(t)$  and  $e_1(t)$ .FIGURE 3: Control input  $u(t)$ .FIGURE 4:  $e_2(t)$  and  $e_3(t)$ .

tracking error tends to zero rapidly. Figure 3 shows the time response of the control input  $u(t)$ . It should be pointed out that the proposed controller, the commonly used term  $\text{sign}(\cdot)$ , is not used in this paper. That is to say, our controller is smooth and bounded, just as indicated in Figure 3. Tracking errors  $e_2(t)$  and  $e_3(t)$  are presented in Figure 4. The fuzzy systems parameters are given in Figure 5. It is to know that

FIGURE 5:  $\theta_1(t)$ ,  $\theta_2(t)$ , and  $\theta_3(t)$ .

these simulation results are matched with Theorem 6, and the proposed method has good robustness.

## 5. Conclusions

In this paper, a command filtered AFBC method has been proposed for Chua's chaotic system with system uncertainties and external disturbances. It has been shown that the proposed method works well without the knowledge of any explicit uncertainty detection. One of the distinctive features of the proposed control approach consists in the fact that the problem of "explosion of complexity" in traditional backstepping design procedure is solved by the proposed first-order filter. In the stability analysis, Lyapunov stability criteria are used. The proposed command filtered AFBC can guarantee the convergence of tracking errors. Simulation results have verified our methods.

## Data Availability

The data used to support the findings of this study are available from the corresponding author upon request.

## Conflicts of Interest

The authors do not have a direct financial relation with any commercial identity mentioned in their paper that might lead to conflicts of interest for any of the authors.

## Acknowledgments

This work is supported by the National Natural Science Foundation of China under Grant no. 11771263 and the Natural Science Foundation of Anhui Province of China under Grant no. 1808085MF181.

## References

- [1] M. Krstic, I. Kanellakopoulos, and P. V. Kokotovic, *Nonlinear and Adaptive Control Design*, vol. 222, Wiley, New York, NY, USA, 1995.

- [2] H. Li, L. Wang, H. Du, and A. Boukroune, "Adaptive fuzzy backstepping tracking control for strict-feedback systems with input delay," *IEEE Transactions on Fuzzy Systems*, vol. 25, no. 3, pp. 642–652, 2017.
- [3] J.-M. Coron, L. Hu, and G. Olive, "Finite-time boundary stabilization of general linear hyperbolic balance laws via Fredholm backstepping transformation," *Automatica*, vol. 84, pp. 95–100, 2017.
- [4] H. Liu, Y. Pan, S. Li, and Y. Chen, "Adaptive Fuzzy Backstepping Control of Fractional-Order Nonlinear Systems," *IEEE Transactions on Systems, Man, and Cybernetics: Systems*, vol. 47, no. 8, pp. 2209–2217, 2017.
- [5] C. L. P. Chen, G.-X. Wen, Y.-J. Liu, and Z. Liu, "Observer-based adaptive backstepping consensus tracking control for high-order nonlinear semi-strict-feedback multiagent systems," *IEEE Transactions on Cybernetics*, vol. 46, no. 7, pp. 1591–1601, 2016.
- [6] A. Stotsky, J. K. Hedrick, and P. P. Yip, "The use of sliding modes to simplify the backstepping control method," in *Proceedings of the American Control Conference*, vol. 3, pp. 1703–1708, IEEE, June 1997.
- [7] D. Swaroop, J. K. Hedrick, P. P. Yip, and J. C. Gerdes, "Dynamic surface control for a class of nonlinear systems," *IEEE Transactions on Automatic Control*, vol. 45, no. 10, pp. 1893–1899, 2000.
- [8] J. A. Farrell, M. Polycarpou, M. Sharma, and W. Dong, "Command filtered backstepping," *IEEE Transactions on Automatic Control*, vol. 54, no. 6, pp. 1391–1395, 2008.
- [9] M. Wang and C. Wang, "Learning from adaptive neural dynamic surface control of strict-feedback systems," *IEEE Transactions on Neural Networks and Learning Systems*, vol. 26, no. 6, pp. 1247–1259, 2015.
- [10] L. Wang, W. Sun, and Y. Wu, "Adaptive fuzzy output feedback control for partial state constrained nonlinear pure feedback systems," *Mathematical Problems in Engineering*, vol. 2018, Article ID 9624938, 12 pages, 2018.
- [11] Y. Li, H. Li, and W. Sun, "Event-triggered control for robust set stabilization of logical control networks," *Automatica*, vol. 95, pp. 556–560, 2018.
- [12] J. Gu and F. Meng, "Some new nonlinear Volterra-Fredholm type dynamic integral inequalities on time scales," *Applied Mathematics and Computation*, vol. 245, pp. 235–242, 2014.
- [13] L. Gao, D. Wang, and G. Wang, "Further results on exponential stability for impulsive switched nonlinear time-delay systems with delayed impulse effects," *Applied Mathematics and Computation*, vol. 268, pp. 186–200, 2015.
- [14] C. Ma, T. Li, and J. Zhang, "Consensus control for leader-following multi-agent systems with measurement noises," *Journal of Systems Science and Complexity*, vol. 23, no. 1, pp. 35–49, 2010.
- [15] W. Sun and L. Peng, "Observer-based robust adaptive control for uncertain stochastic Hamiltonian systems with state and input delays," *Lithuanian Association of Nonlinear Analysts. Nonlinear Analysis: Modelling and Control*, vol. 19, no. 4, pp. 626–645, 2014.
- [16] H. Qin, J. Liu, X. Zuo, and L. Liu, "Approximate controllability and optimal controls of fractional evolution systems in abstract spaces," *Advances in Difference Equations*, p. 322, 2014.
- [17] F. Li and Y. Bao, "Uniform stability of the solution for a memory-type elasticity system with nonhomogeneous boundary control condition," *Journal of Dynamical and Control Systems*, vol. 23, no. 2, pp. 301–315, 2017.
- [18] Y. Guo, "Globally robust stability analysis for stochastic Cohen-Grossberg neural networks with impulse and time-varying delays," *Ukrainian Mathematical Journal*, vol. 69, no. 8, pp. 1220–1233, 2018.
- [19] F. Li and Q. Gao, "Blow-up of solution for a nonlinear Petrovsky type equation with memory," *Applied Mathematics and Computation*, vol. 274, pp. 383–392, 2016.
- [20] X. Lin and Z. Zhao, "Existence and uniqueness of symmetric positive solutions of  $2n$ -order nonlinear singular boundary value problems," *Applied Mathematics Letters*, vol. 26, no. 7, pp. 692–698, 2013.
- [21] H. Wu, "Liouville-type theorem for a nonlinear degenerate parabolic system of inequalities," *Mathematical Notes*, vol. 103, no. 1-2, pp. 155–163, 2018.
- [22] L. Liu, F. Sun, X. Zhang, and Y. Wu, "Bifurcation analysis for a singular differential system with two parameters via topological degree theory," *Nonlinear Analysis: Modelling and Control*, vol. 22, no. 1, pp. 31–50, 2017.
- [23] Y. Sun, L. Liu, and Y. Wu, "The existence and uniqueness of positive monotone solutions for a class of nonlinear Schrödinger equations on infinite domains," *Journal of Computational and Applied Mathematics*, vol. 321, pp. 478–486, 2017.
- [24] R. Xu and X. Ma, "Some new retarded nonlinear Volterra-Fredholm type integral inequalities with maxima in two variables and their applications," *Journal of Inequalities and Applications*, vol. 2017, article no. 187, 2017.
- [25] X. Peng, Y. Shang, and X. Zheng, "Lower bounds for the blow-up time to a nonlinear viscoelastic wave equation with strong damping," *Applied Mathematics Letters*, vol. 76, pp. 66–73, 2018.
- [26] Y. Sun and F. Meng, "Reachable set estimation for a class of nonlinear time-varying systems," *Complexity*, vol. 2017, Article ID 5876371, 6 pages, 2017.
- [27] D. Feng, M. Sun, and X. Wang, "A family of conjugate gradient methods for large-scale nonlinear equations," *Journal of Inequalities and Applications*, vol. 236, 2017.
- [28] X. Du and A. Mao, "Existence and multiplicity of nontrivial solutions for a class of semilinear fractional Schrödinger equations," *Journal of Function Spaces*, vol. 2017, Article ID 3793872, 7 pages, 2017.
- [29] H. Liu and F. Meng, "Some new generalized Volterra-Fredholm type discrete fractional sum inequalities and their applications," *Journal of Inequalities and Applications*, vol. 2016, no. 1, article 213, 2016.
- [30] J. Zhang, Z. Lou, Y. Ji, and W. Shao, "Ground state of Kirchhoff type fractional Schrödinger equations with critical growth," *Journal of Mathematical Analysis and Applications*, vol. 462, no. 1, pp. 57–83, 2018.
- [31] M. Li and J. Wang, "Exploring delayed Mittag-Leffler type matrix functions to study finite time stability of fractional delay differential equations," *Applied Mathematics and Computation*, vol. 324, pp. 254–265, 2018.
- [32] T. Shen, J. Xin, and J. Huang, "Time-space fractional stochastic Ginzburg-Landau equation driven by gaussian white noise," *Stochastic Analysis and Applications*, vol. 36, no. 1, pp. 103–113, 2018.
- [33] J. Wang, Y. Yuan, and S. Zhao, "Fractional factorial split-plot designs with two- and four-level factors containing clear effects," *Communications in Statistics—Theory and Methods*, vol. 44, no. 4, pp. 671–682, 2015.
- [34] R. Xu and Y. Zhang, "Generalized Gronwall fractional summation inequalities and their applications," *Journal of Inequalities and Applications*, vol. 2015, no. 42, 2015.

- [35] Y. Yuan and S.-l. Zhao, "Mixed two- and eight-level fractional factorial split-plot designs containing clear effects," *Acta Mathematicae Applicatae Sinica*, vol. 32, no. 4, pp. 995–1004, 2016.
- [36] L. Zhang and Z. Zheng, "Lyapunov type inequalities for the Riemann-Liouville fractional differential equations of higher order," *Advances in Difference Equations*, vol. 2017, no. 1, p. 270, 2017.
- [37] Y. Pan and H. Yu, "Biomimetic hybrid feedback feedforward neural-network learning control," *IEEE Transactions on Neural Networks and Learning Systems*, vol. 28, no. 6, pp. 1481–1487, 2017.
- [38] T. Wang, Y. Zhang, J. Qiu, and H. Gao, "Adaptive fuzzy backstepping control for a class of nonlinear systems with sampled and delayed measurements," *IEEE Transactions on Fuzzy Systems*, vol. 23, no. 2, pp. 302–312, 2015.
- [39] Y.-J. Liu, Y. Gao, S. Tong, and Y. Li, "Fuzzy approximation-based adaptive backstepping optimal control for a class of nonlinear discrete-time systems with dead-zone," *IEEE Transactions on Fuzzy Systems*, vol. 24, no. 1, pp. 16–28, 2016.
- [40] H. K. Khalil, *Nonlinear Control*, Pearson, New York, NY, USA, 2015.
- [41] Z. Liu, B. Chen, and C. Lin, "Adaptive neural backstepping for a class of switched nonlinear system without strict-feedback form," *IEEE Transactions on Systems, Man, and Cybernetics: Systems*, vol. 47, no. 7, pp. 1315–1320, 2017.
- [42] H. Gao, Y. Song, and C. Wen, "Backstepping design of adaptive neural fault-tolerant control for MIMO nonlinear systems," *IEEE Transactions on Neural Networks and Learning Systems*, vol. 28, no. 11, pp. 2605–2613, 2017.
- [43] J. Yu, P. Shi, and L. Zhao, "Finite-time command filtered backstepping control for a class of nonlinear systems," *Automatica*, vol. 92, pp. 173–180, 2018.
- [44] H. Liu, S. Li, J. D. Cao, A. G. Alsaedi, and F. E. Alsaadi, "Adaptive fuzzy prescribed performance controller design for a class of uncertain fractional-order nonlinear systems with external disturbances," *Neurocomputing*, vol. 219, pp. 422–430, 2017.
- [45] Y. Li, S. Sui, and S. Tong, "Adaptive fuzzy control design for stochastic nonlinear switched systems with arbitrary switchings and unmodeled dynamics," *IEEE Transactions on Cybernetics*, vol. 47, no. 2, pp. 403–414, 2017.
- [46] N. Wang, J.-C. Sun, and M. J. Er, "Tracking-error-based universal adaptive fuzzy control for output tracking of nonlinear systems with completely unknown dynamics," *IEEE Transactions on Fuzzy Systems*, vol. 26, no. 2, pp. 869–883, 2018.
- [47] H. Liu, S. Li, G. Li, and H. Wang, "Adaptive controller design for a class of uncertain fractional-order nonlinear systems: an adaptive fuzzy approach," *International Journal of Fuzzy Systems*, vol. 20, no. 2, pp. 366–379, 2018.
- [48] H. Liu, S. Li, H. Wang, and Y. Sun, "Adaptive fuzzy control for a class of unknown fractional-order neural networks subject to input nonlinearities and dead-zones," *Information Sciences*, vol. 454–455, pp. 30–45, 2018.
- [49] Y. Wang, L. Cao, S. Zhang, X. Hu, and F. Yu, "Command filtered adaptive fuzzy backstepping control method of uncertain nonlinear systems," *IET Control Theory & Applications*, vol. 10, no. 10, pp. 1134–1141, 2016.
- [50] U. Sadek, A. Sarjaš, A. Chowdhury, and R. Svečko, "Improved adaptive fuzzy backstepping control of a magnetic levitation system based on Symbiotic Organism Search," *Applied Soft Computing*, vol. 56, pp. 19–33, 2017.
- [51] Y. Pan and H. Yu, "Dynamic surface control via singular perturbation analysis," *Automatica*, vol. 57, pp. 29–33, 2015.
- [52] J. Ma, Z. Zheng, and P. Li, "Adaptive dynamic surface control of a class of nonlinear systems with unknown direction control gains and input saturation," *IEEE Transactions on Cybernetics*, vol. 45, no. 4, pp. 728–741, 2015.

## Research Article

# A New Approach to Adaptive Stabilization of Stochastic High-Order Nonholonomic Systems

Guangju Li <sup>1</sup> and Kemei Zhang <sup>2</sup>

<sup>1</sup>Institute of Automation, Qufu Normal University, Shandong Province 273165, China

<sup>2</sup>School of Mathematics Sciences, Qufu Normal University, Shandong Province 273165, China

Correspondence should be addressed to Kemei Zhang; zhkm90@126.com

Received 6 May 2018; Accepted 10 July 2018; Published 18 September 2018

Academic Editor: Weihai Zhang

Copyright © 2018 Guangju Li and Kemei Zhang. This is an open access article distributed under the Creative Commons Attribution License, which permits unrestricted use, distribution, and reproduction in any medium, provided the original work is properly cited.

This paper studies the problem of adaptive stabilization for a class of stochastic high-order nonholonomic systems. Under the weaker assumptions, by constructing the appropriate Lyapunov function and combining sign function technique, an adaptive state feedback controller is designed to guarantee global asymptotic stability in probability of the closed-loop system. The effectiveness of the controller is demonstrated by a mechanical system.

## 1. Introduction

Ever since the stochastic stability theory was established by [1, 2], the design and analysis of backstepping controller for stochastic nonlinear systems has achieved remarkable development in recent years; see [1, 3–12] and the references therein. But these papers do not consider stochastic nonholonomic systems.

In this paper, we consider stochastic high-order nonholonomic systems

$$\begin{aligned} dx_0 &= d_0(t, \theta) u_0^{p_0} dt + f_0(x_0, \theta) dt + g_0^\top(x_0, \theta) d\omega, \\ dx_i &= d_i(t, \theta) u_0^{q_i} x_{i+1}^{p_i} dt + f_i(x_0, x, \theta) dt \\ &\quad + g_i^\top(x_0, x, \theta) d\omega, \\ dx_n &= d_n(t, \theta) u_0^{q_n} u^{p_n} dt + f_n(x_0, x, \theta) dt \\ &\quad + g_n^\top(x_0, x, \theta) d\omega, \end{aligned} \quad (1)$$

where  $x_0 \in R$  and  $x = (x_1, \dots, x_n)^\top \in R^n$  are system states,  $u_0$  and  $u$  are control inputs,  $p_i \in R_{odd}^{\geq 1} \triangleq \{p/q | p \text{ and } q \text{ are positive odd integers, and } p \geq q\}$  are odd integers, and  $q_i \geq 0$  are constants,  $i = 1, \dots, n$ .  $\theta \in R^m$  is an unknown constant vector.  $\omega$  is a  $r$ -dimensional standard Wiener process defined on a probability space  $(\Omega, \mathcal{F}, P)$  with

$\Omega$  being a sample space,  $\mathcal{F}$  being a filtration, and  $P$  being a probability measure.  $f_0(x_0, \theta) : R \times R^m \rightarrow R$ ,  $g_0(x_0, \theta) : R \times R^m \rightarrow R^r$ ,  $f_i(x_0, x, \theta) : R \times R^n \times R^r \rightarrow R$ ,  $g_i(x_0, x, \theta) : R \times R^n \times R^r \rightarrow R^r$ ,  $i = 1, \dots, n$ , are locally Lipschitz functions.  $d_i(t, \theta)$ ,  $i = 0, \dots, n$ , are nonlinear control coefficients.

Since many mechanical systems can be modeled by system (1), a series of theoretical results have been obtained. To mention a few, [13–16] investigated the deterministic case of  $g_i = 0$ . Specially when  $d_i = p_i = q_i = 1$  and  $f_i = 0$ , the authors designed a continuous controller by proposing a sliding mode control approach in [13]. When systems contain nonlinear drifts and unknown time-varying coefficients, [15] presented an adaptive control approach to achieve state-feedback stabilization. High-order nonholonomic systems, that is,  $p_i \geq 1$ , were introduced in [16]. The design procedure in [16] combined the idea of a discontinuous change of coordinate and adding a power integrator. However, it did not consider nonlinear parameterizations. Because many practical control systems such as biochemical processes and machines with friction often contain unknown parameters, [14] studied the problem of adaptive stabilization control design for a class of high-order nonholonomic systems with strong nonlinear drifts. Since stochastic noise frequently arises and is inevitable in practical control systems, how to extend these approaches to stochastic high-order nonholonomic systems is a very interesting problem. When  $g_i \neq 0$ , [17] studied the problem of

state feedback stabilization for a class of high-order stochastic nonholonomic systems with disturbed control directions and more general nonlinear drifts. However, nonlinear parameterization and nonlinear drift term in  $x_0$ -subsystem were not discussed in [17]. Unfortunately, all these mentioned results require that the nonlinearities  $f_i(\cdot)$  are dependent on  $(x_1, \dots, x_i)$ . Naturally, an interesting problem is put forward: *For system (1), under weaker assumptions, can a stabilizable state feedback controller be designed?*

In this paper, we will provide a satisfactory answer to this problem. By constructing the appropriate Lyapunov function, skillfully combining parameter separation, sign function, and backstepping design approach, an adaptive state feedback controller is designed to guarantee global asymptotic stability in probability of the closed-loop system. Finally, a simulation example is used to demonstrate the effectiveness of this approach.

The contributions and difficulties of this paper are highlighted from three aspects.

(i) The system under consideration is more general than those investigated in [13–17]. System (1) has unknown control coefficients and permits unknown parameters to enter nonlinear equations. Nonlinear functions  $f_i(\cdot)$  are dependent on  $(x_1, \dots, x_{i+1})$ , which makes discontinuous change of coordinates be inapplicable to the adaptive state feedback control of systems (1). In this paper, we propose a novel design approach to solve this obstacle.

(ii) The unknown growth rates of the upper bounds of  $f_i(\cdot)$  and  $g_i(\cdot)$  are extended; see Remark 13. Therefore, some new mathematical tools, such as sign function and transformation technique, are introduced to simplify the construction of Lyapunov function.

(iii) An practical example for mobile robot with small angle measurement error is modeled and solved by the proposed approach.

This paper is organized as follows. Section 2 gives some preliminaries. Section 3 presents the design and analysis of the adaptive controller, following a practical example in Section 4. Section 5 concludes this paper. The proofs of Propositions 16–19 are given in Appendix.

## 2. Mathematical Preliminaries

Some notations and definitions will be used throughout this paper.  $R^+$  stands for the set of all nonnegative real numbers and  $R^n$  denotes real  $n$ -dimensional space. For vector  $\chi = (\chi_1, \dots, \chi_n)^\top$ ,  $\bar{\chi}_i$  represents  $(\chi_1, \dots, \chi_i)^\top$ . For a given vector or matrix  $x$ ,  $x^\top$  denotes its transpose,  $|x|$  is the Euclidean norm of a vector  $x$ , and  $\text{Tr}\{x\}$  denotes its trace when  $x$  is square.  $\mathcal{C}^i$  denotes the set of all functions with continuous  $i$ th partial derivatives.  $\mathcal{K}$  denotes the set of all functions:  $R^+ \rightarrow R^+$  that are continuous, strictly increasing, and vanishing at zero;  $\mathcal{K}_\infty$  denotes the set of all functions that are of class  $\mathcal{K}$  and unbounded. For any  $y \in R$ , sign function  $\text{sgn}(y)$  is defined as  $\text{sgn}(y) = 1$  if  $y > 0$ ;  $\text{sgn}(y) = 0$  if  $y = 0$  and  $\text{sgn}(y) = -1$  if  $y < 0$ . For simplicity, we denote  $\lceil y \rceil^p = |y|^p \text{sgn}(y)$ . The arguments of functions are sometimes omitted or simplified, for example, a function  $f(x(t))$  is denoted by  $f(x)$  or  $f$ .

In what follows, we present some definitions and lemmas which will be frequently used in the design and analysis of controller. Consider stochastic nonlinear system

$$\begin{aligned} dx &= f(x, \theta) dt + g(x, \theta) d\omega, \\ x(t_0) &= x_0 \in R^n, \end{aligned} \quad (2)$$

where  $\omega$  is a  $r$ -dimensional standard Wiener process defined on a probability space  $(\Omega, \mathcal{F}, P)$ ,  $x \in R^n$  is system state,  $\theta \in R^m$  is an unknown constant vector and the functions  $f: R^n \times R^m \rightarrow R^n$ , and  $g: R^n \times R^m \rightarrow R^{n \times r}$  are locally bounded and locally Lipschitz with respect to  $x$ .

*Definition 1* (see [1]). The equilibrium  $x(t) = 0$  of system (2) with  $f(0, \theta) = 0$ ,  $g(0, \theta) = 0$  is

(i) globally stable in probability if for any  $\varepsilon > 0$ , there exists a class  $\mathcal{K}$  function  $r(\cdot)$  such that  $P\{|x(t)| < r(x_0)\} \geq 1 - \varepsilon$ , for any  $t \geq 0$ ,  $x_0 \in R^n \setminus \{0\}$

(ii) globally asymptotically stable in probability if it is globally stable in probability and  $P\{\lim_{t \rightarrow \infty} |x(t)| = 0\} = 1$ , for any  $x_0 \in R^n$

**Lemma 2** (see [1]). *For system (2), if there exists a  $\mathcal{C}^2$  function  $V(x): R^n \rightarrow R^+$  and class  $\mathcal{K}_\infty$  functions  $\alpha_1(\cdot)$  and  $\alpha_2(\cdot)$ , such that*

$$\begin{aligned} \alpha_1(|x|) &\leq V(x) \leq \alpha_2(|x|), \\ \mathcal{L}V(x) &= \frac{\partial V(x)}{\partial x} f(x, \theta) \\ &\quad + \frac{1}{2} \text{Tr} \left\{ g^\top(x, \theta) \frac{\partial^2 V(x)}{\partial x^2} g(x, \theta) \right\} \\ &\leq -W(x), \end{aligned} \quad (3)$$

where  $W(x)$  is a nonnegative continuous function, then, for any  $x(t_0) \in R^n$ ,

(i) there exists an almost surely unique solution on  $[t_0, \infty)$

(ii) the equilibrium  $x = 0$  is globally stable in probability, and the solution  $x(t)$  satisfies  $P\{\lim_{t \rightarrow \infty} W(x(t)) = 0\} = 1$

**Lemma 3** (see [18]). *For any real-valued continuous function  $h(x, y)$ , where  $x \in R^m$ ,  $y \in R^n$ , there are smooth scalar functions  $c(x) \geq 1$  and  $d(y) \geq 1$ , such that  $|h(x, y)| \leq c(x)d(y)$ .*

**Lemma 4** (see [19]). *Let  $x, y$  be real variables, then for any positive real numbers  $b, c, d$  and continuous function  $a(\cdot) \geq 0$ , one has  $a(\cdot)|x|^c|y|^d \leq b|x|^{c+d} + (d/(c+d))((c+d)/c)^{-c/d} a(\cdot)^{(c+d)/d} b^{-c/d} |y|^{c+d}$ .*

**Lemma 5** (see [20]).  *$f(x) = [x]^a$  is continuously differentiable and  $\dot{f}(x) = a|x|^{a-1}$ , where  $a \geq 1$ ,  $x \in R$ . Moreover,  $df(x(t))/dt = a|x(t)|^{a-1}\dot{x}(t)$ .*

**Lemma 6** (see [20]). *If  $p = a/b \in R_{\text{odd}}^{\geq 1}$ ,  $b \geq 1$ , then  $|x^p - y^p| \leq 2^{1-1/b} [|x|^a - |y|^a]^{1/b}$  for any  $x, y \in R$ .*

**Lemma 7** (see [20]). *For given  $r \geq 0$  and every  $x \in R, y \in R$ ,  $|x + y|^r \leq C_r(|x|^r + |y|^r)$  holds, where  $C_r = 2^{r-1}$  if  $r \geq 1$  and  $C_r = 1$  if  $0 \leq r < 1$ .*

**Lemma 8** (see [20]). *Let  $f : [a, b] \rightarrow R$  be a continuous monotone function with  $f(a) = 0$ ; then  $|\int_a^b f(x)dx| \leq |f(b)||b - a|$ .*

### 3. Design and Analysis of Adaptive Controller

**3.1. Problem Formulation and Assumptions.** The aim of this paper is to design an adaptive state feedback controller for system (1) to guarantee global asymptotic stability in probability of the closed-loop system. We need the following assumptions to achieve this aim.

**Assumption 9.** The sign of  $d_i(t, \theta)$ ,  $i = 0, \dots, n$ , is assumed to be positive, and there exist smooth functions  $0 < \lambda_{i,1}(t) \leq \lambda_{i,2}(t, \theta)$ , such that

$$0 < \lambda_{i,1}(t) \leq d_i(t, \theta) \leq \lambda_{i,2}(t, \theta). \quad (4)$$

**Assumption 10.** For smooth functions  $f_0(x_0, \theta)$  and  $g_0(x_0, \theta)$ , there exist bounded smooth functions  $\alpha_0(x_0, \theta)$ ,  $\beta_0(x_0, \theta)$  such that

$$\begin{aligned} f_0(x_0, \theta) &= x_0 \alpha_0(x_0, \theta), \\ g_0(x_0, \theta) &= x_0 \beta_0(x_0, \theta). \end{aligned} \quad (5)$$

**Assumption 11.** For  $i = 1, \dots, n$ , there exist nonnegative continuous functions  $\alpha_i(x_0, \bar{x}_i, \theta)$ ,  $\beta_i(x_0, \bar{x}_i, \theta)$  and a constant  $\tau$  satisfying  $-r_n < \tau < 0$  such that

$$\begin{aligned} |f_i(x_0, x, \theta)| &\leq \left( |x_1|^{(r_i+\tau)/r_1} + \dots + |x_i|^{(r_i+\tau)/r_i} \right) \alpha_i(x_0, \bar{x}_i, \theta) \\ &\quad + c_i u_0^{q_i} d_i(t, \theta) |x_{i+1}|^{(r_i+\tau)/r_{i+1}}, \end{aligned} \quad (6)$$

$$\begin{aligned} |g_i(x_0, x, \theta)| &\leq \left( |x_1|^{(2r_i+\tau)/2r_1} + \dots + |x_i|^{(2r_i+\tau)/2r_i} \right) \beta_i(x_0, \bar{x}_i, \theta), \end{aligned}$$

where  $r_{n+1}$  is a given positive constant and  $r_1, \dots, r_n$  are recursively defined by  $r_i = p_i r_{i+1} - \tau$  and nonnegative constants  $c_i < 1/2^{p_i-1}$ .

**Remark 12.** Assumptions 10–11 imply that  $f_0(0, \theta) = 0$ ,  $g_0(0, \theta) = 0$ ,  $f_i(0, 0, \theta) = 0$ ,  $g_i(0, 0, \theta) = 0$ ,  $i = 1, \dots, n$ ; that is, origin is the equilibrium of system (1).

**Remark 13.** Assumption 11 enlarges the scope of nonholonomic systems. Specifically, if state  $x_{i+1}$  does not appear in the nonlinear function  $f_i(\cdot)$ , Assumption 11 is degenerated into the following form:

$$\begin{aligned} |f_i(x_0, x, \theta)| &\leq \left( |x_1|^{(r_i+\tau)/r_1} + \dots + |x_i|^{(r_i+\tau)/r_i} \right) \alpha_i(x_0, \bar{x}_i, \theta), \\ |g_i(x_0, x, \theta)| &\leq \left( |x_1|^{(2r_i+\tau)/2r_1} + \dots + |x_i|^{(2r_i+\tau)/2r_i} \right) \beta_i(x_0, \bar{x}_i, \theta), \end{aligned} \quad (7)$$

where  $r_1 = 1$ ,  $r_i = 1 + (i - 1)\tau$  with  $\tau$  being a constant for each  $i = 1, \dots, n$ . Particularly, when  $\tau = 0$ , (7) becomes the following growth condition:

$$\begin{aligned} |f_i(x_0, x, \theta)| &\leq (|x_1| + \dots + |x_i|) \alpha_i(x_0, \bar{x}_i, \theta), \\ |g_i(x_0, x, \theta)| &\leq (|x_1| + \dots + |x_i|) \beta_i(x_0, \bar{x}_i, \theta). \end{aligned} \quad (8)$$

If  $\alpha_i(x_0, \bar{x}_i, \theta)$  and  $\beta_i(x_0, \bar{x}_i, \theta)$  are constants, (8) becomes the linear growth condition in [21]. If  $\alpha_i(x_0, \bar{x}_i, \theta)$  and  $\beta_i(x_0, \bar{x}_i, \theta)$  are smooth nonnegative functions, (8) becomes the linear growth condition in [22, 23]. When  $\tau = -p/q \in (-2/(4n + 1), 0)$  with  $p$  being an even integer and  $q$  being an odd integer, condition (7) becomes the low-order growth condition in [24, 25]. Assumption 11 extends the value of  $\tau$  to an explicit interval rather than a ratio of an even integer over an odd integer.

**Remark 14.** By Lemma 3, there are smooth scalar functions  $\tilde{\lambda}_{i,2}(t) \geq 1$ ,  $\bar{\alpha}_i(x_0, \bar{x}_i) \geq 1$ ,  $\bar{\beta}_i(x_0, \bar{x}_i) \geq 1$ ,  $i = 0, \dots, n$ , and  $\Theta(\theta) \geq 1$  such that

$$\begin{aligned} \lambda_{i,1}(t) &\leq d_i(t, \theta) \leq \tilde{\lambda}_{i,2}(t) \Theta, \\ |f_0(x_0, \theta)| &\leq |x_0| \bar{\alpha}_0(x_0) \Theta, \\ |g_0(x_0, \theta)| &\leq |x_0| \bar{\beta}_0(x_0) \Theta, \\ |f_i(x_0, x, \theta)| &\leq \left( |x_1|^{(r_i+\tau)/r_1} + \dots + |x_i|^{(r_i+\tau)/r_i} \right) \bar{\alpha}_i(x_0, \bar{x}_i) \Theta \\ &\quad + c_i u_0^{q_i} d_i(t, \theta) |x_{i+1}|^{(r_i+\tau)/r_{i+1}}, \\ |g_i(x_0, x, \theta)| &\leq \left( |x_1|^{(2r_i+\tau)/2r_1} + \dots + |x_i|^{(2r_i+\tau)/2r_i} \right) \bar{\beta}_i(x_0, \bar{x}_i) \Theta. \end{aligned} \quad (9)$$

**3.2. Stability and Convergence Analysis.** We state the main result in this paper.

**Theorem 15.** *If Assumptions 9–11 hold for system (1), under an appropriate controller, the origin of the closed-loop system is globally asymptotically stable in probability for any initial condition.*

**Proof.** The proof is based on inductive argument. Firstly, we design an adaptive controller by considering two cases:  $x_0(t_0) \neq 0$  and  $x_0(t_0) = 0$ .

**Case I** ( $x_0(t_0) \neq 0$ ). The structure of system (1) means that the design procedure is divided into two separate parts.

**Part I** (design of controller  $u_0$ ). Let us consider  $x_0$ -subsystem in system (1), define  $\Theta_0 = \lambda_{0,1}^{-1} \max\{\lambda_{0,1}^{-1}, \Theta, \Theta^2\}$ , and choose  $V_0 = x_0^4/4 + (\lambda_{0,1}/2)\tilde{\Theta}_0^2$ , where  $\tilde{\Theta}_0 = \Theta_0 - \hat{\Theta}_0$ . From Remark 14, it follows that

$$\begin{aligned} \mathcal{L}V_0 &= x_0^3 (d_0 u_0^{p_0} + f_0) + \frac{3}{2} \text{Tr} \{g_0 x_0^2 g_0^\top\} - \lambda_{0,1} \tilde{\Theta}_0 \hat{\Theta}_0 \\ &\leq -\frac{a}{\lambda_{0,1}} x_0^4 + \frac{a}{\lambda_{0,1}} x_0^4 + x_0^3 d_0 u_0^{p_0} + \Theta \bar{\alpha}_0(x_0) x_0^4 \end{aligned}$$

$$\begin{aligned}
& + \frac{3}{2} \Theta^2 \bar{\beta}_0^2(x_0) x_0^4 - \lambda_{0,1} \bar{\Theta}_0 \hat{\Theta}_0 \\
& \leq -\frac{a}{\lambda_{0,1}} x_0^4 + \lambda_{0,1} x_0^3 \left( \frac{d_0}{\lambda_{0,1}} u_0^{p_0} + h(x_0) \bar{\Theta}_0 x_0 \right) \\
& \quad - \lambda_{0,1} \bar{\Theta}_0 \left( \hat{\Theta}_0 - x_0^4 h(x_0) \right),
\end{aligned} \tag{10}$$

where  $a$  is a positive constant and  $h(x_0) = a + \bar{\alpha}_0(x_0) + (3/2)\bar{\beta}_0^2(x_0)$  is a positive smooth function. Substituting the adaptive controller

$$\begin{aligned}
u_0 &= - \left( x_0 h(x_0) \sqrt{\bar{\Theta}_0^2 + 1} \right)^{1/p_0}, \\
\dot{\hat{\Theta}}_0 &= x_0^4 h(x_0)
\end{aligned} \tag{11}$$

into (10) leads to

$$\mathcal{L}V_0 \leq -\frac{a}{\lambda_{0,1}} x_0^4. \tag{12}$$

The succeeding proposition characterizes the features of  $x_0$ -subsystem.

**Proposition 16.** *If Assumptions 9-10 hold for  $x_0$ -subsystem, controller (11) guarantees that*

- (i)  $x_0$ -subsystem has an almost surely unique solution on  $[t_0, \infty)$  for any  $x_0(t_0) \neq 0$
- (ii) the equilibrium  $x_0 = 0$  of  $x_0$ -subsystem is globally asymptotically stable in probability
- (iii) the solution of  $x_0$ -subsystem and  $u_0$  does not cross zero for any  $x_0(t_0) \neq 0$

*Proof.* See Appendix.  $\square$

*Part II (design of controller  $u$ ).* In this part, we need to consider  $x_i$ -subsystem in system (1). With the help of Proposition 16, controller  $u$  will be recursively constructed by applying the adding a power integrator approach. Before the beginning of recursive design, we define  $\Theta_1 = \max\{1, \Theta, \Theta^2\}$  and state transformation

$$\begin{aligned}
\xi_1 &= [x_1]^{\sigma/r_1} - [x_1^*]^{\sigma/r_1}, \quad x_1^* = 0, \\
\xi_2 &= [x_2]^{\sigma/r_2} - [x_2^*]^{\sigma/r_2}, \\
x_2^* &= -\phi_1(x_0, x_1, \bar{\Theta}_1) [\xi_1]^{r_2/\sigma}, \\
&\vdots \\
\xi_k &= [x_k]^{\sigma/r_k} - [x_k^*]^{\sigma/r_k}, \\
x_k^* &= -\phi_{k-1}(x_0, \bar{x}_{k-1}, \bar{\Theta}_1) [\xi_{k-1}]^{r_k/\sigma},
\end{aligned} \tag{13}$$

where  $\sigma$  is a positive constant satisfying the relationship  $\sigma \geq \max\{p_1 r_2, \dots, p_n r_{n+1}\}$ ,  $\bar{\Theta}_1$  is the estimate of  $\Theta_1$ , and functions  $\phi_k(\cdot)$  satisfying  $\text{sgn}(\phi_k) = \text{sgn}(u_0^{q_k})$  will be determined later.

To solve the problem caused by sign function, the definition of  $W_k(x_0, \bar{x}_k, \bar{\Theta}_1)$  is given by

$$\begin{aligned}
W_k(x_0, \bar{x}_k, \bar{\Theta}_1) &= \int_{x_k^*}^{x_k} \left[ |s|^{\sigma/r_k} - |x_k^*|^{\sigma/r_k} \right]^{(4l\sigma - \tau - r_k)/\sigma} ds,
\end{aligned} \tag{14}$$

where  $k = 1, \dots, n$  and  $4l$  is an even number and satisfies  $(4l - 2)\sigma \geq \tau + r_k$ .

**Proposition 17.**  *$W_k$  is  $\mathcal{C}^2$  function and satisfies  $C_{k1} |x_k - x_k^*|^{(4l\sigma - \tau)/r_k} \leq W_k \leq C_{k2} |\xi_k|^{(4l\sigma - \tau)/\sigma}$ , where  $C_{k1} = 2^{(\sigma - r_k)(4l\sigma - \tau - r_k)/\sigma r_k} (r_k/(4l\sigma - \tau))$ ,  $C_{k2} = 2^{1 - r_k/\sigma}$ ,  $k = 1, \dots, n$ .*

*Proof.* See Appendix.  $\square$

To obtain the expression of  $u$ , we determine  $\phi_1, \dots, \phi_n$  by induction, the design procedure is implemented as follows.

*Step 1.* Let  $V_1 = W_1 + (1/2)\bar{\Theta}_1^2$ , where  $\bar{\Theta}_1 = \Theta_1 - \hat{\Theta}_1$ . By using (13), (A.3), (A.7), and Lemma 7, we get

$$\begin{aligned}
\mathcal{L}V_1 &\leq [\xi_1]^{(4l\sigma - \tau - r_1)/\sigma} \left( d_1 u_0^{q_1} x_2^{p_1} + f_1 \right) \\
&\quad + \frac{4l\sigma - \tau - r_1}{2r_1} |\xi_1|^{((4l-1)\sigma - \tau - r_1)/\sigma} |x_1|^{(\sigma - r_1)/r_1} |g_1|^2 \\
&\quad - \bar{\Theta}_1 \hat{\Theta}_1 \leq -n \xi_1^{4l} + n \xi_1^{4l} \\
&\quad + [\xi_1]^{(4l\sigma - \tau - r_1)/\sigma} d_1 u_0^{q_1} \left( x_2^{p_1} - x_2^{*p_1} \right) \\
&\quad + [\xi_1]^{(4l\sigma - \tau - r_1)/\sigma} d_1 u_0^{q_1} x_2^{*p_1} - \bar{\Theta}_1 \hat{\Theta}_1 \\
&\quad + \frac{4l\sigma - \tau - r_1}{2r_1} |\xi_1|^{((4l-1)\sigma - \tau - r_1)/\sigma} |x_1|^{(\sigma + r_1 + \tau)/r_1} \bar{\beta}_1^2 \Theta^2 \\
&\quad + [\xi_1]^{(4l\sigma - \tau - r_1)/\sigma} \\
&\quad \cdot \left( |x_1|^{(r_1 + \tau)/r_1} \bar{\alpha}_1 \Theta + c_1 d_1 u_0^{q_1} |x_2|^{p_1} \right).
\end{aligned} \tag{15}$$

Clearly, the application of the fact  $[\xi_1]^{(4l\sigma - \tau - r_1)/\sigma} d_1 u_0^{q_1} x_2^{*p_1} \leq 0$  implies

$$\begin{aligned}
& [\xi_1]^{(4l\sigma - \tau - r_1)/\sigma} u_0^{q_1} d_1 x_2^{*p_1} \\
& + [\xi_1]^{(4l\sigma - \tau - r_1)/\sigma} c_1 d_1 u_0^{q_1} |x_2|^{p_1} \\
& \leq [\xi_1]^{(4l\sigma - \tau - r_1)/\sigma} u_0^{q_1} d_1 x_2^{*p_1} \\
& + |\xi_1|^{(4l\sigma - \tau - r_1)/\sigma} \bar{c}_1 d_1 |u_0|^{q_1} |x_2^*|^{p_1} \\
& + |\xi_1|^{(4l\sigma - \tau - r_1)/\sigma} \bar{c}_1 d_1 |u_0|^{q_1} |\xi_2|^{(r_1 + \tau)/\sigma} \\
& \leq [\xi_1]^{(4l\sigma - \tau - r_1)/\sigma} d_1 u_0^{q_1} (1 - \bar{c}_1) x_2^{*p_1} \\
& + |\xi_1|^{(4l\sigma - \tau - r_1)/\sigma} \bar{c}_1 d_1 |u_0|^{q_1} |\xi_2|^{(r_1 + \tau)/\sigma},
\end{aligned} \tag{16}$$

where  $\bar{c}_1 = 2^{p_1-1}c_1$  is a positive constant. Substituting (16) into (15) and choosing

$$\begin{aligned} x_2^* &= - \left( \frac{1}{\lambda_{1,1} u_0^{q_1} (1 - \bar{c}_1)} \right. \\ &\quad \cdot \widehat{\Theta}_1 \left( \bar{\alpha}_1 + n + \frac{4l\sigma - \tau - r_1}{2r_1} \bar{\beta}_1^2 \right) \Big)^{1/p_1} |\xi_1|^{r_2/\sigma} \quad (17) \\ &\triangleq -\phi_1(x_0, x_1, \widehat{\Theta}_1) |\xi_1|^{r_2/\sigma}, \end{aligned}$$

one has

$$\begin{aligned} \mathcal{L}V_1 &\leq -n\xi_1^{4l} + |\xi_1|^{(4l\sigma - \tau - r_1)/\sigma} d_1 u_0^{q_1} (x_2^{p_1} - x_2^{*p_1}) \\ &\quad + (\Psi_1 - \widehat{\Theta}_1) (\bar{\Theta}_1 + \eta_1) \quad (18) \\ &\quad + \bar{c}_1 d_1 |u_0|^{q_1} |\xi_1|^{(4l\sigma - \tau - r_1)/\sigma} |\xi_2|^{(r_1 + \tau)/\sigma}, \end{aligned}$$

where  $\Psi_1 = \xi_1^{4l} (\bar{\alpha}_1 + n + ((4l\sigma - \tau - r_1)/2r_1) \bar{\beta}_1^2) \geq 0$  and  $\eta_1 = 0$ .

*Step k* ( $k = 2, \dots, n$ ). At Step  $k - 1$ , assume that there exists a  $\mathcal{C}^2$  function  $V_{k-1}$  and virtual controllers  $x_2^*, \dots, x_k^*$  such that

$$\begin{aligned} \mathcal{L}V_{k-1} &\leq -(n - k + 2) \sum_{i=1}^{k-1} \xi_i^{4l} \\ &\quad + |\xi_{k-1}|^{(4l\sigma - \tau - r_{k-1})/\sigma} d_{k-1} u_0^{q_{k-1}} (x_k^{p_{k-1}} - x_k^{*p_{k-1}}) \quad (19) \\ &\quad + (\Psi_{k-1} - \widehat{\Theta}_1) (\bar{\Theta}_1 + \eta_{k-1}) \\ &\quad + \bar{c}_{k-1} d_{k-1} |u_0|^{q_{k-1}} |\xi_{k-1}|^{(4l\sigma - \tau - r_{k-1})/\sigma} |\xi_k|^{(r_{k-1} + \tau)/\sigma}, \end{aligned}$$

where  $\bar{c}_{k-1} = 2^{p_{k-1}-1}c_{k-1}$  is a nonnegative constant and

$$0 \leq \Psi_{k-1} \leq (\xi_1^{4l} + \dots + \xi_{k-1}^{4l}) \varphi_{k-1}, \quad (20)$$

for a  $\mathcal{C}^\infty$  function  $\varphi_{k-1} \geq 0$ . In what follows, we prove that (19) also holds at Step  $k$ . To prove this point, considering  $V_k = V_{k-1} + W_k$ , we deduce from (19) and (A.3)-(A.13) that

$$\begin{aligned} \mathcal{L}V_k &\leq -(n - k + 2) \sum_{i=1}^{k-1} \xi_i^{4l} \\ &\quad + |\xi_{k-1}|^{(4l\sigma - \tau - r_{k-1})/\sigma} d_{k-1} u_0^{q_{k-1}} (x_k^{p_{k-1}} - x_k^{*p_{k-1}}) \\ &\quad + \frac{\partial W_k}{\partial \widehat{\Theta}_1} \widehat{\Theta}_1 + (\Psi_{k-1} - \widehat{\Theta}_1) (\bar{\Theta}_1 + \eta_{k-1}) \\ &\quad + \bar{c}_{k-1} d_{k-1} |u_0|^{q_{k-1}} |\xi_{k-1}|^{(4l\sigma - \tau - r_{k-1})/\sigma} |\xi_k|^{(r_{k-1} + \tau)/\sigma} \\ &\quad + \frac{\partial W_k}{\partial x_0} (d_0 u_0^{p_0} + f_0) + \frac{\partial W_k}{\partial x_k} (d_k u_0^{q_k} x_{k+1}^{p_k} + f_k) \end{aligned}$$

$$\begin{aligned} &+ \frac{1}{2} \left| \frac{\partial^2 W_k}{\partial x_0^2} \right| |g_0|^2 + \sum_{i=1}^{k-1} \frac{\partial W_k}{\partial x_i} (d_i u_0^{q_i} x_{i+1}^{p_i} + f_i) \\ &+ \frac{1}{2} \left| \frac{\partial^2 W_k}{\partial x_k^2} \right| |g_k|^2 + \frac{1}{2} \sum_{i=1}^{k-1} \left| \frac{\partial^2 W_k}{\partial x_i^2} \right| |g_i|^2 \\ &+ \frac{1}{2} \left| \frac{\partial^2 W_k}{\partial x_k \partial x_0} \right| |g_k| |g_0^\top| + \frac{1}{2} \sum_{i=1}^{k-1} \left| \frac{\partial^2 W_k}{\partial x_i \partial x_0} \right| |g_i| |g_0^\top| \\ &+ \frac{1}{2} \sum_{i=1}^{k-1} \left| \frac{\partial^2 W_k}{\partial x_i \partial x_k} \right| |g_i| |g_k^\top| \\ &+ \frac{1}{2} \sum_{i,j=1, i \neq j}^{k-1} \left| \frac{\partial^2 W_k}{\partial x_i \partial x_j} \right| |g_i| |g_j^\top|. \quad (21) \end{aligned}$$

We give the following proposition, whose proof is placed in the Appendix.

**Proposition 18.** *There is a smooth function  $\sigma_k$  such that*

$$\begin{aligned} &|\xi_{k-1}|^{(4l\sigma - \tau - r_{k-1})/\sigma} d_{k-1} u_0^{q_{k-1}} (x_k^{p_{k-1}} - x_k^{*p_{k-1}}) \\ &+ \frac{\partial W_k}{\partial x_0} (d_0 u_0^{q_0} + f_0) + \sum_{i=1}^{k-1} \frac{\partial W_k}{\partial x_i} (d_i u_0^{q_i} x_{i+1}^{p_i} + f_i) \\ &+ \frac{\partial W_k}{\partial x_k} f_k + \frac{1}{2} \left| \frac{\partial^2 W_k}{\partial x_0^2} \right| |g_0|^2 + \frac{1}{2} \left| \frac{\partial^2 W_k}{\partial x_k^2} \right| |g_k|^2 \\ &+ \frac{1}{2} \sum_{i=1}^{k-1} \left| \frac{\partial^2 W_k}{\partial x_i \partial x_k} \right| |g_i| |g_k^\top| + \frac{1}{2} \sum_{i=1}^{k-1} \left| \frac{\partial^2 W_k}{\partial x_i^2} \right| |g_i|^2 \\ &+ \frac{1}{2} \left| \frac{\partial^2 W_k}{\partial x_k \partial x_0} \right| |g_k| |g_0^\top| + \frac{1}{2} \sum_{i=1}^{k-1} \left| \frac{\partial^2 W_k}{\partial x_i \partial x_0} \right| |g_i| |g_0^\top| \quad (22) \\ &+ \frac{1}{2} \sum_{i,j=1, i \neq j}^{k-1} \left| \frac{\partial^2 W_k}{\partial x_i \partial x_j} \right| |g_i| |g_j^\top| \\ &+ \bar{c}_{k-1} d_{k-1} |u_0|^{q_{k-1}} |\xi_{k-1}|^{(4l\sigma - \tau - r_{k-1})/\sigma} |\xi_k|^{(r_{k-1} + \tau)/\sigma} \\ &\leq \frac{12}{13} \sum_{i=1}^{k-1} \xi_i^{4l} + \sigma_k \Theta_1 \xi_k^{4l} \\ &+ \bar{c}_k d_k |u_0|^{q_k} |\xi_k|^{(4l\sigma - \tau - r_k)/\sigma} |\xi_{k+1}|^{(r_k + \tau)/\sigma} \\ &+ |\xi_k|^{(4l\sigma - \tau - r_k)/\sigma} d_k \bar{c}_k |u_0|^{q_k} |x_{k+1}^*|^{p_k}, \end{aligned}$$

where  $\bar{c}_k = 2^{p_k-1}c_k$  is a nonnegative constant. Substituting (22) into (21), we arrive at

$$\begin{aligned} \mathcal{L}V_k &\leq - \left( n - k + \frac{14}{13} \right) \sum_{i=1}^{k-1} \xi_i^{4l} \\ &\quad + (\Psi_{k-1} - \widehat{\Theta}_1) (\bar{\Theta}_1 + \eta_{k-1}) + \frac{\partial W_k}{\partial x_k} d_k u_0^{q_k} x_{k+1}^{p_k} \end{aligned}$$

$$\begin{aligned}
& + \sigma_k \xi_k^{4l} \widehat{\Theta}_1 + \frac{\partial W_k}{\partial \widehat{\Theta}_1} \widehat{\Theta}_1 \\
& + \bar{c}_k d_k |u_0|^{q_k} |\xi_k|^{(4l\sigma - \tau - r_k)/\sigma} |\xi_{k+1}|^{(r_k + \tau)/\sigma} \\
& + |\xi_k|^{(4l\sigma - \tau - r_k)/\sigma} d_k \bar{c}_k |u_0|^{q_k} |x_{k+1}^*|^{p_k}.
\end{aligned}
\tag{23}$$

Obviously, defining  $\Psi_k = \Psi_{k-1} + \xi_k^{4l}(\sigma_k + n - k + 14/13)$  and  $\eta_k = \eta_{k-1} - \partial W_k / \partial \widehat{\Theta}_1$ , it follows from (20) that  $0 \leq \Psi_k \leq (\xi_1^{4l} + \dots + \xi_k^{4l})\varphi_k$ , where  $\varphi_k = \max\{\varphi_{k-1}, \sigma_k + n - k + 14/13\}$  is a nonnegative smooth function. With this in mind, (23) can be rewritten as

$$\begin{aligned}
\mathcal{L}V_k \leq & -\left(n - k + \frac{14}{13}\right) \sum_{i=1}^k \xi_i^{4l} + \left(\Psi_k - \widehat{\Theta}_1\right) \left(\bar{\Theta}_1 + \eta_k\right) \\
& + \frac{\partial W_k}{\partial x_k} d_k u_0^{q_k} x_{k+1}^{p_k} \\
& + \bar{c}_k d_k |u_0|^{q_k} |\xi_k|^{(4l\sigma - \tau - r_k)/\sigma} |\xi_{k+1}|^{(r_k + \tau)/\sigma} \\
& + |\xi_k|^{(4l\sigma - \tau - r_k)/\sigma} d_k \bar{c}_k |u_0|^{q_k} |x_{k+1}^*|^{p_k} \\
& + \xi_k^{4l} \widehat{\Theta}_1 \left(\sigma_k + n - k + \frac{14}{13}\right) + \eta_{k-1} \Psi_{k-1} \\
& - \eta_k \Psi_k.
\end{aligned}
\tag{24}$$

With the help of Lemma 4, one has

$$\begin{aligned}
|\eta_{k-1} \Psi_{k-1} - \eta_k \Psi_k| \leq & \left| \eta_{k-1} \xi_k^{4l} \widehat{\Theta}_1 \left(\sigma_k + n - k + \frac{14}{13}\right) \right| \\
& + \left| \frac{\partial W_k}{\partial \widehat{\Theta}_1} \Psi_k \right| \\
\leq & \frac{1}{13} \sum_{i=1}^k \xi_i^{4l} + \bar{\varphi}_k \widehat{\Theta}_1 \xi_k^{4l},
\end{aligned}
\tag{25}$$

which, together with (24), implies that

$$\begin{aligned}
\mathcal{L}V_k \leq & -(n - k + 1) \sum_{i=1}^k \xi_i^{4l} + \left(\Psi_k - \widehat{\Theta}_1\right) \left(\bar{\Theta}_1 + \eta_k\right) \\
& + [\xi_k]^{(4l\sigma - \tau - r_k)/\sigma} d_k u_0^{q_k} \left(x_{k+1}^{p_k} - x_{k+1}^{*p_k}\right) \\
& + [\xi_k]^{(4l\sigma - \tau - r_k)/\sigma} \left(d_k u_0^{q_k} (1 - \bar{c}_k) x_{k+1}^{*p_k} + [\xi_k]^{(r_k + \tau)/\sigma}\right) \\
& \cdot \widehat{\Theta}_1 \left(\bar{\varphi}_k + \sigma_k + n - k + \frac{14}{13}\right) + \bar{c}_k d_k |u_0|^{q_k} \\
& \cdot |\xi_k|^{(4l\sigma - \tau - r_k)/\sigma} |\xi_{k+1}|^{(r_k + \tau)/\sigma},
\end{aligned}
\tag{26}$$

where  $\bar{\varphi}_k \geq 0$  is a smooth function. It is easy to see that the virtual controller

$$x_{k+1}^* = -\left(\frac{1}{\lambda_{k,1} u_0^{q_k} (1 - \bar{c}_k)}\right)$$

renders

$$\begin{aligned}
\mathcal{L}V_k \leq & -(n - k + 1) \sum_{i=1}^k \xi_i^{4l} \\
& + [\xi_k]^{(4l\sigma - \tau - r_k)/\sigma} d_k u_0^{q_k} \left(x_{k+1}^{p_k} - x_{k+1}^{*p_k}\right) \\
& + \left(\Psi_k - \widehat{\Theta}_1\right) \left(\bar{\Theta}_1 + \eta_k\right) \\
& + \bar{c}_k d_k |u_0|^{q_k} |\xi_k|^{(4l\sigma - \tau - r_k)/\sigma} |\xi_{k+1}|^{(r_k + \tau)/\sigma},
\end{aligned}
\tag{28}$$

which still holds for  $k = n$ . Hence at last step, we can explicitly construct a positive-definite and proper Lyapunov function  $V_n = V_{n-1} + W_n$  and a smooth controller  $x_{n+1}^*$  with form (27) such that

$$\begin{aligned}
\mathcal{L}V_n \leq & -\sum_{i=1}^n \xi_i^{4l} + \left(\Psi_n - \widehat{\Theta}_1\right) \left(\bar{\Theta}_1 + \eta_n\right) \\
& + [\xi_n]^{(4l\sigma - \tau - r_n)/\sigma} d_n u_0^{q_n} \left(u^{p_n} - x_{n+1}^{*p_n}\right) \\
& + \bar{c}_n d_n |u_0|^{q_n} |\xi_n|^{(4l\sigma - \tau - r_n)/\sigma} |\xi_{n+1}|^{(r_n + \tau)/\sigma}.
\end{aligned}
\tag{29}$$

Noting  $\xi_{n+1} = 0$ , by choosing the smooth actual controller  $u$  and the adaptive law for  $\widehat{\Theta}_1$ ,

$$u = x_{n+1}^* = -\phi_n(x_0, \bar{x}_n, \widehat{\Theta}_1) [\xi_n]^{r_{n+1}/\sigma}, \quad \dot{\widehat{\Theta}}_1 = \Psi_n, \tag{30}$$

we get

$$\mathcal{L}V_n \leq -\sum_{i=1}^n \xi_i^{4l}. \tag{31}$$

The succeeding proposition characterizes the features of  $x_i$ -subsystem.

**Proposition 19.** If Assumptions 9–11 hold for system (1), controllers (11) and (30) guarantee that

(i) the closed-loop system has an almost surely unique solution on  $[t_0, \infty)$  for each  $(x_1(t_0), \dots, x_n(t_0), \widehat{\Theta}_1(t_0))$

(ii) the equilibrium of the closed-loop system is globally asymptotically stable in probability,  $P\{\lim_{t \rightarrow \infty} |x(t)| = 0\} = 1$ ,  $P\{\lim_{t \rightarrow \infty} \widehat{\Theta}_1(t) \text{ exist and is finite}\} = 1$  for each  $(x_1(t_0), \dots, x_n(t_0), \widehat{\Theta}_1(t_0))$

*Proof.* See Appendix.  $\square$

Case II ( $x_0(t_0) = 0$ ). When  $x_0(t_0) = 0$ , how to select the controllers  $u_0$  and  $u$  is an interesting topic. If the initial state is zero, one chooses an open loop controller  $u_0 = u_0^* \neq 0$  to drive the state  $x_0$  away from zero; a novel controller  $u = u^*$  can be obtained by the above procedure of original  $x_i$ -subsystem in (1). So there exists  $t_s > 0$  such that  $x_0(t_s) \neq 0$ ; after that, controllers  $u_0$  in (11) and  $u$  in (30) can be used.

In view of the argument above, there exists an adaptive controller, such that the equilibrium of the closed-loop system is globally asymptotically stable in probability for any initial condition. The proof of Theorem 15 is completed.

#### 4. Simulation Example

Consider the bilinear model of a mobile robot with small angle measurement error [26], which is described by

$$\begin{aligned} \dot{x}_c &= \left(1 - \frac{\varepsilon^2}{2}\right) \nu, \\ \dot{y}_c &= \theta \nu + \varepsilon \nu, \\ \dot{\theta} &= \omega, \end{aligned} \quad (32)$$

where  $\varepsilon$  is a small bias in orientation.  $\nu$  and  $\omega$  are two control inputs to denote the linear velocity and angular velocity, respectively. Since stochastic disturbance frequently arises in practical control systems, when the angular velocity  $\omega$  is subject to some stochastic disturbances,  $\omega$  can be expressed as  $\omega(x_c, y_c, \theta) = \omega_1(x_c, y_c, \theta) + \omega_2(x_c, y_c, \theta)\dot{B}(t)$ , where  $B(t)$  is the so-called white noise [2]. Then system (32) is transformed into

$$\begin{aligned} dx_c &= \left(1 - \frac{\varepsilon^2}{2}\right) \nu dt, \\ dy_c &= (\theta \nu + \varepsilon \nu) dt, \\ d\theta &= \omega_1 dt + \omega_2 dB. \end{aligned} \quad (33)$$

For system (33), by taking the state and input transformation  $x_0 = x_c$ ,  $x_1 = y_c$ ,  $x_2 = \theta + \varepsilon$ ,  $u_0 = \nu$ ,  $u_1 = \omega_1$ , one has

$$\begin{aligned} dx_0 &= \left(1 - \frac{\varepsilon^2}{2}\right) u_0 dt, \\ dx_1 &= x_2 u_0 dt, \\ dx_2 &= u_1 dt + \omega_2 dB. \end{aligned} \quad (34)$$

System (34) is a special case of system (1). For simplicity, we assume  $1 - \varepsilon^2/2 > 0$ ,  $\omega_2 = x_2 \sin x_1$ , and  $x_0(0) \neq 0$ .

$$\begin{aligned} x_0(t) &= x_0(t_0) \exp\left(\int_{t_0}^t \left(-d_0(s, \theta) h(x_0(s)) \sqrt{\widehat{\Theta}_0^2 + 1} + \alpha_0(x_0(s), \theta) - \frac{1}{2} \beta_0^\top(x_0(s), \theta) \beta_0(x_0(s), \theta)\right) ds\right) \\ &\quad + \int_{t_0}^t \beta_0^\top(x_0(s), \theta) d\omega. \end{aligned} \quad (A.2)$$

By using Lemma 2.3 in [2], for any  $x_0(t_0) \neq 0$ , there holds  $x_0(t) \neq 0$  for any  $t \geq t_0$ , which implies that

Following the above design process, an adaptive controller can be explicitly given

$$\begin{aligned} u_0 &= -x_0, \\ u_1 &= -\widehat{\Theta}_1 \left(\bar{\varphi}_2 + \sigma + \frac{14}{13}\right) [\xi_1], \\ \dot{\widehat{\Theta}}_1 &= 2\xi_1^4 + \xi_2^4 \left(\sigma + \frac{14}{13}\right), \end{aligned} \quad (35)$$

where  $\xi_1 = [x_1]$ ,  $\xi_2 = [x_2] - 2\widehat{\Theta}_1 u_0^{-1} [\xi_1]$ ,  $\bar{\varphi}_2 = 12|u_0|^{-4/3} (\sigma + 14/13)^{-4/3} (\xi_1^4 + \xi_2^4)$ ,  $\sigma = 231.7u_0^4 \widehat{\Theta}_1^3 + 6\widehat{\Theta}_1 + 12\widehat{\Theta}_1^{4/3} + 231.7$ . By choosing  $\varepsilon = 1$  and initial values  $(x_0(0), x_1(0), x_2(0), \widehat{\Theta}_1(0)) = (2, -0.25, 2, 1)$ , Figure 1 demonstrates the effectiveness of the control scheme.

#### 5. Conclusions

This paper investigates adaptive state feedback stabilization for more general stochastic high-order nonholonomic systems. There still exist some problems to be investigated; for instance, we have the following. (1) The result in this paper can be applied to the case of  $p_i \in R_{odd}^{\geq 1}$ . However, if  $p_i$  is an even number or a ratio of odd integer and even integer, it is unclear whether the control strategy can be applied or not. (2) Recently, some results on stochastic nonlinear systems with SiISS dynamic uncertainty have been obtained [27–35]. An important problem is how to solve adaptive feedback control for stochastic nonholonomic nonlinear systems with SiISS dynamic and parametric uncertainties.

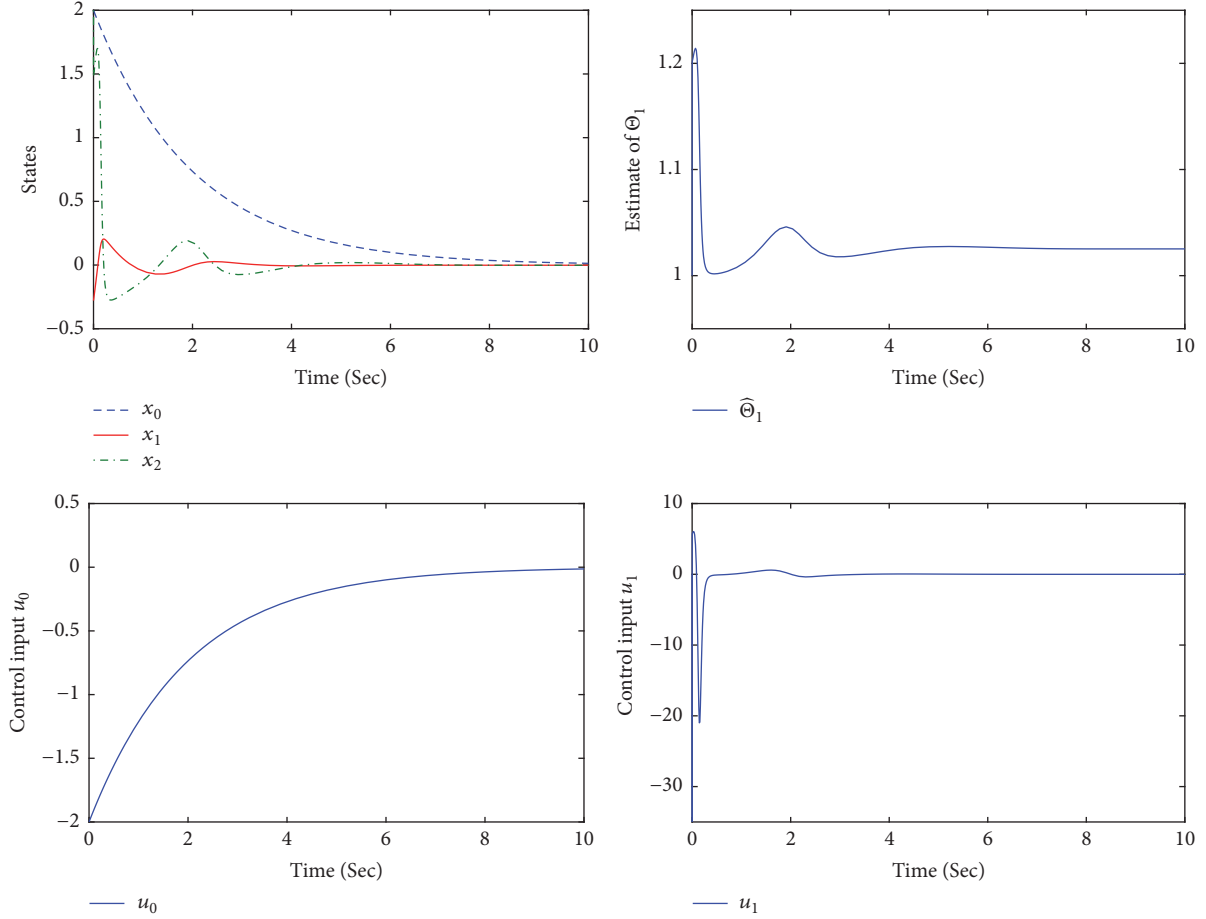
#### Appendix

*Proof of Proposition 16.* It is not hard to prove that  $\widetilde{\Theta}_0$  is bounded. By using (12) and Lemma 2, the equilibrium  $x_0(t) = 0$  of  $x_0$ -subsystem is globally stable in probability and  $P\{\lim_{t \rightarrow \infty} |x_0(t)| = 0\} = 1$  for any  $x_0(t_0) \neq 0$ . By Definition 1, the equilibrium  $x_0(t) = 0$  of  $x_0$ -subsystem is globally asymptotically stable in probability. Substituting (11) into (1), it is easy to obtain

$$\begin{aligned} dx_0 &= \left(-d_0 h(x_0) \sqrt{\widehat{\Theta}_0^2 + 1} + \alpha_0(x_0, \theta)\right) x_0 dt \\ &\quad + \beta_0^\top(x_0, \theta) x_0 d\omega, \end{aligned} \quad (A.1)$$

whose solution is

$u_0$  does not cross zero. The proof of Proposition 16 is completed.  $\square$

FIGURE 1: Trajectories of  $x_0$ ,  $x_1$ ,  $x_2$ ,  $\widehat{\Theta}_1$ ,  $u_0$ ,  $u_1$ .

*Proof of Proposition 17.* From (14) and Lemma 5, we obtain

$$\frac{\partial W_k}{\partial x_k} = [\xi_k]^{(4l\sigma - \tau - r_k)/\sigma}, \quad (\text{A.3})$$

$$\frac{\partial W_k}{\partial x_i} = -\frac{4l\sigma - \tau - r_k}{\sigma} \frac{\partial \left( [x_k^*]^{\sigma/r_k} \right)}{\partial x_i} \cdot \int_{x_k^*}^{x_k} \left| [s]^{\sigma/r_k} - [x_k^*]^{\sigma/r_k} \right|^{((4l-1)\sigma - \tau - r_k)/\sigma} ds, \quad (\text{A.4})$$

where  $i = 1, \dots, k-1$ . Exactly following the same procedure as in the proof of (A.4), we get

$$\frac{\partial W_k}{\partial \widehat{\Theta}_1} = -\frac{4l\sigma - \tau - r_k}{\sigma} \frac{\partial \left( [x_k^*]^{\sigma/r_k} \right)}{\partial \widehat{\Theta}_1} \cdot \int_{x_k^*}^{x_k} \left| [s]^{\sigma/r_k} - [x_k^*]^{\sigma/r_k} \right|^{((4l-1)\sigma - \tau - r_k)/\sigma} ds, \quad (\text{A.5})$$

$$\frac{\partial W_k}{\partial x_0} = -\frac{4l\sigma - \tau - r_k}{\sigma} \frac{\partial \left( [x_k^*]^{\sigma/r_k} \right)}{\partial x_0} \cdot \int_{x_k^*}^{x_k} \left| [s]^{\sigma/r_k} - [x_k^*]^{\sigma/r_k} \right|^{((4l-1)\sigma - \tau - r_k)/\sigma} ds. \quad (\text{A.6})$$

By using (A.3), (A.4), and Lemma 5,

$$\frac{\partial^2 W_k}{\partial x_k^2} = \frac{4l\sigma - \tau - r_k}{r_k} |\xi_k|^{((4l-1)\sigma - \tau - r_k)/\sigma} |x_k|^{\sigma/r_k}, \quad (\text{A.7})$$

$$\begin{aligned} \frac{\partial^2 W_k}{\partial x_i^2} = & \left( \frac{(4l-1)\sigma - \tau - r_k}{\sigma} \right. \\ & \cdot \int_{x_k^*}^{x_k} \left| [s]^{\sigma/r_k} - [x_k^*]^{\sigma/r_k} \right|^{((4l-2)\sigma - \tau - r_k)/\sigma} ds \left( \frac{\partial \left( [x_k^*]^{\sigma/r_k} \right)}{\partial x_i} \right)^2 \\ & \left. - \int_{x_k^*}^{x_k} \left| [s]^{\sigma/r_k} - [x_k^*]^{\sigma/r_k} \right|^{((4l-1)\sigma - \tau - r_k)/\sigma} ds \frac{\partial^2 \left( [x_k^*]^{\sigma/r_k} \right)}{\partial x_i^2} \right) \\ & \cdot \frac{4l\sigma - \tau - r_k}{\sigma}. \end{aligned} \quad (\text{A.8})$$

Similar to (A.8), it follows that

$$\frac{\partial^2 W_k}{\partial x_0^2} = \left( \frac{(4l-1)\sigma - \tau - r_k}{\sigma} \right.$$

$$\int_{x_k^*}^{x_k} \left| [s]^{\sigma/r_k} - [x_k^*]^{\sigma/r_k} \right|^{((4l-2)\sigma - \tau - r_k)/\sigma} ds \left( \frac{\partial \left( [x_k^*]^{\sigma/r_k} \right)}{\partial x_0} \right)^2 \cdot \frac{4l\sigma - \tau - r_k}{\sigma} \tag{A.9}$$

$$- \int_{x_k^*}^{x_k} \left| [s]^{\sigma/r_k} - [x_k^*]^{\sigma/r_k} \right|^{((4l-1)\sigma - \tau - r_k)/\sigma} ds \frac{\partial^2 \left( [x_k^*]^{\sigma/r_k} \right)}{\partial x_0^2}$$

Moreover, it is clear that

$$\frac{\partial^2 W_k}{\partial x_i \partial x_k} = \frac{\partial^2 W_k}{\partial x_k \partial x_i} = -\frac{4l\sigma - \tau - r_k}{\sigma} |\xi_k| \frac{(4l-1)\sigma - \tau - r_k}{\sigma} \frac{\partial \left( [x_k^*]^{\sigma/r_k} \right)}{\partial x_i}, \tag{A.10}$$

$$\frac{\partial^2 W_k}{\partial x_0 \partial x_k} = \frac{\partial^2 W_k}{\partial x_k \partial x_0} = -\frac{4l\sigma - \tau - r_k}{\sigma} |\xi_k|^{((4l-1)\sigma - \tau - r_k)/\sigma} \frac{\partial \left( [x_k^*]^{\sigma/r_k} \right)}{\partial x_0}, \tag{A.11}$$

$$\frac{\partial^2 W_k}{\partial x_i \partial x_0} = \frac{\partial^2 W_k}{\partial x_0 \partial x_i} = \left( \frac{(4l-1)\sigma - \tau - r_k}{\sigma} \int_{x_k^*}^{x_k} \left| [s]^{\sigma/r_k} - [x_k^*]^{\sigma/r_k} \right|^{((4l-2)\sigma - \tau - r_k)/\sigma} ds \frac{\partial \left( [x_k^*]^{\sigma/r_k} \right)}{\partial x_i} \frac{\partial \left( [x_k^*]^{\sigma/r_k} \right)}{\partial x_0} \right. \tag{A.12}$$

$$\left. - \int_{x_k^*}^{x_k} \left| [s]^{\sigma/r_k} - [x_k^*]^{\sigma/r_k} \right|^{((4l-1)\sigma - \tau - r_k)/\sigma} ds \frac{\partial^2 \left( [x_k^*]^{\sigma/r_k} \right)}{\partial x_i \partial x_0} \right) \frac{4l\sigma - \tau - r_k}{\sigma},$$

$$\frac{\partial^2 W_k}{\partial x_i \partial x_j} = \frac{\partial^2 W_k}{\partial x_j \partial x_i} = \left( \frac{(4l-1)\sigma - \tau - r_k}{\sigma} \int_{x_k^*}^{x_k} \left| [s]^{\sigma/r_k} - [x_k^*]^{\sigma/r_k} \right|^{((4l-2)\sigma - \tau - r_k)/\sigma} ds \frac{\partial \left( [x_k^*]^{\sigma/r_k} \right)}{\partial x_i} \frac{\partial \left( [x_k^*]^{\sigma/r_k} \right)}{\partial x_j} \right. \tag{A.13}$$

$$\left. - \int_{x_k^*}^{x_k} \left| [s]^{\sigma/r_k} - [x_k^*]^{\sigma/r_k} \right|^{((4l-1)\sigma - \tau - r_k)/\sigma} ds \frac{\partial^2 \left( [x_k^*]^{\sigma/r_k} \right)}{\partial x_i \partial x_j} \right) \frac{4l\sigma - \tau - r_k}{\sigma},$$

where  $j = 1, \dots, k-1$  and  $j \neq i$ . From the expression of  $x_k^*$ , we know that  $\partial([x_k^*]^{\sigma/r_k})/\partial x_i$ ,  $\partial^2([x_k^*]^{\sigma/r_k})/\partial x_i^2$ ,  $\partial^2([x_k^*]^{\sigma/r_k})/\partial x_i \partial x_j$ ,  $\partial^2([x_k^*]^{\sigma/r_k})/\partial x_i \partial x_0$ ,  $\partial([x_k^*]^{\sigma/r_k})/\partial x_0$ ,  $\partial([x_k^*]^{\sigma/r_k})/\partial \widehat{\Theta}_1$  are continuous functions. It is straightforward to deduce the conclusion that  $W_k(x_0, \bar{x}_k, \widehat{\Theta}_1)$  is  $\mathcal{C}^2$  function.

The rest of proof is divided into two steps. Firstly, we prove the right side of inequality in Proposition 17. In view of Lemmas 6 and 8, one concludes that

$$W_k(x_0, \bar{x}_k, \widehat{\Theta}_1) \leq |\xi_k|^{(4l\sigma - \tau - r_k)/\sigma} 2^{1-r_k/\sigma} \left| [x_k]^{\sigma/r_k} - [x_k^*]^{\sigma/r_k} \right|^{r_k/\sigma} \tag{A.14}$$

$$= 2^{1-r_k/\sigma} |\xi_k|^{(4l\sigma - \tau)/\sigma}.$$

The next work is to prove the left side of inequality. The issue can be solved by considering two different cases. If  $x_k \geq x_k^*$ , then  $[s]^{\sigma/r_k} - [x_k^*]^{\sigma/r_k} \geq 0$ , where  $x_k \geq s \geq x_k^*$ . By Lemma 6, we obtain

$$W_k(x_0, \bar{x}_k, \widehat{\Theta}_1) \geq \int_{x_k^*}^{x_k} \left( 2^{r_k/\sigma - 1} (s - x_k^*) \right)^{(4l\sigma - \tau - r_k)/r_k} ds \tag{A.15}$$

$$= 2^{(r_k - \sigma)(4l\sigma - \tau - r_k)/\sigma r_k} \frac{r_k}{4l\sigma + q_k} (x_k - x_k^*)^{(4l\sigma - \tau)/r_k}.$$

If  $x_k < x_k^*$ , in a similar way,

$$W_k(x_0, \bar{x}_k, \widehat{\Theta}_1) \geq 2^{(r_k - \sigma)(4l\sigma - \tau - r_k)/\sigma r_k} \frac{r_k}{4l\sigma - \tau} (x_k^* - x_k)^{(4l\sigma - \tau)/r_k}. \tag{A.16}$$

Combining (A.15) with (A.16), the proof of Proposition 17 is completed.  $\square$

*Proof of Proposition 18.* Since  $p_{k-1}, k = 2, 3, \dots, n+1$  are odd integers, by using Lemma 6,

$$\left| x_k^{p_{k-1}} - x_k^{*p_{k-1}} \right| \leq 2^{1-r_k p_{k-1}/\sigma} |\xi_k|^{r_k p_{k-1}/\sigma}. \tag{A.17}$$

According to (A.17), Remark 14, and Lemma 4, it follows that

$$\left| \xi_{k-1} \right|^{(4l\sigma - \tau - r_{k-1})/\sigma} d_{k-1} u_0^{q_{k-1}} (x_k^{p_{k-1}} - x_k^{*p_{k-1}}) \leq \frac{1}{13} \xi_{k-1}^{4l} + \sigma_{k1} \Theta_1 \xi_k^{4l}, \tag{A.18}$$

where  $\sigma_{k1}$  is a positive constant. It is easy to deduce from (13) that

$$\left| \frac{\partial \left( [x_k^*]^{\sigma/r_k} \right)}{\partial x_0} \right| \leq |\xi_{k-1}| \left| \frac{\partial \phi_{k-1}^{\sigma/r_k}}{\partial x_0} \right|$$

$$\begin{aligned}
 & + |\phi_{k-1}|^{\sigma/r_k} \left| \frac{\partial \left( -[x_{k-1}^*]^{\sigma/r_{k-1}} \right)}{\partial x_0} \right| \\
 & \qquad \qquad \qquad \vdots \\
 & \leq \sum_{j=1}^{k-2} \prod_{l=j+1}^{k-1} |\phi_l|^{\sigma/r_{l+1}} \left| \frac{\partial \phi_j^{\sigma/r_{j+1}}}{\partial x_0} \right| |\xi_j| + |\xi_{k-1}| \left| \frac{\partial \phi_{k-1}^{\sigma/r_k}}{\partial x_0} \right| \\
 & \leq \sum_{j=1}^{k-1} \psi_{j,1} |\xi_j|,
 \end{aligned} \tag{A.19}$$

where  $\psi_{j,1} = \max\{(\prod_{l=j}^{k-1} |\phi_l|^{\sigma/r_{l+1}}) |\partial \phi_j^{\sigma/r_{j+1}} / \partial x_0|, |\partial \phi_{k-1}^{\sigma/r_k} / \partial x_0|\}$ ,  $j = 1, \dots, k-1$ , are continuous functions. It follows from (A.6), (A.19), Remark 14, and Lemmas 4 and 8 that

$$\begin{aligned}
 \frac{\partial W_k}{\partial x_0} (d_0 u_0^{p_0} + f_0) & \leq (|d_0 u_0^{p_0}| + |f_0|) |\xi_k|^{-\tau/\sigma} 2^{1-r_k/\sigma} \\
 & \cdot \frac{4l\sigma - \tau - r_k}{\sigma} |\xi_k|^{(4l-1)\sigma/\sigma} \sum_{j=1}^{k-1} \psi_{j,1} |\xi_j| \leq \frac{1}{13} \xi_{k-1}^{4l} \\
 & + \sigma_{k2} \Theta_1 \xi_k^{4l},
 \end{aligned} \tag{A.20}$$

where  $\sigma_{k2} \geq 0$  is a smooth function. According to (13) and (A.19), we arrive at

$$\begin{aligned}
 & \left| \frac{\partial^2 \left( [x_k^*]^{\sigma/r_k} \right)}{\partial x_0^2} \right| \\
 & \leq \left| \frac{\partial^2 \phi_{k-1}^{\sigma/r_k}}{\partial x_0^2} \right| |\xi_{k-1}| + \left| \frac{\partial \phi_{k-1}^{\sigma/r_k}}{\partial x_0} \right| \left| \frac{\partial \left( [x_k^*]^{\sigma/r_k} \right)}{\partial x_0} \right| \\
 & + \sum_{j=1}^{k-2} \frac{\partial \left( \prod_{l=j+1}^{k-1} |\phi_l|^{\sigma/r_{l+1}} \left| \frac{\partial \phi_j^{\sigma/r_{j+1}}}{\partial x_0} \right| \right)}{\partial x_0} |\xi_j| \\
 & + \sum_{j=1}^{k-2} \prod_{l=j+1}^{k-1} |\phi_l|^{\sigma/r_{l+1}} \left| \frac{\partial \phi_j^{\sigma/r_{j+1}}}{\partial x_0} \right| \left| \frac{\partial \left( [x_j^*]^{\sigma/r_j} \right)}{\partial x_0} \right| \\
 & \leq \sum_{j=1}^{k-1} \psi_{j,2} |\xi_j|,
 \end{aligned} \tag{A.21}$$

where  $\psi_{j,2} \geq 0$ ,  $j = 1, \dots, k-1$ , are continuous functions. By using (A.9), (A.19), (A.21), Remark 14, and Lemmas 4 and 8, one has

$$\begin{aligned}
 \frac{1}{2} \left| \frac{\partial^2 W_k}{\partial x_0^2} \right| |g_0|^2 & \leq 2^{-r_k/\sigma} \frac{4l\sigma - \tau - r_k}{\sigma} \\
 & \cdot \bar{\beta}_0^2 \Theta_1 x_0^2 \left( |\xi_k|^{-\tau/\sigma} \frac{(4l-1)\sigma - \tau - r_k}{\sigma} |\xi_k|^{(4l-2)\sigma/\sigma} \right)
 \end{aligned}$$

$$\begin{aligned}
 & \cdot \left( \sum_{j=1}^{k-1} \psi_{j,1} |\xi_j| \right)^2 + |\xi_k|^{-\tau/\sigma} |\xi_k|^{(4l-1)\sigma/\sigma} \\
 & \cdot \sum_{j=1}^{k-1} \psi_{j,3} |\xi_j| \leq \frac{1}{13} \xi_{k-1}^{4l} + \sigma_{k3} \Theta_1 \xi_k^{4l},
 \end{aligned} \tag{A.22}$$

where  $\sigma_{k3} \geq 0$  is a smooth function. From (13) and Lemma 7, one arrives at

$$\sum_{i=1}^k |x_i|^{(r_k+\tau)/r_i} \tag{A.23}$$

$$\leq \sum_{i=1}^k \left( |\xi_i|^{(r_k+\tau)/\sigma} + \phi_{i-1}^{(r_k+\tau)/r_i} |\xi_{i-1}|^{(r_k+\tau)/\sigma} \right),$$

$$\sum_{i=1}^k |x_i|^{(2r_k+\tau)/2r_i} \tag{A.24}$$

$$\leq \sum_{i=1}^k \left( |\xi_i|^{(2r_k+\tau)/2\sigma} + \phi_{i-1}^{(2r_k+\tau)/2r_i} |\xi_{i-1}|^{(2r_k+\tau)/2\sigma} \right),$$

where  $\phi_0 = 0$  and  $\xi_0 = 0$ . By (A.3), (A.23) and Lemma 4, it is easy to verify that

$$\begin{aligned}
 \frac{\partial W_k}{\partial x_k} f_k & \leq [\xi_k]^{(4l\sigma - \tau - r_k)/\sigma} \\
 & \cdot \sum_{i=1}^k \left( |\xi_i|^{(r_k+\tau)/\sigma} + \phi_{i-1}^{(r_k+\tau)/r_i} |\xi_{i-1}|^{(r_k+\tau)/\sigma} \right) \Theta_1 \bar{\alpha}_k \\
 & + \bar{c}_k d_k |u_0|^{q_k} |\xi_k|^{(4l\sigma - \tau - r_k)/\sigma} |x_{k+1}|^{p_k} \leq \frac{1}{13} \sum_{i=1}^{k-1} \xi_i^{4l} \\
 & + \sigma_{k4} \Theta_1 \xi_k^{4l} + \bar{c}_k d_k |u_0|^{q_k} |\xi_k|^{(4l\sigma - \tau - r_k)/\sigma} \\
 & \cdot |\xi_{k+1}|^{(r_k+\tau)/\sigma} + \bar{c}_k d_k |u_0|^{q_k} |\xi_k|^{(4l\sigma - \tau - r_k)/\sigma} \\
 & \cdot |x_{k+1}|^{p_k},
 \end{aligned} \tag{A.25}$$

where  $\sigma_{k4} \geq 0$  is a smooth function. Based on (13), one has

$$\begin{aligned}
 \left| \frac{\partial \left( [x_k^*]^{\sigma/r_k} \right)}{\partial x_i} \right| & \leq \left| \frac{\partial \left( \sum_{l=1}^{k-1} \prod_{j=l}^{k-1} \phi_j^{\sigma/r_{j+1}} [x_l]^{\sigma/r_l} \right)}{\partial x_i} \right| \\
 & \leq \sum_{j=i}^{k-1} \phi_j^{\sigma/r_{j+1}} \frac{\sigma}{r_i} \left( |\xi_i|^{(\sigma-r_i)/\sigma} + \phi_{i-1}^{(\sigma-r_i)/r_i} |\xi_{i-1}|^{(\sigma-r_i)/\sigma} \right) \\
 & + \sum_{l=1}^{k-1} \left| \frac{\partial \left( \prod_{j=i}^{k-1} \phi_j^{\sigma/r_{j+1}} \right)}{\partial x_i} \right| \left( |\xi_l| + \phi_{l-1}^{\sigma/r_l} |\xi_{l-1}| \right).
 \end{aligned} \tag{A.26}$$

Similarly, by using (13), (A.4), (A.23), (A.26), Remark 14, and Lemma 4,

$$\begin{aligned} & \sum_{i=1}^{k-1} \frac{\partial W_k}{\partial x_i} (d_i u_0^{q_i} x_{i+1}^{p_i} + f_i) \\ & \leq \sum_{i=1}^{k-1} \sum_{j=1}^{i+1} \Theta_1 \left( |\xi_j|^{(r_i+\tau)/\sigma} + \phi_{j-1}^{(r_i+\tau)/r_i} |\xi_{j-1}|^{(r_i+\tau)/\sigma} \right) \\ & \cdot F \times \frac{4l\sigma - \tau - r_k}{\sigma} 2^{1-r_k/\sigma} \left| \frac{\partial \left( [x_k^*]^{\sigma/r_k} \right)}{\partial x_i} \right| \\ & \cdot |\xi_k|^{((4l-1)\sigma-\tau)/\sigma} \leq \frac{1}{13} \sum_{i=1}^{k-1} \xi_i^{4l} + \sigma_{k5} \Theta_1 \xi_k^{4l}, \end{aligned} \quad (\text{A.27})$$

where  $\sigma_{k5} \geq 0$  is a smooth function and  $F \triangleq \max\{u_0^{q_i}(1 - \bar{c}_i) \bar{\lambda}_{i,2}, \bar{\alpha}_i\}$ . Because of (A.11), (A.19), (A.24), Remark 14, and Lemma 4, the following always holds:

$$\begin{aligned} & \frac{1}{2} \left| \frac{\partial^2 W_k}{\partial x_k \partial x_0} \right| |g_k| |g_0^\top| \leq \sum_{i=1}^k \bar{\beta}_0 \bar{\beta}_k |x_0| \Theta_1 \\ & \cdot \frac{4l\sigma - \tau - r_k}{2\sigma} |\xi_k|^{((4l-1)\sigma-\tau-r_k)/\sigma} \left| \frac{\partial \left( [x_k^*]^{\sigma/r_k} \right)}{\partial x_0} \right| \\ & \cdot \left( |\xi_i|^{(2r_k+\tau)/2\sigma} + \phi_{i-1}^{(2r_k+\tau)/2r_i} |\xi_{i-1}|^{(2r_k+\tau)/2\sigma} \right) \leq \frac{1}{13} \\ & \cdot \sum_{i=1}^{k-1} \xi_i^{4l} + \sigma_{k6} \Theta_1 \xi_k^{4l}, \end{aligned} \quad (\text{A.28})$$

where  $\sigma_{k6} \geq 0$  is a smooth function. Using (A.7), (A.10), (A.24), (A.26), and Lemma 4, one has

$$\begin{aligned} & \frac{1}{2} \sum_{i=1}^{k-1} \left| \frac{\partial^2 W_k}{\partial x_k \partial x_i} \right| |g_k| |g_i^\top| \leq \frac{1}{2} \\ & \cdot \sum_{i=1}^{k-1} \sum_{l=1}^k \sum_{j=1}^i \bar{\beta}_i \bar{\beta}_k \Theta_1 \frac{4l\sigma - \tau - r_k}{2\sigma} |\xi_k|^{((4l-1)\sigma-\tau-r_k)/\sigma} \\ & \times \left| \frac{\partial \left( [x_k^*]^{\sigma/r_k} \right)}{\partial x_i} \right| \left( |\xi_i|^{(2r_k+\tau)/2\sigma} \right. \\ & \left. + \phi_{l-1}^{(2r_k+\tau)/2r_k} |\xi_{l-1}|^{(2r_k+\tau)/2\sigma} \right) \times \left( |\xi_j|^{(2r_i+\tau)/2\sigma} \right. \\ & \left. + \phi_{j-1}^{(2r_i+\tau)/2r_i} |\xi_{j-1}|^{(2r_i+\tau)/2\sigma} \right) \leq \frac{1}{13} \sum_{i=1}^{k-1} \xi_i^{4l} \\ & + \sigma_{k7} \Theta_1 \xi_k^{4l}, \\ & \frac{1}{2} \left| \frac{\partial^2 W_k}{\partial x_k^2} \right| |g_k|^2 \leq \sum_{i=1}^k \bar{\beta}_k^2 \Theta_1 \\ & \cdot \frac{4l\sigma + q_k - r_k}{2\sigma} |\xi_k|^{((4l-1)\sigma-\tau-r_k)/\sigma} |x_k|^{(\sigma+\tau)/r_k} \end{aligned} \quad (\text{A.29})$$

$$\begin{aligned} & \times \left( |\xi_i|^{(2r_k+\tau)/2\sigma} + \phi_{i-1}^{(2r_k+\tau)/2r_k} |\xi_{i-1}|^{(2r_k+\tau)/2\sigma} \right)^2 \\ & \leq \frac{1}{13} \sum_{i=1}^{k-1} \xi_i^{4l} + \sigma_{k8} \Theta_1 \xi_k^{4l}, \end{aligned} \quad (\text{A.30})$$

where  $\sigma_{k7} \geq 0$  and  $\sigma_{k8} \geq 0$  are smooth functions. In terms of (13) and (A.19), it follows that

$$\begin{aligned} & \left| \frac{\partial^2 \left( [x_k^*]^{\sigma/r_k} \right)}{\partial x_i \partial x_0} \right| \\ & \leq \left| \frac{\partial^2 \phi_{k-1}^{\sigma/r_k}}{\partial x_i \partial x_0} \right| |\xi_{k-1}| \\ & + \sum_{j=1}^{k-2} \frac{\partial \left( \prod_{l=j+1}^{k-1} |\phi_l|^{\sigma/r_{l+1}} \left| \frac{\partial \phi_j^{\sigma/r_{j+1}}}{\partial x_0} \right| \right)}{\partial x_i} |\xi_j| \\ & + \sum_{j=1}^{k-2} \prod_{l=j+1}^{k-1} |\phi_l|^{\sigma/r_{l+1}} \left| \frac{\partial \phi_j^{\sigma/r_{j+1}}}{\partial x_0} \right| \left| \frac{\partial \xi_j}{\partial x_i} \right| \\ & + \left| \frac{\partial \xi_{k-1}}{\partial x_i} \right| \left| \frac{\partial \phi_{k-1}^{\sigma/r_k}}{\partial x_0} \right| \\ & \leq \left| \frac{\partial^2 \phi_{k-1}^{\sigma/r_k}}{\partial x_i \partial x_0} \right| |\xi_{k-1}| \\ & + \sum_{j=1}^{k-2} \frac{\partial \left( \prod_{l=j+1}^{k-1} |\phi_l|^{\sigma/r_{l+1}} \left| \frac{\partial \phi_j^{\sigma/r_{j+1}}}{\partial x_0} \right| \right)}{\partial x_i} |\xi_j| \\ & + \sum_{j=1}^{k-2} \prod_{l=j+1}^{k-1} |\phi_l|^{\sigma/r_{l+1}} \left| \frac{\partial \phi_j^{\sigma/r_{j+1}}}{\partial x_0} \right| \left| \frac{\partial \left( [x_j^*]^{\sigma/r_j} \right)}{\partial x_i} \right| \\ & + \left| \frac{\partial \left( [x_{k-1}^*]^{\sigma/r_{k-1}} \right)}{\partial x_i} \right| \left| \frac{\partial \phi_{k-1}^{\sigma/r_k}}{\partial x_0} \right|. \end{aligned} \quad (\text{A.31})$$

Combining (A.12), (A.24), (A.26), (A.31), Remark 14, and Lemma 4 yields

$$\begin{aligned} & \frac{1}{2} \sum_{i=1}^{k-1} \left| \frac{\partial^2 W_k}{\partial x_i \partial x_0} \right| |g_i| |g_0^\top| \leq \sum_{i=1}^{k-1} \sum_{j=1}^i 2^{-r_k/\sigma} \bar{\beta}_0 \bar{\beta}_i |x_0| \Theta_1 \\ & \cdot \frac{4l\sigma - \tau - r_k}{\sigma} |\xi_k|^{((4l-2)\sigma-\tau)/\sigma} \\ & \cdot \left( |\xi_j|^{(2r_i+\tau)/2\sigma} + \phi_{j-1}^{(2r_i+\tau)/2\sigma} |\xi_{j-1}|^{(2r_i+\tau)/2r_i} \right) \\ & \times \left( \frac{(4l-1)\sigma - \tau - r_k}{\sigma} \left| \frac{\partial \left( [x_k^*]^{\sigma/r_k} \right)}{\partial x_i} \right| \sum_{l=1}^{k-1} \psi_{l,1} |\xi_j| \right) \end{aligned}$$

$$+ \left| \frac{\partial^2 \left( [x_k^*]^{\sigma/r_k} \right)}{\partial x_i \partial x_0} \right| |\xi_k| \leq \frac{1}{13} \sum_{i=1}^{k-1} \xi_i^{4l} + \sigma_{k9} \Theta_1 \xi_k^{4l}, \quad (\text{A.32})$$

where  $\sigma_{k9} \geq 0$  is a smooth function. Exactly following the same procedure, tedious calculations conclude that

$$\begin{aligned} & \frac{1}{2} \sum_{i=1}^{k-1} \sum_{j=1}^i \left| \frac{\partial^2 W_k}{\partial x_i^2} \right| |g_i|^2 \\ & \leq \sum_{i=1}^{k-1} \sum_{j=1}^i \bar{\beta}_i^2 \Theta_1 2^{-r_k/\sigma} |\xi_k|^{((4l-2)\sigma-\tau)/\sigma} \\ & \cdot \frac{4l\sigma - \tau - r_k}{\sigma} \left( \left( \frac{\partial \left( [x_k^*]^{\sigma/r_k} \right)}{\partial x_i} \right)^2 \right. \\ & \times \frac{(4l-1)\sigma - \tau - r_k}{\sigma} + \left. \left| \frac{\partial^2 \left( [x_k^*]^{\sigma/r_k} \right)}{\partial x_i^2} \right| |\xi_k| \right) \end{aligned} \quad (\text{A.33})$$

$$\begin{aligned} & \times \left( |\xi_j|^{(2r_i+\tau)/2\sigma} + \phi_{j-1}^{(2r_i+\tau)/2r_i} |\xi_{j-1}|^{(2r_i+\tau)/2\sigma} \right)^2 \\ & \leq \frac{1}{13} \sum_{i=1}^{k-1} \xi_i^{4l} + \sigma_{k10} \Theta_1 \xi_k^{4l}, \\ & \sum_{i,j=1, i \neq j}^{k-1} \frac{1}{2} \left| \frac{\partial^2 W_k}{\partial x_i \partial x_j} \right| |g_i| |g_j| \leq \sum_{i,j=1, i \neq j}^{k-1} \sum_{l=1}^i \sum_{h=1}^j 2^{-r_k/\sigma} \\ & \cdot \frac{4l\sigma - \tau - r_k}{\sigma} \bar{\beta}_i \bar{\beta}_j \Theta_1 |\xi_k|^{((4l-2)\sigma-\tau)/\sigma} \\ & \times \left( \frac{(4l-1)\sigma - \tau - r_k}{\sigma} \left| \frac{\partial \left( [x_k^*]^{\sigma/r_k} \right)}{\partial x_i} \right| \right. \\ & \cdot \left. \left| \frac{\partial \left( [x_k^*]^{\sigma/r_k} \right)}{\partial x_j} \right| + \left| \frac{\partial^2 \left( [x_k^*]^{\sigma/r_k} \right)}{\partial x_i \partial x_j} \right| |\xi_k| \right) \\ & \cdot \left( |\xi_l|^{(2r_i+\tau)/2\sigma} + \phi_{l-1}^{(2r_i+\tau)/2r_i} |\xi_{l-1}|^{(2r_i+\tau)/2\sigma} \right) \\ & \times \left( |\xi_h|^{(2r_j+\tau)/2\sigma} + \phi_{h-1}^{(2r_j+\tau)/2r_j} |\xi_{h-1}|^{(2r_j+\tau)/2\sigma} \right) \\ & \leq \frac{1}{13} \sum_{i=1}^{k-1} \xi_i^{4l} + \sigma_{k11} \Theta_1 \xi_k^{4l}, \end{aligned} \quad (\text{A.34})$$

where  $\sigma_{k10} \geq 0$  and  $\sigma_{k11} \geq 0$  are smooth functions. At last, by using Lemma 4,

$$\begin{aligned} & \bar{c}_{k-1} d_{k-1} |u_0|^{q_{k-1}} |\xi_{k-1}|^{(4l\sigma-\tau-r_{k-1})/\sigma} |\xi_k|^{(r_{k-1}+\tau)/\sigma} \\ & \leq \frac{1}{13} \xi_{k-1}^{4l} + \sigma_{k12} \Theta_1 \xi_k^{4l}, \end{aligned} \quad (\text{A.35})$$

where  $\sigma_{k12}$  is a position constant. Define the nonnegative smooth function  $\sigma_k = \sum_{i=1}^{12} \sigma_{ki}$ , and put (A.18), (A.20), (A.22), (A.25), (A.27)-(A.30), and (A.32)-(A.35) together, the proof of Proposition 18 is completed.  $\square$

*Proof of Proposition 19.* By (31), Proposition 17, and Lemma 2, Proposition 19 is proved.  $\square$

## Data Availability

The data supporting the conclusions of our article are some open access articles that have been properly cited, and the readers can easily obtain these articles to verify the conclusions, replicate the analysis, and conduct secondary analyses. Therefore, we do not create a publicly available data repository.

## Conflicts of Interest

The authors declare that they have no conflicts of interest.

## Acknowledgments

This work was supported by Taishan Scholar Project of Shandong Province of China (no. ts201712040), National Natural Science Foundation of China (no. 61673242), and Shandong Provincial Natural Science Foundation of China (no. ZR2016FM10).

## References

- [1] M. Krstic and H. Deng, *Stabilization of Nonlinear Uncertain Systems*, Springer-Verlag, New York, NY, USA, 1998.
- [2] X. Mao, *Stochastic Differential Equations and Applications*, Horwood Publishing, Chichester, UK, 2007.
- [3] Z. Pan and T. Basar, "Backstepping controller design for nonlinear stochastic systems under a risk-sensitive cost criterion," *SIAM Journal on Control and Optimization*, vol. 37, no. 3, pp. 957-995, 1999.
- [4] Y.-G. Liu and J.-F. Zhang, "Practical output-feedback risk-sensitive control for stochastic nonlinear systems with stable zero-dynamics," *SIAM Journal on Control and Optimization*, vol. 45, no. 3, pp. 885-926, 2006.
- [5] S.-J. Liu, J.-F. Zhang, and Z.-P. Jiang, "Decentralized adaptive output-feedback stabilization for large-scale stochastic nonlinear systems," *Automatica*, vol. 43, no. 2, pp. 238-251, 2007.
- [6] S.-J. Liu, Z.-P. Jiang, and J.-F. Zhang, "Global output-feedback stabilization for a class of stochastic non-minimum-phase nonlinear systems," *Automatica*, vol. 44, no. 8, pp. 1944-1957, 2008.
- [7] L. Liu and X.-J. Xie, "State feedback stabilization for stochastic feedforward nonlinear systems with time-varying delay," *Automatica*, vol. 49, no. 4, pp. 936-942, 2013.
- [8] Q. Wang and C. Wei, "Decentralized robust adaptive output feedback control of stochastic nonlinear interconnected systems with dynamic interactions," *Automatica*, vol. 54, pp. 124-134, 2015.
- [9] K. Zhang, C.-R. Zhao, and X.-J. Xie, "Global output feedback stabilisation of stochastic high-order feedforward nonlinear systems with time-delay," *International Journal of Control*, vol. 88, no. 12, pp. 2477-2487, 2015.

- [10] C.-R. Zhao, K. Zhang, and X.-J. Xie, "Output feedback stabilization of stochastic feedforward nonlinear systems with input and state delay," *International Journal of Robust and Nonlinear Control*, vol. 26, no. 7, pp. 1422–1436, 2016.
- [11] M.-M. Jiang, K.-M. Zhang, and X.-J. Xie, "Output feedback stabilisation of stochastic nonlinear time-delay systems with unknown output function," *International Journal of Systems Science*, vol. 48, no. 11, pp. 2262–2271, 2017.
- [12] H. Sun, Y. Li, G. Zong, and L. Hou, "Disturbance attenuation and rejection for stochastic Markovian jump system with partially known transition probabilities," *Automatica*, vol. 89, pp. 349–357, 2018.
- [13] A. Ferrara, L. Giacomini, and C. Vecchio, "Control of nonholonomic systems with uncertainties via second-order sliding modes," *International Journal of Robust and Nonlinear Control*, vol. 18, no. 4-5, pp. 515–528, 2008.
- [14] F. Z. Gao, F. S. Yuan, H. J. Yao, and X. W. Mu, "Adaptive stabilization of high order nonholonomic systems with strong nonlinear drifts," *Applied Mathematical Modelling*, vol. 35, no. 9, pp. 4222–4233, 2011.
- [15] F. Z. Gao, F. S. Yuan, and H. J. Yao, "Robust adaptive control for nonholonomic systems with nonlinear parameterization," *Nonlinear Analysis: Real World Applications*, vol. 11, no. 4, pp. 3242–3250, 2010.
- [16] W. Lin, R. Pongvuthithum, and C. Qian, "Control of high-order nonholonomic systems in power chained form using discontinuous feedback," *Institute of Electrical and Electronics Engineers Transactions on Automatic Control*, vol. 47, no. 1, pp. 108–115, 2002.
- [17] Q. H. Du, C. L. Wang, and G. Wang, "Adaptive state-feedback stabilization of stochastic high-order nonholonomic systems with nonlinear parameterization," *Transactions of the Institute of Measurement and Control*, vol. 37, no. 4, pp. 536–549, 2015.
- [18] W. Lin and C. Qian, "Adaptive control of nonlinearly parameterized systems: a nonsmooth feedback framework," *IEEE Transactions on Automatic Control*, vol. 47, no. 6, pp. 757–774, 2002.
- [19] B. Yang and W. Lin, "Robust output feedback stabilization of uncertain nonlinear systems with uncontrollable and unobservable linearization," *IEEE Transactions on Automatic Control*, vol. 50, no. 5, pp. 619–630, 2005.
- [20] F. Gao and Y. Wu, "Global stabilisation for a class of more general high-order time-delay nonlinear systems by output feedback," *International Journal of Control*, vol. 88, no. 8, pp. 1540–1553, 2015.
- [21] D. Zhang, C. Wang, G. Wei, and H. Chen, "Output feedback stabilization for stochastic nonholonomic systems with nonlinear drifts and Markovian switching," *Asian Journal of Control*, vol. 16, no. 6, pp. 1679–1692, 2014.
- [22] F. Gao and F. Yuan, "Adaptive stabilization of stochastic nonholonomic systems with nonlinear parameterization," *Applied Mathematics and Computation*, vol. 219, no. 16, pp. 8676–8686, 2013.
- [23] F. Gao, F. Yuan, and Y. Wu, "Adaptive stabilization for a class of stochastic nonlinearly parameterized nonholonomic systems with unknown control coefficients," *Asian Journal of Control*, vol. 16, no. 6, pp. 1829–1838, 2014.
- [24] F. Gao and F. Yuan, "Finite-time stabilization of stochastic nonholonomic systems and its application to mobile robot," *Abstract and Applied Analysis*, vol. 2012, Article ID 361269, 18 pages, 2012.
- [25] F. Gao, F. Yuan, J. Zhang, and Y. Wu, "Further result on finite-time stabilization of stochastic nonholonomic systems," *Abstract and Applied Analysis*, vol. 2013, 8 pages, 2013.
- [26] S. S. Ge, Z. P. Wang, and T. H. Lee, "Adaptive stabilization of uncertain nonholonomic systems by state and output feedback," *Automatica*, vol. 39, no. 8, pp. 1451–1460, 2003.
- [27] H. Deng, M. Krstić, and R. J. Williams, "Stabilization of stochastic nonlinear systems driven by noise of unknown covariance," *IEEE Transactions on Automatic Control*, vol. 46, no. 8, pp. 1237–1253, 2001.
- [28] M.-Y. Cui, X.-J. Xie, and Z.-J. Wu, "Dynamics modeling and tracking control of robot manipulators in random vibration environment," *Institute of Electrical and Electronics Engineers Transactions on Automatic Control*, vol. 58, no. 6, pp. 1540–1545, 2013.
- [29] C. Zhao and X. Xie, "Global stabilization of stochastic high-order feedforward nonlinear systems with time-varying delay," *Automatica*, vol. 50, no. 1, pp. 203–210, 2014.
- [30] X. Xie, N. Duan, and C. Zhao, "A combined homogeneous domination and sign function approach to output-feedback stabilization of stochastic high-order nonlinear systems," *IEEE Transactions on Automatic Control*, vol. 59, no. 5, pp. 1303–1309, 2014.
- [31] H. Ito and Y. Nishimura, "Stability of stochastic nonlinear systems in cascade with not necessarily unbounded decay rates," *Automatica*, vol. 62, no. 12, pp. 51–64, 2015.
- [32] X.-J. Xie, X.-H. Zhang, and K. Zhang, "Finite-time state feedback stabilisation of stochastic high-order nonlinear feedforward systems," *International Journal of Control*, vol. 89, no. 7, pp. 1332–1341, 2016.
- [33] H. Ito and Y. Nishimura, "An iISS framework for stochastic robustness of interconnected nonlinear systems," *Institute of Electrical and Electronics Engineers Transactions on Automatic Control*, vol. 61, no. 6, pp. 1508–1523, 2016.
- [34] X. Xie and M. Jiang, "Output feedback stabilization of stochastic feedforward nonlinear time-delay systems with unknown output function," *International Journal of Robust and Nonlinear Control*, vol. 28, no. 1, pp. 266–280, 2018.
- [35] M.-M. Jiang and X.-J. Xie, "Finite-time stabilization of stochastic low-order nonlinear systems with FT-SISS inverse dynamics," *International Journal of Robust and Nonlinear Control*, vol. 28, no. 6, pp. 1960–1972, 2018.

## Research Article

# Stochastic Stability Analysis of Coupled Viscoelastic Systems with Nonviscously Damping Driven by White Noise

Di Liu <sup>1</sup>, Yanru Wu,<sup>1</sup> and Xiufeng Xie<sup>2</sup>

<sup>1</sup>*School of Mathematics, Shanxi University, Taiyuan 030006, China*

<sup>2</sup>*Applied Science College, Taiyuan University of Science and Technology, Taiyuan 030024, China*

Correspondence should be addressed to Di Liu; di-lau@hotmail.com

Received 27 May 2018; Revised 1 August 2018; Accepted 15 August 2018; Published 16 September 2018

Academic Editor: Xue-Jun Xie

Copyright © 2018 Di Liu et al. This is an open access article distributed under the Creative Commons Attribution License, which permits unrestricted use, distribution, and reproduction in any medium, provided the original work is properly cited.

Nonviscously damped structural system has been raised in many engineering fields, in which the damping forces depend on the past time history of velocities via convolution integrals over some kernel functions. This paper investigates stochastic stability of coupled viscoelastic system with nonviscously damping driven by white noise through moment Lyapunov exponents and Lyapunov exponents. Using the coordinate transformation, the coupled Itô stochastic differential equations of the norm of the response and angles process are obtained. Then the problem of the moment Lyapunov exponent is transformed to the eigenvalue problem, and then the second-perturbation method is used to derive the moment Lyapunov exponent of coupled stochastic system. Lyapunov exponent also can be obtained according to the relationship between moment Lyapunov exponent and Lyapunov exponent. Finally, the effects of various physical quantities of stochastic coupled system on the stochastic stability are discussed in detail. These results are validated by the direct Monte Carlo simulation technique.

## 1. Introduction

Viscoelastic materials are widely used in aerospace, construction, textile, and other industries, because they have a series of excellent properties, including light weight, high strength, wide source, and good shock absorption. These materials' stress depends on the past time history of strain; that is, the stress will increase correspondingly with the increase of time and the bucking will be more likely to occur. Therefore, the research of dynamical behavior of viscoelastic system has received a lot of interests in recent years [1–4].

To better understand the dynamical behavior of the viscoelastic system, many methods had been put forward. McTavish et al. [5] presented GHM method to analyze the linear multiple degree of freedom viscoelastic damping systems. Li et al. [6] studied the decay rate of energy functional of nonlinear viscoelastic full Marguerre-von Kármán shallow shell system. Later, Li [7] also showed the existence and uniqueness of weak solution of this system by applying the Galerkin finite element method. Nieto and Ahmad [8] used the generalized quasi-linearization method to obtain the explicit approximate solutions of an initial and terminal value problem for the

forced Duffing equation with nonviscous damping. Recently, Li and Du [9] studied general energy decay of a degenerate viscoelastic Petrovsky-type plate equation with boundary feedback through a priori estimate and analysis of Lyapunov-like functional.

The dynamic stability as an important field of nonlinear dynamics has attached increasing attention in recent years. Guo et al. [10] derived a new simple sufficient condition of the global asymptotic stability of the integrodifferential systems with delay through constructing suitable Lyapunov functionals combined with the analytical technique. And then Meng et al. [11, 12] obtained a sufficient condition of uniform stability for nonlinear integrodifferential system. However, when we consider the dynamical behavior of the system in a real environment, the stochastic excitation cannot be ruled out, such as wind gusts, earthquakes, and ocean waves [13–15]. Stochastic stability of the system under the stochastic excitation has attracted more and more attention [16–20]. The Lyapunov exponent specially has been researched by many scholars as an important indication for judging the stability of stochastic system. For example, Potapov [21] derived the sufficient condition of the almost-sure asymptotic

stability of elastic and viscoelastic systems by the Lyapunov's direct method. He [22] also studied the stability of elastic and viscoelastic systems under the non-Gaussian excitation. For stochastic stability of high dimensional coupled system, Pavlović et al. [23] proposed the direct Lyapunov method to investigate the almost-sure stochastic stability of a viscoelastic double-beam system under parametric excitation. Then they used the same method to analyze the instability of coupled nanobeam systems subject to compressive axial loading [24]. These works only indicate that the system is almost-surely stable.

According to the theory of large deviation, which was first proposed by Baxendale and Stroock [25], the almost-sure stability of stochastic system does not mean the moment stability. Therefore, it is necessary to study the moment Lyapunov exponent of a stochastic system. The moment Lyapunov exponent can judge not only almost-sure stability but also the moment stability [26]. Nevertheless, analytic solutions of the moment Lyapunov exponent are very difficult to derive. To overcome this, many scholars developed different approximation methods to study the moment Lyapunov exponents of the stochastic system. For example, Sri Namachchivaya and Van Roessel [27] studied the moment Lyapunov exponents of two-degrees-of-freedom coupled elastic oscillators under real noise excitation by combining an asymptotic approximation for the moment Lyapunov exponents. Kozić and his associates [28–30] developed the first-order perturbation approach to obtain weak noise expansion of moment Lyapunov exponents and Lyapunov exponents for a stochastically coupled double-beam system and Timoshenko beam system, respectively. Subsequently, Stojanović and Petković [31] used a perturbation method to study the moment Lyapunov exponents and the Lyapunov exponents of the three elastically connected Euler beams. More recently, Deng [32] applied the averaging method to establish the moment Lyapunov exponent of coupled gyroscopic stochastic system under bounded noise excitation. But it is rare to see studies of the moment Lyapunov exponent of a viscoelastic coupled system with nonviscous damping. Deng [33] investigated stochastic stability of two-degrees-of-freedom coupled viscoelastic system under white noise through moment Lyapunov exponent, but its damping term is viscous.

The purpose of this paper is to study stochastic stability of a viscoelastic coupled system with nonviscous damping subject to Gaussian white noise excitation through moment Lyapunov exponents and Lyapunov exponents, in which the nonviscous damping term is expressed by Boltzmann's superposition integral with a hereditary relaxation kernel. The paper is organized as follows. Section 2 derives the governing equations of motion of a stochastic viscoelastic system with a nonviscous damping. And then solving the problem of the moment Lyapunov exponent is changed into the eigenvalue and eigenfunction problem through a suitable transformation. In Section 3, the zeroth-order and the first-order and second-order perturbation solutions of the moment Lyapunov exponents are derived, respectively, based on the second-order perturbation method. The effects of different physical quantities on the stochastic stability of the coupled system are discussed under the given parameters.

Correspondingly, the results are verified by means of the direct Monte Carlo simulation in Section 4. Finally, conclusions will be drawn in Section 5.

## 2. Problem Formulation

Considering a coupled viscoelastic system with nonviscous damped structure driven by white noise excitation, the governing equations can be expressed as

$$\begin{aligned} \ddot{q}_1 + \omega_1^2 q_1 + \epsilon \beta_1 \int_0^t \gamma(t-\tau) \dot{q}_1(\tau) d\tau + \epsilon H_1 (q_1 - q_2) \\ - \sqrt{\epsilon} K_1 \xi(t) q_1 = 0, \\ \ddot{q}_2 + \omega_2^2 q_2 + \epsilon \beta_2 \int_0^t \gamma(t-\tau) \dot{q}_2(\tau) d\tau + \epsilon H_2 (q_2 - q_1) \\ - \sqrt{\epsilon} K_2 \xi(t) q_2 = 0, \end{aligned} \quad (1)$$

where  $q_1$  and  $q_2$  are generalized displacements.  $\omega_1$  and  $\omega_2$  are natural frequencies.  $\epsilon$  is a small parameter.  $\beta_1$  and  $\beta_2$  are nonviscous damping coefficients.  $H_i$  and  $K_i$  are constants.  $\xi(t)$  is a Gaussian white noise with zero mean and noise intensity  $\sigma^2$ .  $\gamma(t)$  is a relaxation function of nonviscous damping, which can be expressed by

$$\gamma(t) = \frac{1}{\alpha} \exp\left\{-\frac{t}{\alpha}\right\} \quad (2)$$

in which  $\alpha$  is the relaxation parameter. Note that the limit case  $\alpha \rightarrow 0$ , the nonviscous damping force reduces to classical viscous damping.

Let  $q_1 = x_1$ ,  $\dot{q}_1 = \omega_1 x_2$ ,  $q_2 = x_3$ ,  $\dot{q}_2 = \omega_2 x_4$ ; system (1) can be represented as

$$\begin{aligned} \dot{x}_1 &= \omega_1 x_2, \\ \dot{x}_2 &= -\omega_1 x_1 - \epsilon h_1 (x_1 - x_3) - \epsilon \zeta_1 \int_0^t \gamma(t-\tau) \dot{x}_1(\tau) d\tau \\ &\quad + \sqrt{\epsilon} k_1 x_1 \xi(t), \\ \dot{x}_3 &= \omega_2 x_4, \\ \dot{x}_4 &= -\omega_2 x_3 - \epsilon h_2 (x_3 - x_1) - \epsilon \zeta_2 \int_0^t \gamma(t-\tau) \dot{x}_3(\tau) d\tau \\ &\quad + \sqrt{\epsilon} k_2 x_3 \xi(t), \end{aligned} \quad (3)$$

where

$$\begin{aligned} h_1 &= \frac{H_1}{\omega_1}, \\ h_2 &= \frac{H_2}{\omega_2}, \\ k_1 &= \frac{K_1}{\omega_1}, \\ k_2 &= \frac{K_2}{\omega_2}, \\ \zeta_1 &= \frac{\beta_1}{\omega_1}, \\ \zeta_2 &= \frac{\beta_2}{\omega_2} \end{aligned} \quad (4)$$

Using a coordinate transformation,

$$\begin{aligned}x_1 &= a \cos \varphi \cos \theta_1, \\x_2 &= -a \cos \varphi \sin \theta_1, \\x_3 &= a \sin \varphi \cos \theta_2, \\x_4 &= -a \sin \varphi \sin \theta_2.\end{aligned}\quad (5)$$

where  $a$  represents the norm of the response.  $0 \leq \theta_1 \leq 2\pi$  and  $0 \leq \theta_2 \leq 2\pi$  are the angles process of the coupled stochastic system.  $0 \leq \varphi \leq \pi/2$  denotes the coupling or exchange of energy between the coupled system. Equation (3) can be rewritten as

$$\begin{aligned}\dot{\theta}_1 &= \omega_1 + \epsilon \frac{\zeta_1}{a} \frac{1}{\cos \varphi} \cos \theta_1 \int_0^t \gamma(t-\tau) \dot{x}_1(\tau) d\tau \\&+ \frac{\epsilon h_1}{2} (1 + \cos 2\theta_1 - 2 \cos \theta_1 \cos \theta_2 \tan \varphi) \\&- \sqrt{\epsilon} k_1 \cos^2 \theta_1 \xi(t), \\ \dot{\theta}_2 &= \omega_2 + \epsilon \frac{\zeta_2}{a} \frac{1}{\sin \varphi} \cos \theta_2 \int_0^t \gamma(t-\tau) \dot{x}_3(\tau) d\tau \\&+ \frac{\epsilon h_2}{2} (1 + \cos 2\theta_2 - 2 \cos \theta_1 \cos \theta_2 \cot \varphi) \\&- \sqrt{\epsilon} k_2 \cos^2 \theta_2 \xi(t), \\ \dot{\varphi} &= \epsilon \left\{ \frac{h_1}{4} [2(1 - \cos 2\varphi) \sin \theta_1 \cos \theta_2 \right. \\&- \sin 2\varphi \sin 2\theta_1] - \frac{\zeta_1}{a} \sin \varphi \sin \theta_1 \int_0^t \gamma(t-\tau) \\&\cdot \dot{x}_1(\tau) d\tau + \frac{h_2}{4} [-2(1 + \cos 2\varphi) \cos \theta_1 \sin \theta_2 \\&+ \sin 2\varphi \sin 2\theta_2] + \frac{\zeta_2}{a} \sin \varphi \sin \theta_2 \int_0^t \gamma(t-\tau) \\&\cdot \dot{x}_3(\tau) d\tau \left. \right\} + \frac{\sqrt{\epsilon}}{4} (k_1 \sin 2\theta_1 - k_2 \sin 2\theta_2) \\&\cdot \sin 2\varphi \xi(t), \\ \dot{a} &= \epsilon \frac{a}{4} \left\{ h_1 [(1 + \cos 2\varphi) \sin 2\theta_1 \right. \\&- 2 \sin 2\varphi \sin \theta_1 \cos \theta_2] + \frac{\zeta_1}{a} \cos \varphi \sin \theta_1 \int_0^t \gamma(t-\tau) \\&\cdot \dot{x}_1(\tau) d\tau + h_2 [(1 - \cos 2\varphi) \sin 2\theta_2 \\&- 2 \sin 2\varphi \cos \theta_1 \sin \theta_2] + \frac{\zeta_2}{a} \cos \varphi \sin \theta_2 \int_0^t \gamma(t-\tau) \\&\cdot \dot{x}_3(\tau) d\tau \left. \right\} - \frac{\sqrt{\epsilon}}{4} a [k_1 (1 + \cos 2\varphi) \sin 2\theta_1 \\&+ k_2 (1 - \cos 2\varphi) \sin 2\theta_2] \xi(t)\end{aligned}\quad (6)$$

Therefore, the solution forms of  $\theta_i$  can be expressed as  $\theta_i = \omega_i t + \phi_i(t)$  from (6), where  $\theta_i(t)$  is quickly varying process relative to the process  $\phi_i$  due to  $\epsilon \ll 1$ . Therefore, the following approximations will be obtained:

$$\begin{aligned}\theta_i(t-s) &= \omega_i(t-s) + \phi_i(t-s) \approx \theta_i(t) - \omega_i s, \\ \dot{x}_1(t-s) &= \omega_1 x_2(t-s) = -a\omega_1 \cos \varphi \sin \theta_1(t-s) \\ &\approx -a\omega_1 \cos \varphi \sin(\theta_1 - \omega_1 s) \\ &= \omega_1 x_2 \cos \omega_1 s + \omega_1 x_1 \sin \omega_1 s, \\ \dot{x}_3(t-s) &= \omega_2 x_4(t-s) = -a\omega_2 \cos \varphi \sin \theta_2(t-s) \\ &\approx -a\omega_2 \cos \varphi \sin(\theta_2 - \omega_2 s) \\ &= \omega_2 x_4 \cos \omega_2 s + \omega_2 x_3 \sin \omega_2 s.\end{aligned}\quad (7)$$

Substituting (7) into the nonviscous damping, one obtains

$$\begin{aligned}\int_0^t \gamma(t-\tau) \dot{x}_1(\tau) d\tau &= \frac{1}{\alpha} \int_0^t \exp\left\{-\frac{1}{\alpha}s\right\} \dot{x}_1(t-s) ds \\ &= M_1 x_2 + N_1 x_1.\end{aligned}\quad (8)$$

Similarly, the following results also can be derived:

$$\int_0^t \gamma(t-\tau) \dot{x}_3(\tau) d\tau = M_2 x_4 + N_2 x_3, \quad (9)$$

where

$$\begin{aligned}M_1 &= \frac{\omega_1}{1 + \alpha^2 \omega_1^2}, \\ N_1 &= \frac{\alpha \omega_1^2}{1 + \alpha^2 \omega_1^2}, \\ M_2 &= \frac{\omega_2}{1 + \alpha^2 \omega_2^2}, \\ N_2 &= \frac{\alpha \omega_2^2}{1 + \alpha^2 \omega_2^2}.\end{aligned}\quad (10)$$

Substituting (8) and (9) into (6) and letting  $P = a^p = (x_1^2 + x_2^2 + x_3^2 + x_4^2)^{p/2}$  ( $-\infty < p < +\infty$ ), (6) can be written as the following Itô stochastic differential equations:

$$\begin{aligned}d\theta_1 &= m_1(\theta_1, \theta_2, \varphi) dt + \sigma_{11}(\theta_1, \theta_2, \varphi) dW(t), \\ d\theta_2 &= m_2(\theta_1, \theta_2, \varphi) dt + \sigma_{21}(\theta_1, \theta_2, \varphi) dW(t), \\ d\varphi &= m_3(\theta_1, \theta_2, \varphi) dt + \sigma_{31}(\theta_1, \theta_2, \varphi) dW(t), \\ dP &= P m_4(\theta_1, \theta_2, \varphi) dt + P \sigma_{41}(\theta_1, \theta_2, \varphi) dW(t),\end{aligned}\quad (11)$$

where  $W(t)$  is the standard Wiener process; the drift and diffusion coefficients can be rewritten as

$$\begin{aligned}
m_1(\theta_1, \theta_2, \varphi) &= \omega_1 - \epsilon \frac{\zeta_1}{2} [M_1 \sin 2\theta_1 - N_1 (1 \\
&+ \cos 2\theta_1)] + \epsilon \frac{h_1}{2} (1 + \cos 2\theta_1 - 2 \cos \theta_1 \cos \theta_2 \\
&\cdot \tan \varphi) - \epsilon \frac{k_1^2 \sigma^2}{8} (2 \sin 2\theta_1 + \sin 4\theta_1), \\
m_2(\theta_1, \theta_2, \varphi) &= \omega_2 - \epsilon \frac{\zeta_2}{2} [M_2 \sin 2\theta_2 - N_2 (1 \\
&+ \cos 2\theta_2)] + \epsilon \frac{h_2}{2} (1 + \cos 2\theta_2 - 2 \cos \theta_1 \cos \theta_2 \\
&\cdot \cot \varphi) - \epsilon \frac{k_2^2 \sigma^2}{8} (2 \sin 2\theta_2 + \sin 4\theta_2), \\
m_3(\theta_1, \theta_2, \varphi) &= \epsilon \left\{ \frac{h_1}{4} [2(1 - \cos 2\varphi) \sin \theta_1 \cos \theta_2 \right. \\
&- \sin 2\varphi \sin 2\theta_1] + \frac{\zeta_1}{4} \sin 2\varphi [M_1 (1 - \cos 2\theta_1) \\
&- N_1 \sin 2\theta_1] - \frac{h_2}{4} [2(1 + \cos 2\varphi) \cos \theta_1 \sin \theta_2 \\
&- \sin 2\varphi \sin 2\theta_2] - \frac{\zeta_2}{4} \sin 2\varphi \times [M_2 (1 - \cos 2\theta_2) \\
&- N_2 \sin 2\theta_2] + \frac{\sigma^2}{64} [-4k_1^2 (1 + 2 \cos 2\theta_1 + \cos 4\theta_1) \\
&\cdot \sin 2\varphi + k_1^2 (1 - \cos 4\theta_1) \sin 4\varphi - 4k_1 k_2 \sin 2\theta_1 \\
&\cdot \sin 2\theta_2 \sin 4\varphi + 4k_2^2 (1 + 2 \cos 2\theta_2 + \cos 4\theta_2) \\
&\cdot \sin 2\varphi + k_2^2 (1 - \cos 4\theta_2) \sin 4\varphi] \left. \right\}, \\
m_4(\theta_1, \theta_2, \varphi) &= \epsilon \frac{p}{4} \left\langle h_1 [(1 + \cos 2\varphi) \sin 2\theta_1 - 2 \right. \\
&\cdot \sin 2\varphi \cos \theta_2 \sin \theta_1] - \zeta_1 (1 + \cos 2\varphi) \times [M_1 (1 \\
&- \cos 2\theta_1) - N_1 \sin 2\theta_1] + h_2 [(1 - \cos 2\varphi) \sin 2\theta_2 \\
&- 2 \sin 2\varphi \cos \theta_1 \sin \theta_2] - \zeta_2 (1 - \cos 2\varphi) [M_2 (1 \\
&- \cos 2\theta_2) - N_2 \sin 2\theta_2] + \frac{\sigma^2 k_1^2}{32} \{ [10 + 3p \\
&+ 16 \cos 2\theta_1 - 3(p - 2) \cos 4\theta_1] + [8 + 4p \\
&+ 16 \cos 2\theta_1 - 4(p - 2) \cos 4\theta_1] \cos 2\varphi + (p - 2) \\
&\cdot (1 - \cos 4\theta_1) \cos 4\varphi \} + \frac{\sigma^2 k_1 k_2}{8} (p - 2) \times (1 \\
&- \cos 4\varphi) \sin 2\theta_1 \sin 2\theta_2 + \frac{\sigma^2 k_2^2}{32} \{ [10 + 3p \\
&+ 16 \cos 2\theta_2 - 3(p - 2) \cos 4\theta_2] - [8 + 4p
\end{aligned}$$

$$\begin{aligned}
&+ 16 \cos 2\theta_2 - 4(p - 2) \cos 4\theta_2] \cos 2\varphi + (p - 2) \\
&\cdot (1 - \cos 4\theta_2) \cos 4\varphi \left. \right\rangle,
\end{aligned}$$

$$\begin{aligned}
\sigma_{11}(\theta_1, \theta_2, \varphi) &= -\sqrt{\epsilon} k_1 \sigma \cos^2 \theta_1, \\
\sigma_{21}(\theta_1, \theta_2, \varphi) &= -\sqrt{\epsilon} k_2 \sigma \cos^2 \theta_2, \\
\sigma_{31}(\theta_1, \theta_2, \varphi) &= \sqrt{\epsilon} \frac{\sigma}{4} (k_1 \sin 2\theta_1 - k_2 \sin 2\theta_2) \sin 2\varphi, \\
\sigma_{41}(\theta_1, \theta_2, \varphi) &= -\sqrt{\epsilon} \frac{p\sigma}{4} [k_1 (1 + \cos 2\varphi) \sin 2\theta_1 \\
&+ k_2 (1 - \cos 2\varphi) \sin 2\theta_2].
\end{aligned} \tag{12}$$

To obtain the eigenvalue problem for the  $p$ th moment Lyapunov exponents of a four-dimensional linear Itô stochastic system, a linear stochastic transformation [34] is introduced

$$S = T(\theta_1, \theta_2, \varphi) P, \quad P = T^{-1}(\theta_1, \theta_2, \varphi) S, \tag{13}$$

where  $S$  is a new norm process depending on the transformation function  $T(\theta_1, \theta_2, \varphi)$ . The transformation function  $T(\theta_1, \theta_2, \varphi)$  is defined on the independent stationary phase processes  $\theta_1, \theta_2$ , and  $\varphi$  in the ranges  $0 \leq \theta_1 \leq 2\pi, 0 \leq \theta_2 \leq 2\pi, 0 \leq \varphi \leq \pi/2$ . Applying Itô formula, one can obtain

$$\begin{aligned}
dS &= P \left[ \frac{1}{2} \sigma_{11}^2 T''_{\theta_1 \theta_1} + \sigma_{11} \sigma_{21} T''_{\theta_1 \theta_2} + \sigma_{11} \sigma_{31} T''_{\theta_1 \varphi} \right. \\
&+ \frac{1}{2} \sigma_{21}^2 T''_{\theta_2 \theta_2} + \sigma_{21} \sigma_{31} T''_{\theta_2 \varphi} + \frac{1}{2} \sigma_{31}^2 T''_{\varphi \varphi} \\
&+ (m_1 + \sigma_{11} \sigma_{41}) T'_{\theta_1} + (m_2 + \sigma_{21} \sigma_{41}) T'_{\theta_2} \\
&+ (m_3 + \sigma_{31} \sigma_{41}) T'_{\varphi} + m_4 T \left. \right] dt + P (\sigma_{11} T'_{\theta_1} \\
&+ \sigma_{21} T'_{\theta_2} + \sigma_{31} T'_{\varphi} + \sigma_{41} T) dW(t).
\end{aligned} \tag{14}$$

If the transformation function  $T(\theta_1, \theta_2, \varphi)$  is bounded and nonsingular, both processes  $P$  and  $S$  have the same stability behavior. Therefore, transformation function  $T(\theta_1, \theta_2, \varphi)$  is chosen so that the drift term of the Itô differential equation (14) does not depend on the phase processes  $\theta_1, \theta_2$ , and  $\varphi$ , so one can obtain

$$\begin{aligned}
dS &= \Lambda(p) S dt \\
&+ ST^{-1} (\sigma_{11} T'_{\theta_1} + \sigma_{21} T'_{\theta_2} + \sigma_{31} T'_{\varphi} + \sigma_{41} T) dW(t).
\end{aligned} \tag{15}$$

Comparing (14) and (15), such transformation function  $T(\theta_1, \theta_2, \varphi)$  can be written by the following equation:

$$[L_0 + \epsilon L_1] T(\theta_1, \theta_2, \varphi) = \Lambda(p) T(\theta_1, \theta_2, \varphi). \tag{16}$$

where  $L_0$  and  $L_1$  are the following first-order and second-order differential operators:

$$\begin{aligned}
 L_0 &= \omega_1 \frac{\partial}{\partial \theta_1} + \omega_2 \frac{\partial}{\partial \theta_2}, \\
 L_1 &= a_1(\theta_1, \theta_2, \varphi) \frac{\partial^2}{\partial \theta_1^2} + a_2(\theta_1, \theta_2, \varphi) \frac{\partial^2}{\partial \theta_1 \partial \theta_2} \\
 &\quad + a_3(\theta_1, \theta_2, \varphi) \frac{\partial^2}{\partial \theta_1 \partial \varphi} + a_4(\theta_1, \theta_2, \varphi) \frac{\partial^2}{\partial \theta_2^2} \\
 &\quad + a_5(\theta_1, \theta_2, \varphi) \frac{\partial^2}{\partial \theta_2 \partial \varphi} + a_6(\theta_1, \theta_2, \varphi) \frac{\partial^2}{\partial \varphi^2} \\
 &\quad + b_1(\theta_1, \theta_2, \varphi) \frac{\partial}{\partial \theta_1} + b_2(\theta_1, \theta_2, \varphi) \frac{\partial}{\partial \theta_2} \\
 &\quad + b_3(\theta_1, \theta_2, \varphi) \frac{\partial}{\partial \varphi} + c(\theta_1, \theta_2, \varphi),
 \end{aligned} \tag{17}$$

in which

$$\begin{aligned}
 a_1(\theta_1, \theta_2, \varphi) &= \frac{1}{2} k_1^2 \sigma^2 \cos^4 \theta_1, \\
 a_2(\theta_1, \theta_2, \varphi) &= \sigma^2 k_1 k_2 \cos^2 \theta_1 \cos^2 \theta_2, \\
 a_3(\theta_1, \theta_2, \varphi) &= -\frac{k_1 \sigma^2}{4} (k_1 \sin 2\theta_1 - k_2 \sin 2\theta_2) \cos^2 \theta_1 \\
 &\quad \cdot \sin 2\varphi, \\
 a_4(\theta_1, \theta_2, \varphi) &= \frac{1}{2} k_2^2 \sigma^2 \cos^4 \theta_2, \\
 a_5(\theta_1, \theta_2, \varphi) &= -\frac{k_2 \sigma^2}{4} (k_1 \sin 2\theta_1 - k_2 \sin 2\theta_2) \cos^2 \theta_2 \\
 &\quad \cdot \sin 2\varphi, \\
 a_6(\theta_1, \theta_2, \varphi) &= \frac{\sigma^2}{32} (k_1 \sin 2\theta_1 - k_2 \sin 2\theta_2)^2 \sin^2 2\varphi, \\
 b_1(\theta_1, \theta_2, \varphi) &= -\frac{\zeta_1}{2} [M_1 \sin 2\theta_1 - N_1 (1 + \cos 2\theta_1)] \\
 &\quad + \frac{1}{2} h_1 (1 + \cos 2\theta_1 - 2 \cos \theta_1 \cos \theta_2 \tan \varphi) - \frac{k_1^2 \sigma^2}{8} \\
 &\quad \times (2 \sin 2\theta_1 + \sin 4\theta_1) + \frac{k_1 \sigma^2 p}{4} [k_1 (1 + \cos 2\varphi) \\
 &\quad \cdot \sin 2\theta_1 + k_2 (1 - \cos 2\varphi) \sin 2\theta_2] \cos^2 \theta_1, \\
 b_2(\theta_1, \theta_2, \varphi) &= -\frac{\zeta_2}{2} [M_2 \sin 2\theta_2 - N_2 (1 + \cos 2\theta_2)] \\
 &\quad + \frac{1}{2} h_2 (1 + \cos 2\theta_2 - 2 \cos \theta_1 \cos \theta_2 \cot \varphi) - \frac{k_2^2 \sigma^2}{8} \\
 &\quad \times (2 \sin 2\theta_2 + \sin 4\theta_2) + \frac{k_2 \sigma^2 p}{4} [k_1 (1 + \cos 2\varphi)
 \end{aligned}$$

$$\begin{aligned}
 &\quad \cdot \sin 2\theta_1 + k_2 (1 - \cos 2\varphi) \sin 2\theta_2] \cos^2 \theta_2, \\
 b_3(\theta_1, \theta_2, \varphi) &= \frac{h_1}{4} [2(1 - \cos 2\varphi) \sin \theta_1 \cos \theta_2 \\
 &\quad - \sin 2\varphi \sin 2\theta_1] + \frac{\zeta_1}{4} \sin 2\varphi [M_1 (1 - \cos 2\theta_1) \\
 &\quad - N_1 \sin 2\theta_1] + \frac{h_2}{4} [-2(1 + \cos 2\varphi) \cos \theta_1 \sin \theta_2 \\
 &\quad + \sin 2\varphi \sin 2\theta_2] - \frac{\zeta_2}{4} \sin 2\varphi [M_2 (1 - \cos 2\theta_2) \\
 &\quad - N_2 \sin 2\theta_2] + \frac{\sigma^2}{64} [-4k_1^2 (1 + 2 \cos 2\theta_1 + \cos 4\theta_1) \\
 &\quad \times \sin 2\varphi + k_1^2 (1 - \cos 4\theta_1) \sin 4\varphi - 4k_1 k_2 \sin 2\theta_1 \\
 &\quad \cdot \sin 2\theta_2 \sin 4\varphi + 4k_2^2 (1 + 2 \cos 2\theta_2 + \cos 4\theta_2) \\
 &\quad \cdot \sin 2\varphi + k_2^2 (1 - \cos 4\theta_2) \sin 4\varphi] - \frac{\sigma^2 p}{16} (k_1 \sin 2\theta_1 \\
 &\quad - k_2 \sin 2\theta_2) \times [k_1 (1 + \cos 2\varphi) \sin 2\theta_1 + k_2 (1 \\
 &\quad - \cos 2\varphi) \sin 2\theta_2] \sin 2\varphi, \\
 c(\theta_1, \theta_2, \varphi) &= \frac{p}{4} \left\langle h_1 [(1 + \cos 2\varphi) \sin 2\theta_1 - 2 \sin 2\varphi \right. \\
 &\quad \cdot \cos \theta_2 \sin \theta_1] - \zeta_1 (1 + \cos 2\varphi) [M_1 (1 - \cos 2\theta_1) \\
 &\quad - N_1 \sin 2\theta_1] + h_2 [(1 - \cos 2\varphi) \sin 2\theta_2 - 2 \sin 2\varphi \\
 &\quad \cdot \cos \theta_1 \sin \theta_2] - \zeta_2 (1 - \cos 2\varphi) [M_2 (1 - \cos 2\theta_2) \\
 &\quad - N_2 \sin 2\theta_2] + \frac{\sigma^2 k_1^2}{32} \times \{[10 + 3p + 16 \cos 2\theta_1 \\
 &\quad - 3(p - 2) \cos 4\theta_1] + [8 + 4p + 16 \cos 2\theta_1 \\
 &\quad - 4(p - 2) \cos 4\theta_1] \times \cos 2\varphi + (p - 2) (1 \\
 &\quad - \cos 4\theta_1) \cos 4\varphi\} + \frac{\sigma^2 k_1 k_2}{8} (p - 2) (1 - \cos 4\varphi) \\
 &\quad \cdot \sin 2\theta_1 \sin 2\theta_2 + \frac{\sigma^2 k_2^2}{32} \{[10 + 3p + 16 \cos 2\theta_2 \\
 &\quad - 3(p - 2) \cos 4\theta_2] - [8 + 4p + 16 \cos 2\theta_2 \\
 &\quad - 4(p - 2) \cos 4\theta_2] \cos 2\varphi + (p - 2) (1 - \cos 4\theta_2) \\
 &\quad \cdot \cos 4\varphi\} \left. \right\rangle.
 \end{aligned} \tag{18}$$

In the following investigation, the perturbation theory will be used to obtain the solution  $\Lambda(p)$  of (16).

### 3. Moment Lyapunov Exponents

The method of deriving the eigenvalue problem for the moment Lyapunov exponents of a two-dimensional linear Itô stochastic system was first applied by Wedig [34]. The eigenvalue problem for a differential operator of three independent variables  $\theta_1$ ,  $\theta_2$ , and  $\varphi$  will be identified from (16), in which  $\Lambda(p)$  is the eigenvalue and  $T(\theta_1, \theta_2, \varphi)$  is the associated eigenfunction. Meanwhile, the eigenvalue  $\Lambda(p)$  is seen to be the Lyapunov exponent of the  $p$ th moment of system (1) from (15). Applying the perturbation theory, both the moment Lyapunov exponent  $\Lambda(p)$  and the eigenfunction  $T(\theta_1, \theta_2, \varphi)$  are expanded in power series of  $\epsilon$ ; that is,

$$\begin{aligned}\Lambda(p) &= \Lambda_0(p) + \epsilon \Lambda_1(p) + \epsilon^2 \Lambda_2(p) + \dots \\ &\quad + \epsilon^n \Lambda_n(p) + \dots, \\ T(\theta_1, \theta_2, \varphi) &= T_0(\theta_1, \theta_2, \varphi) + \epsilon T_1(\theta_1, \theta_2, \varphi) \\ &\quad + \epsilon^2 T_2(\theta_1, \theta_2, \varphi) + \dots \\ &\quad + \epsilon^n T_n(\theta_1, \theta_2, \varphi) + \dots.\end{aligned}\quad (19)$$

Substituting (19) into (16) and equating terms of the equal powers of  $\epsilon$  lead to the following equations:

$$\begin{aligned}\epsilon^0: L_0 T_0(\theta_1, \theta_2, \varphi) &= \Lambda_0(p) T_0(\theta_1, \theta_2, \varphi), \\ \epsilon^1: L_0 T_1(\theta_1, \theta_2, \varphi) \\ &\quad + L_1 T_0(\theta_1, \theta_2, \varphi) = \Lambda_0(p) T_1(\theta_1, \theta_2, \varphi) \\ &\quad + \Lambda_1(p) T_0(\theta_1, \theta_2, \varphi), \\ \dots \\ \epsilon^n: L_0 T_n(\theta_1, \theta_2, \varphi) \\ &\quad + L_1 T_{n-1}(\theta_1, \theta_2, \varphi) = \Lambda_0(p) T_n(\theta_1, \theta_2, \varphi) \\ &\quad + \Lambda_1(p) T_{n-1}(\theta_1, \theta_2, \varphi) + \dots \\ &\quad + \Lambda_n(p) T_0(\theta_1, \theta_2, \varphi),\end{aligned}\quad (20)$$

where  $T_i(\theta_1, \theta_2, \varphi)$  must be positive and periodic in the range  $0 \leq \theta_1 \leq 2\pi$ ,  $0 \leq \theta_2 \leq 2\pi$ .

**3.1. The Zeroth-Order Perturbation.** Substituting (17) into (20), the zeroth-order perturbation equation is

$$\begin{aligned}\omega_1 \frac{\partial T_0(\theta_1, \theta_2, \varphi)}{\partial \theta_1} + \omega_2 \frac{\partial T_0(\theta_1, \theta_2, \varphi)}{\partial \theta_2} \\ = \Lambda_0(p) T_0(\theta_1, \theta_2, \varphi).\end{aligned}\quad (21)$$

Through  $\Lambda(0) = \Lambda_0(0) + \epsilon \Lambda_1(0) + \epsilon^2 \Lambda_2(0) + \dots + \epsilon^n \Lambda_n(0) = 0$ , thus,  $\Lambda_n(0) = 0$ ,  $n = 1, 2, \dots$  will be obtained. Then (21) does

not contain  $p$ , and the eigenvalue  $\Lambda_0(p)$  is independent of  $p$ . Therefore,  $\Lambda_0(0) = 0$  will lead to  $\Lambda_0(p) = 0$  for arbitrary  $p$ . At this point, (21) will be reduced to

$$\omega_1 \frac{\partial T_0(\theta_1, \theta_2, \varphi)}{\partial \theta_1} + \omega_2 \frac{\partial T_0(\theta_1, \theta_2, \varphi)}{\partial \theta_2} = 0. \quad (22)$$

Using the method of separation of variables, so we can express  $T_0(\theta_1, \theta_2, \varphi)$  as

$$T_0(\theta_1, \theta_2, \varphi) = \Theta_1(\theta_1) \Theta_2(\theta_2) \psi(\varphi), \quad (23)$$

where  $\Theta_1(\theta_1)$ ,  $\Theta_2(\theta_2)$ , and  $\psi(\varphi)$  are functions about  $\theta_1$ ,  $\theta_2$ , and  $\varphi$ , respectively.

Substituting (23) into (22), (22) will become

$$\frac{\omega_1}{\Theta_1} \frac{\partial \Theta_1}{\partial \theta_1} + \frac{\omega_2}{\Theta_2} \frac{\partial \Theta_2}{\partial \theta_2} = 0. \quad (24)$$

Solving the above differential equation (24), one can easily obtain

$$\begin{aligned}\Theta_1(\theta_1) &= C_1 e^{c_1 \theta_1}, \\ \Theta_2(\theta_2) &= C_2 e^{c_2 \theta_2}.\end{aligned}\quad (25)$$

In addition, since function  $T_0(\theta_1, \theta_2, \varphi)$  is periodic about  $\theta_1$  and  $\theta_2$ , the following boundary conditions can be obtained:

$$\begin{aligned}T_0(\theta_1 + 2\pi, \theta_2, \varphi) &= T_0(\theta_1, \theta_2 + 2\pi, \varphi) \\ &= T_0(\theta_1, \theta_2, \varphi).\end{aligned}\quad (26)$$

Substituting (23) and (25) into (26), we can determine the constants  $c_1 = c_2 = 0$ . Therefore,  $T_0(\theta_1, \theta_2, \varphi)$  is a function about only  $\varphi$  to be determined; that is,  $T_0(\theta_1, \theta_2, \varphi) = T_0(\varphi)$ .

The adjoint equation of (22) is

$$-\omega_1 \frac{\partial T_0^*(\theta_1, \theta_2, \varphi)}{\partial \theta_1} - \omega_2 \frac{\partial T_0^*(\theta_1, \theta_2, \varphi)}{\partial \theta_2} = 0. \quad (27)$$

Applying the method of separation of variables to solve (27), one obtains

$$T_0^* = \frac{F(\varphi)}{4\pi^2}, \quad \varphi \in (0, 2\pi), \quad (28)$$

where  $F(\varphi)$  is an arbitrary function.

**3.2. The First-Order Perturbation.** From (20), the first-order perturbation equation is

$$\begin{aligned}L_0 T_1(\theta_1, \theta_2, \varphi) + L_1 T_0(\theta_1, \theta_2, \varphi) \\ = \Lambda_0(p) T_1(\theta_1, \theta_2, \varphi) + \Lambda_1(p) T_0(\theta_1, \theta_2, \varphi),\end{aligned}\quad (29)$$

Based on the analysis results in Section 3.1, one obtains

$$L_0 T_1(\theta_1, \theta_2, \varphi) = \Lambda_1(p) T_0(\varphi) - L_1 T_0(\theta_1, \theta_2, \varphi). \quad (30)$$

Then the solvability condition of (30) is

$$\begin{aligned} \langle \Lambda_1(p) T_0(\varphi) - L_1 T_0(\varphi), T_0^* \rangle &= \frac{1}{4\pi^2} \int_0^{\pi/2} F(\varphi) \\ &\cdot \int_0^{2\pi} \int_0^{2\pi} [\Lambda_1(p) T_0(\varphi) - L_1 T_0(\varphi)] d\theta_1 d\theta_2 d\varphi \\ &= 0, \end{aligned} \quad (31)$$

$$L_1 T_0(\varphi) = c T_0(\varphi) + b_3 \frac{\partial T_0(\varphi)}{\partial \varphi} + a_6 \frac{\partial^2 T_0(\varphi)}{\partial \varphi^2}.$$

Applying the sense of the arbitrary of function  $F(\varphi)$ , (31) will become

$$\begin{aligned} \int_0^{\pi/2} \left[ (\Lambda_1(p) - pQ(\varphi)) T_0(\varphi) \right. \\ \left. - (\mu(\varphi) + p\bar{\mu}(\varphi)) \frac{\partial T_0(\varphi)}{\partial \varphi} \right. \\ \left. - \frac{1}{2} R^2(\varphi) \frac{\partial^2 T_0(\varphi)}{\partial \varphi^2} \right] d\varphi = 0, \end{aligned} \quad (32)$$

where

$$\begin{aligned} Q(\varphi) &= \frac{1}{32} \left\{ \frac{1}{2} (6+p) (k_1^2 + k_2^2) \sigma^2 \right. \\ &\quad - 8(M_1\zeta_1 + M_2\zeta_2) \\ &\quad + [(p+2) (k_1^2 - k_2^2) \sigma^2 - 8(M_1\zeta_1 - M_2\zeta_2)] \\ &\quad \left. \times \cos 2\varphi + \frac{1}{2} (-2+p) (k_1^2 + k_2^2) \sigma^2 \cos^2 2\varphi \right\}, \\ \mu(\varphi) &= -\frac{1}{32} \left\{ [2(k_1^2 - k_2^2) \sigma^2 - 8(M_1\zeta_1 - M_2\zeta_2)] \right. \\ &\quad \left. \cdot \sin 2\varphi - (k_1^2 + k_2^2) \sigma^2 \sin 2\varphi \cos 2\varphi \right\}, \\ \bar{\mu}(\varphi) &= -\frac{1}{32} \left\{ [(k_1^2 - k_2^2) \sigma^2 \sin 2\varphi + (k_1^2 + k_2^2) \sigma^2 \right. \\ &\quad \left. \cdot \sin 2\varphi \cos 2\varphi] \right\}, \\ R^2(\varphi) &= \frac{1}{64} (k_1^2 + k_2^2) \sigma^2 \sin^2 2\varphi; \end{aligned} \quad (33)$$

then (32) is simplified as the following equation:

$$\begin{aligned} L(p) T_0(\varphi) &= \Lambda_1(p) T_0(\varphi), \\ L(p) &= \frac{1}{2} R^2(\varphi) \frac{\partial}{\partial \varphi^2} + [\mu(\varphi) + p\bar{\mu}(\varphi)] \frac{\partial}{\partial \varphi} + pQ(\varphi). \end{aligned} \quad (34)$$

Then the boundary conditions of (34) are determined by considering the adjoint equation for the case of  $p = 0$ ,

$$L^* \bar{m}(\varphi) = 0, \quad L^* = \frac{1}{2} \frac{\partial}{\partial \varphi^2} R^2(\varphi) - \frac{\partial}{\partial \varphi} \mu(\varphi), \quad (35)$$

where  $L^*$  is the Fokker-Planck operator and  $\varphi = 0$  and  $\varphi = \pi/2$  are the entrance boundaries [27]. The eigenfunction  $T_0(\varphi)$  satisfies zero Neumann boundary condition, and  $\Lambda_1(p)$  is the largest eigenvalue of (34) with zeros Neumann boundary. Therefore, the solution of (34) can be calculated from an orthogonal expansion [34]. Under zeros Neumann boundary conditions,  $T_0(\varphi)$  can be expressed by a Fourier cosine series [27]; that is,

$$T_0(\varphi) = \sum_{n=0}^{\infty} z_n \cos 2n\varphi. \quad (36)$$

Substituting (36) into (34), multiplying by  $\cos 2n\varphi$  in both sides and integrating for  $\varphi$ , we can obtain

$$\begin{aligned} \sum_{m=0}^{\infty} a_{m0} z_m &= 2\Lambda_1(p) z_0, \\ \sum_{m=0}^{\infty} a_{mn} z_m &= \Lambda_1(p) z_n, \quad n = 1, 2, \dots, \end{aligned} \quad (37)$$

where

$$a_{mn} = \frac{4}{\pi} \int_0^{\pi/2} L(p) (\cos 2m\varphi) \cos 2n\varphi d\varphi, \quad m, n = 0, 1, 2, \dots, \quad (38)$$

In order to guarantee the existence of the nontrivial solution for each  $z_n$ , the coefficient matrix  $A = (a_{mn})$  must equal zero. Therefore, the problem of calculating  $\Lambda_1(p)$  is translated into calculating the leading eigenvalue of  $A$ . The sequence of approximations will be constructed by the eigenvalues of a sequence of the following submatrices:

$$\begin{aligned} &\left[ \frac{1}{2} a_{00} \right], \\ &\begin{bmatrix} \frac{1}{2} a_{00} & a_{01} \\ \frac{1}{2} a_{10} & a_{11} \end{bmatrix}, \\ &\begin{bmatrix} \frac{1}{2} a_{00} & a_{01} & a_{02} & \dots \\ \frac{1}{2} a_{10} & a_{11} & a_{12} & \dots \\ \frac{1}{2} a_{20} & a_{21} & a_{22} & \dots \\ \vdots & \vdots & \vdots & \ddots \end{bmatrix}, \end{aligned} \quad (39)$$

Obviously, the set of approximate eigenvalues obtained by this method converges to the associated true eigenvalues as  $n \rightarrow \infty$ . In general, we can obtain the approximate

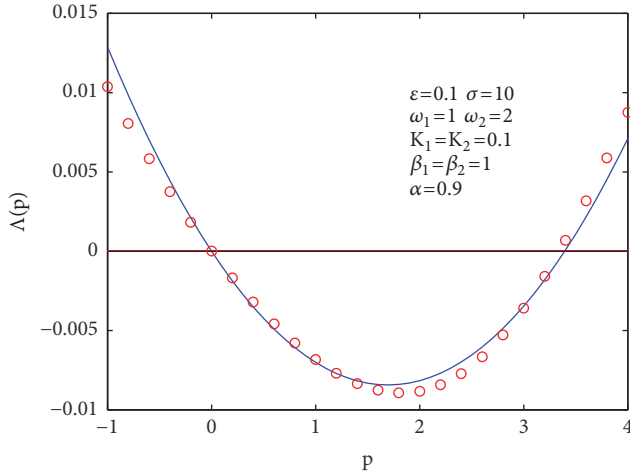


FIGURE 1: Variation of moment Lyapunov exponent with  $p$ . Solid-line in the analytical results of truncation of  $n$ , circle in the numerical results by Monte Carlo.

eigenvalues by truncating  $n$ , which can be written as  $\Lambda_1(p) = a_{00}/2$  and

$$\begin{aligned} \Lambda(p) &= \epsilon \Lambda_1(p) + O(\epsilon^2) = \frac{1}{128} \\ &\cdot \epsilon p \left[ (10 + 3p)(k_1^2 + k_2^2)\sigma^2 - 32(M_1\zeta_1 + M_2\zeta_2) \right] \\ &+ O(\epsilon^2). \end{aligned} \quad (40)$$

The comparison results of approximate analytical moment Lyapunov exponents obtained by truncating  $n$  and the direct Monte Carlo simulation results are shown in Figure 1. It is easily found that the approximate results agree well with the simulation results. Therefore, the first-order perturbation will be reduced to

$$\begin{aligned} \omega_1 \frac{\partial T_1(\theta_1, \theta_2, \varphi)}{\partial \theta_1} + \omega_2 \frac{\partial T_1(\theta_1, \theta_2, \varphi)}{\partial \theta_2} + c(\theta_1, \theta_2, \varphi) \\ = \Lambda_1(p). \end{aligned} \quad (41)$$

Without loss of generality, there is a relationship between two frequencies of the form  $m_1\omega_1 = m_2\omega_2$ , in which  $m_1$  and  $m_2$  are integers. The second frequency can be rewritten as  $\omega_2 = k\omega_1$ . Then the function  $c(\theta_1, \theta_2, \varphi)$  in (41) can be rewritten as

$$\begin{aligned} c(\theta_1, \theta_2, \varphi) &= \Lambda_1(p) + f_0(\theta_1, \theta_2) \\ &+ f_1(\theta_1, \theta_2) \cos 2\varphi \\ &+ f_2(\theta_1, \theta_2) \cos 4\varphi \\ &+ f_3(\theta_1, \theta_2) \sin 2\varphi, \end{aligned} \quad (42)$$

where function  $f_r(\theta_1, \theta_2)$  is the periodic function on  $\theta_1, \theta_2$  and given as

$$\begin{aligned} f_0(\theta_1, \theta_2) &= \frac{p}{4} (h_1 + \zeta_1 N_1) \sin 2\theta_1 \\ &+ \frac{p}{8} (2\zeta_1 M_1 + k_1^2 \sigma^2) \cos 2\theta_1 \\ &+ \frac{p}{4} (h_2 + \zeta_2 N_2) \sin 2\theta_2 \\ &+ \frac{p}{8} (2\zeta_2 M_2 + k_2^2 \sigma^2) \cos 2\theta_2 \\ &+ \frac{3k_1^2 \sigma^2}{128} p(2-p) \cos 4\theta_1 \\ &+ \frac{3k_2^2 \sigma^2}{128} p(2-p) \cos 4\theta_2 \\ &- \frac{k_1 k_2 \sigma^2}{32} p(2-p) \sin 2\theta_1 \sin 2\theta_2, \\ f_1(\theta_1, \theta_2) &= \frac{p}{4} (h_1 + \zeta_1 N_1) \sin 2\theta_1 \\ &+ \frac{p}{8} (2\zeta_1 M_1 + k_1^2 \sigma^2) \cos 2\theta_1 \\ &- \frac{p}{4} (h_2 + \zeta_2 N_2) \sin 2\theta_2 \\ &- \frac{p}{8} (2\zeta_2 M_2 + k_2^2 \sigma^2) \cos 2\theta_2 \\ &+ \frac{k_1^2 \sigma^2}{32} p(2-p) \cos 4\theta_1 - \frac{k_2^2 \sigma^2}{32} p(2-p) \cos 4\theta_2 \\ &+ \frac{p}{32} [8(-\zeta_1 M_1 + \zeta_2 M_2) + (k_1^2 - k_2^2) \sigma^2 (2+p)], \\ f_2(\theta_1, \theta_2) &= -\frac{p(2-p)\sigma^2}{128} (k_1^2 + k_2^2) \\ &+ \frac{p(2-p)\sigma^2}{32} \sin 2\theta_1 \sin 2\theta_2 \\ &+ \frac{p(2-p)\sigma^2}{128} k_1^2 \cos 4\theta_1 \\ &+ \frac{p(2-p)\sigma^2}{128} k_2^2 \cos 4\theta_2, \\ f_3(\theta_1, \theta_2) &= -\frac{h_1 p}{2} \sin 2\theta_1 \cos 2\theta_2 - \frac{h_2 p}{2} \sin 2\theta_2 \cos 2\theta_1. \end{aligned} \quad (43)$$

Note that the general solution  $T_1(\theta_1, \theta_2, \varphi)$  of (41) can not be obtained except in some special cases. Considering the nature

of the coefficients of (41), the series expansion of function  $T_1(\theta_1, \theta_2, \varphi)$  can be presented in the following form:

$$T_1(\theta_1, \theta_2, \varphi) = T_{10}(\theta_1, \theta_2) + T_{11}(\theta_1, \theta_2) \cos 2\varphi + T_{12}(\theta_1, \theta_2) \cos 4\varphi + T_{13}(\theta_1, \theta_2) \sin 2\varphi. \quad (44)$$

Substituting (44) into (41) and equating terms of the equal trigonometry function to give a set of partial differential equations, one obtains

$$\omega_1 \frac{\partial T_{1r}(\theta_1, \theta_2)}{\partial \theta_1} + \omega_2 \frac{\partial T_{1r}(\theta_1, \theta_2)}{\partial \theta_2} + f_r(\theta_1, \theta_2) = 0, \quad (45)$$

$$r = 0, 1, 2, 3,$$

where the function  $T_{1r}(\theta_1, \theta_2)$  can be written as

$$T_{10}(\theta_1, \theta_2) = -\frac{p(2\zeta_1 M_1 + k_1^2 \sigma^2)}{16\omega_1} \sin 2\theta_1 + \frac{p(h_1 + \zeta_1 N_1)}{8\omega_1} \cos 2\theta_1 - \frac{p(2\zeta_2 M_2 + k_2^2 \sigma^2)}{16k\omega_1} \sin 2\theta_2 + \frac{p(h_2 + \zeta_2 N_2)}{8k\omega_1} \cos 2\theta_2 - \frac{3k_1^2 p(2-p)\sigma^2}{512\omega_1} \sin 4\theta_1 - \frac{3k_2^2 p(2-p)\sigma^2}{512k\omega_1} \sin 4\theta_2 + \frac{kk_1 k_2 p(2-p)\sigma^2}{64(1-k^2)\omega_1} \sin 2\theta_1 \cos 2\theta_2 - \frac{k_1 k_2 p(2-p)\sigma^2}{64(1-k^2)\omega_1} \sin 2\theta_2 \cos 2\theta_1 + C_0(\theta_2 - k\theta_1),$$

$$T_{11}(\theta_1, \theta_2) = -\frac{p[8(-\zeta_1 M_1 + \zeta_2 M_2) + (k_1^2 - k_2^2)(2+p)\sigma^2]}{32\omega_1} \theta_1 - \frac{p(2\zeta_1 M_1 + k_1^2 \sigma^2)}{16\omega_1} \sin 2\theta_1 + \frac{p(h_1 + \zeta_1 N_1)}{8\omega_1} \cos 2\theta_1 + \frac{p(2\zeta_2 M_2 + k_2^2 \sigma^2)}{16k\omega_1} \sin 2\theta_2$$

$$- \frac{p(h_2 + \zeta_2 N_2)}{8k\omega_1} \cos 2\theta_2 - \frac{k_1^2 p(2-p)\sigma^2}{128\omega_1} \sin 4\theta_1 + \frac{k_2^2 p(2-p)\sigma^2}{128k\omega_1} \sin 4\theta_2 + C_1(\theta_2 - k\theta_1),$$

$$T_{12}(\theta_1, \theta_2) = \frac{p(2-p)(k_1^2 + k_2^2)}{128\omega_1} \theta_1 - \frac{k_1^2 p(2-p)\sigma^2}{512\omega_1} \sin 4\theta_1 - \frac{k_2^2 p(2-p)\sigma^2}{512k\omega_1} \sin 4\theta_2 - \frac{kk_1 k_2 p(2-p)\sigma^2}{64(1-k^2)\omega_1} \sin 2\theta_1 \cos 2\theta_2 + \frac{k_1 k_2 p(2-p)\sigma^2}{64(1-k^2)\omega_1} \sin 2\theta_2 \cos 2\theta_1 + C_2(\theta_2 - k\theta_1),$$

$$T_{13}(\theta_1, \theta_2) = \frac{p(h_2 - h_1 k)}{2(1-k^2)\omega_1} \sin \theta_1 \sin \theta_2 - \frac{p(h_1 - h_2 k)}{2(1-k^2)\omega_1} \cos \theta_1 \cos \theta_2 + C_3(\theta_2 - k\theta_1), \quad (46)$$

in which  $C_r(\theta_2 - k\theta_1)$  are arbitrary functions of two variables, and we make assumptions as follows:

$$C_r(\theta_2 - k\theta_1) = A_{1r} + B_{1r} \sin(2\theta_2 - 2k\theta_1) + C_{1r} \sin(4\theta_2 - 4k\theta_1), \quad (47)$$

$$r = 0, 1, 2, 3.$$

Here, the unknown constants  $A_{1r}, B_{1r}, C_{1r}$  ( $r = 0, 1, 2, 3$ ) will be determined by using the following conditions:

$$T_{1r}(0, 0) = T_{1r}(0, 2\pi) = T_{1r}(2\pi, 0) = T_{1r}(2\pi, 2\pi) = 0,$$

$$\frac{\partial T_{1r}(0, 0)}{\partial \theta_1} = \frac{\partial T_{1r}(2\pi, 0)}{\partial \theta_1}, \quad (48)$$

$$\frac{\partial T_{1r}(0, 0)}{\partial \theta_2} = \frac{\partial T_{1r}(0, 2\pi)}{\partial \theta_2},$$

$$r = 0, 1, 2, 3.$$

That is,

$$\begin{aligned}
A_{10} &= -\frac{p(h_2 + \zeta_2 N_2 + h_1 k + k \zeta_1 N_1)}{8k\omega_1}, \\
A_{11} &= \frac{p(h_2 + \zeta_2 N_2 - h_1 k - k \zeta_1 N_1)}{8k\omega_1}, \\
A_{12} &= 0, \\
A_{13} &= \frac{p(h_1 - h_2 k)}{2(1 - k^2)\omega_1}, \\
B_{10} &= 0, \\
B_{11} &= -\frac{p\pi [8(-\zeta_1 M_1 + \zeta_2 M_2) + (k_1^2 - k_2^2)(2 + p)\sigma^2] \cos^2 2k\pi}{4 \sin 2k\pi (5 \cos 2k\pi + \cos 6k\pi) \omega_1}, \quad (49) \\
B_{12} &= \frac{p\pi (k_1^2 + k_2^2) (2 - p) \sigma^2 \cos 2k\pi}{16 (3 \sin 2k\pi + \sin 6k\pi) \omega_1}, \\
B_{13} &= 0, \\
C_{10} &= 0, \\
C_{13} &= 0 \\
C_{11} &= \frac{p\pi [8(-\zeta_1 M_1 + \zeta_2 M_2) + (k_1^2 - k_2^2)(2 + p)\sigma^2]}{32 \sin 2k\pi (5 \cos 2k\pi + \cos 6k\pi) \omega_1}, \\
C_{12} &= -\frac{p\pi (k_1^2 + k_2^2) (2 - p) \sigma^2}{64 (4 \sin 4k\pi + \sin 8k\pi) \omega_1},
\end{aligned}$$

**3.3. The Second-Order Perturbation.** To further investigate the effects of parameter  $H_2$  on stochastic stability of system, the second-order perturbation equation of (20) will be used; that is,

$$\begin{aligned}
L_0 T_2(\theta_1, \theta_2, \varphi) + L_1 T_1(\theta_1, \theta_2, \varphi) \\
= \Lambda_1(p) T_1(\theta_1, \theta_2, \varphi) + \Lambda_2(p) T_0(\theta_1, \theta_2, \varphi). \quad (50)
\end{aligned}$$

Based on the solvability condition, one obtains

$$\begin{aligned}
\Lambda_2(p) &= \frac{1}{2\pi^3} \int_0^{\pi/2} \int_0^{2\pi} \int_0^{2\pi} a_1(\theta_1, \theta_2, \varphi) \frac{\partial^2 T_1(\theta_1, \theta_2, \varphi)}{\partial \theta_1^2} \\
&+ a_2(\theta_1, \theta_2, \varphi) \frac{\partial^2 T_1(\theta_1, \theta_2, \varphi)}{\partial \theta_1 \partial \theta_2} \\
&+ a_3(\theta_1, \theta_2, \varphi) \frac{\partial^2 T_1(\theta_1, \theta_2, \varphi)}{\partial \theta_1 \partial \varphi} \\
&+ a_4(\theta_1, \theta_2, \varphi) \frac{\partial^2 T_1(\theta_1, \theta_2, \varphi)}{\partial \theta_2^2}
\end{aligned}$$

$$\begin{aligned}
&+ a_5(\theta_1, \theta_2, \varphi) \frac{\partial^2 T_1(\theta_1, \theta_2, \varphi)}{\partial \theta_2 \partial \varphi} \\
&+ a_6(\theta_1, \theta_2, \varphi) \frac{\partial^2 T_1(\theta_1, \theta_2, \varphi)}{\partial \varphi^2} \\
&+ b_1(\theta_1, \theta_2, \varphi) \frac{\partial T_1(\theta_1, \theta_2, \varphi)}{\partial \theta_1} \\
&+ b_2(\theta_1, \theta_2, \varphi) \frac{\partial T_1(\theta_1, \theta_2, \varphi)}{\partial \theta_2} \\
&+ b_3(\theta_1, \theta_2, \varphi) \frac{\partial T_1(\theta_1, \theta_2, \varphi)}{\partial \varphi} \\
&+ [c(\theta_1, \theta_2, \varphi) - \Lambda_1(p)] T_1(\theta_1, \theta_2, \varphi) d\theta_1 d\theta_2 d\varphi. \quad (51)
\end{aligned}$$

The solution has the following form:

$$\begin{aligned}
\Lambda_2(p) &= \Lambda_{21}(p) \frac{\sin 4k\pi}{2 + \cos 4k\pi} \\
&+ \Lambda_{22}(p) \frac{\cos 4k\pi}{2 + \cos 4k\pi} \\
&+ \Lambda_{23}(p) \frac{1}{2 + \cos 4k\pi}, \quad (52)
\end{aligned}$$

where the values  $\Lambda_{21}(p)$ ,  $\Lambda_{22}(p)$ ,  $\Lambda_{23}(p)$  are given in Appendix A.

Substituting (40) and (52) into (19), the second-order approximate solution of the moment Lyapunov exponent is obtained as

$$\begin{aligned}
\Lambda(p) &= \epsilon \Lambda_1(p) + \epsilon^2 \Lambda_2(p) + O(\epsilon^3) \\
&= \epsilon \left[ \frac{(k_1^2 + k_2^2) \sigma^2}{128} p (3p + 10) - \frac{p}{4} (\zeta_1 M_1 + \zeta_2 M_2) \right] \\
&+ \epsilon^2 \Lambda_2(p) + O(\epsilon^3). \quad (53)
\end{aligned}$$

The corresponding Lyapunov exponents can be expressed as

$$\begin{aligned}
\lambda &= \left. \frac{d\Lambda(p)}{dp} \right|_{p=0} = \epsilon \lambda_1 + \epsilon^2 \lambda_2 + O(\epsilon^3) \\
&= \epsilon \left[ \frac{5}{64} (k_1^2 + k_2^2) \sigma^2 - \frac{1}{4} (\zeta_1 M_1 + \zeta_2 M_2) \right] \\
&+ \epsilon^2 \left( \lambda_{21} \frac{\sin 4k\pi}{2 + \cos 4k\pi} + \lambda_{22} \frac{\cos 4k\pi}{2 + \cos 4k\pi} \right. \\
&\left. + \lambda_{23} \frac{1}{2 + \cos 4k\pi} \right) + O(\epsilon^3), \quad (54)
\end{aligned}$$

where the values  $\lambda_{21}$ ,  $\lambda_{22}$ , and  $\lambda_{23}$  are given in Appendix B.

#### 4. Stochastic Stability Analysis

Through the above-mentioned analysis, the analytic expressions of moment Lyapunov exponents  $\Lambda(p)$  and Lyapunov

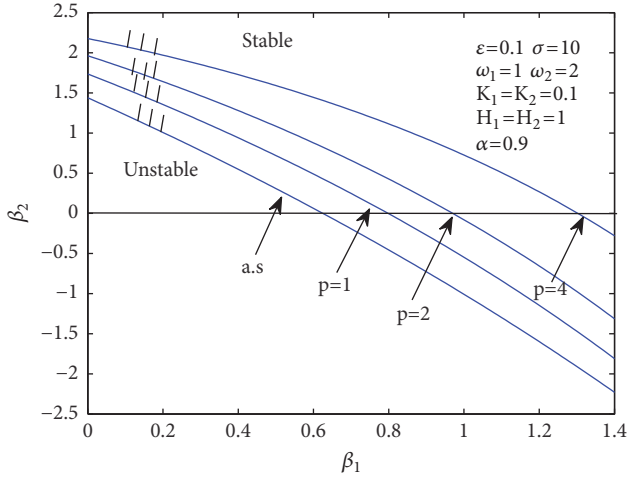


FIGURE 2: Stability regions for almost-sure stability and  $p$ th moment stability with respect to nonviscous damping parameter  $\beta_1, \beta_2$ .

exponents  $\lambda$  have been derived. Next, we use two indices to go on stochastic stability analysis. The  $p$ th moment Lyapunov exponent is defined as

$$\Lambda(p) = \lim_{t \rightarrow \infty} \frac{1}{t} \log E[\|x\|^p], \quad (55)$$

where  $E[\cdot]$  denotes the expected value and  $\|x\|^p$  is a solution process of a random system. If  $\Lambda(p) < 0$ ,  $E[\|x\|^p] \rightarrow 0$  as  $t \rightarrow \infty$ , and it means that the  $p$ th moment Lyapunov exponent is the slope of  $\Lambda(p)$  at the origin; that is,

$$\lambda = \left. \frac{d\Lambda(p)}{dp} \right|_{p=0} = \lim_{t \rightarrow \infty} \frac{1}{t} \log \|x\|, \quad (56)$$

If  $\lambda < 0$ , it indicates that the system is almost-surely stable.

The  $p$ th moment and almost-sure stability boundary can be determined from  $\Lambda(p) = 0$  and  $\lambda = 0$ , respectively. By comparing the second-order perturbation with the first-order perturbation, we find that the moment Lyapunov exponents  $\Lambda(p)$  and the Lyapunov exponents  $\lambda$  under the second-order perturbation contain all the parameter information of the coupled stochastic system. Therefore, we only consider the second-order perturbation in the subsequent research.

The boundaries of the  $p$ th moment and the almost-sure stability with respect to nonviscous damping parameters  $\beta_1$  and  $\beta_2$  are shown in Figure 2. We find that the moment stability boundaries are more conservative than the almost-sure stability boundaries. This means that the almost-sure stability cannot assure the moment stability. And the boundaries of stability for  $p$ th moment would increase with the increase of the order  $p$ .

The effects of relaxation parameter  $\alpha$  on moment Lyapunov exponents are shown in Figure 3. It describes that the stability index and the root  $p$  of  $\Lambda(p) = 0$  will decrease and the system becomes more unstable. Correspondingly, the analytical results and the direct Monte Carlo results are shown in Figure 3(b) for the given  $\alpha$ . And Lyapunov exponent is negative; it means the system is almost-surely stable.

The moment Lyapunov exponents  $\Lambda(p)$  for different nonviscous damping parameter  $\beta_2$  are discussed in Figure 4. It is clear that the bigger values of  $\beta_2$  can enhance the system's stability for  $p > 0$ . Correspondingly, the analytical results and the direct Monte Carlo results are shown in Figure 4(b) for the given different  $\beta_2$ . It illustrates that the system also is almost-surely stable. However, when  $p$  becomes sufficiently large,  $\Lambda(p) > 0$ , the system becomes more unstable.

Next, the effects of  $\epsilon$  on the moment Lyapunov exponents are studied in Figure 5. One easily finds the system is moment stability when  $0 < p < 3$ , and the stability of the system increases with the increase of  $\epsilon$  from 0.01 to 0.1. Afterward, the moment Lyapunov exponents are changed from negative to positive; the system is varied from moment stability to moment instability with the increase of  $p$ . Numerical results are verified by the direct Monte Carlo in Figure 5(b).

Then, in order to discuss the influences of the noise intensity  $\sigma$  on stochastic stability of coupled stochastic system, the moment Lyapunov exponents  $\Lambda(p)$  are shown in Figure 6 with change of values of  $\sigma$ . They describe that the coupled stochastic system could be almost-surely stable. Meanwhile, the moment stability of the coupled system would reduce with the increase of the noise intensity  $\sigma$ .

The variations of the moment Lyapunov exponents for different  $H_2$  are also analyzed. From Figure 7, we find that the coupled stochastic system may be almost-surely stable due to the value of slope  $\Lambda(p)$  less than 0 at the origin. However, the moment stability of system is not assured for  $p < 0$  or  $p$  is sufficiently large due to the moment Lyapunov exponents greater than 0. Besides, one can easily see that the moment stability of the system enhances with the increase of  $H_2$ .

Finally, the effects of  $K_2$  on the moment Lyapunov exponents are investigated and shown in Figure 8. From those figures, the system may be almost-surely stable in terms of the Lyapunov exponents. It is also indicated that the system has the characteristic of the moment stability. And the moment stability of the coupled system will increase with the increase of  $K_2$  under given parameters. The approximate analytical results agree well with numerical simulation results by the direct Monte Carlo.

## 5. Conclusions

In this paper, the moment stability and almost-sure stability of coupled viscoelastic system with nonviscous damping subject to Gaussian white noise excitation are investigated. The nonviscously damped structure is assumed to follow the exponential integral relation, which is possible to model the rate of energy dissipation. Motion equations are transformed into the coupled Itô stochastic differential equations by means of the method of stochastic averaging. Then the linear transformation is introduced to derive the eigenvalue problem. In order to obtain the analytical expressions of eigenvalue, the second-order perturbation method is used. Finally, the effects of Gaussian noise, the relaxation parameter, the nonviscous damping coefficient, and two physical quantities, that is  $H_2, K_2$ , on the moment stability are discussed in detail. Then the corresponding results are verified through the direct Monte Carlo simulation technique. Based on the results above, the

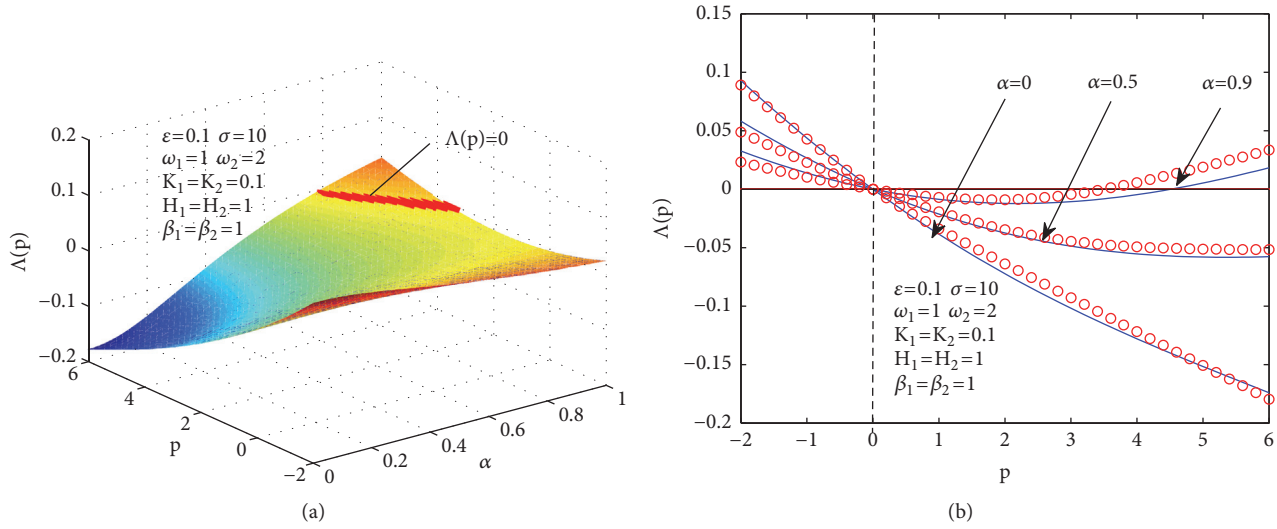


FIGURE 3: Variation of the moment Lyapunov exponent for different  $\alpha$ . Solid-line in the analytical results, circle in the numerical results by Monte Carlo.

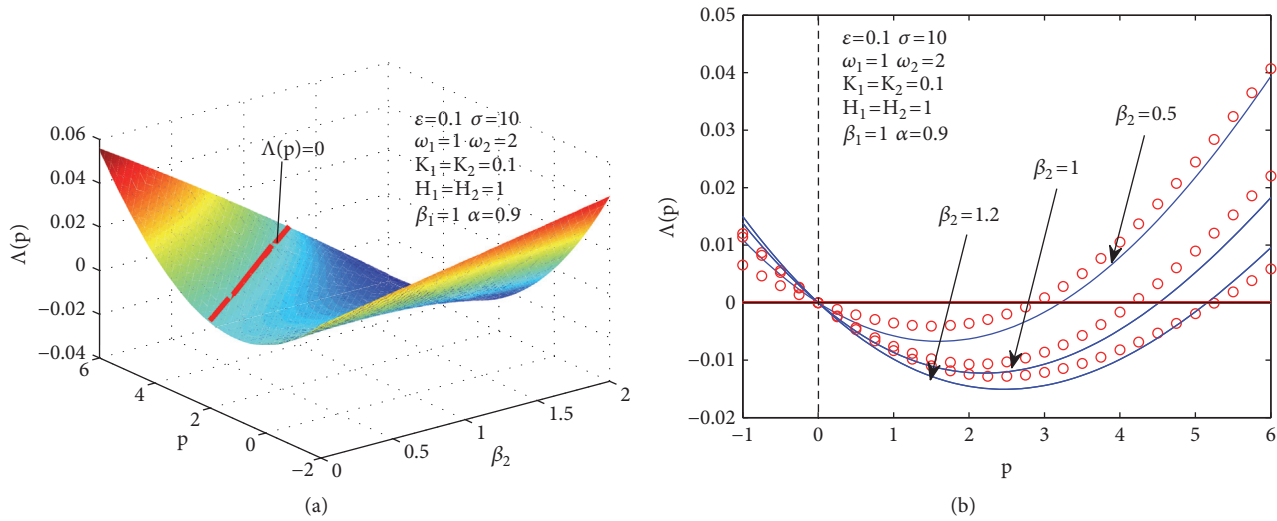


FIGURE 4: Variation of the moment Lyapunov exponent for different  $\beta_2$ . Solid-line in the analytical results, circle in the numerical results by Monte Carlo.

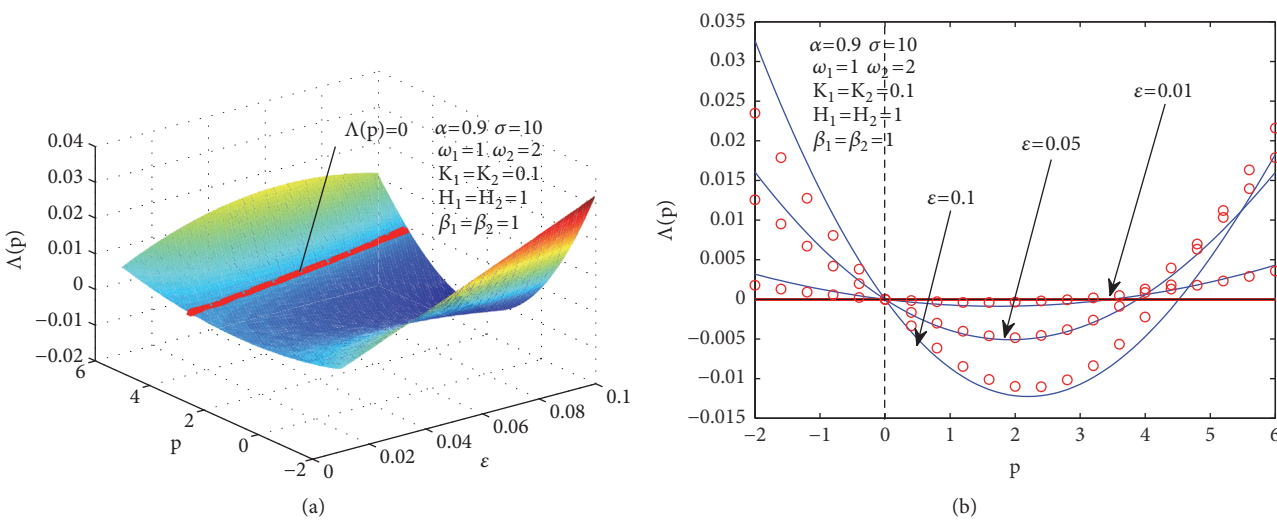


FIGURE 5: Variation of the moment Lyapunov exponent for different  $\varepsilon$ . Solid-line in the analytical results, circle in the numerical results by Monte Carlo.

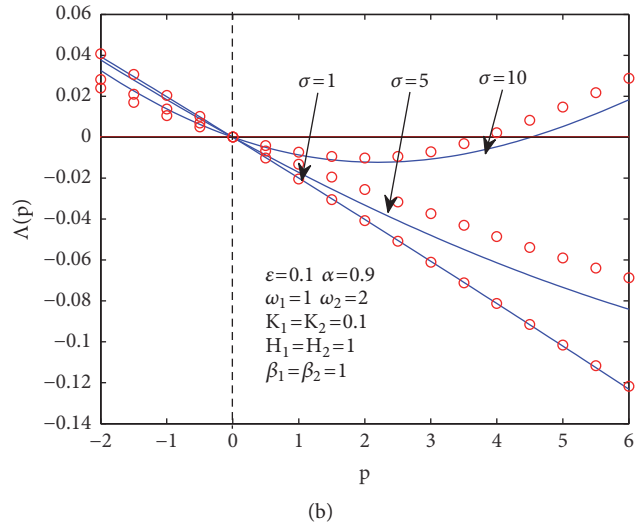
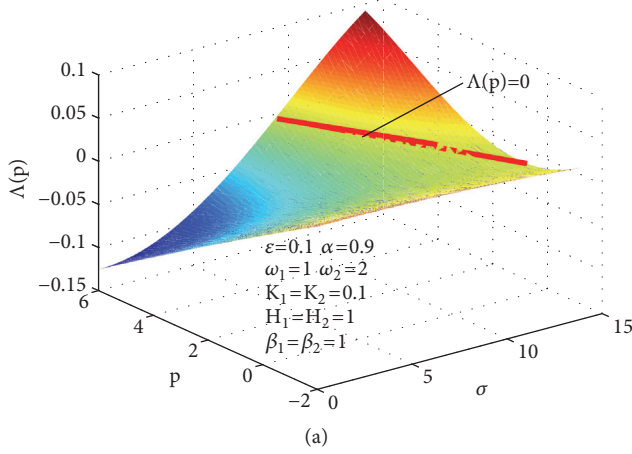


FIGURE 6: Variation of the moment Lyapunov exponent for different  $\sigma$ . Solid-line in the analytical results, circle in the numerical results by Monte Carlo.

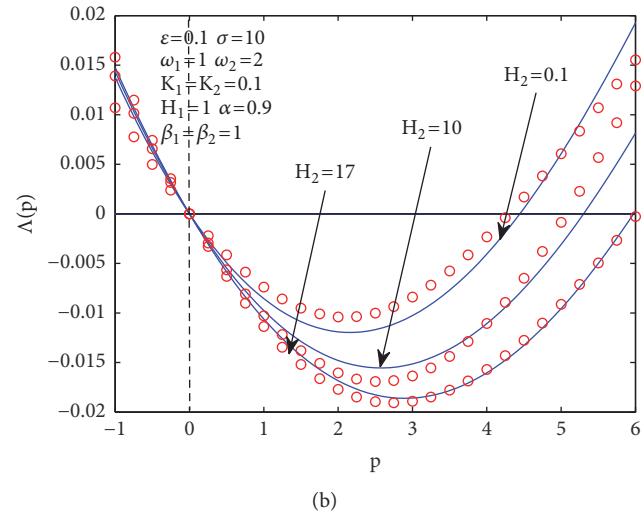
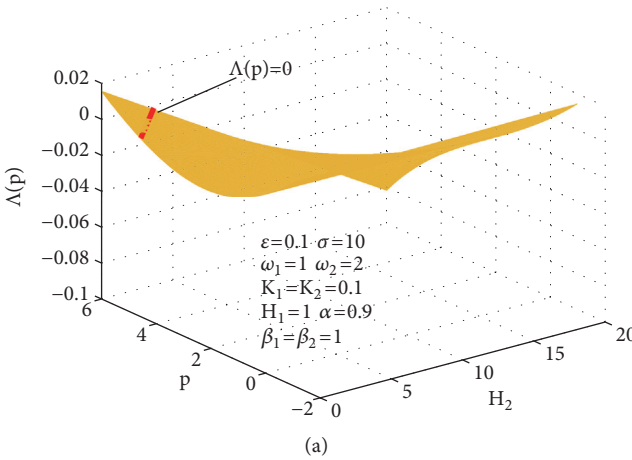


FIGURE 7: Variation of the moment Lyapunov exponent for different  $H_2$ . Solid-line in the analytical results, circle in the numerical results by Monte Carlo.

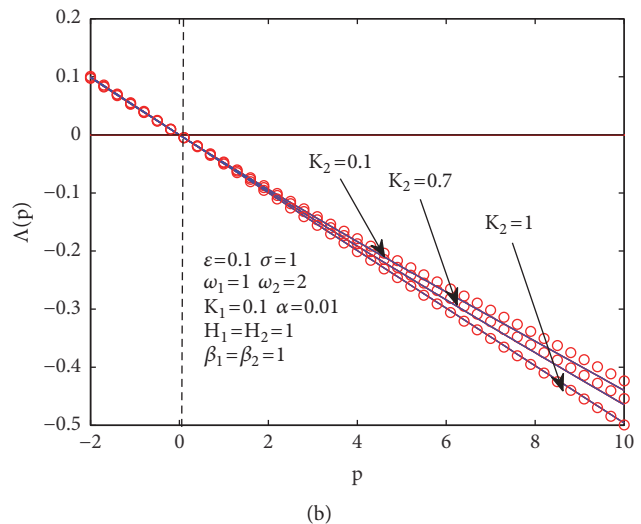
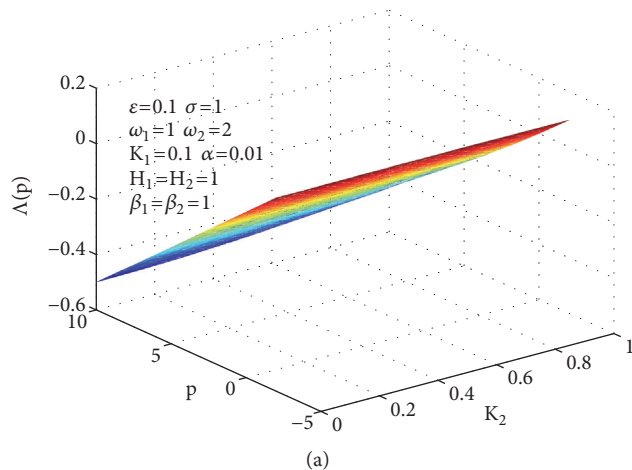


FIGURE 8: Variation of the moment Lyapunov exponent for different  $K_2$ . Solid-line in the analytical results, circle in the numerical results by Monte Carlo.

appropriate parameters will help to strengthen the stability of the coupled viscoelastic system with nonviscous damping.

## Appendix

### A. Values of $\Lambda_{21}(p)$ , $\Lambda_{22}(p)$ , and $\Lambda_{23}(p)$

$$\begin{aligned} \Lambda_{21}(p) = & -\frac{p(2+p)}{262144(-1+k^2)k\omega_1} \left\langle -4096(-1 \right. \\ & + k^2) M_2 \zeta_2 (M_1 \zeta_1 - M_2 \zeta_2) - 128(-1+k^2) \\ & \times \{64kk_1k_2(M_1 \zeta_1 - M_2 \zeta_2) - 4k_1^2(2+p)M_2 \zeta_2 \\ & + k_2^2[(-10+p)M_1 \zeta_1 + 3(6+p)M_2 \zeta_2]\} \sigma^2 \\ & + \{1024k^3k_1k_2(k_1^2 - k_2^2)(2+p) \\ & + 16kk_1k_2[k_1^2(-136 - 62p + p^2) \\ & + k_2^2(120 + 66p + p^2)] + k_2^2(-1+k^2) \\ & \cdot [k_1^2(-312 - 130p + 15p^2) \\ & + k_2^2(328 + 126p - 17p^2)]\} \sigma^4 \rangle \\ \Lambda_{22}(p) = & \frac{p}{98304(-1+k^2)k\omega_1\pi} \left\langle -3072(-1+k^2) \right. \\ & \cdot (2+p)\pi(M_1 \zeta_1 - M_2 \zeta_2) \times [h_2 + N_2 \zeta_2 \\ & + k\pi(M_1 \zeta_1 - M_2 \zeta_2)] + \{256k(k_1^2 + k_2^2)(2+p) \\ & \cdot (4+p)(h_1 - kh_2) - 768k\pi(-1+k^2)k_1^2(10 \\ & + 3p)(h_1 + N_1 \zeta_1) + 384\pi(-1+k^2)(h_2 + N_2 \zeta_2) \\ & \cdot [k_1^2(2+p)^2 - k_2^2(4+p)(6+p)] + 768k\pi^2(-1 \\ & + k^2)(2+p)^2(k_1^2 - k_2^2)(M_1 \zeta_1 - M_2 \zeta_2) - 3k(-1 \\ & + k^2)(-2+p)(2+p)(4+p)\pi^2(k_1^2 + k_2^2)\} \sigma^2 \\ & - 48k(-1+k^2)(2+p)^3\pi^2(k_1^2 - k_2^2)^2 \sigma^4 \rangle \quad (\text{A.1}) \\ \Lambda_{23}(p) = & \frac{p}{49152(-1+k^2)k\omega_1\pi} \left\langle -768(-1+k^2) \right. \\ & \cdot (2+p)\pi(M_1 \zeta_1 - M_2 \zeta_2) \times [3(h_2 + N_2 \zeta_2) \\ & + 4k\pi(M_1 \zeta_1 - M_2 \zeta_2)] + \{256k(k_1^2 + k_2^2)(2+p) \\ & \cdot (4+p) \times (h_1 - kh_2) + 96\pi(-1+k^2)(h_2 \\ & + N_2 \zeta_2) [-3k_1^2(2+p)^2 - k_2^2(92 + 36p + 3p^2)] \\ & - 768k\pi(-1+k^2)k_1^2(10 + 3p)(h_1 + N_1 \zeta_1) \\ & + 768k\pi^2(-1+k^2)(2+p)^2 \times (k_1^2 - k_2^2)(M_1 \zeta_1 \\ & - M_2 \zeta_2) - 3k(-1+k^2)(-2+p)(2+p)(4+p) \\ & \cdot \pi^2(k_1^2 + k_2^2)\} \sigma^2 - 48k(-1+k^2)(2+p)^3\pi^2(k_1^2 \\ & - k_2^2)^2 \sigma^4 \rangle \end{aligned}$$

### B. Values of $\lambda_{21}$ , $\lambda_{22}$ , and $\lambda_{23}$

$$\begin{aligned} \lambda_{21} = & -\frac{1}{16384(-1+k^2)k\omega_1} \left\{ -512(-1+k^2) \right. \\ & \cdot M_2 \zeta_2 (M_1 \zeta_1 - M_2 \zeta_2) - 32(-1+k^2) \\ & \times [32kk_1k_2(M_1 \zeta_1 - M_2 \zeta_2) - 4k_1^2M_2 \zeta_2 \\ & + k_2^2(-5M_1 \zeta_1 + 9M_2 \zeta_2)] \sigma^2 + k_2 [16kk_1^3(-17 \\ & + 16k^2) - 39k_1^2k_2(-1+k^2) + 16kk_1k_2^2(15 \\ & - 16k^2) + 41k_2^3(-1+k^2)] \sigma^4 \} \quad (\text{B.1}) \\ \lambda_{22} = & \frac{1}{6144(-1+k^2)k\omega_1\pi} \left\langle -384\pi(-1+k^2) \right. \\ & \cdot (M_1 \zeta_1 - M_2 \zeta_2) \times [(h_2 + N_2 \zeta_2) + k\pi(M_1 \zeta_1 \\ & - M_2 \zeta_2)] - \{128h_2k^2(k_1^2 + k_2^2) - 96\pi(-1+k^2) \\ & \cdot (k_1^2 - 6k_2^2)(h_2 + N_2 \zeta_2) + 32k[-4h_1(k_1^2 + k_2^2) \\ & + 15k_1^2\pi(-1+k^2)(h_1 + N_1 \zeta_1)] - 192k\pi^2(-1 \\ & + k^2)(k_1^2 - k_2^2)(M_1 \zeta_1 - M_2 \zeta_2) - 3k(-1+k^2) \\ & \cdot \pi^2(k_1^2 + k_2^2)^2\} \sigma^2 - 24k(-1+k^2)\pi^2(k_1^2 - k_2^2)^2 \\ & \cdot \sigma^4 \rangle \quad (\text{B.2}) \\ \lambda_{23} = & \frac{1}{3072(-1+k^2)k\omega_1\pi} \left\langle -96\pi(-1+k^2)(M_1 \zeta_1 \right. \\ & - M_2 \zeta_2) \times [3(h_2 + N_2 \zeta_2) + 4k\pi(M_1 \zeta_1 - M_2 \zeta_2)] \\ & - \{128h_2k^2(k_1^2 + k_2^2) - 24\pi(-1+k^2)(3k_1^2 \\ & - 23k_2^2)(h_2 + N_2 \zeta_2) + 32k[-4h_1(k_1^2 + k_2^2) \\ & + 15k_1^2\pi(-1+k^2)(h_1 + N_1 \zeta_1)] - 192k\pi^2(-1 \\ & + k^2)(k_1^2 - k_2^2) \times (M_1 \zeta_1 - M_2 \zeta_2) - 3k(-1+k^2) \\ & \cdot \pi^2(k_1^2 + k_2^2)^2\} \sigma^2 - 24k(-1+k^2)\pi^2(k_1^2 - k_2^2)^2 \\ & \cdot \sigma^4 \rangle \end{aligned}$$

### Data Availability

All the numerical calculated data used to support the findings of this study can be obtained by calculating the equations in the paper, and the white noise is generated randomly. The codes used in this paper are available from the corresponding author upon request.

## Conflicts of Interest

The authors declare that they have no conflicts of interest.

## Acknowledgments

This work is supported by the National Nature Science Foundation of China (no. 11402139, no. 11572247) and the Outstanding Innovation Programs of Graduate Students in Shanxi (no. 2017BY121). The writers are grateful to the stochastic dynamics team of the Northwestern Polytechnical University for discussions and valuable suggestions during the course of this study.

## References

- [1] A. D. Drozdov, *Viscoelastic structures*, Academic Press, Inc., San Diego, CA, USA, 1998.
- [2] H. Giesekus, "Theory of Viscoelasticity. Von R. M. Christensen. Academic Press, New York-London 1971. 1. Aufl., XI, 245 S., zahlr. Abb.; geb. \$ 13.50.," *Chemie Ingenieur Technik - CIT*, vol. 44, no. 5, pp. 356-356, 1972.
- [3] F. Li, "Limit behavior of the solution to nonlinear viscoelastic Marguerre-von Kármán shallow shell system," *Journal of Differential Equations*, vol. 249, no. 6, pp. 1241-1257, 2010.
- [4] X. Peng, Y. Shang, and X. Zheng, "Lower bounds for the blow-up time to a nonlinear viscoelastic wave equation with strong damping," *Applied Mathematics Letters*, vol. 76, pp. 66-73, 2018.
- [5] D. J. McTavish and P. C. Hughes, "Modeling of linear viscoelastic space structures," *Journal of Vibration and Acoustics*, vol. 115, no. 1, pp. 103-110, 1993.
- [6] F. Li and Y. Bai, "Uniform rates of decay for nonlinear viscoelastic Marguerre-von Karman shallow shell system," *Journal of Mathematical Analysis and Applications*, vol. 351, no. 2, pp. 522-535, 2009.
- [7] F. S. Li, "Global existence and uniqueness of weak solution to nonlinear viscoelastic full Marguerre-von Kármán shallow shell equations," *Acta Mathematica Sinica*, vol. 25, no. 12, pp. 2133-2156, 2009.
- [8] J. J. Nieto and B. Ahmad, "Approximation of solutions for an initial and terminal value problem for the forced Duffing equation with non-viscous damping," *Applied Mathematics and Computation*, vol. 216, no. 7, pp. 2129-2136, 2010.
- [9] F. Li and G. Du, "General energy decay for a degenerate viscoelastic Petrovsky-type plate equation with boundary feedback," *Journal of Applied Analysis and Computation*, vol. 8, no. 1, pp. 390-401, 2018.
- [10] Y. Guo, "Global asymptotic stability analysis for integro-differential systems modeling neural networks with delays," *Zeitschrift für Angewandte Mathematik und Physik*, vol. 61, no. 6, pp. 971-978, 2010.
- [11] F. Meng, L. Li, and Y. Bai, " $\psi$ -stability of nonlinear Volterra integro-differential systems," *Dynamic Systems and Applications*, vol. 20, no. 4, pp. 563-574, 2011.
- [12] L. Li, F. Meng, and P. Ju, "Some new integral inequalities and their applications in studying the stability of nonlinear integro-differential equations with time delay," *Journal of Mathematical Analysis and Applications*, vol. 377, no. 2, pp. 853-862, 2011.
- [13] D. Liu, W. Xu, Y. Xu, and J. Li, "Stochastic responses of viscoelastic system with real-power stiffness under randomly disordered periodic excitations," *Nonlinear Dynamics*, vol. 78, no. 4, pp. 2487-2499, 2014.
- [14] Y. Xu, R. Gu, H. Zhang, W. Xu, and J. Duan, "Stochastic bifurcations in a bistable Duffing-Van der Pol oscillator with colored noise," *Physical Review E: Statistical, Nonlinear, and Soft Matter Physics*, vol. 83, no. 5, 2011.
- [15] Y. Xu, H. Li, H. Wang, W. Jia, X. Yue, and J. Kurths, "The Estimates of the Mean First Exit Time of a Bistable System Excited by Poisson White Noise," *Journal of Applied Mechanics*, vol. 84, no. 9, p. 091004, 2017.
- [16] Y. Guo, "Mean square global asymptotic stability of stochastic recurrent neural networks with distributed delays," *Applied Mathematics and Computation*, vol. 215, no. 2, pp. 791-795, 2009.
- [17] Y. Guo, "Mean square exponential stability of stochastic delay cellular neural networks," *Electronic Journal of Qualitative Theory of Differential Equations*, No. 34, 10 pages, 2013.
- [18] X. Li and X. B. Liu, "Moment Lyapunov exponent and stochastic stability for a binary airfoil driven by an ergodic real noise," *Nonlinear Dynamics*, vol. 73, no. 3, pp. 1601-1614, 2013.
- [19] Y. Xu, Y. Li, and D. Liu, "A method to stochastic dynamical systems with strong nonlinearity and fractional damping," *Nonlinear Dynamics*, vol. 83, no. 4, pp. 2311-2321, 2016.
- [20] C. Floris, "Stochastic stability of damped Mathieu oscillator parametrically excited by a gaussian noise," *Mathematical Problems in Engineering*, vol. 2012, Article ID 375913, 18 pages, 2012.
- [21] V. D. Potapov, "Stability of elastic and viscoelastic systems under a random perturbations of their parameters," *Archive of Applied Mechanics*, vol. 66, no. 4, pp. 273-283, 1996.
- [22] V. D. Potapov, "Stability of elastic and viscoelastic systems under stochastic non-Gaussian excitation," *Acta Mechanica*, vol. 199, no. 1-4, pp. 167-179, 2008.
- [23] I. Pavlović, R. Pavlović, P. Kozić, and G. Janevski, "Almost sure stochastic stability of a viscoelastic double-beam system," *Archive of Applied Mechanics*, vol. 83, no. 11, pp. 1591-1605, 2013.
- [24] I. Pavlović, R. Pavlović, and G. Janevski, "Dynamic instability of coupled nanobeam systems," *Meccanica*, vol. 51, no. 5, pp. 1167-1180, 2016.
- [25] P. H. Baxendale and D. W. Stroock, "Large deviations and stochastic flows of diffeomorphisms," *Probability Theory and Related Fields*, vol. 80, no. 2, pp. 169-215, 1988.
- [26] W. Xie, *Dynamic Stability of Structures*, Cambridge University Press, Cambridge, UK, 2006.
- [27] N. Sri Namachchivaya and H. J. Van Roessel, "Moment Lyapunov exponent and stochastic stability of two coupled oscillators driven by real noise," *Journal of Applied Mechanics*, vol. 68, no. 6, pp. 903-914, 2001.
- [28] P. Kozić, G. Janevski, and R. Pavlović, "Moment Lyapunov exponents and stochastic stability for two coupled oscillators," *Journal of Mechanics of Materials and Structures*, vol. 4, no. 10, pp. 1689-1701, 2009.
- [29] P. Kozic, G. Janevski, and R. Pavlović, "Moment Lyapunov exponents and stochastic stability of a double-beam system under compressive axial loading," *International Journal of Solids and Structures*, vol. 47, no. 10, pp. 1435-1442, 2010.
- [30] G. Janevski, P. Kozić, R. Pavlović, and Z. Golubović, "The moment Lyapunov exponent of a Timoshenko beam under bounded noise excitation," *Archive of Applied Mechanics*, vol. 81, no. 4, pp. 403-417, 2011.
- [31] V. Stojanović and M. Petković, "Moment Lyapunov exponents and stochastic stability of a three-dimensional system on elastic foundation using a perturbation approach," *Journal of Applied Mechanics*, vol. 80, no. 5, 2013.

- [32] J. Deng, "Stochastic stability of gyroscopic systems under bounded noise excitation," *International Journal of Structural Stability and Dynamics*, vol. 18, no. 2, 1850022, 22 pages, 2018.
- [33] J. Deng, W.-C. Xie, and M. D. Pandey, "Moment lyapunov exponents and stochastic stability of coupled viscoelastic systems driven by white noise," *Journal of Mechanics of Materials and Structures*, vol. 9, no. 1, pp. 27–50, 2014.
- [34] W. V. Wedig, "Lyapunov Exponents of Stochastic Systems and Related Bifurcation Problems," in *Stochastic Structural Dynamics: Progress in Theory and Applications*, Elsevier, London, 1988.

## Research Article

# The Adaptive Neural Control for a Class of High-Order Uncertain Stochastic Nonlinear Systems

Xiaoyan Qin 

School of Mathematics and Statistics, Zaozhuang University, Zaozhuang 277160, China

Correspondence should be addressed to Xiaoyan Qin; qin-xiaoyan@163.com

Received 23 May 2018; Accepted 11 July 2018; Published 9 September 2018

Academic Editor: Weihai Zhang

Copyright © 2018 Xiaoyan Qin. This is an open access article distributed under the Creative Commons Attribution License, which permits unrestricted use, distribution, and reproduction in any medium, provided the original work is properly cited.

This paper studies the problem of the adaptive neural control for a class of high-order uncertain stochastic nonlinear systems. By using some techniques such as the backstepping recursive technique, Young's inequality, and approximation capability, a novel adaptive neural control scheme is constructed. The proposed control method can guarantee that the signals of the closed-loop system are bounded in probability, and only one parameter needs to be updated online. One example is given to show the effectiveness of the proposed control method.

## 1. Introduction

Ever since the stochastic stability theory was established by [1–3], the design and analysis of backstepping controller for stochastic nonlinear systems have achieved remarkable development in recent years; see [4–20] and the references therein. Based on the backstepping technique, Pan and Basar [8] firstly studied a class of stochastic nonlinear systems under a risk-sensitive cost criterion. Then, by combining backstepping technique with different nonlinear control methods, [9–13] obtained the state-feedback stabilization results of stochastic nonlinear systems in various structures. In the case of system states being unmeasurable, [14–19] further studied the problem of the output-feedback stabilization for stochastic nonlinear systems with the help of observer design. In addition, by applying the backstepping design and Lyapunov stability analysis, the finite-time control with fast convergence rate has been achieved for stochastic nonlinear systems in [10, 20, 21].

Note that when stochastic nonlinear system is of high-order, it may be nonsmooth and in general not stabilizable. How to deal with this problem is difficult. To handle this case, [9–13, 17, 20] have done remarkable work on stochastic high-order nonlinear systems and obtained different control results. Particularly, the homogeneous domination approach was extended to stochastic nonlinear system in [17], which provides an effective design methods for high-order

stochastic nonlinear systems. However, the above-mentioned results were subjected to the nonlinear dynamics models which are known exactly or unknown parameters existing linearly. Thus, these results cannot be used for the stochastic systems with structured uncertainties. Naturally, one raises the problem of how to design the controller for the high-order stochastic nonlinear systems with structured uncertainties.

To handle the structured uncertainties for the stochastic nonlinear systems, the radial basis function neural network (RBF NN) or the fuzzy logic is used to approximate the uncertain functions, which ensures the growth assumptions can be weakened or removed. Based on these methods and some useful adaptive backstepping control approaches, fruitful results have been introduced and obtained in [22–30] and the references therein. Reference [22] studied the problem of fuzzy backstepping control for a class of stochastic nonlinear strict-feedback systems. Reference [23] considered the adaptive neural network output-feedback control for nonlinear systems with dynamical uncertainties. Reference [25] considered NN output-feedback control for stochastic nonlinear systems with unknown control coefficients. Reference [24] studied NN output-feedback control for stochastic time-delay nonlinear systems with unknown control coefficients. Furthermore, more problems of stochastic nonlinear systems with unmodeled dynamics were studied in [26–30].

Motivated by the aforementioned literatures, one raises the following meaningful problem: *how to relax or remove the*

matching conditions on drift and diffusion terms by RBF NN? And how to design the adaptive NN state-feedback controller for a class of high-order stochastic nonlinear systems with unknown control directions?

In this paper, we will discuss the problem of adaptive neural control for a class of high-order stochastic nonlinear systems with structured uncertainties. By using backstepping recursive approach, Young's inequality, etc., the restrictions on systems nonlinearities are removed and the procedure of the design is simpler. A novel adaptive neural controller is constructed, which assures that the closed-loop system is bounded in probability. In addition, in the design progress, there is only one parameter that needs to be updated online.

The rest of this paper is organized as follows. The notations and some preliminaries are provided in Section 2. In Section 3, we present the main results. In Section 4, we give the simulation example to illustrate the effectiveness of the proposed results, and the conclusion is drawn in Section 5.

## 2. Preliminaries and Problem Formulation

**Notations.**  $R$  denotes the set of all real numbers,  $R^+$  denotes the set of all nonnegative real numbers, and  $R^n$  denotes the real  $n$ -dimensional space.  $C^i$  stands for the family of the functions with  $i$ th continuous partial derivations. For a given vector or matrix  $X$ ,  $X^T$  denotes its transpose,  $Tr\{X\}$  denotes its trace when  $X$  is square, and  $|X|$  is the Euclidean norm of a vector  $X$ . For simplicity, the smooth function  $\varrho(\cdot)$  is sometimes denoted by  $\varrho$ .

Consider a class of high-order stochastic nonlinear systems as follows:

$$dx_i = h_i(t) x_{i+1}^{p_i} dt + \varphi_i(t, \bar{x}_i) dt + g_i(\bar{x}_i) \sum(t) d\omega, \quad i = 1, \dots, n-1, \quad (1)$$

$$dx_n = h_n(t) u^{p_n} dt + \varphi_n(t, \bar{x}_n) dt + g_n(\bar{x}_n) \sum(t) d\omega$$

where  $x = [x_1, \dots, x_n]^T \in R^n$  and  $u \in R$  are the system states and the control input, respectively.  $\bar{x}_i = [x_1, \dots, x_i]^T \in R^i$ ,  $i = 1, 2, \dots, n$  and  $\bar{x}_n = x$ .  $\omega \in R^r$  is an  $r$ -dimensional standard Wiener process defined on the complete probability space  $(\Omega, F, P)$  with  $\Omega$  being a sample space,  $F$  being a filtration, and  $P$  being measure.  $\varphi_i(\cdot)$  and  $g_i(\cdot)$  are unknown smooth functions, with  $\varphi_i(0, 0) = 0$ ,  $g_i(0) = 0$  for  $i = 1, 2, \dots, n$ . The disturbed virtual control coefficients  $h_i(t) : R \rightarrow R$  ( $i = 1, 2, \dots, n$ ) are unknown and continuous functions, respectively;  $\sum(t) : R^+ \rightarrow R^{r \times r}$  is the Borel bounded measurable functions.

**2.1. Preliminary Results.** Next we introduce several technical lemmas which will play an important role in our later control design.

Consider the following stochastic nonlinear system:

$$dx = f(t, x) dt + h(t, x) d\omega \quad (2)$$

where  $f$  and  $g$  are the Borel measurable functions.  $f : R^{n+1} \times R^{n+1} \rightarrow R^n$  and  $g : R^+ \times R^{n+1} \rightarrow R^{n \times r}$  are assumed to be  $C^1$  in their arguments.

**Definition 1** (see [2]). Given  $V(x, t) \in C^{1,2}$  for stochastic nonlinear system (2), the differential operator  $L$  is defined as follows:

$$LV(x, t) = \frac{\partial V}{\partial t} + \frac{\partial V}{\partial x} f + \frac{1}{2} Tr \left( h^T \frac{\partial^2 V}{\partial x^2} h \right) \quad (3)$$

where  $C^{1,2}(R^n \times R^+; R^+)$  denotes all nonnegative functions  $V(x, t)$  on  $R^n \times R^+$ ; i.e.,  $V(x, t)$  satisfies  $C^1$  in  $t$  and  $C^2$  in  $x$ . Simply, the smooth function  $f(\cdot)$  is denoted by  $f$ .

**Definition 2** (see [15]). The solution of stochastic system (2) is said to be bounded in probability if it satisfies

$$\lim_{c \rightarrow \infty} \sup_{0 \leq t \leq \infty} P\{|x(t)| > c\} = 0. \quad (4)$$

**Definition 3** (see [15]). Consider system (2) with  $f(t, 0) = 0$  and  $h(t, 0) = 0$ ; the equilibrium  $x = 0$  is globally stable in probability if, for any  $\varepsilon > 0$ , there exists a class  $K_\infty$  function  $\gamma(\cdot)$  such that

$$P\{|x(t)| < \gamma(|x_0|)\} \geq 1 - \varepsilon, \quad \forall t \geq 0, x_0 \in R^n \setminus \{0\}. \quad (5)$$

**Lemma 4** (Young's inequality [4]). For any  $(x, y) \in R^2$ , the following inequality holds:

$$xy \leq \frac{\varepsilon^p}{p} |x|^p + \frac{1}{q\varepsilon^q} |y|^q. \quad (6)$$

**Lemma 5** (see [15]). Consider the stochastic system (2). Assume that  $f(x, t)$  and  $h(x, t)$  are  $C^1$  in their arguments, and  $f(0, t)$  and  $h(0, t)$  are bounded uniformly in  $t$  if there exist functions  $V(x, t) \in C^{1,2}(R^n \times R^+, R^+)$ ,  $u_1(\cdot), u_2(\cdot) \in K_\infty$  and constants  $a_0 > 0$ ,  $b_0 > 0$  such that

$$\begin{aligned} u_1 |x| \leq V(x, t) \leq u_2 |x|, \\ LV \leq -a_0 V(x, t) + b_0. \end{aligned} \quad (7)$$

Then the solution of (2) is bounded in probability.

The purpose of this paper is to construct a smooth adaptive neural state-feedback controller such that the solution process of system (1) is bounded in probability.

To design the controller for system (1), the following assumptions are needed:

- (A<sub>1</sub>)  $p_1 = p_2 = \dots = p_n = p \geq 1$  are odd integers.
- (A<sub>2</sub>) For any  $Y \in \Omega_Y$ , there exists an ideal constant weight vector  $W^*$  such that  $0 < \|W^*\|_\infty \leq W_{max}$  and  $0 < |\delta| \leq \delta_{max}$ .
- (A<sub>3</sub>) For  $i = 1, \dots, n$ , there are positive constants  $\gamma_{i1}$  and  $\gamma_{i2}$ , such that  $\gamma_{i1} \leq |h_i(t)| \leq \gamma_{i2}$ .
- (A<sub>4</sub>) There exists constant  $M > 0$  such that  $\|\sum^T(t) \sum(t)\|_F^2 \leq M$ .

**Remark 6.** If  $p_1 = p_2 = \dots = p_n = 1$ , system (1) becomes the strict-feedback form. The problem of the feedback control has been studied in [22–24, 26, 27]. However, they did not consider  $p_1 = p_2 = \dots = p_n > 1$ . In this paper, we will consider the problem of the feedback control under the case  $p_1 = p_2 = \dots = p_n > 1$ .

The following radial basis function neural network (RBFNN) will be considered and used to approximate unknown continuous functions:

$$\begin{aligned}\Psi(Y) &: R^n \longrightarrow R, \\ \Psi_{nn}(Y) &= W^T S(Y)\end{aligned}\quad (8)$$

where  $Y \in \Omega_Y \subset R^q$  is the input vector with  $q$  being the neural networks input dimension.  $W = [w_1, w_2, \dots, w_l]^T \in R^l$  denotes the weight vector.  $l > 1$  is the neural network mode number.  $S(Y) = [s_1(Y), s_2(Y), \dots, s_l(Y)]^T$  and  $s_i(Y) = \exp[-\|Y - u_i\|^2/\delta_i]$ ,  $i = 1, 2, \dots, l$  are the basis function vectors. Here  $u_i = [u_{i1}, u_{i2}, \dots, u_{iq}]^T$  is the center of the receptive field, and  $\delta_i$  is the width of the Gaussian function. Equation (8) can approximate any unknown continuous function over the compact set  $\Omega_Y \subset R^q$  with arbitrary accuracy. Namely,

$$\Psi(Y) = W^{*T} S(Y) + \delta(Y), \quad \forall Y \in \Omega_Y. \quad (9)$$

The ideal constant weight vector  $W^*$  is defined as  $W^* := \arg \min_{W \in R^l} \{\sup_{Y \in \Omega_Y} |\Psi(Y) - W^T S(Y)|\}$ , and  $\delta(Y)$  is the approximation error.

From (9), we can easily get

$$\begin{aligned}W^{*T} S(Y) + \delta &\leq |W^{*T} S(Y)| + |\delta| \\ &\leq \sum_{i=1}^l |S_i(Y)| W_{max} + \delta_{max} \leq \Theta \pi(Y)\end{aligned}\quad (10)$$

where  $\pi(Y) = \sqrt{(l+1)(\sum_{i=1}^l S_i^2(Y) + 1)}$ ,  $\Theta = \max(W_{max}, \delta_{max})$ .

To design a state-feedback controller, we first introduce the following transformation:

$$\begin{aligned}\eta_i &= x_i - \alpha_i(\bar{x}_i, \hat{\Theta}), \\ \alpha_i &= -\eta_{i-1} \beta_{i-1}(\cdot). \quad i = 1, 2, \dots, n\end{aligned}\quad (11)$$

where  $\alpha_1 = 0$ ,  $\alpha_i(\cdot)$  is the virtual control law and  $\beta_i(\cdot) > 0$  can be designed in the following form.

Using (11), we have

$$\begin{aligned}d\eta_1 &= dx_1 = h_1 x_2^p dt + \bar{\varphi}_1 dt + G_1 \sum(t) dw \\ d\eta_i &= d(x_i - \alpha_i) \\ &= h_i x_{i+1}^p dt + \bar{\varphi}_i dt - \frac{\partial \alpha_i}{\partial \hat{\Theta}} \dot{\hat{\Theta}} dt + G_i \sum(t) dw \\ &\quad i = 2, \dots, n,\end{aligned}\quad (12)$$

where  $x_{n+1} = u$ ,  $\bar{\varphi}_i = \varphi_i - \sum_{l=1}^{i-1} (\partial \alpha_i / \partial x_l) \varphi_l - \sum_{l=1}^{i-1} (\partial \alpha_i / \partial x_l) x_{l+1}^p - (1/2) \sum_{k,m=1}^{i-1} (\partial^2 \alpha_i / \partial x_k \partial x_m) g_k \sum(t) \sum^T(t) g_m^T$ , and  $G_i = g_i - \sum_{l=1}^{i-1} (\partial \alpha_i / \partial x_l) g_l$ .

### 3. Controller Design and Stability Analysis

**3.1. Controller Design.** In this section, by using the backstepping method and the RBFNN, we construct the adaptive neural controller and approximate the unknown nonlinear functions, respectively.

*Step 1.* Consider the Lyapunov function  $V_1 = (1/4)\eta_1^4 + (1/2)\bar{\Theta}^2$ , where  $\bar{\Theta} = \Theta - \hat{\Theta}$  is the parameter error. By (3) and (12), we have

$$\begin{aligned}LV_1 &= \eta_1^3 (h_1 x_2^p + \bar{\varphi}_1) + \frac{3}{2} \eta_1^2 Tr \left( G_1^T \sum(t) \sum(t) G_1 \right) \\ &\quad - \bar{\Theta} \dot{\hat{\Theta}}.\end{aligned}\quad (13)$$

From Lemma 4 and assumptions (A<sub>2</sub>) – (A<sub>4</sub>), there exists constant  $a_{1j} > 0$ ,  $j = 1, 2$ , such that

$$\eta_1^3 \bar{\varphi}_1 \leq \eta_1^{p+3} \frac{3}{p+3} a_{11}^{3/(p+3)} \bar{\varphi}_1^{(p+3)/3} + \frac{1}{p+3} a_{11}^{p+3} \quad (14)$$

and

$$\begin{aligned}&\frac{3}{2} \eta_1^2 Tr \left( G_1^T \sum(t) \sum(t) G_1 \right) \\ &\leq \frac{3}{2} \eta_1^2 \|G_1\|^2 \left\| \sum(t) \sum(t) \right\|_F^2 \\ &\leq \frac{2}{p+3} a_{12}^{2/(p+3)} \eta_1^{p+3} \|G_1\|^{p+3} M \\ &\quad + \frac{1}{p+3} a_{12}^{p+3} M.\end{aligned}\quad (15)$$

Substituting (14) and (15) into (13), we obtain

$$LV_1 \leq \eta_1^3 h_1 x_2^p + a_1 - \bar{\Theta} \dot{\hat{\Theta}} + \eta_1^{p+3} \Psi_1 \quad (16)$$

where  $\Psi_1 = (3/(p+3))a_{11}^{3/(p+3)}\bar{\varphi}_1^{(p+3)/3} + (2/(p+3))a_{12}^{2/(p+3)}\|G_1\|^{p+3}M$ ,  $a_1 = (1/(p+3))a_{11}^{p+3} + (2/(p+3))a_{12}^{p+3}M$ . Obviously,  $\Psi_1$  is an unknown function since it has unknown function  $\varphi_1$  and  $g_1$ . In practice, it cannot be used directly. Moreover, there exists a neural network  $W_1^{*T} S_1(Y_1)$ ,  $Y_1 = x_1 \in \Omega_{Y_1} \subset R^1$ , such that

$$\Psi_1 = W_1^{*T} S_1(Y_1) + \delta_1(Y_1) \leq \Theta \pi_1(\cdot) \quad (17)$$

where  $\pi_1(\cdot) = \sqrt{(l+1) \sum_{k=1}^l S_{1k}^2} + 1$ . In the view of (16) and (17), we can get

$$\begin{aligned}LV_1 &\leq -\bar{\Theta} \dot{\hat{\Theta}} + \eta_1^3 h_1 (x_2^p - \alpha_2^p) + \eta_1^{p+3} \Theta \pi_1 + \eta_1^3 h_1 \alpha_2^p \\ &\quad + a_1.\end{aligned}\quad (18)$$

Now we choose the virtual control laws

$$\begin{aligned}\alpha_2 &= \left( \frac{-c_1 - \hat{\Theta}\pi_1}{\gamma_{11}} \right)^{1/p} \eta_1 = -\beta_1 \eta_1, \\ \beta_1 &= \left( \frac{c_1 + \hat{\Theta}\pi_1}{\gamma_{11}} \right)^{1/p} > 0\end{aligned}\quad (19)$$

where  $c_1 > 0$  is a constant to be chosen.

Substituting  $\alpha_2$  into (18), it can be rewritten as

$$\begin{aligned}LV_1 &\leq \bar{\Theta} \left( \eta_1^{p+3} \pi_1 - \hat{\Theta} \right) + \eta_1^3 h_1 \left( x_2^p - \alpha_2^p \right) - c_1 \eta_1^{p+3} \\ &\quad + a_1.\end{aligned}\quad (20)$$

By (11), Lemma 4, assumptions  $(A_2)$ ,  $(A_3)$ , and  $(a+b)^n = \sum_{i=0}^n C_n^k a^k b^{n-k}$ , we obtain

$$\begin{aligned}\eta_1^3 h_1 \left( x_2^p - \alpha_2^p \right) &= \eta_1^3 h_1 \left\{ (\eta_2 + \alpha_2)^p - \alpha_2^p \right\} \\ &= \eta_1^3 h_1 \sum_{k=0}^{p-1} C_p^k \alpha_2^k \eta_2^{p-k} = \eta_1^3 h_1 \sum_{k=0}^{p-1} C_p^k (-\eta_1 \beta_1)^k \eta_2^{p-k} \\ &\leq \gamma_{12} \sum_{k=0}^{(p-1)/2} C_p^{2k} |\eta_1^{3+2k}| |\eta_2^{p-2k}| \beta_1^{2k} \\ &\leq \sum_{k=0}^{(p-1)/2} \frac{3+2k}{p+3} \epsilon_{1k}^{(p+3)/(3+2k)} \eta_1^{3+p} \\ &\quad + \sum_{k=0}^{(p-1)/2} \frac{p-2k}{p+3} \epsilon_{1k}^{(p-2k)/(p+3)} \left( C_p^{2k} \beta_1^{2k} \gamma_{12} \right)^{(p+3)/(p-2k)} \\ &\quad \cdot \eta_2^{3+p} \leq \epsilon_1 \eta_1^{p+3} + \gamma_{20} \eta_2^{p+3}\end{aligned}\quad (21)$$

where  $\epsilon_1 \geq \sum_{k=0}^{(p-1)/2} ((3+2k)/(p+3)) \epsilon_{1k}^{(p+3)/(3+2k)}$ ,  $\gamma_{20} \geq \sum_{k=0}^{(p-1)/2} ((p-2k)/(p+3)) \epsilon_{1k}^{(p-2k)/(p+3)} (C_p^{2k} \beta_1^{2k} \gamma_{12})^{(p+3)/(p-2k)}$ , and  $\epsilon_{1k} > 0$  ( $k = 0, 1, \dots, (p-1)/2$ ) are constants.

Substituting (21) into (20), we can get

$$\begin{aligned}LV_1 &\leq \bar{\Theta} \left( \eta_1^{p+3} \pi_1 - \hat{\Theta} \right) - (c_1 - \epsilon_1) \eta_1^{p+3} + \gamma_{20} \eta_2^{p+3} \\ &\quad + a_1.\end{aligned}\quad (22)$$

*Step 2.* We choose the Lyapunov function  $V_2 = V_1 + (1/4)\eta_2^4$  to design the control law  $\alpha_3$ . From (11), (12), and (22), we have

$$\begin{aligned}LV_2 &= LV_1 + \eta_2^3 \left( h_2 x_3^p + \bar{\varphi}_2 - \frac{\partial \alpha_2}{\partial \hat{\Theta}} \dot{\hat{\Theta}} \right) \\ &\quad + \frac{3}{2} \eta_2^2 Tr \left( G_2^T \sum (t) \sum (t) G_2 \right)\end{aligned}$$

$$\begin{aligned}&= \eta_2^3 \left\{ h_2 x_3^p + \bar{\varphi}_2 - \frac{\partial \alpha_2}{\partial \hat{\Theta}} \dot{\hat{\Theta}} \right\} \\ &\quad + \frac{3}{2} \eta_2^2 Tr \left( G_2^T \sum (t) \sum (t) G_2 \right) \\ &\quad + \bar{\Theta} \left( \eta_1^{p+3} \pi_1 - \hat{\Theta} \right) - (c_1 - \epsilon_1) \eta_1^{p+3} + \gamma_{20} \eta_2^{p+3} \\ &\quad + a_1.\end{aligned}\quad (23)$$

From the definition of  $\bar{\varphi}_2$  and Lemma 4, there exist constants  $a_{2j} > 0$ ,  $j = 1, 2$ , such that

$$\eta_2^3 \bar{\varphi}_2 \leq \eta_2^{p+3} \frac{3}{p+3} a_{21}^{3/(p+3)} |\bar{\varphi}_2|^{(p+3)/3} + \frac{1}{p+3} a_{21}^{p+3}\quad (24)$$

and

$$\begin{aligned}&\frac{3}{2} \eta_2^2 Tr \left( G_2^T \sum (t) \sum (t) G_2 \right) \\ &= \frac{3}{2} \eta_2^2 \|G_2\|^2 \left\| \sum (t) \sum (t) \right\|_F^2 \\ &\leq \eta_2^{p+3} \frac{2}{p+3} a_{22}^{2/(p+3)} \|G_2\|^{p+3} M + \frac{1}{p+3} a_{22}^{p+3} M.\end{aligned}\quad (25)$$

By (23), (24), and (25), we can obtain

$$\begin{aligned}LV_2 &\leq \eta_2^3 \left( h_2 x_3^p - \frac{\partial \alpha_2}{\partial \hat{\Theta}} \dot{\hat{\Theta}} \right) + \bar{\Theta} \left( \eta_1^{p+3} \pi_1 - \hat{\Theta} \right) - (c_1 \\ &\quad - \epsilon_1) \eta_1^{p+3} + \gamma_{20} \eta_2^{p+3} + a_1 \\ &\quad + \eta_2^{p+3} \left\{ \frac{2}{p+3} a_{22}^{2/(p+3)} \|G_2\|^{p+3} M \right. \\ &\quad \left. + \frac{3}{p+3} a_{21}^{3/(p+3)} |\bar{\varphi}_2|^{(p+3)/3} \right\} + \frac{1}{p+3} a_{21}^{p+3} + \frac{1}{p+3} \\ &\quad \cdot a_{22}^{p+3} M.\end{aligned}\quad (26)$$

Further, adding and subtracting  $\eta_2^3 f_2$  in the first bracket in (26) and using Lemma 4, there exists a constant  $a_{23} > 0$ , such that

$$-\eta_2^3 f_2 \leq \eta_2^{p+3} \frac{3}{p+3} a_{23}^{3/(p+3)} |f_2|^{(p+3)/3} + \frac{1}{p+3} a_{23}^{p+3}.\quad (27)$$

Then, substituting (27) into (26), we get

$$\begin{aligned}LV_2 &\leq \eta_2^3 \left( h_2 x_3^p - \frac{\partial \alpha_2}{\partial \hat{\Theta}} \dot{\hat{\Theta}} + f_2 \right) + \bar{\Theta} \left( \eta_1^{p+3} \pi_1 - \hat{\Theta} \right) \\ &\quad - (c_1 - \epsilon_1) \eta_1^{p+3} \eta_2^{p+3} \frac{3}{p+3} a_{23}^{3/(p+3)} |f_2|^{(p+3)/3} \\ &\quad + \frac{1}{p+3} a_{23}^{p+3} + \gamma_{20} \eta_2^{p+3} + \eta_2^{p+3} \Psi_2 + \sum_{i=1}^2 a_i\end{aligned}\quad (28)$$

where  $a_2 = (1/(p+3))a_{21}^{p+3} + (1/(p+3))a_{23}^{p+3} + (1/(p+3))a_{22}^{p+3}M$ ,  $\Psi_2 = (2/(p+3))a_{22}^{2/(p+3)}\|G_2\|^{p+3}M + (3/(p+3))a_{21}^{-3/(p+3)}|\bar{\varphi}_2|^{(p+3)/3} + (3/(p+3))a_{23}^{3/(p+3)}|f_2|^{(p+3)/3}$ , and  $f_2 = -(\partial\alpha_2/\partial\Theta)c_0\Theta + (\partial\alpha_2/\partial\Theta)\eta_1^{p+3}\pi_1 - |\partial\alpha_2/\partial\Theta|\eta_2^{p+3}\pi_2$ .

Similar to Step 1, obviously  $\Psi_2$  is an unknown function. Hence there exist the neural networks  $W_2^{*T}S_2(Y_2)$  and  $Y_2 = [\bar{x}_2, \dot{\Theta}] \in \Omega_{Y_2} \subset R^3$  such that

$$\Psi_2 = W_2^{*T}S_2(Y_2) + \delta_2(Y_2) \leq \Theta\pi_2(\cdot) \quad (29)$$

where  $\pi_2(\cdot) = \sqrt{(l+1)\sum_{k=2}^l S_{2k}^2 + 1}$ .

We add and subtract  $h_2\eta_2^3\alpha_3^p$  in the formula (26), respectively, and, substituting (29) into (26), we can get

$$\begin{aligned} LV_2 \leq & \eta_2^3 h_2 (x_3^p - \alpha_3^p) + \eta_2^3 \left( f_2 - \frac{\partial\alpha_2}{\partial\Theta} \dot{\Theta} \right) \\ & + \bar{\Theta} \left( \eta_1^{p+3} \pi_1 - \dot{\Theta} \right) + h_2 \eta_2^p \alpha_3^p - (c_1 - \epsilon_1) \eta_1^{p+3} \\ & + \gamma_{20} \eta_2^{p+3} + \sum_{i=1}^2 a_i + \eta_2^{p+3} \Theta \pi_2. \end{aligned} \quad (30)$$

Now we choose the virtual control law  $\alpha_3 = ((-c_2 - \bar{\Theta}\pi_2 - \gamma_{20})/\gamma_{11})^{1/p}\eta_2 = -\beta_2\eta_2$  and  $\beta_2 = ((c_2 + \bar{\Theta}\pi_2 + \gamma_{20})/\gamma_{11})^{1/p} > 0$ , where  $c_2 > 0$  is a constant to be chosen. Substitution  $\alpha_3$  into (30), (30) can be calculated as

$$\begin{aligned} LV_2 \leq & \eta_2^3 h_2 (x_3^p - \alpha_3^p) + \eta_2^3 \left( f_2 - \frac{\partial\alpha_2}{\partial\Theta} \dot{\Theta} \right) \\ & + \bar{\Theta} \left( \sum_{k=1}^2 \eta_k^{p+3} \pi_k - \dot{\Theta} \right) - (c_1 - \epsilon_1) \eta_1^{p+3} + \sum_{i=1}^2 a_i \\ & - c_2 \eta_2^{p+3}. \end{aligned} \quad (31)$$

By (11), Lemma 4, assumptions  $(A_2) - (A_4)$ , and  $(a+b)^n = \sum_{i=0}^n C_n^i a^i b^{n-i}$ , we have

$$\begin{aligned} \eta_2^3 h_2 (x_3^p - \alpha_3^p) &= \eta_2^3 h_2 \{ (\eta_3 + \alpha_3)^p - \alpha_3^p \} \\ &= \eta_2^3 h_2 \sum_{k=0}^{p-1} C_p^k \alpha_3^k \eta_3^{p-k} = \eta_2^3 h_2 \sum_{k=0}^{p-1} C_p^k (-\eta_2 \beta_2)^k \eta_3^{p-k} \\ &\leq \sum_{k=0}^{(p-1)/2} C_p^{2k} |\eta_2^{3+2k}| |\eta_3^{p-2k}| \beta_2^{2k} \\ &\leq \sum_{k=0}^{(p-1)/2} \frac{3+2k}{p+3} \epsilon_{2k}^{(p+3)/(3+2k)} \eta_2^{3+p} \\ &+ \sum_{k=0}^{(p-1)/2} \frac{p-2k}{p+3} \epsilon_{2k}^{(p-2k)/(p+3)} (C_p^{2k} \beta_2^{2k} \gamma_{22})^{(p+3)/(p-2k)} \\ &\cdot \eta_3^{3+p} \leq \epsilon_2 \eta_2^{p+3} + \gamma_{30} \eta_2^{p+3} \end{aligned} \quad (32)$$

where  $\epsilon_2 \geq \sum_{k=0}^{(p-1)/2} ((3+2k)/(p+3)) \epsilon_{2k}^{(p+3)/(3+2k)}$ ,  $\gamma_{30} \geq \sum_{k=0}^{(p-1)/2} ((p-2k)/(p+3)) \epsilon_{2k}^{(p-2k)/(p+3)} (C_p^{2k} \beta_2^{2k} \gamma_{22})^{(p+3)/(p-2k)}$ ,  $\epsilon_{2k} > 0$ ,  $k = 0, 1, \dots, (p-1)/2$ .

Substituting (32) into (31), we get

$$\begin{aligned} LV_2 \leq & \bar{\Theta} \left( \sum_{i=1}^2 \eta_i^{p+3} \pi_i - \dot{\Theta} \right) - \sum_{i=1}^2 (c_i - \epsilon_i) \eta_i^{p+3} \\ & + \gamma_{30} \eta_3^{p+3} + \eta_2^3 \left( f_2 - \frac{\partial\alpha_2}{\partial\Theta} \dot{\Theta} \right) + \sum_{i=1}^2 a_i. \end{aligned} \quad (33)$$

*Remark 7.* Since  $\dot{\Theta}$  contains  $\eta_1, \eta_2$ , the term  $(\partial\alpha_2/\partial\Theta)\dot{\Theta}$  cannot be used directly to design the virtual control law  $\alpha_2$ . And the function  $f_2$  will be used to compensate for  $(\partial\alpha_2/\partial\Theta)\dot{\Theta}$ . As a result, the term  $\eta_2^3(f_2 - (\partial\alpha_2/\partial\Theta)\dot{\Theta})$  will be considered in the later section.

*Step i* ( $3 \leq i \leq n$ ). We choose the following Lyapunov function  $V_i = V_{i-1} + (1/4)\eta_i^4$ . From (3) and (12), we have

$$\begin{aligned} LV_i &= LV_{i-1} + \eta_i^3 h_i x_{i+1}^p + \eta_i^3 \bar{\varphi}_i \\ &+ \frac{3}{2} \eta_i^2 Tr \left( G_i^T \sum_{t=1}^T (t) \sum (t) G_i \right) + \eta_i^3 \frac{\partial\alpha_i}{\partial\Theta} \dot{\Theta} \end{aligned} \quad (34)$$

where  $V_{i-1} = (1/4)\sum_{j=1}^{i-1} \eta_j^4 + (1/2)\bar{\Theta}^2$ , and

$$\begin{aligned} LV_{i-1} \leq & -\sum_{j=1}^{i-1} (c_j - \epsilon_j) \eta_j^{p+3} + \bar{\Theta} \left( \sum_{j=1}^{i-1} \eta_j^{p+3} \pi_j - \dot{\Theta} \right) \\ & + \sum_{j=2}^{i-1} \eta_j^3 \left( f_j - \frac{\partial\alpha_j}{\partial\Theta} \dot{\Theta} \right) + \gamma_{i0} \eta_i^{p+3} + \sum_{j=1}^{i-1} a_j \end{aligned} \quad (35)$$

where

$$f_j = -\frac{\partial\alpha_j}{\partial\Theta} c_0 \bar{\Theta} + \frac{\partial\alpha_j}{\partial\Theta} \sum_{k=1}^{i-1} \eta_k^{p+3} \pi_k - \eta_j^p \pi_j \sum_{l=2}^j \left| \frac{\partial\alpha_l}{\partial\Theta} \eta_l^3 \right|. \quad (36)$$

Similar to the Steps 1 and 2, from the definition of  $\bar{\varphi}_i$ , Lemma 4, and assumptions  $(A_2) - (A_4)$ , there exist constants  $a_{ij} > 0$ ,  $j = 1, 2$ , such that

$$\eta_i^3 \bar{\varphi}_i \leq \eta_i^{p+3} \frac{3}{p+3} a_{i1}^{3/(p+3)} |\bar{\varphi}_i|^{(p+3)/3} + \frac{1}{p+3} a_{i1}^{p+3} \quad (37)$$

and

$$\begin{aligned} & \frac{3}{2} \eta_i^2 Tr \left( G_i^T \sum_{t=1}^T (t) \sum (t) G_i \right) \\ &= \frac{3}{2} \eta_i^2 \|G_i\|^2 \left\| \sum_{t=1}^T (t) \sum (t) \right\|_F^2 \\ &\leq \eta_i^{p+3} \frac{2}{p+3} a_{i2}^{2/(p+3)} \|G_i\|^{p+3} M + \frac{1}{p+3} a_{i2}^{p+3} M. \end{aligned} \quad (38)$$

Substituting  $LV_{i-1}$ , (37), and (38) into (34), we can get

$$\begin{aligned}
LV_i \leq & \eta_i^3 \left( h_i x_{i+1}^p - \frac{\partial \alpha_i}{\partial \hat{\Theta}} \dot{\hat{\Theta}} \right) + \bar{\Theta} \left( \sum_{j=2}^{i-1} \eta_j^{p+3} \pi_j - \dot{\hat{\Theta}} \right) \\
& - \sum_{j=1}^{i-1} (c_j - \epsilon_j) \eta_j^{p+3} + \gamma_{i0} \eta_i^{p+3} + \sum_{j=1}^{i-1} a_j + \eta_i^{p+3} \\
& \cdot \left\{ \frac{2}{p+3} a_{i2}^{2/(p+3)} \|G_i\|^{p+3} M \right. \\
& \left. + \frac{3}{(p+3)} a_{i1}^{3/(p+3)} |\bar{\varphi}_i|^{(p+3)/3} \right\} + a_i \\
& + \sum_{j=2}^{i-1} \eta_j^3 \left( f_j - \frac{\partial \alpha_j}{\partial \hat{\Theta}} \dot{\hat{\Theta}} \right) + \frac{1}{p+3} a_{i1}^{p+3} + \frac{1}{p+3} \\
& \cdot a_{i2}^{p+3} M.
\end{aligned} \quad (39)$$

Further, add and subtract  $\eta_i^3 f_i$  in the first bracket in (39), and, using the Lemma 4, there exists a constant  $a_{i3} > 0$ , such that

$$-\eta_i^3 f_i \leq \eta_i^{p+3} \frac{3}{p+3} a_{i3}^{3/(p+3)} |f_i|^{(p+3)/3} + \frac{1}{p+3} a_{i3}^{p+3} \quad (40)$$

Then, substituting (40) into (39), we get

$$\begin{aligned}
LV_i \leq & \eta_i^3 \left( h_i x_{i+1}^p - \frac{\partial \alpha_i}{\partial \hat{\Theta}} \dot{\hat{\Theta}} + f_i \right) + \bar{\Theta} \left( \sum_{j=2}^{i-1} \eta_j^{p+3} \pi_j \right. \\
& \left. - \dot{\hat{\Theta}} \right) - \sum_{j=1}^{i-1} (c_j - \epsilon_j) \eta_j^{p+3} + \gamma_{i0} \eta_i^{p+3} + \sum_{j=1}^{i-1} a_j \\
& + \eta_i^{p+3} \left\{ \frac{2}{p+3} a_{i2}^{2/(p+3)} \|G_i\|^{p+3} M \right. \\
& \left. + \frac{3}{(p+3)} a_{i1}^{3/(p+3)} |\bar{\varphi}_i|^{(p+3)/3} \right\} + a_i \\
& + \sum_{j=2}^{i-1} \eta_j^3 \left( f_j - \frac{\partial \alpha_j}{\partial \hat{\Theta}} \dot{\hat{\Theta}} \right) + \frac{1}{p+3} a_{i1}^{p+3} + \frac{1}{p+3} a_{i2}^{p+3} M \quad (41) \\
& + \eta_i^{p+3} \frac{3}{p+3} a_{i3}^{3/(p+3)} |f_i|^{(p+3)/3} + \frac{1}{p+3} a_{i3}^{p+3} \\
& = \eta_i^3 h_i x_{i+1}^p + \bar{\Theta} \left( \sum_{j=2}^{i-1} \eta_j^{p+3} \pi_j - \dot{\hat{\Theta}} \right) \\
& - \sum_{j=1}^{i-1} (c_j - \epsilon_j) \eta_j^{p+3} + \gamma_{i0} \eta_i^{p+3} + \sum_{j=1}^i a_j + \eta_i^{p+3} \Psi_i \\
& + \sum_{j=2}^i \eta_j^3 \left( f_j - \frac{\partial \alpha_j}{\partial \hat{\Theta}} \dot{\hat{\Theta}} \right) + \gamma_{i0} \eta_i^{p+3}.
\end{aligned}$$

where

$$\begin{aligned}
a_i &= \frac{1}{p+3} a_{i1}^{p+3} + \frac{1}{p+3} a_{i2}^{p+3} M + \frac{1}{p+3} a_{i3}^{p+3}, \\
\Psi_i &= \frac{2}{p+3} a_{i2}^{2/(p+3)} \|G_i\|^{p+3} M \\
&+ \frac{3}{(p+3)} a_{i1}^{3/(p+3)} |\bar{\varphi}_i|^{(p+3)/3} \\
&+ \frac{3}{p+3} a_{i3}^{3/(p+3)} |f_i|^{(p+3)/3}
\end{aligned} \quad (42)$$

and

$$f_i = -\frac{\partial \alpha_i}{\partial \hat{\Theta}} c_0 \hat{\Theta} + \frac{\partial \alpha_i}{\partial \hat{\Theta}} \sum_{j=1}^{i-1} \eta_j^{p+3} \pi_j - \eta_i^p \pi_i \sum_{j=2}^i \left| \frac{\partial \alpha_j}{\partial \hat{\Theta}} \eta_j^3 \right|. \quad (43)$$

Since the unknown functions  $\varphi_i$  and  $g_i$  can be derived by  $\Psi_i$ , it cannot be used to design the control law directly. Thus there exist the neural networks  $W_i^{*T} S_i(Y_i)$  and  $Y_i = [\bar{x}_i, \hat{\Theta}] \in \Omega_{Y_i} \subset R^{i+1}$  such that

$$\Psi_i = W_i^{*T} S_i(Y_i) + \delta_i(Y_i) \leq \Theta \pi_i(\cdot) \quad (44)$$

where  $\pi_i(\cdot) = \sqrt{(l+1) \sum_{k=1}^l S_{ik}^2 + 1}$ ,  $f_i = -(\partial \alpha_i / \partial \hat{\Theta}) c_0 \hat{\Theta} + (\partial \alpha_i / \partial \hat{\Theta}) \sum_{j=1}^{i-1} \eta_j^{p+3} \pi_j - \eta_i^p \pi_i \sum_{j=2}^i |(\partial \alpha_j / \partial \hat{\Theta}) \eta_j^3|$ .

We add and subtract  $h_i \eta_i^3 \alpha_{i+1}^p$  in the formula (39), respectively, and, substituting (44) into (39), it has

$$\begin{aligned}
LV_i \leq & \eta_i^3 h_i (x_{i+1}^p - \alpha_{i+1}^p) + \eta_i^3 h_i \alpha_{i+1}^p \\
& + \bar{\Theta} \left( \sum_{j=2}^{i-1} \eta_j^{p+3} \pi_j - \dot{\hat{\Theta}} \right) - \sum_{j=1}^{i-1} (c_j - \epsilon_j) \eta_j^{p+3} \\
& + \gamma_{i0} \eta_i^{p+3} + \sum_{i=1}^i a_j + \eta_i^{p+3} \pi_i \Theta \\
& + \sum_{j=2}^i \eta_j^3 \left( f_j - \frac{\partial \alpha_{j-1}}{\partial \hat{\Theta}} \dot{\hat{\Theta}} \right).
\end{aligned} \quad (45)$$

Choose the virtual control law

$$\begin{aligned}
\alpha_{i+1} &= \left( \frac{-c_i - \bar{\Theta} \pi_i - \gamma_{i0}}{\gamma_{i1}} \right)^{1/p} \eta_i = -\beta_i \eta_i, \\
\beta_i &= \left( \frac{c_i + \bar{\Theta} \pi_i + \gamma_{i0}}{\gamma_{i1}} \right)^{1/p} > 0,
\end{aligned} \quad (46)$$

where  $c_i > 0$  is a constant to be chosen. Then, by substituting  $\alpha_{i+1}$  into (45) and using (11), Lemma 5, and  $(a+b)^n = \sum_{k=0}^n C_n^k a^k b^{n-k}$ , one yields

$$\begin{aligned}
\eta_i^3 h_i (x_{i+1}^p - \alpha_{i+1}^p) &= \eta_i^3 h_i \{ (\eta_{i+1} + \alpha_{i+1})^p - \alpha_{i+1}^p \} \\
&= \eta_i^3 h_i \sum_{k=0}^{p-1} C_p^k \alpha_{i+1}^k \eta_{i+1}^{p-k} = \eta_i^3 h_i \sum_{k=0}^{p-1} C_p^k (-\eta_i \beta_i)^k \eta_{i+1}^{p-k}
\end{aligned}$$

$$\begin{aligned}
 &\leq \sum_{k=0}^{(p-1)/2} C_p^{2k} |\eta_i^{3+2k}| |\eta_{i+1}^{p-2k}| \beta_i^{2k} \\
 &\leq \sum_{k=0}^{(p-1)/2} \frac{3+2k}{p+3} \epsilon_{ik}^{(p+3)/(3+2k)} \eta_i^{3+p} \\
 &+ \sum_{k=0}^{(p-1)/2} \frac{p-2k}{p+3} \epsilon_{ik}^{(p-2k)/(p+3)} (C_p^{2k} \beta_i^{2k} \gamma_{i2})^{(p+3)/(p-2k)} \\
 &\cdot \eta_{i+1}^{3+p} \leq \epsilon_i \eta_i^{p+3} + \gamma_{i+10} \eta_{i+1}^{p+3}
 \end{aligned} \tag{47}$$

where  $\epsilon_i \geq \sum_{k=0}^{(p-1)/2} ((3+2k)/(p+3)) \epsilon_{ik}^{(p+3)/(3+2k)}$ ,  $\gamma_{i+10} \geq \sum_{k=0}^{(p-1)/2} ((p-2k)/(p+3)) \epsilon_{ik}^{(p-2k)/(p+3)} (C_p^{2k} \beta_i^{2k} \gamma_{i2})^{(p+3)/(p-2k)}$ ,  $\epsilon_{ik} > 0$ ,  $k = 0, 1, \dots, (p-1)/2$ .

In the view of (47), (45) can be calculated as

$$\begin{aligned}
 LV_i \leq &\bar{\Theta} \left( \sum_{j=2}^i \eta_j^{p+3} \pi_j - \dot{\hat{\Theta}} \right) - \sum_{j=1}^i (c_j - \epsilon_j) \eta_j^{p+3} \\
 &+ \gamma_{i+10} \eta_{i+1}^{p+3} + \sum_{j=1}^i a_j + \sum_{j=2}^i \eta_j^3 \left( f_j - \frac{\partial \alpha_j}{\partial \hat{\Theta}} \dot{\hat{\Theta}} \right).
 \end{aligned} \tag{48}$$

*Remark 8.* Since  $\hat{\Theta}$  contains  $\eta_j$ ,  $j = 1, 2, \dots, i$ , the term  $(\partial \alpha_j / \partial \hat{\Theta}) \dot{\hat{\Theta}}$  cannot be used directly to design the virtual control law  $\alpha_i$ . And the function  $f_j$  will be used to compensate for  $(\partial \alpha_j / \partial \hat{\Theta}) \dot{\hat{\Theta}}$ . As a result, the term  $\eta_j^3 (f_j - (\partial \alpha_j / \partial \hat{\Theta}) \dot{\hat{\Theta}})$  will be considered in the later section.

Finally, when  $i = n$ ,  $\eta_{n+1} = u$  is the actual control. Choose the actual controller

$$\begin{aligned}
 u &= -\eta_n \beta_n, \\
 \beta_n &= \left( \frac{c_n + \gamma_{n0} + \pi_n \hat{\Theta}}{\gamma_{n1}} \right)^{1/p} > 0
 \end{aligned} \tag{49}$$

where  $c_n > 0$  is a design parameter to be chosen. It can be deduced that

$$\begin{aligned}
 LV_n \leq &-\sum_{j=1}^n (c_j - \epsilon_j) \eta_j^{p+3} + \sum_{j=1}^n a_j \\
 &+ \bar{\Theta} \left( \sum_{j=2}^n \eta_j^{p+3} \pi_j - \dot{\hat{\Theta}} \right) + \sum_{j=2}^n \eta_j^3 \left( f_j - \frac{\partial \alpha_j}{\partial \hat{\Theta}} \dot{\hat{\Theta}} \right)
 \end{aligned} \tag{50}$$

where  $V_n(\eta, \hat{\Theta}) = \sum_{k=1}^n (1/4) \eta_k^4 + (1/2)(\hat{\Theta} - \Theta)^2$ ,  $\eta = (\eta_1, \dots, \eta_n)$ . We finish the controller design procedure.

**3.2. Analysis of Stability.** We have obtained the main result in the following theorem.

**Theorem 9.** Suppose that assumptions  $(A_1) - (A_4)$  hold for the stochastic nonlinear system (1). Furthermore, suppose that the unknown functions  $\Psi_i$  ( $1 \leq i \leq n$ ) can be approximated by the RBF neural networks. Given a control law with the virtual control signals  $\alpha_i$ , it is constructed in (49), and the adaptive law satisfies

$$\dot{\hat{\Theta}} = \sum_{k=1}^n \eta_k^{p+3} \pi_k - c_0 \hat{\Theta} \tag{51}$$

where the design parameter  $c_0 > 0$ . Then the signals of the closed-loop system are bounded in probability.

*Proof.* Choose the Lyapunov function  $V = V_n$  such that

$$\begin{aligned}
 LV \leq &-\sum_{j=1}^n (c_j - \epsilon_j) \eta_j^{p+3} + \sum_{j=1}^n a_j \\
 &+ \bar{\Theta} \left( \sum_{j=2}^n \eta_j^{p+3} \pi_j - \dot{\hat{\Theta}} \right) + \sum_{j=2}^n \eta_j^3 \left( f_j - \frac{\partial \alpha_j}{\partial \hat{\Theta}} \dot{\hat{\Theta}} \right).
 \end{aligned} \tag{52}$$

Substituting the adaptive law (51) into the penultimate term in (52) results in

$$\begin{aligned}
 LV \leq &-\sum_{j=1}^n (c_j - \epsilon_j) \eta_j^{p+3} + \sum_{j=1}^n a_j + c_0 \bar{\Theta} \hat{\Theta} \\
 &+ \sum_{j=2}^n \eta_j^3 \left( f_j - \frac{\partial \alpha_j}{\partial \hat{\Theta}} \dot{\hat{\Theta}} \right).
 \end{aligned} \tag{53}$$

In the following, we will prove that the last term  $\sum_{j=2}^n \eta_j^3 (f_j - (\partial \alpha_j / \partial \hat{\Theta}) \dot{\hat{\Theta}})$  in (53) is negative. It is clear that

$$\begin{aligned}
 -\sum_{j=2}^n \eta_j^3 \frac{\partial \alpha_j}{\partial \hat{\Theta}} \dot{\hat{\Theta}} &= \sum_{j=2}^n \eta_j^3 \frac{\partial \alpha_j}{\partial \hat{\Theta}} c_0 \hat{\Theta} - \sum_{j=2}^n \eta_j^3 \frac{\partial \alpha_j}{\partial \hat{\Theta}} \sum_{i=1}^n \eta_i^{p+3} \pi_i \\
 &= \sum_{j=2}^n \eta_j^3 \frac{\partial \alpha_j}{\partial \hat{\Theta}} c_0 \hat{\Theta} - \sum_{j=2}^n \eta_j^3 \frac{\partial \alpha_j}{\partial \hat{\Theta}} \sum_{i=1}^n \eta_i^{p+3} \pi_i
 \end{aligned} \tag{54}$$

and

$$\begin{aligned}
 -\sum_{j=2}^n \eta_j^3 \frac{\partial \alpha_j}{\partial \hat{\Theta}} \sum_{i=1}^n \eta_i^{p+3} \pi_i &= -\sum_{j=2}^n \eta_j^3 \frac{\partial \alpha_j}{\partial \hat{\Theta}} \sum_{i=1}^{j-1} \eta_i^{p+3} \pi_i \\
 &\quad - \sum_{j=2}^n \eta_j^3 \frac{\partial \alpha_j}{\partial \hat{\Theta}} \sum_{i=j}^n \eta_i^{p+3} \pi_i \\
 &\leq -\sum_{j=2}^n \eta_j^3 \frac{\partial \alpha_j}{\partial \hat{\Theta}} \sum_{i=1}^{j-1} \eta_i^{p+3} \pi_i \\
 &\quad + \sum_{j=2}^n \eta_j^{p+3} \pi_j \sum_{i=2}^j \left| \eta_i^3 \frac{\partial \alpha_i}{\partial \hat{\Theta}} \right|.
 \end{aligned} \tag{55}$$

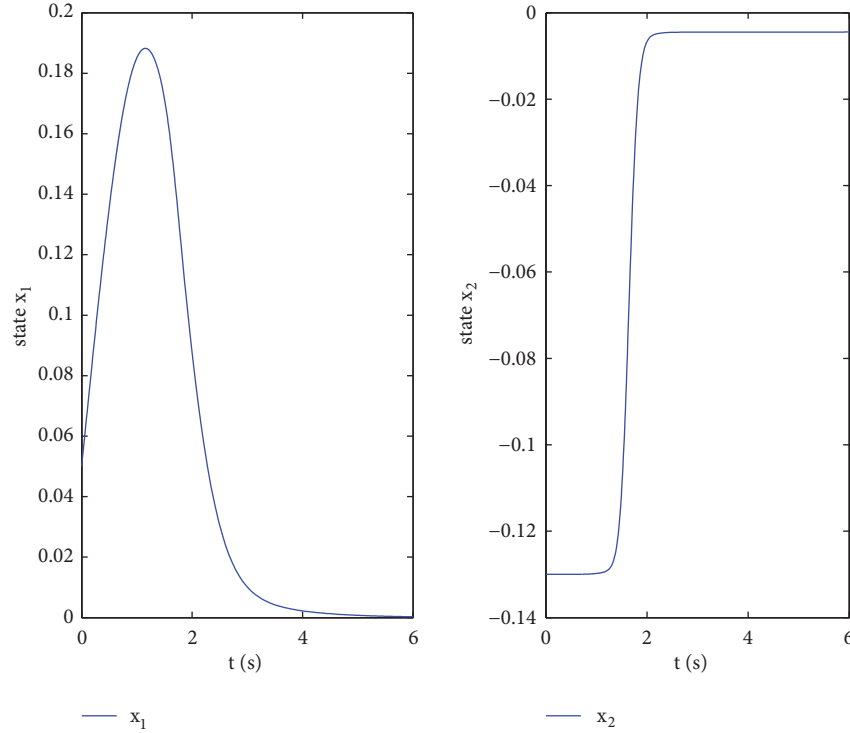


FIGURE 1: The responses of states  $x_1$  and  $x_2$  relative to time.

Substituting (55) into (54), one arrives at

$$\begin{aligned}
-\sum_{j=2}^n \eta_j^3 \frac{\partial \alpha_j}{\partial \Theta} \dot{\Theta} &= \sum_{j=2}^n \eta_j^3 \frac{\partial \alpha_j}{\partial \Theta} \left( c_0 \Theta - \sum_{i=1}^n \eta_i^{p+3} \pi_i \right) \\
&\leq \sum_{j=2}^n \eta_j^3 \frac{\partial \alpha_j}{\partial \Theta} c_0 \Theta - \sum_{j=2}^n \eta_j^3 \frac{\partial \alpha_j}{\partial \Theta} \sum_{i=1}^{j-1} \eta_i^{p+3} \pi_i + \sum_{j=2}^n \eta_j^{p+3} \pi_j \\
&\cdot \sum_{i=2}^j \left| \eta_i^3 \frac{\partial \alpha_i}{\partial \Theta} \right| = -\sum_{j=2}^n \eta_j^3 \\
&\cdot \left\{ -\frac{\partial \alpha_j}{\partial \Theta} c_0 \Theta + \frac{\partial \alpha_j}{\partial \Theta} \sum_{i=1}^{j-1} \eta_i^{p+3} \pi_i - \eta_j^p \pi_j \sum_{i=2}^j \left| \eta_i^3 \frac{\partial \alpha_i}{\partial \Theta} \right| \right\} \\
&= -\sum_{j=2}^n \eta_j^3 f_j.
\end{aligned} \tag{56}$$

By the definition of  $f_i$ , which implies that

$$\sum_{j=2}^n \eta_j^3 \left( f_j - \frac{\partial \alpha_j}{\partial \Theta} \dot{\Theta} \right) \leq 0 \tag{57}$$

and

$$c_0 \Theta \dot{\Theta} = c_0 \Theta (\Theta - \bar{\Theta}) = c_0 \Theta \Theta - c_0 \bar{\Theta}^2 \leq \frac{c_0}{2} \Theta^2 - \frac{c_0}{2} \bar{\Theta}^2 \tag{58}$$

substituting (57) and (58) into (53) yields

$$LV \leq -\sum_{j=1}^n (c_j - \epsilon_j) \eta_j^{p+3} + \sum_{j=1}^n a_j + \frac{c_0}{2} \Theta^2 - \frac{c_0}{2} \bar{\Theta}^2. \tag{59}$$

Furthermore, let  $a_0 = \min\{4(c_j - \epsilon_j), c_0\}$ ,  $j = 1, 2, \dots, n$ , and  $b_0 = \sum_{j=1}^n a_j + (c_0/2)\bar{\Theta}^2$ , and it follows that

$$LV \leq -a_0 V + b_0, \quad t \geq 0. \tag{60}$$

Therefore, according to Lemma 5,  $\eta_i$ ,  $i = 1, 2, \dots, n$ , and  $\bar{\Theta}$  are bounded in probability. Since  $\Theta$  is a constant,  $\bar{\Theta}$  is bounded in probability. It can be obtained that the control law  $\alpha_j$ ,  $j = 1, 2, \dots, n$ , is also bounded in probability because  $\alpha_j$  is the function of  $\eta_j$  and  $\bar{\Theta}$ . So far we get that all the states of the closed-loop system (1) are bounded in probability.  $\square$

#### 4. Simulation Example

In this section, we will give an example to show the effectiveness of the proposed control method in this paper.

*Example 1.* Consider the following stochastic nonlinear system:

$$\begin{aligned}
dx_1 &= \left( 1 + \frac{1}{2} \sin t \right) x_2^3 dt + x_1^3 \sin x_1 t dt \\
&\quad + 3x_1 \sin x_1 \left( 1 + \frac{1}{4} \sin t \right) d\omega \\
dx_2 &= \left( 1 - \frac{1}{4} \sin t \right) u^3 dt.
\end{aligned} \tag{61}$$

Obviously, the system satisfies  $(A_1) - (A_4)$  and  $p_1 = p_2 = 3 > 1$ . Now according to Theorem 9, the virtual control

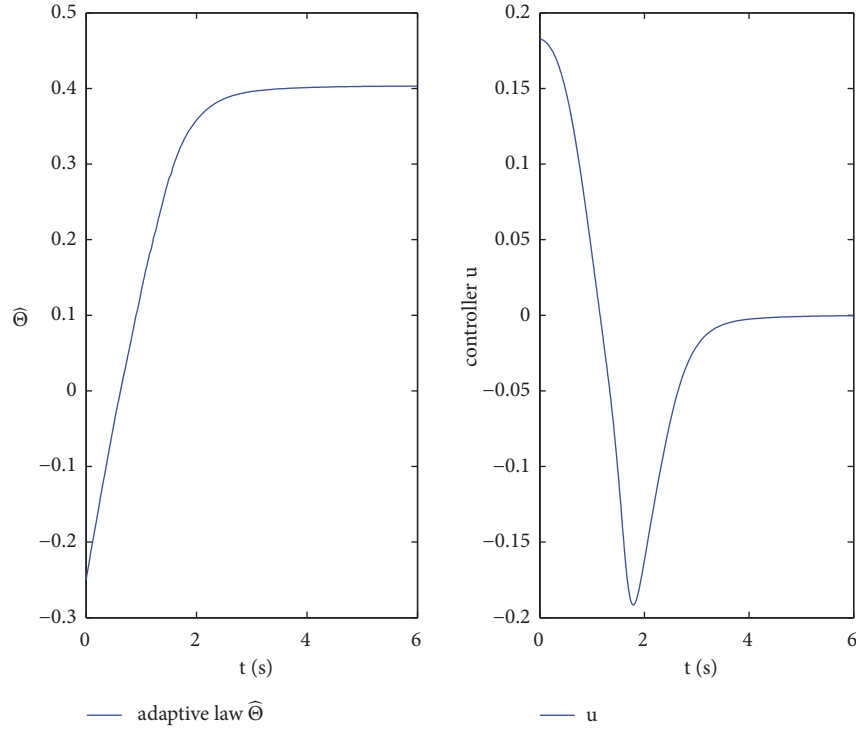


FIGURE 2: The responses of the adaptive law  $\hat{\Theta}$  and the controller  $u$  relative to time.

function  $\alpha_2$ , the control law  $u$ , and the adaptive law  $\hat{\Theta}$  are chosen, respectively, as

$$\begin{aligned}\alpha_2 &= -\eta_1 \beta_1 = -\eta_1 (c_1 + \hat{\Theta} \pi_1)^{1/3}, \\ u &= -\eta_2 \beta_2 = -\eta_2 (c_2 + \hat{\Theta} \pi_2 + \gamma_{20})^{1/3}, \\ \dot{\hat{\Theta}} &= \sum_{i=1}^2 \eta_i^6 \pi_i - c_0 \hat{\Theta},\end{aligned}\quad (62)$$

where  $\eta_1 = x_1$ ,  $\eta_2 = x_2 - \alpha_2$ ,  $Y_1 = \eta_1$ ,  $Y_2 = [\eta_1, \eta_2, \hat{\Theta}]^T$ . In the simulation, neural network  $W_1^{*T} S_1(Y_1)$  includes 7 nodes with centers spaced evenly in  $[-3, -3]$ , neural network  $W_2^{*T} S_2(Y_2)$  includes 81 nodes with centers spaced evenly in  $[-3, -3] \times [-3, -3] \times [0, 3]$ , and all the widths are chosen as 2. The design parameters are chosen as  $c_1 = 2$ ,  $c_2 = 0.5$ ,  $c_0 = 0.1$ .  $\gamma_{20} = \sum_{k=0}^1 ((3-2k)/4) \epsilon_{1k}^{(3-2k)/4} (c_3^{2k} \beta_1^{2k})^{4/(3-2k)}$ , and  $\epsilon_{10} = \epsilon_{11} = 1/4$ . The initial condition  $[x_1(0), x_2(0), \hat{\Theta}(0)] = [0.05, -0.13, -0.25]$ . Figures 1 and 2 show the simulation results. From the figures, we can see that the proposed adaptive control method can guarantee that all the variables for the closed-loop system are bounded.

## 5. Conclusions

This paper has investigated the adaptive neural control for a class of high-order uncertain stochastic nonlinear systems. With the help of backstepping technique and separation technique, a smooth adaptive controller is constructed, and it ensures the closed-loop system is the global bounded in

probability. Only one adaptive learning parameter needed to be updated online. One example has been given to show the effectiveness of the proposed analytical results. A further work is how to design the output-feedback tracking control for more high-order stochastic systems.

## Data Availability

The data used to support the findings of this study are included within the article.

## Conflicts of Interest

The author declares that they have no conflicts of interest.

## Acknowledgments

This paper is supported by Shandong Province Natural Science Foundation of China (No. ZR2016AL05).

## References

- [1] R. Z. Hasminskii, "Stochastic Stability of Differential Equations," *Sijthoff and Noordhoff*, 1980.
- [2] H. Deng, M. Krstić, and R. J. Williams, "Stabilization of stochastic nonlinear systems driven by noise of unknown covariance," *IEEE Transactions on Automatic Control*, vol. 46, no. 8, pp. 1237–1253, 2001.
- [3] X. Mao, *Stochastic Differential Equations and Their Applications*, Chichester: Horwood Publishing, 3rd edition, 2007.
- [4] M. Krstić and H. Deng, *Stabilization of Nonlinear Uncertain Systems*, Communications and Control Engineering, Springer, London, UK, 1998.

- [5] H. Ito and Y. Nishimura, "An iISS framework for stochastic robustness of interconnected nonlinear systems," *Institute of Electrical and Electronics Engineers Transactions on Automatic Control*, vol. 61, no. 6, pp. 1508–1523, 2016.
- [6] H. Sun, Y. Li, G. Zong, and L. Hou, "Disturbance attenuation and rejection for stochastic Markovian jump system with partially known transition probabilities," *Automatica*, vol. 89, pp. 349–357, 2018.
- [7] H. Ito and Y. Nishimura, "Stability of stochastic nonlinear systems in cascade with not necessarily unbounded decay rates," *Automatica*, vol. 62, no. 9, pp. 51–64, 2015.
- [8] Z. Pan and T. Basar, "Backstepping controller design for nonlinear stochastic systems under a risk-sensitive cost criterion," *SIAM Journal on Control and Optimization*, vol. 37, no. 3, pp. 957–995, 1999.
- [9] X. Qin and H. Min, "State feedback stabilisation for stochastic high-order feedforward nonlinear systems with input time-delay," *International Journal of Systems Science*, vol. 49, no. 5, pp. 1012–1020, 2018.
- [10] X.-J. Xie, X.-H. Zhang, and K. Zhang, "Finite-time state feedback stabilisation of stochastic high-order nonlinear feedforward systems," *International Journal of Control*, vol. 89, no. 7, pp. 1332–1341, 2016.
- [11] X. Y. Qin, "State-feedback stabilization for a class of higher-order stochastic nonlinear systems," *Journal of Anhui University. Natural Science Edition. Anhui Daxue Xuebao. Ziran Kexue Ban*, vol. 36, no. 4, pp. 7–12, 2012.
- [12] C. Zhao and X. Xie, "Global stabilization of stochastic high-order feedforward nonlinear systems with time-varying delay," *Automatica*, vol. 50, no. 1, pp. 203–210, 2014.
- [13] F. Gao, Y. Wu, and X. Yu, "Global state feedback stabilisation of stochastic high-order nonlinear systems with high-order and low-order nonlinearities," *International Journal of Systems Science*, vol. 47, no. 16, pp. 3846–3856, 2016.
- [14] Y.-G. Liu and J.-F. Zhang, "Practical output-feedback risk-sensitive control for stochastic nonlinear systems with stable zero-dynamics," *SIAM Journal on Control and Optimization*, vol. 45, no. 3, pp. 885–926, 2006.
- [15] S.-J. Liu, J.-F. Zhang, and Z.-P. Jiang, "Decentralized adaptive output-feedback stabilization for large-scale stochastic nonlinear systems," *Automatica*, vol. 43, no. 2, pp. 238–251, 2007.
- [16] Y.-L. Liu and Y.-Q. Wu, "Output feedback control for stochastic nonholonomic systems with growth rate restriction," *Asian Journal of Control*, vol. 13, no. 1, pp. 177–185, 2011.
- [17] X. Xie, N. Duan, and C. Zhao, "A combined homogeneous domination and sign function approach to output-feedback stabilization of stochastic high-order nonlinear systems," *IEEE Transactions on Automatic Control*, vol. 59, no. 5, pp. 1303–1309, 2014.
- [18] Q. Wang and C. Wei, "Decentralized robust adaptive output feedback control of stochastic nonlinear interconnected systems with dynamic interactions," *Automatica*, vol. 54, pp. 124–134, 2015.
- [19] X. Xie and M. Jiang, "Output feedback stabilization of stochastic feedforward nonlinear time-delay systems with unknown output function," *International Journal of Robust and Nonlinear Control*, vol. 28, no. 1, pp. 266–280, 2018.
- [20] F. Gao and Y. Wu, "Global finite-time stabilisation for a class of stochastic high-order time-varying nonlinear systems," *International Journal of Control*, vol. 89, no. 12, pp. 2453–2465, 2016.
- [21] M.-M. Jiang and X.-J. Xie, "Finite-time stabilization of stochastic low-order nonlinear systems with FT-SISS inverse dynamics," *International Journal of Robust and Nonlinear Control*, vol. 28, no. 6, pp. 1960–1972, 2018.
- [22] C. S. Tong, Y. Li, M. Y. Li, and J. Y. Liu, "Observer-based adaptive fuzzy backstepping control for a class of stochastic nonlinear strict-feedback systems," *IEEE Transactions on Systems, Man, and Cybernetics, Part B (Cybernetics)*, vol. 41, no. 6, pp. 1693–1704, 2011.
- [23] T. Wang, S. C. Tong, and Y. M. Li, "Adaptive neural network output feedback control of stochastic nonlinear systems with dynamical uncertainties," *Neural Computing and Applications*, vol. 23, no. 5, pp. 1481–1494, 2013.
- [24] H.-F. Min and N. Duan, "Adaptive NN output-feedback control for stochastic time-delay nonlinear systems with unknown control coefficients and perturbations," *Nonlinear Analysis: Modelling and Control*, vol. 21, no. 4, pp. 515–530, 2016.
- [25] N. Duan and H.-F. Min, "NN-based output tracking for more general stochastic nonlinear systems with unknown control coefficients," *International Journal of Automation and Computing*, vol. 14, no. 3, pp. 350–359, 2017.
- [26] N. Duan and H.-F. Min, "Decentralized adaptive NN state-feedback control for large-scale stochastic high-order nonlinear systems," *Neurocomputing*, vol. 173, no. 3, pp. 1412–1421, 2016.
- [27] J. Li, W. Chen, and J.-M. Li, "Adaptive NN output-feedback decentralized stabilization for a class of large-scale stochastic nonlinear strict-feedback systems," *International Journal of Robust and Nonlinear Control*, vol. 21, no. 4, pp. 452–472, 2011.
- [28] W.-Q. Li, L. Liu, and G. Feng, "Output tracking of stochastic nonlinear systems with unstable linearization," *International Journal of Robust and Nonlinear Control*, vol. 28, no. 2, pp. 466–477, 2018.
- [29] W. Li, L. Liu, and G. Feng, "Cooperative control of multiple stochastic high-order nonlinear systems," *Automatica*, vol. 82, pp. 218–225, 2017.
- [30] W. Li and J.-F. Zhang, "Distributed practical output tracking of high-order stochastic multi-agent systems with inherent nonlinear drift and diffusion terms," *Automatica*, vol. 50, no. 12, pp. 3231–3238, 2014.

## Research Article

# Adaptive Parallel Simultaneous Stabilization of a Class of Nonlinear Descriptor Systems via Dissipative Matrix Method

Liying Sun <sup>1</sup> and Renming Yang <sup>2</sup>

<sup>1</sup>*School of Mathematics Science, University of Jinan, Jinan 250022, China*

<sup>2</sup>*School of Information Science and Electrical Engineering, Shandong Jiaotong University, Jinan 250357, China*

Correspondence should be addressed to Liying Sun; [ss\\_sunly@ujn.edu.cn](mailto:ss_sunly@ujn.edu.cn)

Received 20 June 2018; Accepted 12 August 2018; Published 30 August 2018

Academic Editor: Xue-Jun Xie

Copyright © 2018 Liying Sun and Renming Yang. This is an open access article distributed under the Creative Commons Attribution License, which permits unrestricted use, distribution, and reproduction in any medium, provided the original work is properly cited.

This paper investigates the adaptive parallel simultaneous stabilization and robust adaptive parallel simultaneous stabilization problems of a class of nonlinear descriptor systems via dissipative matrix method. Firstly, under an output feedback law, two nonlinear descriptor systems are transformed into two nonlinear differential-algebraic systems by nonsingular transformations, and a sufficient condition of impulse-free is given for two resulting closed-loop systems. Then, the two systems are combined to generate an augmented dissipative Hamiltonian differential-algebraic system by using the system-augmentation technique. Based on the dissipative system, an adaptive parallel simultaneous stabilization controller and a robust adaptive parallel simultaneous stabilization controller are designed for the two systems. Furthermore, the case of more than two nonlinear descriptor systems is investigated. Finally, an illustrative example is studied by using the results proposed in this paper, and simulations show that the adaptive parallel simultaneous stabilization controllers obtained in this paper work very well.

## 1. Introduction

In practical control designs, a commonly encountered problem is to design feedback controller(s) to stabilize a given family of parallel systems. It is straightforward to consider each system individually and design a stabilization controller for each system. However, a more economical approach to the problem is to design a single controller, which may take measurements/signals from all members of the family, to stabilize all the systems simultaneously [1, 2]. In this way, the controller implementation cost will be greatly reduced. This control is referred to the parallel simultaneous stabilization. It is noted that this kind of stabilization is different from the traditional simultaneous stabilization problem [3, 4]. The traditional simultaneous stabilization is concerned with designing a control law such that any individual system within the collection of systems can be stabilized by the control law. In other words, the resulting closed-loop system which consists of an individual system and its corresponding controller via its state or output feedback based on that control law is asymptotically stable. It is also noted that the

traditional simultaneous stabilization problem is one of the important research topics in the area of robust control and has received a considerable attention in the past few decades [3–8].

The descriptor system is a natural representation of dynamic systems and describes a larger class of systems than the normal system model [9–16]. In the last three decades, many nice results have been obtained for the controller design of linear descriptor systems; see [9, 10, 13, 14] and references therein. In general, it is not an easy task to design a controller for nonlinear descriptor systems (NDSs) and, accordingly, there are fewer works on NDSs except several special case studies [11, 12, 15, 16]; particularly, it is more difficult to design a parallel simultaneous stabilization controller for a class of nonlinear descriptor systems; the pertinent results were proposed for this case in [1]. For nonlinear differential-algebraic systems, an  $H_\infty$  controller was designed in [15] based on the condition for the existence of  $H_\infty$  controller of nonlinear systems, while the stabilization and robust stabilization of the systems were considered by the feedback linearization approach in [11] and the Hamiltonian function

method in [12], respectively. In [16], based on the linear matrix inequality method, the generalized absolute stability was studied for linear descriptor systems with feedback-connected nonlinearities. Using a nonlinear performance index to the nominal system, a robust adaptive control scheme was presented in [17] for a class of nonlinear uncertain descriptor systems. For the case in which the singular matrix  $E_i = M_i \text{diag}\{I_r, 0\}M_i$  with  $M_i$  being an orthogonal matrix, the parallel simultaneous stabilization and robust adaptive parallel simultaneous stabilization problems were, respectively, studied in [1, 18] for two or a family of nonlinear descriptor systems via the Hamiltonian function method. It should be pointed out that there are, to the best of the authors' knowledge, fewer works on the robust adaptive parallel simultaneous stabilization of NDSs [18].

In this paper, motivated by the Hamiltonian function method [2, 19–29], we apply the structural properties of dissipative matrices to investigate the adaptive parallel simultaneous stabilization and robust adaptive parallel simultaneous stabilization problems for a class of NDSs via output feedback law [30, 31], and propose a new approach, called the dissipative matrix method, to study NDSs. Firstly, under an output feedback law, two NDSs are transformed into two nonlinear differential-algebraic systems by nonsingular transformations, and a sufficient condition of impulse-free is given for two closed-loop systems. Then, the two systems are combined to generate an augmented dissipative Hamiltonian differential-algebraic system by using the system-augmentation technique. Based on the dissipative system, an adaptive parallel simultaneous stabilization controller and a robust adaptive parallel simultaneous stabilization controller are designed for two NDSs, in which the singular matrix  $E_i \geq 0$  ( $\leq 0$ ). Furthermore, the case of more than two NDSs is investigated. Finally, an illustrative example is studied by using the results proposed in this paper, and simulations show that the adaptive parallel simultaneous stabilization controllers obtained in this paper work very well.

The paper is organized as follows. In Section 2, we study the adaptive parallel simultaneous stabilization of two NDSs based on an augmented dissipative Hamiltonian form. Section 3 presents the robust adaptive parallel simultaneous stabilization controller for two NDSs with external disturbances and investigates the case of more than two NDSs. In Section 4, an illustrative example is provided, which is followed by the conclusion in Section 5.

## 2. Adaptive Parallel Simultaneous Stabilization of Two NDSs

This section investigates adaptive parallel simultaneous stabilization problem for two NDSs via dissipative matrix method. Firstly, based on suitable output feedback, two NDSs are transformed into two nonlinear differential-algebraic systems by new coordinate transformations, and then the two systems are combined to generate an augmented dissipative Hamiltonian differential-algebraic system by using the system-augmentation technique, based on which an adaptive parallel simultaneous stabilization controller is designed for the two systems.

Consider the following two NDSs:

$$\begin{aligned} E_1 \dot{x} &= f_1(x, p_1) + g_1(x)u, \\ E_1 x(0) &= E_1 x_0, \\ f_1(0, p_1) &= f_{p_1}(p_1), \\ f_1(0, 0) &= 0, \\ y &= g_1^T(x)x, \\ E_2 \dot{\xi} &= f_2(\xi, p_2) + g_2(\xi)u, \\ E_2 \xi(0) &= E_2 \xi_0, \\ f_2(0, p_2) &= f_{p_2}(p_2), \\ f_2(0, 0) &= 0, \\ \eta &= g_2^T(\xi)\xi, \end{aligned} \quad (1)$$

where  $x = [\tilde{x}_1, \tilde{x}_2, \dots, \tilde{x}_n]^T$ ,  $\xi = [\tilde{\xi}_1, \tilde{\xi}_2, \dots, \tilde{\xi}_n]^T \in \mathbb{R}^n$  and  $y, \eta \in \mathbb{R}^m$  are the states and outputs of the two systems, respectively;  $u \in \mathbb{R}^m$  is the control input;  $p_i \in \mathbb{R}^s$  is an unknown parameter perturbation vector and is assumed to be small enough to keep the dissipative structure unchanged; i.e., if  $R(x) > 0$ , then  $R(x, p_i) > 0$ ;  $f_i(x, p_i) \in \mathbb{R}^n$  is sufficiently smooth vector fields,  $g_1(x), g_2(\xi) \in \mathbb{R}^{n \times m}$ ;  $E_i \in \mathbb{R}^{n \times n}$ ,  $0 < \text{rank}(E_i) = r < n$ , and  $E_i \geq 0$  or  $E_i \leq 0$ ,  $i = 1, 2$ . Without loss of generality, we discuss  $E_i \geq 0$ ,  $i = 1, 2$ .

*Definition 1* (see [32]). A control law  $u = u(x)$  is called an admissible control law if, for any initial condition  $Ex_0$ , the resulting closed-loop descriptor system has no impulsive solution.

**Lemma 2** (see [33]). *If a vector function  $h(x)$  with  $h(0) = 0$  ( $x \in \mathbb{R}^n$ ) has continuous  $n$ th-order partial derivatives, then  $h(x)$  can be expressed as*

$$h(x) = a_1(x)x_1 + \dots + a_n(x)x_n, \quad (3)$$

where  $a_i(x)$ ,  $i = 1, 2, \dots, n$ , are vector functions.

According to Lemma 2, systems (1) and (2) can be transformed into the following form:

$$E_1 \dot{x} = A_1(x, p_1)\alpha_1(x, p_1) + g_1(x)u, \quad (4)$$

$$y = g_1^T(x)x,$$

$$E_2 \dot{\xi} = A_2(\xi, p_2)\alpha_2(\xi, p_2) + g_2(\xi)u, \quad (5)$$

$$\eta = g_2^T(\xi)\xi,$$

where the structural matrix  $A_i(x, p_i) \in \mathbb{R}^{n \times n}$ ,  $\alpha_i(x, p_i) \in \mathbb{R}^n$  is some vector of  $x$  and  $p_i$  satisfying  $\alpha_i(x, 0) = x$ ,  $i = 1, 2$ .

To study the adaptive parallel simultaneous stabilization problem of systems (4) and (5), the following assumptions are given:

$$(A1) \text{rank}[E_i, g_i(x)] = \text{rank}(E_i), \quad \forall x \in \mathbb{R}^n, \quad i = 1, 2;$$

(A2) assume there exists  $\Phi \in \mathbb{R}^{l \times m}$  such that

$$A_i(x, p_i)(\alpha_i(x, p_i) - x) = g_i(x) \Phi^T \theta, \quad (6)$$

$$\forall x \in \mathbb{R}^n, \quad i = 1, 2,$$

where  $\theta \in \mathbb{R}^l$  is an unknown constant vector related to  $p_i$ .

Assumption (A1) implies that fast subsystems of the descriptor systems (1) and (2) have no control  $u$ . Assumption (A2) is the so-called matched condition. In most cases, we can find  $\Phi$  and  $\theta$  such that (6) holds.

Under assumption (A2), systems (4) and (5) are changed as

$$E_1 \dot{x} = A_1(x, p_1)x + g_1(x)u + g_1(x)\Phi^T \theta, \quad (7)$$

$$y = g_1^T(x)x,$$

$$E_2 \dot{\xi} = A_2(\xi, p_2)\xi + g_2(\xi)u + g_2(\xi)\Phi^T \theta, \quad (8)$$

$$\eta = g_2^T(\xi)\xi.$$

**Definition 3.** System (4) is called (strictly) dissipative if the structural matrix  $A(x)$  is (strictly) dissipative; i.e.,  $A(x)$  can be expressed as  $A(x) = J(x) - R(x)$ , where  $J(x)$  is skew-symmetric and  $R(x) \geq 0$  ( $R(x) > 0$ ); system (4) is called feedback (strictly) dissipative if there exists suitable state feedback  $u(x) = \alpha(x) + v$  such that the resulting closed-loop descriptor system is (strictly) dissipative.

**Remark 4.** If  $E_1 \leq 0$ , then systems (7) can be rewritten as

$$E_1' \dot{x} = A_1'(x, p_1)x + g_1'(x)u + g_1'(x)\Phi^T \theta, \quad (9)$$

$$y' = g_1'^T(x)x,$$

where  $E_1' = -E_1 \geq 0$ ,  $A_1'(x, p_1) = -A_1(x, p_1)$ , and  $g_1'(x) = -g_1(x)$ ,  $y' = -y$ .

We can always express  $A_i(x, p_i)$  as  $A_i(x, p_i) = J_i(x, p_i) - R_{i0}(x, p_i)$ , where  $J_i(x, p_i) = (1/2)(A_i(x, p_i) - A_i^T(x, p_i))$  is skew-symmetric and  $R_{i0}(x, p_i) = -(1/2)(A_i(x, p_i) + A_i^T(x, p_i))$  is symmetric,  $i = 1, 2$ . In order to investigate adaptive parallel simultaneous stabilization of systems (4) and (5), we design an output feedback law such that the symmetric part of structural matrix of the closed-loop system can be transformed into positive definite one. Based on this, we have the following result.

**Lemma 5.** Assume that there exists a symmetric matrix  $K \in \mathbb{R}^{m \times m}$  such that

$$-\frac{1}{2}(A_1(x, p_1) + A_1^T(x, p_1)) + K_{11}(x, x) > 0, \quad (10)$$

$$-\frac{1}{2}(A_2(\xi, p_2) + A_2^T(\xi, p_2)) - K_{22}(\xi, \xi) > 0,$$

where  $K_{ij}(x, \xi) = g_i(x)Kg_j^T(\xi)$ ,  $i, j = 1, 2$ . Then, under the following adaptive output feedback law

$$u = -K(y - \eta) - \Phi^T \hat{\theta} + v, \quad (11)$$

$$\dot{\hat{\theta}} = Q\Phi(y + \eta),$$

systems (4) and (5) can be expressed in the following forms:

$$E_1 \dot{x} = (J_1(x, p_1) - R_1(x, p_1))x + g_1(x)Kg_2^T(\xi)\xi + g_1(x)v + g_1(x)\Phi^T(\theta - \hat{\theta}), \quad (12)$$

$$\dot{\hat{\theta}} = Q\Phi(g_1^T(x)x + g_2^T(\xi)\xi),$$

$$y = g_1^T(x)x,$$

$$E_2 \dot{\xi} = (J_2(\xi, p_2) - R_2(\xi, p_2))\xi - g_2(\xi)Kg_1^T(x)x + g_2(\xi)v + g_2(\xi)\Phi^T(\theta - \hat{\theta}), \quad (13)$$

$$\dot{\hat{\theta}} = Q\Phi(g_1^T(x)x + g_2^T(\xi)\xi),$$

$$\eta = g_2^T(\xi)\xi,$$

where  $J_i(x, p_i)$  is skew-symmetric,  $R_i(x, p_i) \in \mathbb{R}^{n \times n}$  is positive definite,  $i = 1, 2$ ,  $\hat{\theta}$  is an estimate of  $\theta$ ,  $Q > 0$  is the adaptive gain constant matrix, and  $v$  is a new reference input.

*Proof.* Substituting (11) into systems (7) and (8), respectively, we can obtain systems (12) and (13), where  $R_1(x, p_1) = -(1/2)(A_1(x, p_1) + A_1^T(x, p_1)) + g_1(x)Kg_1^T(x)$  and  $R_2(\xi, p_2) = -(1/2)(A_2(\xi, p_2) + A_2^T(\xi, p_2)) - g_2(\xi)Kg_2^T(\xi)$ . According to (10), we know that  $R_i(x, p_i) > 0$ . The proof is completed.  $\square$

Since  $E_i \geq 0$  and  $0 < \text{rank}(E_i) = r < n$ , there exists a nonsingular matrix  $M_i \in \mathbb{R}^{n \times n}$  such that

$$M_i^T E_i M_i = \begin{bmatrix} I_r & 0 \\ 0 & 0 \end{bmatrix}, \quad i = 1, 2. \quad (14)$$

Denote

$$x = M_i \bar{x},$$

$$\bar{x} = \begin{bmatrix} x_1 \\ x_2 \end{bmatrix}, \quad M_i = \begin{bmatrix} M_{i11} & M_{i12} \\ M_{i21} & M_{i22} \end{bmatrix},$$

$$M_i^T g_i(x) = \begin{bmatrix} \bar{g}_{i1}(x) \\ \bar{g}_{i2}(x) \end{bmatrix} = \begin{bmatrix} \bar{g}_{i1}(\bar{x}) \\ \bar{g}_{i2}(\bar{x}) \end{bmatrix},$$

$$M_i^T J_i(x, p_i) M_i = \begin{bmatrix} \bar{J}_{i11}(x, p_i) & \bar{J}_{i12}(x, p_i) \\ -\bar{J}_{i12}^T(x, p_i) & \bar{J}_{i22}(x, p_i) \end{bmatrix}$$

$$= \begin{bmatrix} \bar{J}_{i11}(\bar{x}, p_i) & \bar{J}_{i12}(\bar{x}, p_i) \\ -\bar{J}_{i12}^T(\bar{x}, p_i) & \bar{J}_{i22}(\bar{x}, p_i) \end{bmatrix},$$

$$\begin{aligned}
M_i^T R_i(x, p_i) M_i &= \begin{bmatrix} \bar{R}_{i11}(x, p_i) & \bar{R}_{i12}(x, p_i) \\ \bar{R}_{i12}^T(x, p_i) & \bar{R}_{i22}(x, p_i) \end{bmatrix} \\
&= \begin{bmatrix} \bar{R}_{i11}(\bar{x}, p_i) & \bar{R}_{i12}(\bar{x}, p_i) \\ \bar{R}_{i12}^T(\bar{x}, p_i) & \bar{R}_{i22}(\bar{x}, p_i) \end{bmatrix}, \\
\nabla_x H_i(x) &= \frac{\partial H_i(x)}{\partial x}, \\
& \quad i = 1, 2,
\end{aligned} \tag{15}$$

where  $x_1 \in \mathbb{R}^r$ ,  $x_2 \in \mathbb{R}^{n-r}$ ,  $\bar{J}_{i11}(x, p_i) = \bar{J}_{i11}(\bar{x}, p_i)$  and  $\bar{J}_{i22}(x, p_i) = \bar{J}_{i22}(\bar{x}, p_i)$  are skew-symmetric matrices, and  $\bar{R}_{i11}(\bar{x}, p_i) = \bar{R}_{i11}(x, p_i) > 0$ ,  $\bar{R}_{i22}(\bar{x}, p_i) = \bar{R}_{i22}(x, p_i) = \begin{bmatrix} M_{i12}^T & M_{i22}^T \end{bmatrix} R_i(x, p_i) \begin{bmatrix} M_{i12} \\ M_{i22} \end{bmatrix}$ , which implies that  $\bar{R}_{i22}(\bar{x}, p_i) = \bar{R}_{i22}(x, p_i) > 0$ ,  $i = 1, 2$ .

*Remark 6.* That  $R_i(x, p_i) > 0$  is a sufficient not necessary condition of  $\bar{R}_{i22}(x, p_i) > 0$ . In this paper,  $\bar{R}_{i22}(x, p_i) > 0$  can guarantee that the closed-loop descriptor systems (12) and (13) have no impulsive solution. Therefore, (10) is a sufficient condition of systems (12) and (13) to be impulse-free.

From (A1), we have

$$\begin{aligned}
\text{rank} [E_i, g_i(x)] &= \text{rank} M_i^T [E_i, g_i(x)] \begin{bmatrix} M_i & 0 \\ 0 & I \end{bmatrix} \\
&= \text{rank} \begin{bmatrix} I_r & 0 & \bar{g}_{i1}(x) \\ 0 & 0 & \bar{g}_{i2}(x) \end{bmatrix} \\
&= \text{rank} \begin{bmatrix} I_r & 0 \\ 0 & \bar{g}_{i2}(x) \end{bmatrix} = \text{rank}(E_i) \\
&= r,
\end{aligned} \tag{16}$$

that is,  $\bar{g}_{i2}(\bar{x}) = \bar{g}_{i2}(x) = 0$ . Thus, according to (15) and assumption (A1), systems (12) and (13) can be transformed into the following differential-algebraic systems:

$$\begin{aligned}
\dot{x}_1 &= (\bar{J}_{111}(\bar{x}, p_1) - \bar{R}_{111}(\bar{x}, p_1)) x_1 \\
&\quad + (\bar{J}_{112}(\bar{x}, p_1) - \bar{R}_{112}(\bar{x}, p_1)) x_2 \\
&\quad + \bar{g}_{11}(\bar{x}) K \bar{g}_{21}^T(\bar{\xi}) \xi_1 + \bar{g}_{11}(\bar{x}) v \\
&\quad + \bar{g}_{11}(\bar{x}) \Phi^T(\theta - \hat{\theta}), \\
0 &= -(\bar{J}_{112}^T(\bar{x}, p_1) + \bar{R}_{112}^T(\bar{x}, p_1)) x_1 \\
&\quad + (\bar{J}_{122}(\bar{x}, p_1) - \bar{R}_{122}(\bar{x}, p_1)) x_2 \\
&=: \varphi(x_1, x_2, p_1), \\
\dot{\hat{\theta}} &= Q\Phi(\bar{g}_{11}^T(\bar{x}) x_1 + \bar{g}_{21}^T(\bar{\xi}) \xi_1), \\
y &= \bar{g}_{11}^T(\bar{x}) x_1,
\end{aligned} \tag{17}$$

$$\begin{aligned}
\dot{\xi}_1 &= (\bar{J}_{211}(\bar{\xi}, p_2) - \bar{R}_{211}(\bar{\xi}, p_2)) \xi_1 \\
&\quad + (\bar{J}_{212}(\bar{\xi}, p_2) - \bar{R}_{212}(\bar{\xi}, p_2)) \xi_2 \\
&\quad - \bar{g}_{21}(\bar{\xi}) K \bar{g}_{11}^T(\bar{x}) x_1 + \bar{g}_{21}(\bar{\xi}) v \\
&\quad + \bar{g}_{21}(\bar{\xi}) \Phi^T(\theta - \hat{\theta}), \\
0 &= -(\bar{J}_{212}^T(\bar{\xi}, p_2) + \bar{R}_{212}^T(\bar{\xi}, p_2)) \xi_1 \\
&\quad + (\bar{J}_{222}(\bar{\xi}, p_2) - \bar{R}_{222}(\bar{\xi}, p_2)) \xi_2, \\
\dot{\hat{\theta}} &= Q\Phi(\bar{g}_{11}^T(\bar{x}) x_1 + \bar{g}_{21}^T(\bar{\xi}) \xi_1), \\
\eta &= \bar{g}_{21}^T(\bar{\xi}) \xi_1.
\end{aligned} \tag{18}$$

Since  $\bar{J}_{i22}(\bar{x}, p_i) = -\bar{J}_{i22}^T(\bar{x}, p_i)$  and  $\bar{R}_{i22}(\bar{x}, p_i) > 0$ , we know that  $\bar{J}_{i22}(\bar{x}, p_i) - \bar{R}_{i22}(\bar{x}, p_i)$  is invertible [34],  $i = 1, 2$ . Therefore, systems (17) and (18) can be expressed in the following forms:

$$\begin{aligned}
\dot{x}_1 &= (J_{11}(\bar{x}, p_1) - R_{11}(\bar{x}, p_1)) x_1 \\
&\quad + \bar{g}_{11}(\bar{x}) K \bar{g}_{21}^T(\bar{\xi}) \xi_1 + \bar{g}_{11}(\bar{x}) v \\
&\quad + \bar{g}_{11}(\bar{x}) \Phi^T(\theta - \hat{\theta}), \\
0 &= -(\bar{J}_{112}^T(\bar{x}, p_1) + \bar{R}_{112}^T(\bar{x}, p_1)) x_1 \\
&\quad + (\bar{J}_{122}(\bar{x}, p_1) - \bar{R}_{122}(\bar{x}, p_1)) x_2, \\
\dot{\hat{\theta}} &= Q\Phi(\bar{g}_{11}^T(\bar{x}) x_1 + \bar{g}_{21}^T(\bar{\xi}) \xi_1), \\
y &= \bar{g}_{11}^T(\bar{x}) x_1, \\
\dot{\xi}_1 &= (J_{21}(\bar{\xi}, p_2) - R_{21}(\bar{\xi}, p_2)) \xi_1 \\
&\quad - \bar{g}_{21}(\bar{\xi}) K \bar{g}_{11}^T(\bar{x}) x_1 + \bar{g}_{21}(\bar{\xi}) v \\
&\quad + \bar{g}_{21}(\bar{\xi}) \Phi^T(\theta - \hat{\theta}), \\
0 &= -(\bar{J}_{212}^T(\bar{\xi}, p_2) + \bar{R}_{212}^T(\bar{\xi}, p_2)) \xi_1 \\
&\quad + (\bar{J}_{222}(\bar{\xi}, p_2) - \bar{R}_{222}(\bar{\xi}, p_2)) \xi_2, \\
\dot{\hat{\theta}} &= Q\Phi(\bar{g}_{11}^T(\bar{x}) x_1 + \bar{g}_{21}^T(\bar{\xi}) \xi_1), \\
\eta &= \bar{g}_{21}^T(\bar{\xi}) \xi_1,
\end{aligned} \tag{19}$$

where  $J_{i1}(\bar{x}, p_i) - R_{i1}(\bar{x}, p_i) = \bar{J}_{i11}(\bar{x}, p_i) - \bar{R}_{i11}(\bar{x}, p_i) + (\bar{J}_{i12}(\bar{x}, p_i) - \bar{R}_{i12}(\bar{x}, p_i))(\bar{J}_{i22}(\bar{x}, p_i) - \bar{R}_{i22}(\bar{x}, p_i))^{-1} \cdot (\bar{J}_{i12}^T(\bar{x}, p_i) + \bar{R}_{i12}^T(\bar{x}, p_i))$ ,  $i = 1, 2$ .  $J_{i1}(\bar{x}, p_i)$  is skew-symmetric, and  $R_{i1}(\bar{x}, p_i)$  is positive definite, because

$$N \begin{bmatrix} \bar{J}_{i11} - \bar{R}_{i11} & \bar{J}_{i12} - \bar{R}_{i12} \\ -(\bar{J}_{i12}^T + \bar{R}_{i12}^T) & \bar{J}_{i22} - \bar{R}_{i22} \end{bmatrix} N^T$$

$$= \begin{bmatrix} J_{i1} - R_{i1} & 0 \\ * & \bar{J}_{i22} - \bar{R}_{i22} \end{bmatrix}, \quad (21)$$

where

$$N = \begin{bmatrix} I & -(\bar{J}_{i12} - \bar{R}_{i12})(\bar{J}_{i22} - \bar{R}_{i22})^{-1} \\ 0 & I \end{bmatrix}. \quad (22)$$

With assumptions (A1) and (A2), we have the following result.

**Theorem 7.** Consider systems (1) and (2) with their equivalent forms (4) and (5). Assume assumptions (A1) and (A2) hold; if there exist symmetric matrices  $K \in \mathbb{R}^{m \times m}$  and  $\Phi \in \mathbb{R}^{l \times m}$  such that (10) and (6) hold, respectively, then the admissible adaptive parallel controller (11) ( $v = 0$ ) can simultaneously stabilize systems (1) and (2).

$$X = \begin{bmatrix} x_1 \\ \xi_1 \\ \hat{\theta} \end{bmatrix},$$

$$p = \begin{bmatrix} p_1 \\ p_2 \end{bmatrix},$$

$$R(X, p) = \begin{bmatrix} R_{11}(x_1, q_1(x_1), p_1) & 0 & 0 \\ 0 & R_{21}(\xi_1, q_2(\xi_1), p_2) & 0 \\ 0 & 0 & 0 \end{bmatrix}, \quad (24)$$

$$J(X, p) = \begin{bmatrix} J_{11}(x_1, q_1(x_1), p_1) & \bar{g}_{11}(x_1, q_1(x_1)) K \bar{g}_{21}^T(\xi_1, q_2(\xi_1)) & -\bar{g}_{11}(x_1, q_1(x_1)) \Phi^T Q \\ -(\bar{g}_{11}(x_1, q_1(x_1)) K \bar{g}_{21}^T(\xi_1, q_2(\xi_1)))^T & J_{21}(\xi_1, q_2(\xi_1), p_2) & -\bar{g}_{21}(\xi_1, q_2(\xi_1)) \Phi^T Q \\ (\bar{g}_{11}(x_1, q_1(x_1)) \Phi^T Q)^T & (\bar{g}_{21}(\xi_1, q_2(\xi_1)) \Phi^T Q)^T & 0 \end{bmatrix},$$

$$H(X) = \frac{1}{2} (x_1^T x_1 + \xi_1^T \xi_1) + \frac{1}{2} (\theta - \hat{\theta})^T Q^{-1} (\theta - \hat{\theta}).$$

Obviously,  $J(X, p) = -J^T(X, p)$ ,  $R(X, p) \geq 0$ ,  $H(X) \geq 0$ . Therefore, system (23) is a dissipative Hamiltonian system. Choosing  $V(X) = H(X)$ , then  $H(X)$  has a local minimum at  $X_0 = (0^T, 0^T, \hat{\theta}_0^T)^T$ . Then, based on system (23) we have

$$\begin{aligned} \dot{V}(X) &= \frac{\partial^T H(X)}{\partial X} \dot{X} \\ &= \frac{\partial^T H(X)}{\partial X} (J(X, p) - R(X, p)) \frac{\partial H(X)}{\partial X} \\ &= -\frac{\partial^T H(X)}{\partial X} R(X, p) \frac{\partial H(X)}{\partial X} \end{aligned}$$

*Proof.* If assumptions (A1) and (A2) hold, then systems (4) and (5) can be transformed into systems (19) and (20) by the adaptive feedback law (11), which are of index one at the equilibrium point 0 (system (12) is said to have index one at the equilibrium point 0 if  $\partial\varphi(x_1, x_2, p_1)/\partial x_2$  in (17) is nonsingular in a neighborhood of 0); i.e., systems (19) and (20) are impulse-free. According to the implicit function theorem, there exist continuous functions  $q_i(\cdot)$  such that  $x_2 = q_1(x_1)$ ,  $\xi_2 = q_2(\xi_1)$ ,  $q_i(0) = 0$ . Thus, systems (19) and (20) can be rewritten as ( $v = 0$ )

$$\begin{aligned} \dot{X} &= (J(X, p) - R(X, p)) \frac{\partial H(X)}{\partial X}, \\ 0 &= -(\bar{J}_{112}^T(\bar{x}, p_1) + \bar{R}_{112}^T(\bar{x}, p_1)) x_1 \\ &\quad + (\bar{J}_{122}(\bar{x}, p_1) - \bar{R}_{122}(\bar{x}, p_1)) x_2, \\ 0 &= -(\bar{J}_{212}^T(\bar{\xi}, p_2) + \bar{R}_{212}^T(\bar{\xi}, p_2)) \xi_1 \\ &\quad + (\bar{J}_{222}(\bar{\xi}, p_2) - \bar{R}_{222}(\bar{\xi}, p_2)) \xi_2, \end{aligned} \quad (23)$$

where

$$\begin{aligned} &= -x_1^T R_{11}(x_1, q_1(x_1), p_1) x_1 \\ &\quad - \xi_1^T R_{21}(\xi_1, q_2(\xi_1), p_2) \xi_1 \leq 0. \end{aligned} \quad (25)$$

Thus, system (23) converges to the largest invariant set contained in

$$\begin{aligned} \{X : \dot{V}(X) = 0\} &\subset \{X : R_{11}^{1/2}(x_1, q_1(x_1), p_1) x_1 \\ &= 0, R_{21}^{1/2}(\xi_1, q_2(\xi_1), p_2) \xi_1 = 0, \forall t \geq 0\} =: S. \end{aligned} \quad (26)$$

From systems (19) and (20), we know that both  $R_{11}^{1/2}(x_1, q_1(x_1), p_1)$  and  $R_{21}^{1/2}(\xi_1, q_2(\xi_1), p_2)$  are nonsingular, which

implies that  $R_{11}^{1/2}(x_1, q_1(x_1), p_1)x_1 = 0 \implies x_1 = 0$  and  $R_{21}^{1/2}(\xi_1, q_2(\xi_1), p_2)\xi_1 = 0 \implies \xi_1 = 0$ . That is, the largest invariant set only contains one point, i.e.,  $S = \{[0^T, 0^T, \bar{\theta}_0^T]^T\}$ , with which it is easy to see that  $x_1 \rightarrow 0$  and  $\xi_1 \rightarrow 0$ , as  $t \rightarrow \infty$ . Moreover, according to systems (19) and (20), it is clear that  $x_2 \rightarrow 0$  and  $\xi_2 \rightarrow 0$ , as  $t \rightarrow \infty$ . Thus,  $x = M_1 \bar{x} \rightarrow 0$ ,  $\xi = M_2 \bar{\xi} \rightarrow 0$ , as  $t \rightarrow \infty$ . Therefore, under the admissible adaptive parallel control law (11), systems (1) and (2) can be simultaneously stabilized.  $\square$

### 3. Robust Adaptive Parallel Simultaneous Stabilization of Two NDSs and More Than Two NDSs

In this section, we investigate the robust adaptive parallel simultaneous stabilization problem of two NDSs with external disturbances and parameters perturbation and discuss the case of more than two NDSs. Firstly, for a given disturbance attenuation level  $\gamma > 0$ , we design an adaptive parallel  $L_2$  disturbance attenuation output feedback law such that under the law the  $L_2$  gain (from  $w$  to  $z$ ) of the closed-loop system is less than  $\gamma$ . Then, we show that the two systems are simultaneously asymptotically stable when  $w = 0$ .

To design the robust adaptive parallel simultaneous stabilization controller, the following lemma is recalled, first.

**Lemma 8** (see [34]). *Consider a dissipative Hamiltonian system as follows:*

$$\begin{aligned} \dot{x} &= [J(x) - R(x)] \nabla H + g_1(x)u + g_2(x)w, \\ z &= h(x)g_1^T(x) \nabla H, \end{aligned} \quad (27)$$

where  $x \in \mathbb{R}^n$  is the state,  $u \in \mathbb{R}^m$  is the control input,  $w \in \mathbb{R}^q$  is the disturbance,  $J(x)$  is skew-symmetric,  $R(x) \geq 0$ ,  $H(x)$  has a strict local minimum at the system's equilibrium,  $z$  is the penalty function, and  $h(x)$  is a weighting matrix. Given a disturbance attenuation level  $\gamma > 0$ , if

$$R(x) + \frac{1}{2\gamma^2} [g_1(x)g_1^T(x) - g_2(x)g_2^T(x)] \geq 0, \quad (28)$$

then an  $L_2$  disturbance attenuation controller of system (27) can be given as

$$u = - \left[ \frac{1}{2} h^T(x) h(x) + \frac{1}{2\gamma^2} I_m \right] g_1^T(x) \nabla H, \quad (29)$$

and the  $\gamma$ -dissipation inequality

$$\begin{aligned} & \dot{H} + \nabla^T H \begin{bmatrix} R(x) \\ + \frac{1}{2\gamma^2} (g_1(x)g_1^T(x) - g_2(x)g_2^T(x)) \end{bmatrix} \nabla H \\ & \leq \frac{1}{2} \{ \gamma^2 \|w\|^2 - \|z\|^2 \} \end{aligned} \quad (30)$$

holds along the trajectories of the closed-loop system consisting of (27) and (29).

Now, we consider the following NDSs (1) and (2) with external disturbances:

$$\begin{aligned} E_1 \dot{x} &= f_1(x, p_1) + g_1(x)u + d_1 w, \\ E_1 x(0) &= E_1 x_0, \\ f_1(0, p_1) &= f_{p_1}(p_1), \\ f_1(0, 0) &= 0, \\ y &= g_1^T(x)x, \\ E_2 \dot{\xi} &= f_2(\xi, p_2) + g_2(\xi)u + d_2 w, \\ E_2 \xi(0) &= E_2 \xi_0, \\ f_2(0, p_2) &= f_{p_2}(p_2), \\ f_2(0, 0) &= 0, \\ \eta &= g_2^T(\xi)\xi, \end{aligned} \quad (31)$$

where  $w \in \mathbb{R}^q$  is the disturbance,  $d_i(x) \in \mathbb{R}^{n \times q}$ ,  $i = 1, 2$ , other variables are the same as those in systems (1) and (2), and

$$M_i^T d_i(x) = \begin{bmatrix} \tilde{d}_{i1}(x) \\ \tilde{d}_{i2}(x) \end{bmatrix} = \begin{bmatrix} \bar{d}_{i1}(\bar{x}) \\ \bar{d}_{i2}(\bar{x}) \end{bmatrix}. \quad (33)$$

Given a disturbance attenuation level  $\gamma > 0$ , choose

$$z = \Lambda(y + \eta) \quad (34)$$

as the penalty function, where  $\Lambda \in \mathbb{R}^{s \times m}$  is a weighting matrix.

To design the adaptive parallel  $L_2$  disturbance attenuation output feedback control law for systems (31) and (32), the following assumption is given:

$$(A3) \text{ rank } [E_i, d_i(x)] = \text{rank}(E_i), \quad \forall x \in \mathbb{R}^n, \quad i = 1, 2.$$

Assumption (A3) implies that fast subsystems of the descriptor systems (31) and (32) have not been disturbed. Similar to (A1), from (A3) we can obtain that  $\tilde{d}_{i2}(x) = \bar{d}_{i2}(\bar{x}) = 0$ .

Based on Section 2, systems (31) and (32) can be transformed into the following forms:

$$E_1 \dot{x} = A_1(x, p_1) \alpha_1(x, p_1) + g_1(x)u + d_1(x)w, \quad (35)$$

$$y = g_1^T(x)x,$$

$$E_2 \dot{\xi} = A_2(\xi, p_2) \alpha_2(\xi, p_2) + g_2(\xi)u + d_2(x)w, \quad (36)$$

$$\eta = g_2^T(\xi)\xi.$$

Next, we design an adaptive parallel  $L_2$  disturbance attenuation controller for systems (31) and (32).

**Theorem 9.** *Consider systems (31) and (32) with their equivalent forms (35) and (36), the penalty function (34), and the disturbance attenuation level  $\gamma > 0$ . Assume that assumptions (A1)~(A3) hold for systems (35) and (36). If*

(1) there exists a symmetric matrix  $K \in \mathbb{R}^{m \times m}$  such that (10) holds,

(2)  $g_i = d_i$ ,  $i = 1, 2$ ,

then, the following admissible adaptive parallel feedback law

$$u = -K(y - \eta) - \left[ \frac{1}{2} \Lambda^T \Lambda + \frac{1}{2\gamma^2} I_m \right] (y + \eta) - \Phi^T \hat{\theta}, \quad (37)$$

$$\dot{\hat{\theta}} = Q\Phi(y + \eta)$$

can simultaneously stabilize systems (31) and (32).

*Proof.* Rewrite (37) as follows

$$\begin{aligned} u &= -K(y - \eta) - \Phi^T \hat{\theta} + v, \\ \dot{\hat{\theta}} &= Q\Phi(y + \eta), \\ v &= - \left[ \frac{1}{2} \Lambda^T \Lambda + \frac{1}{2\gamma^2} I_m \right] (y + \eta). \end{aligned} \quad (38)$$

Substituting the first part of (38) into systems (35) and (36), according to the proof of Theorem 7 and assumption (A2), we know that systems (35) and (36) are impulse controllable and can be expressed as the following dissipative Hamiltonian form:

$$\begin{aligned} \dot{X} &= [J(X, p) - R(X, p)] \frac{\partial H(X)}{\partial X} + G(X) v \\ &\quad + D(X) w, \\ 0 &= - \left( \bar{J}_{112}^T(\bar{x}, p_1) + \bar{R}_{112}^T(\bar{x}, p_1) \right) x_1 \\ &\quad + \left( \bar{J}_{122}(\bar{x}, p_1) - \bar{R}_{122}(\bar{x}, p_1) \right) x_2, \\ 0 &= - \left( \bar{J}_{212}^T(\bar{\xi}, p_2) + \bar{R}_{212}^T(\bar{\xi}, p_2) \right) \xi_1 \\ &\quad + \left( \bar{J}_{222}(\bar{\xi}, p_2) - \bar{R}_{222}(\bar{\xi}, p_2) \right) \xi_2, \end{aligned} \quad (39)$$

and

$$z = \Lambda G^T(X) \frac{\partial H(X)}{\partial X}, \quad (40)$$

where  $X$ ,  $J(X, p)$ ,  $R(X, p)$ , and  $H(X)$  are given in (23),  $G(X) = [\bar{g}_{11}^T(x_1, q_1(x_1)) \quad \bar{g}_{21}^T(\xi_1, q_2(\xi_1)) \quad 0]^T$  and  $D(X) = [\bar{d}_{11}^T(x_1, q_1(x_1)) \quad \bar{d}_{21}^T(\xi_1, q_2(\xi_1)) \quad 0]^T$ .

Because  $g_i = d_i$ ,  $i = 1, 2$ , it is easy to show

$$\begin{aligned} R(X, p) + \frac{1}{2\gamma^2} [G(X) G^T(X) - D(X) D^T(X)] \\ = R(X, p) \geq 0. \end{aligned} \quad (41)$$

Thus, system (39) with the penalty function (40) satisfies all the conditions of Lemma 8. From Lemma 8, an  $L_2$

disturbance attenuation controller of system (39) can be designed as

$$v = - \left[ \frac{1}{2} \Lambda^T \Lambda + \frac{1}{2\gamma^2} I_m \right] (y + \eta), \quad (42)$$

which is the second part of (38), and, furthermore, the  $\gamma$ -dissipation inequality

$$\dot{H} + \frac{\partial^T H}{\partial X} R(X, p) \frac{\partial H}{\partial X} \leq \frac{1}{2} \{ \gamma^2 \|w\|^2 - \|z\|^2 \} \quad (43)$$

holds along the trajectories of the closed-loop system consisting of (39) and (42).

Therefore, the feedback law (37) is an  $L_2$  disturbance attenuation controller of systems (31) and (32). According to [34], the  $L_2$  gain from  $w$  to  $z$  is less than  $\gamma$ . On the other hand, because  $(\partial^T H / \partial X) R(X, p) (\partial H / \partial X) = x_1^T R_{11}(x_1, q_1(x_1), p_1) x_1 + \xi_1^T R_{21}(\xi_1, q_2(\xi_1), p_2) \xi_1 > 0$ , from (43), we know that system (39) is asymptotically stable when  $w = 0$ ; that is,  $x_1 \rightarrow 0$  and  $\xi_1 \rightarrow 0$  (as  $t \rightarrow \infty$ ). Moreover, it is clear that  $x_2 = q_1(x_1) \rightarrow 0$ ,  $\xi_2 = q_2(\xi_1) \rightarrow 0$  (as  $t \rightarrow \infty$ ). Therefore,  $x = M_1 \bar{x} \rightarrow 0$  and  $\xi = M_2 \bar{\xi} \rightarrow 0$  (as  $t \rightarrow \infty$ ). Thus, the admissible adaptive parallel control law (37) can simultaneously stabilize systems (31) and (32).  $\square$

**Theorem 10.** Consider systems (31) and (32) with their equivalent forms (35) and (36), the penalty function (34), and the disturbance attenuation level  $\gamma > 0$ . Assume that assumptions (A1) ~ (A3) hold for systems (35) and (36). If

(1) there exists a symmetric matrix  $K \in \mathbb{R}^{m \times m}$  such that (10) holds, and

$$\begin{aligned} & - \frac{1}{2} \left( A_1(x, p_1) + A_1(x, p_1)^T \right) + K_{11}(x, x) \\ & + \frac{1}{2\gamma^2} \left[ g_1(x) g_1^T(x) - d_1(x) d_1^T(x) \right] > 0, \\ & - \frac{1}{2} \left( A_2(\xi, p_2) + A_2(\xi, p_2)^T \right) - K_{22}(\xi, \xi) \\ & + \frac{1}{2\gamma^2} \left[ g_2(\xi) g_2^T(\xi) - d_2(\xi) d_2^T(\xi) \right] > 0, \end{aligned} \quad (44)$$

where  $K_{ij}(x, \xi) = g_i(x) K g_j^T(\xi)$ ,  $i, j = 1, 2$ ;

(2)  $g_1 g_2^T = 0$  and  $d_1 d_2^T = 0$ ,

then, the admissible adaptive parallel  $L_2$  disturbance attenuation controller (37) can simultaneously stabilize systems (31) and (32).

*Proof.* From the proof of Theorem 9, we know that under the controller (37), systems (35) and (36) are impulse controllable and can be expressed as (39). From condition (2), it can be seen that

$$\begin{aligned} M_1^T g_1 g_2^T M_2 &= \begin{bmatrix} \bar{g}_{11}(\bar{x}) \\ 0 \end{bmatrix} \begin{bmatrix} \bar{g}_{21}^T(\bar{x}) & 0 \end{bmatrix} \\ &= \begin{bmatrix} \bar{g}_{11}(\bar{x}) \bar{g}_{21}^T(\bar{x}) & 0 \\ 0 & 0 \end{bmatrix} = 0, \end{aligned} \quad (45)$$

that is,  $\bar{g}_{11}(\bar{x})\bar{g}_{21}^T(\bar{x}) = 0$ , and in a similar way, we can obtain  $\bar{d}_{11}(\bar{x})\bar{d}_{21}^T(\bar{x}) = 0$ . Moreover, according to condition (1), we have

$$\begin{aligned} & M_1^T \left( -\frac{1}{2} (A_1(x, p_1) + A_1^T(x, p_1)) \right. \\ & \quad \left. + g_1(x) K g_1^T(x) \right) M_1 + \frac{1}{2\gamma^2} M_1^T [g_1(x) g_1^T(x) \\ & \quad - d_1(x) d_1^T(x)] M_1 \\ & = \begin{bmatrix} \bar{R}_{111}(\bar{x}, p_1) & \bar{R}_{112}(\bar{x}, p_1) \\ \bar{R}_{112}^T(\bar{x}, p_1) & \bar{R}_{122}(\bar{x}, p_1) \end{bmatrix} + \frac{1}{2\gamma^2} \\ & \quad \cdot \begin{bmatrix} \bar{g}_{11}(\bar{x})\bar{g}_{11}^T(\bar{x}) - \bar{d}_{11}(\bar{x})\bar{d}_{11}^T(\bar{x}) & 0 \\ 0 & 0 \end{bmatrix} > 0. \end{aligned} \quad (46)$$

Thus,

$$\begin{aligned} & \bar{R}_{111}(\bar{x}, p_1) + \frac{1}{2\gamma^2} [\bar{g}_{11}(\bar{x})\bar{g}_{11}^T(\bar{x}) - \bar{d}_{11}(\bar{x})\bar{d}_{11}^T(\bar{x})] \\ & := \bar{R}_{111}(\bar{x}, p_1) + C(\bar{x}) > 0. \end{aligned} \quad (47)$$

Since

$$\begin{aligned} & N \begin{bmatrix} \bar{J}_{111} - \bar{R}_{111} - C & \bar{J}_{112} - \bar{R}_{112} \\ -(\bar{J}_{112}^T + \bar{R}_{112}^T) & \bar{J}_{122} - \bar{R}_{122} \end{bmatrix} N^T \\ & = \begin{bmatrix} J_{11} - R_{11} - C & 0 \\ * & \bar{J}_{22} - \bar{R}_{22} \end{bmatrix}, \end{aligned} \quad (48)$$

where  $\bar{J}_{111}$  is skew-symmetric and  $N$  is the same as that in (22), we have

$$\begin{aligned} & \hat{R}_1(\bar{x}, p_1) \\ & := R_{11}(\bar{x}, p_1) \\ & \quad + \frac{1}{2\gamma^2} [\bar{g}_{11}(\bar{x})\bar{g}_{11}^T(\bar{x}) - \bar{d}_{11}(\bar{x})\bar{d}_{11}^T(\bar{x})] > 0. \end{aligned} \quad (49)$$

In a similar way,

$$\begin{aligned} & \hat{R}_2(\bar{\xi}, p_2) \\ & := R_{21}(\bar{\xi}, p_2) \\ & \quad + \frac{1}{2\gamma^2} [\bar{g}_{21}(\bar{\xi})\bar{g}_{21}^T(\bar{\xi}) - \bar{d}_{21}(\bar{\xi})\bar{d}_{21}^T(\bar{\xi})] > 0. \end{aligned} \quad (50)$$

Therefore,

$$\begin{aligned} & R(X, p) + \frac{1}{2\gamma^2} [G(X)G^T(X) - D(X)D^T(X)] \\ & = \begin{bmatrix} \hat{R}_1(x_1, q_1(x_1), p_1) & 0 & 0 \\ 0 & \hat{R}_2(\xi_1, q_2(\xi_1), p_2) & 0 \\ 0 & 0 & 0 \end{bmatrix} \\ & \geq 0. \end{aligned} \quad (51)$$

Thus, system (39) with the penalty function (40) satisfies all the conditions of Lemma 8. From Lemma 8, an adaptive parallel  $L_2$  disturbance attenuation controller of system (39) can be designed as (42), and, furthermore, the  $\gamma$ -dissipation inequality

$$\begin{aligned} & \dot{H} + \frac{\partial^T H}{\partial X} \left\{ R(X, p) \right. \\ & \quad \left. + \frac{1}{2\gamma^2} [G(X)G^T(X) - D(X)D^T(X)] \right\} \frac{\partial H}{\partial X} \\ & \leq \frac{1}{2} \{ \gamma^2 \|w\|^2 - \|z\|^2 \} \end{aligned} \quad (52)$$

holds along the trajectories of the closed-loop system consisting of (39) and (42). Therefore, according to the proof of Theorem 9, the admissible controller (37) can simultaneously stabilize systems (31) and (32).  $\square$

*Remark 11.* We can utilize the results obtained on adaptive parallel simultaneous stabilization and robust adaptive parallel simultaneous stabilization problems for two NDSs to investigate the same problems of more than two NDSs.

Consider the following  $N$  NDSs:

$$\begin{aligned} & E_i \dot{x}^i = f_i(x^i, p_i) + g_i(x^i)u + d_i(x^i)w, \\ & E_i x^i(0) = E_i x_0^i, \\ & f_i(0, p_i) = f_{p_i}(p_i), \\ & f_i(0, 0) = 0, \\ & y_i = g_i^T(x^i)x^i, \end{aligned} \quad (53)$$

$$i = 1, 2, \dots, N,$$

where  $x^i \in \mathbb{R}^{n_i}$ ,  $u \in \mathbb{R}^m$ ,  $w \in \mathbb{R}^q$ , and  $y_i \in \mathbb{R}^m$  are the states, control input, external disturbances, and outputs of the  $N$  systems, respectively;  $p_i$  is an unknown parameter perturbation vector and is assumed to be small enough to keep the dissipative structure unchanged;  $g_i(x^i) \in \mathbb{R}^{n_i \times m}$ ,  $0 \leq E_i \in \mathbb{R}^{n_i \times n_i}$ , and  $0 < \text{rank}(E_i) = r_i < n_i$ ,  $i = 1, 2, \dots, N$ .

Given a disturbance attenuation level  $\gamma > 0$ , choose

$$z = \Lambda \sum_{i=1}^N y_i, \quad i = 1, 2, \dots, N \quad (54)$$

as the penalty function, where  $\Lambda \in \mathbb{R}^{s \times m}$  is a weighting matrix.

Similar to Section 2, we obtain the following forms:

$$\begin{aligned} & E_i \dot{x}^i = A_i(x^i, p_i)\alpha_i(x^i, p_i) + g_i(x^i)u + d_i(x^i)w, \\ & y_i = g_i^T(x^i)x^i, \end{aligned} \quad (55)$$

where  $\alpha_i(x^i, p_i) \in \mathbb{R}^{n_i}$  is some vector of  $x^i$  and  $p_i$  satisfying  $\alpha_i(x^i, 0) = x^i$ ,  $i = 1, 2, \dots, N$ .

Assume that  $(i_1, i_2, \dots, i_N)$  is an arbitrary permutation of  $\{1, 2, \dots, N\}$  and that  $L$  is a positive integer satisfying  $1 \leq L \leq N - 1$ . Let  $T_1 = n_{i_1} + \dots + n_{i_L}$  and  $T_2 = n_{i_{L+1}} + \dots + n_{i_N}$ .

Now, we divide the  $N$  systems into two sets as follows:

$$E_a \dot{X}^a = A_a(X^a, p_a) \Gamma_a(X^a, p_a) + G_a(X^a) u + D_a(X^a) w, \quad (56)$$

$$Y_a = G_a^T(X^a) X^a,$$

$$E_b \dot{X}^b = A_b(X^b, p_b) \Gamma_b(X^b, p_b) + G_b(X^b) u + D_b(X^b) w, \quad (57)$$

$$Y_b = G_b^T(X^b) X^b,$$

where  $X^a = [(x^{i_1})^T, \dots, (x^{i_L})^T]^T \in \mathbb{R}^{T_1}$ ,  $X^b = [(x^{i_{L+1}})^T, \dots, (x^{i_N})^T]^T \in \mathbb{R}^{T_2}$ ,  $p_a = [p_{i_1}^T, \dots, p_{i_L}^T]^T$ ,  $p_b = [p_{i_{L+1}}^T, \dots, p_{i_N}^T]^T$ ,

$$E_a = \text{diag}\{E_{i_1}, \dots, E_{i_L}\},$$

$$E_b = \text{diag}\{E_{i_{L+1}}, \dots, E_{i_N}\},$$

$$A_a(X^a, p_a)$$

$$= \text{diag}\{A_{i_1}(x^{i_1}, p_{i_1}), \dots, A_{i_L}(x^{i_L}, p_{i_L})\},$$

$$A_b(X^b, p_b)$$

$$= \text{diag}\{A_{i_{L+1}}(x^{i_{L+1}}, p_{i_{L+1}}), \dots, A_{i_N}(x^{i_N}, p_{i_N})\},$$

$$\Gamma_a(X^a, p_a) = \text{diag}\{\alpha_{i_1}(x^{i_1}, p_{i_1}), \dots, \alpha_{i_L}(x^{i_L}, p_{i_L})\},$$

$$\Gamma_b(X^b, p_b) \quad (58)$$

$$= \text{diag}\{\alpha_{i_{L+1}}(x^{i_{L+1}}, p_{i_{L+1}}), \dots, \alpha_{i_N}(x^{i_N}, p_{i_N})\},$$

$$Y_a = y_{i_1} + \dots + y_{i_L},$$

$$Y_b = y_{i_{L+1}} + \dots + y_{i_N},$$

$$G_a(X^a) = [g_{i_1}^T(x^{i_1}), \dots, g_{i_L}^T(x^{i_L})]^T,$$

$$G_b(X^b) = [g_{i_{L+1}}^T(x^{i_{L+1}}), \dots, g_{i_N}^T(x^{i_N})]^T,$$

$$D_a(X^a) = [d_{i_1}^T(x^{i_1}), \dots, d_{i_L}^T(x^{i_L})]^T,$$

$$D_b(X^b) = [d_{i_{L+1}}^T(x^{i_{L+1}}), \dots, d_{i_N}^T(x^{i_N})]^T.$$

According to Section 2, (56), (57), and Theorems 9 and 10, we can easily obtain an adaptive parallel simultaneous stabilization controller ( $w=0$ ) and a robust adaptive parallel simultaneous stabilization controller of systems (53).

**Theorem 12.** Consider systems (53) ( $w=0$ ) with their equivalent forms (55) ( $w=0$ ), and assume that assumptions (A1) and (A2) hold ( $i = 1, 2, \dots, N$ ). If there exist a symmetric matrix

$K \in \mathbb{R}^{m \times m}$ , a permutation  $(i_1, i_2, \dots, i_N)$  of  $\{1, 2, \dots, N\}$ , and a positive integer  $L$  ( $1 \leq L \leq N - 1$ ) such that

$$\begin{aligned} R_a(X^a, p_a) &:= -\frac{1}{2} (A_a(X^a, p_a) + A_a(X^a, p_a)^T) \\ &\quad + K_{aa}(X^a, X^a) > 0, \\ R_b(X^b, p_b) &:= -\frac{1}{2} (A_b(X^b, p_b) + A_b(X^b, p_b)^T) \\ &\quad - K_{bb}(X^b, X^b) > 0, \end{aligned} \quad (59)$$

where

$$K_{ij}(X^i, X^j) = G_i(X^i) K G_j^T(X^j), \quad i, j = a, b, \quad (60)$$

then, the adaptive control law

$$\begin{aligned} u &= -K(y_{i_1} + \dots + y_{i_L} - y_{i_{L+1}} - \dots - y_{i_N}) - \Phi^T \hat{\theta} + v, \\ \dot{\hat{\theta}} &= Q \Phi \sum_{i=1}^N y_i \end{aligned} \quad (61)$$

can simultaneously stabilize the  $N$  systems given by (53) ( $w=0$ ), where  $v$  is a new reference input and  $\hat{\theta}$  and  $Q$  are the same as those in (11).

**Theorem 13.** Consider systems (53), the penalty function (54), and the disturbance attenuation level  $\gamma > 0$ . Assume that assumptions (A1) ~ (A3) ( $i = 1, 2, \dots, N$ ) hold. If

- (1) there exist a symmetric matrix  $K \in \mathbb{R}^{m \times m}$ , a permutation  $(i_1, i_2, \dots, i_N)$  of  $\{1, 2, \dots, N\}$ , and a positive integer  $L$  ( $1 \leq L \leq N - 1$ ) such that (59) holds,
- (2)  $g_i = d_i, i = 1, 2, \dots, N$ ,

then, the following robust adaptive parallel controller

$$\begin{aligned} u &= -K(y_{i_1} + \dots + y_{i_L} - y_{i_{L+1}} - \dots - y_{i_N}) \\ &\quad - \left[ \frac{1}{2} \Lambda^T \Lambda + \frac{1}{2\gamma^2} I_m \right] \sum_{i=1}^N y_i - \Phi^T \hat{\theta}, \\ \dot{\hat{\theta}} &= Q \Phi \sum_{i=1}^N y_i \end{aligned} \quad (62)$$

can simultaneously stabilize the  $N$  systems given by (53).

#### 4. An Illustrative Example

In the following, we give an illustrative example to show how to apply Theorem 9 to investigate robust adaptive parallel simultaneous stabilization for two NDSs.

*Example 14.* Consider the following two NDSs:

$$\begin{aligned} E_1 \dot{x} &= f_1(x, p) + g_1(x)u + d_1 w, \\ E_1 x(0) &= E_1 x_0, \\ f_1(0, p) &= f_{1,p}(p), \\ f_1(0, 0) &= 0, \\ y &= g_1^T(x)x, \end{aligned} \quad (63)$$

$$\begin{aligned} E_2 \dot{\xi} &= f_2(\xi, p) + g_2(\xi)u + d_2 w, \\ E_2 \xi(0) &= E_2 \xi_0, \\ f_2(0, p) &= f_{2,p}(p), \\ f_2(0, 0) &= 0, \\ \eta &= g_2^T(\xi)\xi, \end{aligned} \quad (64)$$

where  $x = [\tilde{x}_1, \tilde{x}_2, \tilde{x}_3]^T \in \mathbb{R}^3$ ,  $\xi = [\tilde{\xi}_1, \tilde{\xi}_2, \tilde{\xi}_3]^T \in \mathbb{R}^3$ ,  $u \in \mathbb{R}^2$ ,  $w \in \mathbb{R}^2$ ,

$$\begin{aligned} E_1 &= \begin{bmatrix} 0 & 0 & 0 \\ 0 & 5 & 0 \\ 0 & 0 & 1 \end{bmatrix}, \\ E_2 &= \begin{bmatrix} 2 & 0 & 0 \\ 0 & 2 & 0 \\ 0 & 0 & 0 \end{bmatrix}, \\ f_1(x, p) &= \begin{bmatrix} -\tilde{x}_1 + 2\tilde{x}_2 \\ -2\tilde{x}_1 - \tilde{x}_2^3 - \tilde{x}_2 - 2\tilde{x}_3 - 2p \\ 2\tilde{x}_3 + 2p \end{bmatrix}, \\ f_2(\xi, p) &= \begin{bmatrix} \tilde{\xi}_1^3 - 2\tilde{\xi}_1 - \tilde{\xi}_2 - p - 2\tilde{\xi}_3 \\ -\tilde{\xi}_1 - \tilde{\xi}_2 - p \\ 2\tilde{\xi}_1 - 2\tilde{\xi}_3 \end{bmatrix}, \\ g_1(x) = d_1(x) &= \begin{bmatrix} 0 & 0 \\ 2 & \tilde{x}_2 \\ -2 & 0 \end{bmatrix}, \\ g_2(\xi) = d_2(\xi) &= \begin{bmatrix} 1 & \tilde{\xi}_1 \\ 1 & 0 \\ 0 & 0 \end{bmatrix}. \end{aligned} \quad (65)$$

Choose the penalty function  $z = \Lambda(y + \eta)$ , where  $\Lambda$  is a weighting matrix.

Noticing that  $f_1(0, 0) = f_2(0, 0) = 0$ , we obtain  $\alpha_1(x, p) = (\tilde{x}_1, \tilde{x}_2, \tilde{x}_3 + p)^T$ ,  $\alpha_2(\xi, p) = (\tilde{\xi}_1, \tilde{\xi}_2 + p, \tilde{\xi}_3)^T$ , and

$$\begin{aligned} A_1(x, p) &= \begin{bmatrix} -1 & 2 & 0 \\ -2 & -1 - \tilde{x}_2^2 & -2 \\ 0 & 0 & 2 \end{bmatrix}, \\ A_2(\xi, p) &= \begin{bmatrix} \tilde{\xi}_1^2 - 2 & -1 & -2 \\ -1 & -1 & 0 \\ 2 & 0 & -2 \end{bmatrix}. \end{aligned} \quad (66)$$

It is easy to check that assumption (A2) is satisfied, where  $\Phi = [-1, 0]$  and  $\theta = p$ . According to Theorem 9, we obtain the following forms of systems (63) and (64) by the output feedback  $u = -K(y - \eta) + v$ :

$$\begin{aligned} E_1 \dot{x} &= (J_1(x, p) - R_1(x, p))x + g_1(x)Kg_2^T(\xi)\xi \\ &\quad + g_1(x)v + d_1(x)w + g_1(x)\Phi^T(\theta - \hat{\theta}), \end{aligned} \quad (67)$$

$$y = g_1^T(x)x,$$

$$\begin{aligned} E_2 \dot{\xi} &= (J_2(\xi, p) - R_2(\xi, p))\xi - g_2(\xi)Kg_1^T(x)x \\ &\quad + g_2(\xi)v + d_2(\xi)w + g_2(\xi)\Phi^T(\theta - \hat{\theta}), \end{aligned} \quad (68)$$

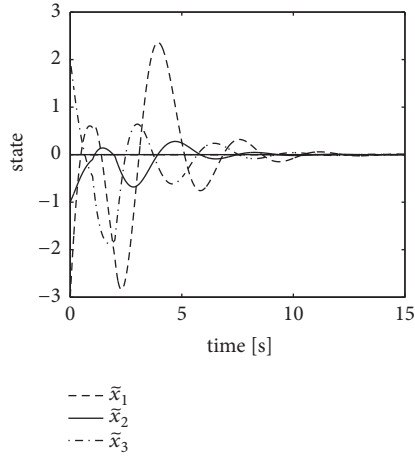
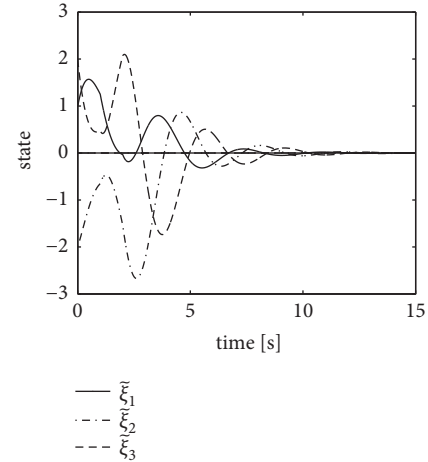
$$\eta = g_2^T(\xi)\xi,$$

where

$$\begin{aligned} K &= \begin{bmatrix} 0.8 & 0 \\ 0 & -1 \end{bmatrix}, \\ J_1(x, p) &= \begin{bmatrix} 0 & 2 & 0 \\ -2 & 0 & -1 \\ 0 & 1 & 0 \end{bmatrix}, \\ R_1(x, p) &= \begin{bmatrix} 1 & 0 & 0 \\ 0 & 4.2 & -2.2 \\ 0 & -2.2 & 1.2 \end{bmatrix}, \\ J_2(\xi, p) &= \begin{bmatrix} 0 & 0 & -2 \\ 0 & 0 & 0 \\ 2 & 0 & 0 \end{bmatrix}, \\ R_2(\xi, p) &= \begin{bmatrix} 1.2 & 0.2 & 0 \\ 0.2 & 0.2 & 0 \\ 0 & 0 & 2 \end{bmatrix}. \end{aligned} \quad (69)$$

Since  $E_1 \geq 0$  and  $E_2 \geq 0$ , we can give nonsingular matrices

$$M_1 = \begin{bmatrix} 0 & 0 & 1 \\ 0 & \frac{\sqrt{5}}{5} & 0 \\ 1 & 0 & 0 \end{bmatrix},$$


 FIGURE 1: Response of the state  $x$ .

 FIGURE 2: Response of the state  $\xi$ .

$$M_2 = \begin{bmatrix} \frac{\sqrt{2}}{2} & 0 & 0 \\ 0 & \frac{\sqrt{2}}{2} & 0 \\ 0 & 0 & 1 \end{bmatrix}. \quad (70)$$

Moreover, it is clear that (A1) and (A3) are also satisfied. Thus, all the conditions of Theorem 9 hold. Therefore, an admissible adaptive parallel simultaneous stabilization controller of systems (63) and (64) can be designed as

$$u = -K(y - \eta) - \left[ \frac{1}{2} \Lambda^T \Lambda + \frac{1}{2\gamma^2} I_m \right] (y + \eta) - \Phi^T \hat{\theta}, \quad (71)$$

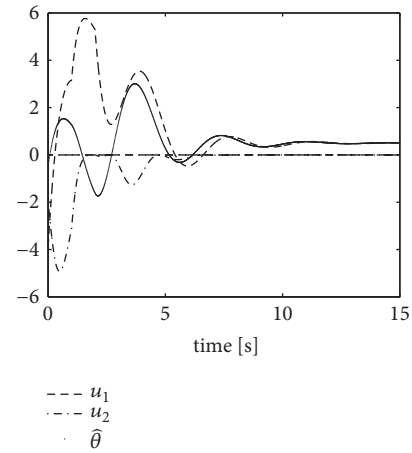
$$\dot{\hat{\theta}} = Q\Phi(y + \eta).$$

In order to test the effectiveness of the controller (71), we carry out some numerical simulations with the following choices: initial condition:  $E_1 x(0) = [0, -5, 2]^T$ ,  $E_2 \xi(0) = [2, -4, 0]^T$ ,  $\hat{\theta}^0 = -0.5$ ; parameter:  $\gamma = 1$ ,  $p = 0.5$ ,  $Q = 1$ , and weighting matrix  $\Lambda = I_2$ . To test the robustness of the controller with respect to external disturbances, we add a square-wave disturbance of amplitude  $[2, -4]^T$  to the systems in the time duration  $[1s \sim 2s]$ . The responses of the states, control signal, and  $\hat{\theta}$  are shown in Figures 1–3, respectively.

It can be observed from Figures 1–3 that the states quickly converge to the origin after the disturbance is removed. The simulation results show that the controller (71) is very effective in simultaneously stabilizing the two systems and has strong robustness against external disturbances and parameters perturbation.

## 5. Conclusion

This paper has investigated the (robust) adaptive parallel simultaneous stabilization problems of a class of nonlinear descriptor systems via dissipative matrix method. Firstly, under a suitable output feedback law, two nonlinear descriptor systems have been changed as two equivalent nonlinear


 FIGURE 3: The control  $u$  and estimate  $\hat{\theta}$ .

differential-algebraic systems by nonsingular transforms, and a sufficient condition of impulse-free has been given for two closed-loop systems. Then, the two systems are combined to generate an augmented dissipative Hamiltonian differential-algebraic system, with which an adaptive parallel simultaneous stabilization controller has been designed for the two systems via the Hamiltonian function method. When there are external disturbances in the two systems, a robust adaptive parallel simultaneous stabilization controller has been presented. Finally, the case of more than two nonlinear descriptor systems has also been investigated in this paper.

## Data Availability

The data used to support the findings of this study are available from the corresponding author upon request.

## Conflicts of Interest

The authors declare that they have no conflicts of interest.

## Acknowledgments

This work is supported by the National Nature Science Foundation of China [61877028, 61374002, 61773015, 61703180] and Shandong Province Key Research and development Project [2018GGX105003].

## References

- [1] L. Sun and Y. Wang, "Simultaneous stabilization of a class of nonlinear descriptor systems via Hamiltonian function method," *Science China Information Sciences*, vol. 52, no. 11, pp. 2140–2152, 2009.
- [2] Y. Wang, G. Feng, and D. Cheng, "Simultaneous stabilization of a set of nonlinear port-controlled Hamiltonian systems," *Automatica*, vol. 43, no. 3, pp. 403–415, 2007.
- [3] W. E. Schmitendorf and C. V. Hollot, "Simultaneous stabilization via linear state feedback control," *Institute of Electrical and Electronics Engineers Transactions on Automatic Control*, vol. 34, no. 9, pp. 1001–1005, 1989.
- [4] M. Vidyasagar, "A state-space interpretation of simultaneous stabilization," *Institute of Electrical and Electronics Engineers Transactions on Automatic Control*, vol. 33, no. 5, pp. 506–511, 1988.
- [5] B. Ho-Mock-Qai and W. P. Dayawansa, "Simultaneous stabilization of linear and nonlinear systems by means of nonlinear state feedback," *SIAM Journal on Control and Optimization*, vol. 37, no. 6, pp. 1701–1725, 1999.
- [6] P. T. Kabamba and C. Yang, "Simultaneous controller design for linear time-invariant systems," *IEEE Transactions on Automatic Control*, vol. 36, no. 1, pp. 106–111, 1991.
- [7] D. E. Miller and T. Chen, "Simultaneous stabilization with near-optimal  $H_{\infty}$  performance," *Institute of Electrical and Electronics Engineers Transactions on Automatic Control*, vol. 47, no. 12, pp. 1986–1998, 2002.
- [8] J.-L. Wu, "Simultaneous  $H_{\infty}$  control for nonlinear systems," *Institute of Electrical and Electronics Engineers Transactions on Automatic Control*, vol. 54, no. 3, pp. 606–610, 2009.
- [9] L. Dai, *Singular Control Systems*, Springer, Berlin, Germany, 1989.
- [10] G. Liu, S. Xu, Y. Wei, Z. Qi, and Z. Zhang, "New insight into reachable set estimation for uncertain singular time-delay systems," *Applied Mathematics and Computation*, vol. 320, pp. 769–780, 2018.
- [11] X. Liu and D. W. Ho, "Stabilization of non-linear differential-algebraic equation systems," *International Journal of Control*, vol. 77, no. 7, pp. 671–684, 2004.
- [12] Y. Liu, C. Li, and R. Wu, "Stabilization and robust stabilization of nonlinear differential-algebraic systems: a Hamiltonian function method," in *Proceedings of the 2006 American Control Conference*, p. 5 pp., Minneapolis, MN, USA, June 2006.
- [13] S. Ma, C. Zhang, and Z. Wu, "Delay-dependent stability and  $H_{\infty}$  control for uncertain discrete switched singular systems with time-delay," *Applied Mathematics and Computation*, vol. 206, no. 1, pp. 413–424, 2008.
- [14] J. Ren and Q. Zhang, "Non-fragile PD state  $H_{\infty}$  control for a class of uncertain descriptor systems," *Applied Mathematics and Computation*, vol. 218, no. 17, pp. 8806–8815, 2012.
- [15] H.-S. Wang, C.-F. Yung, and F.-R. Chang, " $H_{\infty}$  control for nonlinear descriptor systems," *Institute of Electrical and Electronics Engineers Transactions on Automatic Control*, vol. 47, no. 11, pp. 1919–1925, 2002.
- [16] C. Yang, Q. Zhang, and L. Zhou, "Generalised absolute stability analysis and synthesis for Lur'e-type descriptor systems," *IET Control Theory & Applications*, vol. 1, no. 3, pp. 617–623, 2007.
- [17] J.-X. Xu, Q.-W. Jia, and T.-H. Lee, "Adaptive robust control schemes for a class of nonlinear uncertain descriptor systems," *IEEE Transactions on Circuits and Systems I: Fundamental Theory and Applications*, vol. 47, no. 6, pp. 957–962, 2000.
- [18] L. Sun, "Robust adaptive parallel simultaneous stabilization of two nonlinear descriptor systems with disturbance," in *Proceedings of the 33rd Chinese Control Conference, CCC 2014*, pp. 4371–4376, China, July 2014.
- [19] S.-J. Lee, K.-K. Oh, and H.-S. Ahn, "Passivity-based output synchronisation of port-controlled Hamiltonian and general linear interconnected systems," *IET Control Theory & Applications*, vol. 7, no. 2, pp. 234–245, 2013.
- [20] R. Ortega, M. Galaz, A. Astolfi, Y. Sun, and T. Shen, "Transient stabilization of multimachine power systems with nontrivial transfer conductances," *Institute of Electrical and Electronics Engineers Transactions on Automatic Control*, vol. 50, no. 1, pp. 60–75, 2005.
- [21] S. Satoh and K. Fujimoto, "Passivity based control of stochastic port-Hamiltonian systems," *IEEE Transactions on Automatic Control*, vol. 58, no. 5, pp. 1139–1153, 2013.
- [22] T. Shen, R. Ortega, Q. Lu, S. Mei, and K. Tamura, "Adaptive  $L_2$  disturbance attenuation of Hamiltonian systems with parametric perturbation and application to power systems," in *Proceedings of the 39th IEEE Conference on Decision and Control*, pp. 4939–4944, Australia, December 2000.
- [23] W. W. Sun, "Stabilization analysis of time-delay Hamiltonian systems in the presence of saturation," *Applied Mathematics and Computation*, vol. 217, no. 23, pp. 9625–9634, 2011.
- [24] W. Sun and L. Peng, "Observer-based robust adaptive control for uncertain stochastic Hamiltonian systems with state and input delays," *Lithuanian Association of Nonlinear Analysts. Nonlinear Analysis: Modelling and Control*, vol. 19, no. 4, pp. 626–645, 2014.
- [25] W. Sun, Y. Wang, and R. Yang, " $L_2$  disturbance attenuation for a class of time delay Hamiltonian systems," *Journal of Systems Science & Complexity*, vol. 24, no. 4, pp. 672–682, 2011.
- [26] W. Sun and B. Fu, "Adaptive control of time-varying uncertain non-linear systems with input delay: a Hamiltonian approach," *IET Control Theory & Applications*, vol. 10, no. 15, pp. 1844–1858, 2016.
- [27] W. Sun and L. Peng, "Robust adaptive control of uncertain stochastic Hamiltonian systems with time varying delay," *Asian Journal of Control*, vol. 18, no. 2, pp. 642–651, 2016.
- [28] B. Wang, H. Yang, and F. Meng, "Sixth-order symplectic and symmetric explicit ERKN schemes for solving multi-frequency oscillatory nonlinear Hamiltonian equations," *Calcolo. A Quarterly on Numerical Analysis and Theory of Computation*, vol. 54, no. 1, pp. 117–140, 2017.
- [29] Z. Zheng and Q. Kong, "Friedrichs extensions for singular Hamiltonian operators with intermediate deficiency indices," *Journal of Mathematical Analysis and Applications*, vol. 461, no. 2, pp. 1672–1685, 2018.
- [30] S. Li, X. Liu, and X. Dong, "Non-certainty equivalent practically adaptive control for high-order lower triangular systems," *IMA Journal of Mathematical Control and Information*, vol. 32, no. 4, pp. 809–822, 2015.
- [31] X. Yan and X. Song, "Global Practical Tracking by Output Feedback for Nonlinear Systems with Unknown Growth Rate

- and Time Delay," *The Scientific World Journal*, vol. 2014, Article ID 713081, 7 pages, 2014.
- [32] H. Xu and K. Mizukami, "Hamilton-Jacobi equation for descriptor systems," *Systems & Control Letters*, vol. 21, no. 4, pp. 321–327, 1993.
- [33] W. Langson and A. Alleyne, "Infinite horizon optimal control of a class of nonlinear systems," in *Proceedings of the 1997 American Control Conference*, vol. 5, no. 1, pp. 3017–3022, Albuquerque, NM, USA, June 1997.
- [34] Y. Wang, *Generalized Hamiltonian Control Systems Theory Realization, Control and Applications*, Science Press, Beijing, China, 2007.

## Research Article

# Outer Synchronization of a Modified Quorum-Sensing Network via Adaptive Control

Jianbao Zhang <sup>1,2,3</sup>, Wenyin Zhang<sup>1,2</sup>, Denghua Zhang<sup>4</sup>,  
Chengdong Yang <sup>1,2,3</sup>, Kongwei Zhu<sup>1,2</sup> and Jianlong Qiu<sup>2,5</sup>

<sup>1</sup>School of Information Science and Engineering, Linyi University, Linyi 276005, China

<sup>2</sup>Key Laboratory of Complex Systems and Intelligent Computing in Universities of Shandong (Linyi University), Linyi 276005, China

<sup>3</sup>Department of Mathematics, Southeast University, Nanjing 210096, China

<sup>4</sup>College of Science and Technology, North China Electric Power University, Baoding 071000, China

<sup>5</sup>Department of Electrical and Computer Engineering, Faculty of Engineering, King Abdulaziz University, Jeddah 21589, Saudi Arabia

Correspondence should be addressed to Jianbao Zhang; [jianbaozhang@163.com](mailto:jianbaozhang@163.com)

Received 12 May 2018; Revised 27 June 2018; Accepted 25 July 2018; Published 9 August 2018

Academic Editor: Hiroaki Mukaidani

Copyright © 2018 Jianbao Zhang et al. This is an open access article distributed under the Creative Commons Attribution License, which permits unrestricted use, distribution, and reproduction in any medium, provided the original work is properly cited.

Motivated by the quorum-sensing mechanism of bacteria, this paper modifies the network model by adding unknown parameters and noise disturbances and investigates the problem of outer synchronization via adaptive control. In case there exist three unknown parameters, updating laws are presented to identify the unknown parameters with help of Lyapunov stability theory, and the negative effects of noise disturbances are also compensated by designing adaptive controllers. In addition, we simplify the obtained conditions and carry out two succinct and utilitarian corollaries. Finally, numerical simulations are provided to show the validity of the obtained results.

## 1. Introduction

During the past decades, it has been discovered that bacteria, such as *Escherichia coli*, could communicate with each other through producing and monitoring one kind of signaling molecules [1, 2]. The signaling molecules could diffuse into different bacteria or the environment, and the bacteria could coordinate their gene expression and activities in response to the concentration of the signaling molecules. Then, the bacteria are coupled with each other by the intercellular signaling molecules [3] and display various social behaviors such as behaving synchronously [4]. Obviously, the related researches have wide application prospects in biopharmaceutical industry and human health. Now, the mechanism of bacterial communication is widely known as quorum sensing, and more and more researchers began to study collective behavior caused by quorum sensing [5, 6]. In this paper, we modify one of the previous network models coupled through quorum sensing and discuss a typical kind of collective behavior based

on several recent methods developed in the fields of complex networks and nonlinear dynamics.

Recent years have witnessed the great development in the study of complex networks and its collective dynamics [7, 8]. Synchronization is one of the most typical and most extensively studied kinds of collective dynamics, which implies the stability of zero solution of the synchronization error systems. Therefore, from the point of research methods, there are two main effective theoretical methods, i.e., the famous master stability function method [9, 10] and Lyapunov function method [11–13]. The former can be employed to discuss local stability of the synchronous state, and the latter can be used to explore global stability of the synchronous state. Up to now, dozens of different types of synchronization states have been proposed such as complete synchronization [14], cluster synchronization [15, 16], lag synchronization [17, 18], projection synchronization [19, 20], and outer synchronization [21–23]. Thereinto, outer synchronization has attracted many researchers' interest, which describes the synchronization

between two or more networks. For instances, in a model of predator-prey interactions in ecological communities, all the predators form a network system and all the preys form another, and the two networks influence one another's evolution to keep the two species in check [24]. Recently, outer synchronization of the fractional order node dynamics was considered in [21], and outer synchronization under aperiodically adaptive intermittent control was considered in [22]. In many cases, networks can not realize a certain expected synchronization relying on just coupling interaction between different nodes [23]. Therefore, many different kinds of output control methods have been introduced, such as pinning control [25], sliding mode control [26, 27], adaptive control [28, 29], and state feedback control [30]. Thereinto, adaptive control could be used to design controllers for systems with uncertain parameters. Due to great demands from wide applications, many researches have been carried out to investigate synchronization induced by adaptive controllers [31]. It is worth pointing out that there are few researches focused on outer synchronization of networks coupled through quorum sensing.

Motivated by the above discussions, this paper investigates outer synchronization induced by adaptive controllers in quorum-sensing network. At first, we present a modified model of previous quorum-sensing network by adding noise disturbances in case there exist three unknown parameter vectors and the network topology is also unknown. Then, effective adaptive controllers are designed to realize outer synchronization, parameter estimations are designed to identify the unknown parameter vectors, and topology estimations are designed to identify unknown network topology. Based on Lyapunov function method and matrix theory, this paper proves that adaptive outer synchronization is achieved in the quorum-sensing network. To the best of our knowledge, there are few researches focused on this subject by a similar method. In our opinion, there is a certain degree of values both in theory and in practice.

The rest of this paper is organized as follows. In Section 2, the synthetic gene network model coupled through quorum sensing is introduced. In Section 3, several criteria are derived for outer synchronization including the construction of adaptive controllers and parameter estimations. In Section 4, some numerical examples are provided to illustrate the effectiveness of the obtained results. Finally, conclusions are given to summarize the contributions of the paper in Section 5.

## 2. Problem Formulation

The synthetic gene network in *Escherichia coli* was first proposed by Garcia-Ojalvo J et al. [3]. Consider the network consisting of  $N$  cells coupled through quorum sensing. Each cell consists of two basic parts illustrated in Figure 1. The first part is composed of three genes  $a, b, c$  that express their respective proteins  $A, B, C$ , which inhibit the transcription of the three genes  $b, c, a$ , in a cyclic way. The second part of each cell is another gene regulated by protein A, which produces a protein and synthesizes a small molecule known as an autoinducer  $S_i$ . The autoinducer  $S_i$  can diffuse freely

through the cell membrane, which activates the transcription of the genes in first part. For more detailed description, the reader is referred to previous articles [32, 33].

Now, we introduce the quorum-sensing network model. The dynamics of each node consists of the concentrations of three genes and their respective proteins, assume that the  $i$ th cell is described by the following equations:

$$\begin{aligned} \dot{a}_i(t) &= -d_1 a_i(t) + \beta_6 [\mu_6 + C_i^m(t)]^{-1}, \\ \dot{b}_i(t) &= -d_2 b_i(t) + \beta_4 [\mu_4 + A_i^m(t)]^{-1}, \\ \dot{c}_i(t) &= -d_3 c_i(t) + \beta_5 [\mu_5 + B_i^m(t)]^{-1} \\ &\quad + \beta_8 S_i(t) [\mu_7 + S_i(t)]^{-1}, \\ \dot{A}_i(t) &= -d_4 A_i(t) + \beta_1 a_i(t), \\ \dot{B}_i(t) &= -d_5 B_i(t) + \beta_2 b_i(t), \\ \dot{C}_i(t) &= -d_6 C_i(t) + \beta_3 c_i(t), \end{aligned} \quad (1)$$

where  $a_i(t), b_i(t)$ , and  $c_i(t)$  are the concentrations of *mRNA* transcribed from genes  $a, b, c$  in the  $i$ th cell, respectively;  $A_i(t), B_i(t)$ , and  $C_i(t)$  are the concentrations of the corresponding proteins, respectively;  $S_i(t)$  and  $S_e(t)$  are the concentrations of the autoinducer *AI* inside the  $i$ th cell and in the environment. The concentration dynamics of the autoinducer are governed by

$$\begin{aligned} \dot{S}_i(t) &= -d_7 S_i(t) + \beta_7 A_i(t) - \eta (S_i(t) - S_e(t)), \\ \dot{S}_e(t) &= -d_e S_e(t) + \frac{\eta_e}{N} \sum_{j=1}^N (S_j(t) - S_e(t)), \end{aligned} \quad (2)$$

where  $i = 1, 2, \dots, N$ . In the multicell system (1)-(2), the parameters  $d_1, d_2, \dots, d_7$  and  $d_e$  are the dimensionless degradation rates of the chemical molecules;  $\beta_1, \beta_2, \beta_3$  are the translation rates of the proteins from the *mRNAs*;  $\beta_4, \beta_5, \beta_6$  are the dimensionless transcription rates in the absence of repressor;  $\beta_7$  is the synthesis rate of *AI*;  $m = 4$  is the Hill coefficient;  $\beta_8$  is the maximal contribution to the gene  $c$  transcription in the presence of saturating amounts of *AI*;  $\eta$  and  $\eta_e$  measure the diffusion rate of *AI* inward and outward the cell membrane. With the help of the quasi-steady state approximation  $\dot{S}_e(t) = 0$ , one gets that the extracellular *AI* concentration can be approximated as

$$S_e(t) = \frac{q}{N} \sum_{j=1}^N S_j(t), \quad q = \frac{\eta_e}{d + \eta_e}, \quad (3)$$

which reduces (2) to the following form:

$$\dot{S}_i(t) = -(d_7 + \eta) S_i(t) + \beta_7 A_i(t) + \frac{\eta q}{N} \sum_{j=1}^N S_j(t). \quad (4)$$

Equations (1)-(4) describe the concentration state of the  $i$ th cell in the synthetic gene network model coupled through quorum sensing.

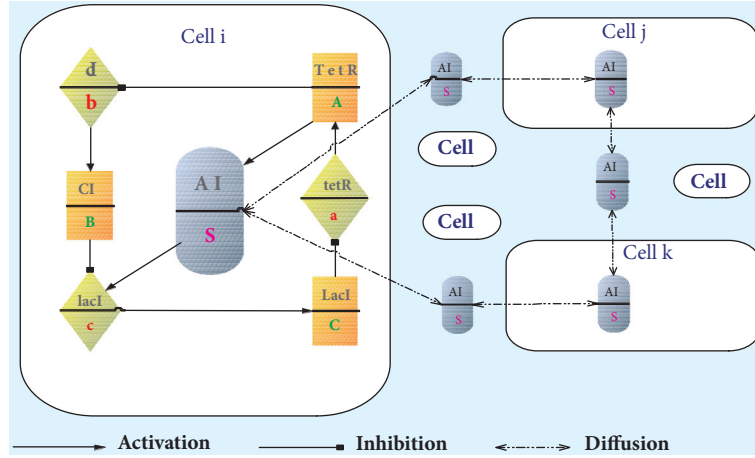


FIGURE 1: Scheme of the repressilator network coupled through signaling molecules, termed quorum sensing. The synchronization scheme of quorum sensing is based on the diffusion of autoinducers (AI) to and from the cells.

Motivated by the quorum-sensing network (1)-(4), we build up a network with three unknown parameter vectors and unknown network topology. The state dynamics are described by the following equations:

$$\begin{aligned}\dot{x}_i(t) &= f_1(x_i(t))\alpha_1 + f_2(x_i(t))\alpha_2 + \beta_8 h(S_i(t)), \\ \dot{S}_i(t) &= -\alpha_3 S_i(t) + \beta_7 A_i(t) + \sum_{j=1}^N c_{ij} S_j(t),\end{aligned}\quad (5)$$

where  $x_i(t) = (a_i(t), b_i(t), c_i(t), A_i(t), B_i(t), C_i(t))^T$ ,  $\alpha_1 = (d_1, d_2, d_3, d_4, d_5, d_6)^T$ ,  $\alpha_2 = (\beta_6, \beta_4, \beta_5, \beta_1, \beta_2, \beta_3)^T$ , and  $\alpha_3 = d_7 + \eta$ , and the diagonal matrix functions

$$\begin{aligned}f_1(x_i(t)) &= -\text{diag}(a_i(t), b_i(t), c_i(t), A_i(t), B_i(t), \\ &C_i(t)), \\ f_2(x_i(t)) &= \text{diag}\left([\mu_6 + C_i^m(t)]^{-1}, [\mu_4 + A_i^m(t)]^{-1},\right. \\ &\left. [\mu_5 + B_i^m(t)]^{-1}, a_i(t), b_i(t), c_i(t)\right), \\ h(S_i(t)) &= (0, 0, S_i(t) [\mu_7 + S_i(t)]^{-1}, 0, 0, 0)^T,\end{aligned}\quad (6)$$

where  $i = 1, 2, \dots, N$ . To meet the demands of broad applications, the matrix  $C = (c_{ij})_{N \times N}$  is a coupling matrix denoting the network topology. The matrix element  $c_{ij}$  is defined as follows: if there is a connection from node  $i$  to node  $j$  ( $i \neq j$ ), then define the coupling strength as  $c_{ij} \neq 0$ ; otherwise,  $c_{ij} = 0$ . Let us assume that there are three unknown parameter vectors existing in the node dynamics,  $\alpha_1$ ,  $\alpha_2$ , and  $\alpha_3$ , and the network topology matrix  $C = (c_{ij})_{N \times N}$  is also unknown.

In order to identify the unknown network topology and parameter vectors, we carry out another network model described by the following equations:

$$\begin{aligned}\dot{\bar{x}}_i(t) &= f_1(\bar{x}_i(t))\bar{\alpha}_1(t) + f_2(\bar{x}_i(t))\bar{\alpha}_2(t) \\ &+ \beta_8 h(\bar{S}_i(t)) + \Delta_1(t) + u_{1i}(t), \\ \dot{\bar{S}}_i(t) &= -\bar{\alpha}_3(t)\bar{S}_i(t) + \beta_7 \bar{A}_i(t) + \sum_{j=1}^N \bar{c}_{ij} \bar{S}_j(t) + \Delta_2(t) \\ &+ u_{2i}(t),\end{aligned}\quad (7)$$

where  $\bar{x}_i(t) = (\bar{a}_i(t), \bar{b}_i(t), \bar{c}_i(t), \bar{A}_i(t), \bar{B}_i(t), \bar{C}_i(t))^T$ ,  $\bar{\alpha}_1(t)$ ,  $\bar{\alpha}_2(t)$ , and  $\bar{\alpha}_3(t)$  are the estimations of the unknown parameter vectors  $\alpha_1$ ,  $\alpha_2$ , and  $\alpha_3$  in the network (5),  $\Delta_1(t)$ ,  $\Delta_2(t)$  are the disturbances, and  $u_{1i}(t)$ ,  $u_{2i}(t)$  are the controllers left to be designed later,  $i = 1, 2, \dots, N$ .

### 3. Adaptive Control Schemes for Outer Synchronization

In this section, several criteria are derived for outer synchronization induced by adaptive control schemes. At first, we need to introduce the following two assumptions.

*Assumption 1.* For any  $x = (x^{(1)}, x^{(2)}, \dots, x^{(6)})^T \in R^6$  and  $S \in R$ , denote

$$\begin{aligned}F(X, \alpha_1, \alpha_2, \alpha_3) &= \left[ (f_1(x)\alpha_1 + f_2(x)\alpha_2 + \beta_8 h(S))^T, \right. \\ &\left. -\alpha_3 S + \beta_7 x^{(4)} \right]^T \in R^7,\end{aligned}\quad (8)$$

where  $X = (x^T, S)^T \in R^7$ . There exists a positive constant  $L$  such that the vector function  $F(X, \alpha_1, \alpha_2, \alpha_3)$  satisfies that

$$\begin{aligned}(Y - X)^T [F(Y, \alpha_1, \alpha_2, \alpha_3) - F(X, \alpha_1, \alpha_2, \alpha_3)] \\ \leq L(Y - X)^T (Y - X)\end{aligned}\quad (9)$$

for any  $X, Y \in R^7$ .

*Assumption 2.* The disturbances  $\Delta_1(t)$  and  $\Delta_2(t)$  are bounded; i.e., there exist two positive constants  $\rho_1, \rho_2$  such that

$$\begin{aligned} \|\Delta_1(t)\| &\leq \rho_1, \\ \|\Delta_2(t)\| &\leq \rho_2. \end{aligned} \quad (10)$$

Now, we design the state feedback controllers of the following form:

$$\begin{aligned} u_{1i}(t) &= -\delta_{1i}(t) e_{1i}(t) - \gamma_{1i}(t) \text{sign}[e_{1i}(t)], \\ \dot{\delta}_{1i}(t) &= k_{1i} e_{1i}^\top(t) e_{1i}(t), \quad k_{1i} > 0, \\ \dot{\gamma}_{1i}(t) &= \xi_{1i} e_{1i}^\top(t) \text{sign}[e_{1i}(t)], \quad \xi_{1i} > 0, \\ u_{2i}(t) &= -\delta_{2i}(t) e_{2i}(t) - \gamma_{2i}(t) \text{sign}[e_{2i}(t)] \\ &\quad + \sum_{j=1}^N p_{ij}(t) \bar{S}_j(t), \\ \dot{\delta}_{2i}(t) &= k_{2i} e_{2i}^2(t), \quad k_{2i} > 0, \\ \dot{\gamma}_{2i}(t) &= \xi_{2i} \text{sign}[e_{2i}(t)] e_{2i}(t), \quad \xi_{2i} > 0, \\ \dot{p}_{ij}(t) &= -\bar{S}_j(t) e_{2i}(t), \end{aligned} \quad (11)$$

where  $e_{1i}(t) = \bar{x}_i(t) - x_i(t)$ ,  $e_{2i}(t) = \bar{S}_i(t) - S_i(t)$ , and  $i = 1, 2, \dots, N$ . Then, one can prove the following theorem based on Lyapunov function method and matrix theory.

**Theorem 3.** Suppose that Assumptions 1 and 2 hold, and the parameter estimations  $\alpha_1(t), \alpha_2(t), \alpha_3(t)$  are designed as follows:

$$\begin{aligned} \dot{\bar{\alpha}}_1(t) &= -\sum_{j=1}^N f_1(\bar{x}_j(t)) e_{1j}(t), \\ \dot{\bar{\alpha}}_2(t) &= -\sum_{j=1}^N f_2(\bar{x}_j(t)) e_{1j}(t), \\ \dot{\bar{\alpha}}_3(t) &= \sum_{j=1}^N \bar{S}_j(t) e_{2j}(t), \end{aligned} \quad (12)$$

and then the synthetic gene network (5)-(7) with controllers (11) and estimations (12) can achieve outer synchronization.

*Proof.* Denote  $X_i(t) = (x_i^\top(t), S_i(t))^\top$ ,  $\bar{X}_i(t) = (\bar{x}_i^\top(t), \bar{S}_i(t))^\top$ ,  $\Delta(t) = (\Delta_1^\top(t), \Delta_2^\top(t))^\top$ , and  $U_i(t) = (u_{1i}^\top(t), u_{2i}^\top(t))^\top$ , and  $\Gamma \in R^{7 \times 7}$  is the inner matrix implying the nodes are coupling through the 7th component, and then the synthetic gene network (5)-(7) can be rewritten as follows:

$$\begin{aligned} \dot{X}_i(t) &= F(X_i(t), \alpha_1, \alpha_2, \alpha_3) + \sum_{j=1}^N c_{ij} \Gamma X_j(t), \\ \dot{\bar{X}}_i(t) &= F(\bar{X}_i(t), \bar{\alpha}_1(t), \bar{\alpha}_2(t), \bar{\alpha}_3(t)) \\ &\quad + \sum_{j=1}^N \bar{c}_{ij} \Gamma \bar{X}_j(t) + \Delta(t) + U_i(t), \end{aligned} \quad (13)$$

Let  $E_i(t) = \bar{X}_i(t) - X_i(t)$ , and the following error system can be obtained:

$$\begin{aligned} \dot{E}_i(t) &= F(\bar{X}_i(t), \bar{\alpha}_1(t), \bar{\alpha}_2(t), \bar{\alpha}_3(t)) \\ &\quad - F(X_i(t), \alpha_1, \alpha_2, \alpha_3) \\ &\quad + \sum_{j=1}^N [\bar{c}_{ij} \Gamma \bar{X}_j - c_{ij} \Gamma X_j] + \Delta(t) + U_i(t). \end{aligned} \quad (14)$$

Using Assumption 1, one has

$$\begin{aligned} E_i^\top(t) [F(\bar{X}_i(t), \bar{\alpha}_1(t), \bar{\alpha}_2(t), \bar{\alpha}_3(t)) \\ - F(X_i(t), \alpha_1, \alpha_2, \alpha_3)] &\leq E_i^\top(t) \\ &\cdot [F(\bar{X}_i(t), \bar{\alpha}_1(t), \bar{\alpha}_2(t), \bar{\alpha}_3(t)) \\ - F(\bar{X}_i(t), \alpha_1, \alpha_2, \alpha_3) + LE_i(t)] &= E_i^\top(t) \\ &\cdot [((f_1(\bar{x}_i(t)) \bar{\alpha}_1(t) + f_2(\bar{x}_i(t)) \bar{\alpha}_2(t))^\top \\ - \bar{\alpha}_3(t) \bar{S}_i(t))^\top + LE_i(t)] &= \sum_{p=1}^2 e_{1i}^\top(t) f_p(\bar{x}_i(t)) \\ &\cdot \bar{\alpha}_p(t) - \bar{\alpha}_3(t) \bar{S}_i(t) e_{2i}(t) + L \sum_{p=1}^2 e_{pi}^\top(t) e_{pi}(t). \end{aligned} \quad (15)$$

Consider the following Lyapunov function:

$$\begin{aligned} V(t) &= \frac{1}{2} \left\{ \sum_{i=1}^N E_i^\top(t) E_i(t) + \sum_{p=1}^3 \bar{\alpha}_p^\top(t) \bar{\alpha}_p(t) \right. \\ &\quad + \sum_{p=1}^2 \sum_{i=1}^N \frac{1}{k_{pi}} [\delta_{pi}(t) - \delta_p^*]^2 \\ &\quad + \sum_{p=1}^2 \sum_{i=1}^N \frac{1}{\xi_{pi}} [\gamma_{pi}(t) - \gamma_p^*]^2 \\ &\quad \left. + \sum_{j=1}^N \sum_{i=1}^N [p_{ij}(t) + \bar{c}_{ij} - c_{ij}]^2 \right\}, \end{aligned} \quad (16)$$

where  $\bar{\alpha}_p(t) = \bar{\alpha}_p(t) - \alpha_p$ ,  $p = 1, 2, 3$ , where  $\delta_p^*, \gamma_p^*$ ,  $p = 1, 2$ , are positive constants chosen arbitrarily. With the help of controllers (11) and estimations (12), the derivative of  $V(t)$  along the trajectories of (5)-(7) can be calculated as follows:

$$\begin{aligned}
 \dot{V}(t) &= \sum_{i=1}^N E_i^\top(t) \dot{E}_i(t) - \sum_{p=1}^2 \bar{\alpha}_p^\top(t) \sum_{j=1}^N f_p(\bar{x}_j(t)) e_{1j}(t) \\
 &\quad + \bar{\alpha}_3^\top(t) \sum_{j=1}^N \bar{S}_j(t) e_{2j}(t) \\
 &\quad + \sum_{p=1}^2 \sum_{i=1}^N [\delta_{pi}(t) - \delta_p^*] e_{pi}^\top(t) e_{pi}(t) \\
 &\quad + \sum_{p=1}^2 \sum_{i=1}^N [\gamma_{pi}(t) - \gamma_p^*] e_{pi}^\top(t) \text{sign}[e_{pi}(t)] \\
 &\quad - \sum_{j=1}^N \sum_{i=1}^N [p_{ij}(t) + \bar{c}_{ij} - c_{ij}] \bar{S}_j(t) e_{2i}(t).
 \end{aligned} \tag{17}$$

Noticing (14) and inequality (15), one has

$$\begin{aligned}
 \dot{V}(t) &\leq L \sum_{p=1}^2 \sum_{i=1}^N e_{pi}^\top(t) e_{pi}(t) \\
 &\quad + \sum_{i=1}^N \sum_{j=1}^N e_{2i}(t) [\bar{c}_{ij} \bar{S}_j(t) - c_{ij} S_j(t)] \\
 &\quad + \sum_{i=1}^N E_i^\top(t) [\Delta(t) + U_i(t)] \\
 &\quad + \sum_{p=1}^2 \sum_{i=1}^N [\delta_{pi}(t) - \delta_p^*] e_{pi}^\top(t) e_{pi}(t) \\
 &\quad + \sum_{p=1}^2 \sum_{i=1}^N [\gamma_{pi}(t) - \gamma_p^*] e_{pi}^\top(t) \text{sign}[e_{pi}(t)] \\
 &\quad - \sum_{j=1}^N \sum_{i=1}^N [p_{ij}(t) + \bar{c}_{ij} - c_{ij}] e_{2i}(t) \bar{S}_j(t) \\
 &\leq L \sum_{p=1}^2 \sum_{i=1}^N e_{pi}^\top(t) e_{pi}(t) + \sum_{i=1}^N \sum_{j=1}^N c_{ij} e_{2i}(t) e_{2j}(t) \\
 &\quad + \sum_{i=1}^N E_i^\top(t) \Delta(t) - \sum_{p=1}^2 \sum_{i=1}^N \delta_p^* e_{pi}^\top(t) e_{pi}(t) \\
 &\quad - \sum_{p=1}^2 \sum_{i=1}^N \gamma_p^* e_{pi}^\top(t) \text{sign}[e_{pi}(t)].
 \end{aligned} \tag{18}$$

Denoting  $e_2(t) = (e_{21}(t), e_{22}(t), \dots, e_{2N}(t))^\top \in R^N$ , one gets

$$\begin{aligned}
 \dot{V}(t) &\leq (L - \delta_1^*) \sum_{i=1}^N e_{1i}^\top(t) e_{1i}(t) \\
 &\quad + e_2^\top(t) [(L - \delta_2^*) I_N + C] e_2(t) \\
 &\quad + \sum_{p=1}^2 \sum_{i=1}^N [e_{pi}^\top(t) \Delta_p(t) - \gamma_p^* e_{pi}^\top(t) \text{sign}[e_{pi}(t)]]
 \end{aligned}$$

$$\begin{aligned}
 &\leq (L - \delta_1^*) \sum_{i=1}^N e_{1i}^\top(t) e_{1i}(t) \\
 &\quad + e_2^\top(t) [(L - \delta_2^*) I_N + C] e_2(t) \\
 &\quad + \sum_{p=1}^2 \sum_{i=1}^N (\rho_p - \gamma_p^*) \|e_{pi}(t)\|_1,
 \end{aligned} \tag{19}$$

where  $\|e_{pi}(t)\|_1 = e_{pi}^\top(t) \text{sign}[e_{pi}(t)]$ . Notice that the constants  $\delta_1^*, \delta_2^*, \gamma_1^*, \gamma_2^*$  are chosen arbitrarily, and we can choose them sufficiently large such that  $L - \delta_1^* < 0$ ,  $\rho_p - \gamma_p^* < 0$ ,  $p = 1, 2$ , and the matrix  $(L - \delta_2^*) I_N + C$  is negative semidefinite. According to this, we have

$$\dot{V}(t) < 0. \tag{20}$$

Thus, based on Lyapunov stability methods, the error dynamical system (14) is globally asymptotically stable. Therefore, the synthetic gene network (5)-(7) with controllers (11) and estimations (12) achieves outer synchronization.

The proof is completed.  $\square$

If one or two of the unknown parameter vectors in the network (5) are given constants, Theorem 3 still holds after modifying the conditions slightly. For instance, supposing that the parameter vectors  $\alpha_1$  and  $\alpha_2$  are given, we modify network (7) as follows:

$$\begin{aligned}
 \dot{\bar{x}}_i(t) &= f_1(\bar{x}_i(t)) \alpha_1 + f_2(\bar{x}_i(t)) \alpha_2 + \beta_8 h(\bar{S}_i(t)) \\
 &\quad + \Delta_1(t) + u_{1i}(t), \\
 \dot{\bar{S}}_i(t) &= -\bar{\alpha}_3(t) \bar{S}_i(t) + \beta_7 \bar{A}_i(t) + \sum_{j=1}^N \bar{c}_{ij} \bar{S}_j + \Delta_2(t) \\
 &\quad + u_{2i}(t).
 \end{aligned} \tag{21}$$

Then the following corollary holds.

**Corollary 4.** Suppose that Assumptions 1 and 2 hold. If the parameter estimation  $\alpha_3(t)$  is designed as follows:

$$\dot{\bar{\alpha}}_3(t) = \sum_{j=1}^N \bar{S}_j(t) e_{2j}(t), \tag{22}$$

then the synthetic gene network (5)-(21) with controllers (11) and estimations (22) can achieve outer synchronization.

If we do not consider the disturbances  $\Delta_1(t)$  and  $\Delta_2(t)$  in network (7), Theorem 3 still holds after modifying controllers (11) slightly. Then, we obtain the following corollary.

**Corollary 5.** Suppose that Assumptions 1 and 2 hold, and the disturbances in network (7) satisfy that  $\Delta_1(t) = 0$  and  $\Delta_2(t) = 0$ . If the controllers  $u_{1i}(t)$ ,  $u_{2i}(t)$  are designed as follows:

$$\begin{aligned}
u_{1i}(t) &= -\delta_{1i}(t) e_{1i}(t), \\
\dot{\delta}_{1i}(t) &= k_{1i} e_{1i}^\top(t) e_{1i}(t), \quad k_{1i} > 0, \\
u_{2i}(t) &= -\delta_{2i}(t) e_{2i}(t) + \sum_{j=1}^N p_{ij}(t) \bar{S}_j(t), \\
\dot{\delta}_{2i}(t) &= k_{2i} e_{2i}^2(t), \quad k_{2i} > 0, \\
\dot{p}_{ij}(t) &= -\bar{S}_j(t) e_{2i}(t),
\end{aligned} \quad (23)$$

where  $i = 1, 2, \dots, N$ , then the synthetic gene network (5)-(7) with controllers (23) and estimations (12) can achieve outer synchronization.

The proof of Corollaries 4 and 5 is similar to that of Theorem 3; therefore, it is omitted here.

#### 4. Numerical Simulations

In this section, we carry out some numerical simulations on the following synthetic gene network consisting of 6 cells:

$$\begin{aligned}
\dot{x}_i(t) &= f_1(x_i(t)) \alpha_1 + f_2(x_i(t)) \alpha_2 + \beta_8 h(S_i(t)), \\
\dot{\bar{x}}_i(t) &= f_1(\bar{x}_i(t)) \bar{\alpha}_1(t) + f_2(\bar{x}_i(t)) \bar{\alpha}_2(t) \\
&\quad + \beta_8 h(\bar{S}_i(t)) + \Delta_1(t) + u_{1i}(t), \\
\dot{S}_i(t) &= -\alpha_3 S_i(t) + \beta_7 A_i(t) + \sum_{j=1}^6 c_{ij} S_j(t), \\
\dot{\bar{S}}_i(t) &= -\bar{\alpha}_3(t) \bar{S}_i(t) + \beta_7 \bar{A}_i(t) + \sum_{j=1}^6 \bar{c}_{ij} \bar{S}_j(t) + \Delta_2(t) \\
&\quad + u_{2i}(t),
\end{aligned} \quad (24)$$

where the functions  $f_1(x_i(t))$ ,  $f_2(x_i(t))$ ,  $h(S_i(t))$  are defined in network (5), the parameters are given as  $(\mu_4, \mu_5, \mu_6, \mu_7) = (0.2, 0.2, 0.2, 0.2)$ ,  $m = 4$ ,  $\beta_7 = 0.018$ ,  $\beta_8 = 1$ ,  $\Delta_1(t)$ ,  $\Delta_2(t)$  are the disturbances, and the coupling matrices are given as

$$\begin{aligned}
C &= \begin{pmatrix} -5 & 1 & 2 & 0 & 1 & 1 \\ 1 & -4 & 0 & 1 & 2 & 0 \\ 2 & 0 & -6 & 2 & 0 & 2 \\ 0 & 1 & 2 & -4 & 1 & 0 \\ 1 & 2 & 0 & 1 & -4 & 0 \\ 1 & 0 & 2 & 0 & 0 & -3 \end{pmatrix}, \\
\bar{C} &= \begin{pmatrix} -6 & 2 & 0 & 1 & 1 & 2 \\ 2 & -6 & 1 & 2 & 1 & 0 \\ 0 & 1 & -5 & 1 & 2 & 1 \\ 1 & 2 & 1 & -5 & 0 & 1 \\ 1 & 1 & 2 & 0 & -5 & 1 \\ 2 & 0 & 1 & 1 & 1 & -5 \end{pmatrix}.
\end{aligned} \quad (25)$$

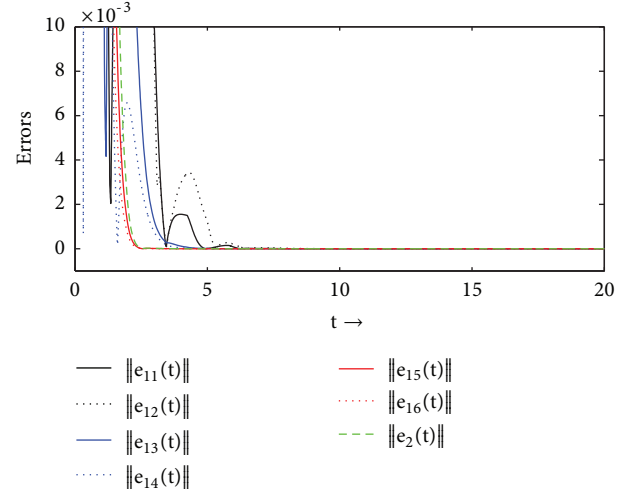


FIGURE 2: Time evolutions of synchronization errors  $\|e_{1i}(t)\|$  and  $\|e_2(t)\|$ ,  $i = 1, 2, \dots, 6$ .

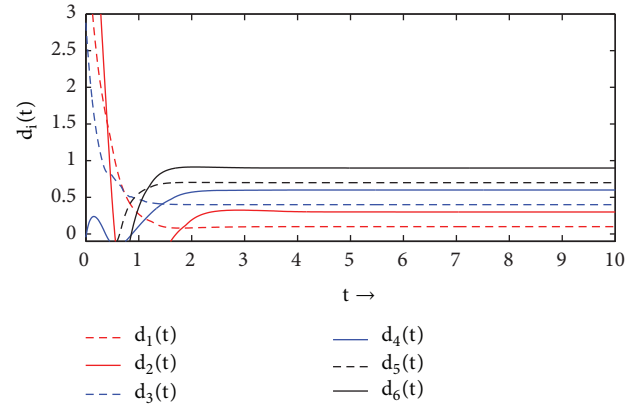


FIGURE 3: Time evolutions of the parameter estimations  $\bar{\alpha}_1(t) = (d_1(t), d_2(t), \dots, d_6(t))^\top$  in (12).

Consider the actual meaning of the network, the true values of the unknown parameters are

$$\begin{aligned}
\alpha_1 &= (0.1, 0.3, 0.4, 0.6, 0.7, 0.9)^\top, \\
\alpha_2 &= (2, 1.9, 1.5, 0.2, 0.6, 0.9)^\top, \\
\alpha_3 &= 0.42,
\end{aligned} \quad (26)$$

estimations (12) are adopted for  $\bar{\alpha}_1(t)$ ,  $\bar{\alpha}_2(t)$ ,  $\bar{\alpha}_3(t)$ , and controllers (11) are adopted for  $u_{1i}(t)$ ,  $u_{2i}(t)$ .

By setting the initial values of network (24) randomly in  $[0, 1]$  and with the feedback gain taken as  $k_{1i} = k_{2i} = 1$ , we plot Figure 2 to show the time evolutions of outer synchronization errors  $\|e_{1i}(t)\| = \|\bar{x}_i(t) - x_i(t)\|$  and  $\|e_{2i}(t)\| = \|\bar{S}_i(t) - S_i(t)\|$ ,  $i = 1, 2, \dots, 6$ . It can be seen that the two errors both go to zero quickly after a short transient period, and network (24) reaches outer synchronization. Figure 3 depicts the time evolutions of the parameter estimations  $\bar{\alpha}_1(t)$ , which displays the perfect identification performance. Figure 4 shows the time evolutions of the parameter estimations

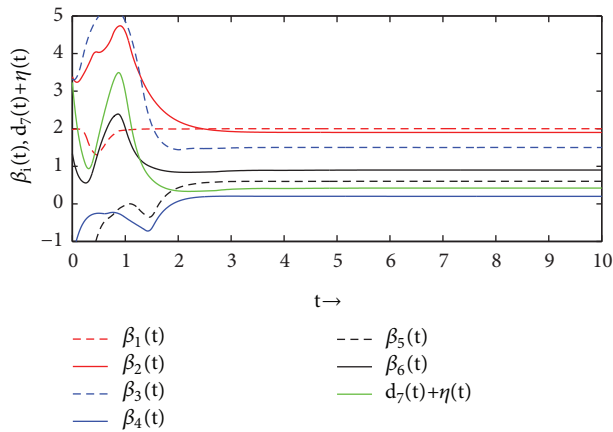


FIGURE 4: Time evolutions of the parameter estimations  $\bar{\alpha}_2(t) = (\beta_1(t), \beta_2(t), \dots, \beta_6(t))^T$  and  $\bar{\alpha}_3(t) = d_7(t) + \eta(t)$  in (12).

$\bar{\alpha}_2(t)$ ,  $\bar{\alpha}_3(t)$ , and further illustrates the effectiveness of the parameter estimations (12). From the three figures, it is clearly observed that the unknown parameters of the network is estimated successfully by the control schemes of Theorem 3.

## 5. Conclusions

This paper builds a model of quorum-sensing network with disturbances, unknown parameter vector, and network topology and investigates the problem of outer synchronization between two quorum-sensing networks. In case that some systems' parameters are unknown in actual applications, adaptive parameter updating laws are designed to estimate the true values of those unknown parameters. Similarly, updating laws are also presented for the unknown elements of the network coupling matrix. Finally, some adaptive controllers are adopted to realize outer synchronization between two quorum-sensing networks. The validity of the proposed control schemes and updating laws is demonstrated by several numerical simulations.

## Data Availability

The authors affirm that all data necessary for confirming the conclusions of the article are present within the article.

## Conflicts of Interest

The authors declare that there are no conflicts of interest regarding the publication of this article.

## Acknowledgments

Project is supported by National Natural Science Foundation of China (nos. 11447005, 61771230, and 61663006), Shandong Provincial Key Research and Development Program of China (no. 2017CXGC0701), Shandong Provincial Natural Science Foundation (no. ZR2016FM40, ZR2016JL021), Jiangsu Planned Projects for Postdoctoral Research Funds

(no. 1701017A), and the Fundamental Research Funds for the Central Universities (no. 9161718004).

## References

- [1] J. D. Dockery and J. P. Keener, "A mathematical model for quorum sensing in *Pseudomonas aeruginosa*," *Bulletin of Mathematical Biology*, vol. 63, no. 1, pp. 95–116, 2001.
- [2] M. E. Taga and B. L. Bassler, "Chemical communication among bacteria," *Proceedings of the National Academy of Sciences of the United States of America*, vol. 100, no. 24, pp. 14549–14554, 2003.
- [3] J. Garcia-Ojalvo, M. B. Elowitz, and S. H. Strogatz, "Modeling a synthetic multicellular clock: repressilators coupled by quorum sensing," *Proceedings of the National Academy of Sciences of the United States of America*, vol. 101, no. 30, pp. 10955–10960, 2004.
- [4] R. Wang and L. Chen, "Synchronizing genetic oscillators by signaling molecules," *Journal of Biological Rhythms*, vol. 20, no. 3, pp. 257–269, 2005.
- [5] E. V. Nikolaev and E. D. Sontag, "Quorum-sensing synchronization of synthetic toggle switches: a design based on monotone dynamical systems theory," *PLoS Computational Biology*, vol. 12, no. 4, Article ID e1004881, 2016.
- [6] B. L. Bassler, "Quorum sensing and its control," *The FASEB Journal*, vol. 30, no. 1, 2016.
- [7] W. Sun, S. Wang, G. Wang, and Y. Wu, "Lag synchronization via pinning control between two coupled networks," *Nonlinear Dynamics*, vol. 79, no. 4, pp. 2659–2666, 2015.
- [8] P. Zhou, S. Cai, J. Shen, and Z. Liu, "Adaptive exponential cluster synchronization in colored community networks via aperiodically intermittent pinning control," *Nonlinear Dynamics*, vol. 92, no. 3, pp. 905–921, 2018.
- [9] L. M. Pecora and T. L. Carroll, "Master stability functions for synchronized coupled systems," *Physical Review Letters*, vol. 80, no. 10, pp. 2109–2112, 1998.
- [10] A. Brechtel, P. Gramlich, D. Ritterskamp, B. Drossel, and T. Gross, "Master stability functions reveal diffusion-driven pattern formation in networks," *Physical Review E: Statistical, Nonlinear, and Soft Matter Physics*, vol. 97, no. 3, Article ID 032307, 2018.
- [11] Z.-Y. Sun, M.-M. Yun, and T. Li, "A new approach to fast global finite-time stabilization of high-order nonlinear system," *Automatica*, vol. 81, pp. 455–463, 2017.
- [12] X.-J. Xie, Z.-J. Li, and K. Zhang, "Semi-global output feedback control for nonlinear systems with uncertain time-delay and output function," *International Journal of Robust and Nonlinear Control*, vol. 27, no. 15, pp. 2549–2566, 2017.
- [13] Y. Li, Y. Sun, and F. Meng, "New criteria for exponential stability of switched time-varying systems with delays and nonlinear disturbances," *Nonlinear Analysis: Hybrid Systems*, vol. 26, pp. 284–291, 2017.
- [14] L. M. Pecora and T. L. Carroll, "Synchronization in chaotic systems," *Physical Review Letters*, vol. 64, no. 8, pp. 821–824, 1990.
- [15] A. Hu, J. Cao, M. Hu, and L. Guo, "Cluster synchronization in directed networks of non-identical systems with noises via random pinning control," *Physica A: Statistical Mechanics and its Applications*, vol. 395, pp. 537–548, 2014.
- [16] J. Zhang, Z. Ma, and G. Chen, "Robustness of cluster synchronous patterns in small-world networks with inter-cluster co-competition balance," *Chaos: An Interdisciplinary Journal of Nonlinear Science*, vol. 24, no. 2, Article ID 023111, 2014.

- [17] H. Liu, W. Sun, and G. Al-mahbashi, "Parameter identification based on lag synchronization via hybrid feedback control in uncertain drive-response dynamical networks," *Advances in Difference Equations*, vol. 2017, no. 1, article 122, 2017.
- [18] Z. Wang, L. Huang, and X. Yang, "Adaptive modified function projective lag synchronization for two different chaotic systems with stochastic unknown parameters," *Mediterranean Journal of Mathematics*, vol. 13, no. 3, pp. 1391–1405, 2016.
- [19] Abdessellem Boulkroune, Sarah Hamel, Farouk Zouari, Abdelkrim Boukabou, and Asier Ibeas, "Output-feedback controller based projective lag-synchronization of uncertain chaotic systems in the presence of input nonlinearities," *Mathematical Problems in Engineering*, vol. 2017, Article ID 8045803, 12 pages, 2017.
- [20] J. Guan, "Function projective synchronization of a class of chaotic systems with uncertain parameters," *Mathematical Problems in Engineering*, vol. 2012, Article ID 431752, 5 pages, 2012.
- [21] M. M. Asheghan and J. n. Míguez, "Robust global synchronization of two complex dynamical networks," *Chaos: An Interdisciplinary Journal of Nonlinear Science*, vol. 23, no. 2, Article ID 023108, 2013.
- [22] S. Cai, X. Lei, and Z. Liu, "Outer synchronization between two hybrid-coupled delayed dynamical networks via aperiodically adaptive intermittent pinning control," *Complexity*, vol. 21, no. S2, pp. 593–605, 2016.
- [23] L. Wang, J. Zhang, and W. Sun, "Adaptive outer synchronization and topology identification between two complex dynamical networks with time-varying delay and disturbance," *IMA Journal of Mathematical Control and Information*, 2018.
- [24] X. Wu, W. X. Zheng, and J. Zhou, "Generalized outer synchronization between complex dynamical networks," *Chaos: An Interdisciplinary Journal of Nonlinear Science*, vol. 19, no. 1, Article ID 013109, 9 pages, 2009.
- [25] C. Yu, J. Qin, and H. Gao, "Cluster synchronization in directed networks of partial-state coupled linear systems under pinning control," *Automatica*, vol. 50, no. 9, pp. 2341–2349, 2014.
- [26] X. Chen, J. H. Park, J. Cao, and J. Qiu, "Adaptive synchronization of multiple uncertain coupled chaotic systems via sliding mode control," *Neurocomputing*, vol. 273, pp. 9–21, 2018.
- [27] Junbiao Guan and Kaihua Wang, "Sliding mode control and modified generalized projective synchronization of a new fractional-order chaotic system," *Mathematical Problems in Engineering*, vol. 2015, Article ID 941654, 9 pages, 2015.
- [28] W. Sun and L. Peng, "Observer-based robust adaptive control for uncertain stochastic Hamiltonian systems with state and input delays," *Lithuanian Association of Nonlinear Analysts. Nonlinear Analysis: Modelling and Control*, vol. 19, no. 4, pp. 626–645, 2014.
- [29] Z.-Y. Sun, C.-H. Zhang, and Z. Wang, "Adaptive disturbance attenuation for generalized high-order uncertain nonlinear systems," *Automatica*, vol. 80, pp. 102–109, 2017.
- [30] X. Xie and M. Jiang, "Output feedback stabilization of stochastic feedforward nonlinear time-delay systems with unknown output function," *International Journal of Robust and Nonlinear Control*, vol. 28, no. 1, pp. 266–280, 2018.
- [31] Yuling Li, Yixin Yin, and Sen Zhang, "Adaptive Control of Delayed Teleoperation Systems with Parameter Convergence," *Mathematical Problems in Engineering*, vol. 2018, Article ID 1046419, 7 pages, 2018.
- [32] M. B. Elowitz and S. Leibler, "A synthetic oscillatory network of transcriptional regulators," *Nature*, vol. 403, no. 6767, pp. 335–338, 2000.
- [33] J. Zamora-Munt, C. Masoller, J. Garcia-Ojalvo, and R. Roy, "Crowd synchrony and quorum sensing in delay-coupled lasers," *Physical Review Letters*, vol. 105, no. 26, Article ID 264101, 2010.

## Research Article

# A Common Value Experimentation with Multiarmed Bandits

Xiujuan Gao , Hao Liang, and Tong Wang 

The School of Economic Mathematics, Southwestern University of Finance and Economics, 611130 Wenjiang, Chengdu, China

Correspondence should be addressed to Tong Wang; 2160202z1008@2016.swufe.edu.cn

Received 21 May 2018; Revised 16 July 2018; Accepted 24 July 2018; Published 30 July 2018

Academic Editor: Ju H. Park

Copyright © 2018 Xiujuan Gao et al. This is an open access article distributed under the Creative Commons Attribution License, which permits unrestricted use, distribution, and reproduction in any medium, provided the original work is properly cited.

We study a value common experimentation with multiarmed bandits and give an application about the experimentation. The second derivative of value functions at cutoffs is investigated when an agent switches action with multiarmed bandits. If consumers have identical preference which is unknown and purchase products from only two sellers among multiple sellers, we obtain the necessary and sufficient conditions about the common experimentation. The Markov perfect equilibrium and the socially effective allocation in  $K$ -armed markets are discussed.

## 1. Introduction

A financial debate has arisen when we need to choose the best goods among multiple products. In Robbins [1], this problem is described as a decision maker facing  $N$  slot machines (called arms) and the maker has to choose one of them at each instantaneous time. Gittins and Jones [2] and Michael et al. [3] calculate the value of pulling an arm, i.e., Gittins index, in discrete time. Comparing the value to the Gittins index of all other arms, Michael et al. [3] present that the optimal strategy for an  $N$ -armed problem is an  $N$ -dimensional discounted Markov decision chain and the value pulling each arm itself is independent of the cutoff. Karatzas [4], Kaspi, and Mandelbaum [5] transform the problem into a standard optimal stopping problem. Bolton and Harris [6] and Bergemann and Välimäki [7] show that when there are  $K \geq 2$  sellers who sell different products and  $N$  consumers whose preferences are identical (but unknown) in the market, the optimal strategies of consumers are to buy the products from the same seller; i.e., it is symmetric equilibria. Cohen and Solan [8] study two-armed bandit problems in the continuous time with the property of Lévy processes and obtain the Hamilton-Jacobi-Bellman (HJB) equation for the problem. They conclude that the optimal strategy is a cutoff strategy when the arms have two types. For other optimal strategies and control approaches, the reader is referred to [9–11] and the references therein.

Jan and Xi [12] investigate that second derivatives of value functions are equal at the cutoff with value matching and

smooth pasting (assume that the value function is  $V(x) \in C^2(R^+)$  and the cutoff is  $x^* \in R^+$ . Value matching:  $V(x^*-) = V(x^*+)$  and smooth pasting:  $V'(x^*-) = V'(x^*+)$  which is discussed in [13, 14], where  $V(x^-) := \lim_{x \rightarrow x^-} V(x)$  and  $V(x^+) := \lim_{x \rightarrow x^+} V(x)$ ), when there are two arms with different types, and conclude that the optimal strategy is an interval strategy in the market. In [12], an application is given about strategic pricing of two vendors in a competitive market. There are  $N \geq 2$  consumers who have the same type either  $H$  or  $L$ . Two vendors produce two different kinds of goods for the two types, respectively. Jan and Xi [12] describe the socially efficient allocation and pricing strategies of two vendors in the market. Moreover, they use value matching, smooth pasting, and second derivatives of value functions to discuss the Markov perfect equilibrium and the socially efficient allocation.

In this article, we investigate multiarmed bandits, while two-armed bandits are studied in [12]. We consider multiple sellers instead of two sellers. In general, there are multiple sellers to sell the same type of goods in the market, but the quality, utilities, and the prices of goods sold by each seller are different. Therefore, changing the number of arms from two to  $K \geq 2$  is reasonable in the market. People believe that purchasing two products has the best effects to type  $H$  or  $L$  in the market. For example, the first seller is the highest utility to type  $H$  but is the lowest utility to type  $L$ . On the contrary, the second seller is the highest utility to type  $L$  but is the lowest utility to type  $H$  and other utilities are between about the two

sellers to types  $H$  and  $L$ . Instinctively, we think that a rational consumer chooses goods only from the first two sellers but this is not perfect or this strategy needs some conditions. We discuss the necessary and sufficient conditions for this strategy.

In order to obtain our conclusions under certain assumptions of the model for multiarmed bandits, using the methods used in [12], we calculate the optimal cutoff points by solving the corresponding ordinary differential equations. Then, we obtain the necessary and sufficient conditions for the strategy of which consumers purchase products from only two sellers among multiple sellers.

The rest of the paper is as follows. In Section 2, we introduce a multiarmed model under certain assumptions and show a conclusion about the model. In Section 3, we give an application for the model. In Section 3.1, we discuss optimal choice of consumers in the case of market equilibrium. Based on the optimal choice of consumers, we derive HJB equations for their utilities functions. Using solutions of the HJB equations, value matching, and smooth pasting, we get the cutoff point at Markov perfect equilibrium and the necessary and sufficient conditions about the common experimentation. In Section 3.2, we get the cutoff point at socially efficient allocation with the same way in Section 3.1. The relationship between the Markov perfect equilibrium and the socially efficient allocation in  $K$ -armed markets is discussed.

## 2. The Model

Jin and Xi [12] consider one agent and a bandit with 2 arms. We study multiarmed bandits and consider the case where there is only one real-valued state  $x(t) \in Y$  and  $Y \in R$  is a connect set. The instantaneous flow payoff of each arm is  $f_j(x)$  at state  $x$ ,  $j = 1, 2, \dots, K$ . Let  $r > 0$  be the discount rate. For each arm  $j$ , there is a probability space  $\{\Omega^j, \mathcal{F}^j, P^j\}$  endowed with filtration  $\{\mathcal{F}_t^j, t \geq 0\}$  and  $T_j(t)$  is the total measure of time to time  $t$  when arm  $j$  has been chosen. From [12], we know that the updating of  $x$  in arm  $j$ , when there are  $K$  arms in the market, satisfies

$$dx_j(t) = \mu_j(x(t-)) dT_j(t) + \sigma_j(x(t-)) dW_j(T_j(t)) + \sum_{i \neq j} \int_{\mathbb{R} - \{0\}} J_j(x(t-), x_i) \mathbb{N}_j(dT_j(t), dx_i), \quad (1)$$

where  $W_j(t)$  is a standard Brownian motion,  $W_j(t)$  is independent of  $W_i(t)$  ( $i \neq j$ ), and  $\mathbb{N}_j$  is a Poisson random measure that is independent of  $W_j$ . The state  $x$  is updated from arm  $i$ ,  $i = 1, 2, \dots, K$  and  $dx(t) = \sum_{i=1}^K dx_i(t)$ . Let  $J_j(x(t-), x_i)$  be the change of the state when there is a Poisson jump. Equation (1) shows that the state changes from  $x_j$  to  $x_i$  ( $i \neq j$ ). Thus, (1) does not contain the case that state  $x_j$  jump from other states. Because state  $x_j$  can jump to any other states and any other states can jump back to  $x_j$ , (1) contains all jump processes that describe the changes of state.

In multiarmed bandit problem, the stochastic process  $\{x_t\}$  is constructed on the product space  $\{\Omega, \mathcal{F}\} := \{\Omega^1, \mathcal{F}^1\} \times$

$\{\Omega^2, \mathcal{F}^2\} \times \dots \times \{\Omega^K, \mathcal{F}^K\}$  with filtration  $\mathcal{F}_t = \bigvee_{i=1}^K \mathcal{F}_{T_i(t)}^i$ . If  $x = x_0$ , the agent chooses an allocation rule  $m_t = \{1, 2, \dots, K\}$  adapted to filtration  $\{\mathcal{F}_t\}_{t \geq 0}$  to solve the following optimal control problem:

$$v(x) = \sup_{m_t} \left\{ \mathbb{E} \int_{t=0}^{\infty} e^{-rt} f_{m_t}(x_t) dt \right\}, \quad (2)$$

$$\begin{aligned} \text{s.t. } dx_t &= \mu_{m_t}(x_t) dt + \sigma_{m_t}(x_t) dW_t \\ &+ \sum_{i \neq m_t} \int_{\mathbb{R} - \{0\}} J_{m_t}(x(t-), x_i) \mathbb{N}_{m_t}(dt, dx_i). \end{aligned} \quad (3)$$

*Assumption 1* (see [12]). Let  $Y$  be a connected set. Assume that  $f_j(x)$ ,  $\mu_j(x)$ ,  $\sigma_j(x)$ , and  $J_j(x, x_i)$  for  $i \neq j$  are  $C^2$  functions of  $x \in Y$ .

*Assumption 2* (see [12]). Assume that the first derivatives of  $f_j(x)$ ,  $\mu_j(x)$ ,  $\sigma_j(x)$ , and  $J_j(x, \cdot)$  with respect to  $x$  are bounded. Namely, there exists  $M > 0$  such that for any  $x \in Y$ ,  $|f'_j(x)| \leq M$ ,  $|\mu'_j(x)| \leq M$ ,  $|\sigma'_j(x)| \leq M$ , and  $|\partial J_j(x, x_i)/\partial x| \leq M$  for each  $i \neq j$ . Using (2) and the dynamic programming principle (the detailed process is in [15]), for any  $h > 0$ , we obtain

$$v(x) = \sup_{m_t} \left\{ \mathbb{E} \int_{t=0}^h e^{-rt} f_{m_t}(x_t) dt + e^{-rh} v(x_h) \right\}. \quad (4)$$

Using Ito's lemma for  $e^{-rt} v(x_t)$  and property of Poisson random measure (the property of Poisson random measure is in [13]), we get

$$\begin{aligned} de^{-rt} v(x_t) &= -re^{-rt} v(x_t) dt + e^{-rt} v'(x_t) dx_t^c + \frac{1}{2} \\ &\cdot e^{-rt} v''(x_t) d[x, x]_t = -re^{-rt} v(x_t) dt \\ &+ e^{-rt} v'(x_t) dx_t^c + \frac{1}{2} e^{-rt} \sigma_{m_t}^2(x_t) v''(x_t) dt \\ &+ \sum_{i=1, i \neq m_t}^{K-1} \left[ \int_{\mathbb{R} - \{0\}} J_{m_t}(x(t-), x_i) \mathbb{N}_{m_t}(dt, dx_i) \right]^2 \\ &+ 2 \sum_{1 \leq p < q \leq K-1} \int_{\mathbb{R} - \{0\}} J_{m_t}(x(t-), x_p) \mathbb{N}_{m_t}(dt, dx_p) \\ &\times \int_{\mathbb{R} - \{0\}} J_{m_t}(x(t-), x_q) \mathbb{N}_{m_t}(dt, dx_q) \\ &= -re^{-rt} v(x_t) dt + e^{-rt} v'(x_t) dx_t^c + \frac{1}{2} \\ &\cdot e^{-rt} \sigma_{m_t}^2(x_t) v''(x_t) dt \\ &+ \sum_{i=1, i \neq m_t}^{K-1} \int_{\mathbb{R} - \{0\}} [v(x + J_{m_t}(x(t-), x_{m_t})) - v(x)] \\ &\cdot \mathbb{N}_{m_t}(dt, dx_i), \end{aligned} \quad (5)$$

where  $dx_t^c = \mu_{m_t}(x_t) dt + \sigma_{m_t}(x_t) dW_t$ .

Then, we have

$$\begin{aligned}
 e^{-rh} v(x_h) &= v(x) + \int_{t=0}^h -re^{-rt} v(x_t) dt \\
 &+ e^{-rt} v'(x_t) dx_t^c + \int_{t=0}^h \frac{1}{2} e^{-rt} \sigma_{m_t}^2(x_t) v''(x_t) dt \\
 &+ \sum_{i=1, i \neq m_t}^{K-1} \int_{t=0}^h [v(x + J_{m_t}(x(t-), x_{m_t})) - v(x)] \\
 &\cdot \mathbb{N}_{m_t}(dt, dx_i).
 \end{aligned} \tag{6}$$

Substituting (6) into (4), using the mean value theorem of integrals and sending  $h \rightarrow 0$ , we get the HJB equation

$$\begin{aligned}
 rv(x) &= \sup_{m_t} \left\{ f_{m_t}(x) + \mu_{m_t}(x) v'(x) + \frac{1}{2} \sigma_{m_t}^2(x) v''(x) \right. \\
 &+ \left. \sum_{i=1, i \neq m_t}^{K-1} \int_{\mathbb{R}-\{0\}} [v(x + J_{m_t}(x(t-), x_i)) - v(x)] \nu_{m_t}(dx_i) \right\},
 \end{aligned} \tag{7}$$

where  $\nu_{m_t}$  is the finite intensity measure of  $\mathbb{N}_{m_t}$ . From [13], we know that there exists a unique solution to (1).

We assume that optimal strategy of consumers is an interval strategy (see [14]). Namely, there exists  $K - 1$  points (cutoffs)  $x^1, x^2, \dots, x^{K-1}$  to partition the space  $Y$  into  $K - 1$  intervals, where  $x^1 \leq x^2 \leq \dots \leq x^{K-1}$ . When  $i, j = 1, 2, \dots, K - 2$  and  $i \neq j$ ,  $(x^i, x^{i+1}) \cap (x^j, x^{j+1}) = \emptyset$ , we assume that if  $x \in (x^{j-1}, x^j)$ , the agent chooses arm  $j$ , where  $j = 1, 2, \dots, K$  and  $x^0 := \inf\{x\}$ ,  $x^K := \sup\{x\}$ . Thus, we have

$$\begin{aligned}
 rv(x) &= f_j(x) + \mu_j(x) v'(x) + \frac{1}{2} \sigma_j^2(x) v''(x) \\
 &+ \sum_{i=1, i \neq j}^{K-1} \int_{\mathbb{R}-\{0\}} [v(x + J_j(x(t-), x_i)) - v(x)] \\
 &\cdot \nu_j(dx_i).
 \end{aligned} \tag{8}$$

Using the conclusions in [12, 14], we have the value matching

$$v(x^{j-}) = v(x^{j+}) \tag{9}$$

and the smooth pasting

$$v'(x^{j-}) = v'(x^{j+}). \tag{10}$$

Now, in the light of the value matching and smooth pasting, we have the following conclusion.

**Theorem 3.** *If  $\sigma_j(x) > 0$  for all  $x \in Y$ ,  $j = 1, 2, \dots, K$ , a necessary condition for optimal solution  $x^j$  is that  $v''(x)$  satisfies  $v''(x^{j-}) = v''(x^{j+})$  for any possible cutoffs  $x^j$ .*

*Proof.* On the basis of assumption  $x \in (x^{j-1}, x^j)$ , an agent chooses arm  $j$ ,  $j = 1, 2, \dots, K$ . It derives that

$$\begin{aligned}
 f_j(x) + \mu_j(x) v'(x) + \frac{1}{2} \sigma_j^2(x) v''(x) \\
 + \sum_{i=1, i \neq j}^{K-1} \int_{\mathbb{R}-\{0\}} [v(x + J_j(x(t-), x_i)) - v(x)] \nu_j(dx_i) \\
 \leq rv(x).
 \end{aligned} \tag{11}$$

For  $x \rightarrow x_j$  and  $x > x_j$ , inequality (11) becomes

$$\begin{aligned}
 f_j(x_j) + \mu_j(x_j) v'(x_{j+}) + \frac{1}{2} \sigma_j^2(x_j) v''(x_{j+}) \\
 + \sum_{i=1, i \neq j}^{K-1} \int_{\mathbb{R}-\{0\}} [v(x_j + J_j(x_j, x_i)) - v(x_{j+})] \\
 \cdot \nu_j(dx_i) \leq rv(x_{j+}).
 \end{aligned} \tag{12}$$

Due to the value matching, we have

$$\begin{aligned}
 f_j(x_j) + \mu_j(x_j) v'(x_{j+}) + \frac{1}{2} \sigma_j^2(x_j) v''(x_{j+}) \\
 + \sum_{i=1, i \neq j}^{K-1} \int_{\mathbb{R}-\{0\}} [v(x_j + J_j(x_j, x_i)) - v(x_{j+})] \\
 \cdot \nu_j(dx_i) \leq rv(x_{j-})
 \end{aligned} \tag{13}$$

and

$$\begin{aligned}
 rv(x_{j-}) &= f_j(x_j) + \mu_j(x_j) v'(x_{j-}) + \frac{1}{2} \sigma_j^2(x_j) \\
 &\cdot v''(x_{j-}) \\
 &+ \sum_{i=1, i \neq j}^{K-1} \int_{\mathbb{R}-\{0\}} [v(x_j + J_j(x_j, x_i)) - v(x_{j-})] \\
 &\cdot \nu_j(dx_i).
 \end{aligned} \tag{14}$$

From the smooth pasting, we obtain  $v''(x_{j+}) \leq v''(x_{j-})$ . In the same way, we get  $v''(x_{j-}) \leq v''(x_{j+})$ . Thus, we have  $v''(x_{j-}) = v''(x_{j+})$  for any  $j = 1, 2, \dots, K$ .  $\square$

Theorem 3 gives a necessary condition under which second derivatives of value functions are equal at every cutoff when there are  $K$  arms in the market.

When  $K = 2$ , i.e., there are two arms in the market; the agent has two states  $x_1$  and  $x_2$  in the model. In this case, we only need to consider that an agent jumps between the two states, i.e.,  $m_t = \{1, 2\}$ . Thus, there is one cutoff, which is discussed in [12].

### 3. Application

The application of Theorem 3 is similar to that in [12]. The difference is that there are  $K \geq 2$  sellers offering different

products in the market. We index these sellers with  $j = 1, 2, \dots, K$ . We assume that all consumers have the same type  $i$ , either  $H$  or  $L$ . Let  $\beta_{jH}$  and  $\beta_{jL}$  be the utilities of consumers who buy good  $j$  with type  $H$  or  $L$ , respectively. We assume  $\beta_{1H} > \beta_{2H} > \dots > \beta_{KH}$  and  $\beta_{1L} < \beta_{2L} < \dots < \beta_{KL}$ , i.e., the more likely the consumers are to buy type  $H$ , the more tendency they choose the previous sellers. Therefore, we denote that  $x \in [0, 1]$  is the common belief that the type is high and then the expected utility of controlling the seller  $j$  is  $f_j(x) := x\beta_{jH} + (1-x)\beta_{jL}$ . If we denote  $a_j := \beta_{jH} - \beta_{jL}$  and  $b_j := \beta_{jL}$ , the utility is represented by

$$f_j(x) = a_j x + b_j, \quad (15)$$

where  $a_j + b_j < a_{j+1} + b_{j+1}$  and  $b_j > b_{j+1}$ .

At any time, all market participants observe all previous outcomes. Because of the influence caused by uncertain external factors, the flow utility  $u_{ji}(t)$  has a noisy signal of the true value (the detailed introduction can be found in [12]).

$$du_{ji}(t) = \xi_{ji} dt + \sigma_j d\widetilde{W}_j(t), \quad (16)$$

where  $\widetilde{W}_j(t)$  is independent of  $\widetilde{W}_i(t)$  ( $i \neq j$ ).

$x$  is related to time and it is described as a learning process in [16], denoted by  $x_t$ . Without loss of generality, we assume

that there are  $n_j$  consumers choosing seller  $j$  and  $\sum_{j=1}^K n_j = N \geq 2$ . From the statements in [6, 7], we have that  $x_t$  satisfies

$$dx_t = \sum_{j=1}^K n_j \Xi_j(x) dW_j(t), \quad (17)$$

where  $W_j(t)$  is independent of  $W_i(t)$  ( $i \neq j$ ) and  $\Xi_j(x) := x^2(1-x)^2(a_j/\sigma_j)$ . We denote  $s_j := a_j/\sigma_j$ .

In the next subsection, the Markov perfect equilibrium and the socially efficient allocation in  $K$ -armed market are discussed.

**3.1. Markov Perfect Equilibrium.** Let  $p_j$  denote the price of goods of seller  $j$ . The price is related to  $x$  at instantaneous time  $t$ . So  $p_j$  is a mapping  $[0, 1] \rightarrow \mathbb{R}$ ,  $j = 1, 2, \dots, K$ . We denote  $\alpha_i$  as the choice of  $i$ th consumer which is related not only to his common belief  $x$ , but also to the prices of the sellers' goods, i.e.,  $\alpha_i : [0, 1] \times \underbrace{\mathbb{R} \times \mathbb{R} \times \dots \times \mathbb{R}}_{\text{The number of } \mathbb{R} \text{ is } K} \rightarrow \{1, 2, \dots, K\}$ . A

symmetric Markov perfect equilibrium is  $\{\alpha, p_1, p_2, \dots, p_K\}$ .

When the choice of the previous  $N - 1$  consumers is observed, the utility of the  $N$ th consumer is maximized. Let  $U(x)$  denote the maximum utility of this consumer and  $n'_j$  denote the number of choosing the  $j$ th seller. We have  $\sum_{j=1}^K n'_j = N - 1$ . There exists  $d \in \{1, 2, \dots, K\}$  subject to  $n'_d = n_d - 1$  and  $n'_i = n_i$ ,  $i \neq d$ . Then, we have

$$rU(x) = \max \left\{ \begin{array}{l} f_1(x) - p_1(x) + \frac{1}{2} \left[ \sum_{i=1}^K n_i \Xi_i(x) + \Xi_1(x) - \Xi_d(x) \right] U''(x) \\ \vdots \\ f_{d-1}(x) - p_{d-1}(x) + \frac{1}{2} \left[ \sum_{i=1}^K n_i \Xi_i(x) + \Xi_{d-1}(x) - \Xi_d(x) \right] U''(x) \\ f_d(x) - p_d(x) + \frac{1}{2} \left[ \sum_{i=1}^K n_i \Xi_i(x) \right] U''(x) \\ f_{d+1}(x) - p_{d+1}(x) + \frac{1}{2} \left[ \sum_{i=1}^K n_i \Xi_i(x) + \Xi_{d+1}(x) - \Xi_d(x) \right] U''(x) \\ \vdots \\ f_K(x) - p_K(x) + \frac{1}{2} \left[ \sum_{i=1}^K n_i \Xi_i(x) + \Xi_K(x) - \Xi_d(x) \right] U''(x) \end{array} \right\}. \quad (18)$$

Due to the price competition, the consumer chooses equal utility for other sellers. Thus, we get

$$\begin{aligned} & f_1(x) - p_1(x) \\ & + \frac{1}{2} \left[ \sum_{i=1}^K n_i \Xi_i(x) + \Xi_1(x) - \Xi_d(x) \right] U''(x) = \dots \\ & = f_{d-1}(x) - p_{d-1}(x) \end{aligned}$$

$$\begin{aligned} & + \frac{1}{2} \left[ \sum_{i=1}^K n_i \Xi_i(x) + \Xi_{d-1}(x) - \Xi_d(x) \right] U''(x) \\ & = f_d(x) - p_d(x) + \frac{1}{2} \left[ \sum_{i=1}^K n_i \Xi_i(x) \right] U''(x) \\ & = f_{d+1}(x) - p_{d+1}(x) \\ & + \frac{1}{2} \left[ \sum_{i=1}^K n_i \Xi_i(x) + \Xi_{d+1}(x) - \Xi_d(x) \right] U''(x) = \dots \end{aligned}$$

$$\begin{aligned}
 &= f_K(x) - p_K(x) \\
 &+ \frac{1}{2} \left[ \sum_{i=1}^K n_i \Xi_i(x) + \Xi_K(x) - \Xi_d(x) \right] U''(x).
 \end{aligned} \tag{19}$$

Therefore, we obtain

$$\begin{aligned}
 f_i(x) - p_i(x) + \frac{1}{2} \Xi_i(x) U''(x) \\
 = f_j(x) - p_j(x) + \frac{1}{2} \Xi_j(x) U''(x),
 \end{aligned} \tag{20}$$

where  $i, j = 1, 2, \dots, K$  and  $i \neq j$ .

Now, we discuss the pricing of goods of sellers. Denote  $V_j(x)$  as the  $j$ th seller's utility. If there are  $n_j$  consumers buying goods  $j$  when the price is  $p_j$ , we have

$$V_j(x) = \mathbb{E} \left[ \int_0^\infty e^{-rt} n_j p_j(x_t) dt \right], \tag{21}$$

where  $dx_t = \sum_{j=1}^K \sqrt{n_j} x_t (1 - x_t) s_j dW_j(t)$ .

From (21), we derive that

$$rV_j(x) = n_j p_j(x) + \frac{1}{2} \left( \sum_{i=1}^K n_i \Xi_i(x) \right) V_j''(x). \tag{22}$$

We get  $n_j = 0$  or  $N$  because all consumers choose only one seller (see [6, 7]). When  $n_j = 0$ , the utility of seller  $j$  is presented in the form

$$rV_j(x) = \frac{N}{2} \Xi_d(x) V_j''(x), \tag{23}$$

where we assume that all consumers choose seller  $d$ , i.e.,  $j \in \{1, 2, \dots, K\} - \{d\}$  and  $n_d = N$ .

When only one consumer chooses seller  $j$ , i.e.,  $n_j = 1$ , the utility of seller  $j$  is

$$\begin{aligned}
 rV_j(x) = p_j(x) \\
 + \frac{1}{2} \left[ (N-1) \Xi_d(x) + \Xi_j(x) \right] V_j''(x).
 \end{aligned} \tag{24}$$

As a rational market participant, when no consumer buys goods, the seller adjusts the price so that the payoff in this case is equal to the payoff when only one consumer chooses this seller. We obtain the price of goods of seller  $j$  in the form

$$p_j(x) = \frac{1}{2} \left( \Xi_d(x) - \Xi_j(x) \right) V_j''(x). \tag{25}$$

From (20), we get the price of seller  $d$  in the form

$$\begin{aligned}
 p_d(x) = f_d(x) - f_j(x) \\
 + \frac{1}{2} \left( \Xi_d(x) - \Xi_j(x) \right) \left( U''(x) + V_j''(x) \right).
 \end{aligned} \tag{26}$$

We have  $N-1$  cutoffs  $x^j$ ,  $j = 1, 2, \dots, N-1$ , where  $0 < x^1 \leq x^2 \leq \dots \leq x^{j-1} < 1$ . When common belief  $x \in (x^{i-1}, x^i)$ , consumer chooses seller  $i$ ,  $i = 1, 2, \dots, K$  ( $x^0 := 0, x^K := 1$ ). If  $x = x^i$ , the utilities of consumers are indifferent when they choose seller  $i$  or  $i+1$  due to value matching. When  $x \neq x^i$ , we have the conclusion

**Theorem 4.** All consumers only choose the first seller or the last seller in the market if and only if cutoffs  $x^j$ ,  $j = 1, 2, \dots, N-1$ , are the same and equal to  $(rD_0 - (b_1 - b_K)) / ((a_1 - a_K) - rD_1)$ , where

$$\begin{aligned}
 D_0 &:= \left( \frac{\gamma_1 + 1}{2} s_1^2 + \frac{\gamma_K - 1}{2} s_K^2 \right) \frac{b_1 - b_K}{r} \frac{C_1 + C_K}{C_1 \cdot C_K}, \\
 D_1 &:= (s_K^2 - s_1^2) \frac{b_1 - b_K}{r} \\
 &+ \left( s_1^2 \frac{\gamma_1 - 1}{2} + s_K^2 \frac{\gamma_K + 1}{2} \right) \frac{a_1 - a_K}{r} \frac{C_1 + C_K}{C_1 \cdot C_K}, \\
 C_1 &:= \frac{1}{2} (N-1) s_1^2 (\lambda_1 - \gamma_1) + \frac{1}{2} s_K^2 (\lambda_1 + \gamma_K), \\
 C_K &:= \frac{1}{2} (N-1) s_K^2 (\lambda_K - \gamma_K) + \frac{1}{2} s_1^2 (\lambda_K + \gamma_1), \\
 \gamma_j &:= \sqrt{1 + \frac{8r}{Ns_j^2}}, \\
 \lambda_1 &:= \sqrt{1 + \frac{8r}{(N-1)s_1^2 + s_K^2}}, \\
 \text{and } \lambda_K &:= \sqrt{1 + \frac{8r}{(N-1)s_K^2 + s_1^2}}.
 \end{aligned} \tag{27}$$

*Proof.* Firstly, we prove the sufficiency. When all cutoffs are equivalent and equal to  $(rD_0 - (b_1 - b_K)) / ((a_1 - a_K) - rD_0)$ , all consumers only choose the first seller or the last seller in the market.

Letting  $x^* := x^1 = \dots = x^{K-1}$ , we have  $x^* = x^1 = x^{K-1}$ . When  $x \in (0, x^1)$ , all consumers choose the first seller. From (25) and (26), we have

$$p_K(x) = \frac{1}{2} \left( \Xi_1(x) - \Xi_K(x) \right) V_K''(x) \tag{28}$$

and

$$\begin{aligned}
 p_1(x) = f_1(x) - f_K(x) \\
 + \frac{1}{2} \left( \Xi_1(x) - \Xi_K(x) \right) \left( U''(x) + V_K''(x) \right).
 \end{aligned} \tag{29}$$

Substituting (29) into (22) yields

$$\begin{aligned}
 rV_1(x) = N \left[ f_1(x) - f_K(x) \right. \\
 \left. + \frac{1}{2} \left( \Xi_1(x) - \Xi_K(x) \right) \left( V_K''(x) - U''(x) \right) \right] + \frac{N}{2} \\
 \cdot \Xi_1 V_1''(x)
 \end{aligned} \tag{30}$$

Substituting (28) and (29) into (22) gives rise to

$$\begin{aligned} rU(x) &= f_K(x) \\ &- \frac{1}{2} (\Xi_1(x) - \Xi_K(x)) (V_K''(x) + U''(x)) \\ &+ \frac{N}{2} \Xi_1 U''(x). \end{aligned} \quad (31)$$

From (23), (30), and (31), for  $x \in (0, x^1)$ , we have

$$\begin{aligned} V_1(x) &= N \frac{f_1(x) - f_K(x)}{r} \\ &+ P_3 x^{(\gamma_1+1)/2} (1-x)^{-(\gamma_1-1)/2} \\ &- NP_2 x^{(\lambda_1+1)/2} (1-x)^{-(\lambda_1-1)/2} \\ V_K(x) &= P_1 x^{(\gamma_1+1)/2} (1-x)^{-(\gamma_1-1)/2} \\ U(x) &= \frac{f_K(x)}{r} + P_2 x^{((\lambda_1+1)/2)(1-x)^{-(\lambda_1-1)/2}} \\ &- P_1 x^{(\gamma_1+1)/2} (1-x)^{-(\gamma_1-1)/2}. \end{aligned} \quad (32)$$

Similarly, for  $x \in (x^{K-1}, 1)$ , it has

$$\begin{aligned} V_1(x) &= Q_1 x^{-(\gamma_K-1)/2} (1-x)^{(\gamma_K+1)/2} \\ V_K(x) &= N \frac{f_K(x) - f_1(x)}{r} \\ &+ Q_3 x^{-(\gamma_K-1)/2} (1-x)^{(\gamma_K+1)/2} \\ &- NQ_2 x^{-(\lambda_K-1)/2} (1-x)^{(\lambda_K+1)/2} \\ U(x) &= \frac{f_1(x)}{r} + Q_2 x^{((\lambda+1)/2)(1-x)^{-(\lambda-1)/2}} \\ &- Q_1 x^{(\gamma_K+1)/2} (1-x)^{-(\gamma_K-1)/2}, \end{aligned} \quad (33)$$

where  $\gamma_j := \sqrt{1 + 8r/Ns_j^2}$ ,  $\lambda_1 := \sqrt{1 + 8r/((N-1)s_1^2 + s_K^2)}$ ,  $\lambda_K := \sqrt{1 + 8r/((N-1)s_K^2 + s_1^2)}$ , and  $P_\xi$  and  $Q_\xi$  are constants,  $\xi = 1, 2, 3$ .

Using value matching, smooth pasting, the second derivative condition, and  $x^* = x^1 = x^{K-1}$ , we have  $V_1(x^*-) = V_K(x^*+)$ ,  $V_1'(x^*-) = V_K'(x^*+)$ ,  $V_1''(x^*-) = V_K''(x^*+)$ , and  $U(x^*-) = U(x^*+)$ . Therefore, we obtain

$$\frac{f_1(x^*) - f_K(x^*)}{r} = \frac{\varphi(x^*)}{C_1} + \frac{\varphi(x^*)}{C_K}, \quad (34)$$

where

$$\begin{aligned} \varphi(x) &:= \left( \frac{\gamma_1+1}{2} s_1^2 + \frac{\gamma_K-1}{2} s_K^2 \right) \frac{b_1 - b_K}{r} \\ &+ \left[ \left( s_K^2 - s_1^2 \right) \frac{b_1 - b_K}{r} \right. \\ &\left. + \left( s_1^2 \frac{\gamma_1-1}{2} + s_K^2 \frac{\gamma_K+1}{2} \right) \frac{a_1 - a_K}{r} \right] x, \\ C_1 &:= \frac{1}{2} (N-1) s_1^2 (\lambda_1 - \gamma_1) + \frac{1}{2} s_K^2 (\lambda_1 + \gamma_K) \end{aligned} \quad (35)$$

and

$$C_K := \frac{1}{2} (N-1) s_K^2 (\lambda_K - \gamma_K) + \frac{1}{2} s_1^2 (\lambda_K + \gamma_1). \quad (36)$$

Define

$$D_0 := \left( \frac{\gamma_1+1}{2} s_1^2 + \frac{\gamma_K-1}{2} s_K^2 \right) \frac{b_1 - b_K}{r} \frac{C_1 + C_K}{C_1 \cdot C_K} \quad (37)$$

and

$$\begin{aligned} D_1 &:= \left( s_K^2 - s_1^2 \right) \frac{b_1 - b_K}{r} \\ &+ \left( s_1^2 \frac{\gamma_1-1}{2} + s_K^2 \frac{\gamma_K+1}{2} \right) \frac{a_1 - a_K}{r} \frac{C_1 + C_K}{C_1 \cdot C_K}. \end{aligned} \quad (38)$$

Thus, we get

$$\frac{f_1(x^*) - f_K(x^*)}{r} = D_0 + D_1 x^* \quad (39)$$

and

$$x^* = \frac{rD_0 - (b_1 - b_K)}{(a_1 - a_K) - rD_0}. \quad (40)$$

When  $x^* := x^1 = \dots = x^{K-1}$ ,  $(x^i, x^{i+1}) = \phi$ ,  $i = 1, 2, \dots, K-2$ , all consumers only choose the first seller or the last seller in the market.

The sufficiency of Theorem 4 is proved.

Now, we prove the necessity. That all consumers choose only the first seller or the last seller in the market means that these cutoffs are the same and equal to  $(rD_0 - (b_1 - b_K))/((a_1 - a_K) - rD_0)$ ,  $x \neq x^*$ . We prove it by contradiction.

Assuming  $x^i \neq x^{i+1}$ , we get  $x^i < x^{i+1}$ ,  $i = 1, 2, \dots, K-2$ . So  $(x^i, x^{i+1}) \cap \{[0, x^*] \cup (x^*, 1]\} \neq \phi$ , i.e.,  $\exists x_0 \neq x^*$ ,  $x_0 \in (x^i, x^{i+1})$ . When the common belief is  $x_0$ , the optimal choice is the  $(i+1)$ th and  $i+1 \neq 1$  and  $i+1 \neq K$ . This is contradiction to the proposition of which all consumers choose only the first seller or the last seller. So  $x^i = x^{i+1}$ ,  $i = 1, 2, \dots, K-2$ . According to the proof of the sufficiency, we have  $x^* = x^1 = x^{K-1} = (rD_0 - (b_1 - b_K))/((a_1 - a_K) - rD_0)$ . The necessity of Theorem 4 is proved.  $\square$

Theorem 4 shows the necessary and sufficient conditions for the consumers' choice. We find that when the consumers only choose the first seller and the last seller, the multiarmed

bandits problem would be attributed to the two-armed bandits. In other words, other sellers gradually disappear in the market because they have no sales. The multiarmed bandit problem is transformed into the two-armed bandits in the situation discussed in [12].

**3.2. Socially Efficient Allocation.** We consider the optimal choice of planners when they face multiarmed bandit problem. Let the total social surplus function be  $w(x)$ . We have

$$w(x) = \sup_{n_1, n_2, \dots, n_K} \left\{ \mathbb{E} \int_0^\infty e^{-rt} \sum_{j=1}^K n_{jt} f_j(x_t) dt \right\} \quad (41)$$

$$\text{s.t. } dx_t = \sum_{j=1}^K \sqrt{n_{jt}} x_t (1 - x_t) s_j dW_j(t). \quad (42)$$

Assume that  $\Pi_j(x)$  is the total social surplus in a neighborhood of  $x$  if a planner choose seller  $j$ . From (41), we have

$$r\Pi_j(x) = N \left[ f_j(x) + \frac{1}{2} \Xi_j(x) \Pi_j''(x) \right], \quad (43)$$

where  $j = 1, 2, \dots, K$ .

Solving the ordinary differential equation (43), we get

$$\Pi_1(x) = N \frac{f_1(x)}{r} + C_1^1 x^{(\gamma_1+1)/2} (1-x)^{-(\gamma_1-1)/2},$$

$$\begin{aligned} \Pi_j(x) &= N \frac{f_j(x)}{r} + C_j^1 x^{(\gamma_j+1)/2} (1-x)^{-(\gamma_j-1)/2} \\ &\quad + C_j^2 x^{-(\gamma_j-1)/2} (1-x)^{(\gamma_j+1)/2} \end{aligned}$$

$$j = 2, \dots, K-1,$$

$$\Pi_K(x) = N \frac{f_K(x)}{r} + C_K^2 x^{-(\gamma_K-1)/2} (1-x)^{(\gamma_K+1)/2}, \quad (44)$$

where  $C_i^1$  and  $C_i^2$ ,  $i = 1, 2, \dots, K$ , are constants.

We denote  $\hat{x}^1, \hat{x}^2, \dots, \hat{x}^{K-1}$  subjecting to  $0 < \hat{x}^1 \leq \hat{x}^2 \leq \dots \leq \hat{x}^{K-1} < 1$  as the cutoffs of the choice for the planner. When  $x \in (\hat{x}^{i-1}, \hat{x}^i)$ , the optimal choice is the  $i$ th seller,  $i = 1, 2, \dots, K$  and  $\hat{x}^0 = 0$ ,  $\hat{x}^K = 1$ . Due to value matching, smooth pasting, and the second derivative conditions, one has

$$\begin{aligned} \Pi_j(\hat{x}_{j-}) &= \Pi_{j+1}(\hat{x}_{j+}), \\ \Pi_j'(\hat{x}_{j-}) &= \Pi_{j+1}'(\hat{x}_{j+}), \\ \Pi_j''(\hat{x}_{j-}) &= \Pi_{j+1}''(\hat{x}_{j+}), \end{aligned} \quad (45)$$

where  $j = 1, 2, \dots, K-1$ .

There are  $(3K-3)$  unknown parameters and  $(3K-3)$  equations in system (45) with  $[x^\beta(1-x)^{1-\beta}]' \neq x^\beta(1-x)^{1-\beta}$ , for all  $\beta > 1$ , i.e., the coefficient matrix of system (45) is nonsingular. Thus, system (45) has a unique solution.

The planner chooses from the first seller or the  $K$ -th seller when  $\hat{x}^1 = \hat{x}^2 = \dots = \hat{x}^{K-1}$ . Let  $x^\dagger := \hat{x}^1 = \hat{x}^2 = \dots = \hat{x}^{K-1}$ . System (45) becomes

$$\begin{aligned} \Pi_1(x^\dagger) &= \Pi_K(x^\dagger), \\ \Pi_1'(x^\dagger) &= \Pi_K'(x^\dagger), \\ \Pi_1''(x^\dagger) &= \Pi_K''(x^\dagger). \end{aligned} \quad (46)$$

We obtain

$$x^\dagger = \frac{(b_1 - b_K) \left( ((\gamma_1 + 1)/2) s_1^2 + ((\gamma_K - 1)/2) s_K^2 \right)}{(a_K - a_1) \left( s_1^2 ((\gamma_1 - 1)/2) + s_K^2 ((\gamma_K + 1)/2) \right) + (b_1 - b_K) (s_1^2 - s_K^2)}. \quad (47)$$

The results in [12] introduce the necessary and sufficient condition under which the Markov perfect equilibrium with cautious strategies is socially efficient with two-armed bandits.

**Corollary 5.** *When  $K \geq 2$ ,  $N \geq 2$ , the consumers' cutoffs are  $x^*$ , and the planner's cutoffs are  $x^\dagger$ , the Markov perfect equilibrium with cautious strategies is socially efficient if and only if  $s_1 = s_K$ . Moreover,  $x^* > x^\dagger$  ( $x^* < x^\dagger$ ) when  $s_1 > s_K$  ( $s_1 < s_K$ ).*

The proof of Corollary 5 is similar to that of Theorem 2 in [12]. We omit its proof.

Corollary 5 shows that the necessary and sufficient conditions under which the Markov perfect equilibrium with cautious strategies is socially efficient when the cutoffs are multiarmed bandits. Jin and Xi [12] present the conditions in

the case of two-armed market. Thus, Theorem 4 extends parts of results in [12].

According to the condition in Corollary 5, when  $(\beta_{1H} - \beta_{1L})/\sigma_1 = (\beta_{KH} - \beta_{KL})/\sigma_K$ , we obtain that the Markov perfect equilibrium with cautious strategies is socially efficient. If  $\sigma_1 = \sigma_K$ , we obtain  $\beta_{1H} - \beta_{KH} = \beta_{1L} - \beta_{KL}$ . In the light of our initial hypothesis, we have  $\beta_{1H} = \beta_{KH}$  and  $\beta_{1L} = \beta_{KL}$ ; i.e., all sellers are identical in the market.

## 4. Conclusion

We study a common value experimentation with multiarmed bandits and present its application. This extends two-armed bandits in [12] to multiarmed bandits. We derive the HJB equation with multiarmed bandits. In the application, we get the necessary and sufficient conditions for the choices of consumers from two sellers. The necessary and sufficient

conditions guarantee that the Markov perfect equilibrium with cautious strategies is socially efficient. In future, we need to solve all the cutoffs in system (45) when these cutoffs are different and give general solutions about these cutoffs.

### Data Availability

No data are used to support the study. Using theoretical derivation and proof, the authors get their conclusions.

### Conflicts of Interest

The authors declare that they have no conflicts of interest.

### Authors' Contributions

The article is a joint work of three authors who contributed equally to the final version of the paper. The authors read and approved the final manuscript.

### Acknowledgments

This work is supported by the Fundamental Research Funds for the Central Universities (JBK120504).

### References

- [1] H. Robbins, "Some aspects of the sequential design of experiments," *Bulletin (New Series) of the American Mathematical Society*, vol. 58, pp. 527–535, 1952.
- [2] J. C. Gittins and D. M. Jones, "A dynamic allocation index in the sequential design of experiments," in *Progress in Statistics*, pp. 241–266, North-Holland, Amsterdam, 1974.
- [3] M. N. Katehakis and J. Veinott, "The multi-armed bandit problem: decomposition and computation," *Mathematics of Operations Research*, vol. 12, no. 2, pp. 262–268, 1987.
- [4] I. Karatzas, "Gittins indices in the dynamic allocation problem for diffusion processes," *Annals of Probability*, vol. 12, no. 1, pp. 173–192, 1984.
- [5] H. Kaspi and A. Mandelbaum, "Lévy bandits: multi-armed bandits driven by Lévy processes," *The Annals of Applied Probability*, vol. 5, no. 2, pp. 541–565, 1995.
- [6] P. Bolton and C. Harris, "Strategic experimentation," *Econometrica*, vol. 67, no. 2, pp. 349–374, 1999.
- [7] D. Bergemann and J. Valimaki, "Experimentation in Markets," *Review of Economic Studies*, vol. 67, no. 2, pp. 213–234, 2000.
- [8] A. Cohen and E. Solan, "Bandit problems with Lévy payoff," *Mathematics of Operations Research*, vol. 38, no. 1, pp. 92–107, 2013.
- [9] X. Yu, X. J. Xie, and N. Duan, "Small-gain control method for stochastic nonlinear systems with stochastic iISS inverse dynamics," *Automatica*, vol. 46, no. 11, pp. 1790–1798, 2010.
- [10] Z.-J. Wu, X.-J. Xie, P. Shi, and Y.-Q. Xia, "Backstepping controller design for a class of stochastic nonlinear systems with Markovian switching," *Automatica*, vol. 45, no. 4, pp. 997–1004, 2009.
- [11] X. Xie and M. Jiang, "Output feedback stabilization of stochastic feedforward nonlinear time-delay systems with unknown output function," *International Journal of Robust and Nonlinear Control*, vol. 28, no. 1, pp. 266–280, 2018.
- [12] J. Eeckhout and X. Weng, "Common value experimentation," *Journal of Economic Theory*, vol. 160, pp. 317–339, 2015.
- [13] D. Applebaum, *Lévy Processes and Stochastic Calculus*, vol. 93 of *Cambridge Studies in Advanced Mathematics*, Cambridge University Press, Cambridge, UK, 2004.
- [14] G. Peskir and A. Shiryaev, *Optimal stopping and free-boundary problems*, Birkhauser Verlag, Basel, Switzerland, 2006.
- [15] J. Yong and X. Y. Zhou, *Stochastic Controls: Hamiltonian Systems and HJB Equations*, vol. 43 of *Applications of Mathematics*, Springer, New York, NY, USA, 1999.
- [16] R. S. Liptser and A. N. Shiryaev, *Statistics of Random Processes II: Applications*, vol. 6, Springer-Verlag, Berlin, 2001.

## Research Article

# Adaptive Fuzzy Output Feedback Control for Partial State Constrained Nonlinear Pure Feedback Systems

Liping Wang <sup>1</sup>, Weiwei Sun <sup>1,2</sup>, and You Wu <sup>1</sup>

<sup>1</sup>*Institute of Automation, Qufu Normal University, Qufu 273165, China*

<sup>2</sup>*School of Engineering, Qufu Normal University, Rizhao 276826, China*

Correspondence should be addressed to Weiwei Sun; [wwsun@hotmail.com](mailto:wwsun@hotmail.com)

Received 9 May 2018; Accepted 4 July 2018; Published 24 July 2018

Academic Editor: Weihai Zhang

Copyright © 2018 Liping Wang et al. This is an open access article distributed under the Creative Commons Attribution License, which permits unrestricted use, distribution, and reproduction in any medium, provided the original work is properly cited.

The adaptive fuzzy output feedback control problem for a class of pure feedback systems with partial state constraints is addressed in this paper. The fuzzy state observers are designed to estimate the unmeasured state while the fuzzy logic systems are used to approximate the unknown nonlinear functions. The proposed adaptive fuzzy output feedback controller can guarantee that the partial state constraints are not violated, and all closed-loop signals remain bounded by use of Barrier Lyapunov Functions (BLFs). A numerical example is presented to illustrate the effectiveness of the results in this paper.

## 1. Introduction

During the last decades, control design of nonlinear systems has attracted increasing interests. All kinds of control techniques have been proposed for both theoretical analysis and practical applications [1–6]. Many practical systems are inherently nonlinear and subject to many forms of constraints such as saturation and physical stoppages. Violation of the constraints may degrade the control performance and even make the system unstable. Therefore, the constraints handling in control design has attracted considerable attention [6–15]. There exist various techniques to tackle the constraints for nonlinear systems like nonlinear reference governor [7], invariance control [9], nonlinear model predictive control [11], etc.

Backstepping methodology is more effective in synthesis of robust and adaptive nonlinear controllers for various systems with parametric or dynamic nonlinearities and uncertainties [16–22]. The work in [20] constructs an adaptive tracking controller by introducing an auxiliary integrator subsystem and using the improved backstepping method such that the closed-loop system has a unique solution that is globally bounded in probability. The concept of Barrier Lyapunov Function (BLF), which is developed via Control Lyapunov Function (CLF) [23] in backstepping design

method, was first proposed in [24]. The characteristic of BLF is that it will approach infinity whenever its arguments approach some limits. Transgression of constraints can be prevented through keeping BLF bounded in the closed-loop system. BLF-based backstepping control has been applied to many constrained nonlinear systems control synthesis [25–29]. Therein, [24, 30, 31] have solved the BLF-based control problem of strict feedback nonlinear systems. The work [27] investigates the output tracking control problem of constrained nonlinear switch systems. The work [29] deals with the problem of adaptive dynamic surface control of nonlinear systems with unknown dead zone in pure feedback form. And the problem with respect to full state constraints is solved in [32, 33].

As we all know, the adaptive fuzzy control has an automatic learning capability which can adjust the adaptive parameters to deal with the uncertainty. Using the approximation property, fuzzy logic systems (FLSs) have been employed to tackle unknown nonlinear systems [26, 28, 34–36]. A control for nonlinear sampled systems with the guaranteed suboptimal performance achieved robust tracking by using fuzzy disturbance observer approach [26]. The work [34] studied an adaptive fuzzy dynamic surface control for nonlinear systems with fuzzy dead zone, unmodeled dynamics, dynamical disturbances, and

unknown control gain functions. And the unknown system functions are approximated by the Takagi-Sugeno-type fuzzy logic systems. The work [36] addressed the adaptive control problem for nonlinear pure feedback systems based on fuzzy backstepping approach. Moreover, [28] constructed the approximation-based adaptive fuzzy tracking controller for non-strict-feedback stochastic nonlinear time-delay systems. As for the adaptive fuzzy observer design, to the best of the authors' knowledge, the existing results consider only the influence of full state constraints, and there is no further discussion about partial state constraints. There is seldom adaptive control method subject to partial state constraints and unmeasured state.

In this paper, we present an adaptive fuzzy backstepping tracking controller for a class of pure feedback nonlinear systems subject to unmeasured states and unknown nonlinear function. Firstly, the fuzzy state observers are designed to estimate the unmeasured state while the fuzzy logic systems are used to approximate the unknown nonlinear functions. Secondly, the proposed adaptive fuzzy output feedback controller can guarantee that the partial state constraints are not exceeded, and all closed-loop signals remain bounded with the using of BLF while the adaptive law for the estimations on uncertain parameters is constructed. A new coordinate transform is introduced during the process. Finally, a numerical example is given to validate our results presented in this paper.

The paper is organized as follows. Section 2 presents the problem formulation and some preliminaries. The main results are proposed in Section 3. Section 4 illustrates the effectiveness of the results by a numerical example.

## 2. Problem Statement and Preliminaries

**2.1. Systems Description.** Consider the following nonlinear pure feedback systems:

$$\begin{aligned}\dot{x}_i &= x_{i+1} + f_i(\bar{x}_i, x_{i+1}), \\ \dot{x}_n &= u + f_n(\bar{x}_n, u), \\ y &= x_1,\end{aligned}\quad (1)$$

where  $\bar{x}_i = [x_1, x_2, \dots, x_i]^T \in \mathbb{R}^i$ ,  $i = 1, 2, \dots, n$ , are the state vectors of the systems,  $u$  and  $y$  are the input and output, respectively. The partition of the full states is constrained, i.e., constrained states  $x_s = [x_1, x_2, \dots, x_{n_s}]^T$  and free states  $x_r = [x_{n_s+1}, x_{n_s+2}, \dots, x_n]^T$ . And the number sequences,  $\{1, 2, \dots, n_s\}$  and  $\{n_s+1, n_s+2, \dots, n\}$ , are both ascending. The states  $x_i(t)$ ,  $i = 1, \dots, n_s$  are required to remain in the set  $|x_i| < k_{q_i}$  with  $k_{q_i}$  being positive constant,  $\forall t \geq 0$ . The nonlinear functions  $f_i(\bar{x}_i, x_{i+1})$ ,  $i = 1, 2, \dots, n-1$  and  $f_n(\bar{x}_n, u)$  are unknown nonlinear smooth functions, supposing that only the output signal is measured and other states are unmeasurable.

This paper is concerned with the problem of adaptive fuzzy output feedback control for system (1). Because of the existing unknown nonlinear functions, the fuzzy logic systems are employed to approximate the unknown nonlinear

functions, and the fuzzy state observers are designed to handle the unmeasurable states. The following lemmas and assumptions related to backstepping design are given which will be used in the further analysis in the sequel.

**Lemma 1** (see [24]). *For any positive constants  $k_b$ , let  $\mathcal{X} := \{z \in \mathbb{R}^l : |z_i| < k_b, i = 1, 2, \dots, n\} \subset \mathbb{R}^n$  and  $\mathcal{N} := \mathbb{R}^l \times \mathcal{X} \subset \mathbb{R}^{n+l}$  be open sets. Consider the system*

$$\dot{\eta} = h(t, \eta), \quad (2)$$

where  $\eta := [w, z]^T \in \mathcal{N}$  is the state, and the function  $h : \mathbb{R}_+ \times \mathcal{N} \rightarrow \mathbb{R}^{n+l}$  is piecewise continuous in  $t$  and locally Lipschitz in  $\eta$ , uniformly in  $t$ , on  $\mathbb{R}_+ \times \mathcal{N}$ . Let  $\mathcal{X}_i := \{z_i \in \mathbb{R} : |z_i| < k_b\} \subset \mathbb{R}$ . Suppose that there exist positive definite functions  $U : \mathbb{R}^l \rightarrow \mathbb{R}_+$  and  $V_i : \mathcal{X}_i \rightarrow \mathbb{R}_+$  ( $i = 1, 2, \dots, n$ ), both of which are also continuously differentiable on  $\mathbb{R}^l$  and  $\mathcal{X}_i$ , respectively, such that

$$V_i(z_i) \rightarrow \infty \quad \text{as } z_i \rightarrow \pm k_b. \quad (3)$$

Let  $V(\eta) := \sum_{i=1}^n V_i(z_i) + U(w)$  and  $z(0) \in \mathcal{X}$ . If the inequality

$$\dot{V} = \frac{\partial V}{\partial \eta} h \leq -\rho V + c, \quad (4)$$

with constants  $\rho > 0$ ,  $c > 0$ , holds in the set  $z \in \mathcal{X}$ , then  $z(t) \in \mathcal{X}$ ,  $\forall t \in [0, \infty)$ .

**Lemma 2** (see [30]). *For any positive constants  $k_b$ , positive integer  $p$ , and any  $z \in \mathbb{R}$  satisfying  $|z| < k_b$ , one has*

$$\log \frac{k_b^{2p}}{k_b^{2p} - z^{2p}} \leq \frac{z^{2p}}{k_b^{2p} - z^{2p}}. \quad (5)$$

*Proof.* We define

$$\begin{aligned}q &= \frac{z^{2p}}{k_b^{2p} - z^{2p}} - \log \frac{k_b^{2p}}{k_b^{2p} - z^{2p}} \\ &= \frac{z^{2p}}{k_b^{2p} - z^{2p}} - \log \left( 1 - \frac{z^{2p}}{k_b^{2p} - z^{2p}} \right).\end{aligned}\quad (6)$$

As  $|z| < k_b$ , we have  $|z|^{2p} < k_b^{2p}$ . Then, we can get the inequalities  $0 \leq z^{2p}/(k_b^{2p} - z^{2p}) < k_b^{2p}/(k_b^{2p} - z^{2p}) = 1 - z^{2p}/(k_b^{2p} - z^{2p})$  and  $0 \leq z^{2p}/(k_b^{2p} - z^{2p}) < 1/2$ . Let  $\varsigma = z^{2p}/(k_b^{2p} - z^{2p})$  and then  $q = -\log(1-\varsigma) + \varsigma$ . The derivative of  $q$  is given as  $\dot{q} = (2-\varsigma)/(1-\varsigma) > 0$ . It shows that  $q$  is continuously increasing and the minimum of  $q$  is  $q_{\min} = 0$ . Thus, we get  $\log(k_b^{2p}/(k_b^{2p} - z^{2p})) \leq z^{2p}/(k_b^{2p} - z^{2p})$ , and  $\log(k_b^{2p}/(k_b^{2p} - z^{2p})) = z^{2p}/(k_b^{2p} - z^{2p})$  if and only if  $z = 0$ .  $\square$

**Lemma 3** (see [37]). *Let  $f(x)$  be a continuous function defined on a compact set  $\Omega$ , and, for any constant  $\varepsilon > 0$ , there exists fuzzy logic system (12) such as*

$$f(x) = \hat{f}(x | \theta) + \varepsilon(x), \quad |\varepsilon(x)| \leq \varepsilon. \quad (7)$$

**Lemma 4** (see [31]). For any  $\beta \in \mathbb{R}^n$  and  $\vartheta > 0$ , the following inequality holds:

$$0 < |\beta| - \beta \tanh\left(\frac{\beta}{\vartheta}\right) \leq \mu\vartheta, \quad \mu = 0.2785. \quad (8)$$

**Assumption 5** (see [24]). For any  $k_{c_i} > 0$ , there exist positive constants  $A_0, Y_1, Y_2, \dots, Y_n$  such that the desired trajectory  $y_d(t)$  and its time derivatives satisfy  $|y_d(t)| \leq A_0 < k_{c_i}$  and  $|y_d^{(i)}(t)| < Y_i$ ,  $i = 1, 2, \dots, n$ , for all  $t \geq 0$ .

**Assumption 6.** There exist known constants  $m_i > 0$  such that

$$|f_i(x_1) - f_i(x_2)| \leq m_i \|x_1 - x_2\|, \quad i = 1, 2, \dots, n. \quad (9)$$

Rewrite (1) as

$$\begin{aligned} \dot{\hat{x}}_i &= x_{i+1} + f_i(\hat{x}_i, \hat{x}_{i+1,f}) + \Delta f_i, \\ \dot{\hat{x}}_n &= u + f_n(\hat{x}_n, u_f) + \Delta f_n, \\ y &= x_1, \end{aligned} \quad (10)$$

where  $\Delta f_i = f_i(\bar{x}_i, x_{i+1}) - f_i(\hat{x}_i, \hat{x}_{i+1,f})$ ,  $i = 1, 2, \dots, n-1$ ,  $\Delta f_n = f_n(\bar{x}_n, u) - f_n(\hat{x}_n, u_f)$ .  $\hat{x}_i$  are the estimates of  $\bar{x}_i$ , which will be obtained by the state observer designed later;  $\hat{x}_{i+1,f}$  and  $u_f$  are the filtered signals for  $\hat{x}_{i+1}$  and  $u$ , respectively. There exist known constants  $\tau_i$ ,  $i = 1, 2, \dots, n$ , such that  $|\hat{x}_{i+1} - \hat{x}_{i+1,f}| \leq \tau_{i+1}$  ( $\tau_1 = 0$ ). The filtered signals are defined as follows:

$$\begin{aligned} \hat{x}_{i,f} &= H_L(s) \hat{x}_i, \\ u_f &= H_L(s) u, \end{aligned} \quad (11)$$

where  $H_L(s)$  is a Butterworth low-pass filter (LPF) [26, 36, 38] with the cutoff frequency  $\omega_c = 1$  rad/s for different values of  $n$ .

**Remark 7.** The filtered signals  $\hat{x}_{i+1,f}$  and  $u_f$  are employed to avoid the so-called algebraic loop problem existing in [29, 39] and to design the state observer and controller for nonlinear pure feedback systems.

**Remark 8.** Based on the statements in [26, 36, 38], most actuators have low-pass property and the replacements  $\hat{x}_{i,f} \approx \hat{x}_i$  and  $u_f \approx u$  are reasonable in the controller design. Therefore, assume that  $|\hat{x}_i - \hat{x}_{i,f}| \leq \tau_i$  with  $\tau_i$  being known constants.

Then (10) can be further rewritten into the following state space form:

$$\begin{aligned} \dot{x} &= Ax + Ky + \sum_{i=1}^{n-1} B_i (f_i(\hat{x}_i, \hat{x}_{i+1,f}) + \Delta f_i) \\ &\quad + B_n (f_n(\hat{x}_n, u_f) + \Delta f_n + u), \end{aligned} \quad (12)$$

where  $x = \begin{bmatrix} x_1 \\ \vdots \\ x_n \end{bmatrix}$ ,  $A = \begin{bmatrix} -k_1 & & & \\ \vdots & I & & \\ -k_n & 0 & \dots & 0 \end{bmatrix}$ ,  $K = \begin{bmatrix} k_1 \\ \vdots \\ k_n \end{bmatrix}$ ,  $B_i = \begin{bmatrix} 0 \\ \vdots \\ 1 \\ \vdots \\ 0 \end{bmatrix}$ ,  $B_n = \begin{bmatrix} 0 \\ \vdots \\ 1 \end{bmatrix}$ . The vector  $K$  is chosen to make matrix  $A$  to

be a strict Hurwitz matrix; i.e., for given a matrix  $Q = Q^T > 0$  there exists a matrix  $P = P^T > 0$  satisfying

$$A^T P + PA = -2Q. \quad (13)$$

**2.2. Design of FLSs and State Observer.** To tackle the unknown nonlinear functions, the fuzzy logic systems are introduced as follows.

Rule  $j$ : if  $x_1$  is  $N_{j_1}$ , and  $x_2$  is  $N_{j_2}$  and  $\dots$  and  $x_n$  is  $N_{j_n}$ , then

$$y(x) \text{ is } M_j, \quad j = 1, 2, \dots, m, \quad (14)$$

where  $y$  is the output of the system,  $N_{j_i}$  and  $M_j$  denote fuzzy sets, and  $m$  represents the number of fuzzy rules.

By using the singleton fuzzifier, center average defuzzification and product inference [25, 28], the final output can be expressed as follows:

$$y(x) = \frac{\sum_{j=1}^m \tilde{y}_j \prod_{l=1}^n \mu_{N_{j_l}}(x_l)}{\sum_{j=1}^m \prod_{l=1}^n \mu_{N_{j_l}}(x_l)}, \quad (15)$$

where  $\tilde{y}_j = \max_{y \in R} \mu_{M_j}(y)$ ;  $\mu_{N_{j_i}}(x_l)$  and  $\mu_{M_j}(y)$  stand for membership functions with respect to fuzzy sets  $N_{j_i}$  and  $M_j$ , respectively.

Define

$$\varphi(x) = \frac{\prod_{l=1}^n \mu_{N_{j_l}}(x_l)}{\sum_{j=1}^m \prod_{l=1}^n \mu_{N_{j_l}}(x_l)} \quad (16)$$

as the basis function vector. The ideal constant weight vector is  $[\tilde{y}_1, \tilde{y}_2, \dots, \tilde{y}_m]^T = [\theta_1, \theta_2, \dots, \theta_m]^T$ ,  $\varphi(x) = [\varphi_1(x), \varphi_2(x), \dots, \varphi_m(x)]^T$ , and  $\varphi_i(x)$  is chosen as Gaussian function; i.e., for  $i = 1, 2, \dots, m$ ,

$$\varphi_i(x) = \exp\left[-\frac{(x - \mu_i)^T (x - \mu_i)}{\eta_i^2}\right], \quad (17)$$

where  $\mu_i = [\mu_{i_1}, \mu_{i_2}, \dots, \mu_{i_n}]^T$  is the center vector, and  $\eta_i$  is the width of the Gaussian function.

Then, the fuzzy output  $y$  in (15) is described as

$$y(x) = \theta^T \varphi(x). \quad (18)$$

Accordingly, assume that the unknown nonlinear functions in (1) are approximated by the following fuzzy logic systems:

$$\hat{f}_i(\hat{x}_i, \hat{x}_{i+1,f} | \hat{\theta}_i) = \hat{\theta}_i^T \varphi_i(\hat{x}_i, \hat{x}_{i+1,f}), \quad 1 \leq i \leq n, \quad (19)$$

where  $\hat{x}_{n+1,f} = u_f$ . The optimal weight vector  $\theta_i^*$  is defined as

$$\begin{aligned} \theta_i^* &= \arg \min_{\theta_i \in \Omega_i} \sup_{(\hat{x}_i, \hat{x}_{i+1,f}) \in U_{i1} \times U_{i2}} \left[ \hat{f}_i(\hat{x}_i, \hat{x}_{i+1,f} | \hat{\theta}_i) \right. \\ &\quad \left. - \hat{f}_i(\hat{x}_i, \hat{x}_{i+1,f} | \theta_i^*) \right], \end{aligned} \quad (20)$$

where  $\Omega_i$  and  $U_{i1} \times U_{i2}$  are compact regions for  $\theta_i$  and  $(\widehat{x}_i, \widehat{x}_{i+1,f})$ , respectively.

Define

$$f_i(x) = \theta_i^{*T} \varphi_i(x) + \varepsilon_i(x) = \widehat{\theta}_i^T \varphi_i(x) + \delta_i(x), \quad (21)$$

where  $\varepsilon_i^*$  and  $\delta_i^*$  ( $i = 1, 2, \dots, n$ ) are known constants satisfying  $|\varepsilon_i| \leq \varepsilon_i^*$  and  $|\delta_i| \leq \delta_i^*$ . Letting  $w_i = \varepsilon_i - \delta_i$ ,  $i = 1, 2, \dots, n$ , it is clear that there is an unknown constant  $w_i^* > 0$  such that  $|w_i| \leq w_i^* = \varepsilon_i^* + \delta_i^*$ .

Based on (12), design a fuzzy state observer as

$$\begin{aligned} \dot{\widehat{x}}_i &= \widehat{x}_{i+1} + \widehat{f}_i(\widehat{x}_i, \widehat{x}_{i+1,f}) + k_i(y - \widehat{x}_1), \\ \dot{\widehat{x}}_n &= u + \widehat{f}_n(\widehat{x}_n, u_f) + k_n(y - \widehat{x}_1), \\ y &= x_1. \end{aligned} \quad (22)$$

Let  $e_i = x_i - \widehat{x}_i$  be an observer error vector. Then from (12) and (22), we have

$$\dot{e} = Ae + \delta + \Delta F, \quad (23)$$

where  $\delta = [\delta_1, \delta_2, \dots, \delta_n]^T$  and  $\Delta F = [\Delta f_1, \Delta f_2, \dots, \Delta f_n]^T$ . Substituting (23) into (22), we have

$$\begin{aligned} \dot{e}_i &= Ae + \delta + \Delta F, \\ \dot{\widehat{x}}_i &= \widehat{x}_{i+1} + \widehat{f}_i(\widehat{x}_i, \widehat{x}_{i+1,f}) + k_i e_1, \\ \dot{\widehat{x}}_n &= u + \widehat{f}_n(\widehat{x}_n, u_f) + k_n e_1, \\ y &= x_1. \end{aligned} \quad (24)$$

Consider the following Lyapunov function candidate:

$$V_0 = \frac{1}{2} e^T P e. \quad (25)$$

Computing the time derivative of  $V_0$ , one has

$$\dot{V}_0 = e^T P \dot{e} = e^T P (Ae + \delta + \Delta F). \quad (26)$$

According to Assumption 6, we get

$$\begin{aligned} \Delta f_i &= |f_i(\bar{x}_i, x_{i+1}) - f_i(\widehat{x}_i, \widehat{x}_{i+1,f})| \\ &\leq m_i \|e\|^2 + m_i |\widehat{x}_{i+1} - \widehat{x}_{i+1,f}| \leq m_i \|e\|^2 + m_i \tau_{i+1} \\ &= m_i \|e\|^2 + \tau'_{i+1}, \end{aligned} \quad (27)$$

where  $\tau'_{i+1} = m_i \tau_{i+1}$ . It is clear that

$$\begin{aligned} \|\Delta F\|^2 &\leq nm^2 \|e\|^2 + \left( \sum_{i=2}^{n+1} \tau'_i \right)^2, \\ e^T P \Delta F &\leq \eta \|P\|^2 \|e\|^2 + \frac{1}{4\eta} nm^2 \|e\|^2 + \eta \|P\|^2 \|e\|^2 \\ &\quad + \frac{1}{4\eta} \left( \sum_{i=2}^{n+1} \tau'_i \right)^2 \\ &\leq 2\eta \|P\|^2 \|e\|^2 + \frac{1}{4\eta} nm^2 \|e\|^2 \\ &\quad + \frac{1}{4\eta} \left( \sum_{i=2}^{n+1} \tau'_i \right)^2. \end{aligned} \quad (28)$$

Using Young's inequality and (28), we get

$$\begin{aligned} \dot{V}_0 &\leq -\lambda_{\min}(Q) \|e\|^2 + \xi \|P\|^2 \|e\|^2 + \frac{1}{4\xi} \|\delta^*\|^2 \\ &\quad + 2\eta \|P\|^2 \|e\|^2 + \frac{1}{4\eta} nm^2 \|e\|^2 + \frac{1}{4\eta} \left( \sum_{i=2}^{n+1} \tau'_i \right)^2. \end{aligned} \quad (29)$$

To simplify the notation, let  $\dot{V}_0 \triangleq -p_0 \|e\|^2 + E_0$ , where  $-p_0 = -\lambda_{\min}(Q) + \xi \|P\|^2 + 2\eta \|P\|^2 + (1/4\eta) nm^2$ ,  $E_0 = (1/4\xi) \|\delta^*\|^2 + (1/4\eta) (\sum_{i=2}^{n+1} \tau'_i)^2$ .

### 3. Main Results

In this section, we propose a generalised design to deal with partial state constraint and the adaptive fuzzy output feedback controller which based on the backstepping technique and fuzzy state observer will be proposed. To guarantee the system performance, the virtual control signals and adaptive laws are designed. A new design procedure is presented which may cover some results related to the full state constraint [37]. To ensure that  $x_i$  remains in the constrained region, we give the feasibility conditions with respect to the design parameters and an initial state region, i.e.,  $x(0) \in \Omega_{x(0)}$ , where  $\Omega_{x(0)} := \{x \in \mathbb{R}^n : -a_i \leq x_i \leq b_i, i = 1, 2, \dots, n\}$  with  $a_i < k_{c_i}$  and  $b_i < k_{c_i}$ .

Let the tracking error

$$z_1 = y - y_d \quad (30)$$

and the variables

$$z_i = \widehat{x}_i - \alpha_{i-1}, \quad i = 2, \dots, n, \quad (31)$$

where  $\alpha_{i-1}$  is a virtual controller to be designed in Step  $i$ .

Define  $K_{z_i} = z_i/(k_{b_i}^2 - z_i^2)$ ,  $k_{b_i} = k_{c_i} - Y_0$  and  $\Omega_{z_i} = \{|z_i| < k_{b_i}, i = 1, 2, \dots, n\}$ . Consider the BLF candidate combined with quadratic Lyapunov function as

$$V_n = V_0 + \sum_{i=1}^{n_s} \frac{1}{2} \log \frac{k_{b_i}^2}{k_{b_i}^2 - z_i^2} + \sum_{i=1}^n \frac{1}{2\gamma_i} \tilde{\theta}_i^T \tilde{\theta}_i + \frac{1}{2\gamma_1} \tilde{\varepsilon}_1^2 + \sum_{i=2}^n \frac{1}{2\gamma_i} \tilde{w}_i^2 + U, \quad (32)$$

where  $U = \sum_{j=n_s+1}^n (1/2)z_j^2$ ,  $j = n_s + 1, \dots, n$ , and  $\log(*)$  stands for the natural logarithm of  $*$ .  $\gamma_1, \gamma_i, \bar{\gamma}_1$ , and  $\bar{\gamma}_i$  are positive constants. It can be proved that  $V_n$  is continuously differentiable and positive definite on  $\Omega_{z_i}$ .

The detailed design procedures are given below.

*Step 1.* According to (19), (21), (24), and (30), the derivative of  $z_1$  is calculated as follows:

$$\dot{z}_1 = \dot{y} - \dot{y}_d = z_2 + \alpha_1 + \theta_1^* \varphi_1 + \varepsilon_1(x) + \Delta F_1 - \dot{y}_d. \quad (33)$$

The Lyapunov function is defined as

$$V_1 = V_0 + \frac{1}{2} \log \frac{k_{b_1}^2}{k_{b_1}^2 - z_1^2} + \frac{1}{2\gamma_1} \tilde{\theta}_1^T \tilde{\theta}_1 + \frac{1}{2\gamma_1} \tilde{\varepsilon}_1^2. \quad (34)$$

Then, substituting (33) into (34), one can have

$$\begin{aligned} \dot{V}_1 &= \dot{V}_0 + \frac{z_1 \dot{z}_1}{k_{b_1}^2 - z_1^2} - \frac{1}{\gamma_1} \tilde{\theta}_1^T \dot{\tilde{\theta}}_1 - \frac{1}{\gamma_1} \tilde{\varepsilon}_1 \dot{\tilde{\varepsilon}}_1 \\ &= \dot{V}_0 + K_{z_1} (z_2 + \alpha_1 + \theta_1^{*T} \varphi_1 + \varepsilon_1(x) + \Delta F_1 - \dot{y}_d) \\ &\quad - \frac{1}{\gamma_1} \tilde{\theta}_1^T \dot{\tilde{\theta}}_1 - \frac{1}{\gamma_1} \tilde{\varepsilon}_1 \dot{\tilde{\varepsilon}}_1. \end{aligned} \quad (35)$$

Design a virtual controller  $\alpha_1$ , adaptive law  $\dot{\tilde{\theta}}_1$ , and  $\dot{\tilde{\varepsilon}}_1$  as

$$\begin{aligned} \alpha_1 &= -\lambda_1 z_1 - \tilde{\theta}_1^T \varphi_1 + \dot{y}_d - \hat{\varepsilon}_1 \tanh\left(\frac{K_{z_1}}{k}\right) - \frac{1}{2} K_{z_1}, \\ \dot{\tilde{\theta}}_1 &= -\sigma_1 \tilde{\theta}_1 + \gamma_1 K_{z_1} \varphi_1, \\ \dot{\tilde{\varepsilon}}_1 &= -\bar{\sigma}_1 \tilde{\varepsilon}_1 + \bar{\gamma}_1 K_{z_1} \tanh\left(\frac{K_{z_1}}{k}\right), \end{aligned} \quad (36)$$

where  $\hat{\theta}_1$  is the estimation of  $\theta_1^*$  and  $\tilde{\theta}_j = \theta_j^* - \hat{\theta}_j$ ,  $\tilde{\varepsilon}_1 = \varepsilon_1^* - \hat{\varepsilon}_1$ ,  $\sigma_1, \bar{\sigma}_1$ , and  $k$  are the positive constants to be designed, respectively. Substituting (36) into (35), it yields

$$\begin{aligned} \dot{V}_1 &= \dot{V}_0 + K_{z_1} (z_2 + \alpha_1 + \theta_1^{*T} \varphi_1 + \varepsilon_1(x) + \Delta F_1 - \dot{y}_d) \\ &\quad - \frac{1}{\gamma_1} \tilde{\theta}_1^T (-\sigma_1 \tilde{\theta}_1 + \gamma_1 K_{z_1} \varphi_1) \\ &\quad - \frac{1}{\bar{\gamma}_1} \tilde{\varepsilon}_1 \left( -\bar{\sigma}_1 \tilde{\varepsilon}_1 + \bar{\gamma}_1 K_{z_1} \tanh\left(\frac{K_{z_1}}{k}\right) \right) \\ &= \dot{V}_0 + K_{z_1} \left( z_2 - \lambda_1 z_1 - \frac{1}{2} K_{z_1} + \Delta F_1 \right) \\ &\quad + \varepsilon_1(x) K_{z_1} - \varepsilon_1^* K_{z_1} \tanh\left(\frac{K_{z_1}}{k}\right) + \frac{\sigma_1}{\gamma_1} \tilde{\theta}_1^T \tilde{\theta}_1 \\ &\quad + \frac{\bar{\sigma}_1}{\bar{\gamma}_1} \tilde{\varepsilon}_1 \tilde{\varepsilon}_1 \\ &\leq \dot{V}_0 + K_{z_1} \left( z_2 - \lambda_1 z_1 - \frac{1}{2} K_{z_1} + \Delta F_1 \right) \\ &\quad + 0.2785k\varepsilon_1^* + \frac{\sigma_1}{\gamma_1} \tilde{\theta}_1^T \tilde{\theta}_1 + \frac{\bar{\sigma}_1}{\bar{\gamma}_1} \tilde{\varepsilon}_1 \tilde{\varepsilon}_1. \end{aligned} \quad (37)$$

*Step i* ( $i = 2, 3, \dots, n_s$ ). The derivative of  $z_i$  is calculated as follows:

$$\begin{aligned} \dot{z}_i &= \dot{\hat{x}}_i - \dot{\alpha}_{i-1} \\ &= z_{i+1} + \alpha_i + \theta_i^* \varphi_i + w_i(x) + k_i e_1 - \dot{\alpha}_{i-1}. \end{aligned} \quad (38)$$

Choose the following Lyapunov function candidates:

$$V_i = V_{i-1} + \frac{1}{2} \log \frac{k_{b_i}^2}{k_{b_i}^2 - z_i^2} + \frac{1}{2\gamma_i} \tilde{\theta}_i^T \tilde{\theta}_i + \frac{1}{2\gamma_i} \tilde{w}_i^2, \quad (39)$$

where  $\tilde{w}_i = w_i^* - \hat{w}_i$ . Similar to (35), one can have

$$\begin{aligned} \dot{V}_i &= \dot{V}_{i-1} + \frac{z_i \dot{z}_i}{k_{b_i}^2 - z_i^2} - \frac{1}{\gamma_i} \tilde{\theta}_i^T \dot{\tilde{\theta}}_i - \frac{1}{\gamma_i} \tilde{w}_i \dot{\tilde{w}}_i \\ &= \dot{V}_{i-1} - \frac{1}{\gamma_i} \tilde{\theta}_i^T \dot{\tilde{\theta}}_i - \frac{1}{\gamma_i} \tilde{w}_i \dot{\tilde{w}}_i \\ &\quad + K_{z_i} (z_{i+1} + \alpha_i + \theta_i^* \varphi_i + w_i(x) + k_i e_1 - \dot{\alpha}_{i-1}). \end{aligned} \quad (40)$$

The virtual controller  $\alpha_i$ , adaptive law  $\dot{\tilde{\theta}}_i$ , and  $\dot{\tilde{w}}_i$  are designed as

$$\begin{aligned} \alpha_i &= -\lambda_i z_i - \tilde{\theta}_i^T \varphi_i - k_i e_1 + \dot{\alpha}_{i-1} - \hat{w}_i \tanh\left(\frac{K_{z_i}}{k}\right) \\ &\quad - \frac{K_{z_{i-1}} z_i}{K_{z_i}}, \\ \dot{\tilde{\theta}}_i &= -\sigma_i \tilde{\theta}_i + \gamma_i K_{z_i} \varphi_i, \\ \dot{\tilde{w}}_i &= -\bar{\sigma}_i \tilde{w}_i + \bar{\gamma}_i K_{z_i} \tanh\left(\frac{K_{z_i}}{k}\right), \end{aligned} \quad (41)$$

where  $\sigma_i$  and  $\bar{\sigma}_i$  are positive constants. Substituting (41) into (40), the following inequality can be obtained:

$$\begin{aligned} \dot{V}_i &= \dot{V}_{i-1} - \frac{1}{\gamma_i} \bar{w}_i \left( -\bar{\sigma}_i \hat{w}_i + \bar{\gamma}_i K_{z_i} \tanh \left( \frac{K_{z_i}}{k} \right) \right) \\ &\quad + K_{z_i} (z_{i+1} + \alpha_i + \theta_i^* \varphi_i + w_i(x) + k_i e_1 - \dot{\alpha}_{i-1}) \\ &\quad - \frac{1}{\gamma_i} \bar{\theta}_i^T (-\sigma_i \hat{\theta}_i + \gamma_i K_{z_i} \varphi_i) \\ &\leq \dot{V}_0 + K_{z_i} z_{i+1} - \sum_{r=1}^i \lambda_r K_{z_r} z_r + \frac{1}{2} \Delta F_1^2 + 0.2785 k \varepsilon_1^* \\ &\quad + 0.2785 k \sum_{r=2}^i w_r^* + \sum_{r=1}^i \frac{\sigma_r}{\gamma_r} \bar{\theta}_r^T \hat{\theta}_r + \frac{\bar{\sigma}_1}{\gamma_1} \bar{\varepsilon}_1 \hat{\varepsilon}_1 \\ &\quad + \sum_{r=2}^i \frac{\bar{\sigma}_r}{\gamma_r} \bar{w}_r \hat{w}_r. \end{aligned} \quad (42)$$

Step  $n_s + 1$ . The derivative of  $z_{n_s+1}$  is calculated as follows:

$$\begin{aligned} \dot{z}_{n_s+1} &= \dot{\hat{x}}_{n_s+1} - \dot{\alpha}_{n_s} \\ &= z_{n_s+2} + \alpha_{n_s+1} + \theta_{n_s+1}^* \varphi_{n_s+1} + w_{n_s+1}(x) \\ &\quad + k_{n_s+1} e_1 - \dot{\alpha}_{n_s}. \end{aligned} \quad (43)$$

The Lyapunov function is chosen as

$$\begin{aligned} V_{n_s+1} &= V_{n_s} + \frac{1}{2} z_{n_s+1}^2 + \frac{1}{2\gamma_{n_s+1}} \bar{\theta}_{n_s+1}^T \bar{\theta}_{n_s+1} \\ &\quad + \frac{1}{2\bar{\gamma}_{n_s+1}} \bar{w}_{n_s+1}^2. \end{aligned} \quad (44)$$

Then, we have

$$\begin{aligned} \dot{V}_{n_s+1} &= \dot{V}_{n_s} + z_{n_s+1} \dot{z}_{n_s+1} - \frac{1}{\gamma_{n_s+1}} \bar{\theta}_{n_s+1}^T \dot{\bar{\theta}}_{n_s+1} - \frac{1}{\bar{\gamma}_{n_s+1}} \\ &\quad \cdot \bar{w}_{n_s+1} \dot{\bar{w}}_{n_s+1} = \dot{V}_{n_s} + z_{n_s+1} (z_{n_s+2} + \alpha_{n_s+1} \\ &\quad + \theta_{n_s+1}^* \varphi_{n_s+1} + w_{n_s+1}(x) + k_{n_s+1} e_1 - \dot{\alpha}_{n_s}) - \frac{1}{\gamma_{n_s+1}} \\ &\quad \cdot \bar{\theta}_{n_s+1}^T \dot{\bar{\theta}}_{n_s+1} - \frac{1}{\bar{\gamma}_{n_s+1}} \bar{w}_{n_s+1} \dot{\bar{w}}_{n_s+1}. \end{aligned} \quad (45)$$

Design a virtual controller  $\alpha_{n_s+1}$ , adaptive law  $\dot{\bar{\theta}}_{n_s+1}$ , and  $\dot{\bar{w}}_{n_s+1}$  as

$$\begin{aligned} \alpha_{n_s+1} &= -\lambda_{n_s+1} z_{n_s+1} - \bar{\theta}_{n_s+1}^T \varphi_{n_s+1} - k_{n_s+1} e_1 + \dot{\alpha}_{n_s} \\ &\quad - \bar{w}_{n_s+1} \tanh \left( \frac{z_{n_s+1}}{k} \right) - K_{z_{n_s}}, \\ \dot{\bar{\theta}}_{n_s+1} &= -\sigma_{n_s+1} \bar{\theta}_{n_s+1} + \gamma_{n_s+1} z_{n_s+1} \varphi_{n_s+1}, \\ \dot{\bar{w}}_{n_s+1} &= -\bar{\sigma}_{n_s+1} \bar{w}_{n_s+1} + \bar{\gamma}_{n_s+1} z_{n_s+1} \tanh \left( \frac{z_{n_s+1}}{k} \right). \end{aligned} \quad (46)$$

Substituting (46) into (45), the following inequality is obtained:

$$\begin{aligned} \dot{V}_{n_s+1} &= \dot{V}_{n_s} + z_{n_s+1} (z_{n_s+2} + \alpha_{n_s+1} + \theta_{n_s+1}^* \varphi_{n_s+1} \\ &\quad + w_{n_s+1}(x) + k_{n_s+1} e_1 - \dot{\alpha}_{n_s}) - \frac{1}{\bar{\gamma}_{n_s+1}} \\ &\quad \cdot \bar{w}_{n_s+1} \left( -\bar{\sigma}_{n_s+1} \bar{w}_{n_s+1} + \bar{\gamma}_{n_s+1} z_{n_s+1} \tanh \left( \frac{z_{n_s+1}}{k} \right) \right) \\ &\quad - \frac{1}{\gamma_{n_s+1}} \bar{\theta}_{n_s+1}^T (-\sigma_{n_s+1} \bar{\theta}_{n_s+1} + \gamma_{n_s+1} z_{n_s+1} \varphi_{n_s+1}) \leq \dot{V}_0 \\ &\quad + z_{n_s+1} z_{n_s+2} - \sum_{r=1}^{n_s} \lambda_r K_{z_r} z_r - \lambda_{n_s+1} z_{n_s+1}^2 + \frac{1}{2} \Delta F_1^2 \\ &\quad + 0.2785 k \varepsilon_1^* + 0.2785 k \sum_{r=2}^{n_s+1} w_r^* + \sum_{r=1}^{n_s+1} \frac{\sigma_r}{\gamma_r} \bar{\theta}_r^T \hat{\theta}_r + \frac{\bar{\sigma}_1}{\gamma_1} \\ &\quad \cdot \bar{\varepsilon}_1 \hat{\varepsilon}_1 + \sum_{r=2}^{n_s+1} \frac{\bar{\sigma}_r}{\gamma_r} \bar{w}_r \hat{w}_r. \end{aligned} \quad (47)$$

Step  $j$  ( $j = n_s + 2, \dots, n-1$ ). The derivative of  $z_j$  is calculated as follows:

$$\begin{aligned} \dot{z}_j &= \dot{\hat{x}}_j - \dot{\alpha}_{j-1} \\ &= z_{j+1} + \alpha_j + \theta_j^* \varphi_j + w_j(x) + k_j e_1 - \dot{\alpha}_{j-1}. \end{aligned} \quad (48)$$

The Lyapunov function is defined as

$$V_j = V_{j-1} + \frac{1}{2} z_j^2 + \frac{1}{2\gamma_j} \bar{\theta}_j^T \bar{\theta}_j + \frac{1}{2\bar{\gamma}_j} \bar{w}_j^2. \quad (49)$$

Then, one can have

$$\begin{aligned} \dot{V}_j &= \dot{V}_{j-1} + z_j \dot{z}_j - \frac{1}{\gamma_j} \bar{\theta}_j^T \dot{\bar{\theta}}_j - \frac{1}{\bar{\gamma}_j} \bar{w}_j \dot{\bar{w}}_j \\ &= \dot{V}_{j-1} - \frac{1}{\gamma_j} \bar{\theta}_j^T \dot{\bar{\theta}}_j - \frac{1}{\bar{\gamma}_j} \bar{w}_j \dot{\bar{w}}_j \\ &\quad + z_j (z_{j+1} + \alpha_j + \theta_j^* \varphi_j + w_j(x) + k_j e_1 - \dot{\alpha}_{j-1}). \end{aligned} \quad (50)$$

Design a virtual controller  $\alpha_{s+1}$ , adaptive law  $\dot{\bar{\theta}}_{s+1}$ , and  $\dot{\bar{w}}_{s+1}$  as

$$\begin{aligned} \alpha_j &= -\lambda_j z_j - \bar{\theta}_j^T \varphi_j - k_j e_1 + \dot{\alpha}_{j-1} - \bar{w}_j \tanh \left( \frac{z_j}{k} \right) \\ &\quad - z_{j-1}, \\ \dot{\bar{\theta}}_j &= -\sigma_j \bar{\theta}_j + \gamma_j z_j \varphi_j, \\ \dot{\bar{w}}_j &= -\bar{\sigma}_j \bar{w}_j + \bar{\gamma}_j z_j \tanh \left( \frac{z_j}{k} \right). \end{aligned} \quad (51)$$

Substituting (51) into (50), the following inequality can be obtained:

$$\begin{aligned}
 \dot{V}_j &= \dot{V}_{j-1} - \frac{1}{\gamma_j} \tilde{\theta}_j^T (-\sigma_j \hat{\theta}_j + \gamma_j z_j \varphi_j) \\
 &\quad + z_j (z_{j+1} + \alpha_j + \theta_j^* \varphi_j + w_j(x) + k_j e_1 - \dot{\alpha}_{j-1}) \\
 &\quad - \frac{1}{\gamma_j} \tilde{w}_j (-\bar{\sigma}_j \hat{w}_j + \bar{\gamma}_j z_j \tanh\left(\frac{z_j}{k}\right)) \\
 &\leq \dot{V}_0 + z_j z_{j+1} - \sum_{r=1}^{n_s} \lambda_r K_{z_r} z_r - \sum_{r=n_s+1}^j \lambda_r z_r^2 + \frac{1}{2} \Delta F_1^2 \\
 &\quad + 0.2785 k \varepsilon_1^* + 0.2785 k \sum_{r=2}^j w_r^* + \sum_{r=1}^j \frac{\sigma_r}{\gamma_r} \tilde{\theta}_r^T \hat{\theta}_r \\
 &\quad + \frac{\bar{\sigma}_1}{\bar{\gamma}_1} \tilde{\varepsilon}_1 \hat{\varepsilon}_1 + \sum_{r=2}^j \frac{\bar{\sigma}_r}{\bar{\gamma}_r} \tilde{w}_r \hat{w}_r.
 \end{aligned} \tag{52}$$

*Step n.* The derivative of  $z_n$  is calculated as follows:

$$\dot{z}_n = \dot{\hat{x}}_n - \dot{\alpha}_{n-1} = u + \theta_n^* \varphi_n + w_n(x) + k_n e_1 - \dot{\alpha}_{n-1}. \tag{53}$$

Define the Lyapunov function as

$$V_n = V_{n-1} + \frac{1}{2} z_n^2 + \frac{1}{2\gamma_n} \tilde{\theta}_n^T \tilde{\theta}_n + \frac{1}{2\bar{\gamma}_n} \tilde{w}_n^2. \tag{54}$$

Then, one can have

$$\begin{aligned}
 \dot{V}_n &= \dot{V}_{n-1} + z_n \dot{z}_n - \frac{1}{\gamma_n} \tilde{\theta}_n^T \dot{\tilde{\theta}}_n - \frac{1}{\bar{\gamma}_n} \tilde{w}_n \dot{\tilde{w}}_n \\
 &= \dot{V}_{n-1} + z_n (u + \theta_n^* \varphi_n + w_n(x) + k_n e_1 - \dot{\alpha}_{n-1}) \\
 &\quad - \frac{1}{\gamma_n} \tilde{\theta}_n^T \dot{\tilde{\theta}}_n - \frac{1}{\bar{\gamma}_n} \tilde{w}_n \dot{\tilde{w}}_n.
 \end{aligned} \tag{55}$$

We choose the control law and the adaptive laws as

$$\begin{aligned}
 u &= -\lambda_n z_n - \tilde{\theta}_n^T \varphi_n - k_n e_1 + \dot{\alpha}_{n-1} - \hat{w}_n \tanh\left(\frac{z_n}{k}\right) \\
 &\quad - z_{n-1}, \\
 \dot{\hat{\theta}}_n &= -\sigma_n \hat{\theta}_n + \gamma_n z_n \varphi_n, \\
 \dot{\hat{w}}_n &= -\bar{\sigma}_n \hat{w}_n + \bar{\gamma}_n z_n \tanh\left(\frac{z_n}{k}\right).
 \end{aligned} \tag{56}$$

Substituting (56) into (55), the following equality can be obtained:

$$\begin{aligned}
 \dot{V}_n &= \dot{V}_{n-1} + z_n (u + \theta_n^* \varphi_n + w_n(x) + k_n e_1 - \dot{\alpha}_{n-1}) \\
 &\quad - \frac{1}{\gamma_n} \tilde{w}_n (-\bar{\sigma}_n \hat{w}_n + \bar{\gamma}_n z_n \tanh\left(\frac{z_n}{k}\right)) \\
 &\quad - \frac{1}{\gamma_n} \tilde{\theta}_n^T (-\sigma_n \hat{\theta}_n + \gamma_n z_n \varphi_n) \\
 &\leq \dot{V}_0 - \sum_{r=1}^{n_s} \lambda_r K_{z_r} z_r - \sum_{r=n_s+1}^n \lambda_r z_r^2 + \frac{1}{2} \Delta F_1^2 \\
 &\quad + 0.2785 k \varepsilon_1^* + 0.2785 k \sum_{r=2}^n w_r^* + \sum_{r=1}^n \frac{\sigma_r}{\gamma_r} \tilde{\theta}_r^T \hat{\theta}_r \\
 &\quad + \frac{\bar{\sigma}_1}{\bar{\gamma}_1} \tilde{\varepsilon}_1 \hat{\varepsilon}_1 + \sum_{r=2}^n \frac{\bar{\sigma}_r}{\bar{\gamma}_r} \tilde{w}_r \hat{w}_r.
 \end{aligned} \tag{57}$$

According to Young's inequality, we have

$$\frac{\sigma_i}{\gamma_i} \tilde{\theta}_i^T \hat{\theta}_i = \frac{\sigma_i}{\gamma_i} \tilde{\theta}_i^T (\theta_i^* - \tilde{\theta}_i) \leq \frac{\sigma_i}{2\gamma_i} (\theta_i^{*T} \theta_i^* - \tilde{\theta}_i^T \tilde{\theta}_i). \tag{58}$$

Then, the derivative of  $V_n$  is given by

$$\begin{aligned}
 \dot{V}_n &\leq \dot{V}_0 - \sum_{r=1}^{n_s} \lambda_r K_{z_r} z_r - \sum_{r=n_s+1}^n \lambda_r z_r^2 + \frac{1}{2} \Delta F_1^2 \\
 &\quad + 0.2785 k \varepsilon_1^* + 0.2785 k \sum_{r=2}^n w_r^* \\
 &\quad + \sum_{r=1}^n \frac{\sigma_r}{2\gamma_r} (\theta_r^{*T} \theta_r^* - \tilde{\theta}_r^T \tilde{\theta}_r) + \frac{\bar{\sigma}_1}{2\bar{\gamma}_1} (\varepsilon_1^{*T} \varepsilon_1^* - \tilde{\varepsilon}_1^T \tilde{\varepsilon}_1) \\
 &\quad + \sum_{r=2}^n \frac{\bar{\sigma}_r}{2\bar{\gamma}_r} (w_r^{*T} w_r^* - \tilde{w}_r^T \tilde{w}_r).
 \end{aligned} \tag{59}$$

Combined with the above analysis, we have come to the following conclusions.

**Theorem 9.** Consider system (1). Assumptions 5 and 6 hold on the sets  $\Omega_{z_i}$ . For the virtual controller  $\alpha_i$ ,  $i = 1, 2, \dots, n-1$ , in (36), (41), and (51) and the actual controller  $u$  in (56) and the adaptive laws in (36), (41), (51), and (56), the following properties hold:

(i) The proposed adaptive control scheme can guarantee that the tracking error converges to a bounded compact set  $\Omega_D = \{|z_1| < D\}$ .

(ii) All the signals in the closed-loop systems are bounded.

(iii) The partial state constraints are not violated.

*Proof.* (i) From Lemma 1, (59) can be rearranged into the form

$$\dot{V} \leq -\rho V + c, \tag{60}$$

where  $\rho = \min\{(4\eta + (1/\eta)\|P\|^2)/8(\lambda_{\min}(Q) - (\xi + 2\eta)\|P\|^2 - (1/4\eta)nm^2 - (1/2)m_1^2), 1/2\lambda_i, 1/\sigma_j, 1/\bar{\sigma}_1, 1/\bar{\sigma}_j\}$ ,  $c = E_n +$

$\sum_{j=1}^n (\sigma_j/\gamma_j)\theta_j^{*T}\theta_j^* + (\bar{\sigma}_1/\bar{\gamma}_1)\varepsilon_1^{*2} + \sum_{j=2}^n (\bar{\sigma}_j/\bar{\gamma}_j)w_j^{*2}$ ,  $E_n = E_0 + (1/2)\tau_2'^2 + k'\varepsilon_1^* + \sum_{j=1}^n k'w_j^{*2}$ , and  $k' = 0.2785k$ . Adding  $e^{\rho t}$  to both sides of the above inequality and integrating it over  $[0, t]$ , it has

$$V(t) \leq \left[ V(0) - \frac{C}{\rho} \right] e^{-\rho t} + \frac{C}{\rho} \leq V(0) + \frac{C}{\rho} \quad (61)$$

$$\triangleq V(0) + C.$$

From the preceding inequality and  $V(t)$ , we can conclude that  $\log(k_{b_j}^2/(k_{b_j}^2 - z_j^2))$ ,  $e_i$ ,  $\hat{\theta}_j$ ,  $\tilde{\varepsilon}_1$ ,  $\tilde{w}_j$  and  $z_j$  are bounded, and  $K_{z_i}$  is bounded. Due to the boundedness of  $\theta_j^*$ ,  $\varepsilon_1^*$ ,  $w_j^*$  and  $\hat{\theta}_j = \theta_j^* - \tilde{\theta}_j$ ,  $\tilde{\varepsilon}_1 = \varepsilon_1^* - \hat{\varepsilon}_1$ ,  $\tilde{w}_j = w_j^* - \hat{w}_j$ , then  $\hat{\theta}_j$ ,  $\hat{\varepsilon}_1$ , and  $\hat{w}_j$  are bounded. It is easy to see that the tracking error converges to a bounded compact set.

(ii) According to (61), we define  $B = \sqrt{2(V(0) + C)/\lambda_{\min}(P)}$ . From the form of  $V(t)$ , we have  $|e_i| \leq \|e\| \leq B$ . Since  $x_1 = z_1 + y_d(t)$  and  $|y_d(t)| \leq Y_0$ , it can be shown that  $|x_1| \leq |z_1| + |y_d(t)| < k_{b_1} + Y_0$ . Suppose  $k_{c_1} = k_{b_1} + Y_0$ , and then  $|x_1| < k_{c_1}$ . To show  $|x_2| < k_{c_2}$ , it needs to confirm that there exists a positive constant  $\bar{\alpha}_1$  such that  $|\alpha_1| \leq \bar{\alpha}_1$ . The boundedness of  $x_1$ ,  $y_d$ ,  $\dot{y}_d$ ,  $\hat{\theta}_1$ ,  $\hat{\varepsilon}_1$ ,  $K_{z_1}$  can be guaranteed because  $\alpha_1 = \alpha_1(x_1, y_d, \dot{y}_d, \hat{\theta}_1, \hat{\varepsilon}_1, K_{z_1})$ . It is easy to know from the definition of  $\alpha_1$  that the supremum of  $\alpha_1$  exists. In view of  $|z_2| < k_{b_2}$  and  $\hat{x}_2 = z_2 + \alpha_1$ , it has  $|\hat{x}_2| < k_{b_2} + \bar{\alpha}_1$ . Due to  $x_2 = \hat{x}_2 + e_2$ , the inequality  $|x_2| \leq |\hat{x}_2| + |e_2| < k_{b_2} + \bar{\alpha}_1 + B$  holds. Let  $k_{c_2} = k_{b_2} + \bar{\alpha}_1 + B$ , and then  $|x_2| < k_{c_2}$ . Similarly, it can show that  $|x_{i+1}| < k_{c_{i+1}}$ ,  $i = 2, 3, \dots, n_s - 1$ , after verifying  $|\alpha_i| \leq \bar{\alpha}_i$ . Since (41), (51), and  $|\alpha_{i-1}| \leq \bar{\alpha}_{i-1}$ , then the controller  $u$  is bounded. From the above analysis, we conclude that all the signals of the closed-loop system  $x$ ,  $\alpha_i$ ,  $u$ ,  $z$ ,  $\hat{\theta}_j$ ,  $\hat{\varepsilon}_1$ ,  $\hat{w}_j$  are bounded.

(iii) From the construction of (61), we get

$$\log \frac{k_{b_1}^2}{k_{b_1}^2 - z_1^2} \leq 2[V(0) - C] e^{-\rho t} + 2C. \quad (62)$$

Taking exponentials on both sides, one has

$$\frac{k_{b_1}^2}{k_{b_1}^2 - z_1^2} \leq e^{2[V(0)-C]e^{-\rho t} + 2C}. \quad (63)$$

Define

$$D = k_{b_1} \sqrt{1 - e^{-2[V(0)-C]e^{-\rho t} - 2C}}. \quad (64)$$

Because  $k_{b_1}^2 - z_1^2 > 0$ , it is easy to get  $|z_1| \leq D$ . If  $V(0) = C$  then  $|z_1| \leq k_{b_1} \sqrt{1 - e^{-2C}} = D$  holds. If  $V(0) \neq C$ , it can be concluded that, given any  $D > k_{b_1} \sqrt{1 - e^{-2C}}$ , there exists  $T$  such that, for any  $t > T$ , it has  $|z_1| \leq D$ . This implies that  $|z_1| \leq k_{b_1} \sqrt{1 - e^{-2C}}$  as  $t \rightarrow \infty$ . That means  $z_1$  can be made arbitrarily small. From above analysis, we can get that  $|x_{i+1}| < k_{c_{i+1}}$  ( $i = 2, 3, \dots, n_s - 1$ ),  $|\alpha_{i-1}| \leq \bar{\alpha}_{i-1}$ , and the controller  $u$  is bounded. The variables  $z_i = \hat{x}_i - \alpha_{i-1}$ , so that  $z_i$  ( $i = 1, 2, \dots, n$ ) is bound, and the systems states are not violated. This completes the proof.  $\square$

## 4. Illustrative Example

In this section, we give an example to show how to apply the results proposed in this paper to investigate the stabilization of nonlinear pure feedback systems subject to partial state constraints.

Let us consider the following nonlinear systems:

$$\begin{aligned} \dot{x}_1 &= x_1 \cos(x_1) + (2x_1^2 + 0.6)x_2, \\ \dot{x}_2 &= x_1 x_2 + u + 0.4 \sin(u), \\ y &= x_1, \end{aligned} \quad (65)$$

where the state constraints are  $|x_1| < 0.5$ ; the reference signal is given as  $y_d = 0.1 \sin(\pi t/3) + 0.1 \cos(t/3)$  for the tracking problem. It is unnecessary to give precise knowledge of the initial state  $x(0)$ . In this simulation, the figures are specific cases. Let  $x_1 = 0.05$ ,  $x_2 = 0.2$ ,  $\hat{x}_1 = 0$ ,  $\hat{x}_2 = 0$ . Fuzzy membership functions for the variables  $\hat{x}_1$ ,  $\hat{x}_2$ ,  $\hat{x}_{2f}$ , and  $u_f$  are given as follows:

$$\begin{aligned} \mu_{F_1'}(\hat{x}_1) &= \exp \left[ -\frac{(\hat{x}_1 - 5 + 2l)^2}{2} \right], \\ \mu_{F_2'}(\hat{x}_2) &= \exp \left[ -\frac{(\hat{x}_2 - 3 + l)^2}{5} \right], \\ \mu_{F_3'}(\hat{x}_{2f}) &= \exp \left[ -\frac{(\hat{x}_{2f} - 3 + l)^2}{5} \right], \\ \mu_{F_4'}(u_f) &= \exp \left[ -\frac{(u_f - 5 + 3l)^2}{7} \right], \end{aligned} \quad (66)$$

$$(l = 1, 2, \dots, 5).$$

From [35], the fuzzy logic systems can be represented as

$$\begin{aligned} \hat{f}_1(\hat{x}_1, \hat{x}_{2f} | \theta_1) &= \theta_1^T \varphi(\hat{x}_1, \hat{x}_{2f}), \\ \hat{f}_2(\hat{x}_1, \hat{x}_2, u_f | \theta_2) &= \theta_2^T \varphi(\hat{x}_1, \hat{x}_2, u_f). \end{aligned} \quad (67)$$

Letting  $k_1 = 5$  and  $k_2 = 5$ , then the state observer can be constructed as

$$\begin{aligned} \dot{\hat{x}}_1 &= \hat{x}_2 + \hat{f}_1(\hat{x}_1, \hat{x}_{2f} | \theta_1) + 5(y - \hat{x}_1), \\ \dot{\hat{x}}_2 &= u + \hat{f}_2(\hat{x}_1, \hat{x}_2, u_f | \theta_2) + 5(y - \hat{x}_1). \end{aligned} \quad (68)$$

The virtual control function  $\alpha_1$  and controller  $u$  as well as the adaptive laws  $\hat{\theta}_1$ ,  $\hat{\theta}_2$ ,  $\hat{\varepsilon}_1$  and  $\hat{w}_2$  are as follows:

$$\begin{aligned}
 \alpha_1 &= -\lambda_1 z_1 - \hat{\theta}_1^T \varphi_1 + \dot{y}_d - \hat{\varepsilon}_1 \tanh\left(\frac{K_{z_1}}{k}\right) - \frac{1}{2} K_{z_1}, \\
 u &= -\lambda_2 z_2 - \hat{\theta}_2^T \varphi_2 - k_2 e_1 + \dot{\alpha}_1 - \hat{w}_2 \tanh\left(\frac{z_2}{k}\right) \\
 &\quad - z_1, \\
 \dot{\hat{\theta}}_1 &= -\sigma_1 \hat{\theta}_1 + \gamma_1 K_{z_1} \varphi_1, \\
 \dot{\hat{\varepsilon}}_1 &= -\bar{\sigma}_1 \hat{\varepsilon}_1 + \bar{\gamma}_1 K_{z_1} \tanh\left(\frac{K_{z_1}}{k}\right), \\
 \dot{\hat{\theta}}_2 &= -\sigma_2 \hat{\theta}_2 + \gamma_2 z_2 \varphi_2, \\
 \dot{\hat{w}}_2 &= -\bar{\sigma}_2 \hat{w}_2 + \bar{\gamma}_2 z_2 \tanh\left(\frac{z_2}{k}\right).
 \end{aligned} \tag{69}$$

Set the design parameters in the above control scheme as

$$\begin{aligned}
 \lambda_1 &= 1, \\
 \lambda_2 &= 2, \\
 \gamma_1 &= 1, \\
 \gamma_2 &= 1, \\
 \bar{\gamma}_1 &= 1, \\
 \bar{\gamma}_2 &= 1; \\
 \sigma_1 &= 1, \\
 \sigma_2 &= 1, \\
 \bar{\sigma}_1 &= 1.5, \\
 \bar{\sigma}_2 &= 0.5, \\
 k &= 0.2.
 \end{aligned} \tag{70}$$

Let  $k_{b_i} = 0.2$ , and from calculation we know it is valid. Choose the initial conditions of adaptive parameters as  $\hat{\theta}_1 = (1, 1, 1, 1, 1)$ ,  $\hat{\varepsilon}_1 = 1$ ,  $\hat{\theta}_2 = (1, 1, 1, 1, 1)$ ,  $\hat{w}_2 = 1$ .

The simulation is given in Figures 1–8. Figure 1 shows the trajectory of the state  $x$ . Figure 2 is the swing curve of the control signal  $u$ . Figure 3 is the state  $x_1$  which remains in the constraint region; it shows the trajectory of the state  $x$ . Figure 4 stands for the variables of  $z_1$  and  $z_2$ , and these error variables can not violate their bounds. Figures 5 and 6 are used to illustrate the trajectories of the system states  $x_1$ ,  $x_2$  and the observer states  $\hat{x}_1$ ,  $\hat{x}_2$ . Figures 7 and 8 show that all the signals in the closed-loop system are bounded. It is clear that the nonlinear pure feedback system subject to partial constraints under the output feedback law is bounded. From the simulation, we can conclude that the results proposed in Theorem 9 are very practicable in stability of nonlinear pure feedback systems with partial constraints. Meanwhile, it is a good tool in analyzing the stability problems of some

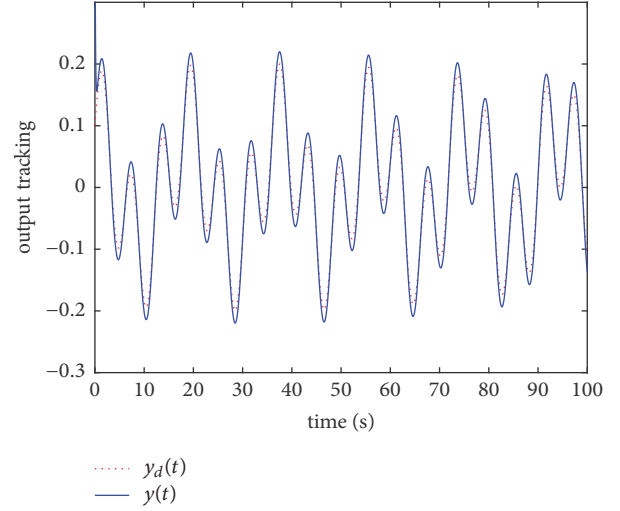


FIGURE 1: The tracking result.

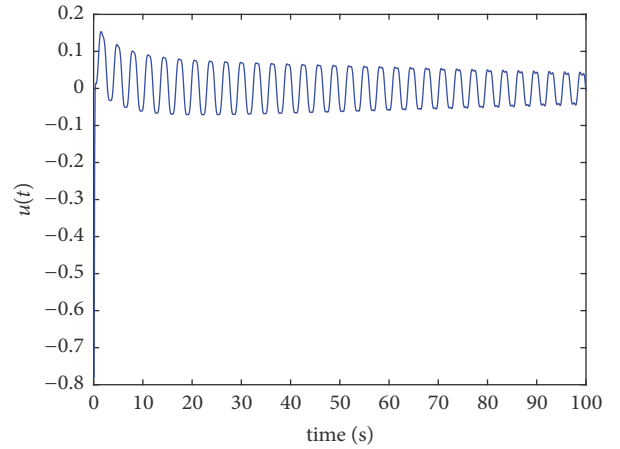


FIGURE 2: The control  $u$ .

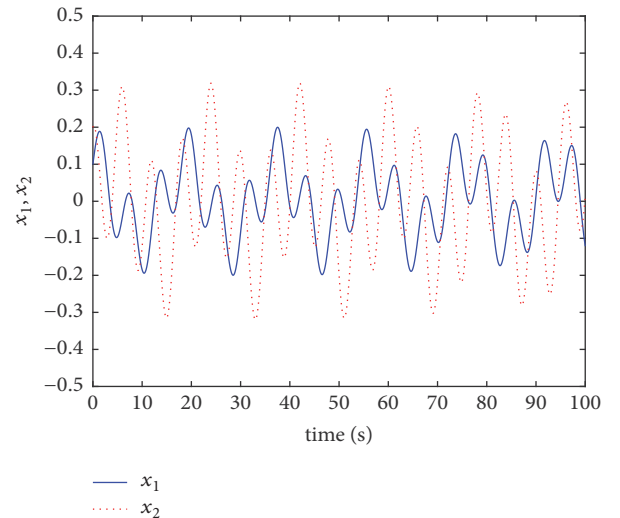


FIGURE 3: States  $x_1$  and  $x_2$ .

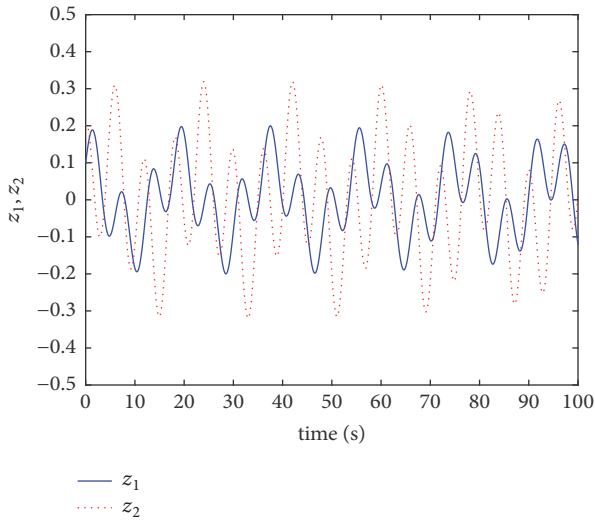


FIGURE 4: Variables  $z_1$  and  $z_2$ .

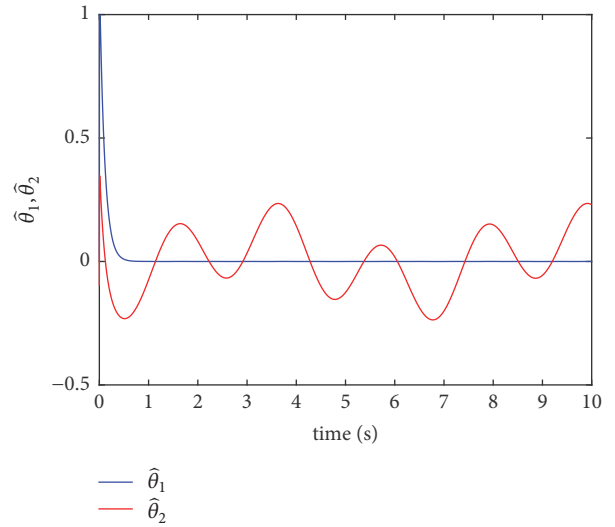


FIGURE 7: Parameter estimates  $\hat{\theta}_1, \hat{\theta}_2$ .

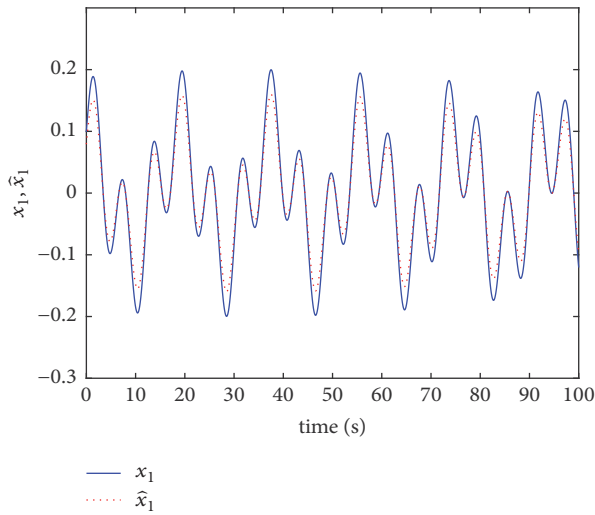


FIGURE 5: States  $x_1$  and  $\hat{x}_1$ .

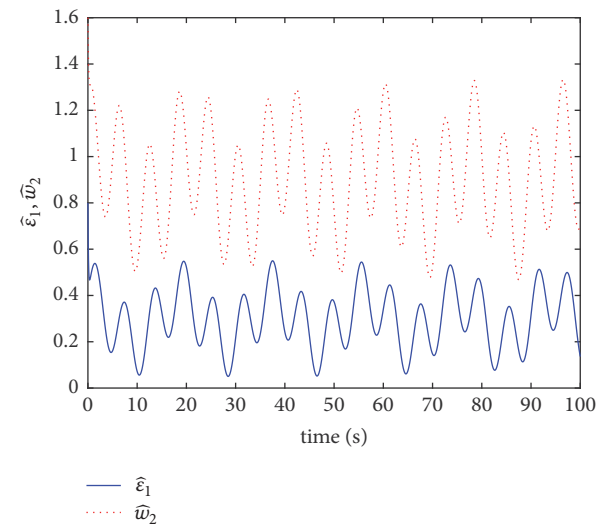


FIGURE 8: Parameter estimates  $\hat{e}_1, \hat{w}_2$ .

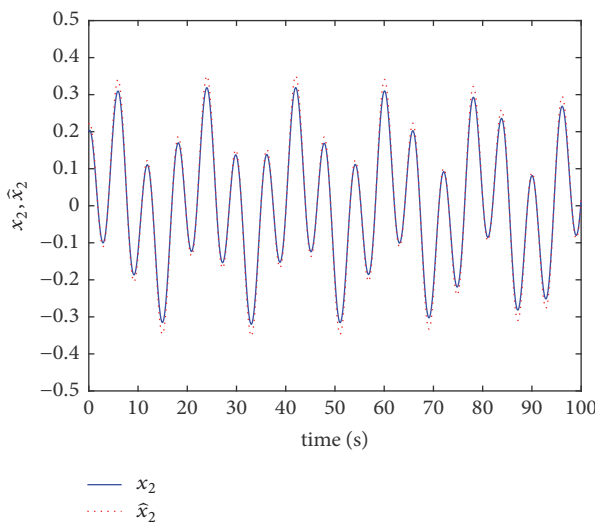


FIGURE 6: States  $x_2$  and  $\hat{x}_2$ .

classes of nonlinear pure feedback systems in the presence of constraint.

### 5. Conclusions

In this paper, the tracking control problem of a class of nonlinear pure feedback systems subject to partial state constraints and adaptive fuzzy output feedback controls has been investigated by use of BLFs and backstepping. The output feedback control law, by which the stability of the closed-loop system is guaranteed, is determined by constraints. Simulations show that the results obtained in this paper are very practicable in analyzing the stability of some classes of nonlinear pure feedback systems.

## Data Availability

No data were used to support this study.

## Conflicts of Interest

The authors declare that they have no conflicts of interest.

## Acknowledgments

This work was supported by the National Natural Science Foundation of China (no. 61703232) and the Natural Science Foundation of Shandong Province (nos. ZR2017MF068, ZR2017QF013).

## References

- [1] L. Guo, L. Liu, and Y. Wu, "Existence of positive solutions for singular fractional differential equations with infinite-point boundary conditions," *Nonlinear Analysis: Modelling and Control*, vol. 21, no. 5, pp. 635–650, 2016.
- [2] F. Li and Y. Bao, "Uniform stability of the solution for a memory-type elasticity system with nonhomogeneous boundary control condition," *Journal of Dynamical and Control Systems*, vol. 23, no. 2, pp. 301–315, 2017.
- [3] S. Rahmani, N. Mendalek, and K. Al-Haddad, "Experimental design of a nonlinear control technique for three-phase shunt active power filter," *IEEE Transactions on Industrial Electronics*, vol. 57, no. 10, pp. 3364–3375, 2010.
- [4] W. Sun and L. Peng, "Observer-based robust adaptive control for uncertain stochastic Hamiltonian systems with state and input delays," *Nonlinear Analysis: Modelling and Control*, vol. 19, no. 4, pp. 626–645, 2014.
- [5] W. Sun and B. Fu, "Adaptive control of time-varying uncertain non-linear systems with input delay: a Hamiltonian approach," *IET Control Theory and Applications*, vol. 10, no. 15, pp. 1844–1858, 2016.
- [6] W. Sun, K. Wang, C. Nie et al., "Energy-based controller design of stochastic magnetic levitation system," *Mathematical Problems in Engineering*, vol. 2017, 6 pages, 2017.
- [7] A. Bemporad, "Reference governor for constrained nonlinear systems," *Institute of Electrical and Electronics Engineers Transactions on Automatic Control*, vol. 43, no. 3, pp. 415–419, 1998.
- [8] G. Chen, J. Xia, G. Zhuang, and J. Zhao, "Improved delay-dependent stabilization for a class of networked control systems with nonlinear perturbations and two delay components," *Applied Mathematics and Computation*, vol. 316, pp. 1–17, 2018.
- [9] T. Hu and Z. Lin, *Control Systems with Actuator Saturation: Analysis and Design*, Birkhäuser, Boston, Mass, USA, 2001.
- [10] H. Li and Y. Wang, "Controllability analysis and control design for switched Boolean networks with state and input constraints," *SIAM Journal on Control and Optimization*, vol. 53, no. 5, pp. 2955–2979, 2015.
- [11] D. Q. Mayne, J. B. Rawlings, C. V. Rao, and P. O. M. Scokaert, "Constrained model predictive control: stability and optimality," *Automatica*, vol. 36, no. 6, pp. 789–814, 2000.
- [12] W. Sun, "Stabilization analysis of time-delay Hamiltonian systems in the presence of saturation," *Applied Mathematics and Computation*, vol. 217, no. 23, pp. 9625–9634, 2011.
- [13] C. Wang, Y. Wu, and J. Yu, "Barrier Lyapunov functions-based adaptive control for nonlinear purefeedback systems with time-varying full state constraints," *International Journal of Control, Automation and Systems*, vol. 15, no. 6, pp. 2714–2722, 2017.
- [14] C. Wang, Y. Wu, and J. Yu, "Barrier Lyapunov functions-based dynamic surface control for pure-feedback systems with full state constraints," *IET Control Theory and Applications*, vol. 11, no. 4, pp. 524–530, 2017.
- [15] J. Xia, G. Chen, and W. Sun, "Extended dissipative analysis of generalized Markovian switching neural networks with two delay components," *Neurocomputing*, vol. 260, pp. 275–283, 2017.
- [16] Z.-P. Jiang, "A combined backstepping and small-gain approach to adaptive output feedback control," *Automatica*, vol. 35, no. 6, pp. 1131–1139, 1999.
- [17] M. Krstic, I. Kanellakopoulos, and P. Kokotovic, *Nonlinear and Adaptive Control Design*, Wiley, New York, NY, USA, 1995.
- [18] B. Ren, S. S. Ge, K. P. Tee, and T. H. Lee, "Adaptive neural control for output feedback nonlinear systems using a barrier Lyapunov function," *IEEE Transactions on Neural Networks and Learning Systems*, vol. 21, no. 8, pp. 1339–1345, 2010.
- [19] X. Xie and M. Jiang, "Output feedback stabilization of stochastic feedforward nonlinear time-delay systems with unknown output function," *International Journal of Robust and Nonlinear Control*, vol. 28, no. 1, pp. 266–280, 2018.
- [20] L. Yao and W. Zhang, "Adaptive tracking control for a class of random pure-feedback nonlinear systems with Markovian switching," *International Journal of Robust and Nonlinear Control*, vol. 28, no. 8, pp. 3112–3126, 2018.
- [21] Z. Q. Zhang, S. Y. Xu, and B. Y. Zhang, "Exact tracking control of nonlinear systems with time delays and dead-zone input," *Automatica*, vol. 52, pp. 272–276, 2015.
- [22] Z. Zhang, S. Xu, and B. Zhang, "Asymptotic tracking control of uncertain nonlinear systems with unknown actuator nonlinearity," *IEEE Transactions on Automatic Control*, vol. 59, no. 5, pp. 1336–1341, 2014.
- [23] K. B. Ngo, R. Mahony, and Z. Jiang, "Integrator backstepping using barrier functions for systems with multiple state constraints," in *Proceedings of the 44th IEEE Conference On Decision and Control, and the European Control Conference 2005*, pp. 12–15, Seville, Spain, 2005.
- [24] K. P. Tee, S. S. Ge, and E. H. Tay, "Barrier Lyapunov functions for the control of output-constrained nonlinear systems," *Automatica*, vol. 45, no. 4, pp. 918–927, 2009.
- [25] M. A. Khanesar, O. Kaynak, S. Yin, and H. Gao, "Adaptive indirect fuzzy sliding mode controller for networked control systems subject to time-varying network-induced time delay," *IEEE Transactions on Fuzzy Systems*, vol. 23, no. 1, pp. 205–214, 2015.
- [26] E. Kim and C. W. Park, "Fuzzy disturbance observer approach to robust tracking control of nonlinear sampled systems with the guaranteed suboptimal performance," *IEEE Transactions on Cybernetics*, vol. 34, pp. 1574–1581, 2004.
- [27] B. Niu and J. Zhao, "Barrier Lyapunov functions for the output tracking control of constrained nonlinear switched systems," *Systems & Control Letters*, vol. 62, no. 10, pp. 963–971, 2013.
- [28] H. Wang, X. Liu, K. Liu, and H. R. Karimi, "Approximation-based adaptive fuzzy tracking control for a class of nonstrict-feedback stochastic nonlinear time-delay systems," *IEEE Transactions on Fuzzy Systems*, vol. 23, no. 5, pp. 1746–1760, 2015.

- [29] T. P. Zhang and S. S. Ge, "Adaptive dynamic surface control of nonlinear systems with unknown dead zone in pure feedback form," *Automatica*, vol. 44, no. 7, pp. 1895–1903, 2008.
- [30] K. P. Tee and S. S. Ge, "Control of nonlinear systems with partial state constraints using a barrier Lyapunov function," *International Journal of Control*, vol. 84, no. 12, pp. 2008–2023, 2011.
- [31] K. P. Tee, B. Ren, and S. S. Ge, "Control of nonlinear systems with time-varying output constraints," *Automatica*, vol. 47, no. 11, pp. 2511–2516, 2011.
- [32] D. P. Li, D. J. Li, Y. J. Liu, S. Tong, and C. L. P. Chen, "Approximation-based adaptive neural tracking control of nonlinear mimo unknown time-varying delay systems with full state constraints," *IEEE Transactions on Cybernetics*, vol. 47, no. 10, pp. 3100–3109, 2017.
- [33] T. Zhang, M. Xia, Y. Yi, and Q. Shen, "Adaptive Neural Dynamic Surface Control of Pure-Feedback Nonlinear Systems With Full State Constraints and Dynamic Uncertainties," *IEEE Transactions on Systems, Man, and Cybernetics: Systems*, vol. 47, no. 8, pp. 2378–2387, 2017.
- [34] H. Su and W. Zhang, "A combined backstepping and dynamic surface control to adaptive fuzzy state-feedback control," *International Journal of Adaptive Control and Signal Processing*, vol. 31, no. 11, pp. 1666–1685, 2017.
- [35] T. Wang, *Adaptive Fuzzy Systems and Control*, Prentice Hall, Englewood Cliffs, NJ, USA, 1994.
- [36] A.-M. Zou, Z.-G. Hou, and M. Tan, "Adaptive control of a class of nonlinear pure-feedback systems using fuzzy backstepping approach," *IEEE Transactions on Fuzzy Systems*, vol. 16, no. 4, pp. 886–897, 2008.
- [37] J. Yi, J. Li, J. Li, and J. Wu, "Adaptive fuzzy output feedback control for a class of nonlinear pure-feedback systems with full state constraints," in *Proceedings of the 2017 36th Chinese Control Conference (CCC)*, pp. 862–867, Dalian, China, July 2017.
- [38] Z. Yang, S. Hara, S. Kanae, and K. Wada, "Robust output feedback control of a class of nonlinear systems using a disturbance observer," *IEEE Transactions on Control Systems Technology*, vol. 19, no. 2, pp. 256–268, 2011.
- [39] D. Wang and J. Huang, "Adaptive neural network control of a class of uncertain nonlinear systems in pure-feedback form," *Automatica*, vol. 42, no. 8, pp. 1365–1372, 2002.

## Research Article

# Adaptive Synchronization for Uncertain Delayed Fractional-Order Hopfield Neural Networks via Fractional-Order Sliding Mode Control

Bo Meng <sup>1,2</sup> and Xiaohong Wang<sup>2</sup>

<sup>1</sup>College of Electrical Engineering and Automation, Shandong University of Science and Technology, Qingdao 266590, China

<sup>2</sup>College of Mathematics and Systems Science, Shandong University of Science and Technology, Qingdao 266590, China

Correspondence should be addressed to Bo Meng; mb0922@sdust.edu.cn

Received 17 May 2018; Accepted 10 July 2018; Published 18 July 2018

Academic Editor: Xue-Jun Xie

Copyright © 2018 Bo Meng and Xiaohong Wang. This is an open access article distributed under the Creative Commons Attribution License, which permits unrestricted use, distribution, and reproduction in any medium, provided the original work is properly cited.

Adaptive synchronization for a class of uncertain delayed fractional-order Hopfield neural networks (FOHNNs) with external disturbances is addressed in this paper. For the unknown parameters and external disturbances of the delayed FOHNNs, some adaptive estimations are designed. Firstly, a fractional-order switched sliding surface is proposed for the delayed FOHNNs. Then, according to the fractional-order extension of the Lyapunov stability criterion, a fractional-order sliding mode controller is constructed to guarantee that the synchronization error of the two uncertain delayed FOHNNs converges to an arbitrary small region of the origin. Finally, a numerical example of two-dimensional uncertain delayed FOHNNs is given to verify the effectiveness of the proposed method.

## 1. Introduction

The research of neural networks (NNs) is quite extensive, reflecting the characteristics of multidisciplinary technology. NNs have many successful applications in the fields of associative memories and image processing. Recently, the discussion on NNs has become a hot topic [1–3]. Guo et al. [4] studied the exponential stability analysis for complex-valued memristor-based bidirectional associative memory (BAM) NNs with time delays. Lv et al. [5] used NNs to discuss the adaptive tracking control for a class of uncertain nonlinear systems. Li et al. [6] studied Hopf bifurcation analysis of complex-valued neural networks model.

Fractional calculus (FC) has a long history. As early as 1695, the concept of fractional differential was mentioned in Leibnitz's letter to L'Hospital. For a long time, FC continues to grow. Podlubny's book [7] systematically introduced the concepts and properties of FC. Bai et al. (see [8–13], and the references therein) studied the existence and uniqueness of solutions for fractional differential equations (FDE). Wang et al. [14–16] studied the numerical analysis of FDE. In recent years, fractional-order systems (FOS) have attracted

wide attentions. The control problems of all kinds of FOS were studied recently [17–21]. Many researchers focused on fractional-order neural networks (FONNs) [22–27]. Cao et al. [28] investigated the existence and uniqueness of the nontrivial solution of NNs and the uniform stability of the FONNs.

The researches on the stability of NNs, FOS, and stochastic systems have attracted the attention of a large number of researchers, and many achievements have been made [29–41]. The sliding mode control (SMC) is a very popular strategy for a general class of nonlinear uncertain systems, with a very large frame of applications fields. Due to the use of the discontinuous function, its main features are the robustness of closed-loop system and the finite-time convergence. Utkin et al. [42] studied the minimum possible value of control based on adaptation SMC methodology. Efe. et al. [43] discussed the fractional fuzzy adaptive SMC. Aghababa [44] designed a chatter-free terminal sliding mode controller for nonlinear fractional-order dynamical systems. The synchronization problems of FOHNNs have captured more and more researchers' attention [45–48]. Xi et al. [22] have discussed SMC for uncertain FOHNNs. Liu et al.

[24] have researched adaptive synchronization of a class of FOHNNs. It is well known that time delay is unavoidable due to finite switching speeds of the amplifiers, and it may cause oscillations or instability of dynamic systems. Wang et al. [26] have discussed the stability analysis of FOHNNs with time delay.

However, to the best of our knowledge, there are few attentions to adaptive synchronization for a class of uncertain delayed FOHNNs subject to external disturbances. The SMC technology was used to solve the above problems in the paper. The rest of this paper is organized as follows: some necessary definitions and lemmas are given in Section 2. The main works including the introduction of fractional-order network model, the fractional-order switched sliding mode surface (SMS), the design of adaptive synchronization controller, and stability analysis are included in Section 3. Section 4 presents a simulation example. Finally, the paper is concluded in Section 5.

## 2. Preliminaries

There are several kinds of definitions for fractional-order derivatives. The definitions of more frequency of use in literatures are Grünwald-Letnikov, Riemann-Liouville, and Caputo definitions [7]. These definitions are generally not equivalent with each other. The Caputo's derivative's Laplace transform requires integer-order derivatives for the initial conditions, which was used in engineering applications frequently. But, the Riemann-Liouville definition's Laplace transform involved fractional-order derivatives for the initial conditions. It was hard to use physically. In the following parts, the Caputo's derivative will be used [24]. Firstly, we give some definitions and lemmas.

*Definition 1* (Riemann-Liouville fractional-order integral [7]). The Riemann-Liouville fractional integral of order  $\alpha$  for a function  $f(t)$  is defined as

$${}_t D_t^{-\alpha} f(t) = \frac{1}{\Gamma(\alpha)} \int_{t_0}^t \frac{f(\tau)}{(t-\tau)^{1-\alpha}} d\tau. \quad (1)$$

where  $\alpha > 0$ ,  $t \geq t_0$ .  $\Gamma(\alpha)$  is Euler's gamma function.

The gamma function  $\Gamma(\alpha)$  is defined for all complex numbers except the nonpositive integers. For complex numbers with a positive real part, it is defined via a convergent infinite integral:

$$\Gamma(\alpha) = \int_0^{+\infty} \tau^{\alpha-1} e^{-\tau} d\tau. \quad (2)$$

*Definition 2* (Caputo fractional-order derivative [7]). The Caputo fractional derivative of order  $\alpha$  for a function  $f(t)$  is defined as

$${}_t D_t^\alpha f(t) = \frac{1}{\Gamma(n-\alpha)} \int_{t_0}^t (t-\tau)^{n-\alpha-1} f^{(n)}(\tau) d\tau. \quad (3)$$

where  $\alpha > 0$ ,  $n$  is an integer satisfying  $n-1 \leq \alpha < n$ . Particularly, for  $0 < \alpha < 1$  case, one can get

$${}_t D_t^\alpha f(t) = \frac{1}{\Gamma(1-\alpha)} \int_{t_0}^t (t-\tau)^{-\alpha} f'(\tau) d\tau. \quad (4)$$

According to Definition 2, for any constants  $L_1 \in \mathbf{R}$  and  $L_2 \in \mathbf{R}$ , the linearity of Caputo's fractional derivative is described by

$${}_t D_t^\alpha (L_1 f(t) + L_2 g(t)) = L_1 {}_t D_t^\alpha f(t) + L_2 {}_t D_t^\alpha g(t). \quad (5)$$

In nonlinear control systems, Lyapunov second method gives a way to analyze the stability of the system without explicitly solving the differential equations. The Lyapunov stability theory for FOS has been developed by Li et al. [33]. One of the main contributions of [33] is the following lemma.

Consider the fractional-order nonlinear system:

$$\begin{aligned} {}_t D_t^\alpha x(t) &= f(x, t), \\ x(t_0) &= x_{t_0}, \end{aligned} \quad (6)$$

where  $x(t) \in \mathbf{R}^n$  is the state vector and  $f(x, t) \in \mathbf{R}^n$  is a Lipschitz continuous nonlinear function.

**Lemma 3** (see [49]). Let  $G(t)$  be a continuous function on  $[0, +\infty)$ , if there exist constants  $\kappa_1 > 0$  and  $\kappa_2 > 0$ , such that

$${}_t D_t^\alpha G(t) \leq -\kappa_1 G(t) + \kappa_2, \quad t \geq 0. \quad (7)$$

Then,

$$G(t) \leq G(0) E_\alpha(-\kappa_1 t^\alpha) + \kappa_2 t^\alpha E_{\alpha, \alpha+1}(-\kappa_1 t^\alpha), \quad t \geq 0. \quad (8)$$

where  $0 < \alpha < 1$ ,  $E_\alpha(\cdot)$  and  $E_{\alpha, \alpha+1}(\cdot)$  are one-parameter Mittag-Leffler function and two-parameter Mittag-Leffler function, respectively.

*Remark 4.* Mittag-Leffler stability means asymptotical stability [32].

**Lemma 5** (see [7]). If  $x(t) \in C^1[0, T]$ , for  $\alpha > 0$  and  $T > 0$ , then the following equations hold:

$${}_0 D_t^\alpha ({}_0 D_t^{-\alpha} x(t)) = x(t). \quad (9)$$

and

$${}_0 D_t^{-\alpha} ({}_0 D_t^\alpha x(t)) = x(t) - \sum_{k=0}^{n-1} \frac{x^{(k)}(t)}{k!} t^k. \quad (10)$$

In particular, for  $0 < \alpha < 1$ ,

$${}_0 D_t^{-\alpha} ({}_0 D_t^\alpha x(t)) = x(t) - x(0). \quad (11)$$

**Lemma 6** (see [21]). Let  $x(t) \in \mathbf{R}^n$  be a continuous and derivable function. Then for any  $t > 0$  the following inequality holds:

$$\frac{1}{2} {}_0^C D_t^\alpha x^T(t) x(t) \leq x^T(t) {}_0^C D_t^\alpha x(t) \quad (12)$$

### 3. Main Results

In this section, considering a system of the uncertain FOHNNs with delay (as a master system)

$$\begin{aligned} {}_0^C D_t^\alpha x_i(t) = & -a_i(t) x_i(t) + \sum_{j=1}^n b_{ij} f_j(x_j(t)) \\ & + \sum_{j=1}^n c_{ij} g_j(x_j(t-\tau)) + I_i. \end{aligned} \quad (13)$$

where  $i = 1, 2, \dots, n$ ,  $0 < \alpha < 1$ ,  $n$  is the number of units in a neural network,  $x_i(t)$  is the state of the  $i$ th unit at time  $t$ ,  $f_j, g_j$  denotes the activation function of the  $j$ th neuron,  $b_{ij}, c_{ij}$  denotes the constant connection weight of the  $j$ th neuron on the  $i$ th neuron,  $a_i > 0$  represents the rate with which the  $i$ th neuron resets its potential to the resting state when disconnected from the network and  $a_i > 0$  is unknown,  $I_i$  denotes the constant external inputs, and  $\tau$  is the transmission constant delay.

Let us discuss the synchronization results, assuming that (13) is a master system and the slave system is defined by the following equation:

$$\begin{aligned} {}_0^C D_t^\alpha y_i(t) = & -a_i(t) y_i(t) + \sum_{j=1}^n b_{ij} f_j(y_j(t)) \\ & + \sum_{j=1}^n c_{ij} g_j(y_j(t-\tau)) + I_i + d_i(t) \\ & + u_i(t). \end{aligned} \quad (14)$$

where  $y_i(t)$  is the state of the  $i$ th unit at time  $t$ ,  $d_i(t)$  is the unknown external disturbance, and  $u_i(t)$  is the control input which will be given later.

Defining the synchronization error  $e_i(t)$  as

$$e_i(t) = y_i(t) - x_i(t) \quad (15)$$

then the error dynamics between the master system (13) and the slave system (14) can be written as

$$\begin{aligned} {}_0^C D_t^\alpha e_i(t) = & -a_i(t) e_i(t) \\ & + \sum_{j=1}^n b_{ij} (f_j(y_j(t)) - f_j(x_j(t))) \\ & + \sum_{j=1}^n c_{ij} (g_j(y_j(t-\tau)) - g_j(x_j(t-\tau))) \\ & + d_i(t) + u_i(t). \end{aligned} \quad (16)$$

*Assumption 7.* Assuming that the nonlinear functions  $f_j$  and  $g_j$  ( $j = 1, 2, \dots, n$ ) satisfy local Lipschitz conditions, and existing positive constants  $L_j^1$  and  $L_j^2$  such that

$$\begin{aligned} |f_j(y_j(t)) - f_j(x_j(t))| & \leq L_j^1 |y_j(t) - x_j(t)|, \\ |g_j(y_j(t-\tau)) - g_j(x_j(t-\tau))| & \\ \leq L_j^2 |y_j(t-\tau) - x_j(t-\tau)|. & \end{aligned} \quad (17)$$

*Assumption 8.* Let the external disturbance  $d_i(t)$  ( $i = 1, 2, \dots, n$ ) be a bounded continuous function, so there exists an unknown positive constant  $\rho_i$  such that

$$|d_i(t)| \leq \rho_i \quad (18)$$

For the sake of simplicity, this article only discusses the constant unknown disturbance.

*3.1. Controller Design.* Generally, designing the process of SMC has two steps. Firstly, an appropriate SMS is designed, which represents the required system dynamic characteristics. In this paper, a switching fractional-order SMS is given as

$$s_i(t) = {}_0^C D_t^{-1} ({}^C D_t^\alpha e_i(t) + p_i e_i(t) + q_i \text{sign}(e_i(t))), \quad (19)$$

where  $i = 1, 2, \dots, n$ ,  $e_i(t)$  is the state of the error system (16), and  $p_i$  and  $q_i$  are positive constants.  $\text{sign}(\cdot)$  is the symbolic function.

$$\text{sign}(e_i(t)) = \begin{cases} 1 & e_i(t) > 0, \\ -1 & e_i(t) < 0, \\ \in [-1, 1] & e_i(t) = 0. \end{cases} \quad (20)$$

According to the SMC theory, when the system operates in SMS, the SMS and its derivative must satisfy

$$\begin{aligned} s_i(t) & = 0, \\ \dot{s}_i(t) & = 0. \end{aligned} \quad (21)$$

As a result, considering ((19)-(21)), one obtains

$$\dot{s}_i(t) = {}_0^C D_t^\alpha e_i(t) + p_i e_i(t) + q_i \text{sign}(e_i(t)) = 0. \quad (22)$$

Then, we have the sliding mode equation (SME)

$${}_0^C D_t^\alpha e_i(t) = -(p_i e_i(t) + q_i \text{sign}(e_i(t))). \quad (23)$$

In the next parts, we construct the SMC law  $u_i(t)$  to make sure the state trajectories of system (16) reach the SMS  $s_i(t) = 0$  and keep on it forever by the SMC method. The fractional-order SMC law is presented as

$$\begin{aligned} u_i(t) = & -(-\hat{a}_i(t) + p_i) e_i(t) - \hat{d}_i(t) - |s_i(t)| \\ & \cdot \left( \sum_{j=1}^n |b_{ij}| L_j^f |e_j(t)| + \sum_{j=1}^n |c_{ij}| L_j^g |e_j(t-\tau)| \right) \\ & - q_i \text{sign}(e_i(t)) - \zeta_i^a s_i(t) - \zeta_i^b \text{sign}(s_i(t)), \end{aligned} \quad (24)$$

where  $\zeta_i^a > 0$  and  $\zeta_i^b > 0$  are constant gains,  $\hat{a}_i(t)$  is the estimation of  $a_i(t)$ ,  $\hat{d}_i(t)$  is the estimation of  $d_i(t)$ , and the unknown parameters  $a_i(t)$  and  $d_i(t)$  are estimated as

$$\begin{aligned} \hat{a}_i(t) & = -\eta_i^a s_i(t) e_i(t), \\ \hat{d}_i(t) & = \eta_i^d s_i(t). \end{aligned} \quad (25)$$

where  $i = 1, 2, \dots, n$ ,  $\eta_i^a > 0$  and  $\eta_i^d > 0$  are adaptation gains.

In order to realize SMC, two steps are required. Firstly, the system trajectories are controlled to reach the SMS  $s_i(t) = 0$ , which is shown in Theorem 9. Secondly, once the system operates in SMS, we should get the stability of the error system (16) and make sure SMS converge to zero in finite time, which is shown in Theorem 12.

**Theorem 9.** For the uncertain delayed FOHNNs (16), if the system is controlled by the SMC law (24) and (25), then the system trajectories will converge to the SMS  $s_i(t) = 0$  in finite time.

*Proof.* Choose the positive definite Lyapunov function candidate

$$V_i(t) = \frac{1}{2}s_i(t)^2 + \frac{1}{2\eta_i^a}(\widehat{a}_i(t) - a_i(t))^2 + \frac{1}{2\eta_i^d}(\widehat{d}_i(t) - d_i)^2. \quad (26)$$

Taking the integer-order derivative of  $V_i(t)$ , we have

$$\dot{V}_i(t) = s_i(t)\dot{s}_i(t) + \frac{1}{\eta_i^a}(\widehat{a}_i(t) - a_i)\dot{\widehat{a}}_i(t) + \frac{1}{\eta_i^d}(\widehat{d}_i(t) - d_i)\dot{\widehat{d}}_i(t). \quad (27)$$

Inserting  $\dot{s}_i(t)$  from (22) into the above equation, one has

$$\dot{V}_i(t) = s_i(t)({}^C_0D_t^\alpha e_i + p_i e_i + q_i \text{sign}(e_i)) + \frac{1}{\eta_i^a}(\widehat{a}_i(t) - a_i)\dot{\widehat{a}}_i(t) + \frac{1}{\eta_i^d}(\widehat{d}_i(t) - d_i)\dot{\widehat{d}}_i(t). \quad (28)$$

Based on (16), we get

$$\begin{aligned} \dot{V}_i(t) = & s_i(t) \left( -a_i e_i(t) \right. \\ & + \sum_{j=1}^n b_{ij} (f_j(y_j(t)) - f_j(x_j(t))) \\ & + \sum_{j=1}^n c_{ij} (g_j(y_j(t-\tau)) - g_j(x_j(t-\tau))) + d_i \\ & \left. + u_i(t) + p_i e_i(t) + q_i \text{sign}(e_i(t)) \right) + \frac{1}{\eta_i^a}(\widehat{a}_i(t) \\ & - a_i)\dot{\widehat{a}}_i(t) + \frac{1}{\eta_i^d}(\widehat{d}_i(t) - d_i)\dot{\widehat{d}}_i(t). \end{aligned} \quad (29)$$

According to Assumption 7, we will obtain

$$\begin{aligned} s_i(t) \sum_{j=1}^n b_{ij} (f_j(y_j(t)) - f_j(x_j(t))) \\ \leq |s_i(t)| \sum_{j=1}^n |b_{ij}| |f_j(y_j(t)) - f_j(x_j(t))| \\ \leq |s_i(t)| \sum_{j=1}^n |b_{ij}| L_j^f |e_j(t)| \end{aligned} \quad (30)$$

Correspondingly, we have

$$\begin{aligned} s_i(t) \sum_{j=1}^n c_{ij} (g_j(y_j(t-\tau)) - g_j(x_j(t-\tau))) \\ \leq |s_i(t)| \sum_{j=1}^n |c_{ij}| L_j^g |e_j(t-\tau)| \end{aligned} \quad (31)$$

Combining ((29)-(31)), we can get the following conclusion:

$$\begin{aligned} \dot{V}_i(t) \\ \leq s_i(t) ((-a_i + p_i) e_i(t) + q_i \text{sign}(e_i(t)) + d_i + u_i(t)) \\ + |s_i(t)| \sum_{j=1}^n |b_{ij}| L_j^f |e_j(t)| \\ + |s_i(t)| \sum_{j=1}^n |c_{ij}| L_j^g |e_j(t-\tau)| \\ + \frac{1}{\eta_i^a}(\widehat{a}_i(t) - a_i)\dot{\widehat{a}}_i(t) + \frac{1}{\eta_i^d}(\widehat{d}_i(t) - d_i)\dot{\widehat{d}}_i(t). \end{aligned} \quad (32)$$

Substituting  $u_i(t)$  from (24) into (32), it yields

$$\begin{aligned} \dot{V}_i(t) \leq & s_i(t) \left( (-a_i + p_i) e_i(t) + q_i \text{sign}(e_i(t)) + d_i \right. \\ & - (-\widehat{a}_i + p_i) e_i(t) - \widehat{d}_i(t) - |s_i(t)| \\ & \cdot \left( \sum_{j=1}^n |b_{ij}| L_j^f |e_j(t)| + \sum_{j=1}^n |c_{ij}| L_j^g |e_j(t-\tau)| \right) \\ & - q_i \text{sign}(e_i(t)) - \zeta_i^a s_i(t) - \zeta_i^b \text{sign}(s_i(t)) + |s_i(t)| \\ & \cdot \left. \sum_{j=1}^n |b_{ij}| L_j^f |e_j(t)| + |s_i(t)| \sum_{j=1}^n |c_{ij}| L_j^g |e_j(t-\tau)| \right) \\ & + \frac{1}{\eta_i^a}(\widehat{a}_i(t) - a_i)\dot{\widehat{a}}_i(t) + \frac{1}{\eta_i^d}(\widehat{d}_i(t) - d_i)\dot{\widehat{d}}_i(t). \end{aligned} \quad (33)$$

Through operation, we get

$$\begin{aligned} \dot{V}_i(t) \leq & s_i(t) \left( (\hat{a}_i(t) - a_i) e_i(t) - (\hat{d}_i(t) - d_i) \right. \\ & \left. - \zeta_i^a s_i(t) - \zeta_i^b \text{sign}(s_i(t)) \right) + \frac{1}{\eta_i^a} (\hat{a}_i(t) - a_i) \dot{\hat{a}}_i(t) \\ & + \frac{1}{\eta_i^d} (\hat{d}_i(t) - d_i) \dot{\hat{d}}_i(t). \end{aligned} \quad (34)$$

Insert (25)

$$\begin{aligned} \dot{V}_i(t) \leq & s_i(t) \left( (\hat{a}_i(t) - a_i) e_i(t) - (\hat{d}_i(t) - d_i) \right. \\ & \left. - \zeta_i^a s_i(t) - \zeta_i^b \text{sign}(s_i(t)) \right) - \frac{1}{\eta_i^a} (\hat{a}_i(t) - a_i) \eta_i^a s_i(t) \\ & \cdot e_i(t) + \frac{1}{\eta_i^d} (\hat{d}_i(t) - d_i) \eta_i^d s_i(t). \end{aligned} \quad (35)$$

Then, one obtains

$$\dot{V}_i(t) \leq -\zeta_i^a s_i^2(t) - \zeta_i^b \text{sign}(s_i(t)) s_i(t). \quad (36)$$

Using  $\text{sign}(s_i(t))s_i(t) = |s_i(t)|$  and property of inequality, we get

$$\dot{V}_i(t) \leq -\zeta_i^b |s_i(t)| < 0, \quad (37)$$

where  $\zeta_i^b > 0$ . Therefore, according to Lyapunov theory, the system states will converge to SMS  $s_i(t) = 0$ . Hence, the proof is achieved completely.  $\square$

*Remark 10.* Theorem 9 gets the error systems trajectories to reach the sliding surface  $s_i(t) = 0$  in finite time.

*Remark 11.* Time delay and external disturbance have little influence on the error system (16).

**3.2. Stability of Sliding Mode.** For the SME (23), we choose the positive definite Lyapunov function

$$V_i(t) = \frac{1}{2} e_i^2(t). \quad (38)$$

Taking the fractional-order derivative of  $V_i(t)$  and using Lemma 6, we get

$$\begin{aligned} {}_0^C D_t^\alpha V_i(t) & \leq e_i(t) {}_0^C D_t^\alpha e_i(t) \\ & = e_i(t) (-p_i e_i - q_i \text{sign}(e_i(t))) \\ & = -p_i e_i^2(t) - q_i e_i(t) \text{sign}(e_i(t)) \\ & = -p_i e_i^2(t) - q_i |e_i(t)| \leq -q_i |e_i(t)| \\ & = -\sqrt{2} q_i V_i^{1/2}(t), \end{aligned} \quad (39)$$

where  $q_i > 0$ . As a result, according to Lemma 3 and Remark 4,  $e_i$  will converge to 0 asymptotically.

Therefore, the state trajectories of system (23) will converge to 0, so one has the following conclusion.

**Theorem 12.** *The sliding mode dynamics system (23) is asymptotically stable, and its states  $e_i(t)$  converge to 0.*

**Corollary 13.** *By Theorems 9 and 12, system (16) is asymptotically stable, which means that system (14) can synchronize system (13).*

## 4. Numerical Simulations

The effectiveness of the obtained theoretical results is shown by the example. Considering the two-dimensional uncertain delayed FOHNNs (as the Master system)

$$\begin{aligned} {}_0^C D_t^\alpha x_1(t) & = -x_1 + 0.5 \sin(x_1(t)) + \sin(x_2(t)) \\ & \quad + 0.5 \tanh(x_1(t - 0.8)) \\ & \quad + \tanh(x_2(t - 0.8)) + 0.2, \\ {}_0^C D_t^\alpha x_2(t) & = -0.5x_2 + \sin(x_1(t)) - 0.5 \sin(x_2(t)) \\ & \quad - 0.5 \tanh(x_1(t - 0.8)) \\ & \quad - \tanh(x_2(t - 0.8)) + 0.3 \end{aligned} \quad (40)$$

where  $\alpha = 0.9$ , the initial conditions are  $x_1(0) = -5, x_2(0) = 5$ .

The form of the slave system is given by

$$\begin{aligned} {}_0^C D_t^\alpha y_1(t) & = -y_1 + 0.5 \sin(y_1(t)) \\ & \quad + \sin(y_2(t)) 0.5 \tanh(y_1(t - 0.8)) \\ & \quad + \tanh(y_2(t - 0.8)) + 0.2 + 0.1 \\ & \quad + u_1(t), \\ {}_0^C D_t^\alpha y_2(t) & = -0.5y_2 - \sin(y_1(t)) - 0.5 \sin(y_2(t)) \\ & \quad - 0.5 \tanh(y_1(t - 0.8)) \\ & \quad - \tanh(y_2(t - 0.8)) + 0.3 + 0.15 \\ & \quad + u_2(t) \end{aligned} \quad (41)$$

Assume that the initial conditions are  $y_1(0) = -3, y_2(0) = 3$ , and  $\alpha = 0.9$ .

Choosing  $p_1 = p_2 = 0.5, q_1 = q_2 = 1.5, L_1^f = L_2^f = L_1^g = L_2^g = 1, \eta_1^a = \eta_2^a = 1.1, \eta_1^d = \eta_2^d = 1.2, \zeta_1^a = \zeta_2^a = 1.1, \zeta_1^b = \zeta_2^b = 1.2$ , one gets

$$\begin{aligned} \dot{\hat{a}}_1(t) & = -1.1e_1(t) s_1(t) \\ \dot{\hat{a}}_2(t) & = -1.1e_2(t) s_2(t) \end{aligned} \quad (42)$$

and

$$\begin{aligned} \dot{\hat{d}}_1(t) & = 1.2s_1(t) \\ \dot{\hat{d}}_2(t) & = 1.2s_2(t) \end{aligned} \quad (43)$$

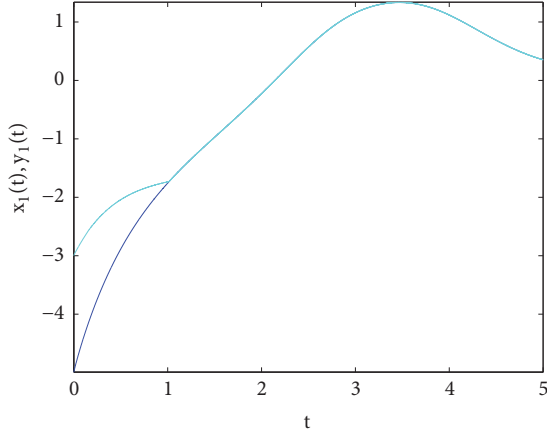


FIGURE 1: Synchronization between  $x_1(t)$  (blue line) and  $y_1(t)$  (green line).

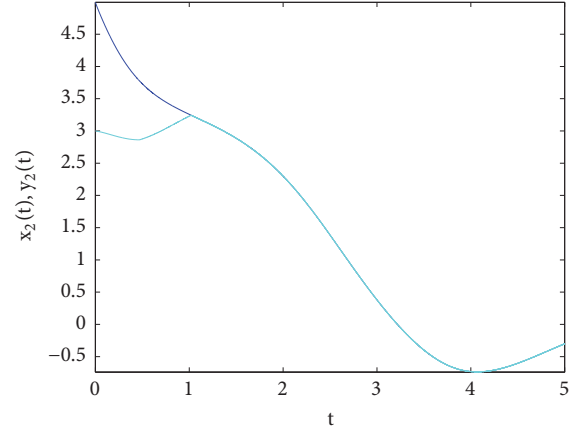


FIGURE 2: Synchronization between  $x_2(t)$  (blue line) and  $y_2(t)$  (green line).

We use (19) and design the SMS

$$\begin{aligned} s_1(t) &= {}_0D_t^{-1} \left( {}_0^C D_t^{0.9} e_1(t) + 0.5e_1(t) + 1.5\text{sign}(e_1(t)) \right) \\ s_2(t) &= {}_0D_t^{-1} \left( {}_0^C D_t^{0.9} e_2(t) + 0.5e_2(t) + 1.5\text{sign}(e_2(t)) \right). \end{aligned} \quad (44)$$

Thus, according to (24), the control inputs are obtained as

$$\begin{aligned} u_1(t) &= (\hat{a}_1(t) - 0.5)e_1(t) - \hat{d}_1(t) - 1.5\text{sign}(e_1(t)) \\ &\quad - 1.1s_1(t) - 1.2\text{sign}(s_1(t)) - |s_1(t)| (0.5|e_1(t)| \\ &\quad + |e_2(t)| + 0.5|e_1(t-0.8)| + |e_2(t-0.8)|), \\ u_2(t) &= (\hat{a}_2(t) - 0.5)e_2(t) - \hat{d}_2(t) - 1.5\text{sign}(e_2(t)) \\ &\quad - 1.1s_2(t) - 1.2\text{sign}(s_2(t)) - |s_2(t)| (-|e_1(t)| \\ &\quad - 0.5|e_2(t)| - 0.5|e_1(t-0.8)| - 1|e_2(t-0.8)|). \end{aligned} \quad (45)$$

The simulation results are depicted in Figures 1–6. Figures 1–3 show the synchronization between two fractional-order neural networks and the time response of the synchronization errors. The time response of the updated parameters and the sliding surfaces are included in Figures 4, 5, and 6, respectively. From the results, we can see that the synchronization errors converge to origin rapidly, and favorable synchronization performance has been achieved.

## 5. Conclusion

The adaptive synchronization problem for FOHNNs with system uncertainties, time delay, and external disturbances has been studied by SMC. Some estimations for system uncertainties and external disturbances are made. Firstly, establishing a switched SMS, the finite-time stability of the SMS to origin is proved according to the fractional-order

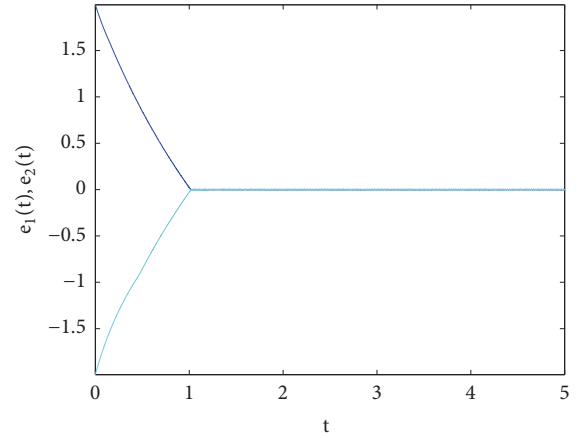


FIGURE 3: Synchronization errors  $e_1(t)$  (blue line),  $e_2(t)$  (green line).

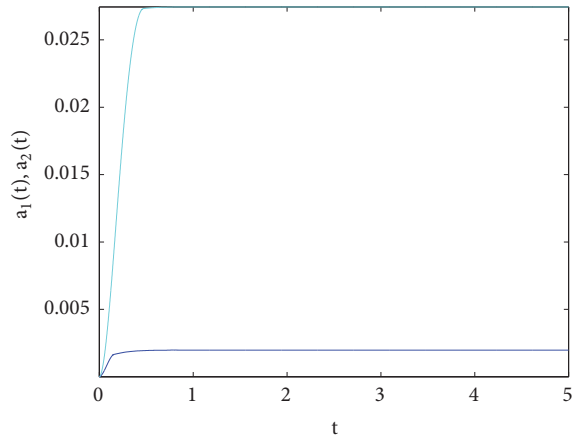


FIGURE 4: The time response of control parameters:  $\hat{a}_1$  (blue line) and  $\hat{a}_2$  (green line).

Lyapunov theory. Secondly, an adaptive synchronization fractional-order sliding mode controller is designed to force the error systems trajectories to reach the switching SMS and remain on it forever. The effectiveness and feasibility of theoretical results are verified by the numerical simulations.

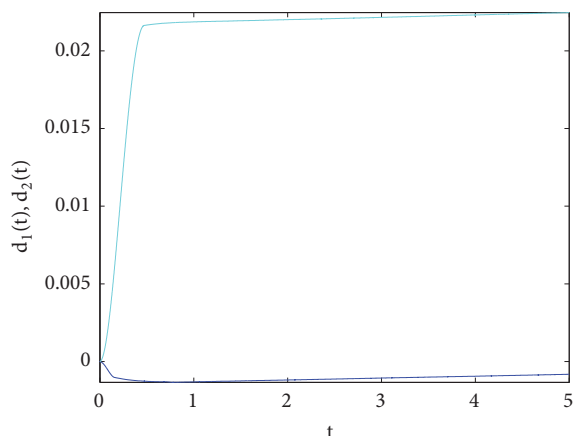


FIGURE 5: The time response of control parameters:  $\hat{d}_1$  (blue line) and  $\hat{d}_2$  (green line).

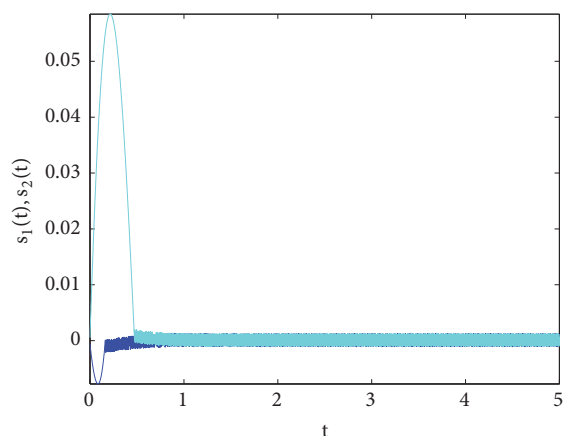


FIGURE 6: The sliding surfaces:  $s_1(t)$  (blue line) and  $s_2(t)$  (green line).

Furthermore, taking advantage of the SMC theory, the stability problems of FOHNNs with both multiple time delays and impulses will be discussed in future works.

### Data Availability

No data were used to support this study.

### Conflicts of Interest

The authors declare that there are no conflicts of interest regarding the publication of this article.

### Acknowledgments

This work was supported by the National Natural Science Foundation of China (no. 61573008), Post-Doctoral Applied Research Projects of Qingdao (no. 2015122), and Scientific Research Foundation of Shandong University of Science and Technology for Recruited Talents (no. 2014RCJJ032).

### References

- [1] G. Velmurugan, R. Rakkiyappan, V. Vembarasan, J. Cao, and A. Alsaedi, "Dissipativity and stability analysis of fractional-order complex-valued neural networks with time delay," *Neural Networks*, vol. 86, pp. 42–53, 2017.
- [2] I. Aizenberg, "Complex-valued neural networks with multi-valued neurons," *Springer*, pp. 39–62, 2011.
- [3] R. Rakkiyappan, G. Velmurugan, and J. Cao, "Multiple  $\mu$ -stability analysis of complex-valued neural networks with unbounded time-varying delays," *Neurocomputing*, vol. 149, pp. 594–607, 2015.
- [4] R. Guo, Z. Zhang, X. Liu, and C. Lin, "Existence, uniqueness, and exponential stability analysis for complex-valued memristor-based BAM neural networks with time delays," *Applied Mathematics and Computation*, vol. 311, pp. 100–117, 2017.
- [5] W. Lv and F. Wang, "Adaptive tracking control for a class of uncertain nonlinear systems with infinite number of actuator failures using neural networks," *Advances in Difference Equations*, Paper No. 374, 16 pages, 2017.
- [6] L. Li, Z. Wang, Y. Li, H. Shen, and J. Lu, "Hopf bifurcation analysis of a complex-valued neural network model with discrete and distributed delays," *Applied Mathematics and Computation*, vol. 330, pp. 152–169, 2018.
- [7] I. Podlubny, "Fractional differential equations," *Mathematics in Science and Engineering*, 1998.
- [8] Y. Cui, "Uniqueness of solution for boundary value problems for fractional differential equations," *Applied Mathematics Letters*, vol. 51, pp. 48–54, 2016.
- [9] Z. Bai, X. Dong, and C. Yin, "Existence results for impulsive nonlinear fractional differential equation with mixed boundary conditions," *Boundary Value Problems*, vol. 1, pp. 63–71, 2016.
- [10] Z. Bai, Y. Chen, H. Lian, and S. Sun, "On the existence of blow up solutions for a class of fractional differential equations," *Fractional Calculus and Applied Analysis*, vol. 17, no. 4, pp. 1175–1187, 2014.
- [11] R. Pu, X. Zhang, Y. Cui, P. Li, and W. Wang, "Positive solutions for singular semipositone fractional differential equation subject to multipoint boundary conditions," *Journal of Function Spaces*, vol. 2017, pp. 1–7, 2017.
- [12] Y. Zou and G. He, "On the uniqueness of solutions for a class of fractional differential equations," *Applied Mathematics Letters*, vol. 74, pp. 68–73, 2017.
- [13] Y. Cu, W. Ma, Q. Sun, and X. Su, "New uniqueness results for boundary value problem of fractional differential equation," *Nonlinear Analysis: Modelling and Control*, pp. 31–39, 2018.
- [14] J. Sabatier, O. P. Agrawal, and A. J. T. Machado, *Advances in fractional calculus*, Springer Netherlands, 2007.
- [15] Z. Wang, "A numerical method for delayed fractional-order differential equations," *Journal of Applied Mathematics*, vol. 2013, Article ID 256071, 7 pages, 2013.
- [16] Z. Wang, X. Huang, and J. Zhou, "A numerical method for delayed fractional-order differential equations: based on G-L definition," *Applied Mathematics & Information Sciences*, vol. 7, no. 2, pp. 525–529, 2013.
- [17] B. Xin and Y. Li, "0-1 test for chaos in a fractional order financial system with investment incentive," *Abstract and Applied Analysis*, Art. ID 876298, 10 pages, 2013.
- [18] Z. Wang, X. Wang, Y. Li, and X. Huang, "Stability and Hopf bifurcation of fractional-order complex-valued single neuron

- model with time delay," *International Journal of Bifurcation and Chaos*, vol. 27, no. 13, 1750209, 13 pages, 2017.
- [19] Z. Wang, X. Huang, and G. D. Shi, "Analysis of nonlinear dynamics and chaos in a fractional order financial system with time delay," *Computers & Mathematics with Applications*, vol. 62, no. 3, pp. 1531–1539, 2011.
- [20] I. Petras, "Modeling and numerical analysis of fractional-order bloch equations," *Computers & Mathematics with Applications*, vol. 61, no. 2, pp. 341–356, 2011.
- [21] N. Aguila-Camacho, M. A. Duarte-Mermoud, and J. A. Galle-gos, "Lyapunov functions for fractional order systems," *Communi-cations in Nonlinear Science and Numerical Simulation*, vol. 19, no. 9, pp. 2951–2957, 2014.
- [22] Y. Xi, Y. Yu, S. Zhang, and X. Hai, "Finite-time robust control of uncertain fractional-order Hopfield neural networks via sliding mode control," *Chinese Physics B*, vol. 27, no. 1, 010202, 2018.
- [23] L. Chen, Y. Chai, R. Wu, T. Ma, and H. Zhai, "Dynamic analysis of a class of fractional-order neural networks with delay," *Neurocomputing*, vol. 111, pp. 190–194, 2013.
- [24] H. Liu, S. Li, H. Wang, Y. Huo, and J. Luo, "Adaptive syn-chronization for a class of uncertain fractional-order neural networks," *Entropy*, vol. 17, no. 10, pp. 7185–7200, 2015.
- [25] G. A. Anastassiou, "Fractional neural network approximation," *Computers & Mathematics with Applications*, vol. 64, no. 6, pp. 1655–1676, 2012.
- [26] H. Wang, Y. Yu, G. Wen, and S. Zhang, "Stability analysis of fractional-order neural networks with time delay," *Neural Processing Letters*, vol. 42, no. 2, pp. 479–500, 2015.
- [27] Y. Fan, X. Huang, Z. Wang, and Y. Li, "Nonlinear dynamics and chaos in a simplified memristor-based fractional-order neural network with discontinuous memductance function," *Nonlinear Dynamics*, vol. 93, no. 2, pp. 611–627, 2018.
- [28] C. Song and J. Cao, "Dynamics in fractional-order neural networks," *Neurocomputing*, vol. 142, pp. 494–498, 2014.
- [29] J. Zhou, C. Sang, X. Li, M. Fang, and Z. Wang, "H $\infty$  consensus for nonlinear stochastic multi-agent systems with time delay," *Applied Mathematics and Computation*, vol. 325, pp. 41–58, 2018.
- [30] J. Wang, K. Liang, X. Huang, Z. Wang, and H. Shen, "Dissipative fault-tolerant control for nonlinear singular perturbed systems with Markov jumping parameters based on slow state feedback," *Applied Mathematics and Computation*, vol. 328, pp. 247–262, 2018.
- [31] H. Gao, J. Xia, G. Zhuang, Z. Wang, and Q. Sun, "Nonfragile finite-time extended dissipative control for a class of uncertain switched neutral systems," *Complexity*, vol. 2017, pp. 1–22, 2017.
- [32] Y. Li, Y. Chen, and I. Podlubny, "Stability of fractional-order nonlinear dynamic systems: Lyapunov direct method and generalized Mittag-Leffler stability," *Computers & Mathematics with Applications*, vol. 59, no. 5, pp. 1810–1821, 2010.
- [33] Y. Li, Y. Chen, and I. Podlubny, "Mittag-Leffler stability of fractional order nonlinear dynamic systems," *Automatica*, vol. 45, no. 8, pp. 1965–1969, 2009.
- [34] H. Ma and Y. Jia, "Stability analysis for stochastic differential equations with infinite Markovian switchings," *Journal of Math-ematical Analysis and Applications*, vol. 435, no. 1, pp. 593–605, 2016.
- [35] Z. Yan and W. Zhang, "Finite-time stability and stabilization of Itô-type stochastic singular systems," *Abstract and Applied Analysis*, vol. 2014, pp. 1–10, 2014.
- [36] Y. Li, W. Zhang, and X. Liu, "Stability of nonlinear stochastic discrete-time systems," *Journal of Applied Mathematics*, vol. 2013, Article ID 356746, 8 pages, 2013.
- [37] Y. Li, Y. Sun, and F. Meng, "New criteria for exponential stability of switched time-varying systems with delays and nonlinear disturbances," *Nonlinear Analysis: Hybrid Systems*, vol. 26, pp. 284–291, 2017.
- [38] Y. Lin and W. Zhang, "Necessary/sufficient conditions for Pareto optimum in cooperative difference game," *Optimal Control Applications and Methods*, vol. 39, no. 2, pp. 1043–1060, 2018.
- [39] Y. Lin, T. Zhang, and W. Zhang, "Pareto-based guaranteed cost control of the uncertain mean-field stochastic systems in infinite horizon," *Automatica*, vol. 92, pp. 197–209, 2018.
- [40] L. Yao and W. Zhang, "Adaptive tracking control for a class of random pure-feedback nonlinear systems with Markovian switching," *International Journal of Robust and Nonlinear Con-trol*, vol. 28, no. 8, pp. 3112–3126, 2018.
- [41] W. Zhang, Y. Lin, and L. Xue, "Linear quadratic Pareto optimal control problem of stochastic singular systems," *Journal of The Franklin Institute*, vol. 354, no. 2, pp. 1220–1238, 2017.
- [42] V. I. Utkin and A. S. Poznyak, "Adaptive sliding mode control, advances in sliding mode control," *Springer Berlin Heidelberg*, pp. 21–53, 2013.
- [43] M. Ö. Efe, "Fractional fuzzy adaptive sliding-mode control of a 2-DOF direct-drive robot arm," *IEEE Transactions on Systems Man and Cybernetics Part B Cybernetics A Publication of the IEEE Systems Man and Cybernetics Society*, vol. 38, no. 6, pp. 1561–1570, 2008.
- [44] M. P. Aghababa, "Design of a chatter-free terminal sliding mode controller for nonlinear fractional-order dynamical systems," *International Journal of Control*, vol. 86, no. 10, pp. 1744–1756, 2013.
- [45] K. Liang, M. Dai, H. Shen, J. Wang, Z. Wang, and B. Chen, "L $_{2}$ -L $_{\infty}$  synchronization for singularly perturbed complex net-works with semi-Markov jump topology," *Applied Mathematics and Computation*, vol. 321, pp. 450–462, 2018.
- [46] Z. Zhang, H. Shao, Z. Wang, and H. Shen, "Reduced-order observer design for the synchronization of the generalized Lorenz chaotic systems," *Applied Mathematics and Computa-tion*, vol. 218, no. 14, pp. 7614–7621, 2012.
- [47] X. Huang, Y. Fan, J. Jia, Z. Wang, and Y. Li, "Quasi-synchronisation of fractional-order memristor-based neural networks with parameter mismatches," *IET Control Theory & Applications*, vol. 11, no. 14, pp. 2317–2327, 2017.
- [48] J. Chen, Z. Zeng, and P. Jiang, "Global Mittag-Leffler stability and synchronization of memristor-based fractional-order neu-ral networks," *Neural Networks*, vol. 51, pp. 1–8, 2014.
- [49] A. Wu and Z. Zeng, "Global Mittag-Leffler stabilization of fractional-order memristive neural networks," *IEEE Transac-tions on Neural Networks and Learning Systems*, vol. 28, no. 1, pp. 206–217, 2017.

## Research Article

# Stability Analysis of Solutions for a Kind of Integro-Differential Equations with a Delay

Jing Zhao <sup>1,2</sup> and Fanwei Meng <sup>1</sup>

<sup>1</sup>School of Mathematical Science, Qufu Normal University, Qufu, 273165, China

<sup>2</sup>Science and Information College, Qingdao Agricultural University, Qingdao 266109, China

Correspondence should be addressed to Fanwei Meng; fwmeng@qfnu.edu.cn

Received 8 May 2018; Accepted 24 June 2018; Published 10 July 2018

Academic Editor: Weihai Zhang

Copyright © 2018 Jing Zhao and Fanwei Meng. This is an open access article distributed under the Creative Commons Attribution License, which permits unrestricted use, distribution, and reproduction in any medium, provided the original work is properly cited.

Stability of zero solution for second-order integro-differential equations with a delay is analyzed and some new results are presented. Through constructing Lyapunov functional, we give the corresponding sufficient conditions on stability of zero solution for two integro-differential equations. Moreover, an illustrative example is considered to support our new results.

## 1. Introduction

Stability and the existence of solutions for nonlinear differential equations have been studied by many scholars [1–20] due to their many applications to problems in information theory, control theory, mechanics, chemistry, physics, and so on. In [5], the authors considered a second-order functional integro-differential equation with multiple delays

$$\begin{aligned} x''(t) + a(t)f(t, x(t), x'(t))x'(t) \\ + g(t, x(t), x'(t)) + \sum_{i=1}^n h_i(x(t - \tau_i)) \\ = \int_0^t C(t, \xi)x'(\xi)d\xi, \end{aligned} \quad (1)$$

and they gave some new conditions on the continuability and boundedness of solutions. Li [6] studied  $\Psi$ -stability of the trivial solutions of the following three nonlinear systems with time delay,

$$x'(t) = f(t, x(t)) + g(t, x(t - \tau(t))), \quad (2)$$

and two Volterra integro-differential equations

$$\begin{aligned} x'(t) = f(t, x(t)) + g(t, x(t - \tau(t))) \\ + p(t, x(t)) \int_0^t q(s, x(s - \tau(s))) ds, \end{aligned} \quad (3)$$

$$\begin{aligned} x'(t) = f(t, x(t)) + g(t, x(t - \tau(t))) \\ + p(t, x(t - \tau(t))) \int_0^t q(s, x(s)) ds. \end{aligned} \quad (4)$$

In [1], Afuwape studied the asymptotic stability and the uniformly ultimate boundedness of the solutions for a kind of third-order delay differential equations and gave some sufficient conditions.

This paper investigates second-order integro-differential equations with a delay and obtains some new results on the stability of zero solution. By constructing Lyapunov functional, the corresponding sufficient conditions are present on stability of zero solution for two integro-differential equations. Moreover, an illustrative example is considered to show that our results are effective.

The rest of this paper is organized as follows. Section 2 presents the main results of this paper. In Section 3, an illustrative example is given to support our new results.

### 2. Main Results

Consider the following integro-differential equation with a delay:

$$\begin{aligned} x'' + f(t, x, x')x' + g(t, x, x') + h(x(t - \tau)) \\ = p(t, x(t)) \int_0^t q(s, x'(s)) ds, \end{aligned} \tag{5}$$

where  $\mathbb{R}_+ = [0, +\infty)$ ,  $\tau > 0$  is a constant,  $f, g : \mathbb{R}_+ \times \mathbb{R}^2 \rightarrow \mathbb{R}$  and  $h : \mathbb{R}_+ \rightarrow \mathbb{R}$  are continuous with  $h(0) = 0$ , and  $p, q : \mathbb{R}_+ \times \mathbb{R} \rightarrow \mathbb{R}$  with  $p(t, 0) = 0$  and  $q(t, 0) = 0$ .

We can rewrite (5) as the system

$$\begin{aligned} x' &= y, \\ y' &= -f(t, x, y)y - g(t, x, y) - h(x) \\ &\quad + \int_{t-\tau}^t h'(x(s))y(s) ds \\ &\quad + p(t, x) \int_0^t q(s, y(s)) ds. \end{aligned} \tag{6}$$

**Theorem 1.** Consider system (6). There exist nonnegative constants  $K^*$ ,  $R$ ,  $b$ ,  $M$ , and  $N$ , a positive number  $l$ , and functions  $P(t), Q(t) : \mathbb{R}_+ \rightarrow \mathbb{R}_+$ , such that the following conditions hold:

- (C<sub>1</sub>)  $h(x)x^{-1} \geq l$  when  $x \neq 0$ ,  $|h'(x)| \leq K^*$ .
- (C<sub>2</sub>)  $g(t, x, 0) = 0$ ,  $g(t, x, y)y^{-1} \geq b$  when  $y \neq 0$ .
- (C<sub>3</sub>)  $|p(t, x)| \leq P(t) \leq M$ ,  $|q(t, y)| \leq Q(t)|y|$ ,  $Q(t) \leq N$ .
- (C<sub>4</sub>)  $N \int_0^\infty P(s)ds + M \int_0^\infty Q(s)ds + K^*(\tau + 1) \leq 2f(t, x, y) + 2b$ .

Then the zero solution of system (6) is stable.

*Proof.* Define a Lyapunov functional  $V(t) = V(t, x, y)$  as

$$\begin{aligned} V(t) &= \frac{1}{2}y^2 + \int_0^x h(\eta) d\eta + \lambda \int_{-\tau}^0 ds \int_{t+s}^t y^2(\theta) d\theta \\ &\quad + \frac{1}{2} \int_0^t ds \int_t^\infty |p(\theta, x(\theta))| Q(s) y^2(s) d\theta, \end{aligned} \tag{7}$$

where  $\lambda$  is a positive constant to be determined. Using condition (C<sub>1</sub>), we have

$$\int_0^x h(\eta) d\eta = \int_0^x \frac{h(\eta)}{\eta} \eta d\eta \geq \int_0^x l\eta d\eta = \frac{l}{2}x^2 > 0, \tag{8}$$

and  $V(t) \geq (l/2)x^2 + (1/2)y^2$ .

Suppose that  $(x(t), y(t))$  is a solution of (6). Then

$$\begin{aligned} \frac{dV}{dt} &= yy' + h(x)y + \lambda \int_{-\tau}^0 [y^2(t) - y^2(t+s)] ds \\ &\quad + \frac{1}{2}Q(t)y^2(t) \int_t^\infty |p(\theta, x(\theta))| d\theta \\ &\quad - \frac{1}{2}|p(t, x(t))| \int_0^t Q(s)y^2(s) ds \\ &= -f(t, x, y)y^2 - g(t, x, y)y + \lambda\tau y^2 \\ &\quad + y(t) \int_{t-\tau}^t h'(x(s))y(s) ds \\ &\quad + y(t)p(t, x(t)) \int_0^t q(s, y(s)) ds \\ &\quad - \lambda \int_{t-\tau}^t y^2(s) ds \\ &\quad + \frac{1}{2}Q(t)y^2(t) \int_t^\infty |p(\theta, x(\theta))| d\theta \\ &\quad - \frac{1}{2}|p(t, x(t))| \int_0^t Q(s)y^2(s) ds. \end{aligned} \tag{9}$$

By conditions (C<sub>1</sub>) and (C<sub>3</sub>) and  $2ab \leq a^2 + b^2$ , we have

$$\begin{aligned} &y(t) \int_{t-\tau}^t h'(x(s))y(s) ds \\ &\leq |y(t)| \int_{t-\tau}^t |h'(x(s))||y(s)| ds \\ &\leq \frac{K^*}{2} \int_{t-\tau}^t [y^2(t) + y^2(s)] ds \\ &= \frac{K^*}{2}\tau y^2 + \frac{K^*}{2} \int_{t-\tau}^t y^2(s) ds, \\ &y(t)p(t, x(t)) \int_0^t q(s, y(s)) ds \\ &\leq |y(t)||p(t, x(t))| \int_0^t |q(s, y(s))| ds \end{aligned} \tag{10}$$

$$\begin{aligned}
 &\leq |p(t, x(t))| |y(t)| \int_0^t Q(s) |y(s)| ds \\
 &\leq \frac{1}{2} |p(t, x(t))| \int_0^t Q(s) [y^2(t) + y^2(s)] ds \\
 &\leq \frac{My^2}{2} \int_0^\infty Q(s) ds \\
 &\quad + \frac{1}{2} |p(t, x(t))| \int_0^t Q(s) y^2(s) ds.
 \end{aligned}
 \tag{11}$$

Then,

$$\begin{aligned}
 \frac{dV}{dt} &\leq \left[ -f(t, x, y) - b + \lambda\tau + \frac{K^*}{2}\tau \right] y^2 \\
 &\quad + \left( \frac{K^*}{2} - \lambda \right) \int_{t-\tau}^t y^2(s) ds \\
 &\quad + \frac{N \int_0^\infty P(s) ds + M \int_0^\infty Q(s) ds}{2} y^2.
 \end{aligned}
 \tag{12}$$

Choosing  $\lambda = K^*/2$ , we have

$$\frac{dV}{dt} \leq \frac{-2f(t, x, y) - 2b + K^*(\tau + 1) + N \int_0^\infty P(s) ds + M \int_0^\infty Q(s) ds}{2} y^2 \leq 0.
 \tag{13}$$

Therefore, the zero solution of system (6) is stable and the proof is completed.  $\square$

Theorem 1 can be generalized to the form with a variable delay  $\tau(t)$ . It only needs a new condition. Then, the following result is obtained.

**Corollary 2.** Consider system (6) with a variable delay  $\tau(t)$ . Conditions (1)-(3) of Theorem 1 are satisfied. Moreover,

- (C<sub>4</sub>')  $N \int_0^\infty P(s) ds + M \int_0^\infty Q(s) ds + ((2-\beta)/(1-\beta))K^*\tau \leq 2f(t, x, y) + 2b$ ,
- (C<sub>5</sub>') there are  $\tau > 0$  and  $0 < \beta < 1$ , such that  $0 \leq \tau(t) \leq \tau$  and  $\tau'(t) \leq 1$ .

Then the zero solution of system (6) with a variable delay  $\tau(t)$  is stable.

*Proof.* The proof is similar to that of Theorem 1. But

$$\begin{aligned}
 \frac{dV}{dt} &\leq \left[ -f(t, x, y) - b + \lambda\tau(t) + \frac{K^*}{2}\tau(t) \right] y^2 \\
 &\quad + \left[ \frac{K^*}{2} - \lambda(1-\beta) \right] \int_{t-\tau(t)}^t y^2(s) ds \\
 &\quad + \frac{N \int_0^\infty P(s) ds + M \int_0^\infty Q(s) ds}{2} y^2.
 \end{aligned}
 \tag{14}$$

Thus, choosing  $\lambda = K^*/2(1-\beta)$ , we have

$$\frac{dV}{dt} \leq \frac{-2f(t, x, y) - 2b + ((2-\beta)/(1-\beta))K^*\tau + N \int_0^\infty P(s) ds + M \int_0^\infty Q(s) ds}{2} y^2 \leq 0.
 \tag{15}$$

Therefore, the zero solution of system (6) with a variable delay  $\tau(t)$  is stable and the proof is completed.  $\square$

Next, we consider another second-order integro-differential system with time delay

$$\begin{aligned}
 &x'' + f(t, x, x')x' + g(t, x, x') + h(x(t)) \\
 &= p(x(t-\tau)) \int_0^t q(s, x'(s)) ds,
 \end{aligned}
 \tag{16}$$

System (16) can be rewritten as follows:

$$\begin{aligned}
 &x' = y \\
 &y' = -f(t, x, y)y - g(t, x, y) - h(x(t)) \\
 &\quad - p(x) \int_0^t q(s, y(s)) ds \\
 &\quad + \int_{t-\tau}^t p'(x(s))y(s) ds \int_0^t q(s, y(s)) ds,
 \end{aligned}
 \tag{17}$$

**Theorem 3.** Consider system (17). There are nonnegative constants  $K, R, L_1, L_2$ , and  $N$ , positive numbers  $l, M$ , and  $M_1$ , and functions  $P(t)$  and  $Q(t)$ , such that the conditions hold:

- (D<sub>1</sub>)  $h(x)x^{-1} \geq l$  when  $x \neq 0$ ,  $|p'(x)| \leq K$ .
- (D<sub>2</sub>)  $f(t, x, 0) = 0, g(t, x, 0) = 0, f(t, x, y)y^{-2} \geq L_1, g(t, x, y)y^{-1} \geq L_2$  when  $y \neq 0$ .
- (D<sub>3</sub>)  $|p(x)| \leq P(t), M_1 \leq P(t) \leq M, |q(t, y)| \leq Q(t)y, Q(t) \leq N$ .
- (D<sub>4</sub>)  $M \int_0^\infty Q(s) ds + ((M + K\tau)N/M_1) \int_0^\infty P(s) ds \leq 2L_2$ .
- (D<sub>5</sub>)  $K\tau \int_0^\infty Q(s) ds \leq 2L_1$ .

Then the zero solution of system (17) is stable.

*Proof.* Define a Lyapunov functional  $V(t) = V(t, x, y)$  as

$$V(t) = \frac{1}{2}y^2 + \int_0^x h(\eta) d\eta + \lambda \int_{-\tau}^0 ds \int_{t+s}^t y^4(\theta) d\theta + \mu \int_0^t ds \int_t^\infty |p(x(\theta))| Q(s) y^2(s) d\theta, \quad (18)$$

where  $\lambda$  and  $\mu$  are two positive constants to be determined. Using condition  $(D_1)$ , we have

$$\int_0^x h(\eta) d\eta = \int_0^x \frac{h(\eta)}{\eta} \eta d\eta \geq \int_0^x l\eta d\eta = \frac{l}{2}x^2, \quad (19)$$

and then  $V(t) \geq (l/2)x^2 + (l/2)y^2$ .

Let  $(x(t), y(t))$  be a solution of (17). Then,

$$\begin{aligned} \frac{dV}{dt} &= yy' + h(x)y + \lambda \int_{-\tau}^0 [y^4(t) - y^4(t+s)] ds \\ &\quad + \mu Q(t) y^2(t) \int_t^\infty |p(x(\theta))| d\theta \\ &\quad - \mu |p(x(t))| \int_0^t Q(s) y^2(s) ds \\ &= -f(t, x, y) y^2 - g(t, x, y) y \\ &\quad - yp(x) \int_0^t q(s, y(s)) ds \\ &\quad + y \int_{t-\tau}^t p'(x(s)) y(s) ds \int_0^t q(s, y(s)) ds \\ &\quad + \lambda \tau y^4 - \lambda \int_{t-\tau}^t y^4(s) ds \\ &\quad + \mu Q(t) y^2 \int_t^\infty |p(x(\theta))| d\theta \\ &\quad - \mu |p(x(t))| \int_0^t Q(s) y^2(s) ds. \end{aligned} \quad (20)$$

Applying conditions  $(D_1)$  and  $(D_3)$  and  $2ab \leq a^2 + b^2$ , we have

$$\begin{aligned} &y \int_{t-\tau}^t p'(x(s)) y(s) ds \int_0^t q(s, y(s)) ds \\ &\leq |y| \int_{t-\tau}^t |p'(x(s))| |y(s)| ds \int_0^t |q(s, y(s))| ds \\ &\leq \frac{K}{2} \int_{t-\tau}^t [y^2(t) + y^2(s)] ds \int_0^t Q(\theta) |y(\theta)| d\theta \\ &\leq \frac{K\tau}{2} y^2(t) \int_0^t Q(\theta) |y(\theta)| d\theta \\ &\quad + \frac{K}{2} \int_{t-\tau}^t y^2(s) \int_0^t Q(\theta) |y(\theta)| d\theta ds \\ &\leq \frac{K\tau}{4} \int_0^t Q(\theta) [y^4(t) + y^4(\theta)] d\theta \end{aligned}$$

$$\begin{aligned} &+ \frac{K}{4} \int_{t-\tau}^t \int_0^t Q(\theta) [y^4(s) + y^2(\theta)] d\theta ds \\ &\leq \frac{K\tau}{4} y^4 \int_0^\infty Q(s) ds + \frac{K\tau}{2} \int_0^t Q(s) y^2(s) ds \\ &\quad + \frac{K}{4} \int_0^\infty Q(s) ds \int_{t-\tau}^t y^4(s) ds, \end{aligned} \quad (21)$$

$$\begin{aligned} &- y(t) p(x(t)) \int_0^t q(s, y(s)) ds \\ &\leq |y(t)| |p(x(t))| \int_0^t |q(s, y(s))| ds \\ &\leq |p(x(t))| |y(t)| \int_0^t Q(s) |y(s)| ds \\ &\leq \frac{1}{2} |p(x(t))| \int_0^t Q(s) [y^2(t) + y^2(s)] ds \\ &\leq \frac{My^2}{2} \int_0^\infty Q(s) ds + \frac{M}{2} \int_0^t Q(s) y^2(s) ds. \end{aligned} \quad (22)$$

By condition  $(D_2)$ , we have

$$\begin{aligned} \frac{dV}{dt} &\leq - \left[ L_1 - \frac{K\tau}{4} \int_0^\infty Q(s) ds - \lambda \tau \right] y^4 \\ &\quad - \left[ L_2 - \frac{M}{2} \int_0^\infty Q(s) ds - \mu N \int_0^\infty P(s) ds \right] y^2 \\ &\quad + \left[ \frac{K}{4} \int_0^\infty Q(s) ds - \lambda \right] \int_{t-\tau}^t y^4(s) ds \\ &\quad + \left[ \frac{M + K\tau}{2} - \mu M_1 \right] \int_0^t Q(s) y^2(s) ds. \end{aligned} \quad (23)$$

Thus, we choose  $\lambda = (K/4) \int_0^\infty Q(s) ds$  and  $\mu = (M + K\tau)/2M_1$ . Using conditions  $(D_4)$  and  $(D_5)$ , we have

$$\begin{aligned} \frac{dV}{dt} &\leq - \left[ L_1 - \frac{K\tau}{2} \int_0^\infty Q(s) ds \right] y^4 - \left[ L_2 \right. \\ &\quad \left. - \frac{M}{2} \int_0^\infty Q(s) ds - \frac{(M + K\tau)N}{2M_1} \int_0^\infty P(s) ds \right] y^2 \\ &\leq 0. \end{aligned} \quad (24)$$

Therefore, the zero solution of system (17) is stable and the proof is completed.  $\square$

**Corollary 4.** Consider system (17) with a variable delay  $\tau(t)$ . Conditions (1)-(3) of Theorem 3 are satisfied. Moreover,

$$(D_5') \quad (2 - \beta)K\tau \int_0^\infty Q(s) ds \leq 4(1 - \beta)L_1,$$

$(D_6)$  there are  $\tau > 0$  and  $0 < \beta < 1$ , such that  $0 \leq \tau(t) \leq \tau$  and  $\tau'(t) \leq 1$ .

Then the zero solution of system (17) with a variable delay  $\tau(t)$  is stable.

*Proof.* The proof is similar to that of Theorem 3. But

$$\begin{aligned} \frac{dV}{dt} &\leq - \left[ L_1 - \frac{K\tau(t)}{4} \int_0^\infty Q(s) ds - \lambda\tau(t) \right] y^4 \\ &\quad - \left[ L_2 - \frac{M}{2} \int_0^\infty Q(s) ds - \mu N \int_0^\infty P(s) ds \right] y^2 \\ &\quad + \left[ \frac{K}{4} \int_0^\infty Q(s) ds - \lambda(1 - \tau'(t)) \right] \int_{t-\tau(t)}^t y^4(s) ds \\ &\quad + \left[ \frac{M + K\tau(t)}{2} - \mu P(t) \right] \int_0^t Q(s) y^2(s) ds \\ &\leq - \left[ L_1 - \frac{K\tau}{4} \int_0^\infty Q(s) ds - \lambda\tau \right] y^4 \\ &\quad - \left[ L_2 - \frac{M}{2} \int_0^\infty Q(s) ds - \mu N \int_0^\infty P(s) ds \right] y^2 \\ &\quad + \left[ \frac{K}{4} \int_0^\infty Q(s) ds - \lambda(1 - \beta) \right] \int_{t-\tau(t)}^t y^4(s) ds \\ &\quad + \left[ \frac{M + K\tau}{2} - \mu M_1 \right] \int_0^t Q(s) y^2(s) ds. \end{aligned} \tag{25}$$

Thus, choosing  $\lambda = (K/4(1 - \beta)) \int_0^\infty Q(s)ds$  and  $\mu = (M + K\tau)/2M_1$ , we have

$$\begin{aligned} \frac{dV}{dt} &\leq - \left[ L_1 - \frac{(2 - \beta)K\tau}{4(1 - \beta)} \int_0^\infty Q(s) ds \right] y^4 - \left[ L_2 \right. \\ &\quad \left. - \frac{M}{2} \int_0^\infty Q(s) ds - \frac{(M + K\tau)N}{2M_1} \int_0^\infty P(s) ds \right] y^2 \\ &\leq 0. \end{aligned} \tag{26}$$

Then, the zero solution of system (6) with a variable delay  $\tau(t)$  is stable and the proof is completed.  $\square$

### 3. An Illustrative Example

In this section, we give an illustrative example to the effectiveness of results obtained in this paper. Moreover, we list a graph of solutions of an integral-differential equation with a delay to verify the correctness of the conclusion.

*Example 1.* Consider the following example:

$$\begin{aligned} x''(t) + 2e^{t+x^2(t)+x'^2(t)}x'(t) + \frac{1}{4}x'(t) + \frac{1}{2}x(t-2) \\ = e^{-2t} \int_0^t e^{-s}x'(s) ds. \end{aligned} \tag{27}$$

In the example,  $f(t, x, y) = 2e^{t+x^2+y^2}$ ,  $g(t, x, y) = (1/4)y$ ,  $h(x) = (1/2)x$ ,  $p(t, x) = e^{-2t}$ ,  $q(t, y) = \int_0^t e^{-s}y(s)ds$ , and a delay  $\tau = 2$ . Obvious, this system is the same form as (5). Moreover,

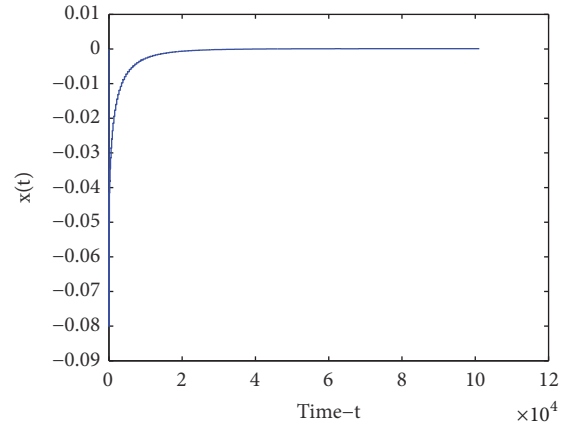


FIGURE 1: Stability of solutions for system (27).

- $(C_1) \ h(x)x^{-1} \geq l = 1/2, |h'(x)| = 1/2 \leq K^* = 1/2;$
- $(C_2) \ g(t, x, 0) = 0, g(t, x, y)y^{-1} \geq b = 1/4;$
- $(C_3) \ |p(t, x)| = P(t) \leq M = 1, |q(t, y)| \leq Q(t)|y|, Q(t) = e^{-t} \leq 1;$
- $(C_4) \ N \int_0^\infty P(s)ds + M \int_0^\infty Q(s)ds + K^*(\tau+1) = \int_0^\infty e^{-2t} dt + \int_0^\infty e^{-t} dt + 1/2 \times 2 = 7/2, 2f(t, x, y) + 2b \geq 4 + 2 \times 1/4 \geq 7/2.$

Thus, all conditions of Theorem 1 are satisfied and the zero solution of system (27) is stable by the obtained result. To show the effectiveness of the result, we carry out a simulation result with the following choices. Initial Condition:  $x(t) = x'(t) = 0$  for  $t \in [-2, 0)$ . The simulation result is shown in Figure 1, which is the stability of solutions for system (27).

### Data Availability

The data used to support the findings of this study are available from the corresponding author upon request.

### Conflicts of Interest

The authors declare that they have no conflicts of interest.

### Authors' Contributions

The first author is the main completer. The second author is the corresponding author and provides the thought of this paper and advice in the process of writing.

### Acknowledgments

This work is supported by the National Natural Science Foundation of China (G11671227, G11701310, and G61403223).

### References

- [1] A. U. Afuwape and M. O. Omeike, "On the stability and boundedness of solutions of a kind of third order delay differential

- equations," *Applied Mathematics and Computation*, vol. 200, no. 1, pp. 444–451, 2008.
- [2] A. Diamandescu, "On the  $\psi$ -stability of a nonlinear Volterra integro-differential system," *Electronic Journal of Differential Equations*, vol. 56, pp. 1–14, 2005.
- [3] A. Diamandescu, "On the  $\psi$ -asymptotic stability of a nonlinear Volterra integro-differential system," *Bulletin Mathematique de la Societe des Sciences Mathematiques de Roumanie*, vol. 46, no. 1-2, pp. 39–60, 2003.
- [4] K. Gopalsamy, *Stability and oscillations in delay differential equations of population dynamics*, Kluwer Academic, Dordrecht, The Netherlands, 1992.
- [5] J. R. Graef and C. Tunç, "Continuability and boundedness of multi-delay functional integro-differential equations of the second order," *Revista de la Real Academia de Ciencias Exactas, Fisicas y Naturales, Serie A: Matematicas*, vol. 109, no. 1, pp. 169–173, 2015.
- [6] L. Li, M. Han, X. Xue, and Y. Liu, " $\Psi$ -stability of nonlinear Volterra integro-differential systems with time delay," *Abstract and Applied Analysis*, pp. 1–5, 2013.
- [7] H. Liu and F. Meng, "Some new nonlinear integral inequalities with weakly singular kernel and their applications to FDEs," *Journal of Inequalities and Applications*, vol. 2015, no. 209, 2015.
- [8] F. Meng, L. Li, and Y. Bai, " $\psi$ -stability of nonlinear Volterra integro-differential systems," *Dynamic Systems and Applications*, vol. 20, no. 4, pp. 563–574, 2011.
- [9] W. Sun, L. Peng, Y. Zhang, and H. Jia, " $H_\infty$  excitation control design for stochastic power systems with input delay based on nonlinear Hamiltonian system theory," *Mathematical Problems in Engineering*, vol. 2015, Article ID 947815, 12 pages, 2015.
- [10] Weiwei Sun, Kaili Wang, Congcong Nie, and Xuejun Xie, "Energy-Based Controller Design of Stochastic Magnetic Levitation System," *Mathematical Problems in Engineering*, vol. 2017, pp. 1–6, 2017.
- [11] W. Sun and L. Peng, "Robust adaptive control of uncertain stochastic Hamiltonian systems with time varying delay," *Asian Journal of Control*, vol. 18, no. 2, pp. 642–651, 2016.
- [12] W. Sun and L. Peng, "Observer-based robust adaptive control for uncertain stochastic Hamiltonian systems with state and input delays," *Lithuanian Association of Nonlinear Analysts. Nonlinear Analysis: Modelling and Control*, vol. 19, no. 4, pp. 626–645, 2014.
- [13] X. Xie and M. Jiang, "Output feedback stabilization of stochastic feedforward nonlinear time-delay systems with unknown output function," *International Journal of Robust and Nonlinear Control*, vol. 28, no. 1, pp. 266–280, 2018.
- [14] X.-J. Xie, Z.-J. Li, and K. Zhang, "Semi-global output feedback control for nonlinear systems with uncertain time-delay and output function," *International Journal of Robust and Nonlinear Control*, vol. 27, no. 15, pp. 2549–2566, 2017.
- [15] R. Xu and Y. Zhang, "Generalized Gronwall fractional summation inequalities and their applications," *Journal of Inequalities and Applications*, vol. 2015, no. 42, 2015.
- [16] R. Xu and F. Meng, "Some new weakly singular integral inequalities and their applications to fractional differential equations," *Journal of Inequalities and Applications*, vol. 2016, no. 78, 2016.
- [17] Y. Wang and L. Liu, "Positive properties of the Green function for two-term fractional differential equations and its application," *Journal of Nonlinear Sciences and Applications. JNSA*, vol. 10, no. 4, pp. 2094–2102, 2017.
- [18] Z. Zheng, X. Gao, and J. Shao, "Some new generalized retarded inequalities for discontinuous functions and their applications," *Journal of Inequalities and Applications*, vol. 7, 2016.
- [19] Y. Zhao, S. Sun, Z. Han, and M. Zhang, "Positive solutions for boundary value problems of nonlinear fractional differential equations," *Applied Mathematics and Computation*, vol. 217, no. 16, pp. 6950–6958, 2011.
- [20] Y. Zhao, Y. Wang, X. Zhang, and H. Li, "Feedback stabilisation control design for fractional order non-linear systems in the lower triangular form," *IET Control Theory & Applications*, vol. 10, no. 9, pp. 1061–1068, 2016.

## Research Article

# Stochastic Optimal Control of Investment and Dividend Payment Model under Debt Control with Time-Inconsistency

Dan Zhu  and Chuancun Yin 

*School of Statistics, Qufu Normal University, Shandong Province 273165, China*

Correspondence should be addressed to Chuancun Yin; [ccyin@mail.qfnu.edu.cn](mailto:ccyin@mail.qfnu.edu.cn)

Received 23 April 2018; Accepted 5 June 2018; Published 9 July 2018

Academic Editor: Weihai Zhang

Copyright © 2018 Dan Zhu and Chuancun Yin. This is an open access article distributed under the Creative Commons Attribution License, which permits unrestricted use, distribution, and reproduction in any medium, provided the original work is properly cited.

This paper considers the optimal debt ratio, investment, and dividend payment policies for insurers with time-inconsistency. The surplus process of an insurance company is determined by the change of asset value and the change of liabilities. The asset can be invested in financial market which contains a risky asset and a risk-free asset, and when the insurer incurs a liability, he/she earns some premium. The objective is to maximize the expected nonconstant discounted utility of dividend payment until a determinate time. This is a time-inconsistent control problem. We obtain the modified HJB equation and the closed-form expressions for the optimal debt ratio, investment, and dividend payment policies under logarithmic utility.

## 1. Introduction

In recent decades, the actuarial science has shown a trend of diversified development. We can see that the relationships between mathematics and risk theory are becoming more and more close; furthermore, a lot of optimal control research problems are becoming very interesting and increasingly important. As a result, some scholars have already studied the optimal investment, optimal reinsurance, optimal dividend, and risk control problems for decades. Specially, as an important way of profit, the optimal investment problems have been widely investigated for many years in literatures. For example, [1] considered an insurance firm that is faced with a stochastic cash flow or random risk process and studied the optimal investment policies with considering exponential utility and minimizing the probability of ruin; for other investment problems also see [2, 3] and so on. The optimal dividend payment has been studied for many years since it was put forward by [4]. For example, [5, 6] investigated the optimal dividend strategies with Brownian motion and the compound Poisson model, respectively, [7, 8] investigated the optimal dividend strategies under spectrally negative Lévy processes and spectrally positive Lévy processes, respectively, [9] studied optimal dividends under nonlinear insurance risk

processes, [10] considered the optimal dividend strategies with capital injections and proportional transaction costs under a jump-diffusion model, and the reader can see more optimal dividend problem in a review about dividend [11]. In addition, researchers not only consider the optimal investment policies or optimal dividends individually but also combine with other optimal control problems. For example, [12–16] considered the optimal investment problems combining with reinsurance. Some researchers also investigated the investment problems with the optimal dividends policies, for example, [17–19].

Recently, the debt management problem has drawn more and more attention by many researchers. In particular, the occurrence of a global financial crisis in 2008 which was brought out by the collapse of US housing market in 2007 had drawn increasing attention to the debt ratio. It is now widely believed that excessive leveraging, and an excessive debt ratio, at key financial institutions helped convert the initial subprime turmoil in 2007 into a full blown financial crisis of 2008. In addition, the failure of AIG (American International Group) told us that the proper debt ratio in an insurance company is very important. Then, many scholars have investigated the optimal debt ratio under different risk models. For example, [20] derived the optimal debt ratio and

dividend payment strategies with reinsurance for an insurer. The paper [21] studied the optimal investment and dividend payment strategies with debt management and reinsurance.

In this paper, we consider the optimal debt ratio, investment, and dividend payment policies for insurers with time-inconsistency. For a very rich number of scholars, they assume that the discount is constant so that the discount function is exponential. However, some scholars argue that the assumption of constant discount rate which means the unchanging of human behavior is unrealistic. Hence, many researchers have studied the so-called time-inconsistent control problems for many years. For example, [22] used Nash equilibrium points to seek the equilibrium policy in dynamic utility maximization under inconsistency; [23] discussed the consumption and portfolio rules for time-inconsistent investors; they derived a modified HJB equation and compared the different styles of investors which are called naive and sophisticated agents. Other studies about time-inconsistency can be seen in [24, 25] and so on. This paper assumes that the discount rate is nonconstant but that a function of time is a nonincreasing function. We assume that the surplus process of an insurance company is determined by the change of asset value and the change of liabilities. The asset can be invested in financial market which contains a risky asset and a risk-free asset, when the insurer incurs a liability, he/she earns some premium. The objective is to maximize the expected nonconstant discounted utility of dividend payment until a determinate time. Then we obtain the closed-form expressions for the optimal debt ratio, investment, and dividend payment policies under logarithmic utility. The model is a generalization of [21] in which the optimal policies with a fixed discount rate are considered. We investigate the optimal policies with a nonconstant discount rate but a nonincreasing function of time.

The remainder of this paper is as follows. Section 2 describes the model and gives the objective function and other basic foundations. In Section 3, we obtain the dynamic equation which so-called modified HJB equation. Finally, we obtain the optimal policies in Section 4.

## 2. The Model

We first give a complete probability space  $(\Omega, \mathcal{F}, P)$  with filtration  $\{\mathcal{F}_t\}_{t \in [0, T]}$  satisfying the usual condition generated by a standard Brownian motion  $\{W(t), t \geq 0\}$ . Let  $X(t)$  denote the surplus of a large insurer. The asset value and liabilities are represented by  $K(t)$  and  $L(t)$ , respectively. The change of surplus process, which is the difference between the change of asset value  $K(t)$  and the change of liabilities  $L(t)$ , can be written as

$$\begin{aligned} dX(t) &= dK(t) - dL(t), \\ X(0) &= x. \end{aligned} \quad (1)$$

Obviously, when the insurer incurs a liability, he earns some premium. Hence, in this paper, we assume the premium rate is  $\theta$  which means that the insurer can collect  $\theta$  dollar when he/she provides a dollar insurance protection. Furthermore, the asset value increasing from the insurance sales during

$[t, t + dt]$  is denoted by  $\theta L(t)dt$ . Naturally, the insurer wants to know that how much  $L(t)$  he can provided. In other words, he wants to know how much of the debt ratio is suitable to the company. Let  $\pi_t = L(t)/X(t)$  denote the debt ratio of the insurance company and  $\pi_t$  also serves as a control variable in this paper. Then, the leverage is described as the ratio between asset values and surplus can be represented as  $1 + \pi_t = K(t)/X(t)$ . With some assumption, we will give the optimal debt ratio in the following.

For the sake of simplicity, we assume there are only a risk-free asset  $P_0(t)$  and a risky asset  $P_1(t)$  in the financial market with prices satisfying

$$\frac{dP_0(t)}{P_0(t)} = rdt, \quad (2)$$

$$\frac{dP_1(t)}{P_1(t)} = \mu dt + \sigma dW(t), \quad (3)$$

where  $r$ ,  $\mu$ , and  $\sigma$  are some positive real numbers satisfying  $r < \mu$ . Assume that the asset is invested in financial market, and the proportional of the asset value is invested in the risky asset at time  $t$  is denoted as  $f_t$ , the rest of the asset is invested in risk-free asset. Intuitively, without considering claims and dividend payment, the surplus process can be denoted by

$$\begin{aligned} dX_1(t) &= [\theta L(t) + K(t)] f_t \frac{dP_1(t)}{P_1(t)} \\ &+ [\theta L(t) + K(t)] (1 - f_t) \frac{dP_0(t)}{P_0(t)}. \end{aligned} \quad (4)$$

Substituting (2) and (3) into (4), we have

$$\begin{aligned} dX_1(t) &= [\theta L(t) + K(t)] \{ [r + (\mu - r) f_t] dt + \sigma f_t dW(t) \}, \\ X_1(0) &= x. \end{aligned} \quad (5)$$

Furthermore, we consider the future claims. We denoted by  $S(t)$  the accumulated claims up to time  $t$ . We have that

$$\begin{aligned} S(t) &= \int_0^t c(s) L(s) ds, \\ S(0) &= 0, \end{aligned} \quad (6)$$

where  $c(s)$  is claim rate. This means the claims are proportional to the amount of insurance liabilities. Let  $D(t)$  be a nonnegative and nondecreasing process representing the sum of the dividends distributed over the time interval  $[0, t]$ . In this paper, our purpose is to investigate the optimal dividend strategy where the dividend payment is proportional to amount of the surplus. Hence, the accumulate dividends can be represented by

$$\begin{aligned} D(t) &= \int_0^t z_s X(s) ds, \\ D(0-) &= 0, \end{aligned} \quad (7)$$

where  $z_t$  is a dividend payment rate and is an  $\mathcal{F}_t$  adapted process. Combining with (5) and considering claims and dividends, the surplus of insurance company is given by

$$\begin{aligned} dX(t) &= dX_1(t) - dS(t) - dD(t) = [\theta L(t) + K(t)] \\ &\cdot \{[r + (\mu - r) f_t] dt + \sigma f_t dW(t)\} - c(t) L(t) dt \\ &- z_t X(t) dt = \{[\theta L(t) + K(t)] [r + (\mu - r) f_t] \\ &- c(t) L(t) - z_t X(t)\} dt + \sigma f_t [\theta L(t) \\ &+ K(t)] dW(t), \quad \text{with } X(0-) = x. \end{aligned} \quad (8)$$

Naturally, we have

$$\begin{aligned} \frac{dX(t)}{X(t)} &= \{[(1 + \theta) \pi_t + 1] [r + (\mu - r) f_t] - c(t) \pi_t - z_t\} dt \\ &+ [(1 + \theta) \pi_t + 1] \sigma f_t dW(t). \end{aligned} \quad (9)$$

Recall that  $\pi_t$  denotes the debt ratio, the insurer wants to determine the optimal liabilities ratio. Thus, in our paper,  $\pi_t$  serve as a control variable. Let  $\mathbb{V} = [0, M], 0 < M < \infty$ . Then, we give the following definition.

*Definition 1.* We say that  $\mathbb{V} = \{\pi_t, f_t, z_t\}_{t \in [0, T]}$  is an admissible set, if

- (i) the process  $\{\pi_t, 0 \leq t \leq T\}$  is a predictable and satisfies that  $\pi_t \in \mathbb{V}$ ;
- (ii) the process  $\{f_t, 0 \leq t \leq T\}$  is a predictable and satisfies that

$$E \int_0^T f_s^2 ds < \infty, \quad T < \infty; \quad (10)$$

- (iii) the process  $\{z_t, 0 \leq t \leq T\}$  is a predictable and satisfy that  $0 \leq z_t < \infty$ .

We also say a policy  $(\pi_t, f_t, z_t)$  is admissible, if  $(\pi_t, f_t, z_t) \in \mathbb{V}$ .

In traditional optimal strategies research, the scholars also assume that the insurer preferences at time  $t$  take the form

$$\begin{aligned} J_1(t, x) &= E_{t,x} \left\{ \int_t^T [e^{-\rho(s-t)} U(z_s X(s))] ds \right. \\ &\left. + e^{-\rho(T-t)} U(X(T)) \right\}, \end{aligned} \quad (11)$$

where  $E_{t,x}$  denotes condition expectation  $E[\cdot | X(t) = x]$ ,  $U(\cdot)$  is a utility function satisfying that  $U' > 0, U'' < 0$ ,  $\rho$  is a discount rate. The insurer wants to choose the optimal policies to maximize  $J_1(t, x)$ , i.e.,

$$\begin{aligned} V_1(t, x) &= \max_{\{\pi_t, f_t, z_t\} \in \mathbb{V}} J_1(t, x), \\ &\text{with } V_1(T, x) = U(x). \end{aligned} \quad (12)$$

For the purpose of obtaining optimal policies, we ought to solve a stochastic control problem, and since the discount rate is constant, the solution is time consistent. However, some scholars argue that the assumption of constant discount rate is unrealistic. Hence, in this paper, we assume that the discount rate is nonconstant, but a function of time  $\nu(s)$  that is a nonincreasing function for  $s \in [0, T]$ . So the discount factor at time  $s$  used to evaluate a payoff at time  $s + t, t \geq 0$ , is  $\zeta(t) = \exp[-\int_0^t \nu(s) ds]$ . Consequently, we assume that the insurer's preference at time  $t$  takes the form of

$$\begin{aligned} J(t, x) &= E_{t,x} \left\{ \int_t^T [\zeta(s-t) U(z_s X(s))] ds \right. \\ &\left. + \zeta(T-t) U(X(T)) \right\}, \end{aligned} \quad (13)$$

which means the insurer's preference is not immutable. The optimal debt ratio, investment, and dividend payment policies consist of solving the following stochastic control problem:

$$V(t, x) = \max_{\{\pi_t, f_t, z_t\} \in \mathbb{V}} J(t, x), \quad \text{with } V(T, x) = U(x). \quad (14)$$

### 3. Dynamic Equation

For any  $\{\pi_t, f_t, z_t\} \in \mathbb{V}$  and any real function  $g(t, x) \in \mathcal{C}^{1,2}([0, \infty) \times [0, \infty))$ , we define a generator  $\mathcal{A}$  about (9) as

$$\begin{aligned} \mathcal{A}g(t, x) &= \frac{1}{2} [(1 + \theta) \pi_t + 1]^2 \sigma^2 f_t^2 x^2 \frac{\partial^2}{\partial x^2} g(t, x) \\ &+ \{[(1 + \theta) \pi_t + 1] [r + (\mu - r) f_t] - c(t) \pi_t - z_t\} \\ &\cdot x \frac{\partial}{\partial x} g(t, x). \end{aligned} \quad (15)$$

For problem (12), in the conventional methods, by dynamic programming principle, the value function satisfies HJB (Hamilton-Jacobi-Bellman) equation (see [21])

$$\max_{\{\pi_t, f_t, z_t\} \in \mathbb{V}} \left\{ \frac{\partial}{\partial t} V(t, x) + \mathcal{A}V(t, x) + e^{-\rho t} U(zx) \right\} = 0, \quad (16)$$

with terminal condition  $V(T, x) = U(x)$ .

For time-inconsistent problem (14), the standard HJB equation cannot be used to obtain the solution. In what follows, we use a modified HJB equation which was used in Marín-Solano and Navas [23] to deal with (14).

We begin with a special discretized version of (14). We divide the  $[0, T]$  into  $N$  periods of constant length  $\varepsilon$ ; in this way we identify  $ds = \varepsilon$ ; therefore the objective of insurer in time  $t = j\varepsilon$  ( $j = 0, 1, 2, \dots, N$ ) will be

$$\begin{aligned} V(j\varepsilon, X(j\varepsilon)) &= \max_{\{\pi_{ke}, f_{ke}, z_{ke}\}} E \left[ \sum_{i=0}^{N-j-1} \zeta(i\varepsilon) U(z_{(i+j)\varepsilon} X((i+j)\varepsilon)) \varepsilon \right. \\ &\left. + \zeta((N-j)\varepsilon) U(X(T)) \right], \end{aligned} \quad (17)$$

From (9), if the surplus is served as discrete, the surplus will have the following form:

$$\begin{aligned} X(k\varepsilon + \varepsilon) &= X(k\varepsilon) \\ &\cdot \{[(1 + \theta)\pi_{k\varepsilon} + 1][r + (\mu - r)f_{k\varepsilon}] - c(t)\pi_{k\varepsilon} \\ &- z_{k\varepsilon}\}\varepsilon + [(1 + \theta)\pi_{k\varepsilon} + 1]\sigma f_{k\varepsilon} [W((k + 1)\varepsilon) \\ &- W(k\varepsilon)], \end{aligned} \quad (18)$$

with  $X(k\varepsilon)$  is given and where  $k = j, \dots, N - 1$ . For (17), in the final period, i.e.,  $j = N$ , we have  $V(T, X(T)) = U(X(T))$ . For  $j = N - 1$ , we have

$$\begin{aligned} &V((N - 1)\varepsilon, X((N - 1)\varepsilon)) \\ &= \max_{\{\pi_{(N-1)\varepsilon}, f_{(N-1)\varepsilon}, z_{(N-1)\varepsilon}\}} E[U(z_{(N-1)\varepsilon}X((N - 1)\varepsilon))\varepsilon \\ &+ \zeta(\varepsilon)V(T, X(T))] \\ &= E[U(z_{(N-1)\varepsilon}^*X((N - 1)\varepsilon))\varepsilon \\ &+ \zeta(\varepsilon)V(T, X(T))]_{\{\pi_{(N-1)\varepsilon}^*, f_{(N-1)\varepsilon}^*, z_{(N-1)\varepsilon}^*\}}, \end{aligned} \quad (19)$$

with

$$\begin{aligned} X(N\varepsilon) &= X((N - 1)\varepsilon) \\ &\cdot \{[(1 + \theta)\pi_{(N-1)\varepsilon} + 1][r + (\mu - r)f_{(N-1)\varepsilon}] \\ &- c(t)\pi_{(N-1)\varepsilon} - z_{(N-1)\varepsilon}\}\varepsilon + [(1 + \theta)\pi_{(N-1)\varepsilon} + 1] \\ &\cdot \sigma f_{(N-1)\varepsilon} [W(N\varepsilon) - W((N - 1)\varepsilon)], \end{aligned} \quad (20)$$

where  $\{\pi_{(N-1)\varepsilon}^*, f_{(N-1)\varepsilon}^*, z_{(N-1)\varepsilon}^*\}$  is the maximizer of the right hand term of the (19). We denote

$$\begin{aligned} &G((N - 1)\varepsilon, X((N - 1)\varepsilon)) \\ &= U(z_{(N-1)\varepsilon}^*X((N - 1)\varepsilon))\varepsilon \Big|_{\{\pi_{(N-1)\varepsilon}^*, f_{(N-1)\varepsilon}^*\}}. \end{aligned} \quad (21)$$

Therefore, the optimal value of (17) can be represented as

$$\begin{aligned} &V(j\varepsilon, X(j\varepsilon)) \\ &= \max_{\{\pi_{j\varepsilon}, f_{j\varepsilon}, z_{j\varepsilon}\}} E[U(z_{j\varepsilon}X(j\varepsilon))\varepsilon + H(j, \varepsilon)], \end{aligned} \quad (22)$$

$$\begin{aligned} &V((j + 1)\varepsilon, X((j + 1)\varepsilon)) \\ &= E[G((j + 1)\varepsilon, X((j + 1)\varepsilon))\varepsilon + H(j + 1, \varepsilon)], \end{aligned} \quad (23)$$

where

$$\begin{aligned} H(j, \varepsilon) &= \sum_{i=1}^{N-j-1} \zeta(i\varepsilon)G((i + j)\varepsilon, X((i + j)\varepsilon))\varepsilon \\ &+ \zeta((N - j)\varepsilon)V(T, X(T)). \end{aligned} \quad (24)$$

Solving  $V(T, X(T))$  in (22) and (23), then using some mathematical techniques to simplify it, we have the lemma as follows.

**Lemma 2.** For initial wealth  $x$ , the equilibrium value  $V(j\varepsilon, X(j\varepsilon))$  of (17) and (18) can be obtained as

$$\begin{aligned} &\zeta((N - j - 1)\varepsilon)V(j\varepsilon, X(j\varepsilon)) \\ &= \max_{\{\pi_{j\varepsilon}, f_{j\varepsilon}, z_{j\varepsilon}\}} E\{\zeta((N - j - 1)\varepsilon)U(z_{j\varepsilon}X(j\varepsilon))\varepsilon \\ &+ \sum_{k=1}^{N-j-1} [\zeta((N - j - 1)\varepsilon)\zeta(k\varepsilon) \\ &- \zeta((N - j)\varepsilon)\zeta((k - 1)\varepsilon)] \\ &\cdot G((k + j)\varepsilon, X((k + j)\varepsilon))\varepsilon + \zeta((N - j)\varepsilon) \\ &\cdot V((j + 1)\varepsilon, X((j + 1)\varepsilon))\} \end{aligned} \quad (25)$$

with  $V(T, X(T)) = U(X(T))$  and

$$\begin{aligned} &X((j + 1)\varepsilon) = X(j\varepsilon) \\ &\cdot \{[(1 + \theta)\pi_{j\varepsilon} + 1][r + (\mu - r)f_{j\varepsilon}] - c(t)\pi_{j\varepsilon} \\ &- z_{j\varepsilon}\}\varepsilon + X(j\varepsilon) \\ &\cdot \{[(1 + \theta)\pi_{j\varepsilon} + 1]\sigma f_{j\varepsilon} [W((j + 1)\varepsilon) - W(j\varepsilon)]\}, \end{aligned} \quad (26)$$

for  $j = 1, 2, \dots, N - 1$ . Equation (25) is the equilibrium dynamic programming equation in discrete time, and we can obtain the solutions by proceeding backward in time from period  $N - 1$  to period 0.

For the continuous time problem of (14), we also derive an equilibrium dynamic programming equation called modified HJB equation. Inspired by the discrete case, the equilibrium value of (14) is defined as the limit when  $\varepsilon \rightarrow 0$  of discrete time equilibrium dynamic programming equation (25). Since  $t = j\varepsilon, T = N\varepsilon$ , with initial wealth  $X(t) = x$ , then  $V(t, x) = V(j\varepsilon, X(j\varepsilon))$ , and by the  $It\hat{o}$  formula, we have

$$\begin{aligned} &V(t + \varepsilon, X(t + \varepsilon)) = V(t, X(t)) \\ &+ \left[ \frac{\partial}{\partial t} V(t, X(t)) + \mathcal{A}V(t, X(t)) \right] \varepsilon \\ &+ [(1 + \theta)\pi_t + 1]\sigma f_t \frac{\partial}{\partial x} V(t, X(t)) \\ &\cdot [W(t + \varepsilon) - W(t)] + o(\varepsilon). \end{aligned} \quad (27)$$

Since  $\zeta(k\varepsilon) = \exp[-\int_0^{k\varepsilon} \nu(s)ds]$ , by Taylor's theorem, then

$$\begin{aligned} &\zeta((N - j)\varepsilon) = \exp\left[-\int_0^{(N-j)\varepsilon} \nu(s)ds\right] \\ &= \zeta((N - j - 1)\varepsilon) [1 - \nu((N - j - 1)\varepsilon)\varepsilon] \\ &+ o(\varepsilon), \end{aligned} \quad (28)$$

$$\begin{aligned} &\zeta((k - 1)\varepsilon) = \exp\left[-\int_0^{(k-1)\varepsilon} \nu(s)ds\right] \\ &= \zeta(k\varepsilon) [1 + \nu(k\varepsilon)\varepsilon] + o(\varepsilon). \end{aligned} \quad (29)$$

Substituting (27), (28) and (29) into (25), we have

$$0 = \max_{\{\pi_t, f_t, z_t\}} E \left\{ U(z_t X(t)) + \frac{\partial}{\partial t} V(t, X(t)) + \mathcal{A}V(t, X(t)) - \nu(T-t)V(t, X(t)) - H(t, X(t)) \right\} \varepsilon + [(1+\theta)\pi_t + 1] \sigma f_t \frac{\partial}{\partial x} \cdot V(t, X(t)) [W(t+\varepsilon) - W(t)] + o(\varepsilon), \quad (30)$$

where

$$H(t, X(t)) = E \left[ \sum_{k=1}^{N-j-1} \zeta(k\xi) \cdot (\nu(k\xi) - \nu((N-j-1)\varepsilon)) G(t+k\xi, X(t+k\xi)) \cdot \varepsilon \right]. \quad (31)$$

Dividing (30) by  $\varepsilon$ , and letting  $\varepsilon \rightarrow 0$  in (30) and (31), we derive the modified HJB equation as

$$\nu(T-t)V(t, x) - \frac{\partial}{\partial t} V(t, x) + H(t, x) = \max_{\{\pi_t, f_t, z_t\}} \{U(z_t x) + \mathcal{A}V(t, x)\}, \quad (32)$$

where

$$H(t, x) = E \left[ \int_0^{T-t} \zeta(s) [\nu(s) - \nu(T-t)] \right]$$

$$\nu(t, x) = E_{t,x} \left\{ \int_t^T [U(z_s X(s)) - \nu(T-s)\nu(s, X(s)) - H(s, X(s))] ds + U(X(T)) \right\} \Bigg|_{\{\pi_t^*, f_t^*, z_t^*\}}, \quad (36)$$

where

$$E_{t,x} \left\{ \int_t^T H(s, X(s)) ds \right\} \Bigg|_{\{\pi_t^*, f_t^*, z_t^*\}} = E_{t,x} \left\{ \int_t^T \int_s^T \zeta(\kappa-s) [\nu(\kappa-s) - \nu(T-s)] G(\kappa, X(\kappa)) d\kappa ds \right\} \Bigg|_{\{\pi_t^*, f_t^*, z_t^*\}}. \quad (37)$$

We know that

$$E_{t,x} \left\{ \int_t^T \nu(T-s) \cdot \int_s^T \zeta(\kappa-s) G(\kappa, X(\kappa)) d\kappa ds \right\} \Bigg|_{\{\pi_t^*, f_t^*, z_t^*\}} = E_{t,x} \left\{ \int_t^T \nu(T-s) \right.$$

$$\cdot G(t+s, X(t+s)) \Bigg] ds = E \left[ \int_t^T \zeta(s-t) \cdot [\nu(s-t) - \nu(T-t)] G(s, X(s)) \right] ds. \quad (33)$$

Therefore, we have the following theorem.

**Theorem 3.** *If  $v(t, x) \in \mathcal{C}^{1,2}$  is the solution to modified HJB equation (32) with  $H$  satisfying (33) and with the boundary condition  $v(T, X(T)) = U(X(T))$ , and there exists an admissible  $\{\pi_t, f_t, z_t\}$  that solves the right side of (32), then  $v(t, x) = V(t, x)$ .*

*Proof.* From Dynkin's formula, we have

$$E_{t,x} [\nu(T, X(T)) - \nu(t, X(t))] = E_{t,x} \left\{ \int_t^T \left[ \frac{\partial}{\partial t} \nu(s, X(s)) + \mathcal{A}\nu(s, X(s)) \right] ds \right\}, \quad (34)$$

and combining with  $v(T, X(T)) = U(X(T))$ , we obtain

$$\nu(t, x) = E_{t,x} \left\{ \int_t^T \left[ -\frac{\partial}{\partial s} \nu(s, X(s)) - \mathcal{A}\nu(s, X(s)) \right] ds + U(X(T)) \right\}. \quad (35)$$

Assuming that  $\{\pi_t^*, f_t^*, z_t^*\}$  satisfies the condition in Definition 1 and solving the right side of (32), then

$$\cdot [\nu(s, X(s)) - \zeta(T-s)U(X(T))] ds \Bigg\} \Bigg|_{\{\pi_t^*, f_t^*, z_t^*\}} = E_{t,x} \left\{ \int_t^T \nu(T-s)\nu(s, X(s)) ds - U(X(T)) + \zeta(T-t)U(X(T)) \right\} \Bigg|_{\{\pi_t^*, f_t^*, z_t^*\}}, \quad (38)$$

and

$$E_{t,x} \left\{ \int_t^T \int_s^T \zeta(\kappa-s) \nu(\kappa-s) G(\kappa, X(\kappa)) d\kappa ds \right\} \Big|_{\{\pi_t^*, f_t^*, z_t^*\}}$$

$$= E_{t,x} \left\{ \int_t^T G(\kappa, X(\kappa)) \int_t^\kappa \zeta(\kappa-s) \nu(\kappa-s) ds d\kappa \right\} \Big|_{\{\pi_t^*, f_t^*, z_t^*\}}$$

$$= E_{t,x} \left\{ \int_t^T G(\kappa, X(\kappa)) [1 - \zeta(\kappa-t)] d\kappa \right\} \Big|_{\{\pi_t^*, f_t^*, z_t^*\}}. \quad (39)$$

Substituting (37), (38), and (39) into (36), we obtain

$$\begin{aligned} v(t, x) &= E_{t,x} \left\{ \int_t^T [U(z_s X(s)) - G(s, X(s)) (1 - \zeta(s-t))] ds + \zeta(T-t) U(X(T)) \right\} \Big|_{\{\pi_t^*, f_t^*, z_t^*\}} \\ &= E_{t,x} \left\{ \int_t^T \zeta(s-t) U(z_s X(s)) ds + \zeta(T-t) U(X(T)) \right\} \Big|_{\{\pi_t^*, f_t^*, z_t^*\}} = V(t, x). \end{aligned} \quad (40)$$

This ends the proof of Theorem 3.  $\square$

#### 4. Optimal Policies

Suppose that the insurer has a log-utility

$$U(x) = \ln(x), \quad (41)$$

Then the modified HJB equation (32) can be rewritten as

$$\begin{aligned} &\nu(T-t) V(t, x) - \frac{\partial}{\partial t} V(t, x) + H(t, x) \\ &= \max_{\{\pi_t, f_t, z_t\}} \left\{ \ln(z_t x) + \frac{1}{2} [(1+\theta)\pi_t + 1]^2 \right. \\ &\quad \cdot \sigma^2 f_t^2 x^2 \frac{\partial^2}{\partial x^2} V(t, x) \\ &\quad + \{[(1+\theta)\pi_t + 1][r + (\mu-r)f_t] - c(t)\pi_t - z_t\} \\ &\quad \left. \cdot x \frac{\partial}{\partial x} V(t, x) \right\}, \end{aligned} \quad (42)$$

with boundary conditions  $V(T, x) = \ln(x)$ .

With the log-utility function, we speculate that the value function has the following form:

$$V(t, x) = A(t) \ln(x) + B(t). \quad (43)$$

Then

$$\begin{aligned} \frac{\partial}{\partial t} V(t, x) &= A'(t) \ln(x) + B'(t), \\ \frac{\partial}{\partial x} V(t, x) &= \frac{A(t)}{x}, \\ \frac{\partial^2}{\partial t^2} V(t, x) &= -\frac{A(t)}{x^2}. \end{aligned} \quad (44)$$

Substituting (43) and (44) into (42), we have

$$\begin{aligned} &\nu(T-t) [A(t) \ln(x) + B(t)] - [A'(t) \ln(x) + B'(t)] \\ &\quad + H(t, x) = \max_{\{\pi_t, f_t, z_t\}} \left\{ \ln(z_t x) - \frac{1}{2} [(1+\theta)\pi_t + 1]^2 \right. \\ &\quad \cdot \sigma^2 f_t^2 A(t) \\ &\quad + \{[(1+\theta)\pi_t + 1][r + (\mu-r)f_t] - c(t)\pi_t - z_t\} \\ &\quad \left. \cdot A(t) \right\}. \end{aligned} \quad (45)$$

For simplicity, we denote  $\Pi_t := (1+\theta)\pi_t + 1$ , intuitively  $\pi_t = (\Pi_t - 1)/(1+\theta)$ ; hence,

$$\begin{aligned} &\nu(T-t) [A(t) \ln(x) + B(t)] - [A'(t) \ln(x) + B'(t)] \\ &\quad + H(t, x) = \max_{\{\pi_t, f_t, z_t\}} \left\{ \ln(z_t x) - \frac{1}{2} \Pi_t^2 \sigma^2 f_t^2 A(t) \right. \\ &\quad + \left\{ \Pi_t [r + (\mu-r)f_t] - \frac{c(t)(\Pi_t - 1)}{1+\theta} - z_t \right\} \\ &\quad \cdot A(t) \Big\} = \max_{\{\pi_t, f_t\}} \left\{ -\frac{1}{2} \Pi_t^2 \sigma^2 \left( f_t - \frac{\mu-r}{\Pi_t \sigma^2} \right)^2 \right. \\ &\quad + \Pi_t \left( r - \frac{c(t)}{1+\theta} \right) \Big\} A(t) + \max_{\{z_t\}} \{ \ln(z_t x) \\ &\quad - z_t A(t) \} + \left[ \frac{\mu-r}{2\sigma^2} + \frac{c(t)}{1+\theta} \right] A(t). \end{aligned} \quad (46)$$

From (46), we can obtain that

$$f_t^* = \frac{\mu-r}{\Pi_t \sigma^2}, \quad (47)$$

$$z_t^* = \frac{1}{A(t)}. \quad (48)$$

Moreover, if  $r > c(t)/(1+\theta)$ , then

$$\begin{aligned} \pi_t^* &= M, \\ \Pi_t^* &= (1+\theta)M + 1; \end{aligned} \quad (49)$$

if  $r < c(t)/(1 + \theta)$ , then

$$\begin{aligned} \pi_t^* &= 0, \\ \Pi_t^* &= 1; \end{aligned} \tag{50}$$

if  $r = c(t)/(1 + \theta)$ , then  $\pi_t^*$  can take any value in  $[0, M]$ .  
By (48),

$$\begin{aligned} H(t, x) &= E \left[ \int_t^T \zeta(s-t) [\nu(s-t) - \nu(T-t)] \right. \\ &\quad \cdot \ln(z_s^* X(s)) \Big] ds = E \left[ \int_t^T \zeta(s-t) \right. \\ &\quad \cdot [\nu(s-t) - \nu(T-t)] \ln \left( \frac{X(s)}{A(s)} \right) \Big] ds. \end{aligned} \tag{51}$$

From (9), we know that

$$X(s) = X(t) \exp \{ \Delta_t(s) \} \tag{52}$$

with

$$\begin{aligned} \Delta_t(s) &= \int_t^s \left\{ [(1 + \theta) \pi_t^* + 1] [r + (\mu - r) f_t^*] \right. \\ &\quad \left. - c(t) \pi_t - z_t^* - \frac{1}{2} [(1 + \theta) \pi_t^* + 1]^2 \sigma^2 f_t^{*2} \right\} dt \\ &\quad + \int_t^s [(1 + \theta) \pi_t^* + 1] \sigma f_t^* dW(t). \end{aligned} \tag{53}$$

Combining (52) and (51), we have

$$\begin{aligned} H(t, x) &= E \int_t^T \zeta(s-t) [\nu(s-t) - \nu(T-t)] \\ &\quad \cdot (\ln X(t) + \Delta_t(s) - \ln A(s)) ds. \end{aligned} \tag{54}$$

Inserting (54) into (46), we obtain that

$$\begin{aligned} &\left\{ \nu(T-t) A(t) - A'(t) - 1 \right. \\ &\quad \left. + \int_t^T \zeta(s-t) [\nu(s-t) - \nu(T-t)] ds \right\} \ln x \\ &= -\nu(T-t) B(t) - B'(t) \\ &\quad - \int_t^T \zeta(s-t) [\nu(s-t) - \nu(T-t)] (\Delta_t(s) \\ &\quad - \ln A(s)) ds + \Pi_t^* \left( r - \frac{c(t)}{1 + \theta} \right) A(t) - \ln A(t) \\ &\quad - 1 + \left[ \frac{\mu - r}{2\sigma^2} + \frac{c(t)}{1 + \theta} \right] A(t). \end{aligned} \tag{55}$$

Equation (55) should be satisfied for any  $x$ ; therefore,

$$\begin{aligned} &\nu(T-t) A(t) - A'(t) - 1 \\ &\quad + \int_t^T \zeta(s-t) [\nu(s-t) - \nu(T-t)] ds = 0, \end{aligned} \tag{56}$$

and using the boundary condition  $A(T) = 1$ , we get

$$A(t) = \zeta(T-t) + \int_t^T \zeta(s-t) ds. \tag{57}$$

So far, we have proved the following theorem.

**Theorem 4.** For problem (14), if the insurer has a log-utility function (41), we can obtain the optimal policies as follows:

$$f_t^* = \frac{\mu - r}{\Pi_t^* \sigma^2}, \tag{58}$$

$$z_t^* = \frac{1}{\zeta(T-t) + \int_t^T \zeta(s-t) ds}. \tag{59}$$

Moreover, if  $r > c(t)/(1 + \theta)$ , then

$$\begin{aligned} \pi_t^* &= M, \\ \Pi_t^* &= (1 + \theta) M + 1; \end{aligned} \tag{60}$$

if  $r < c(t)/(1 + \theta)$ , then

$$\begin{aligned} \pi_t^* &= 0, \\ \Pi_t^* &= 1; \end{aligned} \tag{61}$$

if  $r = c(t)/(1 + \theta)$ , then  $\pi_t^*$  can take any value in  $[0, M]$ .

*Remark 5.* The optimal investment and debt ratio policies are verified the same as the corresponding part in [21] without considering reinsurance. So, we can see that it is the same between time-inconsistency and time-consistency for optimal investment and debt ratio policies. This is because that the investment and debt ratio policies are independent with discount rate in this model.

*Remark 6.* We can see that the optimal dividend payment is the same as [21] without considering reinsurance when the discount rate function  $\nu(s) = \rho$ .

### Data Availability

There are no data used in this study.

### Conflicts of Interest

The authors declare that there are no conflicts of interest regarding the publication of this article.

### Acknowledgments

The research was supported by the National Natural Science Foundation of China (no. 11571198, 11501319, and 11501321), the Project of China Postdoctoral Science Foundation (no. 2015M582064), the Natural Science Foundation of Shandong (nos. ZR2015AL013 and ZR2014AM021), and the Project of Shandong Province Higher Educational Science and Technology Program (no. J15LI05).

## References

- [1] S. Browne, "Optimal investment policies for a firm with a random risk process: exponential utility and minimizing the probability of ruin," *Mathematics of Operations Research*, vol. 20, no. 4, pp. 937–958, 1995.
- [2] C. Yin and C. Wang, "The perturbed compound Poisson risk process with investment and debit interest," *Methodology and Computing in Applied Probability*, vol. 12, no. 3, pp. 391–413, 2010.
- [3] M. Zhou, K. C. Yuen, and C.-c. Yin, "Optimal investment and premium control in a nonlinear diffusion model," *Acta Mathematicae Applicatae Sinica*, vol. 33, no. 4, pp. 945–958, 2017.
- [4] B.-D. Finetti, "Su un'impostazione alternativa della teoria collettiva del rischio," in *Transactions of the XVth International Congress of Actuaries*, vol. 2, pp. 433–443, 1957.
- [5] H. U. Gerber and E. S. Shiu, "Optimal dividends: analysis with Brownian motion," *North American Actuarial Journal*, vol. 8, no. 1, pp. 1–20, 2004.
- [6] H. U. Gerber and E. S. Shiu, "On optimal dividend strategies in the compound Poisson model," *North American Actuarial Journal*, vol. 10, no. 2, pp. 76–93, 2006.
- [7] C. Yin and C. Wang, "Optimality of the barrier strategy in de Finetti's dividend problem for spectrally negative Lévy processes: an alternative approach," *Journal of Computational and Applied Mathematics*, vol. 233, no. 2, pp. 482–491, 2009.
- [8] C. Yin and Y. Wen, "Optimal dividend problem with a terminal value for spectrally positive Levy processes," *Insurance: Mathematics and Economics*, vol. 53, no. 3, pp. 769–773, 2013.
- [9] H. Meng, T. K. Siu, and H. Yang, "Optimal dividends with debts and nonlinear insurance risk processes," *Insurance: Mathematics and Economics*, vol. 53, no. 1, pp. 110–121, 2013.
- [10] C. Yin and K. C. Yuen, "Optimal dividend problems for a jump-diffusion model with capital injections and proportional transaction costs," *Journal of Industrial and Management Optimization*, vol. 11, no. 4, pp. 1247–1262, 2015.
- [11] B. Avanzi, "Strategies for dividend distribution: a review," *North American Actuarial Journal*, vol. 13, no. 2, pp. 217–251, 2009.
- [12] H. Schmidli, "Optimal proportional reinsurance policies in a dynamic setting," *Scandinavian Actuarial Journal*, no. 1, pp. 55–68, 2001.
- [13] Z. Liang, K. C. Yuen, and J. Guo, "Optimal proportional reinsurance and investment in a stock market with Ornstein-Uhlenbeck process," *Insurance: Mathematics and Economics*, vol. 49, no. 2, pp. 207–215, 2011.
- [14] H. Schmidli, "On minimizing the ruin probability by investment and reinsurance," *The Annals of Applied Probability*, vol. 12, no. 3, pp. 890–907, 2002.
- [15] L. Bai and J. Guo, "Optimal proportional reinsurance and investment with multiple risky assets and no-shorting constraint," *Insurance: Mathematics and Economics*, vol. 42, no. 3, pp. 968–975, 2008.
- [16] X. Zhang and T. K. Siu, "Optimal investment and reinsurance of an insurer with model uncertainty," *Insurance: Mathematics and Economics*, vol. 45, no. 1, pp. 81–88, 2009.
- [17] J. Paulsen and H. k. Gjessing, "Optimal choice of dividend barriers for a risk process with stochastic return on investments," *Insurance: Mathematics and Economics*, vol. 20, no. 3, pp. 215–223, 1997.
- [18] H. Meng and T. K. Siu, "On optimal reinsurance, dividend and reinvestment strategies," *Economic Modelling*, vol. 28, no. 1-2, pp. 211–218, 2011.
- [19] P. Azcue and N. Muler, "Optimal investment policy and dividend payment strategy in an insurance company," *The Annals of Applied Probability*, vol. 20, no. 4, pp. 1253–1302, 2010.
- [20] Z. Jin, H. Yang, and G. Yin, "Optimal debt ratio and dividend payment strategies with reinsurance," *Insurance: Mathematics and Economics*, vol. 64, pp. 351–363, 2015.
- [21] Q. Zhao, Z. Jin, and J. Wei, "Optimal investment and dividend payment strategies with debt management and reinsurance," *Journal of Industrial and Management Optimization*, vol. 13, no. 5, pp. 1–26, 2017.
- [22] R. H. Strotz, "Myopia and inconsistency in dynamic utility maximization," *Review of Economic Studies*, vol. 23, no. 3, pp. 165–180, 1955.
- [23] J. Marn-Solano and J. Navas, "Consumption and portfolio rules for time-inconsistent investors," *European Journal of Operational Research*, vol. 201, no. 3, pp. 860–872, 2010.
- [24] Q. Zhao, J. Wei, and R. Wang, "On dividend strategies with non-exponential discounting," *Insurance: Mathematics and Economics*, vol. 58, pp. 1–13, 2014.
- [25] J. Yong, "Time-inconsistent optimal control problems and the equilibrium HJB equation," *Mathematical Control and Related Fields*, vol. 2, no. 3, pp. 271–329, 2012.

## Research Article

# Strong Solutions and Global Attractors for Kirchhoff Type Equation

Xiangping Chen 

Department of Mathematics, Jining University, Qufu, Shandong 273155, China

Correspondence should be addressed to Xiangping Chen; chenxp@jnxu.edu.cn

Received 11 May 2018; Accepted 23 June 2018; Published 8 July 2018

Academic Editor: Xue-Jun Xie

Copyright © 2018 Xiangping Chen. This is an open access article distributed under the Creative Commons Attribution License, which permits unrestricted use, distribution, and reproduction in any medium, provided the original work is properly cited.

We study the long-time behavior of the Kirchhoff type equation with linear damping. We prove the existence of strong solution and the semigroup associated with the solution possesses a global attractor in the higher phase space.

## 1. Introduction

We consider the following nonlinear Kirchhoff type equation with the initial-boundary conditions:

$$\begin{aligned} u_{tt} + u_t + \Delta^2 u + \varphi(u) &= f(x), \\ u(0) &= u_0, \\ u_t(0) &= u_1, \\ u|_{\partial\Omega} = \Delta u|_{\partial\Omega} &= 0, \end{aligned} \quad (1)$$

where  $\Omega$  is a bounded domain in  $R^n$  with smooth boundary,  $\Delta$  denotes the Laplace operator,  $f$  is a given function lying in  $L^2(\Omega)$ , independent of time, and  $\varphi \in C^1(R)$  with  $\varphi(0) = 0$  fulfills the dissipation inequality

$$\liminf_{|u| \rightarrow \infty} \frac{\varphi(u)}{u} > -\lambda_1^2, \quad (2)$$

and

$$\varphi' \geq -l, \quad (3)$$

where  $l > 0$  is a real number and  $\lambda_1$  is the first eigenvalue of  $-\Delta$  on  $L^2(\Omega)$  with Dirichlet boundary conditions

$$\begin{aligned} -\Delta w &= \lambda w, \\ w|_{\partial\Omega} &= 0. \end{aligned} \quad (4)$$

When  $n = 1$ , this problem describes, for instance, the motion of a vibrating string with fixed boundary in a viscous medium. In particular, the function represents the displacement from equilibrium,  $u_t$  is the velocity, and the term  $\varphi(u) - f$  may correspond to a (nonlinear) elastic force. For more details on the model of Kirchhoff, one can refer to [1–3] and the reference therein.

When the coefficient of  $u_t$  is a positive function  $g(u)$ , which depends on  $u$ , then the term  $g(u)u_t$  is a resistance force and the model impresses that the viscous medium embedding the string is stratified. In this case, the existence of the global and exponential attractors has been proven by S. Kolbasin in [4]. The attractor is in the phase space  $H_0^2(\Omega) \times L^2(\Omega)$  and it is bounded in  $[H^4(\Omega) \cap H_0^2(\Omega)] \times H_0^2(\Omega)$ , where  $\Omega$  is a bounded domain in  $R^3$  with smooth boundary.

Similar models have been considered in [5–9], such as plate equation

$$u_{tt} + \sigma(u)u_t + \Delta^2 u + \lambda u + f(u) = g(x), \quad (5)$$

when  $\sigma(u) = \alpha(x)$ , the existence, regularity, and finite dimensionality of a global attractor in  $H_2^2(R^n) \times L^2(R^n)$  with a localized damping and a critical exponent were proven in [5]. For  $\Omega$  a three-dimensional unbounded domain and under suitable conditions on  $\sigma(u)$  and  $f(u)$ , A.Kh. Khanmamedov in [6] showed that this equation possesses a global attractor in  $H^2(R^3) \times L^2(R^3)$ . About Kirchhoff models, long-time dynamics properties were studied by Yang and I. Chueshov in

[7–9] and their references. For example, Yang et al. discussed the long-time behavior of solutions to the Cauchy problem of some Kirchhoff type equations with a strong dissipation in [7, 8] and proved that the dynamical system possesses a global attractor under suitable conditions in the phase space  $X_{1+\delta}$ , where  $X_{1+\delta} = V_{1+\delta} \times V_\delta$ ,  $0 < \delta \leq 1$ .

Thus, to the best of our knowledge, the research about global attractors of the weak solutions for problem (1) with respect to the norm of  $H^2 \times L^2$  is much more; however, the results about the existence of the strong solutions and strong global attractors for (1) are relatively fewer. The purpose of this paper is to supplement some conclusions for the above problem. In particular, we do not demand the function  $\varphi(u)$  to be bounded by polynomials and present here a method different from [9–14]. Furthermore, the global attractor is established in the higher energy space in  $H^4(\Omega) \cap H_0^2(\Omega)$ .

The paper is organized as follows. In Section 2, we recall some notations and some general facts about the dynamical systems theory. In Section 3, we prove well-posedness and the existence of a bounded absorbing set for problem (1). Sections 4 and 5 contain our main results, and we prove the existence of strong solution and a global attractor in the space of higher order.

## 2. Preliminaries

Throughout the paper we will denote

$$\begin{aligned} H &= L^2(\Omega), \\ V &= H_0^1(\Omega), \\ V_1 &= H^2(\Omega) \cap H_0^1(\Omega), \\ V_2 &= D(A) = \{u \in H^2(\Omega) \mid Au \in L^2(\Omega)\}, \end{aligned} \quad (6)$$

where  $A = \Delta^2$ .

The norm and the scalar product in  $L^2(\Omega)$  is denoted by  $\|\cdot\|$  and  $(\cdot, \cdot)$ , respectively, the norm in  $V_i$  is denoted by  $\|\cdot\|_{V_i}$ , ( $i = 0, 1, 2$ ), and the Hilbert spaces  $E_1, E_2$  are

$$\begin{aligned} E_1 &= V_1 \times H, \\ E_2 &= V_2 \times V_1. \end{aligned} \quad (7)$$

For any given function  $u(t)$ , we will write for short  $\xi(t) = (u(t), u_t(t))$  and endow space  $E_1, E_2$  with the standard inner product and norm  $\|\xi_u\|_{E_1}^2 = \|u\|_{V_1}^2 + \|u_t\|_{L^2}^2$ ,  $\|\xi_u\|_{E_2}^2 = \|u\|_{V_2}^2 + \|u_t\|_{V_1}^2$ .

For convenience, the letters  $C$  and  $Q$  present different positive constants and different positive increasing functions, respectively.

We collect some basic concepts and general theorems, which are important for getting our main results. We refer to [14–18] and the references therein for more details.

**Definition 1** (see [16, 18]). Let  $X$  be a Banach space and  $\{S(t)\}_{t \geq 0}$  be a family operator on  $X$ . We say that  $\{S(t)\}_{t \geq 0}$

is a norm-to-weak continuous semigroup on  $X$ , if  $\{S(t)\}_{t \geq 0}$  satisfies

- (i)  $S(0) = \text{Id}$  (the identity);
- (ii)  $S(t)S(s) = S(t+s)$ ,  $\forall t, s \geq 0$ ;
- (iii)  $S(t_n)x_n \rightarrow S(t)x$ , if  $t_n \rightarrow t$ ,  $x_n \rightarrow x$  in  $X$ .

**Definition 2** (see [15]). A  $C^0$  semigroup  $\{S(t)\}_{t \geq 0}$  in a Banach space  $X$  is said to satisfy the condition (C) if, for any  $\varepsilon > 0$  and for any bounded set  $B$  of  $X$ , there exists  $t(B) > 0$  and a finite dimensional subspace  $X_1$  of  $X$ , such that  $\{\|PS(t)x\|_X, x \in B, t \geq t(B)\}$  is bounded and

$$\|(I - P)S(t)x\|_X < \varepsilon, \quad t \geq t(B), \quad x \in B, \quad (8)$$

where  $P : X \rightarrow X_1$  is a bounded projector.

**Theorem 3** (see [14]). Let  $X$  be a Banach space and  $\{S(t)\}_{t \geq 0}$  be a norm-to-weak continuous semigroup on  $X$ . Then  $\{S(t)\}_{t \geq 0}$  has a global attractor in  $X$  provided that the following conditions hold true:

- (i)  $\{S(t)\}_{t \geq 0}$  has a bounded absorbing set  $B_0$  in  $X$ .
- (ii)  $\{S(t)\}_{t \geq 0}$  satisfies the condition (C).

**Theorem 4** (see [16, 18]). Let  $X$  and  $Y$  be two Banach spaces such that  $X \subset Y$  with a continuous injection. If a function  $\varphi$  belongs to  $L^\infty(0, T; X)$  and is weakly continuous with values in  $Y$ , then  $\varphi$  is weakly continuous with values in  $X$ .

**Theorem 5** (see [16, 18]). Let  $X, Y$  be two Banach spaces and  $X^*, Y^*$  be their dual spaces, respectively, such that

$$\begin{aligned} X &\hookrightarrow Y, \\ Y^* &\hookrightarrow X^* \end{aligned} \quad (9)$$

where the injection  $i : X \rightarrow Y$  is continuous and its adjoint,  $i^* : Y^* \hookrightarrow X^*$ , is a densely injective. Let  $\{S(t)\}_{t \geq 0}$  be a semigroup on  $X$  and  $Y$ , respectively, and be a continuous semigroup or a weak continuous semigroup on  $Y$ . Then for any bounded subset  $B$  of  $X$ ,  $\{S(t)\}_{t \geq 0}$  is norm-to-weak continuous on  $S(B)$ .

**Theorem 6** (see [16–18]). Assume that  $\{S(t)\}_{t \geq 0}$  is a semigroup on Banach space  $X$  and satisfies that

- (i)  $\{S(t)\}_{t \geq 0}$  has a bounded absorbing set  $B_0$  in  $X$ ;
- (ii)  $\{S(t)\}_{t \geq 0}$  satisfies condition (C) or  $\{S(t)\}_{t \geq 0}$  is  $\omega$ -limit compact in  $X$ .

And assume furthermore that  $\{S(t)\}_{t \geq 0}$  is norm-to-weak continuous on  $S(B_0)$ . Then  $\{S(t)\}_{t \geq 0}$  has a global attractor  $\mathcal{A}$  in  $X$ ; i.e.,  $\mathcal{A}$  is nonempty, invariant, compact in  $X$  and attracts every bounded subset of  $X$  in the norm topology of  $X$ .

## 3. A Priori Estimate

Next we iterate some main results in [4], which are important for getting a priori estimate.

For any initial data  $u_0 \in v_1, u_1 \in H$ , problem (1) possesses a unique weak solution  $u$ , which satisfies  $u \in C(R_+; V_1), u_t \in C(R_+; H)$ , and, for any  $t \geq 0$ ,

$$\|\xi_u\|_{E_1}^2 \leq Q(\|\xi_u(0)\|_{E_1}) + Q(\|f\|). \quad (10)$$

Furthermore problem (1) generates a dynamical system of solution within the space  $H_0^2(\Omega) \times L^2(\Omega)$ . This system possesses a compact global attractor  $\mathcal{A}$ , which is bounded in  $[H^4(\Omega) \cap H_0^2(\Omega)] \times H_0^2(\Omega)$ .

Choosing  $0 < \varepsilon < 2/3$ , taking the scalar product in  $H$  of the first equation of (1) with  $Av = Au_t + \varepsilon Au$ , we find

$$\begin{aligned} & \frac{d}{dt} \left[ \|\xi_u\|_{E_2}^2 + 2\varepsilon (u_t, Au) - 2(f, Au) + 2(\varphi(u), Au) \right] \\ & + 2\|u_t\|_{V_1}^2 - 2\varepsilon (u_t, Au_t) + 2\varepsilon (u_t, Au) + 2\varepsilon \|u\|_{V_2}^2 \\ & + 2\varepsilon (\varphi(u), Au) - 2\varepsilon (f, Au) - 2(\varphi'(u)u_t, Au) \\ & = 0. \end{aligned} \quad (11)$$

Owing to [4] and Hölder inequality, we obtain

$$\begin{aligned} 2(\varphi'(u)u_t, Au) & \leq |\varphi'(u)| \|u_t\| \|Au\| \\ & \leq \varepsilon \|u\|_{V_2}^2 + Q(R), \end{aligned} \quad (12)$$

where  $R = Q(\|\xi_u(0)\|_{E_1}) + Q(\|f\|)$ . Furthermore we see from (11) that

$$\begin{aligned} & \frac{d}{dt} \left[ \|\xi_u\|_{E_2}^2 + 2\varepsilon (u_t, Au) - 2(f, Au) + 2(\varphi(u), Au) \right] \\ & + (2 - 2\varepsilon) \|u_t\|_{V_1}^2 + 2\varepsilon (u_t, Au) + \varepsilon \|u\|_{V_2}^2 \\ & + 2\varepsilon (\varphi(u), Au) - 2\varepsilon (f, Au) \leq Q(R). \end{aligned} \quad (13)$$

We denote the energy functions as follows:

$$E = \|\xi_u\|_{E_2}^2 + 2\varepsilon (u_t, Au) - 2(f, Au) + 2(\varphi(u), Au). \quad (14)$$

Combining with (13), (12), and  $0 < \varepsilon < 2/3$ , we get

$$\frac{dE}{dt} + \varepsilon E \leq Q(R). \quad (15)$$

By the Gronwall inequality, it follows that

$$E \leq E(\xi(t_0)) e^{-\varepsilon(t-t_0)} + \frac{F(R)}{\varepsilon} (1 - e^{-\varepsilon(t-t_0)}), \quad (16)$$

$\forall t \geq t_0.$

Next, we show that

$$\frac{1}{2} \|\xi_u\|_{E_2}^2 - Q(R, \varepsilon) \leq E \leq \frac{3}{2} \|\xi_u\|_{E_2}^2 + Q(R, \varepsilon). \quad (17)$$

By Hölder inequality, Young's inequality, Poincaré inequality, and [4], we conclude that

$$\begin{aligned} E & \leq \|\xi_u\|_{E_2}^2 + 2\varepsilon \|u_t\|_{V_1} \|u\|_{V_1} + 2\|f\| \|u\|_{V_2} \\ & + 2|\varphi(u)| \|u\|_{V_2} \leq \|\xi_u\|_{E_2}^2 + \frac{1}{2} \|\xi_u\|_{E_2}^2 + Q(R, \varepsilon) \\ & = \frac{3}{2} \|\xi_u\|_{E_2}^2 + Q(R, \varepsilon), \end{aligned} \quad (18)$$

and

$$\begin{aligned} E & \geq \|\xi_u\|_{E_2}^2 - 2\varepsilon c \|u_t\|_{V_1} \|Au\| - 2\|f\| \|Au\| \\ & - 2|\varphi(u)| \|Au\|_{L^2} \\ & = \|\xi_u\|_{E_2}^2 - 2\varepsilon c \left( \frac{1}{4} \|Au\|^2 + \|u_t\|_{V_1}^2 \right) - 2\varepsilon c \frac{3}{8} \|Au\|^2 \\ & - 2\varepsilon c \frac{3}{8} \|Au\|^2 - Q(R, \varepsilon). \\ & = (1 - 2\varepsilon c) \|\xi_u\|_{E_2}^2 - Q(R, \varepsilon) > \frac{1}{2} \|\xi_u\|_{E_2}^2 - Q(R, \varepsilon). \end{aligned} \quad (19)$$

Select  $\varepsilon$  small enough to verify that

$$1 - 2\varepsilon c > \frac{1}{2}. \quad (20)$$

From (16) and (17), we have

$$\begin{aligned} \|\xi_u\|_{E_2}^2 & \leq 2E + Q(R, \varepsilon) \\ & \leq 2E(\xi(t_0)) e^{-\varepsilon(t-t_0)} + \frac{F(R)}{\varepsilon} (1 - e^{-\varepsilon(t-t_0)}) \\ & + Q(R, \varepsilon) \\ & \leq 2 \left( \frac{3}{2} \|\xi_u(t_0)\|_{E_2}^2 + Q(R, \varepsilon) \right) e^{-\varepsilon(t-t_0)} + \frac{F(R)}{\varepsilon} \\ & + Q(R, \varepsilon) \leq 3 \|\xi_u(t_0)\|_{E_2}^2 e^{-\varepsilon(t-t_0)} + Q(R, \varepsilon). \end{aligned} \quad (21)$$

Now if  $B \subset B_{E_2(P_0, \rho)}$ , the ball of  $E_2$ , center at  $P_0$  of radius  $\rho$ , then  $\|\xi_u(t_0)\|_{E_2} \leq \rho$ , provided

$$t - t_0 > \frac{1}{\varepsilon} \ln 3\rho^2. \quad (22)$$

So

$$\|\xi_u\|_{E_2}^2 \leq 1 + Q(R) = \mu. \quad (23)$$

We denote  $\mu = 1 + Q(R)$ .

#### 4. Existence of the Strong Solution

**Theorem 7.** Suppose  $f \in L^2(\Omega)$ ,  $\varphi$  is a  $C^2(R)$  function from  $R$  into  $R$  satisfying (2)-(3) and  $\varphi(0) = 0$ . Then given  $T > 0$ , problem (1) has a unique solution  $u(x, t)$  with

$$\begin{aligned} u & \in L^\infty(0, T; D(A)), \\ u_t & \in L^\infty(0, T; V_1) \end{aligned} \quad (24)$$

for  $u_0 \in D(A)$ ,  $u_1 \in V_1$ . Moreover  $(u, u_t)$  is a weakly continuous function from  $[0, T]$  to  $E_2$ .

*Proof.* We prove the existence of strong solutions by using the Faedo-Galerkin schemes. Assume that there exists an orthonormal basis of  $D(A)$  consisting of eigenvectors  $\omega_i$  of  $A$

in  $D(A)$ ; simultaneously they are also orthonormal basis of  $V$ . The corresponding eigenvalues are  $\lambda_i, i = 1, 2, \dots$ , satisfying

$$A\omega_i = \lambda_i\omega_i, \quad \forall i \in N. \quad (25)$$

For this purpose, according to the basis theory of ordinary differential equations, we build the sequence of Galerkin approximate solutions. They are smooth functions of the form

$$u_N = \sum_{i=1}^N \mu_{Ni} \omega_i, \quad (26)$$

and it satisfies

$$\begin{aligned} \partial_{tt} u_N + P_N(\partial_t u_N) + Au_N + P_N(\varphi(u_N)) &= P_N f, \\ u_N(0) &= P_N u_0, \\ \partial_t u_N(0) &= P_N u_1, \end{aligned} \quad (27)$$

where  $P_m : D(A) \rightarrow V_m$  is the orthogonal projector in  $V_m$ , and  $V_m = \text{span}\{\omega_1, \omega_2, \dots, \omega_m\}$ . Of course for every  $N$  there is the unique solution  $u_N$  to (27).

Choosing  $0 < \varepsilon < 1$ , after multiplying (27) by  $AV_m = Au'_m + \varepsilon_0 Au_m$ , the similar process of (11) leads to

$$\begin{aligned} \frac{d}{dt} \left[ \|\xi_{u_N}\|_{E_2}^2 + 2\varepsilon(u_{Nt}, Au_N) - 2(f, Au_N) \right. \\ \left. + 2(\varphi(u_N), Au) \right] + 2\|u_{Nt}\|_{V_1}^2 - 2\varepsilon(u_{Nt}, Au_{Nt}) \\ + 2\varepsilon(u_{Nt}, Au_N) + 2\varepsilon\|u_N\|_{V_2}^2 + 2\varepsilon(\varphi(u_N), Au_N) \\ - 2(f, Au_N) - 2(\varphi'(u_N)u_{Nt}, Au_N) = 0. \end{aligned} \quad (28)$$

Like the estimates of (12)-(21), we have

$$\|\xi_{u_N}\|_{E_2}^2 \leq 1 + Q(R). \quad (29)$$

It means that the sequence  $\{\xi_{u_N}(t)\}$  is bounded in the space  $L^\infty(0, T; D(A))$  for an arbitrary fixed  $T > 0$ . From (27) we know that

$$\frac{d^2 u_N}{dt^2} = -P_N \frac{du_N}{dt} - Au_N - P_N(\varphi(u_N)) + P_N f. \quad (30)$$

So  $\{\partial_{tt} u_N\}$  is uniformly bounded in  $L^\infty(0, T; H)$ ; then we can extract a subsequence, still denoted by  $u_N$ , such that

$$\begin{aligned} u_N &\rightharpoonup u \quad \text{in } L^2(0, T; D(A)), \\ u'_N &\rightharpoonup u' \quad \text{in } L^2(0, T; H^2), \\ u''_N &\rightharpoonup u'' \quad \text{in } L^2(0, T; H), \\ \varphi(u_N) &\rightharpoonup \varphi(u) \quad \text{in } L^2(0, T; H), \\ P_N f &\rightharpoonup f \quad \text{in } L^2(0, T; H), \quad \text{as } N \rightarrow \infty. \end{aligned} \quad (31)$$

It is easy to pass the limit in (27) and we obtain that  $u$  is a solution of (1), such that

$$\begin{aligned} u(t) &\in L^\infty(0, T; D(A)), \\ u_t(t) &\in L^\infty(0, T; V_1). \end{aligned} \quad (32)$$

Furthermore, from Theorem 4 and [4], we know that  $u$  is a weakly continuous function from  $[0, T]$  to  $E_2$ .

Finally, uniqueness is followed from [4], since any strong solution would be a weak solution.  $\square$

Thus, the dynamical system generated by (1) can be defined in the phase space  $E_2$ , and the corresponding solution semigroup is  $\{S(t)\}_{t>0}$ . By Theorem 7, we have the following results.

**Theorem 8.** *Suppose the conditions of Theorem 7 hold; then there exists a bounded absorbing set  $B$  in  $E_2$  for the semigroup  $\{S(t)\}_{t>0}$ .*

## 5. Global Attractors in $E_2$

We first prove the following compactness results and the norm-to-weak continuity of semigroup.

**Lemma 9.** *Suppose that (2) and (3) hold;  $\varphi(0) = 0, \varphi(u) : D(A) \rightarrow V_1$  is defined by*

$$((\varphi(u), v)) = \int_{\Omega} \Delta \varphi(u) \Delta v dx, \quad (33)$$

$\forall u \in D(A), v \in H_0^2(\Omega)$ . Then  $\varphi$  is continuous compact.

*Proof.* Suppose that  $u_n$  is bounded sequences in  $D(A)$ ; without lose of generality, we assume that  $u_n$  weakly converge to  $u_0$  in  $D(A)$ . By the Sobolev embedding theorem, we know that  $u_n$  is bounded and converges to  $u_0$  in  $L^P(0, T), W^{1,P}(0, T), W^{2,P}(0, T), \forall P \geq 1, \forall T > 0$ . Denote  $u_n - u_0 = \omega_n$ ; by the results of [4] and the Sobolev embedding theorem, we show that  $\varphi'(u), \varphi''(u), \varphi'''(u)$  are uniformly bounded in  $L^\infty$ ; that is, there exists a constant  $M > 0$ , such that

$$\begin{aligned} |\varphi'(u)|_{L^\infty} &\leq M, \\ |\varphi''(u)|_{L^\infty} &\leq M, \\ |\varphi'''(u)|_{L^\infty} &\leq M, \end{aligned} \quad (34)$$

since there exists constant  $0 < \theta < 1$ , such that

$$\begin{aligned} &\left( \int_0^L \left| \frac{\partial^2 (\varphi(u_n) - \varphi(u))}{\partial x^2} \right|^2 dx \right)^{1/2} \\ &\leq \left( \int_0^L \left| \varphi''(u_0 + \theta\omega_n) \frac{\partial^2 (u_0 + \theta\omega_n)}{\partial x^2} \omega_n \right|^2 dx \right)^{1/2} \\ &+ \left( \int_0^L \left| \varphi'''(u_0 + \theta\omega_n) \left( \frac{\partial (u_0 + \theta\omega_n)}{\partial x} \right)^2 \right. \right. \\ &\quad \left. \left. \cdot \omega_n \right|^2 dx \right)^{1/2} \end{aligned}$$

$$\begin{aligned}
 & + \left( \int_0^L \left| \varphi' (u_0 + \theta \omega_n) \frac{\partial^2 \omega_n}{\partial x^2} \right|^2 dx \right)^{1/2} \\
 & + 2 \left( \int_0^L \left| \varphi'' (u_0 + \theta \omega_n) \right. \right. \\
 & \cdot \left. \left. \left( \frac{\partial (u_0 + \theta \omega_n)}{\partial x} \right) \frac{\partial \omega_n}{\partial x} \right|^2 dx \right)^{1/2} \\
 & \leq M \left( \int_0^L \left| \frac{\partial^2 (u_0 + \theta \omega_n)}{\partial x^2} \omega_n \right|^2 dx \right)^{1/2} \\
 & + M \left( \int_0^L \left| \left( \frac{\partial (u_0 + \theta \omega_n)}{\partial x} \right)^2 \omega_n \right|^2 dx \right)^{1/2} \\
 & + M \left( \int_0^L \left| \frac{\partial^2 \omega_n}{\partial x^2} \right|^2 dx \right)^{1/2} \\
 & + 2M \left( \int_0^L \left| \left( \frac{\partial (u_0 + \theta \omega_n)}{\partial x} \right) \frac{\partial \omega_n}{\partial x} \right|^2 dx \right)^{1/2}
 \end{aligned} \tag{35}$$

Because  $u_n$  converges to  $u_0$  in  $L^P(0, T), W^{1,P}(0, T), W^{2,P}(0, T), \forall P \geq 1, \forall T > 0$ , we have

$$\lim_{n \rightarrow \infty} \left( \int_0^L \left| \frac{\partial^2}{\partial x^2} (\varphi(u_n) - \varphi(u_0)) \right|^2 dx \right)^{1/2} = 0 \tag{36}$$

The proof is completed.  $\square$

Similarly, we can prove the following Lemma.

**Lemma 10.** *Let  $g(u, u_t) = \varphi'(u)u_t$  and (2) and (3) hold,  $\varphi(0) = 0$ . Then  $g : D(A) \times V_1 \rightarrow H$  and  $\varphi'(u) : D(A) \rightarrow H$  are continuous compact.*

Since  $D(A) \times V_1 \hookrightarrow V_1 \times L^2$ , from Theorem 5 and [4], we can immediately obtain the following result.

**Lemma 11.** *The semigroup  $\{S(t)\}_{t \geq 0}$  associated with (1) is norm-to weak continuous on  $S(B)$ , where  $B$  is bounded absorbing set of  $\{s(t)\}_{t \geq 0}$  in  $E_2$  and  $S(B)$  is the stationary set of  $B$  defined by*

$$S(B) = \{x \in B \mid S(t) x \in B, \forall t \geq 0\}. \tag{37}$$

Now we give our main results of the paper.

**Theorem 12.** *Suppose that  $f \in L^2(\Omega), \varphi \in C^3(\mathbb{R}, \mathbb{R}), \varphi(0) = 0$ , and (2) and (3) hold. Then the solution semigroup  $\{s(t)\}_{t \geq 0}$  of problem (1) has global attractor  $\mathcal{A}$  in  $E_2$ ; it attracts all bounded subset of  $E_2$  in the norm of  $E_2$ .*

*Proof.* Applying Theorems 7 and 8, we only need to verify that  $\{S(t)\}_{t \geq 0}$  satisfies condition (C) in  $E_2$ .

Let  $\lambda_1, \lambda_2, \dots$  be the eigenvalues of  $A$  in  $D(A)$  and  $\omega_1, \omega_2, \dots$  be the corresponding eigenvectors such that

$$0 < \lambda_1 \leq \lambda_2 \leq \dots \leq \lambda_n \leq \dots, \tag{38}$$

where  $\lambda_n \rightarrow \infty$ , as  $n \rightarrow \infty$  and  $\{\omega_1, \omega_2, \dots\}$  forms an orthogonal basis in  $D(A)$  and  $H_0^2(\Omega)$ .

Let  $V_m = \text{span}\{\omega_1, \omega_2, \dots, \omega_m\}$  and  $P_m$  be the canonical projector on  $V_m$  and  $I$  be the identity. Then, for any  $(u, u_t) \in E_2$ , it has a unique decomposition  $(u, u_t) = (u_1, u_{1t}) + (u_2, u_{2t})$ , where

$$\begin{aligned}
 (u, u_t) &= (P_m u, P_m u_t), \\
 (u_2, u_{2t}) &= (I - P_m)(u, u_t).
 \end{aligned} \tag{39}$$

Since  $f \in L^2(\Omega)$  and  $\varphi' : D(A) \rightarrow H(\Omega)$  are compact continuously verified by Lemma 10, then, for any  $\varepsilon > 0$ , there exists  $N > 0$ , such that, for any  $m > N$ , we have

$$\begin{aligned}
 |(I - P_m) f| &< \frac{\varepsilon}{8}, \\
 \|(I - P_m) f\| &< \frac{\varepsilon}{8},
 \end{aligned} \tag{40}$$

$$\|(I - P_m) \varphi'(u)\| < \frac{\varepsilon}{8}, \quad \forall u \in B_{V_2}(0, \mu),$$

where  $\mu$  is given by (23).

Multiplying (1) by  $Av = Au_{2t} + \alpha Au_2$ , we can get

$$\begin{aligned}
 & \frac{d}{dt} \left[ \|\xi_{u_2}\|_{E_2}^2 + 2\alpha (u_{2t}, Au_2) + 2(\varphi(u), Au_2) \right] \\
 & + 2\|u_{2t}\|_{V_1}^2 - 2\alpha (u_{2t}, Au_{2t}) + 2\alpha (u_{2t}, Au_2) \\
 & + 2\alpha \|u_2\|_{V_2}^2 + 2\alpha (\varphi(u), Au_2) \\
 & = 2(f, Au_{2t}) + 2(\varphi'(u)u_{2t}, Au_2) + 2\alpha (f, Au_2).
 \end{aligned} \tag{41}$$

Applying the Young inequality, Hölder inequality, Sobolev embedding theorem, and (40) and (41), the three terms in the right-hand side of (41) can be estimated as follows:

$$\begin{aligned}
 2(f, Au_{2t}) &\leq 2|(f, Au_{2t})| \leq 2\|(f)_2\|_{V_1} \|u_{2t}\|_{V_1} \\
 &\leq \frac{\varepsilon}{4} \|u_{2t}\|_{H^2}^2 \leq \|u_{2t}\|_{H^2}^2 + C_2 \varepsilon^2; \\
 2(\varphi'(u), Au_2) &\leq 2|(\varphi'(u)u_t, Au_2)| \leq 2 \cdot \frac{\varepsilon}{8} \|u_2\|_{V_2} \\
 &\leq \frac{\alpha}{2} \|u_2\|_{V_2}^2 + C_1 \varepsilon^2; \\
 2\alpha (f, Au_2) &\leq 2\alpha |(f, Au_2)| \leq 2\|(f)_2\|_{V_1} \|u_2\|_{V_1} \\
 &\leq 2C\alpha \cdot \frac{\varepsilon}{8} \|u_2\|_{V_2}^2 \leq \frac{\alpha}{2} \|u_2\|_{V_2}^2 + C_3 \varepsilon^2.
 \end{aligned} \tag{42}$$

Using the above estimates, we transform (41) as follows:

$$\begin{aligned} & \frac{d}{dt} \left[ \|\xi_{u_2}\|_{E_2}^2 + 2\alpha (u_{2t}, Au_2) + 2(\varphi(u), Au_2) \right] \\ & + 2\alpha (u_{2t}, Au_2) + \alpha \|u_2\|_{V_2}^2 + (1-2\alpha) \|u_{2t}\|_{V_1}^2 \\ & + 2\alpha ((\varphi(u))_2, Au_2) \leq C\varepsilon^2, \end{aligned} \quad (43)$$

$$C = C_1 + C_2 + C_3.$$

Choose  $\alpha$  small enough such that  $1-2\alpha > \alpha$  and  $2\alpha > 2\alpha^2$ . Hence (43) can be rewritten as

$$\begin{aligned} & \frac{d}{dt} \left[ \|\xi_{u_2}\|_{E_2}^2 + 2\alpha (u_{2t}, Au_2) + 2(\varphi(u), Au_2) \right] \\ & + \alpha \left[ \|\xi_{u_2}\|_{E_2}^2 + 2\alpha (u_{2t}, Au_2) + 2((\varphi(u))_2, Au_2) \right] \\ & \leq C\varepsilon^2. \end{aligned} \quad (44)$$

Denote  $Y(t) = \|\xi_{u_2}\|_{E_2}^2 + 2\alpha(u_{2t}, Au_2) + 2(\varphi(u), Au_2)$  we arrive at

$$\frac{dY(t)}{dt} + \alpha Y(t) \leq C\varepsilon^2. \quad (45)$$

By Gronwall inequality

$$\begin{aligned} Y(t) & \leq Y(t_1) e^{-\alpha(t-t_1)} + \frac{C\varepsilon^2}{\alpha} (1 - e^{-\alpha(t-t_1)}) \\ & \leq Y(t_1) e^{-\alpha(t-t_1)} + \frac{C\varepsilon^2}{\alpha}. \end{aligned} \quad (46)$$

Next, we show that

$$\frac{1}{2} \|\xi_{u_2}\|_{E_2}^2 - C_4\varepsilon^2 \leq Y(t) \leq \frac{3}{2} \|\xi_{u_2}\|_{E_2}^2 + C_4\varepsilon^2. \quad (47)$$

Indeed, the right inequality is obtained using Hölder inequality, Young inequality, and Lemma 9:

$$\begin{aligned} Y(t) & \leq \|\xi_{u_2}\|_{E_2}^2 + 2\alpha \|u_{2t}\|_{V_1} \|u_2\|_{V_1} \\ & + 2 \|(\varphi(u))_2\| \|Au_2\| \\ & \leq \|\xi_{u_2}\|_{E_2}^2 + 2\alpha\varepsilon \|u_{2t}\|_{V_1}^2 + 2\varepsilon \|Au_2\| \\ & \leq \|\xi_{u_2}\|_{E_2}^2 + \frac{1}{2} \|u_{2t}\|_{V_1}^2 + \frac{1}{2} \|Au_2\| + 2\alpha^2\varepsilon^2 + 2\varepsilon^2 \\ & \leq \frac{3}{2} \|\xi_{u_2}\|_{E_2}^2 + C_4\varepsilon^2. \end{aligned} \quad (48)$$

and the left one is the same, where  $C_4 = 2(1 + \alpha^2)$ .

Thus, combining (46) and (47) and Theorem 8, we deduce

$$\begin{aligned} \|\xi_{u_2}\|_{E_2}^2 & \leq 2Y(t) + 2C_4\varepsilon^2 \\ & \leq 2 \left( \frac{3}{2} R_3^2 + C_4\varepsilon^2 \right) e^{-\alpha(t-t_1)} + \frac{2C\varepsilon^2}{\alpha} + 2C_4\varepsilon^2 \\ & \leq 3R_3^2 e^{-\alpha(t-t_1)} + C_5\varepsilon^2. \end{aligned} \quad (49)$$

Taking  $t - t_1 > t(R_3)$ , it follows that

$$\|\xi_{u_2}\|_{E_2}^2 \leq (1 + C_5\varepsilon^2), \quad (50)$$

where, by (29), we denote  $R^3 = 1 + Q(R)$ ,  $C_5 = C/\alpha + C_4$ ,  $t(R_3) = t_1 + (1/\alpha) \ln 3R_3^2$ .

Together with Theorems 5, 7, and 8, the proof is finished.  $\square$

*Remark 13.* If we transform the first equation of (1) to the following form,

$$u_{tt} + \sigma(u)u_t + \Delta^2 u + \varphi(u) = f, \quad (51)$$

then the term  $\sigma(u)u_t$  accounts for dynamical friction, and we only need to assume the damping coefficient  $\sigma(u)$  is a positive function and by adding some appropriate conditions of continuity, conclusions of Theorem 12 remain valid and the proof's process has no essential difference.

## Data Availability

All data included in this study are available upon request by contact with the corresponding author.

## Conflicts of Interest

The author declares that there are no conflicts of interest.

## Acknowledgments

This work was supported by the National Science Foundation of China (61703181).

## References

- [1] A. Mao and H. Chang, "Kirchhoff type problems in RN with radial potentials and locally Lipschitz functional," *Applied Mathematics Letters*, vol. 62, pp. 49–54, 2016.
- [2] A. Mao and X. Zhu, "Existence and multiplicity results for Kirchhoff problems," *Mediterranean Journal of Mathematics*, vol. 14, no. 2, Art. 58, 14 pages, 2017.
- [3] Q. Gao, F. Li, and Y. Wang, "Blow-up of the solution for higher-order Kirchhoff-type equations with nonlinear dissipation," *Central European Journal of Mathematics*, vol. 9, no. 3, pp. 686–698, 2011.
- [4] S. Kolbasin, "Attractors for Kirchhoff's equation with a nonlinear damping coefficient," *Nonlinear Analysis*, vol. 71, no. 5-6, pp. 2361–2371, 2009.
- [5] A. K. Khanmamedov, "Global attractors for the plate equation with a localized damping and a critical exponent in an unbounded domain," *Journal of Differential Equations*, vol. 225, no. 2, pp. 528–548, 2006.
- [6] A. K. Khanmamedov, "A global attractor for the plate equation with displacement-dependent damping," *Nonlinear Analysis*, vol. 74, no. 5, pp. 1607–1615, 2011.
- [7] Y. Zhijian and W. Yunqing, "Global attractor for the Kirchhoff type equation with a strong dissipation," *Journal of Differential Equations*, vol. 249, no. 12, pp. 3258–3278, 2010.

- [8] Z. Yang and X. Li, "Finite-dimensional attractors for the Kirchhoff equation with a strong dissipation," *Journal of Mathematical Analysis and Applications*, vol. 375, no. 2, pp. 579–593, 2011.
- [9] I. Chueshov, "Long-time dynamics of Kirchhoff wave models with strong nonlinear damping," *Journal of Differential Equations*, vol. 252, no. 2, pp. 1229–1262, 2012.
- [10] F. Li and C. Zhao, "Uniform energy decay rates for nonlinear viscoelastic wave equation with nonlocal boundary damping," *Nonlinear Analysis*, vol. 74, no. 11, pp. 3468–3477, 2011.
- [11] F. Li, Z. Zhao, and Y. Chen, "Global existence uniqueness and decay estimates for nonlinear viscoelastic wave equation with boundary dissipation," *Nonlinear Analysis: Real World Applications*, vol. 12, no. 3, pp. 1759–1773, 2011.
- [12] F. Li, "Limit behavior of the solution to nonlinear viscoelastic Marguerre -von Karman shallow shells system," *Journal of Differential Equations*, vol. 249, no. 6, pp. 1241–1257, 2010.
- [13] M. Sun and Q. Bai, "A new descent memory gradient method and its global convergence," *Journal of Systems Science & Complexity*, vol. 24, no. 4, pp. 784–794, 2011.
- [14] C.-K. Zhong, M.-H. Yang, and C.-Y. Sun, "The existence of global attractors for the norm-to-weak continuous semigroup and application to the nonlinear reaction-diffusion equations," *Journal of Differential Equations*, vol. 223, no. 2, pp. 367–399, 2006.
- [15] Q. Ma, S. Wang, and C. Zhong, "Necessary and sufficient conditions for the existence of global attractors for semigroups and applications," *Indiana University Mathematics Journal*, vol. 51, no. 6, pp. 1541–1559, 2002.
- [16] R. Temam, *Infinite-Dimensional Dynamical Systems in Mechanics and Physics*, vol. 68 of *Applied Mathematical Sciences*, Springer, New York, NY, USA, 2nd edition, 1997.
- [17] Q. Ma and C. Zhong, "Existence of strong solutions and global attractors for the coupled suspension bridge equations," *Journal of Differential Equations*, vol. 246, no. 10, pp. 3755–3775, 2009.
- [18] J. C. Robinson, *Infinite-Dimensional Dynamical Systems: An Introduction to Dissipative parabolic PDEs and the Theory Of Global Attractors*, Cambridge Texts in Applied Mathematics, Cambridge University Press, Cambridge, UK, 2001.

## Research Article

# Disturbance Attenuation via Output Feedback for Nonlinear Time-Delay Systems with Input Matching Uncertainty

Chao Guo<sup>1</sup> and Kemei Zhang<sup>2</sup> 

<sup>1</sup>Institute of Automation, Qufu Normal University, Shandong Province 273165, China

<sup>2</sup>School of Mathematics Sciences, Qufu Normal University, Shandong Province 273165, China

Correspondence should be addressed to Kemei Zhang; zhkm90@126.com

Received 14 April 2018; Accepted 13 June 2018; Published 5 July 2018

Academic Editor: Weihai Zhang

Copyright © 2018 Chao Guo and Kemei Zhang. This is an open access article distributed under the Creative Commons Attribution License, which permits unrestricted use, distribution, and reproduction in any medium, provided the original work is properly cited.

This paper studies the problem of output feedback disturbance attenuation for a class of uncertain nonlinear systems with input matching uncertainty and unknown multiple time-varying delays, whose nonlinearities are bounded by unmeasured states multiplying unknown polynomial-of-output growth rate. By skillfully combining extended state observer, dynamic gain technique, and Lyapunov-Krasovskii theorem, a delay-independent output feedback controller can be developed with only one dynamic gain to guarantee the boundedness of closed-loop system states and the achievement of global disturbance attenuation in the  $L_2$ -gain sense.

## 1. Introduction

The problem of disturbance attenuation via output feedback for nonlinear systems is a relatively meaningful problem in control theory and applications. Compared with the stabilization control and tracking control, fewer results on output feedback disturbance attenuation design have been obtained until now, such as [1–5] and the references therein. It is worth mentioning that, for nonlinear systems with known polynomial-of-output growth rate, the problem of output feedback disturbance attenuation was studied in [5].

In this paper, we consider output feedback disturbance attenuation problem of uncertain nonlinear systems as follows:

$$\begin{aligned} \dot{x}_i(t) &= x_{i+1}(t) + f_i(\theta^*(t), x(t), x(t - \tau_i(t))) \\ &\quad + \varphi_i(\theta^*(t), x(t))^\top \omega(t), \\ &\quad i = 1, \dots, n-1, \\ \dot{x}_n(t) &= u(t) + \nu + f_n(\theta^*(t), x(t), x(t - \tau_n(t))) \\ &\quad + \varphi_n(\theta^*(t), x(t))^\top \omega(t), \\ y(t) &= x_1(t), \end{aligned} \quad (1)$$

where  $x = [x_1, \dots, x_n]^\top \in R^n$ ,  $u \in R$ , and  $y \in R$  are the system state, control input, and output, respectively.  $\nu \in R$  is an unknown constant, representing the input matching uncertainty, and let  $x_{n+1} = \nu$  for notational convenience.  $\theta^*(t) : R^+ \rightarrow R^m$  is a vector of continuous time-varying parameters belonging to an unknown bounded set.  $\tau_i(t) : R^+ \rightarrow R^+$ ,  $i = 1, \dots, n$ , represent the bounded time-varying delays satisfying  $\dot{\tau}_i(t) \leq \kappa < 1$  for an unknown positive constant  $\kappa$ , and the initial condition is  $x(t_0) = \Psi(t_0)$ ,  $t_0 \in [-\bar{\tau}, 0]$  with  $\bar{\tau} = \max_{i=1, \dots, n} \{\tau_i(t), t \geq 0\}$  and  $\Psi$  being a continuous function vector defined on  $[-\bar{\tau}, 0]$ .  $\omega(t) : R^+ \rightarrow R^s$  is disturbance satisfying  $\omega(t) \in L_2[0, +\infty)$ . For  $i = 1, \dots, n$ , functions  $f_i(\cdot)$  and function vectors  $\varphi_i(\cdot)$  are continuous in the first argument and locally Lipschitz with respect to the rest of variables.

**Assumption 1.** For  $i = 1, \dots, n$ , there is an unknown positive constant  $\theta$  and a known positive integer  $p \geq 1$  such that

$$\begin{aligned} |f_i(\cdot)| &\leq \theta (1 + |y(t)|^p) \sum_{j=1}^i |x_j(t)| \\ &\quad + \theta (1 + |y(t - \tau_i(t))|^p) \sum_{j=1}^i |x_j(t - \tau_i(t))|, \end{aligned}$$

$$\|\varphi_i(\cdot)\| \leq \theta(1 + |y(t)|^p). \quad (2)$$

During the past decade years, the problem of global output feedback control for uncertain nonlinear or nonlinear time-delay systems with unknown growth rate has been extensively studied with the aid of the dynamic gain technique, and a series of interesting results have been obtained; see [6–11] and the references therein. Specifically, for nonlinear time-delay systems with unknown polynomial-of-output growth rate, [10] achieved the global output feedback stabilization based on only one dynamic gain.

However, these results do not consider the input matching uncertainty. In many practical control systems, since input matching uncertainty often causes instability or serious deterioration in the performance of systems, output feedback control of nonlinear systems with input matching uncertainty is an attractive topic in recent years; see [12–17] and the references therein. Reference [12] achieved global output feedback regulation of nonlinear systems with zero dynamics and input matching uncertainty, whose nonlinearities are bounded by unmeasured states multiplying known function of output growth rate. References [13, 14] investigated the problem of global adaptive output feedback stabilization of nonlinear systems with input matching uncertainty, whose uncertain nonlinearities only depend on system output. For a class of uncertain time-varying nonlinear systems with input matching uncertainty, whose nonlinearities are strictly restricted, [15] achieved global output feedback stabilization based on two dynamic gains. Lately, a compact design scheme for nonlinear systems with unknown polynomial-of-output growth rate and input matching uncertainty was proposed in [16] based on only one dynamic gain. Reference [17] studied the output tracking problem for a class of stochastic nonlinear systems with unstable modes.

As far as we know, the problem of output feedback disturbance attenuation of uncertain nonlinear systems with input matching uncertainty and unknown multiple time-varying delays, whose nonlinearities are bounded by unmeasured states multiplying unknown constant and polynomial-of-output growth rates, has not yet been considered until now. In this paper, we make an attempt to handle this interesting problem by skillfully combining extended state observer, dynamic gain technique, and Lyapunov-Krasovskii theorem.

Since there simultaneously exist three types of uncertainties in system (1) for the problem of disturbance attenuation, input matching uncertainty, two types of growth rates (unknown constant and polynomial-of-output growth rates), and unknown multiple time-varying delays, some essential technical difficulties to control design will be inevitably produced. (i) The observer in [5, 10] is inapplicable to systems of this paper due to the existence of input matching uncertainty, so a rather difficult work is how to construct a feasible observer. (ii) The analysis method in [16] is unsuitable due to the existence of unknown multiple time-varying delays; hence, another difficulty is how to give a new analysis method. This paper will focus on solving these two difficulties.

This paper is organized as follows. Section 2 gives preliminaries. In Section 3, the design and analysis of output

feedback controller are presented, following a simulation example in Section 4. Section 5 concludes this paper.

## 2. Mathematical Preliminaries

In this paper, the argument of function will be omitted whenever no confusion can arise from the context.  $R$ ,  $R^+$ , and  $R^n$  denote the set of real numbers, the set of all nonnegative real numbers, and the real  $n$ -dimensional space, respectively. For any real vector or matrix  $A$ ,  $A^T$  denotes its transpose;  $A > 0$  denotes that matrix  $A$  is a positive definite matrix;  $\lambda_{\min}(A)$  denotes the minimal eigenvalue of the symmetric matrix  $A$ . For any vector  $x$ ,  $\|x\|_1$  and  $\|x\|$  denote its 1-norm and 2-norm, respectively. Clearly,  $\|x\| \leq \|x\|_1 \leq \sqrt{n}\|x\|$ , where  $n$  is the dimension of  $x$ .  $\text{diag}\{a_1, \dots, a_n\}$  denotes  $n \times n$  diagonal matrix whose element  $(k, k)$  is  $a_k$  and others are zero.  $I_n$  denotes the  $n$ -dimensional identity matrix.  $L_2[0, T)$  and  $L_\infty[0, T)$  denote the appropriate dimension space of square integrable functions and the appropriate dimension space of uniformly bounded functions on  $[0, T)$ , respectively, where  $0 < T \leq +\infty$ .

**Lemma 2** (see [12]). *For any positive real number  $\mu$ , there exist real number  $\sigma_1 > 0$ , symmetric positive definite matrices  $P$  and  $Q$ , and column vectors  $a = [a_1, \dots, a_{n+1}]^T$  and  $k = [k_1, \dots, k_n]^T$  satisfying the following set of inequalities:*

$$\begin{aligned} A^T P + PA &\leq -\sigma_1 I_{n+1}, \\ D_{n+1} P + PD_{n+1} &\geq \mu P, \\ K^T Q + QK &\leq -2\sigma_1 I_n, \\ D_n Q + QD_n &\geq \mu Q, \end{aligned} \quad (3)$$

where  $D_i = \text{diag}\{\mu, 1 + \mu, \dots, i - 1 + \mu\}$ ,  $i = n, n + 1$ , and

$$\begin{aligned} A &= \begin{bmatrix} -a_1 & 1 & \cdots & 0 \\ \vdots & \vdots & \ddots & \vdots \\ -a_n & 0 & \cdots & 1 \\ -a_{n+1} & 0 & \cdots & 0 \end{bmatrix}, \\ K &= \begin{bmatrix} 0 & 1 & \cdots & 0 \\ \vdots & \vdots & \ddots & \vdots \\ 0 & 0 & \cdots & 1 \\ -k_1 & -k_2 & \cdots & -k_n \end{bmatrix}. \end{aligned} \quad (4)$$

**Lemma 3** (Young's inequality). *Let real numbers  $p \geq 1$  and  $q \geq 1$  satisfy  $1/p + 1/q = 1$ , then for any  $x, y \in R$  and any given positive number  $\gamma > 0$ ,  $xy \leq \gamma \|x\|^p + (1/q)(p\gamma)^{-q/p} \|y\|^q$ .*

**Lemma 4** (see [18]). *For  $x, y \in R$  and  $p \geq 1$  is a constant, then  $|x + y|^p \leq 2^{p-1} |x|^p + |y|^p$ .*

**Lemma 5** (Barbalat's lemma, see [19]). *For a continuously differentiable function  $x(t) : \mathbb{R}^+ \rightarrow \mathbb{R}$ , if  $x(t), \dot{x}(t) \in L_\infty$  and  $x(t) \in L_p$  for some  $p \in [1, +\infty)$ , then  $\lim_{t \rightarrow \infty} x(t) = 0$ .*

### 3. Design and Analysis of Output Feedback Controller

**3.1. Control Objective of This Paper.** The objective of this paper is to construct an output feedback controller for system (1) under Assumption 1 such that, by suitably choosing the design parameters,

(i) when  $\omega(t) = 0$  or  $\omega(t) \in L_2[0, +\infty) \cap L_\infty[0, +\infty)$ , all the states of the closed-loop system are bounded and the original system states and their corresponding observer states all converge to zero, and the estimation of the input matching uncertainty converges to its actual value.

(ii) when  $\omega(t) \in L_2[0, +\infty)$ , for any pre-given small real number  $\pi > 0$ , the system output  $y$  has the following property:

$$\int_0^t y^2(s) ds \leq \pi^2 \int_0^t \|\omega(s)\|^2 ds + \rho(\cdot), \quad (5)$$

where  $\rho(\cdot)$  is a nonnegative bounded function.

*Remark 6.* Compared with the problem of disturbance attenuation of free-delay systems in [5],

$$|\psi_i(\cdot)| \leq \theta \left(1 + |y(t)|^p\right) \sum_{j=1}^i |x_j(t)|, \quad (6)$$

$$\|\varphi_i(\cdot)\| \leq \theta \left(1 + |y(t)|^p\right),$$

where  $\theta$  is a known constant, and compared with the problem of stabilization control of time-delay systems in [10],

$$|\phi_i(\cdot)| \leq \theta \left(1 + |y(t)|^p\right) \sum_{j=1}^i |x_j(t)| + \theta \left(1 + |y(t-d(t))|^p\right) \sum_{j=1}^i |x_j(t-d(t))|, \quad (7)$$

where  $d(t)$  is an unknown time-varying delay; it is worth mentioning that none of the systems in [5, 10] take into account the input match uncertainty. Furthermore, compared with the problem of stabilization control of free-delay systems in [16] with input matching uncertainty,

$$|f_i(\cdot)| \leq \theta \left(1 + |y(t)|^p\right) \sum_{j=1}^i |x_j(t)|, \quad (8)$$

where  $\theta$  is an unknown constant. This paper considers the problem of disturbance attenuation for the case in which there simultaneously exist input matching uncertainty, unknown polynomial-of-output growth rate, and unknown multiple time-varying delays; all these factors lead to some essential technical difficulties to control design of the more general systems in this paper.

**3.2. The Design of Observer and Controller for System (1).** Motivated by [14–16], we design the following extended state observer to rebuild the unmeasured states and estimate the input matching uncertainty and construct a coupled controller:

$$\begin{aligned} \dot{\hat{x}}_i &= \hat{x}_{i+1} + a_i L^i (x_1 - \hat{x}_1), \quad i = 1, \dots, n-1, \\ \dot{\hat{x}}_n &= u + \hat{x}_{n+1} + a_n L^n (x_1 - \hat{x}_1), \\ \dot{\hat{x}}_{n+1} &= a_{n+1} L^{n+1} (x_1 - \hat{x}_1), \\ u &= -L^n k_1 \hat{x}_1 - L^{n-1} k_2 \hat{x}_2 - \dots - L k_n \hat{x}_n - \hat{x}_{n+1}, \end{aligned} \quad (9)$$

with  $L$  being a dynamic gain updated by

$$\begin{aligned} \dot{L}(t) &= \max \left\{ -\rho_1 L^2(t) + \rho_2 L(t) \right. \\ &\quad \left. \cdot \left(1 + |y(t)|^p\right)^2, L^{1-2\mu}(t) (x_1(t) - \hat{x}_1(t))^2 \right\}, \quad (10) \\ L(0) &= 1, \end{aligned}$$

where  $\hat{x} = [\hat{x}_1, \dots, \hat{x}_n]^\top \in \mathbb{R}^n$  and  $\hat{x}_{n+1} \in \mathbb{R}$  are the observer states.  $\mu > 0$  is a design parameter and will be first selected such that  $0 < \mu < 1/2p$ ,  $p$  is the same as in Assumption 1. Then, according to Lemma 2, a set  $(\sigma_1, P, Q, a, k)$  can be determined to satisfy the inequalities in Lemma 2, and the vectors  $a$  and  $k$  are selected as the gains of the extended state observer and controller, respectively.  $\rho_1$  and  $\rho_2$  are positive design parameters to be determined. The dynamic gain  $L(t)$  has the following properties for all  $t \geq 0$ :

$$\begin{aligned} \dot{L}(t) &\geq 0, \\ L(t) &\geq 1, \\ L(t) &\geq L(t - \tau_i(t)), \quad i = 1, \dots, n, \\ \dot{L}(t) &\geq -\rho_1 L^2(t) + \rho_2 L(t) \left(1 + |y(t)|^p\right)^2, \\ \dot{L}(t) &\geq L^{1-2\mu}(t) (x_1(t) - \hat{x}_1(t))^2. \end{aligned} \quad (11)$$

*Remark 7.* Since the existence of the input matching uncertainty  $v$  in system (1), the introduction of  $\hat{x}_{n+1}$  in the observer (9) is indispensable to compensate the input matching uncertainty  $v$ . In Theorem 8, we will prove that  $\hat{x}_{n+1}$  ultimately converge to the actual value of the input matching uncertainty  $v$ .

Introduce coordinate transformation

$$\begin{aligned} \varepsilon_i &= \frac{x_i - \hat{x}_i}{L^{i-1+\mu}}, \quad i = 1, \dots, n+1, \\ z_i &= \frac{\hat{x}_i}{L^{i-1+\mu}}, \quad i = 1, \dots, n. \end{aligned} \quad (12)$$

By (1), (9), and (12), we obtain

$$\begin{aligned} \dot{\varepsilon} &= LA\varepsilon + F - \frac{\dot{L}}{L} D_{n+1} \varepsilon, \\ \dot{z} &= LKz + La^* \varepsilon_1 - \frac{\dot{L}}{L} D_n z, \end{aligned} \quad (13)$$

where  $\varepsilon = [\varepsilon_1, \dots, \varepsilon_{n+1}]^\top$ ,  $z = [z_1, \dots, z_n]^\top$ ,  $F = [(f_1 + \varphi_1^\top \omega)/L^\mu, \dots, (f_n + \varphi_n^\top \omega)/L^{n-1+\mu}, 0]^\top$ ,  $a^* = [a_1, \dots, a_n]^\top$ . Let  $V_\varepsilon = m\varepsilon^\top P\varepsilon$  and  $V_z = z^\top Qz$  with  $m = 1 + \|Qa^*\|^2/\sigma_1^2$ . By (11), (13), Lemma 2, and the fact that  $\lambda_{\min}(P)\|\varepsilon\|^2 \leq \varepsilon^\top P\varepsilon$  and  $\lambda_{\min}(Q)\|z\|^2 \leq z^\top Qz$ , we have

$$\begin{aligned} \dot{V}_\varepsilon &\leq -\sigma_1 mL \|\varepsilon\|^2 + 2m\varepsilon^\top PF + m\rho_1 \mu \lambda_{\min}(P) L \|\varepsilon\|^2 \\ &\quad - m\rho_2 \mu \lambda_{\min}(P) (1 + |y|^p)^2 \|\varepsilon\|^2, \end{aligned} \quad (14)$$

$$\begin{aligned} \dot{V}_z &\leq -2\sigma_1 L \|z\|^2 + 2Lz^\top Qa^* \varepsilon_1 + \rho_1 \mu \lambda_{\min}(Q) L \|z\|^2 \\ &\quad - \rho_2 \mu \lambda_{\min}(Q) (1 + |y|^p)^2 \|z\|^2. \end{aligned} \quad (15)$$

By Lemma 3, it is easy to get

$$2Lz^\top Qa^* \varepsilon_1 \leq \sigma_1 L \|z\|^2 + \frac{\|Qa^*\|^2}{\sigma_1} L \varepsilon_1^2. \quad (16)$$

By (2), (12), and the fact that  $L(t) \geq 1$  is a monotone nondecreasing function for  $i = 1, \dots, n$ ,

$$\begin{aligned} \left| \frac{f_i + \varphi_i^\top \omega}{L^{i-1+\mu}} \right| &\leq \frac{\theta(1 + |y|^p)}{L^{i-1+\mu}} \left( \sum_{j=1}^i |x_j| + \|\omega\| \right) \\ &\quad + \frac{\theta(1 + |y(t - \tau_i(t))|^p)}{L^{i-1+\mu}} \sum_{j=1}^i |x_j(t - \tau_i(t))| \\ &\leq \theta(1 + |y|^p) \sqrt{n} (\|\varepsilon\| + \|z\|) + \theta(1 + |y|^p) \|\omega\| \\ &\quad + \theta(1 + |y(t - \tau_i(t))|^p) \\ &\quad \cdot \sqrt{n} (\|\varepsilon(t - \tau_i(t))\| + \|z(t - \tau_i(t))\|). \end{aligned} \quad (17)$$

Using (17) and Lemma 3, it follows that

$$\begin{aligned} 2m\varepsilon^\top PF &\leq 2m \|P\| \|\varepsilon\| \sum_{i=1}^n \left| \frac{f_i + \varphi_i^\top \omega}{L^{i-1+\mu}} \right| \leq (1 + |y|^p)^2 \\ &\quad \cdot (\|\varepsilon\|^2 + \|z\|^2) + d_0 \|\varepsilon\|^2 + g_0 \|\omega\|^2 + \sum_{i=1}^n \frac{1 - \kappa}{n} \\ &\quad \cdot (1 + |y(t - \tau_i(t))|^p)^2 \\ &\quad \cdot (\|\varepsilon(t - \tau_i(t))\|^2 + \|z(t - \tau_i(t))\|^2), \end{aligned} \quad (18)$$

where  $d_0 = (2 + 2/(1 - \kappa))n^3 m^2 \theta^2 \|P\|^2$  and  $g_0 = 2n^2 m^2 \theta^2 \|P\|^2$  are unknown positive constants related to  $\theta$  and  $\kappa$ .

Choose the Lyapunov-Krasovskii functional

$$\begin{aligned} V &= V_\varepsilon + V_z + \sum_{i=1}^n \int_{t-\tau_i(t)}^t \frac{1}{n} (1 + |y(s)|^p)^2 \\ &\quad \cdot (\|\varepsilon(s)\|^2 + \|z(s)\|^2) ds, \end{aligned} \quad (19)$$

and select the design parameters  $\rho_1$  and  $\rho_2$  to satisfy

$$\begin{aligned} \rho_1 &\leq \min \left\{ \frac{\sigma_1}{2m\mu\lambda_{\min}(P)}, \frac{\sigma_1}{2\mu\lambda_{\min}(Q)} \right\}, \\ \rho_2 &\geq \max \left\{ \frac{2}{m\mu\lambda_{\min}(P)}, \frac{2}{\mu\lambda_{\min}(Q)} \right\}. \end{aligned} \quad (20)$$

Then, using (14)-(16), (18)-(20), and  $\dot{\tau}_i(t) \leq \kappa < 1$ ,  $i = 1, \dots, n$ , we arrive at

$$\dot{V} \leq -\frac{\sigma_1}{2} L (\|\varepsilon\|^2 + \|z\|^2) + d_0 \|\varepsilon\|^2 + g_0 \|\omega\|^2. \quad (21)$$

**3.3. Stability and Convergence Analysis.** We state the main result in this paper.

**Theorem 8.** Consider system (1) satisfying Assumption 1, and under the output feedback controller (9) and (10), the closed-loop system consisting of (1), (9), and (10) achieves global disturbance attenuation in the  $L_2$ -gain sense. Moreover, if  $\omega(t) = 0$  or  $\omega(t) \in L_2[0, +\infty) \cap L_\infty[0, +\infty)$ , then  $\lim_{t \rightarrow +\infty} (x(t), \hat{x}(t), \hat{x}_{n+1}(t), u(t)) = (0, 0, \nu, -\nu)$ .

*Proof.* It is observed that the right-hand side of the closed-loop system consisting of (1), (9), and (10) is continuous and locally Lipschitz in  $(x, \hat{x}, \hat{x}_{n+1}, u)$ ; hence, the closed-loop system has a unique solution on the maximal interval  $[0, t_f)$  with  $0 < t_f \leq +\infty$ . Next, we divide the proof into two steps.

*Step I* (the boundedness of  $L(t)$ ,  $\varepsilon(t)$ , and  $z(t)$  on  $[0, t_f)$ )

(i) *Boundedness of  $L(t)$  on  $[0, t_f)$ .* We prove the boundedness of  $L(t)$  on  $[0, t_f)$  by a contradiction argument. Suppose that  $L(t)$  is unbounded on  $[0, t_f)$ ; note the monotone nondecreasing property of  $L(t)$ ; there holds  $\lim_{t \rightarrow t_f} L(t) = +\infty$ . Hence, there is a finite time  $t_1 \in [0, t_f)$  such that  $L(t) \geq \max\{1, 4d_0/\sigma_1\}$ ,  $\forall t \in [t_1, t_f)$ . Then, from (21), it follows that

$$\begin{aligned} \dot{V}(t) &\leq -\frac{\sigma_1}{4} L(t) \|\varepsilon(t)\|^2 - \frac{\sigma_1}{2} L(t) \|z(t)\|^2 \\ &\quad + g_0 \|\omega(t)\|^2, \quad \forall t \in [t_1, t_f), \end{aligned} \quad (22)$$

which, together with  $\omega(t) \in L_2[0, +\infty)$ , implies that  $\varepsilon(t)$  and  $z(t)$  are bounded on  $[t_1, t_f)$  and

$$\begin{aligned} \frac{\sigma_1}{4} \int_{t_1}^{t_f} L(s) \|\varepsilon(s)\|^2 ds &\leq V(t_1) + g_0 \int_{t_1}^{t_f} \|\omega(s)\|^2 ds \\ &< +\infty. \end{aligned} \quad (23)$$

By (12), Lemma 4, and the fact that  $L(t) \geq 1$ , it is obvious that

$$\begin{aligned} -\rho_1 L^2(t) + \rho_2 L(t) (1 + |y(t)|^p)^2 \\ \leq -\rho_1 L^2(t) \\ + 2\rho_2 (1 + |\varepsilon_1(t) + z_1(t)|^p) L^{1+2\mu p}(t). \end{aligned} \quad (24)$$

Then, by  $0 < \mu < 1/2p$  and the boundedness of  $\varepsilon(t)$  and  $z(t)$  on  $[t_1, t_f)$ , there is a finite time  $t_2 \in [t_1, t_f)$ , such that

$-\rho_1 L^2(t) + \rho_2 L(t)(1 + |y(t)|^p)^2 \leq 0$  on  $[t_2, t_f]$ , which, together with (10) and (12), implies that

$$\begin{aligned} +\infty &= L(t_f) - L(t_2) = \int_{t_2}^{t_f} \dot{L}(s) ds \\ &= \int_{t_2}^{t_f} L(s) \varepsilon_1^2(s) ds \leq \int_{t_1}^{t_f} L(s) \|\varepsilon(s)\|^2 ds. \end{aligned} \quad (25)$$

This contradicts with (23). Thus,  $L(t)$  is bounded on  $[0, t_f]$  and suppose  $\lim_{t \rightarrow t_f} L(t) = \bar{L}$  with  $\bar{L} \geq 1$  being a constant.

(ii) *Boundedness of  $z(t)$  on  $[0, t_f]$ .* By (11)-(12), (15)-(16), and (20), we obtain

$$\begin{aligned} \dot{V}_z &\leq -\frac{\sigma_1}{2} \|z\|^2 + \frac{\|Qa^*\|^2}{\sigma_1} \dot{L} \\ &\quad - \rho_2 \mu \lambda_{\min}(Q) (1 + |y|^p)^2 \|z\|^2. \end{aligned} \quad (26)$$

Integrating both sides of (26) with  $L(t) \geq 1$  being a monotone nondecreasing function and  $L(0) = 1$ ,  $\lim_{t \rightarrow t_f} L(t) = \bar{L}$  leads to, on  $[0, t_f]$ ,

$$\begin{aligned} \lambda_{\min}(Q) \|z(t)\|^2 &\leq V_z(t) \\ &\leq V_z(0) - \frac{\sigma_1}{2} \int_0^t \|z(s)\|^2 ds \\ &\quad + \frac{\|Qa^*\|^2}{\sigma_1} (\bar{L} - 1), \end{aligned} \quad (27)$$

from which it follows that,  $\forall t \in [0, t_f]$ ,

$$\begin{aligned} \|z(t)\|^2 &\leq \frac{1}{\lambda_{\min}(Q)} \left( V_z(0) + \frac{\|Qa^*\|^2}{\sigma_1} \bar{L} \right), \\ \int_0^t \|z(s)\|^2 ds &\leq \frac{2}{\sigma_1} \left( V_z(0) + \frac{\|Qa^*\|^2}{\sigma_1} \bar{L} \right), \end{aligned} \quad (28)$$

which implies that  $z(t)$  and  $\int_0^t \|z(s)\|^2 ds$  are bounded on  $[0, t_f]$ .

(iii) *Boundedness of  $\varepsilon(t)$  on  $[0, t_f]$ .* To prove the boundedness of  $\varepsilon(t)$  on  $[0, t_f]$ , we introduce a new change of coordinate

$$\varepsilon_i = \frac{\varepsilon_i}{(L^*)^{i-1+\mu}}, \quad i = 1, \dots, n+1, \quad (29)$$

where the constant is  $L^* \geq 1/m + 2d_1/\sigma_1 + 1 > 1$  with  $d_1$  being a positive constant to be defined. By (13) and (29), we arrive at

$$\dot{\varepsilon} = LL^* A \varepsilon + LL^* a \varepsilon_1 - L \Gamma a \varepsilon_1 + F^* - \frac{\dot{L}}{L} D_{n+1} \varepsilon, \quad (30)$$

where  $\varepsilon = [\varepsilon_1, \dots, \varepsilon_{n+1}]^T$ ,  $\Gamma = \text{diag}\{1, 1/L^*, \dots, 1/(L^*)^n\}$ , and  $F^* = [(f_1 + \varphi_1^T \omega)/(LL^*)^\mu, \dots, (f_n + \varphi_n^T \omega)/(LL^*)^{n-1+\mu}, 0]^T$ .

Choose the Lyapunov function  $V_\varepsilon = \varepsilon^T P \varepsilon$ . By (11), (30), Lemma 2, and the fact that  $\lambda_{\min}(P) \|\varepsilon\|^2 \leq \varepsilon^T P \varepsilon$ ,

$$\begin{aligned} \dot{V}_\varepsilon &\leq -\sigma_1 LL^* \|\varepsilon\|^2 + 2LL^* \varepsilon^T P a \varepsilon_1 - 2L \varepsilon^T P \Gamma a \varepsilon_1 \\ &\quad + 2\varepsilon^T P F^* + L \rho_1 \mu \lambda_{\min}(P) \|\varepsilon\|^2 \\ &\quad - \rho_2 \mu \lambda_{\min}(P) (1 + |y|^p)^2 \|\varepsilon\|^2. \end{aligned} \quad (31)$$

Using (11), (12), (29), and Lemma 3, we obtain

$$\begin{aligned} 2LL^* \varepsilon^T P a \varepsilon_1 &\leq \frac{\sigma_1 LL^*}{4} \|\varepsilon\|^2 + \frac{4(L^*)^{1-2\mu} \|Pa\|^2}{\sigma_1} \dot{L}, \\ -2L \varepsilon^T P \Gamma a \varepsilon_1 &\leq \frac{\sigma_1 LL^*}{4} \|\varepsilon\|^2 + \frac{4\|P \Gamma a\|^2}{\sigma_1 (L^*)^{1+2\mu}} \dot{L}. \end{aligned} \quad (32)$$

Similar to the proof of (18) with  $L^* \geq 1$ , one gets

$$\begin{aligned} 2\varepsilon^T P F^* &\leq (1 + |y|^p)^2 \left( \frac{1}{m} \|\varepsilon\|^2 + \|z\|^2 \right) + d_1 \|\varepsilon\|^2 \\ &\quad + g_1 \|\omega\|^2 + \sum_{i=1}^n \frac{1-\kappa}{n} (1 + |y(t - \tau_i(t))|^p)^2 \\ &\quad \cdot \left( \frac{1}{m} \|\varepsilon(t - \tau_i(t))\|^2 + \|z(t - \tau_i(t))\|^2 \right), \end{aligned} \quad (33)$$

where  $d_1 = n^3 \theta^2 \|P\|^2 (2m + 1 + (m + 1)/(1 - \kappa))$ ,  $g_1 = 2mn^2 \theta^2 \|P\|^2$  are unknown positive constants related to  $\theta$  and  $\kappa$ .

Choose the Lyapunov-Krasovskii functional

$$\begin{aligned} V^* &= V_\varepsilon + V_z + \sum_{i=1}^n \int_{t-\tau_i(t)}^t \frac{1}{n} (1 + |y(s)|^p)^2 \\ &\quad \cdot \left( \frac{1}{m} \|\varepsilon(s)\|^2 + \|z(s)\|^2 \right) ds. \end{aligned} \quad (34)$$

By (20), (26), (31)-(34), the definition of  $L^*$ , and the fact that  $L(t) \geq 1$ , we derive

$$\begin{aligned} \dot{V}^* &\leq -\frac{\sigma_1}{2} LL^* \|\varepsilon\|^2 + L \rho_1 \mu \lambda_{\min}(P) \|\varepsilon\|^2 \\ &\quad - \rho_2 \mu \lambda_{\min}(P) (1 + |y|^p)^2 \|\varepsilon\|^2 \\ &\quad + \frac{2}{m} (1 + |y|^p)^2 \|\varepsilon\|^2 + \eta \dot{L} + 2(1 + |y|^p)^2 \|z\|^2 \\ &\quad + d_1 \|\varepsilon\|^2 + g_1 \|\omega\|^2 \\ &\quad - \rho_2 \mu \lambda_{\min}(Q) (1 + |y|^p)^2 \|z\|^2 + \frac{\sigma_1}{2m} L \|\varepsilon\|^2 \\ &\quad - \frac{\sigma_1}{2m} L \|\varepsilon\|^2 \\ &\leq -\frac{\sigma_1}{2} L \left( L^* - \frac{1}{m} - \frac{2d_1}{\sigma_1} \right) \|\varepsilon\|^2 + \eta \dot{L} + g_1 \|\omega\|^2 \\ &\leq -\frac{\sigma_1}{2} \|\varepsilon\|^2 + \eta \dot{L} + g_1 \|\omega\|^2, \end{aligned} \quad (35)$$

where  $\eta = \|Qa^*\|^2/\sigma_1 + 4(L^*)^{1-2\mu}\|Pa\|^2/\sigma_1 + 4\|P\Gamma a\|^2/\sigma_1(L^*)^{1+2\mu}$  is a positive constant. Similar to the proof of (27), integrating both sides of (35) yields, on  $[0, t_f]$ ,

$$\begin{aligned} \lambda_{\min}(P) \|\epsilon(t)\|^2 &\leq V^*(t) \\ &\leq V^*(0) - \frac{\sigma_1}{2} \int_0^t \|\epsilon(s)\|^2 ds \\ &\quad + \eta(\bar{L} - 1) + g_1 \int_0^t \|\omega(s)\|^2 ds, \end{aligned} \quad (36)$$

from which it follows that,  $\forall t \in [0, t_f]$ ,

$$\begin{aligned} \|\epsilon(t)\|^2 &\leq \frac{1}{\lambda_{\min}(P)} \left( V^*(0) + \eta\bar{L} + g_1 \int_0^t \|\omega(s)\|^2 ds \right), \\ &\int_0^t \|\epsilon(s)\|^2 ds \\ &\leq \frac{2}{\sigma_1} \left( V^*(0) + \eta\bar{L} + g_1 \int_0^t \|\omega(s)\|^2 ds \right), \end{aligned} \quad (37)$$

which together with  $\omega(t) \in L_2[0, +\infty)$  implies that  $\epsilon(t)$  and  $\int_0^t \|\epsilon(s)\|^2 ds$  are bounded on  $[0, t_f]$ . From (29) with the fact that  $L^*$  is a constant, we obtain  $\epsilon(t)$  and  $\int_0^t \|\epsilon(s)\|^2 ds$  are bounded on  $[0, t_f]$ .

*Step II* (we prove that the closed-loop system consisting of (1), (9), and (10) achieves global disturbance attenuation in the  $L_2$ -gain sense). From (12), it is easy to get

$$\begin{aligned} x_i &= L^{i-1+\mu} (\epsilon_i + z_i), \quad i = 1, \dots, n, \\ \hat{x}_i &= L^{i-1+\mu} z_i, \quad i = 1, \dots, n, \\ \hat{x}_{n+1} &= \nu - L^{n+\mu} \epsilon_{n+1}. \end{aligned} \quad (38)$$

When  $\omega(t) \in L_2[0, +\infty)$ , by the boundedness of  $L(t)$ ,  $z(t)$ ,  $\epsilon(t)$  on  $[0, t_f]$  and the fact that  $\nu$  is a constant, it can be derived from (38) that  $x(t)$ ,  $\hat{x}(t)$ , and  $\hat{x}_{n+1}(t)$  are bounded on  $[0, t_f]$ . By (9), it follows that  $u(t)$  is also bounded on  $[0, t_f]$ .

Then, we prove that  $t_f = +\infty$ . The conclusion follows again by a contradiction argument. Suppose  $t_f < +\infty$ , then  $t_f$  would be the finite-escape time of the closed-loop system, which means that at least one component of  $x(t)$ ,  $\hat{x}(t)$ ,  $\hat{x}_{n+1}(t)$ , and  $L(t)$  would tend to infinity at  $t = t_f$ . However,  $x(t)$ ,  $\hat{x}(t)$ ,  $\hat{x}_{n+1}(t)$ , and  $L(t)$  are bounded on the maximal interval  $[0, t_f]$  and hence also bounded at  $t = t_f$  due to the continuity of the solution; this is a contradiction.

$t_f = +\infty$  means that  $L(t)$ ,  $z(t)$ ,  $\epsilon(t)$ ,  $\int_0^t \|z(s)\|^2 ds$ ,  $\int_0^t \|\epsilon(s)\|^2 ds$  are bounded on  $[0, +\infty)$ , which indicates that  $x(t)$ ,  $\hat{x}(t)$ ,  $\hat{x}_{n+1}(t)$ , and  $u(t)$  are bounded on  $[0, +\infty)$ , and  $\int_0^{+\infty} \|z(s)\|^2 ds < +\infty$ ,  $\int_0^{+\infty} \|\epsilon(s)\|^2 ds < +\infty$ . Meanwhile, from (38) with  $y = x_1$ , we obtain  $\int_0^{+\infty} y^2(s) ds < +\infty$ .

Using (21), for any pregiven small real number  $\pi > 0$ ,

$$\dot{V} + \frac{g_0}{\pi^2} y^2 \leq d_0 \|\epsilon\|^2 + g_0 \|\omega\|^2 + \frac{g_0}{\pi^2} y^2. \quad (39)$$

Integrating both sides of (39) leads to,  $\forall t \geq 0$ ,

$$\begin{aligned} \int_0^t y^2(s) ds &\leq \pi^2 \int_0^t \|\omega(s)\|^2 ds + \frac{\pi^2}{g_0} V(0) \\ &\quad + \frac{\pi^2 d_0}{g_0} \int_0^t \|\epsilon(s)\|^2 ds + \int_0^t y^2(s) ds; \end{aligned} \quad (40)$$

choose  $\rho(\cdot) = (\pi^2/g_0)V(0) + (\pi^2 d_0/g_0) \int_0^t \|\epsilon(s)\|^2 ds + \int_0^t y^2(s) ds$ . Obviously,  $\rho(\cdot)$  is a nonnegative bounded function. Then the global disturbance attenuation of the closed-loop system is achieved in the  $L_2$ -gain sense.

Moreover, if  $\omega(t) = 0$  or  $\omega(t) \in L_2[0, +\infty) \cap L_\infty[0, +\infty)$ , by the boundedness of all signals on  $[0, +\infty)$ , from (13), it is obvious that  $\dot{\epsilon}(t)$  and  $\dot{z}(t)$  are also bounded on  $[0, +\infty)$ . Then, by Lemma 5, we conclude that  $\lim_{t \rightarrow +\infty} (\epsilon(t), z(t)) = (0, 0)$ . Therefore, from (9) and (38) with the boundedness of  $L(t)$ , we deduce  $\lim_{t \rightarrow +\infty} (x(t), \hat{x}(t), \hat{x}_{n+1}(t), u(t)) = (0, 0, \nu, -\nu)$ .  $\square$

## 4. Simulation Example

Consider a simple system

$$\begin{aligned} \dot{x}_1 &= x_2 + c_1 x_1^3 (t - \tau_1(t)) + c_2 \ln(1 + x_1^2) \omega, \\ \dot{x}_2 &= u + \nu + c_3 x_1^2 x_2 \\ &\quad + c_4 \ln(1 + x_1^2 (t - \tau_2(t))) x_2 (t - \tau_2(t)) \\ &\quad + c_5 \omega, \\ y &= x_1, \end{aligned} \quad (41)$$

where  $\nu$  is an unknown constant representing the input matching uncertainty, and let  $x_3 = \nu$ .  $c_i, i = 1, \dots, 5$ , are unknown constants, and  $\tau_1(t) = 1 + l_1 \sin(t)$  and  $\tau_2(t) = (1/2)l_2 \cos^2(t)$  represent unknown time-varying delays with  $|l_1| < 1$ ,  $0 < l_2 < 1$  being unknown constants. The system disturbance is  $\omega(t) = 1/(1+t)$ ; obviously,  $\omega(t) \in L_2[0, +\infty)$ . Since  $\ln(1 + x_1^2) \leq 1 + x_1^2$ , Assumption 1 holds with  $\theta = \max\{c_i, i = 1, \dots, 5\}$ ,  $p = 2$ .

From Lemma 2, we choose  $\mu = 0.2 < 1/4$ ,  $a = [3, 3, 1]^T$ ,  $k = [3, 3]^T$ ,  $\sigma_1 = 18$ . Then, by (20), select  $\rho_1 = 0.9$  and  $\rho_2 = 12.8$ . According to Section 3, we get the output feedback controller

$$\begin{aligned} \dot{\hat{x}}_1 &= \hat{x}_2 + 3L(x_1 - \hat{x}_1), \\ \dot{\hat{x}}_2 &= \hat{x}_3 + u + 3L^2(x_1 - \hat{x}_1), \\ \dot{\hat{x}}_3 &= L^3(x_1 - \hat{x}_1), \\ u &= -3L^2 \hat{x}_1 - 3L \hat{x}_2 - \hat{x}_3, \\ \dot{L} &= \max \left\{ -0.9L^2 \right. \\ &\quad \left. + 12.8L(1 + |y|^2)^2, L^{0.6}(x_1 - \hat{x}_1)^2 \right\}, \quad L(0) = 1. \end{aligned} \quad (42)$$

In the simulation, we choose  $c_i = 1, i = 1, \dots, 5$ ,  $\nu = -8$ ,  $l_1 = l_2 = 0.5$  and the initial values  $[x_1(t_0), x_2(t_0)] = [0.5, 0.8]$

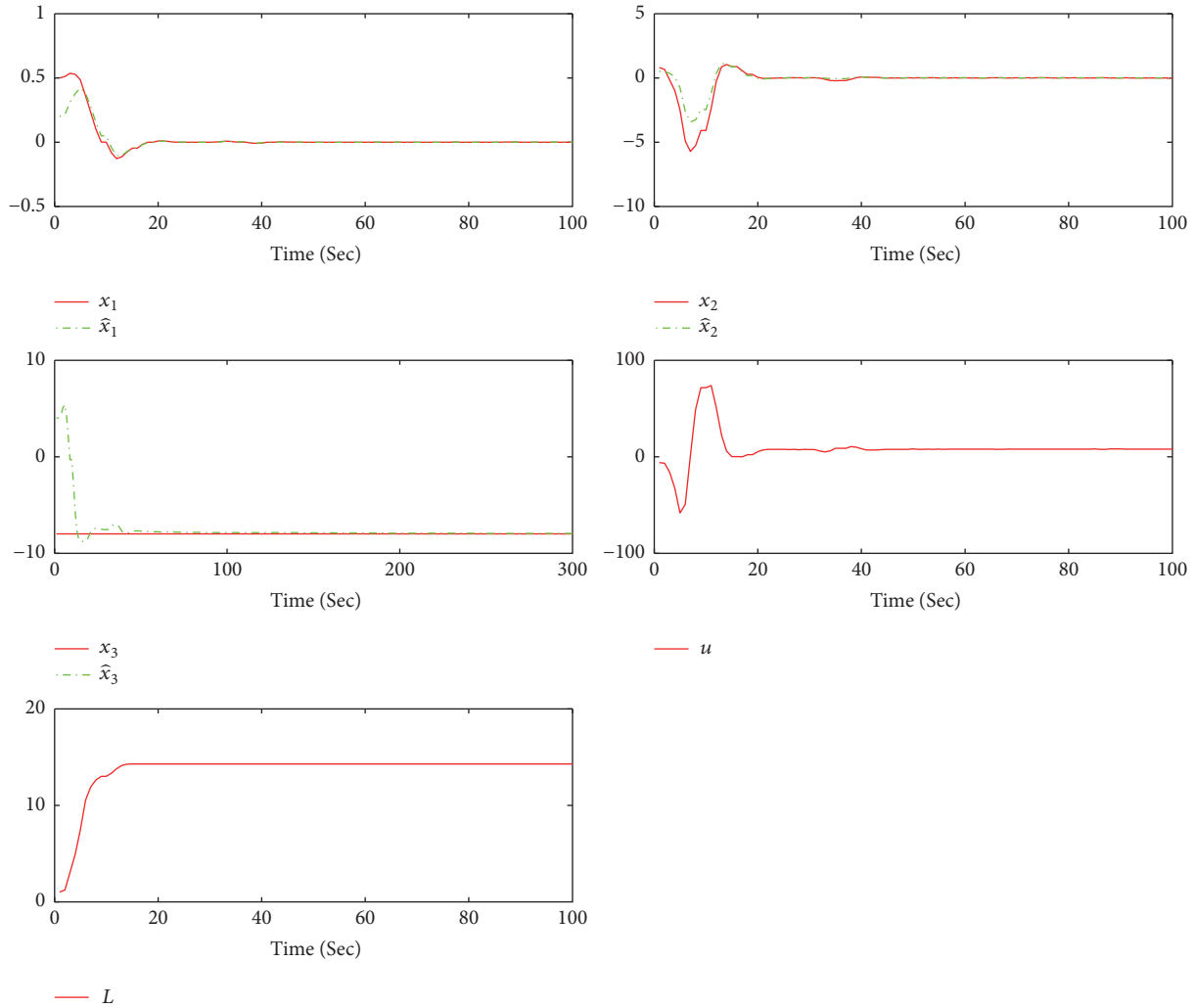


FIGURE 1: The responses of the closed-loop system (41)-(42).

for  $t_0 \in [-1.5, 0]$ ,  $[\hat{x}_1(0), \hat{x}_2(0), \hat{x}_3(0)] = [0.2, 0.5, 4]$ . Figure 1 demonstrates the effectiveness of the control scheme.

### 5. Conclusions

By skillfully combining extended state observer, dynamic gain technique, and Lyapunov-Krasovskii theorem, the problem of output feedback disturbance attenuation for nonlinear systems with input matching uncertainty and unknown multiple time-varying delays is solved in this paper based on only one dynamic gain.

Some interesting problems still remained; e.g., (i) for system (1) with the unknown output function [20–24], can we design an output feedback controller? (ii) Another work is to consider more general input matching uncertainty such as an uncertain harmonic signal.

### Data Availability

The data supporting the conclusions of this manuscript are some open access articles that have been properly cited, and the readers can easily obtain these articles to verify the

conclusions, replicate the analysis, and conduct secondary analyses. Therefore, we do not create a publicly available data repository.

### Conflicts of Interest

The authors declare that they have no conflicts of interest.

### Acknowledgments

This work was supported by the Taishan Scholar Project of Shandong Province of China (no. ts201712040), National Natural Science Foundation of China (no. 61673242), and Shandong Provincial Natural Science Foundation of China (no. ZR2016FM10).

### References

[1] W. Lin, C.-J. Qian, and X.-Q. Huang, “Disturbance attenuation of a class of non-linear systems via output feedback,” *International Journal of Robust and Nonlinear Control*, vol. 13, no. 15, pp. 1359–1369, 2003.

- [2] H. Ito and Z.-P. Jiang, "Robust disturbance attenuation of nonlinear systems using output feedback and state-dependent scaling," *Automatica*, vol. 40, no. 9, pp. 1621–1628, 2004.
- [3] Y.-J. Pan, H.-J. Marquez, and T. Chen, "A new output feedback stabilization controller for the disturbance attenuation of MIMO non-linear systems," *International Journal of Control*, vol. 80, no. 9, pp. 1481–1490, 2007.
- [4] F. Shang, Y. G. Liu, G. Q. Zhang, and C. H. Zhang, "Adaptive disturbance attenuation by output feedback for a class of nonlinear systems," *Acta Automatica Sinica*, vol. 37, no. 12, pp. 1530–1536, 2011.
- [5] F. Shang and Y.-G. Liu, "Adaptive disturbance attenuation via output feedback for nonlinear systems with polynomial-of-output growth rate," *International Journal of Control*, vol. 87, no. 3, pp. 600–611, 2014.
- [6] H. Lei and W. Lin, "Universal adaptive control of nonlinear systems with unknown growth rate by output feedback," *Automatica*, vol. 42, no. 10, pp. 1783–1789, 2006.
- [7] H. Lei and W. Lin, "Adaptive regulation of uncertain nonlinear systems by output feedback: a universal control approach," *Systems and Control Letters*, vol. 56, no. 7-8, pp. 529–537, 2007.
- [8] J.-Y. Zhai and W.-T. Zha, "Global adaptive output feedback control for a class of nonlinear time-delay systems," *ISA Transactions*, vol. 53, no. 1, pp. 2–9, 2014.
- [9] A. Benabdallah, H. Ayadi, and M. Mabrouk, "Global adaptive output stabilization of uncertain nonlinear systems with polynomial output depending growth rate," *International Journal of Adaptive Control and Signal Processing*, vol. 28, no. 7-8, pp. 604–619, 2014.
- [10] X. Zhang and Y. Lin, "Global adaptive output feedback control for a class of uncertain nonlinear time-delay systems," in *Proceedings of the 33rd Chinese Control Conference, CCC 2014*, pp. 2255–2260, China, July 2014.
- [11] X.-L. Jia, X.-K. Chen, S.-Y. Xu, B.-Y. Zhang, and Z.-Q. Zhang, "Adaptive output feedback control of nonlinear time-delay systems with application to chemical reactor systems," *IEEE Transactions on Industrial Electronics*, vol. 64, no. 6, pp. 4792–4799, 2017.
- [12] L. Praly and Z.-P. Jiang, "Linear output feedback with dynamic high gain for nonlinear systems," *Systems and Control Letters*, vol. 53, no. 2, pp. 107–116, 2004.
- [13] Z.-T. Ding, "Asymptotic rejection of unmatched general periodic disturbances with nonlinear Lipschitz internal models," *International Journal of Control*, vol. 86, no. 2, pp. 210–221, 2013.
- [14] Y.-X. Huang and Y.-G. Liu, "Adaptive output-feedback control of nonlinear systems with multiple uncertainties," *Asian Journal of Control*, vol. 20, no. 3, pp. 1151–1160, 2018.
- [15] Y.-C. Man and Y.-G. Liu, "Global output-feedback stabilization for a class of uncertain time-varying nonlinear systems," *Systems and Control Letters*, vol. 90, pp. 20–30, 2016.
- [16] Y.-X. Huang and Y.-G. Liu, "A compact design scheme of adaptive output-feedback control for uncertain nonlinear systems," *International Journal of Control*, pp. 1–9, 2017.
- [17] W.-Q. Li, L. Liu, and G. Feng, "Output tracking of stochastic nonlinear systems with unstable linearization," *International Journal of Robust and Nonlinear Control*, vol. 28, no. 2, pp. 466–477, 2018.
- [18] C.-J. Qian and W. Lin, "A continuous feedback approach to global strong stabilization of nonlinear systems," *Institute of Electrical and Electronics Engineers Transactions on Automatic Control*, vol. 46, no. 7, pp. 1061–1079, 2001.
- [19] H.-K. Khalil, *Nonlinear Systems*, Prentice-Hall, New Jersey, NJ, USA, 2002.
- [20] Z.-J. Li, X.-J. Xie, and K.-M. Zhang, "Output feedback stabilisation for nonlinear systems with unknown output function and control coefficients and its application," *International Journal of Control*, vol. 90, no. 5, pp. 1027–1036, 2017.
- [21] M.-M. Jiang, K.-M. Zhang, and X.-J. Xie, "Output feedback stabilisation of stochastic nonlinear time-delay systems with unknown output function," *International Journal of Systems Science*, vol. 48, no. 11, pp. 2262–2271, 2017.
- [22] M.-M. Jiang, P. Wang, and X.-J. Xie, "Global output feedback stabilisation of nonlinear time-delay systems with unknown output function," *International Journal of Systems Science*, vol. 48, no. 12, pp. 2554–2564, 2017.
- [23] X.-J. Xie, Z.-J. Li, and K.-M. Zhang, "Semi-global output feedback control for nonlinear systems with uncertain time-delay and output function," *International Journal of Robust and Nonlinear Control*, vol. 27, no. 15, pp. 2549–2566, 2017.
- [24] X.-J. Xie and M.-M. Jiang, "Output feedback stabilization of stochastic feedforward nonlinear time-delay systems with unknown output function," *International Journal of Robust and Nonlinear Control*, vol. 28, no. 1, pp. 266–280, 2018.

## Research Article

# The Dynamic Properties of a Nonlinear Economic Model with Extreme Financial Frictions

Huan Wang  and WenYi Huang 

*The School of Economic Mathematics, Southwestern University of Finance and Economics, WenJiang, Chengdu 611130, China*

Correspondence should be addressed to Huan Wang; [harrywang1213@gmail.com](mailto:harrywang1213@gmail.com)

Received 28 April 2018; Accepted 7 June 2018; Published 5 July 2018

Academic Editor: Xue-Jun Xie

Copyright © 2018 Huan Wang and WenYi Huang. This is an open access article distributed under the Creative Commons Attribution License, which permits unrestricted use, distribution, and reproduction in any medium, provided the original work is properly cited.

A generalized economic model with two kinds of agents (farmers and landlords) is investigated. Farmers produce grains by renting lands from landlords. The land which is not rented is cultivated by less productive landlords. The economy is assumed to be with extreme frictions so that there are no markets for agents to trade grains. The rental rate is determined by the equilibrium of the supply and demand. We consider the situation that farmers are likely to take more risk when the rental rate is low and have more risk aversion if the rate goes high. The psychological anticipation is taken into account in the setting of our model. Using the optimal control theory, the dynamic properties of the rental rate and its influence to the endogenous volatility are analyzed. Besides, we clarify that the rental market has an instinctive ability to dominate the anticipation of agents.

## 1. Introduction

Since the Great Depression in 1933, many famous economists, such as Fisher and Keynes, have devoted themselves to the research of the failure of financial markets. Kindleberger [1] clarifies that financial crises are common in history. It seems that the financial frictions for business cycles play an important role in the crisis. Therefore, the desire to give more insight into the financial instability prompts scholars to set up new generalized continuous time equilibrium models. Earlier, Bernanke and Gertler [2] together with Kiyotaki and Moore [3] elaborate several important ways of how financial frictions influence the macroeconomy. One of their main conclusions is that small temporary shocks can have a great impact on the economy.

After the works of [3], He and Krishnamurthy [4, 5] build a kind of typical equilibrium models which allow us to give a research in the full-scale macroeconomic dynamics. Meanwhile, Brunnermeier and Sannikov [6] study the macroeconomic models and get further conclusions. Specifically, Brunnermeier and Sannikov show that the behaviour of the economy with aggregate shocks and financial frictions can be trapped in a less productive level for a long time. In Brunnermeier and Sannikov's model, the endogenous stochastic risks

are set to discuss the behaviour of the economy. The feedback control techniques of stochastic nonlinear systems are found in [7–9].

Although Brunnermeier and Sannikov's work inspires us to study the behaviour of the macroeconomy in a new different way, there are also some drawbacks. Brunnermeier and Sannikov's model can only be solved in a numerical way and some of their predictions go somewhat against empirical evidence. To make up for these drawbacks, Klimenko et al. [10] have developed a dynamic macroeconomic model in a simple setting to analyze the significance of the endogenous risk. With the setting, they get dynamic equations and work out a quasi-closed form solution. They explicitly track down the roots of some important features like poverty trap, which is explained as the paradox of volatility and persistence of exogenous shocks. The implication of endogenous risk for welfare analysis is illustrated [10], while, in [10], they suppose an easy case in which the rental rate has a linear effect on its process. The assumption does not seem to be very practical. As will be illustrated carefully, we take the psychological anticipations of farmers into account and consider a nonlinear effect case.

Following the works in [10], we adopt two kinds of agents: risk-neutral landlords and risk-averse farmers. Landlords,

which are less productive, own the land. Farmers cultivate grains by renting lands from landlords. In the economy, the financial friction is so high that there is no market for the agents to trade. Farmers have to keep the rest of the grains as their precautionary savings. To get rid of defaulting from their rent contracts, farmers have to adapt their scale of activity (the area of lands renting from landlords) to the level of the rental rate. The equilibrium of demand and supply in the rental market determines the process of the rental rate.

One of the remarkable settings in [10] is that the authors suppose there exists a rental market in which the rental rate follows a Markov stationary process, which takes the form similar to Geometric Brownian Motion (GBM). With the equilibrium conditions, Klimenko et al. [10] obtain the closed form solutions and consequently keep on with further analysis. The reason why they choose the form like GBM is that the rental rate is larger than 0 in the real world. Inspired by the works in [10], we take psychological anticipation of farmers into account. If the rental rate is low, farmers would choose to take more risk. On the contrary, farmers would be more risk averse if the rental rate is high. For this sake, the rental rate has an effect on the rental market and then influences its own process. The volatility fluctuates by the rental rate. We consider a rental rate process which differs from that in Klimenko et al. [10]. The closed form solution of the model is obtained. We show that the rental rate market has the ability to adapt itself even if we do not consider the psychological anticipation talked about above.

The rest of the paper is organized as follows. Section 2 gives a brief description of the model. Section 3 describes the equilibrium. Section 4 gives the ways to solve the equilibrium. Section 5 discusses its main properties. Section 6 studies the long-run average behaviour and analyzes the welfare loss problem. The conclusions are given in Section 7.

## 2. Theoretical Framework

**2.1. Basic Statement of the Economy.** In this section, we give the basic setting of the economy which is similar to that in [10]. There are only two types of agents in the economy: farmers and landlords. The landlords own the land, while the farmers can only rent it from the landlords. The rental rate  $q_t$  is endogenously determined in the equilibrium. For convenience, the area of land in the economy is fixed and normalized to 1. We assume that farmers are risk averse and landlords are risk-neutral. Both of the agents have the same discount rate  $\rho$ .

In the economy, the land which is cultivated by farmers yields more crop than that of landlords. More precisely, the flow of output yielding from one unit of land that is cultivated by a representative farmer is described by

$$dy_t = adt + \sigma_0 dB_t, \quad (1)$$

where  $a$  is the average growth rate of farmers and  $\sigma_0$  stands for the aggregate shocks (like climate conditions) exposed in the economy.  $B_t$  is a standard Brownian Motion defined on the probability space  $(\Omega, \mathbb{F}, \mathbb{P})$  with the filtration  $\mathbb{F} = \{\mathcal{F}_t, t \geq 0\}$ .

It is hard to find a representative landlord. For this, we introduce a random variable  $\bar{\alpha}$  which is continuously

distributed over  $[0, a]$ . One unit of land cultivated by an  $\bar{\alpha}$  type of landlord yields the flow of output

$$d\bar{y}_t = \bar{\alpha}dt + \sigma_0 dB_t. \quad (2)$$

In the economy, we assume there exists an extreme financial friction, which means that it is impossible for farmers and landlords to engage in any financial activities. The income of farmers comes from their producing activities and they have no other assets or resources. For some landlords, their productivity is so low that they might be likely to rent the land to farmers and gain rental rate  $q_t$  from the farmers. For other landlords, they will cultivate by themselves. For farmers, they rent lands from landlords with rental rate if it is not so high. Because of the aggregate volatility, the productivity of the two agents varies. Hence, the equilibrium rental rent is fluctuated. In this paper, our goal is to find a Markov stationary equilibrium, where the rental rate  $q_t$  satisfies the following Markov stochastic process:

$$\frac{dq_t}{q_t} = \mu(q_t)dt + \sigma(q_t)q_t^{\beta-1}dB_t, \quad 1 \leq \beta < 2, \quad (3)$$

where the drift  $\mu(q_t)$  and diffusion  $\sigma(q_t)$  are determined by the equilibrium conditions. The parameter  $\beta$  is a constant which takes values between 1 and 2.

As can be seen, the process in (3) is reduced to Klimenko et al. [10] if the parameter  $\beta = 1$ . In Klimenko et al.'s model, the rental rate  $q_t$  has a linear influence on the volatility  $\sigma(q)$ . Here we suppose that the rental rate process takes a form of the CEV model. The volatility is magnified when the rate is low. On the contrary, the volatility is reduced if the rate goes high. As will be clarified, the economy seems to have the instinctive ability to adapt itself whether we take the psychological anticipations into consideration or not.

### 2.2. Decisions of Agents

**Farmers.** At time  $t$ , each farmer chooses his scale of production  $k_t$  and decides how much crop should be consumed, which is denoted by  $c_t$ . Hence, the saving of a representative farmer at time  $t$ , which is denoted by  $s_t$ , is driven by

$$ds_t = k_t(dy_t - q_t dt) - c_t dt. \quad (4)$$

In fact, both  $k_t$  and  $c_t$  depend on the scale of production and the rental rate.

All farmers in the economy are homogeneous and their utility function is logarithmic. Each farmer chooses his optimal consumption  $c_t$  and scale of production  $k_t$  to maximize his all-life expected discounted value of consumption

$$V(s, q) = \max_{c_t, k_t \geq 0} E \left[ \int_0^{+\infty} e^{-\rho t} \ln(c_t) dt \mid s_0 = s, q_0 = q \right], \quad (5)$$

where  $s$  is the farmer's initial stock of saving and  $q$  is the initial rental rate.

**Landlords.** At each time  $t$ , every landlord decides whether to rent out his land or not according to the rental rate. If the

rental rate is more than his own productivity, i.e.,  $q_t \geq \hat{\alpha}$ , he will rent the land out; otherwise he will cultivate by himself.

We assume that all landlords in the economy have infinite elasticity of intertemporal substitution. Each landlord will decide whether to rent the land out or not and consume all his savings immediately at each time  $t$ . Once given a rental rate  $q_t$ , the whole fraction of land leased by landlords is a continuous and increasing function of the rental rate, which is denoted by  $K_S(q_t)$ .

### 3. Equilibrium

In this section, we are supposed to find a way to solve the optimal control problem. Our basic idea is to find the solution of the HJB equation by dynamic programming principle.

**Lemma 1.** *If  $V(s_t, q_t)$  is the maximum expected discounted value of consumption on  $(t, +\infty)$ , then the following equation*

$$V(s, q) = \max_{c_t, k_t \geq 0} E \left[ \int_0^h e^{-\rho t} \ln(c_t) dt + e^{-\rho h} V(s_h, q_h) \mid s_0 = s, q_0 = q \right] \quad (6)$$

holds.

*Proof.* On the temporal interval of  $(0, h)$ , we choose a control process of  $c_t$  and  $k_t$  evolves from  $(0, c_0, k_0)$  to  $(h, c_h, k_h)$ .

(i) For any  $h > 0$ , applying the tower property straightforward, we have

$$\begin{aligned} & E \left[ \int_0^{+\infty} e^{-\rho t} \ln(c_t) dt \mid \mathcal{F}_0 \right] \\ &= E \left\{ E \left[ \int_0^{+\infty} e^{-\rho t} \ln(c_t) dt \mid \mathcal{F}_h \right] \mid \mathcal{F}_0 \right\} \\ &= E \left\{ E \left[ \int_0^h e^{-\rho t} \ln(c_t) dt + e^{-\rho h} \int_h^{+\infty} e^{-\rho(t-h)} \ln(c_t) dt \mid \mathcal{F}_h \right] \mid \mathcal{F}_0 \right\} \\ &= E \left\{ \int_0^h e^{-\rho t} \ln(c_t) dt + e^{-\rho h} E \left[ \int_h^{+\infty} e^{-\rho(t-h)} \ln(c_t) dt \mid \mathcal{F}_h \right] \mid \mathcal{F}_0 \right\} \\ &\leq E \left\{ \int_0^h e^{-\rho t} \ln(c_t) dt + e^{-\rho h} V(s_h, q_h) \mid \mathcal{F}_0 \right\}. \end{aligned} \quad (7)$$

Taking maximum on both sides, we get

$$V(s, q) \leq \max_{c_t, k_t \geq 0} E \left[ \int_0^h e^{-\rho t} \ln(c_t) dt + e^{-\rho h} V(s_h, q_h) \mid \mathcal{F}_0 \right]. \quad (8)$$

(ii) For any  $\varepsilon > 0$ , we can find  $c_t^\varepsilon, k_t^\varepsilon$  such that

$$V(s, q) - \varepsilon \leq E \left[ \int_0^h e^{-\rho t} \ln(c_t^\varepsilon) dt \mid \mathcal{F}_0 \right]. \quad (9)$$

Denoting

$$\hat{c}_t = \begin{cases} c_t, & 0 < t \leq h \\ c_t^\varepsilon, & t > h, \end{cases} \quad (10)$$

$$\hat{k}_t = \begin{cases} k_t, & 0 < t \leq h \\ k_t^\varepsilon, & t > h, \end{cases}$$

we have

$$\begin{aligned} V(s, q) &\geq E \left[ \int_0^{+\infty} e^{-\rho t} \ln(\hat{c}_t) dt \mid \mathcal{F}_0 \right] \\ &= E \left\{ E \left[ \int_0^{+\infty} e^{-\rho t} \ln(\hat{c}_t) dt \mid \mathcal{F}_h \right] \mid \mathcal{F}_0 \right\} \\ &= E \left\{ E \left[ \int_0^h e^{-\rho t} \ln(c_t) dt + e^{-\rho h} \int_h^{+\infty} e^{-\rho(t-h)} \ln(c_t^\varepsilon) dt \mid \mathcal{F}_h \right] \mid \mathcal{F}_0 \right\} \\ &= E \left\{ \int_0^h e^{-\rho t} \ln(c_t) dt + e^{-\rho h} E \left[ \int_h^{+\infty} e^{-\rho(t-h)} \ln(c_t^\varepsilon) dt \mid \mathcal{F}_h \right] \mid \mathcal{F}_0 \right\} \\ &\geq E \left[ \int_0^h e^{-\rho t} \ln(c_t) dt + e^{-\rho h} (V(s_h, q_h) - \varepsilon) \mid \mathcal{F}_0 \right] \\ &= E \left[ \int_0^h e^{-\rho t} \ln(c_t) dt + e^{-\rho h} (V(s_h, q_h)) \mid \mathcal{F}_0 \right] - \varepsilon. \end{aligned} \quad (11)$$

Letting  $\varepsilon \rightarrow 0$  and taking maximum, we obtain

$$V(s, q) \geq \max_{c_t, k_t} E \left[ \int_0^h e^{-\rho t} \ln(c_t) dt + e^{-\rho h} (V(s_h, q_h)) \mid \mathcal{F}_0 \right]. \quad (12)$$

Therefore, we get

$$V(s, q) = \max_{c_t, k_t} E \left[ \int_0^h e^{-\rho t} \ln(c_t) dt + e^{-\rho h} (V(s_h, q_h)) \mid \mathcal{F}_0 \right]. \quad (13)$$

□

**Theorem 2.** Assume  $V(s, q) \in \mathcal{C}^{1,2}$ , and then the value function  $V(s, q)$  of a representative farmer satisfies the following Hamilton-Jacobi-Bellman (HJB) equation

$$\begin{aligned} \rho V = \max_{c, k \geq 0} & \left( \ln c + [k(a - q) - c] V_s + q\mu(q) V_q \right. \\ & \left. + \frac{1}{2} \sigma_0^2 k^2 V_{ss} + \frac{1}{2} q^{2\beta} \sigma(q)^2 V_{qq} + \sigma_0 k q^\beta \sigma(q) V_{sq} \right). \end{aligned} \quad (14)$$

*Proof.* Applying Itô's formula, we have

$$\begin{aligned} d(e^{-\rho t} V(s_t, q_t)) &= e^{-\rho t} \cdot (-\rho) \cdot V(s_t, q_t) dt \\ &+ e^{-\rho t} dV(s_t, q_t) = e^{-\rho t} \left( -\rho V dt + \frac{\partial V}{\partial s} ds_t \right. \\ &+ \frac{1}{2} \frac{\partial^2 V}{\partial s^2} d\langle s \rangle_t + \frac{\partial V}{\partial q} dq_t + \frac{1}{2} \frac{\partial^2 V}{\partial q^2} d\langle q \rangle_t \\ &+ \frac{\partial^2 V}{\partial s \partial q} d\langle s, q \rangle_t \left. \right) = e^{-\rho t} \cdot \left( -\rho V dt \right. \\ &+ V_s (k_t (adt + \sigma_0 dB_t - q_t dt) - c_t dt) \\ &+ \frac{1}{2} V_{ss} k_t^2 \sigma_0^2 dt + V_q (\mu(q_t) q_t dt + \sigma(q_t) q_t^\beta dB_t) \\ &+ \frac{1}{2} V_{qq} \sigma^2(q_t) q_t^{2\beta} dt + V_{sq} k_t \sigma_0 q_t^\beta dt \left. \right) = e^{-\rho t} (A dt \\ &+ B dB_t), \end{aligned} \quad (15)$$

where  $B = \sigma_0 k_t V_s + q_t^\beta \sigma(q_t) V_q$  and

$$\begin{aligned} A &= -\rho V + [k_t (a - q_t) - c_t] V_s \\ &+ q_t \mu(q_t) V_q + \frac{1}{2} k_t^2 \sigma_0^2 V_{ss} \\ &+ \frac{1}{2} q_t^{2\beta} \sigma^2(q_t) V_{qq} \\ &+ \sigma_0 k_t q_t^\beta \sigma(q_t) V_{sq}, \end{aligned} \quad (16)$$

$$\begin{aligned} e^{-\rho h} V(s_h, q_h) &= V(s, q) + \int_0^h d(e^{-\rho t} V(s_t, q_t)) \\ &= V(s, q) + \int_0^h e^{-\rho t} (A dt + B dB_t). \end{aligned} \quad (17)$$

Substituting (17) into (6), we obtain

$$\begin{aligned} V(s, q) &= \max_{c, k_i \geq 0} E \left[ \int_0^h e^{-\rho t} \ln(c_t) dt + V(s, q) \right. \\ &+ \left. \int_0^h e^{-\rho t} (A dt + B dB_t) \mid \mathcal{F}_0 \right]. \end{aligned} \quad (18)$$

Namely,

$$0 = \max_{c, k_i \geq 0} E \left[ \int_0^h e^{-\rho t} (\ln(c_t) + A) dt \mid \mathcal{F}_0 \right]. \quad (19)$$

Noticing that  $(c_t, k_t)$  is procession on  $[0, h]$ , as  $h \rightarrow 0$ ,  $c_t = c$ , and  $k_t = k$  (number, not process), dividing by  $h > 0$ , setting  $h \rightarrow 0$ , and using the mean value theorem, we have

$$\begin{aligned} \rho V &= \max_{c, k \geq 0} \left( \ln c + [k(a - q) - c] V_s + q\mu(q) V_q \right. \\ &+ \left. \frac{1}{2} \sigma_0^2 k^2 V_{ss} + \frac{1}{2} q^{2\beta} \sigma^2(q) V_{qq} + \sigma_0 k q^\beta \sigma(q) V_{sq} \right), \end{aligned} \quad (20)$$

which completes the proof.  $\square$

#### 4. Solution of the Equilibrium

Note that the utility function is logarithmic and the HJB solution  $V(s, q)$  is additively separable. The optimal consumption and scale of productivity are linear functions of the initial savings. We know that the feasible set of each farmer's decision  $(c_t, k_t)$  is homothetic in his initial savings. Hence, we assume that the solution takes the form

$$V(s, q) = \lambda \ln s + \varphi(q), \quad (21)$$

where  $\lambda$  is a constant and  $\varphi(q)$  is a twice differentiable function of  $q$ . If  $V(s, q)$  takes the form above, the property  $V_{sq} = 0$  can be found.

**Theorem 3.** If  $V(s, q) = \lambda \ln s + \phi(q)$ , then the optimal consumption and scale of productivity of each farmer are

$$\begin{aligned} c^*(s, q) &= \rho s, \\ k^*(s, q) &= \frac{a - q}{\sigma_0^2} \cdot \left( \frac{V_{ss}}{V_s} \right)^{-1} = \frac{a - q}{\sigma_0^2} s. \end{aligned} \quad (22)$$

*Proof.* As the term  $V_{sq}$  is vanished, the HJB equation becomes

$$\begin{aligned} \rho V &= \max_{c, k \geq 0} \left( \ln c + [k(a - q) - c] V_s + q\mu(q) V_q \right. \\ &+ \left. \frac{1}{2} \sigma_0^2 k^2 V_{ss} + \frac{1}{2} q^{2\beta} \sigma^2(q) V_{qq} \right). \end{aligned} \quad (23)$$

Our aim is to maximize the function on the right side. To this end, we use the first-order condition with respect to  $c$  and  $k$ , and we get

$$\frac{1}{c^*} - V_s = 0, \quad (24)$$

$$(a - q) V_s + k^* \sigma_0^2 V_{ss} = 0;$$

i.e.,

$$c^* = \frac{1}{V_s} = \frac{s}{\lambda}, \quad (25)$$

$$k^* = \frac{a - q}{\sigma_0^2} \cdot \left( -\frac{V_s}{V_{ss}} \right) = \frac{a - q}{\sigma_0^2} s. \quad (26)$$

Putting the equations above into (14), we have

$$\begin{aligned} \rho(\lambda \ln s + \varphi(q)) &= \ln \frac{s}{\lambda} + \left[ \frac{(a-q)^2}{\sigma_0^2} s - \frac{s}{\lambda} \right] \cdot \frac{\lambda}{s} \\ &+ q\mu(q)\varphi'(q) + \frac{1}{2}\sigma_0^2 \frac{(a-q)^2}{\sigma_0^4} s^2 \\ &\cdot \left( -\frac{\lambda}{s^2} \right) + \frac{1}{2}q^{2\beta}\sigma^2(q)\varphi''(q). \end{aligned} \quad (27)$$

Finally, we get

$$\begin{aligned} &(\rho\lambda - 1)\ln s + \rho\varphi(q) + q\mu(q)\varphi'(q) \\ &- \frac{1}{2}q^{2\beta}\sigma^2(q)\varphi''(q) - \frac{1}{2}\frac{(a-q)^2\lambda}{\sigma_0^2} + \ln \lambda + 1 \\ &= 0. \end{aligned} \quad (28)$$

The equation above holds for any  $s$  and  $q$ . Then we must have

$$\begin{aligned} \rho\lambda - 1 &= 0, \\ \lambda &= \frac{1}{\rho}. \end{aligned} \quad (29)$$

The proof is completed.  $\square$

As is well known, a representative farmer's optimal consumption is a linear function of his saving multiplied by a discount constant  $\rho$ . What is more important is that the farmer's optimal scale of productivity is also a linear function with respect to  $s$ , which is his induced risk tolerance  $(-V_{ss}/V_s)^{-1}$ . So the more saving a farmer has, the more land he will rent. In other words, if a farmer is out of money, he will rent less land from the landlord because he has more risk averseness.

Since the optimal consumption and the scale of rental land are determined, we can go on with the entire economy status. The aggregate stock of saving  $S_t$  satisfies

$$dS_t = K_D(q_t)(dy_t - q_t dt) - \rho S_t dt, \quad (30)$$

where  $K_D(q_t)$  is the demands of lands for all farmers and follows

$$K_D(q_t) = \frac{(a - q_t)}{\sigma_0^2} S_t. \quad (31)$$

To proceed, we give the definition of an equilibrium according to market clearing condition.

*Definition 4.* For any initial natural endowments and rental rate  $q_0$ , an equilibrium is defined by stochastic process with filtration generated by the Brownian motion  $\{B_t, t \geq 0\}$ : the rental rate process  $q_t$  and the aggregate saving process  $S_t$  such that

- (i) the land market clears:  $K_D(q_t) = K_S(q_t)$ ,
- (ii) the market for consumption goods clears.

If the equilibrium that is Markovian in the state  $q_t$  exists, the aggregate stock of savings follows  $S_t = S(q_t)$ . Applying Itô's formula, we have

$$\begin{aligned} dS_t &= \left[ S'(q_t)q_t\mu(q_t) + \frac{1}{2}q_t^2\sigma^2(q_t)S''(q_t) \right] dt \\ &+ \frac{a - q_t}{\sigma_0} S_t dB_t. \end{aligned} \quad (32)$$

Combining (32) with (30) yields

$$\begin{aligned} &\frac{(a - q)^2}{\sigma_0^2} S(q) - \rho S(q) \\ &= q\mu(q)S'(q) + \frac{1}{2}q^{2\beta}\sigma^2(q)S''(q), \\ &\frac{a - q}{\sigma_0} S = \sigma(q)qS'(q). \end{aligned} \quad (33)$$

In addition, the clearing condition implies

$$K_S(q) = \frac{(a - q)}{\sigma_0^2} S(q). \quad (34)$$

**Theorem 5.** *There exists a unique Markov equilibrium in which the rental rate satisfies the following stochastic process:*

$$\frac{dq_t}{q_t} = \mu(q_t) dt + \sigma(q_t)q_t^{\beta-1} dB_t, \quad (35)$$

where

$$\begin{aligned} \sigma(q) &= \frac{(a - q)^2}{q^{\beta-1}\sigma_0 [(a - q)\epsilon_1 + q]}, \\ \mu(q) &= \sigma(q) \\ &\cdot q^{\beta-1} \left\{ \frac{(a - q)^2 \epsilon_1 [(a - q)(2\epsilon_1 - \epsilon_2) + 2q]}{2\sigma_0 [(a - q)\epsilon_1 + q]^2} \right. \\ &\left. - \frac{\rho\sigma_0}{a - q} \right\}. \end{aligned} \quad (37)$$

*Proof.* For convenience, we denote  $\epsilon_1 := q(K'_S(q)/K_S(q))$  (the elasticity of land supply),  $\epsilon_2 := q(K''_S(q)/K'_S(q))$ . Equations (34) and (36) are obtained by solving (33) and (34) directly.  $\square$

We now focus on the properties of (36) and (37). Comparing to the work of Klimenko et al. [10], the only difference is the  $q^{\beta-1}$  part that occurred in the denominator of  $\sigma(q)$ . The paradox of the volatility in Brunnermeier and Sannikov [6] shows up as well. In (37),  $\sigma_0$  has an inverse relationship with  $\sigma(q)$  so that the high exogenous volatility coexists with the low endogenous volatility at the same time. Moreover, we can see that the endogenous volatility  $\sigma$  is a linear function of  $q^{2-\beta}$ ; i.e.,  $\sigma(q) \propto q^{2-\beta}$ . For comparison,  $\sigma(q)$  is a linear function of  $q$ ; i.e.,  $\sigma(q) \propto q$  in [10]. We assume that  $\beta$  takes

value between 1 and 2 to ensure that  $2 - \beta$  is in the interval  $(0, 1)$ . From the graph of function  $f(x) = x^{(2-\beta)}$ , we have that the curve of the endogenous volatility is antrorsely warped by the rental rate  $q$ . When  $q$  is low, it has more impacts on  $\sigma$ . While  $q$  is high, the influence will be pulled down. In Klimenko et al. [10], the influence is linear all the time.

## 5. Properties of the Dynamics

In this section, we are going to discuss the economy in the long term. All properties are determined by the dynamics of the rental rate  $q_t$ . Our main goal is to give deep insight into the process described in Theorem 2. There are only two scenarios of  $q_t$  that may occur: either the rental rate drops very close to 0 and remains at the state of 0 permanently or it fluctuates in the range of  $(0, a)$ . For the first case, we are supposed to investigate the attainability of the boundaries of the process  $q_t$ . For the latter, we will use the ergodic density function to discuss its main properties.

**5.1. Ergodic Density Functions.** If the ergodic density function of process  $q_t$  does exist, we can derive it by solving a Kolmogorov's forward equation. Set

$$\Lambda(q) = \frac{2\mu(q)}{\sigma^2(q)}. \quad (38)$$

As will be clarified, the existence of the ergodic density function and its properties depend on the parameter

$$\Lambda(0) = \frac{2\mu(0)}{\sigma^2(0)} = 2 \left( 1 - \frac{\rho}{\theta^2} \right) \epsilon_1(0) - \epsilon_2(0), \quad (39)$$

where  $\theta = a/\sigma_0$  signifies the risk-adjusted productivity of farmers.

**Theorem 6.** *The properties of the economy depends on  $\Lambda(0)$ :*

(i) *If  $\Lambda(0) \leq 1$ , the ergodic density function does not exist and the economy collapses asymptotically.*

(ii) *If  $\Lambda(0) > 1$ , the process  $q_t$  has the ergodic density distribution*

$$p(q) = \frac{C}{q^2 \sigma^2(q)} e^{\int_0^q (2\mu(s)/\sigma^2(s)) ds}, \quad (40)$$

where  $C$  is a constant such that  $\int_0^a p(s) ds = 1$ . The boundary behaviour of the ergodic density function is characterized by the following:

(i) *When  $\Lambda(0) \geq 2$ ,  $\lim_{q \rightarrow 0} p(q)$  is finite and is infinite otherwise.*

(ii)  $\lim_{q \rightarrow a} p(q) = 0$ .

*Proof.* If the process  $q_t$  has a density  $p(t, x)$ , it satisfies the Kolmogorov differential equation

$$\begin{aligned} \frac{\partial p}{\partial t}(t, q) &= -\frac{\partial}{\partial q} [q\mu(q) p(t, q)] \\ &+ \frac{1}{2} \frac{\partial^2}{\partial q^2} [q^2 \sigma^2(q) p(t, q)]. \end{aligned} \quad (41)$$

If the Markov process  $q_t$  is stationary, the stationary density  $\psi(y)$  must satisfy

$$\psi(y) = \int \psi(x) p(t, x) dx, \quad \forall t > 0. \quad (42)$$

Mimicking the derivation of (41), we deduce  $\psi(y)$  to satisfy

$$0 = -\frac{d}{dq} [q\mu(q) \psi(q)] + \frac{1}{2} \frac{d^2}{dq^2} [q^2 \sigma^2(q) \psi(q)]. \quad (43)$$

By calculation, we have

$$\begin{aligned} \frac{d}{dq} [q\mu(q) \psi(q)] &= \frac{1}{2} \frac{d^2}{dq^2} [q^2 \sigma^2(q) \psi(q)], \\ C_1 + q\mu(q) \psi(q) &= \frac{1}{2} \frac{d}{dq} [q^2 \sigma^2(q) \psi(q)]. \end{aligned} \quad (44)$$

Denoting  $\varsigma(\eta) = e^{-\int (2\mu(\xi)/\xi\sigma^2(\xi)) d\xi}$  to be the integrating factor and  $\zeta(q) = \int_0^q \varsigma(\eta) d\eta$ , we have

$$\begin{aligned} 2C_1 \varsigma(q) + 2\varsigma(q) q\mu(q) \psi(q) \\ &= \varsigma(q) \frac{d}{dq} [q^2 \sigma^2(q) \psi(q)], \\ \varsigma(q) \frac{d}{dq} [q^2 \sigma^2(q) \psi(q)] - 2\varsigma(q) q\mu(q) \psi(q) \\ &= C_2 \varsigma(q), \quad (C_2 = 2C_1) \end{aligned} \quad (45)$$

$$d[\varsigma(q) q^2 \sigma^2(q) \psi(q)] = C_2 \varsigma(q),$$

$$\varsigma(q) q^2 \sigma^2(q) \psi(q) = C_2 \zeta(q) + C_3,$$

$$\psi(q) = \frac{1}{\varsigma(q) q^2 \sigma^2(q)} [C_2 \zeta(q) + C_3].$$

Setting  $m(q) := 1/\varsigma(q) q^2 \sigma^2(q)$ , we get

$$\psi(q) = m(q) [C_2 \zeta(q) + C_3], \quad (46)$$

where  $C_2$  and  $C_3$  are constants to ensure that  $\int_0^a \psi(q) dq = 1$ .  $C_2$  is clarified to be 0 and for  $q = a$  is unattainable in finite time. Therefore, the stationary density of the process  $q_t$  is

$$p(q) = \frac{C}{q^2 \sigma^2(q)} e^{\int_0^q (2\mu(s)/\sigma^2(s)) ds}, \quad (47)$$

where  $C$  is a constant to guarantee that  $\int_0^a p(q) dq = 1$ .

Now we investigate the properties of  $p(q)$  at both ends of the support  $[0, a]$ . In the right neighborhood of the state 0:  $\Theta_0 = (0, \varepsilon]$ , the drift and volatility part of the process  $q_t$  are approximated by

$$\begin{aligned} \sigma(0) &\approx \frac{a}{\sigma_0 \epsilon_1(0)}, \\ \mu(0) &\approx \sigma(0) \left\{ \frac{a^2 [2\epsilon_1(0) - \epsilon_2(0)] - 2\rho\sigma_0^2 \epsilon_1(0)}{2a\sigma_0 \epsilon_1(0)} \right\}. \end{aligned} \quad (48)$$

For  $0 < q_0 < q < \varepsilon$ , the ergodic density function of  $q_t$  is approximated by

$$\begin{aligned} p(q) &\approx \frac{C}{q^2 \sigma^2(0)} e^{\int_{q_0}^q (2\mu(0)/\sigma(0)) ds} \\ &= \frac{C}{q^2 \sigma^2(0)} e^{\int_{q_0}^q (\Lambda(0)/s) ds} = N q^{\Lambda(0)-2}, \end{aligned} \quad (49)$$

where  $N = C/q_0^{\Lambda(0)} \sigma^2(0)$  is a constant.

It is seen that  $\lim_{q \rightarrow 0} p(q) < \infty$  if and only if  $\Lambda(0) \geq 2$ . Moreover, for any  $0 < q_0 < q < \varepsilon$ , in case that the probability distribution does not degenerate when  $q \rightarrow 0$ , we have

$$\int_{q_0}^q p(s) ds \approx \frac{N}{\Lambda(0) - 1} q^{\Lambda(0)-1} < \infty. \quad (50)$$

This condition holds if and only if  $\Lambda(0) > 1$ . If  $\Lambda(0) < 1$ , the ergodic distribution degenerates and the process  $q_t$  ends up in a very close neighborhood of 0 with probability close to 1.

We now talk about the upper boundary behaviour of process  $q_t$ . Consider the left neighborhood of the state  $a$ :  $\Theta_0 = [a - \varepsilon, a)$ . In this status, the drift and volatility of process  $q_t$  are approximated by (see details in Section 5.2)

$$\begin{aligned} q\mu(q) &= -\rho(a - q), \\ q^\beta \sigma(q) &= \frac{(a - q)^2}{\sigma_0}. \end{aligned} \quad (51)$$

The ergodic density function of  $q_t$  is approximated by

$$\begin{aligned} p(q) &\propto \frac{1}{(a - q)^4} e^{-1/(a - q)^2}, \\ \lim_{q \rightarrow a} \frac{1}{(a - q)^4} e^{-1/(a - q)^2} &\stackrel{x=1/(a - q)^2}{=} \lim_{x \rightarrow \infty} \frac{x^2}{e^x} = 0. \end{aligned} \quad (52)$$

This establishes that the density of  $q_t$  vanishes on the occasion that the process  $q_t$  goes very close to its upper boundary  $a$ .  $\square$

**5.2. Attainability of the Boundaries.** For two natural boundaries:  $\underline{q} = 0$  and  $\bar{q} = a$ , we consider the rental rate to stay in the neighborhood of 0. If the economy could reach this state, it means that all farmers have no savings and they choose to rent no land. The landlords will cultivate all the land by themselves. Next, we consider the situation when  $q_t$  fluctuates in the neighborhood of  $a$ . In this case, all landlords are happy to rent their land to farmers. So, the aggregate supply of land in the economy is 1. In the view of the land market clearing condition, the demand of land is also 1. Equation (32) implies that the aggregate saving of farmers is approximated by  $1/(a - q)$ . Inserting this approximation into (32), the dynamics of  $q_t$  in the neighborhood of  $a$  are driven by

$$dq_t = -(a - q_t) \left( \rho dt - \frac{a - q_t}{\sigma_0} dB_t \right). \quad (53)$$

For further verification, we denote some functions according to boundary classification rules in Chapter 15 in [11] the following:

- (i) Scale Function:  $\zeta[b, q] = \int_b^q \zeta(\eta) d\eta$ ;  $\zeta(\eta) = e^{-\int^\eta (2\mu(\xi)/\xi \sigma^2(\xi)) d\xi}$ .
- (ii) Speed Function:  $M[b, q] = \int_b^q m(\eta) d\eta$ ;  $m(\eta) = 1/\eta^2 \zeta(\eta) \sigma^2(\eta)$ .
- (iii)  $\sum(l) = \int_l^q M[\eta, q] d\zeta(\eta)$ .

**Definition 7** (see [11]). A boundary  $l$  is attracting if  $\lim_{q \rightarrow l} \zeta[l, q] < \infty$ .

**Definition 8** (see [11]). A boundary  $l$  is said to be

- (i) attainable if  $\sum(l) < \infty$ ,
- (ii) unattainable if  $\sum(l) = \infty$ .

**Lemma 9** (see [11]). A nonattracting boundary is unattainable in finite time; i.e.,  $\lim_{b \rightarrow l} \zeta[b, q] = \infty$  implies  $\lim_{b \rightarrow l} \sum(b) = \infty$ .

**Theorem 10.** The states  $l = 0$  and  $r = a$  are both unattainable by process  $q_t$  in finite time.

*Proof.* (i) For  $0 < q_0 < q < \varepsilon$ , we have

$$\begin{aligned} \zeta(\eta) &= e^{-(\Lambda(0)/\xi) d\xi} = \left( \frac{q_0}{\eta} \right)^{\Lambda(0)}, \\ m(\eta) &= \frac{\eta^{\Lambda(0)}}{q_0^{\Lambda(0)} \eta^2 \sigma^2(0)} = \frac{1}{q_0^{\Lambda(0)} \sigma^2(0)} \eta^{\Lambda(0)-2} \\ &= \widehat{A}_0 \eta^{\Lambda(0)-2}, \\ \widehat{A}_0 &= \frac{1}{q_0^{\Lambda(0)} \sigma^2(0)}, \\ M[b, q] &= \int_b^q m(\eta) d\eta = \int_b^q \widehat{A}_0 \eta^{\Lambda(0)-2} d\eta \\ &= \frac{\widehat{A}_0}{\Lambda(0) - 1} \cdot (q^{\Lambda(0)-1} - b^{\Lambda(0)-1}), \end{aligned} \quad (54)$$

$$\begin{aligned} \sum(l) &= \int_l^q M[b, q] d\zeta(b) \\ &= \int_l^q \frac{\widehat{A}_0}{\Lambda(0) - 1} \cdot (q^{\Lambda(0)-1} - b^{\Lambda(0)-1}) \cdot \left( \frac{q_0}{b} \right)^{\Lambda(0)} db \\ &= \frac{1}{[\Lambda(0) - 1]^2 \sigma^2(0)} \\ &\quad \cdot \left[ (\Lambda(0) - 1) \ln \frac{l}{q} + \left( \frac{q}{l} \right)^{\Lambda(0)-1} - 1 \right]. \end{aligned}$$

If  $\Lambda(0) > 1$ , we get

$$\begin{aligned} \lim_{l \rightarrow 0} \left( \frac{q}{l} \right)^{\Lambda(0)-1} &= \infty \implies \\ \lim_{l \rightarrow 0} \sum(l) &= \infty. \end{aligned} \quad (55)$$

If  $\Lambda(0) \leq 1$ , we obtain

$$\lim_{l \rightarrow 0} (\Lambda(0) - 1) \ln \frac{l}{q} = \infty \implies \lim_{l \rightarrow 0} \sum (l) = \infty, \quad (56)$$

which implies that the lower boundary  $l = 0$  is unattainable in finite time.

(ii) For  $a - \varepsilon < q < q_0 < a$ , we have  $q\mu(q) = -\rho(a - q)$ ,  $q\sigma(q) = (a - q)^2/\sigma_0$ , and

$$\begin{aligned} \zeta(q) &= e^{-\int_{q_0}^q (2\mu(\xi)/\xi\sigma^2(\xi))d\xi} = e^{\int_{q_0}^q (2\rho\sigma_0^2/(a-\xi)^3)d\xi} \\ &= \bar{A}_0 e^{\rho\sigma_0^2/(a-q)^2}, \end{aligned} \quad (57)$$

where  $\bar{A}_0 = [\rho\sigma_0^2/(a - q_0)^2]^{-1}$ .

Thus, we have

$$\zeta[q, r] = \int_q^r \zeta(\eta) d\eta = \bar{A}_0 \int_q^r e^{\rho\sigma_0^2/(a-\eta)^2} d\eta. \quad (58)$$

Changing the variable by denoting  $x = \sqrt{\rho}\sigma_0/(a - \eta)$ ,  $x_q = \sqrt{\rho}\sigma_0/(a - q)$ , and  $x_r = \sqrt{\rho}\sigma_0/(a - r)$ , we get

$$\begin{aligned} d\eta &= \frac{\sqrt{\rho}\sigma_0}{x^2} dx, \\ \zeta[q, r] &= \bar{A}_0 \int_{x_q}^{x_r} \sqrt{\rho}\sigma_0 \frac{e^{x^2}}{x^2} dx \\ &= \bar{A}_0 \sqrt{\rho}\sigma_0 \left[ -\frac{e^{x^2}}{x} \Big|_{x_q}^{x_r} + \int_{x_q}^{x_r} 2e^{x^2} dx \right] \\ &= \bar{A}_0 \sqrt{\rho}\sigma_0 \left( -\frac{e^{x^2}}{x} + \sqrt{\pi} \operatorname{Erfi}(x) \right) \Big|_{x_q}^{x_r}, \end{aligned} \quad (59)$$

where  $\operatorname{Erfi}(x)$  is the imaginary error function which has derivative  $d\operatorname{Erfi}x/dx = (2/\sqrt{\pi})e^{x^2}$ .

It can be known that  $\zeta[q, r]$  goes to  $\infty$  as  $r$  tends to  $a$ . From Lemma 1 and Definition 7, the state  $a$  is unattainable in finite time.  $\square$

In this section, we mainly talk about the properties of the ergodic density function. We get similar results as that in Klimenko et al. [10]. For the sake of explanation, we are supposed to track down to the model of process of  $q_t$ . The rental rate  $q$  has a nonlinear influence on the parameter  $\sigma$ , which is explicitly described by  $\sigma(q) \propto q^{(2-\beta)}$ . If we track down to the stochastic differential equation of the process  $q_t$ , we find that the influence is counteracted by the SDE itself. This is why we get the same results. In the rest of our paper, we will talk about the process of  $q_t$  in detail.

## 6. Long-Run Average Behaviour, Welfare Loss, and Poverty Trap

**6.1. Long-Run Average Behaviour.** When  $\Lambda(0) > 1$ , we know that there exists an ergodic density function of the

equilibrium rental rate process  $q_t$ . As the time goes to infinity, the time average of the stochastic variable converges. Therefore, the long-run average of  $q_t$  is computed by

$$\bar{q} = \lim_{T \rightarrow \infty} \frac{1}{T} \int_0^T p_s ds = \int_0^a q p(q) dq. \quad (60)$$

If  $\Lambda(0) \leq 1$ , the ergodic distribution degenerates and the process  $q_t$  ends up in a very close neighborhood of 0 with probability near to 1, which indicates  $\bar{q} = 0$ .

**6.2. Welfare Loss.** When the economy is frictionless, all the land is cultivated by the farmers. While the economy has extreme friction, we know that only part of lands is rented by farmers. The welfare loss is clarified to be the difference between the aggregate output in two cases. We are going to give an explicit formula of welfare loss and discuss its main property.

If  $\bar{\alpha} > q_t$ , the landlord will cultivate himself. Otherwise, he rents the land to farmers. Once the rental rate  $q_t$  is determined, the total output process is an integral with respect to the level of  $\bar{\alpha}$

$$dY_t = dy_t \int_0^{q_t} d[K_S(\bar{\alpha})] + d\bar{y}_t \int_{q_t}^a d[K_S(\bar{\alpha})]. \quad (61)$$

In a frictionless economy, the rental rate is fixed at  $q_t = a$  and all land is cultivated by farmers. The possible maximum output is

$$dY_t^{PM} = dy_t \int_0^a d[K_S(\bar{\alpha})] = adt + \sigma_0 dB_t. \quad (62)$$

The possible maximum output minus the total output is the welfare loss in the economy

$$l(q_t) = dY_t^{PM} - dY_t = \int_{q_t}^a (a - \bar{\alpha}) d[K_S(\bar{\alpha})]. \quad (63)$$

Because the ergodic density of  $q_t$  does not exist when  $\Lambda(0) \leq 1$ , we only consider the situation when  $\Lambda > 1$ . In this case, we compute the time average loss by ergodic property

$$\bar{l} = \lim_{T \rightarrow \infty} \frac{1}{T} \int_0^T l_s ds = \int_0^a l(q) p(q) dq. \quad (64)$$

**6.3. Poverty Trap.** Following the ideas in [10], we take the constant-elasticity specification of land supply:  $K_S(q) = (q/a)^\gamma$ , where  $\gamma > 0$ . We derive that  $\epsilon_1(q) = q(K_S'(q)/K_S(q)) = \gamma$  and  $\epsilon_2 = q(K_S''(q)/K_S'(q)) = \gamma - 1$ . Substituting the values of  $\epsilon_1$  and  $\epsilon_2$  into (36) and (37), we have

$$\sigma(q) = \frac{(a - q)^2}{q^{\beta-1}\sigma_0 [(a - q)\gamma + q]}, \quad (65)$$

$$\mu(q) = \sigma(q)$$

$$q^{\beta-1} \left\{ \frac{\gamma(a - q)^2 [(a - q)\gamma + a + q]}{2\sigma_0 [(a - q)\gamma + q]^2} - \frac{\rho\sigma_0}{a - q} \right\}, \quad (66)$$

$$\Lambda(0) = \left( 1 - \frac{2\rho}{\theta^2} \right) \gamma + 1. \quad (67)$$

The poverty trap is mainly caused by the inverse relationship between the endogenous and the exogenous volatility. This occurs in our result as well. When the exogenous volatility  $\sigma_0$  is low, a small shock in the economy gives

rise to the big change of endogenous volatility  $\sigma$ . As a result, the economy will be trapped in a less productive level permanently (see details in Section 4.2 in [10]).

The process of  $q_t$  is

$$\frac{dq_t}{q_t} = \frac{\gamma(a - q_t)^4 [(a - q_t)\gamma + a + q_t] - 2\rho\sigma_0^2(a - q_t)[\gamma(a - q_t) + q_t]^2}{2\sigma_0^2[\gamma(a - q_t) + q_t]^3} dt + \frac{(a - q_t)^2}{\sigma_0[\gamma(a - q_t) + q_t]} dB_t. \quad (68)$$

In (68), the parameter  $\beta$  no longer exists. We are inspired whether people determine behaviour of the market or are controlled by it. Even if we take the agents' psychological anticipation (with parameter  $\beta$ ) into consideration in our model, the rental market always runs in its own way (without  $\beta$ ). This is very meaningful.

## 7. Conclusion

In this paper, we investigate an economy model with extreme friction. In the economy, farmers have to choose their optimal scale of productivity to gain the maximum utility. We obtain conclusions similar to those in Klimenko et al. [10], such as poverty trap, existence conditions of the ergodic density function, and welfare loss. We take the farmers' psychological anticipations into account and adopt a different model of the rental rate process. The closed form of the endogenous volatility is obtained. We analyze how the rental rate influences the endogenous volatility. We find that this consideration does not show up in rental rate process ( $\beta$  does not appear in (68)). This gives us an inspiration that the capital market has some superior powers that are not up to the agents therein.

## Data Availability

The data used to support the findings of this study are available from the corresponding author upon request.

## Conflicts of Interest

The authors declare that there are no conflicts of interest regarding the publication of this paper.

## Authors' Contributions

The article is a joint work of two authors who contributed equally to the final version of the paper. All authors read and approved the final manuscript.

## Acknowledgments

This work is supported by the Fundamental Research Funds for the Central Universities (JBK120504).

## References

- [1] C. Kindleberger, *A Financial History of Western Europe*, vol. 53, Oxford University Press, 2nd edition, 1993.

- [2] B. Bernanke and M. Gertler, "Agency costs, net worth, and business fluctuations," *American Economic Review*, vol. 79, no. 1, pp. 14–31, 1989.
- [3] N. Kiyotaki and J. Moore, "Credit cycles," *Journal of Political Economy*, vol. 105, no. 2, pp. 211–248, 1997.
- [4] Z. He and A. Krishnamurthy, "A model of capital and crises," *Review of Economic Studies*, vol. 79, no. 2, pp. 735–777, 2012.
- [5] Z. He and A. Krishnamurthy, "Intermediary asset prices," *American Economic Review*, vol. 103, no. 2, pp. 1–43, 2013.
- [6] M. K. Brunnermeier and Y. Sannikov, "A macroeconomic model with a financial sector," *American Economic Review*, vol. 104, no. 2, pp. 379–421, 2014.
- [7] X.-J. Xie and W.-Q. Li, "Output-feedback control of a class of high-order stochastic nonlinear systems," *International Journal of Control*, vol. 82, no. 9, pp. 1692–1705, 2009.
- [8] X. Yu and X.-J. Xie, "Output feedback regulation of stochastic nonlinear systems with stochastic iISS inverse dynamics," *Institute of Electrical and Electronics Engineers Transactions on Automatic Control*, vol. 55, no. 2, pp. 304–320, 2010.
- [9] X. Yu, X.-J. Xie, and Y.-Q. Wu, "Decentralized adaptive output-feedback control for stochastic interconnected systems with stochastic unmodeled dynamic interactions," *International Journal of Adaptive Control and Signal Processing*, vol. 25, no. 8, pp. 740–757, 2011.
- [10] N. Klimenko, S. Pfeil, and J.-C. Rochet, "A simple macroeconomic model with extreme financial frictions," *Journal of Mathematical Economics*, vol. 68, pp. 92–102, 2017.
- [11] S. Karlin and H. M. Taylor, *A Second Course in Stochastic Processes*, Academic Press, New York, NY, USA, 1981.

## Research Article

# Global Output Feedback Stabilization for a Class of Nonlinear Cascade Systems

Cai-Yun Liu,<sup>1</sup> Zong-Yao Sun ,<sup>1</sup> Qing-Hua Meng,<sup>2</sup> Chih-Chiang Chen ,<sup>3</sup>  
Bin Cai,<sup>1</sup> and Yu Shao<sup>1</sup>

<sup>1</sup>Institute of Automation, Qufu Normal University, Qufu 273165, China

<sup>2</sup>School of Mechanical Engineering, Hangzhou Dianzi University, Hangzhou 310018, China

<sup>3</sup>Department of Systems and Naval Mechatronic Engineering, National Cheng Kung University, Tainan 70101, Taiwan

Correspondence should be addressed to Zong-Yao Sun; sunzongyao@sohu.com

Received 4 April 2018; Accepted 10 May 2018; Published 2 July 2018

Academic Editor: Weihai Zhang

Copyright © 2018 Cai-Yun Liu et al. This is an open access article distributed under the Creative Commons Attribution License, which permits unrestricted use, distribution, and reproduction in any medium, provided the original work is properly cited.

This paper focuses on the problem of global output feedback stabilization for a class of nonlinear cascade systems with time-varying output function. By using double-domination approach, an output feedback controller is developed to guarantee the global asymptotic stability of closed-loop system. The novel control strategy successfully constructs a unified Lyapunov function, which is suitable for both upper-triangular and lower-triangular systems. Finally, two numerical examples are provided to illustrate the effectiveness of a control strategy.

## 1. Introduction

It is well known that global output feedback stabilization is viewed as one of the most challenging fields of nonlinear control. Researchers have not yet found any unified way to handle the problem of global output feedback stabilization because the measure of states is difficult. Fortunately, with the help of nonseparation principle [1], homogeneous domination approach [2], and backstepping method, many interesting results such as [3–11] have been achieved.

It is worth pointing out that the structures of system output and nonlinear functions determine the possible forms of observer and controller. More specifically, the uncertainty of nonlinearities has led to the emergence of many kinds of observers, including high-gain observer, homogeneous observer, and time-varying observer. For example, [12] solved the problem of global output feedback stabilization based on linear high-gain observer for a class of uncertain nonlinear systems, where controller is independent of higher-order nonlinearities. Under uncertain linear growth condition in [13], a dynamic high-gain observer is proposed without requiring precise information of output function. References [14, 15] achieved system global stabilization by using time-varying observer, which uses the appropriate functions of

time, rather than the dynamic compensator. Since some nonlinear functions satisfy neither the linear growth nor Lipschitz condition in practice, the existing approaches are not suitable. Therefore, [16–19] proposed homogeneous domination method to overcome this obstacle. Based on the existing results, some special observers are proposed, such as dual-observer [20] and reduced-observer [21]. In practice, complex systems are usually composed of simple subsystems. Therefore, cascade systems have become one of the most interesting topics of nonlinear systems. A great deal of research has been devoted to this subject over the last decades, as evidenced by the comprehensive books of [22, 23]. However, when zero-dynamics exist and obey mild conditions, the tracking problem cannot be solved by trivially extending the corresponding results without zero-dynamics; that is, there do not exist appropriate observers to tracking states of cascade systems. As further investigation, researchers now consider cascade connections in which the nonlinear systems are globally stable, but the input subsystem is more complex than just an integrator; for instance, [24–26] successfully investigated output feedback stabilization for uncertain cascade systems under growth condition. Regrettably, their approaches are only suitable for lower-triangular cascade systems. On the other

hand, some literatures [27] achieved global output feedback stabilization when output function depends only on a state. References [28, 29] required that output function be continuous differentiability and initial value equals zero when output is unknown. The above conditions are restrictive; researchers turned to study time-varying output function. For instance, [30] further investigated the problem of global output feedback stabilization for a class of nonlinear systems with unknown measurement sensitivity. Meanwhile, a new method, namely, dual-domination approach, is proposed in [30].

In view of the above argument, an interesting question is proposed simultaneously: *Is it possible to find a new approach to solve the problem of global output feedback stabilization for nonlinear cascade systems with unknown time-varying output function, which is suitable for both upper-triangular and lower-triangular systems?* Based on above analysis and references, we will solve aforementioned question and provide satisfactory answer. There are three troublesome difficulties throughout the paper. The first is to find the appropriate Lyapunov function that is independent of the derivative of output function, since output function is unknown and does not satisfy differentiability. The second is to choose allowable sensitivity error, since it appears in the construction of controller. The third is to design rational observers to successfully track states, since nonlinearities and output function are unknown. A novel observer is proposed, which is different from the existing results [24, 25].

The main contributions of this paper are divided into three aspects: (i) double-domination approach is provided to handle time-varying sensitivity and uncertain nonlinearities, which is suitable for both upper-triangular and lower-triangular systems; (ii) linear observer does not rely on precise information of nonlinearities and output function; (iii) the construction of Lyapunov function avoids the use of the differentiability of output function.

## 2. Preliminaries and Problem Formulation

**2.1. Preliminaries.** We will adopt the following notations throughout this paper.  $\mathbb{R}$  denotes the set of real numbers,  $\mathbb{R}^+$  denotes the set of all nonnegative real numbers, and  $\mathbb{R}^n$  denotes Euclidean space with dimension  $n$ . For any real vector  $x = [x_1, \dots, x_n]^T \in \mathbb{R}^n$ , the norm  $\|x\|_p$  is defined by  $\|x\|_p = (\sum_{i=1}^n x_i^p)^{1/p}$ ,  $1 \leq p < \infty$ . For matrix  $A = (a_{ij})^{n \times n}$ ,  $i = 1, \dots, n$ ,  $j = 1, \dots, n$ ,  $\|A\|$  denotes the norm  $\|A\| = \sqrt{\lambda_{\max}(A^T A)}$ , where  $\lambda_{\max}(A^T A)$  denotes maximum eigenvalue of square matrix  $A^T A$ .  $\mathcal{C}^i$  denotes the set of all functions with continuous  $i$ th partial derivatives. A continuous function  $\alpha : [0, a) \rightarrow [0, \infty)$  is said to belong to class  $\mathcal{K}$  if it is strictly increasing and  $\alpha(0) = 0$ . It is said to belong to class  $\mathcal{K}_\infty$  if  $a = \infty$  and  $\alpha(r) = \infty$  as  $r \rightarrow \infty$ . For a continuously differentiable function  $V : \mathbb{R}^n \rightarrow \mathbb{R}^+$ , it is positive definite if  $V(x) \geq 0$  and  $V(x) = 0$  if and only if  $x = 0$ ; it is radially unbounded if  $V(x) \rightarrow \infty$  as  $\|x\| \rightarrow \infty$ . The arguments of functions are sometimes simplified; for instance, a function  $f(x(t))$  is denoted by  $f(x)$  or  $f$  and  $\|x\|_2$  is denoted by  $\|x\|$ .

In the following, we list three lemmas that play an important role in proving the main results, and their proofs can be found in [31–33].

**Lemma 1** (see [31]). *Let  $c$  and  $d$  be positive constants; given any positive real-valued function  $\gamma(x, y)$ , the following inequality holds:*

$$|x|^c |y|^d \leq \frac{c}{c+d} \gamma(x, y) |x|^{c+d} + \frac{d}{c+d} \gamma(x, y)^{-c/d} |y|^{c+d}. \quad (1)$$

**Lemma 2** (see [32]). *For any  $x = [x_1, \dots, x_n]^T \in \mathbb{R}^n$ , the following inequality holds:*

$$\|x\|_2 \leq \|x\|_1 \leq \sqrt{n} \|x\|_2. \quad (2)$$

**Lemma 3** (see [33]). *For  $x \in \mathbb{R}$  and  $y \in \mathbb{R}$ ,  $p \geq 1$  is an integer, and the following inequality holds:*

$$|x + y|^p \leq 2^{p-1} |x^p + y^p|. \quad (3)$$

**2.2. Problem Formulation.** This paper investigates the nonlinear cascade system described by

$$\begin{aligned} \dot{z} &= f_0(t, z, x, u), \\ \dot{x}_i &= x_{i+1} + f_i(t, z, x, u), \quad i = 1, \dots, n-1, \\ \dot{x}_n &= u + f_n(t, z, x, u), \\ y(t) &= \theta(t) x_1(t), \end{aligned} \quad (4)$$

where  $x(t) = [x_1(t), \dots, x_n(t)]^T \in \mathbb{R}^n$  and  $z(t) \in \mathbb{R}^m$  are system states with the initial values  $x(0) = x_0$ ,  $z(0) = z_0$ ,  $u(t) \in \mathbb{R}$ ,  $y(t) \in \mathbb{R}$  being control input and output, respectively.  $f_0 : \mathbb{R}^+ \times \mathbb{R}^m \times \mathbb{R}^n \times \mathbb{R} \rightarrow \mathbb{R}^m$  is continuous function with  $f_0(t, 0, 0, 0) = 0$  and globally Lipschitz with respect to  $x$ ;  $f_i : \mathbb{R}^+ \times \mathbb{R}^m \times \mathbb{R}^n \times \mathbb{R} \rightarrow \mathbb{R}$ ,  $i = 1, \dots, n$ , are continuous functions with  $f_i(t, 0, 0, 0) = 0$ .  $\theta(t) : \mathbb{R}^+ \rightarrow \mathbb{R}$  is a continuous function that represents time-varying sensitivity.

The following assumptions are needed.

**Assumption 4.** For the continuous function  $\theta(t)$ , there is a known positive parameter  $\bar{\theta}$  satisfying  $|1 - \theta(t)| \leq \bar{\theta} < \tilde{\theta} < 1$ , where  $\bar{\theta}$  is an allowable sensitivity error and  $\tilde{\theta}$  is the upper bound of the allowable sensitivity error.

**Assumption 5.** There exists a positive-definite and radially unbounded function  $U(z) \in \mathcal{C}^2$  such that

$$\begin{aligned} \frac{\partial U}{\partial z} f_0(t, z, 0, u) &\leq -c_1 \|z\|^2, \\ \left\| \frac{\partial U}{\partial z} \right\| &\leq c_2 \|z\|, \end{aligned} \quad (5)$$

where  $c_1 \in (c_1^*, \infty)$ ,  $c_2 \in [0, c_2^*)$ , and  $c_1^*$  and  $c_2^*$  are positive constants.

*Assumption 6.* There exists a constant  $c \geq 0$  such that

$$\begin{aligned} |f_i(\cdot)| &\leq c(\|z\| + |x_{i+2}| + \cdots + |x_n|), \\ & \quad i = 1, \dots, n-2, \\ |f_{n-1}(\cdot)| &\leq c\|z\|, \\ |f_n(\cdot)| &\leq c\|z\|. \end{aligned} \quad (6)$$

*Remark 7.* Since output function contains unknown parameter, it implies that the scope of this paper is more general than [1, 2, 12, 16] whose output function is equal to  $x_1$ .

*Remark 8.* In terms of the appearance of  $\theta(t)$ , two obstacles will be encountered. The first is to find an appropriate observer, which does not use the information of output function. The second is to find the feasible range of  $\theta(t)$ , because the information of  $\theta(t)$  will be used in the design of controller.

### 3. Main Results

*3.1. Output Feedback Controller Design for Upper-Triangular Case.* We now summarise main results of this paper.

**Theorem 9.** For system (4) under Assumptions 4–6, there exists an output feedback controller such that states of the closed-loop system are uniformly bounded over  $[0, +\infty)$  and  $\lim_{t \rightarrow +\infty} x(t) = 0$ .

*Proof.* The proof is in four parts. At first, a linear observer with a domination gain is introduced to reconstruct all the states. Secondly, an output feedback controller composed of another domination gain is constructed to counteract the destabilized terms. Finally, a delicate selection of gains is provided and strict analysis is performed to guarantee that the closed-loop systems are globally asymptotically stable.

*Part I: Design of an Observer.* We construct the following linear observer:

$$\begin{aligned} \dot{\hat{x}}_i &= \hat{x}_{i+1} - \frac{a_i}{L^i} \hat{x}_1, \quad i = 1, \dots, n-1, \\ \dot{\hat{x}}_n &= u - \frac{a_n}{L^n} \hat{x}_1, \end{aligned} \quad (7)$$

where  $a_i > 0$  are coefficients of Hurwitz polynomial  $p_1(s) = s^n + a_1 s^{n-1} + \cdots + a_{n-1} s + a_n$  and the domination gain  $L \geq 1$  will be determined later. Define the estimation error as follows:

$$\varepsilon_i = L^{i-1} (x_i - \hat{x}_i), \quad i = 1, \dots, n. \quad (8)$$

Then, the error equation can be rewritten as

$$\dot{\varepsilon} = \frac{1}{L} A_\varepsilon \varepsilon + \frac{1}{L} D_\varepsilon x_1 + F, \quad (9)$$

where

$$\begin{aligned} \varepsilon &= \begin{bmatrix} \varepsilon_1 \\ \varepsilon_2 \\ \vdots \\ \varepsilon_n \end{bmatrix}, \\ A_\varepsilon &= \begin{bmatrix} -a_1 & 1 & \cdots & 0 \\ \vdots & \vdots & \ddots & \vdots \\ -a_{n-1} & 0 & \cdots & 1 \\ -a_n & 0 & \cdots & 0 \end{bmatrix}, \\ D_\varepsilon &= \begin{bmatrix} a_1 \\ a_2 \\ \vdots \\ a_n \end{bmatrix}, \\ F &= \begin{bmatrix} f_1(\cdot) \\ Lf_2(\cdot) \\ \vdots \\ L^{n-1}f_n(\cdot) \end{bmatrix}. \end{aligned} \quad (10)$$

Since  $A_\varepsilon$  is Hurwitz, there exists a symmetric positive-definite matrix  $P_1 \in \mathbb{R}^{n \times n}$  such that  $A_\varepsilon^T P_1 + P_1 A_\varepsilon = -I$ , where  $I$  is an identity matrix of  $\mathbb{R}^{n \times n}$ . Consider positive-definite and radially unbounded function  $V_\varepsilon(\varepsilon) = \varepsilon^T P_1 \varepsilon$ ; a direct calculation gives

$$\begin{aligned} \dot{V}_\varepsilon &= -\frac{1}{L} \varepsilon^T \varepsilon + 2\frac{1}{L} \varepsilon^T P_1 D_\varepsilon x_1 + 2\varepsilon^T P_1 F \\ &\leq -\frac{1}{L} \|\varepsilon\|^2 + 2\frac{1}{L} \|\varepsilon\| \cdot \|D_\varepsilon\| \cdot \|P_1\| \cdot |x_1| + 2\|\varepsilon\| \\ &\quad \cdot \|P_1\| \cdot \|F\|. \end{aligned} \quad (11)$$

According to Assumption 6 and Lemma 2, we obtain

$$\begin{aligned} \|F\| &= \sqrt{|f_1|^2 + L^2 |f_2|^2 + \cdots + L^{2(n-1)} |f_n|^2} \\ &\leq |f_1| + L |f_2| + \cdots + L^{n-1} |f_n| \\ &\leq cL^{n-1} n \|z\| + \sum_{i=3}^n cL^{i-3} (i-2) |x_i|. \end{aligned} \quad (12)$$

Substituting (12) into (11), one has

$$\begin{aligned} \dot{V}_\varepsilon &\leq -\frac{1}{L} \|\varepsilon\|^2 + 2c \|P_1\| \\ &\quad \cdot \|\varepsilon\| \left( L^{n-1} n \|z\| + \sum_{i=3}^n L^{i-3} (i-2) |x_i| \right) + \frac{2}{L} \|P_1\| \\ &\quad \cdot \|\varepsilon\| \cdot \|D_\varepsilon\| \cdot |x_1|. \end{aligned} \quad (13)$$

In addition, Lemma 1 shows that

$$\frac{2}{L} \|P_1\| \cdot \|\varepsilon\| \cdot \|D_\varepsilon\| \cdot |x_1| \leq \frac{1}{2L} \|\varepsilon\|^2 + \frac{1}{L} K_2 |x_1|^2, \quad (14)$$

and

$$\begin{aligned} & 2c \|P_1\| \cdot \|\varepsilon\| \left( L^{n-1} n \|z\| + \sum_{i=3}^n L^{i-3} (i-2) |x_i| \right) \\ & \leq \sum_{i=3}^n K_i L^{2(i-2)} x_i^2 + \frac{K_1}{L^2} \|\varepsilon\|^2 + \frac{1}{2} cnL^{2n} \|P_1\| \cdot \|z\|^2, \end{aligned} \quad (15)$$

where  $K_1 = c(2n+(n-1)(n-2))\|P_1\| \geq 0$ ,  $K_2 = 2\|D_\varepsilon\|^2\|P_1\|^2 > 0$ , and  $K_i = (1/2)c(i-2)\|P_1\| \geq 0$ ,  $i = 3, \dots, n$ , are independent of a domination gain  $L$ . Therefore, substituting (14) and (15) into (13) yields

$$\begin{aligned} \dot{V}_\varepsilon & \leq -\frac{1}{2L} \|\varepsilon\|^2 + \frac{K_1}{L^2} \|\varepsilon\|^2 + \frac{1}{L} K_2 |x_1|^2 \\ & \quad + \sum_{i=3}^n K_i L^{2(i-2)} x_i^2 + \frac{1}{2} cnL^{2n} \|P_1\| \cdot \|z\|^2. \end{aligned} \quad (16)$$

*Part II: Construction of a Controller.* Consider the following system:

$$\begin{aligned} \dot{x}_1 & = x_2 + f_1(t, z, x, u), \\ \dot{\hat{x}}_i & = \hat{x}_{i+1} + \frac{a_i}{L^i} (\varepsilon_1 - x_1), \quad i = 2, \dots, n-1, \\ \dot{\hat{x}}_n & = u + \frac{a_n}{L^n} (\varepsilon_1 - x_1). \end{aligned} \quad (17)$$

Define the following change of coordinates:

$$\begin{aligned} \xi_1 & = x_1, \\ \xi_i & = \frac{L^{i-1}}{H^{i-1}} \hat{x}_i, \\ v & = \frac{L^n}{H^n} u, \end{aligned} \quad (18)$$

$i = 2, \dots, n,$

where  $H \geq 1$  is a domination gain that will be determined later. Using above coordinate transform, (17) can be rewritten as

$$\begin{aligned} \dot{\xi}_1 & = \frac{H}{L} \xi_2 + \frac{1}{L} \varepsilon_2 + f_1(t, z, x, u), \\ \dot{\xi}_i & = \frac{H}{L} \xi_{i+1} + \frac{a_i}{LH^{i-1}} (\varepsilon_1 - \xi_1), \quad i = 2, \dots, n-1, \\ \dot{\xi}_n & = \frac{H}{L} v + \frac{a_n}{LH^{n-1}} (\varepsilon_1 - \xi_1). \end{aligned} \quad (19)$$

Design the output feedback control law as follows:

$$v = -b_n y - b_{n-1} \xi_2 - \dots - b_2 \xi_{n-1} - b_1 \xi_n, \quad (20)$$

where  $b_i > 0$ ,  $i = 1, \dots, n$ , are coefficients of Hurwitz polynomial  $p_2(s) = s^n + b_1 s^{n-1} + \dots + b_{n-1} s + b_n$ . Substituting (20) into (19), we have

$$\begin{aligned} \dot{\xi} & = \frac{H}{L} A_\xi \xi + \frac{H}{L} D_\xi b_n (1 - \theta(t)) \xi_1 + \frac{B_2}{L} \varepsilon_2 \\ & \quad + \frac{B_1}{LH} (\varepsilon_1 - \xi_1) + \bar{F}, \end{aligned} \quad (21)$$

where

$$\begin{aligned} A_\xi & = \begin{bmatrix} 0 & 1 & \dots & 0 \\ \vdots & \vdots & \ddots & \vdots \\ 0 & 0 & \dots & 1 \\ -b_n & -b_{n-1} & \dots & -b_1 \end{bmatrix}, \\ B_1 & = \begin{bmatrix} 0 \\ a_2 \\ \frac{a_3}{H} \\ \vdots \\ \frac{a_n}{H^{n-2}} \end{bmatrix}, \\ B_2 & = \begin{bmatrix} 1 \\ 0 \\ \vdots \\ 0 \end{bmatrix}, \\ D_\xi & = \begin{bmatrix} 0 \\ \vdots \\ 0 \\ 1 \end{bmatrix}, \\ \bar{F} & = \begin{bmatrix} f_1(\cdot) \\ 0 \\ \vdots \\ 0 \end{bmatrix}. \end{aligned} \quad (22)$$

$A_\xi$  is a Hurwitz matrix that shows that there exists a symmetric positive-definite matrix  $P_2$  such that  $A_\xi^T P_2 + P_2 A_\xi = -I$ . Choose scalar function  $V_\xi(\xi) = \xi^T P_2 \xi$ , which is positive-definite and radially bounded. Noting that  $\|B_2\| = \|D_\xi\| = 1$ , the time derivative of  $V_\xi(\xi)$  along the trajectories of (21) is

$$\begin{aligned} \dot{V}_\xi & = -\frac{H}{L} \xi^T \xi + \frac{2H}{L} \xi^T P_2 D_\xi b_n (1 - \theta(t)) \xi_1 + 2\xi^T P_2 \bar{F} \\ & \quad + 2\xi^T P_2 \left( \frac{B_1}{LH} \varepsilon_1 + \frac{B_2}{L} \varepsilon_2 - \frac{B_1}{LH} \xi_1 \right) \end{aligned}$$

$$\begin{aligned}
 &\leq -\frac{H}{L} \|\xi\|^2 + 2b_n |1 - \theta(t)| \frac{H}{L} \|P_2\| \cdot \|\xi\|^2 + 2 \|\xi\| \\
 &\quad \cdot \|P_2\| \cdot |f_1| + 2 \|\xi\| \cdot \|P_2\| \left( \frac{1}{L} \|\varepsilon\| + \frac{\|B_1\|}{LH} \|\varepsilon\| \right) \\
 &\quad + \frac{2}{LH} \|P_2\| \cdot \|B_1\| \cdot \|\xi\|^2.
 \end{aligned} \tag{23}$$

Firstly, by virtue of Assumption 6 and Lemma 1, it holds that

$$\begin{aligned}
 2 \|\xi\| \cdot \|P_2\| \cdot |f_1| &\leq 2c \|\xi\| \\
 &\quad \cdot \|P_2\| (\|z\| + |x_3| + \dots + |x_n|) \\
 &\leq \frac{c(n-1)}{L^2} \|P_2\| \cdot \|\xi\|^2 \\
 &\quad + c \|P_2\| L^2 (\|z\|^2 + x_3^2 + \dots + x_n^2) \\
 &\triangleq \frac{\bar{K}_1}{L^2} \|\xi\|^2 + \bar{K}_2 L^2 \sum_{i=3}^n x_i^2 \\
 &\quad + \bar{K}_2 L^2 \|z\|^2,
 \end{aligned} \tag{24}$$

where  $\bar{K}_1 = c(n-1)\|P_2\| \geq 0$  and  $\bar{K}_2 = c\|P_2\| \geq 0$ . Furthermore, it is deduced from Lemma 1 that

$$\begin{aligned}
 \frac{2}{L} \|\xi\| \cdot \|P_2\| \cdot \|\varepsilon\| &\leq \frac{1}{8L} \|\varepsilon\|^2 + \frac{8}{L} \|P_2\|^2 \cdot \|\xi\|^2, \\
 \frac{2\gamma}{LH} \|\xi\| \cdot \|P_2\| \cdot \|\varepsilon\| &\leq \frac{1}{8L} \|\varepsilon\|^2 + \frac{8\gamma^2}{LH^2} \|P_2\|^2 \cdot \|\xi\|^2,
 \end{aligned} \tag{25}$$

and because of  $H > 1$ , one can conclude that

$$\|B_1\| = \left( \sum_{i=2}^n \frac{1}{H^{2(i-2)}} a_i^2 \right)^{1/2} \leq \left( \sum_{i=2}^n a_i^2 \right)^{1/2} \triangleq \gamma. \tag{26}$$

Consequently, one obtains

$$\begin{aligned}
 \dot{V}_\xi &\leq -\frac{H}{L} (1 - 2b_n |1 - \theta(t)| \cdot \|P_2\|) \|\xi\|^2 + \frac{1}{4L} \|\varepsilon\|^2 \\
 &\quad + \frac{8\gamma^2}{LH^2} \|P_2\|^2 \cdot \|\xi\|^2 + \frac{8}{L} \|P_2\|^2 \cdot \|\xi\|^2 + \frac{2\gamma}{LH} \|P_2\| \\
 &\quad \cdot \|\xi\|^2 + \frac{\bar{K}_1}{L^2} \|\xi\|^2 + \bar{K}_2 L^2 \sum_{i=3}^n x_i^2 + \bar{K}_2 L^2 \|z\|^2 \\
 &\leq -\frac{H}{L} (1 - 2b_n |1 - \theta(t)| \cdot \|P_2\|) \|\xi\|^2 + \bar{K}_2 L^2 \sum_{i=3}^n x_i^2 \\
 &\quad + \bar{K}_2 L^2 \|z\|^2 + \frac{1}{4L} \|\varepsilon\|^2 \\
 &\quad + \frac{H}{L} \left( \frac{8\gamma^2}{H} \|P_2\|^2 + \frac{8}{H} \|P_2\|^2 + \frac{2\gamma}{H} \|P_2\| + \frac{\bar{K}_1}{L} \right) \\
 &\quad \cdot \|\xi\|^2 \triangleq -\frac{H}{L} (1 - 2b_n |1 - \theta(t)| \cdot \|P_2\|) \|\xi\|^2
 \end{aligned}$$

$$\begin{aligned}
 &+ \bar{K}_2 L^2 \sum_{i=3}^n x_i^2 + \bar{K}_2 L^2 \|z\|^2 + \frac{1}{4L} \|\varepsilon\|^2 \\
 &+ \frac{H}{L} \left( \frac{\bar{K}_3}{H} + \frac{\bar{K}_1}{L} \right) \|\xi\|^2,
 \end{aligned} \tag{27}$$

where  $\bar{K}_3 = 2\gamma(1 + 4\gamma\|P_2\|)\|P_2\| + 8\|P_2\|^2 > 0$  is independent of the domination gains  $L$  and  $H$ .

*Part III: Determination of Domination Gains.* According to above arguments, it follows that

$$\begin{aligned}
 x_1 &= \xi_1, \\
 x_i &= \frac{1}{L^{i-1}} \varepsilon_i + \frac{H^{i-1}}{L^{i-1}} \xi_i, \quad i = 2, \dots, n.
 \end{aligned} \tag{28}$$

Using Lemma 3, there is

$$\begin{aligned}
 x_i^2 &= \left( \frac{1}{L^{i-1}} \varepsilon_i + \frac{H^{i-1}}{L^{i-1}} \xi_i \right)^2 \\
 &\leq \frac{2}{L^{2(i-1)}} \|\varepsilon\|^2 + \frac{2H^{2(i-1)}}{L^{2(i-1)}} \|\xi\|^2,
 \end{aligned} \tag{29}$$

and putting (29) together with (27), we have

$$\begin{aligned}
 \dot{V}_\xi &\leq -\frac{H}{L} (1 - 2b_n |1 - \theta(t)| \cdot \|P_2\|) \|\xi\|^2 + \frac{1}{4L} \|\varepsilon\|^2 \\
 &\quad + \frac{H}{L} \left( \frac{\bar{K}_3}{H} + \frac{\bar{K}_1}{L} \right) \|\xi\|^2 + 2\bar{K}_2 \sum_{i=3}^n \frac{1}{L^{2(i-2)}} \|\varepsilon\|^2 \\
 &\quad + 2\bar{K}_2 \sum_{i=3}^n \frac{H^{2(i-1)}}{L^{2(i-2)}} \|\xi\|^2 + \bar{K}_2 L^2 \|z\|^2 \\
 &\leq -\frac{H}{L} (1 - 2b_n |1 - \theta(t)| \cdot \|P_2\|) \|\xi\|^2 \\
 &\quad + \frac{H}{L} \left( \frac{\widehat{K}_3}{H} + \frac{\widehat{K}_1}{L} \right) \|\xi\|^2 + \frac{1}{L^2} \widehat{K}_4 \|\varepsilon\|^2 \\
 &\quad + \widehat{K}_2 L^2 \|z\|^2 + \frac{1}{4L} \|\varepsilon\|^2,
 \end{aligned} \tag{30}$$

where  $\widehat{K}_1 = \bar{K}_1 + 2\bar{K}_2(H^3 + \dots + H^{2n-3}) \geq 0$ ,  $\widehat{K}_2 = \bar{K}_2 \geq 0$ ,  $\widehat{K}_3 = \bar{K}_3 > 0$ ,  $\widehat{K}_4 = 2(n-2)\bar{K}_2 \geq 0$ . Now, we choose the allowable sensitivity error  $\bar{\theta}$  as

$$\bar{\theta} < \bar{\theta} = \frac{1}{2b_n \|P_2\|}. \tag{31}$$

Because of  $|1 - \theta| \leq \bar{\theta}$ , one has

$$1 - 2b_n |1 - \theta| \cdot \|P_2\| \geq 1 - 2b_n \bar{\theta} \|P_2\| \triangleq \beta. \tag{32}$$

Obviously,  $0 < \beta < 1$  and (30) can be rewritten as

$$\begin{aligned}
 \dot{V}_\xi &\leq -\frac{H}{L} \beta \|\xi\|^2 + \frac{H}{L} \left( \frac{\widehat{K}_3}{H} + \frac{\widehat{K}_1}{L} \right) \|\xi\|^2 + \frac{1}{L^2} \widehat{K}_4 \|\varepsilon\|^2 \\
 &\quad + \widehat{K}_2 L^2 \|z\|^2 + \frac{1}{4L} \|\varepsilon\|^2.
 \end{aligned} \tag{33}$$

Similarly, substituting (29) into (16) yields

$$\begin{aligned}
\dot{V}_\varepsilon &\leq -\frac{1}{2L} \|\varepsilon\|^2 + \frac{K_2}{L} \|\xi\|^2 + \frac{K_1}{L^2} \|\varepsilon\|^2 \\
&\quad + \frac{1}{2} cnL^{2n} \|P_1\| \|z\|^2 + 2 \sum_{i=3}^n \frac{K_i}{L^2} \|\varepsilon\|^2 \\
&\quad + 2 \sum_{i=3}^n \frac{K_i H^{2(i-1)}}{L^2} \|\xi\|^2 \\
&\leq -\frac{1}{2L} \|\varepsilon\|^2 + \frac{1}{L^2} \widehat{K}_5 \|\varepsilon\|^2 + \frac{1}{L} \widehat{K}_6 \|\xi\|^2 + \frac{H \widehat{K}_7}{L^2} \|\xi\|^2 \\
&\quad + \widehat{K}_8 L^{2n} \|z\|^2,
\end{aligned} \tag{34}$$

where  $\widehat{K}_5 = K_1 + 2(K_3 + \dots + K_n) \geq 0$ ,  $\widehat{K}_6 = K_2 > 0$ ,  $\widehat{K}_7 = 2(K_3 H^3 + \dots + K_n H^{2n-3}) \geq 0$ ,  $\widehat{K}_8 = (1/2)cn\|P_1\| \geq 0$ . Applying Assumption 5 and the property of Lipschitz function, one has

$$\begin{aligned}
\frac{\partial U}{\partial z} f_0(t, z, x, u) &= \frac{\partial U}{\partial z} f_0(t, z, x, u) \\
&\quad - \frac{\partial U}{\partial z} f_0(t, z, 0, u) \\
&\quad + \frac{\partial U}{\partial z} f_0(t, z, 0, u) \\
&\leq \left\| \frac{\partial U}{\partial z} \right\| \\
&\quad \cdot \|f_0(t, z, x, u) - f_0(t, z, 0, u)\| \\
&\quad + \frac{\partial U}{\partial z} f_0(t, z, 0, u) \\
&\leq \bar{c}_2 \|z\| \cdot \|x\| - c_1 \|z\|^2,
\end{aligned} \tag{35}$$

where  $\bar{c}_2$  is a positive constant. By Lemma 1, it is easy to obtain that  $\|x\| \leq |x_1| + \dots + |x_n|$ , and, according to Lemma 2, the following inequalities hold:

$$\begin{aligned}
&\bar{c}_2 \|z\| \cdot (|x_2| + \dots + |x_n|) \\
&\leq \frac{c_1}{2} \|z\|^2 + \frac{\bar{c}_2^2}{2c_1} (x_2^2 + \dots + x_n^2), \\
&\bar{c}_2 \|z\| \cdot |x_1| \leq \frac{\bar{c}_2^2}{2L} x_1^2 + \frac{L}{2} \|z\|^2.
\end{aligned} \tag{36}$$

Substituting (36) into (35), one has

$$\begin{aligned}
\frac{\partial U}{\partial z} f_0(t, z, x, u) &\leq -\left(\frac{c_1}{2} - \frac{L}{2}\right) \|z\|^2 \\
&\quad + \frac{\bar{c}_2^2}{2c_1} (x_2^2 + \dots + x_n^2) + \frac{\bar{c}_2^2}{2L} x_1^2.
\end{aligned} \tag{37}$$

According to (29) and the definition of norms, it is easy to deduce that

$$\begin{aligned}
x_1^2 &\leq \|\xi\|^2, \\
x_2^2 + x_3^2 + \dots + x_n^2 &\leq \frac{2(n-1)}{L^2} \|\varepsilon\|^2 + \frac{H}{L^2} 2\widehat{K}_9 \|\xi\|^2,
\end{aligned} \tag{38}$$

where  $\widehat{K}_9 = H + H^3 + \dots + H^{2n-3}$ ; therefore (37) can be further expressed as

$$\begin{aligned}
\frac{\partial U}{\partial z} f_0(t, z, x, u) &\leq -\left(\frac{c_1}{2} - \frac{L}{2}\right) \|z\|^2 + \frac{\bar{c}_2^2 (n-1)}{c_1 L^2} \|\varepsilon\|^2 \\
&\quad + \left(\frac{\bar{c}_2^2 \widehat{K}_9 H}{c_1 L^2} + \frac{\bar{c}_2^2}{2L}\right) \|\xi\|^2.
\end{aligned} \tag{39}$$

Consider positive-definite and radially unbounded function as follows:

$$V = U + V_\varepsilon + V_\xi, \tag{40}$$

and substituting (33), (34), and (39) into (40), there is

$$\begin{aligned}
\dot{V} &\leq -\left(\frac{c_1}{2} - \frac{L}{2} - \widehat{K}_8 L^{2n} - \widehat{K}_2 L^2\right) \|z\|^2 \\
&\quad - \frac{1}{L} \left(\frac{1}{4} - \frac{\widehat{K}_5 + \widehat{K}_4}{L} - \frac{2\bar{c}_2^2 (n-1)}{L}\right) \|\varepsilon\|^2 \\
&\quad - \frac{H}{L} \left(\beta - \frac{\widehat{K}_6 + \widehat{K}_3}{H} - \frac{\widehat{K}_1 + \widehat{K}_7}{L} - \frac{\bar{c}_2^2}{2H} - \frac{\bar{c}_2^2 \widehat{K}_9}{L}\right) \\
&\quad \cdot \|\xi\|^2.
\end{aligned} \tag{41}$$

In order to ensure that  $\dot{V} \leq 0$ , we choose the domination gains  $L$  and  $H$  as follows. Firstly,

$$\beta - \frac{\widehat{K}_6 + \widehat{K}_3}{H} - \frac{\bar{c}_2^2}{2H} \geq \frac{\beta}{2}, \tag{42}$$

implying that

$$H \geq \frac{2\widehat{K}_3 + 2\widehat{K}_6 + \bar{c}_2^2}{\beta}, \tag{43}$$

and, with  $H \geq 1$  in hand, one deduces

$$H \geq \max \left\{ 1, \frac{2\widehat{K}_3 + 2\widehat{K}_6 + \bar{c}_2^2}{\beta} \right\}. \tag{44}$$

As consequence, (41) can be rewritten as

$$\begin{aligned}
\dot{V} &\leq -\left(\frac{c_1}{2} - \frac{L}{2} - \widehat{K}_8 L^{2n} - \widehat{K}_2 L^2\right) \|z\|^2 \\
&\quad - \frac{1}{L} \left(\frac{1}{4} - \frac{\widehat{K}_5 + \widehat{K}_4}{L} - \frac{2\bar{c}_2^2 (n-1)}{L}\right) \|\varepsilon\|^2 \\
&\quad - \frac{H}{L} \left(\frac{\beta}{2} - \frac{\widehat{K}_1 + \widehat{K}_7}{L} - \frac{\bar{c}_2^2 \widehat{K}_9}{L}\right) \|\xi\|^2.
\end{aligned} \tag{45}$$

Secondly, we can select  $L$  to satisfy the following inequalities:

$$\begin{aligned} \frac{1}{4} - \frac{\widehat{K}_5 + \widehat{K}_4}{L} - \frac{2\widehat{c}_2^2(n-1)}{L} &\geq \frac{\beta}{4}, \\ \frac{\beta}{2} - \frac{\widehat{K}_1 + \widehat{K}_7}{L} - \frac{\widehat{c}_2^2\widehat{K}_9}{L} &\geq \frac{\beta}{4}, \end{aligned} \quad (46)$$

and, in light of  $L \geq 1$ , it is straightforward to show that

$$L \geq \max \left\{ 1, \frac{4\widehat{K}_1 + 4\widehat{K}_7 + 4\widehat{c}_2^2\widehat{K}_9}{\beta}, \frac{4\widehat{K}_4 + 4\widehat{K}_5 + 8\widehat{c}_2^2(n-1)}{1-\beta} \right\}, \quad (47)$$

and  $c_1$  satisfies

$$c_1 = \frac{\beta}{4} + c_1^*, \quad c_1^* \geq 2(\widehat{K}_8 L^{2n} + \widehat{K}_2 L^2) + L. \quad (48)$$

Under above choice of domination gains, it is clear that

$$\dot{V} \leq -\frac{\beta}{4} \|z\|^2 - \frac{\beta}{4L} \|\xi\|^2 - \frac{\beta}{4L} \|\varepsilon\|^2. \quad (49)$$

*Part IV: Stability Analysis.* Consider transformed systems (9), (20), and (21). By the existence and continuity of solution, the closed-loop system state composed of  $Y(t) = [z^T, x^T, \widehat{x}^T]^T$  can be defined on a time interval  $[0, t_m)$ , where  $t_m > 0$  may be a finite constant or infinity.

(i) *For the Boundedness of  $Y(t)$ .* Due to the fact that  $v_1(z) \leq U(z) \leq v_2(z)$ ,  $\lambda_{\min}(P)\|x\|^2 \leq x^T P x \leq \lambda_{\max}(P)\|x\|^2$ , where  $v_1$  and  $v_2$  are  $\mathcal{K}_\infty$  functions; we obtain

$$\begin{aligned} V &= U + V_\varepsilon + V_\xi \\ &\geq v_1(z) + \lambda_{\min}(P_1) \|\varepsilon\|^2 + \lambda_{\min}(P_2) \|\xi\|^2 \\ &\geq v_1(z) + \min\{\lambda_{\min}(P_1), \lambda_{\min}(P_2)\} \|\omega(t)\|^2 \\ &\triangleq \varphi_1(\|\omega(t)\|), \end{aligned} \quad (50)$$

and

$$\begin{aligned} V &= U + V_\varepsilon + V_\xi \\ &\leq v_2(z) + \lambda_{\max}(P_1) \|\varepsilon\|^2 + \lambda_{\max}(P_2) \|\xi\|^2 \\ &\leq v_2(z) + \max\{\lambda_{\max}(P_1), \lambda_{\max}(P_2)\} \|\omega(t)\|^2 \\ &\triangleq \varphi_2(\|\omega(t)\|), \end{aligned} \quad (51)$$

where  $\omega(t) = [\varepsilon^T(t), \xi^T(t)]^T$ ,  $\widehat{\omega}(t) = [z^T, \varepsilon^T(t), \xi^T(t)]^T$ , and  $\varphi_1, \varphi_2$  are  $\mathcal{K}_\infty$  functions.

For any  $\epsilon > 0$ , noting that  $\lim_{s \rightarrow +\infty} \varphi_1(s) = +\infty$ , one can always find a constant  $\beta = \beta(\epsilon) > \epsilon > 0$ , such that  $\varphi_2(\epsilon) \leq \varphi_1(\beta)$ . From (49), it follows that  $V(\|\widehat{\omega}(t)\|) \leq V(\|\widehat{\omega}(0)\|)$ ,  $\forall t \in [0, t_m)$ . Then, if  $\|\widehat{\omega}(0)\| < \epsilon$ , it holds that

$$\begin{aligned} \varphi_1(\|\widehat{\omega}(t)\|) &\leq V(\|\widehat{\omega}(t)\|) \leq V(\|\widehat{\omega}(0)\|) \\ &\leq \varphi_2(\|\widehat{\omega}(0)\|) < \varphi_2(\epsilon) \leq \varphi_1(\beta), \end{aligned} \quad (52)$$

$$\forall t \in [0, t_m),$$

which implies that  $\|\widehat{\omega}(t)\| < \beta$ ,  $\forall t \in [0, t_m)$ ; that is,  $\|\widehat{\omega}(t)\|$  is bounded. Therefore, by virtue of estimation errors and coordinates transform, it is easy to get that the state  $Y(t) = [z^T, x^T, \widehat{x}^T]^T$  is bounded on  $[0, t_m)$  as well.

(ii)  $t_m = +\infty$ . This claim can be shown by contradiction; if  $t_m$  is finite, then  $t_m$  would be a finite escape time; that is, the state  $Y(t)$  would tend to  $\infty$  as  $t = t_m$ . However, the continuity of solution guarantees the boundedness of  $Y(t)$  at  $t = t_m$ , since  $Y(t)$  is bounded on  $[0, t_m)$ . This is clearly a contradiction. Therefore, the state of the closed-loop system is uniformly bounded over  $[0, +\infty)$ .

(iii)  $\lim_{t \rightarrow +\infty} x(t) = 0$  and  $\lim_{t \rightarrow +\infty} z(t) = 0$ . Above all, it is clear that

$$\begin{aligned} 0 &\leq \int_0^t \left( \frac{\beta}{4} \|z\|^2 + \frac{\beta}{4L} \|\varepsilon\|^2 + \frac{\beta}{4L} \|\xi\|^2 \right) ds \\ &\leq -\int_0^t \dot{V}(\widehat{\omega}(s)) ds < V(\widehat{\omega}(0)) < +\infty, \quad \forall t \geq 0, \end{aligned} \quad (53)$$

which implies that  $\int_0^\infty ((\beta/4)\|z\|^2 + (\beta/4L)\|\varepsilon\|^2 + (\beta/4L)\|\xi\|^2) ds$  exists and is finite. On the other hand, the boundedness of  $\widehat{\omega}(t)$  over  $[0, +\infty)$  means that  $\dot{\widehat{\omega}}(t)$  is uniformly bounded in  $t$  over  $[0, +\infty)$ . Thus,  $\widehat{\omega}(t)$  is uniformly continuous in  $t$  over  $[0, +\infty)$  and so is  $\widehat{\omega}^2(t)$ . Using well-known Barbalat's Lemma in [22], one obtains  $\lim_{t \rightarrow +\infty} z_i^2(t) = 0$ ,  $\lim_{t \rightarrow +\infty} \xi_i^2(t) = 0$ , and  $\lim_{t \rightarrow +\infty} \varepsilon_i^2(t) = 0$ , which shows that  $\lim_{t \rightarrow +\infty} z(t) = 0$ ,  $\lim_{t \rightarrow +\infty} \xi(t) = 0$ , and  $\lim_{t \rightarrow +\infty} \varepsilon(t) = 0$ . Finally, from (29), it is easy to see that  $\lim_{t \rightarrow +\infty} x(t) = 0$ . This completes the proof.  $\square$

*Remark 10.* A double-domination method is proposed to handle the time-varying output function and nonlinearities in the proof of Theorem 9; that is, two domination gains  $H$  and  $L$  are used to dominate time-varying function  $\theta(t)$  and nonlinearities  $f_i$ , respectively.

*Remark 11.* It should be noted from  $\tilde{\theta} = 1/2b_n\|P_2\|$  that the upper bound  $\tilde{\theta}$  depends on coefficients  $b_1, \dots, b_n$  for the Hurwitz polynomial  $p_2(s)$ . When  $b_1, \dots, b_n$  are specified, the corresponding matrix  $P_2$  as well as the upper bound  $\tilde{\theta}$  can be computed. For example,  $\tilde{\theta} = 0.4420$ , for  $n = 2$ ;  $\tilde{\theta} = 0.1501$ , for  $n = 3$ .

*3.2. Extension to Lower-Triangular Case.* Some subsystems do not satisfy upper-triangular structure in practical application, so we extend the subsystems to lower-triangular form and impose following assumptions on system (4).

*Assumption 12.* For  $i = 1, \dots, n$ , there exists a constant  $c \geq 0$  such that

$$|f_i| \leq c(\|z\| + |x_1| + \dots + |x_i|). \quad (54)$$

**Theorem 13.** For a class of nonlinear cascade system (4) under Assumptions 4, 5, and 12, there exists an output feedback controller, such that states of the closed-loop system are uniformly bounded over  $[0, +\infty)$  and  $\lim_{t \rightarrow +\infty} x(t) = 0$ .

*Proof.* The proof is analogous to the proof of Theorem 9 with an obvious modification. To facilitate comparison, we select same notations as Theorem 9 and many similarities will be omitted.

Firstly, we construct the similar observer as (7)

$$\begin{aligned}\hat{x}_i &= \hat{x}_{i+1} - L^i a_i \hat{x}_1, \quad i = 1, \dots, n-1, \\ \hat{x}_n &= u - L^n a_n \hat{x}_1,\end{aligned}\quad (55)$$

where  $a_i > 0$  and  $L > 1$ . With the help of the previous process, define the estimation error

$$\varepsilon_i = \frac{x_i - \hat{x}_i}{L^{i-1}}, \quad i = 1, \dots, n, \quad (56)$$

and it is straightforward to show that

$$\dot{\varepsilon} = LA_\varepsilon \varepsilon + LG_\varepsilon x_1 + F, \quad (57)$$

and since the definitions of the associated symbol are same as (9), we just give different symbol in the following paper:  $F = [f_1(\cdot), f_2(\cdot)/L, \dots, f_n(\cdot)/L^{n-1}]^T \in \mathbb{R}^{n \times 1}$ . Consider same scalar function  $V_\varepsilon(\varepsilon) = \varepsilon^T P_1 \varepsilon$ , which is proper and radially unbounded. Evidently, following (16), we arrive at

$$\begin{aligned}\dot{V}_\varepsilon &\leq (LK_2 + K_3) x_1^2 + \frac{K_4}{L^2} x_2^2 + \dots + \frac{K_{n+2}}{L^{2n-2}} x_n^2 \\ &\quad - \frac{L}{2} \|\varepsilon\|^2 + K_1 \|\varepsilon\|^2 + K_3 \|z\|^2,\end{aligned}\quad (58)$$

where  $K_1 = cn(n+3)\|P_1\| \geq 0$ ,  $K_2 = 2\|G_\varepsilon\|^2\|P_1\|^2 > 0$ ,  $K_i = (1/2)(n-i+3)c\|P_1\| \geq 0$ ,  $i = 3, \dots, n+2$ , are independent of a domination gain  $L$ .

Secondly, consider system described by

$$\begin{aligned}\dot{x}_1 &= x_2 + f_1(t, z, x, u), \\ \dot{\hat{x}}_i &= \hat{x}_{i+1} + L^i a_i (\varepsilon_1 - x_1), \quad i = 2, \dots, n-1, \\ \dot{\hat{x}}_n &= u + L^n a_n (\varepsilon_1 - x_1).\end{aligned}\quad (59)$$

Then, introduce the following transformations:

$$\begin{aligned}\xi_1 &= x_1, \\ \xi_i &= \frac{\hat{x}_i}{(LH)^{i-1}}, \\ v &= \frac{u}{(LH)^n}, \\ & i = 2, \dots, n,\end{aligned}\quad (60)$$

where  $H \geq 1$  is a domination gain to be determined later. With the help of (60), it is easy to see that system (59) can be rewritten as

$$\begin{aligned}\dot{\xi}_1 &= LH\xi_2 + L\varepsilon_2 + f_1(t, z, x, u), \\ \dot{\xi}_i &= LH\xi_{i+1} + \frac{La_i}{H^{i-1}} (\varepsilon_1 - \xi_1), \quad i = 2, \dots, n-1, \\ \dot{\xi}_n &= LHv + \frac{La_n}{H^{n-1}} (\varepsilon_1 - \xi_1).\end{aligned}\quad (61)$$

If the control law is designed as (20), then substituting (20) into (61) leads to

$$\begin{aligned}\dot{\xi} &= LHA_\xi \xi + LHG_\xi b_n (1 - \theta(t)) \xi_1 + LB_2 \varepsilon_2 \\ &\quad + \frac{L}{H} B_1 (\varepsilon_1 - \xi_1) + \bar{F},\end{aligned}\quad (62)$$

where the definitions of notations are the same as (21). Consider the same quadratic function

$$V_\xi(\xi) = \xi^T P_2 \xi, \quad (63)$$

and, after calculations, we arrive at

$$\begin{aligned}\dot{V}_\xi &\leq -LH\beta \|\xi\|^2 + \frac{L}{4} \|\varepsilon\|^2 + LH \left( \frac{\bar{K}_1}{H} + \frac{\bar{K}_2}{L} \right) \|\xi\|^2 \\ &\quad + \bar{K}_3 \|z\|^2,\end{aligned}\quad (64)$$

where  $\bar{K}_1 = 2\gamma(1+4\gamma\|P_2\|)\|P_2\| + 8\|P_2\|^2 > 0$ ,  $\bar{K}_2 = 3c\|P_2\| \geq 0$ ,  $\bar{K}_3 = c\|P_2\| \geq 0$  are independent of the domination gains  $L$  and  $H$ . It follows from (56) and (60) that

$$\begin{aligned}x_1 &= \xi_1, \\ x_i &= L^{i-1} \varepsilon_i + \hat{x}_i = L^{i-1} \varepsilon_i + (LH)^{i-1} \xi_i, \quad i = 2, \dots, n.\end{aligned}\quad (65)$$

Hence, by Lemma 2, it is easy to obtain the following inequality:

$$\begin{aligned}\frac{1}{L^{2(i-1)}} x_i^2 &= \frac{1}{L^{2(i-1)}} (L^{i-1} \varepsilon_i + (LH)^{i-1} \xi_i)^2 \\ &\leq \frac{1}{L^{2(i-1)}} 2 (L^{2(i-1)} \varepsilon_i^2 + (LH)^{2(i-1)} \xi_i^2) \\ &\leq 2 \|\varepsilon\|^2 + 2H^{2(i-1)} \|\xi\|^2, \quad i = 2, \dots, n.\end{aligned}\quad (66)$$

Putting together (66) and (58), there would always hold

$$\begin{aligned}\dot{V}_\varepsilon(\varepsilon) &\leq -\frac{L}{2} \|\varepsilon\|^2 + \widehat{K}_1 \|\varepsilon\|^2 + (L\widehat{K}_2 + H\widehat{K}_4) \|\xi\|^2 \\ &\quad + \widehat{K}_3 \|z\|^2,\end{aligned}\quad (67)$$

where  $\widehat{K}_1 = K_1 + 2(K_4 + \dots + K_{n+2}) \geq 0$ ,  $\widehat{K}_2 = K_2 + K_3 > 0$ ,  $\widehat{K}_3 = K_3 \geq 0$ ,  $\widehat{K}_4 = 2(K_4 H + \dots + K_{n+2} H^{2n-3}) \geq 0$ . Furthermore, following (39), we arrive at

$$\begin{aligned}\frac{\partial U}{\partial z} f_0 &\leq -\left( \frac{c_1}{2} - \frac{L^2 + \dots + L^{2(n-1)}}{2} \right) \|z\|^2 \\ &\quad + H\widehat{K}_5 \|\xi\|^2 + (n-1)\bar{c}_2^2 \|\varepsilon\|^2,\end{aligned}\quad (68)$$

where  $\widehat{K}_5 = \overline{c}_2^2(H + H^3 + \dots + H^{2n-3})$ . Finally, let

$$V = U + V_\varepsilon + V_\xi, \quad (69)$$

and a direct calculation yields

$$\begin{aligned} \dot{V} \leq & -\left(\frac{c_1}{2} - \frac{L^2 + \dots + L^{2(n-1)}}{2} - \widehat{K}_3 - \overline{K}_3\right) \|z\|^2 \\ & - L \left(\frac{1}{4} - \frac{\widehat{K}_1 + \overline{c}_2^2(n-1)}{L}\right) \|\varepsilon\|^2 \\ & - LH \left(\beta - \frac{\overline{K}_1 + \widehat{K}_2}{H} - \frac{\overline{K}_2 + \widehat{K}_4 + \widehat{K}_5}{L}\right) \|\xi\|^2. \end{aligned} \quad (70)$$

We choose domination gains  $L$  and  $H$  as

$$\begin{aligned} H & \geq \max \left\{ 1, \frac{2\overline{K}_1 + 2\widehat{K}_2}{\beta} \right\}, \\ L & \geq \max \left\{ 1, \frac{4\widehat{K}_1 + 4\overline{c}_2^2(n-1)}{1-\beta}, \frac{4\overline{K}_2 + 4\widehat{K}_4 + 4\widehat{K}_5}{\beta} \right\}, \end{aligned} \quad (71)$$

where  $c_1$  satisfies

$$c_1 = c_1^* + \frac{\beta}{4}, \quad c_1^* \geq 2\overline{K}_3 + 2\widehat{K}_3 + L^2 + \dots + L^{2n-3}, \quad (72)$$

and  $\overline{c}_2$  is a positive constant; there is

$$\dot{V} \leq -\frac{\beta}{4} \|z\|^2 - \frac{\beta}{4} \|\varepsilon\|^2 - \frac{\beta}{4} \|\xi\|^2. \quad (73)$$

The process of stability analysis is analogous to Theorem 9 and is omitted for the sake of space. This completes the proof.  $\square$

*Remark 14.* The process of Theorems 9 and 13 means that Assumptions 4 and 5 are suitable for two cases of triangular systems. The contribution of these assumptions is that  $f_0$  contains all of states of nonlinear cascade systems. Meanwhile, a unified Lyapunov function is successfully constructed and we proposed a novel observer that is different from [24, 26].

## 4. Simulation Example

As application of the design method, two examples are provided as follows.

*Example 1.* Consider nonlinear cascade system:

$$\begin{aligned} \dot{z}(t) &= -2z(t) - x_2(t), \\ \dot{x}_1(t) &= x_2(t) + x_3(t) - \sin(x_1)z(t), \\ \dot{x}_2(t) &= x_3(t) + z(t), \\ \dot{x}_3(t) &= u(t) + z(t), \\ y(t) &= \theta(t)x_1(t), \end{aligned} \quad (74)$$

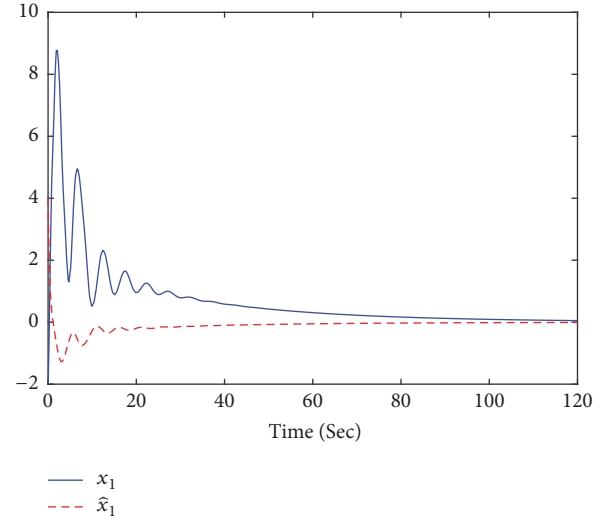


FIGURE 1: The curves of states  $x_1$  and  $\widehat{x}_1$ .

where  $\theta(t) = 1 + 0.15|\sin(6t)|$ . Obviously, systems satisfy Assumptions 4–6 with  $c = 1$ ,  $c_1 = 204$ , and  $c_2 = 20$ . And we choose  $p_2(s) = (s + 0.4)^3$ ; that is,  $b_1 = 1.2$ ,  $b_2 = 0.48$ ,  $b_3 = 0.064$ , and  $\overline{\theta} = 0.1501$ . Besides, for the observer design, we select  $\overline{\theta} = 0.15 < \overline{\theta}$ ,  $a_1 = 4$ ,  $a_2 = 3$ , and  $a_3 = 1$ . In consequence, the control law is given as follows:

$$\begin{aligned} u(t) &= -\frac{b_3 H^3}{L^3} y - \frac{b_2 H^2}{L^2} \widehat{x}_2 - \frac{b_1 H}{L} \widehat{x}_3, \\ \dot{\widehat{x}}_1(t) &= \widehat{x}_2(t) - \frac{a_1}{L} \widehat{x}_1(t), \\ \dot{\widehat{x}}_2(t) &= \widehat{x}_3(t) - \frac{a_2}{L^2} \widehat{x}_1(t), \\ \dot{\widehat{x}}_3(t) &= u(t) - \frac{a_3}{L^3} \widehat{x}_1(t), \end{aligned} \quad (75)$$

where  $L = 2$  and  $H = 7$ . In simulation, initial values are chosen as

$$\begin{aligned} [z, x_1(0), x_2(0), x_3(0), \widehat{x}_1(0), \widehat{x}_2(0), \widehat{x}_3(0)]^T \\ = [-1, -2, 1, 4, 4, -2, -1]^T, \end{aligned} \quad (76)$$

and one gets Figures 1–4, which illustrate that the control law (20) is effective.

*Example 2.* Consider the following nonlinear cascade system:

$$\begin{aligned} \dot{z}(t) &= -z(t) + x_1(t), \\ \dot{x}_1(t) &= x_2(t) + \sin(x_1)z(t), \\ \dot{x}_2(t) &= u(t) + x_1(t), \\ y(t) &= \theta(t)x_1(t), \end{aligned} \quad (77)$$

where  $\theta(t) = 1 + 0.44|\sin(6t)|$ . Evidently, Assumptions 4, 5, and 12 are satisfied with  $c = 1$ ,  $c_1 = 18$ , and  $c_2 = 1$ . And we

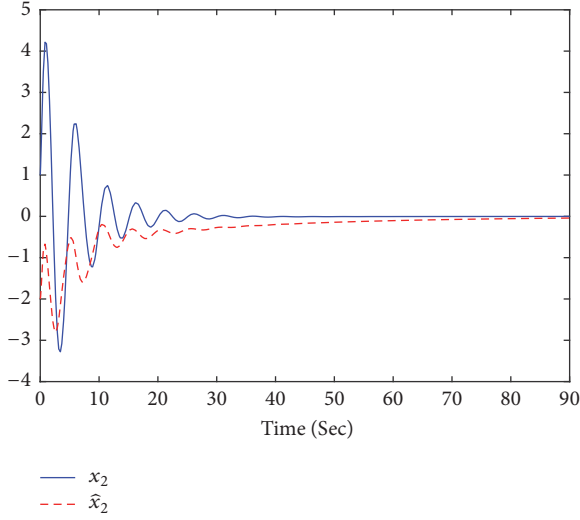


FIGURE 2: The curves of states  $x_2$  and  $\hat{x}_2$ .

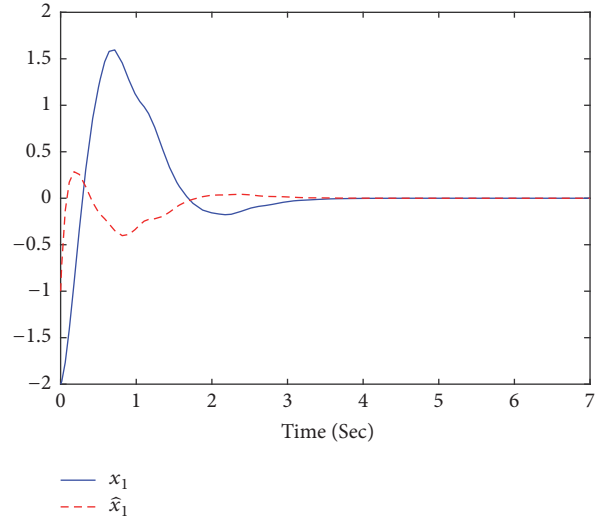


FIGURE 5: The curves of states  $x_1$  and  $\hat{x}_1$ .

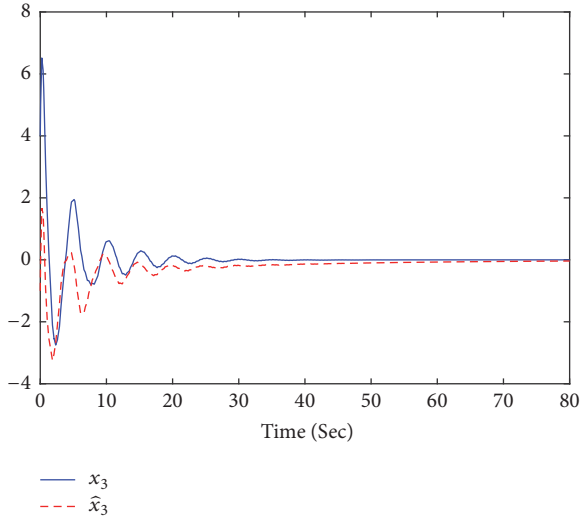


FIGURE 3: The curves of states  $x_3$  and  $\hat{x}_3$ .

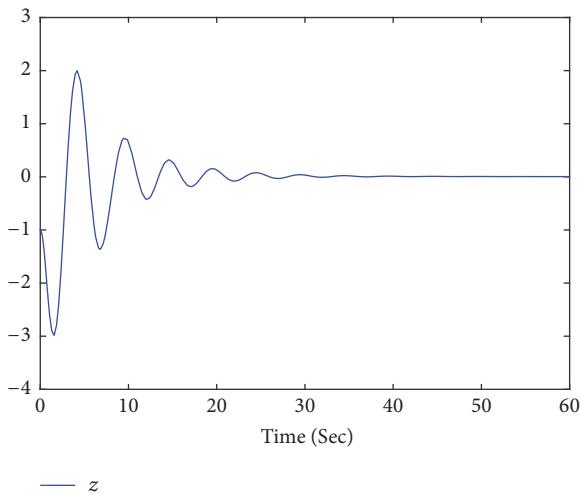


FIGURE 4: The curve of state  $z$ .

choose  $p_2(s) = (s + 0.4)^2$ ; that is,  $b_1 = 0.8$  and  $b_2 = 0.16$ . After sample calculation,  $\bar{\theta} = 0.4420$  and select  $\bar{\theta} = 0.44 < \tilde{\theta}$ ,  $a_1 = 5$ , and  $a_2 = 1$ ; we construct an output feedback controller as follows:

$$\begin{aligned}
 u(t) &= -b_2(LH)^2 y - b_1 LH \hat{x}_2, \\
 \dot{\hat{x}}_1(t) &= \hat{x}_2(t) - a_1 L \hat{x}_1(t), \\
 \dot{\hat{x}}_2(t) &= u(t) - a_2 L^2 \hat{x}_1(t),
 \end{aligned} \tag{78}$$

where  $L = 4$  and  $H = 5$ . In the simulation, we choose the initial values as  $[z(0), x_1(0), x_1(0), \hat{x}_1(0), \hat{x}_2(0)]^T = [3, -2, 4, -1, 1.5]^T$ ; one can obtain the simulation results as shown in Figures 5–8, which exhibit the effectiveness of the control scheme.

### 5. Conclusions

This paper solves the problem of global output feedback stabilization for the nonlinear cascade systems with time-varying output function. The construction of the output feedback controller is based on the double-domination method. There still exist some problems to be investigated. For example, (I) [34–36] solved the problem of finite-time stabilization; it is unclear whether scheme can be applied to solve the finite-time stabilization for nonlinear systems with time-varying output function. (II) References [37, 38] proposed the output feedback controller that ensures that the equilibrium is globally asymptotically stable in probability. Then, is it possible to achieve the stabilization of nonlinear stochastic systems by the proposed strategy of this paper? (III) References [39–45] advanced the solution to the stabilization problem of time-delay systems. However, it is unclear whether this method could be used to address the stabilization of time-delay nonlinear systems. (IV) References [46–48] focus on global adaptive state-feedback stabilization for a class of high-order uncertain nonlinear systems. When  $c$  in Assumption 6

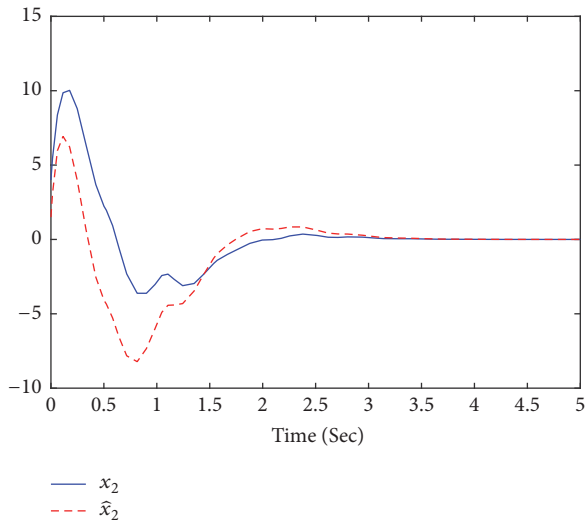


FIGURE 6: The curves of states  $x_2$  and  $\hat{x}_2$ .

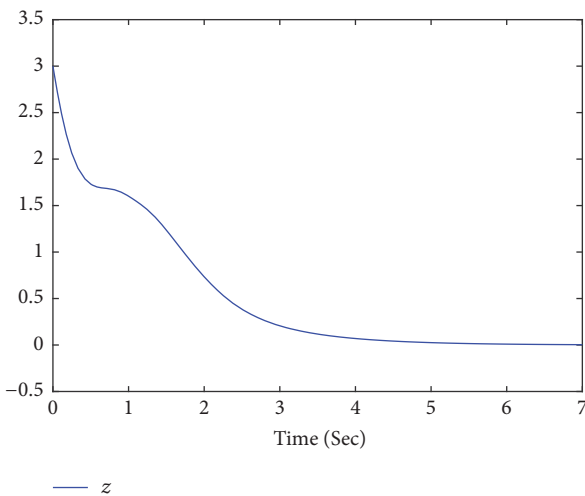


FIGURE 7: The curve of state  $z$ .

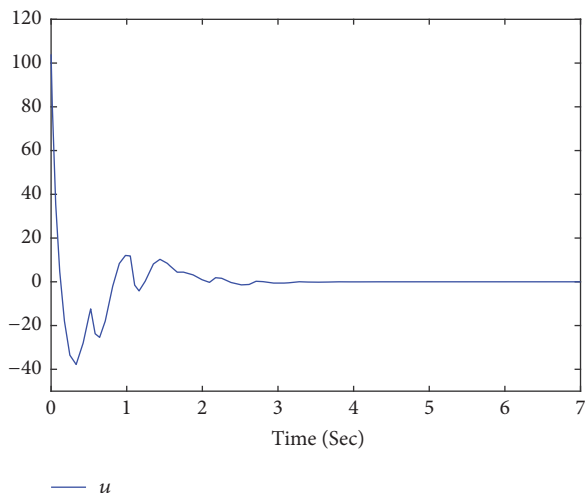


FIGURE 8: The curve of control  $u$ .

is unknown, can the approach of this paper be used to solve the problem of adaptive stabilization?

### Data Availability

The data used to support the findings of this study are available from the corresponding author upon request.

### Conflicts of Interest

The authors declare that they have no conflicts of interest.

### Acknowledgments

This paper is supported by the National Natural Science Foundation of China (61773237, 61374004, and 61473170), China Postdoctoral Science Foundation Funded Project (2017M610414), Shandong Province Quality Core Curriculum of Postgraduate Education (SDYKCI7079), Zhejiang Provincial Natural Science Foundation (LY16E050003), and the Ministry of Science and Technology, Taiwan, under Grant (MOST 106-2218-E-006-026-).

### References

- [1] C. Qian and W. Lin, "Output feedback control of a class of nonlinear systems: a nonseparation principle paradigm," *Institute of Electrical and Electronics Engineers Transactions on Automatic Control*, vol. 47, no. 10, pp. 1710–1715, 2002.
- [2] C. Qian, "A homogeneous domination approach for global output feedback stabilization of a class of nonlinear systems," in *Proceedings of the American Control Conference*, pp. 4708–4715, Portland, Ore, USA, June 2005.
- [3] Z.-Y. Sun, L.-R. Xue, and K. Zhang, "A new approach to finite-time adaptive stabilization of high-order uncertain nonlinear system," *Automatica*, vol. 58, pp. 60–66, 2015.
- [4] N. Wang, C. Qian, and Z.-Y. Sun, "Global asymptotic output tracking of nonlinear second-order systems with power integrators," *Automatica*, vol. 80, pp. 156–161, 2017.
- [5] Z.-Y. Sun, M.-M. Yun, and T. Li, "A new approach to fast global finite-time stabilization of high-order nonlinear system," *Automatica*, vol. 81, pp. 455–463, 2017.
- [6] C.-R. Zhao and X.-J. Xie, "Output feedback stabilization using small-gain method and reduced-order observer for stochastic nonlinear systems," *Institute of Electrical and Electronics Engineers Transactions on Automatic Control*, vol. 58, no. 2, pp. 523–529, 2013.
- [7] Z.-Y. Sun, Z.-G. Liu, and X.-H. Zhang, "New results on global stabilization for time-delay nonlinear systems with low-order and high-order growth conditions," *International Journal of Robust and Nonlinear Control*, vol. 25, no. 6, pp. 878–899, 2015.
- [8] Q. Tan, T. Li, Z. Sun, and Q. Meng, "Output tracking control for generalized high-order nonlinear system with almost disturbance decoupling," *International Journal of Control, Automation, and Systems*, vol. 15, no. 6, pp. 2570–2578, 2017.
- [9] Z.-Y. Sun, T. Li, and S.-H. Yang, "A unified time-varying feedback approach and its applications in adaptive stabilization of high-order uncertain nonlinear systems," *Automatica*, vol. 70, pp. 249–257, 2016.

- [10] T. Li, Z.-Y. Sun, and S.-H. Yang, "Output tracking control for generalised high-order nonlinear system with serious uncertainties," *International Journal of Control*, vol. 90, no. 2, pp. 338–349, 2017.
- [11] B. Yang and W. Lin, "Homogeneous observers, iterative design, and global stabilization of high-order nonlinear systems by smooth output feedback," *Institute of Electrical and Electronics Engineers Transactions on Automatic Control*, vol. 49, no. 7, pp. 1069–1080, 2004.
- [12] C. Qian, "Semi-global stabilization of a class of uncertain nonlinear systems by linear output feedback," *IEEE Transactions on Circuits and Systems II: Express Briefs*, vol. 52, no. 4, pp. 218–222, 2005.
- [13] H. Lei and W. Lin, "Universal adaptive control of nonlinear systems with unknown growth rate by output feedback," *Automatica*, vol. 42, no. 10, pp. 1783–1789, 2006.
- [14] Y. Liu, "Global asymptotic regulation via time-varying output feedback for a class of uncertain nonlinear systems," *SIAM Journal on Control and Optimization*, vol. 51, no. 6, pp. 4318–4342, 2013.
- [15] Y. Man and Y. Liu, "Global output-feedback stabilization for a class of uncertain time-varying nonlinear systems," *Systems & Control Letters*, vol. 90, pp. 20–30, 2016.
- [16] C. Qian and J. Li, "Global output feedback stabilization of upper-triangular nonlinear systems using a homogeneous domination approach," *International Journal of Robust and Nonlinear Control*, vol. 16, no. 9, pp. 441–463, 2006.
- [17] X.-J. Xie and L. Liu, "A homogeneous domination approach to state feedback of stochastic high-order nonlinear systems with time-varying delay," *Institute of Electrical and Electronics Engineers Transactions on Automatic Control*, vol. 58, no. 2, pp. 494–499, 2013.
- [18] G.-D. Zhao and X.-J. Xie, "A homogeneous domination approach to state feedback of stochastic high-order feedforward nonlinear systems," *International Journal of Control*, vol. 86, no. 5, pp. 966–976, 2013.
- [19] X.-J. Xie, N. Duan, and C.-R. Zhao, "A combined homogeneous domination and sign function approach to output-feedback stabilization of stochastic high-order nonlinear systems," *Institute of Electrical and Electronics Engineers Transactions on Automatic Control*, vol. 59, no. 5, pp. 1303–1309, 2014.
- [20] J. Li, C. Qian, and M. T. Frye, "A dual-observer design for global output feedback stabilization of nonlinear systems with low-order and high-order nonlinearities," *International Journal of Robust and Nonlinear Control*, vol. 19, no. 15, pp. 1697–1720, 2009.
- [21] C. Qian and W. Lin, "Recursive observer design, homogeneous approximation, and nonsmooth output feedback stabilization of nonlinear systems," *Institute of Electrical and Electronics Engineers Transactions on Automatic Control*, vol. 51, no. 9, pp. 1457–1471, 2006.
- [22] M. Krstić, I. Kanellakopoulos, and P. Kokotović, *Nonlinear and adaptive control design*, Wiley, New York, NY, USA, 1995.
- [23] A. Isidori, *Nonlinear Control Systems*, Springer, London, UK, 3rd edition, 1989.
- [24] Z.-Y. Chen and J. Huang, "Global output feedback stabilization for uncertain nonlinear systems with output dependent incremental rate," in *Proceedings of the American Control Conference (AAC '04)*, pp. 3047–3052, Boston, Mass, USA, July 2004.
- [25] L. Praly and Z. P. Jiang, "Linear output feedback with dynamic high gain for nonlinear systems," *Systems & Control Letters*, vol. 53, no. 2, pp. 107–116, 2004.
- [26] X. Yan, Y. Liu, and Q. Wang, "Global output-feedback tracking for nonlinear cascade systems with unknown growth rate and control coefficients," *Journal of Systems Science & Complexity*, vol. 28, no. 1, pp. 30–46, 2015.
- [27] G. Li and Y. Lin, "Robust output feedback stabilization of nonlinear systems with low-order and high-order nonlinearities," *International Journal of Robust and Nonlinear Control*, vol. 26, no. 9, pp. 1919–1943, 2016.
- [28] J. Zhai and C. Qian, "Global control of nonlinear systems with uncertain output function using homogeneous domination approach," *International Journal of Robust and Nonlinear Control*, vol. 22, no. 14, pp. 1543–1561, 2012.
- [29] W. Ai, J. Zhai, and S. Fei, "Universal adaptive regulation for a class of nonlinear systems with unknown time delays and output function via output feedback," *Journal of The Franklin Institute*, vol. 350, no. 10, pp. 3168–3187, 2013.
- [30] C. Chen, C. Qian, Z. Sun, and Y. Liang, "Global Output Feedback Stabilization of a Class of Nonlinear Systems with Unknown Measurement Sensitivity," *IEEE Transactions on Automatic Control*, pp. 1-1, 2017.
- [31] C. Zhang, C. Qian, and S. Li, "Global smooth stabilization of a class of feedforward systems under the framework of generalized homogeneity with monotone degrees," *Journal of The Franklin Institute*, vol. 350, no. 10, pp. 3149–3167, 2013.
- [32] H. K. Khalil and J. Grizzle, *Nonlinear Systems*, Macmillan, New York, NY, USA, 1992.
- [33] Z.-Y. Sun, C.-H. Zhang, and Z. Wang, "Adaptive disturbance attenuation for generalized high-order uncertain nonlinear systems," *Automatica*, vol. 80, pp. 102–109, 2017.
- [34] X.-H. Zhang, K. Zhang, and X.-J. Xie, "Finite-time output feedback stabilization of nonlinear high-order feedforward systems," *International Journal of Robust and Nonlinear Control*, vol. 26, no. 8, pp. 1794–1814, 2016.
- [35] M.-M. Jiang and X.-J. Xie, "Adaptive finite-time stabilization of high-order nonlinear systems with dynamic and parametric uncertainties," *Mathematical Problems in Engineering*, Art. ID 5702182, 11 pages, 2016.
- [36] K. Zhang and X.-H. Zhang, "Finite-time stabilisation for high-order nonlinear systems with low-order and high-order nonlinearities," *International Journal of Control*, vol. 88, no. 8, pp. 1576–1585, 2015.
- [37] N. Duan and X.-J. Xie, "Further results on output-feedback stabilization for a class of stochastic nonlinear systems," *Institute of Electrical and Electronics Engineers Transactions on Automatic Control*, vol. 56, no. 5, pp. 1208–1213, 2011.
- [38] Y. Liu, Z. Pan, and S. Shi, "Output feedback control design for strict-feedback stochastic nonlinear systems under a risk-sensitive cost," *Institute of Electrical and Electronics Engineers Transactions on Automatic Control*, vol. 48, no. 3, pp. 509–513, 2003.
- [39] Z.-Y. Sun, S.-H. Yang, and T. Li, "Global adaptive stabilization for high-order uncertain time-varying nonlinear systems with time-delays," *International Journal of Robust and Nonlinear Control*, vol. 27, no. 13, pp. 2198–2217, 2017.
- [40] X.-J. Xie, Z.-J. Li, and K. Zhang, "Semi-global output feedback control for nonlinear systems with uncertain time-delay and output function," *International Journal of Robust and Nonlinear Control*, vol. 27, no. 15, pp. 2549–2566, 2017.
- [41] Z.-Y. Sun, X.-H. Zhang, and X.-J. Xie, "Continuous global stabilisation of high-order time-delay nonlinear systems," *International Journal of Control*, vol. 86, no. 6, pp. 994–1007, 2013.

- [42] S. K. Nguang, "Robust stabilization of a class of time-delay nonlinear systems," *Institute of Electrical and Electronics Engineers Transactions on Automatic Control*, vol. 45, no. 4, pp. 756–762, 2000.
- [43] Z.-B. Song, Z.-Y. Sun, S.-H. Yang, and T. Li, "Global stabilization via nested saturation function for high-order feedforward nonlinear systems with unknown time-varying delays," *International Journal of Robust and Nonlinear Control*, vol. 26, no. 15, pp. 3363–3387, 2016.
- [44] X.-J. Xie and L. Liu, "Further results on output feedback stabilization for stochastic high-order nonlinear systems with time-varying delay," *Automatica*, vol. 48, no. 10, pp. 2577–2586, 2012.
- [45] Z.-Y. Sun, Z.-B. Song, T. Li, and S.-H. Yang, "Output feedback stabilization for high-order uncertain feedforward time-delay nonlinear systems," *Journal of The Franklin Institute*, vol. 352, no. 11, pp. 5308–5326, 2015.
- [46] L.-N. Lv, Z.-Y. Sun, and X.-J. Xie, "Adaptive control for high-order time-delay uncertain nonlinear system and application to chemical reactor system," *International Journal of Adaptive Control and Signal Processing*, vol. 29, no. 2, pp. 224–241, 2015.
- [47] J. Wu, W. Chen, and J. Li, "Global finite-time adaptive stabilization for nonlinear systems with multiple unknown control directions," *Automatica*, vol. 69, pp. 298–307, 2016.
- [48] Z. Sun and Y. Liu, "Adaptive stabilisation for a large class of high-order uncertain non-linear systems," *International Journal of Control*, vol. 82, no. 7, pp. 1275–1287, 2009.

## Research Article

# Consensus Control of Multiagent Systems with High-Order Nonlinear Inaccurate Dynamics and Dynamically Switching Undirected Topologies

Qiang Wang <sup>1,2</sup>, Qingtian Meng,<sup>2</sup> Xiaonan Fang,<sup>3</sup> and Huaxiang Zhang<sup>1</sup>

<sup>1</sup>School of Information Science and Engineering, Shandong Normal University, Jinan 250014, China

<sup>2</sup>School of Physics and Electronics, Shandong Normal University, Jinan 250014, China

<sup>3</sup>School of Information Engineering, Shandong Management University, Jinan 250357, China

Correspondence should be addressed to Qiang Wang; wangqiang5169@163.com

Received 18 April 2018; Accepted 4 June 2018; Published 27 June 2018

Academic Editor: Xue-Jun Xie

Copyright © 2018 Qiang Wang et al. This is an open access article distributed under the Creative Commons Attribution License, which permits unrestricted use, distribution, and reproduction in any medium, provided the original work is properly cited.

This paper investigates the consensus control of a class of high-order nonlinear multiagent systems, whose topology is dynamically switching directed graph. First, the high-order nonlinear dynamics is transformed into the one-order dynamics by structuring a sliding mode plane; then, two consensus control protocols of the one-order dynamics are designed by feedback linearization, one of which is based on PD (proportion and derivative) and the other is based on PID (proportion, integral and derivative). Under these control protocols, it is proved that the consensus of new variable only requires a weaker topology condition; next, we prove that the consensus of the new variable is sufficient to the consensus of the states of multiagent systems, which implies that it only requires a weaker topology condition for the consensus of multiagent systems; finally, the study of an illustrative example with simulations shows that our results as well as designed control protocols work very well in studying the consensus of this class of multiagent systems.

## 1. Introduction

Nonlinear dynamics systems, inaccurate dynamics, and switching systems have been fascinating in the field of control and have attracted considerable attention worldwide. As is known to all, nonlinear dynamics [1–6] are more challenging than their linear peer. Inaccurate dynamics or noises increase the difficulty in analyzing the problem [7–10], and switching models, which some authors devote themselves to [11–15], are intractable. In this paper, we will focus on a class of special nonlinear and switching systems, that is, multiagent systems with nonlinear inaccurate dynamics and dynamically switching undirected topologies, and investigate its consensus conditions. As an important and fundamental issue of the multiagent systems, consensus problem is especially fascinating [16–19], and some specific scenarios on consensus problems are researched by scholars, such as time-delay [20–23], leader following consensus [24–27], and formation [28–31].

The consensus of multiagent systems with a switching interaction topology has been attracting many scholars [32–34]. In [32], the authors considered multiagent systems with first-order integrator dynamics under the switching topology and provided a control protocol under which the dynamics could achieve consensus with a rather weak topology conditions. However, they considered the second-order integrator dynamics in [33] and obtained a condition that needs the stronger topology requirement than the one in [32]; what is more, they pointed out that the condition in [32] was not sufficient to the second-order consensus algorithm with their control protocol. The authors in [34] compared the control protocol in [32] with the one in [33] and pointed out that the topology requirement was dependent on the control protocol. They transformed the high-order linear systems to first-order integrator dynamics by variable substitution and obtained the consensus conditions of high-order linear multiagent systems with a rather weak topology requirement.

The idea in [34] is interesting for high-order systems, which motivate us to consider a class of high-order nonlinear multiagent systems, whose topology is dynamically switching directed graph. We prove that the nonlinear dynamics can achieve consensus with a rather weak topology conditions similar to [32]. First, the high-order dynamics can realize dimensionality reduction by structuring a sliding mode plane; then, two consensus control protocols are designed by feedback linearization, one of which is based on PD (proportion and derivative), and the other is based on PID (proportion, integral, and derivative), such that the new model can achieve the consensus under a rather weak topology condition; next, we prove that the consensus of new control protocols is sufficient to the consensus of nonlinear multiagent systems. Thus, we give a rather weak consensus conditions of high-order nonlinear multiagent systems, in which the union graph has a spanning tree frequently enough. Finally, the study of an illustrative example with simulations shows that our results as well as designed control protocols work very well in studying this class of multiagent systems.

The main contribution of this paper contains: (1) a rather weak topology condition is given for the consensus of nonlinear multiagent systems with switching structure; (2) we present two control protocols for this class of systems, under which the consensus is proved; (3) the reduce-order idea is used to transform the high-order dynamics into one-order dynamics, which simplify the difficulty of problem.

The remainder of the paper is organized as follows. Section 2 is the backgrounds and preliminaries. Section 3 is the main results of the paper. In this section, the high-order nonlinear dynamics is transformed into one-order linear dynamics, and two control protocols are designed. In Section 4, we give an illustrative example to support our new results followed by the conclusion in Section 5.

## 2. Backgrounds and Preliminaries

In [32], Ren and Beard considered a one-order linear system under the switching topology:

$$\dot{x}_i = u_i, \quad (1)$$

and they designed the control protocol as follows:

$$u_i = - \sum_{j \in N_i(t)} a_{ij} (x_i - x_j), \quad (2)$$

it was proved system (1) could achieve consensus under protocol (2) even if the switching topology satisfied a rather weak condition. Specifically to say, it could be formulated as the following lemma.

**Lemma 1.** *Let  $t_1, t_2, \dots$  be an infinite time sequence at which the interaction graph or weighting factors  $a_{ij}$  switch and  $\tau_i = t_{i+1} - t_i \in \gamma, i = 0, 1, \dots$ . Here,  $\gamma$  is an infinite set generated from set  $\bar{\tau}$ , which is a finite set of arbitrary positive numbers. Let  $G(t_i)$  be a switching topology at time  $t = t_i$  and all nonzero entries of the adjacency matrix  $A = [a_{ij}]$  are lower bounded by a positive constant  $\sigma_L$  and upper bounded by a positive constant  $\sigma_M$ . Then the distributed control protocols (2) achieve*

*consensus asymptotically for the multiagent systems specified by (1) if there exists an infinite sequence of uniformly bounded, nonoverlapping time intervals  $[t_i, t_{i+l_j}), l_j \in [1, i_{j+1} - i_j), j = 1, 2, \dots$ , starting at  $t_{i_1} = t_0$ , with the property that each interval  $[t_{i_j+l_j}, t_{i_{j+1}})$  is uniformly bounded and the union of the directed graphs across each interval  $[t_{i_j+l_j}, t_{i_{j+1}})$  has a spanning tree. Furthermore, the consensus value is a constant.*

Furthermore, they considered the second-order integrator in [33]:

$$\begin{aligned} \dot{x}_{i1} &= x_{i2} \\ \dot{x}_{i2} &= u_i, \end{aligned} \quad (3)$$

where  $x_i = [x_{i1}, x_{i2}]$  was the state of Agent  $i$ , and  $u_i$  was the control protocol. They designed the control protocol as

$$u_i = - \sum_{j=1}^n a_{ij} \left[ (x_{i1} - x_{j1}) + r(t) (x_{i2} - x_{j2}) \right], \quad (4)$$

where  $r(t)$  was a positive scalar at time  $t$ . In that book, they provided a result which needed a more stronger connectivity assumption; that is, the interaction graph needed a directed spanning tree at each time instant. Moreover, they provided some simulation examples to illustrate that, under control protocol (4), the assumption of Lemma 1 could not ensure the consensus of second-order consensus generally.

Su and Lin compared the cases as above in [34] and presented a reduced-order idea. They considered the high-order linear multiagent dynamics as follows:

$$\dot{\mathbf{x}}_i = \mathbf{A}\mathbf{x}_i + \mathbf{B}\mathbf{u}_i, \quad i = 1, 2, \dots, m, \quad (5)$$

where  $\mathbf{x}_i \in \mathbf{R}^n$  was the state vector of Agent  $i$ ,  $\mathbf{u}_i$  was the control input the Agent  $i$ , and  $(\mathbf{A}, \mathbf{B})$  was controllable. By transforming the system (5) to one-order dynamics, they presented a control protocol under which the high-order linear multiagent systems could obtain consensus with a rather weak topology.

Inspired by [34], we will consider a class of multiagent systems with  $m$  agents, which each has  $n$ -order nonlinear dynamics described by

$$\dot{x}_i^{(n)} = f(x_i) + b(x_i)u_i, \quad i = 1, 2, \dots, m, \quad (6)$$

where  $x_i \in \mathbf{R}$  is the state of agent  $i$ ,  $u_i \in \mathbf{R}$  is the control input of agent  $i$ , and  $f(x_i)$  or  $b(x_i)$  is inaccurate.

Denoting  $x_{i1} = x_i$ , the dynamics (6) can be rewritten as

$$\begin{aligned} \dot{x}_{i1} &= x_{i2}, \\ \dot{x}_{i2} &= x_{i3} \\ &\dots \\ \dot{x}_{i(n-1)} &= x_{in}, \end{aligned} \quad (7)$$

$$\dot{x}_{in} = f(x_i) + b(x_i)u_i, \quad i = 1, 2, \dots, m,$$

The objective of this study is to design a controller such that the agents described as the system (6) or (7) can

achieve consensus under the dynamically switching directed interaction topologies.

In the following, we will provide some fundamental knowledge on algebraic graph theory, which will be used in the development of this research.

Suppose  $\mathcal{G} = \{\mathcal{V}, \mathcal{E}\}$  be a directed graph of  $N$ -th order with the set of nodes  $\mathcal{V} := \{v_1, v_2, \dots, v_N\}$ , and the set of edges (i.e., ordered pairs of the agents)  $\mathcal{E} \subseteq \mathcal{V} \times \mathcal{V}$ . The matrix  $\mathbf{A} = [a_{ij}]_{N \times N}$  is named the adjacency matrix of the graph  $\mathcal{G}$ , where  $a_{ij}$  is the weight of Agent  $i$  to Agent  $j$ . For any  $i, j \in \mathcal{V}$ ,  $a_{ji} > 0$  if and only if  $j \in \mathcal{N}_i$ , where  $\mathcal{N}_i = \{j | e_{ij} = (v_i, v_j) \in \mathcal{E}\}$ . In this paper we just consider the case of simple graphs, that is,  $e_{ii} \notin \mathcal{E}$ ,  $i = 1, 2, \dots, n$ . The matrix  $\mathbf{D} = [d_{ij}] \in \mathbf{R}^{N \times N}$  is the valency matrix of the topology  $\mathcal{G}$ , where  $d_{ij}$  is defined as

$$d_{ij} = \begin{cases} \sum_{k \in \mathcal{N}_i(t)} a_{ik}, & j = i, \\ 0, & j \neq i. \end{cases} \quad (8)$$

Moreover, the matrix  $\mathbf{L} = \mathbf{D} - \mathbf{A}$  is known as the graph's Laplacian matrix.

### 3. Main Results

This section studies the consensus of the multiagent dynamics (6). We will consider the following scenarios: (I) the dynamics  $f(x_i)$ ,  $i = 1, 2, \dots, m$  is inaccurate, but its estimate is known; (II) the gain  $b(x_i)$ ,  $i = 1, 2, \dots, m$  is inaccurate, but we know its upper bound and its lower bound.

Before giving our main results, another lemma will be useful in our study.

**Lemma 2** (see [34]). *Let  $x(t)$  be a smooth function of  $t$  and assume that  $x(0), \dot{x}(0), \dots, x^{(n-1)}(0)$  are all bounded. Define*

$$s(x, t) = \left( \lambda + \frac{d}{dt} \right)^{n-1} x(t), \quad (9)$$

where  $\lambda > 0$  is a constant. If there exists a scalar  $\Phi > 0$  such that  $|s(x(t), t)| \leq \Phi$  for all  $t \geq 0$ , then there exists a finite  $T_0$ , dependent on the values of  $x(0), \dot{x}(0), \dots, x^{(n-1)}(0)$ , such that

$$\|x^{(i)}(t)\| \leq \frac{2^i \Phi}{\lambda^{n-i-1}}, \quad t \geq T_0, \quad i = 0, 1, \dots, n-1. \quad (10)$$

**3.1. Inaccurate Dynamics in the Systems.** First, we consider the system (6) with undirected topology, assume that  $\hat{f}(x_i)$  is the estimate of  $f(x_i)$ , and the error of estimate is subject to  $F(x_i, \hat{x}_i, \ddot{x}_i, \dots, x_i^{(n-1)})$ , that is,  $|f(x_i) - \hat{f}(x_i)| \leq F$ .

Denote

$$z_i(t) = \left( \lambda + \frac{d}{dt} \right)^{n-1} x_i(t), \quad i = 1, 2, \dots, N, \quad (11)$$

where  $\lambda$  is a positive number.

Then design the control protocol as

$$\begin{aligned} \hat{u}_i = & - \sum_{j=1}^m a_{ij}(t) (z_i - z_j) - C_{n-1}^0 \lambda^{n-1} x_{i2} - C_{n-1}^1 \lambda^{n-2} x_{i3} \\ & - C_{n-1}^2 \lambda^{n-3} x_{i4} - \dots - C_{n-1}^{n-2} \lambda x_{in} - \hat{f}(x_i), \end{aligned} \quad (12)$$

and

$$u_i = \hat{u}_i - F \operatorname{sgn}(z_i), \quad (13)$$

where

$$\operatorname{sgn}(z_i) = \begin{cases} 1, & z_i \geq 0, \\ 0, & z_i < 0, \end{cases} \quad (14)$$

under the protocol (13), and we have the following result.

**Theorem 3.** *Consider the multiagent system of  $m$  agents (6) under the control protocol specified by (13). If the conditions of Lemma 1 are satisfied, then the distributed control protocol (13) achieves consensus asymptotically for the multiagent systems specified by (6) and the consensus is reached at a constant state  $[c, 0, 0, \dots, 0]^T$ .*

*Proof.* Take derivative for (11), and we have

$$\begin{aligned} \dot{z}_i(t) = & \frac{d}{dt} \left\{ \left( \lambda + \frac{d}{dt} \right)^{n-1} x_{i1} \right\} = \frac{d}{dt} \{ C_{n-1}^0 \lambda^{n-1} x_{i1} \\ & + C_{n-1}^1 \lambda^{n-2} x_{i2} + C_{n-1}^2 \lambda^{n-3} x_{i3} + \dots + C_{n-1}^{n-2} \lambda x_{i(n-1)} \\ & + x_{in} \} = C_{n-1}^0 \lambda^{n-1} \dot{x}_{i2} + C_{n-1}^1 \lambda^{n-2} \dot{x}_{i3} + C_{n-1}^2 \lambda^{n-3} \dot{x}_{i4} \\ & + \dots + C_{n-1}^{n-2} \lambda \dot{x}_{in} + f(x_i) + u_i \\ = & - \sum_{j \in \mathcal{N}_i(t)} a_{ij} (z_i - z_j) + f - \hat{f} - F \operatorname{sgn}(z_i), \end{aligned} \quad (15)$$

Choose a Lyapunov function candidate

$$V(z) = \frac{1}{2} z^T z, \quad (16)$$

where  $z = [z_1, z_2, \dots, z_m]^T$ ; then

$$\begin{aligned} \dot{V}(z) = & \dot{z}^T z \\ = & - \sum_{i=1}^m \left( \sum_{j=1}^m a_{ij} (z_i - z_j) z_j + (f - \hat{f}) z_i - F |z_i| \right) \\ \leq & - \sum_{i=1}^m \left( \sum_{j=1}^m a_{ij} (z_i - z_j) z_j + |f - \hat{f}| |z_i| - F |z_i| \right) \\ = & - \sum_{i=1}^m \left( \sum_{j=1}^m a_{ij} (z_i - z_j) z_j + (|f - \hat{f}| - F) |z_i| \right) \\ \leq & - \sum_{j=1}^m \sum_{i=1}^m a_{ij} (z_i - z_j) z_j = - \frac{1}{2} \sum_{i=1}^m \sum_{j=1}^m a_{ij} (z_i - z_j)^2 \\ \leq & 0, \end{aligned} \quad (17)$$

due to  $|f - \hat{f}| \leq F$ .

Letting  $\dot{V}(z) = 0$ , that is,  $\sum_{i=1}^m \sum_{j=1}^m a_{ij} (z_i - z_j)^2 = 0$ , we have  $z_i = z_j$ ,  $i, j = 1, 2, \dots, m$ . According to LaSalle invariant set, the systems converge to the state  $z_i = z_j$ ,  $i = 1, 2, \dots, m$ .

On the other hand, (11) implies  $z_i(t) - z_j(t) = (\lambda + d/dt)^{n-1}(x_{i1}(t) - x_{j1}(t))$ . Since  $z_i, z_j, i, j = 1, 2, \dots, m$  achieves consensus asymptotically, then  $\forall \epsilon > 0, \exists T_1 > 0$ , such that when  $t > T_1, |z_i(t) - z_j(t)| < \epsilon$ . According to Lemma 2, there exists a finite  $T_0 > T_1$ , dependent on the values of  $x_i(T_1), \dot{x}_i(T_1), \dots, x_i^{(n-1)}(T_1), i = 1, 2, \dots, N$ , such that

$$\|x_{i1}^{(k)}(t) - x_{j1}^{(k)}(t)\| \leq 2^k \epsilon / \lambda^{n-k-1}, \quad (18)$$

$$t \geq T_0, k = 0, 1, \dots, n-1,$$

which implies that

$$\|x_{is}(t) - x_{js}(t)\| \leq \epsilon_0, \quad t \geq T_0, s = 1, 2, \dots, n, \quad (19)$$

where  $\epsilon_0 = \max\{2^k \epsilon / \lambda^{n-k-1}, k = 0, 1, \dots, n-1\}$  is an arbitrarily small positive number, which implies that  $x_i(t)$  achieves consensus asymptotically.

Consider the dynamics (7), since  $x_i(t)$  achieves consensus asymptotically, it is easy to obtain that

$$\lim_{t \rightarrow +\infty} \dot{x}_{ik} = 0, \quad k = 1, 2, \dots, n, \quad (20)$$

which implies that  $x_{i1} \rightarrow c$  and  $x_{ik} \rightarrow 0, k = 2, 3, \dots, n$ , thus,  $x_i \rightarrow [c, 0, 0, \dots, 0]^T$ .  $\square$

However, the terms  $F \operatorname{sgn}(z_i)$  have a strong flutter, which may need a strong control power. Next, we will consider the stable under any precision.

*Definition 4.* The system  $\dot{x} = f(x)$  is said to any precision stable if for any designated  $\epsilon_0$ , there exists  $T$ , such that  $\|x(t)\| < \epsilon_0$ , when  $t > T$ .

Consider the set  $B(t) = \{x | s(x, t) \leq \Phi\}$ , where  $\Phi > 0$  is the precision of system state. Letting

$$u_i = \hat{u}_i - F \operatorname{sat}\left(\frac{z_i}{\Phi}\right), \quad (21)$$

where  $u_i$  is the same as (12),

$$\operatorname{sat}\left(\frac{z_i}{\Phi}\right) = \begin{cases} \frac{z_i}{\Phi}, & |z_i| \leq \Phi, \\ \operatorname{sgn}(z_i), & |z_i| > \Phi, \end{cases} \quad (22)$$

under the control protocol (21), we have the following theorem.

**Theorem 5.** Consider the multiagent system of  $m$  agents (6), which is steered by the control protocol specified by (21). If the conditions of Lemma 1 are satisfied, then the protocol (21) achieves any precision stable for the multiagent systems specified by (6).

*Proof.* When  $|z_i|/\Phi > 0$ ,

$$u_i = \hat{u}_i - F \operatorname{sgn}(z_i), \quad (23)$$

from the proof of Theorem 3, the dynamics are convergent to the invariant set  $B(t)$ ; that is, there exists a constant  $T_0$ , when  $t > T_0, z_i(x_i, t) \leq \Phi$ . According to Lemma 2,

$$\|x^{(i)}(t)\| \leq \frac{2^i \Phi}{\lambda^{n-i-1}}, \quad t \geq T_0, i = 0, 1, \dots, n-1. \quad (24)$$

Thus,  $x_i(t) \leq \Phi / \lambda^{n-1}$  for  $i = 1, 2, \dots, m$ .  $\square$

**3.2. Inaccurate Gain in the Systems.** Consider system (6) with the inaccurate gain, that is,  $b(x)$  is unknown, but we know its bounds,  $\underline{b} \leq b(x_i) \leq \bar{b}, i = 1, 2, \dots, N$ , where  $\underline{b}$  and  $\bar{b}$  are positive constant number.

Denoting  $\hat{b} = \sqrt{\underline{b}\bar{b}}$ , and designing

$$u_i = -\hat{b}^{-1} \sum_{j=1}^N (s_i - s_j) - C_{n-1}^0 \lambda^{n-1} x_{i2} - C_{n-1}^1 \lambda^{n-2} x_{i3} - C_{n-1}^2 \lambda^{n-3} x_{i4} - \dots - C_{n-1}^{n-2} \lambda x_{in} - f(x_i), \quad (25)$$

then system (6) can be rewritten as

$$\dot{s}_i = -\sum_{j=1}^N b(x_i) \hat{b}^{-1} a_{ij} (s_i - s_j) \quad (26)$$

Letting  $\hat{\beta} = \sqrt{\bar{b}/\underline{b}}$ , then  $\hat{\beta} > 1$ . Since  $\underline{b} \leq b(x_i) \leq \bar{b}$ , then  $\hat{\beta}^{-1} \leq b(x_i) \hat{b}^{-1} \leq \hat{\beta}$

The control protocol (12) with (11) is constructed by PD Control, which can bring in steady-state error. Thus, another control protocol is designed in order to overcome this deficiency.

Letting

$$z_i(t) = \left(\lambda + \frac{d}{dt}\right)^n \int_0^t x_i(r) dr, \quad i = 1, 2, \dots, N, \quad (27)$$

the control protocol is designed as follows:

$$u_i = -\sum_{j \in N_i(t)} a_{ij} (z_i - z_j) - C_n^0 \lambda^n x_{i1} - C_n^1 \lambda^{n-1} x_{i2} - C_n^2 \lambda^{n-2} x_{i3} - \dots - C_n^{n-1} \lambda x_{in} - f(x_i), \quad (28)$$

and we have the following conclusion.

**Theorem 6.** Consider the multiagent system of  $m$  agents (6), which is steered by the control protocol specified by (28). If and the consensus is reached at a constant state  $[c, 0, 0, \dots, 0]^T$ . If the conditions of Lemma 1 are satisfied, then the distributed control protocol (28) achieves consensus asymptotically for the multiagent systems specified by (6).

*Proof.* Since

$$\begin{aligned}
 \dot{z}_i(t) &= \frac{d}{dt} \left\{ \left( \lambda + \frac{d}{dt} \right)^n \int_0^t x_i(r) dr \right\} \\
 &= \frac{d}{dt} \left\{ C_n^0 \lambda^n \int_0^t x_i(r) dr + C_n^1 \lambda^{n-1} x_{i1} + C_n^2 \lambda^{n-2} x_{i2} \right. \\
 &\quad + \dots + C_n^{n-1} \lambda x_{i(n-1)} + C_n^n x_{in} \left. \right\} = C_n^0 \lambda^n x_{i1} \\
 &\quad + C_n^1 \lambda^{n-1} x_{i2} + C_n^2 \lambda^{n-2} x_{i3} + \dots + C_n^{n-1} \lambda x_{in} + \dot{x}_{in} \\
 &= C_n^0 \lambda^n x_{i1} + C_n^1 \lambda^{n-1} x_{i2} + C_n^2 \lambda^{n-2} x_{i3} + \dots \\
 &\quad + C_n^{n-1} \lambda x_{in} + f(x_i) + u_i = - \sum_{j \in N_i(t)} a_{ij} (z_i - z_j)
 \end{aligned} \tag{29}$$

according to Lemma 1, the dynamics (29) can achieve consensus asymptotically if there exist infinite sequence of uniformly bounded, nonoverlapping time intervals  $[t_j, t_{j+1}]$ ,  $l_j \in [1, i_{j+1} - i_j]$ ,  $j = 1, 2, \dots$  starting at  $t_i = t_0$ , with the property that each interval  $[t_j, t_{j+1}]$  is uniformly bounded and the union of the directed graphs across each interval  $[t_j, t_{j+1}]$  has a spanning tree.

On the other hand, (27) implies  $z_i(t) - z_j(t) = (\lambda + d/dt)^n (\int_0^t (x_{i1}(r) - x_{j1}(r)) dr)$ . Since the dynamics (29) achieve consensus asymptotically, then  $\forall \epsilon > 0, \exists T_1 > 0$ , such that when  $t > T_1$ ,  $|z_i(t) - z_j(t)| < \epsilon$ . According to Lemma 2, there exists a finite  $T_0 > T_1$ , dependent on the values of  $\int_0^{T_1} x_i(r) dr, x_i(T_1), \dot{x}_i(T_1), \dots, x_i^{(n-1)}(T_1), i = 1, 2, \dots, N$ , such that

$$\left\| \int_0^t (x_{i1}(r) - x_{j1}(r)) dr \right\| \leq \frac{\epsilon}{\lambda^n}, \quad t \geq T_0 \tag{30}$$

and

$$\begin{aligned}
 \|x_{i1}^{(k)}(t) - x_{j1}^{(k)}(t)\| &\leq \frac{2^k \epsilon}{\lambda^{n-k-1}}, \\
 t &\geq T_0, \quad k = 0, 1, \dots, n-1.
 \end{aligned} \tag{31}$$

According to the proof of Theorem 3, (31) implies

$$\|x_{is}(t) - x_{js}(t)\| \leq \epsilon_0, \quad t \geq T_0, \quad s = 1, 2, \dots, n. \tag{32}$$

where  $\epsilon_0 = \max\{2^k \epsilon / \lambda^{n-k-1}, k = 0, 1, \dots, n-1\}$  is an arbitrarily small positive number, which implies that  $x_i(t)$  achieves consensus asymptotically.

Consider the dynamics (7); since  $x_i(t)$  achieves consensus asymptotically, it is easy to obtain that

$$\lim_{t \rightarrow +\infty} \dot{x}_{ik} = 0, \quad k = 1, 2, \dots, n, \tag{33}$$

which implies that  $x_{i1} \rightarrow c$  and  $x_{ik} \rightarrow 0, k = 2, 3, \dots, n$ , thus,  $x_i \rightarrow [c, 0, 0, \dots, 0]^T$ .  $\square$

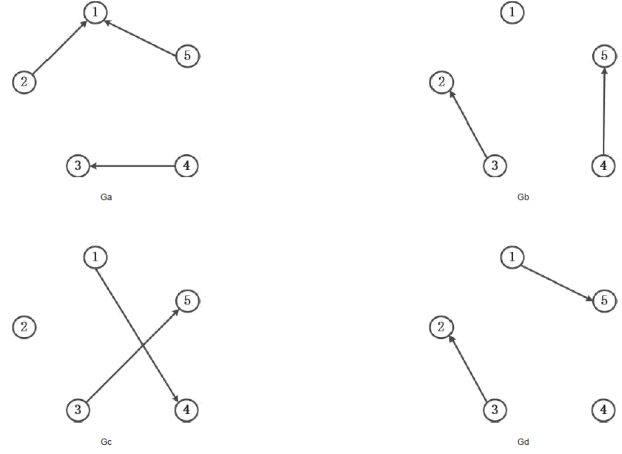


FIGURE 1: The topology of switching directed graph.

*Remark 7.* The method provided in this research is suitable for heterogeneous multiagent systems:

$$x_i^{(n)} = f_i(x_i) + u_i, \quad i = 1, 2, \dots, m, \tag{34}$$

only if the control protocol is designed as

$$\begin{aligned}
 u_i &= - \sum_{j \in N_i(t)} a_{ij} (z_i - z_j) - C_n^0 \lambda^n x_{i1} - C_n^1 \lambda^{n-1} x_{i2} \\
 &\quad - C_n^2 \lambda^{n-2} x_{i3} - \dots - C_n^{n-1} \lambda x_{in} - f_i(x_i).
 \end{aligned} \tag{35}$$

## 4. Illustrative Examples

In this section, we provide an illustrative example to show how to use the method in this research to design control protocol for the consensus of this class of multiagent systems.

*Example 1.* Consider the following 5-agent system running on a circle:

$$\begin{aligned}
 \dot{x}_{i1} &= x_{i2}, \\
 \dot{x}_{i2} &= x_{i3},
 \end{aligned} \tag{36}$$

$$x_{i3} = \sum_{j=1}^3 x_{ij}^2 + u_i, \quad i = 1, 2, 3, 4, 5,$$

whose topology is shown as Figure 1,  $\{Ga, Gb, Gc, Gd\}$  is the set of switching directed graph, it is easy to see that each of them does not obtain a spanning tree. To show the correctness of the above conclusion, we carry out the following numerical simulations. The dynamics start at  $Ga$  and switch to the next one after  $T = 0.01$ , and the switching rules of network topology are as follows:  $Ga \rightarrow Gb \rightarrow Gc \rightarrow Gd \rightarrow Ga \rightarrow Gb \dots$ . It is easy to see that the union graph of the dynamics system (36) has a spanning tree frequently enough.

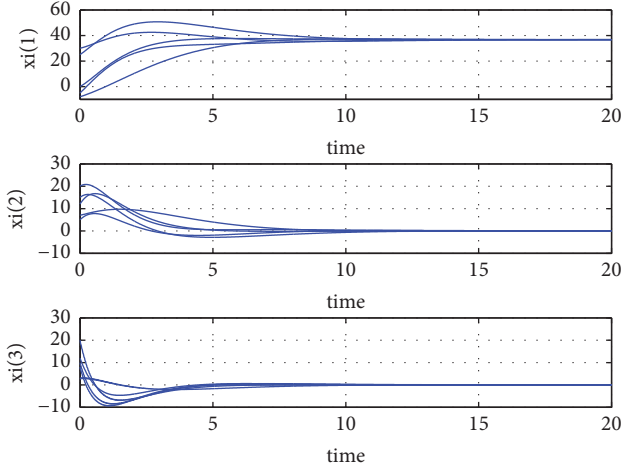


FIGURE 2: The states of agents under the control protocol (37).

Design the control protocol

$$u_i = - \sum_{j \in N_i(t)} (z_i - z_j) - C_2^0 \lambda^2 x_{i2} - C_2^1 \lambda x_{i3} - \sum_{j=1}^3 x_{ij}^2, \quad (37)$$

$$i = 1, 2, 3, 4, 5,$$

where  $z_i(t) = (\lambda + d/dt)^2 x_i(t)$ . Herein, let  $\lambda = 1$  and initial condition  $x_1(0) = [25, 15, 10]^T$ ,  $x_2(0) = [30, 5, 12]^T$ ,  $x_3(0) = [-5, 20, 8]^T$ ,  $x_4(0) = [-8, 7, 3]^T$ ,  $x_5(0) = [0, 12, 20]^T$ .

The simulation results are shown in Figure 2, from which we can see that the states of the 5 agents eventually converge to the same value under the protocol (37) and the final result coincides with the theoretical analysis. Simulation shows that our method is very effective in analyzing the consensus of this kind of multiagent system (36).

In the following, we consider Example 1 with the same switching topology and the same switching rules and design a control protocol obtaining the integration as follows:

$$u_i = - \sum_{j \in N_i(t)} (z_i - z_j) - C_3^0 \lambda^3 \int_0^t x_{i1}(r) dr - C_3^1 \lambda^2 x_{i1} - C_3^2 \lambda x_{i2} - C_3^3 x_{i3} - \sum_{j=1}^3 x_{ij}^2, \quad (38)$$

Under the same initial conditions and  $\lambda = 1$ , the simulation results are shown in Figure 3, from which we can see that the agents converge to each other under the control protocol (38).

## 5. Conclusion

In this paper, the consensus control of a class of high-order nonlinear multiagent systems was investigated, whose topology switched dynamically, and we obtained some consensus results on this class of multiagent systems. Herein, a rather weak topology condition was given for the consensus of nonlinear multiagent systems with switching structure, and

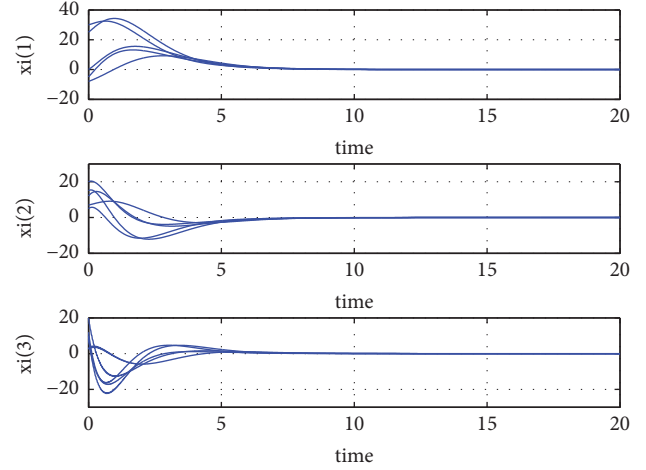


FIGURE 3: The states of agents under the control protocol (38).

two control protocols, one of which was based on PD and the other was based on PID, were presented for this class of systems, and the stabilization was proved; furthermore, a reduced-order method was used to handle the high-order dynamics system, which simplify the difficulty of problem. Simulations showed that our results as well as designed control protocols worked very well in studying the consensus of this class of multiagent systems. However, we just take a step for this class of systems, and some questions, such as how to obtain the estimate  $\hat{f}(x)$ , will be considered in our subsequent research.

## Data Availability

The data used to support the findings of this study are included within the article (Figures 2 and 3).

## Conflicts of Interest

The authors declare that they have no conflicts of interest.

## Acknowledgments

This paper was supported by the National Nature Science Foundation of China [61572298, 61602283, 61702310] and the Natural Science Foundation of Shandong, China (no. ZR2016FB10).

## References

- [1] W. Sun, K. Wang, C. Nie, and X. Xie, "Energy-based controller design of stochastic magnetic levitation system," *Mathematical Problems in Engineering*, Art. ID 7838431, 6 pages, 2017.
- [2] L. Wang and Q.-G. Wang, "A general approach for synchronisation of nonlinear networked systems with switching topology," *International Journal of Systems Science*, vol. 44, no. 12, pp. 2199–2210, 2013.
- [3] W. Sun, G. Pang, P. Wang, and L. Peng, "Robust adaptive control and L2 disturbance attenuation for uncertain Hamiltonian systems with time-delay," *Mathematical Problems in Engineering*, Art. ID 183279, 10 pages, 2013.

- [4] W. Sun and L. Peng, "Observer-based robust adaptive control for uncertain stochastic Hamiltonian systems with state and input delays," *Nonlinear Analysis: Modelling and Control*, vol. 19, no. 4, pp. 626–645, 2014.
- [5] W. Sun and B. Fu, "Adaptive control of time-varying uncertain non-linear systems with input delay: a Hamiltonian approach," *IET Control Theory & Applications*, vol. 10, no. 15, pp. 1844–1858, 2016.
- [6] W. Sun and L. Peng, "Robust adaptive control of uncertain stochastic Hamiltonian systems with time varying delay," *Asian Journal of Control*, vol. 18, no. 2, pp. 642–651, 2016.
- [7] X. Song, J. H. Park, and X. Yan, "Linear estimation for measurement-delay systems with periodic coefficients and multiplicative noise," *Institute of Electrical and Electronics Engineers Transactions on Automatic Control*, vol. 62, no. 8, pp. 4124–4130, 2017.
- [8] X. Song and J. H. Park, "Linear optimal estimation for discrete-time measurement delay systems with multichannel multiplicative noise," *IEEE Transactions on Circuits and Systems II: Express Briefs*, vol. 64, no. 2, pp. 156–160, 2017.
- [9] X. Song and J. H. Park, "Linear minimum mean-square estimation for discrete-time measurement-delay systems with multiplicative noise and Markov jump," *IET Control Theory & Applications*, vol. 10, no. 10, pp. 1161–1169, 2016.
- [10] X. Song and X. Yan, "Duality of linear estimation for multiplicative noise systems with measurement delay," *IET Signal Processing*, vol. 7, no. 4, pp. 277–284, 2013.
- [11] X. Liu, K. Zhang, S. Li, S. Fei, and H. Wei, "Optimal control of switching times in switched stochastic systems," *Asian Journal of Control*, vol. 17, no. 5, pp. 1580–1589, 2015.
- [12] X. Liu, K. Zhang, S. Li, S. Fei, and H. Wei, "Optimal timing control of switched stochastic systems," *IMA Journal of Mathematical Control and Information*, vol. 32, no. 3, pp. 659–674, 2015.
- [13] X. Liu, S. Li, and K. Zhang, "Optimal control of switching time in switched stochastic systems with multi-switching times and different costs," *International Journal of Control*, vol. 90, no. 8, pp. 1604–1611, 2017.
- [14] Y. Zhang and Y.-P. Tian, "Consistency and protocol design of multi-agent systems with stochastic switching topology," *Automatica*, vol. 45, no. 5, pp. 1195–1201, 2009.
- [15] Y. Hong, L. Gao, D. Cheng, and J. Hu, "Lyapunov-based approach to multiagent systems with switching jointly connected interconnection," *Institute of Electrical and Electronics Engineers Transactions on Automatic Control*, vol. 52, no. 5, pp. 943–948, 2007.
- [16] F. Zhang, W. Wang, and H. Zhang, "Distributed design of approximately optimal controller for identical discrete-time multi-agent systems," *Journal of Systems Science & Complexity*, vol. 29, no. 3, pp. 629–641, 2016.
- [17] F. Zhang, H. Zhang, C. Tan, W. Wang, and J. Gao, "A new approach to distributed control for multi-agent systems based on approximate upper and lower bounds," *International Journal of Control, Automation, and Systems*, vol. 15, no. 6, pp. 2507–2515, 2017.
- [18] G. Z. Cui, S. Y. Xu, Q. Ma, Y. M. Li, and Z. Q. Zhang, "Prescribed performance distributed consensus control for nonlinear multi-agent systems with unknown dead-zone input," *International Journal of Control*, vol. 91, no. 5, 2018.
- [19] H. Liu, P. Zhang, B. Hu, and P. Moore, "A novel approach to task assignment in a cooperative multi-agent design system," *Applied Intelligence*, vol. 43, no. 1, pp. 162–175, 2015.
- [20] Z. Wang, H. Zhang, X. Song, and H. Zhang, "Consensus problems for discrete-time agents with communication delay," *International Journal of Control, Automation, and Systems*, vol. 15, no. 4, pp. 1515–1523, 2017.
- [21] Z. Wang, J. Xu, X. Song, and H. Zhang, "Consensus Conditions for Multi-agent Systems Under Delayed Information," *IEEE Transactions on Circuits and Systems II: Express Briefs*, pp. 1–1.
- [22] R. Olfati-Saber and R. M. Murray, "Consensus problems in networks of agents with switching topology and time-delays," *IEEE Transactions on Automatic Control*, vol. 49, no. 9, pp. 1520–1533, 2004.
- [23] H.-Y. Yang, G.-D. Zong, and S.-Y. Zhang, "Movement consensus of delayed multi-agent systems with directed weighted networks," *International Journal of Intelligent Computing and Cybernetics*, vol. 4, no. 2, pp. 265–277, 2011.
- [24] H. Michael, Z. Chen, X. Wang, and J. Lam, "Semi-global observer-based leader-following consensus with input saturation," *IEEE Transactions on Industrial Electronics*, vol. 61, no. 6, pp. 2842–2850, 2014.
- [25] B. Liu, T. Chu, L. Wang, and G. Xie, "Controllability of a leader-follower dynamic network with switching topology," *Institute of Electrical and Electronics Engineers Transactions on Automatic Control*, vol. 53, no. 4, pp. 1009–1013, 2008.
- [26] P. Li, S. Xu, Q. Ma, W. Chen, and Z. Zhang, "Leader-following rendezvous for uncertain Euler–Lagrange multi-agent systems by output feedback," *Journal of The Franklin Institute*, vol. 354, no. 10, pp. 4215–4230, 2017.
- [27] C. Ma, T. Li, and J. Zhang, "Consensus control for leader-following multi-agent systems with measurement noises," *Journal of Systems Science & Complexity*, vol. 23, no. 1, pp. 35–49, 2010.
- [28] Q. Wang, Y. Wang, and H. Zhang, "The formation control of multi-agent systems on a circle," *IEEE/CAA Journal of Automatica Sinica*, vol. 5, no. 1, pp. 148–154, 2018.
- [29] C. Q. Ma and J. F. Zhang, "On formability of linear continuous multi-agent systems," *Journal of Systems Science and Complexity*, vol. 25, no. 1, pp. 13–29, 2012.
- [30] Y. Sun, Y. Tian, and X.-J. Xie, "Stabilization of positive switched linear systems and its application in consensus of multiagent systems," *Institute of Electrical and Electronics Engineers Transactions on Automatic Control*, vol. 62, no. 12, pp. 6608–6613, 2017.
- [31] J. Wang, B. Gong, H. Liu, and S. Li, "Multidisciplinary approaches to artificial swarm intelligence for heterogeneous computing and cloud scheduling," *Applied Intelligence*, vol. 43, no. 3, pp. 662–675, 2015.
- [32] W. Ren and R. W. Beard, "Consensus seeking in multiagent systems under dynamically changing interaction topologies," *IEEE Transactions on Automatic Control*, vol. 50, no. 5, pp. 655–661, 2005.
- [33] W. Ren and R. W. Beard, *Distributed consensus in multi-vehicle cooperative control: theory and applications*, Springer, London, U.K, 2008.
- [34] S. Su and Z. Lin, "Distributed Consensus Control of Multi-Agent Systems with Higher Order Agent Dynamics and Dynamically Changing Directed Interaction Topologies," *IEEE Transactions on Automatic Control*, vol. 61, no. 2, pp. 515–519, 2016.

## Research Article

# Exponential Lagrange Stability for Markovian Jump Uncertain Neural Networks with Leakage Delay and Mixed Time-Varying Delays via Impulsive Control

J. Yogambigai,<sup>1</sup> M. Syed Ali,<sup>1</sup> Quanxin Zhu ,<sup>2,3</sup> and Jingwei Cai<sup>2,4</sup>

<sup>1</sup>Department of Mathematics, Thiruvalluvar University, Vellore, Tamil Nadu 632115, India

<sup>2</sup>School of Mathematical Sciences and Institute of Finance and Statistics, Nanjing Normal University, Nanjing 210023, China

<sup>3</sup>School of Mathematical Sciences, Qufu Normal University, Qufu 273165, China

<sup>4</sup>Basis Department, Jiangsu Polytechnic College of Agriculture and Forestry, Zhenjiang, Jiangsu 212400, China

Correspondence should be addressed to Quanxin Zhu; [zqx22@126.com](mailto:zqx22@126.com)

Received 15 April 2018; Accepted 14 May 2018; Published 20 June 2018

Academic Editor: Qingling Zhang

Copyright © 2018 J. Yogambigai et al. This is an open access article distributed under the Creative Commons Attribution License, which permits unrestricted use, distribution, and reproduction in any medium, provided the original work is properly cited.

The problem of exponential Lagrange stability analysis of Markovian jump neural networks with leakage delay and mixed time-varying delays is studied in this paper. By utilizing the Lyapunov functional method, employing free-weighting matrix approach and inequality techniques in matrix form, we establish several novel stability criteria such that, for all admissible parameter uncertainties, the suggested neural network is exponentially stable in Lagrange sense. The derived criteria are expressed in terms of linear matrix inequalities (LMIs). A numerical example is provided to manifest the validity of the proposed results.

## 1. Introduction

It is known that stability is an important research topic in the mathematical field [1–13]. As a special class of mathematical models, neural networks are similar to the brain synapses link structure; neural networks possess multiple dynamic behaviors [14]. For these reasons, neural frameworks have received considerable attention as a result of their intensive applications in determination of some optimization issue, associative memory, classification of patterns, and other areas [15–18]. Since axonal signal transmission time delays often occur in various neural networks and may also cause undesirable dynamic network behaviors such as oscillation and instability, thus, it is important to study the stability of neural networks. Many practical network systems, such as image processing, communication, fault diagnosis, fixed-point computations, parallel computations, and industrial automation, can be modeled as neural networks (NNs) with time delays [19, 20].

Time-varying delays are used to indicate the promoted speed of signals is finite and uncertain in systems [21–28]. Noting that while signal propagation is sometimes instantaneous and can be modeled with discrete delays, it may also be

distributed during a certain time period so that distributed delays are incorporated into the model [29]. Thus, the issue of stability analysis for neural framework with time-varying delays is investigated via LMI technique by many authors [30–34]. Very recently, a leakage delay, which is the time delay in leakage term of the systems and a considerable factor affecting dynamics for the worse in the systems, has been applied to use in studying the problem of stability for neural networks [35–37]. In fact, the leakage term has also a great impact on the dynamical behavior of neural networks. The authors in [38] investigated the stability problem of neural networks with leakage delays and impulses: a piecewise delay method.

When one models real nervous systems, random disturbance and parameter uncertainties are a unit ineluctable to be thought about. As a result, the connection weights of the neuron depend upon bound resistance and capacitance values that embody uncertainties [34]. Therefore, it is of great importance to consider the random effect on the stability of neural frameworks with parameter uncertainties [39–41]. On the other hand, Markovian jump neural networks can be regarded as a special class of hybrid systems, which

can model dynamic systems whose structures are subject to random abrupt parameter changes resulting from component or interconnection failures, sudden environment changes, changing subsystem interconnections, and so forth [42–45]. A neural network has limited modes, which may jump from one to another at various periods. Thus, neural networks with such a jumping character may transform to each other, according to a Markovian chain [44, 46].

Applications of this kind of neural networks can be found in modeling production systems, economic systems, and other practical systems. But in practice applications, for example, the state of electronic networks is often subject to instantaneous changes at certain instants, this is impulsive phenomenon. Impulsive neural network model belongs to new category of dynamical systems, which is neither continuous nor discrete ones. Examples of impulsive phenomena can also be found in other fields of automatic control system, artificial intelligence, robotics, etc. As we know, neural networks could be stabilized or destabilized by impulsive phenomena [44, 47]. The presence of impulse means that the state trajectory does not preserve the basic properties. One of the most desirable properties of neural framework is the Lyapunov global stability. From a dynamical system point of view, globally stable networks in Lyapunov sense are monostable systems, which have a unique equilibrium attracting all trajectories asymptotically.

However, the equilibrium sometimes does not exist in many real physical systems. When a neural network is used as an associative memory storage or for pattern recognition, the existence of many equilibriums is also necessary. On the other hand, monostable neural networks have been found to be computationally restrictive and multistable dynamics are essential to deal with important neural computations desired. For example, only the neuron with the strongest input should remain active in a winner-take-all network depending on the external input [48, 49]. This is possible only if there are multiple equilibria with some being unstable. As we know, Lagrange stability is one of the most important properties in multistability analysis of the total system which does not require the information of equilibriums [50–54]. The boundedness of solutions and the existence of globally attractive sets lead to a total system concept of stability: (asymptotic) Lagrange stability [55, 56]. Hence we concentrate on studying Lagrange stability of the neural networks with mixed time-varying delays and leakage delay in the presence of uncertainties.

Motivated by the above discussions, it is necessary to study the stability properties in Lagrange sense for impulsive neural networks with parameter uncertainties. To the best of our knowledge, there are no published papers on the Lagrange stability analysis of uncertain Markovian jump neural networks with mixed time-varying delays and leakage delay. To fill this gap, we try to perform an exponential stability in Lagrange sense analysis of conceded neural frameworks with mixed time-varying delays and parameter uncertainties. By using novel Lyapunov-Krasovskii functionals together with the zero function, we establish the Lagrange stability of the neural networks with parameter uncertainties. In particular, these sufficient conditions are communicated as

far as LMIs that can be solved numerically. Finally, a numerical illustration is given to demonstrate the adequacy of the obtained results.

*Notation.*  $\mathbb{R}^n$  denotes the  $n$ -dimensional Euclidean space and  $\mathbb{R}^{m \times n}$  is the set of all  $m \times n$  real matrices. The superscript ' $T$ ' denotes matrix transposition and  $\mathcal{A} \geq \mathcal{B}$  (respectively,  $\mathcal{A} < \mathcal{B}$ ) where  $\mathcal{A}$  and  $\mathcal{B}$  are symmetric matrices (respectively, positive definite);  $\|\cdot\|$  denotes the Euclidean norm in  $\mathbb{R}^n$ . If  $\mathcal{Q}$  is a square matrix, denoted by  $\lambda_{\max}(\mathcal{Q})$  (respectively,  $\lambda_{\min}(\mathcal{Q})$ ) it means the largest (respectively, smallest) eigenvalue of  $\mathcal{Q}$ . Moreover, let  $(\Omega, \mathcal{F}, \{\mathcal{F}_t\}_{t \geq 0}, \mathcal{P})$  be a complete probability space with a filtration  $\{\mathcal{F}_t\}_{t \geq 0}$  satisfying the usual conditions (i.e., the filtration contains all  $\mathbb{P}$ -null sets and is right-continuous). The asterisk  $*$  in a symmetric matrix is used to denote term that is induced by symmetry;  $\text{diag}(\cdot)$  stands for the diagonal matrix;  $I$  and  $0$  denote the identity matrix and zero matrix of appropriate dimensions, respectively.

## 2. Problem Formulation and Preliminaries

Given a complete probability space  $(\Omega, \mathcal{F}, \{\mathcal{F}_t\}_{t \geq 0}, \mathcal{P})$  with a natural filtration  $\{\mathcal{F}_t\}_{t \geq 0}$  satisfying the usual conditions, where  $\Omega$  is the sample space,  $\mathcal{F}$  is the algebra of events, and  $\mathcal{P}$  is the probability measure defined on  $\mathcal{F}$ , let  $\{r_t, t \geq 0\}$  be a right-continuous Markovian chain on the probability space  $(\Omega, \mathcal{F}, \{\mathcal{F}_t\}_{t \geq 0}, \mathcal{P})$  taking values in the finite space  $S = \{1, 2, \dots, m\}$  with generator  $\Phi = \{\phi_{kj}\}_{m \times m}$  ( $k, j \in S$ ) given by

$$\begin{aligned} \mathcal{P}\{r_{(t+\Delta)} = j \mid r_t = k\} \\ = \begin{cases} \phi_{kj}\Delta + 0(\Delta), & \text{if } k \neq j, \\ 1 + \phi_{kk}\Delta + 0(\Delta), & \text{if } k = j. \end{cases} \end{aligned} \quad (1)$$

Here  $\Delta > 0$  and  $\phi_{kj} \geq 0$  is the transition rate from  $k$  to  $j$  if  $j \neq k$ , while  $\phi_{kk} = -\sum_{j \neq k} \phi_{kj}$ .

We consider the Markovian jump uncertain neural networks with both time-varying discrete delays and distributed delays as well as leakage delay and impulsive perturbations:

$$\begin{aligned} \dot{\eta}(t) = & -\mathcal{B}(r_t)\eta(t - \rho) + \mathcal{D}_0(r_t)f(\eta(t)) \\ & + \mathcal{D}_1(r_t)f(\eta(t - \tau(t))) \\ & + \mathcal{D}_2(r_t) \int_{t-d(t)}^t f(\eta(s))ds + \mathcal{F}, \quad t \neq t_h \end{aligned} \quad (2)$$

$$\begin{aligned} \Delta\eta(t_h) = & -\mathcal{H}_h(r_t) \left\{ \eta(t_h^-) - \mathcal{B}(r_t) \int_{t_h-\rho}^{t_h} \eta(s)ds \right\}, \\ & t = t_h, \quad h \in \mathbb{Z}_+ \end{aligned}$$

where  $\eta(t) \in \mathbb{R}^n$  stands for the neuron state vector of the system;  $f(\cdot) \in \mathbb{R}^n$  is the nonlinear activation function, respectively,  $\mathcal{F} = (\mathcal{F}_1, \mathcal{F}_2, \dots, \mathcal{F}_n)^T \in \mathbb{R}^n$  is an external input vector;  $\mathcal{B}(r_t) = \text{diag}(b_1(r_t), b_2(r_t), \dots, b_n(r_t))$  is self-feedback parameter matrix of the neurons, where  $b_i(r_t) > 0$ ;  $\mathcal{D}_0(r_t) = [d_0(r_t)]_{n \times n} \in \mathbb{R}^{n \times n}$ ,  $\mathcal{D}_1(r_t) = [d_1(r_t)]_{n \times n} \in \mathbb{R}^{n \times n}$ ,  $\mathcal{D}_2(r_t) = [d_2(r_t)]_{n \times n} \in \mathbb{R}^{n \times n}$  are connection weight matrices. Also,

$\mathcal{H}_h(r_t)$  is the impulses gain matrix at the moment of time  $t_h$ . The discrete set  $\{t_h\}$  satisfies  $0 = t_0 < t_1 < \dots < t_h < \dots, \lim_{h \rightarrow \infty} t_h = \rho$ .  $\eta(t_h^-)$  denotes the left-hand limits at  $t_h$ . Similarly,  $\eta(t_h^+)$  denotes the right-hand limits at  $t_h$ .  $\rho$  is the leakage delay,  $\tau(t)$  is the discrete time-varying delay, and  $d(t)$  is the distributed time-varying delay.

The initial condition associated with model (2) is  $\eta(s) = \psi(s)$ , where  $s \in [-\beta, 0]$ , and  $\psi$  is differentiable on  $[-\beta, 0]$ , and  $\beta = \max\{\rho, \tau, d\}$ .

The time-varying delays  $\tau(t)$  and  $d(t)$  satisfy

$$\begin{aligned} 0 &\leq \tau(t) \leq \tau, \\ 0 &\leq d(t) \leq d, \end{aligned} \quad (3)$$

where  $\tau$  and  $d$  are constants.

Here  $\mathcal{B}(r_t) = \mathcal{B}(r_t) + \Delta\mathcal{B}(r_t)$ ,  $\mathcal{D}_0(r_t) = \mathcal{D}_0(r_t) + \Delta\mathcal{D}_0(r_t)$ ,  $\mathcal{D}_1(r_t) = \mathcal{D}_1(r_t) + \Delta\mathcal{D}_1(r_t)$  and  $\mathcal{D}_2(r_t) = \mathcal{D}_2(r_t) + \Delta\mathcal{D}_2(r_t)$ .  $\Delta\mathcal{B}(r_t)$ ,  $\Delta\mathcal{D}_0(r_t)$ ,  $\Delta\mathcal{D}_1(r_t)$ , and  $\Delta\mathcal{D}_2(r_t)$  are real-valued unknown matrices representing time-varying parameter uncertainties and are assumed to be of the form

$$\begin{aligned} &[\Delta\mathcal{B}(r_t) \quad \Delta\mathcal{D}_0(r_t) \quad \Delta\mathcal{D}_1(r_t) \quad \Delta\mathcal{D}_2(r_t)] \\ &= \mathcal{M}(r_t) F(r_t) [\mathcal{N}_b(r_t) \quad \mathcal{N}_0(r_t) \quad \mathcal{N}_1(r_t) \quad \mathcal{N}_2(r_t)] \end{aligned} \quad (4)$$

where  $\mathcal{M}(r_t)$ ,  $\mathcal{N}_b(r_t)$ ,  $\mathcal{N}_0(r_t)$ ,  $\mathcal{N}_1(r_t)$ , and  $\mathcal{N}_2(r_t)$  are known real constant matrices for all  $r_t \in S$  and  $F(r_t)$  is the uncertain time-varying matrix satisfying  $F^T(r_t)F(r_t) = I$ ,  $\forall r_t \in S$ .

*Assumption (A).* There is a positive diagonal matrix  $\mathcal{L} = \text{diag}\{l_1, l_2, \dots, l_n\}$  such that  $f(0) = 0$  and

$$|f(\beta_1) - f(\beta_2)| \leq \mathcal{L} |\beta_1 - \beta_2| \quad (5)$$

for  $\beta_1 \neq \beta_2$ .

For convenience, each possible value of  $r_t$  is denoted by  $k$ ,  $k \in S$  in the sequel. Then we have  $\mathcal{B}_k = \mathcal{B}(r_t)$ ,  $\mathcal{D}_{0k} = \mathcal{D}_0(r_t)$ ,  $\mathcal{D}_{1k} = \mathcal{D}_1(r_t)$ ,  $\mathcal{D}_{2k} = \mathcal{D}_2(r_t)$ ,  $\mathcal{H}_{hk} = \mathcal{H}_h(r_t)$ .

*Definition 1* (see [57]). The neural network (2) is said to be uniformly stable in Lagrange sense, if, for any  $\delta > 0$ , there is a positive constant  $H = H(\delta) > 0$  such that  $\|\eta(t, \psi)\| < H$  for any  $\psi \in R_\delta = \{\psi \in C([-\beta, 0], \mathbb{R}^n) : \|\psi\| < H, t \geq 0\}$ .

*Definition 2* (see [57]). If there exists a radially unbounded and positive definite function  $V(\cdot)$ , a nonnegative continuous function  $H(\cdot)$ , and two positive constants  $\gamma$  and  $\varepsilon$  such that, for any solution  $\eta(t)$  of neural network (2),  $V(\eta(t)) > \gamma$  implies  $V(\eta(t)) - \gamma \leq H(\psi)e^{-\varepsilon t}$  for any  $t \geq 0$  and  $\psi \in R_\delta$ , then the neural network (2) is said to be globally exponentially attractive (GEA) with respect to  $V(\eta(t))$ , and the compact set  $\Omega = \{\eta(t) \in \mathbb{R}^n : V(\eta(t)) \leq \gamma\}$  is said to be a GEA set of (2).

*Definition 3* (see [57]). The neural network (2) is globally exponentially stable (GES) in Lagrange sense, if it is both uniformly stable in Lagrange sense and GEA. If there is a need to emphasize the Lyapunov-like functions, the neural network will be called GES in Lagrange sense with respect to  $V$ .

*Definition 4* (see [44]). The function  $V : [t_0, \infty) \times \mathbb{R}^n \times S \rightarrow \mathbb{R}^+$  belongs to class  $\psi_0$  if (a) the function  $V$  is continuous on each of the sets  $[t_{h-1}, t_h) \times \mathbb{R}^n \times S$  and for all  $t \geq t_0$ ,  $V(t, 0, i) \equiv 0$ ,  $i \in S$ ; (b)  $V(t, x, i)$  is locally Lipschitzian in  $x \in \mathbb{R}^n$ ,  $i \in S$ ; (c) for each  $h = 1, 2, \dots$  and  $i, j \in S$ , there exist finite limits

$$\lim_{(t,z,j) \rightarrow (t_h^-, x, i)} V(t_h^-, x, i) \quad \text{and} \quad \lim_{(t,z,j) \rightarrow (t_h^+, x, j)} V(t_h^+, x, j) \quad (6)$$

with  $V(t_h^+, x, j) = V(t_h, x, j)$  satisfied.

**Lemma 5** (see [58]). Let  $\eta, \mu \in \mathbb{R}^n$ ,  $\mathcal{R}$  be a positive definite matrix; then the following inequality holds:

$$\eta^T \mu + \mu^T \eta \leq \eta^T \mathcal{R}^{-1} \eta + \mu^T \mathcal{R} \mu. \quad (7)$$

**Lemma 6** (see [59]). For any constant matrix  $\mathcal{R} > 0$ , any scalars  $\alpha$  and  $\beta$  with  $\alpha < \beta$ , and a vector function  $\eta(t) : [\alpha, \beta] \rightarrow \mathbb{R}$  such that the integrals concerned are well defined, the following inequality holds:

$$\begin{aligned} &\left[ \int_\alpha^\beta \eta(s) ds \right]^T \mathcal{R} \left[ \int_\alpha^\beta \eta(s) ds \right] \\ &\leq (\beta - \alpha) \int_\alpha^\beta \eta^T(s) \mathcal{R} \eta(s) ds. \end{aligned} \quad (8)$$

**Lemma 7** (see [59]). The LMI  $\mathcal{R} = \begin{pmatrix} \mathcal{R}_{11} & \mathcal{R}_{12} \\ \mathcal{R}_{12}^T & \mathcal{R}_{22} \end{pmatrix} < 0$  with  $\mathcal{R}_{11} = \mathcal{R}_{11}^T$ ,  $\mathcal{R}_{22} = \mathcal{R}_{22}^T$  is equivalent to one of the following conditions:

$$\begin{aligned} (i) \quad &\mathcal{R}_{22} < 0, \quad \mathcal{R}_{11} - \mathcal{R}_{12} \mathcal{R}_{22}^{-1} \mathcal{R}_{12}^T < 0; \\ (ii) \quad &\mathcal{R}_{11} < 0, \quad \mathcal{R}_{22} - \mathcal{R}_{12}^T \mathcal{R}_{11}^{-1} \mathcal{R}_{12} < 0. \end{aligned} \quad (9)$$

**Lemma 8** (see [57]). Let  $V(t) \in C([0, +\infty), \mathbb{R})$ , and there are two positive constants  $\delta$  and  $\rho$  such that

$$D^+ V(t) \leq -\delta V(t) + \rho, \quad t \geq 0, \quad (10)$$

and then

$$V(t) - \frac{\delta}{\rho} \leq \left( V(0) - \frac{\delta}{\rho} \right) e^{-\delta t}, \quad t \geq 0. \quad (11)$$

In particular, if  $V(t) \geq \delta/\rho$  for  $t \geq 0$ , then  $V(t)$  exponentially approaches  $\rho/\delta$  as  $t$  increases.

**Lemma 9** (see [60]). Let  $\mathcal{D}$ ,  $\mathcal{E}$ , and  $\mathcal{F}(t)$  be real matrices of appropriate dimensions, and  $\mathcal{F}(t)$  satisfies  $\mathcal{F}^T(t)\mathcal{F}(t) = I$ . Then, the following inequality holds for any constant  $\varepsilon > 0$ :

$$\mathcal{D} \mathcal{F}(t) \mathcal{E} + \mathcal{E}^T \mathcal{F}^T(t) \mathcal{D}^T = \varepsilon \mathcal{D} \mathcal{D}^T + \varepsilon^{-1} \mathcal{E}^T \mathcal{E}. \quad (12)$$

### 3. Main Results

The following theorem presents a Lagrange stability condition for the Markovian jump neural networks (2) with uncertainties (i.e.,  $\Delta\mathcal{B}(r_t) \neq 0$ ,  $\Delta\mathcal{D}_0(r_t) \neq 0$ ,  $\Delta\mathcal{D}_1(r_t) \neq 0$ ,  $\Delta\mathcal{D}_2(r_t) \neq 0$ ).

**Theorem 10.** Under assumption (A), for given constants  $\tau, d, \delta > 0$ , there exist positive definite matrices  $\mathcal{W}_1, \mathcal{W}_2, \mathcal{W}_3, \mathcal{W}_4, \mathcal{R}_{1k}, \mathcal{R}_2, \mathcal{R}_3$ , positive diagonal matrices  $\mathcal{Q}, \mathcal{S}$ , and any appropriate dimensional matrices  $\mathcal{P}_1, \mathcal{P}_2, \mathcal{X}_{11}, \mathcal{X}_{12}, \mathcal{X}_{13}, \mathcal{X}_{22}, \mathcal{X}_{23}, \mathcal{X}_{33}$  such that the following linear matrix inequalities (LMIs) hold:

$$\mathcal{X} = \begin{bmatrix} \mathcal{X}_{11} & \mathcal{X}_{12} & \mathcal{X}_{13} \\ * & \mathcal{X}_{22} & \mathcal{X}_{23} \\ * & * & \mathcal{X}_{33} \end{bmatrix} > 0, \quad (13)$$

$$\begin{bmatrix} \mathcal{R}_{1k} & (I - \mathcal{H}_{hk})^T \mathcal{R}_{1l} \\ * & \mathcal{R}_{1l} \end{bmatrix} \geq 0, \quad (14)$$

$$h \in \mathbb{Z}_+, \text{ [here } r_{ih} = l \text{]}$$

$$\Psi = \Psi_{(r,s)} < 0 \quad (15)$$

$$(r, s = 1, 2, \dots, 14),$$

where

$$\begin{aligned} \Psi_{1,1} = & -\mathcal{R}_{1k}\mathcal{B}_k - \mathcal{B}_k\mathcal{R}_{1k} + \delta\mathcal{R}_{1k} + \sum_{j=1}^m \phi_{kj}\mathcal{R}_{1j} \\ & + \delta\mathcal{R}_2 + \tau\mathcal{X}_{11} + \mathcal{X}_{13} + \mathcal{X}_{13}^T + \mathcal{L}\mathcal{Q}\mathcal{L} \\ & + \varepsilon_2\mathcal{N}_{bk}^T\mathcal{N}_{bk}, \end{aligned}$$

$$\Psi_{1,2} = \tau\mathcal{X}_{12} - \mathcal{X}_{13} + \mathcal{X}_{23}^T,$$

$$\Psi_{1,3} = \mathcal{R}_{1k}\mathcal{D}_{0k} - \varepsilon_2\mathcal{N}_{bk}^T\mathcal{N}_{0k},$$

$$\Psi_{1,4} = \mathcal{R}_{1k}\mathcal{D}_{1k} - \varepsilon_2\mathcal{N}_{bk}^T\mathcal{N}_{1k},$$

$$\Psi_{1,5} = \mathcal{R}_{1k}\mathcal{D}_{2k} - \varepsilon_2\mathcal{N}_{bk}^T\mathcal{N}_{2k},$$

$$\Psi_{1,6} = \mathcal{B}_k\mathcal{R}_{1k}\mathcal{B}_k - \delta\mathcal{R}_{1k}\mathcal{B}_k - \sum_{j=1}^m \phi_{kj}\mathcal{R}_{1j}\mathcal{B}_k,$$

$$\Psi_{1,10} = \mathcal{R}_{1k}^T\mathcal{M}_k,$$

$$\Psi_{1,11} = \mathcal{R}_{1k},$$

$$\Psi_{2,2} = \tau\mathcal{X}_{22} - \mathcal{X}_{23} - \mathcal{X}_{23}^T + \mathcal{L}\mathcal{S}\mathcal{L},$$

$$\Psi_{3,3} = d\mathcal{R}_3 - \mathcal{Q} + \varepsilon_1\mathcal{N}_{0k}^T\mathcal{N}_{0k} + \varepsilon_2\mathcal{N}_{0k}^T\mathcal{N}_{0k},$$

$$\Psi_{3,4} = \varepsilon_1\mathcal{N}_{0k}^T\mathcal{N}_{1k} + \varepsilon_2\mathcal{N}_{0k}^T\mathcal{N}_{1k},$$

$$\Psi_{3,5} = \varepsilon_1\mathcal{N}_{0k}^T\mathcal{N}_{2k} + \varepsilon_2\mathcal{N}_{0k}^T\mathcal{N}_{2k},$$

$$\Psi_{3,6} = -\mathcal{D}_{0k}^T\mathcal{R}_{1k}\mathcal{B}_k,$$

$$\Psi_{3,7} = \mathcal{D}_{0k}^T\mathcal{P}_1^T,$$

$$\Psi_{3,8} = \mathcal{D}_{0k}^T\mathcal{P}_2^T - \varepsilon_1\mathcal{N}_{0k}^T\mathcal{N}_{bk},$$

$$\Psi_{4,4} = -\mathcal{S} + \varepsilon_1\mathcal{N}_{1k}^T\mathcal{N}_{1k} + \varepsilon_2\mathcal{N}_{1k}^T\mathcal{N}_{1k},$$

$$\Psi_{4,5} = \varepsilon_1\mathcal{N}_{1k}^T\mathcal{N}_{2k} + \varepsilon_2\mathcal{N}_{1k}^T\mathcal{N}_{2k},$$

$$\Psi_{4,6} = -\mathcal{D}_{1k}^T\mathcal{R}_{1k}\mathcal{B}_k,$$

$$\Psi_{4,7} = \mathcal{D}_{1k}^T\mathcal{P}_1^T,$$

$$\Psi_{4,8} = \mathcal{D}_{1k}^T\mathcal{P}_2^T - \varepsilon_1\mathcal{N}_{1k}^T\mathcal{N}_{bk},$$

$$\Psi_{5,5} = -\frac{e^{-\delta d}}{d}\mathcal{R}_3 + \varepsilon_1\mathcal{N}_{2k}^T\mathcal{N}_{2k} + \varepsilon_2\mathcal{N}_{2k}^T\mathcal{N}_{2k},$$

$$\Psi_{5,6} = -\mathcal{D}_{2k}^T\mathcal{R}_{1k}\mathcal{B}_k,$$

$$\Psi_{5,7} = \mathcal{D}_{2k}^T\mathcal{P}_1^T,$$

$$\Psi_{5,8} = \mathcal{D}_{2k}^T\mathcal{P}_2^T - \varepsilon_1\mathcal{N}_{2k}^T\mathcal{N}_{bk},$$

$$\Psi_{6,6} = \delta\mathcal{B}_k\mathcal{R}_{1k}\mathcal{B}_k + \sum_{j=1}^m \phi_{kj}\mathcal{B}_k\mathcal{R}_{1j}\mathcal{B}_k - \frac{e^{-\delta\rho}}{\rho}\mathcal{R}_2,$$

$$\Psi_{6,10} = -\mathcal{R}_{1k}^T\mathcal{M}_k\mathcal{B}_k,$$

$$\Psi_{6,12} = \mathcal{B}_k\mathcal{R}_{1k},$$

$$\Psi_{7,7} = \tau e^{\delta\tau}\mathcal{X}_{33} - \mathcal{P}_1 - \mathcal{P}_1^T,$$

$$\Psi_{7,8} = -\mathcal{P}_1\mathcal{B}_k - \mathcal{P}_2^T,$$

$$\Psi_{7,9} = \mathcal{P}_1^T\mathcal{M}_k, \Psi_{7,13} = \mathcal{P}_1,$$

$$\Psi_{8,8} = -\mathcal{P}_2\mathcal{B}_k - \mathcal{B}_k\mathcal{P}_2^T + \varepsilon_1\mathcal{N}_{bk}^T\mathcal{N}_{bk},$$

$$\Psi_{8,9} = \mathcal{P}_2^T\mathcal{M}_k,$$

$$\Psi_{8,14} = \mathcal{P}_2,$$

$$\Psi_{9,9} = -\varepsilon_1 I,$$

$$\Psi_{10,10} = -\varepsilon_2 I,$$

$$\Psi_{11,11} = -\mathcal{W}_1,$$

$$\Psi_{12,12} = -\mathcal{W}_2,$$

$$\Psi_{13,13} = -\mathcal{W}_3,$$

$$\Psi_{14,14} = -\mathcal{W}_4, \quad (16)$$

and other  $\Psi_{(r,s)}$  are equal to zero.

Then the Markovian jump uncertain neural network (2) is globally exponentially stable in Lagrange sense. Moreover, the set

$$\Omega = \left\{ \eta(t) \in \mathbb{R}^n : \|\eta(t)\| \leq \left( \frac{\mathcal{F}^T (\mathcal{W}_1 + \mathcal{W}_2 + \mathcal{W}_3 + \mathcal{W}_4) \mathcal{F}}{\delta\lambda_{\min}(\mathcal{R}_1)} \right)^{1/2} e^{\rho\|\mathcal{B}_k\|} \right\} \quad (17)$$

is an estimation of globally exponentially attractive set of (2).

*Proof.* Consider the following Lyapunov-Krasovskii functional candidate for model (2) as

$$V(r_t, t) = \sum_{a=1}^5 V_a(r_t, t), \quad (18)$$

where

$$\begin{aligned} V_1(r_t, t) &= \left( \eta(t) - \mathcal{B}_k \int_{t-\rho}^t \eta(s) ds \right)^T \\ &\quad \cdot \mathcal{R}_{1k} \left( \eta(t) - \mathcal{B}_k \int_{t-\rho}^t \eta(s) ds \right), \\ V_2(r_t, t) &= \int_{-\rho}^0 \int_{t+\theta}^t e^{\delta(s-t)} \eta^T(s) \mathcal{R}_2 \eta(s) ds d\theta, \\ V_3(r_t, t) &= \int_{-d}^0 \int_{t+\theta}^t e^{\delta(s-t)} f^T(\eta(s)) \mathcal{R}_3 f(\eta(s)) ds d\theta, \\ V_4(r_t, t) &= \int_{-\tau}^0 \int_{t+\theta}^t e^{\delta(\tau+s-t)} \dot{\eta}^T(s) \mathcal{X}_{33} \dot{\eta}(s) ds d\theta, \\ V_5(r_t, t) &= \int_0^t \int_{\theta-\tau(\theta)}^{\theta} e^{\delta(s-t)} \vartheta^T(\theta, s) \mathcal{X} \vartheta(\theta, s) ds d\theta, \end{aligned} \quad (19)$$

and  $\vartheta(\theta, s) = [\eta^T(\theta) \quad \eta^T(\theta - \tau(\theta)) \quad \dot{\eta}^T(s)]^T$ .

Computing the time derivative of  $V_1(r_t, t)$ , along the trajectories of model (2), and using Lemma 5, we obtain

$$\begin{aligned} \dot{V}_1(r_t, t) &= \left( \eta(t) - \mathcal{B}_k \int_{t-\rho}^t \eta(s) ds \right)^T \mathcal{R}_{1k} (\dot{\eta}(t) \\ &\quad - \mathcal{B}_k \dot{\eta}(t) + \mathcal{B}_k \eta(t - \rho)) + (\dot{\eta}(t) - \mathcal{B}_k \eta(t) \\ &\quad + \mathcal{B}_k \eta(t - \rho))^T \mathcal{R}_{1k} \left( \eta(t) - \mathcal{B}_k \int_{t-\rho}^t \eta(s) ds \right) \\ &\quad + \sum_{j=1}^m \phi_{kj} \left( \eta(t) - \mathcal{B}_k \int_{t-\rho}^t \eta(s) ds \right)^T \mathcal{R}_{1j} \left( \eta(t) \right. \\ &\quad \left. - \mathcal{B}_k \int_{t-\rho}^t \eta(s) ds \right), \\ &\leq -\delta V_1(r_t, t) + \delta \left( \eta(t) - \mathcal{B}_k \int_{t-\rho}^t \eta(s) ds \right)^T \\ &\quad \cdot \mathcal{R}_{1k} \left( \eta(t) - \mathcal{B}_k \int_{t-\rho}^t \eta(s) ds \right) + \left( \eta(t) \right. \\ &\quad \left. - \mathcal{B}_k \int_{t-\rho}^t \eta(s) ds \right)^T \mathcal{R}_{1k} - \mathcal{B}_k \eta(t) \\ &\quad + \mathcal{D}_{0k} f(\eta(t)) + \mathcal{D}_{1k} f(\eta(t - \tau(t))) \\ &\quad + \mathcal{D}_{2k} \int_{t-d(t)}^t f(\eta(s)) ds + \mathcal{F} + -\mathcal{B}_k \eta(t) \end{aligned}$$

$$\begin{aligned} &+ \mathcal{D}_{0k} f(\eta(t)) + \mathcal{D}_{1k} f(\eta(t - \tau(t))) \\ &+ \mathcal{D}_{2k} \int_{t-d(t)}^t f(\eta(s)) ds + \mathcal{F} \Big)^T \mathcal{R}_{1k} \left( \eta(t) \right. \\ &\quad \left. - \mathcal{B}_k \int_{t-\rho}^t \eta(s) ds \right) + \sum_{j=1}^m \phi_{kj} \left( \eta(t) \right. \\ &\quad \left. - \mathcal{B}_k \int_{t-\rho}^t \eta(s) ds \right)^T \mathcal{R}_{1j} \left( \eta(t) \right. \\ &\quad \left. - \mathcal{B}_k \int_{t-\rho}^t \eta(s) ds \right), \\ &\leq -\delta V_1(r_t, t) + \eta^T(t) \left( -\mathcal{R}_{1k} \mathcal{B}_k - \mathcal{B}_k \mathcal{R}_{1k} + \delta \mathcal{R}_{1k} \right. \\ &\quad \left. + \mathcal{R}_{1k} \mathcal{W}_1^{-1} \mathcal{R}_{1k} + \sum_{j=1}^m \phi_{kj} \mathcal{R}_{1j} \right) \eta(t) + \eta^T(t) \\ &\quad \cdot \mathcal{R}_{1k} \mathcal{D}_{0k} f(\eta(t)) + f^T(\eta(t)) \mathcal{D}_{0k}^T \mathcal{R}_{1k} \eta(t) \\ &\quad + \eta^T(t) \mathcal{R}_{1k} \mathcal{D}_{1k} f(\eta(t - \tau(t))) \\ &\quad + f^T(\eta(t - \tau(t))) \mathcal{D}_{1k}^T \mathcal{R}_{1k} \eta(t) + \eta^T(t) \\ &\quad \cdot \mathcal{R}_{1k} \mathcal{D}_{2k} \int_{t-d(t)}^t f(\eta(s)) ds \\ &\quad + \left( \int_{t-d(t)}^t f(\eta(s)) ds \right)^T \times \mathcal{D}_{2k}^T \mathcal{R}_{1k} \eta(t) + \eta^T(t) \\ &\quad \cdot \left( \mathcal{B}_k \mathcal{R}_{1k} \mathcal{B}_k - \delta \mathcal{R}_{1k} \mathcal{B}_k - \sum_{j=1}^m \phi_{kj} \mathcal{R}_{1j} \mathcal{B}_k \right) \\ &\quad \cdot \int_{t-\rho}^t \eta(s) ds + \left( \int_{t-\rho}^t \eta(s) ds \right)^T \left( \mathcal{B}_k \mathcal{R}_{1k} \mathcal{B}_k \right. \\ &\quad \left. - \delta \mathcal{B}_k \mathcal{R}_{1k} - \sum_{j=1}^m \phi_{kj} \mathcal{B}_k \mathcal{R}_{1j} \right) \eta(t) - f^T(\eta(t)) \\ &\quad \cdot \mathcal{D}_{0k}^T \mathcal{R}_{1k} \mathcal{B}_k \times \int_{t-\rho}^t \eta(s) ds - \left( \int_{t-\rho}^t \eta(s) ds \right)^T \\ &\quad \cdot \mathcal{B}_k \mathcal{R}_{1k} \mathcal{D}_{0k} f(\eta(t)) - f^T(\eta(t - \tau(t))) \\ &\quad \cdot \mathcal{D}_{1k}^T \mathcal{R}_{1k} \mathcal{B}_k \times \int_{t-\rho}^t \eta(s) ds - \left( \int_{t-\rho}^t \eta(s) ds \right)^T \\ &\quad \cdot \mathcal{B}_k \mathcal{R}_{1k} \mathcal{D}_{1k} f(\eta(t - \tau(t))) \\ &\quad - \left( \int_{t-d(t)}^t f(\eta(s)) ds \right)^T \mathcal{D}_{2k}^T \mathcal{R}_{1k} \end{aligned}$$

$$\begin{aligned}
& \times \mathcal{B}_k \int_{t-\rho}^t \eta(s) ds - \left( \int_{t-\rho}^t \eta(s) ds \right)^T \\
& \cdot \mathcal{B}_k \mathcal{R}_{1k} \mathcal{D}_{2k} \int_{t-d(t)}^t f(\eta(s)) ds \\
& + \left( \int_{t-\rho}^t \eta(s) ds \right)^T \times \left( \delta \mathcal{B}_k \mathcal{R}_{1k} \mathcal{B}_k \right. \\
& \left. + \mathcal{B}_k \mathcal{R}_{1k} \mathcal{W}_2^{-1} \mathcal{R}_{1k} \mathcal{B}_k + \sum_{j=1}^m \phi_{kj} \mathcal{B}_k \mathcal{R}_{1j} \mathcal{B}_k \right) \\
& \cdot \int_{t-\rho}^t \eta(s) ds + \mathcal{F}^T (\mathcal{W}_1 + \mathcal{W}_2) \mathcal{F}.
\end{aligned} \tag{20}$$

Calculating the time derivative of  $V_b(r_t, t)$  ( $b = 2, 3, 4, 5$ ), we have

$$\begin{aligned}
\dot{V}_2(r_t, t) &= -\delta \int_{-\rho}^0 \int_{t+\theta}^t e^{\delta(s-t)} \eta^T(s) \mathcal{R}_2 \eta(s) ds d\theta \\
&+ \rho \eta^T(t) \mathcal{R}_2 \eta(t) - \int_{t-\rho}^t e^{\delta(s-t)} \eta^T(s) \mathcal{R}_2 \eta(s) ds \\
&\leq -\delta V_2(r_t, t) + \rho \eta^T(t) \mathcal{R}_2 \eta(t) \\
&- e^{-\delta\rho} \int_{t-\rho}^t \eta^T(s) \mathcal{R}_2 \eta(s) ds \leq -\delta V_2(r_t, t) \\
&+ \rho \eta^T(t) \mathcal{R}_2 \eta(t) - \frac{e^{-\delta\rho}}{\rho} \left( \int_{t-\rho}^t \eta(s) ds \right)^T \\
&\cdot \mathcal{R}_2 \left( \int_{t-\rho}^t \eta(s) ds \right),
\end{aligned} \tag{21}$$

$$\begin{aligned}
\dot{V}_3(r_t, t) &\leq -\delta V_3(r_t, t) + df^T(\eta(t)) \mathcal{R}_3 f(\eta(t)) \\
&- \frac{e^{-\delta d}}{d} \left( \int_{t-d(t)}^t \eta(s) ds \right)^T \mathcal{R}_3 \left( \int_{t-d(t)}^t \eta(s) ds \right),
\end{aligned} \tag{22}$$

$$\begin{aligned}
\dot{V}_4(r_t, t) &= -\delta \int_{-\tau}^0 \int_{t+\theta}^t e^{\delta(\tau+s-t)} \dot{\eta}^T(s) \mathcal{X}_{33} \dot{\eta}(s) ds d\theta \\
&+ \tau e^{\delta\tau} \dot{\eta}^T(t) \mathcal{X}_{33} \dot{\eta}(t) \\
&- \int_{t-\tau}^t e^{\delta(\tau+s-t)} \dot{\eta}^T(s) \mathcal{X}_{33} \dot{\eta}(s) ds \leq -\delta V_4(r_t, t) \\
&+ \tau e^{\delta\tau} \dot{\eta}^T(t) \mathcal{X}_{33} \dot{\eta}(t) - \int_{t-\tau}^t \dot{\eta}^T(s) \mathcal{X}_{33} \dot{\eta}(s) ds,
\end{aligned} \tag{23}$$

$$\begin{aligned}
\dot{V}_5(r_t, t) &= \int_{t-\tau(t)}^t e^{\delta(s-t)} \vartheta^T(t, s) \mathcal{X} \vartheta(t, s) ds \\
&- \delta \int_0^t \int_{\theta-\tau(\theta)}^{\theta} e^{\delta(s-t)} \vartheta^T(\theta, s) \mathcal{X} \vartheta(\theta, s) ds d\theta
\end{aligned}$$

$$\begin{aligned}
& \leq -\delta V_5(r_t, t) + \int_{t-\tau(t)}^t \vartheta^T(t, s) \mathcal{X} \vartheta(t, s) ds \\
&= -\delta V_5(r_t, t) + \tau(t) \left[ \eta^T(t) \mathcal{X}_{11} \eta(t) \right. \\
&+ \eta^T(t) \mathcal{X}_{12} \eta(t - \tau(t)) + \eta^T(t - \tau(t)) \mathcal{X}_{12}^T \eta(t) \\
&+ \eta^T(t - \tau(t)) \mathcal{X}_{22} \eta(t - \tau(t)) \left. \right] + \eta^T(t) \left( \mathcal{X}_{13} \right. \\
&+ \mathcal{X}_{13}^T \eta(t) + \eta^T(t) \left( -\mathcal{X}_{13} + \mathcal{X}_{23}^T \right) \eta(t - \tau(t)) \\
&+ \eta^T(t - \tau(t)) \left( -\mathcal{X}_{13}^T + \mathcal{X}_{23} \right) \eta(t) + \eta^T(t - \tau(t)) \\
&\cdot \left( \mathcal{X}_{23}^T + \mathcal{X}_{23} \right) \eta(t - \tau(t)) \\
&+ \int_{t-\tau}^t \dot{\eta}^T(s) \mathcal{X}_{33} \dot{\eta}(s) ds.
\end{aligned} \tag{24}$$

From assumption (A), it follows that

$$0 \leq \eta^T(t) \mathcal{L} \mathcal{Q} \mathcal{L} \eta(t) - f^T(\eta(t)) \mathcal{Q} f(\eta(t)), \tag{25}$$

$$\begin{aligned}
0 &\leq \eta^T(t - \tau(t)) \mathcal{L} \mathcal{S} \mathcal{L} \eta(t - \tau(t)) \\
&- f^T(\eta(t - \tau(t))) \mathcal{S} f(\eta(t - \tau(t))).
\end{aligned} \tag{26}$$

Left-multiplying two sides of (2) by  $\dot{\eta}^T(t) \mathcal{P}_1$ , we obtain

$$\begin{aligned}
\dot{\eta}^T(t) \mathcal{P}_1 \dot{\eta}(t) &= -\dot{\eta}^T(t) \mathcal{P}_1 \mathcal{B}_k \eta(t - \rho) \\
&+ \dot{\eta}^T(t) \mathcal{P}_1 \mathcal{D}_{0k} f(\eta(t)) \\
&+ \dot{\eta}^T(t) \mathcal{P}_1 \mathcal{D}_{1k} f(\eta(t - \tau(t))) \\
&+ \dot{\eta}^T(t) \mathcal{P}_1 \mathcal{D}_{2k} \int_{t-d(t)}^t f(\eta(s)) ds \\
&+ \dot{\eta}^T(t) \mathcal{P}_1 \mathcal{F}.
\end{aligned} \tag{27}$$

Taking the transpose on two sides of (27), we have

$$\begin{aligned}
\dot{\eta}^T(t) \mathcal{P}_1^T \dot{\eta}(t) &= -\eta^T(t - \rho) \mathcal{B}_k^T \mathcal{P}_1^T \dot{\eta}(t) + f^T(\eta(t)) \mathcal{D}_{0k}^T \mathcal{P}_1^T \dot{\eta}(t) \\
&+ f^T(\eta(t - \tau(t))) \mathcal{D}_{1k}^T \mathcal{P}_1^T \dot{\eta}(t) \\
&+ \left( \int_{t-d(t)}^t f(\eta(s)) ds \right)^T \mathcal{D}_{2k}^T \mathcal{P}_1^T \dot{\eta}(t) \\
&+ \mathcal{F}^T \mathcal{P}_1^T \dot{\eta}(t).
\end{aligned} \tag{28}$$

Adding (27) to (28) and using Lemma 5, we get

$$\begin{aligned}
 0 \leq & \dot{\eta}^T(t) \left( -\mathcal{P}_1 - \mathcal{P}_1^T + \mathcal{P}_1 \mathcal{W}_3^{-1} \mathcal{P}_1 \right) \dot{\eta}(t) \\
 & - \dot{\eta}^T(t) \mathcal{P}_1 \mathcal{B}_k \eta(t - \rho) - \eta^T(t - \rho) \mathcal{B}_k \mathcal{P}_1^T \dot{\eta}(t) \\
 & + \dot{\eta}^T(t) \mathcal{P}_1 \times \mathcal{D}_{0k} f(\eta(t)) \\
 & + f^T(\eta(t)) \mathcal{D}_{0k}^T \mathcal{P}_1^T \dot{\eta}(t) \\
 & + \dot{\eta}^T(t) \mathcal{P}_1 \mathcal{D}_{1k} f(\eta(t - \tau(t))) \\
 & + f^T(\eta(t - \tau(t))) \mathcal{D}_{1k}^T \mathcal{P}_1^T \dot{\eta}(t) \\
 & + \dot{\eta}^T(t) \mathcal{P}_1 \mathcal{D}_{2k} \int_{t-d(t)}^t f(\eta(s)) ds \\
 & + \left( \int_{t-d(t)}^t f(\eta(s)) ds \right)^T \mathcal{D}_{2k}^T \mathcal{P}_1^T \dot{\eta}(t) \\
 & + \mathcal{F}^T(t) \mathcal{W}_3 \mathcal{F}
 \end{aligned} \tag{29}$$

Similarly, we obtain the zero inequality from (2) by multiplying  $\eta^T(t - \rho) \mathcal{P}_2$  and using Lemma 5 as follows:

$$\begin{aligned}
 0 = & -\eta^T(t - \rho) \mathcal{P}_2 \dot{\eta}(t) - \dot{\eta}^T(t) \mathcal{P}_2^T \eta(t - \rho) - \eta^T(t - \rho) \\
 & \cdot \left( \mathcal{P}_2 \mathcal{B}_k + \mathcal{B}_k \mathcal{P}_2^T \right) \eta(t - \rho) + \eta^T(t - \rho) \\
 & \cdot \mathcal{P}_2 \mathcal{D}_{0k} f(\eta(t)) + f^T(\eta(t)) \mathcal{D}_{0k}^T \mathcal{P}_2^T \eta(t - \rho) \\
 & + \eta^T(t - \rho) \mathcal{P}_2 \mathcal{D}_{1k} f\left(\eta(t - \tau(t))\right) \\
 & + f^T(\eta(t - \tau(t))) \mathcal{D}_{1k}^T \mathcal{P}_2^T \eta(t - \rho) \\
 & + \eta^T(t - \rho) \mathcal{P}_2 \mathcal{D}_{2k} \int_{t-d(t)}^t f(\eta(s)) ds \\
 & + \left( \int_{t-d(t)}^t f(\eta(s)) ds \right)^T \mathcal{D}_{2k}^T \mathcal{P}_2^T \eta(t - \rho) + \eta^T(t - \rho) \\
 & \cdot \mathcal{P}_2 \mathcal{F} + \mathcal{F}^T(t) \mathcal{P}_2^T \eta(t - \rho) \leq -\eta^T(t - \rho) \\
 & \cdot \mathcal{P}_2 \dot{\eta}(t) - \dot{\eta}^T(t) \mathcal{P}_2^T \eta(t - \rho) + \eta^T(t - \rho) \\
 & \cdot \left( -\mathcal{P}_2 \mathcal{B}_k - \mathcal{B}_k \mathcal{P}_2^T + \mathcal{P}_2 \mathcal{W}_4^{-1} \mathcal{P}_2 \right) \eta(t - \rho) \\
 & + \eta^T(t - \rho) \mathcal{P}_2 \mathcal{D}_{0k} f(\eta(t)) + f^T(\eta(t)) \\
 & \cdot \mathcal{D}_{0k}^T \mathcal{P}_2^T \eta(t - \rho) + \eta^T(t - \rho) \\
 & \cdot \mathcal{P}_2 \mathcal{D}_{1k} f\left(\eta(t - \tau(t))\right) \\
 & + f^T(\eta(t - \tau(t))) \mathcal{D}_{1k}^T \mathcal{P}_2^T \eta(t - \rho) \\
 & + \eta^T(t - \rho) \mathcal{P}_2 \mathcal{D}_{2k} \int_{t-d(t)}^t f(\eta(s)) ds
 \end{aligned}$$

$$\begin{aligned}
 & + \left( \int_{t-d(t)}^t f(\eta(s)) ds \right)^T \mathcal{D}_{2k}^T \mathcal{P}_2^T \eta(t - \rho) \\
 & + \mathcal{F}^T(t) \mathcal{W}_4 \mathcal{F}.
 \end{aligned} \tag{30}$$

Combining (20)-(26), (29), and (30), we obtain

$$\begin{aligned}
 \dot{V}(r_t, t) \leq & -\delta V(r_t, t) + \xi^T(t) \Theta \xi(t) \\
 & + \mathcal{F}^T(t) (\mathcal{W}_1 + \mathcal{W}_2 + \mathcal{W}_3 + \mathcal{W}_4) \mathcal{F},
 \end{aligned} \tag{31}$$

where  $\xi(T) = [\eta^T(t) \ \eta^T(t - \tau(t)) \ f^T(\eta(t)) \ f^T(\eta(t - \tau(t))) \left( \int_{t-d(t)}^t f(\eta(s)) ds \right)^T \ \left( \int_{t-\rho}^t \eta(s) ds \right)^T \ \dot{\eta}^T(t) \ \eta^T(t - \rho)]^T$ , and

$$\Theta = \left( \Theta_{ij} \right)_{8 \times 8}, \tag{32}$$

in which  $\Theta_{1,1} = -\mathcal{R}_{1k} \mathcal{B}_k - \mathcal{B}_k \mathcal{R}_{1k} + \delta \mathcal{R}_{1k} + \mathcal{R}_{1k} \mathcal{W}_1^{-1} \mathcal{R}_{1k} + \sum_{j=1}^m \phi_{kj} \mathcal{R}_{1j} + \delta \mathcal{R}_2 + \tau \mathcal{X}_{11} + \mathcal{X}_{13} + \mathcal{X}_{13}^T + \mathcal{L} \mathcal{Q} \mathcal{L}$ ,  $\Theta_{1,2} = \tau \mathcal{X}_{12} - \mathcal{X}_{13} + \mathcal{X}_{23}^T$ ,  $\Theta_{1,3} = \mathcal{R}_{1k} \mathcal{D}_{0k}$ ,  $\Theta_{1,4} = \mathcal{R}_{1k} \mathcal{D}_{1k}$ ,  $\Theta_{1,5} = \mathcal{R}_{1k} \mathcal{D}_{2k}$ ,  $\Theta_{1,6} = \mathcal{B}_k \mathcal{R}_{1k} \mathcal{B}_k - \delta \mathcal{R}_{1k} \mathcal{B}_k - \sum_{j=1}^m \phi_{kj} \mathcal{R}_{1j} \mathcal{B}_k$ ,  $\Theta_{2,2} = \tau \mathcal{X}_{22} - \mathcal{X}_{23} - \mathcal{X}_{23}^T + \mathcal{L} \mathcal{S} \mathcal{L}$ ,  $\Theta_{3,3} = d \mathcal{R}_3 - \mathcal{Q}$ ,  $\Theta_{3,6} = -\mathcal{D}_{0k}^T \mathcal{R}_{1k} \mathcal{B}_k = \mathcal{D}_{0k}^T \mathcal{P}_1^T$ ,  $\Theta_{3,8} = \mathcal{D}_{0k}^T \mathcal{P}_2^T$ ,  $\Theta_{4,4} = -\mathcal{S}$ ,  $\Theta_{4,6} = -\mathcal{D}_{1k}^T \mathcal{R}_{1k} \mathcal{B}_k$ ,  $\Theta_{4,7} = \mathcal{D}_{1k}^T \mathcal{P}_1^T$ ,  $\Theta_{4,8} = \mathcal{D}_{1k}^T \mathcal{P}_2^T$ ,  $\Theta_{5,5} = -(e^{-\delta d} / d) \mathcal{R}_3$ ,  $\Theta_{5,6} = -\mathcal{D}_{2k}^T \mathcal{R}_{1k} \mathcal{B}_k$ ,  $\Theta_{5,7} = \mathcal{D}_{2k}^T \mathcal{P}_1^T$ ,  $\Theta_{5,8} = \mathcal{D}_{2k}^T \mathcal{P}_2^T$ ,  $\Theta_{6,6} = \delta \mathcal{B}_k \mathcal{R}_{1k} \mathcal{B}_k + \mathcal{B}_k \mathcal{R}_{1k} \mathcal{W}_2^{-1} \mathcal{R}_{1k} \mathcal{B}_k + \sum_{j=1}^m \phi_{kj} \mathcal{B}_k \mathcal{R}_{1j} \mathcal{B}_k - (e^{-\delta \rho} / \rho) \mathcal{R}_2$ ,  $\Theta_{7,7} = \tau e^{\delta \tau} \mathcal{X}_{33} - \mathcal{P}_1 - \mathcal{P}_1^T + \mathcal{P}_1 \mathcal{W}_3^{-1} \mathcal{P}_1$ ,  $\Theta_{7,8} = -\mathcal{P}_1 \mathcal{B}_k - \mathcal{P}_2^T$ ,  $\Theta_{8,8} = -\mathcal{P}_2 \mathcal{B}_k - \mathcal{B}_k \mathcal{P}_2^T + \mathcal{P}_2 \mathcal{W}_4^{-1} \mathcal{P}_2$ , and the rest of  $\Theta_{ij}$  are zero.

Now we consider the change of  $V(r_t, t)$  at impulse time  $t = t_h, h \in \mathbb{Z}_+$ . By (2), we have

$$\begin{aligned}
 \eta(t_h) - \mathcal{B}_k \int_{t_h - \rho}^{t_h} \eta(s) ds \\
 = \eta(t_h^-) - \mathcal{H}_{hk} \left[ \eta(t_h^-) - \mathcal{B}_k \int_{t_h - \rho}^{t_h} \eta(s) ds \right] \\
 - \mathcal{B}_k \int_{t_h - \rho}^{t_h} \eta(s) ds \\
 = (I - \mathcal{H}_{hk}) \left[ \eta(t_h^-) - \mathcal{B}_k \int_{t_h - \rho}^{t_h} \eta(s) ds \right].
 \end{aligned} \tag{33}$$

Moreover, it follows from (14) that

$$\begin{aligned}
& \begin{bmatrix} \mathcal{R}_{1k} & (I - \mathcal{H}_{hk})^T \mathcal{R}_{1l} \\ * & \mathcal{R}_{1l} \end{bmatrix} \geq 0 \iff \\
& \begin{bmatrix} I & -(I - \mathcal{H}_{hk})^T \\ * & I \end{bmatrix} \begin{bmatrix} \mathcal{R}_{1k} & (I - \mathcal{H}_{hk})^T \mathcal{R}_{1l} \\ * & \mathcal{R}_{1l} \end{bmatrix} \begin{bmatrix} I & 0 \\ -(I - \mathcal{H}_{hk}) & I \end{bmatrix} \geq 0 \iff \\
& \begin{bmatrix} \mathcal{R}_{1k} - (I - \mathcal{H}_{hk})^T \mathcal{R}_{1l} (I - \mathcal{H}_{hk}) & 0 \\ * & \mathcal{R}_{1l} \end{bmatrix} \geq 0 \iff \\
& \mathcal{R}_{1k} - (I - \mathcal{H}_{hk})^T \mathcal{R}_{1l} (I - \mathcal{H}_{hk}) \geq 0
\end{aligned} \tag{34}$$

Combining (33) and (34), we obtain

$$\begin{aligned}
V_1(r_{t_h}, t_h) &= \left[ \eta(t_h) - \mathcal{B}_k \int_{t_h-\rho}^{t_h} \eta(s) ds \right]^T \\
&\cdot \mathcal{R}_{1k} \left[ \eta(t_h) - \mathcal{B}_k \int_{t_h-\rho}^{t_h} \eta(s) ds \right] \\
&= \left[ \eta(t_h^-) - \mathcal{B}_k \int_{t_h-\rho}^{t_h} \eta(s) ds \right]^T (I - \mathcal{H}_{hk})^T \\
&\cdot \mathcal{R}_{1k} (I - \mathcal{H}_{hk}) \left[ \eta(t_h^-) - \mathcal{B}_k \int_{t_h-\rho}^{t_h} \eta(s) ds \right] \\
&\leq \left[ \eta(t_h^-) - \mathcal{B}_k \int_{t_h-\rho}^{t_h} \eta(s) ds \right]^T \\
&\cdot \mathcal{R}_{1k} \left[ \eta(t_h^-) - \mathcal{B}_k \int_{t_h-\rho}^{t_h} \eta(s) ds \right] = V_1(r_{t_h^-}, t_h^-).
\end{aligned} \tag{35}$$

This yields

$$V(r_{t_h}, t_h) \leq V(r_{t_h^-}, t_h^-), \quad h \in \mathbb{Z}_+.$$
 \tag{36}

Obviously, by employing Lemma 6, we see that  $\Psi < 0$  in (15) is equivalent to  $\Theta < 0$ . Thus, it follows from (31) that

$$\begin{aligned}
\dot{V}(r_t, t) &\leq -\delta V(r_t, t) \\
&+ \mathcal{F}^T(t) (\mathcal{W}_1 + \mathcal{W}_2 + \mathcal{W}_3 + \mathcal{W}_4) \mathcal{F}.
\end{aligned} \tag{37}$$

Combining Lemma 7 and (37), we get

$$\begin{aligned}
V(r_t, t) &- \frac{\mathcal{F}^T(t) (\mathcal{W}_1 + \mathcal{W}_2 + \mathcal{W}_3 + \mathcal{W}_4) \mathcal{F}}{\delta} \\
&\leq \left( V(r_0, 0) \right. \\
&\left. - \frac{\mathcal{F}^T(t) (\mathcal{W}_1 + \mathcal{W}_2 + \mathcal{W}_3 + \mathcal{W}_4) \mathcal{F}}{\delta} \right) e^{-\delta t}.
\end{aligned} \tag{38}$$

On the other hand, we obtain

$$\begin{aligned}
V(r_0, 0) &= \left( \eta(0) - \mathcal{B}_k \int_{-\rho}^0 \eta(s) ds \right)^T \mathcal{R}_{1k} \left( \eta(0) \right. \\
&\left. - \mathcal{B}_k \int_{-\rho}^0 \eta(s) ds \right) \\
&+ \int_{-\rho}^0 \int_{\theta}^0 e^{\delta s} \eta^T(s) \mathcal{R}_2 \eta(s) ds d\theta \\
&+ \int_{-d}^0 \int_{\theta}^0 e^{\delta s} f^T(\eta(s)) \mathcal{R}_3 f(\eta(s)) ds d\theta \\
&+ \int_{-\tau}^0 \int_{\theta}^0 e^{\delta(\tau+s)} \dot{\eta}^T(s) \mathcal{X}_{33} \dot{\eta}(s) ds d\theta \\
&\leq \left[ (1 + \rho \|\mathcal{B}_k\|)^2 \|\mathcal{R}_{1k}\| + \frac{\rho}{\delta} \|\mathcal{R}_2\| \right. \\
&+ \frac{d}{\delta} \|\mathcal{R}_3\| \max_{1 \leq i \leq n} \{I_i^2\} \left. \sup_{s \in [-h, 0]} \|\psi(s)\|^2 \right. \\
&+ \left. \left[ \frac{\tau}{\delta} e^{\delta \tau} \|\mathcal{X}_{33}\| \right] \sup_{s \in [-h, 0]} \|\dot{\psi}(s)\|^2 \right].
\end{aligned} \tag{39}$$

Let

$$\begin{aligned}
\mathbf{H} &= \left[ (1 + \rho \|\mathcal{B}_k\|)^2 \|\mathcal{R}_{1k}\| + \frac{\rho}{\delta} \|\mathcal{R}_2\| \right. \\
&+ \left. \frac{d}{\delta} \|\mathcal{R}_3\| \max_{1 \leq i \leq n} \{I_i^2\} \right] \sup_{s \in [-h, 0]} \|\psi(s)\|^2 \\
&+ \left[ \frac{\tau}{\delta} e^{\delta \tau} \|\mathcal{X}_{33}\| \right] \sup_{s \in [-h, 0]} \|\dot{\psi}(s)\|^2.
\end{aligned} \tag{40}$$

From (38), we have

$$\begin{aligned}
V(r_t, t) &- \frac{\mathcal{F}^T(t) (\mathcal{W}_1 + \mathcal{W}_2 + \mathcal{W}_3 + \mathcal{W}_4) \mathcal{F}}{\delta} \\
&\leq \mathbf{H} e^{-\delta t}.
\end{aligned} \tag{41}$$

Hence, the Markovian jump neural network is globally exponentially attractive.

From definition of  $V(r_t, t)$ , we have

$$V(r_t, t) \geq \lambda_{\min}(\mathcal{R}_{1k}) \left\| \eta(t) - \mathcal{B}_k \int_{t-\rho}^t \eta(s) ds \right\|^2. \quad (42)$$

It follows from (41) and (42) that

$$\begin{aligned} \left\| \eta(t) - \mathcal{B}_k \int_{t-\rho}^t \eta(s) ds \right\| &\leq \left( \frac{\mathbf{H}}{\lambda_{\min}(\mathcal{R}_{1k})} \right. \\ &\left. + \frac{\mathcal{F}^T(t) (\mathcal{W}_1 + \mathcal{W}_2 + \mathcal{W}_3 + \mathcal{W}_4) \mathcal{F}}{\delta \lambda_{\min}(\mathcal{R}_{1k})} \right)^{1/2}. \end{aligned} \quad (43)$$

Furthermore,

$$\begin{aligned} \|\eta(t)\| &\leq \left( \frac{\mathbf{H}}{\lambda_{\min}(\mathcal{R}_{1k})} \right. \\ &\left. + \frac{\mathcal{F}^T(t) (\mathcal{W}_1 + \mathcal{W}_2 + \mathcal{W}_3 + \mathcal{W}_4) \mathcal{F}}{\delta \lambda_{\min}(\mathcal{R}_{1k})} \right)^{1/2} + \|\mathcal{B}_k\| \\ &\cdot \int_{t-\rho}^t \|\eta(s)\| ds. \end{aligned} \quad (44)$$

From the well-known Gronwall inequality, we get

$$\begin{aligned} \|\eta(t)\| &\leq \left( \frac{\mathbf{H}}{\lambda_{\min}(\mathcal{R}_{1k})} \right. \\ &\left. + \frac{\mathcal{F}^T(t) (\mathcal{W}_1 + \mathcal{W}_2 + \mathcal{W}_3 + \mathcal{W}_4) \mathcal{F}}{\delta \lambda_{\min}(\mathcal{R}_{1k})} \right)^{1/2} e^{\rho \|\mathcal{B}_k\|}. \end{aligned} \quad (45)$$

Therefore, the Markovian jump neural network (2) is uniformly stable in Lagrange sense. So, the Markovian jump neural network (2) is globally exponentially stable in Lagrange sense. Moreover, we know from (41) and (42) that a globally exponentially attractive set of (2) is as follows:

$$\begin{aligned} \Omega &= \left\{ \eta(t) \in \mathbb{R}^n \mid V(r_t, t) \right. \\ &\leq \left. \frac{\mathcal{F}^T(t) (\mathcal{W}_1 + \mathcal{W}_2 + \mathcal{W}_3 + \mathcal{W}_4) \mathcal{F}}{\delta} \right\} \subseteq \left\{ \eta(t) \right. \\ &\in \mathbb{R}^n \mid \|\eta(t)\| \\ &\leq \left( \frac{\mathcal{F}^T(t) (\mathcal{W}_1 + \mathcal{W}_2 + \mathcal{W}_3 + \mathcal{W}_4) \mathcal{F}}{\delta \lambda_{\min}(\mathcal{R}_{1k})} \right)^{1/2} \\ &\left. \cdot e^{\rho \|\mathcal{B}_k\|} \right\}. \end{aligned} \quad (46)$$

The proof is completed.  $\square$

Theorem 10 provides a Lagrange stability criteria for Markovian jump neural networks with uncertainties (i.e.,  $\Delta \mathcal{B}(r_t) \neq 0, \Delta \mathcal{D}_0(r_t) \neq 0, \Delta \mathcal{D}_1(r_t) \neq 0, \Delta \mathcal{D}_2(r_t) \neq 0$ ). In

the following results we derived the Lagrange stability conditions for the Markovian jump neural networks without uncertainties (i.e.,  $\Delta \mathcal{B}(r_t) = \Delta \mathcal{D}_0(r_t) = \Delta \mathcal{D}_1(r_t) = \Delta \mathcal{D}_2(r_t) = 0$ ).

**Theorem 11.** Under assumption (A), for given constants  $\tau, d, \delta > 0$ , there exist positive definite matrices  $\mathcal{W}_1, \mathcal{W}_2, \mathcal{W}_3, \mathcal{W}_4, \mathcal{R}_{1k}, \mathcal{R}_2, \mathcal{R}_3$ , positive diagonal matrices  $\mathcal{Q}, \mathcal{S}$ , and any appropriate dimensional matrices  $\mathcal{P}_1, \mathcal{P}_2, \mathcal{X}_{11}, \mathcal{X}_{12}, \mathcal{X}_{13}, \mathcal{X}_{22}, \mathcal{X}_{23}, \mathcal{X}_{33}$  such that the following linear matrix inequalities (LMIs) hold:

$$\mathcal{X} = \begin{bmatrix} \mathcal{X}_{11} & \mathcal{X}_{12} & \mathcal{X}_{13} \\ * & \mathcal{X}_{22} & \mathcal{X}_{23} \\ * & * & \mathcal{X}_{33} \end{bmatrix} > 0, \quad (47)$$

$$\begin{bmatrix} \mathcal{R}_{1k} & (I - \mathcal{H}_{hk})^T \mathcal{R}_{1l} \\ * & \mathcal{R}_{1l} \end{bmatrix} \geq 0, \quad (48)$$

$$h \in \mathbb{Z}_+, \text{ [here } r_{t_h} = l]$$

$$\begin{aligned} \check{\Psi} &= \check{\Psi}_{(r,s)} < 0 \\ &(r, s = 1, 2, \dots, 12), \end{aligned} \quad (49)$$

where

$$\check{\Psi}_{1,1} = -\mathcal{R}_{1k} \mathcal{B}_k - \mathcal{B}_k \mathcal{R}_{1k} + \delta \mathcal{R}_{1k} + \sum_{j=1}^m \phi_{kj} \mathcal{R}_{1j}$$

$$+ \delta \mathcal{R}_2 + \tau \mathcal{X}_{11} + \mathcal{X}_{13} + \mathcal{X}_{13}^T + \mathcal{L} \mathcal{Q} \mathcal{L},$$

$$\check{\Psi}_{1,2} = \tau \mathcal{X}_{12} - \mathcal{X}_{13} + \mathcal{X}_{23}^T,$$

$$\check{\Psi}_{1,3} = \mathcal{R}_{1k} \mathcal{D}_{0k},$$

$$\check{\Psi}_{1,4} = \mathcal{R}_{1k} \mathcal{D}_{1k},$$

$$\check{\Psi}_{1,5} = \mathcal{R}_{1k} \mathcal{D}_{2k},$$

$$\check{\Psi}_{1,6} = \mathcal{B}_k \mathcal{R}_{1k} \mathcal{B}_k - \delta \mathcal{R}_{1k} \mathcal{B}_k - \sum_{j=1}^m \phi_{kj} \mathcal{R}_{1j} \mathcal{B}_k,$$

$$\check{\Psi}_{1,9} = \mathcal{R}_{1k},$$

$$\check{\Psi}_{2,2} = \tau \mathcal{X}_{22} - \mathcal{X}_{23} - \mathcal{X}_{23}^T + \mathcal{L} \mathcal{S} \mathcal{L},$$

$$\check{\Psi}_{3,3} = d \mathcal{R}_3 - \mathcal{Q},$$

$$\check{\Psi}_{3,6} = -\mathcal{D}_{0k}^T \mathcal{R}_{1k} \mathcal{B}_k$$

$$\check{\Psi}_{3,7} = \mathcal{D}_{0k}^T \mathcal{P}_1^T,$$

$$\check{\Psi}_{3,8} = \mathcal{D}_{0k}^T \mathcal{P}_2^T,$$

$$\check{\Psi}_{4,4} = -\mathcal{S},$$

$$\begin{aligned}
\check{\Psi}_{4,6} &= -\mathcal{D}_{1k}^T \mathcal{R}_{1k} \mathcal{B}_k, \\
\check{\Psi}_{4,7} &= \mathcal{D}_{1k}^T \mathcal{P}_1^T, \\
\check{\Psi}_{4,8} &= \mathcal{D}_{1k}^T \mathcal{P}_2^T, \\
\check{\Psi}_{5,5} &= -\frac{e^{-\delta d}}{d} \mathcal{R}_3, \\
\check{\Psi}_{5,6} &= -\mathcal{D}_{2k}^T \mathcal{R}_{1k} \mathcal{B}_k, \\
\check{\Psi}_{5,7} &= \mathcal{D}_{2k}^T \mathcal{P}_1^T, \\
\check{\Psi}_{5,8} &= \mathcal{D}_{2k}^T \mathcal{P}_2^T, \\
\check{\Psi}_{6,6} &= \delta \mathcal{B}_k \mathcal{R}_{1k} \mathcal{B}_k + \sum_{j=1}^m \phi_{kj} \mathcal{B}_k \mathcal{R}_{1j} \mathcal{B}_k - \frac{e^{-\delta \rho}}{\rho} \mathcal{R}_2, \\
\check{\Psi}_{6,10} &= \mathcal{B}_k \mathcal{R}_{1k}, \\
\check{\Psi}_{7,7} &= \tau e^{\delta \tau} \mathcal{X}_{33} - \mathcal{P}_1 - \mathcal{P}_1^T, \\
\check{\Psi}_{7,8} &= -\mathcal{P}_1 \mathcal{B}_k - \mathcal{P}_2^T, \\
\check{\Psi}_{7,11} &= \mathcal{P}_1, \\
\check{\Psi}_{8,8} &= -\mathcal{P}_2 \mathcal{B}_k - \mathcal{B}_k \mathcal{P}_2^T, \\
\check{\Psi}_{8,12} &= \mathcal{P}_2, \\
\check{\Psi}_{9,9} &= -\mathcal{W}_1, \\
\check{\Psi}_{10,10} &= -\mathcal{W}_2, \\
\check{\Psi}_{11,11} &= -\mathcal{W}_3, \\
\check{\Psi}_{12,12} &= -\mathcal{W}_4,
\end{aligned}$$

and other  $\check{\Psi}_{(r,s)}$  are zero. (50)

Then, the Markovian jump neural network (2) (with  $\Delta \mathcal{B}(r_t) = \Delta \mathcal{D}_0(r_t) = \Delta \mathcal{D}_1(r_t) = \Delta \mathcal{D}_2(r_t) = 0$ ) is globally exponentially stable in Lagrange sense. Moreover, the set

$$\begin{aligned}
\Omega &= \left\{ \eta(t) \in \mathbb{R}^n \mid \|\eta(t)\| \right. \\
&\leq \left. \left( \frac{\mathcal{F}^T (\mathcal{W}_1 + \mathcal{W}_2 + \mathcal{W}_3 + \mathcal{W}_4) \mathcal{F}}{\delta \lambda_{\min}(\mathcal{R}_1)} \right)^{1/2} e^{\rho \|\mathcal{B}_k\|} \right\}
\end{aligned} \tag{51}$$

is an estimation of globally exponentially attractive set of (2).

*Proof.* Define the Lyapunov-Krasovskii functional candidate as  $V(r_t, t)$  as defined in Theorem 10. By employing the same method in Theorem 10, we can easily prove the desired result.  $\square$

*Remark 12.* Now, we consider the following neural network, as a special case of neural network (2) that reduces to

a delayed neural network without Markovian jump parameters described by

$$\begin{aligned}
\dot{\eta}(t) &= -\mathcal{B}_k \eta(t - \rho) + \mathcal{D}_{0k} f(\eta(t)) \\
&\quad + \mathcal{D}_{1k} f(\eta(t - \tau(t))) \\
&\quad + \mathcal{D}_{2k} \int_{t-d(t)}^t f(\eta(s)) ds + \mathcal{F}, \quad t \neq t_h
\end{aligned} \tag{52}$$

$$\begin{aligned}
\Delta \eta(t_h) &= -\mathcal{H}_{hk} \left\{ \eta(t_h^-) - \mathcal{B}_k \int_{t_h-\rho}^{t_h} \eta(s) ds \right\}, \\
t &= t_h, \quad \kappa \in \mathbb{Z}_+
\end{aligned}$$

Using the same method in Theorem 10, we can get the following results

**Corollary 13.** Under assumption (A), for given constants  $\tau, d, \delta > 0$ , there exist positive definite matrices  $\mathcal{W}_1, \mathcal{W}_2, \mathcal{W}_3, \mathcal{W}_4, \mathcal{R}_{1k}, \mathcal{R}_2, \mathcal{R}_3$ , positive diagonal matrices  $\mathcal{Q}, \mathcal{S}$ , and any appropriate dimensional matrices  $\mathcal{P}_1, \mathcal{P}_2, \mathcal{X}_{11}, \mathcal{X}_{12}, \mathcal{X}_{13}, \mathcal{X}_{22}, \mathcal{X}_{23}, \mathcal{X}_{33}$  such that the following linear matrix inequalities (LMIs) hold:

$$\mathcal{X} = \begin{bmatrix} \mathcal{X}_{11} & \mathcal{X}_{12} & \mathcal{X}_{13} \\ * & \mathcal{X}_{22} & \mathcal{X}_{23} \\ * & * & \mathcal{X}_{33} \end{bmatrix} > 0, \tag{53}$$

$$\begin{bmatrix} \mathcal{R}_{1k} & (I - \mathcal{H}_{hk})^T \mathcal{R}_{1k} \\ * & \mathcal{R}_{1k} \end{bmatrix} \geq 0, \quad h \in \mathbb{Z}_+, \tag{54}$$

$$\begin{aligned}
\widehat{\Psi} &= \widehat{\Psi}_{(r,s)} < 0 \\
(r, s &= 1, 2, \dots, 14),
\end{aligned} \tag{55}$$

where

$$\begin{aligned}
\widehat{\Psi}_{1,1} &= -\mathcal{R}_{1k} \mathcal{B}_k - \mathcal{B}_k \mathcal{R}_{1k} + \delta \mathcal{R}_{1k} + \delta \mathcal{R}_2 + \tau \mathcal{X}_{11} \\
&\quad + \mathcal{X}_{13} + \mathcal{X}_{13}^T + \mathcal{L} \mathcal{Q} \mathcal{L} + \varepsilon_2 \mathcal{N}_{bk}^T \mathcal{N}_{bk},
\end{aligned}$$

$$\widehat{\Psi}_{1,2} = \tau \mathcal{X}_{12} - \mathcal{X}_{13} + \mathcal{X}_{23}^T,$$

$$\widehat{\Psi}_{1,3} = \mathcal{R}_{1k} \mathcal{D}_{0k} - \varepsilon_2 \mathcal{N}_{bk}^T \mathcal{N}_{0k},$$

$$\widehat{\Psi}_{1,4} = \mathcal{R}_{1k} \mathcal{D}_{1k} - \varepsilon_2 \mathcal{N}_{bk}^T \mathcal{N}_{1k},$$

$$\widehat{\Psi}_{1,5} = \mathcal{R}_{1k} \mathcal{D}_{2k} - \varepsilon_2 \mathcal{N}_{bk}^T \mathcal{N}_{2k},$$

$$\widehat{\Psi}_{1,6} = \mathcal{B}_k \mathcal{R}_{1k} \mathcal{B}_k - \delta \mathcal{R}_{1k} \mathcal{B}_k,$$

$$\widehat{\Psi}_{1,10} = \mathcal{R}_{1k}^T \mathcal{M}_k,$$

$$\widehat{\Psi}_{1,11} = \mathcal{R}_{1k},$$

$$\widehat{\Psi}_{2,2} = \tau \mathcal{X}_{22} - \mathcal{X}_{23} - \mathcal{X}_{23}^T + \mathcal{L} \mathcal{S} \mathcal{L},$$

$$\widehat{\Psi}_{3,3} = d \mathcal{R}_3 - \mathcal{Q} + \varepsilon_1 \mathcal{N}_{0k}^T \mathcal{N}_{0k} + \varepsilon_2 \mathcal{N}_{0k}^T \mathcal{N}_{0k},$$

$$\widehat{\Psi}_{3,4} = \varepsilon_1 \mathcal{N}_{0k}^T \mathcal{N}_{1k} + \varepsilon_2 \mathcal{N}_{0k}^T \mathcal{N}_{1k},$$

$$\begin{aligned}
 \widehat{\Psi}_{3,5} &= \varepsilon_1 \mathcal{N}_{0k}^T \mathcal{N}_{2k} + \varepsilon_2 \mathcal{N}_{0k}^T \mathcal{N}_{2k}, \\
 \widehat{\Psi}_{3,6} &= -\mathcal{D}_{0k}^T \mathcal{R}_{1k} \mathcal{B}_k, \\
 \widehat{\Psi}_{3,7} &= \mathcal{D}_{0k}^T \mathcal{P}_1^T, \\
 \widehat{\Psi}_{3,8} &= \mathcal{D}_{0k}^T \mathcal{P}_2^T - \varepsilon_1 \mathcal{N}_{0k}^T \mathcal{N}_{bk}, \\
 \widehat{\Psi}_{4,4} &= -\mathcal{S} + \varepsilon_1 \mathcal{N}_{1k}^T \mathcal{N}_{1k} + \varepsilon_2 \mathcal{N}_{1k}^T \mathcal{N}_{1k}, \\
 \widehat{\Psi}_{4,5} &= \varepsilon_1 \mathcal{N}_{1k}^T \mathcal{N}_{2k} + \varepsilon_2 \mathcal{N}_{1k}^T \mathcal{N}_{2k}, \\
 \widehat{\Psi}_{4,6} &= -\mathcal{D}_{1k}^T \mathcal{R}_{1k} \mathcal{B}_k, \\
 \widehat{\Psi}_{4,7} &= \mathcal{D}_{1k}^T \mathcal{P}_1^T, \\
 \widehat{\Psi}_{4,8} &= \mathcal{D}_{1k}^T \mathcal{P}_2^T - \varepsilon_1 \mathcal{N}_{1k}^T \mathcal{N}_{bk}, \\
 \widehat{\Psi}_{5,5} &= -\frac{e^{-\delta d}}{d} \mathcal{R}_3 + \varepsilon_1 \mathcal{N}_{2k}^T \mathcal{N}_{2k} + \varepsilon_2 \mathcal{N}_{2k}^T \mathcal{N}_{2k}, \\
 \widehat{\Psi}_{5,6} &= -\mathcal{D}_{2k}^T \mathcal{R}_{1k} \mathcal{B}_k, \\
 \widehat{\Psi}_{5,7} &= \mathcal{D}_{2k}^T \mathcal{P}_1^T, \\
 \widehat{\Psi}_{5,8} &= \mathcal{D}_{2k}^T \mathcal{P}_2^T - \varepsilon_1 \mathcal{N}_{2k}^T \mathcal{N}_{bk}, \\
 \widehat{\Psi}_{6,6} &= \delta \mathcal{B}_k \mathcal{R}_{1k} \mathcal{B}_k - \frac{e^{-\delta \rho}}{\rho} \mathcal{R}_2, \\
 \widehat{\Psi}_{6,10} &= -\mathcal{R}_{1k}^T \mathcal{M}_k \mathcal{B}_k, \\
 \widehat{\Psi}_{6,12} &= \mathcal{B}_k \mathcal{R}_{1k}, \\
 \widehat{\Psi}_{7,7} &= \tau e^{\delta \tau} \mathcal{X}_{33} - \mathcal{P}_1 - \mathcal{P}_1^T, \\
 \widehat{\Psi}_{7,8} &= -\mathcal{P}_1 \mathcal{B}_k - \mathcal{P}_2^T, \\
 \widehat{\Psi}_{7,9} &= \mathcal{P}_1^T \mathcal{M}_k, \\
 \widehat{\Psi}_{7,13} &= \mathcal{P}_1, \\
 \widehat{\Psi}_{8,8} &= -\mathcal{P}_2 \mathcal{B}_k - \mathcal{B}_k \mathcal{P}_2^T + \varepsilon_1 \mathcal{N}_{bk}^T \mathcal{N}_{bk}, \\
 \widehat{\Psi}_{8,9} &= \mathcal{P}_2^T \mathcal{M}_k, \\
 \widehat{\Psi}_{8,14} &= \mathcal{P}_2, \\
 \widehat{\Psi}_{9,9} &= -\varepsilon_1 I, \\
 \widehat{\Psi}_{10,10} &= -\varepsilon_2 I, \\
 \widehat{\Psi}_{11,11} &= -\mathcal{W}_1, \\
 \widehat{\Psi}_{12,12} &= -\mathcal{W}_2, \\
 \widehat{\Psi}_{13,13} &= -\mathcal{W}_3, \\
 \widehat{\Psi}_{14,14} &= -\mathcal{W}_4,
 \end{aligned}$$

and other  $\widehat{\Psi}_{(r \times s)}$  are zero.

(56)

Then, the uncertain neural network (2) is globally exponentially stable in Lagrange sense. Moreover, the set

$$\Omega = \left\{ \eta(t) \in \mathbb{R}^n \mid \|\eta(t)\| \leq \left( \frac{\mathcal{F}^T (\mathcal{W}_1 + \mathcal{W}_2 + \mathcal{W}_3 + \mathcal{W}_4) \mathcal{F}}{\delta \lambda_{\min}(\mathcal{R}_{1k})} \right)^{1/2} e^{\rho \|\mathcal{B}_k\|} \right\} \quad (57)$$

is an estimation of globally exponentially attractive set of (2).

*Remark 14.* In this paper we studied exponential Lagrange stability for Markovian jump uncertain neural networks with leakage delay and mixed time-varying delays via impulsive control. The stability of neural networks was studied by applying the differential inequality and Lyapunov method [30–34]. And the authors considered Lyapunov stability, where the Lyapunov stability of equilibrium point can be regarded as a special case of the Lagrange stability. In addition we considered model uncertainties, Markovian jumping parameters, and leakage delay in the concerned networks since it will affect the stability of the systems. Thus our results are more general than the results in the literature.

#### 4. Numerical Example

This section provides numerical result to demonstrate the effectiveness of the presented strategy.

*Example 1.* Consider the following delayed uncertain Markovian jump neural networks with 2 modes:

$$\begin{aligned}
 \dot{\eta}(t) &= -\mathcal{B}_k \eta(t - \rho) + \mathcal{D}_{0k} f(\eta(t)) \\
 &\quad + \mathcal{D}_{1k} f(\eta(t - \tau(t))) \\
 &\quad + \mathcal{D}_{2k} \int_{t-d(t)}^t f(\eta(s)) ds + \mathcal{F}, \quad t \neq t_h \quad (58)
 \end{aligned}$$

$$\Delta \eta(t_h) = -\mathcal{H}_{hk} \left\{ \eta(t_h^-) - \mathcal{B}_k \int_{t_h - \rho}^{t_h} \eta(s) ds \right\},$$

$$t = t_h, \quad h \in \mathbb{Z}_+$$

$$\mathcal{B}_1 = \begin{bmatrix} 1 & 0 \\ 0 & 1 \end{bmatrix},$$

$$\mathcal{D}_{01} = \begin{bmatrix} 0.2 & -1 \\ 0 & -3 \end{bmatrix},$$

$$\mathcal{D}_{11} = \begin{bmatrix} -0.2 & -0.2 \\ 0.2 & -0.3 \end{bmatrix},$$

$$\mathcal{D}_{21} = \begin{bmatrix} -0.3 & -0.8 \\ 0.4 & -0.1 \end{bmatrix},$$

$$\mathcal{B}_2 = \begin{bmatrix} 1 & 0 \\ 0 & 1 \end{bmatrix},$$

$$\mathcal{D}_{02} = \begin{bmatrix} 2 & 1 \\ -1 & 0.2 \end{bmatrix},$$

$$\mathcal{D}_{12} = \begin{bmatrix} -0.3 & -0.4 \\ 0.4 & -0.5 \end{bmatrix},$$

$$\mathcal{D}_{22} = \begin{bmatrix} 0.4 & -0.2 \\ -0.2 & 0.4 \end{bmatrix},$$

$$\mathcal{H}_{h1} = \mathcal{H}_{h2} = \begin{bmatrix} 0.4 & 0 \\ 0 & 0.4 \end{bmatrix},$$

$$\mathcal{M}_1 = \begin{bmatrix} 0.2 & 0 \\ 0 & 0.2 \end{bmatrix},$$

$$\mathcal{N}_{b1} = \mathcal{N}_{01} = \mathcal{N}_{11} = \mathcal{N}_{21} = \begin{bmatrix} 0.1 & 0 \\ 0 & 0.1 \end{bmatrix},$$

$$\mathcal{M}_2 = \begin{bmatrix} 0.5 & 0 \\ 0 & 0.5 \end{bmatrix},$$

$$\mathcal{N}_{b2} = \mathcal{N}_{02} = \mathcal{N}_{12} = \mathcal{N}_{22} = \begin{bmatrix} 0.2 & 0 \\ 0 & 0.2 \end{bmatrix},$$

$$\mathcal{F} = \begin{bmatrix} 0.5 \\ 0.2 \end{bmatrix},$$

$$L = \text{diag} \{0.5, 0.5\}.$$

(59)

In order to obtain Lagrange stability, we take  $\tau = 0.8$ ,  $d = 0.5$ ,  $\delta = 0.5$ , and  $\rho = 0.5$  and apply Theorem 10; we get feasible solutions to LMIs (14) and (15) as follows:

$$\mathcal{R}_{11} = \begin{bmatrix} 0.1899 & -0.1535 \\ -0.1535 & 0.2065 \end{bmatrix},$$

$$\mathcal{R}_{12} = \begin{bmatrix} 0.6008 & 0.0496 \\ 0.0496 & 0.6771 \end{bmatrix},$$

$$\mathcal{R}_2 = \begin{bmatrix} 1.2472 & -0.8560 \\ -0.8560 & 1.2001 \end{bmatrix},$$

$$\mathcal{R}_3 = \begin{bmatrix} 8.2198 & -0.7129 \\ -0.7129 & 6.6828 \end{bmatrix},$$

$$\mathcal{W}_1 = \begin{bmatrix} 514.8650 & 0.0785 \\ 0.0785 & 514.9600 \end{bmatrix},$$

$$\mathcal{W}_2 = \begin{bmatrix} 514.6668 & 0.0266 \\ 0.0266 & 514.6908 \end{bmatrix},$$

$$\mathcal{W}_3 = \begin{bmatrix} 514.8894 & -0.0147 \\ -0.0147 & 514.8409 \end{bmatrix},$$

$$\mathcal{W}_4 = \begin{bmatrix} 515.2687 & -0.0025 \\ -0.0025 & 515.1238 \end{bmatrix},$$

$$\mathcal{Q} = \begin{bmatrix} 8.4321 & 0 \\ 0 & 8.4321 \end{bmatrix},$$

$$\mathcal{S} = \begin{bmatrix} 6.0806 & 0 \\ 0 & 6.0806 \end{bmatrix},$$

$$\mathcal{P}_1 = \begin{bmatrix} 1.1608 & 0.0506 \\ 0.0506 & 0.7860 \end{bmatrix},$$

$$\mathcal{P}_2 = \begin{bmatrix} 1.1608 & 0.0506 \\ 0.0506 & 0.7860 \end{bmatrix},$$

$$\mathcal{X}_{11} = \begin{bmatrix} 2.2685 & -0.0457 \\ -0.0457 & 2.3587 \end{bmatrix},$$

$$\mathcal{X}_{12} = \begin{bmatrix} -3.5666 & -0.0549 \\ -0.0549 & -3.6697 \end{bmatrix},$$

$$\mathcal{X}_{13} = \begin{bmatrix} -2.1441 & -0.0331 \\ -0.0331 & -2.2075 \end{bmatrix},$$

$$\mathcal{X}_{22} = \begin{bmatrix} 2.5925 & 0.0542 \\ 0.0542 & 2.6978 \end{bmatrix},$$

$$\mathcal{X}_{23} = \begin{bmatrix} 2.1427 & 0.0326 \\ 0.0326 & 2.2061 \end{bmatrix},$$

$$\mathcal{X}_{33} = \begin{bmatrix} 0.3626 & 0.0263 \\ 0.0263 & 0.4137 \end{bmatrix}.$$

(60)

From Theorem 10, we know that the uncertain neural networks concerned are globally exponentially stable in Lagrange sense, and

$$\Omega = \{\eta(t) \in \mathbb{R}^n \mid \|\eta(t)\| \leq 12.0212\} \quad (61)$$

is an estimation of globally exponentially attractive set of (2).

## 5. Conclusion

The problem of Lagrange stability analysis has been investigated in this paper for uncertain Markovian jump neural networks with mixed time-varying delays and leakage delay. By choosing a Lyapunov-Krasovskii functional, the improved delay-dependent criteria are based on the Lagrange stability approach with attractive set. The Lagrange stability criterion has been obtained by solving a set of LMIs, which can guarantee the global exponential stability of the concerned system. A numerical example is given to illustrate the validity and feasibility of the obtained theoretical results.

## Data Availability

No data were used to support this study.

## Conflicts of Interest

The authors declare that they have no conflicts of interest.

## Acknowledgments

This work was jointly supported by the National Natural Science Foundation of China (61773217, 61374080), CSIR, 25(0274)/17/EMR-II dated 27/04/2017, the Natural Science Foundation of Jiangsu Province (BK20161552), Qing Lan Project of Jiangsu Province, the Priority Academic Program Development of Jiangsu Higher Education Institutions, and Advanced Study and Training of Professional Leaders of Higher Vocational Colleges in Jiangsu (2017GRFX019).

## References

- [1] G. Wang, "Existence-stability theorems for strong vector set-valued equilibrium problems in reflexive Banach spaces," *Journal of Inequalities and Applications*, 2015:239, 14 pages, 2015.
- [2] Y. Bai and X. Mu, "Global asymptotic stability of a generalized SIRS epidemic model with transfer from infectious to susceptible," *Journal of Applied Analysis and Computation*, vol. 8, no. 2, pp. 402–412, 2018.
- [3] L. Gao, D. Wang, and G. Wang, "Further results on exponential stability for impulsive switched nonlinear time-delay systems with delayed impulse effects," *Applied Mathematics and Computation*, vol. 268, pp. 186–200, 2015.
- [4] Y. Li, Y. Sun, and F. Meng, "New criteria for exponential stability of switched time-varying systems with delays and nonlinear disturbances," *Nonlinear Analysis: Hybrid Systems*, vol. 26, pp. 284–291, 2017.
- [5] L. G. Wang, K. P. Xu, and Q. W. Liu, "On the stability of a mixed functional equation deriving from additive, quadratic and cubic mappings," *Acta Mathematica Sinica*, vol. 30, no. 6, pp. 1033–1049, 2014.
- [6] L. G. Wang and B. Liu, "Fuzzy stability of a functional equation deriving from additive, quadratic, cubic and quartic functions," *Acta Mathematica Sinica*, vol. 55, no. 5, pp. 841–854, 2012.
- [7] F. Li and Y. Bao, "Uniform stability of the solution for a memory-type elasticity system with nonhomogeneous boundary control condition," *Journal of Dynamical and Control Systems*, vol. 23, no. 2, pp. 301–315, 2017.
- [8] Y.-H. Feng and C.-M. Liu, "Stability of steady-state solutions to Navier-Stokes-Poisson systems," *Journal of Mathematical Analysis and Applications*, vol. 462, no. 2, pp. 1679–1694, 2018.
- [9] J. Hu and A. Xu, "On stability of F-Gorenstein flat categories," *Algebra Colloquium*, vol. 23, no. 2, pp. 251–262, 2016.
- [10] W. W. Sun, "Stabilization analysis of time-delay Hamiltonian systems in the presence of saturation," *Applied Mathematics and Computation*, vol. 217, no. 23, pp. 9625–9634, 2011.
- [11] X. Zheng, Y. Shang, and X. Peng, "Orbital stability of solitary waves of the coupled Klein-Gordon-Zakharov equations," *Mathematical Methods in the Applied Sciences*, vol. 40, no. 7, pp. 2623–2633, 2017.
- [12] C. Liu and Y.-J. Peng, "Stability of periodic steady-state solutions to a non-isentropic Euler-Maxwell system," *Zeitschrift für angewandte Mathematik und Physik*, vol. 68, no. 5, Art. 105, 17 pages, 2017.
- [13] X. Zheng, Y. Shang, and X. Peng, "Orbital stability of periodic traveling wave solutions to the generalized Zakharov equations," *Acta Mathematica Scientia B*, vol. 37, no. 4, pp. 998–1018, 2017.
- [14] S. Haykin, *Neural Networks: A Comprehensive Foundation*, NJ, USA, Prentice-Hall, 1998.
- [15] Y. Guo, "Global asymptotic stability analysis for integro-differential systems modeling neural networks with delays," *Zeitschrift für Angewandte Mathematik und Physik*, vol. 61, no. 6, pp. 971–978, 2010.
- [16] Y. Guo, "Global stability analysis for a class of Cohen-Grossberg neural network models," *Bulletin of the Korean Mathematical Society*, vol. 49, no. 6, pp. 1193–1198, 2012.
- [17] A. Abdurahman, H. Jiang, and K. Rahman, "Function projective synchronization of memristor-based Cohen-Grossberg neural networks with time-varying delays," *Cognitive Neurodynamics*, vol. 9, no. 6, pp. 603–613, 2015.
- [18] K. Shi, S. Zhong, H. Zhu, X. Liu, and Y. Zeng, "New delay-dependent stability criteria for neutral-type neural networks with mixed random time-varying delays," *Neurocomputing*, vol. 168, pp. 896–907, 2015.
- [19] Y. Guo, "Mean square exponential stability of stochastic delay cellular neural networks," *Electronic Journal of Qualitative Theory of Differential Equations*, No. 34, 10 pages, 2013.
- [20] Y. Guo, "Exponential stability analysis of travelling waves solutions for nonlinear delayed cellular neural networks," *Dynamical Systems. An International Journal*, vol. 32, no. 4, pp. 490–503, 2017.
- [21] W. Sun and L. Peng, "Observer-based robust adaptive control for uncertain stochastic Hamiltonian systems with state and input delays," *Nonlinear Analysis: Modelling and Control*, vol. 19, no. 4, pp. 626–645, 2014.
- [22] L. G. Wang and B. Liu, "The Hyers-Ulam stability of a functional equation deriving from quadratic and cubic functions in quasi- $\beta$ -normed spaces," *Acta Mathematica Sinica*, vol. 26, no. 12, pp. 2335–2348, 2010.
- [23] Y. Guo, "Nontrivial periodic solutions of nonlinear functional differential systems with feedback control," *Turkish Journal of Mathematics*, vol. 34, no. 1, pp. 35–44, 2010.
- [24] L. Li, F. Meng, and P. Ju, "Some new integral inequalities and their applications in studying the stability of nonlinear integro-differential equations with time delay," *Journal of Mathematical Analysis and Applications*, vol. 377, no. 2, pp. 853–862, 2011.
- [25] M. Li and J. Wang, "Exploring delayed Mittag-Leffler type matrix functions to study finite time stability of fractional delay differential equations," *Applied Mathematics and Computation*, vol. 324, pp. 254–265, 2018.
- [26] G. Liu, S. Xu, Y. Wei, Z. Qi, and Z. Zhang, "New insight into reachable set estimation for uncertain singular time-delay systems," *Applied Mathematics and Computation*, vol. 320, pp. 769–780, 2018.
- [27] W. Sun, Y. Wang, and R. Yang, "L2 disturbance attenuation for a class of time delay Hamiltonian systems," *Journal of Systems Science & Complexity*, vol. 24, no. 4, pp. 672–682, 2011.

- [28] W. Qi, Y. Kao, X. Gao, and Y. Wei, "Controller design for time-delay system with stochastic disturbance and actuator saturation via a new criterion," *Applied Mathematics and Computation*, vol. 320, pp. 535–546, 2018.
- [29] Y. Guo, "Mean square global asymptotic stability of stochastic recurrent neural networks with distributed delays," *Applied Mathematics and Computation*, vol. 215, no. 2, pp. 791–795, 2009.
- [30] S. Boyd, L. El Ghaoui, E. Feron, and V. Balakrishnan, *Linear Matrix Inequalities in System and Control Theory*, SIAM, Philadelphia, Pa, USA, 1994.
- [31] R. Anbuvithya, K. Mathiyalagan, R. Sakthivel, and P. Prakash, "Passivity of memristor-based BAM neural networks with different memductance and uncertain delays," *Cognitive Neurodynamics*, vol. 10, no. 4, pp. 339–351, 2016.
- [32] Y. Guo, "Globally robust stability analysis for stochastic Cohen-Grossberg neural networks with impulse and time-varying delays," *Ukrainian Mathematical Journal*, vol. 69, no. 8, pp. 1049–1060, 2017.
- [33] R. Sathy and P. Balasubramaniam, "Stability analysis of fuzzy Markovian jumping Cohen-Grossberg BAM neural networks with mixed time-varying delays," *Communications in Nonlinear Science and Numerical Simulation*, vol. 16, no. 4, pp. 2054–2064, 2011.
- [34] M. Syed Ali, "Robust stability of stochastic uncertain recurrent neural networks with Markovian jumping parameters and time-varying delays," *International Journal of Machine Learning and Cybernetics*, vol. 5, no. 1, pp. 13–22, 2014.
- [35] K. Gopalsamy, "Leakage delays in BAM," *Journal of Mathematical Analysis and Applications*, vol. 325, no. 2, pp. 1117–1132, 2007.
- [36] Q. Zhu, J. Cao, T. Hayat, and F. Alsaadi, "Robust stability of Markovian jump stochastic neural networks with time delays in the leakage terms," *Neural Processing Letters*, vol. 41, pp. 1–27, 2015.
- [37] M. Syed Ali, S. Arik, and M. Esther Rani, "Passivity analysis of stochastic neural networks with leakage delay and Markovian jumping parameters," *Neurocomputing*, vol. 218, pp. 139–145, 2016.
- [38] R. S. Kumar, G. Sugumaran, R. Raja, Q. Zhu, and U. K. Raja, "New stability criterion of neural networks with leakage delays and impulses: a piecewise delay method," *Cognitive Neurodynamics*, vol. 10, no. 1, pp. 85–98, 2016.
- [39] M. Syed Ali and M. Esther Rani, "Passivity analysis of uncertain stochastic neural networks with time-varying delays and Markovian jumping parameters," *Network: Computation in Neural Systems*, vol. 26, no. 3–4, pp. 73–96, 2015.
- [40] O. M. Kwon, M. J. Park, J. H. Park, S. M. Lee, and E. J. Cha, "Passivity analysis of uncertain neural networks with mixed time-varying delays," *Nonlinear Dynamics*, vol. 73, no. 4, pp. 2175–2189, 2013.
- [41] S. Zhu, Y. Shen, and G. Chen, "Exponential passivity of neural networks with time-varying delay and uncertainty," *Physics Letters A*, vol. 375, no. 2, pp. 136–142, 2010.
- [42] Y. Liu, W. Liu, M. A. Obaid, and I. A. Abbas, "Exponential stability of Markovian jumping Cohen-Grossberg neural networks with mixed mode-dependent time-delays," *Neurocomputing*, vol. 177, pp. 409–415, 2016.
- [43] Q. Zhu and J. Cao, "Exponential stability of stochastic neural networks with both Markovian jump parameters and mixed time delays," *IEEE Transactions on Systems, Man, and Cybernetics, Part B: Cybernetics*, vol. 41, no. 2, pp. 341–353, 2011.
- [44] Q. Zhu and J. Cao, "Stability analysis of markovian jump stochastic BAM neural networks with impulse control and mixed time delays," *IEEE Transactions on Neural Networks and Learning Systems*, vol. 23, no. 3, pp. 467–479, 2012.
- [45] M. Syed Ali, "Stability of Markovian jumping recurrent neural networks with discrete and distributed time-varying delays," *Neurocomputing*, vol. 149, pp. 1280–1285, 2015.
- [46] M. Syed Ali, N. Gunasekaran, and Q. Zhu, "State estimation of T-S fuzzy delayed neural networks with Markovian jumping parameters using sampled-data control," *Fuzzy Sets and Systems*, vol. 306, pp. 87–104, 2017.
- [47] G. Chen, O. van Gaans, and S. Verduyn Lunel, "Fixed points and  $p$ th moment exponential stability of stochastic delayed recurrent neural networks with impulses," *Applied Mathematics Letters*, vol. 27, pp. 36–42, 2014.
- [48] G. Seiler and J. A. Nossek, "Winner-Take-All Cellular Neural Networks," *IEEE Transactions on Circuits and Systems II: Analog and Digital Signal Processing*, vol. 40, no. 3, pp. 184–190, 1993.
- [49] H. Wersing, W.-J. Beyn, and H. Ritter, "Dynamical stability conditions for recurrent neural networks with unsaturating piecewise linear transfer functions," *Neural Computation*, vol. 13, no. 8, pp. 1811–1825, 2001.
- [50] Q. Luo, Z. Zeng, and X. Liao, "Global exponential stability in Lagrange sense for neutral type recurrent neural networks," *Neurocomputing*, vol. 74, no. 4, pp. 638–645, 2011.
- [51] A. Wu, Z. Zeng, C. Fu, and W. Shen, "Global exponential stability in Lagrange sense for periodic neural networks with various activation functions," *Neurocomputing*, vol. 74, no. 5, pp. 831–837, 2011.
- [52] X. Wang, M. Jiang, and S. Fang, "Stability analysis in Lagrange sense for a non-autonomous Cohen-Grossberg neural network with mixed delays," *Nonlinear Analysis. Theory, Methods & Applications. An International Multidisciplinary Journal*, vol. 70, no. 12, pp. 4294–4306, 2009.
- [53] B. Wang, J. Jian, and M. Jiang, "Stability in Lagrange sense for Cohen-Grossberg neural networks with time-varying delays and finite distributed delays," *Nonlinear Analysis: Hybrid Systems*, vol. 4, no. 1, pp. 65–78, 2010.
- [54] Z. Tu, J. Jian, and K. Wang, "Global exponential stability in Lagrange sense for recurrent neural networks with both time-varying delays and general activation functions via LMI approach," *Nonlinear Analysis: Real World Applications*, vol. 12, no. 4, pp. 2174–2182, 2011.
- [55] Z. Tu, J. Jian, and B. Wang, "Positive invariant sets and global exponential attractive sets of a class of neural networks with unbounded time-delays," *Communications in Nonlinear Science and Numerical Simulation*, vol. 16, no. 9, pp. 3738–3745, 2011.
- [56] X. Liao, Q. Luo, and Z. Zeng, "Positive invariant and global exponential attractive sets of neural networks with time-varying delays," *Neurocomputing*, vol. 71, no. 4–6, pp. 513–518, 2008.
- [57] X. Liao, Q. Luo, Z. Zeng, and Y. Guo, "Global exponential stability in Lagrange sense for recurrent neural networks with time delays," *Nonlinear Analysis: Real World Applications*, vol. 9, no. 4, pp. 1535–1557, 2008.
- [58] H. Wu, X. Liao, W. Feng, and S. Guo, "Mean square stability of uncertain stochastic BAM neural networks with interval time-varying delays," *Cognitive Neurodynamics*, vol. 6, no. 5, pp. 443–458, 2012.

- [59] K. Gu, "An integral inequality in the stability problem of time-delay systems," in *Proceedings of the 39th IEEE Conference on Decision and Control*, vol. 3, pp. 2805–2810, Sydney, Australia, December 2000.
- [60] B. Chen, X. Liu, C. Lin, and K. Liu, "Robust  $H_\infty$  control of Takagi–Sugeno fuzzy systems with state and input time delays," *Fuzzy Sets and Systems*, vol. 160, no. 4, pp. 403–422, 2009.

## Research Article

# Adaptive Tracking Control for a Class of Manipulator Systems with State Constraints and Stochastic Disturbances

Wei Sun <sup>1,2</sup>, Wenxing Yuan,<sup>1</sup> Jing Zhang,<sup>1</sup> and Qun Sun <sup>3</sup>

<sup>1</sup>School of Mathematics Science, Liaocheng University, Liaocheng 252000, China

<sup>2</sup>Key Laboratory of Measurement and Control of CSE, Ministry of Education, School of Automation, Southeast University, Nanjing 210096, China

<sup>3</sup>School of Mechanical and Automotive Engineering, Liaocheng University, Liaocheng 252000, China

Correspondence should be addressed to Wei Sun; [tellsunwei@sina.com](mailto:tellsunwei@sina.com)

Received 7 April 2018; Revised 13 May 2018; Accepted 24 May 2018; Published 20 June 2018

Academic Editor: Xue-Jun Xie

Copyright © 2018 Wei Sun et al. This is an open access article distributed under the Creative Commons Attribution License, which permits unrestricted use, distribution, and reproduction in any medium, provided the original work is properly cited.

An adaptive controller is constructed for a class of stochastic manipulator nonlinear systems in this paper. The states are constrained in the compact set. A tan-type Barrier Lyapunov Function (BLF) is employed to deal with state constraints. The proposed control scheme guarantees the output error convergence to a small neighbourhood of zero. All the signals in the closed-loop system are bounded. The simulation results illustrate the validity of the proposed method.

## 1. Introduction

Adaptive control of strict-feedback nonlinear systems has received a lot of attention since the appearance of recursive backstepping design [1] and feedforward design [2, 3]; a great deal of work has been done for this class of systems in the past decades; for example, see [4–9]. Constraints are widespread in many real systems such as robotic manipulators and physical engineering systems. Therefore robotic manipulators have received increasing attention over the last few years. For this reason, many methods have been used to handle the issue of constraints, for example, [10–16]. In detail, in [10], the author studies the neural network adaptive control design for robotic systems with the velocity constraints and input saturation. An adaptive finite-time controller is considered in [11] for a class of strict-feedback nonlinear systems with parametric uncertainties and full state constraints. In [12], the problem of position control of manipulators operating in the task space under state constraints has been addressed. Literatures [15, 16] discussed the trajectory and tracking control problems of the mobile manipulator with constrained end-effector and adaptive controllers are proposed.

The practical systems are inevitable to contain the stochastic disturbance and it can cause instability of system.

So the stability of stochastic nonlinear systems has attracted great attention [17–19]. In [20], the author has proposed the state equations of the stochastic dynamics of an open-chain manipulator in a fluid environment. This paper has given an algorithm for the discretization of the state equations and explained how the interaction between a fluid and a manipulator can be taken into account in the control of manipulators. The work [21] studies the problem of output feedback stabilization for a class of stochastic feedforward nonlinear systems with state and input delays and the unknown output function. In [22], the stochastic response of a mobile robotic manipulator has been investigated. This paper has studied the sensitivities of the joints responses to base velocity, the surface roughness coefficients, manipulator configuration, and damping in detail.

In this paper, an adaptive tracking controller will be designed for stochastic manipulator nonlinear systems with full state constraints. A backstepping technique with a tan-type Barrier Lyapunov Function (BLF) will be constructed to address the state constraints problem and all the states in stochastic nonlinear systems are not violated. The error signals have converged to an arbitrarily small neighbourhood of zero and all the signals in the closed-loop system are bounded.

## 2. System Description

*2.1. Problem Statement and Preliminary Results.* Consider the one-link manipulator which contains motor dynamics and stochastic disturbances. The model is described as [9]

$$\begin{aligned} D\ddot{q} + \theta\dot{q} - N \sin(q) &= \tau_r + \tau_d, \\ M\dot{\tau}_r + H\tau_r &= u - k_m\dot{q}, \end{aligned} \quad (1)$$

where  $q, \dot{q}, \ddot{q}$  are the link position, velocity, and acceleration, respectively;  $\tau_r$  denotes the torque produced by the electrical system;  $\tau_d$  is the known torque stochastic disturbance;  $u$  is the electromechanical torque control input;  $D$  is a known mechanical inertia;  $\theta$  is unknown coefficient of viscous friction at the joint;  $N$  is a known constant related to the mass of the load and the coefficient of gravity;  $M$  is the known armature inductance;  $H$  is the known armature resistance;  $k_m$  is the known back electromotive force coefficient;  $m$  is the link mass; and  $l$  is the length of the link which is known. Then, following change of coordinates  $\xi_1 = q$ ,  $\xi_2 = \dot{q}$ ,  $\xi_3 = \tau_r$ , we can get

$$\begin{aligned} d\xi_1 &= \xi_2 dt, \\ d\xi_2 &= \frac{1}{D} (\xi_3 - \theta\xi_2 + 10 \sin(\xi_1)) dt + \frac{1}{D} \sin(\xi_1) \xi_1 d\omega, \\ d\xi_3 &= \frac{1}{M} (u - k_m\xi_2 - H\xi_3) dt, \\ y &= \xi_1. \end{aligned} \quad (2)$$

All the states are constrained in the compact set as  $\Omega_\xi := \{\xi_i(t) \in R, |\xi_i(t)| \leq k_{c_i}\}$ , where  $i = 1, 2, 3$ ,  $k_{c_i}$  are positive constants.

Given a reference trajectory  $q_d$ , the control objective is to design an adaptive control algorithm such that  $q$  tracks the desired trajectory  $q_d$  as much as possible; all the signals in closed-loop systems are bounded; the state constraint requirements are not violated. To facilitate control system design, the following assumption and lemma are proposed.

*Assumption 1.* The reference trajectory  $y_d(t)$  and its derivatives up to the  $n$ -th ones are continuous and bounded. That is, for any constant  $k_{c_i} > 0$ , there exist positive constants  $Y_i, i = 0, \dots, n$ , such that  $|y_d(t)| \leq Y_0 < k_{c_1}$ ,  $|y_d^{(i)}(t)| \leq Y_i, i = 1, \dots, n$ .

*Remark 2.* This assumption is reasonable. Assumption 1 is the worst case one. The requirement on derivatives is widely fixed in backstepping control [23]. This is because the standard backstepping technique requires the reference signal to be continuous and derivable to design the desired controller.  $y_0 < k_{c_1}$  in assumption is always true in practice for the requirement of output tracking control. A similar assumption is also considered in [24, 25].

Next, consider the following stochastic nonlinear system:

$$dx = f(x) dt + g(x) d\omega, \quad (3)$$

where  $x \in R^n$  is the system state vector;  $f(x) \in R^n$  and  $g(x) \in R^{n \times r}$  satisfy the locally Lipschitz functions and the linear growth condition and  $f(0) = 0, g(0) = 0$ ;  $\omega$  is an  $r$ -dimensional standard Wiener process.

*Definition 3* (see [2]). For any Lyapunov function  $V(x, t) \in C^{2,1}$ , we define the differential operator  $L$  as follows:

$$L[V(x, t)] = \frac{\partial V}{\partial t} + \frac{\partial V}{\partial x} f + \frac{1}{2} \text{Tr} \left\{ g^T \frac{\partial^2 V}{\partial x^2} g \right\}, \quad (4)$$

where  $\text{Tr}(\cdot)$  is the matrix trace.

**Lemma 4** (see [26]). *There exist a  $C^{2,1}$  function  $V$ , two constants  $\gamma > 0, \rho > 0$ , and  $K_\infty$  class functions  $\alpha_1, \alpha_2$  satisfying  $\alpha_1(\|x\|) \leq V(x) \leq \alpha_2(\|x\|)$  and  $LV(x) \leq -\gamma V(x) + \rho$ ; then, there is a unique strong solution which satisfies*

$$E[V(x)] \leq V(x_0) e^{-\gamma t} + \frac{\rho}{\gamma}. \quad (5)$$

## 3. Control Design and Stability Analysis

*Step 1.* Define the tracking error  $e_1 = \xi_1 - y_d, e_2 = \xi_2 - \alpha_1$ , where  $\alpha_i$  are the virtual controllers and  $|\alpha_i| < \bar{\alpha}_i$  with  $\bar{\alpha}_i$  are positive constants, and  $e_i \in \Omega_e := \{e_i \in R, |e_i| < k_{b_i}, i = 1, \dots, n\}$  with  $k_{b_1} = k_{c_1} - Y_0 > 0, k_{b_i} = k_{c_i} - \bar{\alpha}_{i-1} > 0$ . We can get

$$de_1 = d\xi_1 - dy_d = (e_2 + \alpha_1 - \dot{y}_d) dt. \quad (6)$$

Consider a candidate BLF as follows:

$$V_1 = \frac{k_{b_1}^4}{\pi} \tan\left(\frac{\pi e_1^4}{4k_{b_1}^4}\right). \quad (7)$$

Based on Definition 3, one has

$$LV_1 = \frac{e_1^3}{\cos^2(\pi e_1^4/4k_{b_1}^4)} (e_2 + \alpha_1 - \dot{y}_d). \quad (8)$$

Design the virtual controller  $\alpha_1$  as

$$\alpha_1 = -\frac{K_1 \sin(\pi e_1^4/4k_{b_1}^4) \cos(\pi e_1^4/4k_{b_1}^4)}{e_1^3} + \dot{y}_d, \quad (9)$$

where  $K_1 > 0$  is a design parameter. Substituting (9) into (8), we can obtain

$$LV_1 \leq -K_1 \tan\left(\frac{\pi e_1^4}{4k_{b_1}^4}\right) + \frac{e_1^3}{\cos^2(\pi e_1^4/4k_{b_1}^4)} e_2. \quad (10)$$

*Step 2.* Define the tracking error  $e_3 = \xi_3 - \alpha_2$ ; the following can be obtained:

$$\begin{aligned} de_2 &= d\xi_2 - d\alpha_1 \\ &= \frac{1}{D} (e_3 + \alpha_2 - \theta\xi_2 + 10 \sin(\xi_1)) dt \\ &\quad + \frac{1}{D} \sin(\xi_1) \xi_1 d\omega \\ &\quad - \left( \frac{\partial \alpha_1}{\partial \xi_1} \xi_2 + \sum_{i=1}^2 \frac{\partial \alpha_1}{\partial y_d^{(i-1)}} y_d^{(i)} \right) dt. \end{aligned} \quad (11)$$

Choose a candidate BLF as follows:

$$V_2 = V_1 + \frac{k_{b_2}^4}{\pi} \tan\left(\frac{\pi e_2^4}{4k_{b_2}^4}\right) + \frac{1}{2}\tilde{\theta}^2. \quad (12)$$

Here  $\tilde{\theta} = \hat{\theta} - \theta$ ,  $\hat{\theta}$  denotes the estimation of  $\theta$ . Based on Definition 3, we can obtain

$$\begin{aligned} LV_2 = & LV_1 + \frac{e_2^3}{\cos^2(\pi e_2^4/4k_{b_2}^4)} \left( \frac{1}{D} (e_3 + \alpha_2 - \theta \xi_2 + 10 \right. \\ & \cdot \sin(\xi_1)) - \frac{\partial \alpha_1}{\partial \xi_1} \xi_2 - \sum_{i=1}^2 \frac{\partial \alpha_1}{\partial y_d^{(i-1)}} y_d^{(i)} \left. \right) \\ & + \frac{3k_{b_2}^4 e_2^4 \cos(\pi e_2^4/4k_{b_2}^4) + 2\pi e_2^6 \sin(\pi e_2^4/4k_{b_2}^4)}{2k_{b_2}^4 \cos^3(\pi e_2^4/4k_{b_2}^4)} \left( \frac{1}{D} \right. \\ & \cdot \sin(\xi_1) \xi_1 \left. \right)^2 + \tilde{\theta} \dot{\tilde{\theta}} \leq LV_1 + \tilde{\theta} \dot{\tilde{\theta}} \\ & + \frac{e_2^3}{\cos^2(\pi e_2^4/4k_{b_2}^4)} \left( \frac{1}{D} (\alpha_2 - \hat{\theta} \xi_2 + 10 \sin(\xi_1)) \right. \\ & - \frac{\partial \alpha_1}{\partial \xi_1} \xi_2 - \sum_{i=1}^2 \frac{\partial \alpha_1}{\partial y_d^{(i-1)}} y_d^{(i)} \\ & + \frac{3k_{b_2}^4 e_2 \cos(\pi e_2^4/4k_{b_2}^4) + 2\pi e_2^3 \sin(\pi e_2^3/4k_{b_2}^4)}{2k_{b_2}^4 \cos(\pi e_2^4/4k_{b_2}^4)} \left( \frac{\xi_1}{D} \right. \\ & \cdot \sin(\xi_1) \left. \right)^2 \left. \right) + \frac{e_2^3 e_3}{D \cos^2(\pi e_2^4/4k_{b_2}^4)} \\ & - \frac{\tilde{\theta} e_2^3 \xi_2}{D \cos^2(\pi e_2^4/4k_{b_2}^4)}. \end{aligned} \quad (13)$$

Design the virtual controller  $\alpha_2$  as

$$\begin{aligned} \alpha_2 = & -\frac{K_2 D \sin(\pi e_2^4/4k_{b_2}^4) \cos(\pi e_2^4/4k_{b_2}^4)}{e_2^3} + \hat{\theta} \xi_2 - 10 \\ & \cdot \sin(\xi_1) + D \frac{\partial \alpha_1}{\partial \xi_1} \xi_2 + D \sum_{i=1}^2 \frac{\partial \alpha_1}{\partial y_d^{(i-1)}} y_d^{(i)} \\ & - \frac{3k_{b_2}^4 e_2 \cos(\pi e_2^4/4k_{b_2}^4) + 2\pi e_2^3 \sin(\pi e_2^3/4k_{b_2}^4)}{2Dk_{b_2}^4 \cos(\pi e_2^4/4k_{b_2}^4)} \\ & \cdot \xi_1^2 \sin^2(\xi_1), \end{aligned} \quad (14)$$

where  $K_2 > 0$  is a design parameter. An tuning function is chosen as  $\tau_1 = e_2^3 \xi_2 / D \cos^2(\pi e_2^4/4k_{b_2}^4)$ . Substituting (14) into (13) yields

$$\begin{aligned} LV_2 \leq & -\sum_{i=1}^2 K_i \tan\left(\frac{\pi e_i^4}{4k_{b_i}^4}\right) + \tilde{\theta} (\dot{\tilde{\theta}} - \tau_1) \\ & + \frac{e_2^3 e_3}{D \cos^2(\pi e_2^4/4k_{b_2}^4)}. \end{aligned} \quad (15)$$

Step 3. Defining the tracking error  $e_3 = \xi_3 - \alpha_2$ , we have

$$\begin{aligned} de_3 = & d\xi_3 - d\alpha_2 = \frac{1}{M} (u - k_m \xi_2 - H \xi_3) dt \\ & - \left( \frac{\partial \alpha_2}{\partial \xi_1} \xi_2 + \frac{\partial \alpha_2}{\partial \xi_2} \left( \frac{1}{D} (\xi_3 - \theta \xi_2 + 10 \sin(\xi_1)) \right) \right. \\ & + \sum_{i=1}^3 \frac{\partial \alpha_2}{\partial y_d^{(i-1)}} y_d^{(i)} + \frac{\partial \alpha_2}{\partial \hat{\theta}} \dot{\hat{\theta}} \\ & \left. + \frac{1}{2} \frac{\partial^2 \alpha_2}{\partial \xi_2^2} \left( \frac{1}{D} \sin(\xi_1) \xi_1 \right)^2 \right) dt. \end{aligned} \quad (16)$$

Construct a candidate BLF as follows:

$$V_3 = V_2 + \frac{k_{b_3}^4}{\pi} \tan\left(\frac{\pi e_3^4}{4k_{b_3}^4}\right). \quad (17)$$

Based on Definition 3, computing  $LV_3$ , we can figure out

$$\begin{aligned} LV_3 = & LV_2 + \frac{e_3^3}{\cos^2(\pi e_3^4/4k_{b_3}^4)} \left( \frac{1}{M} (u - k_m \xi_2 - H \xi_3) \right. \\ & - \frac{\partial \alpha_2}{\partial \xi_1} \xi_2 + \frac{\partial \alpha_2}{\partial \xi_2} \left( \frac{1}{D} (\xi_3 - \theta \xi_2 + 10 \sin(\xi_1)) \right) \\ & + \sum_{i=1}^3 \frac{\partial \alpha_2}{\partial y_d^{(i-1)}} y_d^{(i)} + \frac{\partial \alpha_2}{\partial \hat{\theta}} \dot{\hat{\theta}} \\ & \left. + \frac{1}{2} \frac{\partial^2 \alpha_2}{\partial e_2^2} \left( \frac{1}{D} \sin(\xi_1) \xi_1 \right)^2 \right) \leq \frac{e_2^3 e_3}{D \cos^2(\pi e_2^4/4k_{b_2}^4)} \\ & + \frac{e_3^3}{\cos^2(\pi e_3^4/4k_{b_3}^4)} \left( \frac{1}{M} (u - \xi_2 - 0.5 \xi_3) - \frac{\partial \alpha_2}{\partial \xi_1} \xi_2 \right. \\ & + \frac{\partial \alpha_2}{\partial \xi_2} \left( \frac{1}{D} (\xi_3 - \theta \xi_2 + 10 \sin(\xi_1)) \right) \\ & + \sum_{i=1}^3 \frac{\partial \alpha_2}{\partial y_d^{(i-1)}} y_d^{(i)} + \frac{\partial \alpha_2}{\partial \hat{\theta}} \dot{\hat{\theta}} \\ & \left. + \frac{1}{2} \frac{\partial^2 \alpha_2}{\partial e_2^2} \left( \frac{1}{g_m} \sin(\xi_1) \xi_1 \right)^2 \right) + \sum_{i=1}^2 K_i \tan\left(\frac{\pi e_i^4}{4k_{b_i}^4}\right) \\ & + \tilde{\theta} (\dot{\tilde{\theta}} - \tau_1). \end{aligned} \quad (18)$$

Design the controller  $u$  as follows:

$$u = M \left( -\frac{K_3 \sin(\pi e_3^4/4k_{b_3}^4) \cos(\pi e_3^4/4k_{b_3}^4)}{e_3^3} + \sum_{i=1}^3 \frac{\partial \alpha_2}{\partial y_d^{(i-1)}} y_d^{(i)} + \frac{\partial \alpha_2}{\partial \hat{\theta}} \dot{\hat{\theta}} + \frac{1}{2} \frac{\partial^2 \alpha_2}{\partial e_2^2} \left( \frac{1}{D} \sin(\xi_1) \xi_1 \right)^2 \right. \\ \left. - \hat{\theta}^T \frac{1}{D} \frac{\partial \alpha_2}{\partial \xi_2} \xi_2 + \frac{\partial \alpha_2}{\partial \xi_1} \xi_2 + \frac{\partial \alpha_2}{\partial \xi_2} \frac{1}{D} \xi_3 - \frac{\vartheta_{e_2} g_2 e_3}{\vartheta_{e_3}} \right), \quad (19)$$

where  $K_3 > 0$  is a design parameter. Choosing  $\tau_2 = \tau_1 + (1/D)(\partial \alpha_2 / \partial \xi_2) \xi_2$  and substituting (18) and (19) into (15) result in

$$LV_3 \leq -\sum_{i=1}^3 K_i \tan\left(\frac{\pi e_i^4}{4k_{b_i}^4}\right) + \tilde{\theta}(\dot{\hat{\theta}} - \tau_2). \quad (20)$$

The adaptive law is given as  $\dot{\hat{\theta}} = \tau_2 - \sigma \hat{\theta}$  with a design parameter  $\sigma$ . Then, we can obtain

$$LV_3 \leq -\sum_{i=1}^3 K_i \tan\left(\frac{\pi e_i^4}{4k_{b_i}^4}\right) - \sigma \tilde{\theta} \hat{\theta} \\ \leq -\sum_{i=1}^3 K_i \tan\left(\frac{\pi e_i^4}{4k_{b_i}^4}\right) + \frac{\sigma \theta^2}{2} - \frac{\sigma \tilde{\theta}^2}{2}. \quad (21)$$

Choose  $\eta_1 = \min\{K_1\pi/k_{b_1}^2, K_2\pi/k_{b_2}^2, K_3\pi/k_{b_3}^2, \sigma\}$ ; then (21) can be rewritten as

$$LV_3 \leq -\eta_1 \left( \sum_{i=1}^3 \frac{k_{b_i}^2}{\pi} \tan\left(\frac{\pi e_i^4}{4k_{b_i}^4}\right) + \frac{1}{2} \tilde{\theta}^2 \right) + C_1, \quad (22)$$

where  $C_1 = \sigma \theta^2 / 2$ ; that is,

$$LV_3 \leq -\eta_1 V_3 + C_1. \quad (23)$$

**Theorem 5.** Consider system (1) under Assumption 1; the controller  $u$  is given in (19), and the adaption law  $\dot{\hat{\theta}} = \tau_2 - \sigma \hat{\theta}$ . Then, the following are guaranteed:

- (1) The full state constraints are not violated.
- (2) All the signals in the closed-loop system are bounded.
- (3) The error signals  $e_i(t)$  will converge to  $\Xi = \{e_i : E(|e_i|^4) \leq (4k_{b_i}^4/\pi) \tan^{-1}((V_3(0) + C_1/\eta_1)(\pi/k_{b_i}^4))\}$ .

*Proof.* Define a candidate BLF as follows:

$$V_3 = \sum_{i=1}^3 \frac{k_{b_i}^4}{\pi} \tan\left(\frac{\pi e_i^4}{4k_{b_i}^4}\right) + \frac{1}{2} \tilde{\theta}^2. \quad (24)$$

From (23), we can get that

$$LV_3 \leq -\eta_1 V_3 + C_1. \quad (25)$$

Based on Lemma 4, we know that

$$0 \leq (E[V_3(t)]) \leq V_3(0) e^{-\eta_1 t} + \frac{C_1}{\eta_1}. \quad (26)$$

Then, the following inequality holds:

$$E\left(\frac{k_{b_i}^4}{\pi} \tan\left(\frac{\pi e_i^4}{4k_{b_i}^4}\right)\right) \leq (E[V_3(t)]) \\ \leq V_3(0) e^{-\eta_1 t} + \frac{C_1}{\eta_1}. \quad (27)$$

Hence,

$$E(|e_i|^4) \leq \frac{4k_{b_i}^4}{\pi} \tan^{-1}\left(\left(V_3(0) e^{-\eta_1 t} + \frac{C_1}{\eta_1}\right) \frac{\pi}{k_{b_i}^4}\right) \\ \leq \frac{4k_{b_i}^4}{\pi} \tan^{-1}\left(\left(V_3(0) + \frac{C_1}{\eta_1}\right) \frac{\pi}{k_{b_i}^4}\right). \quad (28)$$

Hence, the size of  $(4k_{b_i}^4/\pi) \tan^{-1}((V_3(0) + C_1/\eta_1)(\pi/k_{b_i}^4))$  can be made small enough by choosing appropriate parameters. On the other hand, from the above inequality, we can obtain that  $E[V_3(t)]$  is limited by  $C/\eta_1$ . Then, we know that  $V_3(t)$  is bounded. So  $\tilde{\theta}$  is bounded and  $\hat{\theta} = \tilde{\theta} + \theta$  is bounded. Then we know that  $e_i$ ,  $y_d$ ,  $\alpha_i$ , and  $u$  are bounded. From  $e_1 = \xi_1 - y_d$  and  $|y_d| \leq Y_0$ , we know that  $|\xi_1| \leq |e_1| + |y_d| < k_{b_1} + Y_0 = k_{c_1}$ . From  $e_2 = \xi_2 - \alpha_1$  and  $|\alpha_1| \leq \bar{\alpha}_1$ , we can obtain that  $|\xi_2| \leq |e_2| + |\alpha_1| < k_{b_2} + \bar{\alpha}_1 = k_{c_2}$ . In a similar way, we can obtain  $|\xi_3| < k_{c_3}$ . Thus, the full state constraints are not violated.  $\square$

## 4. Simulation

In this section, simulation is introduced to demonstrate the effectiveness of the proposed scheme.

$$d\xi_1 = \xi_2 dt,$$

$$d\xi_2 = \frac{1}{D} (\xi_3 - \theta \xi_2 + 10 \sin(\xi_1)) dt \\ + \frac{1}{D} \sin(\xi_1) \xi_1 d\omega, \quad (29)$$

$$d\xi_3 = \frac{1}{M} (u - K_m \xi_2 - H \xi_3) dt,$$

$$y = \xi_1,$$

where  $D = 1$ ,  $M = 1$ ,  $N = 10$ ,  $B = 1$ ,  $H = 0.5$ , and  $k_m = 1$ . All the states are constrained in the compact set as  $\Omega_\xi := \{\xi_i(t) \in \mathbb{R}, |\xi_i(t)| \leq 1.5\}$ . The reference signal is chosen as  $y_d = 0.5 \sin t$ .

In the simulation, the design parameters are chosen as  $\xi_i(0) = 0.1$ ,  $K_i = 1$ ,  $i = 1, 2, 3$ ,  $\hat{\theta}(0) = 0.1$ ,  $k_{b_1} = k_{b_2} = 1$ ,  $k_{b_3} = 0.9$ , and  $k_{b_4} = 1.1$ . The results of the simulation are shown in Figures 1–4. The output tracking  $q$  and  $q_d$  is illustrated in Figure 1. It can be seen that the position state  $q$  can precisely

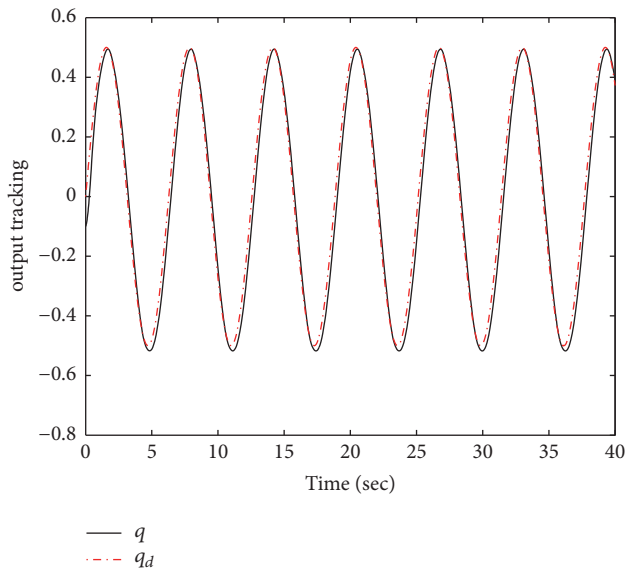


FIGURE 1: The trajectories of  $q$  and  $q_d$ .

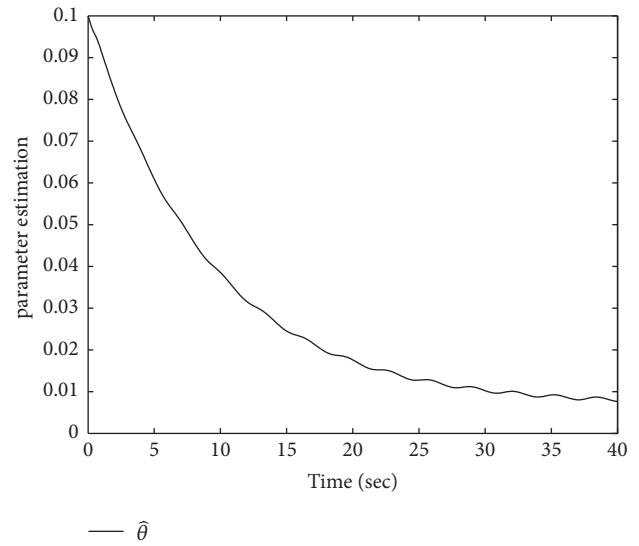


FIGURE 3: The estimation of  $\hat{\theta}$ .

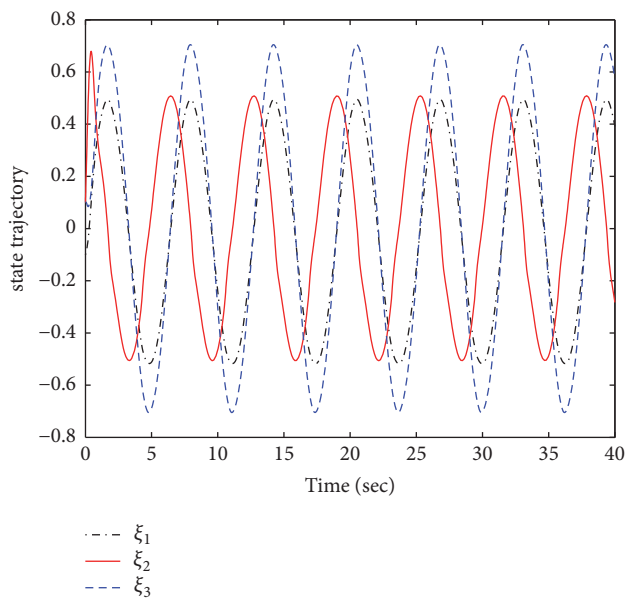


FIGURE 2: The trajectories of  $\xi_1$ ,  $\xi_2$ , and  $\xi_3$ .

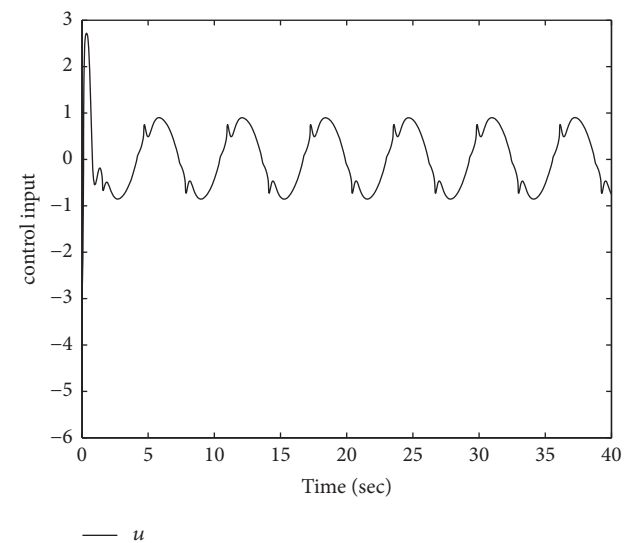


FIGURE 4: The trajectory of control input  $u$ .

track the desired trajectory  $q_d$ . It is shown in Figure 2 that all the states are strictly constrained in  $\{\xi_i \mid -1.5 \leq \xi_i(t) \leq 1.5\}$ ,  $i = 1, 2, 3$ . The parameter updating law  $\hat{\theta}$  and input  $u$  are all bounded as shown in Figures 3 and 4. The simulation results demonstrate the effectiveness of the proposed adaptive control scheme.

### 5. Conclusions

This study carries out the adaptive tracking control for a class of stochastic manipulator nonlinear systems. An adaptive controller is proposed to ensure that the mean square of the tracking error can be made arbitrarily small. Simulation

results are presented to illustrate the effectiveness of the proposed control strategy.

### Data Availability

In this paper, only numerical simulation is given; all the data are produced by Matlab program. No other data were used to support this study.

### Conflicts of Interest

The authors declare that they have no conflicts of interest.

## Acknowledgments

This research was supported by the National Natural Science Foundation of China under Grants 61603170, 61573177, and 61773191; the Natural Science Foundation of Shandong Province for Outstanding Young Talents in Provincial Universities under Grant ZR2016JL025; the Natural Science Foundation of Shandong Province of China ZR2018MF028; and Special Fund Plan for Local Science and Technology Development led by Central Authority.

## References

- [1] M. Krstic and P. V. Kokotovic, "Adaptive nonlinear design with controller-identifier separation and swapping," *Institute of Electrical and Electronics Engineers Transactions on Automatic Control*, vol. 40, no. 3, pp. 426–440, 1995.
- [2] C.-R. Zhao and X.-J. Xie, "Global stabilization of stochastic high-order feedforward nonlinear systems with time-varying delay," *Automatica*, vol. 50, no. 1, pp. 203–210, 2014.
- [3] H. Fujimoto, Y. Hori, and A. Kawamura, "Perfect tracking control based on multirate feedforward control with generalized sampling periods," *IEEE Transactions on Industrial Electronics*, vol. 48, no. 3, pp. 636–644, 2001.
- [4] Z.-Y. Sun, M.-M. Yun, and T. Li, "A new approach to fast global finite-time stabilization of high-order nonlinear system," *Automatica*, vol. 81, pp. 455–463, 2017.
- [5] Q. Zhou, H. Li, C. Wu, L. Wang, and C. K. Ahn, "Adaptive Fuzzy Control of Nonlinear Systems with Unmodeled Dynamics and Input Saturation Using Small-Gain Approach," *IEEE Transactions on Systems, Man, and Cybernetics: Systems*, vol. 47, no. 8, pp. 1979–1989, 2017.
- [6] W. Si, X. Dong, and F. Yang, "Decentralized adaptive neural control for high-order stochastic nonlinear strongly interconnected systems with unknown system dynamics," *Information Sciences*, vol. 424, pp. 137–158, 2018.
- [7] W. Sun and Y. Wu, "Modeling and finite-time tracking control for mobile manipulators with affine and holonomic constraints," *Journal of Systems Science and Complexity*, vol. 29, no. 3, pp. 589–601, 2016.
- [8] Z.-Y. Sun, C.-H. Zhang, and Z. Wang, "Adaptive disturbance attenuation for generalized high-order uncertain nonlinear systems," *Automatica*, vol. 80, pp. 102–109, 2017.
- [9] H. F. Ho, Y. K. Wong, and A. B. Rad, "Adaptive fuzzy approach for a class of uncertain nonlinear systems in strict-feedback form," *ISA Transactions*, vol. 47, no. 3, pp. 286–299, 2008.
- [10] H. Rahimi Nohooji, I. Howard, and L. Cui, "Neural network adaptive control design for robot manipulators under velocity constraints," *Journal of The Franklin Institute*, vol. 355, no. 2, pp. 693–713, 2018.
- [11] C. Wang, Y. Wu, and J. Yu, "Barrier Lyapunov functions-based dynamic surface control for pure-feedback systems with full state constraints," *IET Control Theory & Applications*, vol. 11, no. 4, pp. 524–530, 2017.
- [12] M. Galicki, "An adaptive non-linear constraint control of mobile manipulators," *Mechanism and Machine Theory*, vol. 88, pp. 63–85, 2015.
- [13] N. Chen, F. Song, G. Li, X. Sun, and C. Ai, "An adaptive sliding mode backstepping control for the mobile manipulator with nonholonomic constraints," *Communications in Nonlinear Science and Numerical Simulation*, vol. 18, no. 10, pp. 2885–2899, 2013.
- [14] Y.-S. Lu and Y.-Y. Lin, "Smooth motion control of rigid robotic manipulators with constraints on high-order kinematic variables," *Mechatronics*, vol. 49, pp. 11–25, 2018.
- [15] W. Dong, "On trajectory and force tracking control of constrained mobile manipulators with parameter uncertainty," *Automatica*, vol. 38, no. 9, pp. 1475–1484, 2002.
- [16] Z. Li, S. S. Ge, M. Adams, and W. S. Wijesoma, "Robust adaptive control of uncertain force/motion constrained nonholonomic mobile manipulators," *Automatica*, vol. 44, no. 3, pp. 776–784, 2008.
- [17] W. Zhang and B. Chen, "H-representation and applications to generalized Lyapunov equations and linear stochastic systems," *IEEE Transactions on Automatic Control*, vol. 57, no. 12, pp. 3009–3022, 2012.
- [18] X.-J. Xie, N. Duan, and C.-R. Zhao, "A combined homogeneous domination and sign function approach to output-feedback stabilization of stochastic high-order nonlinear systems," *Institute of Electrical and Electronics Engineers Transactions on Automatic Control*, vol. 59, no. 5, pp. 1303–1309, 2014.
- [19] W. Zhang, Y. Zhao, and L. Sheng, "Some remarks on stability of stochastic singular systems with state-dependent noise," *Automatica*, vol. 51, pp. 273–277, 2015.
- [20] M. J. Richard and B. Lévesque, "Stochastic dynamical modelling of an open-chain manipulator in a fluid environment," *Mechanism and Machine Theory*, vol. 31, no. 5, pp. 561–572, 1996.
- [21] Z.-G. Liu and Y.-Q. Wu, "Modelling and adaptive tracking control for flexible joint robots with random noises," *International Journal of Control*, vol. 87, no. 12, pp. 2499–2510, 2014.
- [22] U. O. Akpan and M. R. Kujath, "Stochastic response of a flexible mobile robotic manipulator structure," *Computers & Structures*, vol. 59, no. 5, pp. 891–898, 1996.
- [23] M.-Y. Cui, X.-J. Xie, and Z.-J. Wu, "Dynamics modeling and tracking control of robot manipulators in random vibration environment," *Institute of Electrical and Electronics Engineers Transactions on Automatic Control*, vol. 58, no. 6, pp. 1540–1545, 2013.
- [24] X. Jin, "Adaptive fault tolerant control for a class of input and state constrained MIMO nonlinear systems," *International Journal of Robust and Nonlinear Control*, vol. 26, no. 2, pp. 286–302, 2016.
- [25] W. He, Y. Chen, and Z. Yin, "Adaptive neural network control of an uncertain robot with full-state constraints," *IEEE Transactions on Cybernetics*, vol. 46, no. 3, pp. 620–629, 2016.
- [26] W. Chen, L. Jiao, J. Li, and R. Li, "Adaptive NN backstepping output-feedback control for stochastic nonlinear strict-feedback systems with time-varying delays," *IEEE Transactions on Systems, Man, and Cybernetics, Part B: Cybernetics*, vol. 40, no. 3, pp. 939–950, 2010.

## Research Article

# A Novel Fifth-Degree Strong Tracking Cubature Kalman Filter for Two-Dimensional Maneuvering Target Tracking

Zhaoming Li <sup>1</sup>, Wenge Yang <sup>2</sup> and Dan Ding <sup>2</sup>

<sup>1</sup>Graduate School, Space Engineering University, Beijing 101416, China

<sup>2</sup>Department of Electrical and Optical Engineering, Space Engineering University, Beijing 101416, China

Correspondence should be addressed to Dan Ding; [ddnjr@163.com](mailto:ddnjr@163.com)

Received 12 April 2018; Accepted 31 May 2018; Published 20 June 2018

Academic Editor: Hiroaki Mukaidani

Copyright © 2018 Zhaoming Li et al. This is an open access article distributed under the Creative Commons Attribution License, which permits unrestricted use, distribution, and reproduction in any medium, provided the original work is properly cited.

A novel fifth-degree strong tracking cubature Kalman filter is put forward to improve the two-dimensional maneuvering target tracking accuracy. First, a new fifth-degree cubature rule, with only one point more than the theoretical lower bound, is used to approximate the intractable nonlinear Gaussian weighted integral in the nonlinear Kalman filtering framework, and a novel fifth-degree cubature Kalman filter is proposed. Then, the suboptimal fading factor is designed for the filter to adjust the filtering gain matrix online and force the residual sequences mutually orthogonal, thus improving the ability of the filter to track the mutation state, and the fifth-degree strong tracking cubature Kalman filter is derived. The suboptimal fading factor is calculated in a new method, which reduces the number of calculations for the cubature points from three times to twice without calculating the Jacobian matrix. The simulation results indicate that the proposed filter has the ability to track the maneuvering target and achieve higher target tracking accuracy and thus verifies the effectiveness of the proposed filter.

## 1. Introduction

For the last several decades, the target tracking has momentous applications in many fields, such as navigation guidance, military application, and sensor networks [1]. In target tracking problem, the process model is generally linear, while the measurement model, mainly including the measured range and bearing angle, is nonlinear [2, 3]. The essence of the target tracking is to use a series of measured ranges and bearing angle information to estimate the position and velocity of the target in real time; hence, it belongs to the nonlinear filtering problem, which has always been dealt with using the nonlinear Kalman filters [4].

In nonlinear Kalman filters, the extended Kalman filter (EKF) [5] is the most widely used one. In EKF, the nonlinear function is approximated using the first-order Taylor series expansion and, then, the standard Kalman filter is applied [6]. EKF is simple in principle; however, its filtering accuracy and stability may reduce for the strong nonlinear system, and it needs to calculate the Jacobian matrix, which is difficult to accomplish at times. Julier [7] adopts a set of sigma points to approximate the posterior probability density

function (PDF) and proposes the unscented Kalman filter (UKF). UKF is a derivative-free filter and can achieve third-degree filtering accuracy [8, 9]. However, there exist some tunable parameters in the selection of sigma points, and the inappropriate selection may reduce the filtering accuracy. In addition, the weight on the center point may be negative for the high-dimensional system, which may degrade the numerical stability of the filter [10, 11]. Arasaratnam [12, 13] puts forward the cubature Kalman filter (CKF), where the intractable integral in nonlinear Kalman filter is decomposed into the spherical integral and the radial integral, which are approximated using different numerical integration rules. CKF contains a set of cubature points with equal weights; thus the numerical stability is guaranteed [14–16]. CKF can be regarded as a special case of UKF [17]; however, CKF gives the rigorous reason for the selection of parameters for the first time. In order to improve the accuracy of CKF, Jia [18] adopts the symmetric spherical interpolation and moment matching method to calculate the spherical integral and radial integral, respectively, and proposes the fifth-degree CKF. And then, Wang [19] employs the transformation group of the regular simplex instead of the symmetric spherical interpolation to

derive the fifth-degree spherical simplex-radial CKF. These two filters improve the filtering accuracy effectively.

However, the conventional nonlinear Kalman filters cannot achieve the effective tracking of the maneuvering target. In order to improve the ability of the filter to fast track the mutation state, Zhou [20] proposes the strong tracking filter (STF) on the basis of EKF. The STF uses the suboptimal fading factor to realize the real time adjustment of the gain matrix to force the residual sequences mutually orthogonal [21, 22]; it has the ability to track the mutation state while inheriting the inherent defects of EKF. Correspondingly, the strong tracking UKF (STUKF) and strong tracking CKF (STCKF) are put forward in succession. There are two methods to calculate the suboptimal fading factor in these two types of filters. On the one hand, the fading factor is still calculated using the Jacobian matrix [23–25], which may bring some trouble in strong nonlinear systems. On the other hand, the fading factor is calculated using the equivalent expressions derived by the statistical regression method [26, 27], in which the predicted measurement covariance and the cross-covariance are contained. It results in the nonlinear transformation carried out for three times, which increases the amount of calculation while loses a certain precision.

In this paper, a novel fifth-degree strong tracking cubature Kalman filter (5-STCKF) is proposed to further improve the two-dimensional maneuvering target tracking accuracy. A new fifth-degree cubature rule is utilized to approximate the intractable nonlinear Gaussian weighted integral, and a novel fifth-degree cubature Kalman filter is put forward. To improve the ability of the filter to track the mutation state, the suboptimal fading factor is designed to adjust the filtering gain matrix online and force the residual sequences mutually orthogonal and the 5-STCKF is derived. The suboptimal fading factor is calculated in a new method, which reduces the number of calculations for the cubature points from three times to twice without calculating the Jacobian matrix. The proposed 5-STCKF has the ability to track the mutation state and can achieve better performance compared with the 5-CKF and 5-SSRCKF in maneuvering target tracking applications. In addition, the number of cubature points needed in the 5-STCKF is less than those in the 5-CKF and 5-SSRCKF. The simulation results verify the validity of the filter.

The rest of this paper is organized as follows: the novel fifth-degree cubature Kalman filter is proposed in Section 2, the novel fifth-degree strong tracking cubature Kalman filter is derived in Section 3, the simulation results and analysis are presented in Section 4, and the conclusion is given in Section 5.

## 2. A Novel Fifth-Degree Cubature Kalman Filter

The following discrete time nonlinear system is considered:

$$\begin{aligned} \mathbf{x}_k &= \mathbf{f}(\mathbf{x}_{k-1}) + \mathbf{w}_{k-1} \\ \mathbf{z}_k &= \mathbf{h}(\mathbf{x}_k) + \mathbf{v}_k \end{aligned} \quad (1)$$

where  $\mathbf{x}_k \in \mathbf{R}^n$  denotes the state vector at time  $k$ ,  $\mathbf{z}_k \in \mathbf{R}^p$  represents the measurement vector, and  $\mathbf{f}(\cdot)$  and  $\mathbf{h}(\cdot)$  denote

the known nonlinear process and measurement functions, respectively.  $\mathbf{w}_k$  is the zero mean Gaussian white process noise, with the covariance being  $\mathbf{Q}_k$ , and  $\mathbf{v}_k$  is the zero mean Gaussian white measurement noise, with the covariance being  $\mathbf{R}_k$ .

Given the measurements  $\mathbf{Z}_k = \{\mathbf{z}_1, \mathbf{z}_2, \dots, \mathbf{z}_k\}$ , the minimum mean square error (MMSE) estimate of the state  $\mathbf{x}_k$  with the estimate error covariance is given below:

$$\hat{\mathbf{x}}_k^{MMSE} = E(\mathbf{x}_k | \mathbf{Z}_k) = \int \mathbf{x}_k p(\mathbf{x}_k | \mathbf{Z}_k) d\mathbf{x}_k \quad (2)$$

$$\mathbf{P}_x = \int (\mathbf{x}_k - \hat{\mathbf{x}}_k^{MMSE})(\mathbf{x}_k - \hat{\mathbf{x}}_k^{MMSE})^T p(\mathbf{x}_k | \mathbf{Z}_k) d\mathbf{x}_k \quad (3)$$

where  $p(\mathbf{x}_k | \mathbf{Z}_k)$  denotes the posterior PDF.

For nonlinear Kalman filters, the posterior PDF is assumed to be Gaussian distribution and the following five integrals in the filtering framework are required to be calculated [12]:

$$\hat{\mathbf{x}}_k^- = \int_{\mathbf{R}^n} \mathbf{f}(\mathbf{x}_{k-1}) N(\mathbf{x}_{k-1}; \hat{\mathbf{x}}_{k-1}^+, \mathbf{P}_{k-1}^+) d\mathbf{x}_{k-1} \quad (4)$$

$$\begin{aligned} \mathbf{P}_k^- &= \int_{\mathbf{R}^n} \mathbf{f}(\mathbf{x}_{k-1}) \mathbf{f}^T(\mathbf{x}_{k-1}) N(\mathbf{x}_{k-1}; \hat{\mathbf{x}}_{k-1}^+, \mathbf{P}_{k-1}^+) d\mathbf{x}_{k-1} \\ &\quad - \hat{\mathbf{x}}_k^- (\hat{\mathbf{x}}_k^-)^T + \mathbf{Q}_k \end{aligned} \quad (5)$$

$$\hat{\mathbf{z}}_k = \int_{\mathbf{R}^n} \mathbf{h}(\mathbf{x}_k) N(\mathbf{x}_k; \hat{\mathbf{x}}_k^-, \mathbf{P}_k^-) d\mathbf{x}_k \quad (6)$$

$$\begin{aligned} \mathbf{P}_{z,k} &= \int_{\mathbf{R}^n} \mathbf{h}(\mathbf{x}_{k-1}) \mathbf{h}^T(\mathbf{x}_{k-1}) N(\mathbf{x}_k; \hat{\mathbf{x}}_k^-, \mathbf{P}_k^-) d\mathbf{x}_k \\ &\quad - \hat{\mathbf{z}}_k \hat{\mathbf{z}}_k^T + \mathbf{R}_k \end{aligned} \quad (7)$$

$$\mathbf{P}_{xz,k} = \int_{\mathbf{R}^n} \mathbf{x}_k \mathbf{h}^T(\mathbf{x}_k) N(\mathbf{x}_k; \hat{\mathbf{x}}_k^-, \mathbf{P}_k^-) d\mathbf{x}_k - \hat{\mathbf{x}}_k^- \hat{\mathbf{z}}_k \quad (8)$$

where  $N(\mathbf{x}; \hat{\mathbf{x}}, \mathbf{P}_x)$  denotes the Gaussian distribution with mean  $\hat{\mathbf{x}}$  and covariance  $\mathbf{P}_x$ ,  $\hat{\mathbf{x}}_k^-$  and  $\mathbf{P}_k^-$  represent the prior state estimate and estimate error covariance, respectively,  $\hat{\mathbf{z}}_k$  is the predicted measurement, and  $\mathbf{P}_{z,k}$  and  $\mathbf{P}_{xz,k}$  denote the measurement covariance and cross-covariance, respectively.

It can be seen from (4) to (8) that the key problem in nonlinear Kalman filters is to calculate the intractable integral in the form of  $I_N = \int_{\mathbf{R}^n} \mathbf{g}(\mathbf{x}) N(\mathbf{x}; \hat{\mathbf{x}}, \mathbf{P}_x) d\mathbf{x}$ , where  $\mathbf{g}(\mathbf{x})$  is arbitrary nonlinear function. In general, it is hard to achieve the analytical solution of  $I_N$ , and the numerical approximation should be considered. For this, the integral  $I_e = \int_{\mathbf{R}^n} \mathbf{g}(\mathbf{x}) \exp(-\mathbf{x}^T \mathbf{x}) d\mathbf{x}$  is taken into account first.

There already exist some cubature rules, including the third-degree spherical-radial cubature rule and fifth-degree spherical-radial cubature rule, to calculate  $I_e$ , and it is proved that the fifth-degree cubature rule can achieve higher accuracy than the third-degree one. For more details, please refer to [12, 18].

In this paper, through linear transformation, a novel fifth-degree cubature rule for calculating the integral  $I_N$  is given below.

It is pointed out in [28] that  $I_e$  can be calculated approximately using the following fifth-degree cubature rule:

$$\begin{aligned}
 I_e = & A \underbrace{[g(\eta, \eta, \dots, \eta) + g(-\eta, -\eta, \dots, -\eta)]}_{2C_n^1} \\
 & + B \underbrace{\sum_{perm} [g(\lambda, \xi, \dots, \xi) + g(-\lambda, -\xi, \dots, -\xi)]}_{2C_n^1} \\
 & + C \underbrace{\sum_{perm} [g(\mu, \mu, \gamma, \dots, \gamma) + g(-\mu, -\mu, -\gamma, \dots, -\gamma)]}_{2C_n^2}
 \end{aligned} \quad (9)$$

where perm means all distinct permutations,  $C_n^1$  and  $C_n^2$  represent the binomial coefficients that equal to  $n$  and  $n(n-1)/2$ , respectively, and the parameters  $\eta$ ,  $\mu$ , and  $\gamma$  satisfy the following equations. For more details, please refer to [28, 29].

$$\frac{\mu}{\gamma} = -3 \pm \sqrt{16 - 2n} \quad (10)$$

$$\gamma^2 = \frac{3 \pm \sqrt{7 - n}}{2(16 - n \mp 4\sqrt{16 - 2n})} \quad (11)$$

$$\eta^2 = \frac{n(n-7) \mp (n^2 - 3n - 16)\sqrt{7-n}}{2(n^3 - 7n^2 - 16n + 128)} \quad (12)$$

However, (9) is not suitable for calculating  $I_N$  in its current form. In order to simplify (9), we define  $\mathbf{e}$  as an  $n$ -order identity matrix and the matrix subscript  $[\cdot]_i$  is utilized to denote the  $i$ th column and, then, (9) can be written in the following form:

$$\begin{aligned}
 I_e = & A \left[ \mathbf{g} \left( \sum_{i=1}^n \eta \mathbf{e}_i \right) + \mathbf{g} \left( -\sum_{i=1}^n \eta \mathbf{e}_i \right) \right] \\
 & + B \sum_{i=1}^n \left[ \mathbf{g} \left( \lambda \mathbf{e}_i + \sum_{j=1, j \neq i}^n \xi \mathbf{e}_j \right) \right. \\
 & \left. + \mathbf{g} \left( -\lambda \mathbf{e}_i - \sum_{j=1, j \neq i}^n \xi \mathbf{e}_j \right) \right] \\
 & + C \sum_{i=1}^{C_n^2} \left[ \mathbf{g} \left( \mu \mathbf{e}_j + \mu \mathbf{e}_k + \sum_{l=1, l \neq j, l \neq k}^n \gamma \mathbf{e}_l \right) \right. \\
 & \left. + \mathbf{g} \left( -\mu \mathbf{e}_j - \mu \mathbf{e}_k - \sum_{l=1, l \neq j, l \neq k}^n \gamma \mathbf{e}_l \right) \right], \\
 & j < k; j, k = 1, 2, \dots, n
 \end{aligned} \quad (13)$$

Further, we define the following variables:

$$\mathbf{p} = \sum_{i=1}^n \eta \mathbf{e}_i \quad (14)$$

$$\mathbf{q}_i = \lambda \mathbf{e}_i + \sum_{j=1, j \neq i}^n \xi \mathbf{e}_j \quad (15)$$

$$\mathbf{s}_i = \mu \mathbf{e}_j + \mu \mathbf{e}_k + \sum_{l=1, l \neq j, l \neq k}^n \gamma \mathbf{e}_l \quad (16)$$

Then, (13) is transformed into the following simplified form:

$$\begin{aligned}
 I_e = & A [\mathbf{g}(\mathbf{p}) + \mathbf{g}(-\mathbf{p})] + B \sum_{i=1}^n [\mathbf{g}(\mathbf{q}_i) + \mathbf{g}(-\mathbf{q}_i)] \\
 & + C \sum_{i=1}^{C_n^2} [\mathbf{g}(\mathbf{s}_i) + \mathbf{g}(-\mathbf{s}_i)]
 \end{aligned} \quad (17)$$

It can be proved that  $I_N$  has the following equivalent form [12]:

$$I_N = \frac{1}{\sqrt{\pi^n}} \int_{\mathbf{R}^n} \mathbf{g} \left( \sqrt{2\mathbf{P}_x \mathbf{x}} + \hat{\mathbf{x}} \right) \exp(-\mathbf{x}^T \mathbf{x}) d\mathbf{x} \quad (18)$$

such that  $I_N$  can be approximated using the cubature rule below:

$$\begin{aligned}
 I_N = & \frac{A}{\sqrt{\pi^n}} \left[ \mathbf{g} \left( \sqrt{2\mathbf{P}_x \mathbf{p}} + \hat{\mathbf{x}} \right) + \mathbf{g} \left( -\sqrt{2\mathbf{P}_x \mathbf{p}} + \hat{\mathbf{x}} \right) \right] \\
 & + \frac{B}{\sqrt{\pi^n}} \sum_{i=1}^n \left[ \mathbf{g} \left( \sqrt{2\mathbf{P}_x \mathbf{q}_i} + \hat{\mathbf{x}} \right) + \mathbf{g} \left( -\sqrt{2\mathbf{P}_x \mathbf{q}_i} + \hat{\mathbf{x}} \right) \right] \\
 & + \frac{C}{\sqrt{\pi^n}} \sum_{i=1}^{C_n^2} \left[ \mathbf{g} \left( \sqrt{2\mathbf{P}_x \mathbf{s}_i} + \hat{\mathbf{x}} \right) + \mathbf{g} \left( -\sqrt{2\mathbf{P}_x \mathbf{s}_i} + \hat{\mathbf{x}} \right) \right] \\
 = & \sum_{i=1}^{n^2+n+2} \omega_i \mathbf{g}(\hat{\mathbf{x}}^{(i)})
 \end{aligned} \quad (19)$$

where the cubature points and corresponding weights are given below and the specific values of  $A$ ,  $B$ , and  $C$  are given in [29].

$$\begin{aligned}
 \hat{\mathbf{x}}^{(i)} = & \begin{cases} \sqrt{2\mathbf{P}_x} [\mathbf{p}, -\mathbf{p}]_i + \hat{\mathbf{x}}, & i = 1, 2 \\ \sqrt{2\mathbf{P}_x} [\mathbf{q}, -\mathbf{q}]_{i-2} + \hat{\mathbf{x}}, & i = 3, \dots, 2n+2 \\ \sqrt{2\mathbf{P}_x} [\mathbf{s}, -\mathbf{s}]_{i-2n-2} + \hat{\mathbf{x}}, & i = 2n+3, \dots, n^2+n+2 \end{cases} \\
 \omega_i = & \begin{cases} \frac{A}{\sqrt{\pi^n}}, & i = 1, 2 \\ \frac{B}{\sqrt{\pi^n}}, & i = 3, \dots, 2n+2 \\ \frac{C}{\sqrt{\pi^n}}, & i = 2n+3, \dots, n^2+n+2 \end{cases}
 \end{aligned} \quad (21)$$

where  $\mathbf{q} = [\mathbf{q}_1, \mathbf{q}_2, \dots, \mathbf{q}_n]$  and  $\mathbf{s} = [\mathbf{s}_1, \mathbf{s}_2, \dots, \mathbf{s}_{C_n^2}]$  represent the matrices constituted by  $\mathbf{q}_i$  and  $\mathbf{s}_i$ , respectively.

Take  $n = 6$  as an example, which will be used in the simulation section; the parameters in (19) are listed in Table 1.

*Remark 1.* The number of points needed in the fifth-degree cubature rule proposed in [18] is  $2n^2 + 1$ , and that in the spherical simplex cubature rule proposed in [19] is  $n^2 + 3n + 3$ . However, the number of points needed in the proposed

TABLE 1: Parameters of the cubature rule with  $n=6$ .

Parameters	Values
$\eta$	1
$\lambda$	$\sqrt{2}$
$\xi$	0
$\mu$	-1
$\gamma$	1
$A$	$0.0078125 \pi^{n/2}$
$B$	$0.0625 \pi^{n/2}$
$C$	$0.078125 \pi^{n/2}$

cubature rule (19) is  $2 + 2C_n^1 + 2C_n^2 = n^2 + n + 2$ , which is less than those of the aforementioned two filters and only one more than the theoretical lower bound of the fifth-degree rules, that is,  $n^2 + n + 1$  [29].

*Remark 2.* The cubature rule (19) can be applied in the condition that  $2 \leq n \leq 7$ , and for the conventional two-dimensional maneuvering target tracking problem, the maximum state dimension is seven (including two position variables, two velocity variables, two acceleration variables, and an optional turn rate); hence, the proposed cubature rule is suitable in the application of maneuvering target tracking.

Based on the cubature rule and the points and weights, the novel fifth-degree cubature Kalman filter is proposed in the nonlinear Kalman framework as follows.

*Step 1* (filter initialization). Take the initial values  $\hat{\mathbf{x}}_0^+$  and  $\mathbf{P}_0^+$  into consideration.

Cycle  $k = 1, 2, \dots$ , and complete the following steps.

*Step 2* (time update). The posterior state estimate  $\hat{\mathbf{x}}_{k-1}^+$  and estimate error covariance  $\mathbf{P}_{k-1}^+$  are used instead of  $\hat{\mathbf{x}}$  and  $\mathbf{P}_x$  in (20) to calculate the cubature points  $\hat{\mathbf{x}}_{k-1}^{(i)}$ , which are propagated using the nonlinear process function  $\mathbf{f}(\cdot)$  to obtain the following points  $\mathbf{X}_k^{(i)}$ :

$$\mathbf{X}_k^{(i)} = \mathbf{f}(\hat{\mathbf{x}}_{k-1}^{(i)}) \quad (22)$$

The prior state estimate and the estimate error covariance are calculated below:

$$\hat{\mathbf{x}}_k^- = \sum_{i=1}^{n^2+n+2} \omega_i \mathbf{X}_k^{(i)} \quad (23)$$

$$\mathbf{P}_k^- = \sum_{i=1}^{n^2+n+2} \omega_i (\mathbf{X}_k^{(i)} - \hat{\mathbf{x}}_k^-) (\mathbf{X}_k^{(i)} - \hat{\mathbf{x}}_k^-)^T + \mathbf{Q}_{k-1} \quad (24)$$

where  $\omega_i$  is given in (21).

*Step 3* (measurement update). The prior state estimate  $\hat{\mathbf{x}}_k^-$  and estimate error covariance  $\mathbf{P}_k^-$  are used instead of  $\hat{\mathbf{x}}$  and  $\mathbf{P}_x$  in (20) to calculate the cubature points  $\hat{\mathbf{x}}_k^{(i)}$ , which are

propagated using the nonlinear measurement function  $\mathbf{h}(\cdot)$  to obtain the following points  $\mathbf{Z}_k^{(i)}$ :

$$\mathbf{Z}_k^{(i)} = \mathbf{h}(\hat{\mathbf{x}}_k^{(i)}) \quad (25)$$

The predicted measurement  $\hat{\mathbf{z}}_k$ , the predicted measurement covariance  $\mathbf{P}_{z,k}$  and the cross-covariance  $\mathbf{P}_{xz,k}$  are calculated as follows, respectively:

$$\hat{\mathbf{z}}_k = \sum_{i=1}^{n^2+n+2} \omega_i \mathbf{Z}_k^{(i)} \quad (26)$$

$$\mathbf{P}_{z,k} = \sum_{i=1}^{n^2+n+2} \omega_i (\mathbf{Z}_k^{(i)} - \hat{\mathbf{z}}_k) (\mathbf{Z}_k^{(i)} - \hat{\mathbf{z}}_k)^T + \mathbf{R}_k \quad (27)$$

$$\mathbf{P}_{xz,k} = \sum_{i=1}^{n^2+n+2} \omega_i (\hat{\mathbf{x}}_k^{(i)} - \hat{\mathbf{x}}_k^-) (\mathbf{Z}_k^{(i)} - \hat{\mathbf{z}}_k)^T \quad (28)$$

The Kalman filtering gain  $\mathbf{K}_k$ , the posterior state estimate  $\hat{\mathbf{x}}_k^+$ , and the posterior estimate error covariance  $\mathbf{P}_k^+$  are calculated, respectively.

$$\mathbf{K}_k = \mathbf{P}_{xz,k} \mathbf{P}_{z,k}^{-1} \quad (29)$$

$$\hat{\mathbf{x}}_k^+ = \hat{\mathbf{x}}_k^- + \mathbf{K}_k (\mathbf{z}_k - \hat{\mathbf{z}}_k) \quad (30)$$

$$\mathbf{P}_k^+ = \mathbf{P}_k^- - \mathbf{K}_k \mathbf{P}_{z,k} \mathbf{K}_k^T \quad (31)$$

### 3. A Novel Fifth-Degree Strong Tracking Cubature Kalman Filter

The maneuvering target tracking problem can be regarded as a mutation state tracking problem. It can be seen from (30) that once the state has an abrupt change, the residual  $\boldsymbol{\varepsilon}_k = \mathbf{z}_k - \hat{\mathbf{z}}_k$  may increase thereupon, and if  $\mathbf{K}_k$  remains minimum as it tends to be as the filter is stable, the proposed fifth-degree cubature Kalman filter may lose the ability to track the mutation state. Therefore, we should adjust  $\mathbf{K}_k$  online to satisfy the following two criterions:

$$(a) E \left[ (\mathbf{x}_k - \hat{\mathbf{x}}_k^+) (\mathbf{x}_k - \hat{\mathbf{x}}_k^+)^T \right] = \min \quad (32)$$

$$(b) E (\boldsymbol{\varepsilon}_{k+j} \boldsymbol{\varepsilon}_k^T) = 0, \quad j = 1, 2, \dots \quad (33)$$

The first criterion ensures the optimal filter, and the second criterion, which is called the orthogonality principle [20], plays a key role in tracking the mutation state. It has been proved that the residual series in Kalman filter are mutually orthogonal, which can be regarded as metrics to evaluate the performance of the filter. If we adjust  $\mathbf{K}_k$  online to force the criterion (b) established once the state takes an abrupt change, the filter has the ability to track the mutation state then and is named strong tracking filter.

It has been proved that (33) has the following expression:

$$E (\boldsymbol{\varepsilon}_{k+j} \boldsymbol{\varepsilon}_k^T) = \mathbf{H}_{k+j} \mathbf{F}_{k+j} \left[ \prod_{i=k+1}^{k+j-1} (\mathbf{I} - \mathbf{K}_i \mathbf{H}_i) \mathbf{F}_i \right] (\mathbf{P}_k^- \mathbf{H}_k^T - \mathbf{K}_k \mathbf{V}_k) \quad (34)$$

where  $\mathbf{F}_k = \partial \mathbf{f} / \partial \mathbf{x} |_{\mathbf{x}=\hat{\mathbf{x}}_{k-1}^+}$  and  $\mathbf{H}_k = \partial \mathbf{h} / \partial \mathbf{x} |_{\mathbf{x}=\hat{\mathbf{x}}_k^-}$  denote the Jacobian matrix and  $\mathbf{V}_k = E(\boldsymbol{\varepsilon}_k \boldsymbol{\varepsilon}_k^T)$  represents the residual covariance.

It can be seen from (34) that, in order to force  $E(\boldsymbol{\varepsilon}_{k+j} \boldsymbol{\varepsilon}_k^T) = 0$ , the following must hold:

$$\mathbf{P}_k^- \mathbf{H}_k^T - \mathbf{K}_k \mathbf{V}_k = 0 \quad (35)$$

By using the statistical linear regression method, the following can be achieved:

$$\begin{aligned} \mathbf{P}_{z,k} &= E \left[ (\mathbf{z}_k - \hat{\mathbf{z}}_k) (\mathbf{z}_k - \hat{\mathbf{z}}_k)^T \right] \\ &= E \left[ (\mathbf{H}_k (\mathbf{x}_k - \hat{\mathbf{x}}_k^-) + \mathbf{v}_k) \left( (\mathbf{x}_k - \hat{\mathbf{x}}_k^-)^T \mathbf{H}_k^T + \mathbf{v}_k^T \right) \right] \\ &= \mathbf{H}_k E \left[ (\mathbf{x}_k - \hat{\mathbf{x}}_k^-) (\mathbf{x}_k - \hat{\mathbf{x}}_k^-)^T \right] \mathbf{H}_k^T + E(\mathbf{v}_k \mathbf{v}_k^T) \\ &= \mathbf{H}_k \mathbf{P}_k^- \mathbf{H}_k^T + \mathbf{R}_k \end{aligned} \quad (36)$$

$$\begin{aligned} \mathbf{P}_{xz,k} &= E \left[ (\mathbf{x}_k - \hat{\mathbf{x}}_k^-) (\mathbf{z}_k - \hat{\mathbf{z}}_k)^T \right] \\ &= E \left[ (\mathbf{x}_k - \hat{\mathbf{x}}_k^-) (\mathbf{H}_k (\mathbf{x}_k - \hat{\mathbf{x}}_k^-) + \mathbf{v}_k)^T \right] \\ &= E \left[ (\mathbf{x}_k - \hat{\mathbf{x}}_k^-) (\mathbf{x}_k - \hat{\mathbf{x}}_k^-)^T \right] \mathbf{H}_k^T = \mathbf{P}_k^- \mathbf{H}_k^T \end{aligned} \quad (37)$$

Combined with (37), (35) is transformed into the following form:

$$\mathbf{P}_{xz,k} - \mathbf{K}_k \mathbf{V}_k = 0 \quad (38)$$

Then, by substituting (29) into (38), we have

$$\mathbf{P}_{xz,k} - \mathbf{K}_k \mathbf{V}_k = \mathbf{K}_k \mathbf{P}_{z,k} - \mathbf{K}_k \mathbf{V}_k = \mathbf{K}_k (\mathbf{P}_{z,k} - \mathbf{V}_k) = 0 \quad (39)$$

On account of  $\mathbf{K}_k$  which is a nonzero matrix, (39) turns into

$$\mathbf{P}_{z,k} - \mathbf{V}_k = 0 \quad (40)$$

In order to adjust  $\mathbf{K}_k$  online, the time-varying suboptimal fading factor is introduced into the prior estimate error covariance and (24) is modified as follows:

$$\mathbf{P}_k^- = \lambda_k \left[ \sum_{i=1}^{n^2+n+2} \omega_i (\mathbf{X}_k^{(i)} - \hat{\mathbf{x}}_k^-) (\mathbf{X}_k^{(i)} - \hat{\mathbf{x}}_k^-)^T + \mathbf{Q}_{k-1} \right] \quad (41)$$

where  $\lambda_k \geq 1$  is the time-varying suboptimal fading factor.

Similarly,  $\mathbf{P}_{z,k}$  and  $\mathbf{P}_{xz,k}$  are modified according to (36) and (37) as below:

$$\mathbf{P}_{z,k} = \lambda_k \sum_{i=1}^{n^2+n+2} \omega_i (\mathbf{Z}_k^{(i)} - \hat{\mathbf{z}}_k) (\mathbf{Z}_k^{(i)} - \hat{\mathbf{z}}_k)^T + \mathbf{R}_k \quad (42)$$

$$\mathbf{P}_{xz,k} = \lambda_k \sum_{i=1}^{n^2+n+2} \omega_i (\hat{\mathbf{x}}_k^{(i)} - \hat{\mathbf{x}}_k^-) (\mathbf{Z}_k^{(i)} - \hat{\mathbf{z}}_k)^T \quad (43)$$

By substituting (42) into (40), we obtain that

$$\lambda_k \sum_{i=1}^{n^2+n+2} \omega_i (\mathbf{Z}_k^{(i)} - \hat{\mathbf{z}}_k) (\mathbf{Z}_k^{(i)} - \hat{\mathbf{z}}_k)^T + \mathbf{R}_k - \mathbf{V}_k = 0 \quad (44)$$

Define  $\mathbf{M}_k = \sum_{i=1}^{n^2+n+2} \omega_i (\mathbf{Z}_k^{(i)} - \hat{\mathbf{z}}_k) (\mathbf{Z}_k^{(i)} - \hat{\mathbf{z}}_k)^T$  and  $\mathbf{N}_k = \mathbf{V}_k - \mathbf{R}_k$ , and (44) turns into

$$\lambda_k \mathbf{M}_k = \mathbf{N}_k \quad (45)$$

By calculating the trace of both sides of (45), we achieve the following suboptimal fading factor:

$$\lambda_k = \begin{cases} \lambda_0, & \lambda_0 \geq 1 \\ 1, & \lambda_0 < 1, \end{cases} \quad (46)$$

$$\lambda_0 = \frac{\text{tr}(\mathbf{N}_k)}{\text{tr}(\mathbf{M}_k)}$$

The residual covariance  $\mathbf{V}_k = E(\boldsymbol{\varepsilon}_k \boldsymbol{\varepsilon}_k^T)$  can be estimated as follows:

$$\mathbf{V}_k = \begin{cases} \boldsymbol{\varepsilon}_1 \boldsymbol{\varepsilon}_1^T, & k = 1 \\ \frac{\rho \mathbf{V}_{k-1} + \boldsymbol{\varepsilon}_k \boldsymbol{\varepsilon}_k^T}{1 + \rho}, & k \geq 2 \end{cases} \quad (47)$$

where  $\rho$  denotes the forgetting factor and is generally set to be  $0.95 \leq \rho \leq 0.99$ .

In practical applications,  $\mathbf{N}_k$  is often modified as  $\mathbf{N}_k = \mathbf{V}_k - \beta \mathbf{R}_k$ , where  $\beta \geq 1$  denotes the softening factor to smooth the state estimate.

Thus, the novel fifth-degree strong tracking cubature Kalman filter is derived by substituting (42), (43) instead of (27), and (28) and (41) into (31), and the calculation process is listed in Figure 1.

*Remark 3.* In the previous nonlinear strong tracking filters,  $\mathbf{P}_{z,k}$  and  $\mathbf{P}_{xz,k}$  are contained in the calculation of  $\lambda_k$  [26, 27] and results in the cubature points being calculated three times in a filtering cycle, which may reduce the filtering accuracy due to the loss of the higher order moment information. However, in the proposed 5-STCKF,  $\mathbf{M}_k$  and  $\mathbf{N}_k$  are calculated using a different method and the cubature points are calculated only twice in a filtering cycle as the conventional CKF, which may achieve more accurate estimate and better computational efficiency.

*Remark 4.* There is no need to calculate the Jacobian matrix; thus, the proposed 5-STCKF is a derivative-free filter.

## 4. Simulation Results and Analysis

In this section, a maneuvering target tracking simulation is taken to test the performance of the proposed filter

*4.1. Maneuvering Target Tracking Models.* The dynamic model of the two-dimensional maneuvering target is given below:

$$\mathbf{x}_k = \mathbf{F} \mathbf{x}_{k-1} + \boldsymbol{\Gamma} \mathbf{u}_{k-1} + \mathbf{G} \mathbf{w}_{k-1} \quad (48)$$

where  $\mathbf{x}_k = (x_k, \dot{x}_k, y_k, \dot{y}_k)^T$  denotes the target state,  $\mathbf{u}_k = (\ddot{x}_k, \ddot{y}_k)^T$  represents the control input, and  $\mathbf{w}_{k-1}$  is the zero mean Gaussian process noise.  $\mathbf{F}$ ,  $\boldsymbol{\Gamma}$ , and  $\mathbf{G}$  denote the state

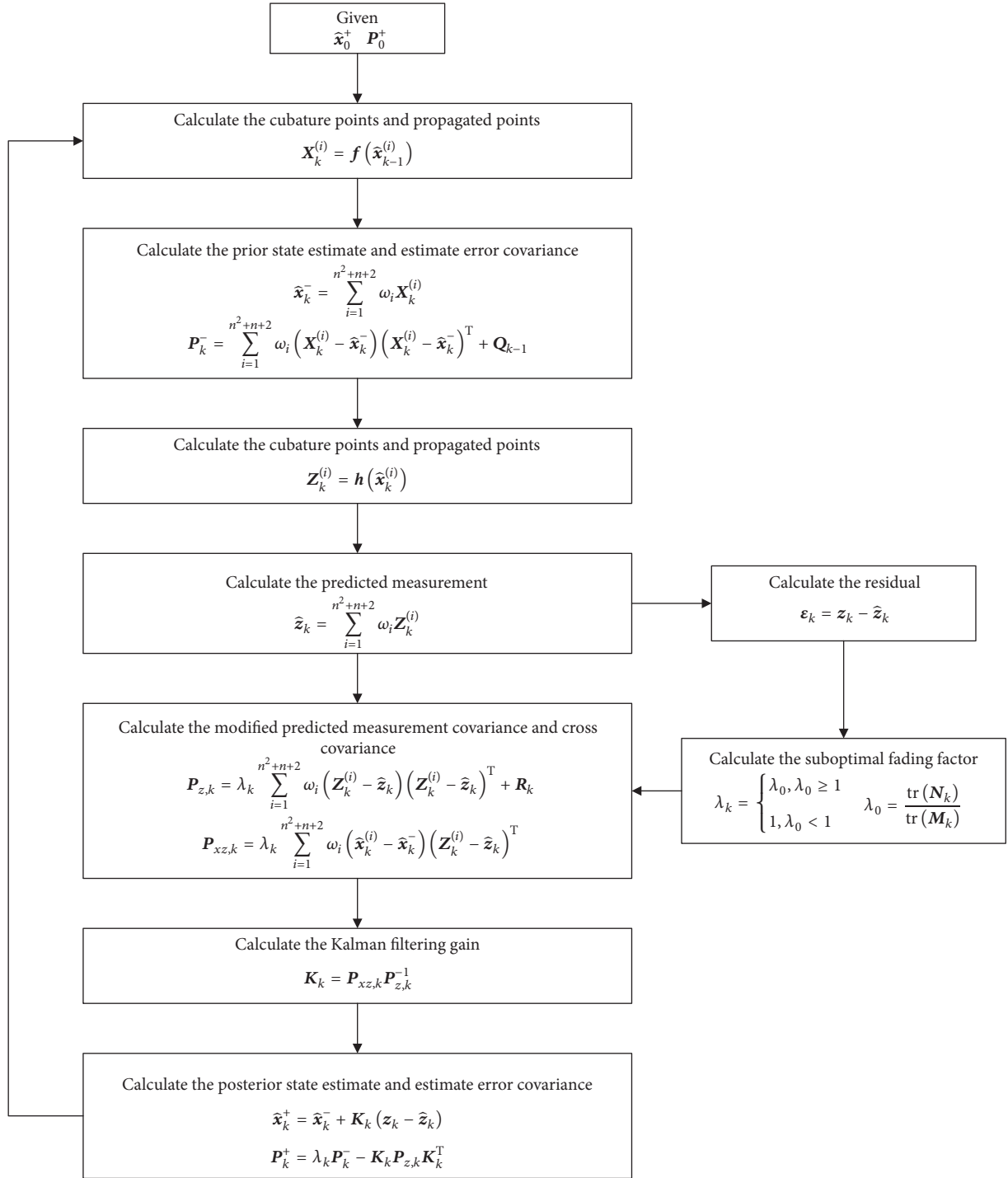


FIGURE 1: The calculation process of the proposed 5-STCKE.

transformation matrix, the control input matrix, and the noise input matrix, respectively, which are given below:

$$\mathbf{F} = \begin{bmatrix} 1 & T & 0 & 0 \\ 0 & 1 & 0 & 0 \\ 0 & 0 & 1 & T \\ 0 & 0 & 0 & 1 \end{bmatrix},$$

$$\mathbf{\Gamma} = \mathbf{G} = \begin{bmatrix} \frac{T^2}{2} & 0 \\ T & 0 \\ 0 & \frac{T^2}{2} \\ 0 & T \end{bmatrix}$$

(49)

where  $T$  is the time interval.

For the tracking system, the target state and the control input are unknown; in this case, the target state and the control input can be used to form the augmented state vector  $\mathbf{x}_k^a = (\mathbf{x}_k^T, \mathbf{u}_k^T)^T$ , and (48) is modified as follows:

$$\mathbf{x}_k^a = \mathbf{F}^a \mathbf{x}_{k-1}^a + \mathbf{G}^a \mathbf{w}_{k-1} \quad (50)$$

where  $\mathbf{F}^a$  and  $\mathbf{G}^a$  denote the augmented state transformation matrix and noise input matrix, respectively, which are given below:

$$\mathbf{F}^a = \begin{bmatrix} \mathbf{F} & \mathbf{\Gamma} \\ \mathbf{0}_{2 \times 4} & \mathbf{I}_2 \end{bmatrix}, \quad (51)$$

$$\mathbf{G}^a = \begin{bmatrix} \mathbf{G} \\ \mathbf{0}_{2 \times 2} \end{bmatrix}$$

The measurement model is given as follows:

$$\mathbf{z}_k = \begin{bmatrix} \sqrt{x_k^2 + y_k^2} \\ \text{atan } 2(y_k, x_k) \end{bmatrix} + \mathbf{v}_k \quad (52)$$

where  $\text{atan } 2$  denotes the four-quadrant inverse tangent function and  $\mathbf{v}_k$  is the zero mean white Gaussian measurement noise.

**4.2. Simulation Results and Analysis.** In this simulation, the initial location of the target is  $(x_0, y_0) = (100, 400)$  and the initial velocity of the target is  $(\dot{x}_0, \dot{y}_0) = (15, 20)$ . The location of the radar is  $(100, 0)$ . The total simulation time is 400s, and the target takes a high maneuvering with the acceleration given below. The trajectory of the target and the location of the radar is shown in Figure 2.

$$\mathbf{u}_k = \begin{cases} (0, 0)^T, & 0 < k \leq 40 \\ (6, -8)^T, & 40 < k \leq 120 \\ (-3, 7)^T, & 120 < k \leq 200 \\ (5, 2)^T, & 200 < k \leq 400 \end{cases} \quad (53)$$

The initial filtering state is  $\hat{\mathbf{x}}_0^+ = (100, 15, 400, 20, 0, 0)^T$ , and the initial covariance is  $\mathbf{P}_0^+ = \text{diag}(2500, 400, 2500, 100, 10, 10)$ . The process noise covariance is  $\mathbf{Q}_k = 0.1 \times \text{diag}(1, 1)$ , and the standard deviations of range measurement noise and bearing measurement noise are 25m and  $0.02^\circ$ , respectively. The forgetting factor is  $\rho = 0.98$ , and the softening factor is set to be  $\beta = 6$ .

The CKF, the proposed 5-CKF, the STCKF in [26] (denoted as STCKF-1), the STCKF (CKF combined with the new strong tracking filter structure in this paper), and the proposed 5-STCKF are taken into account in this simulation. The metrics used to compare the performance of various

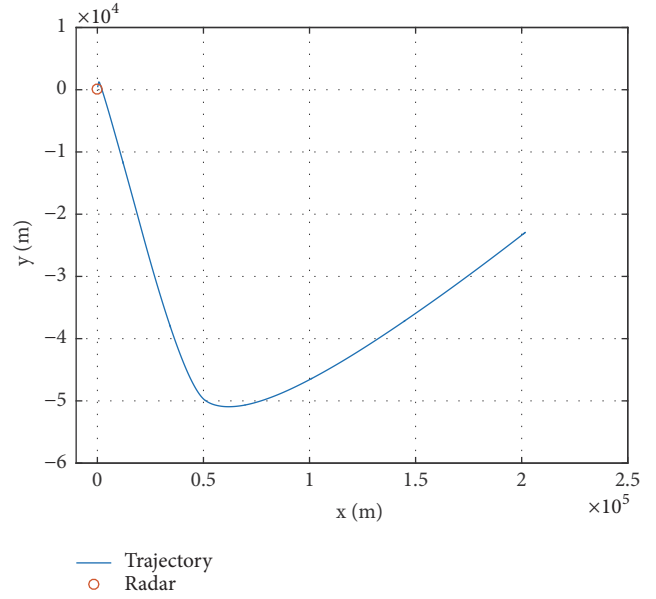


FIGURE 2: The trajectory of the target and the location of the radar.

filters are the root mean square error (RMSE) and average RMSE (ARMSE), which are defined as follows:

$$RMSE_{pos}(k) = \sqrt{\frac{1}{M} \sum_{m=1}^M \left( (x_k - \hat{x}_{m,k}^+)^2 + (y_k - \hat{y}_{m,k}^+)^2 \right)} \quad (54)$$

$$ARMSE_{pos} = \frac{1}{N} \sum_{k=1}^N RMSE_{pos}(k) \quad (55)$$

where  $M$  denotes the number of Monte-Carlo runs,  $N$  represents the total simulation times,  $x_k$  and  $y_k$  denote the true position at time  $k$ , and  $\hat{x}_{m,k}^+$  and  $\hat{y}_{m,k}^+$  denote the estimated position at time  $k$  in the  $m$ th Monte-Carlo simulation. The velocity RMSE and velocity ARMSE are defined similarly.

The Monte-Carlo simulations are implemented 200 times, and the results are shown in Figures 3–6. It can be seen from Figures 3 and 4 that the position RMSE and velocity RMSE of all the filters have a sudden jump at 40s, 120s, and 200s on account of the maneuverings taken. However, the RMSEs of the three strong tracking filters achieve convergence after a short time, while those of the CKFs achieve divergence, indicating that the three strong tracking filters have the ability to track the maneuvering target, while the CKF and 5-CKF cannot. The reason is that the suboptimal fading factor in the strong tracking filters can adjust the filtering gain matrix in real time to force the residual sequences mutually orthogonal, thus to enhance the ability of the filter to track the mutation state, while no fading factor exists in the CKF and 5-CKF. From Figures 5 and 6, we see that the three strong tracking filters can estimate the accelerations effectively, while CKF and 5-CKF cannot achieve the estimations of the accelerations.

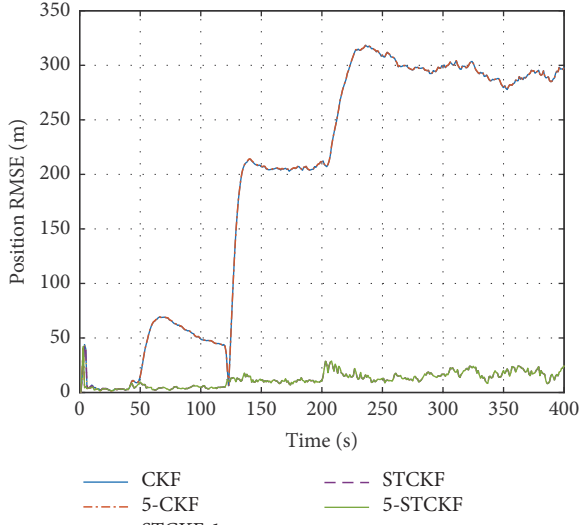


FIGURE 3: Position RMSEs of the five filters.

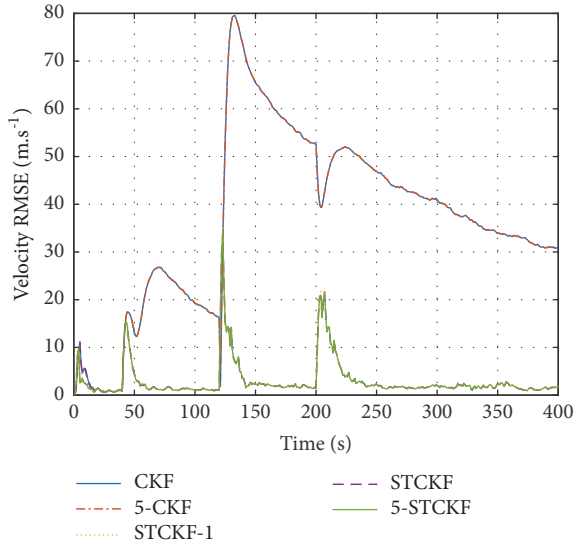


FIGURE 4: Velocity RMSEs of the five filters.

TABLE 2: Position ARMSEs and velocity ARMSEs of the five filters.

Filters	Position ARMSE/m	Velocity ARMSE/(m.s <sup>-1</sup> )
CKF	194.2629	36.4900
5-CKF	194.2501	36.4539
STCKF-1	12.1252	3.1578
STCKF	12.0985	3.1417
5-STCKF	11.9466	3.0843

The position ARMSE and velocity ARMSE are listed in Table 2. As shown in the figures, the RMSEs of the CKF and 5-CKF are significantly larger than those of the other three strong tracking filters. The RMSEs of STCKF are smaller than that of STCKF-1, indicating that the new strong tracking filter structure proposed in this paper is better than that in [26]; the reason is that the proposed

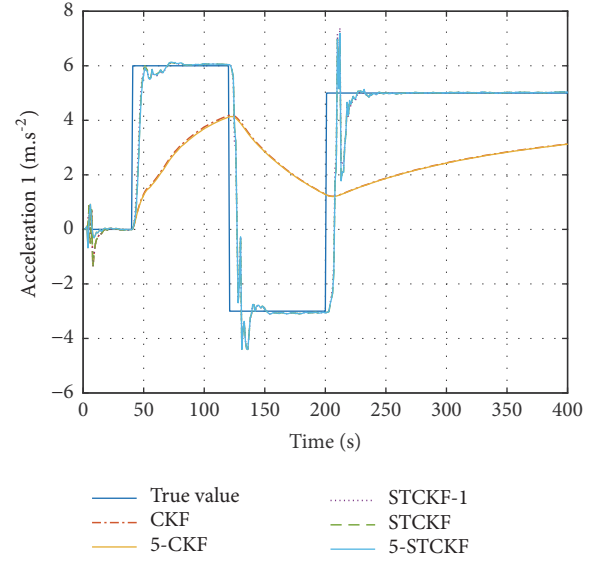


FIGURE 5: Estimated acceleration 1 of the five filters.

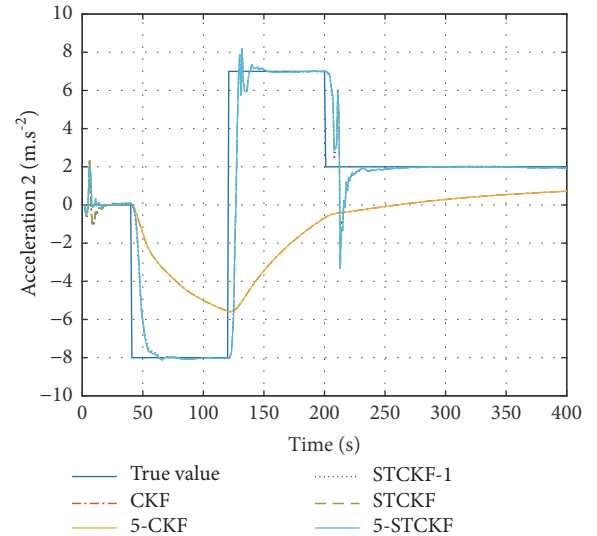


FIGURE 6: Estimated acceleration 2 of the five filters.

structure reduces the calculation for cubature points from three times to twice, which reduces the loss of higher order moment information. Compared with STCKF, the 5-STCKF improves the position ARMSE and velocity ARMSE by 1.26% and 1.83%, respectively, indicating that the novel fifth-degree cubature rule is more accurate in approximating the Gaussian weighted integral than conventional third-degree cubature rule.

## 5. Conclusion

In this paper, a novel 5-STCKF is put forward to improve the two-dimensional maneuvering target tracking accuracy. For this, the intractable nonlinear Gaussian weighted integral is approximated using a novel fifth-degree cubature rule, and the suboptimal fading factor is designed in a new method

to adjust the filtering gain matrix online and force the residual sequences mutually orthogonal, thus to improve the ability of the filter to track the mutation state. Simulation results show that the conventional CKF cannot track the maneuvering target, while the 5-STCKF has the ability to track the maneuvering target, and compared with STCKF, 5-STCKF can achieve higher target tracking accuracy.

## Data Availability

The simulation results data used to support the method of this study are available from the corresponding author upon request.

## Conflicts of Interest

The authors declare no conflicts of interest.

## Acknowledgments

This work was supported partly by the National High Technology Research and Development Program of China (2015AA7026085).

## References

- [1] H. Wu, S. Chen, B. Yang, and K. Chen, "Feedback robust cubature Kalman filter for target tracking using an angle sensor," *Sensors*, vol. 16, p. 629, 2016.
- [2] L. Jia-qiang, Z. Rong-hua, C. Jin-li, Z. Chun-yan, and Z. Yan-ping, "Target tracking algorithm based on adaptive strong tracking particle filter," *IET Science, Measurement & Technology*, vol. 10, no. 7, pp. 704–710, 2016.
- [3] H. Wu, S. Chen, B. Yang, and X. Luo, "Range-parameterised orthogonal simplex cubature Kalman filter for bearings-only measurements," *IET Science, Measurement & Technology*, vol. 10, no. 4, pp. 370–374, 2016.
- [4] P. H. Leong, S. Arulampalam, T. A. Lamahewa, and T. D. Abhayapala, "A Gaussian-sum based cubature Kalman filter for bearings-only tracking," *IEEE Transactions on Aerospace and Electronic Systems*, vol. 49, no. 2, pp. 1161–1176, 2013.
- [5] K. Reif, S. Gunther, E. Yaz, and R. Unbehauen, "Stochastic stability of the discrete-time extended Kalman filter," *IEEE Transactions on Automatic Control*, vol. 44, no. 4, pp. 714–728, 1999.
- [6] M. L. Psiaki, "Backward-smoothing extended Kalman filter," *Journal of Guidance, Control, and Dynamics*, vol. 28, no. 5, pp. 885–894, 2005.
- [7] S. Julier, J. Uhlmann, and H. F. Durrant-Whyte, "A new method for the nonlinear transformation of means and covariances in filters and estimators," *IEEE Transactions on Automatic Control*, vol. 45, no. 3, pp. 477–482, 2000.
- [8] K. Xiong, H. Y. Zhang, and C. W. Chen, "Performance evaluation of UKF-based nonlinear filtering," *Automatica*, vol. 42, no. 2, pp. 261–270, 2006.
- [9] K.-M. Roh, S.-Y. Park, and K.-H. Choi, "Orbit determination using the geomagnetic field measurement via the unscented kalman filter," *Journal of Spacecraft and Rockets*, vol. 44, no. 1, pp. 246–253, 2007.
- [10] K. P. B. Chandra, D.-W. Gu, and I. Postlethwaite, "Square root cubature information filter," *IEEE Sensors Journal*, vol. 13, no. 2, pp. 750–758, 2013.
- [11] J. Zarei and E. Shokri, "Convergence analysis of non-linear filtering based on cubature Kalman filter," *IET Science, Measurement & Technology*, vol. 9, no. 3, pp. 294–305, 2015.
- [12] I. Arasaratnam and S. Haykin, "Cubature Kalman filters," *Institute of Electrical and Electronics Engineers Transactions on Automatic Control*, vol. 54, no. 6, pp. 1254–1269, 2009.
- [13] I. Arasaratnam, S. Haykin, and T. R. Hurd, "Cubature Kalman filtering for continuous-discrete systems: theory and simulations," *IEEE Transactions on Signal Processing*, vol. 58, no. 10, pp. 4977–4993, 2010.
- [14] L. Zhang, H. Yang, H. Lu, S. Zhang, H. Cai, and S. Qian, "Cubature Kalman filtering for relative spacecraft attitude and position estimation," *Acta Astronautica*, vol. 105, no. 1, pp. 254–264, 2014.
- [15] Y. Zhang, Y. Huang, N. Li, and L. Zhao, "Embedded cubature Kalman filter with adaptive setting of free parameter," *Signal Processing*, vol. 114, pp. 112–116, 2015.
- [16] K. Zhang and G. Shan, "Model-switched Gaussian sum cubature Kalman filter for attitude angle-aided three-dimensional target tracking," *IET Radar, Sonar & Navigation*, vol. 9, no. 5, pp. 531–539, 2015.
- [17] L. Chang, B. Hu, A. Li, and F. Qin, "Transformed unscented Kalman filter," *Institute of Electrical and Electronics Engineers Transactions on Automatic Control*, vol. 58, no. 1, pp. 252–257, 2013.
- [18] B. Jia, M. Xin, and Y. Cheng, "High-degree cubature Kalman filter," *Automatica*, vol. 49, no. 2, pp. 510–518, 2013.
- [19] S. Wang, J. Feng, and C. K. Tse, "Spherical simplex-radial cubature Kalman filter," *IEEE Signal Processing Letters*, vol. 21, no. 1, pp. 43–46, 2014.
- [20] D. H. Zhou, Y. G. Xi, and Z. J. Zhang, "A suboptimal multiple fading extended Kalman filter," *Acta Automatica Sinica*, vol. 17, no. 6, pp. 689–695, 1991.
- [21] M. L. Bai, D. H. Zhou, and H. Schwarz, "Identification of generalized friction for an experimental planar two-link flexible manipulator using strong tracking filter," *IEEE Transactions on Robotics and Automation*, vol. 15, no. 2, pp. 362–369, 1999.
- [22] Q. Ge, T. Shao, S. Chen, and C. Wen, "Carrier tracking estimation analysis by using the extended strong tracking filtering," *IEEE Transactions on Industrial Electronics*, vol. 64, no. 2, pp. 1415–1423, 2017.
- [23] M. Narasimhappa, S. L. Sabat, and J. Nayak, "Adaptive sampling strong tracking scaled unscented Kalman filter for denoising the fibre optic gyroscope drift signal," *IET Science, Measurement & Technology*, vol. 9, no. 3, pp. 241–249, 2015.
- [24] W. Zhang, M. Zhu, and Z. Chen, "An adaptive SLAM algorithm based on strong tracking UKF," *Robot*, vol. 32, no. 2, pp. 190–195, 2010.
- [25] B. Xia, H. Wang, M. Wang, W. Sun, Z. Xu, and Y. Lai, "A new method for state of charge estimation of lithium-ion battery based on strong tracking cubature kalman filter," *Energies*, vol. 8, no. 12, pp. 13458–13472, 2015.
- [26] L. Wang, L. Wu, Y. Guan, and G. Wang, "Online sensor fault detection based on an improved strong tracking filter," *Sensors*, vol. 15, no. 2, pp. 4578–4591, 2015.
- [27] H. Liu and W. Wu, "Strong tracking spherical simplex-radial cubature kalman filter for maneuvering target tracking," *Sensors*, vol. 17, no. 4, article 714, 2017.

- [28] D. L. Wei, Z. S. Cui, and J. Chen, "Uncertainty quantification using polynomial chaos expansion with points of monomial cubature rules," *Computers & Structures*, vol. 86, no. 23-24, pp. 2102–2108, 2008.
- [29] J. Lu and D. L. Darmofal, "Higher-dimensional integration with Gaussian weight for applications in probabilistic design," *SIAM Journal on Scientific Computing*, vol. 26, no. 2, pp. 613–624, 2004.